NEM 94

EUROEM

HPEM

BORDEAUX FRANCE - MAY 30 - JUNE 4 1994

EURO ELECTROMAGNETIC

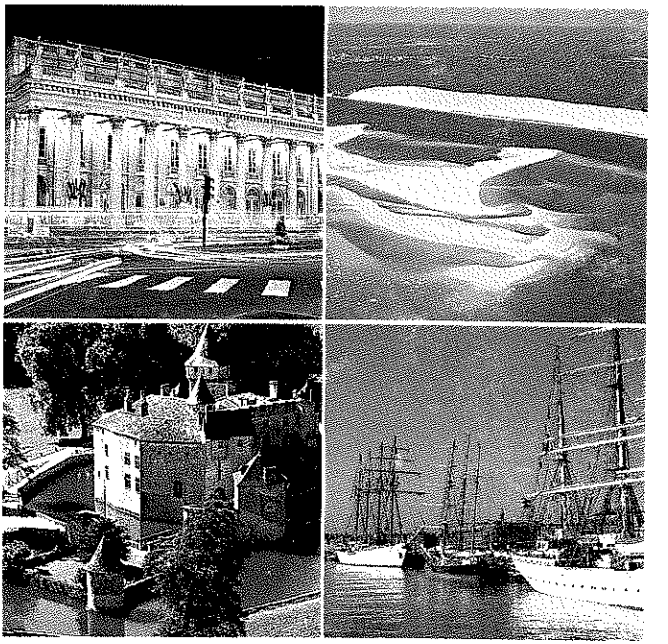

International Symposium on Electromagnetic Environments and Consequences

BOOK OF ABSTRACTS

PERMANENT NEM COMMITTEE

URSI INTERNATIONAL UNION OF RADIO SCIENCE

INSTITUTE OF ELECTRICAL AND ELECTRONICS EN

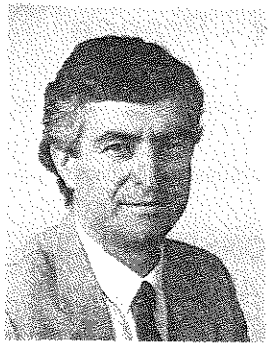

Welcome to the EUROEM 94 International Symposium on ***Electromagnetic Environments and Consequences*** which held in Bordeaux, France, during the week May 29 - June 4, 1994.

EUROEM 94 is organized with the technical sponsorship of the permanent NEM Committee, and with the technical cosponsorship of the ***Institute of Electrical and Electronics Engineers*** (IEEE) - Antennas and Propagation Society - Electromagnetic Compatibility society - Nuclear and plasma Science Society PSAC - Electron Device Society, the ***International Union of RadioScience*** (URSI), and in cooperation with a number of scientific and technical organizations around the world.

EUROEM 94 is the principal forum for the exchange of scientific and technical information on ***Electromagnetic Environments and Consequences.***

The technical program last six days from Monday May 30 through Saturday June 4. It consists of seventy oral sessions and two poster sessions offering more than five hundred invited and contributed papers coming from thirty seven nations. In addition several workshops and panel discussions will be organized. Six short courses will cover particular subjects ; on Wednesday June 1 and Friday June 3, distinguished speakers will address the major technical topics.

The industrial exhibition is an important aspect of the technical program. Any participant is invited to visit approximately one hundred companies proposing new technologies, equipments and services. The exhibition will be open from Monday May 30 through Thursday June 2, 1994.

In addition, two technical visits are proposed. One is a tour of the Braud et Saint-Louis, Nuclear Power Plant operated by Électricité de France ; the other one is a visit of the civil aircraft industry in Toulouse.

We have put together an attractive and entertaining social program for you, your family and friends. The different tours conducted by bilingual guides will bring you in the heart of Bordeaux, to the wine country and to the Atlantic coast and its wild nature. We strongly suggest the proposed touristic pass to optimize your pleasure.

Make your visit to Bordeaux an extended vacation to enjoy the south west part of France. Stay with your family in a medieval or Renaissance castle in the wine country or in the Périgord Valley and visit the 15000 year old paintings at the Lascaux caves. Come and visit Rocamadour and enjoy truffles, foie gras and the best cheeses or simply relax and enjoy the sun on the Atlantic coast.

On behalf of the EUROEM 94 Committees, I invite you to enjoy the EUROEM 94 International Symposium for a week of high quality scientific and technical exchange and for a week of authentic french life style.

D.J. SERAFIN
EUROEM 94 Chairman

EUROEM - EuroElectroMagnetics
May 30 - June 4, 1994 - Bordeaux - France

iis symposium has convened in major cities accross the USA on a regular basis since 1973 (... Stanford 88, buquerque 90, Chicago 92).

ie 1994 symposium is, for the first time, held outside of the U.S.A., in Europe and will address a wide range of tech-cal topics with the theme :

ELECTROMAGNETIC ENVIRONMENTS AND CONSEQUENCES

ECHNICAL SPONSORSHIP :

EM Permanent Committee

ECHNICAL CO-SPONSORSHIP :

EE - Institute of Electrical and Electronics Engineers

- Antennas and Propagation Society
- Electromagnetic Compatibility Society
- Nuclear and Plasma Science Society (PSAC)
- Electron Devices Society

RSI - International Union of RadioScience

HOST ORGANIZATION

Délégation Générale pour l'Armement (D.G.A.)
Direction des Recherches, Etudes et Techniques
Centre d'Etudes de Gramat - 46500 GRAMAT FRANCE
Tél : (33) 65 10 54 32 - Telex : 531679 F - Fax : (33) 65 10 54 33

COOPERATION WITH :

tère de l'Enseignement Supérieur et de la Recherche	*France*
nse Research Agency	*United Kingdom*
lesministerium der Verteidigung	*Germany*
erlands Organization for Applied Scientific Research	*Netherlands*
nce Materiel Administration	*Sweden*
ipement de l'Armement	*Switzerland*
nse Nuclear Agency	*U.S.A.*
ips Laboratory	*U.S.A.*
y Research Laboratory	*U.S.A.*
nse Research Establishment	*Canada*
al Research Laboratory	*U.S.A.*
al Air Systems Command	*U.S.A.*
t Aviation Authorities	*Europe*
tre Nat de la Recherche Scientifique	*France*
ce Nat Etudes & Recherches Aéronautiques	*France*
Centre National d'Etudes Spatiales	*France*
Centre National d'Etudes des Télécoms	*France*
Commissariat à l'Energie Atomique	*France*
European Space Agency	*Europe*
Federal Aviation Administration	*U.S.A.*
Groupement des Industries Françaises Aéronautiques et Spatiales	*France*
Électricité de France	*France*
Syndicat des Industries de Matériel Professionnel d'Électronique et de Radiocommunications	*France*
Association Astronautique et Aéronautique de France	*France*
Union Technique de l'Automobile, du Motocycle et du Cycle	*France*
Groupement des Industries Concernées par les Matériels de Défense Terrestre	*France*
Secrétariat Général de la Défense Nationale	*France*
Los Alamos National Laboratory	*U.S.A.*

GENERAL AND SCIENTIFIC ORGANIZATION

SYMPOSIUM CHAIRMAN

D.J. SERAFIN - DGA - Centre d'Etudes de Gramat - 46500 GRAMAT FRANCE
Phone : (33) 65 10 54 06 or 46 - Fax : (33) 65 10 54 33 or 09

SCIENTIFIC COMMITTEE

N.K. AGARWAL	*India*	W.J. KARZAS	*U.S.A*
F.J. AGEE	*U.S.A.*	J.L. LABOUREYRAS	*Franc*
J.L. AUCOUTURIER	*France*	A. LANUSSE	*Franc*
G. BAKER	*U.S.A.*	P. LEFORT	*Franc*
W.L. BAKER	*U.S.A.*	D. LEUTHAEUSER	*Germa*
C. BAMIERE	*France*	B. MILLER	*U.S.A*
P.R. BARNES	*U.S.A.*	E. MILLER	*U.S.A*
C.E. BAUM	*U.S.A.*	F. MOLINET	*Franc*
G. BEKEFI	*U.S.A.*	J. NITSCH	*Germa*
B.H. BERNSTEIN	*U.S.A.*	M. OREFICE	*Ita*
J.C. BOLOMEY	*France*	W. RADASKY	*U.S.A*
J.L. BOULAY	*France*	Y. RAHMAT-SAMII	*U.S.A*
H.S. CABAYAN	*U.S.A.*	P.W. REIP	*U.*
K.F. CASEY	*U.S.A.*	D. ROBSON	*U.*
M. D'AMORE	*Italy*	D.J. SERAFIN	*Franc*
P. DEGAUQUE	*France*	I. SMITH	*U.S.A*
M. DOUCET	*France*	G. SOPER	*U.S.A*
A. DROUILLAT	*France*	B.T. SZENTKUTI	*Switzerlan*
P. FUERXER	*France*	W. TABBARA	*Franc*
R.L. GARDNER	*U.S.A.*	A. TAFLOVE	*U.S.A*
M. GLYNN	*U.S.A.*	C.D. TAYLOR	*U.S.A*
V.L. GRANATSTEIN	*U.S.A.*	F. TESCHE	*U.S.A*
D.R. HULL	*U.K.*	P. USLENGHI	*U.S.A*
B. JECKO	*France*	E. VANCE	*U.S.A*
C. JONES	*U.S.A.*	E. WENAAS	*U.S.A*
J. JOUSSOT-DUBIEN	*France*	R. WHITE	*U.S.A*
M. KANDA	*U.S.A.*	T.J. WIETING	*U.S.A*
T. KARLSON	*Sweden*		

INTERNATIONAL COMMITTEE

Chairman : M. IANOZ - Switzerland - Co-Chairman : C.E. BAUM - U.S.A.

N.K. ARGAWAL	*India*	L. LIBELLO	*U.S.A*
P. BRUGUIERE	*France*	J. MILLETTA	*U.S.A*
N.J. CARTER	*U.K.*	W. OCHS	*German*
M. D'AMORE	*Italy*	D.M. PARKES	*U.K*
C.D. DE HAAN	*Netherlands*	J.J. RODARO	*Franc*
E. DE LOS REYES	*Spain*	J. SHILLOH	*Israe*
A.M. DE OLIVIERA SANTOS	*Brazil*	J.W. STONE	*U.K*
D.V. GIRI	*U.S.A.*	U.D. STRÄEHLE	*German*
A. KÄLIN	*Switzerland*	B.I. WALHGREN	*Swede*
S. KASYHAP	*Canada*	M.W. WIK	*Swede*
E. KROGAGER	*Denmark*		

ECHNICAL PROGRAM COMMITTEE

airman : J.C. BOLOMEY - France - Co-Chairman : D.J. SERAFIN - France

.C. ALLIOT - *O.N.E.R.A.*
'. AURIOL - *Ecole Centrale de LYON*
I. BAUDRAND - *E.N.S.E.E.I.H.T.*
'. BENIGUEL - *I.E.E.A.*
.P. BOEUF - *Université TOULOUSE*
.M. BUZZI - *Ecole Polytechnique*
.P. CATANI - *C.N.E.S.*
3. CHAMPIOT - *Electricité de FRANCE*
'. CHRISTOPHE - *O.N.E.R.A.*
). DAFIF - *Université LIMOGES*
'. DEGAUQUE - *Université LILLE*
.P. DESMETTRE - *A.N.V.A.R.*
M. DILL - *D.G.A.*
). DUPOUY - *D.G.A.*
3. EUMURIAN - *THOMSON CSF*
3. FAILLON - *THOMSON CSF*
3. FICHEUX - *U.T.A.C.*
'. FLOURENS - *GERAC*
I. C. GAUTHEROT - *D.G.A.*
). GAUTHIER - *C.N.E.S.*
3. GERMAIN - *C.E.A.*
E. GOZZI - *D.G.A.*
H. GRAUBY - *GERAC*
J. HAMELIN - *Ministère de l'Industrie, des Postes, des Télécoms et du Commerce Extérieur*
M. HOWYAN - *D.G.A.*
B. JECKO *Université LIMOGES*
H. KIRCHNER - *THOMSON CSF*
J. LAUNSPACH - *C.E.A.*
J.P. LHOTE - *D.G.A.*
A. LITAUER - *ALCATEL*
R. MALABIAU - *D.G.A.*
J.D. MILLET - *D.G.A.*
F. MOLINET - *MOTHESIM*
J. PIGNERET - *NUCLETUDES*
A. PRIOU - *D.G.A.*
M. RENARD - *D.G.A.*
M. ROSENBERG - *D.G.A.*
W. TABBARA - *Université PARIS*
A. TOUBOUL - *Université BORDEAUX*
P. VERLHAC - *NUCLETUDES*
B. VEYRET - *Université BORDEAUX*
A. ZEDDAM - *FRANCE TELECOM*

TECHNICAL PROGRAM

LENARY SESSIONS

Vednesday June 1 - 10 h 50
Chairman : G.K. Soper - Principal Deputy Assistant to the secretary of defense (Atomic Energy) Pentagone, Washington DC - U.S.A.

10 h 50 : Do Weak Electromagnetic Fields Cause Bioeffects ? Why Is There Such Skepticism ? What Are Possible Answers ?
T.A. Litovitz - Catholic University of America - U.S.A.

11 h 15 : Electromagnetic Detection, Location & Identification of Unexploded Ordonance For Environmental Cleanup
A.E. Hooper. - U.S. Army Yuma Proving Ground - U.S.A.
D. Brown - Aberdeen Proving Ground - U.S.A.

11 h 40 : Integration of Electromagnetic Threats
J. Ma. Pierre - Defense Nuclear Agency - U.S.A.

12 h 05 : Electro-Static Discharge on Spacecrafts : The Genesis, The Risks & The Protections
L. Inzoli - ESA / ESTEC - Netherlands

Friday June 3 - 10 h 30
Chairman : D.J. Serafin - D.G.A. - Centre d'Etudes de Gramat - France

10 h 30 : IEC Standardization of Immunity to HEMP
M.W. Wik - Defence Materiel Administration - Sweden

11 h 00 : High Power Microwaves in Russia
G.A. Mesyats Vice President of the Russian Academy of Sciences and
V.E. Fortov - Russian Academy of Sciences - Russia
S. Korovin - High Currents Electronic Institute Tomsk - Russian Academy of Sciences - Russia

11 h 30 : Up to Date State of the NEMP Problems and Topical Research Directions
V.M. Loborev - Russian Federation Defence Ministry - Russia

12 h 00 : Implications for computational electromagnetics of evolving computer technology
E.K. Miller - Los Alamos National Laboratory - U.S.A.

ANALYSIS OF RETARDED TIME FINITE DIFFERENCE TECHNIQUES

Jim Gilbert
Metatech Corporation
Goleta, California

In the calculation of EMP environments and interactions, it is often useful to go into a moving coordinate system which is traveling at the speed of light, or even faster. The advantage of this is that the number of spatial and time steps can be greatly reduced without loss of calculational accuracy; the disadvantages are that it is often necessary to use implicit differencing techniques involving the inversion of matrices and that care must be taken not to lose accuracy in these inversions. These techniques are best suited for the calculation of EMP environments and coupling to simple structures such as idealized overhead lines where the geometric configuration of conductors is invariant under translations. In this paper we will first discuss the use of implicit techniques in general terms, describing the techniques, limitations and dispersion relations. We will then show how the retarded time technique for overhead line calculations can be extended to include a branched power transmission network in a retarded time implicit network.

The simplest example of a multidimensional retarded time code is a Cartesian finite difference code in two dimensions, and we will take the retarded time direction along the x-axis. Maxwell's equations in retarded time become

$$\frac{\partial F}{\partial x} = \frac{\partial E_z}{\partial y}$$

$$\frac{1}{c}\frac{\partial G}{\partial \tau} - \frac{1}{2}\frac{\partial G}{\partial x} = -\frac{1}{2}\frac{\partial E_z}{\partial y}$$

$$\frac{1}{c}\frac{\partial E_z}{\partial \tau} = \frac{1}{2}\frac{\partial}{\partial y}(F - G)$$

where $F=E_y+cB_z$ is a wave propagating in the +x direction and $G=E_y-cB_z$ is a wave propagating in the -x direction. The equation for the forward going wave F no longer depends on time, but is integrated forward in x. The equation can be put into finite difference form using a centered technique which is different than the centering for explicit techniques - all fields are taken at the same point in x, and F and G occur at mesh points in y, with E_z at half mesh points in y. An implicit technique must be used in the y direction, and the solution in the x-direction can be performed in either an implicit or an explicit fashion. As with the explicit techniques discussed in an accompanying paper, the accuracy can be

determined by the the dispersion relation. A plot of the group velocity is shown in Figure 1.

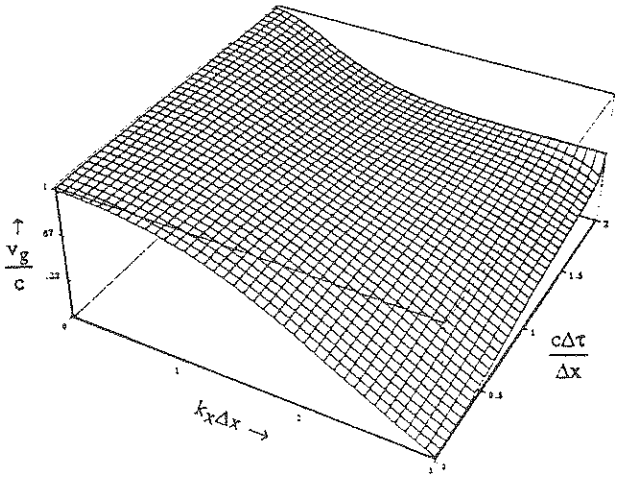

Figure 1. Group velocity of waves perpendicular to retarded time direction.

The presentation will include the dispersion relation for the full implicit case as well as discussing applicability to spherical coordinate systems and oblique incidence of ionizing radiation on a surface. The application the retarded time technique to the calculation of HEMP coupling to an overhead line network illustrates many of the advantages and disadvantages. First consider coupling to a line over a perfectly conducting ground. The equations are best left in terms of the original voltages and currents instead of being put in terms of forward and backward going waves as in the previous example. The transmission line equations become

$$L\frac{\partial I}{\partial \tau}+\frac{\partial V}{\partial x}-\frac{\mu}{c}\frac{\partial V}{\partial \tau}=E_{inc}$$
$$C\frac{V}{\partial \tau}+\frac{\partial I}{\partial x}-\frac{\mu}{c}\frac{\partial I}{\partial \tau}=0$$

where $\mu=\cos\theta$ and θ is the angle between the retarded time axis and the segment of the transmission line. For single lines, the finite difference equations are tridiagonal (five diagonal if an imperfectly conducting ground is included), but making a network breaks this property. Direct inversion of the matrices involved become too inefficient for practical problems, but a numerical trick can be used to reduce the problem to one of inverting tridiagonal matrices for each individual line between nodes, together with inverting a full matrix whose rank is the number of nodes. To describe this procedure, designate the current at the left end of line segment i as I_i^- and that on the right as I_i^+. At each time step, three calculations of each line segment can be used to define the constants A, B and C in

$$I_i^+ = A_i^+ + B_i^+ V_i^- + C_i^+ V_i^+$$
$$I_i^- = A_i^- + B_i^- V_i^- + C_i^- V_i^+$$

where V_i^- and V_i^+ are the voltages at the left and right ends of the ith segment. At each node, the total current must be conserved, and this gives rise to a matrix equation for the node voltages. Since a practical problem can involve several dozen nodes, but many hundreds of finite difference cells, the saving is considerable. The full paper will show examples of calculations performed using this technique.

CAD DATA EXCHANGE AND AUTOMATED MESH GENERATION FOR 3D TIME DOMAIN SOLUTIONS OF MAXWELL'S EQUATIONS

by

Rodney A. Perala* and Henry S. Weigel, IV
Electro Magnetic Applications, Inc.
7655 W. Mississippi Avenue, Suite 300, Lakewood, Colorado 80226 USA
303-980-0070

and

Joe Walsh
FEGS, P. O. Box 838, Duluth, GA 30136-0838 USA
404-497-8947

and

John Rawlinson
FEGS. Ltd., Oakington House Oakington
Cambridge CB4 5AH ENGLAND

The 3D Time Domain Finite Difference (TDFD) solution of Maxwell's Equations is well known and proven to be an efficient and accurate method for solving complex interaction problems. Because the method is a direct solution of the differential equations, there are no fundamental physical approximations which could detract from the solutions' accuracy. In fact, there are really only two sources of error for the solution of these equations:

1. Discretization errors in time and space
2. Accuracy of the scattering object description

The discretization errors determine the bandwidth of the computation. These errors are commonly thought of as acceptably small for results within this bandwidth.

The object description errors are of great significance when one is interested in solving for the EM interaction of a complex system. One example of this is a commercial aircraft, for which one might be interested in solving for both the interior and exterior response. With the TDFD method, this is typically done by gridding the entire aircraft, exterior and interior, and solving the entire problem at once. Interior structures can be extremely detailed, and without automated tools, a considerable amount of work may be involved in obtaining a physical description of the interior. In this process, there is much opportunity for errors to occur in simply developing the analysis model.

In addition, when an analysis model has been defined, there is the problem of generating the 3D mesh. To do this without automated tools is extremely tedious and is again subject to error. Capabilities presently exist to perform 3D analysis on many hundreds of megacells, thus making mesh generation of a complex object of this size prohibitively complex to do without automation.

In this paper we describe facilities which can automate both the analysis model building and the mesh generation. The analysis model can be directly and automatically developed from CAD descriptions. The facility in fact also has the capability for automated post processing, integrated with the analysis model data structure through a Graphical User Interface (GUI).

The GUI has the capability of importing CAD object descriptions, developing an analysis model from the CAD description, automatically meshing the analysis model, interfacing this with the TDFD code, and performing post processing data visualization.

In the paper we discuss the issues involved regarding the requirements for CAD data exchange. The difference between the CAD description and the analysis model are described, as well as the problems involved in developing a suitable analysis model from the CAD description. Sources of error in the mesh generation process are observed, and their possible impact on analysis accuracy.

Examples of this process will be given. A simple example of a cylinder is shown in the figure below, which first shows a suitable analysis model, followed by an automatically generated suitable TDFD mesh.

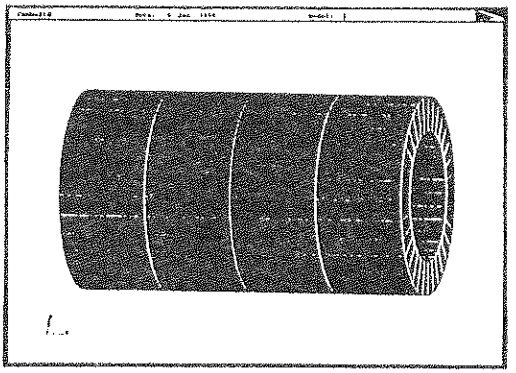

a. Analysis Model of a Simple Cylinder

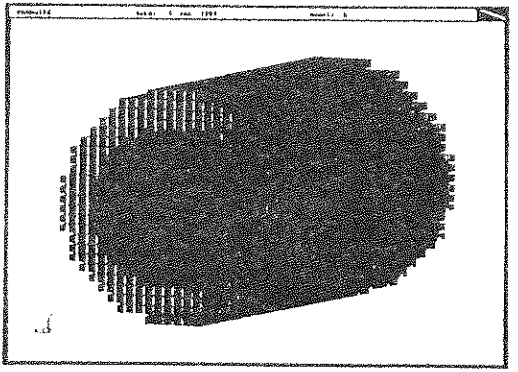

b. Automatically Meshed Model of the Same Cylinder

F.D.T.D. METHOD COUPLED WITH NON ORTHOGONAL SYSTEM OF COORDINATES APPLIED TO SCATTERING PROBLEMS

J.M. Barres, C. Faure, J. Chandezon
L.A.S.M.E.A.
CNRS, URA 830
Université Blaise Pascal
63177 AUBIERE

B. Pecqueux, R. Vezinet
Délégation Générale
pour l'Armement
Centre d'Etudes de Gramat
46500 GRAMAT

Finite Difference Time Domain (F.D.T.D.) method yields the evolution in time of the fields, given a known excitation, and leads to a complete understanding of transient phenomena and near fields. The main default of F.D.T.D. coupled with a cartesian mesh (YEE, IEEE trans. Ant. Propagat., vol. AP-14, no 3, 302-307,1966) lies in the fact that the boundary conditions applied to field components leads to a stepped-edge approximation of curve surfaces.
This process may be improved using the Contour Path Method (A. TAFLOVE, G.A. KRIEGSMANN, EECS and ESAM Depts, Northwestern Univ., Final Rep., 1987): the classical cartesian mesh is kept, but the cells adjacent to the scatterer are deformed to take better into account its real shape.
In this paper, we present a F.D.T.D. algorithm coupled with a tensorial formalism which permits to express accurately the boundary conditions, by using a non orthogonal system of coordinates adapted to the form of the target.

One of the greatest difficulty involved by using curvilinear coordinates is the implementation of the truncation condition at the boundaries of the mesh. Numerical codes for calculating the radiation boudary condition are the most efficient when they are applied in a cartesian mesh. Therefore, we integrate a non orthogonal system of coordinates into a cartesian one. The transition from the first to the second is made by defining a function u of change of coordinates. Figure 1 shows the 2D mesh (roughly represented) in the case of a square of which one side is deformed by a gaussian ($f(x)$).

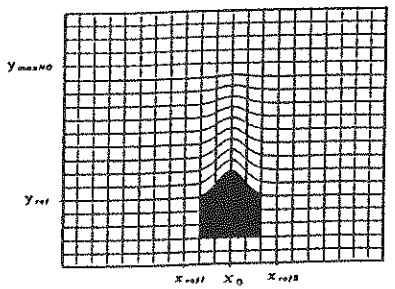

cartesian coordinates	curvilinear coordinates
$x^1 = x$	$x^{1'} = x$
$x^2 = y$	$x^{2'} = u$
$x^3 = z$	$x^{3'} = z$

$$u = \frac{x^2 - f(x^1)}{y_{maxNO} - f(x^1)}(y_{maxNO} - y_{ref}) + y_{ref}$$

Figure 1

The metric tensor in a non orthogonal mesh can be calculated whether analytically if the contour of the object corresponds to a known function (or if it may be approximated by Fourier series), or numerically if only the parametric coordinates in a cartesian mesh are known.
We use the Maxwell-Minkowski formalism (covariant formalism) which have the advantage to be invariant in the case of changing system of coordinates (E.J. POST, Formal structure of electromagnetics, Amsterdam, 1962 - J. CHANDEZON, thèse d'état, Université de Clermont-Ferrand, 1979). Boundary conditions are then expressed exactly, considering the continuity of the covariant tangential component E_i (or H_i if the object is not a perfect conductor) on the surface of the target (corresponding to a line of coordinates). The assembling of different system of coordinates is obviously possible only when the continuity of the covariant components is verified at their interfaces. The time step is calculated by the formula given by M. FUSCO (IEEE Trans. Ant. Prop., vol. 38, no 1, 1990), which is an extension to a curvilinear mesh of the stability condition applied in a cartesian mesh.

The study of propagation of an incident wave through the mesh gives good results, subject to a suitable compromise between the deformation height and the size of the non-orthogonal mesh area. The study of convergence, according to dicretization step, also gives complete satisfaction. Figure 2 shows the H_z component above the object presented on figure 1 at the abscissa $x = x_0$. Calculations are carried with the three following methods: staircasing, contour path and covariant formalism. The excitation is a half period sinusoid TE wave, introduced in the cartesian mesh. The time step used is $\Delta\tau = c\Delta t = 0.3$ and the number of cycles is 830 ; the size of the space is $300\delta \times 300\delta$ where δ is the spatial step in the cartesian mesh ($\delta = \lambda/30$); the size of one side of the square is 60δ, the height of the deformation is 10δ.

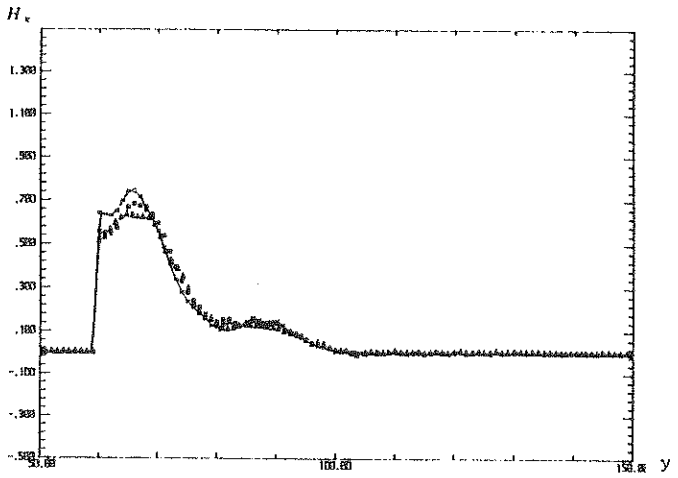

* staircaising • contour path ▲ covariant formalism

Figure 2

FIELDS DISTRIBUTIONS INSIDE A CLOSED GUIDE USING THE FINITE DIFFERENCES METHOD

Rosber Neves Almeida Júnior
Humberto Abdalla Júnior *
Antonio José Martins Soares

Departamento de Engenharia Elétrica
Caixa Postal 04591
Universidade de Brasília
70910-900 DF - Brasil

In the study of the electromagnetic theory it is important to know the distribution of the electric and magnetic fields inside a wave guide. From these it is possible to know how the device works and realize some of its characteristics. This knowledge is also important in teaching as it allows the student to see how the theory works and what will happen inside the guide if one or more parameters change. A computer program was developed to find two dimension fields distributions inside a closed guide with an arbitrary number of layers of different permittivities and an arbitrary number of conductors. These layers and conductors can also be arbitrarily positioned. The fields are traced in a two dimension graph and the potential can be also traced in a three dimension graph. The wave inside the guide is supposed to be a TEM or quasi-TEM one.

In order to know the fields distribution inside a generic device, the Laplace equation has to be solved with the boundary conditions of the guide. Sometimes this equation can be solved analytically using the symmetry of the guide. However, in many cases the analytical solution is quite complex and then a numeric solution is the way to solve the equation.

In this study the finite differences method was chosen for solving Laplace equation due for its simplicity and easy computer implementation.

The application of finite differences to solve this problem restricts the propagation modes in the guide to the TEM or quasi-TEM ones, since for these cases the distribution along the z direction does not change ($\partial\phi/\partial z=0$) and only two dimensions will be needed to represent the field inside the guide. With this consideration the Laplace equation reduces to:

$$\frac{\partial^2\phi}{\partial x^2}+\frac{\partial^2\phi}{\partial y^2}=0$$

A program which runs on an IBM-PC compatible computer has been developed to solve the Laplace equation in generic guide configurations like normal, inverted and suspended microstrips or normal and suspended striplines, for example. Some results obtained with that program are shown in Fig. 1 where a coupled line with two conductors and a dielectric layer with $\varepsilon_r = 2.31$ has its fields distribution drawn.The fields distributions were divided in odd and even modes. As the position of the

lines are arbitrary, the coupled line is not centralized. The line could also be drawn in the middle o the non-unitary dielectric layer.

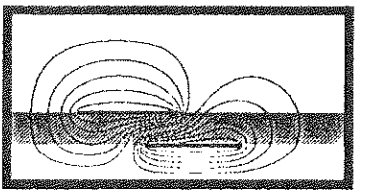

Fig 1a - Magnetic Field (odd mode)

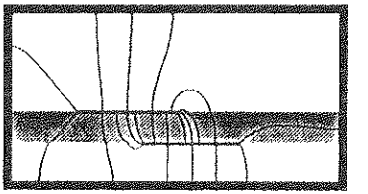

Fig 1b - Electric Field (odd mode)

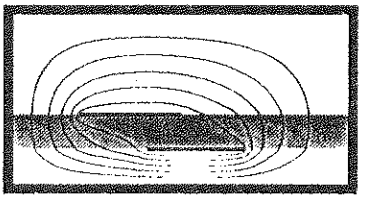

Fig 1c - Magnetic Field (even mode)

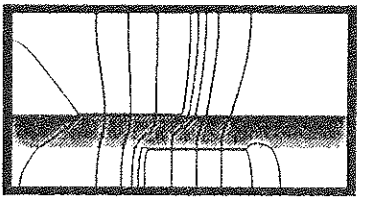

Fig 1d- Electric Field (even mode)

The developed program can also draw a 3D graph to represent the potential distribution a shown in Fig. 2

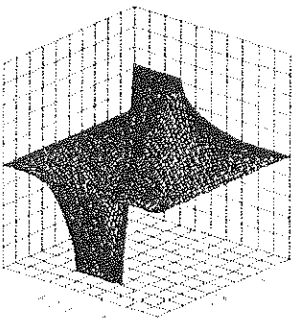

Fig 2a (odd mode)

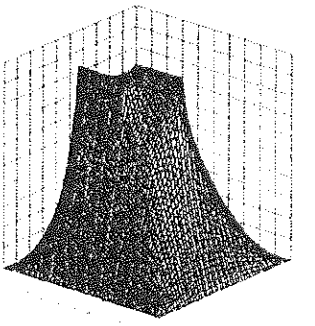

Fig 2b (even mode)

The graphs of Fig. 2a and 2b are similar to the ones of Fig.1a and 1c respectively. In the 3D graphs the potential is represented in the vertical axis while the box's dimensions are represented in the horizontal plane.

Looking at the above figures it is possible to see what happens inside the guide when the field distributions are splited in the two modes. The behavior of the field and flux lines can be easily observed as well as the influence of the insertion of a layer with different permittivity on the fields configuration. The program allows the modification of any of the device parameters. For each modification a corresponding graphic output will be provided.

A PERFECTLY MATCHED LAYER FOR FREE-SPACE SIMULATION IN FINITE-DIFFERENCE COMPUTER CODES

JEAN-PIERRE BERENGER

Centre d'Analyse de Défense 16 bis, Avenue Prieur de la Côte d'Or 94114 Arcueil, France

Most problems solved by the FDTD method are open ones, involving theoretically boundless space extension. So, especial conditions have to be applied on the outer boundaries of the computational domain to absorb the outgoing waves. Various techniques have been used in computer codes to achieve such a simulation of free-space. As it appears through literature, the first one was the *radiating boundary* (Merewether 1971 - THREDE code, Holland 1977). Another one, widely used in France, was the *matched layer* (DIFRAC code, Bérenger 1977 - THREDII code, Holland 1983) which consists in surrounding the computational domain with an absorbing layer whose impedance matches that of free-space. A third technique appeared with the one-way approximation of the wave equation (Engquist-Majda 1977) applied later in the FDTD method (Mur 1981). This last technique seems to be the most used today. However, none of the techniques of free-space simulation is faultless, a wave is absorbed reflectionless in particular cases only, for instance if it is plane and propagates perpendicularly to the boundary. Such imperfections reduce the accuracy of results in some problems and imposes constraints on others as the well known need of setting boundaries sufficiently far from the scatterer when solving wave-structure interaction problems. In order to remove such inconveniences, a new technique of free-space simulation has been developed, which is referred as PML technique.

In a first step, a brief overview of the theory of the PML technique will be provided (a detailed description was submitted to *Journal of Computational Physics*). This technique is based on the use of an absorbing layer which is perfectly matched in the sense that theoretically no reflection occurs at an interface lying between vacuum and layer. In other words, at any frequency and any incidence angle, the reflection coefficient is zero at a vacuum-layer interface. The key of such a reflectionless medium is the splitting of each component of the electromagnetic field into two sub-components.

In a second step we will present some computations performed to evaluate how the theoretical reflectionless properties of the PML layer are preserved in practical FDTD computations. Such computations show that a small amount of numerical reflection is observed, but with a magnitude that can be reduced by tuning some parameters of the layer. So, the PML technique can easily yield practical reflection coefficients far shorter than those produced by the classical matched layer or by the second order of the one-way wave equation.

The last step will be devoted to realistic applications of the PML technique, and especially the wave-structure interaction problems will be adressed. For solving these last problems, it will be shown that the PML technique allows to suppress vacuum around the scatterer, contrary to the other techniques of free-space simulation. So, though the layer has to be some cells thick to avoid numerical reflections, the computational requirements can be drastically reduced by using the PML technique. Such reductions will be illustrated by means of various scatterers of practical interest (airplane, ground vehicule, wire antennas,...).

APPLICATION OF THE RECIPROCITY THEOREM IN FINITE DIFFERENCE TIME DOMAIN SOLUTION OF MAXWELL'S EQUATION

By

Paul M. McKenna* and Poh H. Ng

ELECTRO MAGNETIC APPLICATIONS, INC.
7655 West Mississippi Avenue, Suite 300
Lakewood, CO 80226 USA
Phone: 303-980-0070
Fax: 303-980-0836

The Lorentz Reciprocity Theorem is a result from classical electrodynamics which relates the action at a distance (field) of one source to the action of another source. If the two sources J1 and J2 can be thought of as infinitesimal, then we can show, via the reciprocity theorem, that

$$E1*J2 = E2*J1$$

where E1 and E2 are the fields produced by the sources J1 and J2, respectively. This result is regularly used in antenna theory to show the equivalence of an antenna under transmission and reception, among other applications. We have applied the reciprocity theorem to investigate the problems of plane wave coupling to a free space scattering objects in the time domain, which is of interest to the HEMP, HPM and HIRF communities. A typical example is the excitation of an internal wire by fields penetrating the enclosing structure. The main interest in this case is to determine the largest possible response of the wire to an incident pulse. For a given structure and an incident pulse waveform, the response of the wire is determined by the polarization and propagation vectors of the pulse. Thus, the largest response of the wire could be determined by a parametric variation of these two vectors. However, another approach is to drive the wire with a chosen source and examine the radiated fields in various directions to find the largest radiated field. Then by the reciprocity theorem, these are then the propagation and polarization vectors which will produce the largest response in the wire. Since, theoretically, this needs to be done only once, with the additional overhead of computing the radiated fields, significant savings in computational efforts is possible.

The finite difference time domain (FDTD) method is useful in computing electromagnetic fields near the scattering object. Due to limitation in computer memory it is not practical to compute the radiation fields. However, the equivalence principle can be utilized to calculate the radiation fields analytically. For the projection of the FDTD fields to locations outside the FDTD volume, a surface enclosing the scatterer is chosen within the FDTD volume space. The equivalent electric and magnetic sources, which are calculated from the FDTD fields on the surface, are then used to compute the radiation field at the appropriate time at the location of interest. The implementation of the equivalence principle is complicated by the staggered grid typically used in FDTD as well as the need to minimize computer resources required.

A Critical Look at Time Domain Maxwell Solvers for Electromagnetics

Raj Mittra
Electromagnetic Communication Laboratory
University of Illinois at Urbana-Champaign
Urbana, IL , U.S.A 61801

ABSTRACT

In this paper we present an overview of some recent developments in Time Domain Techniques for solving the problems of electromagnetic scattering from arbitrarily-shaped and inhomogeneous bodies, radiation from antennas on complex structures, and the modeling of microwave and digital circuits. Because of the versatility of the time domain methods, as evidenced by their ability to model complex scatterers as well as electronic circuits that often possess intricate geometries and or have highly inhomogeneous material properties, and because the need to invert a matrix is obviated in the direct solution of Maxwell's equations using the time domain approaches, these methods are currently finding widespread applications in electromagnetics. Of course, the time domain methods are in direct competition with the two widely-used frequency domain approaches, e.g., the Method of Moments and the finite element method(FEM), and the user must make an intelligent decision as to the 'best' method by which to deal with a particular problem.

Despite the many advantages of the time domain methods, the classical finite difference time domain (FDTD) approach, which is also the most widely-used one, has a number of fundamental limitations and there have been many recent attempts to overcome these by various means, e.g., using the Finite Element Time Domain (FETD) approach instead of the FDTD method. One of the main objectives of this paper is to review these various developments and to discuss their present status.

The paper then moves on to present a number of interesting and useful applications that illustrate the power, the utility, as well as the problems that arise in the application of the time domain methods. Some example applications are: (i) scattering by periodic structures which require the imposition of the Floquet condition at the cell boundaries; (ii) underwater or underground imaging of buried at very low frequencies, 1 Hz to 30 KHz range, typically referred to as the quasi-static range; (iii) analysis of resonant antennas, e.g., microstrip patches in a complex environment; (iii) scattering by a large complex structure, e.g., an aircraft; (iv) analysis of inhomogeneous-filled cavities; (v) design of microwave

and industrial heating systems: (vi) extraction of equivalent circuits of transmission line discontinuities arising in microwave and digital circuits: and. (vii) electromagnetic compatibility problems. e.g.. coupling into a cable bundle located in a complex environment.

The paper finishes by drawing some conclusions on the basis of the numerical results presented in the paper for some of the above examples.

CONSOLIDATION OF ANALYTICAL TECHNIQUES IN SYSTEM ASSESSMENT

Robert L. Gardner
Phillips Laboratory
PL/WS
3550 Aberdeen SE
Kirtland AFB, NM, 87117-5776

Abstract

One of the pressing problems of high power electromagnetics (HPE) research is the prediction of the penetration of electromagnetic fields deep into real systems. Interest in making these predictions has increased with the complexity of HPE threats. Candidate threats include lightning, other systems (EMC), high power microwaves, and the currently less interesting nuclear EMP. A number of techniques have been applied to the problem, including statistical methods, large numerical simulations, and topological decomposition. In this paper, we will discuss an application of the BLT equation to system assessment presented six years ago [Paxton and Gardner, Proceedings of EMC Zurich, 1987, page 58J4] and its application to current problems.

The first step in this calculation is to develop the methodology of applying simple transmission line concepts to systems. Simple solutions have been developed for the treatment of propagation along bundles of many combed wires. These solutions use two methods. The first method is to derive an equivalent set of constitutive relations for a cylinder of closely packed conductors. This method is to be compared to a uniaxial cylinder solution, which is the second method. These solutions are adequate for propagation along combed cable bundles, but do not treat the complexities that normally occur in real cable layouts. Discontinuities can be treated using generalized junctions.

Junctions are formed, for example, when two parts of a cable bundle separate either on termination or as part of a generalized cable harness. In this paper, a few simple examples are presented that illustrate the behavior these junctions. Cases are treated which show preferential reflection of differential mode signals

over common mode currents on the bundle. Another example shows certain characteristics of cable breakout boxes.

All of these junction treatments and propagators can be combined into a code that is capable of treating distribution of current within a real system. Predictions of experiments performed on a real communications satellite are used as a case study. Since an analytic propagator is used in the code, run times are extremely fast for geometries that are mostly extended in one dimension.

The type of solved geometry is shown in the figure below. While this geometry appears simple, a similar one was used to predict the behavior of current injection experiments on a real satellite. Sensor measurements agreed with the predictions within about a factor of two for slow excitation.

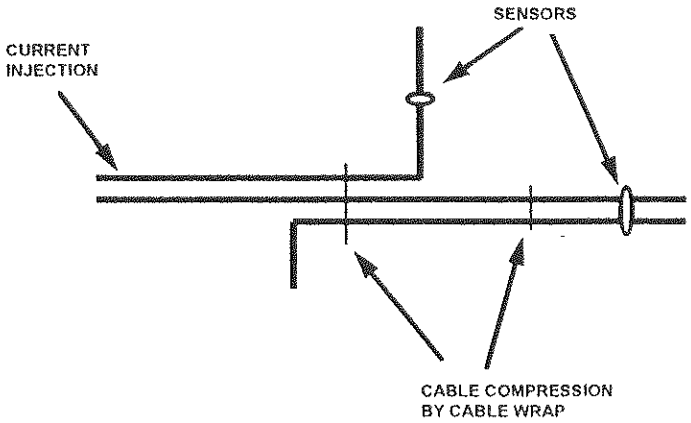

COUPLING ANALYSIS BY A RAPID NEAR FIELD MEASUREMENT TECHNIQUE

B. Chevalier*, J.L. Lasserre
Délégation Générale pour l'Armement
Direction des Recherches, Etudes et Techniques
Etablissement Technique Central de l'Armement
Centre d'Etudes de Gramat
46500 GRAMAT FRANCE

F. Lucas
Satimo
Zone de Courtaboeuf
91952 Les ULIS Cedex FRANCE

1. INTRODUCTION

The interaction between an electromagnetic wave and a target happens through antennas and shielding defects (apertures, connectors...).

If it is quite easy to determine the coupling via the antennas (front door), it is more difficult to estimate the same quantity for a component or a specific equipment inside a structure (back door).

Usual experimental methods simulate as faithfully as possible the coupling conditions: direct illumination of the object. However, these techniques present some constraints.

So, we have chosen an indirect method to determine the coupling using near field measurements. A spherical measurement device has been chosen because of the complexity of the systems to be tested.

2. THE COUPLING CROSS SECTION

To characterize the coupling between the incident wave and the structure, we introduce the notion of Coupling Cross Section (CCS):

$$\sigma = \frac{W_r}{P_{inc}}$$

where σ is the CCS (cm^2), W_r the received power at the considered point (W), and P_{inc} the incident power density (W/cm^2).

The antenna theory is used to determine the CCS. The object is considered in reception and transmission mode (fig. 1).

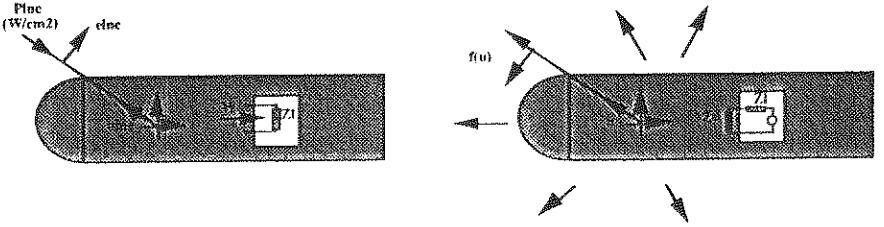

figure 1 : CCS definition for a device under a microwave illumination and the reciprocal problem

For a test point, the CCS is given by:

$$\sigma(u) = \frac{\lambda^2}{4\pi} \rho_{ch}\, \rho_{pol}(u).G(u)$$

where λ is the wavelength, ρ_{ch} and ρ_{pol} respectively the load and polarization factors, and G(u) the gain is direction u.

So, the CCS depends on three primary parameters: frequency, attitude angle and polarization.

3. NEAR FIELD MEASUREMENT DEVICE

The development of a near field measurement device, the SOCRATE facility, has made possible the entire analysis of CCS

between 100 MHz and 4 GHz. This device has been set in an anechoic chamber to simulate free space environment.

The frequency range is divided in two subbands - 100 MHz to 1 GHz and 1 GHz to 4 GHz - using different measurement techniques. In the lower band, the measurements are achieved by means of a single wide band antenna moved mechanically on the meridian. For the upper band, the measurements are performed by means of a semi circular array of 128 dual polarized probes using the modulated scattering technique (J. Ch. Bolomey, B. J. Crown & al, IEEE Trans. AP 36, n°6, June 1988, pp 804 - 813).

4. COUPLING CROSS SECTION ANALYSIS

4.1 Principle of determination of the CCS

We need to measure two quantities to determine the CCS of a device: - the input impedance at the considered feeding point
- the near field radiated by the device.

The input impedance is simply measured with a network analyser. The SOCRATE facility permits to measure the near field on a sphere around the object.

Firstly, the probes of SOCRATE are calibrated using antennas of reference for which the radiated patterns are known. After that, we can measure the corrected near field radiated by the device under test. A spherical near field to far field transformation is then used to obtain the radiated pattern. Using the reciprocity theorem, the CCS is then calculated from the input impedance and the radiated pattern of the device under test.

4.2 Results

To show the interest of SOCRATE for coupling analysis, we have chosen a cylinder (496mm×245mm) presenting four apertures: 3 slots and a circular aperture (fig. 2)

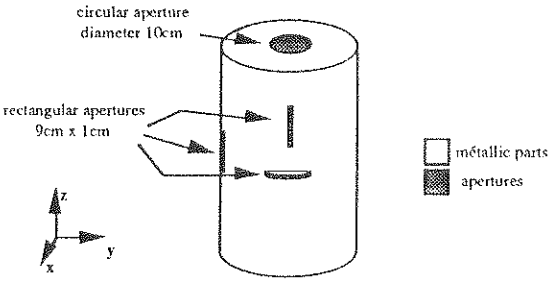

figure 2 : Generic object

The figure 3 shows the CCS obtained at several frequencies: 920 MHz, 930 MHz (TM_{010} mode), 940 MHz, 1.5 GHz (TM_{110} mode) and 2.5 GHz (TM_{111} mode). These diagrams are the combination of the two polarizations along θ and ϕ.

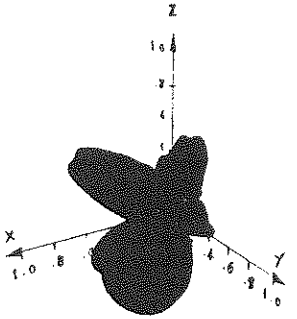

a) f = 920 MHz, max = 1.6 cm²

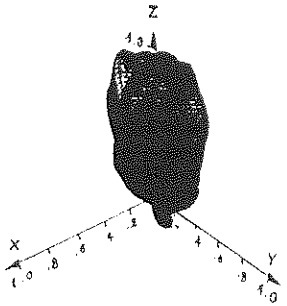

b) f = 930 MHz, max = 30 cm²

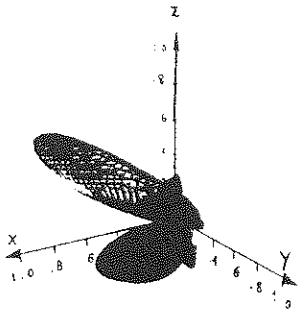

c) f = 940 MHz, max = 1.7 cm²

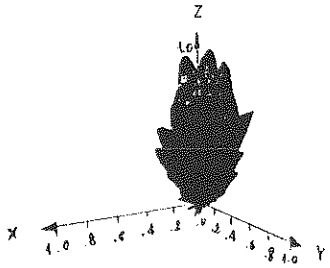

d) f = 1.5 GHz, max = 30 cm²

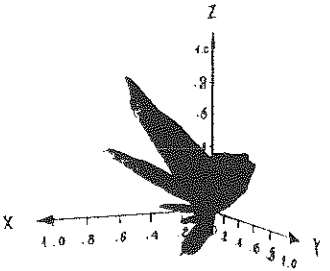

e) f = 2.5 GHz, max = 20 cm²

figure 3 : Coupling cross sections

The CCS diagrams of figure 3 show important variations of attitude angles and coupling levels with frequency, even for very small variations of the frequency around a mode of the cavity (fig. 3 a, b and c). Moreover, the diagrams become more directive for higher frequencies.

Each polarization can be isolated in order to determine, for each frequency, the preferential polarization for the coupling and its associated attitude angle (fig. 4).

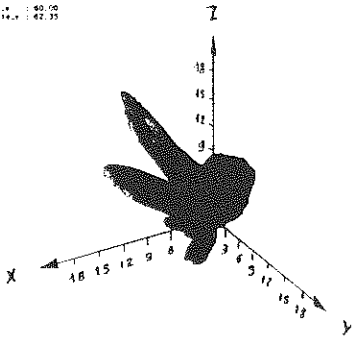

a) θ polarization, max = 19 cm²

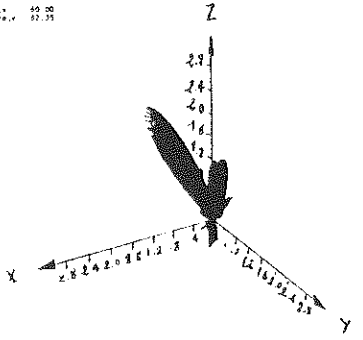

b) ϕ polarization, max = 2 cm²

figure 4 : CCS at f = 2.5 GHz

4. CONCLUSION

We have presented in this paper a method for coupling analysis using rapid near field measurements.

The results presented show the interest of such a method to determine, for a given target, the worst cases of stress by an electromagnetic wave: frequencies, preferential attitude angles and polarizations for coupling.

Associated with this coupling analysis, the C.E.G. is developing a method for the diagnosis of leakage points using a near field to very near field transformation.

The combined use of these two analyses will allow to define the hardening necessary to protect the systems against electromagnetic threats.

COUPLING OF A PLANE WAVE AND A FINITE SLOTTED CYLINDER: INTERNAL AND EXTERNAL NEAR FIELD DISTRIBUTIONS

L.F. Libelo and F.S. Libelo*,# L & L Associates, Bethesda, MD. USA
C.L. Andrews, *Prof. Emeritus*, SUNY, Albany, NY. USA

An experimental electromagnetic coupling investigation of a thin walled, metallic circular cylinder of finite length, closed at both ends and containing a single, symmetrically located, finite length slot in the side wall, aligned parallel to the axis of the cylinder, was carried out. Results obtained for monochromatic CW illumination at normal, symmetric incidence along the cylinder diameter through the center of the slot will be shown.

Measured scans were made of the normalized squared amplitude of the components of the total electric field along the cylinder diameter passing through the center of the slot. Clearly the corresponding linear amplitude distributions can be readily obtained from these. The scans ranged from the inside back wall across the interior of the cylinder and through the slot center to some distance out in front of the cylinder.

To obtain the E-field distributions sensors were constructed by using conducting epoxy to bond short straight sections of thin copper wire on opposite ends of miniature zero biased Schottky diodes. The lengths of the rectifying antennas were carefully controlled to make them inefficient at the frequencies of interest. Simple optical techniques were utilized to ensure maintenance of the alignment of the sensors all along the line of scan. The detected rectified signals were transmitted by long narrow strips of magnetic recording tape of very high impedance at these frequencies. The tapes were also appropriately bonded to the sensors by conducting epoxy. Due to the high impedance the signal transmitted to the recording system remained quite independent of the orientation of the tape leads in the region of the incident and scattered fields. This very important characteristic is essential for obtaining reliable field data.

Field distributions were taken for slots one half-wavelength long for each value of the angle of the slot subtended at the cylinder axis ranging from about 10^{o} to 180^{o}. Due to time limitations only a selected set of results will be presented. Results for two cases will be shown. The first gives the component of E-field parallel to the cylinder axis (the E_z component) for the

incident radiation polarized parallel to the longitudinal slot. The second gives the component of E-field perpendicular to the plane determined by the cylinder axis and the diameter along which the scan was performed (the E_y component) but, in this case, the incident radiation was polarized normal to the cylinder axis. The squared field amplitudes were always normalized relative to the values in the absence of the slotted cylindrical cavity. Results for incident radiation at frequencies below the cutoff of the lowest pure cavity mode, just above the corresponding TE_{111}, and above the TM_{011} cutoffs will be shown.

A large number of interesting characteristics are evident in the resulting measured data. The relative efficiency of coupling through the slot for the two polarization directions is clearly noted for the case when only diffusion into the cylinder can occur as well as for the situation where standing waves can be supported inside. Effects of slot angle size can be observed. Persistence of the cavity characteristics for what would normally be presumed to be large openings is somewhat surprising. Intriguing complex behavior of the system in the vicinity of the slot stands out quite dramatically in many of the E-field scans.

The more general study revealed a host of other very interesting properties displayed by the system in the B-field data as well as for scans of E and B field components measured along different directions, and for different polarizations for the incident radiation, inside and outside the slotted cylinder. Experimental investigation of the system with a circular aperture for various aperture diameters was also carried out. These results shall be reported on at a later date.

Also with Montgomery County Public Schools, Rockville MD. USA

ELECTROMAGNETIC PULSE COUPLING INTO A METALLIC APERTURE WITH SMALL OPENINGS

Hsing-Yi Chen*, I-Young Tarn, and Yeou-Jou Hwang

Department of Electrical Engineering
Yuan-Ze Institute of Technology
Nei-Li, Taoyuan Shian, Taiwan 32026
Telephone: (03) 463-8800 ext. 283
Fax: (03) 463-9355

Analysis of electromagnetic pulse (EMP) penetration via improperly seated shielded aperatures into cavities is an important study in designing computer hartdware systems, TV monitors, high sensitivity instruments, and military application systems. In this paper, the finite-difference time-domain (FDTD) method (K. S. Yee, IEEE Trans. AP-14, 302-307, 1966) was used to study the EMP coupling into one metallic aperture through a small hole by nuclear electromagnetic pulse (NEMP) waves. The intensity of electric field close to NEMP generators can reach to a very high value of 60-100 kV/m. The rise time is on the order of 10-30 ns in the NEMP waves, while the pulse durations is on the order of 100-300 ns. Approximately, the incident electric fields of NEMP waves were expressed by $E(t) = 52\times(e^{-4\times10^6 t} - e^{-4.762\times10^8 t})$ kV/m used for the calculations by using the FDTD technique as shown in Fig. 1. The frequency of the NEMP waves was assumed to be 50 MHz. A rectangular aperture was made of aluminum material with dimensions of 30× 30×40 cm in each side as shown in Fig. 2. The thickness of each plate of the aperture was assumed to be 1 cm and one small hole with an area of 10×10 cm was opened in the frontplate. The electric field was sampled at a point in the center of the metallic aperture. The time-domain behavior of the electric field inside the metal aperture excited by the NEMP waves was obtained by the FDTD method as shown in Fig. 3. It was found that: i) the maximum electric field of 383 V/m was induced inside the aperture, ii) the time-domain response oscilated with the frequency of the NEMP waves and damped out in about 400 ns.

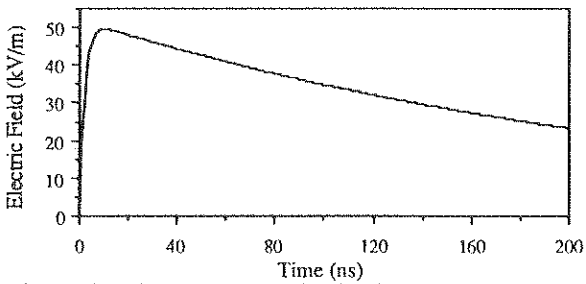

Fig.1 The NEMP wave used for the simulations. The incident electric field was assumed to be $E_z(t) = 52 \times (e^{-4\times10^6 t} - e^{-4.762\times10^8 t})$ kV/m.

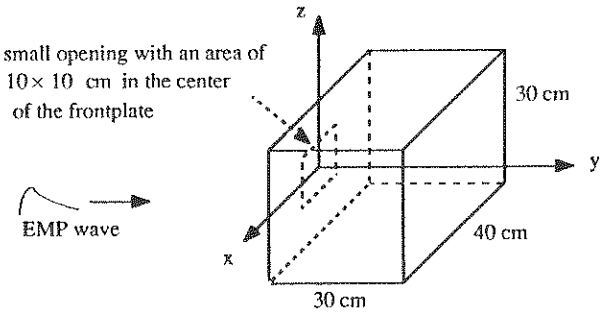

Fig. 2 An aluminum aperture with dimensions of 30× 30×40 cm in each side was used for the simulations by the FDTD method. The thickness of each plate of the aperture was assumed to be 1 cm. The time-domain behavior of electric field was sampled by a point located at x=0, y=15, and z= 0 cm.

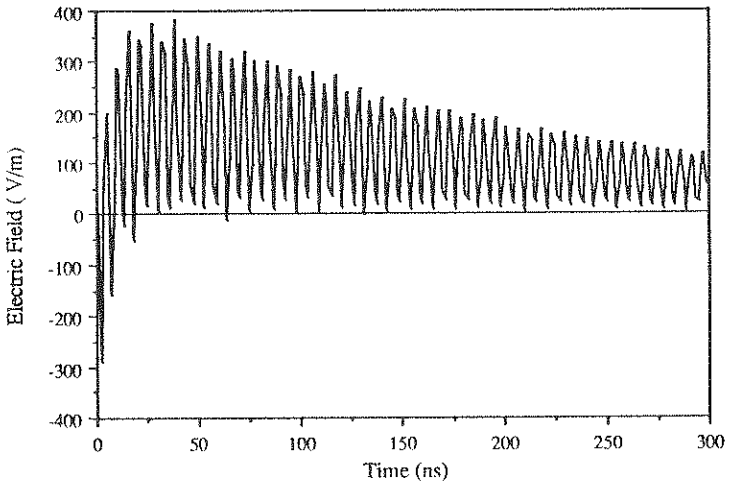

Fig. 3 The time response of the electric field samlped at point (0, 15 cm, 0) inside the metal aperture.

COUPLING OF AN EM WAVE TO A WIRE IN A CAVITY VARIATIONS WITH WIRE POSITION

D.Lecointe[+*], W.Tabbara[+,++], J.L.Lasserre[+++]

[+]Division Onde - L.S.S./Service d'Electromagnétisme,[++]Université Paris VI Supélec, Plateau de Moulon, 91192 Gif sur Yvette, France.
[+++]C.E.G., Service AEM, Groupe HF, 46500 Gramat, France.

I. PROBLEM AND FORMULATION

An electromagnetic plane wave penetrates through an aperture in the wall of a rectangular cavity and induces a voltage on an impedance placed at the lower end of a vertically oriented wire attached to the bottom of the cavity. For apertures with its sizes small with respect to the wavelength ($\leq 0.4\ \lambda$), the problem is equivalent to the radiation, in a closed cavity, of an electric and a magnetic dipoles placed at the aperture location. When the reaction of the cavity walls on the aperture is neglected, the dipoles moments are functions of the geometry of the aperture and of the incident field. When the reaction is taken into account, the moments are considered as unknowns and determined simultaneously with the induced currents on the wire. An integral equation approach, based on the Green's function of the cavity, and combined with a moment method, is used to determine the currents and/or the dipoles moments. This approach has been validated by comparison with experimental data provided by the Centre d'Etudes de Gramat and the results published elsewhere.

II. RESULTS

We shall here focus our attention mainly on the coupling strength as a function of the wire position and on the identification of the resonances related to these positions and to the walls reaction on the aperture. And we shall also consider the influence of the direction of incidence of the incoming plane wave.

We have considered four positions as shown in the insert of the figure. Before the first resonance, the behavior of the voltage is as expected : it decreases as the distance wire to aperture increases. Some resonances are not sensitive to the wire location. Among them, the resonances of the cavity and those which appears when the reaction of the cavity walls on the aperture is not neglected. When the wire is close to the aperture, there exist enough coupling to create a resonance even when the walls reaction is not considered. This happens at 755 MHz (anti resonance) for a wire at location 2, and at 780 MHz (resonance). The latter has its amplitude greatly magnified when the walls reaction is taken into account.

We have observed the same effects when the wire is at location 1 at 770 MHz (anti resonance similar to the 755 MHz one for location 2) and 780 MHz (resonance),. except that the 780 MHz resonance does not appear if the walls reaction is neglected.

Concerning the angle of arrival of the incident wave, it has no significant effects on the induced voltage over a range of values [-40°, +40°].

Figure 1 : INFLUENCE OF THE WIRE POSITION

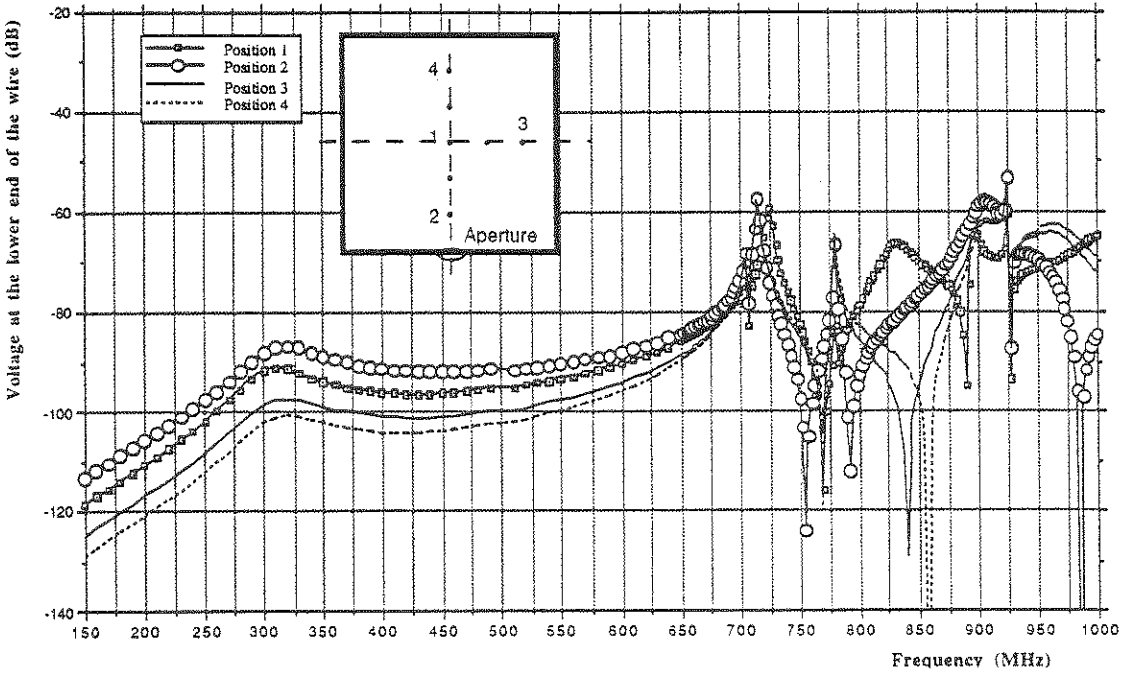

MEASUREMENTS OF ELECTROMAGNETIC FIELDS AT THE WORKPLACE: ALUMINIUM CASTHOUSE (ELECTROMAGNETIC CASTING) AND ALUMINIUM REDUCTION PLANT

Alfred F. Steinegger, HSConsultant, CH - 3973 Venthône, SWITZERLAND

The recent discussion of the possible health effects of electromagnetic fields has suffered from confusion. For example, the biological effects of magnetic fields depend not only on the magnetic field strength (which is directly proportional to the current intensity and distance from the current conductor) but also substantially on the frequency of the current. In this presentation measured data are presented for workplaces in an aluminium casthouse where electromagnetic casting is done and in an aluminium smelter. The question of possible health effects is discussed with reference to the corresponding limit values.

- **Magnetic fields in the electromagnetic casting process (EMC) of aluminium**

In this continuous process there is no mechanical contact of the liquid metal with a mould during solidification. The still liquid head of the ingot, before solidification by cooling takes place, is confined only by the electromagnetic field strength. The necessary magnetic field is produced by a current of 6 '000 A at 2 '500 Hz. The measurements were made at different places in the working environment and in the converter room. During casting there is no need to go into the converter room.

Table 1: Measured data 1 m above the floor level in the working area and 1.5 m in the converter room.

Regular work	5.2 ± 7.7 µT (range 0.5 - 26.9)
Occasional work	2.8 ± 0.7 µT (range 1.0 - 3.4)
Regular work, most of the time	0.4 ± 0.8 µT (range 0.03 - 3.4)
Converter room	33.1 ± 60.5 µT (range 0.11 - 191)

Inside the mould, which is not accessible during the casting process, 3.1 ± 2.4 mT (range 0.54 - 5.2) were measured. During casting the presence of a person directly above the mould, where we have 3.5 and 5.2 µT is not required. From these data we see that the electromagnetic exposure of the workers for routine work ranges is well below the corresponding Threshold Limit Value (TLV - ACGIH) of 24 µT for the frequency of 2 '500 Hz. The values for most of the time during casting, which takes about 6 hours a day, approx. one fifth of the corresponding TLV, are of the same magnitude as from exposure to magnetic fields in everyday life in a non-professional environment, for instance in kitchens and bathrooms, where the typical range is 0.1 - 22 µT with max. values up to 700 µT.

- **Magnetic fields in the aluminium smelting process**

High currents, up to 200 KA of direct current are used in producing aluminium by the electrolytic process. For a plant with 100 KA values of 2.5 - 10 mT at different locations of the typical working area were derived by calculation. These

data have been confirmed by stationary measurements at the same places about 1 m above the ground level. At some "hot spots" where the operator stays only occasionally, the values were between 10 and 20 mT.

Personal dosimeters permit a better evaluation of the exposure at these workplaces. Personal monitors for static magnetic fields, however, are not yet commercially available. For that reason we used a prototype probe analyzer built according to the indications by the Aluminiumindustriens Miljøskretariat / University of Oslo, which has kindly been made available to us. The instrument used was calibrated with an instrument of known accuracy. In combination with a data logger it was possible to get data for a better evaluation of the exposure by dosimetry. The measured value was registered every two seconds. The results of two measuring campaigns, over one hour and over a whole shift, are summarized in Table 2 , and Fig. 1.

Table 2: Results of personal monitoring in the potroom

	1 hour	8- hour shift
Number of values	1088	12 7 44
Number of values > 12 mT	50	134
B max [mT]	40.9	53.0
Mean value B eff [mT]	7.25	4.42
Mean value B [mT]	4.42	3.27

Fig. 1: Distribution of the results of personal monitoring

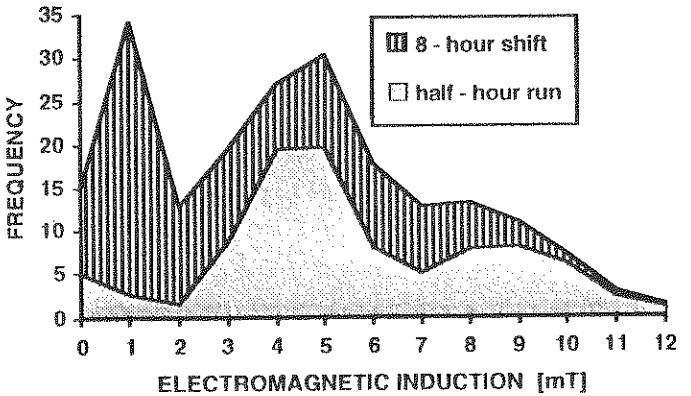

If we compare these results with the corresponding limit values, we see that the exposure for routine work in a 1000 KA smelter is considerably lower.

Table 3: Commonly used limit values of static magnetic fields

		1993 - 1994 TLV (ACGIH)	DIN/ V VDE 0848
Whole body TWA*	workplace	60	75
Ceiling limit	workplace	2000	2000
Cardiac pacemakers		1.0	
General public	whole body 24 h / day		1.26
	whole body 6 h / day		12.6

* 8 - hour Time-Weighted Average

Usually static magnetic fields are superposed by time variable components which result from the rectification of the alternative current. For that reason, the spectrum of frequencies was analysed between 0 and 2 '400 Hz. The highest values were observed in the direct neighborhood of the rectifier room (see Table 4). They decrease rapidly with distance. All results are much lower than the corresponding frequency-dependent ACGIH limit values for occupational exposure.

Table 4: Stationary measurement (max. values) of superposed oscillating currents [in μT] from 50 to 2 '400 Hz in the potroom, rectifier and control room

f [Hz]	50	300	600	1200	1500	1800	2100	2400
Rectifier room	55.27	30.61	4.41	1.72	0.78	0.06	0.06	0.44
Control room	14.45	4.76	2.00	0.16	0.14	0.02	0.06	0.05
Pot, 9 m dist.from rectifier	12.85	14.79	6.05	<	0.62	1.05	0.14	<
Pot, 18 m dist.from rectifier	<	0.45	0.18	0.14	<	0.08	<	0.02
Limit values (ACGIH)	1200	200	100	50	40	33	29	25

ELECTROMAGNETIC FIELDS , BIOLOGICAL EFFECTS AND RISKS AND HAZARDS FOR HUMAN HEALTH

Dr COURT
CENTRE DE RECHERCHES DU SERVICE DE SANTE DES ARMEES
I.C.N.I.R.P.
GROUPE SSA - CEA/DSV-DPTE.

The levels of electromagnetic fields (EMF) to which human health is exposed, increase progressively with the development of civil and military industries, the growth of electrical power generation, all transmission systems (telecommunication, TV, broadcasting), radar and detection systems, all medical applications and their general use in occupational situations. Very low, in the middle of last century, just before the industrial era, the actual human and environmental exposure is made of a complex mix of EMF with a very wide frequency range. Simultaneously the sociological perception of the biological effects of EMF and their hazards are not very well adapted, often exagerated and distorted, sometimes manipulated by conflicting interests; with the discovery and the first scientific discussions of magnetism, the evaluation of Marat's work and the pseudo medical manipulation of Messmer, just before the French Revolution, by Lavoisier and the Royal Academy of Sciences has provoked similar reactions..... Actually the positions are so contrasted ; simultaneously, sometimes same considerations from rare and debated biological results without known mechanism or inconsistent epidemiological data, create deplorable confusions and entertain some degrees of anxiety.

The interaction and biological effects of EMF, differ in different regions of the EM spectrum and it is important to distinguish three separate regions, static electric and magnetic fields, EMF up to 100 KHz and RF above 100 KHz.

With static electric and magnetic fields, there is little evidence of any adverse effect of static electric fields on human health except possible those associated with surface charge. There is any adverse effect in relation to short-term exposure to static magnetic fields of up to 2T. For the static magnetic field of up at least 1T, any carcinogenetic or mutagenetic effects appear. No consistent effects on rodent behavior appear after exposure to up to 12 $kV.m^{-1}$ and there is any effect on hematopoïetic and reproduction and prenatal or post natal

survival after exposure to fields of up to 340 $kV.m^{-1}$. Changes in the EEG electroencephalogram or in the behavior of primates were reported between 2 and 9 T , but there is no unequivocal evidence from animal studies that chronic exposure to static magnetic fields of 1-2 T over days to years has any adverse effect.

With electric and magnetic fields up to 100 KHz extremely and low frequency electric fields induce time varying electric changes on the surface of the body and electric fields and currents inside the body. The magnitude of the induced current density depends on the electical properties of tissues, on body size and orientation and increases linearly with increasing frequency. The threshold of perception of the effects of surface charge is 15-20 $kV.m^{-1}$ for hair vibration, as low as about $kV.m^{-1}$ for hair vibration, as low as about 1,3,5 $kV.m^{-1}$ for microstocks to grounded objects. In the frequency range 1-1000 Hz induced current densities greater than about 10 $mA.m^{-2}$ may affect electrically excitable cells (muscular and nervous system cell particularly.)

Time varying electromagnetic fields up-to 100 KHz (including power frequencies) are not mutagenic or carcinogenetic. The influence of prolonged exposure to electric fields on the production and secretion of melatonine, a possible inhibor of tumour growth has been not confirmed and the possible effects of exposure on circadian rythmes and on prenatal and post natal development are without consistency.

With radiofrequency effects above 100 kHz the power absorption per unit mass of tissue increases and penetration decreases, but the coupling of RF to the body is variable with the body size relative to the wavelength and the orientation relative to the field.The maximum (resonant) absorption conditions occur at around 40 MHz for an average man and when the radiation wavelength is smaller than the dimensions of the body, it is possible to have the reflexion and refraction of radiation in localised hot spots. The absorption is confirmed to skin when frequencies are greater than about 10 GHz.

The effect of exposure to RF frequencies above 100 kHz is thermal and the concept used to describe absorption rate and specific effect is SAR or specific absorption rate, with two notions, the value normalised over the whole body mass or the whole body averaged SAR or the localised value over a small mass of tissue. The man tolerate short-term rises in body temperature by up about 1°C corresponding to a specific absorption rate SAR of 1 $W.kg^{-1}$ up to 4 $W.kg^{-1}$ for short periods, but the tolerance is variable with age, the thermoregulatory ability and the physical, the exercices and the clinical conditions

It is possible to hear pulse-modulated RF and microwave radiation between about 200 MHz and 6.5 GHz the perception threshold for pulses shorter than 30 μs.is variable with the energy density per pulse # 400 mJ . m^{-2}. The perception for a pulse is a click, for continuous modulated impulsions train, a buzzing noise.

It is possible to describe :

- endocrin responses to acute EMF exposure but all responses are non specific and in relation to the heat,

- effects of RF on hematopoitic and reproduction function but all effects are the expression of stress-heat- mediated response,

- the heating effect on the lens of the eye, but the threshold temperature in the lens for cataract induction for prolonged exposure is between about 41 and 43° C, with corresponding local SAR # 100 - 140 W.kg-1

- an teratogenic effect with a significative rise in maternal body temperature, but exposure at less than W.kg^{-1} had no effect.

- any increase in mutation or chromosome aberration when the central temperature is maintened in physiological limits and many experimental results suggest that RF is not mutagenic, unlikely to initiate cancers and there is any risk in carcinogenetic processes.

Generally the epidemiological studies concerning residential exposure or occupational exposure to EMF and their influence on the morbidity, the mortality, the risk of cancer does not suggest that EM field exposure in normal conditions is a risk or hazard.

Several epidemiological data on the children's cancer (hematological diseases and brain tumors) are absolutely unable to establish surely a link between EMF exposure and a carcinogenetic effect :

- Electromagnetic field measurement were rarely made
- The exposure were assessed on the basis of non sure informations
- The biases in the selection of controls are frequent and no evaluated.
- The general morbidity and other etiologic factors are not always studied with precisions.

There is no firm evidence of the existence of a carcinogenetic hazard from exposure of paternal gonads.

Actually the limits for occupational and public exposure, established by IEEE, NATO and IRPA Guidelined on Protection Against Non-Ionizing Radiation represent the best value to allow the general use of EMF under safe conditions.

Actually with moderation and strict scientific evaluation, it is possible to propose studies on the biological effects of ultra short pulsed modulated EMF, to promote theoretical and some experimental studies point towards the cell membrane, the cell transformation studies and to privelege the epidemiological studies with an approach · study of workers occupationally exposed to different EMF.

CURRENT AND SAR INDUCED IN A HUMAN HEAD MODEL BY THE ELECTROMAGNETIC FIELDS IRRADIATED FROM A CELLULAR PHONE

Jong-Chwen Wang* and Hsing-Yi Chen

Department of Electrical Engineering
Yuan-Ze Institute of Technology
Nei-Li, Taoyuan Shian, Taiwan 32026
Telephone: (03) 463-8800 ext. 283
Fax: (03) 463-9355

Recently, there has been an increasing public concern about the health risk of electromagnetic (EM) waves emitted from cellular phones. Do cellular phones really cause brain tumors? Before answering this question, the most important thing for researchers may be to conduct innovative studies associated with analytical and numerical quantification of the biological effects caused by EM waves and to further study their potential hazards. In this paper, the near field finite-difference time-domain method (K. S. Yee, IEEE Trans. AP-14, 302-307, 1966), was used to calculate the current and specific absorption rate (SAR) distributions in an inhomogeneous model of a human head exposed to the electromagnetic waves irradiated from a cellular phone. The human head was simulated by a model of 57,263 block cells with inhomogeneous dielectric constant and conductivity. The cellular phone was modeled by an equivalent dipole antenna with an equivalent resistor of 120 ohms located at the center gap between the two arms of this dipole antenna. The transmitted power of the cellular phone was assumed to be 0.6 watts at a frequency of 835 MHz. For the head near the dipole antenna in the range of 1.0~2.5 cm, the maximum currents and SARs induced in the head were found in the ranges of 356~551 mA and 1.228~2.627 W/kg (as shown in Figs. 1-3), respectively. It was also found that the maximum SAR induced in the head was below the IEEE's upper safety limit of 1.6 W/kg for the head to keep a distance from the dipole antenna by longer than 2.0 cm. From Patrick Reilly's report (Electrical Stimulation and Electropathology, Cambridge University Press, Cambridge, United Kingdom, 1992), the neuroelectric thresholds may exceed thermal thresholds if the waveform of the electric current is inefficient for electrical stimulation, such as with sinusoidal currents of very high frequency (> 10^5 Hz), or pulsed currents of very short duration. According to Reilly's empirical formula for the myelinated nerve model, an asymptotic form can be approximately expressed by $I_t = I_0 (f/f_e)^a$. In the asymptotic form, $I_0 \approx 0.4$ mA, f_e=5400 Hz, and a = 0.8 regardless of stimulus duration. Then the I_t is calculated to be 5668 mA at f= 835 MHz, which required to influence neural activity is larger than the maximum induced current of 551 mA calculated for the head near the antenna by 1.0 cm. Finally, further work in this area should be done, to allow researchers to focus on conditions of maximum absorption in the head for study of the biological effects.

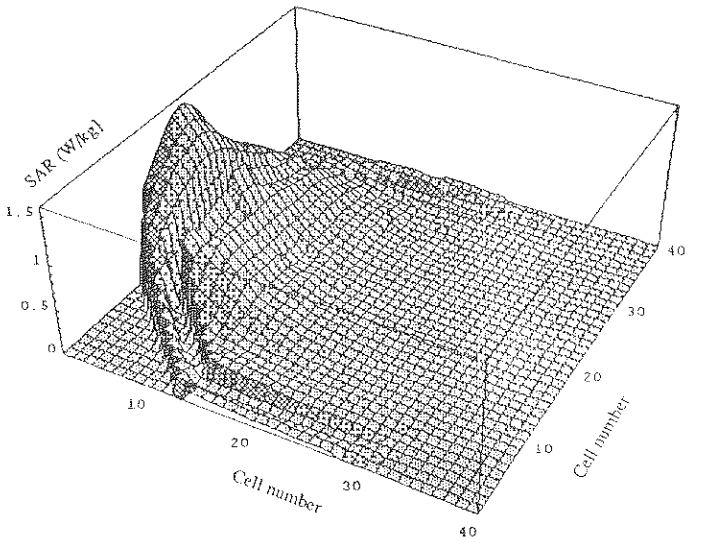

Fig. 1 SAR distributions in the 25th layer counted from the bottom of the head. The distance between the antenna and the head was assumed to be 2.0 cm.

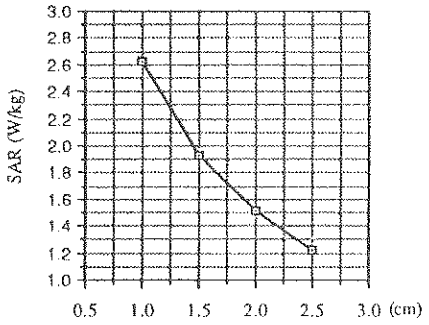

Fig. 2 Maximum SARs induced in the head for the case of an equivalent resistance R_a = 120 ohms used in the dipole antenna.

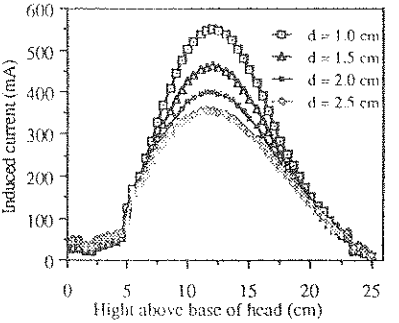

Fig. 3 Current distributions in the head for the case of an equivalent resistance R_a = 120 ohms used in the dipole antenna. d is the distance between the dipole antenna and the head.

MICROWAVE EXPOSURE OF FOREST TREES AND LICHENS

P. Schmutz (*), J. B. Bucher and D. Tarjan

Federal Institute of Forest, Snow and Landscape Research, CH-8903 Birmensdorf, Switzerland

J. Siegenthaler and Ch. Stäger

R & D Department, GD PTT, CH-3030 Berne, Switzerland

M. Urech

PULS Environmental Consulting, CH-3007 Berne, Switzerland

In the past years, forest damage in connection with 'forest decline' was occasionally attributed to the increasing presence of radio wave and microwave radiation in the environment. In Switzerland, case studies near radio stations and microwave links found no correlation between forest health and exposure to electromagnetic waves in the power flux density (PFD) range between 10E-5 and 10E-12 mW/cm2.

Fig.1

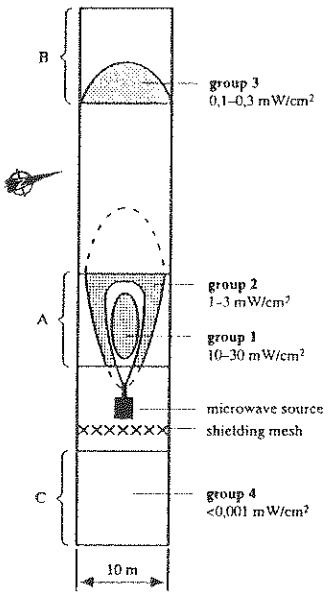

The present study investigated the effects of microwaves with high PFD on young trees. Four-year-old spruce (*Picea abies*) and three-year-old beech (*Fagus sylvatica*) seedlings were planted in an alternate pattern in three fields (A, B and C, cf. Fig. 1) with a distance of 86 cm between neighbouring trees. Field A and B were exposed to microwaves generated by a 600 W magnetron source of 2.45 GHz, focussed by a horn antenna. Field C was shielded from the microwave source by a metal mesh. The trees were permanently exposed to PFD's of between 0.0007 and 30 mW/cm2 depending on their location, for the period of three and a half years. Heating effects of the microwave radiation were estimated by measuring the temperature-dependent hydrolysis of sucrose solutions exposed in sealed ampoules at different locations in the fields. The typical solution temperatures increased with increasing PFD up to 4 C above control solutions exposed to 0.0007 mW/cm2 (Fig. 2).

During the whole exposure period, the microwave radiation caused no visual symptoms on the trees, such as foliage chlorosis and necrosis or premature leaf abscision. The dates of bud break were indepedent of PFD. Trees were grouped into four exposure classes (Fig. 1), and from each class 10 trees were randomly selected for further analyses. Needle dry weight per shoot length on spruce branches was independent of PFD. This confirmed the visual judgement that even the highest microwave PFD's did not affect crown transparency. Photosynthesis in beech leaves appeared to be similar at all PFD's, as indicated by chlorophyll fluorescence measurements. The nutrient status of spruce needles was not dependent on microwave PFD. The concentrations of calcium and sulfur in beech leaves were significantly reduced at higher PFD's during the first two years of exposure (Fig. 3). However, even in the class exposed to PFD's above 10 mW/cm2 these nutrients were still in the normal range for beech. In the third year of exposure, the effect disappeared. The transient reduction of Ca concentrations is interesting, since mammal cells were reported to excrete Ca when exposed to low-frequency modulated radio waves (Blackman et al., 1985. Bioelectromagnetics 6, p. 1 - 11).

In addition to the trees, transplants of the lichen species *Parmelia tiliacea* and *Hypogymnia physodes* were exposed to the microwaves. After 300 days of exposure both species showed significantly reduced growth at a PFD of 50 mW/cm2 compared to transplants exposed to 5 and 0.0007 mW/cm2. It is currently under investigation whether this response was due to thermal effects.

The present study revealed no evidence of microwave-induced damage on forest trees. On the other hand, lichens responded to high PFD's with reduced growth, the threshold lying between 5 and 50 mW/cm2. In further investigations, the effects of frequency bands and of modulated microwaves should be tested, which was beyond the scope of the present study.

Fig. 2

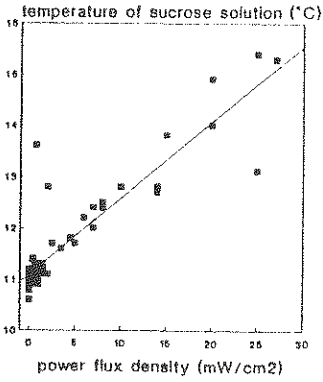

Fig. 3

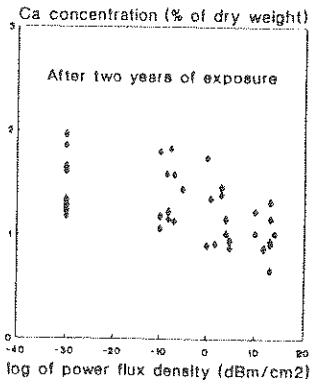

POLARIZATION PROBLEM IN THE DUAL FREQUENCY APPLICATOR

Adnen RAJHI, Tasuku TAKAGI
Depart. of Electric. Commun. Tohoku Univ. Japan

I- Introduction

The polarization state in hyperthermia applicators plays an important role specially in the heating of the subcutaneous fat tissue as shown in Fig. 1, where the tangential electric field to the layred fat-muscle tissue is preferred due to the low heating rate of the subcutaneous fat tissue but in other hands the normal electric field can allow deep heating rather than the tangential. In order to optimize the heating pattern, we find the necessity to design dual frequency applicator in which both electric field are tangentially polarized in the φ and z direction. In this paper we analyze the global polarization state of a two monochromatique EM waves.

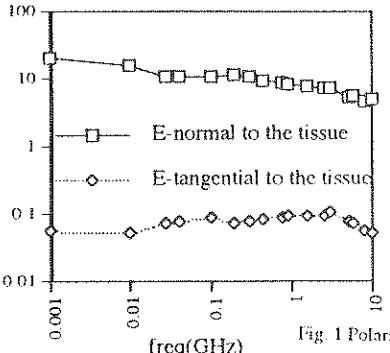

Fig. 1 Polarization effect in the subcutaneous fat tissue

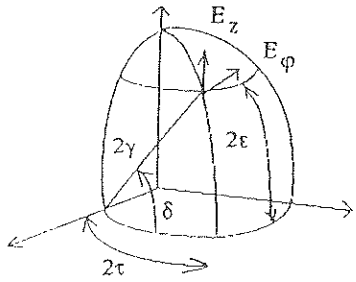

Fig. 2 The poincare sphere

II- Polarization state and stokes parameters

Generally, the polarization state of an EM monochromatic wave can be described by a point on the poincare sphere as shown in Fig. 2, in which the longitude and latitude of the point are related to the parameters of the polarized wave; and it can be shown that the describing set of the polarization state for the two linearly polarized waves ($\vec{E}_\varphi$, $\vec{E}_z$) can be expressed in terms of stockes parameters s_i by

$$s_0 = |E_\varphi|^2 + |E_z|^2$$

$$s_1 = s_0 \cos 2\varepsilon \cos 2\tau = |E_\varphi|^2 - |E_z|^2$$

$$s_2 = s_0 \cos 2\varepsilon \sin 2\tau = 2\,|E_\varphi|\,|E_z| \cos \delta$$

$$s_3 = s_0 \sin 2\varepsilon = 2\,|E_\varphi|\,|E_z| \sin \delta$$

with τ orientation angle of the polarization, ε ellipticity angle, $\gamma = \mathrm{Tan}^{-1}(\frac{E_z}{E_\varphi})$.

Using the principle of the additivity of stockes parameters which satisfy the relation $s_0^2 \geq s_1^2 + s_2^2 + s_3^2$; and the polarization of the two combined monochromatic EM waves can result to an elliptically polarized wave or unpolarized as will be explained in the following ssection

III- The resulting polarization state

Consider two linearly polarized (ε =0) applicators ($\vec{E}_\varphi$, $\vec{E}_z$) with constant amplitudes ($|E_\varphi|$, $|E_z|$) and constant phases ($\delta\varphi$, δz) and assuming that $\delta = \delta z - \delta\varphi$, $\delta\omega = \omega_2 - \omega_1$ and $\xi = \delta\vec{k}.\vec{r} + \delta\omega t$; then two cases of interest appear : when the two applicators are operating at the same frequency (Fig. 3-a Shows the variation of the mean value of the square of the resulting electric field denoted by $I(\theta)$ with θ the angle between $\vec{E}_\varphi$ and $\vec{E}$ for different sets of polarization angles (τ_φ , τ_z)) and when they are operating at different frequencies(Fig. 3-b shows the variation of $I(\theta , \xi)$ with respect to ξ for the different polarization sets; and a comparison is given in Fig. 4 for the two cases.

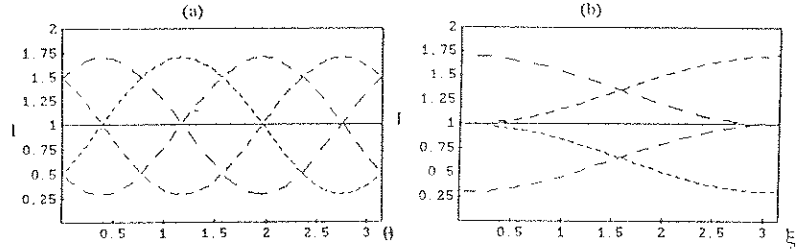

Fig. 3 Variation of the electric intensity (a) when the two applicators operating at the same frequency and (b) at different frequencies.

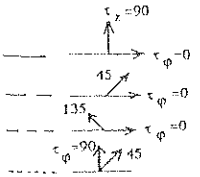

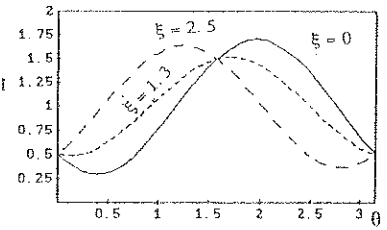

Fig.4 Comparison of the electric intensity for the two cases.

IV- Conclusion

A single frequency applicators have a fixed polarization state and by using a secondary applicators it has been shown that the polarized field can be shifted with respect to the angle θ and with respect to the difference phase due to the different frequencies. Using the principle of the additivity of the stockes parameters shows that the composite wave can be decomposed into an unpolarized part (when the intensity is independent of θ and ξ) and an elliptically polarized part having m as a degree of polarization given by $m = \frac{(s_1^2 + s_2^2 + s_3^2)^{1/2}}{s_0}$; m and the electric vector size of the ellipse is controlled by the frequency bandwidth $\delta\omega$.

EFFECT OF LOW LEVEL RADIOFREQUENCY FIELDS MODULATED AT BRAIN WAVE FREQUENCY ON ATPASE SYSTEM OF DEVELOPING RATS

Kumud K. Kunjilwar[1] and J. Behari
School of Environmental Sciences
Jawaharlal Nehru University,
New Delhi-110067, INDIA

ABSTRACT

We examined the effect of acute as well as chronic exposures of rats to three consecutive harmonics at 36.75 MHz, 73.5 MHz and 147 MHz amplitude modulated (AM) at brain wave frequencies such as 16 and 76 Hz (30-35 days, 3h/day; Av. whole body SAR 0.1-0.14 W/Kg) on ATPase system in developing rat brain. A significant increase in Na^+/K^+-ATPase activity was found in exposed rats compared to the control ones (Fig.1) while a significant decrease in Ca^{2+}-ATPase activity was seen in the exposed rats compared to the control (Fig. 2 A & B). Fig. 1 depicts the net Na^+-K^+-ATPase activity (µmoles of Pi/min/mg) in chronically exposed rats brain as well control ones Fig. 2 depicts net Ca^{2+}-ATPase activity (µmoles/mg/hr) in various exposed and control rats brain. Significant change in ATPase activities was observed in all the cases while at 147 MHZ (AM 16 Hz) the effect was most predominant. However an acute exposure of rats (upto 3 hours) produced no significant change in ATPase activities. A short term single exposure (upto 60 minutes) of total brain membranes in vitro did not show any significant change in ATPase activities. The observed change in Na^+-K^+-ATPase appears to be due to change in ouabain binding of site and which in turn reduces the ability of ouabain to act as an inhibitor of Na^+-K^+-ATPase. It is interesting to observe that significant changes are found even for power level lower than those recommended by Environmental Protection Agency for public safety, USA.

KEYWORDS :- Amplitude modulated, Radiofrequency, Carrier wave, sub-harmonics, Na^+/K^+-ATPase, Ca^{2+}-ATPase.

FIGURE NO. - 1

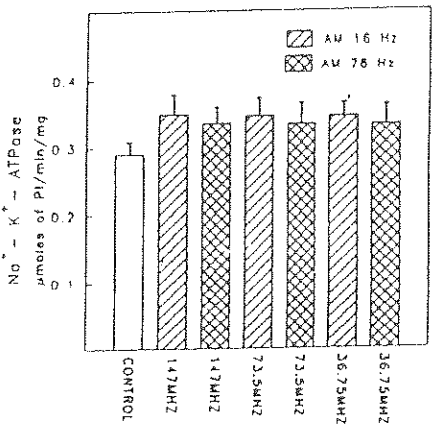

FIGURE NO. - 2

A

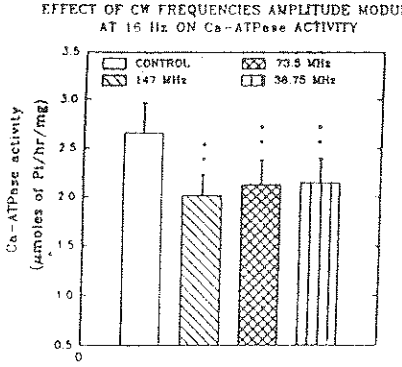

B

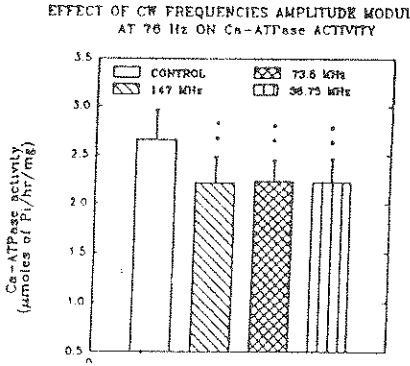

IONIC CONDUCTIVITY AS THE MECHANISM OF MICROWAVE ABSORPTION BY BIOLOGICAL MEMBRANES

Galina I.Ovchinnikova, Julia F.Korosteleva

Physics Department
Moscow State University
119899, Moscow Russia

It may be considered as the experimental fact that iological membranes exhibit superionic conductivity R.E.Lechner, ISSC,1993,Russia]. On the other hand it was shown n [K.Funke,Phys.Lett.53A,3,215,1975] that materials with uperionic conductivity have characteristic features in microwave ielectric response. It means that one can expect the same icrowave spectra features in biological membranes. These eatures consist of sharp decrease in active part of dielectric ermittivity which reaches negative values accompanied by an ldditional relative maximum of conductivity.

To describe the microwave spectra features let us suppose hat the mechanism of superionic conductivity is the jump one and

$$-11$$

hat the jump time is about 10 s. It is evident that this time is ie same order as the microwave period time.

In this case the current induced by moving charges will not e any more just the capacity current as it has been considered efore. The active current component will bring the additional icrowave absorption and cause the biological response of nvestigated system.

Additional active and reactive current components may be ount as the dielectric permittivity and conductivity of some

edia. The frequency dependence comes through transit time.

To prove the identity of offered absorption mechanism the esults were correlated with experimental measurements in requency range where the measurements exist. As an example for omparison the tissues and bones dielectric permitivity and onductivity were chosen. It is shown that there is a good orrelation between calculations and measurements.

"A TRANSPORTABLE 500 kV/0.9 ns-RISE TIME NEMP GENERATOR"

by W. Pont
TNO Physics and Electronics Laboratory
P.O. Box 96864, 2509 JG The Hague, The Netherlands

INTRODUCTION

To simulate a Nuclear EMP corresponding to the new demands, a pulser must be able to generate a pulse with a very short rise time corresponding to frequencies in the Giga Hertz region within the working volume of the NEMP simulator. In order to do so, the pulser should have very small dimensions, and act more or less like a point source. Otherwise non-TEM modes are already exited by the pulser itself.
The described generator therefore has cross-sectional dimensions of only 10 cm at the connection of the switch with the wave launcher. The oil-filled fast output circuit furthermore consists of a strip-line capacitor and a SF6-pressurized rail-gap switch.
This fast pulse circuit is driven by a 500 kV/5 ns rise time pulse generator. A 20 feet, non-metallic, container houses the whole generator system.

Constructing such very fast generators learns that there are many limitations, such as minimum dimensions, insulation, series inductance and speed of the switch. So each part of the system must be designed very carefully, nearly up to the limits of what is physically possible.
The described fast circuit has been made in a strip-line structure from the beginning to the end. Figure 1 explains this.

To match the 90 Ω wave launcher to the generator, the characteristic impedance of the strip-line structure is kept 90 Ω constant up to the output electrode of the switch. The input electrode is connected to the strip-line capacitor via a very short, low inductance conductor.
The rise time of the generated pulse depends strongly on the fast circuit inductance, the characteristics of the output switch, the way of driving the circuit, and the quality of the output transition.

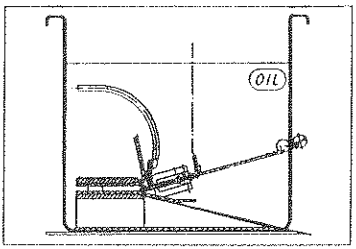

Fig. 1: Fast pulse circuit in strip-line structure.

THE SWITCH

An elliptical curved, 6 cm wide stainless steel rail-gap in SF6, in self breakdown mode, was chosen. The actual closing of this output switch is determined by two mechanisms:
a) *Statistical time-lag.* This is the time needed to form a free electron in the gap volume.
b) *Formative time-lag.* This is the time to build up the discharge current to its maximum value.

These time-lags can be decreased considerably by operating the switch under over-voltage conditions, by driving the circuit with a 5 ns-rise time pulse generator (type 8080 of Physics International Company) via a resistor. For a short time this stressing voltage can be much higher than the static breakdown voltage of the gap.
The rise time related to the switch can be calculated from:

$$t_{gap} = 2.2 \cdot 88 \left(\frac{\rho}{\rho_o}\right)^{1/2} \cdot (Z_c + Z_l)^{-1/3} \cdot E^{-4/3} \qquad [ns]$$

Where ρ/ρ_0 is the ratio of the SF6-gas density to that of air, E is the electric field in the gap in MV/m, $Z_c + Z_l$ is the total circuit impedance. For a single gap (0.9 cm at 10 bar of SF6) and a voltage of 500 kV, the rise time calculated from the upper equation is 0.56 ns. For a total rise time of 0.9 ns, the inductance-related rise time must be not larger than 0.7 ns. This means that the total circuit inductance must be equal or less than 30 nH; this can only be realized in a coaxial structure. Therefore the strip-line shape has been chosen. For a further decrease of this inductance the rail-gap principle was applied. By applying the charging voltage, of the strip-line capacitor, to the same point where the switch is connected, some time is saved by pre-stressing the gap.

THE STRIP-LINE CAPACITOR

It is formed by aluminium ground and top plates, with a specially shaped[1] centre conductor plate insulated by two plates of dielectric material. Considered as a piece of transmission line, the output-pulse amplitude depends on the characteristic impedance Z_c of this line. The lower Z_c, the higher the pulse amplitude, because of the higher reflection coefficient, when the charged strip-line is switched to the load Z_l (90 Ω), see also figure 2. For a low Z_c the dielectric insulator must have a high ε and must be thin and/or the line must have a large width. These data are in contradiction with high voltage insulation and speed. So, eventually 1.2 cm thick polythene was chosen with a moderate ε_r (2.35) but with a very low loss for high frequencies ($tg\delta = 0.0001$) and high dielectric strength (700 kV/cm). A sandwich construction was used to half Z_c to about 4 Ω.

Once the switch closes, nearly 92% of the voltage is reflected to the open rear of the strip-line. So a stair-case like output pulse is generated (figure 2), each step having 92% of the amplitude of the previous one, and a length of less than 2 ns. Notice that the pulse duration is a function of the reflection coefficient, and the length of the strip-line. Because the pulse duration of the 8080 driver is much longer than the wanted pulse, the measured output pulse has a longer tail than the calculated pulse (figure 2). This could be improved by pulse compression technics.

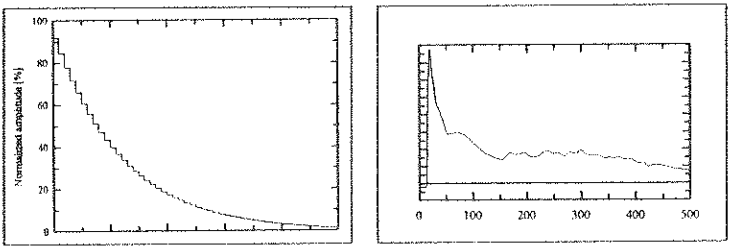

Fig. 2: The generated output pulse; calculated 1) and measured 2).

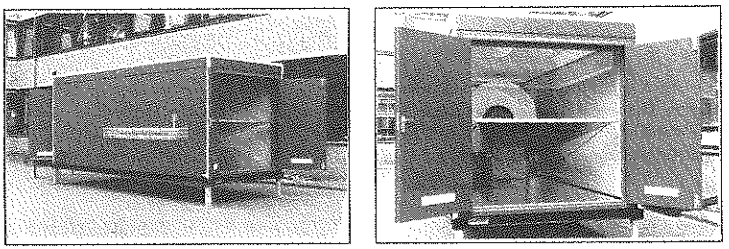

Fig. 3: The complete generator installed in a transportable non-metallic container.

---

1) The plate forms about half a circle, to have equal travelling times, back and forward, of the reflected voltage step to the point the switch input-electrode is connected.

Producing High-Voltage Pulses Using MC-Generators

T.Shikura *, M.Miyamoto
Fuji Electric Corporate R&D Ltd.
7, Yawata-kaigandori, Ichihara, Chiba, 290, Japan

Ⅰ.Introduction

Pulsed power sources to generate high-power pulses are widely employed in the researches in different fields of modern physics and techniques. Recently, the generators have been designed which supply high power in the load over the range of about a few MV and pulse durations of 10^{-6} to 10^{-7} s. However, such generators are very expensive and great in size and weight. Therefore, the use of Magnetic Compression explosive generators (MC-generators) hold the greatest advantages, because they are economical, convenient and less in size and weight. In this paper, more emphasis is forcused on the possibilities of using MC-generators to provide the pulsed high-voltage sources.
The MC-generators are usually low impedance sources and are well suited to drive a wide variety of low impedance loads. On the other hand, high impedance loads could take advantage of the positive future of MC-generators if suitable power conditioning systems were available to generator's load section.
In the earlier researches, some pulsed transformers are tested and/or simulated for that system. However, such devices are great in size in case of herical type generators are used.
In this paper, we show the calculation results of more compact system to produce high voltage-pulses.

Ⅱ.Calculation Circuit

Figure 1 shows the calculation circuit for high voltage generation. In this circuit, initial current flows through a generator inductance and interrupter SW_{off}. If SW_{off} and closing switch SW_{on} is operated, then current is interrupted by SW_{off}, voltage induces at entrance of transmission line T.L.. This induced voltage propagates to the end of line, the voltage will become twice at the end because of missmaching.
In our calculation, the interrupter,such as opening switch, and closeing switch is assumed to variable resistance that the resistance changes linealy.

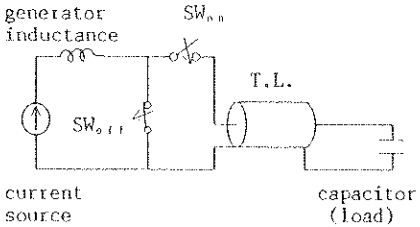

Fig.1 calculation circuit

Ⅲ.Results

Figure 2 shows the relationship between final resistance R_{off} of interrupter and capacitor voltage without T.L.. The output voltage increases as resistance becomes large. For high performance switches, such as plasma compression switch using explosives, the rate of resistance

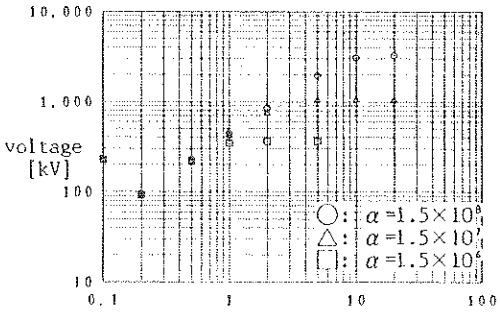

Fig.2 Output voltage without T.L.

increase α is the range of about 1.5×10^8 (Ω/s) and its resistance is several hundred m Ω. Therefore, obtainable output voltage will be a few hundred kV. Figure 3 shows the output voltage of the circuit with T.L. which characteristic impedance Z and its propagation time τ is 10 Ω and 1 μs, respectively. In case of the circuit with T.L., the voltage becomes twice of that of without T.L..

Figure 4 shows the relation between the output voltage and characteristic impedance. The output voltage becomes the maximum values in the range of Z=10 ~ 50Ω. The calculated waveform in τ =10ns, α =1.5×10^8, Z=10Ω, is shown in Fig.5(a). The voltage waveform is an impulse which a high frequency component, which is relate to the propagation time of the L., is superimposed.

If we can positively utilize t 's sinusoidal wave, we may get mor. high-voltage.

Figure 5(b) shows the voltage waveform in the circuit with inductor connected in seriall to capacitor, which inductance is the value ajusted above frequency to the dominant one between capacitor and inductor to above one.

By using this method, we will get a few times greater than that of non-inductor circuit.

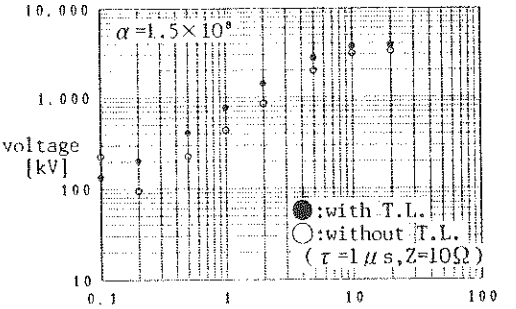

Fig.3 Output voltage with T.L.

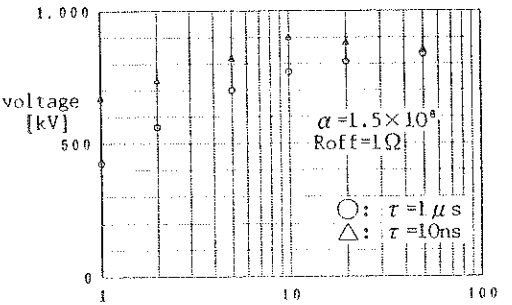

Fig.4 Output voltage vs Z

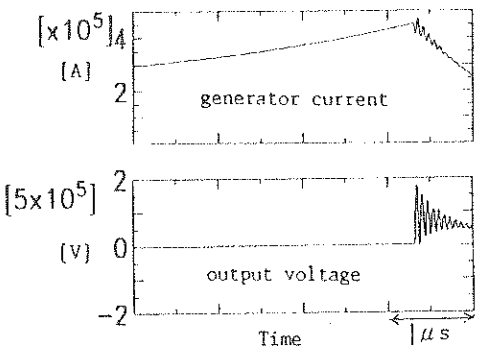

(a) with transmission line

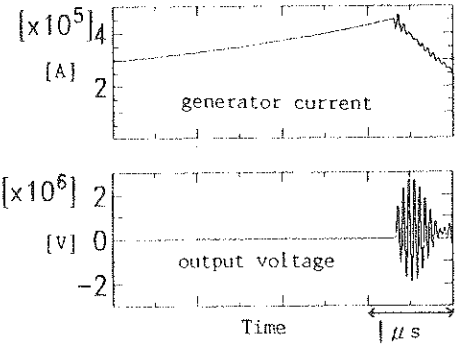

(b) with transmission line and tuning inductor

Fig.5 Voltage waveform

MODIFICATIONS OF THE STRAIGHT CHANNEL ELECTRON MULTIPLIER FOR THE PURPOSE OF HIGH-CURRENT ELECTRON EMISSION

Yu.M.Saveljev *, A.Maitland
C.E.Little and D.M.Parkes

University of St Andrews, Department of Physics and Astronomy
North Haugh, St.Andrews, Fife, KY16 9SS, Scotland, UK

One of the main features of the channel electron multiplier (CEM) is that the total gain does not depend on the absolute length L and diameter d but only the length-to-diameter ratio γ=L/d. To date, applications of CEMs have been confined almost exclusively to image intensification and mass spectrometry. For both applications the emphasis is on miniaturization to form microchannel multipliers as plates of parallel tubes (image) or single tubes (mass spectrometry). Microchannel plates for image intensification have aimed to produce the required high resolution by reducing d to few micrometers. The question of scaling to large diameters does not appear to have been considered. The advantages of such scaling lead to the possibility to create a new kind of electron source which can operate as a cold cathode in poor vacuum conditions with multiplication factors of 10^6 and more. Moreover, the input electron gun may be of low current and voltage with high-frequency modulation. A schematic diagram of the possible electron source on the base of the CEM is shown in Fig.1. The present work aimes to estimate parameters of the CEM as a new high-current large-aperture electron source.

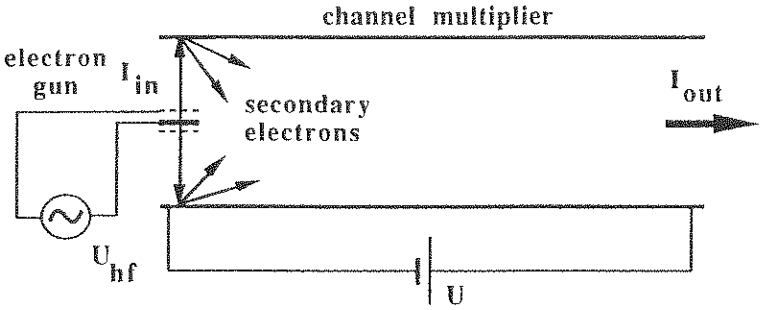

Fig.1

To estimate the geometrical characterisics of the CEM we assume the following properties of the secondary emissive material: the secondary emission coefficient δ reaches its maximum δ_m=2.5 at the primary electron energy V_m=350eV; α=0.6, V_a=5eV and the shape of the δ(V) curve is controlled by a "large" β-function (the detailed description of the above parameters is presented in: YU.SAVELJEV and A.MAITLAND, present issue). If the total channel gain is $G=I_{out}/I_{in}=10^6$ and d=10cm then γ=46, L=460cm and U=2.1kV are required. Such a length is clearly unpractical.

We may reduce L by increasing the transverse secondary electron energy by one of the following methods. The first employs a positively biased grid placed near the channel inner wall. In the second method there is a thin wire at the channel axis and a third version introduces a positive space charge within the channel volume. Appropriate potential distributions are shown in Fig.2. Obviously, these methods allow substantial increase of the transverse electron energy and hence the monochromatic approximation may be used.

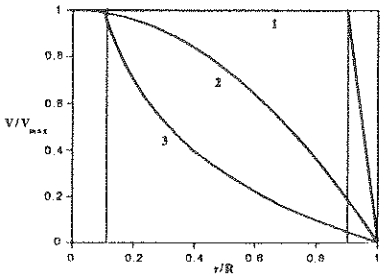

Fig.2 Potential distributions in the cross-section plane of the modified CEMs.
1-grid, 2-positive space charge, 3-wire.

Analysis on the assumption that the electron space charge is completely neutralized shows that the expressions for the channel gain are similar to those obtained for conventional CEM's. It is required only to replace the initial electron energy by the effective energy, V_f, given by the product of figure of merit f that describes the effectiviness of each method used and the appropriate potential V_g (grid), V_w (wire) or V_c (positive space charge) :

$$G = \exp(g\gamma) \qquad g = \frac{4V_L}{V_d}\ln\delta \qquad V_f = f_g V_g$$

$$V_f = f_w V_w$$

$$V = V_0 + \frac{V_d^2}{4V_f} \qquad \cos\theta = \sqrt{\frac{V_0}{V}} \qquad V_f = f_c V_c$$

At $V_f \geq 200$-300V parameter f begin to be constant, i.e. $f_g \approx 1.0$ (grid), $f_w \approx 0.1$ (wire) and $f_c \approx 0.45$ (positive space charge).

Since the gain parameter depends strongly on the value of V_f the total channel length can be decreased substantially by one or other of these methods. At $V_f = 250$V and the channel conditions mentioned above, the length-to-diameter ratio required is 4.6 and L=46cm rather than the 460cm required for the case of conventional CEM. For a given total gain, further decrease in L may be shown to be possible by taking into account boundary effects.

We have seen that transversly modified CEM's may be scaled to give high-current, large-aperture electron sources which can be quite compact. Such devices may be applied in many different applications such as high-voltage accelerators or microvawe technology.

INVESTIGATION OF A CORONA-PLASMA TRIGGERED PSEUDOSPARK SWITCH

M. Legentil*, V. Puech*, J.C. Thomaz*, L.C. Pitchford§, N. Ouadoudi§ and J.P. Boeuf§

*: Laboratoire de Physique des Gaz et des Plasmas (CNRS URA 073), Université Paris-Sud, 91405 Orsay Cedex, France
§: Centre de Physique Atomique de Toulouse (CNRS URA 277), Université Paul Sabatier, 31062 Toulouse Cedex, France

Pseudospark discharges are transient hollow cathode discharges in special geometries which, under proper conditions, display an abrupt transition to a highly conducting state a short time after the application of a trigger. Pseudosparks have unique properties - hold off voltages of 10's of kV, peak currents in the range 10-100 kA with a current rise in the order of 10^{11}-10^{12} A/s (often circuit limited), and fast recovery times allowing high repetition rate - which are very appealing for the development of a new class of high power switches for a variety of industrial and defense applications. Triggering is accomplished by a variety of means for injecting charges in the hollow cathode backspace including electrical or optical schemes. Although pseudospark switches have been developed to the point that they are now commercially available for certain applications, work remains to be done to determine the best combination of physical and triggering conditions and to develop a simple and reliable triggering scheme suitable for high frequency operation with long life and having a low cost with no standby power consumption demands.

In the present communication, we report a series of experiments and calculations related to a novel pseudospark triggering technique using a corona-plasma electrode to feed electrons into one of the pseudospark hollow electrodes. A schematic cross sectional view of a corona-plasma triggered pseudospark switch is shown in Fig.1. The pseudospark consists of two symmetric cylindrical hollow electrodes with central apertures in the plane and parallel plates facing each other. The corona-plasma electrode consists of a trigger electrode, a thick plate of dielectric and, in the vicinity of the dielectric surface, a grid in electrical contact with the inner part of the pseudospark hollow electrode. When a fast rising voltage pulse is applied to the trigger electrode, electrons are emitted at the gas-dielectric-grid interface (triple point) by field emission. The solution of Poisson's equation yields the electric field at the surface of the dielectric and shows that a field enhancement of two orders of

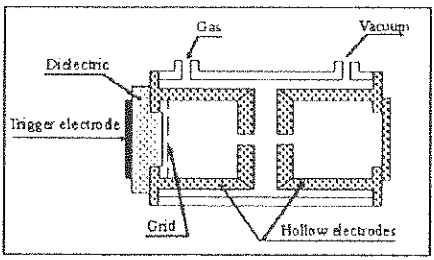

Figure 1: Schematic cross sectional view of a corona-plasma triggered pseudospark.

magnitude can be reached for ϵ values higher than 1000, *i.e.* in ceramics such as barium titanate. Using such a ceramic as a dielectric, a corona-plasma electrode has been proved able to trigger the pseudospark discharge in a very large range of parameters with less than 4 mJ spend in the trigger section. Some preliminary investigations of the high repetition rate possibilities of this pseudospark triggering technique have been performed with an undamped electric circuit (C=24 nF charged under 10 kV) producing a current reversal of about 80%. The corona-plasma triggered pseudospark has been able to run, in a continuous mode at a repetition rate frequency of 100 Hz, during 4 hours ($> 10^6$ shots) without any misfiring or self break of the main discharge. At higher repetition rates, an important temperature increase of the pseudospark structure has limited the experiments to a burst mode with up to 10^5 shots per burst. In that mode, the corona-plasma triggered pseudospark has been run without failure up to a frequency of 1 kHz, a frequency limited only by the available electronic control unit.

To identify the importance of the physical parameters which can influence the time to breakdown and the jitter of the corona-plasma triggered pseudospark we will compare the experimental results to the predictions of a model calculation based on a two dimensional, self consistent code coupling the Poisson equation for the electric field to a fluid description of the electron and ion transport equations. An important feature of the model is that the ionization source term in the fluid equations is determined through a Monte-Carlo simulation allowing the inclusion of the non local properties of the high energy electrons. As a result, the model is an hybrid fluid-particle model (J.P. Boeuf and L.C. Pitchford, IEEE Trans. Plasma Sci. 19, 286-296,1991) which gives an accurate description of the space and time dependent evolution of the electric field and charged particle densities in the pseudospark hollow electrodes.

For all the experimental conditions, the pseudospark switch has been triggered with the corona-plasma electrode operating either on the hollow cathode or on the hollow anode side of the pseudospark. Moreover, for each of these two locations, the hollow electrode on which the corona-plasma electrode was implemented could be grounded or connected to a positive or negative high voltage, showing that the corona-plasma trigger is a very versatile device for the pseudospark discharge initiation. In this preliminary investigation, the cumulative number of pseudospark discharges switched with this technique is above 10^7, and work is in progress to optimize and to assess the limitations of this corona-plasma trigger which appears as a low cost, simple, efficient and reliable technique for the development of long life, high repetition rate pseudospark switches.

Acknowledgements: The authors wish to thank Professor M.A. Gundersen from University of Southern California (US) for many discussions about pseudospark physics and technology. Financial support from DRET through contract 91/054 is greatly acknowledged.

THE MITTON - A HIGH-VOLTAGE CLOSING AND OPENING SWITCH

N A Ridge*, P F Hirst, A Maitland.
J F Allen Laboratories, Department of Physics and Astronomy, University of St Andrews, North Haugh, St Andrews, Fife, KY16 9SS, Scotland.

D M Parkes.
RF Techniques Section, Defence Research Agency, St Andrews Road, Malvern, Worcs., WR14 3PS, England.

The MITTON is a high-voltage closing and opening switch. The MITTON operates on the left-hand side of the Paschen curve, like hydrogen thyratrons, where small electrode spacing and low pressures allow operation at high breakdown voltages. The MITTON, shown schematically in Figure 1, essentially consists of an annular ceramic envelope containing two high voltage gaps which are separated by a drift space. The drift space is formed by a ceramic cylinder on the outside, and a metal cylinder on the inside of the switch. A thermionic cathode is situated in the base of the switch along with a hydrogen reservoir to control the gas pressure. The breakdown voltage of the switch is determined by the sum of the breakdown voltages of the high voltage gaps (approximately 30 kV for each 3 mm gap at 0.1 torr hydrogen.)

The MITTON is triggered into conduction by a non-contact triggering method; the electric fields, necessary to ionise the low pressure gas within the switch are generated by a microwave source of sufficient power (10 kW, 1 μs) to produce electric fields greater than the Paschen minimum for rf breakdown in the drift space. The switch is charged initially to a voltage below the breakdown voltage. When the microwave signal is applied to the wire helix, which surrounds the drift space, the microwave fields cause ionisation of the gas. The resultant plasma then diffuses into the high voltage gaps, through the slotted grids, triggering the switch into conduction. The switch passes a large current (circuit limited) with a low sustaining voltage ("arc drop"). The uniformity of the microwave-induced plasma leads to the formation of a highly uniform cylindrical current path, which is inherently of low inductance. Anode voltage fall-times (90% - 10%) of less than 10 ns (limited by the diagnostics) have been measured at charging voltages of 12 kV.

Opening is achieved through the application of a negative bias voltage (approximately 600 ns FWHM and 0.5 - 1.5 kV amplitude) to the large area grid structure which bounds the drift space on three sides. The bias voltage required to achieve switch opening increases as the initial discharge current increases. The application of a negative bias voltage to the grid leads to the formation of a positive ion sheath (a region of lower electrical conductivity than the plasma) between the plasma and the grid, thereby causing an increase in the switch impedance that leads to a simultaneous reduction of the switch current. This non-equilibrium situation eventually results in the current falling to zero, (switch opening) even though there is still a high voltage applied to the anode via the charging capacitor. Figure 2 shows an oscilloscope trace of the MITTON opening phase, where Va represents the anode voltage, Id, the discharge current, and Vb, the bias voltage. For the trace shown, the switch starts to open when the applied bias voltage is 1 kV, at a discharge current of 11 amps. The anode voltage rises to 10.5 kV as the discharge current falls to zero.

The ability to switch off current will allow the MITTON to operate at high repetition rates. Switch opening times of about 0.5 μs, at currents of up to 11 amps, have been measured for charging voltages of 11 kV. The above opening time represents a theoretical maximum repetition rate of 2 MHz.

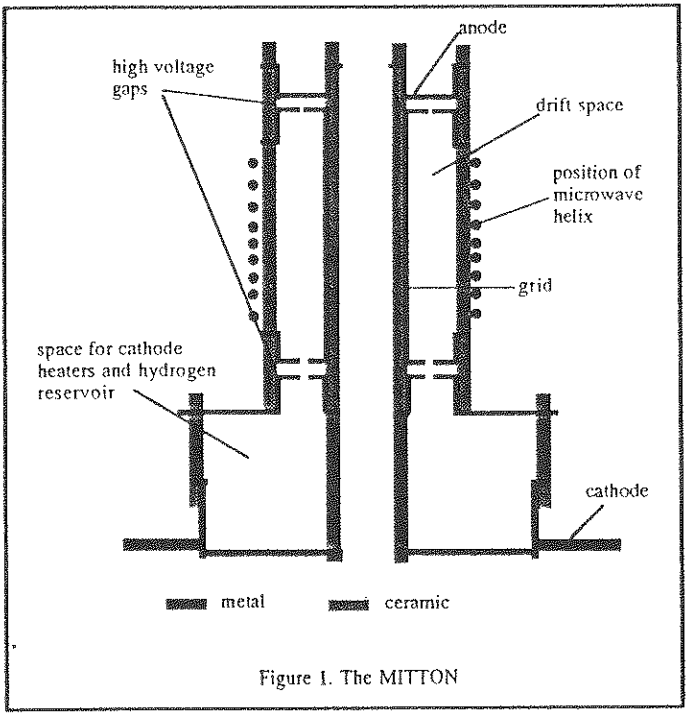

Figure 1. The MITTON

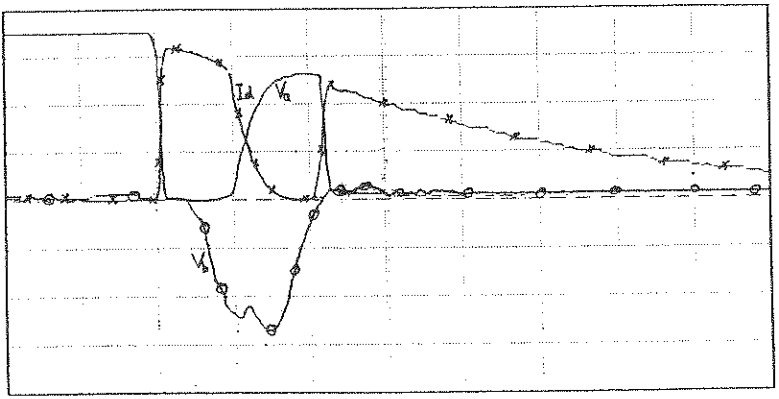

Figure 2. Oscilloscope trace of MITTON opening phase

— Anode voltage, Va; 4 kV/div
-*- Discharge current, Id; 4 amps/div
-o- Bias voltage, Vb; 500 V/div
Timebase; 500 ns/div

ELECTROMAGNETIC COMPATIBILITY IN ELECTROTHERMAL GUN RESEARCH INSTALLATIONS.

E. Thornton* and C.R. Spikings.
British Aerospace Operations Ltd.,
Sowerby Research Centre,
FPC 30, PO Box 5,
Filton, Bristol, BS12 7QW, UK.

Electric gun installations, like other high power pulse generators are a potential source of electrical interference. In large systems on test ranges the electromagnetic emission can be a costly nuisance causing misfires and interference on diagnostic records. However much more serious hazards can result from interference in the control system and from the nearby presence of sensitive materials.

The design of high power capacitor banks, including that of multi-module sequentially triggered banks for electric guns is now a relatively mature technology, with considerable emphasis on the control of earth (ground) loops and on em compatibility in the trigger and control systems.

Sponsored by Royal Ordnance, Nottingham, a 500 kJ capacitor bank has been designed and installed at the Sowerby Research Centre (Spikings and Thornton, Electrothermal Launcher Experiments at SRC. 4th International Symposium on Electromagnetic Launch Technology, Celle, Germany, May 2-6 1993). More recently Maxwell have designed and installed a 2.4 MJ bank at the RO test range at Faldingworth.

EM diagnostic measurements were made on the 500 kJ bank using electric and magnetic field probes. The bank is installed in a small, partly underground bunker, which restricted probe positions to within 2m of the bank, itself of typically 2m dimensions. Electric and magnetic field values of the order of $1 kVm^{-1}$ and 50 μTesla respectively were measured. These results are discussed in terms of the electromagnetic energy induced in conductors in the position of the probes.

Further measurements were made during installation of the Maxwell bank at RO Faldingworth. Here it was possible to make probe measurements at a larger number of positions, but even so the large size of the bank limited measurements to close-in near field, mostly at radial positions much less than the bank dimensions. Accurate interpretation of the fields as a function of radial distance is therefore difficult, but we believe that a significant interpretation can still be made.

The results from the two independently designed installations show low figures of em emission, with negligible signals at higher frequencies. This is perhaps indicative of the care taken in conductor layout and in the extensive

decoupling in both systems, resulting in reliable triggering and lack of diagnostic interference. A power attenuation factor in excess of 120 dB between the main pulse and control and diagnostic signals is achieved without the use of shielded rooms.

The self-test technique of em compatibility testing is particularly suited to pulse power technology, where very high effective attenuation factors are required. Simulation sources, particularly CW of sufficiently high power are not available, and the primary pulse is therefore the logical test source. It is usually well characterised, and associated with an available, high performance diagnostic recording system.

We have described a single shot system, but there are many repetitive pulse systems for which these techniques are equally appropriate. The relevant features of the pulse generating system are a temporary energy store, fast, high current switching, a trigger system and a control system. These features are particularly characteristic of modern traction systems as well as power controls and switched mode power supplies.

A ROTATING SPARK GAP ASSEMBLY FOR HIGH REPETITION RATE FAST SWITCHING

S. Bower*, F. Jones and S. Ella,
EEV Limited, Carholme Road, Lincoln, LN1 1SF, U.K.

K. Trafford, DRA, St. Andrew's Road, Malvern, WR14 3PS, U.K.

There is considerable interest at present in extending the repetition rate capabilities of very fast switches for high voltage operation. It is known that conventional two electrode spark gaps are capable of operation under optimum conditions at repetition rates of up to 1kHz whilst maintaining their fast switching capabilities, but as repetition rate is increased beyond these values recovery problems are found to occur. Rotating spark gaps have been used in the past to avoid these recovery problems by the movement of a fresh gap into the discharge area between switching operations.

The results of tests on a three gap multi-electrode rotating assembly are described. Measurements of breakdown voltage and switching time under both d.c. and pulse charged conditions at repetition rates of 1kHz and above are reported. The performance of the device as a fast switch is evaluated and operational problems discussed.

EFFECTS OF ELECTROMAGNETIC DISTURBANCES ON OPERATIONAL AMPLIFIERS

R. LESTIENNE, J. BAUDET, B. DEMOULIN and P. DEGAUQUE
Universite des Sciences et Technologies de LILLE
Laboratoire de Radiopropagation et Electronique
UA CNRS 837
Bâtiment P3
59655 VILLENEUVE D'ASCQ Cédex - FRANCE

The operational amplifiers (O.A.) may be disturbed either temporarily or even destroyed by electromagnetic sources. Indeed the coupling of the electromagnetic waves on the printed circuit board behaves usually as distributed voltage generators. Furthermore in case of a line-to-line coupling on the circuit itself, equivalent noise current generators can be applied on the input or output of the O.A.

At first, we consider the response of the O.A. when it is excited by low level disturbances such that no lasting effect occurs. Experimentally, the disturbances are applied on the output of the device, on its - input or on the power supply lines. For each case, various types of O.A. have been tested such as the series LM 741, LM 324 and MC 34084. As an example, Curves in Figure 1 show the voltage at the output of these O.A. when the - input is disturbed by a transient signal. It is generated from the coupling between two lines on the same circuit board, a TTL signal flowing on one line, the second one being connected to this - input of the O.A.

The O.A. response is a damped sinudoid whose amplitude and frequency depend on the intrinsic parameters of the device. A physical interpretation based on the modelization of the internal circuits are proposed. In a second part, high amplitude signals will be considered. Indeed it appears that if this amplitude is just below the destruction level of the device, lasting effect occurs. A typical example is the change of its voltage gain. A

parametric study shows the relation between the amplitude, tje width of the pulse on the nominal characteristics of the device.

In the last part of this presentation, the effect of an illumination of the circuit board by continuous sine wave at frequencies near 1 GHz is considered. The circuit is placed inside a mode-stirred chamber and the amplitude of the signals induced on the inputs of the O.A. will be experimentally determined. The advantages and drawbacks of the method are pointed out.

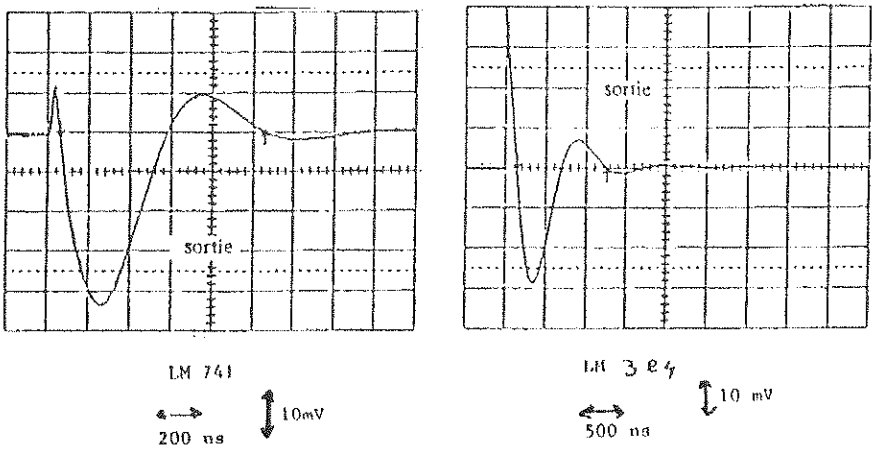

Fig. 1

TOPOLOGICAL ANALYSIS OF THE E.M.I. INVOLVED IN DIGITAL SIGNAL PROCESSING HIGH DENSITY INTERCONNECTIONS

H. MISSON*, S. CHARRUAU, A. TOUBOUL*

SEXTANT Avionique
rue Toussaint Catros
33160 ST MEDARD EN JALLES

IXL-Université Bordeaux I (CNRS URA 846)
351 cours de la Libération
33405 TALENCE Cedex

This paper concerns a general topological analysis of the Electromagnetic interferences (E.M.I.) inside the high density interconnections required for digital signal processing (D.S.P.). The economical constrains of industrial operations lead to predict the E.M.I. effects at the earlier step of the D.S.P. design by the way of solving in a matrix form the transmission line equations (T.L.E.) over the whole interconnection network. E.M.I. parasites are created on lines having at least one segment in the vicinity of a disturbing line which is itself disturbed by at least one another so on up to the initially disturbing lines. So, the T.L.E. matrices are almost empty. Besides, the C.A.D. systems usually aimed at the interconnection design make the no n null elements of the T.L.E. matrices randomly distributed, so strongly hardening the numerical computation. The goal of the topological analysis of E.M.I. is to provide an efficient ordering of the non null elements of the T.L.E. matrices close to their diagonal before any numerical computation.

The presentation of this E.M.I. topological analysis begins by defining the necessary basic terms and properties concerning the E.M.I. vicinities of 3D electrical conductors. A partitioning process of a whole D.S.P. interconnection network is proposed in respect with the topological properties of E.M.I. Then the required ordering of the non null elements of the T.L.E. matrices is got by a clever numbering of the segments of all the lines based on the topological properties of E.M.I..

For ending, this topological analysis of E.M.I. led to a package implemented in the environment of a C.A.D. system.

TOPOLOGICAL SENSITIVITY OF ELECTRONIC COMPONENTS SUBMITTED TO A POWERFUL MICROWAVE PULSE

J.MOUTON J.CHARTIER
CEA - DAM - FRANCE -

Abstract

Unlike a photon ionizing pulse, an electromagnetic pulse exhibits shallow penetration on conducting structure. Electronics components placed in metallic boxes should be insensitive to a microwave agression.

Experimentation shows that they are perturbated or destroyed by tracks or connecting cables induced currents. For most of components as bipolar transistors, JFET,diodes...., a level of sensitivity is defined which agrees with the amount of electrical energy they can stand without damage

This notion of "Intrinsic sensitivity" is not suffucient to characterize the level of vulnerability of an equipment. It is more advisable to use the notion of "Topological sensitivity", as a substitute, which qualifies components in their electrical surrounding, considering the agression residual coupling energy which penetrates the system.

Presented experimental results deal with sensitivity of an operational amplifier LF 356, exposed to a microwave power pulse.

Component is included in a printed circuit board astable multivibrator, located in a metallic copper cavity. Two high immunity EM cables allow measurements before, during and after illumination. Different configurations have been tested:

- screening-tightness effect of the experimental cavity.
- EM coupling effect upon the connector tracts outside the component.
- EM coupling effect on the internal structure(with case cutoff).
- direct coupling effect on each entry port of the component.

The microwave generator is a Thomson klystron operated by CEA/CESTA research center.

The generated pulse, at 3GHz, lasted 6 µs with power ajustable from 27KW to 10MW. Necessary power density necessary to destroy the component fluctuates from 300 to 500 W/cm^2 with the configuration under study.

EMP induced failures and hardening analysis tools for electronic equipments

H. ZUGAJ * , J. PIGNERET
NUCLETUDES - BP 117, 91944 LES ULIS, FRANCE

Theoretical vulnerability analysis, carried out within the framework of equipments hardening projects against EMP and lightning effects, are conducted in order to :

- assess the components safety margins, i.e. the ratio between damage thresholds and calculated electrical stress,
- design and check any necessary modification into the circuits to remove the identified weaknesses and ensure hardening.

What is mainly needed to carry out the assessments is to get damage models suitable to a large class of devices and stress waveforms. Among the models which have been developped since the early seventies, one calculating method, described by TASCA [1] and WILLIAMS [2], appears especially adapted :

$$\text{safety margin} = 10 \log [\max S(t)] \quad \text{in dB}$$

$$S(t) = \int_0^t P(t') \cdot \frac{d}{d(t-t')} \left| \frac{1}{P_F(t-t')} \right| dt'$$

$P(t')$: instantaneous power dissipated in the component

$P_F(t-t')$: power of a rectangular pulse with Δt duration leading to component failure

The quality of the assessment relies on :

- an accurate simulation of the transient electrical responses $P(t')$ of the components,
- a good correlation between the calculated responses and the component failure data (P_F for rectangular pulse $\Delta t = t-t'$).

The object of this paper is to present a new methodology, engineering oriented, to obtain accurate and efficient predictions. The tool is built by associating a component data base, a circuit analysis program and some dedicated softwares : the S(t) solver and a management/documentation module.

The main points of this method are the following :

- The component failure phenomena is supposed to be simulated by a "thermal like" model. The experience shows that, for stress under a few hundred volts, this assumption is convenient.

- Analysis is performed using the average component failure levels. Hardening margins are to be considered in order to reach the equipment survival level with a given confident rate :

  operational safety margin = 10 log [max S(t)] - hardening margin

- An assessment, by min and max threshold estimation, has to be performed for components exhibiting current polarity dependent failure levels.

At the present step of development, the tool can be used for almost every circuit topology and electrical stress shapes. Emphasis has been put on interactivity operation to speed up the hardening process. Unproper electrical device characterization, under and near failure threshold can lead to significant errors in low margin circuits.

Validation networks, built around fuses, CTP, rectifiers, and stressed by complex waveforms, have been simulated, and the results have been compared to measurements. The full paper discuss the remaining factors limiting the accuracy.

An example of synthetic analysis output produced by the tool is given below :

Circuit : ampli.C1	Stress : sinus.S1	HM : 10 dB
device designation	component type	SM (dB)
A1	OP-15J	- 7 dB
A2	OP-15J	+ 4 dB
T1-1	TRANS : MAT02	+ 12 dB
T1-2	TRANS : MAT02	+ 18 dB
D1	DIODE : THD6916	+ 7 dB

HM : hardening margin SM : operational safety margin

Failure analysis can be performed through graphical outputs examination : shape and time of failure occurence.

References : [1] EMP Radiation and protective techniques - 1976

[2] HDL-TR-1833 - Mars 1978

Ground/ Power Plane and Interconnect Modeling for EMC Analysis in High Speed Designs

Ravender Goyal
Mentor Graphics Corporation
8005, SW Boeckman Road
Wilsonville, OR 97070- 7777
USA
Phone: (503) 685- 1781
Fax: (503) 685- 1282

Computer system clocks are increasing conservatively by a factor of 2 every year from 100 MHz in 1993- 94 to about 1 GHz by the end of the decade. DEC's new Alpha-APX microprocessor currently runs at about 100- 200 MHz and a 1- 2 GHz version is planned for 1994. Intel's Pentium processor released in 1993 runs at 70- 100 MHz clock rate and later versions are expected to run at significantly higher clock rates. Fujitsu is targeting a RISC processor at 1 GHz by the end of 1994. Similarly, data rates of 2 GB/s or more are common in digital communication systems such as PCN (Personal Computer Network), Cellular and Optical Fiber systems. The signal edge rates or the slew rates in these systems are significantly higher in nano- second or even sub- nano second range, which in return means design management at significantly high frequencies, typically in the range of several GHz.

The packaging densities are also increasing dramatically as shown in Figure 1, to accommodate complex functionality on a single module/ IC. This requires densely packaged interconnects working at high clock rates, which results in the signal distortion and signal crosstalk between adjacent lines.

On an average, in high speed PCB systems (above 30 MHz clock rate) the interconnects contribute to approximately 35%- 45% of the total input to output delay. Also, the IC packages slow down the function of an IC, as shown in Figure 2, anywhere by 10% to 50% depending on the IC clock rate. This makes the use of bare IC chips attractive in high speed systems and thus the use of MCM technology. However, the interconnect delay and the effects of non- ideal ground and power planes remain significant and it is important to manage their adverse effects on the overall performance of the module. Interconnects begin to behave as distributed transmission lines and coupled lines at clock rates above 40 MHz.

High performance and high density designs must take signal integrity, interconnect delay, and power and ground plane effects into consideration. We have developed unique approaches in describing electrical constraints and circuit topologies in PCB & MCM layout environment and defining timing and signal integrity rules within the topology. These electrical rules drive intelligent placement and routing algorithms for both auto/interactive and automatic functions. The auto-interactive tools guide the user as they leverage their experience in solving tough problems.

In this paper we will present design techniques for interconnect and power/ ground plane modeling of the structures and design rules typically used in PCB & MCM, which significantly improve the system performance and provide first time correct designs

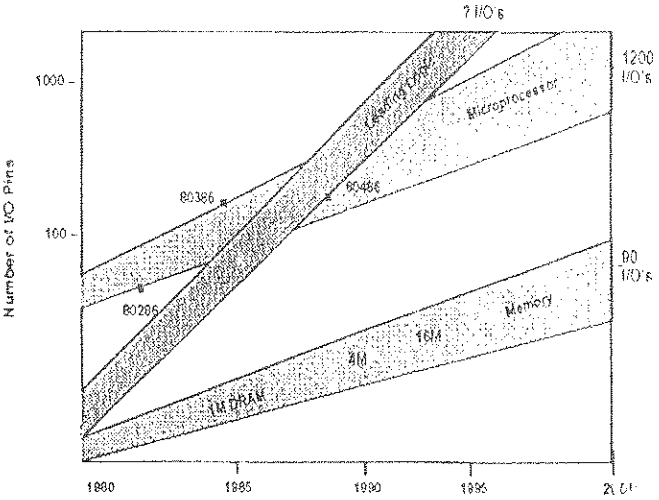

Figure 1

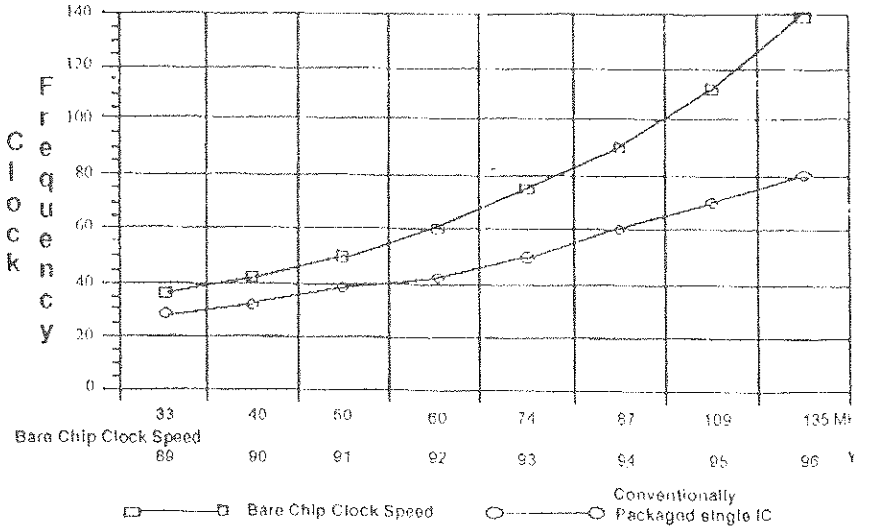

Figure 2

PHYSICAL ANALYSIS AND OPTIMIZATION OF OVERVOLTAGE PROTECTION CROWBAR SEMICONDUCTOR DEVICES

DEPEE Jean-Yves*, EHLINGER René, CHANTE Jean-Pierre
Laboratoire CEGELY-ECPA - URA 829
INSA Bâtiment 401
69621 VILLEURBANNE CEDEX
tel: 72 43 87 25
fax: 72 43 85 30

With the evolution of technologies, electron devices are more and more integrated and work now at very high frequencies. Unfortunately these devices are more and more sensitive to transient overvoltage phenomena. These phenomena may be natural (lightning phenomena) or may be due to a parasitized electromagnetic environment.

It is very important to be able to prevent the device degradation by limiting the voltage across them. Most of the protection devices are used in parallel with the sensitive circuits. The protection device impedance decreases with an increasing voltage, which eliminates the excessive energy.

Among the protection devices, some seem to be interesting in future: the semiconductor protection crowbar devices. They behave like avalanche diodes below a given current value called the breakover current (Ibo). Beyond this current, the impedance falls down (negative resistance behaviour). After elimination of the transient surge, the component comes back to high impedance state when the current decreases below the holding current (Ih).

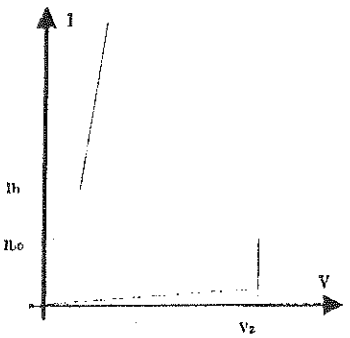

Current versus voltage curve
for protection crowbar semiconductor devices

The current voltage curve indicated above is similar to the one describing a discharge gas tube behaviour. The voltage limitation (avalanche voltage for the semiconductor device,

disruptive voltage for the gas tube) is more accurate for the semiconductor crowbar device even at high voltage increase speed (dV/dt). For the discharge tubes, the ionisation phenomena are slower and the disruptive voltage increases at high dV/dt. On the other hand, the overflow capabilities are larger in the case of a gas tube (maximum current value for a 8/20µs current wave. 100A with a semiconductor crowbar device, 10kA with a tube).

For a better understanding of the static and dynamic phenomena that limit the overflow capabilities we perform a physical simulation of the semiconductor protection crowbar device behaviour.

Therefore we use the SILVACO software: GIGA-2-D, able to solve in two dimensions the semiconductor equations (Poisson, continuity and temperature equations).

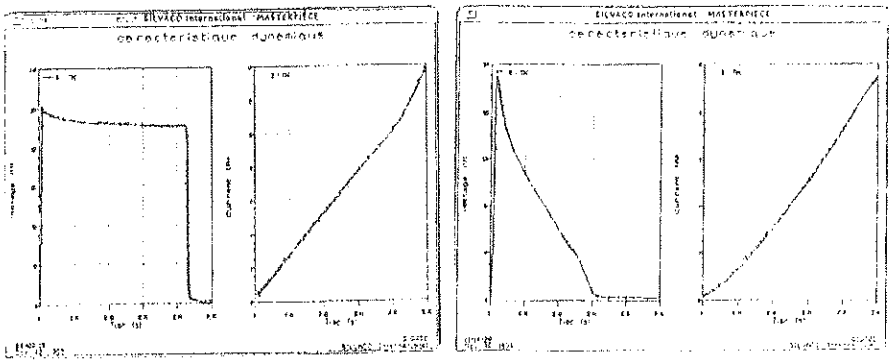

Current and voltage evolution for two types of structure
after an overvoltage application

We thus enlighten two types of overvoltage protection structures able to realise voltage limitation and fast impedance decrease. For these two types of structures the voltage evolution at breakover phenomenon are quite different (clamping voltage time, voltage fall down speed).

The analysis of the different processes involved in these two structures enabled us to identify in each case the parameters determining the avalanche voltage and the breakover current.

By a simulation taking care of the temperature conditions we are now able to optimise a structure adapted for high current flow. Therefore we try to find the best trade-off between the doping values and the layers size.

We will extend later this analysis to the turn-off process. We will analyse the influence of the structure pattern on the storage charge location and on the storage charge evacuation phenomena.

EMI CONTROL BY SOFTWARE FOR A RF COMMUNICATION SYSTEM

* G.K. SAHA
Brig. Dr. G.K. DEB
Electronics Research & Development Centre,
P-1, Taratala Road, Calcutta - 700 088, INDIA.

ABSTRACT

This paper presents the design and development of Software to control Electromagnetic Interference [EMI] of a RF communication system. Transient electromagnetic [EM] fields i.e. lightning electromagnetic pulse [LEMP] and nuclear electromagnetic pulse [NEMP] resulting from the lightning and nuclear detonation respectively, pose a formidable threat to modern electrical and electronic systems. Traditional methods by which EMI can be controlled typically deal with hardware based solutions such as : grounding, shielding, bonding, balancing, isolation, circuit insulation by separation, lengthening the discharge path of say an Electro Static Discharge [ESD] event, use of secondary shield, a spark arrestor, proper capacitor placement, back-to-back diodes at circuit inputs etc., to prevent overvoltages. The use of clamping devices such as zener diodes may be used as transient suppressors. But all these various hardware immunity techniques force the design to grow in size and weight resulting in System unreliability. In an era of increasing restrictions on physical (i.e. weight and size) budgets and financial resources, the System Design Engineer needs creative alternatives to produce designs that are consistent with increasingly restrictive requirements. However, Computer Software/ Firmware which is properly designed, can control EMI without increasing size, weight, and hardware cost. In this paper, an indepth investigation has been made to examine how a properly designed software helps in reduction of the EMI potential and thus assures EMI hardness to a RF communication system. A typical RF system (shown in fig.1) with a source, possibly some software controlled processing and an RF subsystem, radiates a signal which is picked up by a receiver. The receiver may process the information using a combination of microprocessors, user look up table [LTB], and software code or logic. In order to find out whether received signal frequency [F], pulse width [PW] and pulse repetition interval [PRI] truly match a record in a predefined LTB, a processing software has been properly designed. The basic processing logic is shown in figure 2.

Some action, namely Track is performed depending on the result of this match. Computer Software has been properly designed with enhanced logic to continually verify that faults are detected in data/ program flow and then necessary recovery action is taken. This properly designed processing software is of high reliability & accuracy and hence reduces an EMI situation with potentially disastrous consequences resulting from simple basic processing logic. This Software with enhanced logic can control EMI and provide a significant role for proper EMC management during the life span of a RF communication system and thus maximum EMI hardening and maintenability have been established by this properly designed software.

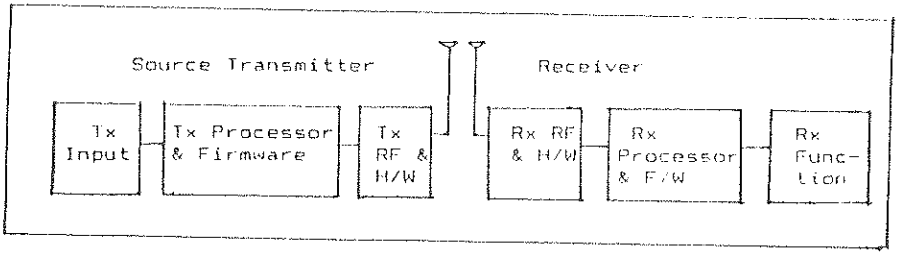

Fig. 1.

Algorithm 1. A user data look up table [LTB] contains records of information like F, PW, PRI. This algorithm shows the basic processing logic to find out a true match of F, PW, PRI of received signal with a predefined record in LTB.

```
Step 1.  Read :  Search signal F, PW, PRI.

Step 2.  If F=F(LTB) and PW=PW(LTB), then:
            If PRI=PRI(LTB), then:
               TRACK.
            Else:
               Go to step 1.
            [ End of inner If structure. ]
         Else:
            Go to step 1.
         [ End of outer If structure. ]
```

Fig. 2.

THE ORGANIZATION OF SIGNALS IN CABLES AND ITS BENEFITS IN FUTURE WIRING SYSTEMS

P. J. Morrison*, R. Sutton, M. Longtin, J. Tigner,
M. Vandersluis, L. Beers, T. Styer, F. Dunbar, J. Champion
Science Applications International Corporation
McLean, Virginia, USA

One of the last stumbling blocks in modern systems integration, especially for aircraft, is the combination of wiring and cable harnesses with the rest of the electrical and electronics subsystems. An organized wiring system, as defined here, allows the integration of these from the initial planning and design phases through construction, delivery, and maintenance. The advantage of this approach is the control, to a degree not before possible, of the wire-to-wire crosstalk and externally coupled signals; consequently, design margins can be severely relaxed.

This approach is uniquely matched to computer design and manufacturing techniques in a systems perspective since an organized wiring system consists of a physical assemblage, such as a cable ribbon harness, combined with an intelligent system to distribute the electromagnetic signals across the harness so as to minimize crosstalk. If this is done properly the result is a considerable savings in system weight, complexity, and design time. This occurs in conjunction with a concomitant increase in manufacturability, and reduced construction time will lower costs, and maintainability. One of the missing links in this chain has been the ability to organize signals in a harness and then to calculate the crosstalk in each wire to demonstrate the utility of the chosen organization. This means that system design will include wiring between "black boxes" as part of the initial process and ultimately will result in proceeding directly from design to manufacturing with a minimum of engineering mock-ups and laboratory breadboards. This paper will present the results of the combination of a knowledge based organizational system for system signals combined with a calculational tool to determine the expected crosstalk for a given organization. These have been combined in turn with databases of signal parameters and cable physical parameters in an interactive, personal computer based engineering tool.

An organized wiring system consists of a deliberate and thought-out wiring path for each particular signal, relative to other signals in a multiconductor harness, so as to possess positive attributes not possible in the usual randomized cable wiring construction. Some of the positive attributes are physical: the use of a pre-determined path, cable connections via standardized integration units, and the use of a small set of standardized cable cross-sections (e.g., number of wires, shields). These can allow the integration of the wiring system with other CAD/CAM tools available to wiring engineers; the present effort summarized in this paper includes integration with the CATIA package (an engineering CAD package used by Boeing aircraft and others) so that the wiring design is now part of the integrated design process, as other physical parts of an aircraft are. Other attributes, which embody the bulk of this presentation, are electrical. They include locating signals in a harness so that they will not interfere with each other (e.g. segregation of susceptible and noisy signals) while at the same

time minimizing the use of deliberate ground guard wires and separate shields, other than harness overshields. The physical optimization results in ease in manufacturability and maintainability while the electrical optimization results in considerable weight savings. The combination of the two will result in simplicity of design, further weight savings, allowance for future expendability and alteration at minimal cost.

In such a configuration, the coupling paths must be understood and calculable; this is the virtue of an organized system. The physical signal path is known for the entire length of the cable run, as are the paths of all other signals. The physical organization of the cable requires that the electrical parameters of all wires (capacitance and inductance matrices) are known and so the calculation of crosstalk becomes possible. The calculational methodology follows a state of the art calculation of the electrical parameter matrices and solution of the multiconductor transmission-line equations for shielded lines (C. Paul, and B. Bowles, IEEE Transactions on Electromagnetic Compatibility, V. 33, p. 149, Aug. 1991). This will be detailed in the paper. This includes high frequency effects due to transmission line response, the finite resistance of internal and external shields, and crosstalk through loads, resulting in a general matrix solution of the problem. The software interface includes access to and development of electrical and physical data bases of signals and harnesses, allows the imposition of design margins, arbitrary terminations and interconnections, manual or automatic signal organization (based on a knowledge-based rule module), and a graphic output of the crosstalk results along with the input signal parameters and a scaled physical cross-section of the harness. Two representative screen prints of the software tool are appended to this abstract.

Future efforts in the development of this tool include the possibility of Built-In Test as part of the wiring system along with adaptive reprogramming of wiring paths in the event of point failures. Also in need of exploration are load design for crosstalk optimization and the area of lightning protection in this design.

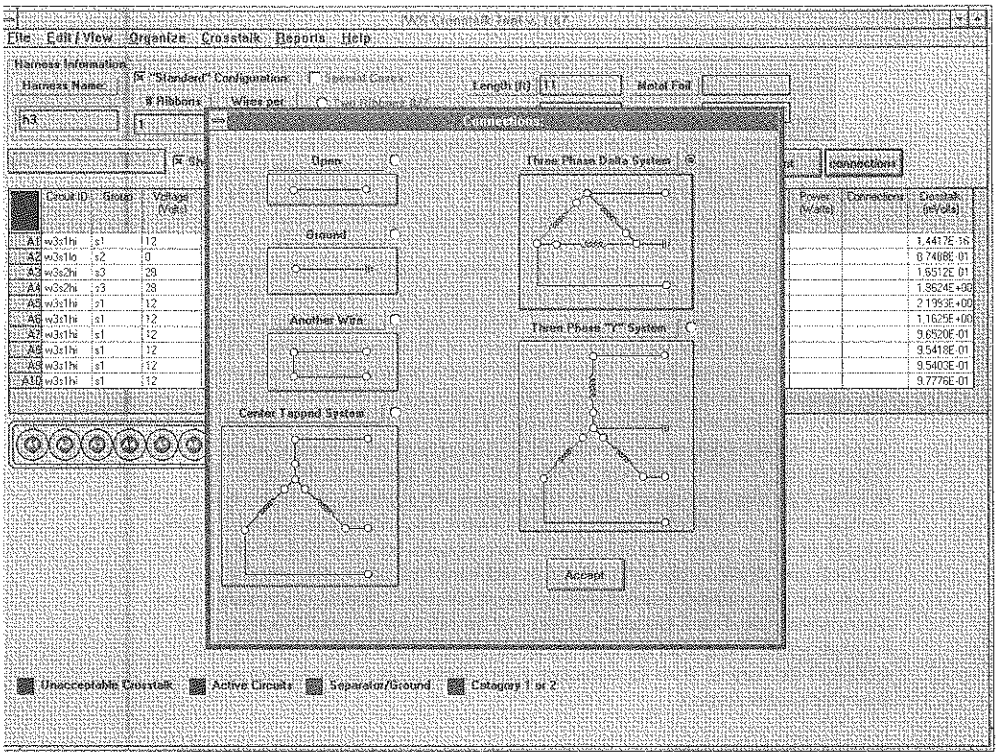
File Edit / View Organize Crosstalk Reports Help
Harness Information
Harness Name:
"Standard" Configuration
Length (ft) 11
Metal Foil
h3
Ribbons
Wires per
Connections
Open
Three Phase Delta System
Ground
Another Wire
Three Phase "Y" System
Center Tapped System
Accept
connections
Unacceptable Crosstalk
Active Circuits
Separator/Ground
Category 1 or 2

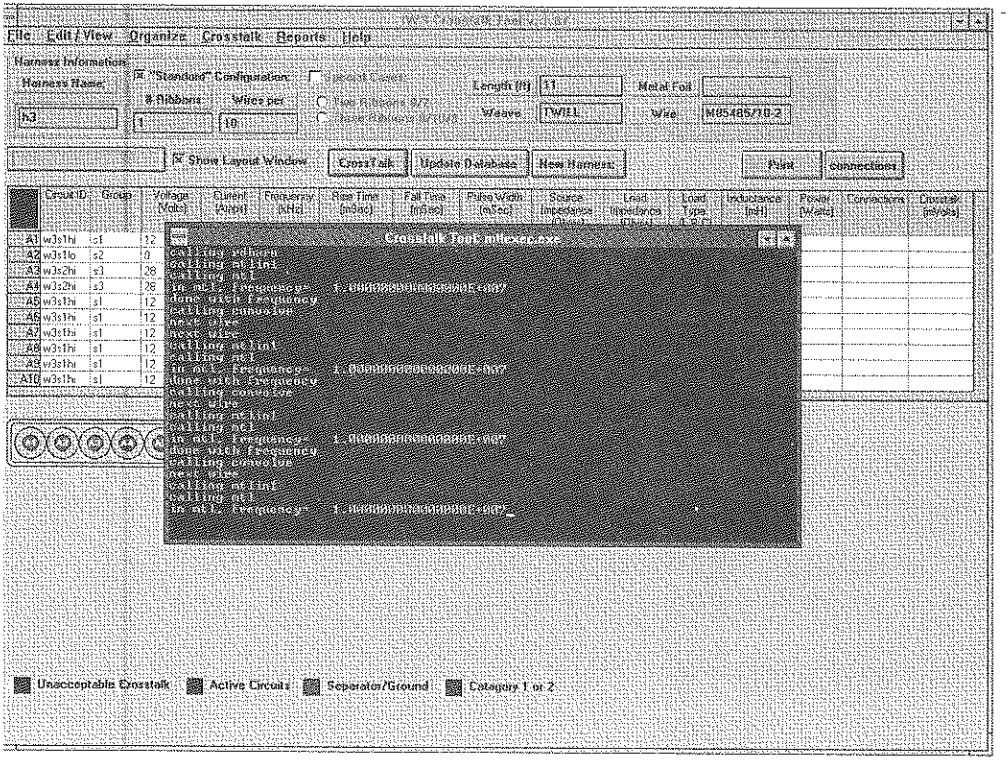
File Edit / View Organize Crosstalk Reports Help
Harness Information
Harness Name:
"Standard" Configuration
Length (ft) 11
Metal Foil
h3
Ribbons
Wires per
Weave TWILL
Wire M85485/10-2
Show Layout Window
CrossTalk
Update Database
New Harness
Print
connections
Crosstalk Test Window
Unacceptable Crosstalk
Active Circuits
Separator/Ground
Category 1 or 2

New Lightning and NEMP Protection Technics

C. GIRARD *, Alcatel Cable / D.E.E.
Y. BOURDET , Alcatel Cable / D.E.E.

Technological progress in the design and production of components, combined with the implementation of new circuit arrangements, now make use of new protection technics possible. These tecnnics protect against the induced effects of lightning and NEMP, applied to wire and coaxial networks.

The purpose of these new technics is to:

- improve the electrical performance of the protective devices, by decreasing the level of residual voltages that highly susceptible equipment has to withstand;
- reduce the protective device cost and volume as compared to those the previous generations.

Protection of energy transport networks

The conventional technic implemented for the protection of energy transport networks is outlined in the diagram below, for one phase:

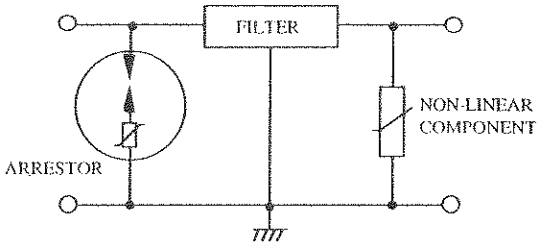

This type of protective device uses peak clipping components at the input and output of the circuit, and a low-pass filter.

This technic has the following drawbacks:

- a fairly high level of residual voltage (about 800 V) for lightning strokes (low frequency disturbances). The peak clipping components' thresholds shall have to be selected beyond the rated voltage of the energy transport network;
- capacitive leakage current from the filter in the range of 2 to 10 A, which forbids its direct use in networks, whose neutral line is grounded or presents an impedance. In this case, the protective device is located between two transformers, the second of which redistributes the neutral;
- large volume, high cost and fairly cumbersome implementation.

The protection technique we propose is shown by the diagram below for one phase:

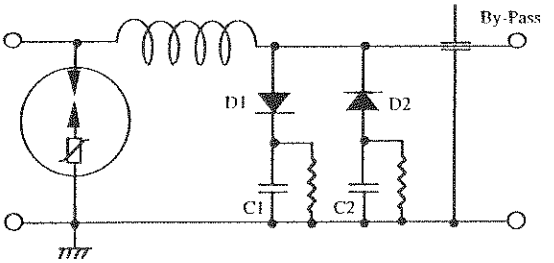

Similar to the previous version, this protection circuit includes an input arrestor for clipping the energy level of the incoming disturbances.

The second stage consists of an "active filter" made up of components L, D_1, C_1 (or L, D_2, C_2).

Once the power is turned on, the high-valued capacitors C_1 and C_2 charge to their respective maximum and minimum network voltages.

Then diodes D_1 and D_2 turn off.

When an over voltage appears, diode D_1 or D_2 (depending on the over voltage polarity) becomes conductive and the LC filters works efficiently (having the high capacitance values, i.e. 100 to 500 µF).

After the disturbance has vanished, the diodes turn off again. Resistors R_1 ands R_2 are provided to discharge capacitors C_1 and C_2.

With this principle, the residual voltage level of the lightning (low frequency) waves can be reduced down to 100 or 150 V.

The leakage current is reduced down to 150 mA, but it could be further reduced by adding the following circuit:

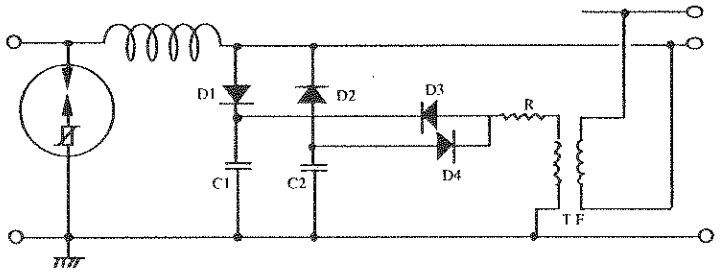

A small transformer is used. Its primary winding obtains power from two of the phases. Its secondary winding, slightly increases the voltage level s by 10% above the network's voltage. This voltage, rectified by diodes D_3 and D_4, charges the capacitors to a higher value than that of the network level. This thereby turns diodes D_1 and D_2 permanently off (except in case of an over voltage).

This arrangement brings the leakage current down to nearly zero. It offers many advantages to those users who want to detect any failures on their networks.

From a maintenance point of view,a supplementary step worth considering would consist of integrating an electronic monitoring device directly inside this protection unit. Its primary function the function of which would be to warn the user whenever one of the circuit's components fails.

The principle is summerized in the figure below:

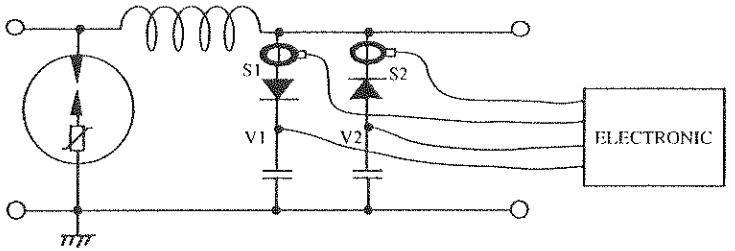

An electronic unit permanently monitors 4 parameters: the two current levels in diodes by means of two sensors S_1 and S_2, and the two voltage levels V_1 and V_2 across the capacitors. This information is used to detect a defective component. The status of this electronic monitoring device's essential function can be displayed either locally, or via a remote site (through a fiber optic link)

ELEMENTS FOR AN HARDENING OF THE ARABEL MULTI FUNCTION RADAR ANTENNA

Christian CAREL

THOMSON-CSF
Division Radiocommunications
Guerre Electronique et Sécurité
66, rue du Fossé Blanc - B.P. 156
92231 GENNEVILLIERS Cedex

ARABEL is an X-band Multi-Function Radar. Its antenna is one of the most exposed to environments FSAF family sub-system : the french naval SAAM and the french-italian ground mobile SAMP/T fire control unit.

One particular point of interest of the antenna is the lens composed by more three thousand dipole-phase shifter-dipole (dpd), way for front door penetration.

The goal of the communication is to describe studies developed to estimate the EMP hardeness for the first prototype by a both bottom-up and top-down approach. The differents stages are :

- an experimental approach for the burn-out and susceptibility threshold of elementary components (resistor, capacitor, diodes, integrated circuits) ;

- an experimental study of the voltage induced on a dpd point of entry by radiated field illumination. A comparison with a 9 dpd response set on a mini-gider, with and without cap, permit to estimate first the decreasing of sensitivity due to element integration and second the shielding effectiveness for the cap ;

- a global test of a scale one mock-up lightened under a strip-line at full EMP level. The voltage measurement comparison with those of two previous stages leads to a margin estimate for the mock-up.

- the prototype lens margin is obtained by convolution of the external surface field calculated by a 3D finite difference code with the mock-up field response.

A WAVE ABSORBER COMPOSED OF DOUBLE-LAYER PARALLEL ARRAYS OF ZIGZAG CARBON CLOTH BELTS

HIROSHI UJIIE
(Tohoku Institute of Technology ,Sendai,JAPAN)

ABSTRACT

A new way to utilize the carbon cloth for the wave absorber is proposed and its properties are discussed from the standpoints of matching,absorption,polarization and oblique incidence.

1. Structure

The procedure of construction is the following:

◊ A carbon cloth is cut down into many carbon cloth belts with a same width(W);
◊ Each belt is cut into a zigzag shape;
◊ These carbon cloth belts are arrayed in parallel at a proper iterval(d) by dielectric spacers, this aggrigation is named as "basic absorber";
◊ Two basic absorbers are piled up at a right angle each other,(Fig.1).

This double-layer carbon cloth belts arrays is the new wave absorber proposed in this paper.

2. Discussions

(1) Matching

It is so easy to cut down the carbon cloth into any shape that various types of impedance matching to the free space are available. The carbon cloth array can be seen as many fine lines array for the normal incidence, so the reflecting area by the carbon is extremely small.Therefore this absorber is able to have a superior impedance matching to the free space.

(2) Absorption

The amount of absorption depends on the width of carbon cloth belt(W),the array interval(d) and the intrinsic resistance of the carbon cloth(R) that represents approximately the effects of length and density of carbon fibers in the cloth. Fig.2 shows a measured absorption curve of the basic absorber (R=0.98[Ω-cm] carbon cloth and styroform spacers).

The absorption level is controllable widely by the interval(d), accordingly the thickness(=W) of the basic absorber is able to be much thiner compared with the carbon powder distributed absorber, by a proper choice of the array interval.

(3) Polarization

The basic absorber has sufficient absorption only for a linearly polarized wave. Enough absorption for the incident wave with any polarization can be obtained by piling up two basic absorbers at a right angle each other. The measured results about the double-layer absorber show almost the same absorption for three incidences (vertical,horizontal and 45°inclined polarizations).

(4) Oblique incidence

The response to the oblique incidence is examined by the scattering pattern measurement about a test absorber (S=20λ×20λ,λ:wave length). Fig.3 shows a scattering pattern for the incident angle of 30 °. The measured results show less reflection in comparison with a carbon powder distributed pyramidal absorber on the general market. An explanation on the superior response to the oblique incidence is shown in the illusturation (Fig.4).

3. Conclusion

The potentials of the proposed absorber are the following:

- Simple structure and easy fablication;
- Superior impedanc matching to the free space;
- Wide cotrollability of absorption;
- Superior response to the oblique incidence.

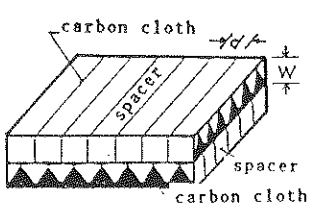

Fig.1 Structure

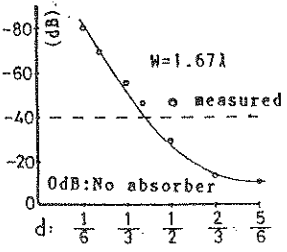

Array interval(λ)

Fig.2 Absorption

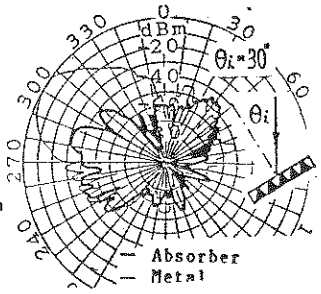

Fig.3 Scattering pattern

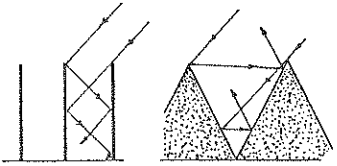
1 proposed 2 pyramidal

Fig.4 Response to oblique incidence

USING THE FIELD EMISSION EFFECT FOR INCREASING SCREENING EFFICIENCY

Loudmila V.Vavriv*, Vladimir V.Knyazev, Andrey E.Serebryannikov
Molniya Research and Engineering Institute, Kharkov, Ukraine

The screening is one of the main methods in providing protection of radioelectronic equipment from destabilizing action of electromagnetic radiation of different physical origin (LEMP, NEMP, etc.).In "traditional" screening the weakening of external noise fields is reached through the damping in the material of screening envelope. The realization of this method faces definite difficulties when the protection of aerospace objects from powerful and super powerful nanosecond electromagnetic fields are required.

For the high-frequency portion of spectrum the main mechanism of penetration is not a diffusion through envelope walls, but is an infiltration through small technological irregularities such as mechanical joints, welded seams and elements necessary for the airborne instruments (radio windows, etc.).

Besides, the availability of geometric irregularities leads to the local field amplification. This results in decreasing the screening efficiency of high frequency components. Thereat, the screening efficiency in low frequency portion of spectrum remains practically unchanged. Local decrease of the fields' levels near the irregularities is one of the methods used for the pointed-out factors compensation. This problem can be solved through the use of special materials for the manufacturing of screens. These materials should possess the property of field emission (M.I.Elison, G.F.Vasiliev Field emission, Moscow,1958). The latter effect is strongly manifested only in the vicinity of irregularities. Besides, the tungsten and molybdenum whose use gives the best effect from the point of view of electron simulation intensity are very expensive. Therefore it is recommended in practice to combine "traditional" screening with the metal deposition possessing field emission properties in places of expected local amplification of a field. The high intensity of this method is reached when the amplitudes of external noise field are equal to 10^5 -10^6 V/m and higher. The mechanism of external field damping is reduced to the formation of plasma layer in the vicinity of irregularities owing to electrons' emission from the surface. When the electromagnetic pulses pass through the plasma layer the amplitudes of harmonic components with the frequencies that not exceed plasma frequency decay according to the exponential low in the first approximation (V.V.Nicol'sky, T.I.Nicol'skaya Electrodynamics and waves' propagation). Since the value of plasma frequency has order of 10^8 - 10^{10} Hz for the metals possessing the property of the field emission the levels of EMP high-frequency components the most dangerous for radioelectronics would be significantly reduced. The technical realization of the method suggested for increasing the screening efficiency is protected by the patent.

EFFECT OF DESIGN CHANGES OF DOOR-FLANGE ASSEMBLIES ON THEIR SHIELDING EFFECTIVENESS

L. Dreux, P. Bonamour, M. Sternberg, B. Lepetit *
AEROSPATIALE 12, rue Pasteur BP76
92152 Suresnes Cedex FRANCE

1 - INTRODUCTION

Airframe materials are usually metallic or metallized composite materials. Therefore, they provide a high shielding effectiveness. This shielding effectiveness is an increasingly important feature of airframes, since the electromagnetic environment which an aircraft must be able to sustain is increasingly high. However, details of the structure can lower this shielding effectiveness : for example, joints between panels of different materials, or between the airframe and access doors, which are used to maintain equipments located in avionics compartments.

In the case of the access door, this lower shielding results from the penetration of external electromagnetic fields through the slot which exists between the door and the flanges of the compartment. One performant way to solve the problem is to fill this gap with a conductive gasket. Yet a conductive gasket has several disavantages : high cost, short lifetime in corrosive environmental conditions, difficult industrial use (special preparation of material surfaces is needed to reach the maximum effectiveness). It can therefore be useful to study, maybe less performant, but more convenient solutions.

Two mechanisms of degradation of shielding effectiveness exist :

- narrow cavity resonances
- broader slot resonances.

We show hereafter how this latter phenomenon is influenced by design changes in the door-flange assembly, in particular :

- the size of the overlapping between the door and the structure,
- the addition of conductive braids between the door and the structure.

2 - EXPERIMENTAL SET-UP

We use a metallic box, opened on its front. An assembly which simulates the door of the aircraft is put on the front of the box. This assembly includes a non conductive gasket between a door and a flange (figure 1). The walls inside the box are covered with electromagnetic absorbers to reduce resonances in the cavity.

The shielding effectiveness is defined as the ratio between the amplitudes of the fields inside the box, with the door respectively closed and opened. A 100 V/m vertically polarized electric field is used to illuminate the box. The amplitude of the fields inside the box is measured in the range 20 MHz - 1 GHz with an electrical passive sensor connected to a spectrum analyser by an optical link.

3 - EFFECTS OF THE OVERLAPPING

Three sizes are considered : 5 mm, 15 mm and 30 mm (see figure 1). The results of the measurements (figure 2) show that an increase of the overlapping increases the overall shielding effectiveness and the slot resonance frequency. These phenomena can be explained with a numerical model (finite elements method) which computes the surface currents and fields inside the box.

4 - EFFECTS OF CONDUCTIVE BRAIDS

Bonding braids can be put on hinges or on door latches to increase the electrical conductivity between the structure and the door and to change the distribution of currents around the slot. Results of measurements are shown on figure 3, for 3 configurations : no bonding braid, two and four bonding braids. The slot resonances are less intense, but cavity resonances are enhanced. The quality factor of the cavity is better with the bonding braids.

5 - CONCLUSION

We have described several simple design changes of door-flange assemblies which improve their shielding effectiveness. None of them is as efficient as the use of a conductive gasket. Some may be

sufficient for the electromagnetic environment to be considered. Further studies on the effect of the gasket thickness could provide additional interesting results.

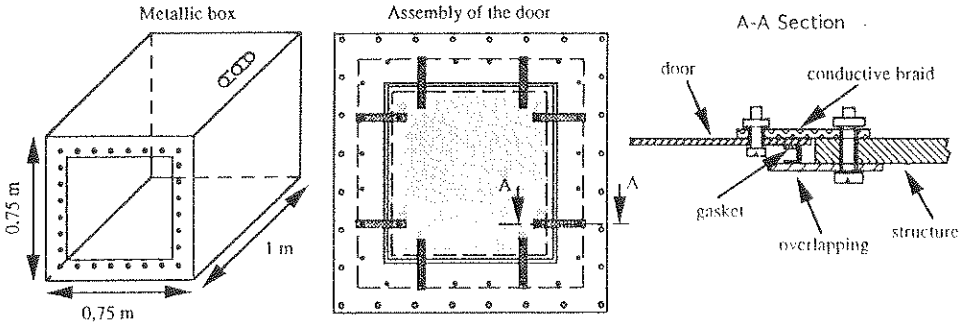

Figure 1 : Experimental set-up

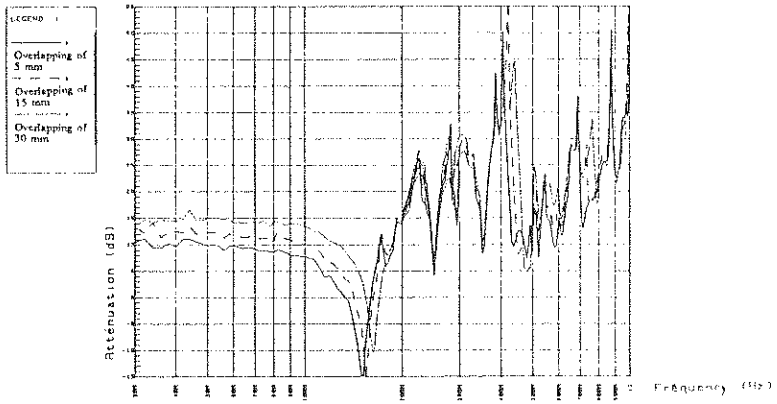

Figure 2 : Effects of the overlapping

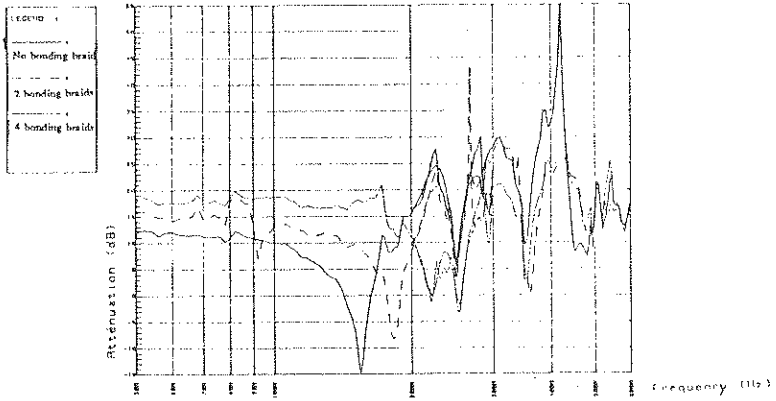

Figure 3 : Effects of conductive braids

GERAC
ELECTROMAGNETISME

THE SENIOR PARTNER IN ELECTROMAGNETIC COMPATIBILITY

ENGINEERING : SOME OF OUR REFERENCES

- major participation in lightning and HIRF certification of AIRBUS planes,
- development of EMC specifications for Channel Tunnel electronic equipment,
- substantial engagement in preparing the HA-EMP Hardening Guide (French DOD),

DIGITAL SIMULATIONS : SOME OF OUR PRODUCTS

- **3D codes :**
  - structures in any material,
  - perfect or not perfectly-conducting floor,
  - non linear events,
  - ...
- **2D codes**
- **Cable coupling codes**
- **Modelling protection items**

TESTS : SOME OF OUR FACILITIES

- **Standard tests** : The whole equipment to run the major standard tests in lightning, EMC, HA and LA-EMP.

- **Non standard tests :**

  Double exponentials
  - shape (tm/td) : from 5 ns / 200 ns to 5 µs / 150 ms
  - amplitudes (Vco/Icc) : from 100 V / 20 A to 100 000 V / 10 A

  Damped sinusoids :
  - frequencies from 10 kHz to 100 MHz :
  - amplitudes up to 10 000 V / 100 A

GERAC - BP 19 - 46500 GRAMAT - Tél. 65 38 79 23 - PARIS : (1) 41 07 51 51 - TOULOUSE : 61 39 93 75

A REVIEW OF THE PHENOMENOLOGY OF HIGH POWER MICROWAVE EFFECTS ON ELECTRONIC COMPONENTS[1]

Robert J. Antinone
BDM Federal, Inc.
1801 Randolph Road S.E.
Albuquerque, NM 87106 USA

In most cases the effects of high power microwaves (HPM) on electronic systems start with the interaction of coupled signals with one or more electronic components within the system. Understanding the phenomenology of how HPM signals affect electronic components is fundamental to understanding how HPM affects electronic systems. This paper reviews our current understanding of the response of common electronic components to HPM signals.

The initial studies of the effects of HPM on electronic components were based on the studies of electromagnetic pulse (EMP) effects on such components. Researchers recognized two types of effects, permanent effects such as degradation and damage and transient effects such as disturbance and upset. In the EMP case damage or degradation is usually caused by absorbing excessive power from the pulse, and researchers hypothesized that this same mechanism would apply to the HPM case. This proved to be true in many cases although the amount of incident power absorbed at microwave frequencies may be much different from the amount absorbed at EMP frequencies. Other EMP damage mechanisms such as latchup also proved to be important in the HPM case although the incident power required to trigger latchup may be different between the two cases.

During the late 1960's Wunsch and others developed models to explain the relationship between the duration of an EMP pulse and the power required to cause damage. These models have proven applicable to the HPM case as well. However, these models describe only a portion of the response problem. The parasitic reactances associated with the component have greater effect on its response at typical HPM frequencies than they do at typical EMP frequencies. Likewise, multiple signal paths within the component may be more difficult to understand at microwave frequencies.

[1] This work sponsored by the U.S. Air Force Phillips Laboratory under prime contract F29601-89-C-0008 through Kaman Sciences Corporation under subcontract KD-SC-8013

In the case of disturbance and upset our past experience with EMP has not been as helpful in understanding the HPM response of components. EMP signals are often in the normal operating band of common electronic components, while HPM signals usually are out of the normal band. Thus, the response mechanism is fundamentally different. Whereas the component responds directly to EMP excitation, the component must first convert the HPM signal to one it can use. The component usually does this by the process of rectification. Any nonlinearity will rectify the incident HPM signal and recover its envelope. The component then responds to the envelope.

The efficiency of the rectification process controls how well the component responds to the HPM signal. Different components will respond differently, and efficiency will vary with frequency. Components based on Schottky diode technology may respond better at higher frequencies than components based on silicon junctions. Figure 1 shows some typical HPM disturbance data.

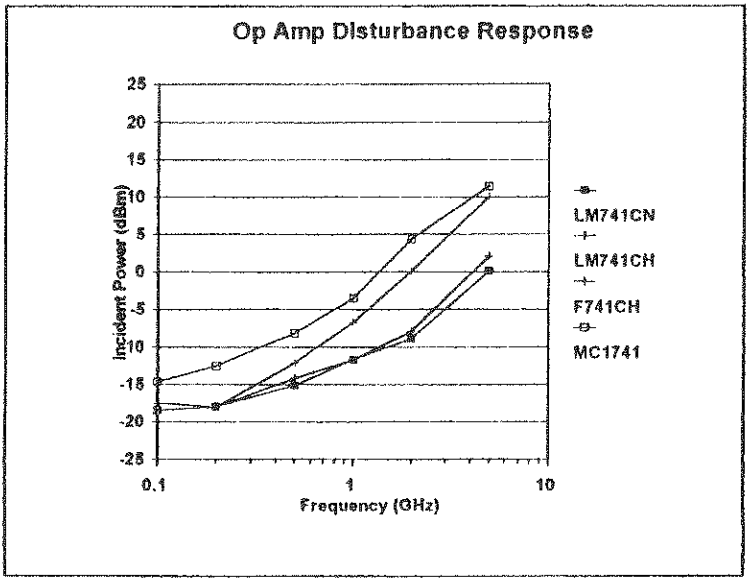

Figure 1. HPM disturbance data for typical operational amplifiers.

HPM FUNCTIONAL RESPONSE TESTING AND ITS APPLICATION TO THE INTERFERENCE OF SMART MUNITIONS

Raymond A. Meinhart*
Klaus Ruffing
EMC Technical Center
WTD 81, Dept. 321
91171 Greding, Germany

Jürgen Bohl*
DIEHL GmbH & Co., Dept. M-ELK
Fischbachstr. 16
90552 Röthenbach, Germany

Within the framework of any high power microwave (HPM) susceptibility methodology, the functional response testing of a live system in its simulated operational environment against radio-frequency (RF) irradiation is critical to validate predictions and help plan future tests. This testing is unique in that it provides a direct indication of the type and magnitude of functional degradation due to RF radiation at a relatively low required power. A specific technique for this type of testing has been developed and applied to the testing of various smart missile/munition systems to determine the critical RF parameters required to interfere with the electronics of these systems. The testing technique along with the results of these munition studies, including aspects of autonomous versus semi-autonomous systems, front and back door coupling, munition guidance and control, flight simulation, and hardening, are presented in this paper.

The primary purpose of functional response testing is not to damage or even necessarily upset the function of the system under test. Instead, it is to probe the realm of possible effects that RF irradiation may bring about. This is not to say that upset is unwanted or unlikely or, for especially sensitive equipment, that damage will not occur, but these are secondary goals. The key word for this type of testing is "response." This implies any deviation of critical internal voltages and/or currents from their normal operating range. These signals are typically monitored via a minimally invasive and non-perturbing means such as fiber-optic transmitter/receiver systems. This type of testing was applied to various munition/missile systems and the experience gained during these tests compiled into a specific test process to directly measure the RF response of a system during irradiation.

Smart munitions can face high power microwave hazards generated by either natural, civil, or military environments. In order to understand these interactions better, their subsystems and sensors are presented along with a comparison of semi-autonomous and fully autonomous systems with respect to their subsystems and flight profiles.

These systems normally incorporate intentional (front door) as well as unintentional (back door) paths for microwave transmission. A front door path, for example, could be the millimeter-wave seeker subsection with antenna. Furthermore, nearly all smart missile/munition

systems need wings for aerodynamic lift and control fins to maneuver the system to the target. These protruding structures can be regarded as antennas responding to electric fields. The slots for these structures provide a back door path for the magnetic fields generated by the corresponding current in these appendages. Throughout the entire flight path of the missile, the RF energy is passed to the inside of the system via the fins, wings, and slots, and can thereby cause interference dependent on the field strength, polarization, frequency, and the carrier modulation frequency. This energy is further propagated through the system via the wiring and electronic components. Resonances corresponding to the missile's physical dimensions can also influence its mission.

After stabilization, the missile guidance and control system is required to guide the missile to the target area and to acquire and hit the target with subsequent final homing. The different layers of the guidance and control loop of smart munitions are each designed with different tasks. Comparatively, these control loops are either more or less sensitive to electromagnetic radiation interference and can lead to the loss of the target.

Investigation results are shown for different smart munition systems irradiated with electromagnetic fields up to 600 Volts/meter between 100 MHz and 18 GHz. During these live tests, defined flight events were continually processed by the missile. The results show not only the overall system vulnerability, but also the coupling effects of the electromagnetic field to the internal wiring and subsystems. Further results show how the different coupling effects can be avoided. Flight path simulation models were also implemented by introducing RF perturbations at specific points in the control loop to measure the induced effect on missile flight. Final consideration was given to how one protects against this demonstrated interference during the development stages of such a system.

MICROWAVE COUPLING MEASUREMENTS ON A SMALL OBJECT.

Peter G. Landgren
BOFORS MISSILES
Karlskoga Sweden

Introduction

This paper will discuss two different coupling measurements performed in the microwave region, 1-18 GHz. First a detailed description of the normal way of doing coupling measurements will be given. This will be followed by a presentation of coupling measurements utilising a mode stirred chamber. Finally a comparison will be made.

Background

In connection with a larger program to develop test methods for general microwave susceptibility testing of small objects, a sub task was to analyse how to do coupling measurements. For this reason a test object was needed. Many coupling measurements have previously been done on simple objects like tubes with simple hatches and alike. The decision was taken to use a real missile for these tests.

Test object

The missile had to be modified to be able to install test points. Two types of test points were used. Five points were short, 4 mm, monopole antennas made of semi-rigid coax. Four test points were voltage measurements on specific subunits in the missile. Also one dummy test point was added later. Only the five field test points will be discussed in this paper.

The positions of the test points were determined after an analysis of the test object concerning joints, subunits, and the possibility to install. Not all electronic boards were in place, but some of the most important was.

Normal test

The first test was done in an anechoic chamber. The missile was illuminated from three different directions and with vertical and horizontal polarisation. Frequency range was 0.5 (2) - 18 GHz. The measurement system consisted of one microwave network analyser feeding horn antennas. To increase dynamic range, low noise pre-amplifiers (25-42 dB) were used at the analyser input terminal.

Results:

The graph shows attenuation as function of frequency for horizontal and vertical polarisation. Some smoothing of the curves has been done.

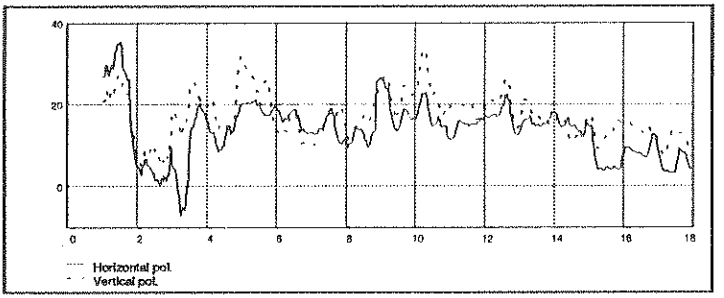

Mode stirred chamber test

The same test object was used with the additional dummy test point added. The reason for this was to see if there was any systematic coupling in the test set up.

Results

The same method was used as above. Note the dummy test point.

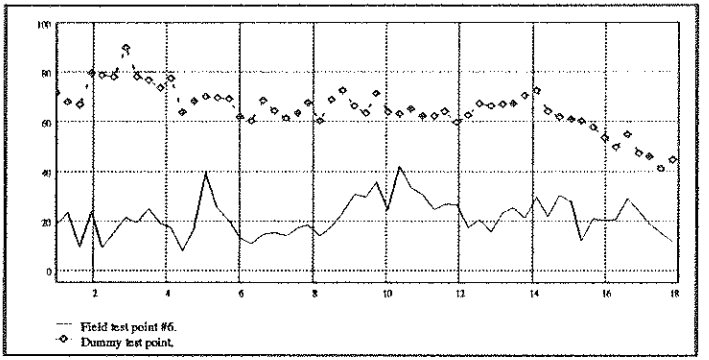

Comparison

Both methods give similar results. However there might be a tendency to lose some resonances when using a mode stirred chamber.

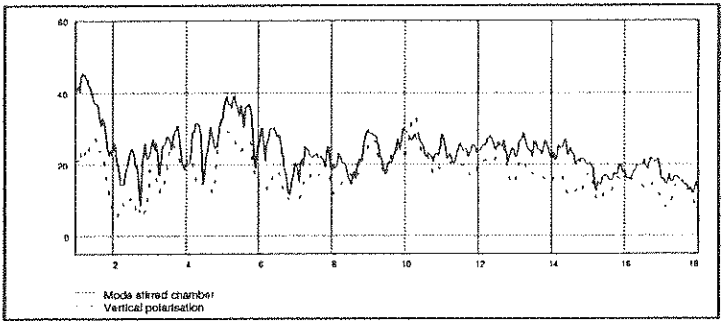

Conclusion

All measurements were done with too many frequency points, 8000 for the normal and 27217 for the mode stirred chamber. This gives a way to analyse how much data really is needed to get good results.

In addition to what is given in this paper a great number of experiments were performed to try to understand the different coupling paths and mechanisms, propagation within the missile and cavity resonance phenomena.

Gyrotron Experiments Using Cold and Thermionic Cathodes

AW Cross, SN Spark, K Ronald, ADR Phelps and W He

Department of Physics and Applied Physics
University of Strathclyde
Glasgow, G4 0NG, U.K.

A comparative investigation of the oscillating characteristics of a step-tunable (20 to 45GHz) gyrotron with the change in the electron beam source is reported. This was achieved by directly comparing the oscillating characteristics of a gyrotron based on a cold cathode with second gyrotron which utilised a thermionic cathode as a means of generating the electron beam.

The cold cathode electron beam source consisted of a 12mm outer diameter stainless steel hollow rod with a sharpened knife edge configured within a two electrode diode. The physical mechanism responsible for electron emission was thought to be due to field emission at microscopic irregularities which covered the cathode knife edge resulting in the localised heating and vaporisation of the material. This creates a surface plasma from which the electron beam may be formed. The field-immersed, field emission cold cathode generated large currents ≈800A with the application of both single and repetitive pulsed potentials of magnitude ≈-75kV. This system produced mm-waves in the frequency range 24 to 100GHz at power levels ≈6MW. The mm-wave pulse duration of the cold cathode gyrotron was limited to ≈400ns. It has previously been shown that the limit on the relativistic electron beam pulse duration was due to "plasma disruption" at the cathode[1]. This is a process by which the accumulation of plasma at the cathode in conjunction with its expansion across the anode-cathode gap results in the degradation and eventual termination of the relativistic electron beam. With the use of a thermionic cathode continuous electron emission is possible. This allows the extension of the relativistic electron beam pulse duration beyond the 100ns to 400ns limit presently imposed by "plasma disruption" of the diode. A high power (≈100kW), long pulse (≈50μs to 100μs) gyrotron has subsequently been developed utilising an electron beam forming system based on a MIG-type thermionic cathode built by EEV Co fig(1). The operating parameters of both gyrotrons are compared in table 1.

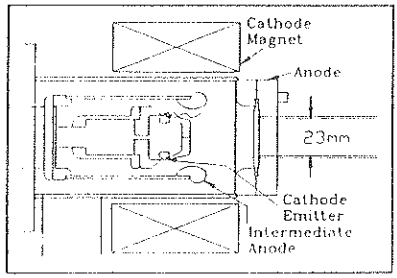

Figure 1. Scale drawing of MIG type thermionic cathode.

	Gyrotron: Cold Cathode	Gyrotron: Thermionic Cathode
I_{Source}	800A	20A
V_{beam}	75kV	60kV
mm-Wave Power	6MW	100kW
Pulse Duration	100ns	50 to 100μs
Frequency Range	20 to 100GHz	20 to 45GHz

Table 1. Gyrotron operating parameters

Powering the thermionic cathode gyrotron with a (5μF, 723J) Marx bank, producing a cathode pulsed potential of magnitude -60kV, resulted in the generation of a 20A electron beam which had characteristic 1/e decay time of ≈100μs. This resulted in the generation of a 50μs and a

100μs duration mm-wave output pulse at a central intra-cavity B field value of 1.175T and 1.650T respectively. At central intra-cavity B fields of 1.175T and 1.650T, the cavity modes of oscillation were identified from the measured near-field radiation patterns with their corresponding critical starting currents required for mode excitation measured as a function of B field. The TE_{02} mode, cut-off frequency ≈29.1GHz, was identified at an intra-cavity B field of 1.175T with a corresponding critical starting current of 1.5A, fig(2). The TE_{03} mode, cut-off frequency 42.2GHz, was identified at an intra-cavity B field of 1.650T with a measured starting current of 0.5A.

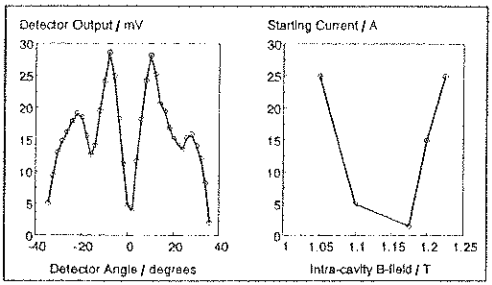

Figure 2. TE_{02} near field radiation pattern and starting current with respect to intra-cavity B-field.

A heterodyne diagnostic system was used to measure the frequency and line width of both the TE_{02} and the TE_{03} modes. The TE_{02} mode was measured oscillating at a full-width, half-height line width of 1.3MHz, at a centre frequency of (29.7±0.3)GHz fig(3). Similarly, the TE_{03} mode was found to be oscillating at four separate cavity resonant frequencies, with a centre frequency of (42.5±0.3)GHz. Each resonance had a measured bandwidth of ≈5MHz, with a frequency separation of ≈20MHz. This 20MHz frequency separation matches that of the longitudinal cavity modes.

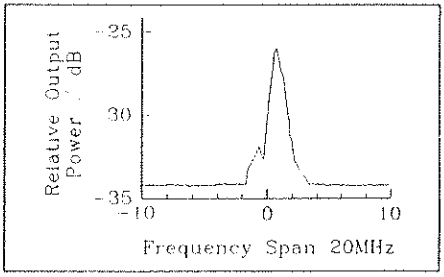

Figure 3. Heterodyne frequency measurement of TE_{02} mode, centre frequency 29.7GHz.

The gyrotron output power was measured using a broad band power meter. The energy content per pulse was determined via the absorption of the mm-waves in a calibrated thermocouple calorimeter, with the mm-wave pulse duration monitored using a Ka-band crystal detector. An energy content per mm-wave pulse of ≈12J, with a corresponding output power of ≈120kW was measured. A gyrotron operating efficiency of ≈10% was deduced. It can therefore be concluded that the change in the electron beam source from a field-immersed, field emission, cold cathode to a MIG type thermionic cathode did not significantly effect the gyrotron operating efficiency. As the thermionic cathode gyrotron and the cold cathode gyrotron were based on identical ill-defined, oxygen-free, high conductivity (OFHC) copper cavities, this suggests that in this experiment it is the interaction cavity and not the electron beam source which dominates gyrotron operating efficiency.

Acknowledgements

Support for this research was provided by DRA agreement 2065/61 and an SERC research grant. The authors thank the EEV company and the SERC for providing an SERC CASE studentship for Mr A W Cross. Helpful discussions with M. Esterson, H. P. Bohlen, D.M. Parkes and K. Trafford are gratefully acknowledged.

References

1. Ronald K, Spark S N, Phelps A D R and He W, 1993, "High Speed Diagnostic Study of Pulsed, Cold Cathode, Gyrotrons," *Proc. 18th Int. Conf. Infrared and Millimeter Waves*, SPIE 2104, 454-455

APPLICATION OF MULTIDIMENSIONAL ELECTROMAGNETIC SCALE MODELING TECHNIQUES FOR ASSESSMENT OF HPM EFFECTS.

Capt TN Pranesha, I.N
Cdr Pritam Lal, I.N
Lcdr T Jagannath, I.N

ABSTRACT

1. Although it is customary in scattering and antenna measurements to use same medium in both the scale and model systems from considerations of convenience. The general concept and principles of scale modelling allow, without loss of generality, change in medium also. The change in medium of full scale system to scale model systems amounts to change in electric and magnetic scale factors in addition to conventionally familiar mechanical and temporal scale factors. Flexibility in selection of all the four scale factor increases the complexity of scale modelling and imposes additional problems in measurement of conventional scattering or antenna related parameters. However, it renders it feasible to build scaled systems suitable for use in assessment of high field interaction problems.

2. This paper examines the suitability of multi dimensional scale modelling approach in the HPM context. Beginning with defining the conditions for an EM Scale model to simulate an arbitrary target system and allowing freedom in selection of mechanical, temporal, electric and magnetic scale factors, the relationship between the full scale system operating in the free space to the scale model operating in the selected model medium is established in terms of medium characteristics and corresponding scale factors. Usefulness of such relationships in conduct of measurements of interest in the context of high intensity field interaction with model system of practical interest is then examined. A survey of materials which are potentially suited for use in multi dimensional scale modelling is also attempted based on available data on high voltage insulating oils and materials. An outline approach on conduct of tests on the multi dimensional scale model is also addressed.

EFFECTS MODELLING AND ANALYSIS
A METHODOLOGY FOR ASSESSMENT OF IMPACT OF HPM THREAT

Capt TN Pranesha, I.N
Cdr LM Khanna, I.N
Lcdr SN Behera, I.N

Abstract

1. With the likely advent of HPM weapons as a viable tactical offensive option in the warfare, the requirement for review of existing offensive and defensive deployment concepts, with specific reference to the impact of intense HPM threat on critical electronic war assets, assumes importance. The conventional approach of evaluation in realistic simulated environments would not be feasible in this context in view of the complexity of threat and multiplicity of concurrent phenomena which need to be accounted for to achieve comprehensive simulated environment suitable to the specific issues in hand and the resultant large outlays in terms of capital cost and lead time requirements for development of necessary infrastructure and techniques. The need is for a quick assessment of likely impact of this newer threat on existing electronic warfare assets and deployment concepts with a reasonable degree of confidence rather than achieving insight into the threat interaction phenomenon itself. The emergent field of Effects Modelling appears to render a viable tool for adaptation in this vital area.

2. After a brief account on the conceptual framework associated with Effects Modelling, application of these concepts to the context of electromagnetic interaction is attempted. The basic approach consists of evolving parameters of threat model and system interaction model emanating from transient EM event and EM interaction of transient field on the system with given topology and connectivity conditions and the use of these parameters in overall risk analysis. Although the basic HPM threat model is represented in terms of heuristically graded effect vector, further refinement of the same is feasible through inclusion of factors like value of the concerned effects to the enemy, opportunity cost etc. Similarly basic system interaction model could be represented in terms of effect (impact) at any selected port which also, in turn, could be heuristically graded and appended with known parameters pertaining to asset importance, current protection level etc, to evolve system vulnerability function. Finally the HPM risk analysis for each operationally significant context may be carried out using the threat and vulnerability functions obtained from the above steps.

High Gain GaAs Photoconductive Semiconductor Switches for Impulse Sources

G. M. Loubriel, F. J. Zutavern, R. R. Gallegos,
W. D. Helgeson, and M. W. O'Malley
High Power Electromagnetics Department
Sandia National Laboratories
Albuquerque, NM 87185-1153

Abstract: The ability of high gain GaAs Photoconductive Semiconductor switches (PCSS) to deliver fast risetime pulses when triggered with small laser diode arrays makes them suitable for their use in ultra- wideband, impulse transmitters. Other aspects of the switches that are relevant to this and other applications are switch lifetime (longevity), switch opening time (carrier lifetime), switching jitter, and the required laser energy. This talk will emphasize the results obtained with high gain GaAs switches for ultra wideband applications. We have demonstrated that the GaAs switches can be used to produce either a monocycle or a monopulse with a period or total duration of about 3 ns. For the monopulse, the voltage switched was above 100 kV, producing over 1 kA through a 50 Ω load (50 MW); at a burst repetition rate of 1 kHz. The optical trigger used was a pair of fiber optic coupled laser diode arrays with an energy of 90 nJ per pulse (each).

The reduction in the amount of required trigger energy has been traced to a reduction in the voltage risetime. We tested this effect in a experiment where the first to last timing spread was recorded for a 3 by 2 matrix of different voltage risetimes (210, 590, and 865 ns) and different laser energies (90 nJ and 1.8 μJ). The lasers did not trigger the switch for the 865 ns risetime. The 90 nJ did not trigger the switch when the voltage risetime was 590 ns. The 1.8 μJ did trigger the switch when the risetime was 590 ns but only about half the time. For the 213 ns risetime both laser energies resulted in triggering with low jitter. The experiment clearly shows a relationship between the risetime of the voltage across the switch and the required trigger energy and switch jitter. Thus, it may be possible to reduce jitter and laser energy requirement by using faster voltage charging.

When the system is triggered simultaneously with two laser diode arrays two current filaments are observed. By delaying one filament with respect to the other, the infrared photoluminescence from the filaments was recorded in a time resolved fashion. We measured a speed of 2 cm/ns for the tip of the filament. Pictures of the filaments will be presented.

This work was supported by the United States Department of Energy under contract DE-AC04-94AL8500 and by the Air Force Phillips Laboratory under contract FMBA 93-334 DOE.

THE DECADE HIGH POWER GENERATOR†

G. Frazier*, S. Ashby, K. Childers, C. Deeney,
D. Drury, J. Goyer, D. Kortbawi, I. Roth, P. Sincerny, C. Stallings
Physics International Company
2700 Merced Street
San Leandro, CA 94577

L. Schlitt
Leland Schlitt Consulting Services
2725 Briarwood Drive
Livermore, CA 94550

DECADE is a 35 TW pulsed power generator designed to drive both large area bremsstrahlung diode arrays and imploding plasma loads. For a one square meter array of bremsstrahlung diodes, the machine will deliver up to 2.5 MJ of electrical energy at a peak voltage of 1.8 MV. DECADE will drive up to 25 MA into a plasma radiation source load.

The DECADE generator (Figure 1) consists of sixteen independent pulsed power modules. Each module has a 500 kJ Marx generator that pulse charges a water transfer capacitor. The transfer capacitor discharges into a water output line through an array of triggered gas switches. The water output line then pulse charges the final inductive store/opening switch pulse compression stage. When the opening switch opens, the inductive store discharges into either an independent diode load or into a vacuum convolute that connects all sixteen modules to single imploding plasma load.

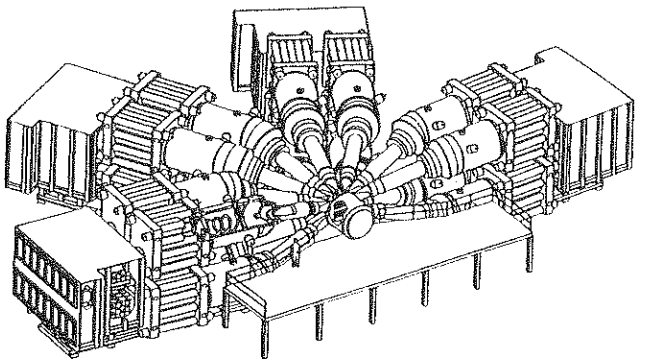

Figure 1. Illustration of the complete DECADE machine. For scale, note the man standing on the platform.

† Work supported by the U.S. Defense Nuclear Agency.

DECADE is designed to produce x-rays from both bremsstrahlung and plasma radiation sources. The bremsstrahlung radiation will be produced in both a large-area and a high-dose configuration. In the large-area configuration, the average dose will be 20 kRad (in silicon), delivered over an area of 1 square meter. The maximum endpoint voltage for this case will be 1.5 MV, and the radiation pulse-width (FWHM) will be 40 ns. The high-dose configuration will deliver 80 kRad into 1500 cm^2. For this case, the end-point voltage is 1.8 MV; the radiation pulse width is also 40 ns. The dose will be reproducible, so that 9 of 10 shots are within 10% of the average.

The plasma radiation will be produced from aluminum wire arrays and argon gas puffs. For aluminum k-line x-rays (1.6 keV), the total yield will be 400 kJ. The argon k-line x-rays at 3.2 keV will have a total yield of 200 kJ. In both cases, the radiation pulse width will be less than 30 ns.

To produce the bremsstrahlung radiation, DECADE will deliver 2.5 MJ to the load in 40 ns, with a peak voltage of 1.8 MV, a diode current of 22 MA, and a diode power of 35 TW. This corresponds to performance on a single module of 160 kJ coupled into a bremsstrahlung diode. The plasma radiation will require a peak current into a short circuit of 25 MA.

DECADE will operate at a rate of 3 shots per day, 12 shots per week, and will be available for users 60% of the year. It will be command-fired to within ± 30 ns, with a delay time between 10 μs and 10 minutes.

The DECADE design is based on engineering data from a half-energy prototype module. The first of 16 full-energy modules has been built and is presently undergoing testing. The complete DECADE machine will be operational in March 1996. The design of DECADE is discussed and results from module tests are presented.

FAST RISE-TIME COAXIAL-TO-CONIC TRANSITION*

D.P. Snowden and S.Y. Tang
Mission Research Corporation, San Diego CA, USA
V.A.J. van Lint, Private Consultant, La Jolla CA, USA

As part of a program to upgrade the Defense Nuclear Agency's (DNA's) ARES electromagnetic pulse simulator at Kirtland AFB, New Mexico, USA, a new coaxial-to-conic transition was designed, built and tested. The purpose of this new transition is to support the faster-rising pulse provided by a new pulse forming network installed at the same time. It was required that the transition be capable of operating at peak voltages up to 3 MV.

It was necessary that the new transition mate with the existing 48-inch O.D. coaxial input (operating at an impedance of 110 Ω in oil) and with the existing expanding biplane at the output of the transition (also at 110 Ω). In addition it was a design requirement that the transition provide a constant impedance at the oil-gas interface in the system. Finally in order to limit the cost of the modification it was decided to design the new transition so that it could be mounted in the existing oil/gas box.

In order to envision the structure of the electrodes in the transition region, consider that the outer coaxial electrode is split longitudinally along its top surface and the electrode is unfolded gradually and symmetrically to form the lower electrode of the conic section. Simultaneously the inner coaxial electrode is expanded horizontally to become the upper electrode. In addition the lower electrode is bent to slope downward and the upper electrode is sloped upward. Proper adjustment of electrode dimensions over the unfolding/expanding region will yield a constant wave impedance.

The detailed shape of the transition section was scaled from the dimensions of a similar transition developed earlier for an electromagnetic pulser (STRTF) designed for and built at the Harry Diamond Laboratories in Adelphi, MD, USA. A one-fifth scale model of the present transition was constructed to allow measurement of the impedance and pulse rise time and to assess the changes required in the initial design to yield the best uniform impedance and rise time.

Constant impedance at the oil-gas interface is achieved by using a pseudo-graded dielectric over a distance downstream from the oil box, where the effective dielectric constant varies smoothly from 2.3 (the value for the oil) to 1 (the value for the gas). As the effective dielectric constant decreases, the width of the upper electrode increases so that the line impedance is constant. The grading of the effective dielectric constant is achieved by use of alternating layers of polyethylene and gas oriented normal to the propagation direction. The thicknesses of these layers is small compared to the wavelength of the highest frequency components of interest, allowing an average dielectric constant to be meaningful. The ratio of the

* Work performed for Pulse Sciences, Incorporated in support of Defense Nuclear Agency Contract DNA001-92-C-0196

thicknesses of the adjacent gas and polyethylene layers increases in the downstream direction gradually reducing the effective dielectric constant in that direction.

A one-tenth scale model of the interface region was fabricated to allow testing and refinement of the graded dielectric region. From the results of tests on this model an algorithm was developed which allowed design of the layer pairs utilizing commercially available thicknesses of polyethylene. Several graded regions were then constructed for testing in the one-fifth scale model.

The figure shows typical time dependent electric fields at three locations. These data were measured in the one-fifth scale model; similar results were obtained with the full-scale transition. The on-axis field (mid-plane, center) reproduces the input pulse with only small degradation in the rise time (the driving pulse for these measurements had a rise time of 0.067 ns). On the upper electrode the pulse rises and then decrease beyond the peak, while on the ground plane electrode, after the initial rise there is a delay followed by a continued rise. These measurements suggest the presence of a toroidal, pseudo TM_{01} mode which arrives slightly after the principal mode. This mode would be zero on axis, would be of opposite sign to the principal mode near the upper electrode and of the same sign as that mode near the ground plane. Measurements in the full-scale system also showed an antisymmetric horizontal component of the electric field off axis on the mid plane, also in agreement with this interpretation. This mode is evidently generated in the unfolding section. Another low voltage measurement in the full scale system confirmed this interpretation: A conductor placed midway between the upper and ground electrodes just beyond the unfolding section suppressed this mode.

Results of detailed pulsed field measurements in the full scale system will be presented as well as a discussion of means which could be used to reduce or eliminate the generation of this mode.

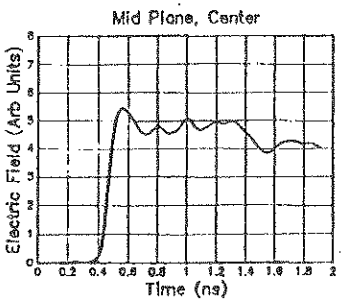

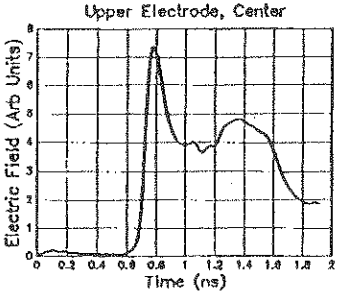

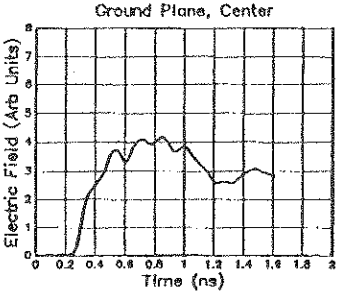

SANDIA NATIONAL LABORATORIES' HIGH POWER ELECTROMAGNETIC IMPULSE SOURCES

L. F. Rinehart*, M. T. Buttram, G. J. Denison, J. M. Lundstrom,
W. R. Crowe, J. F. Aurand, P. E. Patterson
Dept. 1248
Sandia National Laboratories
Albuquerque N.M. 87185 USA

ABSTRACT

Three impulse sources have been developed to cover a wide range of peak power, bandwidth and center frequency requirements. Each of the sources can operate in single shot, rep-rate, or burst modes. These devices are of rugged construction and are suitable for field use. This paper will describe the specifications and principals of operation for each source.

The sources to be described are: SNIPER (Sub-Nanosecond ImPulsE Radiator), a coaxial Blumlein pulser with an in-line (series) peaking switch; EMBL (EnantioMorphic BLumlein), a bipolar parallel plate Blumlein with a crowbar type (parallel) peaking switch; and the LCO (L-C Oscillator) a spark-switched L-C oscillator with damped sinusoidal output.

SNIPER and EMBL are ultra-wideband sources which produce a very fast high voltage transition. When differentiated by the antenna, an impulse whose width corresponds to the transition time is radiated. The LCO operates with a center frequency up to 800 MHz and up to 100 MHz bandwith. Because the LCO output is relatively narrow band RF, high gain antennas may be employed to produce very high radiated field strengths.

SNIPER

SNIPER is a 250 kV ultra-wideband source producing 1.25 GW peak power into a 50 ohm load. The oil-insulated Blumlein is switched by a hydrogen gas spark gap. Hydrogen exhibits very fast dielectric recovery, allowing full power operation at >1 kHz and reduced power operation up to 5 kHz. The line output is 3 ns FWHM. A purged oil dielectric peaking gap in the center conductor of the coaxial Blumlein output sharpens the leading edge of the pulse to about 200 ps. This switch operates at 10 to 15 MV/cm electric stress level to produce the fast risetime.

The Blumlein and modulator fit into a 45 cm diameter by 75 cm length cylindrical container.

EMBL

The enantiomorphic (mirror image) Blumlein, EMBL, operates at 750 kV to produce >11 GW peak power into 50 ohms. EMBL is a four line, single switch arrangement of two oppositly charged parallel plate Blumleins. The Blumleins are in a "Marxed" configuration in which they would share a (fifth) ground line between them. The two lines would erect in opposite polarities with respect to this line.

Since both the charging and output are bipolar, an actual ground line is unnecessary. Instead, the ground line is omitted and exists as a virtual ground plane. This plane is also a plane of symmetry, the two Blumleins being mirror images above and below it.

Because the device stores 54 Joules per shot, rep-rate is power supply limited to 700 Hz in 1 second bursts (40 kW ave. power during the burst). EMBL uses bipolar charging to improve efficiency by reducing the energy stored in stray capacitance around the modulator transformer and Blumlein. With bipolar charging energy is stored in stray capacitance at 1/2 the full charge voltage (1/4 the energy).

The EMBL Blumlein output pulse is 3.5 ns FWHM. The pulse is crowbarred at peak voltage by a gas spark gap so that it's trailing edge is sharpened to <200 ps. There is essentially no difference in spectral content between sharpening the leading or trailing edge of the pulse. The 3 dB bandwidth of the radiated pulse (about 200 ps FWHM) extends from 0.2 to 1.2 GHz, and is peaked at 800 MHz. The EMBL Blumlein, peaking switch, and modulator fit in a 40 cm square by 1.7 m long container.

LCO

The LCO transmitter comprises a small spark switched "pancake" L-C oscillator which directly drives a very "fat" 1/2 wave dipole. The dipole is situated at the focus of a parabolic cylinder sub-reflector, and the dipole and sub-reflector package is positioned at the focus of a larger (3.7 m diameter) parabolic dish. Overall gain for the system is 20 dB with a 12 degree (3dB) beamwidth. The modulator, L-C oscillator, dipole, and sub-reflector are enclosed in a plastic box filled with insulating gas (SF6).

A typical UHF LCO transmitter we have constructed runs at 700 MHz center frequency with 100 MHz bandwidth. The device can run for several minutes at >1 kHz rep-rate.

100 TW, 1 MJ X-RAY SOURCES

B. ETLICHER, H. LAMAIN, P. AUVRAY, L. FRESCALINE, C. ROUILLE, J.-M. BUZZI, A. CHUVATIN,

Laboratoire de Physique des Milieux Ionisés, Laboratoire du CNRS, Ecole Polytechnique, 91128 Palaiseau, France

J.-F. LEON, F. LASALLE, A. MOREL, J.C. LAVAL, M. LALANDE, M. VIE

Centre d'Etude de Gramat, 46500 Gramat, France

In this presentation, we analyze the possibility to generate very high power X-ray sources, in the MJ range, by fast compression of Z-pinch plasma. Recent progress in the load design, which can undertake present instability limitations, will be presented in detail from experiments done on generators with store energy in the range 0.01-1 MJ. Important progress are still needed to understand more carefully and optimize the dynamical process of the Z-pinch compression and also to built new type of ultra high power generator (100 TW) with higher efficiency, compact and cheaper design to undertake limitations of standard technologies.

Work partially supported by DRET under contract #92.134 and ETCA/CEG under contract #420/115/01.

STACKED BLUMLEIN PULSE GENERATORS: VERSATILE SOU OF HIGH POWER REPETITIVE WAVEFORMS

F. Davanloo,* D. L. Borovina and C. B. Collins
Center for Quantum Electronics, University of Texas at Dallas
P.O. Box 830688, Richardson, TX 75083-0688

F. J. Agee
Philips Laboratory
PL/WSR
Kirtland AFB, NM 87117-6008

L. E. Kingsley
Army Research Laboratory,EPSD
Ft. Monmouth, NJ 07703-5601

The stacked Blumlein pulse power sources developed at the University of Texas at Dallas consist of several triaxial Blumleins stacked in series at one end. The lines are charged in parallel and synchronously commuted with a single switching element at the other end. In this way, relatively low charging voltages are multiplied to give the desired discharge voltage across an arbitrary load without the need for complex Marx bank circuitry. In this report, the generation of high power thyratron switched waveforms with pulse durations in the range of 80-600 ns is demonstrated without degradation of the voltage gains. Opportunities for tactically packaging these pulsers are also investigated by studying dielectric lifetimes and Blumleim spacings on small scale prototypes and a significant reduction in size and weight is demonstrated. The promising capabilities of photoconductive switches for the use in these Blumlein pulsers are discussed.

To fulfill the demand for pulse power sources producing several hundred kV pulses at moderately high repetition rates, the UTD group first introduced and implemented a new approach in 1988 to combine the functions of pulse shaping and voltage multiplication using stacked Blumleins. This yielded a pulser which was capable of delivering high voltage pulses with fast risetimes at high repetition rate. The pulser consisted of eight triplate Blumleins which were charged in parallel at one end and switched by a single hydrogen thyratron. Output voltages up to 200 kV at 0.5 kA current were available from this device. Subsequently a second prototype stacked Blumlein generator was reported which produced voltages in excess of 0.5 MV. An x-ray diode matched to this pulse power source allowed the production of intense x-ray pulses containing useful fluxes of photons having energies around 400 keV. These x-ray systems have been used to excite the fluorescence from high-pressure rare gas plasmas. The deposition of hundreds of millirad of x-rays in nanosecond pulses into tens of atmosphere of argon gas resulted in a strong excitation of the VUV spectra that depended upon the generation of highly ionized precursors (F. DAVANLOO, R.K. KRAUSE, J.D. BHAWALKAR & C.B. COLLINS, Proceedings of the 8th International Pulsed Power Conference, 1991, pp.971-974).

The stacked Blumlein pulsers consisted of three separate but integrated subassemblies: (1) the switching assembly, (2) pulse-forming Blumleins, and (3) the pulse-stacking module. Each of the sections may be removed and can be modified and/or serviced independently. The purpose of the switching assembly is to distribute the switching current to each of the Blumleins in a manner to avoid both transit time inequalities and path constric-

tions. The thyratron housing and current returns were constructed in a way to reduce overall inductance of the switch circuit.

In this work, performances of 2-line stacked Blumlein pulse generator with Blumlein lengths of 9.2 m, 17 m, 32.6 m and 48.2 m and line impedance of 50 Ω were characterized. The full capacitance of the system was charged in 150 μs with a pulse-power supply. Commutation was effected by the four-gap EEV CX 2025X Deuterium thyratron at repetition rates of 1 - 100 Hz. Voltage and current pulses were measured with a tapped, water resistor voltage divider and a fast current monitor, respectively. Outputs of these pulse measuring devices were connected to a Tektronix 7912AD transient digitizer.

In the resistive loading condition of operation, the output from the pulsers were connected to nominally matched loads built from a stack of ten 10 Ω non-inductive carbon disc resistors. The output voltage waveforms were measured across the first carbon resistor in the load stack and then were multiplied by a factor of 10. The voltage waveforms for the resistive loading conditions of operation and Blumlein lengths of 9.2 m, 17 m, 32.6 m and 48.2 m are shown in Fig. 1. The voltage waveforms in this figure indicate voltage gains of about 1.9.

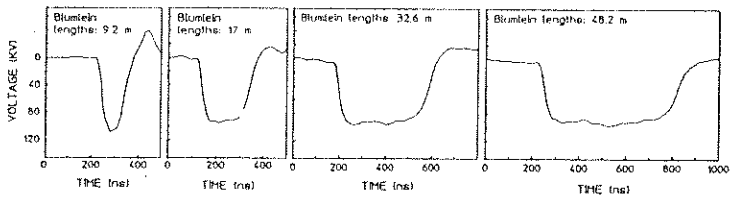

Figure 1. Resistive load voltage waveforms for the stacked 2-line devices with Blumlein line lengths of 9.2 m, 17 m, 32.6 m and 48.2 m and line impedances of 50 Ω. These particular waveforms correspond to a charging voltage of 50 kV.

A comparison of waveforms obtained from the pulser with Blumlein lengths of 9.2 m and 48.2 m, as seen in Fig. 1, indicates that the extension of Blumlein lengths resulted in generation of waveforms with pulse durations of about 500 ns longer without degradation in voltage gains.

In this work, it is also demonstrated that the stacked Blumlein pulser can be developed into light and compact devices without degradation in their performances. The feasibility of an intense pulsed power source based upon these novel stacked Blumlein pulsers commuted with photoconductive switches is detailed.

HIGH VOLTAGE PULSE SHARPENING USING NONLINEAR FERROELECTRIC CERAMIC DIELECTRICS

S. A. Fairlie* and C. E. Little

J. F. Allen Research Laboratories
Dept. of Physics and Astronomy
University of St. Andrews
North Haugh
St. Andrews
Fife
KY16 9SS
Scotland

Many ferroelectric ceramics commonly used as high voltage capacitor dielectrics exhibit a nonlinear capacitance voltage characteristic, is the relative dielectric constant falls with increasing applied electric field. This arises as a consequence of operating these materials close to their Curie temperatures in order to maximise their permittivities. A ferroelectric has a large peak in relative dielectric constant close to its Curie temperature, but in this region there is generally also a high sensitivity to applied electric field. Usually this nonlinearity is regarded as a problem by commercial capacitor manufacturers and much effort is expended to produce ceramic dielectric compositions with characteristics that are as independent of applied electric field and temperature as possible.

Recently however these strongly nonlinear ferroelectric ceramics have been applied to the sharpening of the leading edges of high voltage electric pulses to produce very fast voltage risetimes. When these materials are used as the dielectric in transmission lines, the electric field dependent nonlinear capacitance causes different parts of an incident pulse to propagate with different phase velocities. If the nonlinearity is sufficiently marked then the phase velocity at a point on an incident pulse will depend on the voltage at that point so that the high voltage parts of the wave front travel faster and 'catch-up' with the more slowly propagating base of the pulse. In this way pulses with very sharp shock-front leading edges can be generated.

Experiments are described demonstrating pulse sharpening action in transmission lines containing these nonlinear ferroelectric ceramic dielectrics using nanosecond pulses with peak voltages of up to 40 kV. The source impedance of the system varies in the range 5 Ω to 50 Ω implying peak currents of up to a few kA. The pulse sharpening performance of these lines is analysed and discussed and the factors that limit the minimum risetimes that can be achieved are identified. The characteristics required by an "ideal" dielectric material in this application are also derived.

HEB/Collider Freewheel Diode Abort Kicker Power Supplies

K. R. Rust and C. A. Wilson
Accelerator Division
Superconducting Super Collider Laboratory
2550 Beckleymeade
Dallas, Texas 75237
(214) 708-3335

ABSTRACT

The Superconducting Super Collider rings (CW, CCW) will accelerate protons from an injection energy of 2 TeV to an experimental energy of 20 TeV. The Collider abort kicker magnet power supplies will be required to abort the beams in the instances of a filling sequence malfunction or a superconducting magnet getting warm requiring a quench protect circuit to fire. The current to be delivered to the abort magnets range from 1.3 kA to 13 kA which corresponds to the energy levels that will be aborted. During the acceleration time, the power supply will be required to track the beam energy level which will be increasing for 1000 seconds. The abort gap is 4 μs wide. The maximum filling time of the magnet, to full field, is 3.5 μs for a synchronous abort. The abort power supply current is also required to droop to 80% of the required kick strength. This droop will be used to deflect the beam on one axis while a painter magnet deflects the beam on the other axis for 18 cycles. This painting action is necessary to protect the beam stop from damage due to the high energy that will be delivered by the beam. A freewheel diode circuit is one way to accomplish the goal of the HEB and the Collider abort kicker power supplies. Diode turn-on characteristics and forward-voltage drop of several high-voltage diodes will be discussed along with the design of a freewheel diode prototype circuit for the Collider and HEB abort power supplies.

TERAWATT ELECTRONICS

V. Serlin* and M. Friedman
Plasma Physics Division
Naval Research Laboratory
Washington, DC, USA

Using novel techniques, electromagnetic energy can be stored, compressed, and then released with peak power levels in the terawatt range. This energy can be used to either efficiently generate terawatt RF pulses with frequencies up to 10 GHz, or accelerate a high current (≈ 1kA) particle beam to a GeV energy. Because of the very high peak power and very short (sub-nanosecond) individual pulses, there are potentially revolutionary applications to electronics warfare.

The physics and technology of modulated intense relativistic electron beams (IREBs) was developed at the Naval Research Laboratory (NRL). We were able to generate modulated IREBs in the frequency range of 50MHz-3.5GHz, and extract the beam energy in the form of RF radiation. About 15 GW of RF power was extracted into the atmosphere at 1.3 GHz and 1.7 GW at 3.5 GHz. We have also used this RF to power directly a compact high-gradient electron accelerator, achieving a 60 Mev electron beam with a current of 200 Amperes and an average electric field of 60 MV/m. Scaling laws, however, indicate that with the present geometry, we are approaching the limits of RF power output at these frequencies.

Consequently, we are currently building a new Relativistic Klystron Amplifier (RKA) operating in a 'triaxial' geometry, in which a large diameter (66cm) annular IREB is propagated between two coaxial grounded conductors. In this geometry the input electron beam current is significantly higher than previously. The beam impedance can be as low as 1 ohm, however, initially we will use a beam current of ~100 kA at 500 kV. The output power is constant throughout the operating frequency range of 50MHz-10GHz.

This device will be able to produce an RF energy pulse in the tens of Gigawatts for about 140 nanoseconds. Rather than extracting this RF power into the atmosphere, it can be stored temporarily in an RF structure and subsequently quickly dumped into a load, increasing the power by time compression. The energy transfer from the modulated IREB to the storage structure can be achieved with an efficiency exceeding 50%, according to our calculations. The energy storage

capability of this structure per pulse, can be approximately estimated with the simple formula $U=PQ/\omega$, where P is the power input, Q is the quality factor of the structure, and $\omega/2\pi$ is the frequency of the RF. Since P ~ 10GW, Q ~ 1000-25000, and $\omega/2\pi$ ~ 1 GHz, the stored energy U ~ 1-10 kJ per pulse. Of course, this energy can only be stored for a short duration and has to be quickly dumped into a load. An attractive storage system is a backward travelling wave structure with a relatively low group velocity, V_g. This structure will have a high efficiency if its length L is such that L/V_g ~ pulse duration of the IREB. During the loading of the RF energy into the structure, the system is "clean" - no electrons are present. Therefore, the electric field that can be sustained is many times the empirical Kilpatrick limit (35 MV/m at 1.3 GHz).

Once the structure is fully loaded with RF energy, a single pulse or a train of pulses of particles will traverse it and drain the stored energy. A simple model based on TEM transmission line theory shows that the efficiency of the RF energy transfer should exceed 50%. Since this phase of the process occurs after the original modulated IREB pulse has ended, the load is automatically decoupled from the source. In conventional accelerators this decoupling is usually achieved with high power isolators.

The useful output from this device can take several forms:

- a train of terawatt electron bunches that can be used to generate a terawatt narrowband RF pulse.
- a single terawatt electron bunch that can be used to generate a terawatt wideband RF pulse.
- various electron and ion beams with kA currents, TW peak powers, and GeV energies.

* This work is supported by BMDO/Army Research Laboratory and the Naval Research Laboratory

DEVELOPMENT AND CHARACTERIZATION OF NEW PEAKING CAPACITOR ARMS FOR MEMPS

A. W. Kälin* and B. R. Brändli,
Defence Technology and Procurement Agency,
NEMP-Laboratory, AC-Zentrum, CH-3700 Spiez, Switzerland

D. V. Giri, Pro-Tech, 3708 Mt. Diablo Boulevard, Suite 215, Lafayette, CA 94549 USA

1. Introduction

The objective of this paper is to perform an electrical characterization of the existing peaking capacitor arms in the Swiss MEMPS (*M*obile *EMP S*imulator) facility and eventually to develop improved peaking capacitors. The improvement we seek is in the frequency performance of these capacitors, while preserving other performance criteria such as high voltage and capacitance value. The improved design is the dihedral capacitor and has been described in ("High-Frequency Capacitors" by D.V.Giri and C.E.Baum, Energy Storage and Dissipation Note 10, March 15, 1990). In the following sections, we describe the experimental techniques in evaluating the frequency performance of these capacitors and the results for the existing capacitors. The results of the dihedral capacitor performance are expected to be available in due course and will be included in the presentation of this paper.

2. Problems with Capacitors in Use

An elemental capacitor in a typical peaking capacitor arm consists of two metallic foils separated by multiple layers of dielectric strips. It has been observed from measurements that open-circuit resonances exist in the capacitor which limits the useful frequency range of operation. The series resonances, where the capacitor becomes a short circuit do not present any problem, but the open circuit resonances (typically occurring at 10's of MHz) limit their use. The losses also increase as more and more elemental capacitors are series connected. The above reference has also modelled the present peaking capacitance design with transmission lines leading to an estimation of these inherent resonances. The new design overcomes the frequency limitation by using physically smaller elemental capacitors and connecting them in parallel to form an unit dihedral capacitor. Unit dihedral capacitors are then series connected to fabricate a peaking capacitor arm. The present design and the new dihedral designs are schematically shown in figures 1 and 2 below.

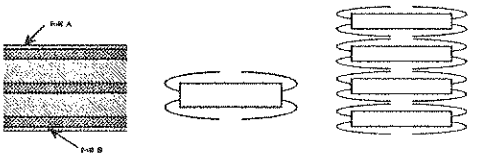

a) one element b) wound capacitor c) stack

Figure 1. Existing peaking capacitor in MEMPS

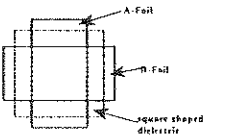

Figure 2. Dihedral or $D_{2,d}$ Capacitors

3. Experimental Procedure and Results

The frequency response of the peaking capacitors used in MEMPS are evaluated using the experimental setup shown in figure 3. It consists of a rectangular coaxial transmission line, whose inner conductor can be a rectangular metallic pipe (approximately a 50 Ohm line) or a single peaking capacitor arm.

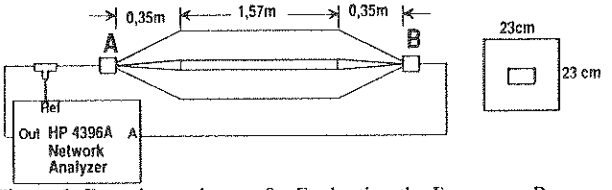

Figure 3. Experimental setup for Evaluating the Frequency Response of the Peaking Capacitors

A TDR measurement was initially performed on the peaker line in the above figure to ensure that the transitions at the two ends are reasonably close to 50 Ohms and that there are no other significant discontinuities along the line. The above figure is self explanatory and the results of connecting a 2m coaxial cable in place of the peaker line, peaker line with inner conducting tube and the peaker line with a MEMPS peaker arm are displayed in figures 4a, 4b and 4c respectively.

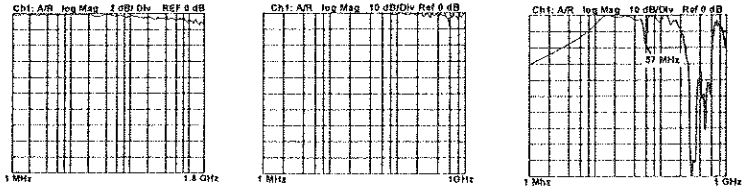

a) 2m long coaxial cable b) Perfectly conducting inner tube c) MEMPS peaker arm

Figure 4. Experimental Results

It is evident that the MEMPS peaker arm has an open circuit resonance at about 57 MHz, which is inadequate to propagate the higher frequencies in a pulse with risetime of 5 ns. It is recalled that the peaker arms form the biconical surface in the MEMPS pulser configuration. It can be shown that the product of the risetime (10 to 90%) and the 3dB cutoff frequency of a pulse is (1/2.875). So a 5 ns pulse has a 3dB frequency cutoff at 70 MHz and the peaker is required to operate well upto 100 MHz or so. The new design of the dihedral peaking capacitors is being fabricated and is expected to have its first open circuit resonance in 100's of MHz. These results will be included in our presentation.

Any replacement of the existing peaking capacitor arms in MEMPS must meet the performance requirements in terms of a) higher frequencies, b) high voltage requirement , c) proper capacitance value in the available volume of space. Once the new dihedral capacitors are validated for their high-frequency performance, the other criteria such as the capacitance value in the given volume and high-voltage considerations are relatively easier to meet.

"LIGHTWEIGHT, TACTICAL PRIME POWER FOR MOBILE PULSED POWER APPLICATIONS"

T. R. Childers*, H. S. Coombe, and J. H. Ferrick

Integrated Power Sources Team
Belvoir Research, Development and Engineering Center (BRDEC)
Ft. Belvoir, VA. 22060-5606.

Since the early 1970s, BRDEC has been actively involved in the development of prime power concepts, components and systems for various tactical pulsed power applications. Through these efforts, various approaches have arisen which facilitate the development of lightweight, mobile, diesel fueled tactical prime power sources (both short duty and continuous duty). This paper will discuss these approaches and options as well as recent specific developments which illustrate the application of various compact prime power design techniques.

Traditionally, one of the biggest roadblocks in the development of fieldable, mobile pulsed power systems has been the size and weight of the prime power equipment. Continuing technology advances and system integration concepts have allowed us to realize the goal of lightweight prime power systems suitable for tactical applications.

Prime power source components for pulsed systems convert available energy (usually diesel fuel) into electric power which can be used to feed the energy storage and pulse conditioning components. US Army policy directs the use of common, kerosene based fuels on the battlefield. Prime power components typically include the following: 1. an engine to convert fuel (chemical energy) into rotating mechanical power, 2. an alternator to produce electrical power, and 3. a power converter to produce the d.c. power required by the first stage of the load. A Transformer-Rectifier (T-R) unit is often used to convert low to medium voltage a.c. from the alternator into the d.c. voltage required by the power conditioning. Traditionally, most pulsed loads have required High Voltage DC (HVDC) from 10 to 100s of kV. However, BRDEC is currently involved in a prime power effort for a high power solid state radar which ultimately requires Low Voltage DC (LVDC) of about 10 V.

Turbines are at present the best option for developing very high power density prime power systems, and continuing advances in engine materials and designs promise to increase their power density and fuel efficiency in the coming years. Turbines in the 1 - 3 MW power range typically weigh about 180 - 550 kg (roughly 7.7 kW/kg). Pulsed applications which require lower average powers or which have less stringent size/weight requirements can utilize reciprocating diesel engines. Diesel engines in the same power range weigh about 2,000 to 5,500 kg (roughly 0.9 kW/kg). Diesel-fueled rotary engine technology appears promising for providing additional design flexibility between turbine and reciprocating engines, however, large diesel-fueled rotaries require further development and are not currently in production.

Advances in materials and designs have allowed development of reliable, High Speed, High Frequency (HSHF) alternators. HSHF alternators have much higher power densities than traditional low speed alternator designs. These advanced HSHF alternators can be designed so that they are directly coupled to turbines, eliminating the weight and cost of a gearbox. BRDEC has developed a prototype HSHF alternator (rated 3 MW and 700-1,000 Hz) which can be direct driven by the US Army T-55 turbine. This oil cooled alternator weighs 390 kg and operates at 10,500 to 15,000 r/min with a power density of 7.7 kW/kg. In comparison, a 3 MW commercial, off-the-shelf 1,800 r/min, 60 Hz alternator would weigh about 6,800 kg with a power density of 0.44 kW/kg.

For the T-R unit, continuing advances in power semiconductor technology have significantly reduced the size and weight of the rectifier portion of the system. High voltage, high average current diode devices now available allow for the design of very compact T-R units. The high frequency from the HSHF alternator leads to significant reduction in transformer core weight, one of the heavier components in high power T-R units. BRDEC has developed an oil cooled 3 MW rated T-R unit for pulsed applications with a weight of 340 kg and a power density of 8.8 kW/kg.

In the late 1980s, BRDEC undertook work on a 1 MW average power pulsed power source development concept. This required the development of very lightweight prime power source components suitable for integration into an compact carrier. This was a short duty prime power system designed to recharge a pulsed capacitor. The components include a diesel-fueled turbine directly driving a HSHF alternator at 30,000 r/min. Alternator power is transformed and rectified to HVDC. The HVDC then charges a pulsed capacitor which feeds a Pulse Forming Network (PFN). The reactance of the alternator and T-R unit were designed so that the currents during the early part of the capacitor charging cycle were kept within manageable levels. This effort provides a good illustration of the importance of system level integration between the prime power and pulser sub-systems.

The majority of DoD loads require 60 Hz and BRDEC is exploring concepts which couple compact HSHF alternators with Power Frequency Converter (PFC) circuits to provide 60 Hz. Continuing advances in solid state power switch technology have given rise to concepts using compact, solid state d.c. link circuits with Pulse Width Modulated (PWM) output. The circuit would convert the high frequency from the HSHF alternator to 60 Hz. Integrated Gate Bi-polar Transistor (IGBT) and Gate Turn-Off (GTO) power switches have both been explored for this converter. The HSHF alternator and d.c. link combination may offer significant size/weight reductions over commercial off-the-shelf 60 Hz alternators. Future power switch advances such as higher power MOS-Controlled Thyristors (MCTs) may allow for greater weight reductions. The HSHF-PFC combination may offer significant size/weight savings over traditional 1,800 r/min, 60 Hz alternators. These size/weight savings could be applied to prime power equipment ranging from 10s of kW to multi-megawatts.

In summary BRDEC has and is continuing to develop concepts and hardware for compact, tactical prime power systems which will aid in the development and field deployment of a wide range of mobile pulsed power systems.

MEASURED EQUATION OF INVARIANCE AND ITS APPLICATIONS IN FREQUENCY AND TIME DOMAINS

Kenneth K. Mei* and Yaowu Liu

Department of Electrical Engineering and Computer Sciences
University of California
Berkeley, CA 94720

The measured equation of invariance (MEI) is a technique to terminate the finite difference/element equations at mesh boundaries without invoking an absorbing boundary condition or a global integration. The terminating equations at the mesh boundaries using MEI are strictly local and are robust even the mesh is terminated very close to the object boundary. So MEI method can drastically reduce the computation time and memory when used with the finite element/difference method. Furthermore, it can make the task of mesh generation much easier. The concept of MEI is based on the postulate that the local linear relation between neighboring nodal fields are invariant to excitations. Based on this postulate as a first principle, the linear equations at the mesh boundaries are found without finite differencing the differential equation, which fails at the mesh boundary. MEI is a new concept in field computation, in that it breaks away from the traditional approach of deriving discrete nodal equations from differential equations, rather it derives the discrete equations from a set of solutions, which are associated to the object solution by geometry. MEI has been successfully applied to scattering, antennas and microstrip structures in frequency domain (Mei et al, IEEE Trans. Antennas and Prop. to be published Mar.'94).

In this paper, the frequency domain MEI will be reviewed and results on wave scattering using MEI will be shown for metal and dielectric scatterers. It will also be shown that MEI is applicable to very large targets whose dimension reach thousands of wavelength in 2D.

In this paper it is shown that the same postulates used in the frequency domain are applicable to time domain as well, i.e., we can terminate the FDTD mesh very close to the object boundary by linear equations retrieved from known solutions, via measuring functions and metrons. It is shown that using time domain MEI on a rectangular metal scatterer the FDTD mesh can be terminated at only two space segments away from the object boundary, where all conventional absorbing boundary conditions fail. Numerical test results are shown to verify the postulates that the local linear space-time equations are invariant to incident fields. Therefore, one set of equation at the mesh boundary can be used for all incident fields.

Comparisons of time domain MEI (TDMEI) and conventional absorbing boundary conditions (ABC) are made at mesh boundaries far enough from the object boundary. It is shown that TDMEI and ABC provide different coefficients for the boundary space-time equations. TDMEI equations are functions of locations and ABC are not. TDMEI equations are functions of the scatterer geometries and ABC are not. These differences are consistent with the original postulates put forth by Mei.

The time domain MEI is not only a contribution to make the FDTD method faster and leaner, but is also a potentially new venue to treat boundary configurations difficult for conventional approaches, such as mesh terminations crossing material interfaces or crossing obliquely with a transmission line.

APPLICATION AND VALIDATION OF THE TIME DOMAIN THREE DIMENSIONAL FINITE DIFFERENCE METHOD TO A WIDE VARIETY OF ELECTROMAGNETIC COUPLING PROBLEMS

BY

R. A. PERALA*, T. H. RUDOLPH, P. M. McKENNA
Electro Magnetic Applications, Inc.
P. O. Box 260263
Denver, Colorado 80226-0263
USA

The objective of this paper is to present several examples of the Three Dimensional Time Domain Finite Difference method (TDFD) applied to several electromagnetic coupling problems. These include lightning, nuclear EMP, and magnetic field shielding effectiveness. Systems include aircraft, partially buried facilities, and communication shelters. Emphasis is placed on comparison of numerical results to experimental results in order to validate the method.

The interaction of EM fields with systems is generally a complex process. This is because systems are generally complex three dimensional structures made out of a wide variety of materials such as metals, composites, dielectrics, and other lossy materials. Geometrical shapes are complex, requiring that analysis approaches can't rely upon simple canonical models, such as spheres or cylinders.

In order to evaluate E^3 effects on systems, one has the option of using testing or analysis, or a combination of both. Testing is an expensive process, especially for large systems such as aircraft or facilities, and in the future, testing costs are expected to increase. Analysis, on the other hand, will become more cost effective in the future. This is occurring for two primary reasons. First, the capability of analysis methods is constantly being improved. It is now quite possible to perform detailed 3D calculations of EM interaction with complex systems. Second, computing power is rapidly increasing, and computing costs are decreasing. The net result is that as time goes on, analysis becomes an increasingly valuable tool in the electromagnetic community.

The objective of this paper is to illustrate the application of the TDFD approach to a wide variety of situations. First, the method and its capabilities are described. Then, numerical and experimental results are compared for the following situations:

- NASA F-106B In-Flight Natural Lightning External Response
- USAF/FAA CV-580 In-Flight Natural Lightning External Response
- NASA F-106B In-Flight Natural Lightning Internal Cable Response
- NASA F-106B Self-Consistent Nonlinear Triggered Lightning Response
- Saab JAS39 Lightning Response of Carbon Fiber Wing Box
- Saab JAS39 Lighting Validation Test
- NEMP Interior Response of an S-280 Tactical Shelter
- MIL-STD-285 Magnetic Field Shielding Effectiveness of an S-280 Tactical Shelter
- Lighting Response of a Semi-Buried Munitions Storage Igloo

Examples are given in Figures 1 and 2. Figure 1 shows the responses of a thunderstorm research aircraft, and Figure 2 shows comparisons for Nuclear EMP interactions with a tactical shelter. These results, and others to be given in the presentation, indicate good accuracy and illustrate the method's usefulness for EM validation of systems.

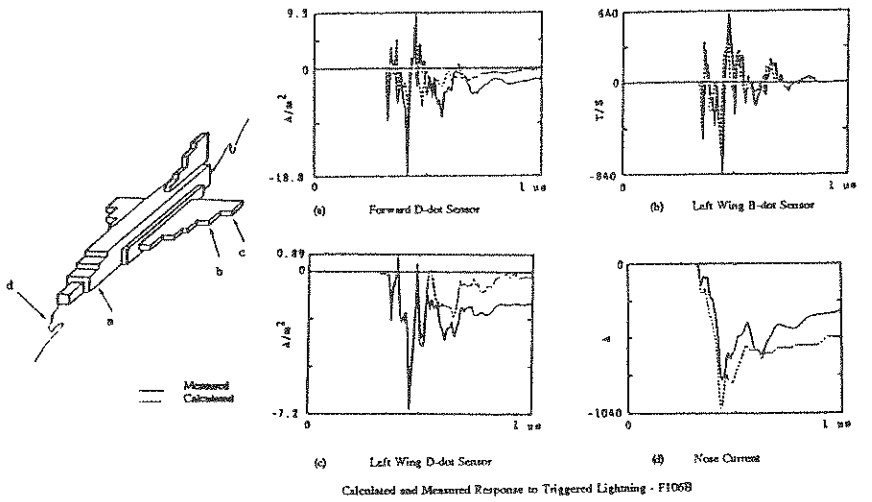

Figure 1 Comparison of NASA F106B In-Flight Natural Lightning External Response

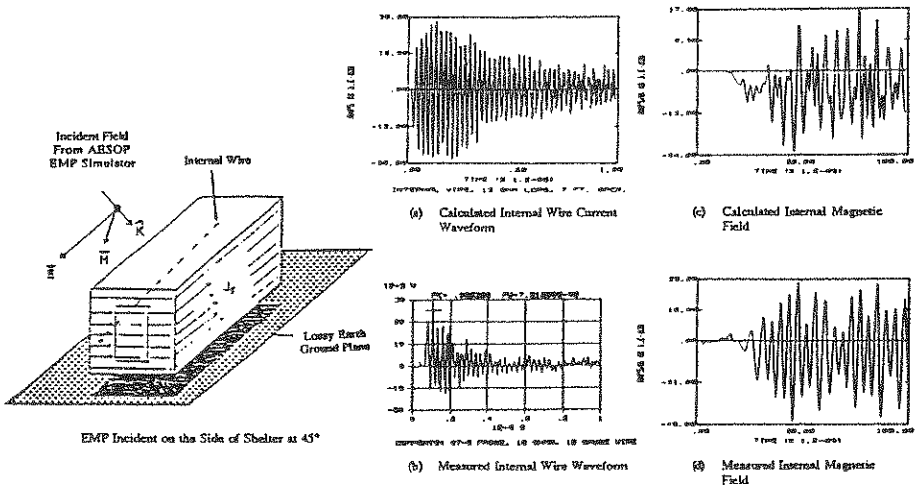

Figure 2 Comparison for Nuclear EMP Excitation of a Tactical Shelter

FINITE-DIFFERENCE, TIME-DOMAIN SOLUTIONS TO THE MAXWELL EQUATIONS USING NON-ORTHOGONAL, BOUNDARY CONFORMING GRIDS

Ronald J. Chase
U.S. Army Research Laboratory

Recent years have seen a resurgence in applications of finite-difference time-domain (FDTD) techniques to solutions of electromagnetic (EM) coupling/scattering problems. The majority of these applications have employed the well known numerical algorithm originally published by K.S. Yee. In this traditional approach, the physical space is modeled by a staggered set of rectangular cells in the computational space, the field equations are approximated by algebraic equations on the cells, and the fields are computed by advancing discrete increments in time. The simplicity of this technique and the capability of modeling materials with inhomogeneities, anisotropy, and nonlinearities undoubtably accounts for the widespread popularity of this approach.

One disadvantage of using a rectangular mesh in the computational volume is the inaccurate representation of curved boundaries of objects. This results in a "staircase" boundary approximation, that in some applications introduces unacceptable error. A boundary conforming mesh would remove this impediment, and also offer the possibility of reducing the number of cells needed to adequately model the object. Since the early 1980's several researchers have directed their attention to developing practical, efficient boundary conforming meshes.

The work investigated here applies developments in numerical grid generation to applications of the Yee algorithm in two dimensions. The types of grids investigated had "nearly orthogonal" square curvilinear grid structure, in which a coordinate line (surface in 3D) is coincident with each segment of the boundary of the physical region. In some instances, this type of irregular grid may be implemented around the scatterer, and transitioned into rectangular cells away from the object. The Maxwell equations are transformed numerically according to standard rules of differential calculus, and solved in the gridded system. Emphasis has been placed on determining the factors that affect the convergence rate, and efficiency of the solutions.

NUMERICAL ELECTROMAGNETIC ANALYSIS OF EMP SIMULATORS: A COMPARATIVE STUDY

S. Kashyap and A. Louie
Defence Research Establishment Ottawa
Ottawa, Ontario, Canada

ABSTRACT

This paper deals with the analysis of three types of wire EMP simulators. The behaviour of electromagnetic fields at various locations as a function of simulator shape is studied. A modified version of the Numerical Electromagnetic Code (NEC) is used for the computations.

INTRODUCTION

Parallel-plate wire structures with tapered input and output ends have been extensively used for testing EMP susceptibility of large systems. Lately there has been some interest in conical-shaped simulators (J. J. A. Klaasen, IEEE Trans. on EMC, vol 35-3, 329-338, 1993). Most of the fields in such simulators are concentrated between the upper and the lower sets of wires. The uniformity and rise time of the fields are affected by geometric parameters, such as angle and length of the tapers and the length of the mid-section. Detailed knowledge of the behaviour of the fields is essential in designing simulators for making reliable EMP susceptibility measurements.

PROCEDURE

Figure 1 shows the shapes of three simulators considered. They all have the same length (90m), same width (20m) and the same height (10m). In all three cases the electromagnetic quantities of interest are computed for a six-wire model. The first model has an input taper, an output taper, and a horizontal section all of the same length (30m). The second model has equal input and output tapers (45m), but no middle section. The third model has an input taper of 60m and an output taper of 30m. The symbols Ξ, Δ, and Γ are used to identify the simulators respectively. Excitation is provided as a voltage source on the first segment of each of the 6 wires

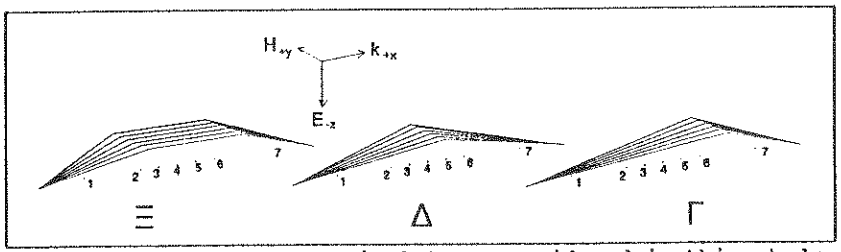

Figure 1. The three EMP simulators considered in this study.

of the input taper. The termination is a 100Ω load in each case. All three simulators have a perfectly conducting ground plane.

A modified version of the Numerical Electromagnetic Code (NEC) (G. J. Burke and A. J. Poggio, Naval Ocean Systems Command, Technical Document 116, 1977) is used for the computations. The wires are divided into segments of 0.25 m or less, and have a 1 cm diameter. These wire parameters satisfy the NEC simulation criteria for reasonable accuracy for frequencies up to 256 MHz. The analysis makes use of the symmetry and the number of segments is reduced to one-quarter of the total number. The computations are performed from 4 to 256 MHz with a 4 MHz step. The resulting current densities are used to compute the electric field at various locations within the volume of the simulators. This constitutes the frequency-domain response. An inverse Fourier transform of the product of the frequency-domain response and the spectrum of the EMP gives the time-domain response. Figure 2 shows some of the results: the electric field intensity at a point in the middle of the horizontal section of the first simulator and under the apex for the other two simulators. The contributions from different sections which make up the total field are identified. The amplitude and the rise time of the field at this and other locations in the volume of the simulator are affected by the angle and length of the tapers and the length of the mid-section. This effect will be discussed in detail. Leakage of EM fields around the simulators will also be discussed.

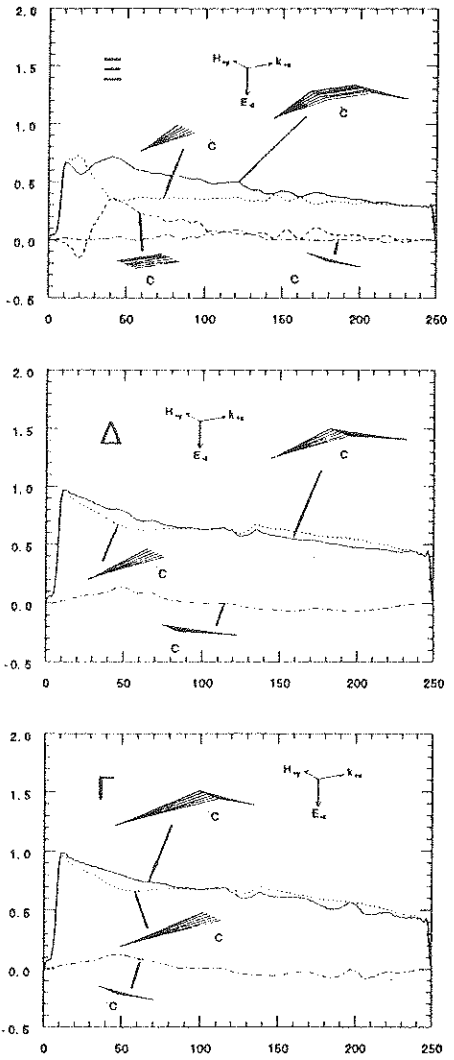

Figure 2. Total E_z-field and the contributions from various sections of the simulators. Abscissa = time in ns; ordinate = normalized E_z-field.

FINITE ELEMENT METHOD FOR NUMERICAL STUDY OF ELECTROMAGNETIC RESONANCES IN AIRCRAFTS INCLUDING ELECTRICAL WIRES

S. AMRAM*, P. BONAMOUR
AEROSPATIALE 12, rue PASTEUR 92152 SURESNES, FRANCE

The study of the direct and non direct effects of lightning or HIRF (High Intensity Radiated Fields) on complex structures such as a helicopter or an airplane is generally achieved through difficult and costly tests. Moreover, these tests are often far away from the real flight conditions. Thus, a theoretical modelling of the coupling of an electromagnetic wave with an aircraft may decrease the amount of testing and lead to more accurate results. A numerical method (AS-ELFI) [C.Brochard et S.Dahirel, *Manuel d'utilisation d'ELFI3S*, internal note Aerospatiale DS, 1993] based on a variational formulation, discretized by finite elements, has been developped within AEROSPATIALE. The proposed approach allows for the study of the electromagnetic frequency response of 3D structures made of homogeneous, isotropic dielectric media and perfectly conducting surfaces. The present paper deals with a model including electrical wires [A.Mazari, *Thèse de doctorat de Paris VI*, 1991], using the 'thin wire approximation' [R.Degauque, J.Hamelin, *Compatibilité electromagnétique* , Dunod 1990]. This formulation on wires permits to model cables with a lineic impedance, or wire antennas excited by a generator.

The present implementation of the formalism, illustrated here by two examples, has several advantages :

- -The 3D structures are defined by an unstructured mesh of surface triangular finite elements, which gives a very accurate model of the geometry.
- -The mesh is in perfect adequation to local field variations
- -The cabling routes are also defined accurately by beam elements. The method permits to model numerous wires of various diameters and electromagnetic characteristics.

First the method has been validated [S.Amram, *Implantation des fils dans ELFI3S*, internal note, 1993] by studying the input impedance of a center-fed wire antenna. The results of calculations performed with this canonical example have been compared to results taken from Schelkunoff [*Antennas*, J.Wiley and Sons, London 1952] showing a very good agreement.

The usefulness of the method is illustrated on a complex structure, a helicopter including two wires. The helicopter structure is supposed to be infinitely thin and made of a perfectly conductive metal as well as the wires. Of the two wires, one is connected to the aircraft surface and the other floating inside. The aircraft is illuminated by a linearly polarized plane wave in the 5 to 135 MHz range. The incident wave vector is in the xOy plane and makes a 45° angle with both x and y axes. The polarization is horizontal (the E vector is in the plane xOy). The main interest of the structure described above is that it allows the study of various resonance phenomena arising from both the helicopter (cavity resonances) and the wires.
The type of surface mesh involved in our 3D model is made of triangles (figure 1). A commonly used condition for this mesh is that the size of the triangles ought to be of the order of $\lambda/5$. We have used a mesh whose triangle size is 0.3m , which corresponds to a maximum frequency of 200 MHz. For the wires the mesh criterium is $\lambda/10$.

The simpler problem of the helicopter alone (e.g. without wires) can be described more generally as that of a resonant cavity, since the overall dimensions of a helicopter are of the same order of magnitude as the wavelength in the considered range. Figure 2 presents a plot of the electric field magnitude, for a given point inside the helicopter, as a function of frequency. A striking feature of this plot is that there is no resonance frequency below 68 MHz. This can be physically understood if we think of the helicopter as a rectangular waveguide with a propagation axis along its longitudinal axis. The typical heigth and width of the helicopter define indeed a cut-off frequency of approximately 68 MHz. Above the cut-off frequency, numerous modes of cavity resonance are found.

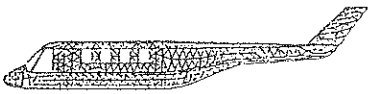

Fig.1 : mesh of a helicopter

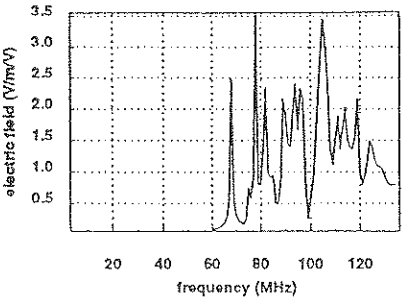

Fig.2 : Electrical field at a given point inside the helicopter; horizontal polarization
resonances (MHz) : 82, 89, 94, 96, 105, 111, 114, 119, 124

Now, we just illuminate the 'floating' wire (length l=7.92m) and we observe the current on the element of the wire identical to the observation point in the previous study (figure 3).

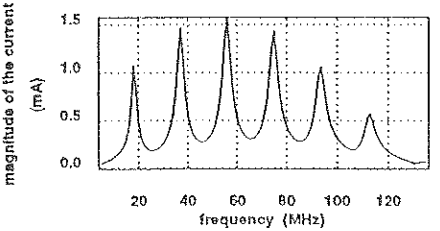

Fig.3 : Electrical current on the 'floating'wire
horizontal polarization; resonances (MHz) : 18, 37, 56, 75, 94, 113

As one would expect , the resonances obtained correspond to incident wavelengths satisfying the relation $l=n\lambda/2$, n integer ranging from 1 to 6. Finally the full structure with the two wires is considered. The figure 4 and 5 illustrate the electromagnetic coupling of both types of structures. The current in the same element as before is represented in figure 4. Below 75 MHz we find again the resonances of the wire whose length is 7.92m. Above this cut-off frequency a mixture of wire and cavity resonances appears. But the wire resonances seem to be more intense than the others. We observe exactly the same phenomena on the second wire whose length is 9.16m (figure 5).

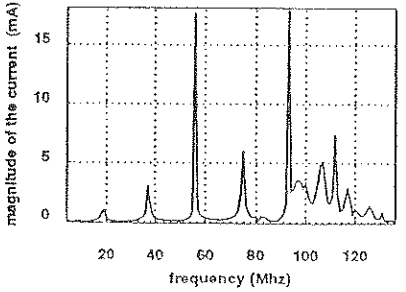

Fig.4 : Electrical current on the 'floating'wire
horizontal polarization
resonances (MHz) : 18, 37, 56, 75, 82, 94
97, 107, 112, 117, 121, 126, 131

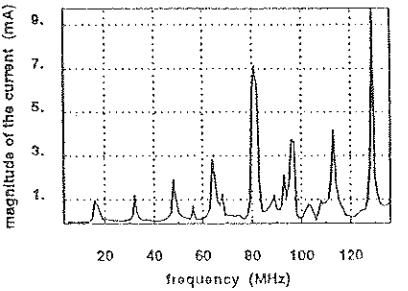

Fig.5 : Electrical current on the 'connected' wire
horizontal polarization
resonances (Mhz) : 16, 32, 48, 64, 82,
88, 93, 96, 102, 113, 129

EM Response of a Missile

S. Kashyap, J. Seregelyi and A. Louie
Defence Research Establishment Ottawa
Ottawa, Ontario, Canada
K1A 0Z4

ABSTRACT

This paper deals with the analysis and measurement of the interaction of electromagnetic waves with a missile aboard a ship. Results of computations and measurements of surface current density and electric field intensity are presented at various locations on and around the missile. The agreement between the computed and measured results is very good.

INTRODUCTION

The electromagnetic compatibility of various weapon systems aboard a ship is of serious concern. The performance of these weapon systems must be ensured by hardening against the electromagnetic environment caused by a source such as an EMP or a shipboard antenna.

The prediction of electromagnetic fields present around the weapon system and of the surface currents induced on the surface of the weapon system is important in assessing the EM compatibility and in designing protective measures.

PROCEDURE

Figure 1a shows a model of a missile. A vertically polarized plane electromagnetic wave is assumed to be incident on the missile. The surface current density and the electric field intensity at various locations on and around the missile are computed. The analysis is based on a moment method solution of the electric field integral equation (EFIE) (S. M. Rao et al, IEEE Antennas and Prop., vol AP-30, 409-418, 1982). It is a simple and efficient numerical procedure for the study of electromagnetic scattering by arbitrarily shaped bodies. The surface of the object is modelled geometrically as a finite union of planar triangular patches ("faces"). For each frequency and with a chosen orientation of an incident plane wave, a numerical solution is computed. The electromagnetic scattering properties of the body are then described uniquely by the collection of surface current densities ("basis functions") across the common edges of face pairs. This collection of currents is stored in a file, and may then be used to compute any other electromagnetic scattering property associated with the object, such as current density at any surface location and orientation, electric field at any point, or radar cross section at any view angle.

Fields on and around the missile and the surface current densities at various locations are calculated at 1 MHz interval, from 1 to 256 MHz. This constitutes the frequency-domain response. It provides information on the structure resonances, the distribution of surface current density and electric field intensity at different frequencies. The time-domain response is obtained by multiplying the frequency-domain response with the spectrum of the incident pulse such as the EMP, and taking an inverse Fourier transform.

A full-scale model of the missile was constructed. The model was exposed to EMP in the DREMPS facility (J.Seregelyi et al, Proc. IEEE EMC Symp., 465-466, 1993). The electric fields on and around the missile and the surface current densities were measured at various locations. The measurement results were compared with the computations. Figure 1b shows one of the comparisons. It shows the computed and the measured values of the time derivative of the surface current density at a location on the missile. Further details will be presented showing that, in general, there is good agreement between the computations and the measurements.

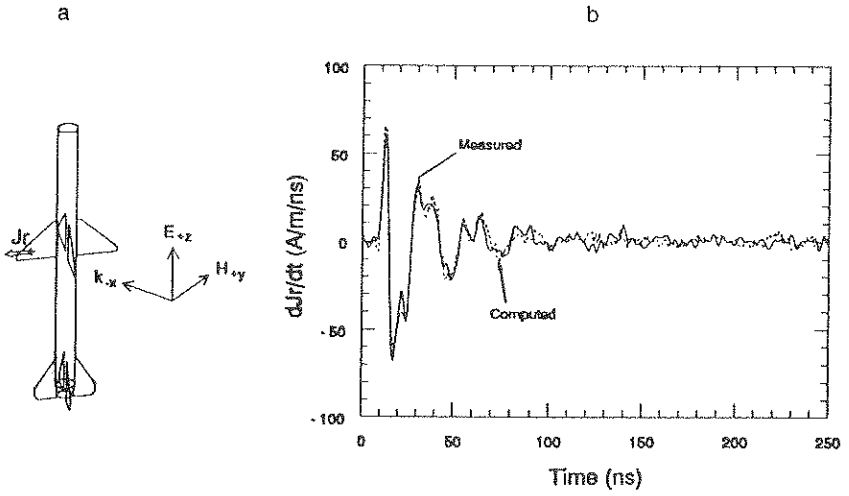

Figure 1. Time derivative of radial surface current density dJ_r/dt, on a back mid-fin of the missile.

Adaptive meshing in 3D for the FDTD Algorithm and application to aperture problems

S.Taylor , A.M.Milne and D.J.Evans
FGE Ltd
Chiltlee Manor,
Liphook,
Hampshire,
England

We present here details of an adaptive gridding algorithm for the Finite Difference Time Domain method as implemented in the FGE code INGRID. The algorithm allows regions of refined mesh to be embedded within coarser grids to allow local target features to be modelled in fine detail without the computational overhead of a fine mesh everywhere. The method is used in fully 3D problems but is easiest illustrated in 2D. The coarse zone and fine zone regions are in contact along a line of H nodes (see fig 1) which are all updated on the fine mesh.

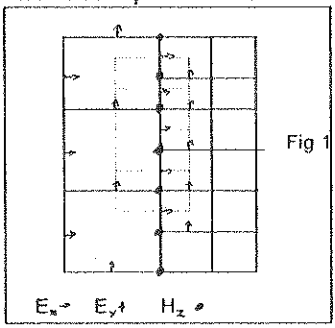

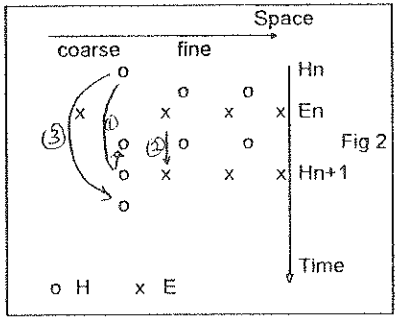

The large squares are lines joining up the coarse zone H nodes and the small squares the equivalent fine zone lines. The dotted lines show the Faraday contours used to update the boundary H nodes. These make use of E nodes which are available within the fine mesh and by suitable interpolation on the coarse mesh.

The refinement ratio at each level is two and the fine mesh undergoes two time steps for each coarse mesh step. The Time advancement at the boundary is illustrated in figure 2.

On step 1 a normal H update takes place on both meshes . On step 2 an E update takes place on the fine mesh using a time interpolated H value from the coarse mesh. In step 3 an extended time step is undertaken to give the required coarse zone H value for the second fine mesh E update. All other steps are as the normal Yee algorithm

As an example of the use of the method we consider the ingress of EM energy into a box with a thin slot in it. The thickness of the box is determined by the FDTD cell size and may be an overestimate of the real system as a result of meshing constraints. This

thickness determines the depth of the slot and for a TM wave into the slot the attenuation through the slot is exponential with depth. We show results here for the field measured within the box using local adaptive meshing to allow the slot to be half the depth of a coarse zone calculation.

These results are the time domain response (figure 3) inside the box with and without adaptive meshing of the slot and the Fourier transform of the results (Figure 4). These show the effect of the attenuation. The coarse zone mesh allows much less ingress than locally adapted thin slot. They also show that the adaptive meshing algorithm gives stable results and does not affect the resonant frequencies of the box.

Figure 3 : Ey Inside Box

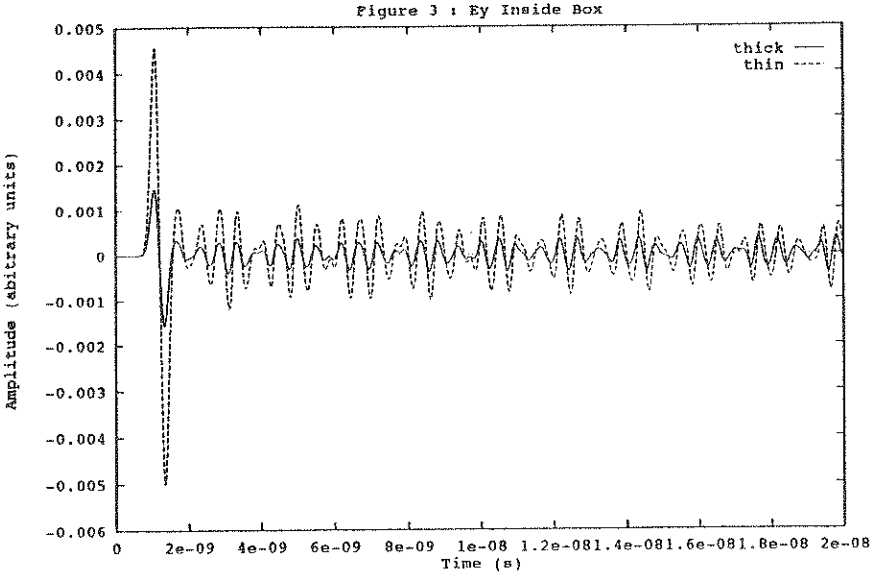

Figure 4 : Ey Inside Box

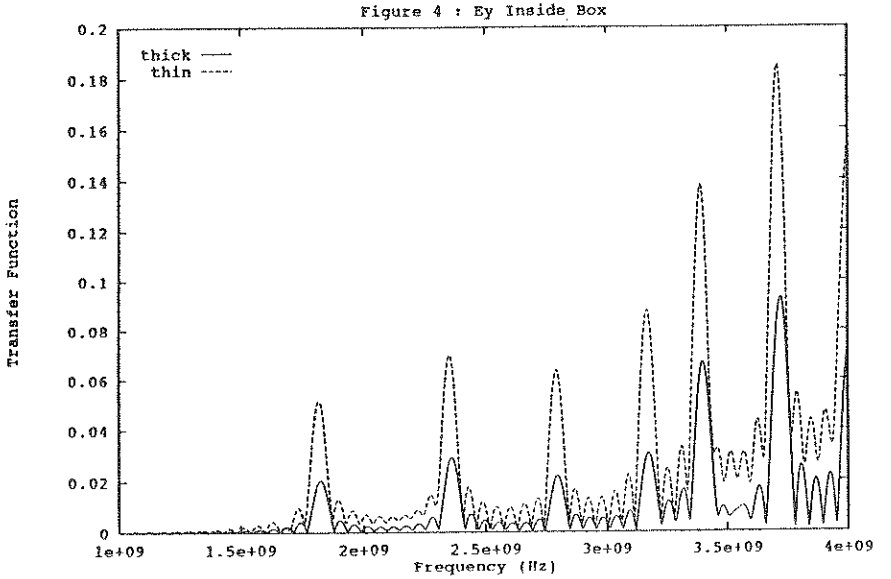

Analysis of the Diffracting Centers of a complex 3-dimensional structure

I. De Leeneer*, E. Schweicher
Royal Military Academy
MMWW-OMRA
30,Renaissance Avenue
1040 BRUSSELS - Belgium

A. Barel
Vrije Universiteit Brussel
Applied Sciences-dept ELEC
Pleinlaan 2
1050 BRUSSELS-Belgium

1 Introduction

Most Radar Cross Section calculations are done on specific objects, with well known geometrical characteristics. This means that if one chooses to treat a different geometry, the theoretical considerations and simplifications will probably change, and so will the practical implementation . The aim of this work is to develop a method, which will treat 3-dimensional objects of any shape. Special geometrical features like systematic modelling of the object, removal of the hidden faces, or the recognition of diffracting centres will be done automatically. The extra computer time, needed for these supplementary treatments, will as much as possible be kept to an acceptable value.
In this work, we will only consider the monostatic Radar Cross Section. We will treat objects of the size of an aircraft, and use frequencies going from 10 to 40 GHz. This brings us in the Optical region, and allows the use of High Frequency asymptotic methods like Physical Optics (PO) for the reflections, and Michaeli's Equivalent Current Method (ECM) for the diffractions.
We will not go into details for what concerns the evaluation of the reflected field. For details, see: J. Preissner, V. Stein: Special Problems in Applying the Physical Optics Method for Backscatter Computation of Complicated Objects, IEEE Trans. AP, V36, No2, February 1988.

2 General Method

• The geometry of the object is defined by the triangles modelling its external surface. We chose this option, because this gives rise to only one kind of reflection, namely the reflection on a flat surface, and because of the ease in using existing finite element software, which allows an interactive modelling and an immediate triangular meshing of the 3-dimensional surface. The object will be saved in two files, one containing the co-ordinates of all the nodes, another giving for each triangle its three node numbers. By this way, the object is represented by two ASCII files, which augments the portability of these data.
• Before any other treatment, the wedges will be detected. This is followed by the selection of those wedges who will have a non negligible contribution. This will reduce the time used for diffraction calculations. For these wedges, the aspect angle independent parameters (like the inner angle) are determined. This has to be done only once, allowing a gain in computer time.
• The hidden faces algorithm will be launched. This is a very time consuming part, but cannot be avoided. This algorithm will select the visible triangles, which are those who will contribute to the reflected field. It will also select the visible wedges. Here, attention has to be paid to the fact that a hidden triangle still can contribute to a visible wedge!
• Finally, only the wedges who are "sharp" enough to be the source of a non negligible diffracted field will be retained, and their aspect angle dependent parameters are determined.
• The resulting diffracted field is calculated, which will allow the determination of the Radar Cross section. Here a problem can arise, if the object consists of thousands of triangles. Indeed, we obtain a summation of a great amount of data, and this will often lead to numerical instabilities. Several approaches are actually examined, to reduce this instability.

3 Problems

3.1 Modelling

The triangular patches merely approach the real surface. As a starting point, based on standard antenna literature, we agreed to allow a $\frac{\lambda}{16}$ deviation of the modelled surface compared to the real surface, where λ represents the wavelength. We will study the validity of this assumption.
Another problem arises where the object has a small radius of curvature. Indeed, Physical Optics approaches the reflecting plane by an "infinite" plane, which is achieved practically when the triangles' dimensions are not smaller then 5λ. But we still want to keep the $\frac{\lambda}{16}$ accuracy! Both conditions cannot be fulfilled when the radius of curvature is small. Instead of using hybrid methods, who combine the asymptotic solutions to locally more rigorous solutions, we tried to substitute the strongly curved parts by one or several wedges, and considered their diffracted field. To test out this approach, we used a cylinder of finite extent, and varied its radius of curvature.

3.2 Wedge Analysis

Because we modelled the object by triangles, we will consider each frontier between two triangles as a wedge. The problem of the *detection* of the wedges reduces itself to the detection, for each triangle, of its neighbouring triangles. This is done prior to the hidden faces removal, because a hidden triangle still can determine a visible wedge. But in this case we also consider all the fictitious wedges, introduced by our triangular modelling. We will analyse the influence and the relative importance of these supplementary wedges, which still count for the curvature of the object.
If the wedge inner angle becomes too large (approaching the limit of 180 degrees, where we have a flat plate), its diffracted field becomes negligible. We will determine a limit, separating the wedges *to keep*, from the others.

4 Experiments

We treat a cylinder of finite length, and use Physical Optics for the reflections, and Michaeli's Equivalent Current Method for the diffractions. We compare the Radar Cross Section obtained in the following cases:
- The cylinder is considered as a whole. For the diffractions, only the real (end-point) curved edges are considered.
- The same cylinder is modelled by triangular patches. To compare the influence of the fictitious wedges, their separate contributions are determined.
- The same cylinder is modelled by a different number of patches. This will influence the modelling accuracy of the cylinder, while the inner angle of the fictitious wedges will change. So we will be able to determine the best compromise between the number of modelling patches and the influence of the treatment of the fictitious wedges, and check if the $\frac{\lambda}{16}$ limitation is acceptable.
- Several cylinders with very small radii of curvature are considered, to see if we can replace the strongly curved parts by a succession of wedges. In this case, elliptic cylinders are used.

5 Conclusions.

If one chooses to be geometry independent, several supplementary problems have to be solved, before one can perform a Radar Cross Section calculation. This paper deals with the preliminary treatments necessary to the determination of the diffracted field. The different experiments were just recently started, and the data obtained by now are insufficient to lead to conclusions. We expect however to find that the fictitious wedges cannot be disregarded, and that the part of an elliptic cylinder having a very small radius of curvature can be approximated by diffracting wedges.

SCATTERING OF ELECTROMAGNETIC WAVES BY DIELECTRIC BODIES

By
Maj.Osman YILDIRIM
Lecturer
Turkish Air Force Academy
HAVA HARP OKULU
Electrical and Electronics Department
34807, Yeşilyurt, İstanbul, TURKEY

Telephone home : 574 36 63
Job : 663 24 90-4339

ABSTRACT

The scattering of electromagnetic waves by homogeneous isotropic dielectric geometric shapes have been investigated using a quasistatic approximation. In this paper, the modified Rayleigh- Gans Approach is developed and applied to a circular thin disk, cylinder, thin rod object whose physical sizes are small compared to wavelength.

Techniques described by Le Vine (D.M.Le Vine, IEEE Trans. AP-32(1), 6-12, 1984) were used to determine the fields scattered by bodies in the far zone. The scattered field relationships were then used to obtain the radar coss-section equations in closed form and also the total, absorption and scattering cross-sections computed by using internal fields.

We present a metlod to calculate scattering properties of dielectric bodies that are small compared to wavelength in at least one direction, that is, for very thin or flat particles. If this thinness criterion is satisfied, the results are valid in all frequency regions. Our results are in good agreement with literature (R.Schiffer, K.O.Thielheim, J.Appl. Phys., 50(4), 2476-2483, 1979).

By using a quasistatic approximation Mathematical representation of scattering and absorption by a small particle is a sort of generalizing of Rayleigh-Gans. In addition scattering by an arbitrarily oriented an ellipsoid, same is used to obtain results of

circular disk, thin cylinder and sphere. As a special case, our result converges the result in the literature (K.Shimizu, J.Opt.Soc.Am.73(4), 1983).

In the calculation of amplitude function, by changing the value of L's(polarizability factor), one can obtain the internal field components for different shapes (H.C.Van De Hulst, Dover Press, 1981). Scattering amplitude is calculable since the internal field is known.

Recently, numerical techniques, such as the extended boundary condition method and other coupled integral equations method of solutions (O.Yıldırım, I.Akduman, 7th European Elect. Struc.Conf., Politecnico di Torino, Italy, 1993) have been applied to different geometries of scattering problems.

SAFIR:
AN OPERATIONAL SYSTEM FOR THUNDERSTORM EARLY LOCALIZATION AND LIGHTNING HAZARD WARNING

Philippe RICHARD
DIMENSIONS, 13790 Rousset, FRANCE

During the 80's research programs in the field of lightning physics and thunderstorm phenomenology have been conducted at the French National Agency for Aerospace Research (ONERA). They were based in particular on the development of electromagnetic techniques for the fine spatial and temporal analysis of atmospheric discharges. This research has conducted to the development of the SAFIR system, a new generation of lightning localization system, performing the real time localization of thunderstorms and the early warning for lightning hazards. This system, is now manufactured by the Dimensions Company and is used operationnally by weather services, electric utilities, military and space centers, for thunderstorm nowcasting and early lightning warning.

The SAFIR system operational principle is that all along the development of a thunderstorm cell, the electrical activity of the thundercloud (in terms of internal micro-discharges, intra-cloud lightnings and cloud-to-ground lightnings), is closely related to the different stages of evolution of the cell and to the thunderstorm severity.

SAFIR early warning performances are made possible by the high frequency electromagnetic detection of all electrical discharges which occur within the storm cloud as it builds-up and grows; these discharges are a precursor phenomenon allowing a storm cloud to be identified and located up to 1 hour before producing cloud-to-ground strikes, and its path and severity to be predicted. These internally occuring events are indicative of thunderstorm severity, they enable to identify severe storms and to assess the potential for weather hazards such as cloud-to-ground lightning.

A basic SAFIR system covers an area of 90,000 square kilometres and comprises 3 detection stations (distant of about 100 km) and a central station. Each detection station performs the angular location of electromagnetic sources associated with lightning discharges by using VHF interferometry. Informations are transmitted to the central station which calculates, by triangulation, the 2D spatial localization of lightning flashes and performs the identification of thunderstorm cells and nowcasting for lightning hazards.

The purpose of this communication is to present the principles of the SAFIR system in relation with thunderstorm electrical phenomenology, and to illustrate its performances for lightning strike hazards early warning.

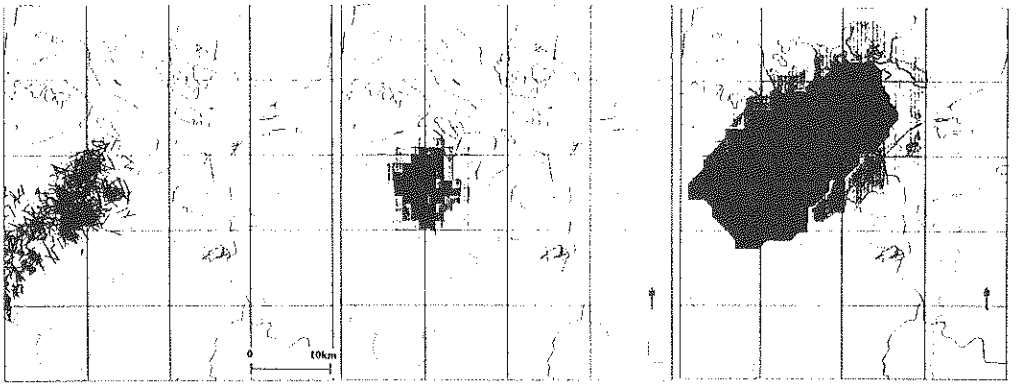

MAPPING OF TOTAL LIGHTNING ACTIVITY | DENSITY MAPPING OF ELECTRICAL ACTIVITY | NOWCASTING OF CELLS EVOLUTIONS

SAFIR Real Time Display

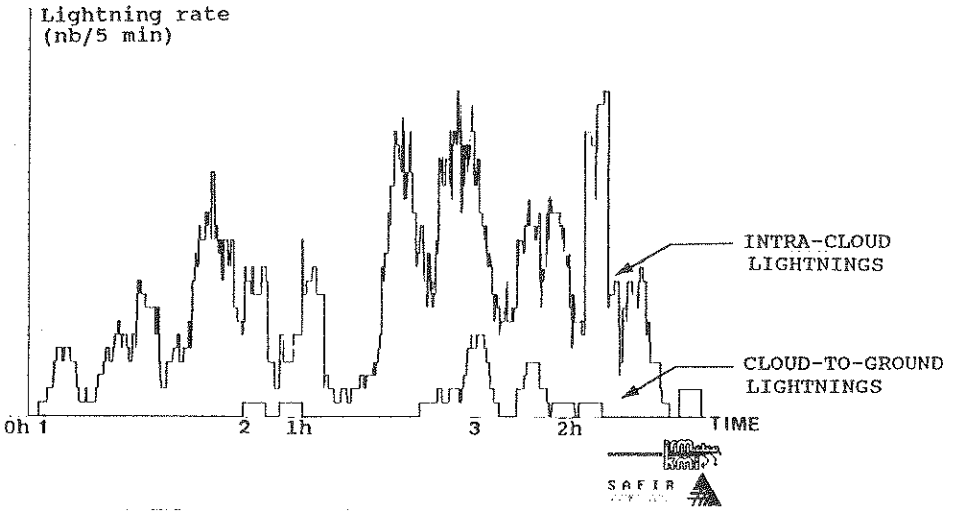

1. First Intra Cloud flash (to)
2. First Cloud to Ground flash (to + 45 minutes)
3. Maximum of Cloud to Ground activity (to + 1h40min)

Typical evolution with time of the number of intra-cloud and cloud-to-ground lightnings produced by a thunderstorm

On the Peak Electromagnetic Fields That Are Radiated by Lightning Return Strokes Aloft

E. Philip Krider
Institute of Atmospheric Physics
The University of Arizona, Tucson, Arizona 85721

In recent years, upward discharges have been observed between the tops of thunderclouds and the lower ionosphere [R.C. Franz, R.J. Nemzek & J.R. Winckler, Science 249, 48-51, 1990; O.H. Vaughan, Jr., R. Blakeslee, W.L. Boeck, B. Vonnegut, M. Brook & J. McKune, Jr., Mon. Wea. Rev. 120, 1459-1461, 1992], and lightning-stimulated airglow emissions have been recorded at altitudes near 90 km [W.L. Boeck, O.H. Vaughan, Jr., R.Blakeslee, B.Vonnegut & M. Brook, Geophys. Res. Lett. 19, 99-102, 1992]. Evidence for lightning-caused heating and ionization in the lower ionosphere (70-110 km) has also been obtained [U.S. Inan, D.C. Shafer, W.Y. Yip & R.E. Orville, J. Geophys. Res 93, 11,455-11,472, 1988; R.L. Dowden & C.D.D. Adams, J. Atmos. Terr. Phys. 55, 1335-1359, 1993]. Among the mechanisms that have been proposed to explain these phenomena is a direct coupling of lightning radiation fields to the ionospheric plasma [U. S. Inan, T.F. Bell & J.V. Rodriguez, Geophys. Res. Lett. 18, 705-708, 1991; J.V. Rodriguez, U.S. Inan & T.F. Bell, Geophys. Res. Lett. 19, 2067-2070, 1992; Y.N. Taranenko, U.S. Inan & T.F. Bell, Geophys. Res. Lett. 19, 1815-1818, 1992, Geophys. Res. Lett. 20, 1539-1542, 1993]. Unfortunately, there have been very few measurements of the amplitudes of lightning fields in the upper atmosphere in the salient frequency interval., *i.e.*, from a few to a few hundred kilohertz, and there have been no measurements of the angular distributions that propagate upward. The largest sources of lightning radiation in the ELF-VLF-LF bands are the return strokes in cloud-to-ground flashes. Because of the new interest in how such fields interact with the larger geophysical environment, and also interact with aircraft and spacecraft aloft, we have attempted to estimate the peak amplitudes of return stroke fields aloft and the associated radiation pattern.

The geometry of our problem is sketched in Figure 1. We use a spherical coordinate system with its origin at the point where the return stroke begins. Because fields (and currents) from return strokes peak in times that are of the order of microseconds or less, the length of the stroke at the time of the peak will be limited to hundreds of meters or less, even if the velocity is close to the speed of light. If such a channel is viewed from a distance, R, that is of the order of hundreds of kilometers, it will appear to be an infinitesimal dipole.

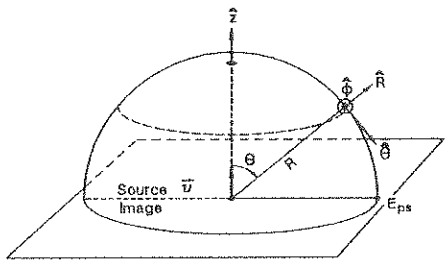

Figure 1. Spherical coordinate system with its origin at the point where the return stroke begins on the ground.

Estimates of the peak field amplitude that will be radiated by a vertical return stroke propagating upward, with the dipole approximation, are shown in Table 1 [E.P. Krider, J. Geophys. Res. 97, 15,913-15,917, 1992; J. Atmos. Electr. (Japan), in press, 1994] for typical stroke speeds, v, relative to the speed of light, c. [Note: The v/c of 0.99 can be regarded as an extreme value.] These estimates assume that the

transmission-line model for the stroke current is valid up to the time of the peak. Note how a peak current of 30 kA radiates 6, 12, 21 and 64 V/m at a distance of 100 km when v/c = 0.33, 0.67, 0.90, and 0.99, respectively, assuming that there is no attenuation in the atmosphere or on the surface. Since the electron mean free path at 100-km altitudes is on the order of 1 m, such fields are large enough to produce substantial heating and ionization in the lower ionosphere [J.V. RODRIGUEZ, U.S. INAN & T.F. BELL, Geophys. Res. Lett. 19, 2067-2070, 1992; Y.N. TARANENKO, U.S. INAN & T.F. BELL, Geophys. Res. Lett., 19, 1815-1818, 1992 & 20, 1539-1542, 1993].

TABLE 1. The maximum amplitude of $\vec{E}_p$ in V/m (in the $\hat{\theta}$ -direction) that a vertical return stroke radiates into the upper half-space for various values of v/c and I_p. All values have been computed at a range (R) of 100 km, assuming that there is no attenuation. θ_m is the polar angle of the maximum amplitude. Numbers in parentheses are percentages of negative first strokes that exceed the tabulated value of peak current [K. BERGER, R. B. ANDERSON & H. KRONINGER, Electra 80, 23-37, 1975].

v/c	θ_m (degrees)	Peak Current 14 kA (95%)	30 kA (50%)	80 kA (5%)
0.33	90	2.8	6	16
0.67	90	5.6	12	32
0.90	29	9.8	21	56
0.99	8.2	30	64	170

The angular distributions of the peak field are shown in Figure 2 for the same values of v/c as in Table 1. When v/c is small, the field has a $\sin\theta$ distribution that peaks on the ground ($\theta = \pi/2$). At large v, however, the maximum lifts off the ground and becomes substantially more vertical.

Our conclusion is that return strokes in natural lightning will indeed radiate large fields into the upper half-space and, on those occasions when the velocity is very close to the speed of light, a heavily ionizing field near the vertical. It is conceivable that, in an extreme case, the upward propagating field will be large enough to trigger a discharge between the cloud top and the lower ionosphere.

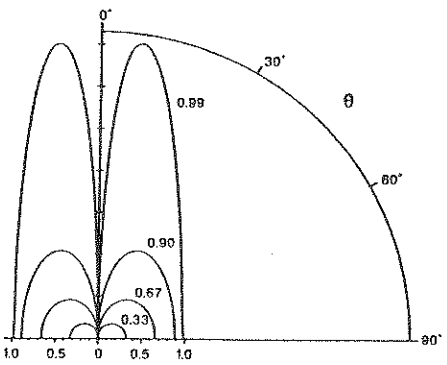

Figure 2. Polar plot of the relative amplitude of the peak field radiated into the upper half-space. The values of v/c are given by each curve, and there is symmetry about the vertical axis.

A MODEL FOR PREDICTING TRIGGERING OF LIGHTNING BY LAUNCH VEHICLES, MISSILES, AND AIRCRAFT

By

Rodney A. Perala*, Dale A. Steffen, Terence H. Rudolph,
Gregory J. Rigden, Hank S. Weigel

ELECTRO MAGNETIC APPLICATIONS, INC.
7655 West Mississippi Avenue, Suite 300
Lakewood, CO 80226
Phone: 303-980-0070
Fax: 303-980-0836

Triggering of Lightning by aerospace vehicles has been of great interest for some time. The incidents involving Atlas Centaur-67 and Apollo 12 have shown the importance of understanding this phenomenon. Also, NASA, Air Force, FAA and French in-flight research programs have demonstrated the commonplace phenomenon of aircraft triggered lightning. There therefore needs to be a model which can be used to predict the likelihood of this occurrence.

This paper is a follow-up on previous research in these matters published at previous conferences (R.A. Perala, et.al., 1988, 1991 and 1992 International Aerospace and Ground Conference on Lightning and Static Electricity). The work has now been completed on developing these models, which involved both experimental and numerical efforts. In this paper we present an overall model applied to launch vehicles, developed especially for the Titan IV vehicle, but the principles apply to other vehicles as well. The model considers the following parameters:

- Altitude
- Velocity
- Plume properties
- Corona to arc transition conditions
- Dynamic air pressure
- Ambient static electric field

We give specific examples of application of this model to launch vehicles, and explain how the model may be applied to aircraft as well.

One of the critical aspects of triggering of lightning by launch vehicles is the effect of the plume on triggering conditions. In previous papers we have presented some of our concepts of how the plume interacts with a thunderstorm field. In this paper, we describe the experiments and analysis which were done to validate the concept we have previously reported.

We report on several experiments which were accomplished, as follows:

- The charging of an isolated laboratory flame in an impressed electric field
- Charging of a solid rocket motor (with shuttle propellant) in an artificially impressed field

Numerical modeling was used to understand and interpret the experiments. Plume chemistry models were used to predict ion and electron density profiles of the plume. These results were then used in conjunction with electrostatic modeling of the motor/plume in order to determine motor charging time constants. Plume RF attenuation measurements at 10 GHz were used to calibrate the plume chemistry models.

The most significant finding of this research is that the volume of the plume which governs the electrostatic behavior of the launch vehicle is bounded by the plume conductivity contour of between 10^{-9} and 10^{-10} mhos/m. This has a great impact on triggering conditions, which apparently can occur at rather low thunderstorm field levels.

In particular, we have derived an equation which predicts lightning triggering levels for the Titan IV launch vehicle, as an analytical expression for the minimum triggered lightning ambient field threshold, E_a, as a function of altitude, A:

$$E_a = \frac{E_o\left[e^{-0.0312A} + 0.086^{e^{-0.0194(A-25)^2}}\right]}{(0.4A^2 + 250)}$$

where A is in units of kilofeet. A plot of this equation is provided in the figure below for altitudes between 5 and 55 thousand feet. Somewhere below 5 thousand feet, probably between 2 and 3 thousand, the effects of the earth become significant and the equation is no longer valid. As a conservative approach the minimum triggered lightning ambient field at these lower altitudes is given the value at 5 thousand feet as shown in the figure. The analytical expression allows the extension of the altitude range as desired. The end value of 55,000 feet is selected to bound the altitude of relative hazardous weather phenomena and the accompanying triggered lightning danger zone.

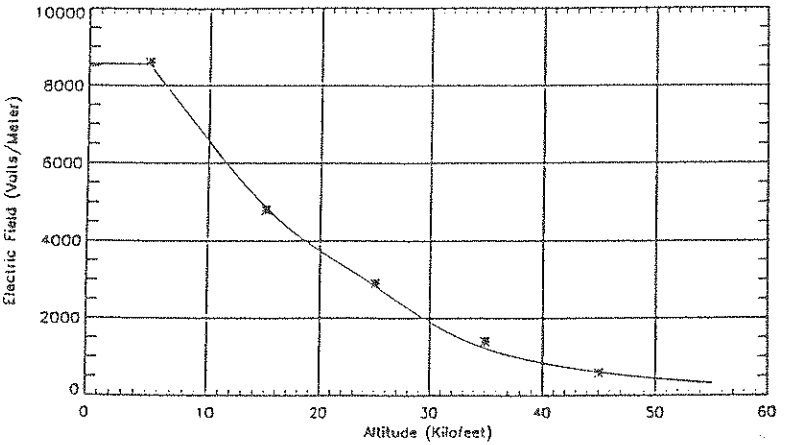

A Plot of the Above Equation Providing the Minimum Triggered Lighting Ambient Electric Field as a Function of Altitude

RADIO FREQUENCY (RF) TESTING OF LIGHTNING PROTECTION SYSTEMS

Richard S. Collier
Electro Magnetic Applications Inc
7655 West Mississippi Avenue St 300
Lakewood CO USA 80226-4332

ABSTRACT

Radio Frequency (RF) techniques have been developed for testing and evaulating Lightning Protection Systems for buildings and other structures; and the RF measurements provide a method for predicting lightning threats to these buildings. The resulting output uses computer modeling and RF data to map zones in and around the structure which may be considered "safe" for various types of assets in lightning environments, considering the level of protection and the susceptibility of assets in question.

This proceedure is evaluated by comparing RF test results with data from triggered lightning data obtained at the EPRI and Ft. McClellan triggered lightning facilities. The building at Ft. McClellan is a concrete with rebar structure, floor and walls, with a variety of metal connections and a metal roof. The experimental house at the EPRI site is essentially an unshielded structure of ordinary building materials and represents a different electromagnectic coupling to a potential lightning strike.

Three Dimensional Finite Difference computer models have been constructed for both of these experimental facilities. The construction of both of these facilities was visually monitored, and the particular construction details were included in the computer models. The models are designed to describe the results of both RF and Triggered Lightning excitation to the building and surrounding environment. The computer models contain adjustable parameters which include soil and concrete conductivities and dielectric constants and the contact resistance between the soil and underground cables and between concrete and iron rebar elements and also other wire, cable and metal terminations and connections. Some of these parameters are frequency dependent. The computer model uses appropriate average values of these parameters over the primary frequency range of interest - which for lightning events is in the 100 KHz to 20 MHz range. This is the frequency range of the RF testing measurements.

The RF testing measurments are used for comaparison to update and refine the computer model, which is used to predict the response to triggered lightning for the various experimental configurations of the buildings. PC VGA color monitor graphics displays of CRAY2 generated data show calculated electric and magnetic field intensities on arbitrary isometric and cross-sectional views of the buildings and surrounding areas at specific time frames during a lightning strike. These displays allow visual observation of "hot spots" and "safe areas" in relation to the location of specific assets which are being protected. Time dependent plots also show field magnitude waveforms at particular

chosen locations in and around the buildings.

The model is presently set up for the linear regime (up to the point where non-linear arcing occurs at some point in the system). The model can also roughly predict when non-linear arcing can occur - which is primarily dependent on breakdown electric field intensities which develope in the soil and concrete.

As a result of the RF and model comparisons, a rationale is obtained for defining Threat Categories, e.g. Low, Medium, High, in terms of upper and lower limits on the Electric and Magnetic Field, their time derivitives, and the action integrals of these quantities as the the drivers for potential damaging power absorption of given assets. Susceptibilities of Given Assets are obtained from the manufacturers of the assets and/or the results from EMI testing in Laboratories. Assets can include explosives, electronics, construction materials and personnel.

The Evaluation of LEMP Effect on 33 kV Primary Feeder Overhead Line Using New Model for Lightning Channel

R.Moini, B.Kordi , M.Abedi*
AmirKabir University of Technology
Electrical Engineering Department
No 424,Hafez Ave.,TEHRAN,I.R.IRAN
Phone:(+98)216139480,FAX:(+98)216406469

Abstract :

In this paper an attempt will be made to introduce a new model based on monopole antenna for lightning channel.This model has been deduced from experimental and theoretical works by Nucci et al[1,2].The paper will also present the induced voltage and current on three phase over head line (33kV), caused by lightning , stroke a ground nearby the line , using proposed model.
This accurate modelling will help the design engineers to have outstanding view on protection scheme to protect the overhead lines against lightning.

Formulation of the problem :

For calculating electromagnetic field radiated by lightning channel , fig(1) has been used.Lightning channel is modeled by monopole antenna which one end is located on the earth surface. The generator of the antenna has been selected in such way that time-space transient current caused by generator in any point along the antenna shows the current distribution of lightning channel which is consistent with Nucci et al research works (figs 2&3).For evaluation of time-space transient current , electric field integral equation in time domain using moment method has been applied [3].It is clear that with extension of above model , the induced voltage and current on power line nearby the modelled lightning channel , can be examined to predict the transient overvoltages.Fig(1) also shows the location of proposed antenna (lightning channel) and three phase high voltage over head line.Comparing the results obtanied through our model and previous model [4,5] we can conclude:

-The accuracy of our model is much higher.
-In our model horizontal and vertical radiation of electric field can be examined without losing accuracy due to large distance.
-In our model coupling between different wires can be included , because of the nature of moment method.
-In our model induced voltage and current can be deduced in any point of line .
-The resistive and reactive load can be included in any end of power line.
-In our model the earth can be considered as a nonideal conductor .

Conclusion :

With our model the induced voltage and current in over head lines caused by lightning stroke can be evaluated easily , simply and accurately.Therefore line protection scheme can be designed properly.

References:

[1]:C.A.Nucci,G.Diendorfer,M.A.Uman,F.Rashidi,M.Ianoz,C.Mazetti,Jour.of Geograp.Res.,vol.95,No D12,1990.
[2]:C.Nucci,F.Rashidi,M.Ianoz,C.Mazetti,IEEE Trans. on EMC,vol.35,No 1,1993.
[3]:J.Herault,R.Moini,A.Reineix,B.Jecko,IEEE Trans. on Ant. Prop.,vol. 38,No 8,1990.
[4]:M.Abedi,B.Vahidi,Proc. of High Tech. in Power Industry IASTED,Int. Conf.,Taiwan 1991.
[5]:R.Moini,B.Kordi,B.Vahidi,M.Abedi,A.C.E.S94,Monterey,U.S.A.,1994.

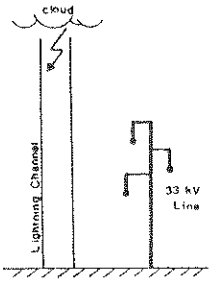

fig. 1 Three dimensional XYZ coordinate with Return Stroke Channel and 3 phase power conductors

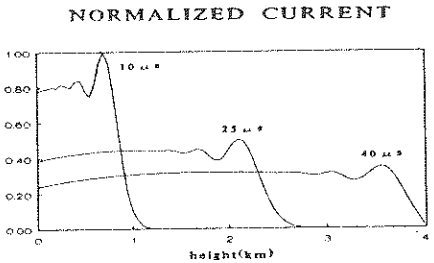

fig. 2 Distribution of lightning current along the channel at different times

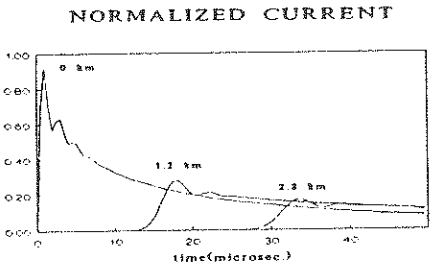

fig. 3 Current time wave shape at 3 different heights

PRELIMINARY ANALYSIS OF CLOSE ELECTROMAGNETIC FIELDS PRODUCED BY TRIGGERED LIGHTNING DURING 1993 FLORIDA CAMPAIGN

*A. BEN RHOUMA°, P. AURIOL° and S. RATHOIN °
A. EYBERT BERARD°°,J.P. BERLANDIS°° and B. BADOR°°

°CEGELY (CNRS 829) - ECL 36 AV Guy de Collongue BP 163, 69131 ECULLY Cédex
°°CEA/DRN/DTP/STI.LASP 17 rue des Martyrs 38054 GRENOBLE CEDEX9

In the literature the triggered lightning measurements of the electromagnetic fields in a short range around the striking point are not common. However, their temporal evolution is not yet well known. In 1993, a triggered lightning campaign was carried out by PTI (Power Technologies Inc) and CEA group, under EPRI funding (Electrical Power Research Institute). The CEA group was also in charge of lightning current characterisation and electromagnetic field measurements at close range (50m and 110m from the triggered discharge. I, E and H measurements were performed respectively by coaxial shunt and 4 Thomson space field sensors (2 for E and 2 for H). The sensors were connected via 5 optical Thomson "Melopée" devices to Lecroy digitisers and data were stored on hard disc. 26 return strokes, greater than 4kA, were recorded. The crest values of the current amplitudes of the different return strokes were located in a window from 5.8 to 38.6 kA, with more than 50% of all strokes exceeding 12.4 kA.

The rising time between 10% and 90% of the crest value of the current waveform was in average about 550ns. For electromagnetic field waveforms, this time depends on the distance at which these fields were measured. For example, for the magnetic field measured at 110m from the striking point, this time is about 30% greater than that of the same field measured at 50m.

CEA and CEGELY (group in charge of the electromagnetic field analysis), show that the different records obtained during this campaign confirm the proportionality between the crest values of the magnetic field waveforms and those of the corresponding current ones. Figure 1 shows for the distances of 50m and 110m, a comparison between the measured values of the magnetic field and the calculated ones with the Ampere law ($H=I/2\pi d$), versus the current amplitude, for the strike 9320 which generated 7 return strokes. The amplitude of the magnetic field, measured at a distance of 110m from the striking point is in average about 57% of the amplitude obtained at 50m from the same point.

The electric field waveforms obtained are in agreement with theory. However, in these waveforms we can note the contribution of the electrostatic component of the field, which is represented by a slight linear evolution after the first few microseconds from the beginning of the return stroke. Figure 2 shows the electric field variation corresponding to the approaching leader and the return stroke of the third flash in the strike 9320 at both distances. The variation of the electric field amplitude with distance is function of the contribution of the different components of the field which are in $1/d$, $1/d^2$ and $1/d^3$. For the waveforms represented in figure 2, the amplitude of the field measured at 50m is about 44% greater than that measured at 110m.

Owing to the tortuosity of the channel and the finite conductivity of the soil, the magnetic field can have a non zero vertical component, and the electric field a non zero horizontal one. These components are of great importance in the calculation of the induced voltages on cables, but, at short distances from the striking point, they have never been measured before. In 1993, during the same campaign, University of Florida was involved in electromagnetic field measurements (vertical E and horizontal H) at 30 meters from the striking point. So we have now a significant data base about electromagnetic measurements between 30 and 110 meters from the discharge.

We also present in this paper a single case of simultaneous horizontal and vertical magnetic field components at 110m. This record was obtained for a flash which had a maximum current amplitude of 7.1 kA. Figure 3 shows the waveforms obtained in this record where we can ascertain that the vertical component amplitude is about the half of the horizontal one. (In the literature a ratio of about 1/50 was found for the vertical and horizontal electric field components for natural lightning at a distance of 7km). In our final paper, simulation results about this last point can eventually by presented.

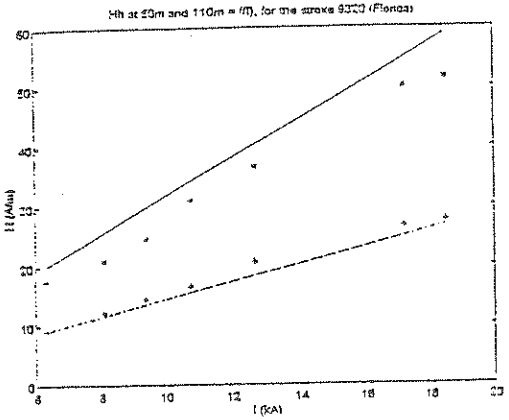

Figure n°1:

measured and calculated values of H at 50m (*), (__) and at 110m (÷),(_.) for the strike 9320.

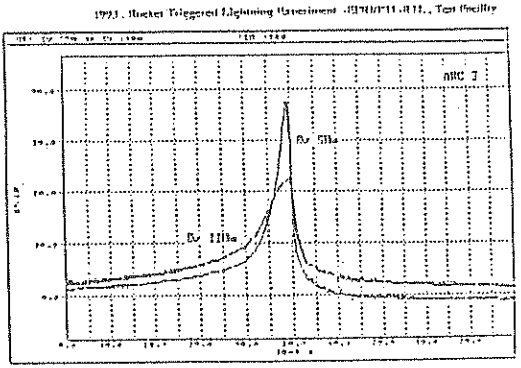

Figure n°2:

leader and return stroke electric field variation at 50m and 110m for the third flash of the strike 9320.

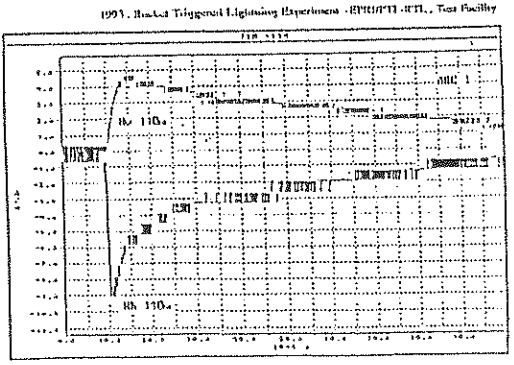

Figure n°3:

vertical and horizontal magnetic field components measured at 110m for the strike 9334.

ROCKET TRIGGERED LIGHTNING -KENNEDY SPACE CENTER & BEYOND

William Jafferis
BJC
4140 Hickory Hill Blvd.
Titusville, Florida 32780
Telephone 407-269-6943 Fax 407- 264-0876

Introduction: The Kennedy Space Center covers an area of 1000 Km², and is in one of the highest isokraunic levels in the country. Outdoor operations involving space vehicles, towers, explosives and fuel storage, aerial and buried cabling and piping connecting widely distributed sensitive electronic and mechanical equipment: all subjected to critical schedules making lightning a serious hazard. The hazard was recognized in the very early days of space center by Dr. Kurt Debus , the center director . To eliminate effects to operations and assure maximum safety to all personnel, flight and ground support equipment Dr. Kurt Debus recommended the development of a lightning protection system for all launch processing facilities and a system to detect charged clouds capable of producing lightning within the operational area. Both systems, lightning protection and detection where considered *STATE OF THE ART* and as such, the advice Dr. Debus recommended was to use the best experts and research scientist available and develop local instrumentation capable of measuring lightning events so that the effectiveness of these systems could be verified.

Experience has shown that solutions to these problems are very difficult and time consuming. A project was started that would use rocket triggering to create natural lightning in a laboratory setting, permitting accurate time correlated measurement of pertinent data enabling in-depth studies. In addition data from the extensive instrumentation and meteorological system provided to satisfy operational requirements would be available to researchers in a time correlated fashion. This research facility was called **KSC ATMOSPHERIC SCIENCE FIELD LABORATORY** and was active from 1984 through 1991. The facility was closed for budgetary reasons. This paper will discuss the results of these operations as well of the resulting rocket triggering facilities located in north central Florida and north central Alabama.

Rocket Triggered Lightning Program at Camp Blanding , Florida: The **Electric Power Research Institute and Power Technology Incorporated** participated in **ASFL/RTLP 87.88** studies of power equipment. The results were very successful and **EPRI/PTI** requested a large scale experiment involving aerial and buried electric power transmission cables. When **KSC** closed down **ASFL** center director agreed to loan the necessary equipment and material to **EPRI** if a suitable site was found. The State of Florida agreed to lease a portion of Florida State Army property, which has the necessary air clearance and rocket storage facility. The site, 250 Km² located on the western edge of Camp Blanding or 10 Km east of Starke, Florida. Operations began in June 1993 and were conducted by **PTI** assisted by the French group from CEA at Grenoble

Rocket Triggered Lightning Program at Pelham Range, Fort McClellan, Alabama: The **SANDIA NATIONAL LABORATORY** supported by the **U.S. ARMY** participated in **ASFL/RTLP 1990.** Studies of materials and field testing their rocket triggering system to be used at facilities located at Fort Mclellan Anniston, Alabama. The site , 200 Km^2 in area is on Pelham Range located north west of Anniston and has been operational during the summers of 1991 and 1992. Air space is not a problem as operations can be conducted at any time.

LIGHTING SAFETY EVALUATION OF LAUNCH COMPLEXES, LIGHTNING MITIGATION SYSTEMS AND PERSONNEL SAFETY

Louis Ullian
Deputy Director of Safety
45th Space Wing
United States Air Force
Patrick AFB, Florida

Ronald J. Wojtasinski*
Principle Investigator
Richard L. Gaudio II
Science and Technology Corporation
Cape Canaveral, Florida

The paper presents a systematic engineering approach to evaluating electromagnetic effects of lightning on aerospace launch systems. The EM environment is applied to various electromagnetic models from the literature of launch structures, facilities and systems. Determining the operational requirement of the systems which must function during a lightning event and personnel functions required allows the design and evaluation of lightning mitigating techniques.

The related hazards to personnel and equipment are derived for an aerospace launch facility. The appropriateness of applicable codes and specifications can then be evaluated. The paper evaluates personnel and equipment hazards on launch complexes at Cape Canaveral Florida caused by lightning. The threat of lightning constrains work activities on the launch complexes and the processing of a aeorospace vehicles for flight. During the summer months, sixty percent of the work time can be lost because of thunderstorms within five miles of the launch complex. The paper comments on hazards caused during lightning strikes, the adequacy of facilities to conduct lightning currents safely and, lightning grounding and facility grounding. Lightning interception by lightning rods and lightning interceptor systems are considered in this application. The possible benefits derived by the reduction of lightning effects as a consequence of the interceptor system.

The analysis calculates current flows and voltage gradients on the structure and around the earth grounds to determine step voltage and touch voltages. Effects on telephone, video and control systems was analyzed for personnel and equipment hazard. Personnel hazards were identified for telephones and camera systems. Closed circuit television systems were disabled by lighting transients because of shielding practice. An operational hazard analysis identifies lightning hazardous operations. The personnel were safe within the confines of launch structures during a lightning and within designated protected areas.

Voltage hazards were created at the peripheral grounding

locations of lightning down conductors and transmitted along the security fence. The direct current component of the lightning strike current was eliminated from the launch structure but effects of fast rise times remained.

The conclusion is the effectiveness of lightning protection standard design practice is generally adequate. Generally the good practice of protecting cables and equipment with a lightning current carrying shield is violated placing equipment at risk needlessly.

The manned operations at the launch facility could be significantly increased during thunderstorm alerts from previous conservative operations practice. For high value activities and personnel protection from lightning effects, the detailed design of lightning protection must be in response to specific operational requirements to ensure the protection of resources and people.

The paper highlights inconsistencies with practice, theory, data and experience. Issues of discussion are:

1. Voltage gradients developed in structures versus acceptable levels of exposure voltage to humans?
2. Telephone grounding and over voltage protection practice in structures. The protection of equipment and people?
3. An "effective faraday cage", for shielding personnel?
4. Earth "grounding" and equipotential planes and hazardous voltages?
5. Voltage potentials, development and coupling mechanisms.
6. Lightning Mitigation, how effective?
7. Operational safety requirements for personnel safety; practical parameters.
8. Operations hazard analysis for lightning.

KEY WORDS: lightning, protection, safety, personnel, electric shock, standards, evaluation, launch, facilities, grounding, shielding, operations, electromagnetic, modeling.

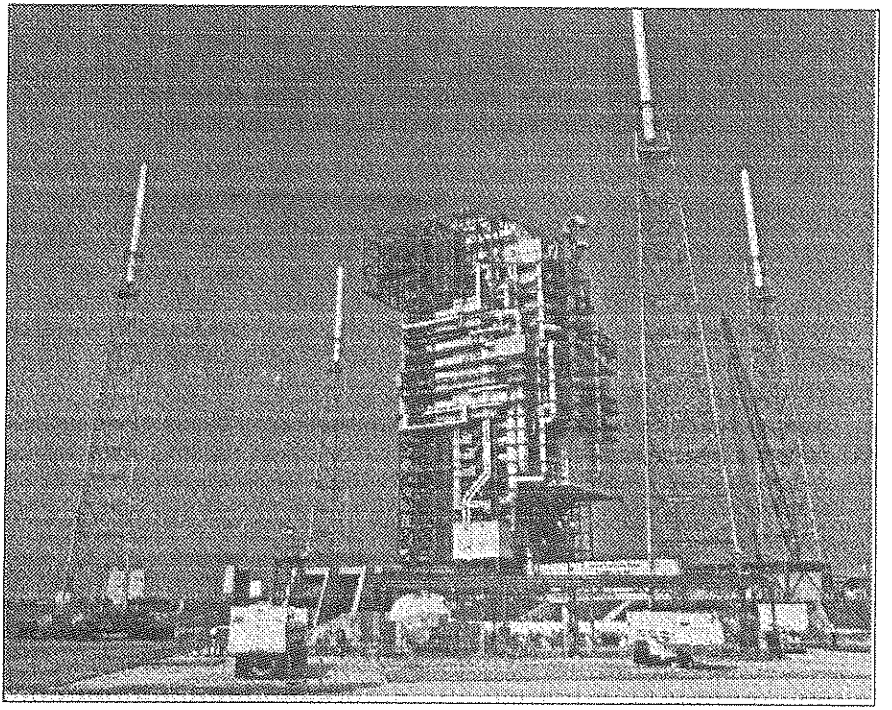

Figure 1. Lightning Mitigation System.

EVALUATION OF ELECTROMAGNETIC ENVIRONMENT AROUND A STRUCTURE DURING A LIGHTNING STROKE.

Carlos A. F. Sartori **José Roberto Cardoso,Ph. D.**
Student member,IEEE *** Member,IEEE ***
Escola Politécnica da Universidade de São Paulo

ABSTRACT

One of the most important problem related to Electromagnetic Compatibility analisys is the evaluation of the electromagnetic environment around a structure struck by a direct lightning.

Beyond the classified areas, where the insurance aspects related to explosion harzards are very important, the evaluation of the effects resulting from lightning has been assuming a special concern in our modern society due to the use of high susceptibility equipments, like electronic ones, in many social activities in a wide variety of functions.

This work was proposed due to the necessity of developing an electromagnetic field calculation methodology in the interior of a lightning protection system during a lightning stroke, suitable for the evaluation of energy and interference level associated with them.

The objective of the present work is to carry out a discretization technique in the space and time that meets the need of calculating the current distribution in a lightning protection system and the flux density or magnetic field inside the protected volume.

For this propose was developed a three-dimensional element or cell, where the central node corresponds to a junction of transmission lines, forming a impedance descontinuity in each line. Figure 1 shows this element.

The response of the cell to incident voltage pulses and the current distribution were determined by transmission line and wave propagation theory.

Then, using the dipole and images theory was calculated the contribution of each reflected and incident current of the element to the magnetic field.

The total magnetic field as a function of the time, in any point of the space, can then be determined by superposition, after subdividing the protection system conductors into a finite number of elementery units, represented by the proposed three-dimensional element or cell.

It was assumed in the present model some simplifications that could be reduced in a second round, without damage to the general philosophy adopted up to this moment. Among these simplifications are the calculation of transmition line

parameters through traditional formulas, not taking in account the non-linear ionization phenomena, and the simulation of the lightning stroke by a unidirectional current source.

Some numerical results are shown in order to evaluate the physical and mathematical consistence of the proposed methodology.

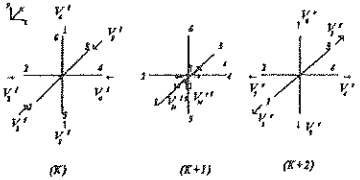

Figure 1: Impulse response of the proposed three-dimensional element at instants k, k+1 and k+2

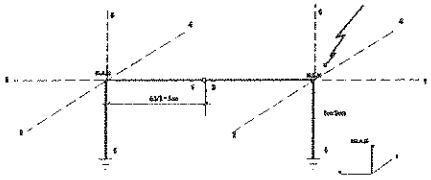

Figure 2 : Sketch of a structure struck by a lightning at point (0,0,0) and of the applied three-dimensional elements .

In the example shown in the fig. 2, caracteristic impedances of vertical and horizontal lines are assumed as 112Ω and 245Ω, earth resistence (Rat) as 5Ω and the current source is represented by the function :

I = 5 t (kA) for t≤2 μs and I=10 [0.5 t - 0.51 (t - 2)] (kA) for t〉2μs.

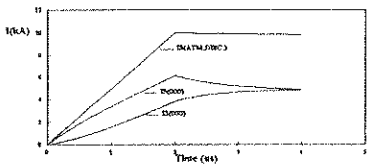

Figure 3 : Current distribution in the cell (000)

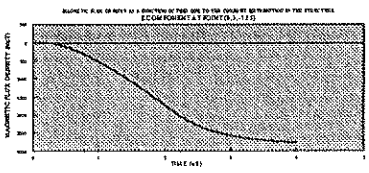

Figure 4 : Magnetic flux density B (μT) as a function of time (μs) at point (0,3,-1.25) m, due to the current distribution in the structure represented in the figure 2.

ABSTRACT

LIGHTNING-INDUCED ELECTROMAGNETIC PULSE (LEMP) AND ITS EFFECT INSIDE A CATENARY SYSTEM

T. J. Lie*, R. Briët, J. C. Chai
The Aerospace Corp.
El Segundo, California, USA

1. Introduction

The objectives of this work are (1) to reformulate the description of the electromagnetic pulse (EMP) from a nearby lightning stroke from a perspective of coupling to electronics, and (2) to estimate the attenuated lightning-induced EMP (LEMP) inside a catenary system at a US launch site. In the present work, a lightning stroke refers to a vertical upward current pulse along a channel of finite height from a perfectly conducting ground.

The reformulated EMP-model relates solely to the finite electromagnetic energy packet released from the lightning stroke; it does not consider either the initial or final ambient electrostatic fields of the lightning event. Thus, a LEMP starts out in time at an electric field level of zero and ends up back to zero after the event. This feature contrasts the picture of existing models, where a point charge accumulates at the high-end tip of the lightning channel to build up a permanent electrostatic field. While the existing models include slowly varying electrostatic ambient field, the EMP-model takes into account only the rapidly varying part that is responsible for coupling to electronics.

The catenary system considered in the present work is that of the US Launch Complex 40/41 at Cape Canaveral. It will be shown that it functions as an effective Faraday Cage in the low frequency region below 5 kHz, while in the high frequency region above 1 MHz, approximately 5% of the electric field manages to penetrate the system.

2. Basic Features of the EMP-Model

The lightning model described in the 1975 paper by Uman, McLain and Krider (Am J Phys, 43, 33, 1975) basically represents the existing models. This basic model of lightning is referred to hereafter as the UMK-model contrasting the EMP-model of the present work.

Figure 1 illustrates comparison of the vertical electric field calculated by these two models, where the lightning channel height is assumed to be 4 km, the same height used in the 1975 UMK paper. The lightning current stroke is that

of Component A of US military standard MIL-STD-1795A, which has the shape of a double exponential pulse with a maximum amplitude of 200 kA.

Figure 1
E-Field (vertical) of Lightning Stroke
of Component A per US MIL-STD-1795A
(at 1 km away, 150 ft above ground)

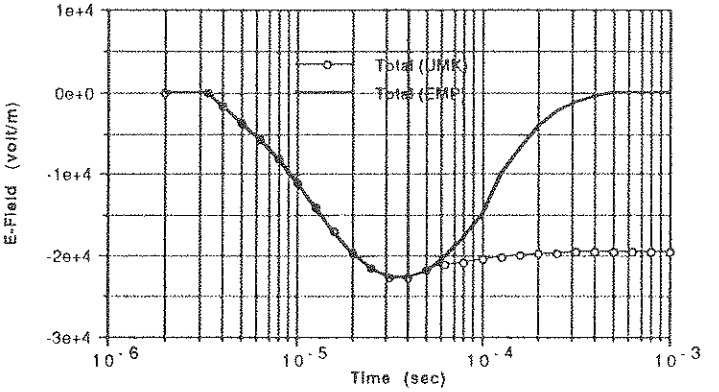

The observation point for this calculation is at a horizontal distance of 1 km from the lightning and 150 ft (46 m) above the ground. The total charge involved in the lightning stroke is about 20 Coulombs. Thus, the UMK-model yields, as Figure 1 confirms, a final ambient vertical electric field of about 20 kvolt/m.

A characteristic feature of the UMK-model is that lightning leaves behind a permanent ambient field, which is an electrostatic field due to the charges accumulated at both the high-end tip of the lightning channel and its image of the opposite sign. Such an electrostatic field is absent in the EMP-model, which is also noted in a 1978 article by Le Vine and Meneghini (J Geophys Res 83, 2377, 1978).

Thus, the UMK-model appears to present lightning as a charging process, thus creating an electrostatic field to counteract the preexisting electrostatic ambient field. In the EMP-model, on the other hand, the charges of the lightning current, as they arrive at the channel end, are shielded out by an existing large charge reservoir in thunderclouds that is responsible for the preexisting ambient field.

The difference between the two models can be mathematically attributed to the difference in the scalar potential. In the UMK-model, the scalar potential contains a term for the accumulated point charges at the channel end-points. In the EMP-model, on the other hand, this term is eliminated, because these charges are negated by the existing large charge reservoir of the opposite sign at the channel height. In this way, the EMP-model disregards the slowly varying electric field that is irrelevant to electronic coupling.

3. Shielding Effects of Catenary System

Figure 2 compares the vertical E-field spectrum of the lightning EMP (solid line) and the corresponding E-field (dashed line) under the catenary system of the US Launch Complex 40/41 at Cape Canaveral. The observation point is 1 km away from the lightning and 150 ft above ground. It is apparent that the catenary system provides an effective Faraday Cage in the low frequency region below 5 kHz, while in the high frequency region above 1 MHz, the E-field penetration is about 5%.

Figure 2
LEMP E-Field (vertical) Spectrum Comparison of Free-Field and Catenary-Field (at 1 km away, 150 ft above ground)

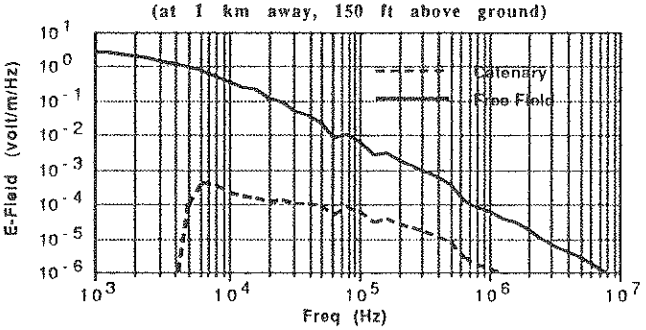

The inverse transform to the time domain of the catenary E-field spectrum is shown in Figure 3. It indicates that the E-field value at the cited particular distance lies below the maximum environmental safety level of 27 volt/m, which is a nominally quoted field for electro-explosive device (EED) of launch vehicles.

Figure 3
LEMP E-Field (vertical) inside Catenary System (at 1 km away, 150 ft above ground)

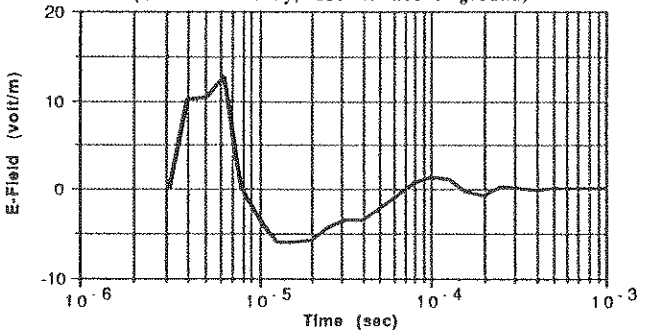

IMPROVEMENTS OF THE ELECTROGEOMETRICAL MODEL FOR LIGHTNING PROTECTION OF STRUCTURES BY MEANS OF LIGHTNING ROD CONDUCTORS

Gérard BERGER
Laboratoire de Physique des Décharges
CNRS - SUPELEC
Plateau de Moulon
91192 Gif-sur-Yvette Cedex
France

Claude GARY
Ingénieur Honoraire
Electricité de France
1 Avenue du Général de Gaulle
92140 CLAMART
France

Lightning attachment to structures consists in the junction of a downward negative leader and an upward connecting leader launched from the given structure, for instance from a lightning rod conductor. This process has been clearly demonstrated in nature or high voltage laboratory as well. However, quantitative criteria of the process remained inadequate.

The protective model at present used and advocated in the international standards derives from the electrogeometrical model elaborated by researchers of the CIGRE Working Group 33-01. This model appeals to the striking distance concept. Such a striking distance is assessed to depend only on the expected crest current intensity of the first return stroke and not on geometry parameters or electrical impedance of the grounded object.

After a review of the main features of the model at the moment, we develop in this paper a new approach of improvements which takes into account the height of the grounded objects and their capability to initiate the upward connecting discharge. This new model, which will demand further investigations in nature or laboratory, allows to validate the existing empirical relationships between the striking distance and the return stroke crest currents derived from long term observations on high voltage transmission lines. Moreover, it gives consistency to values of the upward leader inception field deduced from convenient high voltage laboratory experiments performed on various lightning rod conductors, thus solving the scaling factors problematics often put forward against high voltage laboratory simulations.

OPTIMIZING FERRITE TILE INSTALLATIONS FOR SHIELDED ENCLOSURE ANECHOIC UPGRADES

Edward F. Dyer PE
Head, Electromagnetic Test Engineering Section
NASA Goddard Space Flight Center, Code 754.2
Greenbelt, MD 20771 USA

ABSTRACT

Radiated interference and susceptibility measurements in shielded enclosures are seriously affected by the facilities geometry and the reflective/absorptive characteristics of the enclosure surfaces. Electromagnetic compatibility (EMC) tests performed at our two NASA Goddard Space Flight Center shielded enclosure facilities have often led to conflicting opinions regarding pass/fail determination of flight hardware, resulting in expensive retests and possibly unnecessary design upgrades. Excessive levels of generated radiated noise is often measured at/near room-resonance frequencies, with wide variations in levels observed dependent on test antenna locations. Susceptibility test signal levels also vary by 20-30 dB dependent on test antenna location and signal frequency, with these variations again being most pronounced at/near room resonance transmission modes.

This paper discusses the performance improvements either obtained or expected by installing ferrite tiles of different designs in three testing facilities, two of which have already been modified, and one of which is planned for modification in the 1995-6 time frame. Two of the facilities take advantage of selective tile installation at transmission nodes to minimize cost and weight involved in complete surface installations. One facility required concurrent reduction in external power line noise harmonics from entering the test area, whereas the design driver for another was the need for minimizing the inherent room VSWR when conducting 200-V/m susceptibility tests. One room is also a Class 10,000 clean room requiring special design considerations for maintaining the room cleanliness. The smallest of the rooms was completely tiled, whereas the two larger rooms were/are planned to be selectively tiled, requiring transmission mode analyses (based on Greens Theorem) to insure optimum tile placement.

Different RF bonding and earth grounding techniques were employed in the two larger rooms as well as different tile mounting techniques. The largest room modifications have not been completed, so that only design plans and goals can be presented for this room. This particular room is also planned to have false

walls of RF transparent material installed to which the ferrite tile will be mounted, so that its design parameters are unique from the other two facilities. One of the facilities is located and owned by the Westinghouse Electric Corporation in Baltimore, MD and has been in use for several years. The smaller of the NASA facilities combines carbon-loaded polyurethane wedge blocks mounted on silver-based-epoxy-mounted ferrite tiles for optimum absorption. Track-mounted rolling absorber panels front the large equipment access doors.

Electromagnetic Compatibility tests have been performed in shielded enclosures for years, in order to prevent either ingress or egress of radiated electromagnetic signals. Virtually all of these enclosures are ineffective at shielding power line harmonics. Very few enclosures offer sufficient free test space to allow installation of the larger polyurethane cones that will absorb RF energy below about 1-GHz, even if the cost, dirty environment, and limited life were acceptable. Ferrite tiles offer many advantages, but are still expensive, offer only modest absorption capability (including virtually none at frequencies below 10-MHz), and add substantially to support structure static floor loading. However, tiles do have the advantages of offering a clean environment, minimal reduction in test area available after tile upgrading of existing enclosures, and reasonable effectivity in the frequency bands that most often contribute to interference/susceptibility problems. And, when used in conjunction with the carbon-impregnated polyurethane blocks, the combination of absorbers offer high performance broadband anechoic capability, as well as a reasonable compromise on test area sacrifice.

Commercially available ferrite tile models have typically been designed for absorption of specific frequency bands - particularly, the television broadcast bands (so as to prevent commercial television signal reflections from causing ghost interference in large commercial buildings). EMC applications require a broadband absorption capability rather than the relatively narrow absorption capability of the typical tile. Consequently, for quantitative applications, it is essential that the performance of the room be well documented once the tile has been installed due to the non-linear nature of its absorption performance capabilities. Tile configurations necessary for achieving a minimum of 20-dB absorption of the three highest-level transmission modes of normally-incident electromagnetic waves in the frequency range from 30-MHz through 1-GHz were calculated using Green's Theorem for each mode and tiles were then installed on only the portion of the wall area determined necessary by the analysis.

FEASIBILITY OF TEST EQUIPMENTS FOR PRODUCING STRENGTHENED ELECTRIC AND MAGNETIC FIELDS

Pascal MEISSE*, Eric DAUCHY
GERAC
B.P. 19, 46500 Gramat
FRANCE

1. INTRODUCTION

The coupling of an electromagnetic plane wave on a conductive structure induces a tangential magnetic field $\vec{H}_t$ and a normal electric field $\vec{E}_n$ at its surface. Experiments and numerical codes showed that equipments located at the ends or the middle of great size structures (airplanes, missiles, ships, ...) are submitted to, respectively, strengthened electric or magnetic fields, i.e these fields can be up, respectively, 20 or 6 times greater than the nominal level of the incident plane wave and the equivalent wave impedance is very superior or very inferior to 377 Ω. The waveform of the strengthened fields is, in first approximation, a damped sinusoid. For instance, for the NEMP, the peak level is 50 kV/m to 1 MV/m for E field and 130 to 800 A/m for H field. The pseudo-frequency f_0 is 3 MHz to 30 MHz.
Nowadays, the test equipments for reproducing such fields need great size simulators, based on the principle of a radiated plane wave associated with a large conductive structure. They are difficult to implement and require high voltage DC power supply (more than 1 MV). To test small equipments, usually located on the previous structures, the use of these simulators is too expensive. So, two test equipments, well adapted to the experiments on such equipments, have been developped. They are easy to implement and require lower DC power supply (not exceeding 200 kV).

2. STRENGTHENED MAGNETIC FIELD TEST EQUIPMENT

The strengthened magnetic field is obtained by a resonant circuit LC. The capacitor C is variable from 50 pF to 5 nF. The inductor L is a copper foil, connected in parallel to the capacitor. The H field is confined inside the foil, what gives important levels. The equipment under test is located in the useful volume, according to the schematic diagram of the figure 1.
H and E fields have been measured in the centre of the useful volume. The ratio E/H, which is the wave impedance, is less than 0.5 Ω. The waveform of the component Hy is a damped sinusoid (figure 2). Its peak value is reported in table I, for several frequencies.

DC power supply (kV)	Pseudo-frequency (MHz)	Peak level (A/m)
5	3	595
10	10	345
10	20	180
10	26	130
10	29	110

TABLE I : H field peak level versus frequency

For each frequency, a 800 A/m H field peak level can be obtained by using a 100 kV DC power supply. To confirm this test equipment, the H field cartography inside the foil has been realized. Except for the area near the switch, the H field is homogeneous inside the volume.

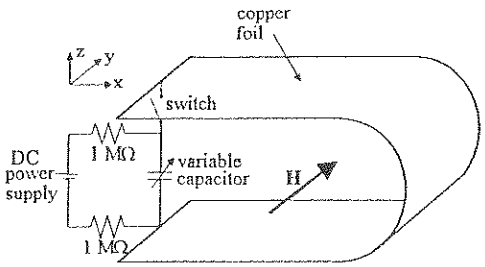

Figure 1 : Schematic diagram of the H field test equipment

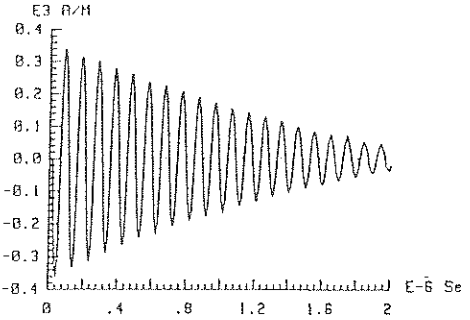

Figure 2 : H field waveform at 10 MHz and DC power supply of 10 kV

3. STRENGTHENED ELECTRIC FIELD TEST EQUIPMENT

To get a strengthened electric field, a wire structure of length L_s is used (figure 3). The structure is short-circuited at one end and is open circuited at the other one. The generator waveform is a double exponential, and is injected at the short-circuited end. The equipment (size : 30 cm x 20 cm x 10 cm) is located at the open circuited end. The resonance frequency f_r of the structure is given by the relationship :

$$f_r = \frac{c}{4(L_s + h)}$$

where c is the light velocity in the air.

For a length L_s between 1.6 m and 18 m, the frequency range is 18 MHz to 3 MHz. For this frequency range and for a 4 kV DC power supply level, the E field peak level is about 20 kV/m. This field is homogeneous in the three directions. The H field peak level is 2 A/m, what gives an equivalent wave impedance of 10 kΩ. The waveform depends on the length L_s (figure 4).

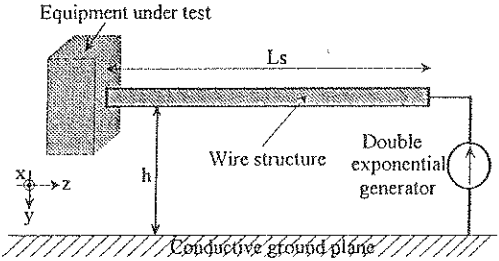

Figure 3 : Schematic diagram of the E field test equipment

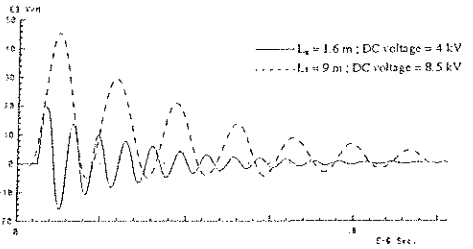

Figure 4 : E field waveform versus length L_s

By increasing the DC power supply level to 8.5 kV, the measured E field becomes 47 kV/m. So, it is proportional to DC power supply. By using a 200 kV DC power supply level, a 1 MV/m E field peak level can be obtained.

ACKNOWLEDGMENTS

The authors wish to thank the Centre d'Etudes de Gramat (CEG) which has supported this study.

NAVAL AIR WARFARE CENTER AIRCRAFT DIVISION DIRECT DRIVE: SYSTEM STATUS/RESEARCH AND DEVELOPMENT

Kurt Sebacher* and Sam Frazier
Naval Air Warfare Center Aircraft Division
Patuxent River, Maryland, USA

The Naval Air Warfare Center Aircraft Division (Patuxent River) is a lead DoD facility used for testing military aircraft to Electromagnetic Environmental Effects (E^3). Inductively coupled bulk current injection direct drive test techniques are used to determine, characterize, or develop subsystem strength as part of a system level test. Bulk current injection direct drive testing is further used to quantify the aircraft's survivability or characterize vulnerabilities. The test sequence involves stimulating the system in a free field electromagnetic environment while measuring desired test point waveforms (stress). The waveform is then reproduced and amplified to threat/threat plus margin levels and induced on the desired test point. Upset levels (strength) are then determined. The margin of strength over stress determines the subsystems level of survivability.

The use of inductively coupled bulk current injection direct drive testing has many roles in the Navy's E^3 program. E^3 survivability disciplines such as MIL-STD-461/462, lightning, EMP, EMR/EMV, HPM, and UWB either use direct drive testing or may in the near future. The emergence of state-of-the-art arbitrary waveform generators, high powered broadband amplifiers, efficient broadband couplers, and powerful data processing tools have enabled the Navy to develop a wideband direct drive capability that precisely reproduces composite waveforms. The direct drive development goal of the Navy is the capability to combine all available E^3 stress response data into a single bounded stress envelope. Then adequately recreate this envelope in single events and amplify to levels which demonstrate survivability or characterize strength. To reach this goal the Navy has embarked on several research efforts. This paper will discuss these efforts.

The idea of inductively coupled bulk current injection direct drive testing though simple in concept has been difficult in execution. Exact waveform replication along with frequency and amplitude limitations have hindered the effectiveness of this test technique. However, some recent findings at the Naval Air Warfare Center Aircraft Division, Phillips Laboratory

(USAF) and Kaman Sciences have enabled bulk current injection direct drive to become more effective. The direct drive system has been outfitted with a new arbitrary waveform generator, a larger wattage amplifier, and custom built couplers. Signal processing techniques are used to enhance the drive waveform for better waveform replication and test effectiveness. Test waveforms are exactly replicated using load impedance measurements and a real time normalization process.

MIL-STD-2169A bulk current injection direct drive test capability has been achieved through a joint effort between the Navy, Phillips Lab and Kaman Sciences. Arbitrary waveform generators are limited in high frequencies to 200 MHz. A new technique has been developed in which the output of a white noise source is conditioned to provide a high frequency broadband signal. The waveform is designed by (frequency varying) filtering the white noise spectrum followed by (time varying) pulse modulation of the continuous filtered noise signal. The prototype system is being tested at Phillips Laboratory and the Naval Air Warfare Center Aircraft Division (Patuxent River). Upgrades to be considered for future versions include a series of filters or "super graphic equalizer" for more control of waveform shaping.

The improved bulk current injection direct drive system has allowed the Naval Air Warfare Center Aircraft Division (Patuxent River) to verify the compliance of DOD aircraft to E^3 threats more efficiently and effectively. Aircraft subsystem's margin of survivability/vulnerability can now more easily be determined.

Several direct drive issues still need to be investigated and resolved. Pulse forming networks need to be developed to increase the amplitudes used for lightning direct drive testing. Coupling methods such as radiated, direct, distributed, and differential will be researched and tested to increase test correlation confidence. The use of multiport/multisource direct drive testing will also enhance correlation. Bulk current injection direct drive testing is fast becoming an accepted and widely used test method. Modernizing an existing direct drive system will significantly improve E^3 test capabilities.

A NEW TECHNIQUE FOR HIGH FREQUENCY DIRECT DRIVE BASED ON A WHITE NOISE SOURCE

S. Frazier* and K. Sebacher
Naval Air Warfare Center, Aircraft Division
Patuxent River, MD

D. Lawry and W.D. Prather
Phillips Laboratory/WSR
Kirtland AFB, NM

G.I. Hoffer, S. Kokorowski and D.P. McLemore
Kaman Sciences Corporation
Alameda, CA; Santa Monica, CA and Albuquerque, NM

Direct drive techniques have long played an important role in the study of the effects of electromagnetic environments on electronic systems. In the past a commonly accepted method for determining conducted susceptibilities has been the injection of single damped sinusoids. However, this approach is inadequate for the simulation of broadband transients. The more recently developed technique employing arbitrary waveform generators (AWGs) has not been extended to high frequencies due to hardware operating speed limitations. In this paper a new technique is discussed in which the output of a white noise source is conditioned to provide a high frequency, broadband signal suitable for direct drive testing.

Commercial white noise sources, based on semiconductor diodes, are available and are commonly used in testing and ECM applications. These sources can provide various bandwidths with frequencies ranging from less than 1 Hz to greater than 100 GHz. Products extend from bare diodes to fully integrated, programmable noise sources. The output from one of these devices is a continuous signal with time domain amplitudes varying randomly according to a Gaussian distribution. These characteristics lead to a nearly constant frequency domain magnitude (over the bandwidth of the source) and a randomly varying phase.

A prototype noise source generator has been constructed for evaluation in direct drive applications; a block diagram of this system is shown in Figure 1. The source is a Noise Com NC 6110, which has an white noise output flat to ±2.5% from 100 Hz to 1.5 GHz and a total output power of 10 dBm. An example of the measured output from this unit is show in Figure 2. The filter is any one of a number of simple filters constructed in the laboratory. These filters have center frequencies ≥100 MHz and roll off above and below the peak at 20, 40, or 60 dB/decade. The choice of filter depends on the general shape of the coupling spectrum to be simulated. The pulse source used to provide the waveform envelope is either a square wave generator and a pulse-forming filter or an arbitrary

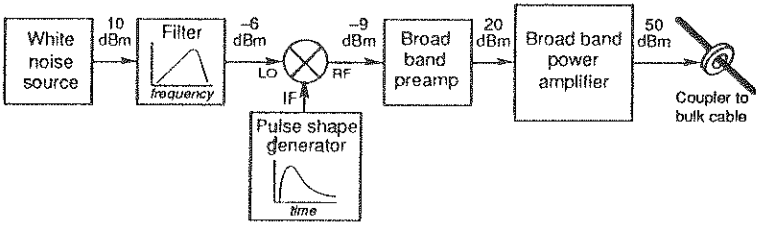

Figure 1. Block diagram of prototype white noise source direct drive generator.

waveform generator. The filtered white noise and the pulse envelope are fed into the LO and IF ports, respectively, of a double balanced mixer with rf bandwidth of 10 MHz to 1.5 GHz. The pulse modulated noise signal appears at the RF port of the mixer. This signal is then amplified to the desired level, and fed into a broadband (>1 GHz) inductive coupler for injection onto a test article cable. The approximate power levels at each stage in this process are indicated in the diagram.

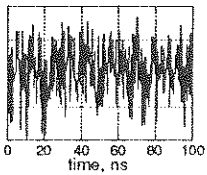

Figure 2. Output of Noise Com white noise source.

The measured transfer function of one of the filters employed is shown in Figure 3a. The effect of this filter on the white noise signal is illustrated in Figure 3b. Finally, Figure 3c shows an example of the pulsed waveform obtained when the filtered white noise is modulated with an envelope shape generated by an AWG. The transfer function for a filter with a higher frequency peak is given in Figure 4a, and an example of the resulting pulse-modulated waveform is shown in Figure 4b.

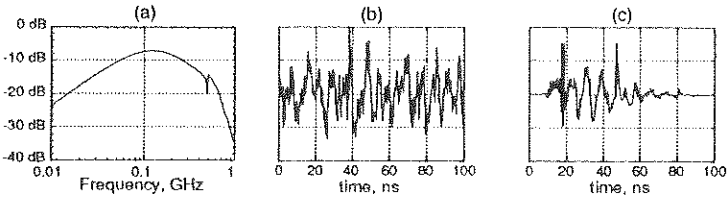

Figure 3. (a) Magnitude of filter transfer function with peak at about 100 MHz. (b) White noise signal after passing through 100 MHz filter. (c) Filtered noise after pulse modulation.

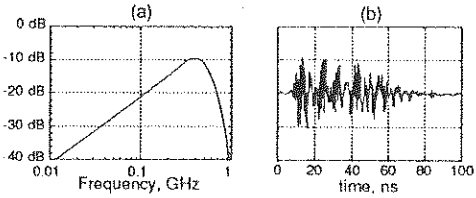

Figure 4. (a) Transfer function magnitude for filter with peak at 400 MHz. (b) White noise signal after 400 MHz filter and pulse modulation.

The random character of the white noise signal results in considerable pulse-to-pulse variation in the output waveforms. The waveform norms, however, are relatively constant. For example, the standard deviation is typically about 20% of the mean for the peak amplitude and about 10% for the root action integral. The random variation of the details of the direct drive waveforms may even be beneficial for the simulation of coupled transients at high frequencies where coupling exhibits a random behavior.

COMPACT TRAVELLING-WAVE ESD SIMULATOR

L. M. MacLeod* and K. G. Balmain
Dept. of Electrical and Computer Engineering
University of Toronto, Canada

The electrostatic discharge (ESD) simulator under consideration in this work represents the human body. An ESD event can contain high frequency components (associated with a fast risetime). Since the body acts as a distributed system at high frequencies, the traditional lumped-element ESD simulators cannot adequately represent the high frequency response. A travelling-wave approach is thus required. A travelling-wave ESD simulator has been constructed from a lossy dielectric material (Eccosorb VF-60), and the ESD waveform generated by this simulator has been found to compare well with the human ESD event.

The drawback of the travelling-wave ESD simulator is that the simulator is large, since its dimensions must be comparable with those of the human body. The purpose of the work presented here is to determine whether the travelling-wave ESD simulator can be made smaller without affecting its discharge properties. The resulting compact simulator would be more convenient for equipment ESD susceptibility testing than the full-size simulator.

Figure 1 shows the travelling wave ESD simulator in its original state and with a shortened arm and a compacted body. The full-size simulator consists of a finger (9 cm by 1 cm), an arm (60 cm by 5 cm) and a body panel (130 cm by 60 cm). The discharge site is at the finger tip. The work presented here does not consider the ESD arc itself, focusing instead on the representation for the human body.

The focus of the compaction process is the simulator arm. Since the simulator material (and the human arm) is lossy, the ESD current waveform attenuates as it propagates along the arm. If the signal attenuates very rapidly, the arm can be shortened since the currents at the end of the arm would be very small. In this work, signals in the range from 100 MHz to 6 GHz are considered. Below 100 MHz, the ESD simulator arm is much shorter than a wavelength and thus the travelling-wave effect is not so important.

A thin-wire Method of Moments computer program is used to predict the currents flowing on the ESD simulator arm. The arm is represented by a wire grid loaded with resistors and capacitors. Results are verified by comparing the computed results with measurements made with a vector network analyzer. Both one-port and two-port comparisons are made. Port 1 is at the finger tip (where the discharge occurs) and port 2 is on a square loop probe that is next to the simulator arm (and can be moved parallel to the arm).

The computed results show that at high frequencies (6 GHz) the current

attenuates very quickly, and thus the simulator arm can be shortened considerably. However, at lower frequencies (100 MHz) the current does not attenuate so rapidly. Based on the simulation results, a truncation point for the simulator arm is determined (the shortened arm is 30 cm long). Measurements confirm that the full-size arm can be replaced by the truncated arm (see Figure 2). The body of the compact ESD simulator is then reduced in area to maintain the same capacitance as the full-size simulator. Measurements confirm that with the simulator body attached to the arm, the simulation is still adequate. Thus it has been shown that compaction of the travelling-wave simulator is feasible.

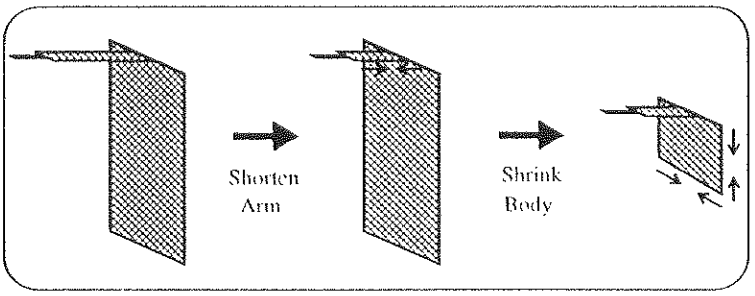

Figure 1. Travelling-wave simulator compaction process.

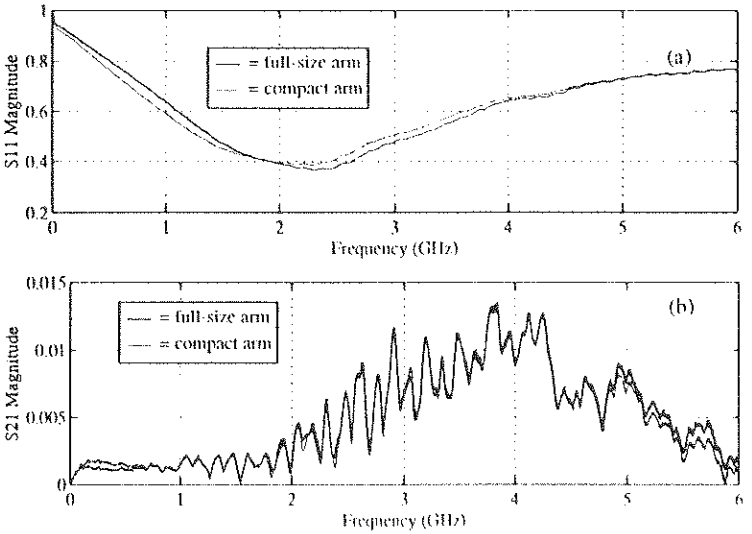

Figure 2. Verification of arm truncation point: (a) reflection coefficient at finger tip; (b) two-port measurement between finger tip and loop probe that is 25 cm from the finger tip.

SPHERICAL NEAR-FIELD FACILITY FOR MICROWAVE COUPLING ASSESSMENTS IN THE 100 MHZ- 6 GHZ FREQUENCY RANGE

Ph.Garreau, G.Cottard, F.Lucas
SATIMO, Le Pin, rue de la Terre de Feu, ZA Courtabœuf
91952 Les Ulis, France

J.Ch.Bolomey
SUPÉLEC, Electromagnetics Department, Plateau de Moulon
91192 Gif-sur-Yvette Cedex, France

ABSTRACT

Microwave coupling assessments require specific equipment. Indeed, as it is now well known, coupling cross sections are very sensitive to parameters such as incidence angle, frequency and polarization. Accordingly, the operational conditions corresponding to the worst vulnerability cases have to be carefully determined before conducting high power testing. For this reason, at least two levels of investigation must be considered. The first one is devoted to low power coupling measurements while the second one corresponds to true scale assessment within conditions as close as possible to the expected threat. The first phase has been shown to be efficiently conducted via Near-Field techniques. A Near-Field spherical facility, SOCRATE, has been designed and realized for the Centre d'Études de Gramat (CEG/DGA) for this special purpose. Initially devoted to the 100 MHz- 4 GHz frequency band, the equipment has been successfully used up to 6 GHz.

This paper presents the architecture of the Near-Field facility and its associated equipment. Basically, SOCRATE allows to make Near-Field measurements on a 4 meters diameter sphere which is convenient to test objects up to 2 meters long. Such a probing geometry is obtained by combining the rotation of the object under test around the polar axis, while field measurements are performed on a semi-circular arc. After one revolution of the object under test, the Near-Field distribution is known on a sphere. Two probing schemes are used, according the frequency range. In a "low" frequency range extending from 100 MHz to 1 GHz, the measurements are performed with a single probe, which consists of two orthogonal resistively loaded dipoles. The probe is mounted on a carriage moving on a circular mechanical support. The probe is connected to an HP 8510 network analyser. For the "high" frequency range, extending from 1 GHz to approximately 6 GHz, a modulated probe array is used to speed up the duration of the measurements. The probe array consists of 128 dual-polarized elements, consisting of short crossed dipoles loaded by PIN

diodes. According to the modulated scattering technique, the modulated signal resulting from the On-Off switching of the diodes is collected by an array of spiral elements. The output of the collector array is connected to the microwave receiver. The microwave signal is converted to an intermediate frequency of 20 MHz by means of an HP 8510 network analyser. Then a double coherent detection is performed, successively, at the intermediate frequency and at the modulation frequency. The use of a probe array is paricularly convenient for the "high" frequency band for which the number of measurement points become high. Indeed, if D is the diameter of the smallest sphere, centered on the center of the facility and surrounding all the object under test, the number of points of measurement is roughly $e\pi D/2\lambda$. For example, for a 1 meter long object, the time required to explore one frequency is 3 minutes at 3 GHz. As compared to the mechanical scan velocity which is 10 cm/s in the "low" frequency range, the modulated probe array provides 200 equivalent cm/s at 3 GHz. Coupling cross-sections have been measured on generic objects with simple shapes and on true scale missile subsystems. Typical coupling cross sections of the order of 10^{-6} cm^2 can be measured.

Initially devoted to coupling cross-section measurements, the SOCRATE facility has found a broader field of applications in the domain of microwave coupling measurements. As shown in a companion paper, the Near-Field data can be processed in view of the diagnostic of complex radiating objects to determine their Ports Of Entry (POE). In addition, SOCRATE proved to be very usefull for microwave metrology general purposes. The different antennas to be associated with high power sources devoted for high power assessments can be fully characterized: the field distribution at the test object location can be easily determined from measured Near-Field data, making possible to evaluate the microwave field homogeneity in the test area as well as the leakage to be expected and the identification of the most hazardous areas which will require adequate protection through absorbers or shieldings. Furthermore, the bandwidth of SOCRATE allows broad frequency band operations, including in-band and out-of-band characterizations. The flexibility of SOCRATE Near-Field facility will be illustrated by several examples relevant to microwave coupling configurations.

CHARACTERIZING THE TIME DOMAIN ELECTROMAGNETIC FIELDS OF A WIDE ANGLE BICONICAL ANTENNA RESTING ON A GROUND PLANE

John G. Stewart* and Bruce T. Benwell
United States Army
Army Research Laboratory
ATTN: AMSRL-WT-ND
2800 Powder Mill Road
Adelphi, MD 20783

ABSTRACT

The US Army Research Laboratory (ARL) has designed a second generation vertically polarized high altitude electromagnetic pulse (VEMPS II) simulator to simulate a fast risetime EMP environment. The VEMPS II simulator consists of a vertically oriented biconical antenna resting on earth ground. The simulator's antenna is approximately 30m in height with a diameter of 15m.

While awaiting the fielding of this simulator, ARL, in conjunction with the Centre d'Etudes de Gramat (CEG) at Gramat, France, has performed a series of experiments on a 1/10th scale model (SM) of VEMPS II as part of a USA/French Data Exchange Agreement (DEA-A-80-F-1265). The goal of these experiments was to determine the necessity of resistively loading the antenna as well as to characterize the EM environment within the simulators projected test volume.

The first phase of this effort consisted of using continuous wave evaluation techniques to characterize the EM fields and radial current distribution generated by this antenna with and without resistive loading. The results of this effort were presented at NEM'91.

The second phase of this effort, to be reported at this time, consisted of performing a comprehensive characterization of the time domain EM environment within the projected test volume, with and without resistive loading. For these tests the antenna was driven with a fast risetime pulse source. Fields were also measured above and at large distances from the antenna for environmental reasons. Figure 1 shows the simulator's test volume as well as the test points needed to achieve the test objectives.

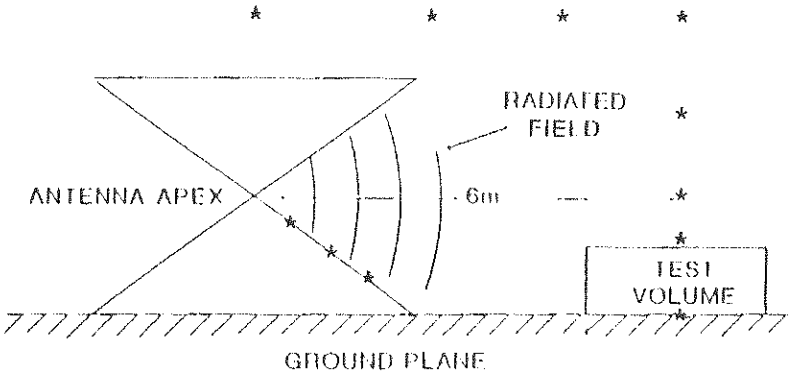

FIGURE 1. VEMPS II SCALE MODEL RESTING ON GROUND PLANE

* TEST POINTS

This paper discusses the experimental program, methodologies used to assure that valid data were collected, and the results of the phase II time domain field measurements.

SIMULATION ADEQUACY LEVELS AND THE CORRECT CHOICE OF TEST PULSES PARAMETERS

Andrey E.Serebryannikov*, Loudmila V.Vavriv, Larisa A.Matsokina
Molniya Research and Engineering Institute
Kharkov, Ukraine

The correct choice of test pulses parameters are one of the main problems in the EMC theory and practice. The parameters should be chosen proceeding from the requirements of the tests' adequacy to the natural conditions, under which the object is subjected to the influence of powerful electromagnetic noises. This problem is especially vital for the tests of aerospace engineering objects, where the requirements of reliable functioning of equipment are the highest. The peculiarities of electromagnetic situation (EMS) shaping and mutual correlation of different effecting mechanisms should be taken into account during the choice of pulses' parameters and simulation methods.

The set of terms is suggested which serves as a basis for the correct methodological approach to the choice of simulated fields' parameters, test rigs and techniques. For the radio electronic equipment carrying objects subjected to the tests on the whole we shall introduce the following notions. The complete adequacy is a complete reproduction of EMS and of the operational conditions in the simulator. In the most practical cases this level can be realized only approximately (approximate complete adequacy). It's connected with the improbability of consideration of all factors during simulation that influence the EMS shaping under natural conditions. This type of adequacy is realized through the choice of relationship between the dimensions of the test object and dimensions of the shaping-system of the simulator.

The partial (local) adequacy is a simulation of natural EMS on a local area of surface or on a local part of volume. It can be locally accurate. The realization of this level is performed through the synthesis of the natural EMS in the field shaping system of the simulator by the choice the parameters of test pulses under the prescribed geometry of field shaping system. It was shown that the problem of a synthesis can be solved for some envelopes of peculiar geometry during the tests in the simulators with guided waves.

The extreme adequacy takes a separate place. The realization of this level presupposes that parameters of the simulated EMS are no less dangerous comparing with the case of natural conditions. This level has a sense only in the case when the tested object contains only linear or quasilinear circuits and elements or when nonlinear elements have characteristics under which the amplification of the external field doesn't lead to the decreasing of currents and fields levels that directly effect the inputs of the elements used in radioelectronics.

The external adequacy presupposes the equality of the fields' components on the surface of the screening envelope both during operation and simulation. Its realization can be required for the envelopes where small irregularities are the main passes for the inside penetration of noises. The external adequacy can be both complete and partial.

The internal adequacy presupposes that EMS inside the screening envelope in the same during the simulation as in case of operation; the external EMS may not correspond to the operational conditions. It also can be complete or partial. "Element by element" adequacy is a simulation of currents and fields' parameters producing destabilizing action directly on the input of the separate radioelectronics' elements similar to those in the natural conditions.

The choice of the pulses' parameters and of the test technique is performed depending on the adequacy level to be realized. The correct approach to these problems presupposes the availability of the reliable experimental and calculation estimations of EMS in the natural conditions. These estimations can result in the averaged parameters, the most probable or the worst (for example, experimental data for LEMP). The use of the worst parameters has a sense only in a case of availability of linear or weak nonlinear elements and circuits. Otherwise, it is necessary to take into consideration the statistical character of noises through the multiple action on the object during simulation; the parameters of the pulses vary in some range, peculiar for the given type of noises. This test technique is the most universal. Since the process of EMS shaping in the natural conditions has a statistical character (the process of lightning discharge shaping, for example) the test technique is very promising. It presupposes the modeling of probabilities' distribution law close to the prescribed one in the same modeling installation. The alternative approach is based on the use of pulses' generators that have narrow spread of parameters in comparison with the characteristic width of the curve of the probabilities' distribution of noise parameters. In this case the simulators must provide for the possibility of parameters' rearrangement, for example, using the correcting circuits.

The radioelectronic equipment carrying objects have been subjected to the tests both in whole and for the separate elements and units. The necessity of the whole object tests is stipulated by the impossible consideration of mutual correlation of all factors of interaction of elements and circuits. On the other hand, the complexity of the simulation of powerful fast transition electromagnetic fields in large volumes are compensated by the possible of producing of more rigid parameters (from the point of view of action on radioelectronics) in smaller volumes. Therefore, it is recommended in practice in general case to the subject aerospace objects to the tests by the multiple action on the whole object and on the separate (the most important) units and blocks, but at more rigid parameters. One of the ways to predict the levels of currents and fields, affecting directly the radioelectronic elements are a physical modeling (including scaled modeling in time and space). The mathematical modeling gives reliable results only in a limited number of cases. The necessity of realization of one of the described levels or techniques is stipulated by many factors including the degree of rigid requirements for the equipment being operated.

HIGH ENERGY CONDUCTED DISTURBANCES IN THE TELECOMMUNICATION CUSTOMER PREMISES

B. Djebari* , L. Guerin , M. Gleonec

FRANCE TELECOM/CNET/LAB/QFE
Route de Trégastel, BP 40
F - 22300 LANNION CEDEX

Summary - This paper presents the statistical results of the CELSIUS project launched by France Télécom, by September 1992, in nine customer premises. The conducted high energy disturbances stressing Telecommunication Terminal Equipment (TTE) in customer premises, are measured simultaneously on telecommunication and mains ports, through the common and differential mode voltages (up to 10 kV peak). A large data base is already available and processed to give statistical results.

1. GENERAL

Telecommunication networks are widely exposed to high energy disturbances which are lightning and induction. In France, the network distribution is made mainly in the countryside, by overhead cables and, is often close to power lines (along the roads), source of induction. It can be noticed that induction on telecommunication lines is always severe for the equipment.

In the stormy season many equipment are damaged mainly by the nearby lightning return stroke, inducing by the mean of the EM field, common mode disturbances in the cables. Direct stroke to telecommunication lines is uncommon and, when it happens, causes big damage to the cables and to the connected equipment.

The network operator has to guarantee the safety of people, the protection and the immunity of the network equipment. This is can easily be achieved by a better knowledge of the EM environment. Statistical analysis is very useful for the optimisation of the EM requirements and the cost of the equipment.

Few years ago France Télécom had conducted COPELIA project in telecommunication centres, in order to have statistical knowledge of the high energy conducted EM disturbances on the subscriber lines. This study had given the statistical distribution of the parameters of the lightning pulses(peak voltage, rise time, duration) and of he induction from power lines.

At the subscriber side the Telecommunication Terminals Equipment (TTE) were mainly simple telephone sets stressed by conducted disturbances only on the telecommunication port. Today most of the TTE are sophisticated electronic equipment powered locally by the mains and then, submitted also to conducted disturbances on this port

European directives for TTE made a separation between the public network area and the customer side. European standards give the requirements of TTE in the field of safety and EMC. Then, it is clear, today the responsibility of the network operator becomes strong in terms of control of the disturbances coming in the customer promises, especially when the safety of people is involved.

2. CELSIUS PROJECT

In order to have a statistical knowledge of the conducted electromagnetic disturbances stressing the TTE in the customer premises, France Télécom launched in September 1992 a national measurement campaign called CELSIUS project. Nine modified Transient Monitoring System (TMS) recorders made by the Australian KEL Aerospace Company had been installed in nine customer premises measurement sites spread in France (see figure 1). The recorder is designed to measure mainly, lightning and induction pulses. The four channels of the recorder are configured with the help of high voltage probes, to measure, up to 10 kV peak, the conducted common and differential mode disturbances on the

telecommunication and the mains ports. Switching pulses on the mains can then also be measured. Each TMS recorder has 30 minutes battery backup, modem, and is controlled, through the switched public network, by a computer located in Lannion. The data transfer is programmed each two days.

3. STATISTICAL RESULTS

A data base of thousands of events is available now including the stormy end of September 1992 and the complete 1993 stormy season. It is processed to give the statistical results on the telecommunication and the mains ports.

The figure 2 shows the cumulative distribution of the events (trigger event on at least one channel), on the telecommunication line along the year for the nine measurement sites. It can be noticed that the number of the events increases in the stormy season.

This paper presents the details of the CELSIUS project statistical results on telecommunication and mains ports. Transient records like lightning and induction on telecommunication line; and lightning or switching on mains are described statistically by their parameters (peak amplitude, dv/dt and time duration).

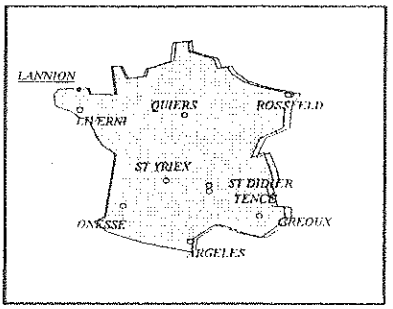

Figure 1 : CELSIUS project measurement sites location

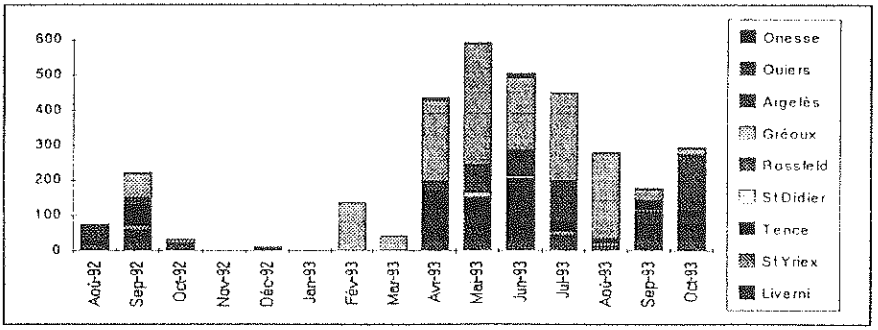

Figure 2 : Cumulative distribution of the events on the telecommunication ports during the year.

MEASUREMENTS OF RADIATED ELECTROMAGNETIC DISTURBANCES GENERATED BY HIGH-SPEED TRAINS IN SPAIN

Crespo R.(*), Soto F., Sancha J.L.	REE
Sánchez S., Lafuente A.	ASINEL
Ruiz J.L., Fernández C.	SEVILLANA DE ELECTRICIDAD
Amantegui J.	IBERDROLA

REE is RED ELECTRICA DE ESPAÑA, S.A.
Pº del Conde de los Gaitanes, 177
28109 - Alcobendas (MADRID)
SPAIN

The high-speed train (AVE), from Madrid to Sevilla (470 km), is in operation since April 1992. AVE is feeding by three HV transmission lines at 220 and 132 kV level. These three lines are exclusively devoted to the electric supply of the catenary, done with a rate voltage of 25 kV AC through single-phase 20 MVA transformers 220/25 or 132/25 kV, placed in nine 220 kV substations (along 332 km) and three 132 kV substations (along 138 km).

The level of the electromagnetic interferences generated by the AVE varies depending on electric current, train speed, distance from railway, weather conditions, pantographs and contact wires (Sancha J.L. et allia, PQA'92, Atlanta USA, Sep. 1992 and Power System Electromagnetic Compatibility, CIGRE Symposium, Lausanne, Oct. 1992).

Due to a supply of these characteristics is used for the first time in Spain, there is not any Spanish technical standard that fixes the maximum levels of the disturbances caused by high-speed trains.

Because of AVE is the first high-speed train running in Spain, REE (responsible of the Spanish System Network), SEVILLANA and IBERDROLA (private electric utilities) and ASINEL (Spanish laboratory) are developing a research project in order to evaluate AVE disturbance impact.

The present paper describes the metodologhy and the equipments used on the radiated disturbances measurement.

The metodologhy is based on the electric (E) and magnetic (B) fields measurement, and includes two steps: firstly, it is carried out one spectrum analysis to determine the frequencies that appear in greater disturbances and after that, selective receivers are used on studying the interference signals in each frequency. Likewise, magnetic field (B) is measured at 50 Hz frequency.

The measurements were obtained close to the railway, outside and inside the supply substations.

The results obtained of these measurements are presented and compared with international suggested values and another experiences with high-speed trains in Europe.

CONDUCTIVE INTERFERENCE OF ELECTRIC RAILWAYS ON CIRCUITS WITH EARTH RETURN

Wojciech Machczyński
Technical University of Poznań, Poland

1. Introduction

The electromagnetic compatibility of the components of electric traction system is a criterion participating more and more in the decisions of network planning and operation. Acceptance or inadmissibility of the effects of electric railway systems on nearby earth return circuits (cables, pipelines) requires the quantification of these physical effects.

Electric railways can generally affect nearly earth return circuits through two different mechanisms : inductive and conductive couplings. The inductive coupling has already been accurately studied in a number of publications, whereas some aspects of the conductive coupling should be investigated.

Existing mathematical algorithms for the computation of a conductive interference from external flow field on nearby underground earth return circuits can only deal with rather simple field and circuit configurations.

The purpose of the paper, which is a continuation of previous considerations of the author, is to present a method able to simulate the conductive interference of any given complexity from external electric flow field produced in the vicinity of the electrified railways.

A method of calculation is based on a copmplete field method of solution of the transmission-line problem. The analysis given is applicable to any railway system in which tracks may be represented by a single earth return circuit with current energisation. It is assumed in the paper that the system considered is linear, that the earth is homogeneous and that the effects of currents in the underground installations on the track current can be disregarded. Quasistationary behaviour is assumed implicitly. The technical application of the method is illustrated by an example of computer simulation.

2. Scalar potential in the earth due to current in conductor with earth return

The knowledge of the earth potential of the electric flow field in the vicinity of the tracks is required for the method. The potential may be obtained by means of the technique used in the earth return circuits theory, when the conductor with longitudinal current flow is considered.

The distribution of the longitudinal current depends on the mode of the current excitation in the conductor. In the stray current theory the current (shunt) energisation of the conductor with earth return lying on the surface of the earth, Fig.1a, is of great importance.

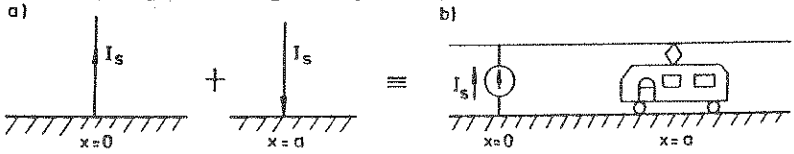

Fig.1. Basic circuits. a) Current energisation of the conductor with earth return, b) electrified railway system

The relation of the potential in the earth owing to the current flowing in the conductor with the current energisation is numerically solved only. Efficient techniques of calculation have been applied in the computation algorithm developed.

3. Model of an electrified railway system

The system shown in Fig.1a may be applied directly by superposition in building up electrified railway system as in Fig.1b. In this system tracks are represented by a single conductor - equivalent to a rail continuously in contact with the earth through the track ballast. The conductor is energised with the currents I_g and $-I_g$ by a feeder station and a load at points $x = 0$ and $x = a$, respectively.

It should be noted that the basic model may be applied directly by superposition if there are a number of loads to be considered.

4. Computer results - example

The usefulness and efficiency of the computation algorithm developed shall be demonstrated by the example of a pipeline buried in a DC stray current area. The pipeline $L = 3.6$ km with the parameters $\Gamma = 0.208$ 1/km and $Z_0 = 0.68\ \Omega$, terminated at end points through resistances 1 and 2 Ω, is buried at the depth $d = 1$ m in the soil with the conductivity $\kappa = 0.01$ S/m.

The potentials and the current (per unit of feeder station current) along the pipeline have been calculated and shown in Fig.2. The earth potential V_E due to stray currents of the DC electrified railway system has been also shown in the Fig.2.

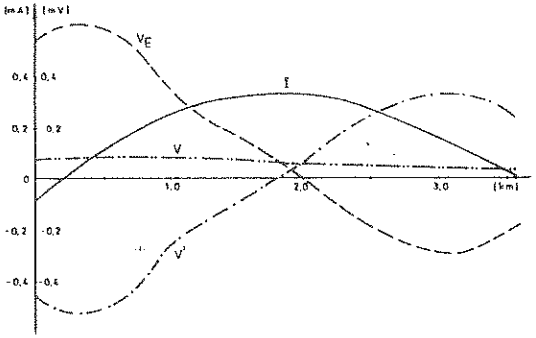

Fig.2. Potential and current distributions in the pipeline due to stray currents

Fig.2 shows that the potential difference between the pipeline and the sorrounding soil (V') exceeds in any points the tolerable corrosion limit i.e. + 100 mV ($I_g \geq 500$ A). The protective measures should be undertaken to avoid the stray current corrosion of the pipeline.

5. Final remarks

A method and a computer program have been developed for the calculation of the potential distribution in a system of underground metal installations buried in the vicinity of electrified railway systems.

The computer simulation of the harmful effects that the electric traction may have on nearby underground structures may be useful in planning of localisation of the installations affected by stray currents and in designing the protective measures against the stray currents as well.

The extensive parametric analysis to examine the roles of various factors which affect the interference levels caused in extensive metal underground conductors by conductive effects may be performed using the method described.

A MODEL FOR EXAMINING ELECTROMAGNETIC PERTURBATIONS AND INTERFERENCE IN TELECOMMUNICATIONS SYSTEMS

Dr. Fred J. Ricci
Virginia Tech
Northern Virginia Graduate Center
2990 Telestar Court
Falls Church, VA 22042

Abstract:

The problem of Electromagnetic Perturbations and Interference in Telecommunications Systems as been of concern in telecommunications systems for years.

Recently, we have developed a number of computer simulation models to help analyze the Electromagnetic effects in telecommunications systems. These models were developed for both commercial and military systems to examine such phenomena as: power transients, multipath interference, phase and amplitude perturbations, atmospheric absorption losses, etc.

The results of the simulations have enabled recommendations to be made regarding hardening, protection and maintenance. Listed below is a summary of some of the phenomena simulated.

1. Phase Perturbations. This research considered the causes and effects of phase perturbations in a telecommunication system. It involves the generation of waveforms via various modulation techniques and the susceptibility of these wave forms to phase perturbations. It also discusses the effect of the phase variations on signal transmission and demodulation.

2. Amplitude Perturbations. This research considered the causes and effects of amplitude perturbations in a telecommunication system. The intent of this was come to address those phenomena which are external to the systems themselves. Examples of these phenomena are multipath interference, rain attenuation and atmospheric absorption losses.

2.1 Multipath Interference. This research considered the effects of electromagnetic energy reaching a receiving antenna by multiple paths. This phenomena addressed the following cases:

a. Interference due to specular reflections from the ground or other obstructions in the path of the electromagnetic energy propagation.

b. Atmospheric conditions causing frequency selective fading due to multiple paths propagating through the atmosphere.

3. System to System Interference. This research considered the interference caused by one telecommunications system to another. Specific topics under this category will include fundamental frequency interference, harmonic frequency interference, intermodulation interference and antenna coupling. Radio Frequency (RF) characteristics of all system components (transmitters, receiver and antennas) were addressed.

3.1 Receiver RF Characteristics. This research addressed the RF characteristics of a receiver such as demodulation, receiver sensitivity, receiver bandwidth and receiver rejection.

3.2 Transmitter RF Characteristics. This research addressed the RF characteristics of a transmitter output power and transmitter bandwidth.

3.3 Antenna RF Characteristics. This research addressed the RF characteristics of an antenna such as gain, directivity, beamwidth and polarization.

3.4 Antenna Coupling. This research addressed the degree of coupling between system antennas. This coupling will be determined by antenna polarization matches/mismatches, antenna gain in the direction of other system and physical separation of the antennas.

4. Fundamental Frequency Interference. Systems which have the same operational frequency will typically interfere with each other if located in close proximity. This research addressed degrees of interference encountered based on system component RF characteristics.

5. Intermodulation Interference. Nonlinear characteristics of transmitting systems can cause intermodulation products to be generated. These products can cause interference to a receiving system. This research addressed degrees of intermodulation interference encountered based on system component RF characteristics.

As a result of the simulation carried out in this research, a number of recommendations are made with regard to hardness, protection and maintenance. Specific results resulting from this research effort will be presented at the symposium.

PROPAGATION OF ELECTROMAGNETIC INTERFEREN CAUSED BY HV LINES

L.Jermendy
Institute for Electrical Power Research
Budapest, Hungary

Interference on transmission lines can occur both as a result of corona on conductors and due to partial discharges and corona on insulators, breakdown and spark-over of defective insulators, corona on line fittings, as well as due to sparking in bad contacts of line fittings and insulators in strings. Measurements on transmission lines have shown that in a number of cases line fittings and insulator strings are interference sources in the presence of gaps and sharpened elements. Discharges occur between metal parts with bad contacts. These bad contacts may be caused by corrosion, dirt and dry pollution.

A large number of capacitive discharge type sources were found at one section of the double circuit 400 kV transmission line. The propagation of the summarized TVI signals are shown in Fig.1.

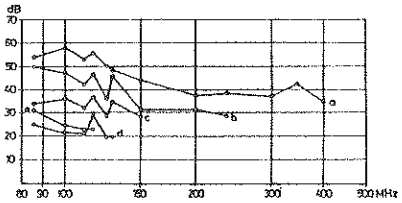

Fig.1. Attenuation of TVI along the 400 kV transmission line
Curve a - sources on both circuits
b - sources only on the circuit near to the antenna
c - at a distance of 180 m from the last source
d - at a distance of 560 m from the last source
e - at a distance of 1200 m from the last source (influenced by other sources)

The plotted values indicate the strong interference propagating more than 1 km along the line. If on both circuits many discharges appear, disturbing values can be recorded in a wide frequency range up to 400-500 MHz.

The electromagnetic vawes generated by small discharges on high voltage propagate also in the direction perpendicular to the line, and therefore can disturb the reception far from the transmission line as well. In the worst situation the reception arial has to be directed into the line if the transmitter is over it.

Usual values of TVI as a function of frequency are shown with the parameter of the distance in air. From the given four curves of Fig. 2. the attenuation of air at higher frequency can be estimated.

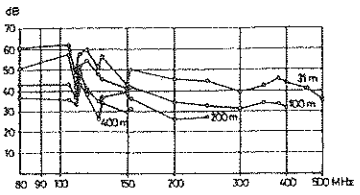

Fig.2.Frequency spectra of TVI generated by gap discharges on the 400 kV transmission line

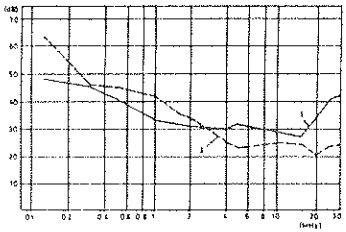

Fig.3. Lateral profiles of interference from 400 kV transmission line lines at 0,5 MHz (1 - for lines with defective spacers, 2 - for lines with corona on conductors, 3- calculated characteristics taking accoun of corona on conductors; seé formula)

The gap discharge generates interference which holds a considerable level at a great distance from the line. Values obtained from measurements on operating lines are a sum of interference from various sources. Fig.3. shows lateral profiles of interference from double-circuit 400 kV lines with delta-phase arrangement at 0,5 MHz. Curve 1 was obtained for a line with defective spacers. Curve 3 was plotted on the basis of calculations according to the well-known formula:

$$E''_n = E'_n + 20\ k \log R'/R''$$

where

E'_n, E''_n - interference level,
R', R'' - distances from the nearest phase of the line,
k - the lateral attenuation factor.

Based on the measurement results obtained on 400 kV transmission lines with delta-phase configuration the lateral attenuation factor k is equal to 1,7. When an interference source on the line is only corona on conductor (curve 2.), an attenuation character coincides with the wide spread dependence (curve 3).

HIGH POWER MILLIMETER WAVE TRANSIT-TIME AMPLFIER

M. Joseph Arman

Phillips Laboratory, Electromagnetic Sources Division

3550 Aberdeen Ave. SE

Kirtland AFB, NM, 87117-5776, USA

The need for High Power Millimeter Wave sources in the gigawatt range is on the rise in many disciplines and applications including communications, radar, and the military. Sources based on resonant cavities are power limited due to the physical size of the source which diminishes with the wavelength.

The author has explored the possibility of amplifying low level millimeter wave radiations to the gigawatt levels in a resonant cavity with no limitations on the physical size of the cavity. First a large 30cm diameter 15cm long cylindrical resonant cavity, Figure 1, is brought to resonance by launching a low level TM wave of a frequency matching that of one of the high level characteristic TM modes of the cavity. This mode is chosen to be in the millimeter range, TM_{066} for instance. After the saturation is reached, a high energy multi-kiloamp intense relativistic electron beam is injected axially into the resonant cavity where it interacts with the standing wave radiation in the cavity, and, under proper conditions, radiates coherently at the frequency of the resonating rf leading to amplification. The current chosen here is 4 kiloamp and the voltage of the beam is 500kV.

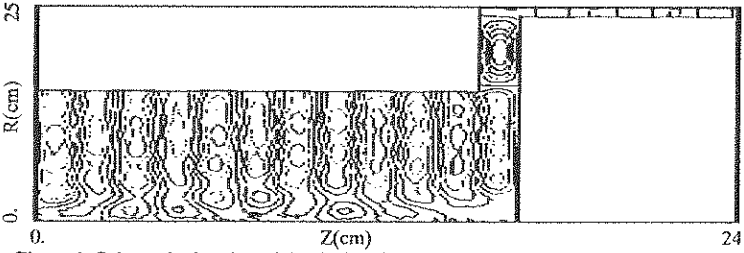

Figure 1 Schematic drawing of the device shown with the contour plots of E_r

The amplification process can be qualitatively understood in the following way. The beam electrons that enter the cavity at an accelerating phase, with proper velocity, will reach the second node just as the fields have changed sign, thus accelerating again. This process repeats at the next node and so on until the electrons reach the end of the cavity with their velocity augmented and a crossing time that is less than that of free drift. On the other hand, the electrons entering the cavity at a decelerating phase, will go through every half-wavelength decelerating and reach the exit with their energy reduced and a crossing time that is larger than that of the free drift. A calculation of the changes in the kinetic energy of these particles shows that the longer they stay in the cavity the more kinetic energy they exchange, so that the electrons entering at the decelerating phase lose more energy than the accelerating ones gain leading to a net loss of energy for the beam.

Matching of the transit time to the period of the rf is crucial for coherent radiation. The amplification saturates when electrons are slowed down enough to fall out of phase with the resonating fields and the transit time no longer matches the rf period.

As a result of the consecutive acceleration and deceleration that the beam is periodically subjected, it becomes modulated in the momentum space, ultimately giving rise to a densely bunched beam in the configuration space upon exit, Figure 2. This gives rise to the possibility of further radiation from the reduced beam in an adjacent cavity, maximizing the overall efficiency.

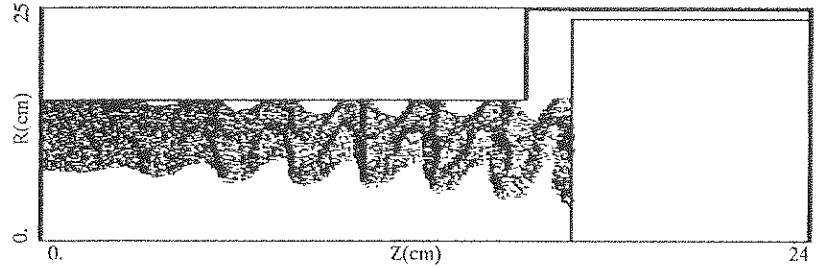

Figure 2 The beam is highly bunched as it leaves the system. The coaxial load also shown.

The loading can be achieved either radially through a radial waveguide or axially though a coaxial line. A coaxial load is the method chosen in the preliminary studies merely to simplify the simulation and to preserve the azimuthal symmetry necessary for a 2-D simulation.

Figure 3 is a plot of the extracted power as a function of time. After the initial surge, the peak power settles down to 2 GW. The rms power will be approximately 1 GW giving an rms efficiency of 50%. Fourier analysis of Figure 3 shows no competing modes present in the cavity, an indication of robust and stable operation.

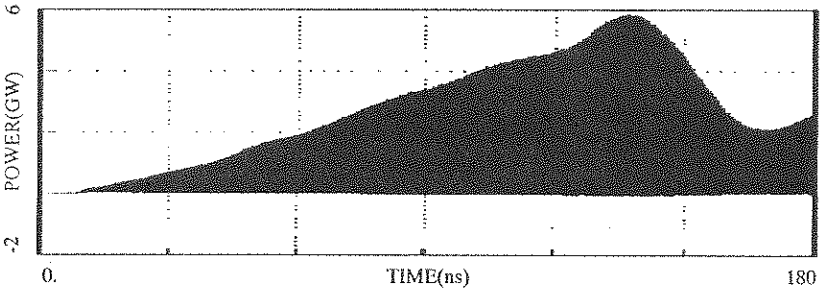

Figure 3 Extracted power as a function of time

This concept requires no external magnetic fields for guiding the electron beam so the device will be relatively small and portable.

The simulations presented here were carried out using the 2-D PIC code MAGIC. The 3-D PIC code SOS will be used for three-dimensional simulations of the problem.

MODELING AND ANALYSIS OF A NOVEL TUNNEL LADDER MILLIMETER-WAVE STRUCTURE

Thomas M. Wallett and A. Haq Qureshi*
NASA Lewis Research Center, Cleveland, Ohio 44135

Of a variety of structures considered in recent years for possible applications at millimeter-wave frequencies, one that has received attention is a thin tunnel ladder circuit which was presented conceptually by Karp (A. Karp, Proc. IRE, vol. 43, pp. 41-46, 1955). Similar structures consisting of parallel line arrays were also analyzed by Pierce (J. R. Pierce, IRE Trans. Electron Devices, vol. ED-2, pp. 13-24, 1955) and others. The actual tunnel ladder structure is a novel, high impedance structure of hexagonal tunnel geometry which does not lend itself to a closed form analysis.

We have carried out an analysis of the structure by approximating the actual hexagonal tunnel cross section as an ellipse (Figure 1). Electromagnetic wave propagation in the ridged wave guide containing the tunnel ladder structure was analyzed in elliptic cylindrical coordinates using Mathieu functions and their derivatives. The power through the structure was calculated from the corresponding electric and magnetic fields.

A 29 GHz structure was fabricated using two ladders, each having a depression in the middle of the rungs, placed together to form the tunnel ladder structure of hexagonal geometry. The structure was placed in a ridged wave guide supported by two boron nitride dielectric slabs glued to the upper and lower ridges with the rungs on both ladders aligned. Resonant frequencies of the structure were measured from 10 GHz to 35 GHz using an HP 8510C network analyzer.

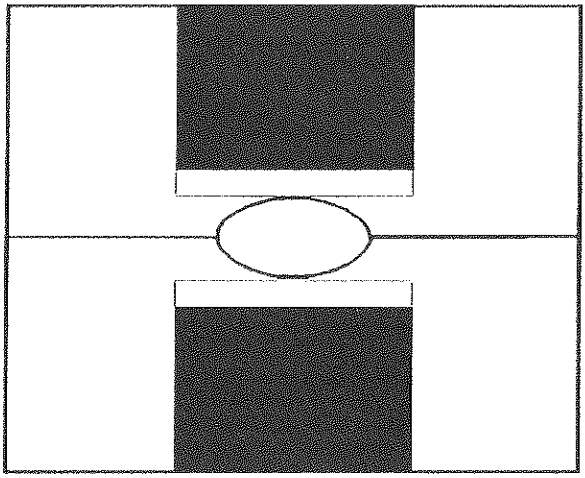

Figure 1 - Idealized elliptical tunnel ladder structure supported by dielectric slabs.

The structure was also modeled as an elliptic tunnel ladder of the same tunnel area and the same ladder thickness using the MAFIA code (Figure 2).

Results obtained from the theoretical analysis, experimental measurements, and the computed model are compared for the resonant frequencies, frequency shifts due to the insertion of a perturbing dielectric rod, and the interaction impedances.

The ability to predict structure characteristics without first fabricating extremely small structures for very high frequencies has been demonstrated by these investigations. It was found that it is easier, faster, more versatile and, eventually cost effective to model microwave structures using computer-aided design codes than to fabricate, test, and evaluate the prospective structures experimentally to determine their potential use in microwave devices. Furthermore, structure geometry can be varied easily in the computer analysis of the model to achieve desired characteristics.

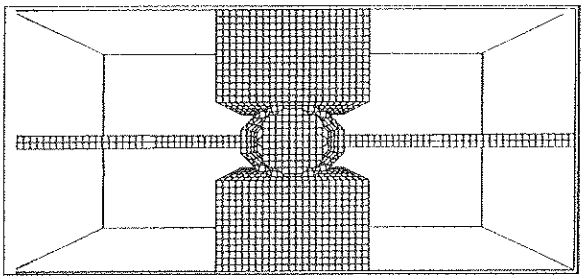

Figure 2 - Computer-generated mesh simulating the tunnel ladder structure.

Experimental CARM Characterisation

SJ Cooke, SN Spark, AW Cross, W He, H Yin and ADR Phelps

Department of Physics and Applied Physics
University of Strathclyde, Glasgow, G4 0NG, U.K.

Operation of the cyclotron autoresonance maser (CARM) currently under development at Strathclyde University is reported. Experimental characterisation of the device is compared with model predictions, for operating parameters given in table 1. The design is based on an enhanced field emission cold cathode electron source and conventional magnet systems for operation in short pulse, high PRF operation. A number of novel components incorporated into the design are described.

The CARM interaction promises to provide a means to achieve high power, high frequency radiation in the mm-wave region. Its advantages for this purpose arise from the large Doppler frequency upshift over gyrotron devices and the autoresonant nature of the interaction, leading to high efficiency and low magnetic field operation. Much interest in the CARM oscillator has been introduced with the success of recent experiments[1,2].

Accelerating potential	~500 kV
Electron current	100 A
Relativistic factor, γ	~2.0
Cavity magnetic field	0.3 - 0.38 T
Cyclotron frequency, ω_c	3 - 4 GHz
Doppler upshift factor	4 - 7
Operating frequency	12 - 20 GHz
Bandwidth	2-3 GHz
Power in TE_{11} mode	5 MW
Pulse duration	100 ns
Pulse repetition frequency	100 - 300 Hz

Table 1. Operating parameters of CARM experiment.

1) CARM Experiment

The specification and device characteristics will be reported for CARM oscillation in the 12-20 GHz band. In contrast to previously reported CARM devices, pulse repetition frequencies (PRF's) greater than 100 Hz have been employed. For applications to plasma heating and plasma diagnostics, where large average powers are required, pulse repetition rates of at least this order are necessary.

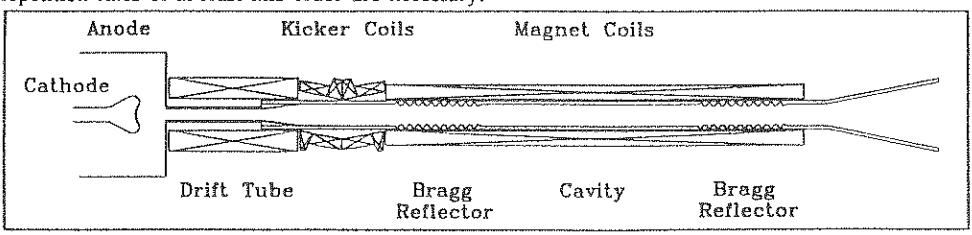

Figure 1: Schematic outline of CARM oscillator

2) Trajectory modelling

Electron trajectories within each of the major device components, figure 1, have been modelled, incorporating the effects of space-charge self-consistently by iterative solution of Poisson's equation. Diode and magnetic lens parameters were optimised to give narrow beam-velocity and energy distributions, and comparison made with experimental data. Modelling of the kicker shows a potentially wide tunability of the transverse beam velocity, shown for a bundle of beam trajectories by $\alpha = v_\perp / v_\parallel$ in figure 2. Numerical predictions of the kicker operation are compared with electron beam diagnostic results.

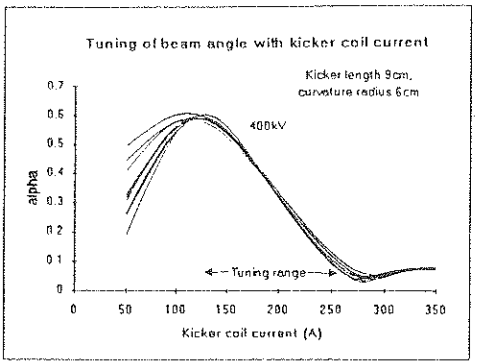

Figure 2: Tunable range of beam angle

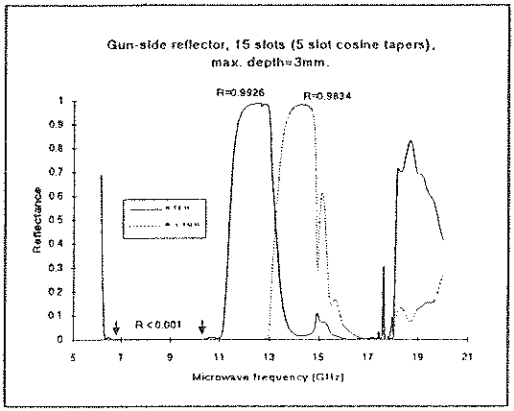

Figure 3. Calculated reflection coefficients of the TE_{11} and the TM_{11} modes as a function of frequency.

3) CARM Interaction

The CARM oscillator relies upon a convective instability and therefore requires a cavity to be defined. Operation is greatly assisted with the use of resonant Bragg reflectors to provide frequency-selective feedback at the CARM frequency and suppress low-frequency parasitic gyrotron oscillation. A periodic stepped-wall waveguide structure, provides resonant mode coupling with excellent electron-beam transport. A multi-mode scattering matrix code was developed to model the device characteristics (figure 3). Deep corrugations provide strong coupling in a compact reflector, with taper sections optimised to give excellent reflection and transmission characteristics as shown.

Acknowledgements

We would like to thank the SERC and the DRA for support of this work. D.M.Parkes and K.Trafford provided encouragement and stimulating discussions.

References

1. V.L.Bratman, G.G.Denisov, M.M.Ofitserov, S.V.Samsonov, O.V.Arkhipov, V.I.Kazacha, A.K.Krasnykh, E.A.Perelstein and A.V.Zamrij, 1992, "Cyclotron autoresonance maser with high Doppler frequency up-conversion", *International Journal of Infrared and Millimeter Waves*, 13, 1857-1873.

2. S.Alberti, B.G.Danly, G.Gulotta, E.Giguet, T.Kimura, W.L.Menninger, J.L.Rullier and R.J.Temkin, 1993, "Experimental Study of a 28GHz High-power Long Pulse Cyclotron Autoresonance Maser Oscillator", *Physical Review Letters*, 71, 2018-2021.

MAGNETIC FLUX COMPRESSORS FOR HIGH POWER VIRCATOR SYSTEM

V.B. Mintsev
Institute of Chemical Physics
142432, Chernogolovka, Russia

V.E.Fortov
High Energy Density Research Center
127412, Moscow, Russia

Pulsed power vircator systems are considered to be one of the most powerful relativistic generators of microwave radiation. Future advances in this field are limited now by characteristics of electrofeeding systems - the capacitor banks being very complex, bulky and expensive engineer construction.

In present paper explosively driven magnetic flux compressors (MFC) are considered as a pulsed power feeding system for triode with virtual cathode. Various electrical schemes for matching of vircator and MFC impedances are discussed. The transformer less scheme based on MFC with magnetic flux trapping seems to be more perspective. Parameters of electrical scheme elements and MFC are determined from requirements to the vircator impulse waveform. It is shown, that to realize 1 MeV electron beam, MFC should produce 10 kJ energy impulse in time ≤ 10 μs. The constructions of MFC on such parameters are considered. The experimental results in generation of 100 MW microwaves radiation impulses with the aid of high explosive, which were presented for the first time on Megagauss-VI conference, are discussed in detail.

THE EFFECT OF ELECTRON BEAM FORMATION ON THE EFFICIENCY OF CYCLOTRON RADIATION IN MAGNETIC CUSP

A.B.Ivanov, V.M.Michailov, E.V.Nesterov, V.P.Tarakanov*
Russian Academy of Science, High Energy Density Research Center,
Moscow, Russia, e-mail:karat@tarak.msk.su

rule, in simulation models and experimental realizations of rotrons (Kuzelev M.V., Rukhadze A.A., Usp. Phys. Nauk, v.152, 285,1987; 'Relativistic high-frequency electronics',edit.by V.Gaponov-Grehov,v.1-7,1979-1992, Gorky, IPF AN USSR), the gnetic field in resonator is considered to be uniform and ansversal component of the electrons velocity - weakly lativistic. Under such conditions, the recovery of electrons

>from the cyclotron resonance with electromagnetic wave caused by the loss of energy and saturation of instability usially occures at the distances much longer then the wave-length of radiation. This way, the length of saturation defines the optimal length of resonator in gyrotrons. The increase of the beam current and especially the transversaal velocity causes the reduction of length of saturation. So (as was proposed by Alterkop B.A., V.M.Michailov, Rukhadze A.A., V.P.Tarakanov, Phys. Plasmy, v.18, No.6, p.733-738,1992), by use of applied external magnetic field increasing along the axis of waveguide practically full transfer of beam energy ito the rotational energy is done and the length of resonator is sufficiently reduced.

In this case, the maximum of radiation is observed from the region of reflecting of the electrons because in this region the beam is transformed into the gas of oscillators, for which the cyclotron instability has a maximum increment.

The velocity homogenety of beam in the inlet of waveguide is one of the most important factors influenced on the effectiveness of radiation. Velocity distribution, on the contrary, depends on the history of electrons motion in accelerator. This is why, for alculation of efficiency of microwave generation it is necessary o take into consideration the zone of acceleration of electrons. diod with magnetic insulation was chosen as an accelerator for uther analysis.

umerical simulation was accomplished with help of code KARAT Tarakanov V.P., User's Manual for Code KARAT, BRA inc., VA, USA, 992). The electrons are started their motion with small initial nergy on the edge of cylyndrical cathode. Then, annular electron eam is injected into the cylindrical waveguide through the split n the thick anode, which, as well as waveguide walls, was onsidered to have ideal electrical conductivity, and was ropageted through magnetic cusp. Transmitted through the cusp articles were directed onto the wavwguide wall by decreasing agnetic field. It was assumed, that particles were absorbed in he thick anode and the walls of waveguide. The right face of aveguide provides radiation of the electromagnetic wave into ree space.

ıe efficiency of induced radiation was calculated by the spatial ıtegration of Pointing vectors near the right face of waveguide. : was found, that generation efficiency reaches the ıasistationary value 20%. For given parameters of the system, ıe energy in TE wave is by an order magnitude greater then the ıergy in TM wave.

ıe experimental installation includes inductive energy storages, ode with magnetic insulation as an accelerator of electrons and lindrical waveguide with magnetic cusp formed by specially signed magnetic coils. The induced radiation is transmitted rough the conical horn into free space. The efficiency of diation was measured by means of calorimeter technique.

mparision between analytical, numerical and experimental sults was accomplished.

ANALYSIS OF MAGNETIC FIELD IN THE VICINITY OF POWER TRANSFORMERS

Mukund Muralidhar * George G. Karady
Arizona State University

Magnetic fields produced by power lines, household wiring, and power appliances are becoming sources of public concern regarding potential health hazards. The fields generated by transmission lines and household appliances have been studied extensively. Preliminary studies indicate that motors and transformers are the major sources of magnetic fields in electrical appliances. Literature survey shows that transformer generated magnetic fields has not been studied sufficiently. The purpose of this paper is to characterize the field generated by transformers and study the effect of various parameters.

The magnetic field of different transformers was measured using standard techniques. The measurement system consisted of:

a) Sensor: has three coils orthogonal to each other and measures the derivative of field in the x, y, and z directions. The frequency range is 30 Hz to 300 kHz.
b) Integrator: three of them integrate the field derivatives and give field components.
c) Magnetic Tape Recorder: is an eight channel analog recorder. It records the three field components simultaneously along with a synchronizing signal. Depending on the speed of the tape the upper limit of the frequency range varies from 1.25 kHz to 20 kHz.
d) Digital Storage Oscilloscope: has two channels with a real time bandwidth of 40 MHz. Each field component is transferred to the scope using the synchronizing signal as trigger.
e) IBM PC 286: the digitized data from the scope is transferred to the PC using the GURU data acquisition software.
f) Fast Fourier Transform (FFT) Spectrum Analyzer: has one channel with frequency range from dc to 100 kHz. The amplitude of 400 harmonics are calculated by FFT.

The data from the PC was transferred to the VAX 860 mainframe computer where a code written in FORTRAN 77 evaluates the parameters of interest.

To develop a field map around the transformer, a three-dimensional net was formed. Due to symmetry, the field was measured in only one quadrant. Fig. 1 shows the measurement locations. The front view shows the measurement points on the coil side and the side view shows the measurement points on the core side. The approximate distance between measurement locations was one inch. The field was measured at no load, and full load conditions. Furthermore the effect of supply voltage variation was also studied. The harmonic content of the field was measured using a spectrum analyzer.

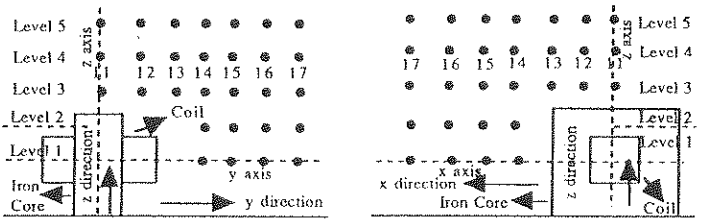

a. Front View (showing coil side). b. Side View (showing core side).

Fig. 1. Front View and Side View of Transformer Showing Measurement Locations.

Typical results are presented for a small transformer rated 100 VA, 120/10 V at full load conditions. Figs. 2a and 2b show the field as a function of horizontal distance on the coil side and core side respectively for different heights above the center of the transformer. From the figures it is seen that the field reduces with distance. The field on the core side is much higher than the field on the coil side. On the coil side only one component of the leakage flux is dominant (B_x component), while on the core two components are dominant (B_x and B_z). Figs. 3a and 3b show the waveshape of the different components for level 2, location 14 (coil

side) and location 41 (core side). The figures indicate that on the coil side the x-component is nearly ten times larger than the other two components. On the core side the y-component is negligible compared with the other two components.

The waveshape of some of the components is similar to the waveshape of the magnetizing current. The frequency spectrum of the field components was measured using a spectrum analyzer. Significant harmonics were present upto 1.5 kHz. The transformer load was varied from no load to full load of 10 A to determine the effect on the field. The variation in the field was found negligible. This shows that the field around the transformer is primarily caused by the leakage flux. Variation of the supply voltage from 0 V to 120 V (keeping load current constant) produced large variations in the field. This is because as the supply voltage increases, the flux in the core increases, therefore the leakage flux increases and so the field also increases.

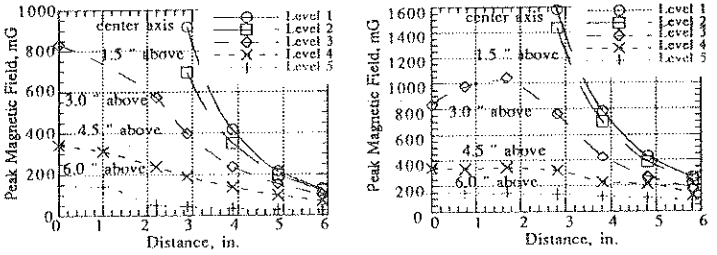

a. Measurement Locations on Coil Side.

b. Measurement Locations on Core Side.

Fig. 2. Magnetic Field B versus Distance at Different Heights Above the Transformer.

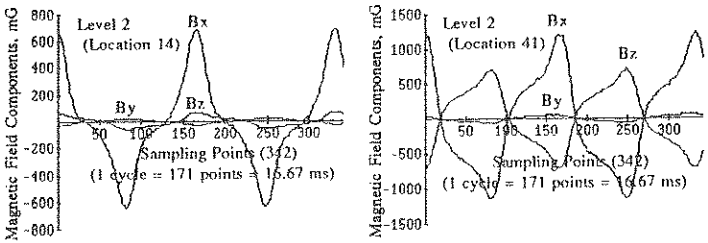

a. Coil Side.

b. Core Side.

Fig. 3. B_x, B_y, and B_z Components of Magnetic Field as a Function of Time.

The results show that field strengths of significant magnitudes are present near the transformer and hence emphasize the importance of characterization of the field in the vicinity of the transformer. Also the field has to be evaluated by one of the numerical techniques, like for example, finite element method. This would provide an analytical tool by which the field in the vicinity of the transformer can be evaluated using design specifications.

The following conclusions are drawn from the study:

1. The field is mainly determined by the flux in the core. Reduction in the leakage flux of the transformer through better designs would reduce the field strength.
2. The load has a negligible effect on the field.
3. The field on the core side is higher than the field on the coil side.
4. The field strength could be reduced by enclosing the transformer within a shield.

RELATIVISTIC MAGNETRONS AND KLYSTRONS AT HIGH REPETITION RATES AND HIGH AVERAGE POWERS

James Benford
Physics International Company
2700 Merced Street
San Leandro, CA 94577

Generation of microwaves at high power has progressed largely in single shot devices, yet applications require repetitive operation at substantial repetition rates which means high average power. Therefore, the technical challenge is two-fold: to increase the repetition rate and to extend the pulse duration. This means we must sustain high electric fields on a repetitive basis and over longer durations while avoiding RF breakdown and gap closure. This talk describes experiments on long pulse operation and repetitive operation of both relativistic magnetrons and relativistic klystron amplifiers. Together they represent the major classes of HPM sources: cross-field devices and linear beam tubes. Repetitive experiments use CLIA, a compact voltage adder, generating 750 kV, 10 kA using magnetic switching to produce 100 ns pulses. We have operated a water cooled L-band magnetron at repetition rates as high as 250 Hz with no breakdown or pulse shortening giving 6.3 kW average *microwave* power. A short burst at 1 kHz operated at ~ 25 kW. In this regime operation is not limited by gas buildup between pulses, by electrode erosion or by microwhisker depletion. A relativistic klystron has been operated in essentially the same conditions. To achieve longer pulse durations we are improving the quality of surface conditions by a variety of techniques, operating at low (10^{-8} torr) vacuum base pressure, tailoring electrode shapes and optimizing external loading We use a pulse power source with FWHM of 500 ns and a base to base duration of 800 ns. Thus far we have produced high power magnetron pulses with durations of 200 ns and propagated a beam in the RKA which shows stable operation for the entire pulse duration. This talk presents a perspective on the technical issues and results of the ongoing experiments.

HIGH POWER MICROWAVE CHERENKOV OSCILLATORS USING HIGH CURRENT RELATIVISTIC ELECTRON BEAMS

*S.D. Korovin, S.D. Polevin, I.V. Pegel, V.V. Rostov, A.M. Roitman
Institute of High Current Electronics, Tomsk, Russia,
and
V.L. Bratman, G.G. Denisov, A.V. Smorgonsky
Institute of Applied Physics, Nizhny Novgorod, Russia

This paper is devoted to theoretical and experimental investigations of high power microwave oscillators using high current nanosecond electron beams. The main goal of this work was to study stimulated Cherenkov radiation of intense relativistic electron beams in different systems and to create high power single mode microwave oscillators with efficient transfer of electron beam kinetic energy to electromagnetic waves.

The influence of non-synchronous waves and additional (non-Cherenkov) resonances on the process of microwave generation in a 3 cm relativistic BWO are discussed. Experimental data presented in this paper indicate that the efficiency of 3 cm relativistic BWO can achieve 40% with pulsed microwave power - 10^9 W. The enhancement of microwave power and efficiency of microwave generation was achieved using the non-uniformity of the phase velocity of the synchronous wave, and non-uniform coupling coefficient between the electrons and the electromagnetic wave.

We studied oversized Cherenkov oscillators with 8 mm wavelength. One of them was a 120 MW OROTRON with TM_{13} mode of the circular waveguide. Another one was a two stage two electron beam Cherenkov oscillator. The maximum microwave power in this experiment was 500 MW with a pulse duration of 10-15 ns.

All of our experiments were carried out using SINUS high current nanosecond electron accelerators. The performance parameters of our accelerators are as follows: electron energy 100 to 2000 keV, beam current 1 to 20 kA, pulse duration 5 to 50 ns, repetition rate up to 200-300 pps. These accelerators were also used to experimentally study the10 ns, 500 MW, 100 pps relativistic BWO.

"HUGHES' PLASMA-ASSISTED RF SOURCES"

J.M. Butler*, D.M. Goebel, J. Santoru, P.W. Sumner, and R.M. Watkins
Hughes Research Laboratories
3011 Malibu Canyon Road
Malibu, CA 90265

R.L. Eisenhart
Hughes Missile Systems Company
Canoga Park, CA 91304

High-peak, high-average power microwave oscillator and amplifier systems are under development at Hughes Research Laboratories for use in future jammer, directed energy, and material processing applications. These Plasma-Assisted, Slow-Wave Oscillator (PASOTRON™) and recently demonstrated amplifier systems utilize an electron beam-to-RF energy conversion mechanism similar to a conventional Backward-Wave Oscillators (BWO) and Traveling-Wave Tube (TWT) amplifiers. The sources, however, employ a high pulse-repetition-frequency capable E-gun and plasma-filled Slow-Wave Structure (SWS) to produce and propagate long, high-power beam pulses which require no axial-magnetic fields for transport. Through the innovative integration of plasma generation and control techniques with conventional RF technology, Hughes has developed a unique family of RF sources which bridge the gap between low-power, long-pulse conventional tube technology and high-power, short-pulse relativistic tube technology.

Experimental results are presented documenting the high-energy performance of S-, C-, and X-band oscillator systems. A schematic of the experimental PASOTRON apparatus is shown in Fig. 1. Spontaneously generated RF pulses up to 100-μsec long are reported at power levels in the 1-to-5 MW range. Calculations show an integrated RF energy per pulse of up to 500 J, and electron-beam to microwave-radiation power-conversion efficiency of ~20%. The PASOTRON oscillates at a center frequency tunable with beam voltage and maintains a narrow instantaneous bandwidth typically <10 MHz in width.

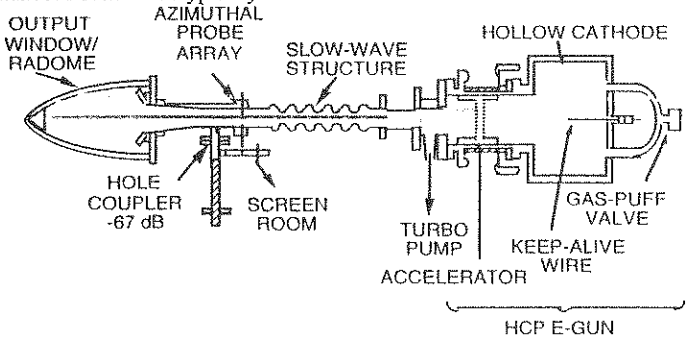

Figure 1. Schematic diagram of PASOTRON test apparatus.

Experimental parameter studies of a single-stage amplifier based on Hughes' PASOTRON technology are also reported. In this system, represented in the schematic of Fig. 2, long-electron-beam pulses are coupled with a 120-μsec long, 8.9-to-9.9 GHz RF-drive signal provided by a 10-kW TWT. As the beam and the drive signal propagate through the SWS, amplification of the input-RF-drive signal is achieved. Data is reported showing the dependence of the amplifier's gain, efficiency, and instantaneous bandwidth on beam voltage and current, RF drive frequency and amplifier structure length. Results show amplifier gain of 10-to-18 dB, phase stability of .005°/V, and a tunable bandwidth of 1%.

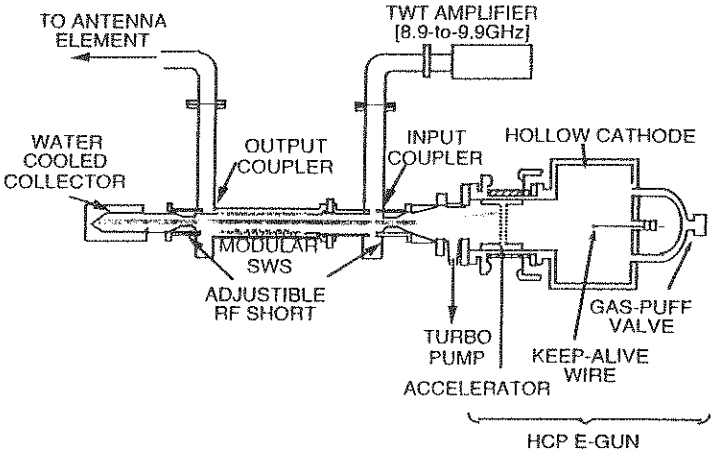

Figure 2. Schematic diagram of Plasma-Assisted X-band amplifier apparatus.

The long electron beam pulses utilized in both oscillator and amplifiers system's are obtained from a Hughes Hollow-Cathode Plasma (HCP) E-gun, which employs a low-pressure glow discharge to provide a stable, high current-density electron source. Electrons from the HC plasma are extracted by a multi-aperature electron beam-extraction system and accelerated into a gas-filled cylindrical waveguide. In most high-power BWOs and TWTs, axially-directed magnetic fields are required to transport the high current beams because electrostatic space-charge forces can lead to the rapid radial expansion of the beam diameter. In the PASOTRON, radial space-charge forces responsible for beam expansion are eliminated by allowing the beam to generate a background plasma by ionizing a low-pressure gas. In the absence of space-charge forces and an external magnetic field, the beam's self-magnetic field can cause the beam radius to compress through a process commonly known as the Bennett Pinch Effect. Hence, as the electron beam travels through the plasma-filled waveguide, it compresses in diameter before entering the SWS. As the electron beam propagates through the SWS a resonant interaction occurs between a SWS electromagnetic waveguide mode and the beam to efficiently generate RF radiation. For a given electron beam, a SWS can be designed to operate over a specified frequency range as either an oscillator or an amplifier.

*This work was support by Hughes Independent Research and Development Fund and the Air Force Office of Scientific Research contract #F49620-92-C-0015

HIGH POWER SMITH-PURCELL FREE-ELECTRON AMPLIFIERS DEVELOPMENT

Dmitry M. Vavriv
Institute of Radio Astronomy, 4 Krasnoznamennaya St.,
310002 Kharkov, UKRAINE

ABSTRACT. Comparison studies of single- and two-resonator Smith-Purcell free-electron amplifiers have been carried out. The limiting output characteristics (output power, gain, efficiency) of such amplifiers over the millimeter and submillimeter wave bands have been determined. The results of experiments are analyzed and the most promising amplifier designs are proposed.

1.INTRODUCTION. The use of the Smith-Purcell effect (S.J.SMITH & E.M.PURCELL, Phys.Rev., V.92, No 4, 1069, 1953) in electronics made it possible to produce the effective sources of oscillations over the millimeter and submillimeter wave bands. The further progress in instruments of this type is associated to a large extent with possible development amplifiers in the above mentioned wave bands. However, the results of experimental investigations of such type of amplifiers have shown little promise from the point of view of their efficiency, output power. In this paper, we provide an explanation for these difficulties and propose a more promising way of the developing the Smith-Purcell amplifiers.

The problem is that an oscillatory system of the amplifiers being studied is usually the same as that of similar generators, namely, a single open resonators formed by two metallic mirrors one of which is covered by a diffraction grating (Fig.1a). This construction is known to satisfy best the peculiarities of the interaction between an electron beam and the resonator field in the case of auto generators. We have found that, by contrast to achieve an acceptable output characteristics of the amplifiers, it is necessary to say no to the traditional single-resonator constructions, and come to multi-resonator ones, e.g., such as that shown on Fig. 1b. This, naturally, complicates the development and design of the devices.

The results concerning output characteristics of different types of the Smith-Purcell amplifiers were obtained by solving the self-consistent system of Maxwell's and particles motion equations. Space charge field, nonlinear and nonstationary effects have been taken into account (D.M.VAVRIV & O.A.TRETYAKOV, Theory of Resonant Amplifiers with Distributed Interaction of O-type, Kiev: Naukova Dumka, 1989). The mathematical model created permits to describe almost all the phenomena observed in the experiments, and makes it possible to investigate various modes of amplifiers operation.

2.RESULTS. The single-resonator device of Fig.1 is the reflection-type amplifier. Relatively high values of the gain are observed only in the vicinity of the threshold of oscillations self-excitation. However here, the bandwidth of the amplifier is too small. The results obtained have also shown that the maximum efficiency which can be realized in this case is not higher than 3%.

Taken together, these findings of the investigation indicate that the single-resonator amplifiers have little to offer as high power amplifiers. These results are in good agreement with the experimental data (V.K.KORNIJENKO & V.S.MIROSHNICHENKO, Izv.Vuzov - Radioelektr., V.26, No 3, 93, 1983).

The drawbacks of the single-cavity amplifiers result mainly from the fact that it is impossible to provide both good beam bunching and extraction of the HF energy from the beam by using one and the same interaction space. These processes are to be separated in space. To achieve this objective, one has to use multi-resonator constructions of the amplifier, as in the case of the klystrons with distributed interaction.

The amplifiers characteristics can be substantially improved by using even the two-resonator design as in Fig. 1b. High power amplifiers can be developed, provided that suitable parameters of the resonators and the beam are chosen. It was found that the rather high gain values of the order of 30 - 40 db can be reached with the bandwidths of approximately 1%. The electronic efficiency and the power output P of such amplifiers can be as high as

$$\text{Efficiency} = 0.8\ v_0 / (R_y\ f)$$

$$\text{Power} = 0.05\ \varepsilon_0 (m/e)^2\ v_0^7 / (f^2\ R_y^2)$$

where v_0 is the initial beam velocity, R_y is the radius of the field spot on the diffraction grating of the output resonator, e and m are the charge and mass of electron, respectively, ε_0 is the permittivity of free space.

These results are best illustrated by a specific example. If beam voltage is 100 kV and R_y =5mm then efficiency may be as great as 50% and output power ranges up to about 1 MW at the frequency f=60GHz. The distinctive property of such amplifiers is that the power output essentially depends on the beam velocity which gives possibility of increasing the value of P relatively easy.

3.CONCLUSION. The single-resonator design used for the Smith-Purcell oscillators shows little promise for the development of the high power amplifiers on its base. The application of the two- or multi- resonator systems is only way of creating promising amplifiers of millimeter and submillimeter wave bands. These systems are candidates for the development of high power Smith-Purcell amplifiers which may have practical usage.

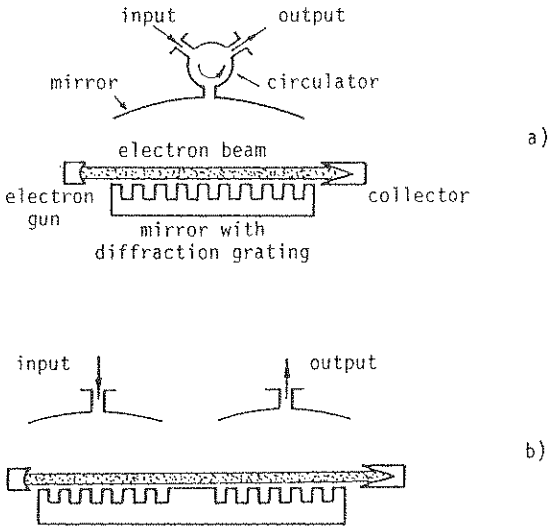

Fig.1. Schematic diagram of the Smith-Purcell amplifiers with (a) single- and (b) two-resonator designs.

FREQUENCY-TUNABLE MICROWAVE SOURCES

L. Brown* and A. Maitland
J. F. Allen Research Laboratories,
The Department of Physics and Astronomy,
The University of St. Andrews,
North Haugh, St. Andrews, Fife KY16 9SS,
Scotland, U.K.

D. M. Parkes
DRA, Electronics Division, RSRE,
St. Andrews Road, Malvern,
Worcs. WR14 3PS, England, U.K.

Significant changes in high power microwave (HPM) technologies have been witnessed throughout the last few decades, not least in the field of HPM sources. A great number of new source types have been proposed and developed. Many are high power versions of the conventional microwave sources such as magnetrons, travelling-wave tubes and klystrons. Others rely almost entirely for their successful operation upon new mechanisms which were rarely exploited before the early 1970s and which are both numerous and diverse in nature.

The incentive behind this increase in the number of tube types is a need to meet ever increasing demands for higher output powers at higher efficiencies. This drive is almost certain to continue with researchers still aiming to increase peak powers, average powers and pulse durations. One of the more dramatic developments that may be attributed to this goal is the introduction of relativistic electron beams in both conventional and relatively new source types. Not only has this resulted in dramatic leaps in output power, but it has also cleared a pathway to the understanding and utilization of a number of mechanisms associated with relativistic energies.

While a significant amount of research is being carried out with regard to increasing the operating frequencies of existing tubes, an associated field, frequency tunability, has perhaps not received the attention it deserves. Source bandwidths and tuning speeds have not enjoyed the significant improvements such as have been observed in the output power arena. This may be attributable to the fact that tuning capacity is often a by-product of a configuration that has ultimately been designed for its power generating capabilities. Through skilful engineering, the tuning capacities of existing sources have been maximised, but the field is still regarded by many as a secondary research issue. As a result, present tuning methods are often restricted, cumbersome and slow.

Oscillators, which by their very nature are designed to operate at sharply defined frequencies, are the least likely candidates for provision of wide bandwidths and rapid tuning. The magnetron provides a typical example. If the operating parameters are maintained at constant values, then tuning of the output cavities will produce bandwidths of approximately 1% or less. Further, tuning is likely to be performed by mechanical means. Gyrotrons provide an example of oscillators which may be step-tuned. This technique allows for

frequency selection by changing the value of a basic operating parameter. In either case, both tuning range and tuning speed are limited.

Amplifiers have demonstrated the greater capacity for tunability to date. Concentrated research in the field of frequency tunability could do well to commence with an investigation of amplifier structures, which by their very nature are wideband. Nevertheless, advances in amplifier bandwidths have not been overly spectacular to date. The majority of amplifiers achieve bandwidths of approximately 5 - 10%, with the exception of the free-electron laser configuration which has achieved bandwidths of approximately 30%. Nevertheless, a number of tubes possess potential for greater tunability. Amplifier investigations may have to overcome problems related to overmoding of slow wave structures. Improved means of narrowband frequency selection will have to be found.

From a tunability viewpoint, microwave tubes may be broadly classified as user controlled or source dependent according to the degree of accuracy with which an operator may select a particular output frequency. User controlled tubes permit absolute external control over frequency. In source dependent tubes, power is the main concern and tunability tends to be a secondary consideration. Such tubes are of limited use in applications where stringent user control over frequency is a requirement. In general, source development has been aimed at producing high powers or wide bandwidths but not both. In seeking to attain extended tuning capacity at high powers, we must ask to what extent the one must be compromised in order to attain the other.

With increased emphasis being placed on pulse-to-pulse (frequency-agile) applications it is our belief that the above issues will become of greater importance to microwave source manufacturers. Through necessities dictated by applications, tuning requirements will become wider and faster. An emphasis may be placed on improved mode selection techniques while the bandwidth capability of existing slow wave structures will require extension. Present microwave generation mechanisms may require tailoring to meet this new demand. For these reasons, we present an overview of existing HPM sources which have demonstrated a variety of bandwidths. We review the mechanisms by which microwaves are generated and tuned, and we classify tube types according to their suitability for frequency-tunable and/or frequency-agile applications.

SCALING LAWS FOR ESTIMATING VERY CLOSE-IN SOURCE REGION EMP AND COUPLING

William J. Karzas
Consultant
7423 W. Manchester Avenue, # 7
Los Angeles, CA 90045-2375

Some time ago it became necessary to estimate the fields and coupling very close to the source of near-ground nuclear EMP. Detailed finite-difference machine computations were in-hand only for radial distances significantly farther out than the desired locations and for various reasons it was not considered reasonable to carry out extensive new calculations. Thus some kind of extrapolation from the existing data became necessary.

While it was simple to extrapolate the driving gamma ray flux, extrapolating the induced electric (and magnetic) fields was less straightforward because we were in a regime where the self-consistent effect (modification of the driving Compton electron motions by the fields they produce) is significant. The procedure decided on was to calculate the electric and magnetic fields at the close-in points without considering the self-consistent interaction (this can be done without expending great effort), and then to use some theoretically derived algorithms to modify them. This approach is reasonable since the intense air conductivity produced by the radiation effectively makes the fields at a given close-in point independent of conditions more than a few skin depths removed. Thus, fields everywhere in space need not be modified for self consistency to make the correction at a few points.

Electric Field Limiting: First we note that a few skin depths away from the ground or any other surfaces, the produced fields are electric only and radial, as if conditions were spherically symmetric. In this case, the Compton electron motion is modified by a radially inward force. Since near the ground typical Compton electrons have MeV energies and travel a few meters before they lose their energy to ionization we can expect energy loss to the electric field to be significant for fields of the order of hundreds of kilovolts per meter. When this occurs the resultant fields will be reduced. A simple analysis is presented with these results:

Let a be the ratio, for non-self-consistent conditions, of the energy drop against the electric field (across the Compton range) divided by the initial Compton energy.

$$a = \frac{e E_0 \lambda_0}{W_0} .$$

Then ε, the ratio of self-consistent to non-self consistent early-time saturated electric field magnitude, is given by the solution of the following equation:

$$\varepsilon^2 (1 + a\varepsilon) = 1 , \quad \text{with} \quad \varepsilon = \frac{E}{E_0} .$$

For strong electric-field limiting, $a \gg 1$, so that

$$E = E_0 \varepsilon \approx E_0 a^{-1/3} .$$

Similarly, the magnitude of the Compton current and air conductivity are electric-field limited:

$$J \approx J_0 \varepsilon^{-2} \approx J_0 a^{-2/3}, \text{ and } \sigma = \sigma_0 (1 + a\varepsilon)^{-1/2} \approx \sigma_0 a^{-1/3}$$

These results are also valid near a conducting surface normal to the gamma flux, and thus can be used to estimate induced charge density.

Magnetic Field Limiting: Of greater interest, perhaps, is the current induced on conductors originating close-in to the source. Within a region a few skin depths thick near conducting surfaces parallel to the gamma Compton currents, the radial (parallel) electric field is very small. In particular, a diffusion theory-like calculation, with ξ the distance normal to the surface and δ the skin depth, gives:

$$E_r \approx \frac{|J|}{\sigma} \left| 1 - e^{-\frac{\xi^2}{\delta^2}} \right|$$

$$H_\phi \approx |J| \delta \, e^{-\frac{\xi^2}{\delta^2}}$$

$$E_\xi \approx \frac{\omega}{c\sigma} H_\phi = \frac{\varepsilon_0 \omega}{\sigma} Z_0 H_\phi$$

Thus, the magnetic field is generated by surface currents of about one skin depth worth of Compton current. This outgoing magnetic field pulse carries with it a transverse electric field E_ξ appropriate to the impedance of a conducting medium.

This magnetic field will dominate the Compton electron motion near the surface of interest. (Since the parallel electric field is reduced, electric field limiting does not occur.) The electrons will be turned with $R_L(H)$, the Larmor radius in the magnetic field.

Letting b be the ratio of electron range to Larmor radius (both for non-self-consistency), another simple analysis gives η, the ratio of self-consistent to non-self-consistent magnetic field as the solution of:

$$b\eta^2 = \sin b\eta \text{ or } 1, \text{ as } b\eta < \text{ or } > \frac{\pi}{2} .$$

For typical, 1 MeV, Compton electrons, the self-consistent magnetic field is

$$B \approx (2 I B_0)^{1/2}, \text{ with the fields in Gauss.}$$

Limited Induced Currents: On a cylinder of radius r parallel to the flux, the limited induced current in terms of the non-self-consistent result is

$$I \approx 100 \sqrt{I_0(A)\, r(m)} \text{ Amp.}$$

Some comparisons with detailed numerical calculations will be presented.

Source Region Invited Session

IMPACT OF COMPTON ELECTRON LIFETIME EFFECTS ON SREMP SOURCES

By

C.W. Jones*
T.W. Larkin
W. A. Radasky
K.S. Smith
Metatech Corporation
Albuquerque, New Mexico

Nearly all solutions for ground burst Source Region EMP (SREMP) assume that the Compton current J (A/m^2) and the air ionization Q (ion pairs/$m^3 \cdot s$) possess time histories which are identical to the local gamma ray flux waveform. This assumption is actually an approximation which assumes that Compton electron ranges (and lifetimes) in sea-level air are very short compared to the rise and decay times of the photon pulse. This approximation is therefore dependent on the relationship between the photon time history, its spectrum, and the air density. Modern flash x-ray simulators have improved to the extent that rise times are now faster than 10 ns with energy spectra containing substantial content above 4 MeV (e.g., HERMES III). These characteristics are clearly of interest for considering finite electron lifetime effects.

This paper will examine a set of photon time waveforms with monoenergetic gamma energies to evaluate the Compton currents, ionization rates and the ratio J/Q as a function of time. These calculations are performed by first evaluating the delta function response of a single energy photon flux through the process of creating and tracking a distribution of Compton electrons. Full relativistic electron tracking procedures are considered as well as the secondary ionization energy loss mechanisms. The delta function responses are then convoluted with time histories of interest to produce detailed calculations of the radial Compton current and air ionization rate.

Sample results from our calculations are summarized in Table I below. The table indicates the constant J/Q ratio found under the assumption of short electron lifetimes and compares them to time-dependent values calculated for a simple 6 × 12 ns pulse (rise time × pulse width). The time-dependent values are sometimes significantly higher than the constant values and will typically result in higher SREMP electric fields.

Table 1. Comparison of detailed electron lifetime calculations with the short lifetime approximation.

E_γ (MeV)	0.5	1.0	2.0	4.0	6.0
Short Electron Lifetime Approximation	6.6(-24)*	1.0(-23)	1.4(-23)	1.6(-23)	1.9(-23)
Finite Electron Lifetimes (t = 10 ns)	7.0(-24)	1.2(-23)	2.0(-23)	2.5(-23)	2.6(-23)

*All values are the ratio of J/Q in $(A/m^2)/(\text{ion pairs}/(m^3 \cdot s))$ for air density of 1 kg/m^3.

COMPTON DIODES RESPONSE TO 14 MEV NEUTRONS

*F.Amaudric du Chaffaut
A.Stark (Service C.E.M. B.P.12 - 91680 Bruyères le Châtel FRANCE)

INTRODUCTION

For solving Maxwell's equations and for computing E.M.fields in a medium, it's necessary to know the conductivity and the currents inside this medium. In this study we are specially interesting in the I.E.M coming from the interaction between neutrons and air.

As neutrons are crossing air they give energy to charged particules, and at the same time, "γ" rays are created. Then "γ" rays give energy to the matter and produce recoil electrons current. The computation of the air ionization and its conductibility with the associated electrons current has been made, for a hundred meters high aerian explosion with the Tripoli 2 code for one neutron source (Ref:: C.E.A. CONF 9706 - Vergnaud, J.P.Ulpat, J.C.Nimal, G.Faucheux). The computed current intensity is straight connected to the incident neutron flux, then it's very important to measure this flux precisely. In this study we present a calculation of a Compton Diode response to 14 MeV neutrons. Then we compare the computed sensitivity to this one got experimentally.

I COMPUTATION OF THE COMPTON DIODE RESPONSE TO 14 MEV NEUTRONS

Compton diode is composed of three main parts:

the intake window
the coming out window
and the central electrode which is called collector (cf following figure)

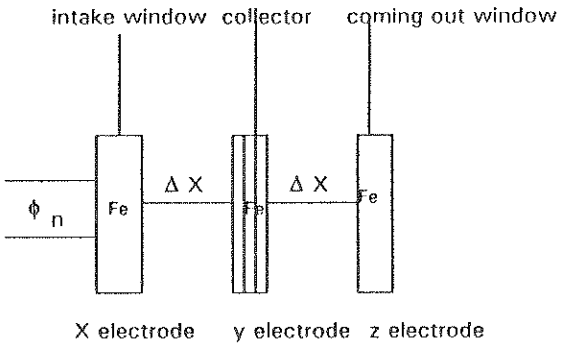

COMPTON DIODE DIAGRAM

γ"rays create electrons (Compton effect, photoelectric effect). Then the topic of this study is to compute the electric signal induced on the collector.
The calculation is composed of three main steps:

1- for each plate we compute the "γ" rays number emitted in each band of energy with two cross section data tables.

2- for each area facing another one we compute the "γ" rays going in and out.

3- finally using "γ" rays flux and DELLIN and MAC CALLUN tables we calculate electrons currents.

We find that the theoritical sensibility value does'nt change a lot according to the used cross sections.

II EXPERIMENTAL NEUTRON SENSIBILITY of the COMPTON DIODE

The method we have used is the following one:
We have measured a 14 MeV Neutrons source on one hand with the compton diode and on the other hand with a standard detector, "the recoil protons telescope", the sensibility of which is kown very exactly.

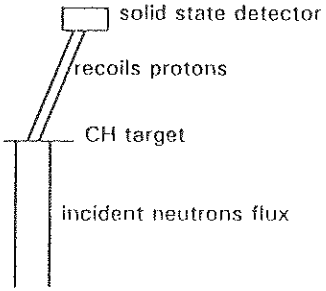

Principle of the Recoil Protons Telescope

We have found a gap of about 10% between theoritical and experimental sensibility value of the compton diode.

CONCLUSION

The very simple model we have used for computing the neutrons sensibility of the compton diode gives us a value compatible with the experimental value. This result is very important, it shows that compton diode generally used as "γ" sensor, can be a very good neutron detector. The main quality of this sensor is its simplicity. It runs in high doses level, without feeding voltage. It would be interesting to carry on this study in computing compton diode sensibility according to incident neutrons energy.

SREMP* SIMULATION USING ASTERIX FLASH X-RAY FACILITY** RADIATION FIELD DATA AND ANALYSIS

M. VIE, E. DELAHAYE*, G. NOUVEL,
CENTRE D'ETUDES DE GRAMAT, F-46500 GRAMAT, FRANCE

ASTERIX is a french 7 MeV end point voltage flash X-Ray (réf. P. EYL & Al. IEEE Pulsed Power Conference June 1989, Montery CA) used for SREMP studies.

From current and voltage diagnostics delivered at the diode, we have computed electronic distribution resolved in angle, energy and time.

This numerical simulation is performed using MAGIC, a two dimensional electromagnetic particle in cell code (B. Goplen & Al., MRC/WDC-R-201, oct. 89).

The previous electron source is used to compute the X-Ray distribution at the external side of the converter versus energy (fig. 1), angle (fig. 2) and time. X-Ray source calculations are made by using the CEG Monte Carlo code Electre 6 - Phoebus 6 (NOUVEL & Al., RADECS MONTPELLIER, sept. 91).

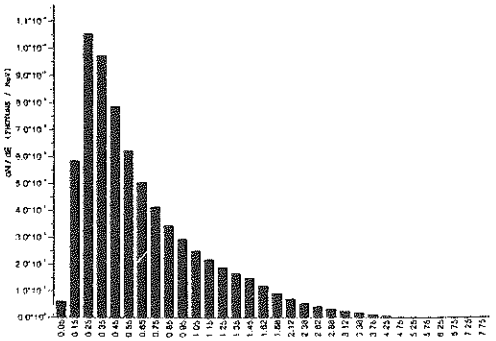

E(MeV)

Fig. 1 : TOTAL PHOTON DISTRIBUTION VS ENERGY

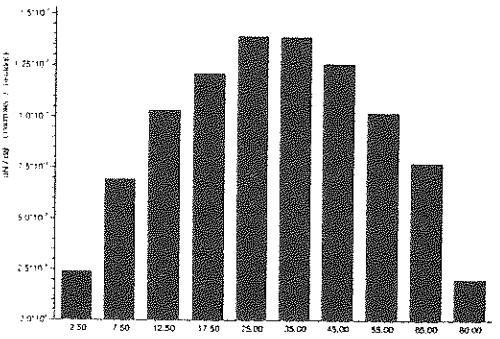

θ (degree)

Fig. 2 : TOTAL PHOTON DISTRIBUTION VS ANGLE

Total ionizing dose is then computed inside an experimental dosimeter made of 8 mm Silica modelled like silicon and 3 mm Aluminium encapsulation.

---

* Source Region ElectroMagnetic Pulse

** This work has been supported by the French Delegation Generale pour l'Armement

RELATIVISTIC MAGNETRONS AND KLYSTRONS AT HIGH REPETITION RATES AND HIGH AVERAGE POWERS

James Benford
Physics International Company
2700 Merced Street
San Leandro, CA 94577

Generation of microwaves at high power has progressed largely in single shot devices, yet applications require repetitive operation at substantial repetition rates which means high average power. Therefore, the technical challenge is two-fold: to increase the repetition rate and to extend the pulse duration. This means we must sustain high electric fields on a repetitive basis and over longer durations while avoiding RF breakdown and gap closure. This talk describes experiments on long pulse operation and repetitive operation of both relativistic magnetrons and relativistic klystron amplifiers. Together they represent the major classes of HPM sources: cross-field devices and linear beam tubes. Repetitive experiments use CLIA, a compact voltage adder, generating 750 kV, 10 kA using magnetic switching to produce 100 ns pulses. We have operated a water cooled L-band magnetron at repetition rates as high as 250 Hz with no breakdown or pulse shortening giving 6.3 kW average *microwave* power. A short burst at 1 kHz operated at ~ 25 kW. In this regime operation is not limited by gas buildup between pulses, by electrode erosion or by microwhisker depletion. A relativistic klystron has been operated in essentially the same conditions. To achieve longer pulse durations we are improving the quality of surface conditions by a variety of techniques, operating at low (10^{-8} torr) vacuum base pressure, tailoring electrode shapes and optimizing external loading We use a pulse power source with FWHM of 500 ns and a base to base duration of 800 ns. Thus far we have produced high power magnetron pulses with durations of 200 ns and propagated a beam in the RKA which shows stable operation for the entire pulse duration. This talk presents a perspective on the technical issues and results of the ongoing experiments.

HIGH POWER MICROWAVE CHERENKOV OSCILLATORS USING HIGH CURRENT RELATIVISTIC ELECTRON BEAMS

*S.D. Korovin, S.D. Polevin, I.V. Pegel, V.V. Rostov, A.M. Roitman
Institute of High Current Electronics, Tomsk, Russia,
and
V.L. Bratman, G.G. Denisov, A.V. Smorgonsky
Institute of Applied Physics, Nizhny Novgorod, Russia

This paper is devoted to theoretical and experimental investigations of high power microwave oscillators using high current nanosecond electron beams. The main goal of this work was to study stimulated Cherenkov radiation of intense relativistic electron beams in different systems and to create high power single mode microwave oscillators with efficient transfer of electron beam kinetic energy to electromagnetic waves.

The influence of non-synchronous waves and additional (non-Cherenkov) resonances on the process of microwave generation in a 3 cm relativistic BWO are discussed. Experimental data presented in this paper indicate that the efficiency of 3 cm relativistic BWO can achieve 40% with pulsed microwave power - 10^9 W. The enhancement of microwave power and efficiency of microwave generation was achieved using the non-uniformity of the phase velocity of the synchronous wave, and non-uniform coupling coefficient between the electrons and the electromagnetic wave.

We studied oversized Cherenkov oscillators with 8 mm wavelength. One of them was a 120 MW OROTRON with TM_{13} mode of the circular waveguide. Another one was a two stage two electron beam Cherenkov oscillator. The maximum microwave power in this experiment was 500 MW with a pulse duration of 10-15 ns.

All of our experiments were carried out using SINUS high current nanosecond electron accelerators. The performance parameters of our accelerators are as follows: electron energy 100 to 2000 keV, beam current 1 to 20 kA, pulse duration 5 to 50 ns, repetition rate up to 200-300 pps. These accelerators were also used to experimentally study the10 ns, 500 MW, 100 pps relativistic BWO.

"HUGHES' PLASMA-ASSISTED RF SOURCES"

J.M. Butler*, D.M. Goebel, J. Santoru, P.W. Sumner, and R.M. Watkins
Hughes Research Laboratories
3011 Malibu Canyon Road
Malibu, CA 90265

R.L. Eisenhart
Hughes Missile Systems Company
Canoga Park, CA 91304

High-peak, high-average power microwave oscillator and amplifier systems are under development at Hughes Research Laboratories for use in future jammer, directed energy, and material processing applications. These Plasma-Assisted, Slow-Wave Oscillator (PASOTRON™) and recently demonstrated amplifier systems utilize an electron beam-to-RF energy conversion mechanism similar to a conventional Backward-Wave Oscillators (BWO) and Traveling-Wave Tube (TWT) amplifiers. The sources, however, employ a high pulse-repetition-frequency capable E-gun and plasma-filled Slow-Wave Structure (SWS) to produce and propagate long, high-power beam pulses which require no axial-magnetic fields for transport. Through the innovative integration of plasma generation and control techniques with conventional RF technology, Hughes has developed a unique family of RF sources which bridge the gap between low-power, long-pulse conventional tube technology and high-power, short-pulse relativistic tube technology.

Experimental results are presented documenting the high-energy performance of S-, C-, and X-band oscillator systems. A schematic of the experimental PASOTRON apparatus is shown in Fig. 1. Spontaneously generated RF pulses up to 100-μsec long are reported at power levels in the 1-to-5 MW range. Calculations show an integrated RF energy per pulse of up to 500 J, and electron-beam to microwave-radiation power-conversion efficiency of ~20%. The PASOTRON oscillates at a center frequency tunable with beam voltage and maintains a narrow instantaneous bandwidth typically <10 MHz in width.

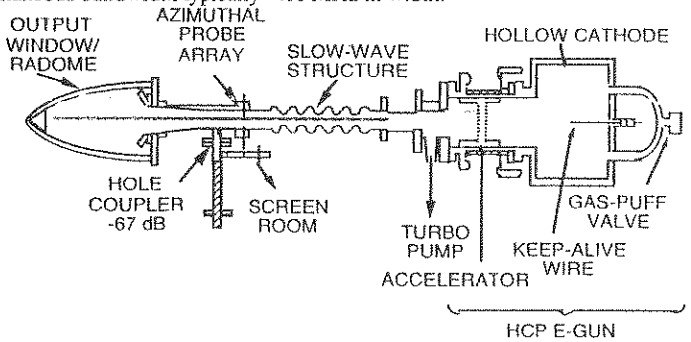

Figure 1. Schematic diagram of PASOTRON test apparatus.

Experimental parameter studies of a single-stage amplifier based on Hughes' PASOTRON technology are also reported. In this system, represented in the schematic of Fig. 2, long-electron-beam pulses are coupled with a 120-μsec long, 8.9-to-9.9 GHz RF-drive signal provided by a 10-kW TWT. As the beam and the drive signal propagate through the SWS, amplification of the input-RF-drive signal is achieved. Data is reported showing the dependence of the amplifier's gain, efficiency, and instantaneous bandwidth on beam voltage and current, RF drive frequency and amplifier structure length. Results show amplifier gain of 10-to-18 dB, phase stability of .005°/V, and a tunable bandwidth of 1%.

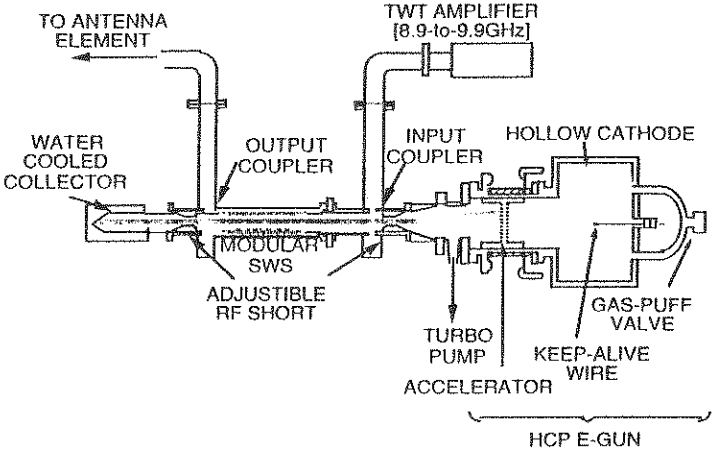

Figure 2. Schematic diagram of Plasma-Assisted X-band amplifier apparatus.

The long electron beam pulses utilized in both oscillator and amplifiers system's are obtained from a Hughes Hollow-Cathode Plasma (HCP) E-gun, which employs a low-pressure glow discharge to provide a stable, high current-density electron source. Electrons from the HC plasma are extracted by a multi-aperature electron beam-extraction system and accelerated into a gas-filled cylindrical waveguide. In most high-power BWOs and TWTs, axially-directed magnetic fields are required to transport the high current beams because electrostatic space-charge forces can lead to the rapid radial expansion of the beam diameter. In the PASOTRON, radial space-charge forces responsible for beam expansion are eliminated by allowing the beam to generate a background plasma by ionizing a low-pressure gas. In the absence of space-charge forces and an external magnetic field, the beam's self-magnetic field can cause the beam radius to compress through a process commonly known as the Bennett Pinch Effect. Hence, as the electron beam travels through the plasma-filled waveguide, it compresses in diameter before entering the SWS. As the electron beam propagates through the SWS a resonant interaction occurs between a SWS electromagnetic waveguide mode and the beam to efficiently generate RF radiation. For a given electron beam, a SWS can be designed to operate over a specified frequency range as either an oscillator or an amplifier.

*This work was support by Hughes Independent Research and Development Fund and the Air Force Office of Scientific Research contract #F49620-92-C-0015

HIGH POWER SMITH-PURCELL FREE-ELECTRON AMPLIFIERS DEVELOPMENT

Dmitry M. Vavriv
Institute of Radio Astronomy, 4 Krasnoznamennaya St.,
310002 Kharkov, UKRAINE

ABSTRACT. Comparison studies of single- and two-resonator Smith-Purcell free-electron amplifiers have been carried out. The limiting output characteristics (output power, gain, efficiency) of such amplifiers over the millimeter and submillimeter wave bands have been determined. The results of experiments are analyzed and the most promising amplifier designs are proposed.

1.INTRODUCTION. The use of the Smith-Purcell effect (S.J.SMITH & E.M.PURCELL, Phys.Rev., V.92, No 4, 1069, 1953) in electronics made it possible to produce the effective sources of oscillations over the millimeter and submillimeter wave bands. The further progress in instruments of this type is associated to a large extent with possible development amplifiers in the above mentioned wave bands. However, the results of experimental investigations of such type of amplifiers have shown little promise from the point of view of their efficiency, output power. In this paper, we provide an explanation for these difficulties and propose a more promising way of the developing the Smith-Purcell amplifiers.

The problem is that an oscillatory system of the amplifiers being studied is usually the same as that of similar generators, namely, a single open resonators formed by two metallic mirrors one of which is covered by a diffraction grating (Fig.1a). This construction is known to satisfy best the peculiarities of the interaction between an electron beam and the resonator field in the case of auto generators. We have found that, by contrast to achieve an acceptable output characteristics of the amplifiers, it is necessary to say no to the traditional single-resonator constructions, and come to multi-resonator ones, e.g., such as that shown on Fig. 1b. This, naturally, complicates the development and design of the devices.

The results concerning output characteristics of different types of the Smith-Purcell amplifiers were obtained by solving the self-consistent system of Maxwell's and particles motion equations. Space charge field, nonlinear and nonstationary effects have been taken into account (D.M.VAVRIV & O.A.TRETYAKOV, Theory of Resonant Amplifiers with Distributed Interaction of O-type, Kiev: Naukova Dumka, 1989). The mathematical model created permits to describe almost all the phenomena observed in the experiments, and makes it possible to investigate various modes of amplifiers operation.

2.RESULTS. The single-resonator device of Fig.1 is the reflection-type amplifier. Relatively high values of the gain are observed only in the vicinity of the threshold of oscillations self-excitation. However here, the bandwidth of the amplifier is too small. The results obtained have also shown that the maximum efficiency which can be realized in this case is not higher than 3%.

Taken together, these findings of the investigation indicate that the single-resonator amplifiers have little to offer as high power amplifiers. These results are in good agreement with the experimental data (V.K.KORNIJENKO & V.S.MIROSHNICHENKO, Izv.Vuzov - Radioelektr., V.26, No 3, 93, 1983).

The drawbacks of the single-cavity amplifiers result mainly from the fact that it is impossible to provide both good beam bunching and extraction of the HF energy from the beam by using one and the same interaction space. These processes are to be separated in space. To achieve this objective, one has to use multi-resonator constructions of the amplifier, as in the case of the klystrons with distributed interaction.

The amplifiers characteristics can be substantially improved by using even the two-resonator design as in Fig. 1b. High power amplifiers can be developed, provided that suitable parameters of the resonators and the beam are chosen. It was found that the rather high gain values of the order of 30 - 40 db can be reached with the bandwidths of approximately 1%. The electronic efficiency and the power output P of such amplifiers can be as high as

$$\text{Efficiency} = 0.8\ v_0 / (R_y\ f)$$

$$\text{Power} = 0.05\ \varepsilon_0 (m/e)^2\ v_0^7 / (f^2\ R_y^2)$$

where v_0 is the initial beam velocity, R_y is the radius of the field spot on the diffraction grating of the output resonator, e and m are the charge and mass of electron, respectively, ε_0 is the permittivity of free space.

These results are best illustrated by a specific example. If beam voltage is 100 kV and R_y =5mm then efficiency may be as great as 50% and output power ranges up to about 1 MW at the frequency f=60GHz. The distinctive property of such amplifiers is that the power output essentially depends on the beam velocity which gives possibility of increasing the value of P relatively easy.

3.CONCLUSION. The single-resonator design used for the Smith-Purcell oscillators shows little promise for the development of the high power amplifiers on its base. The application of the two- or multi- resonator systems is only way of creating promising amplifiers of millimeter and submillimeter wave bands. These systems are candidates for the development of high power Smith-Purcell amplifiers which may have practical usage.

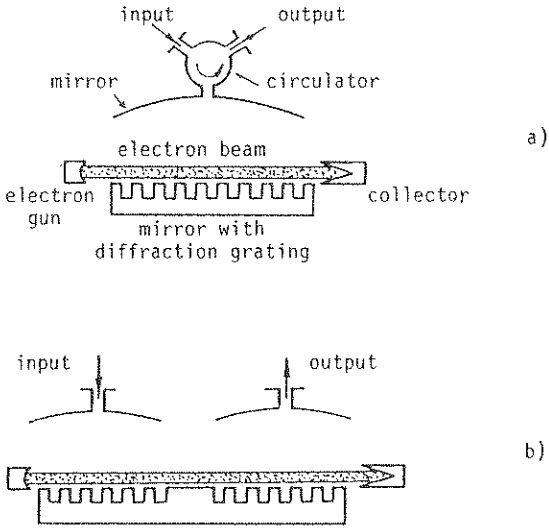

Fig.1. Schematic diagram of the Smith-Purcell amplifiers with (a) single- and (b) two-resonator designs.

FREQUENCY-TUNABLE MICROWAVE SOURCES

L. Brown* and A. Maitland
J. F. Allen Research Laboratories,
The Department of Physics and Astronomy,
The University of St. Andrews,
North Haugh, St. Andrews, Fife KY16 9SS,
Scotland, U.K.

D. M. Parkes
DRA, Electronics Division, RSRE,
St. Andrews Road, Malvern,
Worcs. WR14 3PS, England, U.K.

Significant changes in high power microwave (HPM) technologies have been witnessed throughout the last few decades, not least in the field of HPM sources. A great number of new source types have been proposed and developed. Many are high power versions of the conventional microwave sources such as magnetrons, travelling-wave tubes and klystrons. Others rely almost entirely for their successful operation upon new mechanisms which were rarely exploited before the early 1970s and which are both numerous and diverse in nature.

The incentive behind this increase in the number of tube types is a need to meet ever increasing demands for higher output powers at higher efficiencies. This drive is almost certain to continue with researchers still aiming to increase peak powers, average powers and pulse durations. One of the more dramatic developments that may be attributed to this goal is the introduction of relativistic electron beams in both conventional and relatively new source types. Not only has this resulted in dramatic leaps in output power, but it has also cleared a pathway to the understanding and utilization of a number of mechanisms associated with relativistic energies.

While a significant amount of research is being carried out with regard to increasing the operating frequencies of existing tubes, an associated field, frequency tunability, has perhaps not received the attention it deserves. Source bandwidths and tuning speeds have not enjoyed the significant improvements such as have been observed in the output power arena. This may be attributable to the fact that tuning capacity is often a by-product of a configuration that has ultimately been designed for its power generating capabilities. Through skilful engineering, the tuning capacities of existing sources have been maximised, but the field is still regarded by many as a secondary research issue. As a result, present tuning methods are often restricted, cumbersome and slow.

Oscillators, which by their very nature are designed to operate at sharply defined frequencies, are the least likely candidates for provision of wide bandwidths and rapid tuning. The magnetron provides a typical example. If the operating parameters are maintained at constant values, then tuning of the output cavities will produce bandwidths of approximately 1% or less. Further, tuning is likely to be performed by mechanical means. Gyrotrons provide an example of oscillators which may be step-tuned. This technique allows for

frequency selection by changing the value of a basic operating parameter. In either case, both tuning range and tuning speed are limited.

Amplifiers have demonstrated the greater capacity for tunability to date. Concentrated research in the field of frequency tunability could do well to commence with an investigation of amplifier structures, which by their very nature are wideband. Nevertheless, advances in amplifier bandwidths have not been overly spectacular to date. The majority of amplifiers achieve bandwidths of approximately 5 - 10%, with the exception of the free-electron laser configuration which has achieved bandwidths of approximately 30%. Nevertheless, a number of tubes possess potential for greater tunability. Amplifier investigations may have to overcome problems related to overmoding of slow wave structures. Improved means of narrowband frequency selection will have to be found.

From a tunability viewpoint, microwave tubes may be broadly classified as user controlled or source dependent according to the degree of accuracy with which an operator may select a particular output frequency. User controlled tubes permit absolute external control over frequency. In source dependent tubes, power is the main concern and tunability tends to be a secondary consideration. Such tubes are of limited use in applications where stringent user control over frequency is a requirement. In general, source development has been aimed at producing high powers or wide bandwidths but not both. In seeking to attain extended tuning capacity at high powers, we must ask to what extent the one must be compromised in order to attain the other.

With increased emphasis being placed on pulse-to-pulse (frequency-agile) applications it is our belief that the above issues will become of greater importance to microwave source manufacturers. Through necessities dictated by applications, tuning requirements will become wider and faster. An emphasis may be placed on improved mode selection techniques while the bandwidth capability of existing slow wave structures will require extension. Present microwave generation mechanisms may require tailoring to meet this new demand. For these reasons, we present an overview of existing HPM sources which have demonstrated a variety of bandwidths. We review the mechanisms by which microwaves are generated and tuned, and we classify tube types according to their suitability for frequency-tunable and/or frequency-agile applications.

SCALING LAWS FOR ESTIMATING VERY CLOSE-IN SOURCE REGION EMP AND COUPLING

William J. Karzas
Consultant
7423 W. Manchester Avenue, # 7
Los Angeles, CA 90045-2375

Some time ago it became necessary to estimate the fields and coupling very close to the source of near-ground nuclear EMP. Detailed finite-difference machine computations were in-hand only for radial distances significantly farther out than the desired locations and for various reasons it was not considered reasonable to carry out extensive new calculations. Thus some kind of extrapolation from the existing data became necessary.

While it was simple to extrapolate the driving gamma ray flux, extrapolating the induced electric (and magnetic) fields was less straightforward because we were in a regime where the self-consistent effect (modification of the driving Compton electron motions by the fields they produce) is significant. The procedure decided on was to calculate the electric and magnetic fields at the close-in points without considering the self-consistent interaction (this can be done without expending great effort), and then to use some theoretically derived algorithms to modify them. This approach is reasonable since the intense air conductivity produced by the radiation effectively makes the fields at a given close-in point independent of conditions more than a few skin depths removed. Thus, fields everywhere in space need not be modified for self consistency to make the correction at a few points.

Electric Field Limiting: First we note that a few skin depths away from the ground or any other surfaces, the produced fields are electric only and radial, as if conditions were spherically symmetric. In this case, the Compton electron motion is modified by a radially inward force. Since near the ground typical Compton electrons have MeV energies and travel a few meters before they lose their energy to ionization we can expect energy loss to the electric field to be significant for fields of the order of hundreds of kilovolts per meter. When this occurs the resultant fields will be reduced. A simple analysis is presented with these results:

Let a be the ratio, for non-self-consistent conditions, of the energy drop against the electric field (across the Compton range) divided by the initial Compton energy.

$$a = \frac{e E_0 x_0}{W_0} .$$

Then ε, the ratio of self-consistent to non-self consistent early-time saturated electric field magnitude, is given by the solution of the following equation:

$$\varepsilon^2 (1 + a\varepsilon) = 1 , \quad \text{with} \quad \varepsilon = \frac{E}{E_0} .$$

For strong electric-field limiting, $a >> 1$, so that

$$E = E_0 \varepsilon \approx E_0 a^{-1/3} .$$

Similarly, the magnitude of the Compton current and air conductivity are electric-field limited:

$$J = J_0 \varepsilon^{-2} \approx J_0 a^{-2/3}, \text{ and } \sigma = \sigma_0 (1 + a\varepsilon)^{-1/2} \approx \sigma_0 a^{-1/3}$$

These results are also valid near a conducting surface normal to the gamma flux, and thus can be used to estimate induced charge density.

Magnetic Field Limiting: Of greater interest, perhaps, is the current induced on conductors originating close-in to the source. Within a region a few skin depths thick near conducting surfaces parallel to the gamma Compton currents, the radial (parallel) electric field is very small. In particular, a diffusion theory-like calculation, with ξ the distance normal to the surface and δ the skin depth, gives:

$$E_r \approx \frac{|J|}{\sigma} \left| 1 - e^{-\frac{\xi^2}{\delta^2}} \right|$$

$$H_\phi \approx |J| \delta \, e^{-\frac{\xi^2}{\delta^2}}$$

$$E_\xi \approx \frac{\omega}{c\sigma} H_\phi = \frac{\varepsilon_0 \omega}{\sigma} Z_0 H_\phi$$

Thus, the magnetic field is generated by surface currents of about one skin depth worth of Compton current. This outgoing magnetic field pulse carries with it a transverse electric field E_ξ appropriate to the impedance of a conducting medium.

This magnetic field will dominate the Compton electron motion near the surface of interest. (Since the parallel electric field is reduced, electric field limiting does not occur.) The electrons will be turned with $R_L(H)$, the Larmor radius in the magnetic field.

Letting b be the ratio of electron range to Larmor radius (both for non-self-consistency), another simple analysis gives η, the ratio of self-consistent to non-self-consistent magnetic field as the solution of:

$$b\eta^2 = \sin b\eta \text{ or } 1, \text{ as } b\eta < \text{ or } > \frac{\pi}{2} .$$

For typical, 1 MeV, Compton electrons, the self-consistent magnetic field is

$$B \approx (21 B_0)^{1/2}, \text{ with the fields in Gauss.}$$

Limited Induced Currents: On a cylinder of radius r parallel to the flux, the limited induced current in terms of the non-self-consistent result is

$$I \approx 100 \sqrt{I_0(A)\, r(m)} \text{ Amp.}$$

Some comparisons with detailed numerical calculations will be presented.

Source Region Invited Session

IMPACT OF COMPTON ELECTRON LIFETIME EFFECTS ON SREMP SOURCES

By

C.W. Jones*
T.W. Larkin
W. A. Radasky
K.S. Smith
Metatech Corporation
Albuquerque, New Mexico

Nearly all solutions for ground burst Source Region EMP (SREMP) assume that the Compton current J (A/m^2) and the air ionization Q (ion pairs/$m^3 \cdot s$) possess time histories which are identical to the local gamma ray flux waveform. This assumption is actually an approximation which assumes that Compton electron ranges (and lifetimes) in sea-level air are very short compared to the rise and decay times of the photon pulse. This approximation is therefore dependent on the relationship between the photon time history, its spectrum, and the air density. Modern flash x-ray simulators have improved to the extent that rise times are now faster than 10 ns with energy spectra containing substantial content above 4 MeV (e.g., HERMES III). These characteristics are clearly of interest for considering finite electron lifetime effects.

This paper will examine a set of photon time waveforms with monoenergetic gamma energies to evaluate the Compton currents, ionization rates and the ratio J/Q as a function of time. These calculations are performed by first evaluating the delta function response of a single energy photon flux through the process of creating and tracking a distribution of Compton electrons. Full relativistic electron tracking procedures are considered as well as the secondary ionization energy loss mechanisms. The delta function responses are then convoluted with time histories of interest to produce detailed calculations of the radial Compton current and air ionization rate.

Sample results from our calculations are summarized in Table 1 below. The table indicates the constant J/Q ratio found under the assumption of short electron lifetimes and compares them to time-dependent values calculated for a simple 6×12 ns pulse (rise time $\times$ pulse width). The time-dependent values are sometimes significantly higher than the constant values and will typically result in higher SREMP electric fields.

Table 1. Comparison of detailed electron lifetime calculations with the short lifetime approximation.

E_γ (MeV)	0.5	1.0	2.0	4.0	6.0
Short Electron Lifetime Approximation	6.6(-24)*	1.0(-23)	1.4(-23)	1.6(-23)	1.9(-23)
Finite Electron Lifetimes (t = 10 ns)	7.0(-24)	1.2(-23)	2.0(-23)	2.5(-23)	2.6(-23)

*All values are the ratio of J/Q in $(A/m^2)/(\text{ion pairs}/(m^3 \cdot s))$ for air density of 1 kg/m^3.

COMPTON DIODES RESPONSE TO 14 MEV NEUTRONS

*F.Amaudric du Chaffaut
A.Stark (Service C.E.M. B.P.12 - 91680 Bruyères le Châtel FRANCE)

INTRODUCTION

For solving Maxwell's equations and for computing E.M.fields in a medium, it's necessary to know the conductivity and the currents inside this medium. In this study we are specially interesting in the I.E.M coming from the interaction between neutrons and air.

As neutrons are crossing air they give energy to charged particules, and at the same time, "γ" rays are created. Then "γ" rays give energy to the matter and produce recoil electrons current. The computation of the air ionization and its conductibility with the associated electrons current has been made, for a hundred meters high aerian explosion with the Tripoli 2 code for one neutron source (Ref:: C.E.A. CONF 9706 - Vergnaud, J.P.Ulpat, J.C.Nimal, G.Faucheux). The computed current intensity is straight connected to the incident neutron flux, then it's very important to measure this flux precisely. In this study we present a calculation of a Compton Diode response to 14 MeV neutrons. Then we compare the computed sensitivity to this one got experimentally.

I COMPUTATION OF THE COMPTON DIODE RESPONSE TO 14 MEV NEUTRONS

Compton diode is composed of three main parts:

the intake window
the coming out window
and the central electrode which is called collector (cf following figure)

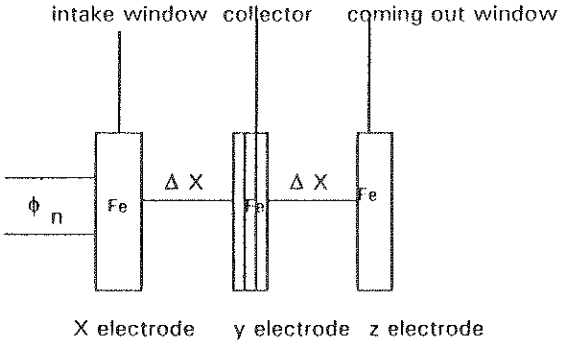

COMPTON DIODE DIAGRAM

γ"rays create electrons (Compton effect, photoelectric effect). Then the topic of this study is to compute the electric signal induced on the collector.
The calculation is composed of three main steps:

1- for each plate we compute the "γ" rays number emitted in each band of energy with two cross section data tables.

2- for each area facing another one we compute the "γ" rays going in and out.

3- finally using "γ" rays flux and DELLIN and MAC CALLUN tables we calculate electrons currents.

We find that the theoritical sensibility value does'nt change a lot according to the used cross sections.

II EXPERIMENTAL NEUTRON SENSIBILITY of the COMPTON DIODE

The method we have used is the following one:
We have measured a 14 MeV Neutrons source on one hand with the compton diode and on the other hand with a standard detector, "the recoil protons telescope", the sensibility of which is kown very exactly.

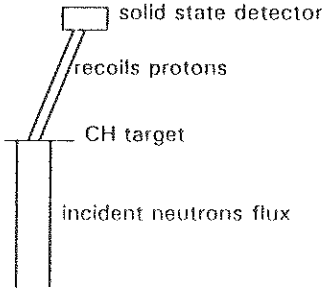

Principle of the Recoil Protons Telescope

We have found a gap of about 10% between theoritical and experimental sensibility value of the compton diode.

CONCLUSION

The very simple model we have used for computing the neutrons sensibility of the compton diode gives us a value compatible with the experimental value. This result is very important, it shows that compton diode generally used as "γ" sensor, can be a very good neutron detector. The main quality of this sensor is its simplicity. It runs in high doses level, without feeding voltage. It would be interesting to carry on this study in computing compton diode sensibility according to incident neutrons energy.

SREMP* SIMULATION USING ASTERIX FLASH X-RAY FACILITY** RADIATION FIELD DATA AND ANALYSIS

M. VIE, E. DELAHAYE*, G. NOUVEL,
CENTRE D'ETUDES DE GRAMAT, F-46500 GRAMAT, FRANCE

ASTERIX is a french 7 MeV end point voltage flash X-Ray (réf. P. EYL & Al. IEEE Pulsed Power Conference June 1989, Montery CA) used for SREMP studies.

From current and voltage diagnostics delivered at the diode, we have computed electronic distribution resolved in angle, energy and time.

This numerical simulation is performed using MAGIC, a two dimensional electromagnetic particle in cell code (B. Goplen & Al., MRC/WDC-R-201, oct. 89).

The previous electron source is used to compute the X-Ray distribution at the external side of the converter versus energy (fig. 1), angle (fig. 2) and time. X-Ray source calculations are made by using the CEG Monte Carlo code Electre 6 - Phoebus 6 (NOUVEL & Al., RADECS MONTPELLIER, sept. 91).

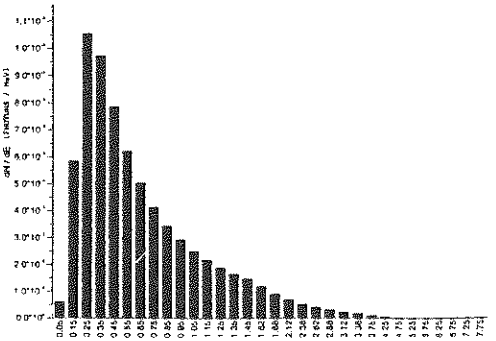

E(MeV)

Fig. 1 : TOTAL PHOTON DISTRIBUTION VS ENERGY

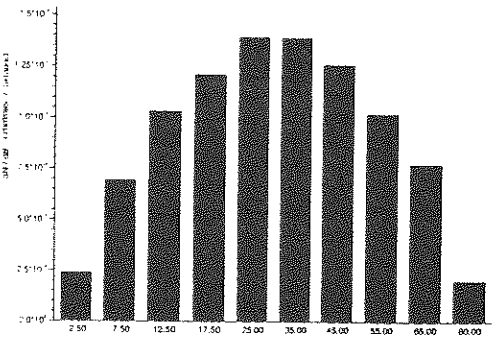

θ (degree)

Fig. 2 : TOTAL PHOTON DISTRIBUTION VS ANGLE

Total ionizing dose is then computed inside an experimental dosimeter made of 8 mm Silica modelled like silicon and 3 mm Aluminium encapsulation.

---

* Source Region ElectroMagnetic Pulse

** This work has been supported by the French Delegation Generale pour l'Armement

Calculated total dose results are given versus radius on the converter R(cm) and versus the silicon depth Y(10^{-2} cm) (figure 4).

We have used RPL* silica and TL** LiF dosimeters distributed on the converter exit surface. The measured discrepancy between LiF and silica dosimeters is less than 15 %.

The data versus calculation are in agreement in the range of 10 % except for the first and the fourth radius where the discrepancy can reach 40 % (Fig. 5).

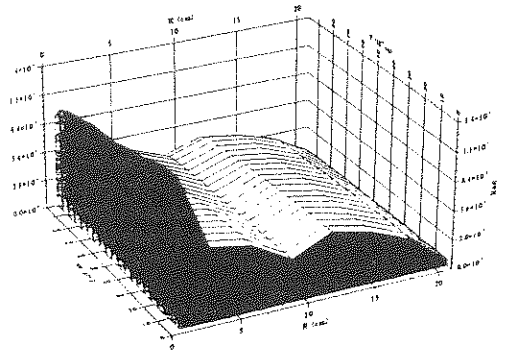

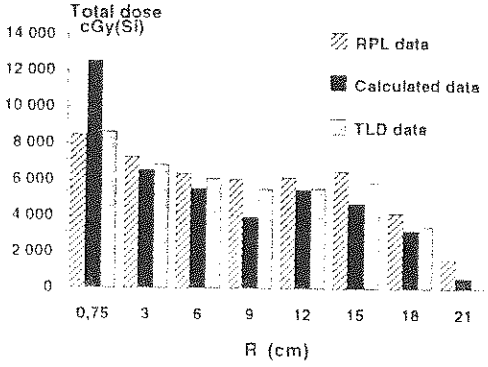

Fig. 4 : CALCULATED TOTAL DOSE VS RADIUS (R) ON THE CONVERTER AND VS DEPTH OF SILICON (Y)

Fig. 5 : EXPERIMENTAL AND CALCULATED TOTAL DOSE DATA COMPARISON

Time, angle and energy electron and photon distribution data show an ASTERIX's nominal behaviour in agreement with previously published works with AURORA, HERMES III and MAXIBEAM 6-150 (KORNAHL & AL., IEEE Pulsed Power Conference, 1987).

The photons beam properties will be used to compute the compton current density and fields inside the ASTERIX's test cell for Source Region Electromagnetic Pulse Coupling.

---

* Radio PhotoLuminescent

** ThermoLuminescent

OVERVIEW OF LOW ALTITUDE EMP GENERATION AND COUPLING TO SYSTEM

Christian CAREL

THOMSON-CSF
Division Radiocommunications
Guerre Electronique et Sécurité
66, rue du Fossé Blanc - B.P. 156
92231 GENNEVILLIERS Cedex

The objective of this communication consists in a general presentation (based on open litterature) about this physics mecanisms which occur during a low altitude nuclear event and which lead to low altitude EMP generation, propagation and coupling to system.

During the presentation the following points will be approached :

- Radiation sources ; their interactions with environment ;
- Compton electrons production ; the source current ;
- Air ionization ; air chemistry ; the conduction current ;
- Self consistent behavior of the currents with electromagnetic fields ;
- Maxwell's equations ;
- Outside source region electromagnetic fields ;
- Coupling to long line and 3D systems.

SHORT-PULSE INTERACTION WITH COMPOSITE MATERIALS: PHASE-SPACE DATA PROCESSING

Leopold B. Felsen
Department of Electrical Engineering
Polytechnic University
Six MetroTech Center
Brooklyn, NY 11201 USA

Abstract

When materials are excited with short-pulse (SP) electromagnetic (EM) waves, the time domain (TD) response furnishes a rich data base because of the very wide bandwidths (VBW) accommodated in a single experiment. The initially highly resolved SP signal is modulated and distorted during its interaction with the material, which generally has temporally dispersive EM properties. When the material properties change with time, spatial dispersion appears as well. Interpretation of the TD response in terms of the wave phenomena that are responsible is essential either for extracting the material properties from a test sample, or for modifying the configuration and/or excitation of a known material in order to shape the output signal. In layered composites, the wave-based interpretation has to take into account the material dispersion as above and the structural (configurational) dispersion due to the layering; structural dispersion, as manifested by guided modes or spatial resonances, is present even when the layer materials are not temporally dispersive.

The direct TD interpretation of the dispersively distorted data via wave-oriented TD processing is a new challenge for the analyst. Because SP-induced phenomenology differs drastically from that in the frequency domain (FD), the conventional transformation from TD to FD loses the relevant physics because of the subsequently required VWB synthesis. Instead, using TD wave objects as basis elements in the processing retains the relevant physics. The problem can be approached systematically by projecting the space-time dependent data base onto appropriate subdomains of the eight-dimensional configuration $(\underset{\sim}{r}, t)$ - spectrum $(\underset{\sim}{k}, \omega)$ phase space, where $\underset{\sim}{r}$ is the position vector in space and $\underset{\sim}{k}$ is the corresponding wave vector in the spectral domain. Space-time ray techniques and TD leaky mode techniques are invoked to develop the phase space tracks of the signal due to material or structural dispersion. Windowed and multiresolution transforms of the data are shown to implement the phase space projection. These concepts are illustrated on various examples.

COLLECTIVE EFFECTS IN AN ELECTRON PLASMA SYSTEM CATALYZED BY ELECTROMAGNETIC LOCALIZED WAVES

Dr. Richard W. Ziolkowski
Electromagnetics Laboratory
Department of Electrical and Computer Engineering
The University of Arizona
Tucson, AZ 85721
(602) 621-6173 (office), (602) 621-8076 (fax)
ziolkowski@ece.arizona.edu

The characteristics of the beams generated by ultra-wide bandwidth electromagnetic systems are central to their practical applications. These characteristics include the rate of beam divergence, the beam intensity, and the energy efficiency. Analytical bounds on the characteristics of localized wave beams that are associated with arbitrary pulse-driven multi-derivative array systems have been derived and are supported with a variety of numerical calculations and experiments. These bounds will be briefly reviewed. The discussion will consider the equivalent concepts in the time domain of sidelobes, the depth of focus, and the intensity versus energy focusing properties associated with properly designed localized wave pulsed-beams. Particular attention will be given to the design of focused pulsed-beams whose properties are advantageous for interactions with conductive materials.

It has been demonstrated that there is a possibility of the existence of an essentially single species plasma state represented by a stable packet of charged particles moving collectively through space-time. It will be shown that such a long-lived, collective plasma state, bosonic in nature, can be catalyzed by an electromagnetic localized wave. Condensation to this state is shown to occur on a very short time scale. The model treats the particle packet as a warm electron plasma (fluid) and self-consistently incorporates the resulting electromagnetic field. It is analogous to models of superconductors where the phonon states mediate the condensation process. In fact a localized wave analysis of type II superconductors can be performed; this analysis will be mentioned briefly. Predicted characteristics of the localized particle packet and its associated electromagnetic fields compare favorably with recent experimental data.

We will examine the possibility of exciting one of these collective electron packets in or near a conductor with a focused, electromagnetic localized wave pulsed-beam. Emphasis will be given to realizable sets of plasma and field parameters. Implications to material characterization and remote sensing applications be discussed.

TRANSIENT EFFECTS ON DISPERSIVE MATERIALS

Ph. LEVEQUE* - B. JECKO

I.R.C.O.M. - Equipe "Electromagnétisme"
Faculté des Sciences - U.R.A. au C.N.R.S. n°356
123, Avenue Albert Thomas 87 060 LIMOGES CEDEX

The propagation of transient electromagnetic fields in dispersive dielectric or ferrite media is studied. The dielectric media are assumed to be linear, isotropic, homogeneous and can be described by the Debye or Lorentz model. The saturated ferrite media are assumed to be linear, anisotropic, homogeneous and can be described by the Polder tensor. The frequency-dependant finite difference time domain $(FD)^2$ TD method is used to calculated the response of pulses in dispersive media, using two conceptually different approaches.

- Convolution integral technique

The first approach uses a convolution integral ; in the time domain, the flux density ($\vec{D}$ or $\vec{B}$) is the convolution of the dielectric or magnetic tensor with the field ($\vec{E}$ or $\vec{B}$). This convolution is untractable in the nearest neighbor FDTD approach. Therefore this term is performed recursively, exploiting the exponential nature of the time domain susceptibilities.

- Differential equation technique

The second approach relates the field $\vec{E}$ (respectively $\vec{B}$) to the flux density $\vec{D}$ (respectively $\vec{B}$) via an ordinary differential equation. For example, the electric flux density $\vec{D}$ is given by $\vec{D} = \varepsilon_\infty \vec{E} + \vec{P}$ and the equation for an electric polarization $\vec{P}$ in a medium with orientation polarization characteristics, corresponding to the Debye model, is given by a first order differential equation. Also we can obtain the relation between $\vec{E}$ and $\vec{D}$ using the finite difference approximation.

Applications

To validate this method, we consider a microstrip patch antenna with a lossy dielectric substrate, assumed to have an orientation polarization and we study the dispersive material effects on the classical characteristics of antennas, deduces from Fourier transform. Especially we can obtain the dissipated power in the substrate. An other application concern the saturated ferrite microstrip antennas. First the method has been validated for a two dimensionnal problem of a guided wave. Second a comparison between theoretical results and experiment is done considering a rectangular patch antenna with a biased ferrite substrate. Finally a ferrite circulator is studied.

As application, this time domain approach allows to examine the electromagnetic behaviour of dispersive materials illuminated by electromagnetic pulse. Moreover, it is possible to consider the dispersive characteristics of a physical ground (especially the frequency dependance of permittivity) for the transient studies.

In conclusion, a powerful method has be developed to consider dispersive materials. It has been found that the F.D.T.D. method is capable of predicting transients that are associated with propagation in dispersive media such as Debye or Lorentz media, or anisotropic saturated ferrites. Thus, it is possible to simulate propagation in realistic materials in the time domain.

MACROSCOPIC DESCRIPTION OF MATTER

A.N. Serdyukov

Principle problems of macroscopic electrodynamics of bianisotropic media are discussed.

A detailed analysis of macroscopic electrodynamics symmetry has been carried out. Relations of reciprocity for macroscopic parameters of bianisotropic media, which are illustrated by examples of dual symmetrical electrodynamics of naturally gyrotropic, magnetically active and moving media, have been formulated.

A relationship between different methods of phenomenological description of natural gyrotropy has been stated.

It has been proved a universal summation rule consisting in the fact, that integral at all frequencies from the real part of magnetoelectric gyration pseudotensor being equal to zero.

ELECTROMAGNETIC SCATTERING IN COMPOSITE MEDIA

J.P. PARNEIX, F. DE DARAN, V. VIGNERAS-LEFEBVRE

Laboratoire de Physique des Interactions Ondes-Matière (PIOM)
CNRS, URA 1506
E.N.S.C.P.Bordeaux, 351 Cours de la Libération
33405 Talence Cédex, France

The growth of new materials with specific electromagnetic properties (absorbing or transparent materials), most often leads to the utilization of heterogeneous structures. The numerous parameters arising in their conception, such as the size, the nature or concentration of the different constituents, makes necessary a modelization that precedes the conception. The classical mixture laws usually fail when the concentrations of inclusions are strong or when the inclusion sizes are in the same order as the wavelength.

In this paper, we present a model using the multiple scattering formalism. The general wave propagation equation is first solved in the case of a single sphere, using the Mie theory. The formalism allows us to easily separate the parameters associated with the nature of the particle from the elements connected with the spatial point where the field is calculated. The multiple scattering is studied by using an iterative method. First, we calculate the field scattered by each sphere, as if the sphere was alone in the incident field. This first order scattered field serves in its turn as an incident field that will be scattered by the spheres, and so on, until the solution converges.

Numerical results for the backscattering, forward scattering and more generally the scattering diagrams of single spheres of different nature (perfectly conducting, lossy dielectric -homogeneous or stratified-, chiral, etc...) are presented, as well as the scattering diagram of systems of colinear or coplanar spheres. The effects of coupling between the spheres on absorption properties are investigated in details. The numerical data are compared to bistatic free-space measurements achieved by using vectorial network analyzers.

BROADBAND CHARACTERIZATION OF A Ni Zn FERRITE/Ba TiO_3 COMPOSITE USING THE 14mm DIAMETER COAXIAL AIR LINE T/R TECHNIQUE

Richard G. Geyer, James Baker-Jarvis,
John H. Grosvenor, Jr. and Claude M. Weil*
Electromagnetic Fields Division (813.08),
National Institute of Standards and
Technology,
Boulder, CO 80303

The Transmission/Reflection (T/R) method is a widely used measurement technique for characterizing the dielectric and magnetic properties of homogeneous and isotropic solid materials over broad ranges of the RF/microwave spectrum. Improved algorithms, based on an iterative solution, have been developed for this technique at NIST. These yield measurement accuracies of the order of +-5% for low-to-medium permittivity (ϵ_r' < 50) and medium-to-high loss materials.

This talk will discuss the application of this technique to the characterization of a heterogeneous composite mixture consisting of a nickel-zinc ferrite embedded in a barium titanate matrix. This material was developed for use in lossy feed-thru filters designed for EMI reduction applications, as part of a NIST-industry collaboration. Using a 14mm diameter coaxial air line, measurements of both complex permittivity and permeability were conducted over the RF spectral range of 1 - 2000 MHz. NIST characterized a total of nine separate samples with differing volumetric fractions of the ferrite media ranging from 0 to 100% in 12.5% increments.

Samples with low ferrite loading in the range 0 to 25%, presented a major measurement challenge owing to their very high permittivity values. For example, the 0% ferrite-loaded sample (pure Ba TiO_3) exhibited an ϵ_r' value of approximately 1500 at frequencies less than 100 MHz. The application of the coaxial air line T/R technique to the measurement of materials with permittivity levels exceeding 100 generally results in major inaccuracies caused by the inevitable presence of an air gap between sample and the coax line inner conductor. This gap always biases measured data low and must be corrected for. The magnitude of this error and methods of correcting for it will be discussed at length.

As part of this study, we examined the fit of the measured data to a modified Maxwell-Garnet model which predicts the properties of a magnetic dipole-loaded matrix. Reasonably good agreement was noted.

PARTICULAR WAVES IN CHIRAL MEDIA

Semchenko I.V.

Gomel State University

Sovetskaya St.,Bld.104, 246699, Gomel,Belarus

Telephones (0232) 577520, 576557

E-mail:root % tpf.gsu.gomel.by @ relay.ussr.eu.net.

Particular waves in various chiral media are treated which have the symmetry characterized by the absence of any inversion center. Such symmetry of a medium is caused either by the structure of individual molecules or by the spatial spiral arrangement of molecules. Phenomenological material equations for chiral media, including the relationship between the electrical induction and the magnetic field intensity and the relationship between the magnetic induction and the electric field intensity, have been used. Cases of scalar and tensor susceptibilities describing the properties of chiral media have been examined. Calculations are made using direct or coordinateless techniques of the tensor calculus.Also, the technique of transition to the twisted coordinate system accompanying the rotation of molecules of the chiral medium are used.

It is demonstrated that the particular waves can appear in the region of the medium absorption. The dielectric permeability of themedium at these frequencies acquires small magnitudes close to naught and becomes comparable with the parameter characterizing the chirality of the medium. A possibility is demonstrated that a particular circularly polarized wave having the polarity sign governed by the sign of the chirality parameter of the medium,can exist in the bi-isotropic media. The bi-isotropic medium is monorefrective at the frequency at which this wave originates, i.e.,no other waves can be excited at this frequency. This particular wave is characterized by electric and magnetic fields different from naught. Yet,the Pointing vector of this wave reduces to naught and the wave does not transport any energy in the space. Longitudinal waves of the plasma type can also exist in the bi-isotropiuc medium at some other frequency. A wave with the random ellipticity and infinite phase velocity independent of the coordinates,is alsopossible. Particular waves can be excited by an electromagnetic wave incident externally upon the bi-isotropic medium and may also result from the Vavilov-Cherenkov effect.

Also, spirally structured particular waves in the chiral media have been investigated. This structure results from the spiral ordering of molecules or other microelements of the medium. The type of the particular waves in the medium depends upon the relationship between the period of the spiral structure and the length of electromagnetic waves in the vacuum.

PROPAGATION IN UNIAXIAL BIANISOTROPIC COMPOSITE MATERIALS

Sergei A. Tretyakov*, Alexander A. Sochava, and Tatiana G. Kharina
St. Petersburg State Technical University, Radiophysics Department
Polytekhnicheskaya 29, 195251 St. Petersburg, Russia
(Phone: +7-812-552-7685, Fax: +7-812-552-6086)

In the last few years, novel biisotropic and bianisotropic composite materials for advanced microwave applications were extensively studied with remarkable progress. Samples of isotropic chiral composites were fabricated and measured by several laboratories. Theoretical studies of still more complex and general structures showed that also non-reciprocal biisotropic materials and specific bianisotropic structures (*omega composites*, see M.M.I. Saadoun and N. Engheta, Microw. and Optic. Technol. Lett., 5, 184, 1992) can offer novel and most interesting possibilities for microwave technology. Uniaxial omega composites with Ω-shaped conductive inclusions distributed in an isotropic matrix in a certain order appear to be prospective for anti-reflection coverings (S.A. Tretyakov and A.A. Sochava, Electron. Lett., 29, 1048, 1993).

In this presentation we report the results of the studies of wave propagation in general uniaxial materials with Ω particles *and* with intrinsic handedness, i.e. in uniaxial chiral omega structures. Since both the chiral materials and the omega structures possess interesting novel features, it is promising to study properties of more general media, which are the subject of this presentation.

The material equations modelling the most general uniaxial media can be expressed in terms of uniaxial constitutive dyadics, which define the relations between the field vectors:

$$\overline{D} = \epsilon_0(\epsilon_t\overline{\overline{I}}_t + \epsilon_a\bar{z}_0\bar{z}_0)\cdot\overline{E} + j\sqrt{\epsilon_0\mu_0}\,(-\kappa_t\overline{\overline{I}}_t - \kappa_a\bar{z}_0\bar{z}_0 + K\overline{\overline{J}})\cdot\overline{H},$$
$$\overline{B} = \mu_0(\mu_t\overline{\overline{I}}_t + \mu_a\bar{z}_0\bar{z}_0)\cdot\overline{H} + j\sqrt{\epsilon_0\mu_0}\,(\kappa_t\overline{\overline{I}}_t + \kappa_a\bar{z}_0\bar{z}_0 + K\overline{\overline{J}})\cdot\overline{E},$$

where the unit vector $\bar{z}_0$ points in the direction of the geometrical axis, $\overline{\overline{I}}_t = \bar{x}_0\bar{x}_0 + \bar{y}_0\bar{y}_0$ is the two-dimentional transverse unit dyadic, and $\overline{\overline{J}} = \bar{z}_0 \times \overline{\overline{I}}_t = \bar{y}_0\bar{x}_0 - \bar{x}_0\bar{y}_0$ is the 90 degree rotator in the transverse $(x-y)$ plane.

Chirality of the material is measured by the parameters κ_t and κ_a. The dimentionless material constant K modelles the field coupling due to the omega particles.

First, we consider eigenwaves in unbounded uniform general uniaxial media. They are, in general, elliptically polarized. Since the opposite directions of the geometrical axis z are physically non-equivalent, the polarization patterns depend on the sign of the propagation factor in the z-direction. Next, the theory of reflection and transmission in plane layers is developed based on the vector transmission-line model. Numerical examples clarify the effects of chirality and omega coupling on the reflection and transmission properties of plane general uniaxial layers.

Practical possibilities to realise complex omega composites are discussed, and an approximate analytical model of dependence of the constitutive dyadics on the geometrical microstructure is presented.

ELECTROMAGNETIC PROPERTIES OF COMPOSITE MATERIALS, THEORETICAL ADVANCES : A HELP FOR DESIGNING COMPOSITES FOR APPLICATIONS

Thierry ROBIN and Bernard SOUILLARD*
X-RS, Parc-Club, 28, rue Jean Rostand,
F - 91893 ORSAY Cedex, FRANCE.
Also at :
Centre de Physique Théorique, Ecole Polytechnique,
F - 91128 PALAISEAU Cedex, FRANCE.

We consider the electromagnetic (optical, infrared, microwaves,...) properties of composites made with inclusions of different materials and forms in a matrix.Such composites have many applications : radar stealth, electromagnetic compatibility, infrared controlled emissivity, electromagnetic shielding, radomes, ...

Despite of much work, a complete theoretical approach for this very difficult problem was still lacking. The existing theories worked only for a small range of concentrations and/or for a small range of frequencies of incident radiation and a rather large proportion of experimental results is not clearly understood.

Different approaches have been developed to calculate the electromagnetic properties of heterogeneous materials. Most theoretical approaches to describe the frequency dependent electromagnetic properties are based on "*effective medium*" type of approximation that compute the permittivity of an equivalent homogeneous material. Conducting grains are supposed to be much smaller than the wavelength and are treated as separated.

These theories have been shown to work quite well for low concentrations or for low contrast. But it has been increasingly recognized that they could not describe correctly the electromagnetic properties of dielectric-conductor or dielectric-semiconductor composites at intermediate concentrations, for example near the insulator-conductor threshold. In this case, according to us, the main reason for their failure at higher concentrations, and in particular in the vicinity of the insulator-conductor threshold, relies on the fact that many inclusions can be close enough to form aggregates where the current can flow or where there is a strong electromagnetic interaction via induced polarization between the inclusions (see the figure).

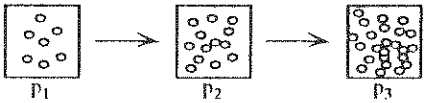

Since 1989, we developed a new theory. In contrast to other theories our approach takes fully into account the microscopic structure of the composite and in particular the aggregation in the composite. We thus gave our theory the name : "Theory of Aggregates". It can treat most materials and gives qualitative and quantitative good results for all concentrations of inclusions, especially in the domains of the parameters where other theories are wrong but that are essential for the applications.

We will present the recent advances of the theory. In particular, we will expose the results of our model in different cases for the form and the material of the inclusions :
- form: spheres, fibers, disks,...
- material: dielectric, good or poor conductor, semiconductor, conducting polymer,...

Finally, we will discuss different cases for the resulting composite material :
- isotropic,
- anisotropic,
- bi-anisotropic,...

We will show that the theory can be a good help for designing new composites materials with specific electromagnetic properties. The theory cannot totally avoid experimental work but it can significantly reduce the number of experimental attempts.

It can be also a help for understanding the properties of existing materials. For example, it is sometimes very interesting to know the electromagnetic properties of a composite designed for a specific frequency band in different bands.

SPECIAL WAVES IN ELECTRODYNAMICS OF BIANISOTROPIC MEDIA

G.S. Mityurich, A.N. Serdyukov*

A theory has been developed and characteristics of specific electromagnetic waves in bianisotropic crystals and artificial media when one of the main tensor values of dielectric (magnetic) permeability being in the region of small values have been investigated.

THE TIME BEHAVIOUR OF THE HIGH ORBIT SPACECRAFT CHARGING AND ITS CONNECTION WITH THE MAGNETOSPHERE DYNAMICS

Popov G.V.(*) and Degtjarev V.I.
Inst.Solar-Terr.Phys. RAS
664033 Irkutsk, P.O.Box 4026, Russia

The electrostatic charging of spacecrafts (SC) is an extremely complex phenomenon, which attracts the attention of different branches of the fundamental and applied science. So, for example, for engineers and users of SC the charging is a process which has as consequences some hazard discharges and payloads mulfunctions. As for the magnetosphere physics, it view at the charging of SC as at a phenomenon closely related with properties and dynamics of the magnetospheric plasma.

The report outlines main approaches and results obtained in ISTP RAS in treating experimental data on charging of high orbit Russian satellites. In-flight experiments were performed on different orbits: geostationary, high-elliptic "Molniya"-type and high circular (about 20,000 km) orbit . Measurements of surface electrostatic fields on SC's were made by a group from the Novosibirsk University and probes installed at different satellites were identical.

The following aims were stated in treating and interpreting the primarily experimental data:

- To evaluate, if any, main regularities in time behaviour of the SC electrostatic sheath.
- To compare regularities revealed with existing theoretical understandings of the Lengmuir-probe behaviour.
- To identify physical agents, which control the amplitude and time variations of electrostatic fields on the SC surfice.
- To find links between the time variation of the SC-charging and processes in the magnetosphere.

The main approach used in the data treating is a typical one for the magnetosphere physics, namely:

- Data on electric field were appended by data on charged particles fluxes measured on same spacecrafts (these experments were performed by Moscow University group) and by data of ground based measurements of geophysical values. Combined together these data sets allowed to restore the general picture of the magnetosphere processes, taking place during time intervals of interest.
- Experimental data were grouped in accordance with the level of magnetospheric activity: results specific for quiet days were separated and these results were used as a reference level for the disturbances evaluation.
- The so called "Index of charging disturbances" (IE) was introduced for the discription of the 3-dimension electrostatic sheath of the SC, which in a method of its evaluation and its physical meaning is similar to the well-known AE-index.

As a result of treating experimental data from geostationary communication satellites "Gorizont" regular daily variation of the charging was obtained, which reflect the daily crossing by SC of different regions of the magnetosphere. Disturbances of charging, closely related to typical for substorms injection events were established also. Simultaneous observations of charging of two geostationary SC's allowed to track the propagation in space of effects from injections on the SC-charging. A very interesting and not fully understood feature was revealed in regular charging variations: electric fields on the SC surface did not respond to the SC crossings of the plasmapause, when the plasma acting on the SC changed its parameters abruptly and substantially.

Main regularities in time variations of SC charging discovered for geostationary orbit were confirmed in general by treating data obtained at other high orbits. Of course, regular variations change from one type of the orbit to another.

The investigation of electrostatic field disturbances revealed the direct causal connection of them with magnetosperic disturbances. The "tree of causal relations" was constructed including IE index and ground based measured indices reflecting the geophysical values (geomagnetic field, riometric absorption, ionosphere parameters and other) disturbances. This made it possible to put forward the idea how to monitor and forecast the SC charging disturbances on the basis of ground based measurements of geophysical values disturbances.

The report pays a special attention to some questions of the international coordination of the SC charging investigations. The point is that nowaday there exists a considerable difference in aims and approaches of "fundamental" and "applied" investigators of the SC charging. These differences cause difficulties in the mutual uderstanding, and the result is that engineers do not use in full achievements of the magnetosphere physics and, inversely, specialists in the magnetosphere physics do not know clearly how to use there results for the benefit of applied aspects of the SC charging problem. Some proposals are listed aimed to eliminate the gap between fundamental and applied investigations.

SIMULATION OF "SPACE EXPERIMENTS" IN THE LABORATORY

Antonov V.M., Ponomarenko A.G.*, Zakharov Yu.P.
Institute of Laser Physics, Siberian Branch of the Russian Academy of Sciences, 630090 Novosibirsk, RUSSIA

In our report we present the main results of the investigations during the past 20 years which have been directed to the development of ideology and justification of the possibility for conducting a "space experiment" (SE) under laboratory conditions.

The simulation program has the following items:
1. nonstationary processes in the space and near-Earth plasmas;
2. active space experiments (ASE) to investigate the background medium and to look for new physical effects;
3. electromagnetic interaction of spacecrafts (SC) with the background medium;
4. power sources and technology.

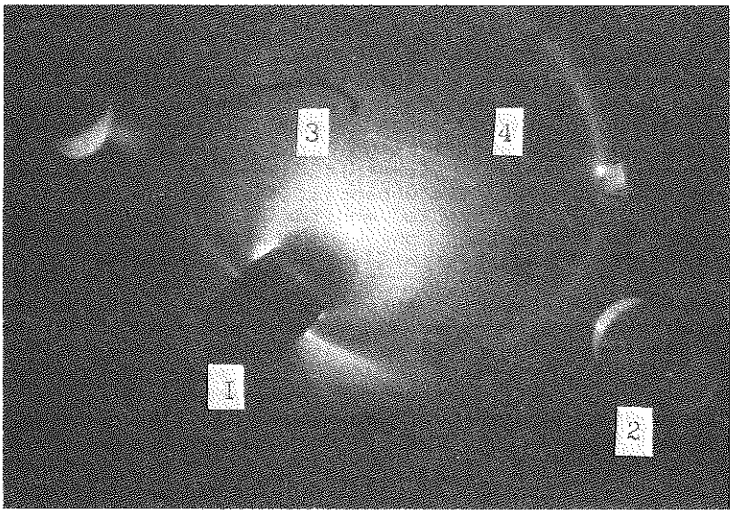

To fulfill the program we have developed an experimental facility named KI-1 (Space Investigations-1) consisting of a high-vacuum chamber with diameter 1,5 m and length 5 m , terrella scale models with characteristic dimensions 5÷20 cm and magnetic moment 10^6-2 10^7 G cm^3, a background plasma injector (50 kJ) and quasi-stationary magnetic field 1 kG, high-power sources of laser radiation with energy 0,1-1 kJ at pulse duration 10^{-7} 10^{-6} s, wide-aperture electron and ion beams with energy 10-300 keV, cur-

rent 1-10 kA and pulse duration 10^{-6}-10^{-4} s, an automized diagnostic complex used for the probe, electromagnetic and optical measurements with high time-space resolution.

According to sections 1 and 2 the experiments and numerical calculations are being carried out for the foundation of a "limited simulation" concept while modelling such fundamental processes as electrodynamics and stability of magnetospheres, space explosions (of Super-nova type), collisionless shock waves, double layers, transients' generation, plasma instabilities and so on. It is obvious that all these problems should be carefully investigated to obtain a dynamic model of the medium, surrounding spacecrafts.

As an example of the possibilities of the KI-1 facility in the Figure mentioned above we present a photograph of the laser plasma explosion, qualitatively illustrating the process of the formation of artificial radiation belts and motion of plasma products in the earth magnetic field (1-terrella scale model, 2-focusing mirror, 3-target, 4-measurement probes).

According to section 3 the techniques of the laboratory simulation of spacecraft charging processes at the geostationary orbit has been developed. We have investigated the dynamics of electrization, the electric discharge formation, electromagnetic pulse excitation and the level of solar batteries' degradation with the complex effect of such space factors as hot and cold plasmas, proper external atmosphere, ultraviolet radiation of the Sun with allowance for electrophysical properties and design peculiarities of the surface materials, plasma and gas jets of the engine setups.

According to section 4 we have investigated the problem of the interaction of the artificial magnetosphere with the background plasma which may arise at launching powerful inductive energy storages into space.

Using the results of the investigations on sections 1 - 3 we have developed the following methods:
- test and calibration of the spacecraft apparatus probes for the measurements of the environment parameters;
- determination of the conditions for the SC charging neutralization by the pulse laser plasma flows;
- control for the SC charging level with the help of dissipating centres and grid screens and some others.

PLASMA SOURCES, ION PROPULSION AND PLASMA CONTACTORS: AN ACTIVE INTERACTION WITH THE SPACE PLASMA ENVIRONMENT

G.F. Cirri, G. Matticari*, A. Matucci
Proel Tecnologie, Firenze (Italy)

The use of plasma sources on board of Earth Orbiting Spacecrafts has been proposed, in recent years, to perform scientific and technology experiments as well as for operational payloads in application missions.

Energetic plasma sources (300-3000 eV) can be successfully exploited for generating thrust and for studying both the propagation and the interactions of a plasma beam within the environmental plasma.

Besides, low energy plasma sources (10 - 50 eV) can be advantageously utilized to prevent or limit the surface charge build-up on spacecrafts by providing an efficient way to "ground" the whole spacecraft to the plasma environment, as well as, when required, for the neutralization of the ion beam produced by ion thrusters.

In this paper the technology developments and on-ground experimental activities at PROEL TECNOLOGIE, both on high-energy and low-energy plasma sources, are presented with refer to:

- Electron Cyclotron Resonance (ECR) ion thruster.
- Neutralizer / Plasma contactor, based on the "hollow cathode" technology.
- Axial Plasma Source, based on the Stationary Plasma Technology.

The ECR radiofrequency (RF) ion thruster is based on an innovative technology whose development is underway at PROEL TECNOLOGIE under ASI contract.

The design goals of this technology are addressed to the minimization of propellant demand (coping with satellite power allocation), to the extension of useful lifetime and to the improvements of beam characteristics, also to avoids problems relevant to spacecraft / space environment interactions.

The ECR thruster, proposed for a thrust in the millinewton range (namely $2 \div 8$ mN), is envisaged for applications on small satellites (or lightsats) in the range $300 \div 800$ kg.

The neutralizer / plasma contactor technology has been initially developed by PROEL (under ESA contract) for the neutralization of the ion beam produced by the German thruster RIT 10 (see Fig. 1). The neutralizer qualification has been recently completed for the ARTEMIS mission. As original application, the plasma contactor extended family ($1 \div 10$ A), based on the "hollow cathode" neutralizer technology, has been developed by PROEL under ASI contract to be applied to Tethered Space Systems and to spacecraft charging prevention. Recently a ground demonstration test of this technology has been successfully carried out sponsored by ESA: the original capability to provide a "ground path" between the spacecraft and the plasma environment has been clearly pointed out.

A plasma contactor has been used indeed to neutralize the artificially induced charge on floating metallic objects in a high vacuum environment. Experiments were made both with

continuous charge injection and simple event charging; transient waveforms associated with the plasma contactor switching on and off have been recorded.

In this paper, the main results of these experiments are presented.

Concerning the plasma sources for scientific applications, PROEL has carried out, in collaboration with MAI-RIAME of Moscow, an extensive characterization activity on a Stationary Plasma Axial Source of Russian design. The beam emitted by the source has been investigated both with refer to the plasma parameters (density, potentials and temperature) and with refer to the current density distribution and beam shape / divergency. This beam extensive characterization, accomplished at PROEL labs, has to be retained as a preliminary ground activity in view of possible in-flight experiments finalized to investigations on energetic (artificial) plasma beam / ionospheric environment interactions.

The significant results of the experimental activity on the Stationary Plasma Axial Source are, as well, provided in the paper.

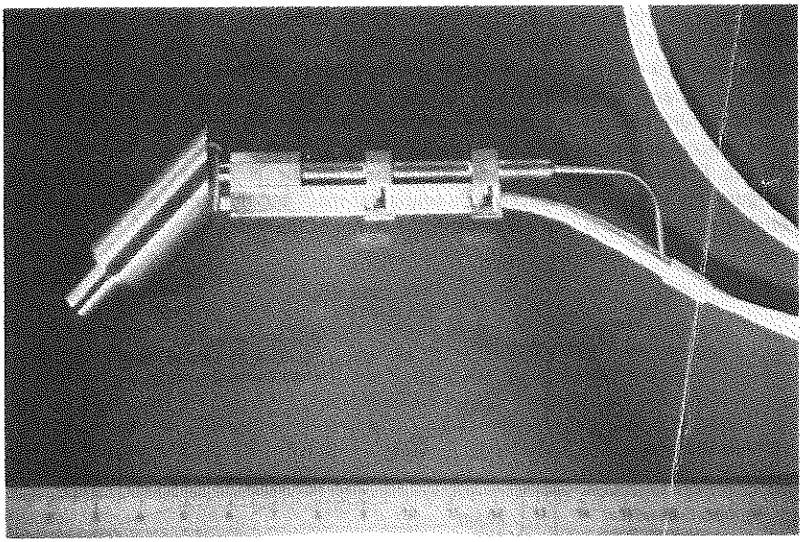

Fig. 1: The neutralizer / plasma contactor technology developed by PROEL TECNOLOGIE

ULF/VLF/ELF ORBITING LONG TETHER ANTENNAS

Carlo Bonifazi (*), Francesco Svelto, and Jean Sabbagh
Agenzia Spaziale Italiana (ASI)
Viale Regina Margherita 202
00198 Roma, Italy

(*)TSS Core Science Equipment - ASI Principal Investigator

The study of electromagnetic waves propagation in the ionosphere in the ULF/VLF range can take a significant advantage by the use of long orbiting antennas which use the Earth gravity-gradient force. These type of antennas, hereon referred to as tethered antennas, can reach lengths of few tens of km.. Orbiting space tether systems have recently reached the level of flight demonstration with SEDS and TSS programs. In fact, the first known demonstration of tethered spacecraft occurred in mid-1960s during NASA's GEMINI Program. On two occasions a Gemini spacecraft (Gemini VI and VII) was tethered to its Agena second stage over a 100-foot distance, with one gravity-gradient oriented and the other slowing spinning. In addition, the 1980s saw several sub-orbital sounding rocket experiments which successfully utilized the tethered concept for electrodynamic applications. What makes the concept of a tethered satellite pratical is the inherent stability of a deployed tethered satellite. Specifically, a tethered satellite system (in circular orbit) can establish a stable configuration where both spacecraft's centers of mass and the tether axis align with a line pointing along the local vertical towards the center of the Earth.

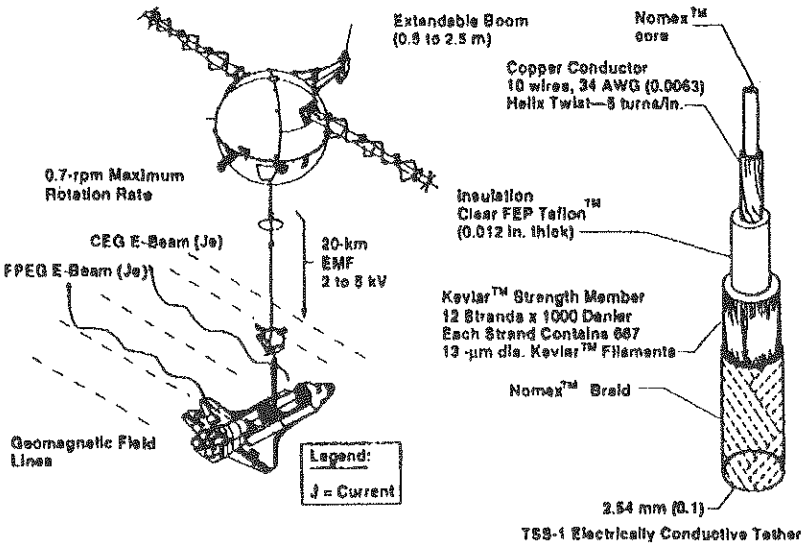

This stable configuration is achieved by the tension in the tether resulting from differences between gravitational and centrifugal forces at the upper and lower end of the tether system. Any perturbation away from this stable configuration orients the tether tension to pull it back to vertical. The magnitude of the tension is surprisingly small, i.e., for a predicted full (20 km)deployment of the TSS-1 tether was of the order of 50 N. It is also possible to take advantage of more complex libration motions - e.g., due to atmospheric drag - to the benefit of science measurements. For example, it may be feasible to consider orienting an electrodynamic tether along the local magnetic field vertical in the auroral regions, for measurement of the natural electric field.

The global current closure mechanism in the TSS strongly affects the actual power that can be radiated. There are different theories for the current closure path through the ionospheric plasma. Someone is speculating that TSS-like configurations will produce a current flowing along the magnetic field lines to the lower ionosphere in the form of Alfven waves, where they will close across the magnetic field due to the high electron-neutral collision frequency. More recently, laboratory experiments at the University of California at Los Angeles (UCLA) by Stenzel seem to suggest Wistler waves to be current-carrier rather than Alfven waves.

A picture of the global interaction of a large conducting body moving in a magnetoplasma was first indicated by Drell et al.. At a given instant, the two terminations of the system apply potential pulses of opposite polarization to the magnetic flux tubes they intercept (i.e., positive at the satellite and negative at the Orbiter for the TSS-1). This process results in a charge transfer between the two terminations and the ambient plasma. This perturbation generates waves out of the system, which transport away the space charge set up between the end flux tubes. The superposition of the waves generated, at successive times, on different flux tubes, forms two wings of opposite charge polarization left behind by the two terminations of the system.

The first Tethered Satellite System (TSS-1) Electrodymanic mission has been launched aboard the Space Shuttle STS-46 on July 31, 1992, as a joint mission between the United States and Italy. A 500-kg, spherical Satellite (1.6 m diameter), attached to the Orbiter by a thin (0.24 cm), conducting, insulated wire (Tether), has been reeled upwards from the Orbiter payload bay to a distance of 257 m, rather than the expected 20 km, when the Shuttle was at a projected altitude of 300 km. The first TSS mission was intended to demonstrate some of the unique applications of the TSS as a tool for research by conducting exploratory experiments in space plasma physics. Electrodynamic goals included evaluation of system current-voltage(I-V) response, the study of controllable field-aligned current and waves structures (simulating natural processes of the planetary ionospheres and magnetospheres), sheath physics, and spacecraft charging.

The paper will describe the TSS, whose reflight is now scheduled on October, 1995, and its basic applications as an antenna for ground base observations in the ULF-VLF-ELF frequency bands.

ELECTROSTATIC DISCHARGE PLASMA PROPAGATION AND INTERACTION MODELLING

A. Soubeyran *, J.P. Estienne
Matra Marconi Space France
31 rue des Cosmonautes, Z.I. du Palays, 31077 Toulouse Cedex, France

L. Talaalout
Centre National d'Etudes Spatiales
18 av. E. Belin, 31400 Toulouse Cedex, France

Introduction

When immersed into the space plasma environment, spacecraft elements acquire a certain charging level. As a result of either infra or inter elements differential potential, electrostatic fields may reach high enough values to exceed breakdown values. Several mechanisms are in fact likely possible, which lead to apparently different type of electrostatic discharges (ESD : "blow-off", "punch-through", "inverted voltage gradient"). Although these mechanisms are not yet fully understood, empirical risky levels have been derived for different configurations, mainly from ground experiments.

Discharge coupling

After this initiation, the phenomenon involved in the development of the discharge and its effects on electronic systems is far from being subdued. After more than twenty years of in-flight electronic perturbations recording, it remains today almost impossible to identify positively the ESD origin of anomalies (apart from statistical correlation with charging level), essentially due to the lack of understanding in coupling mechanisms between discharges and electronic devices. Two ways can be basically followed by the discharge to couple into electrical circuits :

1- Direct transfer of charged particles (conductive path): replacement currents (blow-off and image charges) and collected currents (flash-over) near the discharge site (which may reach sometimes at least meter extensions)

2- Electromagnetic coupling (radiative path) : parasitic reception by wires and antennae (mainly high frequency)

The blow-off current

Only the first point was so far widely addressed by numerical modelling, restricted in fact essentially to replacement currents, that is the direct injection of current into structure or circuits, using a circuit analyser resolution of lumped element models. This is on one hand because of the relative simplicity of this restricted problem and on another hand due to available experimental measurements of the blow-off current. Unfortunately it does not generally bring a correct evaluation of the actual threatening currents, thus explaining the high margins taken to protect electronics and failures in spite of all.

New unified approach

As a result of a long term effort in MMS, partly supported by CNES and ESA, advanced numerical simulation tools are under development to model the results of new conceptual analysis pertaining to the discharge propagation and coupling phase. These new developments are directed first of all toward the previously untreated areas, namely the electromagnetic pulse associated to a discharge on one hand and the collection of flash-over currents on the other hand.

The electromagnetic pulse

As a first attempt, the electromagnetic pulse can be modelled as the result of the blow-off current flowing in a large wire crossing the surface of the spacecraft and extending away from it. Such a model permits to use a Boundary Integral Equation formulation for MAXWELL equation resolution in vacuum (Method of Moments used in MAXSIM software developed at MMS for ESA). It is also possible to approximate in experimental conditions. Although representing a large improvement with respect to previous simulations, this approach is however not fully satisfactory because there are interactions between the ejected current and the corresponding e.m. field. It was the reason to move toward a much better simulation based on a volume resolution of the coupled MAXWELL and VLASOV transport equation. Especially efficient numerical technics are being developed to be applied on an unstructured finite element grid meshing : C.F.D. based flux method for MAXWELL equations and the same for VLASOV equation after a conversion into an hyperbolic system using appropriate base functions to project the distribution function on, separating the velocity dependant part (MATESD software developed at MMS for CNES).

The flash-over current

With respect to the flash-over current, it is more and more considered that not only negative particles but also positive ones are generated during a discharge event, so that we are dealing in fact with a plasma. This plasma seems likely dense enough in some cases to expand far away (meters) from the original discharge site, perhaps triggering secondary discharges and involving a very low space impedance leading to an extended short-circuit-like stress, lasting up to several microseconds (e.g. inverted voltage gradient discharge). When arising near an electrical power source (solar arrays, battery etc...), thus a phenomenon could imply major degradation, like permanent real short-circuits as observed on solar arrays, as a results of high circuit stress and possible power line ringing. A preliminary numerical application of this concept leads actually to a stress confirmed by experimental results.

Conclusion

It looks like that we now arrive at a breakthrough point were the conjunction between a good experimental basis, new physical concepts derived for example from high vacuum insulation analysis and advanced numerical capabilities permits now to achieve a comprehensive and unified approach of discharge phenomena. Decisive design improvements in the near future will be based on on-going modelling developments.

SUMMARY OF TRANSIONOSPHERIC PROPAGATION STUDIES

L. BERTEL*, C. GRIMAULT
Université de Rennes 1 - Laboratoire Radiocommunications - URA CNRS 834
Campus de Beaulieu - 35042 Rennes Cedex

The purpose of this article is to summarize transionospheric propagation studies. The medium is considered linear. The links examined are from a station to a moving or geostationary satellite, and vice-versa. The working frequencies addresses by the summary are from 20 MHz (HF range)to 60 GHz (millimeter range).

Firstly, a description is given of the physical phenomena occurring during propagation : mean stratification, anisotropy, dispersivity and non-stationarity leading to non-homogeneity and turbulence. Their impact on reception is assessed in terms of :

- anisotropy effect : the presence of the magnetic field makes the medium anisotropic. Outside quasi-transverse zones (the equatorial region), this property results in two propagation modes, a fact that must be taken into consideration at reception. This causes a rotation of the polarisation plane (Faraday effect), which in turn influences the choice of antenna an polarization,

- path fading a distinction is made in respect of the various effects encountered (plasma, but also gas and hydrometeors), in order to single out specifically ionospheric fading,

- propagation time : an altimetry measurement from a point below a satellite derived from the measurement requires correction, methods for which are described,

- angle of arrival (refraction effect) : a description is given of the expressions by which the angular discrepancy between the true direction of arrival (ground or satellite) and a rectilinear path may be calculated,

- doppler shift, of different orders depending on the working frequency (spatial or ionospheric doppler effect of different orders).

Results are presented in the form of mathematical expressions. They are both simple to apply and, in some cases, original. The respective influences of frequency, electron density, terrestrial magnetic induction and satellite orbit appear clearly in the phenomena described.

The second part of the article deals with the phenomenon of scintillation of waves propagating through the ionosphere. Variations in a signal passing through the medium are caused by the formation of, and changes in, irregularities, and by their drift relative to the ground. There are a number of possible approaches to the study of scintillation ; the aspects dealt with here are the morphology and geography of irregularities, and the theory of propagation through an irregular plasma layer, in terms of the direct problem. The physical mechanism responsible for the generation of irregularities is not discussed ; nor is wave reflection from irregular plasma, or the transionospheric radar aspect.

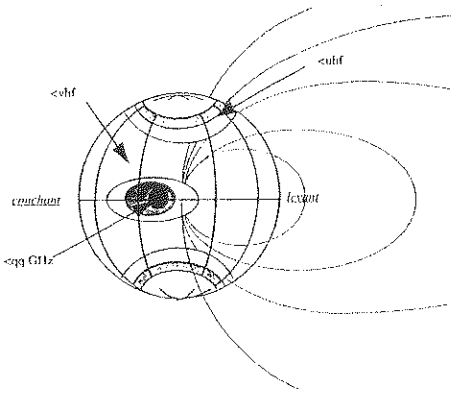

SCINTILLATION MORPHOLOGY (from Aarons)

Scintillation characteristics are variable in both time and space. Their disparities are due to the plasma-specific processes which cause irregularities, and vary from region to region. Distinctions are drawn between high and mid-latitude regions, and the equatorial regions. The parameters responsible for discrepancies are described as are scintillation characteristics depending on location, time of day, season, and solar and magnetic activity.

While ionospheric irregularities may be said to be field-aligned and controlled, the medium remains essentially random. Thus, the statistical approach seems natural to describe the medium and also, from many points of view, to build a propagation theory. The statistical properties and relations describing the medium are set forth.

Regardless of the point of observation the irregularity spectrum is of the "power law" type, between two dimensions referred to as the internal and external scales. The characteristics of the spectrum and the scales are given, and it will be seen that there is an intermediary scale below which the gradient of the spectrum is steeper (in the equatorial regions), and that the anisotropy of the spectrum appears to be linked to the size of the irregularities (auroral regions).

The theory of propagation through a turbulent plasma layer may be approached in several ways. The phase screen method does not take the perturbation of the wave front within the medium into account. Solving the parabolic equation, an approximation of the scalar wave equation under certain conditions, meets that requirement, but is not possible as a general case. Rytov's approximation provides solutions, but is by its very nature a single-scattering solution, applicable to the case of weak turbulence. Solving for a highly turbulent system requires the Markov's approximation, which yields a differential equation giving the received field moments. Both approaches are set forth, and their respective limits demonstrated. With greater computing power available, numerical methods have become very helpful in understanding such phenomena, particularly in highly turbulent systems. Though such methods lack the interpretational relevance offered by analytical solutions, they eliminate the need for the approximations associated with statistical theories. The F.T.D.T. or Split-Step Fourier methods are described, together with examples of applications.

As a conclusion, the article proposes a signal model that is both analytical and statistical.

IMPULSE RADAR PROPAGATION ACROSS A IONIZED MEDIUM

M. FOURNIER*, M. SOIRON*, Y. BENIGUEL**

* LCTAR, 6 rue Nieuport, 78141 VELIZY-VILLACOUBLAY, FRANCE
** IEEA, 13 promenade Paul Doumer, 92400 COURBEVOIE, FRANCE

A study of the deleterious effects of a ionized medium on the propagation of radar signals is presented. Two models have been developped to solve the problem depending on the data available.

In a first order approach, we use the total electron content (TEC) of the medium. It is assumed that the complex propagation constant can be expanded as a second order Taylor series. The ionized medium is characterized by the maximum phase shift of the transmitted signal, the group velocity, the dispersivity and the Faraday rotation. All these parameters are deduced from the TEC value. Analytical expressions have been obtained for the envelope and the frequency modulation of the convolution of the received and transmitted signals.

This theory has been applied to a gaussian envelope pulse, gaussian and rectangular envelope pulses with linear frequency modulation and to a PSK code. As an example curves plotted on figure below show the distorsion of a gaussian envelope pulse taking into account a magnetic field for a linearly polarized signal. The convolution result of received and transmitted signals has been plotted for several values of the Faraday rotation angle.

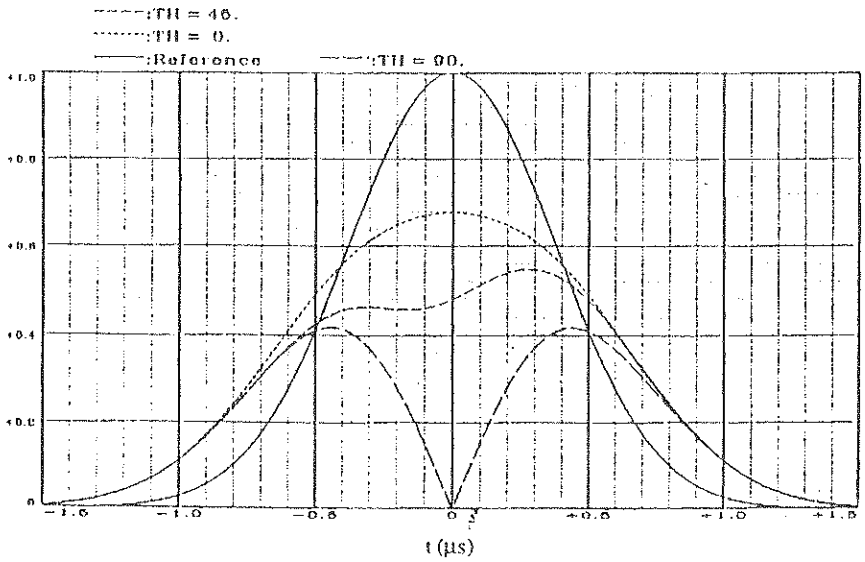

Matched filter response
for an electronic density equal ten times the ionospheric electronic density

The solution of the parabolic equation allows to obtain a second order model. The medium is described by its index spectral probability density for which a power law or a Bessel function approximation is assumed. The derivation of the equation provides the two-position two-frequency coherence function of the transmitted field. A simple solution may be derived in the plane wave approximation. The global solution is obtained numerically. From this function, we deduce the coherence distance, the coherence bandwidth and the coherence time of the medium. These values limit the antenna gain pattern, the modulation bandwidth and the integration time and consequently decrease the efficiency of the system. The anisotropy of the medium modifies the spectral probability density of the index of the medium. A geometrical factor must be added in the equations to include this effect.

The impulse response of the medium is obtained as the inverse Fourier transform of the coherence function. This function is shown below, versus a normalized time with respect to the coherence bandwidth value. Several curves have been plotted varying the phase standard variation which may be obtained from the statistical parameters describing the medium.

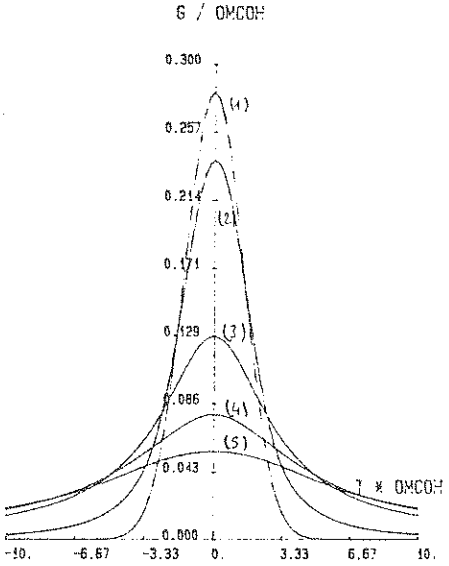

impulse response of the medium increasing σ_ϕ
5 r. (1), 500 r. (2), 2500 r. (3), 5000 r. (4), 7500 r. (5)

The fourth order moment of the signal may also be derived from the parabolic equation. Calculations are very cumbersome in the general case. Simplifications may be achieved in the case of small fluctuations.

POST-NUCLEAR SATELLITE COMMUNICATION CHANNEL FROM NUCLEAR MEDIUM TO TRANSMISSION THROUGH PROPAGATION

B. DURAND*
Centre d'Études de Systèmes et de Techniques Avancées
37, av du Général de Gaulle
35170 BRUZ

F. SIMONET
CEA-CESTA
BP2
33114 LE BARP

I- Introduction

Few studies have already investigated the nuclear effects on satellite communication ("Space Communication and Nuclear Scintillation" - Ed. Nirode C. Mohanty-1990). Fast derivations of the results have been made possible with assumptions on the spatial and temporal electron density variations in the nuclear medium and with assumptions on wave propagation through it to compute the Generalized Power Spectrum defined as the Fourier transform of the wave electric field correlation function (Wittwer -1980- DNA-5662D)

However, a more precise description of signal disturbances is required in satellite communications to study degradations on a link and to develop modern technics which decrease these degradations. To this end, CELAR (Centre d'ELectronique de l'ARmement) has defined the required characteristics of the post-nuclear channel for further use in the transmission scope.

Besides, CEA (Commissariat à l'Énergie Atomique) has been working on the effects of endo and exo-atmospheric nuclear bursts for many years; various new numerical codes have been developped to characterize nuclear media and to quantify wave distorsions by propagating through the nuclear media.

Thanks to the various ability of the two teams (CEA and CELAR), a useful study of the nuclear channel can thoroughly managed from a nuclear medium characterization to a transmission exploitation.

In the next part, nuclear effects on wave propagation are defined in relation with geometrical considerations. Then the parameters needed for transmission studies are given as well as the way to get them thanks to propagation codes.

Finally, we discuss on the impact of these parameters on the design of transmission system.

II- Geometrical considerations and physical effects

For a given satellite link, wave distorsions are related through the refractive index formulation to the wave frequency, to the non-uniform ionization encountered along the wave path.

The non uniform ionization of ionosphere produced by a nuclear burst is strongly dependant on the power and altitude of the burst. For example, low altitude burst induces fireball with sharp electron density gradient and high altitude burst induces large amount of striations aligned with the terrestrial magnetic field. Various nuclear scenarios are then to be studied. The computation of the non-uniform ionization, its time evolution and its motion are made with hydro- and magnetohydro-dynamical codes taking into account chemical processes.

For a given nuclear scenario, 2D or 3D ray tracing codes, 2D Multiple Phase Screen (MPS) code or a mixed "ray-MPS" code (F. Simonet, F. Pierronne - 2nd Journées d'Etudes SEE- Perros Guirec 1994) is used to compute the perturbed wave amplitude and phase on the ground station level (downlink) or on the satellite level (uplink) after propagation through the nuclear medium.

III- Propagation parameters to be studied

From the amplitude and phase computed on a receiver level for each wave frequency in a bandwidth, the correlation functions of the scattering channel are calculated to get the coherence length, time and bandwidth.

However, one must be careful in using these functions in relation with the Wide Sense Stationary Uncorrelated Scattering (WSSUS) assumption (AGARD CP 442 (1989) J.S. Belrose, R. Bultitude, D. Clark). In fact, some simulations have shown a stationary behaviour of the channel but only in small areas. A similar study must be made in the frequency domain for the correlation of scattering.

Besides, the attenuation which degrades a link budget is evaluated.

Finally, statistical analysis of the amplitude and phase variations are required in each stationary area. By this way, the characteristics of fadings (the nature, the length and the depth of the fading) and the Doppler shifts are studied.

In a second time, the receiver antenna aperture filtering effects have to be integrated and analyzed (C. Grimault - 2nd Journées d'Etudes SEE- Perros Guirec 1994).

IV- Use of propagation parameters for the design of a satellite communication system.

In a stationary area, the channel capacity and the cut-off rate can be calculated. In a non-selective flat fading channel, the channel capacity (Shannon) becomes random (IEEE Trans-com. nov 1990 - M. Filip, E. Vilar). For a conventional satellite link, the cumulative distribution function of the normalized channel capacity $(\frac{C}{B})$ is given by :

$$F_{\frac{C}{B}}(\alpha) = \int_{\frac{S}{N}\Big|_0 - (2^{\alpha}-1)_{dB}}^{+\infty} p_L(l)dl$$

where $L = L_u(\alpha + \beta L_d)$, α and β depends on $(\frac{C}{N_0})_{u,0}$ and $(\frac{C}{N_0})_{d,0}$ (link budget in a clear sky) and L_u, L_d are the attenuation on the uplink and downlink with their particular probability density.

For a given link budget, a such formulation shows that it could be possible to reach a higher troughput on a scattering channel even if the channel capacity sometimes becomes weak.

The main goal of a transmission engineer is now to find transmission technics to reach the channel capacity or the cut-off-rate under constraints (bandwidth or/and power).

For a given data rate, modulations which have a spectral efficiency (in bit/s/Hz) in respect with the relation $\frac{1}{T_c} << B << B_c$ (B is the bandwidth of the signal, T_c and B_c are the coherence time and bandwidth) must be used. For high data rates, technics like Continuous Phase Modulation (CPM) and/or Pulse Shaping can be used.

Besides, FEC (Forward Error Corrector) codes (block or trellis codes) increase the performance of a transmission system; for a given code, its robustness depends on the statistical characteristics of fadings. For instance, the 'hamming distance' and the length of a block code must be chosen in relation with the length of fading, the depth of fading and their probabilities. For convolutional codes, interleavers are necessary on a dispersive channel and its size depends on the coherence time. To efficiently battle with deep fadings, a block code as the outer code and a convolutional code as a inner code (concatened codes) could be used in a slow-varying channel. But, a FEC code increases the required system bandwidth due to the code rate.

Recently, a new area of technics has been investigated: the association of codes and modulations (coded modulation). These techniques allow better performance at no cost in bandwidth. Different types of coded modulations are studied (Treillis Codes Modulations -TCM, and Block Coded Modulation BCM) for slow time-varying channels; the optimum signal constellation must be calculated in relation with the statistical characteristics of fadings.

A FEC code offers diversity by spreading information on a higher number of symbols. A frequency diversity can be realized by spreading data on a bandwidth larger than the coherence bandwidth: spread spectrum techniques with direct sequence or frequency hopping could be used, as well as multi-carrier techniques (J. C. Belfiore, O. Risse, M. Testard - CELAR -1993).

Two or more antennas systems for one receiver can be used to create space diversity. The gap between the two antennas depends on the coherence length of the channel ("Space Communication and Nuclear Scintillation" - Ed. Nirode C. Mohanty-1990).

In a scattering channel, the synchronization (time frequence, phase) of a given waveform must be carefully analyzed and robust algorithms must be developped taking into account Doppler shift, phase noise, and fading characteristics.

Finally, in the case of a non-stationary behaviour of the nuclear channel, a model is required to take this problem into account. If a finite number of stationary areas are defined, a simple model based on a Markov chain can be chosen; each state of the Markov chain is allocated to a stationary area of the channel with its coherence time, bandwidth and length. The relation between two states i and j is defined by the probability P_{ij} to go from the state i to the state j.

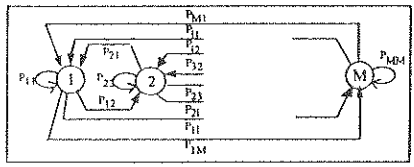

Then, the evaluation of the bit error probability (P_e of one link is given by :

$$P_e = \sum_{i=1}^{M} P_i W_i$$

where W_i is the probability of being in the i stationary state and P_i is the bit error probability in this state.

Besides, the non-stationarity of the channel can be studied to develop new technics based on the adaptativity of the waveform. Few levels in adaptativity are possible. For data transmission based on 'packets transmission', ARQ (Automatic-Repeat-Request) technics are interesting. The size of packet must be studied in relation with the size of stationary areas and coherence time. It could be also possible to use punctured codes as well as shortened codes, and to adapt the depth of puncturing according to the type of fading (Testard- CELAR/ITES/TR/10345 - 1994).

Such technics need protocols to control the adaptativity. This is then interesting only if the stationarity of the channel changes much slower than the transmission delay which is high for satellite communication (250 ms).

V- Conclusion

The steps of a "post-nuclear satellite communication channel" study have been discussed. They include a characterization of nuclear effects on ionosphere, then an evaluation of the wave propagation perturbations and then the use of the signal degradations to define a robust transmission system.

We have pointed out the need of a precise description of the channel which can be reached by the linking of some numerical codes for each step of the study.

VI-Acknowledgement

The authors gratefully thank CAD (Centre d'Analyse de Défense) and CELAR for their support and their trust on the works concerning this topic.

THE PROPAGATION OF ELECTROMAGNETIC WAVES IN THE TWO DIMENSIONAL IRREGULAR WAVEGUIDE

*Bichutskaya T., Makarov G.
Inst. of Physics, St. Petersburg Univ., Russia

The focusing effect of a large scale irregularity on the electromagnetic field in the waveguide is investigated by fullwave-ray method with help of the differential equation for a beam divergence. The displacement of paths of normal waves on the complex plane is estimated. The conditions of implementation of the longitudinal approximation for the calculation of amplitude and phase of field in two-dimensional irregular waveguide are defined.

The earth-ionosphere waveguide becomes irregular if the ionosphere is disturbed by the line of terminator or solar proton events or any other. The characteristics of upper wall of irregular waveguide are altering all the way of changing of the ionosphere ionization. To consider the field in the case where a wavelength is smaller than the horizontal scale of the ionosphere disturbance the ray/full-wave method is can be used.

In the ray/full-wave method the full-wave theory is used to determine a local modes parameters and a ray traces are employed to describe the signal's horizontal structure. In this method is used the horizontal scale of the disturbance which is much greater than its vertical scale. E.C.FIELD et al.(Radio sci.21,511,1986) employed this method to calculate the two dimensional ray traces and to estimate the loss energy for ELFsignal qualitatively. We developed this method to estimate the electromagnetic field amplitude and phase in the irregular earth-ionosphere waveguide quantitavely.

The solution of Maxwell's equations for one of the components of electromagnetic TM-field can be reduced to solving an inhomogeneous wave equation in the partial derivatives. The solving of this equation is written as the mode sum in which the coefficients containing the dependence of horizontal coordinates are determined by the horizontal ray method.

The vertical problem is formulated in each cross-section of irregular waveguide. The local characteristics of the low ionospheric boundary are determined by integrating the vertical differential equations describing the field in the ionosphere. The initial values of the problem of vertical integrating in the ionosphere are evaluated with a help a WKB method on the upper boundary of the substantial domain ionosphere. The ionospheric impedance referred to the lower boundary of the substantial domain is recalculated at the effective ionospheric reflection height . The impedance of ionosphere at the effective reflection height has the faint dependence on the wave incidence angle (or eigenvalue). The result from integrating of the differential equations in the ionosphere determines the effective reflection height and the ionosphere impedance - the parameters that are need to resolve the vertical problem in the each cross-section of the irregular

waveguide. Obtained values of the height and the impedance of the ionospheric boundary are treated as a variable parameters, each of them is a function of horizontal variables in the irregular region of the waveguide. The local modes characterized by complex eigenvalues and by eigenfunctions of the transverse operator and utilized as basis functions are need to resolve a horizontal problem.

The coefficients containing the dependence of horizontal coordinates are described by the system of independent equations in partial derivatives if to neglect the mode coupling. To solve this system of equations it can be used the geometrical optics method. The horizontal distribution of field phase and amplitude in zero aproximation can be determined from the eiconal equation and the transfer equation. In this problem the really part of horizontal wave number is analogous to a refractive index and its imaginary part determines the absorption of field. The second order differential equation for a beam divergence added to the equations into the ray variables describing the ray traces are integrated numerically. The ray traces can be determined in the complex plane because the horizontal wave number is complex.

The influence of the space disturbance of the ionosphere by a center-symmetrical ionization at the field dependence on a horizontal coordinates was been estimated numerically . The computations have been made for the disturbance center both placed at the direct propagation path from the transmitter to the receiver and displaced from this path. The results show the change of ray traces and the field amplitude and phase as a functions of the longitudinal and transversal horizontal coordinates relative to a path propagation . The displacement of ray traces in the complex plane has a nonmonotonic character in dependence of the exit angle of a ray that is in accordance with the focusing effect of irregularity.

The field amplitude disturbance as a function of the longitudinal coordinate goes through a maximum in a place of the ionization disturbance center. The field amplitude is not restored to undisturbed value if the lateral scale of the ionization disturbance is more surpassing the first Fresnel zone. In the case where the lateral scale of ionospheric disturbance has the order of the first Fresnel zone the field amplitude is restored to undisturbed value. In this case the field amplitude disturbance has a local character.

The disturbance of the field phase as a function of the longitudinal coordinate has an integral character. It is summarized in all way of ionospheric disturbance and is remained constant in a rest of a path to the receiver. The field phase disturbance is weakly dependent on the lateral scale of the ionization disturbance. The disturbance of field phase watches on the scale and value of disturbed horizontal wave number along a path propagation.

The dependence of the field amplitude disturbance on the lateral horizontal coordinate is characterized by the focusing effect at the path passing on the symmetric line of the irregularity in the case where the lateral scale of the irregularity has the order of the first Fresnel zone. A shadowing zone is determined by a geometric shadow of the irregularity.

COLLISIONAL ABSORPTION DURING MICROWAVE PROPAGATION THROUGH THE ATMOSPHERE

J.P. Boeuf* and Ph. Belenguer
CNRS, Centre de Physique Atomique de Toulouse
Université P. Sabatier, 118 Route de Narbonne
31062 Toulouse Cedex, France

High power pulsed microwave beams can generate electron avalanches where free electrons, driven by the microwave fields, produce ionization through collisions with air molecules. Part of the electromagnetic energy carried by the wave is absorbed through electron-molecule energy transfer (electron impact ionization and other inelastic collisions). For high enough electric fields, the exponential multiplication of electrons can lead to the total absorption of the electromagnetic energy. Although the physical phenomena involved in the avalanche process are reasonably understood, a number of questions concerning microwave energy absorption and microwave breakdown need to be clarified. In this paper, we choose to address the following points:

1) - Is it possible to describe microwave absorption by using a simple breakdown criterion or is it necessary to go through the complex problem of solving Maxwell's equations coupled to the electron transport equations ?
2) - In the limit of high altitudes (low pressure) and short pulses is it necessary to use a fully kinetic description of electron transport or can we simply use macroscopic coefficients to describe the electron multiplication process ?
3) - The free electron density (and diffusion) being very small at low altitudes, air-breakdown under these conditions leads to the formation of small plasmas, or plasmoids, localized around the seed electrons; how does this affect the wave energy absorption rate ?

Different physical and numerical models of the collisional absorption of a microwave pulse propagating through the atmosphere have been developed to address and illustrate these questions. The paper is divided in three parts.

In a first part we present some results from a 1D model of the wave propagation and collisional absorption. Typical conditions considered are: wave frequency from 1 to 100 GHz, pulse duration from 1 ns to 1 μs, altitudes between 0 and 100 km. The model is based on a fluid description of the electron transport

phenomena (continuity, momentum transfer and energy equations) coupled with Maxwell's equations for the electromagnetic fields (linearly polarized wave). The set of fluid equation describing electron transport must be closed by some assumptions on the electron velocity distribution functions. Different closure assumptions have been used and the corresponding results compared together. This first model is similar to the one developed by Yee et al. (J.H. Yee, R.A. Alvarez, D.J. Mayhall, D.P. Byrne and J. De Groot, Phys. Fluids, 29, 1238, 1986). Results from this model show how the initial shape of a microwave pulse is modified during the propagation due to collisional energy absorption and give the fractional wave energy absorbed as a function of altitude.

In a second part, a simpler approach, based on the classical breakdown criterion is presented and discussed. The breakdown criterion simply assumes that air-breakdown occurs when the electron multiplication within the avalanche reaches 10^8. By using the concept of effective field, E_{eff} (the dc field which would give the same multiplication as the ac field), the breakdown criterion leads to a universal curve, the breakdown curve, giving E_{eff}/N as a function of $N\tau$ (N is the gas density and τ the pulse duration). The results obtained from the breakdown criterion are compared with those deduced from the more detailed model above. We also show, by using a Monte Carlo simulation of the electron transport in the microwave field, that the use of a macroscopic, precalculated, ionization coefficient and the concept of effective field give a reasonably accurate estimation of the breakdown field even in the region of high E/N and short $N\tau$.

In a third part we present some results from a 2D fluid model of the formation and extension of a localized plasma (plasmoid) at low altitudes, under a microwave pulse, for conditions where the pulse duration is longer than the breakdown time. The model is similar in essence to the one described by V.B. Gildenburg, I.S. Gushchin, S.A. Dvinin et A.V. Kim, Sov. Phys. JETP 70, 645, 1990. Results show that once the density of the avalanche reaches a critical density, the plasma continues to grow and extend mainly in the directions parallel to the electric field. The rms electric field can reach very high values in the fronts of the plasmoid and decreases in the bulk plasma. The model allows to estimate the energy absorbed by plasmoids. It is shown that a large part of the initial wave energy can be transmitted even for pulse durations several times longer than the breakdown time.

Acknowledgements

This work has been supported by Centre d'Etudes de Gramat.

EUROEM 94, Bordeaux, May 1994

BODY-FITTED PIC SOFTWARE FOR MICROWAVE DEVICE MODELLING

J W Eastwood*, W Arter and R W Hockney

AEA Technology, Culham Laboratory,
Abingdon, Oxon. OX14 3DB, England

INTRODUCTION

This paper describes three dimensional body-fitted Particle-In-Cell (PIC) software for modelling the interaction of electromagnetic fields and flows of relativistic charged particles. This software offers powerful new capabilities for electromagnetic PIC modelling.

The 'Virtual Particle' (VP) algorithms used arise from a finite element approximation of the tensor formulation of the Action. The implementation breaks the computational volume into a set of curvilinear hexahedra, and uses transfinite interpolation to generate the element nets in each block. The combination of isoparametric hexahedral elements and multiblock decomposition leads to algorithms ideally suited to MIMD computers.

The software was designed for three dimensional modelling of microwave sources and microwave transmission, where the interaction of electromagnetic waves with charged particle flow is important, although it can equally well be applied to other time dependent problems normally tackled by finite difference, time domain (FDTD) codes.

NUMERICAL METHOD

VP algorithms are derived using finite elements in both space and time. Current is assigned from 'virtual particles' placed at points specially interpolated between positions at successive time levels, a procedure which automatically leads to charge conservation. In general curvilinear coordinates $(\bar{x}^1, \bar{x}^2, \bar{x}^3)$ the Action integral is

$$I = \int dt\, d\bar{x}^1\, d\bar{x}^2\, d\bar{x}^3 \left\{ \frac{1}{2}(E_i\, d^i - H_i\, b^i) + J^i\, A_i - \rho\phi \right\} + I_K$$

where I_K is the kinetic lagrangian, $E_k = -\frac{\partial \phi}{\partial \bar{x}^k} - \frac{\partial A_k}{\partial t}$, $b^i = \epsilon^{ijk}\frac{\partial A_k}{\partial \bar{x}^j}$, $d^i = \epsilon_o\sqrt{g}g^{ij}E_j$, and $H_i = \frac{1}{\mu_o\sqrt{g}}g_{ij}b^j$. The 'superparticle' current is given by the sum over all particles:

$$J^i = \sum_p q_p \delta(\bar{x}^1 - \bar{x}^1_p)\delta(\bar{x}^2 - \bar{x}^2_p)\delta(\bar{x}^3 - \bar{x}^3_p)\dot{\bar{x}}^i$$

Treating I as a functional of the vector potential A_i, the scalar potential ϕ and particle coordinates $\{x_r\}$ leads to Euler-Lagrange equations representing Maxwell's equations and relativistic particle motion; the discrete approximations to these differential equations are obtained by substituting test function

approximations for ϕ, A_i and x_p and taking variations with respect to the nodal amplitudes. The result for the field nodal amplitudes, after assembling the element contributions, is

$$\partial_t b^i = -e^{ijk}\partial_j E_k, \;\; \partial_i b^i = 0$$

$$\partial_t d^i = e^{ijk}\partial_j H_k - J^i, \;\; \partial_i d^i = Q$$

The discrete VP equations in the quantities b^i,d^i, E_k,H_k,J^i and Q are identical in any coordinate system. Geometrical and material (permeability and permittivity) information appears only in the constitutive relations $E_i = G^E_{ij} d^j$, $H_i = G^H_{ij} b^j$. Similarly, the formulae for the assignment and interpolation of the contravariant current emerging from the Action integral are coordinate independent.

Components of the particle equations of motion are integrated using the leapfrog scheme in a locally tangent coordinate system, then transforming the components to the curved space coordinates at the new particle positions.

MESH GENERATION AND MIMD

The multiblock subdivision of the computational domain minimises the amount of global data and interprocessor message passing, and simplifies load balancing across processors. Each slave block only requires data from its neighbours, and the master control program only requires information about the block surfaces ('glue patches') which join the slave blocks together. This arrangement gives a large computational intensity and a weak Amdahl limit to speedup on distributed memory MIMD computers. Moreover, the simple logical cube addressing within each block leads to fast serial processing.

Without compromising efficient MIMD processing, one can further demand that boundary conditions *only* apply at the surfaces of blocks; this eliminates the addressing problems in embedding surfaces within blocks, and allows surface data to be passed to the control program through the 'glue patch' tables. Further saving of computer storage and time arise from keeping metric information and material property data only in those blocks where they are needed. When many small blocks are used to describe a complex object, load balancing is achieved by assigning several blocks to one processor.

FINAL REMARKS

This paper outlines the extension of the VP algorithms to general geometry and their implementation on parallel computers. The result is a particularly simple coordinate invariant form for the field equations and a current assignment scheme which has the same charge conserving property as its orthogonal counterpart.

The multiblock decomposition is well suited to distributed memory MIMD computers. Both the electromagnetic and particle parts of the calculation have little message passing between blocks and small scalar overheads, so large speedups are possible even for nonuniform particle distributions and complex device shapes.

Some microwave tube calculations and results from parallel computer benchmarking will be presented.

MODELING OF EM WAVES PENETRATION THROUGH SLOTS AND SEAMS.

RUDOLPH T.*
Electro Magnetic Applications
Lakewood-DENVER

TIXIER J.N.* PECQUEUX B. VEZINET R.
Centre d'Etudes de Gramat
46500 GRAMAT

The purpose of this paper is the development of a numerical method for the representation of slot coupling, usable in a finite difference code and its relation with experimental studies.

Apertures which need a special treatment in the FDTD context are resonant apertures when one of the dimensions (width) can not be gridded.

The method presented here is an improvement of the Thin Slot Formalism of Merewether and Fisher by the use of a "ratio-technique" which corrects the field across the slot to give a good transmission of the EM energy.

The point of interest in a slot is the transverse electric field as shown in Figure 1:

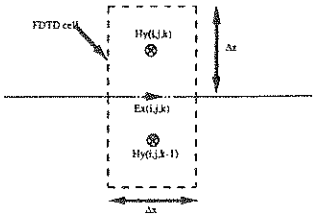

Figure 1 : Fields of interest in a slot in infinite thin plane.

First, we can consider Ex(i,j,k) uniform in the line Δx. Then this component can be calculated as the average of the actual Ex field over the line Δx.

But if we look at a different view shown in figure 2, one can see that Ex should be interpreted as the average value over the area ΔyΔz. Thus we have two interpretations for the same field, which give different values in regions where fields are rapidly varying, as slots (figure 3).

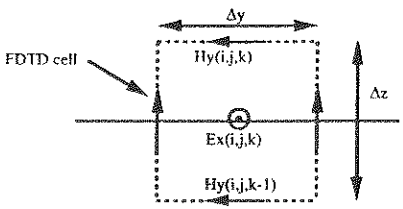

Figure 2 : average value over area.

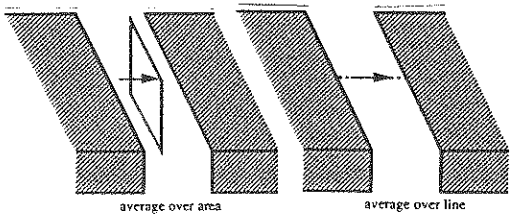

Figure 3 : Two different interpretations.

As the value usually used in FDTD codes is the surface interpretation, we must correct the electric field computed in Ampere's law (1) to obtain the line average. The advance equation of Hz becomes (w represents the width of the slot) :

$$-\mu\,\delta Hz/\delta t=[Ey(i+1,j,k)-Ey(i,j,k)]\Delta y-Ex(i,j+1,k)\Delta x+RwEx(i,j,k) \qquad (1)$$

To calculate this ratio(R), a conformal mapping is used for thin and thick slots.

The first results shown in figures 4 and 5 has been obtained for a slot in thin and thick plane. We can note good agreements between the formalism and the reference case where the width of the slot is gridded. The excitation is made by a plane wave with a zero to peak rise time of 3ns.

w=3cm
d=0
L=40cm
Δx=5cm

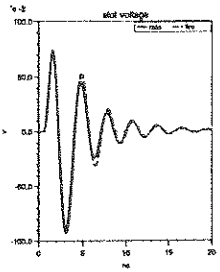

Figure 4 : slot in thin plane.

w=3cm
d=3cm
L=40cm
Δx=5cm

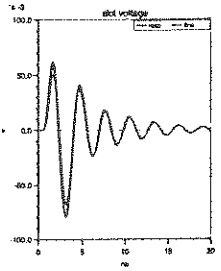

Figure 5 : slot in thick plane.

A method to relate numerical and experimental studies is to measure the input impedance of a slot, (ratio of voltage in the center of the slot to the current injected in the frequency domain), parameter function of the width in an analytical formula obtained by King and Blake (The self-Impedance of a symmetrical Antenna, IRE, vol30, No7, July 1942).

The validation of this experiment appears in figure 6 where the measurement of the input impedance is compared with numerical results with good agreements.

The curves presented in figure 7 shows coupling through a slot in a Faraday cage when the excitation is made by a normally incident plane wave with electric field polarized across the slot.

w=1mm
d=2mm
L=40cm

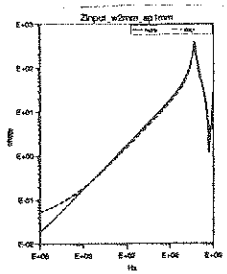

Figure 6 : input impedance.

w=1mm
d=2mm
L=40cm

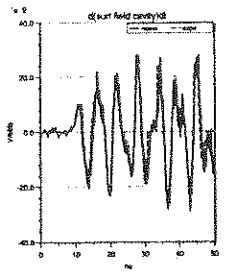

Figure 7 : coupling in a cavity.

As a conclusion, we can say that the formalism gives good results and can be related with experiment by the measurement of input impedance for simple slots.

Nevertheless, we must know exactly if this kind of measurement can be done in more realistic structures and if the notion of transfer impedance could be more acceptable in this case.

Furthermore, the modeling of loaded slot should not use the same technique and current studies are made to employ simultaneously the thin slot formalism (without ratio) and a composite materials formalism to simulate loaded slots. The problem is also to find a connection between numerical and experimental results (maybe also with the transfer impedance).

CALCULATION OF APERTURE COUPLING BY MEANS OF NUMERICAL ELECTROMAGNETIC CODES. A COMPARISON BETWEEN FD-TD, EFIE AND THE ITERATIVE WCG-FFT METHOD

C.D de Haan*, M.G.E Brand and A.P.M. Zwamborn
TNO Physics & Electronics Laboratory,
P.O. Box 96864,
2509 JG The Hague, The Netherlands.
e-mail: C.D.de Haan@fel.tno.nl

1. Introduction

During the past several years considerable effort has been put into the development of computational techniques for handling the scattering and diffraction of electromagnetic waves by an object. We can distinguish between global techniques (e.g., the use of wave function expansion and integral equation) and local techniques (finite-difference and finite-elements methods).
In this paper we describe and compare three numerical techniques that are used for solving complicated electromagnetic scattering and coupling problems. Firstly, we present the finite-difference time-domain (FD-TD) method, which is a local technique. Secondly, we present the electric field surface integral equation (EFIE) formulation that is solved by employing the triangular patch model in the method of moments. Subsequently, we present the weak form of the domain integral equation that is solved by using the iterative conjugate gradient FFT (WCG-FFT) method. Noted that EFIE and WCG-FFT are both global frequency-domain techniques. For a number of realistic test cases, the numerical results are compared with respect to numerical accuracy and efficiency.

2. Finite-difference time-domain

In the FD-TD method, which was proposed by Yee (1966) and developed further by Taflove and Umashankar [2] and many other authors, the time and space derivatives in the Maxwell curl equations are approximated by centered finite differences on a Cartesian mesh.
At t=0 all the fields in the computational domain are initialized at zero and a plane wave is started. By taking discrete time steps the time evolution of the fields in the domain is generated. The incident wave is tracked as it propagates through the domain and interacts with the object under consideration. Time stepping is continued untill all the fields have the same sinusoidal time dependence (sinusoidal steady state). In order to compute frequency domain quantities such as bistatic radar-cross section or EM fields inside an enclosure, time stepping is continued until accurate amplitude and phase information can be extracted out of the time domain response.

3. Electric field integral equation

The scattering of arbitrary-shaped perfectly-conducting bodies is solved using a surface integral equation formulation for the electric field. The electric field (surface) integral equation is solved by using the method of moments in which the testing functions of the electric field and the expansion functions of the electric surface current density are both appropriate triangular-patch functions. This technique is described by Glisson [2]. The system of equations is then solved by using a LU factorization algorithm. EFIE is applicable to both open and closed surfaces.

4. Weak form of the domain integral equation

The domain integral equation that is obtained in its strong form is weakened by testing it with appropriate testing functions and expanding the electric vector potential with appropriate expansion functions. The advantages of this procedure are, firstly, that the grad-div operator acting on the vector potential is integrated analytically over the domain of the object only and, secondly, that we have maintained the simple convolution structure of the vector potential. The integral equation is formulated in terms of the electric flux density. The continuity of the normal component of the electric flux density yields a correct implementation of the normal component of the electric field at the interfaces of (strong) discontinuity. No surface integrals that are directly related to surface-charges are introduced. The weak domain integral equation is solved using an iterative conjugate gradient scheme in which the convolution integral is computed efficiently by using the Fast Fourier Transform algorithm. This procedure is introduced by Zwamborn and van den Berg in [3].

5. Numerical results and conclusions

We will briefly discuss the applicability of each method for the numerical approximation of three-dimensional scattering problems, such as microwave coupling to a complex object. We firstly compare FD-TD and WCG-FFT with the analytical solution (Mie series) that are carried out for a strongly inhomogeneous dielectric sphere. Secondly, we present numerical computations for the three methods that are carried out for a perfectly conducting disc. Here, we compare the computed bistatic radar cross section with the analytical solution. Subsequently, we use a perfectly conducting box with an aperture as a simple object to study coupling effects. For this test case we compare the computed electric field inside the object as the incident field penetrates through an aperture. All the computations are carried out on the Convex C230 mini-supercomputer. Using this computer, we compare all three methods with respect to numerical accuracy and efficiency and briefly discuss the advantages and disadvantages of each method.

References

[1] A. Taflove and K.R. Umashankar, ``Review of FDTD numerical modeling of electromagnetic wave scattering and radar cross section", *Proceedings of the IEEE*, Vol. 77, pp.~682-699, May 1989.

[2] A.W. Glisson, ``Recentadvances in frequency domain techniques for electromagnetic scattering problems," *IEEE Trans.on Magnetics*, Vol. 25, No 4, July 1989.

[3] A.P.M. Zwamborn and P.M. van den Berg, ``The three-dimensional weak form of the conjugate gradient FFT method for solving scattering problems," *IEEE Trans. Microwave Theory Techn.*, MTT-40, pp.~1757-1766, September 1992.

LIMIT PARAMETERS OF THE PULSE RESPONSE IN THE PROBLEMS OF TRANSIENT ELECTROMAGNETICS

Andrey E.Serebryannikov*, Loudmila V.Vavriv
Molniya Research and Engineering Institute, Kharkov, Ukraine
Konstantin V.Avramov
Kharkov Polytechnical Institute, Kharkov, Ukraine

The data concerning limit parameters of pulse response are necessary for the correct choice of sampling frequency and discretization step to solve the problems of transient electromagnetics using FFT or other discrete algorithms. These data are also necessary for the creation of spectral analysis apparatus. As an example, this problem is easy to solve in case of linear circuits when the expansion of response spectrum is impossible in comparison with the external action. This condition is not met in the problems of non stationary electrodynamics, when the processes of resonance scattering take place. The interference in some volumes (illuminated areas of scatterer) results in spectrum expansion to the area of higher frequencies. Thus the problem is reduced to the estimation of boundary frequency for the response spectrum ω_r in case of absence of complete a priory information about its characteristics. This contradicts the generally accepted sampling procedure where the parameters of the sampled signal are considered to be a priory known.

Several alternative methods used for the estimation of boundary frequency of the response spectrum have been considered. One of them is assumed that the partial energy integrals of response and external action are equal. The boundary frequency of the external action ω_0 is considered to be a known one, and it realizes the sampling procedure with the prescribed accuracy. The errors caused by the limitation of the real signal with the nonfinite spectrum are equal in both cases. In the general case, when a priory data are not available (it was only assumed, that the considered functions refer to those that are integrated in square), the problem is reduced to the solution of equation relatively ω_r using the numerical methods. Such an approach was justified because it is the only way to exclude the loss of data concerning high-frequency portion of response spectrum and the calculations performed for the solution of equations in the frequency domain can lead to the unjustified losses of computational time if the estimation of ω_r is not available. The problem is significantly simplified if the maximum value of the transfer response can be determined proceeding from the physical consideration or this response can be restricted by the simple integrated functions. The partial amplitude integrals have also been used instead of partial energy ones. The more strict approach presupposes that the sampling error of initial action is unknown and it is not equal to the error of response sampling. In this case the problem on estimation of boundary spectra's frequency is reduced to the problem on accuracy of signal representation using the finite Kotelnikov series (M.M.Gel'man, etc. Discrete transform and coding of width-band signals, Moscow, 1985). The availability of data concerning the boundary frequency of response spectra allows for the estimation of other ultimate parameters such as amplitudes and increment time. These methods were used during the solution of a number of nonstationary problems of internal and external electrodynamics.

A SIMULATION TOOL FOR SYSTEM LEVEL TRANSIENT EMC ANALYSIS ON SATELLITES

L. Inzoli - ESTEC XE DIVISION - Noordwijk - NL*
F. Svelto - ASI - Agenzia Spaziale Italiana - Roma - IT
M. Bandinelli, F. Bessi, S. Chiti, L. Giorgi - IDS SpA - Pisa - IT

Abstract

Among transient threats that could compromise the success of a satellite's mission, the most dangerous and common is electrostatic discharge (ESD). This phenomenon, due to differential voltages among different points of the satellite's surface, produces both radiate electromagnetic (e.m.) fields and current, characterized by a wide frequency band. The nonuniform charging of the satellite's surface is due to its operative environment, in particular the satellite's surfaces are not uniformly exposed to the incident flux of particles and to the earth's magnetospheric plasma.

Due to high performance requested from such a system and due to its high cost, a particular test phase is devoted to the ESD hazard at system level. The detection and correction of some problems in this phase of the programme can involve expensive changes in the system structure. Moreover the test's definition is not good enough because it can't reproduce the exact flight configuration of the satellite; it is very complex, for example, to deploy solar panels in an anechoic chamber, or to perform the test in a vacuum environment, under electron irradiation.

For the above mentioned reasons it could be important to have a software tool able to detect some problems, relevant to transient disturbances at system level, in a preliminary phase of the programme and furthermore to perform an e.m. analysis on a configuration as close as possible to the operative one.

Moreover the comparison between the test set-up and the operative configuration, that could be performed using this tool, can help in tuning the meaningful parameters of satellite qualification tests for electrostatic discharge.

The prototype simulation tool presented in this paper, is constituted of three basic modules relevant to the three fundamental operations necessary to perform the analysis:

- modelling the actual geometrical and constitutive configuration;
- solving the e.m. problem;
- processing the raw data obtained by the e.m. analysis.

The e.m. analysis is performed by means of a numerical procedure, based on a frequency domain Method Of Moments (MOM) technique. The procedure can model characteristic satellite structures and materials by means of patches, wires and attachments suitably interconnected. Starting from the MOM main outputs (current distribution, near and far field, ...) many other results (for example, coupling of interferences on the load impedance of a shielded cable) can be obtained resorting to simulation techniques specially devoted.

The simulation tool, as described in a previous paper (L. Inzoli, F. Svelto, M. Bandinelli, F. Bessi, S. Chiti, L. Giorgi, Proc. of "3rd ESA EUROPEAN WORKSHOP on ELECTROMAGNETIC COMPATIBILITY and COMPUTATIONAL ELECTROMAGNETICS", 279-284, Oct. 1993), has been validated on simple and canonical configurations resorting to:

- literature data;
- cross comparisons with other numerical codes such as the Numerical Electromagnetic Code (NEC);
- preliminary measured data.

In order to obtain a deeper validation, on realistic configurations, a measurement activity specially devoted to the ESD problem, has been planned out and performed at the Centro Elettrotecnico Sperimentale Italiano (CESI). In particular, the tests have been carried out with set-up configurations of increasing complexity, either from the geometrical point of view or for the eccitation type.

The main scope of this paper is to show and discuss the comparisons between simulation results and measured data together with some remarks relevant to the modelling of test set-up and its parassitic parameters.

RECORDING OF THE SPACECRAFT ELECTRIZATION CONSEQUENCES ON POLAR ORBIT OF 1000 KM ALTITUDE

* Vasily I. Gorlov, Deputy Department manager
Oleg G. Vasilyev, Leading Engineer

The operating experience of more than hundred Low-Earth Orbit (LEO) system spacecraft (SC) developed by Design Bureau/ASA Polyot for military and economic purposes demonstrates a number of unexpected malfunctions and failures of on-board equipment. Some of them may be explained by SC electrization.

Caused by implementing in new developments of more updated equipment, more affectable by interferences, Polyot Design Bureau planned a number of experimental programs in space for research of SC interaction with space, including LEO SC electrization on polar orbits, affecting SC normal operation.

In February, 1991, an experiment "TEST-1" begun, concerning electrization affect on SC "Cosmos-2123" of "Zikada" system injected into polar orbit with inclination 82.5 degrees and altitude 1000 km.

The SC was loaded with the following scientific equipment:

"Zond-3", developed and manufactured by NIIT, for recording of quasistatic and transitory electric field intensity, transitory field frequency, electric discharges number and plasma charge current.

"ADA", developed and manufactured by NIIPME MAI, for developing the method and device for recording of electric charge impulse amplitude and time parameters.

"KD", developed and manufactured by NIIPME MAI, MAI and MEI for ferpic optimization for quasistatic electric field intensity recording.

The sensor equipment was interfaced with on-board telemetry system by scientific equipment control block "BUNA".

In addition the SC was equipped by impulse plasma compensating unit "IPK-5", developed by NIIPME MAI, intended for possibility of SC surface potential compensation by plasma jet of 2 Hz frequency, but caused by its' failure before the launch, it was dismounted. "IPK-5" will be tested on "TEST-2" equipment on equal SC in the nearest future.

The summary of the results is the following:

- During the period recorded the maximum electrostatic field intensity amplitude changed on 40 KV/m in range -20 +20KV/m

- In 24 hour period the electrostatic field amplitude varied from -3 +2KV/m to -10 +20KV/m

- The electrostatic field intensity amplitude change of 5KV/m per second was accompanied by electrostatic charge development with their rate and amplitude increase and disturbance occurences in information channels.

- Electromagnetic interference peaks with period 5-70 seconds were monitored on sensor equipment located on the outer surface of SC. The peaks had over-limit amplitude and high frequency.

- The substantial affect of electrization processes on SC normal functioning was demonstrated.

The research is going on. In the beginning of 1994 an additional experiment will be held on the next SC on the orbit of the system.

SPACELAB MULTI-LAYER INSULATION ELECTROSTATIC DISCHARGE CONTROL

Danny R. Graves* - McDonnell Douglas Aerospace
Robert A. Green - McDonnell Douglas Aerospace

Spacelab is a system of enclosed laboratory modules and space-exposed pallets which are carried to and from orbit by the Space Transportation System (STS). Spacelab remains in the payload bay of the STS Orbiter throughout the flight.

Multi-layer insulation (MLI) is utilized in the Spacelab Passive Thermal Control System. The Spacelab MLI designs are similar to designs used in the Orbiter and other spacecraft. The materials and construction of MLI make it susceptible to electrostatic charging.

MLI is a system of reflective (low emittance) metallic radiation shield layers alternating with non-metallic separator layers. A typical MLI cross section is shown in Figure 1. The outer cover is made of a durable Teflon coated glass fiber cloth, referred to as beta cloth, which typically has a metallic grid sewn into the surface. Directly beneath the beta cloth is the light block layer which is typically single metallized (metal on one side only) Kapton with the non-metallic side facing the beta cloth. Below the light block layer is a system of alternating double metallized reflector layers and Dacron net separators with the first layer below the light block and the last layer before the inner cover being a separator net. The inner cover is made of Nomex cloth with a carbon fiber grid sewn into the surface. The whole system is sewn together around the edges to form the MLI blanket.

Spacelab MLI surfaces can acquire excess electrostatic charge through triboelectrification (frictional charging due to materials with different dielectric constants rubbing together) and/or charging due to interaction with the space plasma environment. Data from previous space flight experiments indicates that space plasma charging is more of a concern in geo-synchronous or polar orbit than in the low-

earth orbit of Spacelab. Therefore, triboelectrification is the major charging mechanism for Spacelab MLI surfaces.

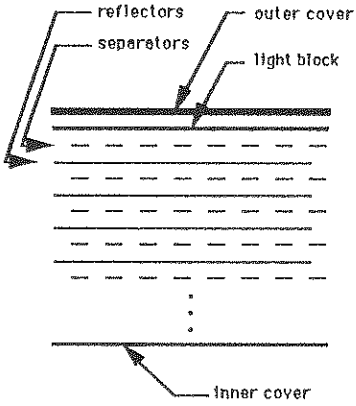

Figure 1. Typical cross-section of Spacelab MLI.

Triboelectrification of the MLI surfaces can occur during the highly vibrational launch/ascent phase of the mission as well as the highly turbulent descent/landing phase of a mission. If triboelectric charging of a surface has occurred and bonding is not adequate to drain the charge in a sufficiently short time period, the potential for an electrostatic discharge (ESD) exists.

Spacelab's major reason for MLI ESD control is to prevent ignition of hydrogen gas which may have leaked into the payload bay from Orbiter plumbing. Such an ignition could have catastrophic results and is of primary concern during ascent/descent when the Orbiter payload bay doors are closed.

In order to preclude an electrostatic discharge, MLI must be electrically bonded to structure ground. This paper describes current Spacelab MLI bonding methods and requirements, difficulties encountered in implementing these bonding methods, present techniques of overcoming bonding difficulties, and possible future methods of overcoming bonding difficulties.

COMPARISON OF ELECTROMAGNETIC FIELDS RADIATED BY ELECTROSTATIC DISCHARGES FOR ADVANCED TEST APPLICATIONS

C. Imposimato* A. Manara M. Zuntini L.Inzoli
(CESI - Italy) (ESA/ESTEC - Holland)

Abstract

Aim of this paper is to critically summarize and compare the radiation measurements from a square, vertical, metallic plate (i.e. 0.5 m per side), connected to the ground reference via a 1 MΩ resistance and excited by electrostatic discharges on the back side. In such configuration the radiating element is used to mask both the spark gap and the simulator, limiting uncontrolled radiation into measuring field sensors. This set-up is normally used, without specific characterization, for commercial device testing.
The field sensors were positioned both very close to the plate and far from the plate (from 10 cm to 50 cm stepped every 10 cm and up to 4 m), in order to evaluate the field map: the source ESD discharge voltage were 20 kV on spark gap and also in later stage 5 kV spark gap to be compared with the current literature values. These measurements were performed in the CESI anechoic chamber which meets the validation requirements for alternative test sites as specified in ANSI C63.4-1991 (dimensions: 23x16x12 m - absorbers: 244 cm long) in order to reduce the contamination of the data due to reflections from walls and other scatterers (the plate tends indeed to resonate at about 200 MHz, under excitation by the spark with chamber walls). (See figure 1 for the test set-up).
Furthermore, some measurements were repeated in more typical laboratory environment conditions. In fact, the above mentioned set-up, which is normally used to characterize the behavior of equipment for civil or industrial applications when radiated ESD tests are performed, does not explicitly require an anechoic room.

Now, first, the measured fields are compared with the typical fields radiated by MIL-STD-1541 sparker, as well known from the literature and used for the radiated ESD test required by ESA and NASA space systems. The aim is to verify how it is possible to improve, for some application, the radiated ESD test performed with the "plate method", as alternative method for spatial applications.
On the basis of our investigation, the most relevant advantage in applying the "plate method" consists of a more predictable and faster transient field. In addition, a larger surface of the equipment can be tested at very high frequency. For instance, the near electric field produced by the plate excited by 20 kV electrostatic discharge can reach values up to about 40 kV/m if the field sensor is placed down to 10 cm from the plate.

As second aim, starting from these results, the analysis was extended to take into account the new RS105 (radiated susceptibility, transient electromagnetic field) test required by MIL-STD-461D with the plate method test.
Because the waveshape of the transient in RS105 is quite similar to ESD and the electric field strength required by RS105 is of the same order of magnitude (50 kV/m), we can establish a reasonable correlation between the requirement RS105 and ESD. Furthermore, because we envisage to perform the same measurements of field characterization placing some equipment near to an ESD excited plate and alternatively under a NEMP antenna, we will present, in this paper, a qualitative experimental comparison between the severity involved by the two tests. We believe indeed that, when RS105 or ESD test will be required, at least for small equipment, similarity in design and test requirement can be efficiently used.

SIMULATED EFFECTS OF STRONG IONOSPHERIC SCATTERING ON GPS SYSTEM PERFORMANCE

P.N. Vijayakumar and T.R. Tyagi

(National Physical Laboratory, New Delhi-110012, India)

ABSTRACT: Strong ionospheric scintillations have been observed at VHF and GHz frequencies in the Indian low-latitude sector during the high solar activity periods of 1988-1991. These are known to produce wide band interference in satellite radio communication systems. Often, these scintillations are found to be non-gaussian in character and tend to possess a high degree of correlation over a given bandwidth of interest. The problem of this kind of correlated-noise interference is rather serious, especially, at GHz frequencies which are prone to strong scattering by spiky ionospheric structures, or the so called ionospheric glints, which are nothing but sharp gradients in ionospheric plasma densities. In this paper we evaluate the performance of GPS receiving systems which employ dual frequency correlation technique for determining the differential group delay (ΔT) introduced by the ionosphere. The determination of ΔT could be seriously affected when the two GPS L-Band frequencies viz L1 (1575.42 MHz) and L2 (1227.6 MHz) are strongly scattered by spiky ionospheric structures present around 350 km height range. In our present computer simulation two dimensional parabolic equation is numerically solved to obtain complex wave field distribution of L1 and L2 signals after scattering by a model phase screen producing diffraction effects in free space. Cross correlations of phase fluctuations and amplitude fluctions of L1 and L2 signals are considered separately to evaluate the performance of code free GPS receiver intended for ionospheric applications. Possible remedial measures through digital signal processing techniques are suggested.

ON BOARD ANTENNAS MODELLED BY USING SIMPLE RADIATING ELEMENTS

M. Domingo, R.P. Torres, M.F. Cátedra
Grupo de Sistemas y Radio
Dpto. Electrónica. Universidad de Cantabria
Avda. los Castros s/n. Santander 39005. SPAIN
Phone: +34 42 201493, Fax: +34 42 201402

ABSTRACT

The analysis of the performance of antennas on board of satellites, aircrafts, ships, etc., is an acute problem that needs simple and versatile models of the antennas. In this communication a method to obtain these models by using simple radiating elements (electric and/or magnetic dipoles) is presented.

SUMMARY

The analysis of the performance of antennas on board of structures such as satellites, aircrafts, ships, etc., where lots of equipments and systems share a quite reduced space, requires flexible numerical models of the different kind of antennas.

From the point of view of developing a general code that allows the analysis of on board antennas and that facilitates the change of their relative positions, two main requirements are needed: an accurate and efficient electromagnetic code that takes into account the effects of the structure where the antennas are placed and the development of simple models of the antennas that allow to obtain their fundamental electromagnetic characteristics without a great computational cost.

The radiation pattern of the antenna to be modeled is measured when it is placed in front of several metallic structures such as squared plates, circular plates and cylindrical sections. The numerical models consist on a set of electric and magnetic dipoles which radiates the same pattern than the measured antenna. The model must be coherent with changes of the geometry and the frequency. To obtain these models it is necessary to combine a previous knowledge of the basic elemental dipoles behaviour with a parametrization of the problem capable of being applied to numerical optimization techniques.

The radiation pattern of the set of dipoles can be obtained by using a high frequency approach as GTD if the conducting structures are electrically large. In this case a fast program has been implemented. When the electrical

dimension of ground planes are small it is necessary to use rigorous methods to calculate the radiation pattern of the dipoles near to conducting structures. The methods used to solve these situations are based upon the Conjugate Gradient algorithm along with the Fast Fourier Transform (M.F. Cátedra, J.G. Cuevas, L. Nuño. IEEE-AP, 1744-1752, 1988 and J.C. Arredondo, F. Ruíz, M.F. Cátedra. JINA'90, 104-107, 1990). This method solves the Electrical Field Integral Equation (EFIE)

$$\vec{E}^i(\vec{r}) = \int \vec{J}(\vec{r}')\, G(\vec{r}, \vec{r}')\, dS' \qquad (1)$$

where $\vec{E}^i$ is the field impressed by the dipoles in the ground plane.

The radiated field is obtained as the sum of the field radiated directly by the dipoles and the scattering field produced by the impressed field in the plate:

$$\vec{E}^i = \vec{E}^d + \vec{E}^s \qquad (2)$$

The models optimization process implies to compute many times the scattered field. The CG-FFT method is efficient enough to be used in these optimization tasks.

The above method to generate models of antennas has been applied to a high number of typical aircraft antennas. A big set of measurements has been carried out to validate the method. Furthermore, statistical studies of the accuracy of the models obtained have been performed and will be presented.

2D and 3D Finite Element Formulation for High Power Microwave antennas

L. Nicolas, J.L. Yao-bi
CEGELY - URA CNRS 829
BP163 Ecully cedex
France

S.J. Salon, K.A. Connor
Rensselaer Polytechnic Inst.
Troy, NY 1280-3590
USA

B.G. Ruth, L.F. Libelo
Army Research Lab.
Adelphi, MD 20783-1197
USA

Abstract: We present a 2D and 3D nodal-based finite element formulation for the analysis of high power microwave antennas. It is written directly in terms of the electric field or the magnetic field vector. Open boundary is modeled using absorbing boundary conditions. The formulation includes conductor interfaces and far field calculations

Introduction. The purpose of the work reported here is to describe an analysis tool that can provide a two- or three-dimensional model of the operation of Vlasov/Nakajima type mode convertors. The specific application of such devices is for lauching well-defined beams from high power low order mode sources. Electromagnetic field information is obtained with a finite element model that utilizes an absorbing boundary condition. Three-dimensional analysis is necessary to fully characterize the operation of these wave launchers. However two-dimensional modeling may give some useful information.

Justification of the choices about the formulation: finite element method, nodal elements and absorbing boundary condition.

- The finite element method (F.E.M.) is very well adapted for modeling anisotropic and non-linear phenomena (constitutive parameters of the media depend on the direction, the frequency and the magnitude of the applied field). This is especially crucial for high power microwaves.

- Nodal elements have very desirable properties: they are very well known and thus easy to use, they conform exactly to curved surfaces and they minimize the time of computation. Spurious modes may be eliminated in 3D using a penalty function. The discontinuity of the normal field at material interfaces may be explicitly enforced.

- The F.E. domain has to be truncated as much as possible, especially in 3D where three unknowns are used for each node. The second order Engquist-Majda absorbing boundary condition (A.B.C.) has been shown previously to give accurate results (L.NICOLAS and all, IEEE Trans. on Mag., MAG29 n°2, 1830-1834).

The 3D F.E. formulation.

As shown previously (L. NICOLAS and all, IEEE Trans. on Mag., MAG29 n°2, 1642-1645), the Galerkin form of the Helmoltz equation for the magnetic field is:

$$\iiint_V \left(\nabla W \times \frac{1}{\varepsilon_r} \nabla \times \mathbf{H} \right) dv + \iiint_V W k_0^2 \mu_r \mathbf{H}\, dv - \iiint_V (\nabla . \mathbf{H})(\nabla W)\, dv +$$
$$\iint_S W (\nabla . \mathbf{H})\, ds - \iint_S \mathbf{n} \times \left(W \frac{1}{\varepsilon_r} \nabla \times \mathbf{H} \right) ds = j\omega\varepsilon_0 \iiint_V W \mathbf{J}\, dv$$

This includes the penalty function used to force the magnetic field to be divergence-free. The surface terms are evaluated on the boundary of the F.E. mesh: surfaces of perfect conductors, which are not meshed, and outer surfaces of the F.E. domain, which have to be rectangular. This last feature is due to the second order Engquist-Majda A.B.C. that we use to modelize the open boundary. The boundary condition on perfect electric conductors is implicit for the magnetic field.

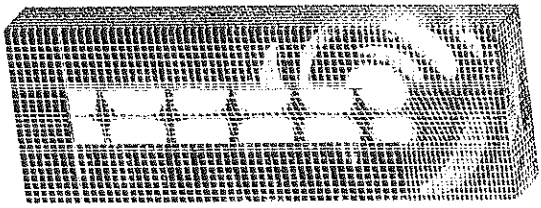

Fig. 1: 3D modeling of a Vlassov-type antenna with a 60° slant-cut angle - TM01 mode - 5.5. GHz

The 2D approximation.

In 2D, both geometric and physical quantities are uniform in the z-direction, perpendicular to the studied cross-section. The direction of propagation of the wave is then contained in this cross-section, and the magnetic field becomes perpendicular to this plane (case of a T.M. propagation): $\mathbf{H} \equiv Hz$, and the previous expression becomes:

$$\iint_S \left(\nabla W \cdot \frac{1}{j\omega\varepsilon} \nabla H + j\omega\mu W . H \right) ds - \int_\Gamma W . \frac{1}{j\omega\varepsilon} \frac{\partial H}{\partial n} \, d\Gamma = - \iint_S W . J \, d\Gamma$$

The far field calculation.

The far field -outside the F.E. mesh- is calculated using an integral-type method (L. NICOLAS, proc. of Compumag 93, 308-309). Equivalent electric and magnetic surface current are first obtained on a surface surrounding the antenna inside the F.E. domain. This is performed using the F.E. near field. The far field may then be calculated using some common approximations.

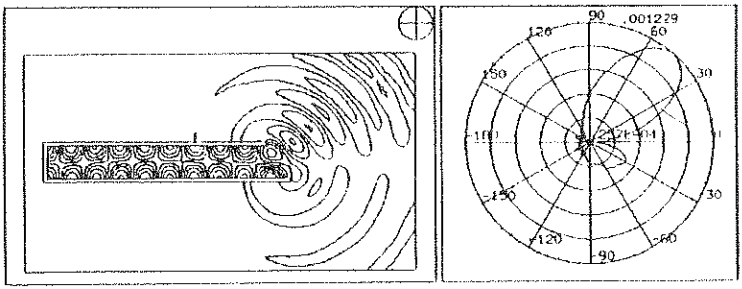

Fig.2: 2D modeling and far field corresponding to the example shown in Fig.1

Observation of Chaos in a Microwave Circuit

Chance M. Glenn* and Scott Hayes
U.S. Army Research Laboratory
Adelphi, MD, USA 20783

Chaotic behavior has been observed in a microwave circuit that consists of a shunt PIN diode cascaded with a 0.68-dB/MHz rolloff bandpass filter (see fig. 1). The chaos manifests itself as a broad-band power spectral density output signal given a narrow band input signal. The chaos appears and disappears as the incident power to the circuit is increased, suggesting bifurcations and periodic windows in the chaotic region. Data are included that illustrate classic characteristics of chaos, such as period doubling and broad-band spectral characteristics.

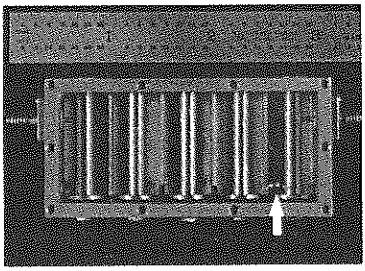

Figure 1. *Microwave circuit realized with cylindrical cavity resonators (note PIN diode at right-most resonator).*

A chaotic system can generate complex, seemingly random, yet completely structured behavior, depending upon the system parameters and initial conditions. Any system, whether chaotic or not, can be described in terms of state variables (such as independent currents and voltages in electronic circuits). These time-dependent variables, when plotted in an orthogonal coordinate system, form what are commonly called *state-space trajectories*. These trajectories describe the global behavior of the system as it evolves in time. The region that these trajectories tend to, over a period of time, is called the *attractor*. In a chaotic system, the state space trajectories diverge exponentially, thus initial states close to each other will rapidly move apart. However, because the system is bounded, the trajectories must fold back onto themselves (a chaotic attractor is often termed a *strange attractor*). When it is not possible to extract two or more independent state variables (as was the case with the microwave circuit), a projection of the attractor can be formed through a time delay embedding. Time-delay embedding is a technique wherein the state variables are derived from the output signal: $x \rightarrow v(t)$, $y \rightarrow v(t+\delta_1 t)$, $z \rightarrow v(t+\delta_2 t)$; for a three-dimensional system, where $v(t)$ is the time-dependent voltage and δ_i is the i^{th} time delay increment. The reconstructed attractor will be geometrically similar to one generated by conventional means to within a smooth change of coordinates. This technique was used to create two-dimensional projections (*phase portraits*) of the various attractors produced by the microwave circuit.

A system in chaos tends to be extremely sensitive to initial conditions, small perturbations, and minute changes to the system parameters. The microwave circuit is a driven system so that drive signal power (P_{in}), and the frequency (f_{in}) are parameters that the chaos responds to. As f_{in} was fixed at 1.575 GHz and P_{in} was increased, we began to see various behavior such as periodic, quasi-periodic, and chaotic motion. Figure 2 shows a period doubling (2,4,8) sequence observed as P_{in} was varied from 19 to 20 mW (spectral content was also measured to verify this). This type of behavior tended to precede chaos. Figure 3 is an example of a fully chaotic state occurring at P_{in} = 37 mW. The bandwidth limitation of the oscilloscope did not allow the state space trajectories to be fully resolved, thus they appear hazy. The chaotic states that appeared and disappeared (from 13 to 110 mW) were predominately stable and repeatable.

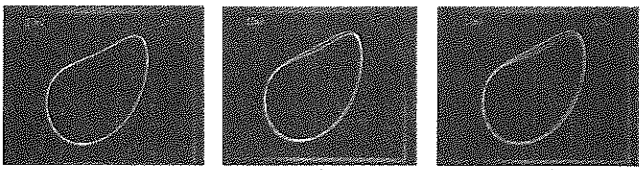

(a) (b) (c)

Figure 2. *Measured phase portraits for (a) period 2, (b) period 4, and (c) period 8.*

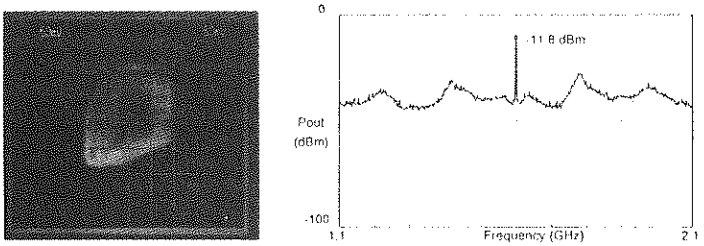

(a) (b)

Figure 3. *Measured (a) phase portrait and (b) frequency spectra of chaos occurring at* P_{in} = *37 mW.*

Several examples of periodic, quasi-periodic, toroidal, chaotic, and intermittent behavior, which were observed experimentally with this microwave circuit, will be decribed. The ability to produce several types of chaotic behavior, in conjunction with the distributed nature of the circuit, leads the authors to believe that microwave circuit is a high-dimensional system. Presently, chaos is an undesirable behavior in electronic systems; however, much work is being done in the area of periodic stabilization and control.

A MM-GTD ANALYSIS OF COUPLING AND RADIATION OF ANTENNAS ON RESONANT SIZE BODIES MODELLED BY PARAMETRIC SURFACES

L. Valle, F. Rivas, M.F. Cátedra
Grupo de Sistemas y Radio
Departamento de Electrónica. Universidad de Cantabria.
Avda. Los Castros s/n. 39005 Santander. Cantabria. SPAIN
Phone: +34 42 201493, Fax: +34 42 201402

ABSTRACT

The purpose of this communication is to present a technique for the treatment of the analysis of the coupling and radiation patterns of antennas on board of perfectly conducting bodies. The bodies are modeled using NURBS surfaces (D.F. Rogers, J.A. Adams. "Mathematical Elements for Computer Graphics". McGraw-Hill International Editions, 1990) and they are large compared to the wavelength. NURBS surfaces are quit useful when complex geometries are involved, as in the case of aircrafts, because with just a few of them a very realistic representation of the body is made. In fact, NURBS surfaces are currently used in many industrial applications for import, create, transform, rendering and export geometrical data of the bodies. For computational reasons (more stability) NURBS surfaces are transformed in equivalent Bézier patches (G. Farin. "Curves and Surfaces for Computer Aided Geometric Design". Academic Press, 1988).

SUMMARY

The electromagnetic characterization of antennas mounted on or near three-dimensional surfaces by the Moment Method (MM) is significantly limited by computer storage of the matrix coupling. This communication examines a hybrid technique which combines the MM with the GTD approximation. This MM-GTD approximation provides a way of extending the usefulness of the MM when electrically large bodies are considered. The antenna is defined like a numerical model formed by a set of electric and/or magnetic dipoles (P. Martínez, M. Domingo, R.P. Torres, M.F. Cátedra. VIII Symposium Nacional de la URSI. 733-737. Valencia, Spain 1992) when the working frequency is large in terms of the size of the body. The antenna is represented by point-sources located near a point of the body named focus. Only the subdomains illuminated by the focus are numerically fed.

In the present approach the element Z_{ij} of the MM matrix is only considered if the current defined in the subdomain j is close to i. The concept of "close" is measured in terms of the number of Fresnel zones considered around the subdomain i. Working in this way, it is only necessary to store and

to compute the coupling between a few pairs of sudomains. The computational efficiency is improved when large bodies are analyzed.

The code is particularized to the treatment of antennas situated near conducting bodies and the focus must be in the proximity of a Bézier patch of the geometry. In the four boundary-lines of this patch current basis functions have been defined (L. Valle, F. Rivas, M.F. Cátedra. To appear in IEEE Transactions on Antennas and Propagation).

In these subdomains (antenna subdomains) the current will be strong due to its proximity to the focus of the antenna and for this reason this current will be considered in the computation directly coupled with all the illuminated subdomains of the geometry not only with the close ones.

The resulting direct coupling matrix is not quasi diagonal but randomly sparse with only four rows full (the corresponding to the antenna subdomains). This fact supposes to use a lot of zero terms in the coupling matrix. To avoid this the matrix is represented by two new matrices. The first one only has four rows and as many column as illuminated sudomains. The second one contains as many rows as subdomains defined in the geometry minus four and for each row, the number of columns is less or equal than the maximal number of subdomains close to a given subdomain. When the body is electrically large, this last number will be always smaller than the number of illuminated subdomains and in conclusion the memory requirements of the method are highly reduced. To obtain the current, an efficient algorithm based in the Gradient Conjugate Method is considered to solve the system of equations.

Finally, to compute the radiated field at an arbitrary point in the space it is necessary to consider the contribution of the direct ray, which comes from the source and the scattering field due to the current excited in all the parts of the body. The method has been successfully validated by comparison with measurements or with results of pure MM codes. Currently is being used in the industry.

METHOD OF SYNTHESIS OF DIRECTIONAL COUPLERS WITH BIG COUPLING

Dmitry Stepanov
Vinnitsa Polytechnic Institute

for mail: av. Younost 20/73 F93, 286030 VINNITSA, Ukraine

One of widespread methods of waveguide coupling to provide branching, power control and others is use directional couplers (DC) with big coupling. There is offered in the paper method of synthesis of such devices, allow to considerably improve its characterystics and to determine the borders of appliement of small coupling methods. The method include nonstandart way of near field interaction accounting. The method may be applied as for singlemode DC as for multimode DC.

Offered method is based on specific model of DC describe real processes on DC the way, that allow to account tham by use the special fictious DC is called as equivalent DC. The main thesises of the model are:

- every coupler is regard as an outstanding and concentrated radiation source,
- any output power is regard as a sum of some parts, corresponded to the energy passage ways to this output in accordance to its phases.

These thesises allow to introduce the equivalent DC in wich couplers couplings correspond to the shares of the mentioned ways. The equivalent DC has the next properties:

1) power in the primary equivalent line is constant,
2) reflections of couplers are absent,
3) reradiations from line to line are absent after the first one get place.

These properties of equivalent DC coincide to the properties of widespread small coupling models of DC synthesis. This circumstance allow to separate the task of big coupling synthesis at the three relatively undepended tasks:

1) synthesis of equivalent DC by small coupling methods,
2) transition from the equivalent DC to the real one according to the equations of link,
3) accounting or approximation the near field interactions between couplers in DC.

This separation of task of synthesis at the three ones allow to solve each of tham apart, they are nonsolvcable if together at direct synthesis with accounting of real DC effects.

The equivalent DC has also very convenient for use property - property of superposition: in the case of some equivalent couplers are coinside, the result of this will be equivalent coupler with the coupling equal to the sum of ones, this property allow to minimize equivalent DC to the number of couplers in real DC in the most kinds of DC. The equalization of numbers of couplers in real and equivalent DC allow to link real and equivalent couplers the only way. Transition from real couplers to the equivalent ones is provided by the next formule at the approximation of directionality of DC:

$$B_i = C_i \prod_{j=1}^{i-1}(1-C_j) - 2C_i \sum_{K=1}^{i-2} C_K \varkappa_K \sum_{n=K+1}^{i-1} \varkappa_n C_n - C_i \Big(\sum_{K=1}^{i-1} \varkappa_K C_K\Big)^2 -$$

$$- \frac{1}{(1-\mathcal{X}_i)} \sum_{k=2}^{i-1} [(1-\mathcal{X}_k)C_k \sum_{n=1}^{k-1} (1-\mathcal{X}_n)C_n (1-\mathcal{X}_{i+n-k})C_{i+n-k}, \quad (1)$$

where Bi - equivalent couplers, Ci - real ones. $\mathcal{X}_i$ - directionalyties of couplers.

On use (1) the diagram showing the difference between figured couplings with and without accounting of real processes in DC obtained (fig.1)

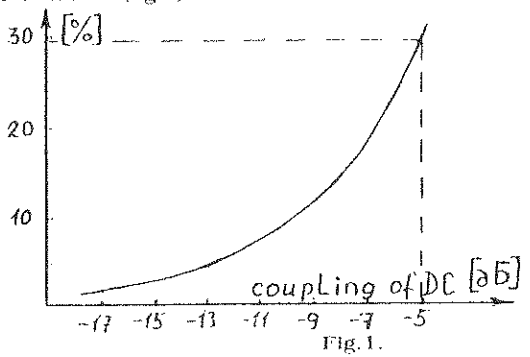

Fig.1.

This diagram shows the value of error of small coupling methods of synthesis in dependence of value of DC coupling and allow to define the borders of applicement of such methods in dependence of given accuracy of synthesis and coupling.

The other important moment for synthesis of DC is accounting of near field interactions (NFI) between couplers. We avoid the strict solving of the task by electrodynamic methods are too complicated for, and don't give opportunity for use tham in direct synthesis, but only in analysis.

We offer to use method based on experimental data is enough convenient and simple. The results of NFI in it are formylated by the frecuency characterystics:

$$\dot{X}^r(\omega) = \dot{Y}^r(\omega) - \dot{Z}^r(\omega) \quad , \quad (2)$$

where $\dot{X}^r(\omega)$ - result of NFI between couplers of r multitude, $\dot{Y}^r(\omega)$ - frecuency characterystic from experiment (accounted NFI), $\dot{Z}^r$ - one without such accounting is figured by methods of small coupling.

As for the whole DC, its accounting of NFI is formulated by the next formule:

$$\dot{X}(\omega) = \dot{X}^{r_1}(\omega) + \ldots + \dot{X}^{r_n}(\omega) \quad , \quad (3)$$

where - r_i multitudes of interactioned couplers describe compliitely interactions in DC.

It may be shown, that if r_i and links in tham are the same, share of each of tham in NFI result will be proportional to the value of coupling of definite coupler in the multitude. This gives an opportunity to account or to approximate NFI in synthesis.

The dignity of offered method is opportunity of direct synthesis of DC with big coupling, widening of domain of applicement of existed methods of small coupling and defenition of tham, opportunity of accounting or approximation of NFI in synthesis.

TRANSIENT RADIATION OF A CIRCULAR LOOP WITH A REALISTIC EXCITATION

R. H. ROCHEROLLES S.C.R.I.P.

After a short introduction, the second part is devoted to the calculation of the transient radiated field of the electric dipôle and of the magnetic dipôle. The third part is devoted to the formulation of the excitation current in a quite usual concrete example. The fourth part is devoted to the field radiated by a circular loop when it is excited by the current pulse described in the third part. In conclusion, the radiation of the linear dipôles is compared to that of the loop, and some attractive properties of the loop are outlined.

I - Introduction

" In early 1969, Prof. T. T. Wu stated : " It is worth emphasizing that our knowledge about the transient response of antennas is very meagre indeed " ".(G. FRANCESCHETTI and C. H. PAPAS, IEEE Trans. Ant. Prop., vol AP 22, n°5, 651-661, 1974) These two scientists from Caltech published 68 basic references from 1958 to 1973 and presented a number of very interesting procedures and results.

II - Transient Radiated Fields of the Dipôles.

In the classical approach of the antenna theory, one calculates first the vector potentials of an oscillating charge, and then derivates the radiated fields : E_r , E_θ , H_φ , for the electric dipôle, and H_r , H_θ , E_φ , for the magnetic dipôle, in the frequency domain.

By a Fourier transform of these six field equations FRANCESCHETTI and PAPAS presented the equations of the radiation of these dipôles in the far field, that is to say for the 1/r terms, in the time domain.

Two years later, an excellent paper (K. J. LANGENBERG, IEEE Trans. Ant. Prop. 236-239, March 1976) extended the results to the near-field radiation zone without the knowledge of the corresponding time harmonic components. Using a Laplace transform at the early stage of the vectors potentials, the author gave the theoretical solution for the transient radiation of a small circular loop. Then, he discussed the importance of finite rise times instead of ideal step function current, as is done in the next chapter of the present paper.

In this work, we use a Laplace transform at the six field equations level and we obtain by a simple calculation the near, middle, and far-field terms of the six field components.

$$E_r = 60.\ell \left[\frac{c}{r^3} \int I.dt + \frac{I}{r^2} \right]. \cos\theta$$

$$E_\theta = 30\ell \left[\frac{c}{r^3} \int I.dt + \frac{I}{r^2} + \frac{1}{r}\frac{\dot{I}}{c} \right]. \sin\theta$$

$$H_\varphi = \frac{\ell}{4\pi} \left[\frac{I}{r^2} + \frac{1}{r}\frac{\dot{I}}{c} \right]. \sin\theta$$

for the electric doublet of moment $J_y = I.l$

$$H_r = \frac{iS}{2\pi}\left[\frac{I}{r^3} + \frac{1}{r^2}\cdot\frac{\dot{I}}{c}\right]\cos\theta$$

$$H_\theta = \frac{S}{4\pi}\left[\frac{I}{r^3} + \frac{1}{r^2}\cdot\frac{\dot{I}}{c} + \frac{1}{r}\cdot\frac{\ddot{I}}{c^2}\right]\sin\theta$$

$$E_\varphi = 30S\left[\frac{1}{r^2}\cdot\frac{\dot{I}}{c} + \frac{1}{r}\cdot\frac{\ddot{I}}{c^2}\right]\sin\theta$$

for the magnetic doublet of moment M = I.S

III - Formulation of the current pulse.

Physical considerations of the power circuit help us to propose a good simulation of the current in a quite usual practical case. (fig 1)

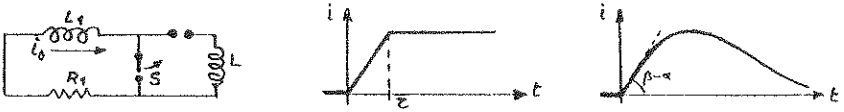

We suppose that the energy is first accumulated in the inductance L_1 in the form $\frac{1}{2} L_1 . i_0^2$. At the time t=0 the switch S is opened, and the current is then circulating in the serial circuit $L_1 + L$. The current variation makes surtension on the switch and creates a plasma whose resistance grows with time. After a delay τ , arcing swith off.

For simplification, we take a linear growing current from t=0 to t= τ, because the exact law of current growing is not important here, but only the elbow of the curve at t=0 which creates a discontinuity of the first derivative. It is noteworthy that this discontinuity is always realised when a spark-gap is in a place in the circuit. (fig 2)

The current pulse may be formulated by : $i = e^{-\alpha t} - e^{-\beta t}$

where α stand for current extinction and β stand for the rise time. α is generally much smaller than β . The slope at t=0 is $\beta - \alpha \cong \beta$. One has only to make $\beta = \frac{1}{\tau}$ to get a good loop current model.(fig 3)

IV - Circular Loop Radiation in the Far-field zône.

Remaining terms H_θ and E_φ are proportional to the second time derivative of the current. The first time derivative is $y'(t) = -\alpha e^{-\alpha t} + \beta e^{-\beta t}$ and $y'(0) = \beta - \alpha$. There is apparently no difficulty, but a step is in ambush at t=0. For this reason the time derivative of $y'(t)$ is not $\alpha^2 e^{-\alpha t} - \beta^2 e^{-\beta t}$ and $y''(0)$ is not $\alpha^2 - \beta^2$. There is a Dirac impulse at t=0 which gives very high values to H_θ and E_φ , and adds a constant term $\beta - \alpha$ to their frequency spectrum.

V - Specific Properties of the Loop Radiated Fields.

The area under the Dirac function at t=0 is $\beta - \alpha$. According to the cited authors, the duration τ' of the practical Dirac impulse is under the control of the loop radius. The peak value of the second time derivative at t=0 is $\frac{\beta-\alpha}{\tau'} \sim \frac{\beta}{\tau'} \simeq \frac{1}{\tau \cdot \tau'}$ It may be very high. In the far-field zône, fields radiated by an electric dipôle are proportional to $\frac{\dot{I}}{c}$. Fields radiated by a magnetic dipôle are proportional to $\frac{\ddot{I}}{c^2}$. Their ratio is proportional to $\frac{\tau'}{c}$. If τ' is smaller than 3 ns, the circular loop is winning.

THE EFFECTS OF VOLUME, SHAPE AND FILL FACTOR ON THE IEMP RESPONSE OF ELECTRONIC EQUIPMENT BOXES

By

Gregory J. Rigden and Rodney A. Perala*

ELECTRO MAGNETIC APPLICATIONS, INC.
7655 West Mississippi Avenue, Suite 300
Lakewood, CO 80226 USA
Phone: 303-980-0070
Fax: 303-980-0836

The objective of this effort was to calculate the internal electromagnetic pulse (IEMP) response of electronic equipment boxes as a function of volume, shape, and fill factor. The responses calculated consisted of internal electric and magnetic fields along with wire and circuit board trace element currents and voltages. A total of six boxes of varying shapes and sizes possessing a few wires up to multiple complex circuit boards were modeled. The box volumes ranged from 3 to 384 liters.

To investigate the effects of shape and volume, two wires were inserted into each of the six boxes. One wire stretched between the midpoints of the two opposing faces of largest area and the other between the faces of smallest area. One wire was slightly shifted to prevent intersection at the box center. Each wire was insulated from the box at one end and connected through a 50 Ohm resistor at the other to simulate a measuring device. Each box was illuminated with two different gamma pulse waveforms incident along the respective internal wire directions.

The peak wire responses for gamma ray incidence upon the face of largest area generally exceeded those for the small face incident direction while the peak responses of the wire parallel to the incident direction exceeded those of the perpendicular wire. A direct proportionality relation was discovered between the peak wire response magnitude and the corresponding box volume. The constant of proportionality depended upon the gamma source. The peak internal electric and magnetic field values were roughly proportional to the area of the box face that was perpendicular to the incident direction, although affected somewhat by box resonances.

A similar behavior was observed when the wires were replaced by circuit boards. The peak circuit board responses were similar to the wires while the internal fields were enhanced by the presence of metal such as circuit board grounding planes. This field enhancement, however, was local and limited in spatial extent. The concept of fill factor was investigated by inserting several complex circuit boards into one of the smaller boxes. The results of this endeavor revealed the impact of installing the many boards to have limited affect on the internal wire or trace peak responses.

INDOOR MULTIPATH FADING REDUCTION WITH AN ADAPTIVE PHASED ARRAY

Ahmed T. Denidni*, Gilles Y. Delisle**
*Electrical Engineering Dept., Laval University, Ste-Foy, Qué, G1K 7P4.
**INRS-Télécommunications, Ile-des-Soeurs, Qué, H3E 1H6.

Abstract

In recent years, many studies have shown that the received channel in a wireless indoor communication system is known to vary significantly according to multipath propagation. This phenomena is due to the fact that there is frequently no line-of-sight-signal between the transmitter and the receiver, but rather several propagation paths. These signals combined constructively or destructively to produce the output signal.

Multipath fading compensation techniques can be used in a wireless indoor system, such as equalization. The various time length that an equalizer can compensate if all time delays are considered is limited and insufficient. In a wireless indoor environment, not only the reference signal is absent but it cannot also logically be considered that the desired signal direction is known a priori. The main reason for this being is that the environment is similar to the one found in the mobile radio channel where multiple instantaneous changes are encountered.

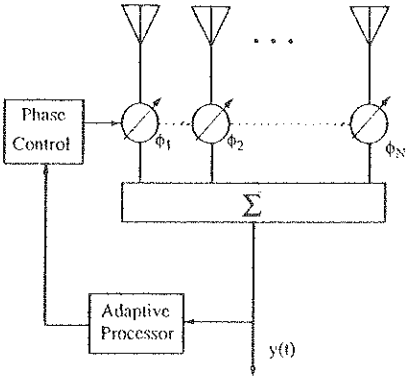

Fig 1: Block diagram of a N phased array

To reduce the effects of the multipath fading, a new type of

This work was supported by the Canadian Institute for Telecommunications Research (CITR)

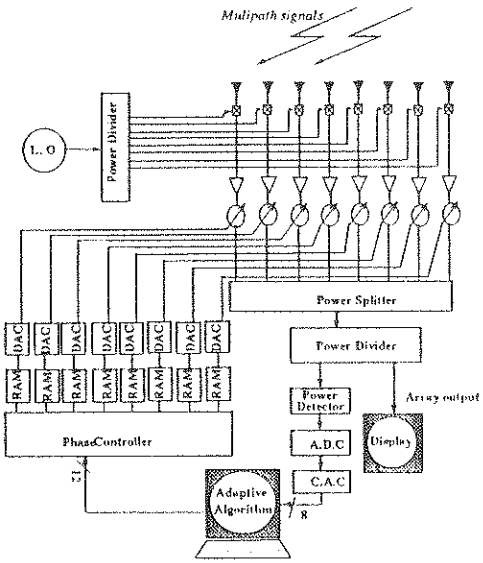

Fig. 2 : Block diagram of experimental system.

phased array is proposed. Basically an adaptive phased array, as shown in Fig. 1, is composed of a number of identical array element with their outputs weighted only in phase. Then, to produce the system output, all outputs are added in a combiner to produce the system output. To adjust the phase at each antenna of the array, our system contains an internal feedback loop based on a non-linear "on-off" method and the objective is to maximize the array output power. In this approach, the algorithm does not require any reference signal and the desired signal is chosen to be the strongest one from multiple incident waves on the antenna array. The adaptive algorithm can be applied to a multi-input system whose output power is expressed as a function of the adjustable phase angles.

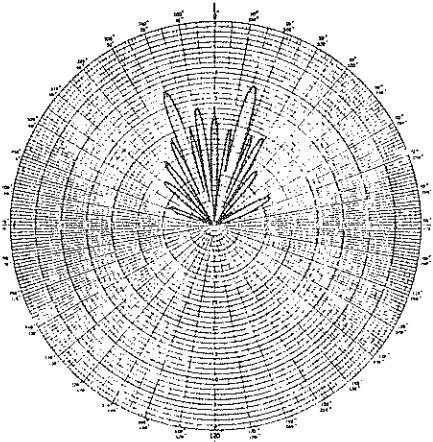

Fig. 3:Array pattern after adaptation.

A 20 GHz physical implementation with discrete components of a prototype phased array has been implemented as shown in Fig. 2. Both analytical and experimental results obtained with such an array are discussed in comparison with those predicted by the theory. Experimental examples of such results are shown on Fig. 3 where the adapted array pattern is adapted for an incoming signal at 20°.

CALCULATION AND MEASUREMENT OF BOX IEMP FOR CANONICAL CONFIGURATIONS INCLUDING SCATTERING OBJECTS

Dr. James R. Elliott* and Gregory J. Rigden
Electro Magnetic Applications, Inc.
P.O. Box 260263
Denver, CO 80226
USA
(303) 980-0070

and

Dr. Walter Kornahl
Wehrwissenschaftliche Dienstelle Der Bundeswehr für ABC-Schutz
Postfach 11 42
3042 Munster
Deutchland

The photon environment associated with the tactical nuclear source region generates photocurrents which give rise to electromagnetic fields. When this occurs within an empty enclosure with conducting walls it is often referred to as box IEMP. The magnitude of the response is known to depend on the size of the box as well as the gamma dose rate and its time derivative. Experiments have confirmed the ability to model the IEMP response for many configurations using spatially uniform photocurrents and ionization associated with a nominal 1 MeV gamma ray environment.

However, there may be cases when the enclosure walls or scattering objects of various materials may introduce significant variations from the nominal and uniform excitation with the volume. It may also happen that the system generated electromagnetic pulse (SGEMP) due to radiation interactions with the box or its contents is not clearly distinguishable from the empty box IEMP. The objective of the study reported in this paper is to use both numerical modeling and measurements at a flash X-ray simulator to investigate these complications.

The modeling began with a radiation transport Monte Carlo code (the Integrated Tiger Series codes, Version 3.0). For a given box/scatter configuration the energy/charge deposition and the three components of electron fluence were sampled throughout the interior volume. In addition, the code was augmented in order to capture the time dependence associated with energy/charge deposition and the electron fluence. A significant modification in rise time is possible when the enclosure transit time exceeds the nominal rise time of the gamma dose rate.

A time domain finite difference solution to Maxwell's equations was employed local photocurrents, ionization and time dependence based on the Monte Carlo results. Results are obtained for three configurations:

1. wire terminated in 50 Ohms on one end and shorted to box wall on other end
2. wire terminated in 50 Ohms on one end and isolated from box wall on other end
3. wire terminated in 50 Ohms on one end and attached to suspended metal plate on other end

Two different sized boxes were modeled for a 1 ns rise time pulse and for a slower pulse representing the simulator waveform.

Measurements were made at the WWD flash X-ray simulator for these same two boxes and three configurations as well as for several other sized boxes. The simulations also employed different scattering materials within and at the boundaries of the boxes.

Interesting regularities were observed in both modeling and measurements. These will be characterized as a function of box size, material and test wire configuration. Results for uniform, nominal sources are compared to those deriving from local sources calculated from the ITS programs. Measured results are used for model validation. The presence of significant scattering objects within the boxes reveals the blending of SGEMP and IEMP effects.

EVALUATION OF THE EFFECT OF ELECTROMAGNETIC PULSE ON THE LINEAR SYSTEM

V.G.Boronichev, INTERSWIAZ firm, Saint-Petersburg, Russia
G.K.Boronichev, LONIIR, Saint-Petersburg, Russia
L.M.Martynov, the Ministry of Communications, Moscow, Russia

A b s t r a c t

In practice in many cases there is limited information about shape of the pulse effecting the system. For example a pulse generated by lightning or nuclear explosion causes in some communication the pulse of current or voltage which in its turn can affect radioelectronic equipment connected to above mentioned communication. At this the information about pulse shape affected the radioelectronic equipment is limited, e.g. only the data about affect module is more or less reliable. In this work the response of linear system on pulse affect limited by module, which real form is unknown, is evaluated.

The formulated task can be solved on base of Duamel integral. Let $f(t-\tau)$ be an impact with a module equal to 1, and its signs be alternated according to the law $\operatorname{sign}\left[\frac{dh(t)}{dt}\right]$; $h(t)$ -a transient system function. Let time intervals when the signs of function are constant be $t_1 - 0$; $t_2 - t_1$; $t_3 - t_2$.

Then $$h(\infty)_{max\ max} = 2\left[h(t_1) - h(t_2) + h(t_3) - h(t_4) + \cdots\right] \qquad (1)$$

As t_1, t_2, t_3 are time moments at which sign of $\frac{dh(\tau)}{d\tau}$ is changed and therefore $\frac{dh(t)}{dt}$ derivative is equal to 0, so values of $h(t_i)$ included in brackets are equal to extrema of oscillations appearing in a system at a single impact. Therefore if the impact on a system has 1 module, so the maximum amplitude of its response of x will be equal:

$$x_{max\ max} = 1h(\infty)_{max\ max}$$

This approach can be shown on some examples.

1. Linear system of the first order: Let forced oscillations at the system be described by the equation:

$$T\dot{u} + Ku = f(t), \quad |f(t)| \leq 1$$

If such system is affected by a single impact and $u(0)=0$, a transient process $u(t)$ will be aperiodic and its maximum value

will be equal to $\frac{1}{k}$. So

$$u_{max\ max} = 1/k$$

2. A system of the second order: Let forced oscillations at the system be described by the equation:

$$\ddot{u} + 2\alpha\dot{u} + \beta^2 u = f(t);\ u(0)=\dot{u}(0)=0$$

A transient process u(t) if the roots of characteristic equation are complex can be shown in the following way:

$$u(t) = \frac{1}{\beta^2}\left[1 - e^{-\alpha t}\sin(\omega_1 t + \psi)\right]\ ;\quad \omega_1^2 = \beta^2 - \alpha^2$$

At this, time intervals at which u(t) is sign-constant are constant and can be found from the expression:

$$t_{n+1} - t_n = \frac{\pi}{\omega_1}\ ,\ \text{where } n=0,1,2,3....$$

Then using (1) and introducing a designation of $\gamma = e^{-\pi\frac{\alpha}{\omega_1}}$ we will finally have:

$$u_{max\ max} = \frac{1}{\beta^2}\cdot\frac{1+\gamma}{1-\gamma}$$

The regarded approach can be easily spread over systems of higher orders, but in this case a specific application software package should be developed to use it.

Practical realization of a proposed method if evaluation of linear system response on a restricted by module impact can be come to the following procedures:

1. Impact module is defined
2. Transient system function is defined experimentally or analytically.
3. Maximum possible amplitude of a system response is evaluated by formula (1).

This last gives the base for conclusion about potential possibility for a system to be affected by a powerfull electromagnetic pulse.

MATHEMATICAL MODELLING OF ELECTROBIOLOGICAL INTERACTIONS

Andrzej Krawczyk* and Tadeusz Skoczkowski
Institute of Electrical Engineering,
Pożaryskiego 28, 04-703 Warsaw, Poland

ABSTRACT

The interactions of electromagnetic fields and biological structures are of great interest both from medical and technological points of view. The medical aspect is well-known (even intuitively) while bio-electrotechnology is being developed just at recent time. Especially it is readily seen when dealing with electric field and its influence on living cells. Biologists and biochemists are mainly interested in the voltage induced in the cell membrane (*transmembrane voltage*). This gives the information about forces acting on membrane which cause the phenomenon called *dielectrophoresis*. The other phenomenon which joins electromagnetic field and biological structures is *electroporesity* when the pores in a membrane are caused by electric field. The latter case requires carefully carried calculations since the transmembrane voltage decides on the phenomenon. The paper, however, does not aim at biological effect; our goal is to show how the system "electric field - living cell" should be mathematically modelled. It should be stressed that the research in bio-electromagnetism is on very initial step as concerns the calculation methods. This results from two facts: the first is that so far there were no links between people working on computational electromagnetism and biologists and the second comes from the complex nature of biological structures. The modelling of them is more complicated and not well-documented as it is with technical products, like electric machines.

A living cell may be represented by multilayered, spherical structure that is piecewise homogeneous. It consists of the cell interior, the membrane and the conducting wall which is made of glycocalix chains. The cell is suspended in electrolyte which, from computational point of view, constitutes the infinite, unbounded region. The structure of a cell is, in fact, much more complex - the membrane is made of two lipid layers and contains ion channels. Therefore, the geometry of an object is more complicated than that above described. Also, the material parameters (conductivity and electric permeability) are not constant. However, for analytical computation the model is the only possible. To analyze the real object one needs to use some numerical modelling which will be commented below.

Both for constant and alternating fields the electric field in each region is calculated as the solution of Laplace's equations expressed in spherical coordinates and coupled by interface conditions:

$$\frac{\partial}{\partial r}(r^2\frac{\partial \Phi|_j}{\partial r}) + \frac{1}{\sin\theta}\frac{\partial}{\partial \theta}(\sin\theta\frac{\partial \Phi|_j}{\partial \theta}) = 0 \qquad (1)$$

with interface conditions:

$$\Phi|_j = \Phi|_{j+1} \qquad (2)$$

$$\alpha_j \frac{\partial \Phi}{\partial r} \mid_j = \alpha_{j+1} \frac{\partial \Phi}{\partial r} \mid_{j+1} \tag{3}$$

where j is the description of medium, α_j are the parameters which represent material properties and field frequency ($\alpha_j = \sigma_j + i\omega\epsilon_j$).

The solution of eqn (1) has an analytical form and it may serve as the test approach.

Such an analysis may cause some doubts as concern alternating field because one could expect eddy currents and then Helmholtz's (or parabolic) equation should be considered. But, taking into account low conductivities of all the media, the process is static from the mathematical point of view. The dynamics of the process, *i.e.* the variation im time, is represented by continuity of current, thus by interface conditions (3).

Eqn (1) is valid as long as the spherical model is concerned. For real cases the field equation should be written in threedimensional Cartesian coordinates and is as follows:

$$\nabla^2 \Phi = 0 \tag{4}$$

with the interface conditions (2) and (3).

To solve the above equation one can use one of the numerical approach and in the paper the boundary element method (BEM) is adopted. The method seems to be the most proper for the case as dimensions of particular domains are unproportional which makes the finite element method (FEM) useless. Then, eqn (4) is transformed by means of Green's identity into the boundary integral equation with Green's function which, in the case, is equal to

$$G = \frac{1}{4\pi r} \tag{5}$$

where r is the distance between source point and field point.

The boundary-integral equation is as follows:

$$\frac{\Omega}{4\pi}\Phi_i + \int_S \Phi \cdot \mathrm{grad}(\frac{1}{4\pi r})\frac{\partial r}{\partial n} dS = \int_S \frac{\partial \Phi}{\partial n} \cdot (\frac{1}{4\pi r}) dS \tag{6}$$

where Ω is the solid angle on the boundary at the point i, S is the surface of domain considered.

The problem belongs to the class of the so called open boundary and nonhomogeneous problems, so that the final matrix is rather complex but the method gives the solution which is well-picturing the field.

The results obtained from both analytical and numerical approaches are presented and discussed. Further investigations regarding eddy currents and the thermal effect of the cell is also discussed.

GEOMAGNETIC ACTIVITY-RELATED STUDIES IN CLINICAL COSMOBIOLOGY

E. Stoupel*, Toor Heart Institute, Beilinson Medical Center, Petah Tigva, Sackler Faculty of Medicine, Tel Aviv University, Tel Aviv, Israel

Studies conducted over the last twenty five years have confirmed a significant relationship between daily and/or monthly levels (I^{o} - IV^{o}) of geomagnetic activity (GMA) measured in nanotesla units and the natural history of clinical physiological and pathological events. The main findings based on our observations (1978-1993) may be summarized as follows:

1. Central nervous system and behavior:
a) migraine attacks - more intensive ath higher GMA ($r=0.96$, $p<0.002$ for 486 attacks reported in 1987);
b) epileptic seizures - higher incidence in females and a trend towards a higher number of admissions for all patients at GMA IV^{o} (stormy). (1991)
c) Dizziness - equal male/female ratio at GMA I^{o}; a strong trend towards higher male/female ratio (1.5) at GMA IV^{o} (1991).
d) Stroke-adversely related to GMA only in males aged 65 or less ($r=-0.97$, $p=0.027$. (1993)
e) Suicide - adversely related to GMA ($r=-0.222$, $p=0.03$, for 2,359 deaths. (1993)
f) First admission of psychiatric patients ($n=1829$) adverse relationship with monthly ($n=113$) GMA index ($r=-0.22$, $p<0.05$;). (1991)

2. Neuroendocrine system:
a) prolactin level higher at GMA III-IV^{o}.
b) growth hormone level - lower at GMA III-IV^{o}.
c) corticosteroid level 17-KS higher, 11-KS lower, at high GMA. (1983)

3. Intraocular pressure:
Low at GMA IV^{o}, especially in persons 65 years and older. (1993)

4. Cardiovascular parameters and coagulation system:
a) in-hospital cardiovascular mortality $r=-0.23$, $p<0.0001$ for 5667 patients - negative correlation with I^{o}-IV^{o} levels of GMA.
b) Nonmyocardial infarction-related-hospital cardiovascular mortality - $r=-0.23$, $p=0.01$ for 4094 patients. (1991)

c) arterial blood pressure/diastolic in healthy and hypertensive persons - higher at daily GMA III°-IV°. (1980)
d) sudden death-adversely related to GMA - more in quiet (I°) GMA ($p<0.01$). (1993)
e) frequency of ventricular extrasystoles ($p<0.01$) paroxysmal atrial fibrillation ($r=-0.976$ $p=0.02$ with I°-IV° level of GMA; 653 admissions; 1993) ventricular tachycardia rate adversely related to GMA.
f) Prothrothrombin index, platelet count and aggregation - high at highest GMA; clotting time - trend towards prolongation at higher GMA. (1980)
g) Monthly pregnancy-induced hypertension $-r=-0.4$, $p=0.01$ for 628 cases in 60 months. (1990)
f) localization of myocardial infarction (MI): Anterior/Inferior wall infarction ratio correlated with GMA ($r=0.94$, $p<0.01$ for 1657 cases) inferior wall more MI at GMA I° (quiet). (1988)

5. White blood cells:
a) leukocyte adhesiveness and aggregation in the peripheral blood lower at GMA IV ($p<0.001$). (1993)
b) basophil count in the peripheral blood adversely correlation with GMA ($r=0.54$, $p<0.01$). (1980)

6. In many studies obvious gender differences in the relationship to GMA:.

7. The natural history of many kinds of complex pathologies (MI - stroke) is offered by opposing multidirectional relationships with GMA: blood platelet aggregation and heart rhythm disturbances, platelet aggregation and bleeding time, platelet leucocyte adhesiveness and aggregation, etc. Together with the progress of medicine these factors neutralize the GMA relationship with ingredients involved in the pathogenesis of these diseases and their distribution in time.

8. It is possible that the increase in some biological medical events at low GMA does not entail a direct relationship, and thus may be other environmental mediatory factors affecting the studied organisms.

9. Most of the quantitative differences at all 4 GMA levels were in the range of 8 - 10%. Such changes can be crucial for people with borderline reserves. This population is growing with ever increasing life span in the community.

FREQUENCY DEPENDENT EFFECTS OF P E M F ON CIANOBACTERIA

N. Pekaric-Nadj*, Z. Obreht and V. Dosen,
Faculty of Technical Sciences, University of Novi Sad,
21000 Novi Sad, Vojvodina, Yugoslavia

The blue-green algae or cianobacteria raised great interest recently for their possible role as a natural fertilizer. The aim of this work was to look for the effects of the pulsating electromagnetic field (PEMF) on cianobacteria. The inoculum for this experiment was made of an immeasurably small amount of cianobacteria (Nostoc, strain 2C1B). The cianobacteria were taken from the sand layer, where they were kept dried for five years, and placed in 3000 ml of nutritive medium (standard solution BG-11 with nitrogen in a form of nitrites). Everything was mixed and homogenized on vortex. Eleven groups of 5 Erlenmeyer flasks were filled with 50 ml solution each. The first (control) group was sham exposed and the rest 10 groups were exposed to the PEMF with the different repetition rate.

The PEMF was generated by the microprocessor controlled generator and a suitable applicator which produced vertically oriented homogenous magnetic field. The generator emitted always the same single pulses (70 μs long square pulses with 1 mT peak value), but with the different repetition rate. Respective frequencies for 10 experimental groups were 8, 15, 24, 35, 45, 50, 55, 60, 65, and 75 pulses per second (pps). All groups were exposed to PEMF only once for 30 minutes, at the beginning of the experiment. Immediately after, all groups were placed in the zone with the controlled light intensity. They were grown in the same medium for the next 30 days, at the room temperature and in the local geomagnetic field. After that the analysis was performed double blindly. Following data were monitored:

1. Absolute biomass (after McKinney, 1941)
2. Relative number of single cells (deterioration of natural filaments)
3. Relative protein concentration (after Loway, 1951)
4. Relative ammonium concentration (after Solorzano, 1969).

Results of the analysis showed that the biomass of algae was significantly decreased by frequencies 55, 60 and 65 pps. For the same frequencies characteristic filaments, present in the control, were considerably disturbed. Single cells were observed in the visible field of the microscope, as may be seen from Figure 1. Analysis also showed that at these frequencies the significant increase in extra cellular protein and ammonium concentration was present, probably as a result of the cell destruction. On the other hand biomass was significantly increased on frequency 35 pps. As observed by microscope 35 pps strongly provoked the development of the other organisms - green algae in each of 5 flasks. From that fact we concluded that a little contamination with green algae must have been present in the initial inoculum, and that PEMF of 35 pps provided optimal conditions for their development.

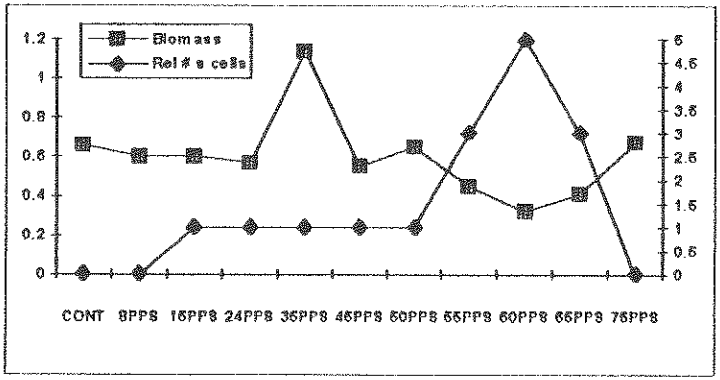

Figure 1. The influence of the different pulse rate on the biomass (μg chlorophyll per ml) and number of single cells in the visible field of microscope (Nostoc, strain 2C1B).

The same experiment was repeated with five additional strains of cianobacteria. Two of these strains were not growing in the control flasks and in the experimental flasks at some frequencies. It seems that stimulation with the PEMF of some frequencies (particularly 8 and 75 pps) helped these strains of dried algae to recover. The results for the remaining three strains were similar to those showed on Figure 1. For each strain we found destructive effects of PEMF around 60 pps. Judged by bare eyes beneficial effects of the frequencies 8 and 75 pps were always present.

LIGHTNING ENERGY ABSORPTION IN HUMANS AND PERSONNEL SAFETY UNDER LIGHTNING CONDITIONS

J.C. Chai, H.A. Heritage*, and H. Z. Wilson
The Aerospace Corporation, P.O. Box 92957, Los Angeles, CA 90009, USA
Telephone (310) 336-8341; FAX (310) 336-5581

Summary

It has been widely accepted that most human deaths associated with electricity are due to electric current pulses through the heart, causing a heart condition known as ventricular fibrillation. There has been an abundance of measurements performed in laboratories to determine this threshold level The majority of these measurements were, however, limited to pulse widths from milliseconds to a few seconds. The responses in humans to electromagnetic excitations, on the other hand, were found to be of much shorter durations. An example of this is the human interaction with electromagnetic pulses (EMP)which depends on human body impedance and soil conductivity over a wide frequency range; another example is the lightning-induced current in humans which also depends upon the location of lightning current injection.These analytical evidences make it difficult to infer a safety zone for humans under lightning conditions based upon existing measurements/data alone.

With the completion of an overhead catenary wire array lightning protection system at Launch Complex 40/41 of Cape Canaveral Air Force Station in Florida, USA, the condition of safety for the personnel remaining on the launch complex during lightning storms becomes an issue of utmost importance. A safety procedure defining safety zones for personnel working in the new configuration is therefore needed. To address this need, this paper surveys data in the open literature, and expresses the thresholds, above which discomfort, injury or ventricular fibrillation for humans occurs, in terms of energies, instead of *safe* step (or touch) voltages. Furthermore, utilizing the author's previous analytical results for human responses to lightning currents over various distances, this paper calculates the lightning energies induced in the chest region of a human body. This stress energy is calculated for a range of human resistances, and is presented in a series of plots as a function of soil conductivities, human body response currents or distances to the lightning injection point on the ground (see Figures 1 and 2). The comparison of the stress energy to the nominal thresholds energy of 10-joule for human injury or even death, shows that step voltages are not the main cause for human injuries/deaths under lightning conditions. This paper then proceeds to examine streamering effects due to the induced E-field on humans situated within the overhead catenary

wire array. It is found that under a specific scenario, the induced E-field on humans can be of sufficient amplitudes and duration to sustain the propagation of streamers, and pose a major safety hazard. This study concludes by proposing *analytical* safety zones for humans which take into consideration the physical launch site configuration and essential parameters of the lightning interaction.

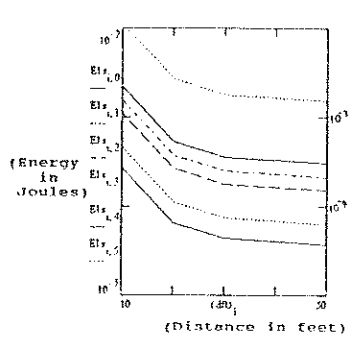

Figure 1. Lightning energies (E1s) induced in human chest region for various human resistances as a function of distance (dft) to the injection current. The ground resistivity in this case is 100 ohms-meter.

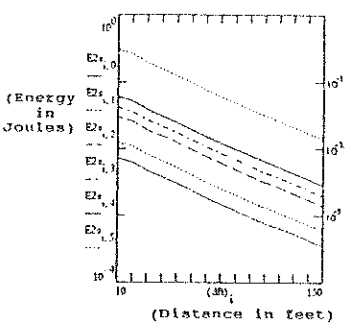

Figure 2. Lightning energies (E2s) induced in human chest region for various human resistances as a function of distance (dft) to the injection current. The ground resistivity in this case is 1500 ohms-meter.

ROTATIONAL ELECTROMAGNETIC FIELD AROUND TRANSMISSION LINES

N. Pekaric-Nadj*, M. Prsa, V. Kojic and V. Dragic
Faculty of Technical Sciences, University of Novi Sad
21000 Novi Sad, Vojvodina, Yugoslavia

Many studies now under progress, try to find the possible relation between 50/60 Hz electromagnetic fields in residences and the different kinds of cancer. Attention is paid to the magnetic fields which depend mainly on currents and wire configuration. The field intensities in residences are usually characterized in several categories such as "high", "very high", "low", "very low", depending mainly on the field intensity. In our opinion for the residences placed directly under the three phase transmission lines, the field intensity is not the main factor, but presence of the rotating field may play an essential role.

One can easily meet rotating fields in the vicinity of the three phase transmission lines. If the respective currents of the lines are
$I1(t) = Im \cos \omega t$,
$I2(t) = Im \cos (\omega t - 2\pi/3)$ and
$I3(t) = Im \cos (\omega t - 4\pi/3)$,
as a consequence magnetic field in the vicinity of the lines has two (or in general three) orthogonal components which differ in intensity and phase. Resulting vector rotates in space with frequency f=50/60 Hz and the field is ellipticaly polarized. Although the field intensity of 1-10 μT may seem little, its effects are significant (M. Kato et al., Bioelectromag., V.14, No.2, 97-107, 1993.). There are at least two hypotheses for great effectiveness of such field . As it is formed from the two orthogonal components, the possibility for the AC/DC resonance in geomagnetic field is increased (Liboff et al., M. Blank's ed. El. & Mag. in Biol. & Med., 623-628, 1993.). The other hypothesis arises from the non uniformity of the cell membrane. The rotating field may find its way easier to enter the cell (J. Zawilska , J. Nowak, Neurosci. Lett. 118,17-20, 1990.).

In order to evaluate which area under the lines may be affected

by the rotational field generated by the transmission lines we made a simple numerical model. For 110 kV lines, with nominal currents 200 amps, for the lines 10 m above the ground and conductors separated 6 meters from each other, the zone affected by the rotational field is approximately cylinder with the radius of 10 m measured from the central conductor. In the case of 400 kV and 1000 amps nominal current the zone with the rotational field is twice wider. Some numerical results for major and minor axis of the coresponding ellipses are illustrated in Figure 1.

On the other hand standard magnetic field meters with three axes probes are not able to detect if the field is rotational or not, because in the case of the rotational field standard meter detects only the intensity which corresponds to the major axis of the ellipse. For this reason we designed a microprocessor based meter of our own which is able to detect the presence of the rotational field.

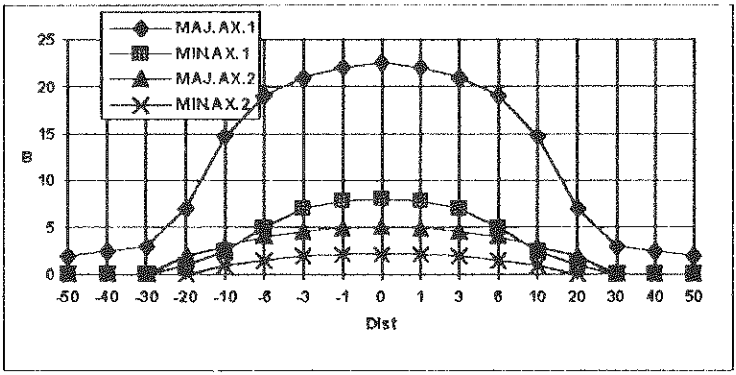

Figure 1. Magnetic flux density B(μT) as a function of the distance (in meters) from the central conductor. MAJ.AX.1 and MIN.AX.1 represent major and minor axes of the ellipse which corresponds to 1000 amps three phase transmission line. MAJ.AX.2 and MIN.AX.2 equally represent major and minor axis of the ellipse which corresponds to 200 amps transmission line. Conductors are in the same plane, separated 6 m , 10 m above the ground.

When the new corridors for transmission lines are planed we suggest that at least the zones with the rotational fields are left free of residences.

KMP ELECTRONICS

SPÉCIALISTE DES ÉQUIPEMENTS D'ÉMISSION DE PUISSANCE ET RÉCEPTION POUR LA COMPATIBILITÉ ÉLECTROMAGNÉTIQUE ET LES TESTS DE SUSCEPTIBILITÉ

Amplificateurs de puissance MOS-FET

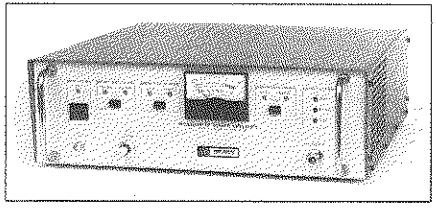

Large bande :
10 KHz à 1 GHz
Forte puissance :
1 Kwatt et plus
selon la bande - Interface IEEE, contrôle à distance
Selon norme IEC Pub 801-3 et 6.

Antennes d'émission/ réception

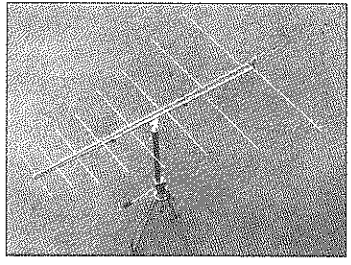

Log-périodiques,
log-spirales, biconiques,
dipoles, boucles, cornets.

Instrumentations IEM/IRF/TEMPEST

Récepteurs de détection
Tempest - Applications
toutes normes.

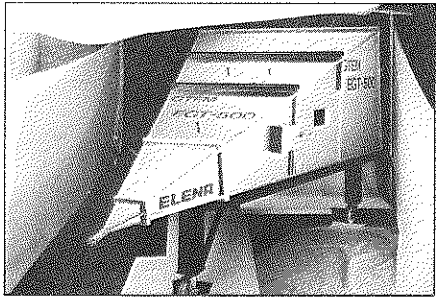

Cellules TEM et GTEM

8 modèles TEM,
DC à 1 GHz
300 watts
de puissance
admissible,
3 modèles GTEM,
DC à 2 GHz
100 à 1000 watts
de puissance admissible - 16 Kvolts pulse.

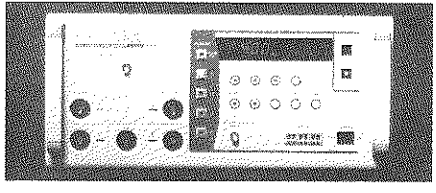

Générateurs de décharges électrostatiques

0,2 à 30 Kvolts,
temps de montée
0,7 à 1 nsec.

Générateurs de bursts rapides

250 à 4500 volts, cycle 2,5 - 5 et 10 KHz.

Simulateurs de perturbations IEM

Selon norme IEC Pub 801-5.

BP 64 - 9, allée Beausoleil - 92145 Clamart Cedex - Tél. : (1) 46 45 09 45 - Fax : (1) 46 45 24 03

TRANSIENT SCATTERING OF EM-PULSES BY SIMPLE AND COMPLEX TARGETS IN THE COMBINED TIME-FREQUENCY DOMAIN USING IMPULSE RADAR

H. C. Strifors,*[1] S. Abrahamson,[2] B. Brusmark,[2] and G. C. Gaunaurd[3]

[1]National Defense Research Establishment (FOA 2), S-172 90 Sundbyberg, Sweden
[2]National Defense Research Establishment (FOA 3), P.O. Box 1165
S-581 11 Linköping, Sweden
[3]Naval Surface Warfare Center, Research Department, White Oak (Code R-34)
Silver Spring, MD 20903-5000, USA

ABSTRACT

In the experimental part of the present work we study the transient scattering of short ultra-wideband (UWB) electromagnetic pulses by targets of simple and complex shape using an impulse radar. The impulse radar system, designed by ERA Technology, UK, transmits pulses of length 1 ns with a repetition frequency of 250 GHz and peak power of 50 W. The frequency content of the transmitted pulses covers the band of 0.2-2 GHz with the (dipole) antennas used, which is then further restricted by the analog bandwidth of 1 GHz of the digitizing signal analyzer. To suppress noise, the time-series considered are each composed of 64 ensemble averaged sampled waveforms. Antenna coupling and clutter returns are eliminated by first measuring the background without any target present and then subtracting it from each of the following time-series with a target present. The measurements are performed in an anechoic chamber at the National Defense Research Establishment (FOA 3).

The complex-shaped targets are plastic scale-models of aircraft with artificially metallized surfaces. The aircraft are chosen to be a B-52 bomber and a C-130 transport. For comparison, we also use simple-shaped targets such as a metal sphere and a dielectric, air-filled spherical shell. We display the various signature representations for these targets, both theoretically predicted, and as observed from measured data. The actual shape of the interrogating, incident pulse is theoretically modeled using a digital filter design technique together with pulse returns from a reference target (a metal sphere). The theoretically predicted radar cross sections (RCSs) of the simple targets are then compared with recorded and digitally processed data to demonstrate the accuracy of the experimentally obtained data.

We then extend the signature representations of these targets to the combined time-frequency domain. While the standard Fourier analysis allows the decomposition of a signal into individual frequency components and the establishment of the relative intensity of each component, it does not describe *when* those frequencies occurred. As we have demonstrated earlier, representations of the signature of an object in the combined time-frequency domain could add information needed or desired for target identification purposes. A useful such representation, which is also conveniently computed using a fast Fourier transform (FFT) technique, is the Wigner distribution (WD). To control the occurrence of "cross terms" a time-window is introduced, in this case a Gaussian window. The resulting pseudo-Wigner distribution (PWD) is shown to be capable of extracting informative signature features, about the targets within the frequency band of the incident pulses, in agreement with the general time-development of the resonance features present in that fre-

quency band. The investigation is extended to targets of complex shape, i.e., the scale models of a B-52 and a C-130. The monostatic RCSs of the complex-shaped targets are measured when the targets are illuminated at a few different aspect angles. It becomes clear that the analysis of backscattered pulses in the combined time-frequency domain by means of the PWD with an appropriate width of the time-window will improve the target identification capability furnished by the ordinary RCS of the considered scatterers. All PWD results will be presented in informative two and three-dimensional plots.

The theoretical determination of RCSs of scatterers of simple shape is a well-studied problem area. Traditionally, the analytical treatment has used material compositions of the scatterers with only small amounts of absorption of incident signal power, if any at all. By coating a given target with a thin layer with suitable electromagnetic properties the RCS can be reduced to a smaller or larger extent, and it is of interest to investigate not only the radar cross-section reduction (RCSR), but also its effect on the transient scattering of pulses of short duration. Therefore, we study the transient (monostatic) scattering of short UWB electromagnetic pulses when the target is a metal sphere with a coating made of a hypothetical material that substantially reduce the RCS of the metal sphere. The shape of the incident pulses is selected to be the one that nicely model the performance of the actual impulse radar system. We compute the signature in the combined time-frequency domain using the PWD, and we compare the results with those above for an uncoated metal sphere.

TRANSFORMS AND SYMMETRIES IN TARGET IDENTIFICATION

Carl E. Baum
Phillips Laboratory/WSR
3550 Aberdeen Ave SE
Kirtland AFB NM 87117-5776

This paper considers the use of window and wavelet transforms for the analysis of transient/broad-band electromagnetic scattering data. By appropriate choice of window position and width target substructures can be isolated under favorable conditions. The resulting target features and their associated scattering signatures can be used in target identification, both from the properties of the individual signatures and their relative time of arrival at the observer for a scattering-center analysis.

By a target feature let us mean some geometrical shape including constitutive parameters of some substructure or piece of the target. A special case of this is the target as a whole. Associated with particular features there are target signatures by which we mean temporal waveforms, or more generally properties of the scattering dyadic, including polarization. Various symmetries of the features (and target as a whole) produce symmetries in the signatures which help parameterize (decompose) the signatures and help in target identification.

Particle physicists have often referred to the elementary-particle zoo to describe the menagerie of such "beasts". Furthermore, symmetry plays an important role in elementary-particle theory. By analogy we can speak of a target-feature zoo or target-feature/signature zoo. As discussed in this paper symmetry also plays an important role in this zoo. In a manner similar to which elementary particles are grouped by quantum symmetries, let us group our feature/signature pairs according to the symmetries involved. So let us divide our target features zoo into N_h habits. Some of the habitats and their significances for target features and signatures are:

habitat	consequences
time translation (t) and linearity	s plane representations and filters
dilation (t_1)	exhibition of dilation symmetric substructures
window location (t_o)	substructure viewed as though on infinite structure (space translation)

reciprocity	symmetric $\ddot{A}$ in backscatter, principal axes for polarization
rotation/reflection (point symmetry groups)	symmetries in $\ddot{A}$, polarization

Specific features can involve more than one symmetry habitat (intersection of habitats).

An important concept is the idea of partial symmetries associated with target substructures. This leads to a set of convenient decompositions of the target-feature signatures which aid in identification of a particular target in its various aspects (orientations) with respect to the observer. These are exhibited by the t_o parameters of the triwave kernel, both in the form of the window Laplace/Fourier transform and wavelet transform. This windowing isolates one region of time, and under favorable conditions a corresponding region of space on the target for consideration. This windowing is multiplication in time domain, and can be compared to a filter which multiplies in frequency domain (and is equivalently a convolution in time domain). One can combine the two. For example, one can isolate a substructure resonance which can also be modified by a pulse with zeros at the natural frequencies (either before or after windowing) and thereby both identify the resonance and narrow the pulse for scattering-center analysis. Dispersion curves, such as for waveguides have also been observed in the phase-space diagrams coming out of these transforms. If one has some information concerning these characteristics, then in principle filters can be formed to modify this behavior in a manner analogous to poles in the complex frequency plane, again helping with the identification.

Suppose that one has characterized some set of targets by the various entities in the target-feature zoo. Note that various of the corresponding signatures factor with certain of the factors being aspect independent (at least over some range of angles of incidence in backscattering). Then one can try to fit such signature functions to the target scattering and thereby identify the target. Of course, in a realistic radar application there is significant noise which complicates the problem. Various techniques such as filtering, windowing, and averaging can be used to reduce the noise. Finally, probability techniques can be used to help bring the information out of the remaining noise.

T-PULSES AND WAVELETS

T. K. Sarkar*
H. Wang
Department of Electrical and Computer Engineering
Syracuse University
Syracuse, New York 13244-1240 USA
Phone: 315-443-3775
Fax: 315-443-2583
E-mail: TKSARKAR@RODAN.SYR.EDU

M. Wicks
Rome Laboratory
Griffiss Air Force Base
New York 13441 USA

M. Salazar-Palma
Dept. Senales, Sistemas y Radio Communicaciones
Universida Politecnica de Madrid
Madrid 28034, Spain

Abstract: One attractive feature of wavelets, is that as a basis function, they have compact supports both in the original and in the transform domain for all practical purposes. However, it is extremely difficult to make such constructs from a strictly theoretical viewpoint as a function cannot simultaneously be strictly limited both in the original and in the transform domain. However, from a practical point of view, one can produce a time limited waveform whose spectral energy (say 99%) is concentrated in a particular band. Moreover, wavelets have no 'dc' components. Hence a numerical waveshaping procedure needs to be designed so as to generate waveforms with no d.c. components and they be time limited with 99% of their energy concentrated in a particular band.

From a users point of view, additional constraints are necessary. For example, in radar applications, it is desirable to have waveforms which has no intersymbol interference - i.e. the waveform is orthogonal to its shifted versions. This will guarantee that the neighboring cells do not influence the results and hence would guarantee pulse to pulse orthogonality. A numerical optimization technique has been designed to generate waveshapes with such properties. Such waveshapes has been termed "T-pulses" - or time limited pulses which are practically band limited. A detailed mathematical description of this construct is available in [IEEE Transactions on Acoustic, Speech and Signal Processing, April 1988, pp. 608].

One of the objective of this paper is to demonstrate the equivalence between T-

pulses and wavelets. The goal is to use T-pulses for obtaining acquiring broadband target characteristic. This can be achieved by either illuminating the target by an impulse and obtain the impulse response of the target. An alternate approach would be to take a narrow frequency band and sweep it across the target spectrum using conventional antennas and receivers. The T-pulse provides the methodology to provide wideband information in the frequency domain. Hence, narrow band target signatures which are "finger prints" of the target can be easily identified utilizing the T-pulse technique.

Examples will be presented to illustrate how T-pulses can be used for efficient radar target identification applications.

Wave-Oriented Data Processing: Linking Data with Phenomenology

L.B. Felsen and L. Carin
Department of Electrical Engineering
Polytechnic University
Six MetroTech Center
Brooklyn, NY 11201

Abstract

Generating prediction, classification and identification algorithms for increasingly complex propagation and scattering scenarios is one of the major challenges for the modeling community. Extracting desired information from a measured or numerically computed signal at the observer requires a choice of basis (parametrization) for data processing. Although the received signal is established by wave interaction with the ambient environment, the effect on the signal due to this interaction is usually not taken into account explicitly by conventional processing. To link scattering phenomenology with data, we have been exploring the ultra-wideband (UWB)/short pulse (SP) regime in order to establish the most comprehensive data base. This has led to new parametrizations of configuration induced dispersion directly in the time domain (TD). The wave-oriented data processing is implemented by accessing appropriate subdomains of the eight-dimensional (space time)-(wavenumber-frequency) phase space. Wave phenomenology in the phase space is sorted out by subjecting the data to windowed Fourier (FT) or Radon transforms which yield the local spectral amplitudes, wavenumbers and frequencies in space-time. By forward or backpropagation, depending on the scenario, these local spectra connect the observer with the scatterer. After the wave physics has been identified via the windowed FT, other algorithms that have better resolution or multiresolution, like wavelets, can be applied to highlight essential features. To learn the rules of this game, we have begun to look at simple scattering scenarios driven by truncated strict, smoothly perturbed, and randomly perturbed periodicity, which leave Bragg-modulated footprints in the phase space and identify the FD and TD dispersion, as well as truncation effects. Other scenarios involve targets in clutter, and SP induced leaky modes

The analytical approach is based on rigorous formulations, from which asymptotics extracts the wave objects that establish phenomenology. We have referred to this as observable-based parametrization (OBP). The quality of the asymptotic OBP's, in the FD and TD, is assessed through comparison with numerical reference data generated by Method of Moments and Finite Difference Time Domain algorithms. To close the phenomenological loop between the data and scattering environment, the OBP footprints in the phase space are extracted from the numerical reference data by the techniques described in the first paragraph. The analytic procedures will be briefly reviewed, followed by application to various canonical and non-canonical model configurations. The results furnish entries in an OBP-phase space dictionary, with which signatures from unknown targets can be compared for classification and identification.

A UNIFORM DIELECTRIC LENS FOR LAUNCHING A SPHERICAL WAVE INTO A PARABOLOIDAL REFLECTOR

Carl E. Baum
and
Joseph J. Sadler
Phillips Laboratory
and
Alexander P. Stone*
University of New Mexico

ABSTRACT

In this paper we consider dielectric-lens designs for the specific case of launching an approximate spherical TEM wave onto an impulse radiating antenna (IRA). The desire for faster and faster pulse rise times means that one needs to establish the TEM-mode field distributions over the cross-section of the feed. In this case one would require that such pulses be treated as waves, and in general wants to match these waves from one region to another with a minimum of distortion and reflection.

The lenses considered here are treated from an "equal-time" point of view. This is a transit-time condition on ray paths and is imposed to ensure the correct spherical wavefront. Thus some reflections are introduced at boundaries. However these reflections can be small in certain cases, and the wave passing into the second medium can be a good approximation to a dispersionless TEM wave.

Illustrations and numerical tables are presented from which examples of these lenses may be constructed.

Impulse Radiating Antennas

Everett G. Farr*
Farr Research

Carl E. Baum
Phillips Laboratory

Considerable progress has recently been made in the study of methods for radiating impulse-like waveforms. We summarize in this paper the various antennas one can use to radiate a fast impulse, and the techniques available to analyze them.

A reflector IRA consists of a paraboloidal reflector fed by a TEM feed, which attaches to the reflector through an impedance (Figure 1). The impedance is chosen so that at low frequencies the antenna forms a $\vec{p} \times \vec{m}$ dipole with a cardioid antenna pattern. Thus, even at low frequencies the antenna has some directional properties. At higher frequencies, the antenna performs like a classical plane-wave aperture.

The lens IRA consists of a TEM feed with a lens in the aperture (Figure 2). The lens creates a planar phase front, so the high-frequency performance is similar to that of a reflector IRA. However, the low-frequency behavior is similar to that of a short electric dipole, so there is no directionality in the pattern at low frequencies. Furthermore, if the aperture is large, the dielectric lens weighs a great deal. On the other hand, a lens IRA does not have feed blockage. Thus, a lens IRA may be appropriate in cases where the aperture is small and where low-frequency directionality is not important. Note that if the TEM feed is long enough, a lens may not be necessary, depending upon the bandwidth required. In this case, the resulting antenna is a simple TEM horn.

In this paper we provide simple models for the radiated far field on boresight for both lens and reflector IRAs. Such models provide a simple way of comparing performance between the various designs. In the case of the reflector IRA, the step response consists of a prepulse, followed by an impulse with the opposite sign. The impulse is calculated by aperture integration, and the prepulse is calculated by a stereographic projection of the conical transmission line. It is interesting that the area of the impulse is equal and opposite in sign to that of the prepulse. Since the area of a radiated waveform must be zero, this is a necessary (but not sufficient) condition for being a good first approximation to the actual radiated field.

When designing reflector IRAs, one must choose a feed impedance. In doing so, one must trade off low feed impedance, which provides the best gain, against aperture blockage. We provide a method for trading off these factors, and we calculate the optimal feed impedance for a variety of feed configurations. In order to carry this out, a reasonable definition of transient gain is required. We develop a definition of

transient gain that has the important characteristic that it is as useful in transmission as it is in reception (i.e., satisfies reciprocity). Such a definition allows us to develop a meaningful radar equation in the time domain.

Many of the aperture fields that appear in this type of antenna satisfy a new symmetry, which we call self-reciprocal symmetry. In those cases where this is true, one can provide very simple expressions for the early-time radiated field on boresight.

Finally, we provide a method of analyzing the radiated field from IRAs off-boresight. This technique allows one to calculate an antenna pattern for these antennas. An interesting result of these calculations is that for a reflector IRA the pattern is considerably narrower in the E-plane than in the H-plane.

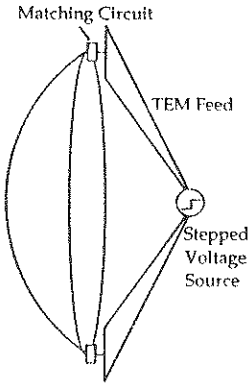

Figure 1. A reflector Impulse Radiating Antenna (IRA).

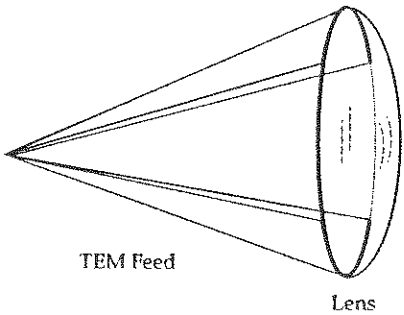

Figure 2. A lens IRA.

K-Space Imaging Algorithms applied to UWB SAR

S. R. Cloude, P. D. Smith, A. Milne
Applied Electromagnetics Ltd,
St. Andrews, KY16 9LU, Scotland
Tel/fax : 334 77598

P. Bellamy, C. Thornhill
DRA
St. Andrews Rd.
Gt. Malvern
Worcs, WR14 3PS
Tel : 684 892733

Abstract

There has recently been a great deal of interest in developing methods for adapting Ultra Wide Band (UWB) Radar systems for 2-dimensional image construction. These radars aim to exploit the inherently high range resolution yet low centre frequency of UWB radar to achieve high quality range and cross-range imaging of buried and hidden structures. However, due to their inherently wide bandwidth, conventional Synthetic Aperture methods based on the concept of Doppler matched filters and target phase histories are not applicable. For this reason most effort has been centred on using direct time domain construction methods based on diffraction migration techniques.

However, by formulating the imaging process in k-ω space significant improvements in image quality can be achieved over the direct time domain methods. In these methods we essentially maintain information about the magnitude and direction of the k vector for a wide range of $|k|$ values to effect an image reconstruction based on Fourier processing. In this paper we outline such an approach and illustrate its application to UWB radar imaging by using numerical predictions from a time domain finite difference code.

We discuss factors limiting resolution such as aperture sampling requirements, antenna pattern effects and variability of UWB target scattering. We also show how 3-dimensional imaging is possible by utilising appropriate projections in k space.

HIGH POWER ELECTROMAGNETICS AND CHIRP PULSE COMPRESSION IN TRANSMIT AND RECEIVE MODES

Albert W. Biggs
Electrical and Computer Engineering Dept., EB 262-B
The University of Alabama at Huntsville
Huntsville, AL 35899, USA
(Phone: 1-205-895-6459, Fax: 1-205-895-6803)

"Chirp" was first used by B. Oliver in an internal Bell Lab memo, "Not with a Bang, but with a Chirp," in 1951. It describes how radar detection ranges are increased without loss of resolution or increase of peak power. Transmitted radar pulses, with long periods T and low peak power (Chirp), have Frequency Modulated (FM) carriers that sweep frequencies across bandwidth B during each period. The pulses are backscattered from clouds, meteors, or buried ancient structures to radar receivers and compressed with matched filters into (sin X)/X shapes as narrow pulses with high peak powers (Bang). Pulse compression ratios are ratios of original pulse period T to collapsed pulse width (1/B), or BT. Typical BT ratios vary from values of 10 to 100,000. The product BT is the increase in peak power due to pulse compression. With BT equal to 20, 100 watts before compression increases to 2 kilowatts after compression. Chirped pulse compression is achieved in transmit modes with wide band antennas, such as log periodic dipole arrays (LPDA), where the matched filters are the antennas.

Computer generated curves of amplitude and phase spectra are presented for variable Chirp signal pulse width, reduced periods after compression, and frequency intervals during a period of the original pulse. Pulse compression ratios BT from 20 to 120, in increments of 20, are seen with one microsecond pulse periods T, and frequency bandwidths B of 20 to 120 megahertz in 20 megahertz increments. The compressed pulse period decreases from 50 nanoseconds (BT = 20) to 8 nanoseconds (BT = 120). Differences in these and previously published curves were found because use of more accurate computer

generated Fresnel Integral values. The effect of Doppler frequencies on Chirped pulse waveforms is seen with +10 to -10 megahertz Doppler frequencies in 2 megahertz increments. This family of Doppler shifted outputs of the matched filter are like the ambiguity function for the linear FM signal.

Linear FM signals and pulsed waveforms are substantially distorted by LPDAs because of frequency dispersion in phase-frequency and amplitude-frequency spectra. Frequency bandwidths B of these antennas are limited by the bandwidth ratio P, given by f_2 / f_1 (upper frequency/lower frequency), to 2.5 due to deterioration of input characteristics at low frequencies to antenna pattern distortion at high frequencies (L.Y. Astanin and G. A. Burrel, *Zarubezhnaya Radioelecktronika 9*, 3-27, 1981). If LPDA antennas are modeled as filters, possessing both amplitude versus frequency and phase versus frequency responses, then their phase conjugate functions can be shown to produce pulse compression distorted by frequency dispersion. The technique for chirping is an application of matched filter design found in radar systems (M. I. Skolnik, *Introduction to Radar Systems*, McGraw Hill, pp. 369-375, 1980).

The pulse distortion and FM frequency errors in LPDAs can be greatly reduced by three different techniques. The phase-frequency response of the LPDA can be corrected by changing the logarithm's periodicity to arithmetic periodicity, by altering only the equation of the change of coordinates and lengths of the dipoles. The disadvantage of this technique is that the "arithmetic" periodic dipole array (APDA) has a small deterioration in B in comparison with the LPDA. In this paper, a modulation technique is described which compresses ultra wideband (UWB) signals on conventional LPDAs.

Although the modulation technique applies only to linear FM signals, the same methodology can greatly reduce pulse distortion when the pulse waveform is known.

WIDEBAND NOISE RADARS for X- and K_a-WAVEBANDS

K.A. LUKIN

Institute of Radiophysics and Electronics
Ukrainian Academy of Sciences
12 Acad. Proskura St., Kharkov, 31Ø085, UKRAINE.
Tel.(ØØ7-Ø57)-244-8349, Fax. (ØØ7-Ø57)-244-1105
E-mail: ire%ire.kharkov.ua@relay.ussr.eu.net

At some cases it is very difficult technically to provide the necessary characteristics for the radars, using the traditional pulsed signals. Moreover, it is well known that in comparing with pulsed signal radars the Noise Radars have a number of advantages. In particular, the continuous working regime and correlation processing provide the high sensitivity of the Noise Radar and as a consequence, the possibility of usage of very small output power for radiated signals, which could be provided by compact power supply equipment. These provide a small sizes, weights and environmentally save characteristics of the Noise Radars. Such kind of radars also will have good parameters from the EMC point of view: high reliability, frequency compatibility and noise-proof characteristics.

However, there are two principal difficulties, not allowing to create the Noise Radars:

- design of the controlled wide-band oscillators producing the noise signals of the chosen frequency band;
- design of the correlators for the correlation processing of the chaotic signals with large enough Fourier spectrum bandwidth and for long enough distances.

From other hand, the expected advantages and recent achievements in computing and GaAs-chips engineering force the investigators and give them new possibilities to construct the Noise Radars with desirable characteristics.

In this paper the preliminary results of the investigations of problem under consideration, carrying out in the Laboratory of Nonlinear Dynamics of Electronic Systems in the Institute of Radiophysics and Electronics of Ukrainian Academy of Sciences are presented. The laboratory models of Wide Band Noise Radars in X- and K_a-wave bands were designed, constructed and tested.

For producing the noise carrier signals the solid state oscillators of the two kinds were designed on the base of IMPATT-diodes and Gun-diodes, as well as for obtaining the high power noise signals the corresponding oscillator was constructed on the base of weak-resonant BWO (B.P.Efimov, K.A.Lukin, V.A.Rakitaynsky. Journal of Techn. Phys., 12,2388-2400,1988; Pisma v Journal of Techn.Phys.18,9-12,1989). Both kinds of noise oscillators were designed on the base of the modern principles of dynamical stochastization of the nonlinear systems. Chaotic regime was provided by special design of the microwave resonator, as well as by usage of the special operating regime. Solid state noise oscillators allows to produce continuous chaotic signals with output

power up to 100 mW and controlled frequency bandwidth from 30MHz to 300 MHz. Vacuum noise oscillators produce the wide tunable noise signals with bandwidth from 50MHz to 1000MHz and output power up to 15 W in continuous regime.

For correlation processing of the received noise signals the Digital-Analog Time Integrating Correlator was designed and constructed on the base of fast digital components with clock frequency 500MHz. This allows (at least theoretically) to process the signals with highest frequency up to 250MHz. To avoid the necessity of analog-digital converters usage the known principle of the noise signals clipping was used. The Digital Delay Lines (DDL) of two kinds were designed, namely: DDL on the base of shift registers - for short distances and DDL with usage of fast RAM memory - for the long ones. Real correlator designed allows to process the noise signals with bandwidth about 200MHz.

Another kind of Noise Radar, using so called double spectrum processing of the reflected signal was also designed, constructed and tested. This radar uses the measurements or computer analysis of the Fourier power spectrum of received and transmitted signals sum and the following measurements of the power spectrum of the video output signal of the first spectrum analyzer. This gives possibility to use a serial wide band spectrum analyzers (allowing to process the noise signals with a bandwidth around 2 GHz) instead of special correlators.

Experimental investigations of the Noise Radars designed showed that they provide the distance resolution value of 75cm with accuracy about 30cm and allow to measure the target velocity with accuracy about 10cm/s in the range from 0.3m/s to 10m/s. The regular operating of these radars was observed under effect of the external electromagnetic noise, providing the voltage level on the mixer-diode, exceeding the useful signal by 30 dB for integration time about 0.5 ms.

Possible application areas of the Wide Band Noise Radars:

- in Millimeter and Centimeter Wave Navigation Systems with high distance resolution and environmentally save characteristics;
- Millimeter and Centimeter Wave Meteorological Radars;
- Noise Reflectometer for measurement of the cut-off layer position in fusion plasma reactors (tokamak,torsatron);
- Millimeter wave All-Weather Observing Systems with high distance resolution and environmentally save characteristics (for aircrafts, trains and cars).

First real application of the Noise Radar designed now is supposed to realize in the system for measurements of the cut-off layer position in fusion plasma reactor - torsatron URAGAN-2M (Physical Engineering Institute, Kharkov, Ukraine)

PLANE WAVE COUPLING TO A SYSTEM MADE OF SHIELDED AND UNSHIELDED MULTICONDUCTOR CABLES INTERCONNECTED BY LINEAR NETWORKS.

K.Kerroum, F.Paladian, J.Fontaine
LASMEA
URA CNRS n°830
Université Blaise Pascal
63177 AUBIERE Cedex
FRANCE

A.Zeddam, O.Daguillon
France Télécom - CNET
2, route de Trégastel
BP 40
22301 LANNION CEDEX
FRANCE

Frequency analysis of interaction between an external electromatic field and an arbitrary system of multiconductor transmission lines (MTL) above an imperfect conducting ground is presented. The system is made of L uniform or nonuniform MTL with Ni (i=1...L) conductors: quasi-TEM propagation is assumed for each MTL and coupling between different MTL is neglected. For each linear multiport network connecting the MTL containing Nj (j=1...M) external nodes, we have used following matrix equation:

$$[P'].[V'] + [Q'].[I'] = [E'] \quad (j = 1 \ldots M)$$

This system representing boundary conditions is a combined representation of Thevenin's and Norton's schemes. We assum Nj equal to the total number of conductors of all MTL connected to the jth network.

Solutions are given by a supermatrix system combining the matrix equations of the L MTL and those of the M networks:

$$[\Lambda].[X] = [B]$$

with a total number of equations equal to:

$$K = C + D = 2\sum_{i=1}^{L} N_i + \sum_{j=1}^{M} N_j$$

with: C= D = K/2.

For cascaded system this system can be written under the form:

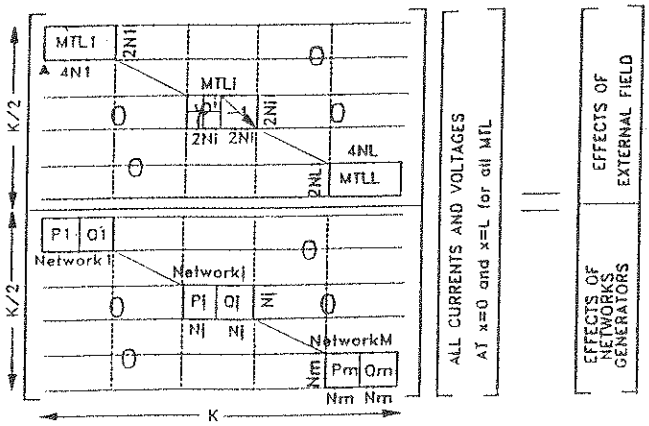

Supermatrix [A] contains two matrix bloks [A1] and [A2] each of dimension ((K/2)xK) corresponding to MTL equations and bounding conditions at networks respectively.
Supervector [X] contains unknown voltages and currents at conductors ends.
Supervector [B] contains K/2 components corresponding to generators located at networks and K/2 components relative to external perturbation.

Time domain voltages and currents can be obtained through the Fourier Transform. This formalism can be generalized to multiconductor shielded cables.

Consider for example the two following configurations with a shielded and a unshielded transmission bus. Time domain experimental results obtained under EMP simulator in CNET Lannion (France) are presented: current Ib on shield and common mode voltage VMC1 on conducteur (1) at x=0.
Configuration (1) is given by figure 1 and corresponding results are given figure 2 and 3.

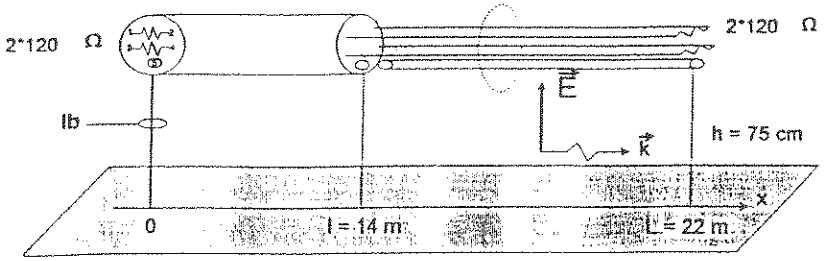

Figure 1

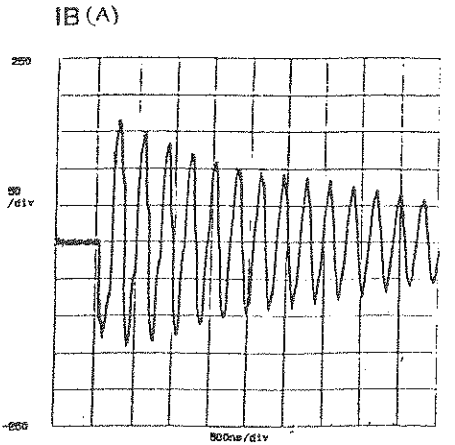

Figure 2

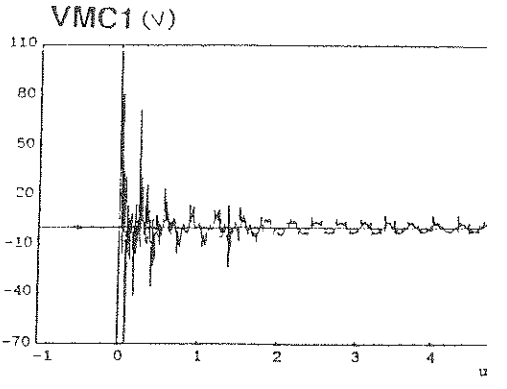

Figure 3

Configuration (2) is a Y shape form as given in figure 4 and corresponding results are presented figures 5 and 6.

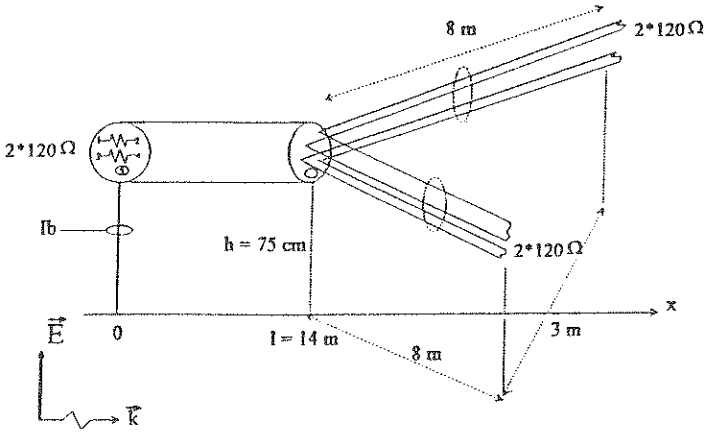

Figure 4

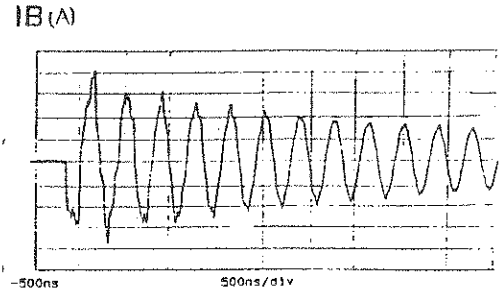

Figure 5

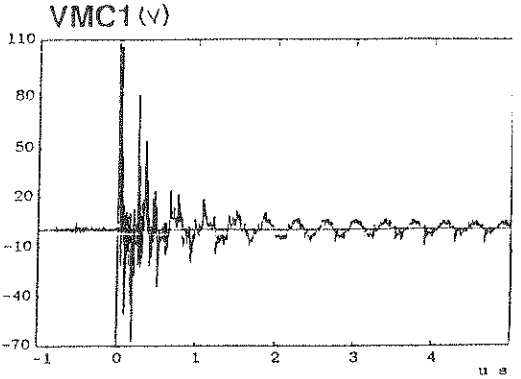

Figure 6

Numerical results will be present during the session.

EVALUATION OF THE SURFACE AND TRANSFER IMPEDANCE TENSORS FOR FULLY ANISOTROPIC MULTILAYER SLABS FOR PLANE WAVE ILLUMINATION

By

Paul M. McKenna* and Terence Rudolph

ELECTRO MAGNETIC APPLICATIONS, INC.
7655 West Mississippi Avenue, Suite 300
Lakewood, CO 80226 USA
Phone: 303-980-0070
Fax: 303-980-0836

With the expanding use of composite materials and special coatings for many systems, it is necessary to develop methods of analyzing the shielding and coupling properties of these materials, which may also have significant anisotropies. From a modeling standpoint, it is not possible to resolve individual layers of these materials when computing the coupling to a realistic system in three dimensions. One method for overcoming this limitations to appeal to the concepts of the surface and transfer impedances of these (multilayered) materials. A useful and analytically tractable case of interest is plane wave illumination of a plane slab, composed of multiple, possible anisotropic, layers. The solution of the electromagnetic fields for a single layer (isotropic or anisotropic) can be written as a boundary value problem:

$$\begin{bmatrix} hx(d) \\ -hy(d) \\ ex(d) \\ -ey(d) \end{bmatrix} = [M] \begin{bmatrix} hx(-d) \\ -hy(-d) \\ ex(-d) \\ -ey(-d) \end{bmatrix}$$

where M is the matrix exponential function for the single layer. To extend this to multiple layers, note that a matrix exponential function for each layer and require continuity for the fields at each interface, so that the appropriate multilayer (I layers) slab boundary value problem can be written as:

$$\begin{bmatrix} hx(d) \\ -hy(d) \\ ex(d) \\ -ey(d) \end{bmatrix} = [M1]*[M2]*\ldots*[MI] \begin{bmatrix} hx(-d) \\ -hy(-d) \\ ex(-d) \\ -ey(-d) \end{bmatrix}$$

where Mi (i=1, ...,I) represents the single layer matrix exponential function for the ith layer. This is simply the analog of the forward propagation matrix technique for isotropic layers applied to anisotropic layers. The matrix product of the single layer matrix exponentials is very complicated formally, but simple to compute if one iterates over layers and accumulates the successive product layer by layer. Once the iteration over all layers is complete, the accumulated product matrix can be treated in the same fashion as the single layer matrix exponential function and thus be used to derive the surface and transfer impedance tensors.

INDUCED HARMONIC CURRENTS IN RECEIVING STRUCTURE CONNECTED TO TIME VARYING LOAD

Bernard GUILLOU HYPERFIELD Engineering S.A
22 Avenue des Fauvettes 33700 MERIGNAC TEL:56.47.87.87 FAX:56.13.02.26

ABSTRACT

This work presents practical analytical and numerical considerations for engineers who want study on desk computers, harmonic currents effects induced in three dimensionnal (3D) one port linear receiving structures (typically antennas) connected to time varying loads . The antenna works in a receiving mode and is illuminated by an incident sinusoidal plane wave at frequency Fo. Due to time varying impedance changes in the connected load, currents at frequencies others than Fo can be induced in the load circuit and antenna structures. This allows to unwanted waves to re-radiate in the around space. (J. A LANDT, E. MILLER, IEEE AP-31 1,121-126,1983).
The paper described analytical and numerical schemes used to modelize the problem:

As a first step, the well known Norton equivalent circuit representation of the receiving structure is used to get, the short-circuit source current and radiating impedance in frequencial domain (T. K. LIU , F.M. TESCHE, IEEE AP-24 2,131-139,1976).
This step can be done with a own or commercial available softwares, which generally uses a numerical moment method for resolving an electric or magnetic field integro-differential boundary equation. These former softwares respectivelly allow frequential analysis for, apertures antennas on conducting body of revolution (L.N MEDGYESI, J.H MULLEN, IEEE AP,1976), or for 3D wires structures (A.R DJORDJEVIC & ALL, AWAS User's Manual, Artech House, 1990) on PC desk computers. This way offers great availability and inexpensive computation costs .

The second step of analysis is treated in the time domain, where the load current-versus-voltage law is written. In this paper, we consider essentialy time varying resistors as possible connected load . However , time varying capacitor has also been treated . Sinusoidal modulation law around the mean resistor value is choosed to test the numerical scheme, but others more general time domain characteristic law could be handled by the software.
The third step of the analysis is the numerical links between, frequential and time domain currents or voltage values. This step is achieved with the use of a Discret Fast Fourier Transform (DFT) . This way to realise time-to-frequency conversion is similar to the standard harmonic balance technique.(R. GILMORE ,IEEE MTT-34 12,1294-1307,1986). The used iteratively algorithm for general time domain resistor laws is described in the paper. In addition, for the the specific case of the sinusoïdal modulation , we present recurrence formulations for the discrete values of the resistor voltage spectrum.

The software which uses the three described steps has been written, and computations for a 3D fictitious antenna structure shown in figures 1 have been done to investigate the harmonic current effects. Figures 2 and 3 show the radiation impedance and the short-circuit current curves obtained in this case.
A parameter study has been realised for several values ot the relative modulation factor m when the time varying resistor law is given by Ro x (1+ (m/2) x sin(2 π Fm t)), where Ro is the mean value, m defined by m = (R(t) max - R(t) min) / Ro) and Fm the load modulation frequency . For Fo nearly 450 MHz, m = 2 , Fm= 50 MHz, Ro=500 ohms, figures 4(a), 4(b), 4(c), 4(d), 4(e) show respectively the data entries, convergence curve stopped at iteration 32 (relative distance error near 0.1 %), resistor voltage spectrum amplitude and real and imaginary time domain current components induced in the load resistor.

To conclude, this paper shows that computations of induced harmonic currents on 3D receiving structures connected to time varying loads are practically realisable on PC desk computers. With the obtained results , evaluation of re-radiation fields strengths at others frequencies than the incident wave frequency are easily achieved.

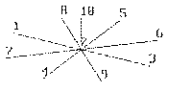

FIGURE No: 1a

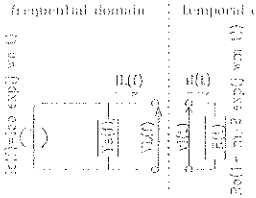

Norton equivalent circuit representation of the receiving structure with time varying load

FIGURE No: 1 b

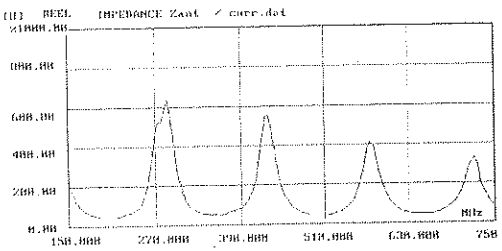

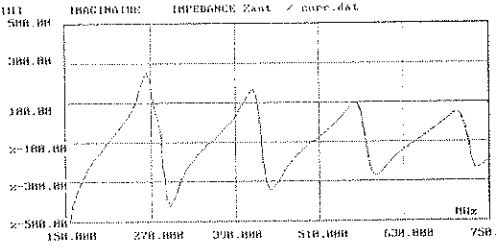

FIGURE No: 2

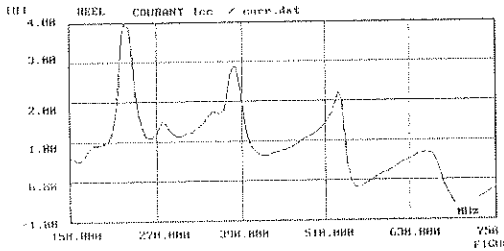

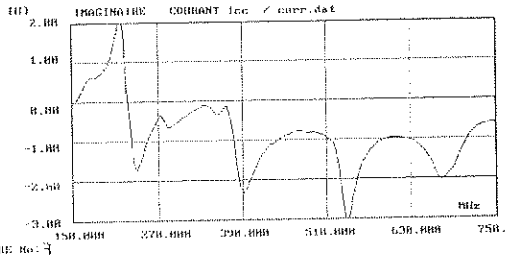

FIGURE No: 3

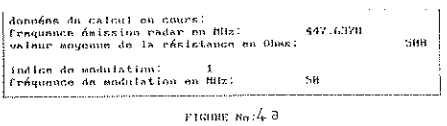

FIGURE No: 4 a

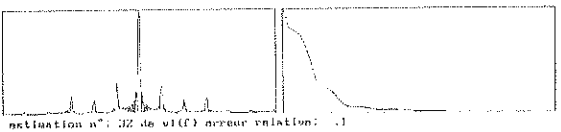

FIGURE No: 4 b

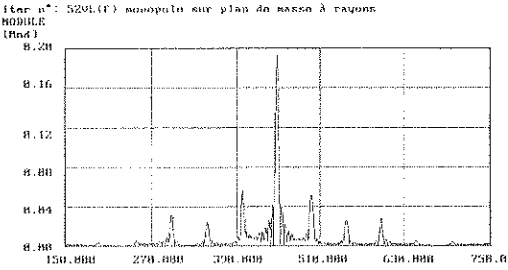

FIGURE No: 4 c

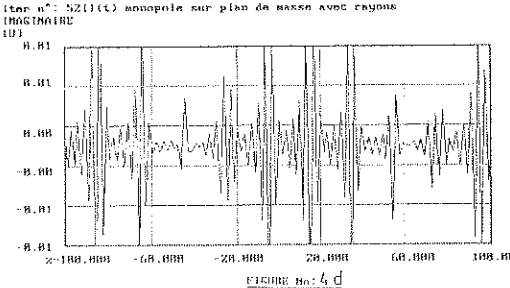

FIGURE No: 4 d

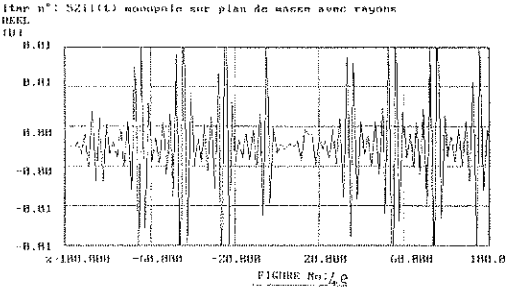

FIGURE No: 4 e

A VERY SHORT ELECTROMAGNETIC PULSE COUPLING WITH A VERTICAL WIRE PARAMETRIC STUDY EXPERIMENTAL AND THEORITICAL APPROACHES COMPARAISONS

M. Bourzeix* J.P. Percaille B. Pecqueux
Délégation Générale pour l'Armement
Direction des Recherches, Etudes et Techniques
Centre d'Etudes de Gramat 46500 GRAMAT , FRANCE

SUMMARY

The determination of the antennas response is a major point of interest in electromagnetic vulnerability of weapons systems studies.

Most of the antennas protection devices uses non linear components. So, the open circuit voltage : Voc , short circuit current: Isc and specifically dVoc/dt are studied.

Simulating different incidence angles is very uneasy on real scale. It's the reason why , here , reduced scale experiments are used and compared with theoretical approaches.

The response of a vertical wire representative of an antenna submitted to a fast electromagnetic pulse (Rise time = 100 ps)has been studied.

The antenna response equivalent generator has been determined.

Voc , Isc and specifically dVoc/dt have been studied for different incidence angles of the incident field and different wire heights (See figure 1).

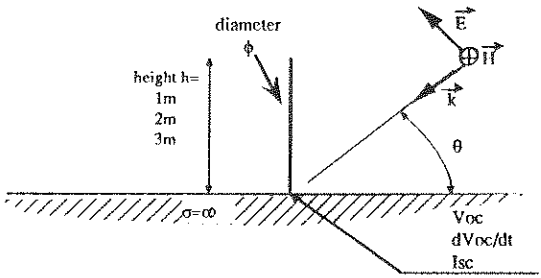

Figure 1 : generic sketch of the study

Two theoretical approaches have been used and compared with experimental results.

A conclusion about the validity of these technics is presented

COUPLING OF AN ELECTROMAGNETIC WAVE TO A METALLIC BOX THROUGH TWO TYPES OF APERTURE

R.Chotard*(1), R.Léveillé(1), V.Levillain(2), W.Tabbara(3), G.Afquié(4)

(1) PSA, Direction des Etudes et Techniques Automobiles, Division Carosserie, 18 rue des Fauvelles, 92250 La Garenne-Colombes, France.
(2) AEROSPATIALE Espace et Défense, Groupe Etudes et Dimensionnements de la Direction Technique, 66 rue de Verneuil-BP2,78133 Les Mureaux Cedex, France.
(3) Lab.Signaux et Systèmes et Université Paris VI, Supélec, Plateau de Moulon, 91192 Gif sur Yvette, France.
(4) Université. Paris VI, Lab. Electronique Analogique et Micro-ondes, 75252 Paris Cedex 05, France.

I. THE MODEL AND THE EXPERIMENTAL SETUP

We consider, the coupling of an electromagnetic wave to a metallic box through two types of aperture. In configuration 1 (C1), the lid, is heightened by 1 mm leaving a 1320 mm perimeter aperture. The rectangular aperture is closed. In configuration 2 (C2), the box is closed and the rectangular aperture of 180x5 mm^2 is opened in the front side. A vertically/horizontally polarised plane wave hits the box front face at normal incidence. We are interested in the amplitude of the electric field at a point in the middle of a side wall as shown on Figure 1.

The model is based on an integral representation of the electromagnetic field, and a surface finite element method is used to determine the electric and magnetic currents on the structure. The field is then computed at any point inside the box. The "Raviart and Thomas" finite elements are used here in order to solve the resulting integral equation.

In the experimental setup, the source is a horn antenna located one meter in front of the box which lays on a ground plane. The electric field is measured with a 12 mm high whip antenna attached to a connector. The measured values are normalised by those of the incident field at the front side.

II. RESULTS

We consider here two cases of strong coupling : a vertically polarised incident wave in C1, and a horizontally polarised one in C2. The results should be read having in mind that the model does not take into account the losses in the cavity walls. Hence, the calculated field levels at resonant frequencies will be greater than the measured ones. In both configurations the resonances belong to two groups : on one hand the cavity resonances, and on the other hand the slot resonances. Those in the first group are at 707 MHz and 866 MHz (Figure 2). In C1, the slot resonances are at 227 MHz, 454 MHz, 682 MHz, 909 MHz and they occur when the perimeter of the slot is equal to $n\lambda$. In C2, the aperture first resonance is at 833 MHz where its length is equal to 0.5λ. The results on Figure 3 show instead a value of 800 MHz, this is due to the width of the aperture equal to 5 mm. The computations emphasise the need to take into account, in C1 the thickness of the lid and the box border as well as the border width, and in C2 the thickness of the front side.

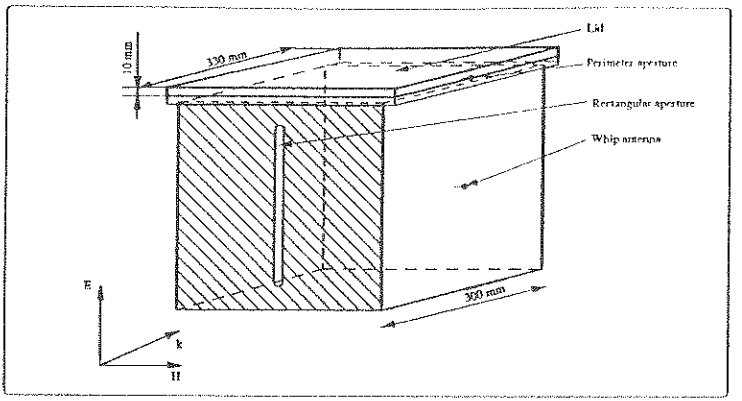

FIGURE 1

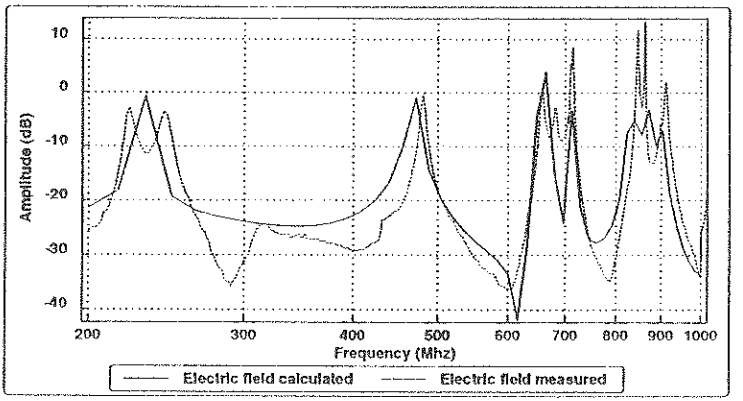

FIGURE 2

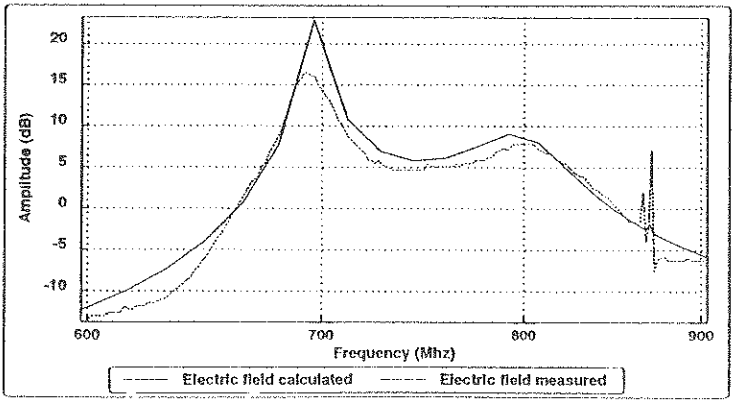

FIGURE 3

Electromagnetic Topology: accurate characterisations of topological networks Application to an EMPTAC aircraft experiment

J.P. Parmantier *, V. Gobin, F. Issac,
O.N.E.R.A.
29, avenue de la division Leclerc
92320 CHATILLON

I. Junqua, Y. Daudy, J.M. Lagarde
Centre d'Etudes de Gramat
46500 GRAMAT

The objective of the talk is to show the precision one may obtain in the topological characterisation of a canonical network and how to use it to constitute in advance a qualitative data bank on the wiring of a complex structure. By "canonical" network, we intend a network made of simple elementary multiconductor lines (one, two, three wire cables, shielded or unshielded), laying on a metallic plane, geometric configuration widely encountered in the specification tests for equipment. In this talk we'll mainly show how such a configuration may be used to constitute a consistent data bank for further in-situ experiment. We'll illustrate the interest of the method with the presentation of a pre-experiment performed in France to prepare another experiment on the EMPTAC aircraft (see paper entitled "Application of EM Topology on an experiment on the EMPTAC aircraft").

In EM Topology, multiconductor lines are characterised as tubes thanks to R, L, C parameter matrices. These parameters are generally measured with an "impedance bridge". The results obtained are consistent for low frequency and each measurement requires a specific load configuration between the different wires constituting the multiconductor line. But, to performed very accurate calculations on multiconductor line models it is necessary to take into account the frequency dependence of R, L, C parameters. We propose a method based on the measurement of S-parameters at one extremity of the line, using a network analyser.

One interest of the experimental procedure comes from the simplicity of the load configuration required and this suggests that it would be possible to develop an automatic device in the future. At the extremity where the measurements are performed, all wires are loaded on 50 Ω; at the other extremity, two configurations must be considered: a full short-circuit and a full open circuit. The so determined short-circuit and open circuit S-parameters are then numerically treated to derive the R, L, C parameters as a function of the frequency. Other parameters, very useful for the characterisation of multiconductor transmission lines, such as the characteristic impedance and the propagation matrices, or the eigen mode and propagation velocity vectors, are moreover derived at the same time. For complex multiconductor lines, this method is not efficient anymore for frequencies involving the resonance of the line, and the parameters must be extrapolated.

The improvement of such a characterisation is illustrated by the study we performed to prepare the experiment on the EMPTAC aircraft (see figure 1). The network, we had to manage with in this experiment was running inside the cockpit and inside a forward shielded volume (Network A).

To understand the topology of the wiring and to analyse the different types of coupling involved in the aircraft, we decided to study first the coupling on a simple new cable network (Network B). This network had to reproduce the topology of Network A, that is to say, the same types of connections, the same location inside the aircraft, and also the same types of common mode and differential coupling between wires). For this, Network B was made of two and three wire cables; more precisely the three wire cable inside the cockpit was shielded as it was for Network A (see figure 2).

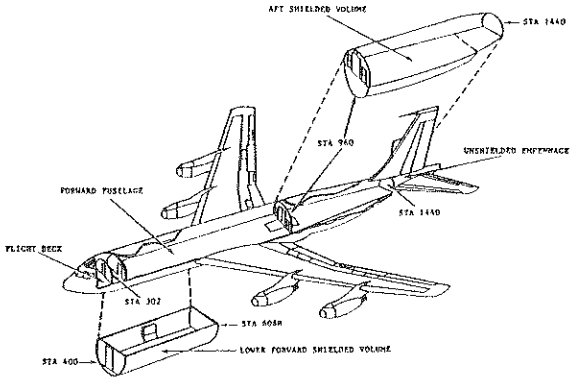

Fig. 1: EMPTAC sections.

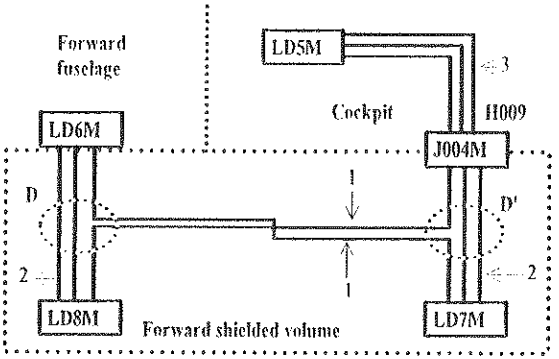

Fig. 2: Electrical scheme of network B.

To perform a quantitative topological analysis, we installed Network B on a metallic plane and used CRIPTE code to achieve predictive calculations. All wires have been flattened on the plane. Each tube of the network has been characterised with S-parameter measurements on short and open circuits. The sections of unflattened lines, at the level of the terminal box connectors, have been modelled as a tube with an equivalent length. The terminal boxes have been modelled in terms of circuit S-parameters. Several examples will be presented showing the improvements one may obtain by introducing the frequency dependence in the tube models.

Injections have also been performed on the network with a current probe located at different points of the "cockpit" shielded cable. For this, the shield of the cable has been considered as a wire in the model: this method allows to calculate at the same time the current distribution on the shield and on the internal wires, whatever the terminal connection of the shield is.

Finally, we'll present how these results have been used to determine the new topological characterisation of the tubes of Network B, once introduced inside the forward shielding volume in the EMPTAC aircraft.

Various solutions for introducing electromagnetic source terms in a topological modelling

V. Gobin *, J.P. Parmantier, F. Issac,
O.N.E.R.A.
29, avenue de la division Leclerc
92320 CHATILLON

I. Junqua, Y. Daudy, J.M. Lagarde
Centre d'Etudes de Gramat
46500 GRAMAT

During the last few years, capabilities of numerical modelling have been improved both in the 3D domain (finite difference codes, time and frequency integral equation formalism, ...) and in the 2D domain (multiconductor line formalism, network codes, ...). In the meantime, the improvement of experimental methods of simulation went on. To be able to handle actual CEM problems, a connection between the various parallel approaches appears to be necessary. Electromagnetic Topology is a theory that help to analyse the coupling on complex structures by breaking the global problem into a simpler one. The studies on that item allowed ONERA to built a numerical code (CRIPTE) that synthesises the elementary problems thanks to a multiconductor line network formalism. A lot of theoretical and experimental validations of this methodology were carried out during the last years, involving a collaboration between ONERA and CEG. Along the different campaigns (in France, on different structures including an aircraft wing and in the USA on the EMPTAC aircraft), problems of different kinds appeared and were solved. They can be separated into two classes:

- analysis of the propagation into the structure itself leading to the multiconductor line network topological characterisation.

- analysis of the electromagnetic fields leading to the equivalent current and voltage sources to apply on topological network models.

The purpose of this paper is to focus on the second point and present the solutions that were used during the ONERA/CEG collaboration to solve the various difficulties encountered :

1) Coupling through small apertures

The problem can be solved thanks to the dipole theory. In general, two equivalent voltage and current generators have to be introduced on a multiconductor line to simulate an EM coupling, respectively:

$$V_{eq} = j\omega\alpha\vec{H}_{cc} \qquad I_{eq} = j\omega\beta\vec{E}_{cc}$$

where 'cc' is for the short-circuit fields. During successive experiments (on a caisson) and on a MIRAGE III aircraft wing) the coefficients have been determined experimentally, using a local EM illumination on the aperture (with a stripline or another antenna). The measurement of the short-circuit current and the open-circuit voltage at one end of a test line led to α et β. The evaluation of the actual generators with the structure under the simulators available in Gramat was obtained using a calibration of the short-circuit fields.

2) Coupling through large apertures

For a large aperture, the distribution of the fields on its surface is needed and it is not realistic to proceed anymore as in section 1. A solution is then to apply the Thevenin theory at the output port connectors of the excited volume. On these ports, one has to measure the voltages induced on the various wires of the bundle and to evaluate (by measure or calculation) the impedance of the lines seen from theses. Then, a new topological network including the equivalent junction and its equivalent Thevenin generator may be built. The drawback is that the information in this zone is lost, but the method remains still efficient for the other zones of the structure. It can also be applied when one is just interested in a specific area of a complex structure. Validations of the methodology will be presented.

3) Modelling of a current probe injection

A common methodology for testing complex bundles is to use a current injection probe. The problem is then to introduce this specific EM source in the topological model. A calibration of the probe may be performed on a very short line by measuring an equivalent S parameter matrix (connecting the tested wire and the generator feeding the probe). To simulate the injection on an actual line network, one has just to introduce this specific junction in the topological network problem solved by CRIPTE.

4) Coupling on a shielded cable

The case of a shielded cable illumination can be solved thanks to the transfer impedance concept. The voltage generator is proportional to the current in the shield:

$$V_{eq} = Z_t I_{Shield}$$

During the EMPTAC campaign (see paper entitled "Application of EM Topology on an experiment on the EMPTAC aircraft), the model of a global source on a shielded cable running in the cockpit was introduced with success by measuring the current at eight locations of the cable in a very complex environment. The EM level at any port of the internal wires was then correctly reproduced by the calculations.

5) Determination of the source generator model for an illumination under a simulator

When a structure such as an aircraft is illuminated by a simulator, it is very difficult to determine the equivalent generator to introduce in the model of an inner cable. During the 1993 EMPTAC campaign, a new method was successfully applied. First, the characterisation of the topology of the shielded cable running in the cockpit has been carried out, leading to the line parameters of the shield in the structure. The same was done for the internal wires inside the shield. Then the CRIPTE code was used to calculate the current at one point of the shield when an unit lumped voltage generator is applied on all wires (including the shield), near the windscreen of the cockpit. Thus a transfer function between the voltage generator and the current on the shield was obtained. It remained to measure the current on the shield under the Elipticus simulator available at the Philips Laboratory in Albuquerque to obtain the actual voltage generator which summarises the effect of the illumination. Once obtained, this generator is *independent* (this is a consequence of the induction theorem) of the nature of wires and of the loads on wires (shielded included). So, it was used to *predict* the induced voltage and current levels on different locations in the aircraft.

During the last few years, Electromagnetic Topology method has been applied by ONERA and CEG on more and more complex structures. Both experimental measurements and numerical modelling have been used to study the sensitivity of the structure to an electromagnetic interference. When facing a difficulty, a single measurement or a single calculation was not able to lead to a correct solution, but their combination was generally the key of the problem. In some cases, a part of the structure under test was considered *as a sensor* and a numerical modelling has been used to interpret its response. In the future, the synthesis between experiments and modelling should allow a better quantitative prediction of EMC problem and help to find optimised solutions.

Towards An Integrated FDTD/Electromagnetic Topology Tool

Joe LoVetri*, Doru Mardare
Department of Electrical Engineering
The University of Western Ontario
London, Ontario, Canada, N6A 5B9
(email: joe@gauss.engga.uwo.ca)

Methods of Topological Modelling

The use of electromagnetic topology concepts to analyze the electromagnetic compatibility of complex systems is very appealing in that the concepts can be applied at many levels of conceptualization. For example, volume/surface based topology can be used to analyze systems in an approximate sense at a very high level (J. LoVetri & G.I. Costache, *IEEE Trans. on EMC*, vol. 33, no. 3, pp 241-251, Aug. 1991). The volumes in the topology are characterized as either *field*, *circuit* or *interaction path nodes* and the associated *interaction sequence diagram* keeps track of the possible interaction paths. Nodes are then given electromagnetic attributes which define the node's susceptibility and disturbance level or shielding effectiveness. The interaction modelling is handled at the *transfer function* level and necessitates the use of *fuzzy* transfer functions in order to model the inherent uncertainty in this type of modelling (J. LoVetri & W. H. Hennecker, *1992 IEEE Int. Symp. on EMC Symposium*, Anaheim, Ca, pp. 127-130, August, 1992). Another high level approach is the use of scattering matrix norms to represent the electromagnetic attributes (C. E. Baum, *Electromagnetics*, 6, pp 33-45, 1986).

When modelling at a system level, sources of error include: coarseness of the topological decomposition; type and approximation of the electromagnetic attribute values (fuzzy variables, norms); propagation of disturbances through the topology; and comparison of disturbance impinging at a node to the node's susceptibility level. The main motivation for modelling at this level is to determine the important interaction paths in a complex system.

The multiconductor transmission line (MTL) approach, i.e. tubes and junctions, with the associated BLT equation (C.E. Baum, T.K. Liu, and F.M. Teche, *Interaction Note 350*, Nov. 1978), can be used at a lower level to get a more detailed description of interactions in the electronic systems within the volume/surface topology. The BLT approach assumes a priori knowledge of the characteristic impedance of the multiconductor transmission lines and it assumes that the S-parameter scattering matrices, which model the MTL junctions, are known, measured, or approximated in some way (J.P. Parmantier, G. Labaume, J.C.Alliot, P. Degauque, *Recherche Aerospatiale*, 1990-5). The analysis is usually made in the frequency domain and is the basis of the frequency and time domain norm approximations referred to previously.

A "combined approach" based on using the methods of dynamic systems theory to reduce the order of the system has also been investigated (V. Ya. Kontorovich, E. I. Glushankov, S. L. Primak, *Zurich EMC'93*, pp. 307-310, 1993).

FDTD and Electromagnetic Topology

Time-domain modelling of the propagation of signals along multiconductor transmission lines and at their junctions has been well investigated (A.R.Djordjevic, T.K.Sarkar, R.F. Harrington, *Proc. IEEE*, vol.75, no.6, 1987). The lines are assumed to be completely described by frequency independent transmission line parameters L, C, R and G per unit length (i.e. quasi-TEM analysis). The MTL's, or tubes, can be described by a system of partial differential equations in the time domain and so explicit finite difference equations are obtained and solved subject to the boundary and initial conditions. If the tube junctions are modelled using an electromagnetic field FDTD procedure then a priori knowledge of the junction scattering matrices is not required. For lines with frequency-dependent parameters a convolution procedure can be incorporated into the FDTD procedure at a cost of added program complexity.

Both, the modelling of MTL's and the modelling of electromagnetic fields using FDTD are well understood. The important consideration here is the interface between the two regimes. For example voltages and the currents on the MTL's must be transferred to EM fields once the energy enters the FDTD domain and vice-versa. The first case can be handled by formulating the FDTD equations to include source terms. The second case, where fields are converted to voltages and currents, is not a unique problem and has been considered previously for applications where FDTD is interfaced to a SPICE type circuit simulation program (R. Mittra, W. D. Becker, P. H. Harms, *IEEE Trans. Cir. Sys. I*, Vol. 39, No. 11, pp. 964-973, November 1992). Various techniques of implementing these transformations will be investigated and results presented.

The advantages of using a field modelling tool in conjunction with an electromagnetic topology tool are many. Junctions which have not been characterized experimentally can be simulated, on-line, with the FDTD modeler. Field models will only be generated where the EM Topology Tool determines there is a critical path in the interaction sequence diagram.

Conclusions

The combination of the FDTD field modeler and EM topology methods is a realistic possibility for the solution electromagnetic interaction problems. The high level methods of EM topology are used to reduce the problem size and the lower level, more accurate, methods of FDTD are used to obtain quantitative predictions and refinements to the topology models. The compatibility of these techniques will be discussed.

REFLECTIONS ON A UNIFIED APPROACH TO ELECTROMAGNETIC PROTECTION

Robert A. Pfeffer*, U.S. Army Nuclear and Chemical Agency,
7150 Heller Loop Suite 101, Springfield, VA 22150-3198
Jürgen B. Nitsch and Richard J. Sturm, NBC Research and Development Institute,
P.O.Box 1142, D-29623 Munster

Introduction. In the near future sensitive electronic military equipment will be required to operate in severe electromagnetic environment (EME) containing frequencies from D.C. to GHz. Those non-ionizing radiation environments include electrostatic discharge (ESD), p-static, lightning, electromagnetic interference/compatibility (EMI/EMC), electromagnetic pulse (NEMP), high intensity radiated fields (HIRF), and high power microwaves (HPM).

Since all EME effects are based on Maxwell's equations, the equation of motion (Lorentz' law) and material equations it is not surprising that the same arose against all EME hardening philosophy shielding and penetration protection. Unfortunately in the past considerable effort was taken to harden critical systems to these environments seperately. As a consequence, hardening of a system became very costly and partially even inefficient. Therefore it appears to be mandatory to unify the protection process aiming at an approach which might become adopted by a wider community. In our presentation we generally sketch a possible approach which will include five major steps: description of the EME and their threats, the coupling process, the hardening procedure and simulation, documentation and implementation structure.

Environments and threats. Usually any one system has to meet more than one environment. A helicopter, e.g., could be given the requirement to operate when exposed to near and/or direct strike lightning, EMP, and HIRF over its lifetime, while mobile C3I could have an operational requirement to meet EMI/EMC, EMP, and lightning.

EME can conveniently be broken down into four categories:

- static (ESD, p-static, direct lightning)
- single pulse (lightning (near strike), NEMP, HPM)
- repetitive pulses, bursts (HPM, NNEMP)
- cw (EMI / EMC, HIRF)

Especially the EME for category two and four could be characterized by only one (reasonable worst case) enveloping curve in the time domain and in the frequency domain, respectively, leading to fewer criteria.

Coupling also very sensitively depends on the system itself. Therefore a coupling analysis has to be performed on each, distinguishing strictly between transient and cw - excitation, i.e. between homogeneous *plus* inhomogeneous solutions of the system-equations and enforced oscillations of the system. In this context the coupling parameters in terms of norms play an important role. They likewise should include the effects of repetitive pulses.

Hardening and simulation. Hardening options for virtually all EME have remained the same: shielding, nonsusceptable data links (e.g. fiber optics), and penetration control (e.g. filters, MOVs, surge arrestors, and zener diodes).

Because most electronic devices fail from overvoltage followed by sufficient energy or from power delivered to the device, engineers developed the use of shielding and penetration protection to reduce the coupled signals below normal operating levels.

Simulation usually consists of three major techniques: current injection, pulse testing and cw. The consolidation of environment criteria and coupling data makes it possible to simplify the test process and to conduct all EME testing at one facility.

Documentation. Currently there is a host of documentation, sometimes even containing conflicting information, which is given to the system developers. Too many standards, specifications, handbooks and manuals lead to increasing costs and confuse engineers and managers rather than simplify the hardening process. Therefore future documentation must be consistently written and reduced to a necessary minimum in number.

Implementation Structure. As a practical matter major cost savings are derived from the most efficient use of existing facilities by consolidating simulator capabilities whenever possible and by establishing a single organization to develop all EME performance requirements and to act as an interface with the developer.

Summary. A unified approach to EME protection is a low risk, cost reducing alternative to the traditional approach to system hardening. Since civilian requirements are considerably different from military ones, one can not expect a *single stringent* approach. However, it has to be ensured, due to the commonalty among all the EME, that there will evolve a *unified* set of protection measures based on a set of *consistent* hardening requirements which will allow to unify also the test procedures.

Application of Electromagnetic Topology on an experiment on the EMPTAC aircraft

I. Junqua *, Y. Daudy, J.M. Lagarde
Centre d'Etudes de Gramat
46500 GRAMAT

J.P. Parmantier , V. Gobin, F. Issac,
O.N.E.R.A.
29, avenue de la division Leclerc
92320 CHATILLON

After several validations performed on canonical structures, the formalism of Electromagnetic Topology enables today to process some parts of industrial structures. ONERA and Centre d'Etudes de Gramat (CEG) showed the efficiency of this approach all along common experiments. These researches were focused on theoretical modelling and on experimental characterisation of various elements constituting topological networks (see paper entitled "Introduction of industrial type cable networks in topological problems: application on a Mirage III wing"). In this talk, we present the results of an experiment performed on an aircraft in October and November 1993, in the context of MWDDEA 7336, in collaboration between ONERA, CEG and the Phillips Laboratory (Albuquerque, USA).

The structure under study was the "EMPTAC" ("Electromagnetic Pulse Test-bed Aircraft"), a Boeing 707 used in the eighties by the US Air Force on Kirtland base, in Albuquerque, in order to carry out various studies on hardening methods for E.M design and maintenance. Therefore, major modifications were made on this aircraft in order to simulate a critical electrical function representative of the one existing in the B1B aircraft. Thus, two shielded zones were built: a forward shielded volume and an aft shielded volume. The wiring located inside these shielded volumes is connected by means of a shielded cable network. These modifications on the structure were performed following "Qualitative Electromagnetic Topology rules", but no predictive calculations relative to "Quantitative Electromagnetic Topology" had been carried out till now.

As a first experiment, we decided to limit the work to the coupling in the lower shielded volume. Therefore, the initial cable network was disconnected at the level of the fuselage. The cable network under study was constituted of a shielded cable running inside the cockpit, then connecting the cable network located in the lower forward shielded volume: the whole network was named network A. Although the actual whole modified EMPTAC network presents a very clean geometry (on the EMT point of view), it still remained complex for a first approach on a complex aircraft. This is the reason why the topological method was first applied to a simplified network (Network B) which was built and tested in France ,then integrated afterwards in the aircraft. This network was made up of simple lines (two and three wire cables instead of bundles with 22 or 12 wires in the existing network A) (see paper entitled "Electromagnetic Topology: accurate characterisation of topological networks. Application to an EMPTAC aircraft experiment").

Once Network B installed in the aircraft, the topological network characteristics (tubes) were modified in order to take into account the fact that cables were not flattened anymore against the reference plane. No new measurement to characterise them "in situ" has been necessary; the parameters of cables of Network B located in the lower forward shielded volume were perfectly deduced from the data base determined in France, by splitting up the initial topological network in various tubes modelling the running of the cables flattened or not flattened on the reference plane. The shielded cable running in the cockpit was split up in 8 tubes which characteristics were deduced from a reflectometry measurement made at one extremity of the shield.

Moreover local injections with a current probe tested in France were performed in the aircraft. In fact, theses local injections enabled the validation of the "in-situ" of Network B. Global illuminations of the aircraft under an antenna named "Ellipticus antenna" and at our disposal in the Phillips Laboratory were performed in the frequency domain: measured voltages were calculated in real time with the CRIPTE code. Thanks to the knowledge of the shielded cable topology, source terms to apply on the shielded cable model were calculated by means of a transfer function between a current measured on the shield and a current calculated when the cable is excited by a unit generator (see paper entitled "Various solutions for introducing EM source terms in a topological modelling"). Several configurations of shield connection on the structure were studied (short-circuit and open-circuit) (Fig. 1). The topological approach gave us the evidence that the lower shielded volume was not so perfectly hardened. Indeed, the residual noise of the lower shielded volume was measured by disconnecting the shielded cable located in the cockpit and was compared to calculations assuming that interference was originated in the cockpit.

Network A was completely characterised and tested in the aircraft. R, L, C parameters of each tubes were numerically calculated thanks to geometrical characteristics (conductor radius, dielectric radius, dielectric permittivity), the random twisting of each bundle being simulated with CRIPTE. For any local excitation with a current probe and global excitation under the antenna, the same source terms as the ones defined for Network B could be introduced for the simulation of Network A.

The great success of this experimentation is that Electromagnetic Topology, because of its combination of measurements and calculations and because of its modular approach, can be a useful and efficient tool to analyse EM coupling in complex structures. Moreover, the quality of simulations, as well as the deduced results, constitute a method which will be of great help for the conception of optimised EMC structure.

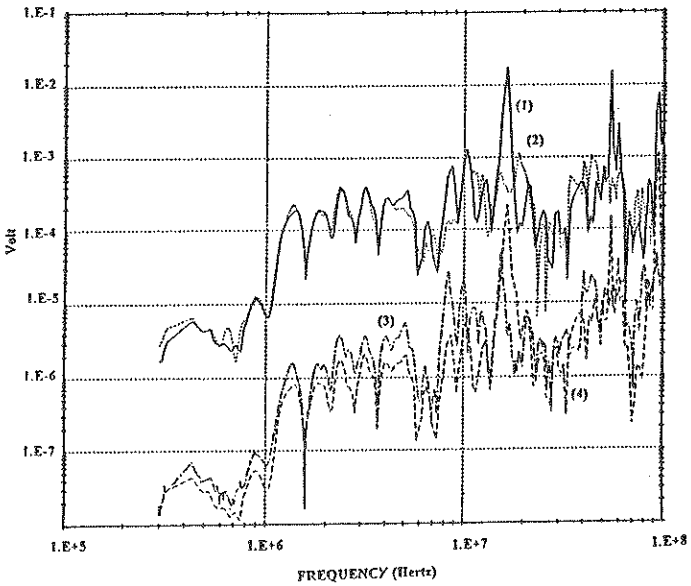

Fig. 1: calculated and measured voltage at the extremity of the shielded cable
- short-circuited shield:
- (1) measurement
- (2) calculation
- open-circuited shield:
- (3) measurement
- (4) calculation

A UNIFIED TOPOLOGICAL APPROACH TO ELECTROMAGNETIC ENVIRONMENTS (EME) PROTECTION

ABSTRACT

GEORGE BAKER, HEADQUARTERS DNA
J. PHILIP CASTILLO*, Logicon RDA
Edward F. Vance, SRI International

This paper presents an approach to the potential unification of protection technology for a wide spectrum of electromagnetic environments (EME). Of particular interest is the protection of complex electronic systems. An electromagnetic topological approach will be applied in developing a consistent shielding protection method. A general source/victim geometry will be considered (figure 1).

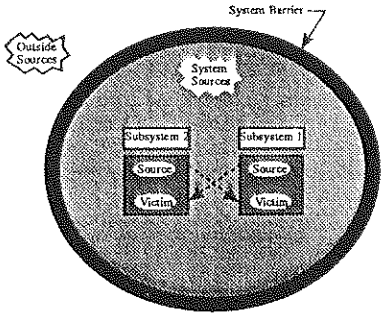

Figure 1

Applicable electromagnetic topological protection techniques will be presented. Next, the varying characteristics of the various EME, for electromagnetic sources both internal and external to the system, will be described. The EME considered (figure 2) in this paper include the following:

- EMI/EMC(Electromagnetic Interference/Compatibility
- LEMP (Lightning Electromagnetic Pulse)
- NEMP (Nuclear EMP)
- HPM (High Power Microwaves)

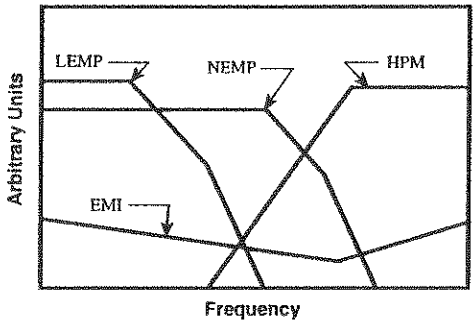

Figure 2

Existing protection practices will be discussed. Incompatibilities and suggested remedies among these practices will be included. Lastly, a generalized topological approach and the basic technological needs for applying the unified approach will be presented.

INTRODUCTION OF INDUSTRIAL-TYPE CABLE NETWORKS IN A TOPOLOGICAL PROBLEM APPLICATION TO A FIGHTER AIRCRAFT WING

J.P. Parmantier* – F. Issac
V. Gobin – P. Besnier
O.N.E.R.A
8 rue des Vertugadins
92190 MEUDON

I. Junqua – Y. Daudy
J.M. Lagarde
Centre d'Etudes de Gramat
46500 GRAMAT

1. INTRODUCTION

Since 1991, the "Office Nationale d'Etudes et de Recherches Aérospatiales" (O.N.E.R.A) and the "Centre d'études de Gramat" (C.E.G) have carried out several experimentations in order to apply and validate the Electromagnetic Topology formalism (E.M.T) to structures of growing complexity, submitted to an electromagnetic interference. This formalism, theoretically derived from the Multiconductor Transmission Line model, has been implemented by O.N.E.R.A (C.R.I.P.T.E code) and used to predict voltages and currents induced on a cable network running inside a perturbated system.

The purpose of this abstract is to present a complete topological study performed in 1993 on a MIRAGE 3 ing fitted out with a complex industrial-type harness. The related procedure followed all along this study is constituted of several steps:

- Cable network topological characterization,
- Cable network electrical characterization,
- System response to a current injection,
- System response to a global illumination under a simulator.

The potentiality of E.M.T, applied to this system is, then, evaluated by validating each step of the procedure after comparisons between measurements and joined topological simulations, performed in real-time.

2. SYSTEM UNDER TEST DESCRIPTION

The studied self-made harness is running inside the MIRAGE 3 wing gutter, free of mechanical control surface, and is constituted of cables of different natures, representing essential aeronautical functions:

- 5 pairs of bifilar and 3-wire cables representing flight controls system,
- 2 pairs of 2 mononofilars providing 2 lights,
- 1 coaxial cable for the antenna,
- 1 twisted shielded cable representing a weapon system function,
- 2 monofilars for a D.C supply function.

This cable network is connected at its extremities to black boxes of 50 Ohm loads, simulating equipment.

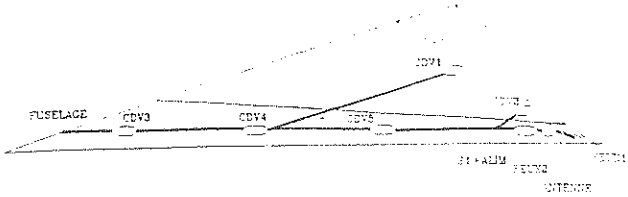

Fig. 1: Running of the harness in the MIRAGE 3 wing

The gutter, in which the harness is running, being considered as the main topological volume, the topological

network can be, then, directly derived from the geometry of the studied harness (branching).

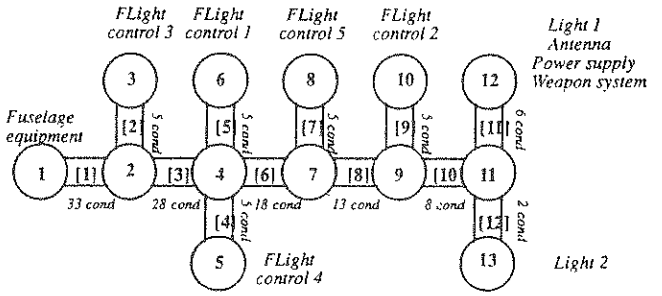

Fig. 2: Topological network

3. HARNESS ELECTRICAL CHARACTERIZATION

The complexity of the harness can be reduced by gathering any conductors providing the same electrical function, making themselves sub–harnesses. In one sense, the total harness is made of 13 sub–harnesses, weakly twisted as it is commonly the case in aeronautics. Nevertheless, the great number of conductors constituting any sub–harness does not enable an experimental characterization, in terms of line parameters (resistance, inductance and capacitance). In order to overcome this difficulty, a method, based on the measurement of a representative set of line parameters and on the running properties of the harness inside the structure, has been developed (*Fig. 3*).

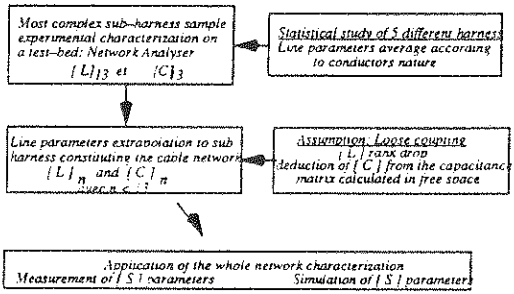

Fig. 3: Harness electrical characterization

4. SYSTEM RESPONSE TO AN ELECTROMAGNETIC PERTURBATION

Once the harness has been correctly characterized, in terms of line parameters, the next step consists in evaluating the potentiality of E.M.T to predict induced perturbations on equipments connected to the harness. To achieve this aim, two kinds of electromagnetic perturbation are studied: a current injection and a global illumination.

4.1 Current Injection

To perform this current injection, a current probe, driven by a network analyser, is inserted at 2 successive locations on the harness. The topological model of this agression consists in introducing, in the numerical simulation, a lumped voltage generator on each conductor submitted to the current injection. This voltage generator, independant of the perturbated conductors, is derived from a set of [S] parameters measurements of the current probe on a test–bed. Measurements, by means of a network analyser, of voltages induced on each equipment, have been compared with the joined topological simulations.

4.2 Global Illumination

The MIRAGE 3 wing is, then, submitted to an electromagnetic global illumination under an E.M.P semi-rhombic simulator. Since the MIRAGE 3 wing is considered as well shielded, frames on the wing surface are removed so that significant levels of induced voltages can be measured at harness extremities. The coupling of the external perturbation on the conductors located underneath these small apertures are expressed as distributed voltages and currents generators. They are related to the electromagnetic fields existing on short-circuited apertures and to coupling coefficients dependent on apertures geometry and on the location of the perturbated conductors against the apertures. A data base of these coupling coefficients has been previously defined by means of their measurements on a test-bed in various geometrical configurations.

5. CONCLUSION

The complexity of this industrial-type harness enabled the development of different methods of cable network electrical characterization and of electromagnetic source terms determination, combining simulations, measurements and statistical approach. These methods have been successfully validated by introducing these parameters in the topological model of this specific problem, in various configurations.

In order to apply E.M.T for the analysis of electromagnetic coupling inside a realistic system such as a complete aircraft, canonical experimentation and reflection must be achieved. In this perspective, future works will be achieved by O.N.E.R.A and C.E.G, in order to face industrial-type E.M.C problems.

CONTROL OF ELECTROMAGNETIC ENVIRONMENT BASED ON THE COMBINED APPROACH

Dr. Eugeny I. Glushankov, Prof. Valery Ya. Kontorovich*,
Nick Soveiko, Sergey L. Primak.

Abstract

Present paper deals with the problems of controlling the Electromagnetic Environment (EME) in large dimensioned electrical and radio systems.

EME control means here that we are introducing certain modification and/or complete elimination of existing interconnections within the system under consideration. This modification is done on the basis of EMI analysis and is intended to provide an interference-free system, i.e. a system that satisfies the stated EMC criteria.

Complete analysis of systems with certain complexity in a variety of practical cases is still hardly possible due to enormous amount of computations. For example, a secondary power supply system of a vessel consists of 150 analogue paths. Each path together with transmission lines and spurious elements can be represented by 20-30th order system, which results in approximately 3,000-4,500th order system as a whole. EMI analysis in such a system becomes now a routine task and of course it is not always possible to involve a supercomputer for it.

Meanwhile, EMI analysis does not always require exact values of currents, voltages, etc. to be determined - numerical estimations are quite sufficient. Up to nowadays there are some principal methods in that field, allowing significant decrease of considered systems order by the cost of obtaining only estimations of required values. Electromagnetic Topology proposed by C. Baum et al [1] and developed in subsequent papers, e.g. [2], is the first one. The second approach is based on the System Dynamics concepts and was applied by V. Kontorovich to the solution of EMC problems in complicated radio systems [3]. So-called Combined Approach was introduced on the basis of those methods, principal concepts of this approach were considered in [4].

A decomposed system represented in the form of (super)-matrix differential equation is taken as an initial point for the EMI analysis based on the Combined Approach.

The first step in EMI analysis is construction of the Interaction Sequence Diagram (ISD) which simplifies structural decomposition of complicated systems. It is advantageous (if possible) to separate the tubes in such a way that the waves are travelling in one direction within each tube. this allows us

to separate vectors of excitation and response for each junction thus further simplifying decomposition and aggregation. Separate tubes and junctions are allocated for spurious paths in order to construct separate comparison systems for this parts of the system.

At the next step we construct comparison systems (CS) for the junctions. For each junction a multiply input - multiply output CS is constructed with number of inputs/outputs equal to the number of tubes coincident to the junction.

Then those CS are aggregated and EMC criteria checkup is performed in a usual way [3]. Whether the criteria is not satisfied, control is introduced into the system. From the solution of CS one can derive constraints for the norms of interconnection matrices. Based on this constraints the interconnection matrices are modified or synthesized in general to eliminate the unwanted interference. The modified interconnection matrices are used e.g. to introduce supplementary shielding, filtering circuits, etc into the system. In other cases some kind of external controlling excitation is to be applied to the system. This is actually control of EME in the considered system. Whether it is not possible to find out some kind of modification to make the system interference-free, this system is treated as essentially non-satisfying the EMC criteria.

Description of the proposed techniques is illustrated by a number of practical examples.

References

[1] C.E. Baum, T.K. Liu, F.M. Tesche, On The Analysis Of General Multiconductor Transmission Line Networks. Interaction Notes, Note 350, November 1980.

[2] J. LoVetry, G. Costache, An Electromagnetic Interaction Modelling Advisor. IEEE Trans. on EMC, vol. 33, No 3, August 1991.

[3] V.Ys. Kontorovich, Solution of EMC problems by System Dynamics Theory // 8th International Zurich Symposium and Technical Exhibition on EMC, Zurich, 1989, pp. 51-54.

[4] V.Ya. Kontorovich, Eu.I. Glushankov, S.L. Primak, Analysis of Electromagnetic Interference Effect on Complex Systems: Combined Approach // 10th International Zurich Symposium and Technical Exhibition on EMC, Zurich, 1993, pp. 307-310.

An Example of a High-Power Microwave System: Mark 0 Phaser

D.V.Giri, Pro-Tech, 3708 Mt.Diablo Blvd.,Suite 215, Lafayette, CA 94549-3610
and
Prof.Y.Rahmat-Samii, Dept. of Elec.Engineering., UCLA, Los Angeles, CA 90024

I.Introduction

Various considerations for the design of a high-power microwave (HPM) system (phaser) have been addressed in thepast [C.E.Baum, Sensor and Simulation Note 306, and D.V.Giri,Circuit and Electromagnetic System Design Note 40]. The term "phaser" stands for pulsed high-amplitude sinusoidal electromagnetic radiation. This class of phasers is defined by

$$P_S = 10^N \quad \text{in GW} \tag{1}$$

where P_S is the useful power from an HPM source. The above definition is useful at a nominal frequency of 1 GHz. The objective of this paper is to describe in detail the design considerations of a Mark 0 Phaser. It is emphasized that we are concerned with single-shot operation of the phaser. Phasers are not necessarily intended to destroy the target, but deny a successful mission. Given that semiconductors devices are physically small and only take about a microsecond to dissipate heat, microwave weapons with pulse widths of the order ofa microsecond or less operating in a single-shot mode are appropriate and relevant.

2. Mark 0 Phaser at ~ 1 GHz

The Mark 0 Phaser described here is a 1.1 GHz; 1 GW average power, 100 ns pulse duration that can be readily assembled. A relativistic magnetron source is commercially available [J.Benford, Physics International Company, San Leandro, CA] with the following capability:

frequency = 1.1GHz	wavelength = 0.2727m	period = 0.909 ns
peak power = 1.8 GW	average power = 0.9 GW (single shot operation)	
waveguide = WR-650	pulse width = 60ns (containing 66 cycles)	

It should be possible to make the following modifications to this ccommercially available source:
i) obtain a peak power of 2 GW, corresponding to an average power of 1 GW
ii) use WR-975 waveguide instead of WR-650 (power handling capacity)
iii) increse the pulse width to about 100ns to obtain about 100 cycles for improved coupling.

The rectangular waveguide out of the HPM source is indicated in figure 1 along with the pyramidal feed horn and the various interfaces between vacuum, SF6 and outside air.

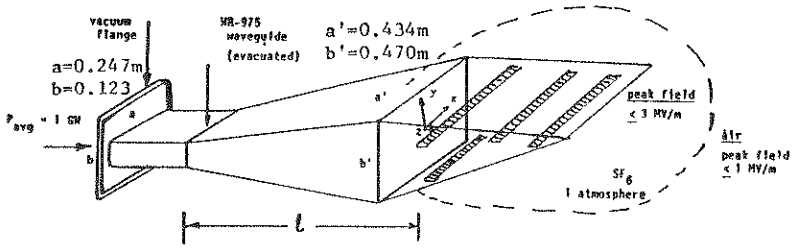

Figure 1. Feed horn for the Mark 0 Phaser

One also needs to measure the forward and reflected powers by a suitably designed side-wall directional coupler. The design og the coupler will be discussed. The reflector geometry with an offset feed is shown in figure 2. the radiation pattern of the reflector antenna in figure 3. Far field parameters are listed in Table 1.

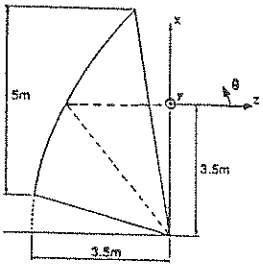

Figure 2. Reflector geometry with an offset feed

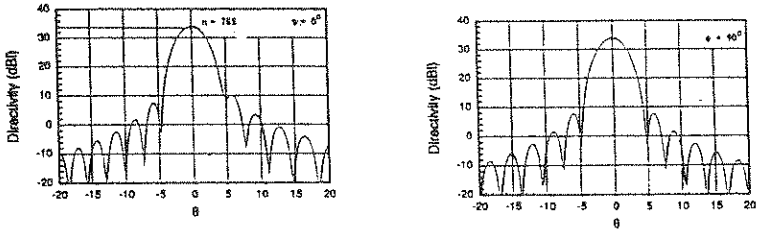

Figure 3. Radiation pattern of the reflector antenna

TABLE 1. Far field parameters of the reflector antenna

R km	E_{peak} (far field) kV/M	P_{avg} (far) kW/m^2	fluence U J/m^2
1	12.8	220	2.2×10^{-2}
3	4.3	24	2.4×10^{-3}
10	1.3	2.2	2.2×10^{-4}
20	0.64	0.54	0.5×10^{-4}

As an example, Mark 0 Phaser 1.1GHz) with ~ 20 sq.m antenna produces a field of 1.3 km at a distance of 10 km. The pulse length is 100ns containing about 110 cycles. One can estimate the induced voltage pulse at antenna terminals of a generic target system to quantify the coupling. The energy contained in the voltage pulse leads to an estimation of the engy deposited in a receiving diode for example, if the circuit details are available. In addition, precise fluence levels delivered to unprotected electronic instrumentation via back door coupling is a system specific issue with many factors governing this type of potential damage. It is however evident that even truck mountable systems with a 1 GW source have adequate field strengths at several km to potentially cause damage via both front and back door coupling mechanisms. It then becomes clear what a progression of such phasers can do in terms of damaging unprotected systems.

ANALYTICAL TECHNIQUES FOR CALCULATING MICROWAVE COUPLING

F.C. Yang* and K.S.H. Lee
Kaman Sciences Corporation
2800 28th Street, Suite #370
Santa Monica, CA 90405
(310) 450-5772
FAX (310) 450-2553

Abstract

To predict the interaction of high frequency signals with a complex object is difficult, if not impossible. The interaction is a sequence of events, first coupling to an object exterior, penetration through POEs (points of entry), and then propagation inside the object. Different types of POEs can be broadly categorized into back doors and front doors. Front door interaction can generally be analytically formulated for predictions and likewise for back door interaction directly via a conducting wire. Back door interaction first via apertures, then into a cavity, and finally to electronics is the most difficult to predict.

When the wavelength of a high frequency signal is small compared to various interior and exterior dimensions of an object, the concept of a mode-tuned chamber may be applied to estimate the interior fields, once the penetrated power is obtained (K.S.H. LEE & F.C. YANG, EMP Interaction Note 482, September 1989). Analytical techniques can be employed to calculate the penetrated power and also the coupling of the interior fields to electronics. In such a calculation, the quality factor of the interior cavity will be involved when applying the mode-tuned chamber concept for field estimates. For some cases the quality factor can be analytically estimated; otherwise, one will have to rely on measurements or existing data bases and applying analytical extrapolation.

When the wavelength of a high frequency signal is large or comparable to the interior and exterior dimensions of a system, alternative techniques need to be used. The available techniques are quasi-static approximations and can involve the use of the quality factor. However, the cavity fields will be much more position dependent than the high frequency case discussed above. The computational requirements will thus be more labor-intensive.

The analytical prediction approach mentioned above may use the techniques of trends, bounds and statistics (TBS).

The trend technique may be defined as some averaged behavior of the interaction as a function of a certain parameter such as frequency. Or

it may be defined as some asymptotic solutions to Maxwell's equations for a certain parameter as being large or small. Examples will be given to illustrate how such trends can be obtained (K.S.H. LEE & F.C. YANG, IEEE EMC Vol. 34, No. 3, August 1992).

The technique of predicting the upper bound of the coupling behavior has two advantages: (a) it involves only a few parameters of the interaction problem, and (b) certain bounds can be derived rigorously from first principles. Examples of bounds will be given (K.S.H. LEE & F.C. YANG, EMP Interaction Note 491, September 1992; L.K. WARNE & K.C. CHEN, IEEE EMC Vol. 32, No. 3, August 1990).

Microwave interaction is highly complex, and hence any form of predictions will have variations and uncertainties arising from random variations of the system and/or source parameters and from a lack of knowledge of these parameters. One method to deal with these variations and uncertainties is the method of statistics. Examples will be given to illustrate how certain statistical parameters can be extracted from calculational or measurement results with the aid of some physical understanding of the interaction process involved. Such parameters are very useful not only for summarizing system coupling data base but also for predicting other object's responses.

NONLINEAR SPACE-CHARGE WAVES IN A UNIFORM SLOW-WAVE STRUCTURE

Kendall F. Casey* and Brian A. Baertlein
Ballena Systems Corporation
5820 Stoneridge Mall Road, Pleasanton, CA 94588 USA

In this paper we consider the kinematic problem of one-dimensional space-charge wave propagation on a thin (surface current) beam in an axially uniform and lossless structure which can support a slow electromagnetic wave. The general theoretical formulation of this problem was carried out by Casey and Baertlein (*Electromagnetics*, vol. 11, pp. 337–355, 1991) and numerical results were presented for the case of an annular beam in a perfectly conducting cylindrical waveguide. We extend those earlier results by considering propagation within a conducting cylindrical waveguide having an inductively reactive wall. Such a waveguide can support a slow electromagnetic mode whose propagation speed can be close to, or match, the speed of the beam. The beam and wave can therefore intimately interact. It is of interest to explore this interaction, which is the basis for the operation of many types of high-power microwave sources.

We assume that the structure is uniform in the z-direction and that the current flow is restricted to this axial direction and is independent of the transverse coordinates. The surface current density $J_{sz}(t - z/v_p)\vec{a}_z$ and the surface charge density $\rho_s(t - z/v_p)$ then take the forms

$$J_{sz}(\hat{t}) = \rho_{s0}\left[v_0 + v_p g(\hat{t})\right] \tag{1}$$

$$\rho_s(\hat{t}) = \rho_{s0}\left[1 + g(\hat{t})\right] \tag{2}$$

where v_0 is the dc beam velocity and ρ_{s0} the dc surface charge density, v_p is the phase velocity of a propagating signal, $\hat{t} = t - z/v_p$, and the function $g(\hat{t})$ satisfies (in the nonrelativistic limit) the nonlinear singular integral equation

$$g(\hat{t})\frac{1 + g(\hat{t})/2}{[1 + g(\hat{t})]^2} = \frac{e\rho_{s0}}{m(v_0/v_p - 1)^2}\int_{-\infty}^{\infty} G(\hat{t} - \hat{t}')g(\hat{t}') \tag{3}$$

The quantities e and m denote respectively the electron charge and mass.

The kernel $G(\hat{t} - \hat{t}')$ is the Green's function which relates the axial electric field on the beam to the surface current density:

$$E_z(\hat{t}) = -\int_{-\infty}^{\infty} G(\hat{t} - \hat{t}')\frac{dJ_{sz}}{d\hat{t}'}d\hat{t}' \tag{4}$$

This function has the general form

$$G(\hat{t}) = Z_0 \sum_{n=1}^{\infty} A_n e^{j\omega_n|\hat{t}|} \tag{5}$$

where Z_0 is the intrinsic impedance of free space and the coefficients A_n are dimensionless; the frequency ω_n is that of the nth waveguide mode propagating at phase velocity v_p. We remark that the ω_n are real for slow-wave modes (that is, modes for which $v_p < c$ where c denotes the speed of light) and imaginary ($\omega_n = j\alpha_n$ with α_n real and positive) for fast-wave modes; and that no slow-wave mode is supported in a closed waveguide with perfectly conducting walls.

Given the Green's function for a specific structure, the integral equation (3) can be solved numerically. One can also develop approximate solutions. To do so, first rewrite the integral equation in terms of the function $h(\hat{t})$, defined by

$$h(\hat{t}) = g(\hat{t})\frac{1 + g(\hat{t})/2}{[1 + g(\hat{t})]^2} \tag{6}$$

The inverse relation is

$$g(\hat{t}) = -1 + \frac{1}{\sqrt{1 - 2h(\hat{t})}} \tag{7}$$

Next, construct an approximate Green's function which includes only the lowest-order waveguide mode(s), and apply to both sides of the integral equation for $h(\hat{t})$ the operator which reduces the approximate Green's function to a delta function. The result is a nonlinear differential equation for $h(\hat{t})$ which can, with further approximation, be solved in terms of the Jacobi elliptic functions. These approximate analytic solutions reveal the principal features of the exact numerical solutions, which include periodic and solitary waves.

We will present approximate analytical, and exact numerical, results for the behavior of space-charge waves propagating on an annular current beam within a closed cylindrical waveguide which has an inductively reactive wall and which is thus able to support a single axially symmetric slow electromagnetic wave. Particular attention will be given to those situations in which (1) the propagation velocity of the slow wave is close to that of the beam and (2) solitary-wave solutions are possible.

A SIMULATION OF THE ELECTROMAGNETICS OF ELECTRON PHOTOEMISSION

Dr. William Page*
US Air Force
Phillips Laboratory

Brian Fisk
Kaman Sciences Corporation

Laser light incident on metal surface can cause electron emission by various processes. The emitted electrons have a velocity distribution determined by the emission process and by intensity modulation of the incident laser beam. The motion of these electrons consistent with their associated fields have been computationally studied and will be discussed. There have been similar previous studies for pulsed X-ray photoemission by Longmier and Carron and others. Carron has also developed an approximate analytical theory for the special case of sinusoidal modulated laser induced emission.

A simple and fast numerical simulation of the radiation caused by electrons with arbitrary emission velocity distributions, which move away from the surface of their origin and then back, has been written. The simulation has been used to determine the effects on the radiated field due to variations in the incident illumination. The case where the incident radiation is considered to be sinusoidal, hence the parameters which can vary are the illumination intensity, the frequency of the sine wave, and the energy of the photons will be discussed. The first two parameters affect the number of photoelectrons which are emitted as a function of time and the last parameter affects the kinetic energy, or the initial velocity, of the emitted electrons.

The simulation is one-dimensional in the sense that the electron motion is restricted to be perpendicular to the plane of emission. There is no magnetic field and the electric field is restricted to be perpendicular to the plane of emission. For the cases of interest, where the illumination is over a spot on a large piece of metal, this model has been called the "cookie-cutter" model. It is equivalent to taking the answer that one would get from taking the effect for an infinitely illuminated plane and by considering only the motion of the electrons above the spot of interest. An alternative way of viewing this is to ignore all edge effects. Given that the only electromagnetic field which is non-zero is the perpendicular electric field, it is easy to formulate the evolution of the fields and the currents due to the photoelectrons. The only one of Maxwell's equations which yields a non-trivial equation is Ampere's Law. Since the magnetic field is zero, Ampere's equation gives a relationship between the current and the electric field. When this equation is integrated in time, it yields an equation which indicates that the electric field at any point in time and space is proportional to the time integral of the total current which has flowed past that point. The photoelectrons' motion is affected by the field pulling the electrons back towards the emitting surface and the resulting field and the motion of the photoelectrons are coupled.

In order to determine a radiated electromagnetic field from the model used above, the dipole moment at each time is computed for the given distribution of electrons. Once the total dipole moment is found, the radiated electric field is determined by the second time derivative of the dipole moment at the appropriate retarded time. Comparisons of this one-dimensional model with a two-dimensional simulation indicate that, for a spot which is not too small nor too large and for an observer who is not too close to the edge of the spot, the one-dimensional model yields reasonable results. A larger spot size

reduces the importance of edge effects, which have been ignored, but if the spot is too large with respect to the wavelength of the incident radiation, the effects of phasing over the spot can be important. The condition of a distant observer reduces the effects of the near and intermediate fields in comparison with the far fields.

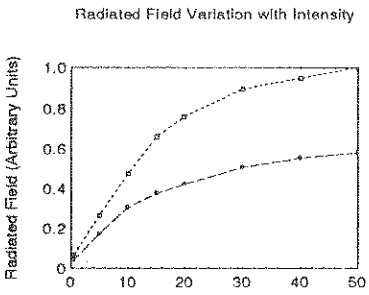

FIGURE 1

As mentioned above, there are three parameters of the incident light which determine the behavior of the emitted electrons and, ultimately, the field radiated. First, the variation with intensity will be considered. Somewhat surprisingly, the dipole moment does not vary much with the incident intensity. This can be rationalized by recalling that the dipole moment is dependent on two things: the number of electrons and the distance they travel. While increasing the incident intensity of the light increases the total number of photoelectrons, it also results in much larger electric fields at the surface of the metal which pull the emitted electrons back more quickly. Hence, the photoelectrons do not travel as far. These two opposing effects roughly cancel each other out leaving the dipole moment approximately independent of the incident light intensity. In order to determine the variation of the second time derivative of the dipole moment and, hence, the radiated field, a more careful analysis is required. Carron has performed such an analysis and has shown that, for sufficiently large incident intensities, the radiated field should increase as the square root of the initial intensity. This behavior is clearly observed in figure 1.

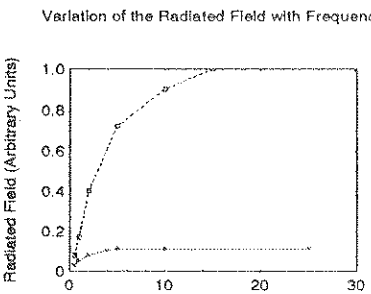

FIGURE 2

The variation of the radiated field with the source frequency also follows the analytic predictions. In this case, the behavior is separated into two cases: regions of the parameter space where the source is sufficiently slow that the electrons can react to it and regions where they cannot. This criteria can be made quantitatively by computing a "plasma frequency" and comparing the source time variation with this plasma frequency. When such an analysis is performed, the radiated field varies as the square root of the source frequency when the electrons have time to respond to the incident illumination while there is no variation once this point has been exceeded. This variation is also clearly seen in figure 2.

Carron's theory also predicts the behavior of the radiated field with variations in the electron energy. It predicts a square root dependence in some cases and a three quarters power in others. The dependence on the electron energy in the simulation results is more difficult to pick out than the behavior of the previous two parameters.

A PLASMA SHIELD DEMONSTRATION EXPERIMENT FOR PROTECTION AGAINST RF ENERGY

Alfred L. Sharp *
Phillips Laboratory
3550 Aberdeen SE, Albuquerque, NM 87117-5776
Dr John E. Brandenburg
Research Support Instruments, Inc.
635 Slaters Lane, Alexandria, VA 22314

One of the potential susceptibilities that must be considered for space based satellite systems is degradation and jamming from low power RF electromagnetic (EM) sources. This paper describes a protection concept based on the use of a self-generated plasma surrounding the satellite or sensitive component that will serve as a shield against a broad range of EM radiation. Basic shield design parameters are discussed, and experimental results described. Potential for scaling the laboratory results to full size satellites will be reviewed, and performance of the plasma using various gasses will be quantified.

The concept of a plasma shield is one of trapping a shell of plasma at approximately glow discharge parameters ($n_e \geq 10^{11}$ cm^{-3} and 1eV electron temperatures) around a satellite or critical component in space that will serve as a shield against EM radiation either for radar identification or direct damage. The basic physics of the concept is well understood theoretically and has been demonstrated experimentally in the DIMEX-I (DIpole Magnetic Electromagnetic eXclusion) experiment. This experiment demonstrated that plasmas of glow discharge parameters could be trapped in a stable mode in dipole magnetic fields such as those produced by common ferrite magnets. The plasmas were made in a pulsed mode, which verified a long, ≈1 msec period of stable confinement followed by a period of decay characterized by a Bohm diffusion time. The plasma was observed to spontaneously form a "shell" density profile, enclosing but not impinging on an object. Steady state plasmas at lower densities were also produced. The method of trapping was not optimal, and the experiments, while successful, were limited by the small size of the vacuum chamber available. A follow-on experiment to scale the DIMEX to steady state in a large vacuum chamber was the next step.

The current DIMEX-II experiment had a basic goal of demonstrating a glow discharge plasma trapped around a dipole magnet as a useful and scalable technology for satellite protection. In order to be a useful technology it must be able to run steady state and be efficient in terms of power consumption. In order to be truly scalable, the plasma must be demonstrated in a large chamber far away from the chamber walls to simulate space conditions, and be able to operate under conditions of space vacuum with gas being provided by the device itself. For these reasons the apparatus for the current experiment was designed to sustain a steady state plasma and be mountable in a variety of vacuum chambers. The final and largest of these chambers (2 meter diameter) was located at the Naval Research Laboratory (NRL) and allowed testing of the DIMEX under simulated space conditions of very low background pressure and vacuum chamber walls located

many magnetic scale lengths away. From this experiment we have been able to assemble a large data base for design of a future space experiment.

The primary apparatus used in the DIMEX-II experiment was a cylindrical aluminum casing containing a magnet and electrodes to create a trapped electron population for ionizing Argon or Xenon gas and a source of gas that can be controlled to allow small amounts of Argon or Xenon to diffuse from the cylindrical magnet. Ionization was created by creating a "planar magnetron" arrangement on the magnet case surface and by puffing gas from holes into the magnetron discharge. This method of creating a plasma was quite successful and allowed operation of the device under space conditions. In addition, an antenna was fixed to the surface of the magnet and was used to measure plasma density when an RF generator outside the chamber was used to irradiate the DIMEX-II apparatus. Measurements thus obtained were used to confirm plasma blocking of the RF energy. Measurements of plasma densities were also made using Langmuir probes. The magnet assembly was 4cm in radius and 10cm in length. A ring of soft iron guided the flux surfaces away from the supporting rod at the base so that it would interfere as little as possible with the plasma. Measurements were collected by the use of a supporting rod that carried power, gas, and diagnostic cables into the DIMEX-II apparatus itself. The supporting rod contained a small tube for gas, a pair of wires to control a bias voltage for the magnetron discharge, and a coaxial cable for carrying the RF signals received by the RF detector.

The DIMEX-II was a laboratory scale experiment of plasma protection technology that demonstrated the following capabilities:

1. Formation of a plasma shell able to deflect RF radiation enclosing but not directly impinging on most surfaces of an isolated object in a space like environment in steady state.

2. Steady state operation at $n_e \geq 5 \times 10^{10}$ peak densities with monitoring of power and gas consumption to be from 150-360W at approximately 2cc/sec STP gas consumption.

3. Rapid on and off capability, the plasma could be ignited and extinguished in a fraction of a second.

4. Plasma equilibrium in a large vacuum chamber where plasma was free of wall effect, and was localized around the device.

5. Attenuation of 2.0 GHz signals by 50% reaching the surface of the magnet in steady state. For a full scale device, approximately 40db signal attenuation is anticipated.

6. Operation with both Argon and Zenon under space conditions, equivalent to more than 120km altitude, and the sustaining of discharge by gas feed from the device rather than neutral background.

The DIMEX-II experiment was entirely successful in meeting its project goals and has advanced the technology of controlled plasmas for space applications and EM protection.

THE SWEDISH HIGH POWER MICROWAVE (HPM) PROJECT

S Jonsson*, National Defence Research Establishment
P.O. Box 1165, S-581 11 LINKÖPING - SWEDEN

K-G Lövstrand, Defence Materiel Administration
P.O. Box 13400, 580 13 LINKÖPING - SWEDEN

Background, Goal and Purpose

In recent years HPM-weapons have been discussed increasingly. Two of the reasons are the possibilities to generate microwave power well into the GW region with energy per pulse reaching kJ-levels and the continuing miniaturization of electronic circuits making them increasingly sensitive to microwave radiation. There are also reports about weapon development and even use of them in war operations. It is therefore necessary to assess the threat of these weapons, the vulnerability of own systems, protection needs and possibilities.

The *goal* of the project is to make the defence authorities aware of the threat and to create the technical potential to meet, with minimum delay, the new demands when needed. Thus the *purpose* is to develop methods and means for system vulnerability analysis and protection. This implies studying the threat development, the phenomenology of HPM penetration and effects, protection methods and components. As it is of prime interest to distribute the information among the defence organizations, industry included, broad participation in the project is encouraged.

Participating Agencies and Resources.

The HPM project is organised with participation from the High Command, the National Defence Research Establishment (FOA), the Electronics, Aircraft and Testing Departments of the Defence Materiel Administration (FMV) and several defence industries e.g. SAAB Military Aircraft and Bofors AB.

The intentionally broad project organization opens efficient channels from the research work into materiel procurement groups and industrial R&D projects. The main theoretical and experimental resources, shared by the participating agencies and industries, are:

- A high power microwave test facility (MTF) with five spot frequency transmitters in the L, S, C, X and K_u bands, output peak power 1-25 MW, antenna gain 20-30 dB, single pulse or up to 1 kHz repetition rate. The MTF is mobile and can be used outdoors or coupled to an anechoic chamber for high intensity (1-50 MW/m^2) testing.
- A large anechoic shielded room 33mx16mx10.5m. The room, also used for radar research, is well equipped for precision low level swept coupling measurements of microwave radiation (LLSC).
- Several anechoic rooms, also used for EMC-work, each of which are equipped with microwave generators, TWT power amplifiers, network analysers etc.
- A mode stirred chamber 2.4mx2.4mx6m.
- Several component test fixtures for electronic component testing.
- FDTD and other computer codes implemented on a Cray-XMP computer.

Project Program.

The HPM-program is based on earlier and continuing R&D on HPM, HIRF, EMP and EMC at FOA and the industries. An especially important work has been done at the SAAB Military Aircraft within their military aircraft program. Included in the first part of the long term program is:

- A survey of various threat situations and characterization of the possible threat.

- Development of methods and techniques for determination of front- and backdoor coupling and for system vulnerability assessment.
- Survey of defence materiel for definition of objects for detailed studies.
- Development of preliminary specifications and HPM protection methods.
- Definition and detailed planning of a major HPM test facility.
- Development of component test methods.

Plans for the second part of the program:

- The major test facility will be established.
- HPM threat situations and the corresponding threat characters will be revised.
- Regular component testing will be performed.
- Several system vulnerability assessments will be performed.
- Some system hardening experiments will be performed.

Results (Examples)

Work within the project has, apart from this Symposium, been reported at several conferences, e.g.:

- Microwave coupling into a slotted cavity has been studied using a generic object (M.G. BÄCKSTRÖM & J. LORÉN, 3rd Int. Conf. on Electromagnetics in Aerospace Appl., Torino, Italy, 1993). Figure 1 shows the good agreement between measured and calculated cross-section values.

- A study of transmit/receive (TR) cells as a protection device have been accomplished (K. MADSÉN, URSI XXIVth General Assembly, Kyoto, Japan, 1993). It turns out that TR-cells are performing well also when the pulse has very short risetime (< 1 ns) and the frequency is out of the normal working band, cp. fig. 2.

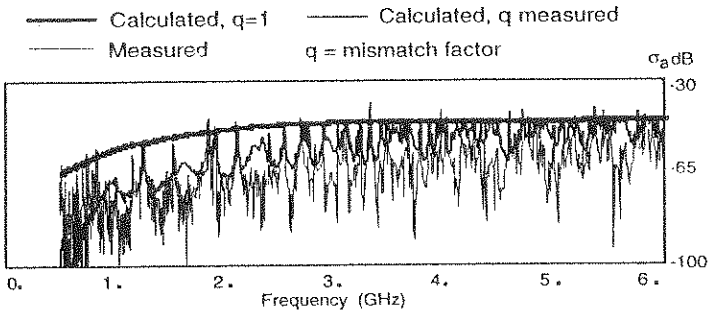

Fig. 1. Cross-section for generic object.

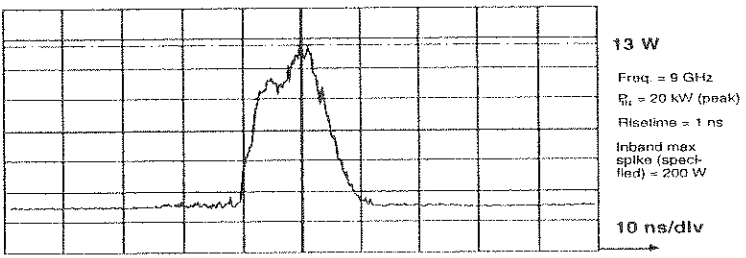

Fig. 2. Spike leakage through 5 GHz TR-cell

GENERIC RESPONSE TO HIGH POWER MICROWAVES

Arthur Nanenson* and Terence J. Wieting, Code 6650
U. S. Naval Research Laboratory, Washington, DC 20375
and
Nathan Seeman, S.F.A. Associates, Landover MD

This paper points out the apparent presence of a generic probability distribution for the high power microwave (HPM) upset of diverse systems. HPM data have been treated with the methods of Hardness Assurance, such as cumulative plots on probability paper and one-sided tolerance limits. We here illustrate the need for treating HPM data with relatively new statistical techniques such as step-stress analysis. For those who may be unfamiliar with the topics, the full paper will present discussions of lognormal distributions, probability paper and one-sided tolerance limits.

1. Background

In 1988 it was observed that the probability distribution of stress-to damage for HPM impinging on a number of very diverse systems followed a smooth curve with little dependence on the particular kind of system. A rather unusual probability distribution was proposed at the time, but it was later noted that the strange distribution resulted from failure to report negative test data on systems which remained undamaged at the maximum test stress. Evidently, what was observed was the truncated portion of a lognormal distribution. One lesson from this episode is the importance of reporting negative results and the importance of stating the maximum stress applied to unaffected systems. Moreover, it is necessary to report the two bounds of stress, between which a system upsets rather than simply an average stress. Such "step-stress" data must generally be treated using "step-stress" analysis. However, the most intriguing conclusion is that there may be a generic lognormal distribution, which to first order can be used to approximate the damage or upset probability of very diverse systems.

2. Data from The Naval Research Laboratory (NRL) And from Expert Estimates

Figure 1 shows a cumulative probability plot of NRL data for different IR seeking missiles. When displayed on lognormal probability paper, the data approximately follow a straight line indicating a lognormal distribution. Any grouping of data points by missile type is of only minor statistical significance, and thus the probability distribution for stress-to-upset is roughly the same for the different missiles. Given the very diverse nature of the missiles investigated, it is unlikely, in the absence of a generic rule, that they would all exhibit such a peculiar similarity. We sought further corroboration of our conclusions from theoretical estimates made by a team of experts on missile upset and damage. Working separately, these experts evaluated many diverse RF and IR seeking missiles. Though there was no particular agenda for and no particular anticipation of a generic distribution, when the data were displayed as a cumulative plot on lognormal probability paper, a lognormal distribution emerged. Again, there was no statistically significant grouping of data by missile type, IR/RF mode of operation, analyst or place of manufacture. Thus, unbiased expert opinion corroborates our suggestion of a generic probability distribution.

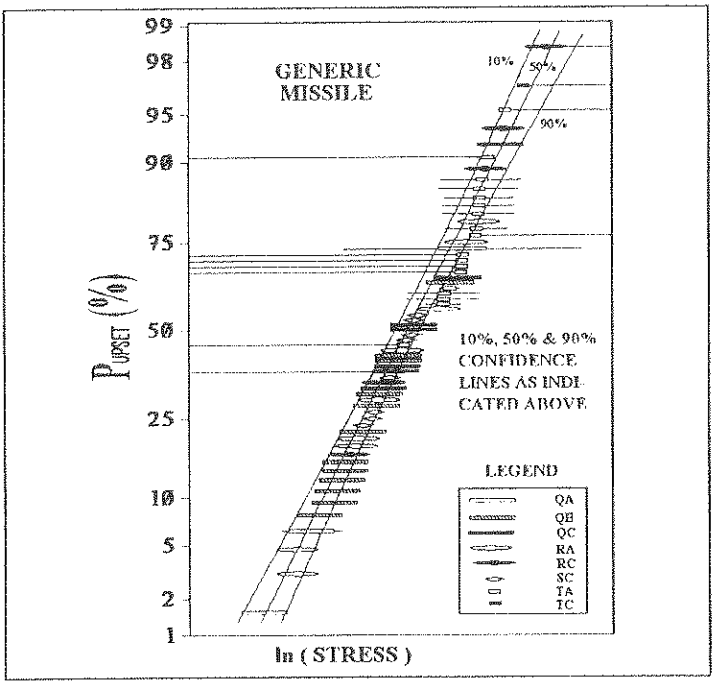

Figure 1. Cumulative Probability Plot on Lognormal Probability Paper for NRL Data on HPM Upset of IR Seeking Missiles. The X-axis is in arbitrary units. A horizontal line on a point indicates stress limits between which upset occurred. Lines extending from the data point to the left edge of the plot indicate that only an upper bound was determined. Lines from the data point to the right edge indicate that only a lower bound was determined.

3. Conclusions

NRL data, expert opinion and damage data from 1988 combine to strongly suggest generic probability distributions for the HPM upset and damage of complex systems. In arriving at these conclusions, the full article will emphasize techniques of analysis such as step-stress calculations and one-sided tolerance limits (for probabilities and confidences). The advantages of cumulative probability plots displayed on probability paper (compared with more conventional S-shaped curves) will also be pointed out.

HPM AGAINST RADAR; A GENERIC MODEL.

M.-Y. LIENHART (*)
THOMSON CSF Surface Detection Systems Division
Base d'Antennes de Limours - 91470 LIMOURS (FRANCE)
B. ARNAUD, N. SAMAMA
THOMSON Shorts Systems
9, Rue des Mathurins - BP 150 - 92223 BAGNEUX CEDEX (FRANCE)

1. Introduction

Prediction of effects of HPM on targets needs extensive parametric studies because of the large number of parameters to optimize. In particular, electromagnetic transmission needs to focus on:

- antenna characteristics: transmitted power, aperture illumination function, effective radiated power, sidelobes;
- air breakdown, versus frequency, pulse length and atmospheric conditions;
- coupling phenomena lead to take into account the receiving antenna, the filter, and the non-linear characteristics of the limiter and the most sensitive components.

We have developped a generic model, called DUEL: Destruction or Upset by Electromagnetic Lightning. This model allows optimization of a HPM system, in order to achieve the most efficient effects on a target. A side result of this model is an estimation of the fratricide effects near the HPM system. That is particularly important to optimize the display of an operational system.

2. Program description

The program is modular and is composed of five main subprograms:

- **ARME** is dedicated to modelisation of an HPM antenna. The transmitting antenna is supposed to be a HPM pyramidal horn. We start with the waveform feeding the horn. The frequency spectrum of the pulse is calculated with a FFT. The aperture field distribution is approximated by the fundamental mode TE01 with a quadratic phase correction; at a given point P, the radiated field is calculated using the plane-wave spectrum method (2-D FFT) and the far-field approximation. We assume here that the radiation process is linear. Applying the superposition theorem, we calculate the field spectrum at P, then the pulse waveform through inverse FFT.
- **PROPA** models the physics of atmospheric propagation, including linear and non-linear phenomena. The path from the transmitting horn to the receiving antenna is sampled with regular spaces. The first sample is at the near field / far field transition of the transmitter. At each sample point, the interaction between the HPM waveform and the atmosphere is calculated. Only electrons are considered. The method is a compromise between Mc Donald's model and Lawrence Livermore's model. It is less time-consuming, while enabling prediction of the waveform distortion on its path through atmosphere. The transport coefficients of Lupan were chosen and validated with a more complex model. Our model properly describes the propagation of a plane wave through atmosphere for altitudes lower than 60 km, and frequencies between 100 MHz and 40 GHz. In the far-field of the transmitting antenna, the field is a spherical wave. At each space sample, the field's decrease as 1/r is calculated. Thus, breakdown issues are concentrated in the vicinity of the transmitting antenna.
- **CIBLE** models a receiving antenna of the target. A large-aperture, high-gain antenna is considered for front-door, in-band coupling. Such an antenna is typical of ground- or sea-based radars. Its characterization relies upon its plane-wave spectrum, sampled and truncated, at the central frequency. The equivalent Thevenin circuit is used in the global model.

Our calculations were done in S-band, for the transmitting and receiving antennas.

- **SALUT** models the microwave receiving circuits (band-pass filter, diode limiter) and components (PIN diode of the limiter, low-noise amplifier transistor). The filter's bandwidth (-3dB) is about 10%; its central frequency can be adjusted. The limiter is characterized by its output/input power transfer function, which relies upon a small-signal model and a large-signal model. The incident RF power values on the PIN diode and the bipolar transistor determine their respective temperatures, as a function of time. Their thermal destruction can be predicted.
- **GRAPHIQUE** is a group of subprograms dedicated to representation of an amount of results in a user-friendly way.

3. Results

A few results concerning breakdown in atmosphere, and diode and transistor heating, are given here. For a plane wave propagating at low altitude, in standard atmosphere, in S-band, we calculate the power and energy surface density, as a function of pulse length:

T_I (ns)	10	20	50	100	200	500
P_{CL} (MW/cm²) THOMSON	5,1	4,0	3,1	2,5	2,2	1,9
E_{CL} (MJ/cm²) THOMSON	50	80	150	250	430	900
E_{CL} (MJ/cm²) CABAYAN	55	90	160	270	450	900

Our results are in good agreement with the results of Dr CABAYAN (Livermore).

As a result of our parametric studies, we can display contours of temperature growth of the limiter's diode (left) and the LNA transistor (right) as a function of azimuth and elevation of the incident wave vector, in the target's axes. A 10 GW, 500 ns S-band pulse is transmitted. The horn is pointed toward the target. The distance is 2 km. As expected, the contours are parallel to the receiving antenna's radiating pattern. The hazardous solid angle corresponds to the main lobe of the cosecant pattern.

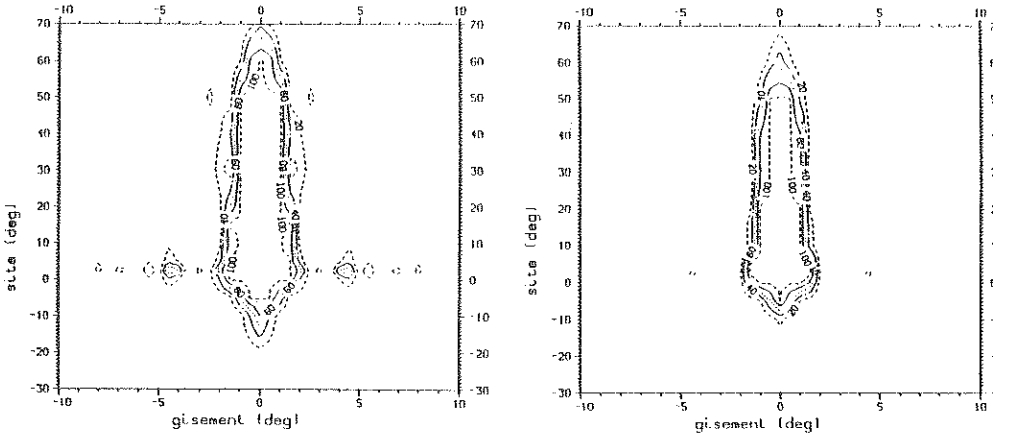

4. Acknowledgments

This work was performed with support of "Direction des Recherches, Etudes et Techniques" (DRET, France) under contract 90/444.

THE FIER HPM TEST FACILITY

JP.BRASILE, G. JEAN-FRANCOIS, M. SIMON
THOMSON SHORTS SYTEMES
9, Rue des Mathurins - BP 150 - 92223 BAGNEUX CEDEX (FRANCE)

1 - Introduction

An HPM test facility "the FIER " has been designed and built by THOMSON SHORTS SYSTEMES .This facility produce :

-High Power Microwave (HPM)
-High Intensity Radiated Fields (HIRF)

The major objectives are :

-Vulnerability tests (HIRF use)
-Technological demonstrator (high voltage,high current,HPM)
-Physical experiments

The facility consists of four major units that are : a High Voltage Generation (HVG) ; a Microwave Generation (MG) ; a Microwave Radiation Area (MRA) and a Control and Diagnostics System (CDS)

2 - Description

HIGH VOLTAGE GENERATION (HVG) : The HVG consist of:

-a HV power supply unit (100 kV)

-a fast compact Marx generator (3 kJ ; 0.4 to 1.2 MV ; Equivalent capacitance 4.17 nF ; SF6 gas insulation - O Bècle et al ,8th IEEE International Pulse Power Conf. pp998-1000 San Diego 1991),single shot.

-a voltage pulse forming line (deionised water line with self breaking SF6 gas master switch 12 Ω ,capacitance 2.77 nF ; pulse length 50ns.)

MICROWAVE GENERATION (MG) : The MG consist of:

-a relativistic magnetron in S band
-a focusing (1 Tesla) with its power supply
-3 Horns antennas (16 dB) fed by waveguides under vacuum
-auxiliaries (vacuum,cooling.....)

MG is placed in a concrete shield room to protect from X ray radiation. The main dimensions are :

Diameter	: 1,3 m	(with focusing magnet)
Length	: 1,8 m	(RF generator)
Weight	: 2,5 t	(with focusing magnet)
Total length	: 7 m	(complete setup)

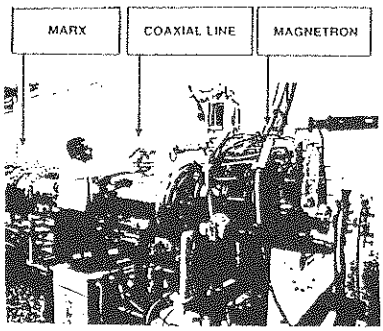

MICROWAVE RADIATION AREA (MRA) :
The MRA consists of an anechoic chamber

- length 22 m
- width 10 m
- high 5.5 m

3 horns antennas feeded by the 3 magnetron outputs waveguides radiate in the chamber .

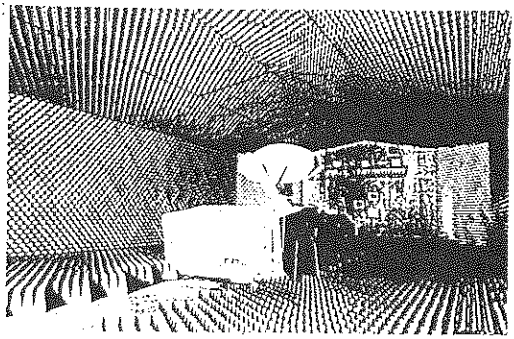

CONTROL AND DIAGNOSTICS SYSTEM (CDS) : The CDs consist of a shielded sceen room that contains control panels and instrumentation.

3 - Results

The FIER performance measured characteristics are:

-RF outpout power with a range from 60 MW to 1 GW for 3 outputs and with a total energy of 25 J per pulse

-RF Frequency for 3 frequencies : 2.8 GHz ;3.2 GHz and 3.7 GHz

-Magnetron current in the range from 4 kA to 20 kA

-Axial magnetic field in the range from 0.4 T to 1T

-Magnetron applied high voltage in the range from 400 kV to 900 KV

Typical traces are as follows:

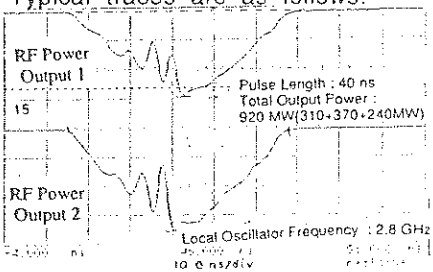

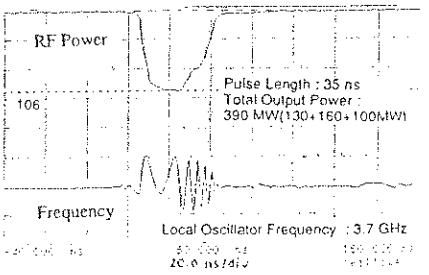

Radiated Field characteristics are for a single output :

Frequency (GHz)	2.8	3.2	3.7
Peak Power (MW)	350	150	200
Pulse Width (ns)	55	35	35
Rise Time (ns)	3 to 20	5 to 8	3 to 15
Illuminated Spot-3 dB (m2)			
- at 3 m from antenna	1.4	1	0.8
- at 6 m from antenna	5.5	4.2	3.1
- at 10 m from antenna	15.3	11.6	8.6
- at 14 m from antenna	30	22.7	16.8
Power Density / Peak Field (W/cm2) / (kV/m)			
- at 3 m from antenna	13570 / 320	7600 / 240	13550 / 320
- at 6 m from antenna	3400 / 160	1900 / 120	3390 / 160
- at 10 m from antenna	1220 / 95	680 / 70	1220 / 95
- at 14 m from antenna	620 / 70	350 / 50	620 / 70

COMPARISON OF ANTENNA FACTOR CALIBRATION OF A TUNED DIPOLE BETWEEN TWO ANTENNA METHOD AND NIST METHOD

Sisir K. Das *, P.H. Rao, K.T. Selvan
V. Venkatesan, K.M. Krishnaiah and P. Ramakrishna

SAMEER - Centre for Electromagnetics
2nd Cross Road, C.I.T. Campus
Taramani, Madras - 600 113, India

Motohisa Kanda

National Institute of Standards & Technology (NIST)
325, Broadway, Boulder
Colorado 80303, USA

ABSTRACT

The paper describes the calibration technique of a horizontally polarized tuned dipole antenna for its antenna factor and compares the results obtained using two different methods. These are two antenna method and NIST dipole method. The measurements were carried out in an FCC accredited open area test site with metal ground plane. The test set up is shown in Fig. 1. In two antenna method the antenna factor was found using two identical antennas and finding the gain G from the following expressions:

$$G_t = G_r = G = \frac{1}{2}\left[20\log_{10}\left(\frac{4\pi r}{\lambda}\right) + 10\log_{10}\left(\frac{P_r}{P_t}\right)\right] \quad (1)$$

$$AF = 20\log_{10}\left(\frac{9.7}{\lambda\sqrt{G}}\right) \quad (2)$$

where λ is the operating wavelength, P_t & P_r are the transmitted and received power, r is the distance between the antennas.

In NIST method a standard field E at the site of AUT was generated and measured using the NIST dipole (Fig. 2). The rf signal induced in the dipole was detected by a diode and open circuit dc output voltage measured using a high impedance dc voltmeter after filtering it using a RC filter. Before the measurement, NIST dipole was calibrated by injecting rf signal through a T-junction (Fig. 3) and measuring dc voltage output without the presence of antenna elements. From this calibration (Fig. 4) curve an unknown electric field strength can be found by measuring dc output voltage and calculating the field strength from the corresponding calibrated value of V_{rf}:

$$E = \frac{V_{rf}}{h_e} \qquad (3)$$

where $h_e = \tan\left(\frac{\pi h}{\lambda}\right)$, the effective height of the dipole of length 2h. Received voltage V output from the AUT was measured and antenna factor of the AUT is calculated from the ratio E/V. The measurement was carried out at 200 MHz and values of the antenna factor are shown in table-1.

Table - 1

Antenna Factor of a tuned dipole at 200 MHz

Method	Antenna Factor (dB)
Two antenna method	12.5
NIST method	12.3

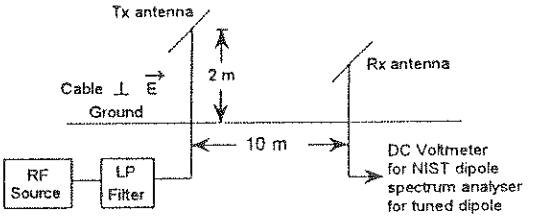

Fig. 1 Experimental set up for calibrating horizontal dipole

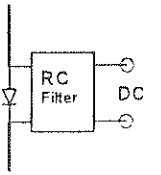

Fig. 2 NIST dipole

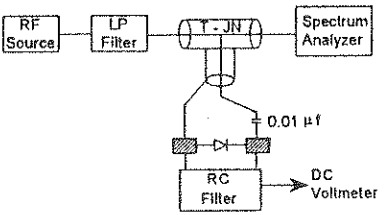

Fig. 3 Calibration of NIST dipole

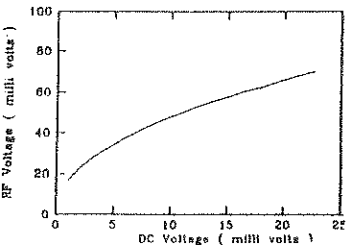

Fig. 4 NIST dipole Vrf vs. Vdc

REALIZATION OF A MEASUREMENT SYSTEM FOR THE SIMULTANEOUS DETERMINATION OF THE SIX COMPONENTS OF AN ELECTROMAGNETIC NEAR FIELD FOR THE FREQUENCIES FROM 75 kHz TO 30 MHz

K.-H. Gonschorek, S. Helmers
Technical University Hamburg-Harburg
Department of theoretical electric engineering
Harburger Schlosstrasse 20
21071 Hamburg

A. Gille*, J.-L. ter Haseborg
Technical University Hamburg-Harburg
Department of measurement engineering / EMC
Harburger Schlosstrasse
21071 Hamburg

Introduction

Electromagnetic waves are more and more used in a lot of domains like, for example, the wireless communication. Due to the increasing number of electronic equipment, radiating electromagnetic fields, several new problems concerning the electromagnetic compatibility (EMC) occure. Another important aspect is the protection of human beings, who are exposed to an electromagnetic field.

Therefore it is necessary to know the fieldstrength of electromagnetic fields in certain areas. Especially for the protection of persons, working near radiating instruments, the knowledge of the short-range field is important. The calculation in the short-range field is difficult because of the complicated structure of the field next to the source. In measurements, the general problem is to measure the electric and the magnetic field separately. An electromagnetic field has three components of the electric and three components of the magnetic field.

In this paper, a measurement system is presented, based on the developments by Kanda, which is able to measure all six components of an electromagnetic field in the band of frequencies from 75 kHz to 30 MHz (F. GASSMANN : Messung d. echten Strahlungsdichte durch gleichzeitige E- und H- Felderfassung im Bereich 75 kHz bis 30 MHz, EMV '92, 3. Int. Fachmesse und Kongreß f. elektromagn. Verträglichkeit). The measureable amplitude of the fieldstrength is from 0,5 V/m up to 500 V/m and from 4 mA/m up to 4 A/m. Thus this system measures about ten times more sensitive than the sensor presented by GASSMANN. In varying the amplification of the measured voltages it is even possible to detect fields with the magnitude of about 100 mV/m and 0.8 mA/m.

Theory

The principle of the presented system is a double loaded angular loop as shown in figure 1. The voltage, caused by the electric field, has the same z-direction at the two resistors. The magnetic field induces a current circulating in the loop. For that reason, the voltages at the resistors have z-directions in opposite sense. The sum of the two voltages $\Sigma = U_1 + U_2 = 2\,U_e$ is therefore proportional to the electric field and the difference $\delta = U_1 - U_2 = 2\,U_m$ corresponds to the magnetic fieldstrength.

With three orthogonal loops it is possible to measure all six components of an electromagnetic field.

The problem is to measure the voltages, because the tap describes an other loop which may disturb the original field. The solution is the transition from a loop to a half-loop over ground. In theory an ideal conducting ground represents a reflecting plane, so a half-loop over ground can be described as a complete loop theoretically.

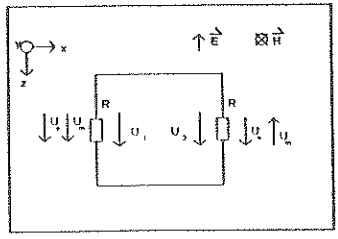

Figure 1 : Double charged loop

Sensor

Three stirrups must be arranged orthogonal over a conducting plane. A cube would be a conceivable form, but it is not suitable because of the strong and irregular reflections at the edges of the cube. For that reason, the form of a sphere is chosen (figure 2). The sphere has a diameter from 15 cm, the material is copper, 2 mm

thick. Three stirrups are sufficient for the measurement as shown at the system from GASSMANN. But three stirrups cannot be arranged symmetrically on the sphere. The presented sensor is constructed with six stirrups, all orthogonal to each other. So the electromagnetic field will be disturbed symmetrically and the isotropy should be better than with a sensor with three stirrups.

As described above, it is necessary to choose two of the six voltages at a time to form the sum and the difference. This voltages must be send to a detector. The transmitter route is a light circuit, so it does not disturb the original electromagnetic field.

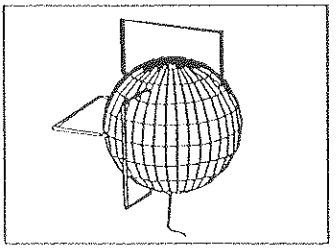

Figure 2 : Sensor

For measuring the magnetic field the size of the stirrup is decisive, for measureing the electric field the value of the resistor is important. The higher the value, the higher the voltage, induced by the electric field. The voltage, caused by the magnetic field, is independent of the value of the resistor. Therefore a critical load exists, where the sum Σ and the difference δ of the voltages have about the same value (figure 3). For this load, the value of U_1 is much greater than the voltage U_2.

The value of the resistance should not be near the value of the critical load, because the voltage U_2 is too small in relation to the voltage U_1 to have any influence on the results.

Inside the sphere the following components of the system are placed :

- switch, for choosing the two voltages of one of the stirrups
- subtractor and adder
- emitter for sending the measured voltage over the light circuit
- accumulators for the power supply of the electronic components

The substractor is realised with two transimpedance-amplifiers. By connecting one of the voltages alternated at the positive and at the negative entrance to one of the transimpedance-amplifiers, the circuit arrangement realizes an substractor and an adder at a time. The transimpedance-amplifiers have a bandwidth of 475 MHz. An amplification of the obtained voltages with the factor 10 is possible, so a more sensitive measurement could be effected.

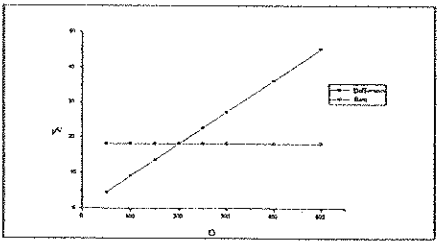

Figure 3 : Critical load

Measurements with the sensor in comparison with the theoretically calculated values will be presented and discussed.

Conclusions

There is a great interest and necessarity in measuring electric and magnetic fields on or in the near of biological dielectrics, especially for the investigation of the influences of electromagnetic fields for human bodies. These influences are not exactly studied yet. Accurate E-field sensors exist already, but a real problem is the reliable determination of the H-field. Due to the fact, that the electric and the magnetic field have different influences on biological dielectrics, the presented measuring principle is suitable for a sensor, utilised for these studies. The sensor itself should be smaller and adapted at the special forms and characteristics of biological dielectrics. It is intended to realize a measurement system for the detection of electric, magnetic and electromagnetic fields on plain and curved dielectric surfaces.

System Level Coupling Measurements using a 1000 Ohm Compact Voltage Probe

Kenneth R. Calahan
Los Alamos National Laboratory

Michael D. Rogers
BDM Federal, Inc

Abstract

Five years ago, Los Alamos National Laboratory (LANL) began measuring the coupling efficiency of fast transient electromagnetic waveforms to contemporary military systems. The transient waveforms of interest, depending on the waveform, covered many decades in the frequency domain, with the highest possible frequency being 1 GHz. One of the key goals was to measure the coupled waveform at the connecting pin of a specific component. This presented a potentially difficult situation because many of the desired measurements would be located within line-replaceable units (LRUs) which tend to be very compact and have little excess space in which to install instrumentation. Additionally, we could not change the original shielding configuration of the LRU. This problem is particularly difficult if one tries to use commercially available probes. The final challenge which we faced was that of not electrically loading the circuit, powered and unpowered, with the installed probe.

To make electronic measurements at the component level of an electronic circuit, one can use either a voltage or current probe as the sensor and then feed that signal into a recording device. Traditionally, current probes have been used to measure currents on wire bundles and individual wires within a military system. Current probes are very attractive because of their ease of use and non-intrusive measurement technique. Their shortcoming is their size. The most compact commercial current probes available are relatively large (typically .5"x.5"x1"). This is not small enough to get into the available spaces within some LRUs. Additionally, current probes are very difficult to use for measurements on printed circuit cards. These difficulties associated with current probes forced us to look at voltage probes.

Recently, Dr. Victor Van Lint, of MRC, was attempting to measure the coupling of fast transients to small systems such as desktop computers and portable radios. He, too, was faced with the challenge of putting probes into small places. In response to that challenge, Dr. Van Lint developed a voltage probe with a 1000 ohm resistor at the test point end of the semi-rigid cable and integrated the resistor into the semi-rigid cable. This design helped minimize the impact on the circuit under

test and mitigate parasitic capacitances and inductances caused by the resistor leads and their associated connection to the resistor. We recognized the value and flexibility of this measurement technique and began using the 1000 ohm voltage probe in our test efforts. The 1000 ohm voltage probe proved to be invaluable for field testing, primarily because it could be easily, and inexpensively, built from raw materials at the test location to meet the changing demands of a test effort. Over time, the basic design of the probe has been improved and procedures for proper installation and use of the probe have been developed. The current LANL design, of the MRC voltage probe, is shown in Figure 1.

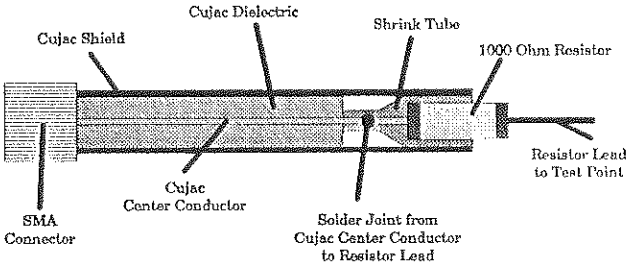

Figure 1. Cross-sectional Drawing of the 1000 Ohm Voltage Probe.

This paper will focus on the field assembly, calibration and application of the 1000 ohm voltage probe. Specific emphasis will be placed on the proper installation on the probe for both power-on and power-off applications plus grounding considerations and techniques for penetration into shielded sub-systems. The paper will detail the proper assembly of the 1000 ohm voltage probe and an easily fabricated calibration fixture, which can be use to characterize the actual frequency response of a newly fabricated 1000 ohm voltage probe.

BROADBAND AND ULTRASENSITIVE ELECTROMAGNETIC SENSORS FOR NEMP, EMC AND LIGHTNING : THEORY AND EXPERIMENTAL RESULTS

EUMURIAN Grégoire
Chef du Service IMD Instrumentation
THOMSON-CSF/RGS
Département Electromagnétique et Nucléaire

PAMPALONE Fabrizio
Responsable du laboratoire IEM
THOMSON-CSF/RGS
Département Electromagnétique et Nucléaire

Classic passive sensors used for NEMP, EMC or lightning present certain drawbacks :

- Inadequate bandwidth, requiring use to several sensor for broadband measurements
- low sensitivity for small size and high frequency sensors
- large size regardless the wavelength to obtain sensitivity.

Active and semi-active sensor designs allow coverage of the 1 kHz - 1 GHz and 200 kHz - 20 GHz bandwidths, with a single miniature sensor ; the use of specially designed optical link and remote control of ranges permits to obtain high dynamic ranges of measurement, from some $mV/_m$ to $1MV/_m$ in time domain, or CW measurements with extreme sensitivity, in the $\mu V/_m$ range within 1 Hz analysis bandwidth.

For measurements on reduced scale models, the active and semi-active sensor concept allow construction of small size sensors, respectively less than 8 cm and 2 cm height.

To obtain no perturbation of incident field during a measurement, the active sensor concept is used in integrated E-field or H-field broadband sensors, including in a spherical design the antenna electrodes, remote controlled attenuators, amplifiers, battery powering, control unit and optical modem.

This type of active integrated modem-sensors allow CW measurements in the 10 kHz - 1 GHz frequency range with extreme sensitivity of 0.5 $\mu V/m$ within 1 Hz or transient (time domain) analysis of fast electromagnetic phenomena with rise time less than 400 ps.

INFRARED IMAGES of SCATTERED ELECTROMAGNETIC FIELDS FROM SCALE MODEL AIRCRAFT

John Norgard*, Joseph Sadler
Ronald Sega**, William Prather

Microwave Research Group
USAF Phillips Laboratory (PL/WSR)
3550 Aberdeen Avenue SE
Kirtland AFB, NM 87117-5776

* Also with the University of Colorado at Colorado Springs
** Also with NASA/JSC Houston

ABSTRACT

Recent experimental work has been performed using low power microwave (LPM) continuous wave sources to determine the electromagnetic (EM) scattering characteristics of scale model aircraft under high power microwave (HPM) pulsed field conditions. These scale model scattering tests are helpful in understanding the general scattering characteristics of a full-sized aircraft under similar conditions. The scattering data collected on a scale model aircraft can also be used as a "pre-test" look at the actual full scale aircraft before it is fully instrumented and tested at an outdoor test site or in an anechoic chamber.

For the scale model tests, a non-destructive, minimally-perturbing infrared (IR) imaging technique was used to measure the scattered fields. Two-dimensional cross-sectional views of the scattered electric fields from the scale model aircraft were determined using this technique. The IR measurement technique involves the observation of microwave/millimeter wave energy deposited in an electrically lossy IR detection screen in the plane over which the electric field is to be measured. Joule heating of the detector material results in IR emissions which can be detected by an IR imaging system. The IR detection screen material is calibrated such that a given temperature rise (above the ambient temperature of the material) corresponds to a particular incident electric field intensity level.

As an example, the diffraction patterns of the electric fields scattered from a scale model F16 aircraft under various test conditions were determined using this IR measurement technique. The model is a 1:32 scale model of the actual aircraft. The model was irradiated with the near and far fields of a microwave horn antenna. The angle of incidence, polarization, and frequency of the incident radiation were varied. The polarization of the incident pulse was parallel to or perpendicular to the axis of the model.

These tests were performed in the Anechoic Chamber at the Microwave Test Group at the USAF Phillips Laboratory. The IR detector screen for these tests was constructed out of Teledeltos paper (a carbon impregnated thin film). Styrofoam forms were cut out to conform to the shape of the F16 in the axial and transverse profiles listed above. The carbon paper was attached to one side of the styrofoam forms. A non-conducting fixture was made to hold the F16 model (with the attached IR detection screens) in the various configurations listed above.

Low level CW testing of the scale model F16 was performed. IR maps of the electric field diffraction pattern in several axial and transverse planes of the aircraft were obtained. The model F16 was tested in the 2 to 40 GHz frequency range. The model was irradiated with both horizontally and vertically polarized radiation. The incident radiation was oriented for nose on, trail on, and broadside angles of incidence.

IR thermograms were taken in four transverse planes of the aircraft: i) in front of the wing, through the cockpit, ii) through the wing section, iii) behind the wing, and iv) through the middle of the tail section.

IR thermograms also were made in two axial planes of the aircraft: i) in the plane of the cross section of the aircraft and ii) in a plane through the middle of the wing.

REMOTE GEOMAGNETIC FIELD MONITOR

Paul R. Barnes*
Oak Ridge National Laboratory
Oak Ridge, TN USA

Fred M. Tesche
Dallas, TX USA

The earth is continuously emersed in the solar wind, a rarified plasma of protons and electrons emitted from the sun. Diurnal variations and small fluctuations in the solar wind cause small variations in the earth's ambient magnetic field. These ambient field variations are important in the analysis of magnetic depth soundings and aerial magnetic surveys. Larger geomagnetic field fluctuations occur during solar storms. Solar flares that erupt during sunspot activity shower the earth with x-rays and charged particles about two days after the eruption. If properly oriented, this plasma cloud can interact with the earth's magnetic field and result in a geomagnetic disturbance (GMD) known as a solar geomagnetic storm. Very intense solar storms produce the brilliant northern auroras and cause significant distortions in the earth's magnetic field that upset communications and electric power systems. A severe solar storm on March 13, 1989 blacked out the entire Hydro-Quebec power system and 6 million people were without electricity. The vulnerability of electric power systems in the Northeast United States could increase during the late 1990's due to the trend of transmitting large amounts of power over long distances to meet the electricity demands of this region. The severe storms expected during the next few years could cause major problems with significant economic impacts.

The U.S Department of Energy (DOE) has installed instrumentation to monitor solar storms. This geomagnetic field monitor is operated by the Oak Ridge National Laboratory (ORNL). It is located in a remote area of the Oak Ridge reservation away from long lines, traffic, pipes, etc. to permit accurate geomagnetic field measurements. It monitors both magnetic and electric fields at a relatively high sample rate of up to 1 sample per second. The monitor is located in an area with no telephone or power service. A Cellular phone data link is being used to download the monitor computer via modem to a data storage computer at ORNL. Power is provided by a solar power system consisting of a photovoltaic array, a charging circuit, and batteries.

Data from this monitor along with data from the U. S. Geological Survey and the Electric Power Research Institute will be used to characterize solar storms. This data will play an important role in reducing the vulnerability of electric power systems to solar storms by providing comprehensive data on the temporal and spatial characteristics of geomagnetic field variations and fill important gaps in our fundamental understanding of this phenomena which is a first step in the development of mitigation methods. Once severe solar storms are well characterized, operational strategies and component and network protection can be designed to enhance electric power system reliability.

This paper describes the monitor design and special problems encountered by the requirement that the system be located in a remote area. A sample of the measured data and comparison with predicted results are also presented.

TIME DOMAIN SHIELDING EFFECT MEASURING TECHNIQUES

Gregor Stricker*, Lars Jendernalik, Christian Pfeiler; Universität Dortmund
Lehrstuhl für Hochspannungstechnik und elektrische Anlagen,
44221 Dortmund

EMC analysis of electrical systems often requires information about the shielding effect of cases. The shielding factor of real cases is highly determined by discontinuities like bushes or cooling ducts. As theoretical treatment of such problem is mostly extensive but coarse, measurement of shielding factor is of high importance, e. g. proof of shielding enclosures. Due to the not totally given comparability of different measuring techniques the stated shielding factor of real cases is somehow uncertain.

Typically shielding factor is measured in frequency domain. Therefore powerful and expensive amplifiers and aerials are needed. Moreover measurement using transient electromagnetic field is possible. Fig. 1a shows the magnetic field strength inside the test volume of a TEM-cell operating with high voltage pulses (Wittler, M.: Zum Einsatz von TEM-Zellen im Hochspannungsimpuls-betrieb. Dortmund 1992). The field strength inside a 19" electronic case placed inside the test volume is plotted in fig. 1b. By comparing the peak values a useful estimation of the shielding factor can be deduced from these plots: $a_H \approx 20\log(\hat{H}_A / \hat{H}_I) \approx 40\text{dB}$. Additionally frequency dependence of the shielding factor can be evaluated by fourier transformation. This measuring technique requires a fast digital recorder and a TEM-cell for high voltage pulse operation, which is rarely available in most laboratories. Therefore a plain shielding effect measuring technique is investigated.

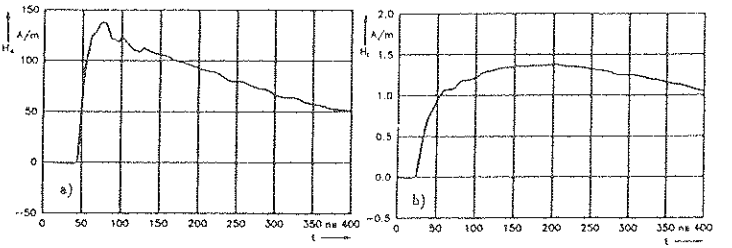

Fig 1: *Magnetic field strength inside the test volume of a TEM-cell (a) and inside a 19" electronic case (b)*

An alternative method measuring the shielding effect shows fig. 2. A fast mains independent pulse generator with a repeating frequency of about 10 Hz radiates an electromagnetic field using a wire loop. A measuring detector with a loop

aerial indicates the field strength. The shielding factor can be evaluated by comparing the frequency dependent peak values of a measurement with and without the casing. Loop aerial and measuring detector are available in many laboratories. A mains independent pulse generator can simply be constructed by a dc-ac converter, a GREINACHER-cascade and a pulse forming circuit. As the rise time of the pulse is about some nanoseconds the upper limiting frequency is equal to customary test receivers (about 30 MHz).

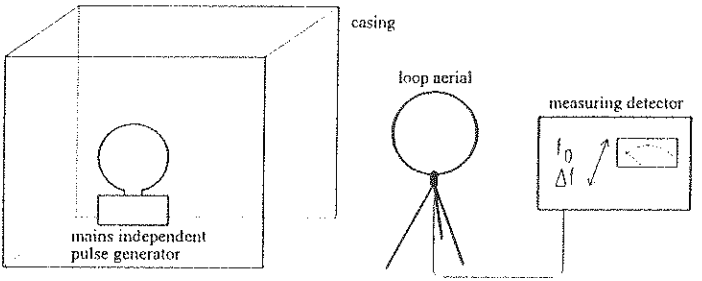

Fig 2: *Shielding factor measuring arrangement using pulsed electromagnetic fields generated inside the tested shielding enclosure*

Fig 3 plots the shielding factor of the 19" electronic case evaluated using the technique described above (fig 2). The shielding effect of the casing deduced from fig 1. is confirmed. Moreover the alternative technique does not need any additional shielding breach for a measuring line. Therefore it is a useful alternative to customary techniques.

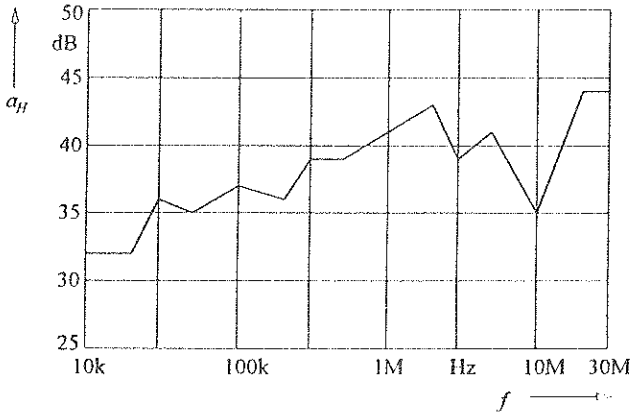

Fig 3: *Measured shielding factor of the 19" electronic case*

CRUCIALLY NEW TYPE OF MICROELECTRONIC SENSOR

Larisa P.Pereverzeva and Yuri M.Poplavko
Kiev Polytechnic Institute, 252056 Kiev UKRAINE.

The future of sensors technique is the "intelligent sensor" in which microelectronic processor is integrated with sensitive elements. However, most of such devices have to use complex combination of various materials: one of them changes its electrical properties under influence of metered parameter while others are semiconductor processor (providing amplification, filtering, read out functions) and some packings, interfaces, electrodes etc. The rigid bound of several materials with a sharp distinction between their chemical and thermal properties poses a lot of problems for technology.

In this work a new way is proposed which permits to use a one-crystal semiconductor sensor at least for thermal and acoustic imaging. This method is based on new effect - thermopiezoelectric response (TPER) which provides possibility of "pyroelectric"behaviour of any piezoelectric (Yu.POPLAVKO and L.PEREVERZEVA, Ferroelectrics, 130, 361-366, 1992; Russian Journal Techn.Phys. 62,93-98, 1992). Of course, this action includes volume piezoeffect as well. The principle idea lies in the fact that one of the most promising semiconductors GaAs are among piezoelectrics. Moreover, semi-insulating GaAs is practically dielectric and it is usually used as a wafer for thin-layer epitaxial semiconductor microelectronics. Essentially, the problem is as follows: how to transform a passive i-GaAs wafer into an"active" thermal- or mechanical-to-electric energy transducer.It is well known that only the crystal of pyroelectric symmetry is operable as a such transducer whereas GaAs and another sphalerite crystals are nothing more than piezoelectric. Figures 1-3 show how to get an artificial pyroelectric response from piezoelectrics of GaAs symmetry.

Usual pyroelectricity is based on spontaneous polarization Ps temperature dependence, Fig. 1. It is important to keep in mind that pyroelectric coefficient p_1 includes the secondary coefficient $p"_1$from the piezoelectrically transformed strains(Fig.2)where e_{1m} is piezocoefficient and a_m is thermal expansion coefficient. Unit cell of GaAs crystal possesses an intrinsic electric polarity which is totally compensated for stress-free sphalerite unit

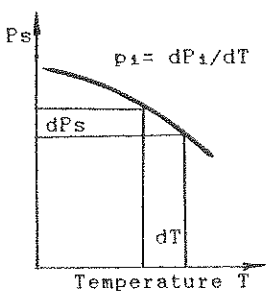

FIGURE 1

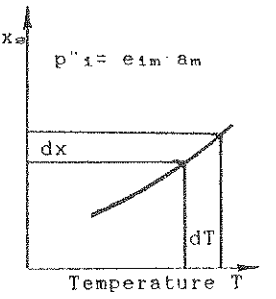

FIGURE 2

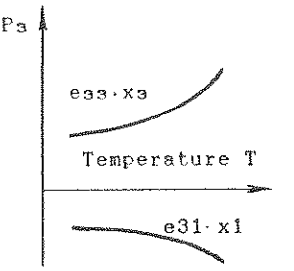

FIGURE 3

cell because four 3-fold polar axes are crossing at the angle of 109.5°. But this self-compensated polarity could be artificially decompensated due to partial limitation of strains under special boundary conditions.Therein lies the TPER, which manifestation is shown on Fig.3.Thin crystal plate of (111)-cut shows longitudinal piezoeffect $P_3=e_{33}\,x_3$ where"3"is [111]-axis and transverse piezoeffect $P_3 = (e_{31}+e_{32})x_3$. The sum of piezoelectric coefficients $e_{31}+ e_{32}+ e_{33}= 0$ so any scalar influences totally compensate each other if crystal is free to expand. This compensation is shown on Fig.3 for GaAs crystal thermal treatment for longitudinal strain component $x_3= a\cdot dT$ and transverse components $x_1= x_2= a\cdot dT$. If the last ones are forbidden by planar clamping the polarization $P_3 = =e_{33}\cdot a\cdot dT$ imitates "pyroelectricity". Fig.3 transforms into Fig.2 so TPER is equivalent to secondary pyroeffect.

Partial clamping was realized by many ways: in our first dynamic experiments the CO_2-laser was used for crystal heating by the modulated thermal beam. Piezoelectric plates or rods were free suspended so a natural electromechanic clamping has been realized. The 0.1 mm thickness i-GaAs plate produces about 2 V/K that corresponds to "pyrocoefficient"= $dP/dT = 1.5\cdot10^{-8}$ C/m^{2}K with voltage sensitivity Sv= 0.02 m^{2}C^{-1}. Our investigations show that some of III-V semiconductors (which is capable to form solid solutions with GaAs) have these parameters 10 times more and above all they are much closer to dielectrics than i-GaAs. By comparison, in the best pyroelectric crystals voltage sensitivity Sv = 0.6-0.4 m^{2}C^{-1} while maximum Sv for III-V compounds is hardly probable more than 0.2 m^{2}C^{-1}. But a water-soluble pyroelectric-champion TGS so as the crystals of $LiTaO_3$-type are difficult to integrate with semiconductor matrix processor. Moreover, all pyroelectric cells in the hybrid-type "pyroprocessor" should have different sensitivity so the effect from these matrix fall short of this ideal.

In one of static experiment the semi-insulating GaAs crystal plate should be stick to substrate with a low thermal expansion coefficient, for instance to fused silica. This is rather convenient for measurements but for device application the special etching process would suffice to provide the planar limitation of strains.In both cases only the thermally induced thickness strain should be possible and just in the direction of [111]-polar axis Thus, the boundary conditions could transform the piezoelectric crystal into "pyroelectric" one.Techniques for producing a volume piezoeffect in i-GaAs wafer is analogues to artificial pyroelectricity. The usual problem of pyroelectric integrated sensor is to provide a negligible thermal contact between pyroelectric crystal and high thermoconductive silicon wafer. The device really need a comlicated system of packings. But in our case the GaAs-type wafer itself is a "pyroelectric" transducer while amplifiers and other microelectronics is no more than very thin epitaxial leyers with ultra low thermal mass.

In conclusion, artificial pyroelectricity in GaAs-type crystals would give rise to a new generation of pyroelectric sensors. Single-element pyroelectric sensor consists of i-GaAs (111)-cut wafer-thermotransducer and FET amplifier integrated on the same wafer which is operating as a "pyrogate". Hundreds of "pyrotransistors" on the same wafer would form matrix thermal image processor which sensitivity increases as square root from cells number (if their properties are identical). The modern microelectronic technology can guarantee the same properties of each cells of such processor and provide read out circuits.

A LARGE GTEM CELL FOR EMC MEASUREMENTS

P. Wilson, F. Gassmann, R. Müller*
EMC Baden Ltd.
CH-5405 Baden, Switzerland

C. Zehntner, H. Haldemann
Defence Technology and Procurement Agency
EMC Laboratory, CH-3000 Bern, Switzerland

EMC Baden, under a contract with the Swiss Defence Technology and Procurement Agency (GRD), is presently realizing a large GTEM 3750 cell for emission and susceptibility testing, both CW and pulse. A GTEM cell, as shown in figure 1, is essentially a flared section of 50 Ω rectangular coaxial transmission line terminated by a broadband load. The termination is a hybrid design consisting of a low frequency matched 50 Ω load and high frequency cone absorber. Such cells are commercially available up to a size of 1750 mm, where 1750 designates the end height of the inner conductor (measured vertically to the floor at the termination). Thus, the planned cell with a final inner conductor height of 3750 mm is some two times larger than existing cells, as indicated by figure 2 which shows the partially constructed cell. Both the increased size and certain performance requirements, such as high input power capability, make modifications to the standard cell design necessary. This paper will highlight the 3750 cell now being realized, its expected performance and the added design considerations. Particular attention will be given to the input module and termination designs.

GTEM cells are attractive as test chambers for a number of reasons. They are shielded enclosures and thus isolated. They are broadband (> 1 GHz) and require no antennas, as the cell itself acts as a transducer. GTEM cells can be used to both generate high field levels and detect small emission signals. And the linear phase characteristics of such cells mean that they can be used in both the CW and pulse mode. The planned GTEM 3750 cell will accept up to 10 kW of input power yielding field levels of 200 V/m over a 3.5 m height. Higher field levels are available by moving the EUT (Equipment Under Test) towards the input section (e.g. at 1500 mm ~ 500 V/m).

The main advantage of this specific GTEM cell is that large objects can be tested for frequencies up to 1 GHz and beyond.

Standard size GTEM cell terminations consist of a large resistor array, typically made with 1-2 W carbon resistors, and carbon-loaded-foam cone absorber. The GTEM 3750 cell is to handle up to 10 kW of input power; thus, on the order of 10,000 standard 1 W resistors would be necessary to form the array. Clearly, such an array would be difficult and expensive to produce. An alternative is to use custom design ceramic "tube" resistors. These have the advantage of high power capability and low inductance. The number of tubes required is relatively low (compared to a standard array) and, should a failure occur, replacing resistors is simple.

As a check, a standard sized cell (GTEM 1500) was retrofitted with tube resistors to check whether field uniformity and performance would be maintained. The results show equivalent performance versus the standard resistor array design.

Another area which has received particular attention is the input module. The high power and accuracy requirements of the 3750 cell necessitate an exacting design. The basic task is to transition from a circular to rectangular coaxial cross section while maintaining a 50 Ω characteristic impedance. This was accomplished using finite element simulations. The resulting transition section has a VSWR of less than 0.5 %.

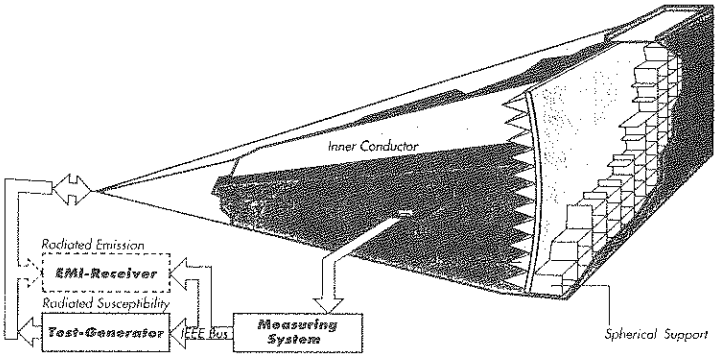

Fig. 1 GTEM cell (standard size 1500), typical application

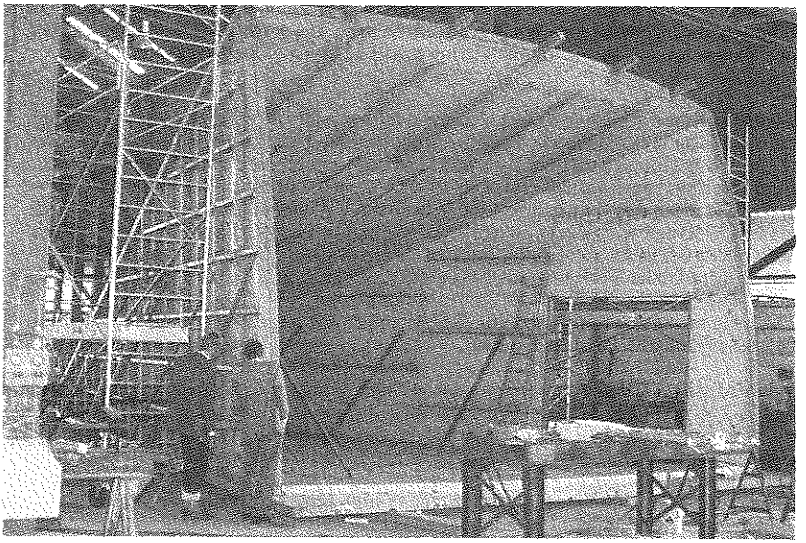

Fig. 2 The GTEM 3750 cell presently under construction.

A Fully Automated Shielding Effectiveness Monitoring System for Continuous Operation Implementing a Digital Synchronous Detector Receiver

F. Broydé *, E. Clavelier
EXCEM
12, Chemin des Hauts de Clairefontaine
78580 MAULE - FRANCE

The present abstract describes the main characteristics of a family of shielding effectiveness monitoring system designed for continuous error-free operation, implementing a digital synchronous detector receiver. The technology of these systems, called VIG 3, stems from the same developpement effort as the VIG 2 technology which was based on analog signal processing (Broydé & Clavelier, Proc. of the 1991 IEEE Int. Symp. on EMC, pp 106-108). However, it features completely new principles and characteristics.

A system according to the VIG 3 technology includes two main sub-systems as shown on fig. 1 : the transmitter sub-system including the transmitter unit (1) and its antenna system (2) on one side of the screened room under test (6), and the receiver sub-system including the receiver unit (3) and its antenna system (4) on the other side of the screened room (6). A multi-channel fiber optic link (5) conveys various frequency and phase information beween the two sub-systems. According to the specific requirement, the location (inside or outside the screened room under test) of the transmitter and receiver sub-systems may be exchanged. The transmitter and receiver have multiple frequency conversion circuits, such that they all use the same frequency references. This scheme is very attractive because it allows perfect stability of the receiver with respect to the transmitter, and a very narrow bandwidth is therefore possible in the receiver. After the over-sampling of a very low frequency last intermediate frequency, VIG 3 implements a sophisticated digital signal processing circuit for the final synchronous detection : a noise-assessment algorithm selects the output of a filter in a cascade of IIR digital filters in a power of 2 bandwidths sequence. This allows an optimum response time for a given accuracy.

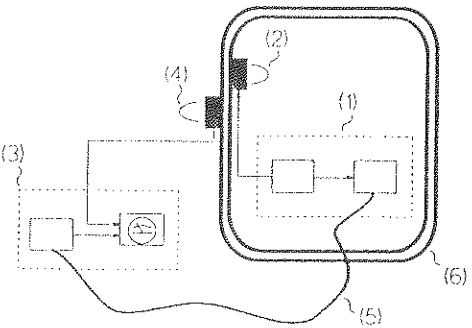

Figure 1 : the VIG 3 principle

The very narrow bandwidth at which a VIG 3 system can operate (1 mHz for instance) brings in itself a very good immunity against the various sources around the receiver. Moreover, the fiber optic links also allow the automatic change of frequency, of antennas in both antenna systems, of power level at the transmitter, etc, in order to reduce, through the processing of various measurement data, the probability of undetected leak, and the probability of false alarms.

The figure 2 shows the installation of a VIG 3 system in a very large hardened telecommunication center with several large rooms. In this case the VIG 3 / model 1 system was selected, which may operate at three frequencies (one in the LF band, one in

the HF band, and one in the UHF band), and is able to select one antenna among 113 antennas in the receiver and in the transmitter sub-systems. The selection of antennas is obtained with antenna switching units which can be installed far away from the receiver and transmitter and be remotely controlled by them, in order to optimize the cabling requirements. LF and HF measurements are very useful for proximity measurements near doors, connectors, etc, while UHF data are useful for a global control of the screening efficiency, thanks to their good propagation and uniformity (helped by multiple reflexions) inside the enclosure.

The VIG 3 technology of shielding monitoring systems exhibits many desirable features for the continuous control of EMP hardened facilities :

— fully automatic measurement and interpretation ;
— very good availability ;
— very high probability of leak detection ;
— very low probability of false alarm.

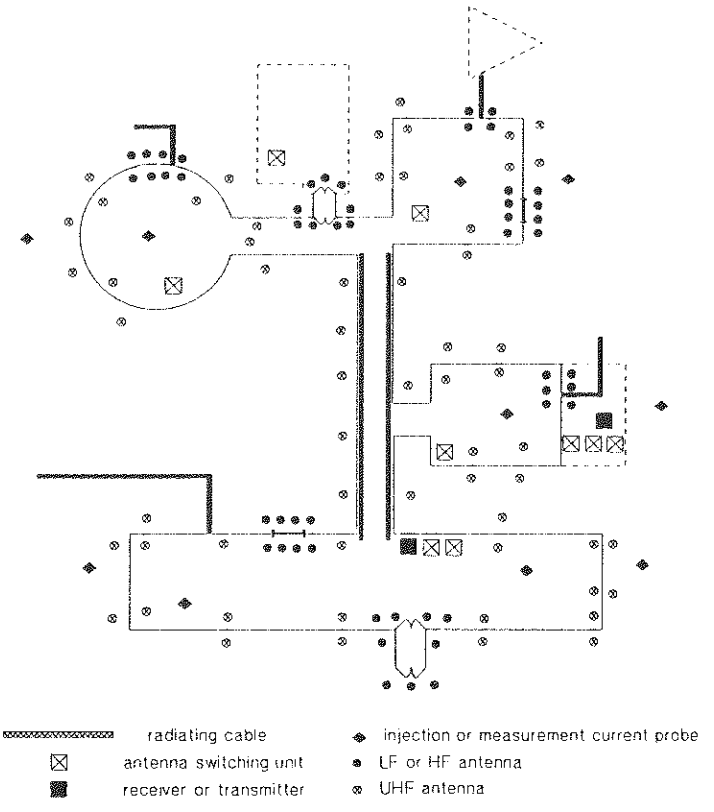

Figure 2 : installation of a VIG 3 system in a very large hardened telecommunication center with several large rooms.

APPARATUS FOR THE FARADAY ROTATION MEASUREMENT IN THE OPTICAL ACTIVE MEDIA.

George A Stanciu

Department of Physics, Polytechnica University of Bucharest

Splaiul Independentei 313 , C P 77206 , Romania.

Introduction.

It is known that if a linear polarized electromagnetic wave propagates trough a medium placed under the influence of a longitudinal magnetic field (with magnetic induction B parallel with the direction of wave's propagation) initial direction of wave's polarization is rotated with an angle called Faraday rotation. In the resonant case , when wave's frequency has a value very close of the transition frequency corresponding of the transition between two atomic levels having the populations n_n and n_m , Faraday rotation angle depends of wave's frequency ,of medium's length and of the refraction indices (n_n and n_m), associated with emitted wave between Zeeman splitted levels of the atom introduced in the magnetic field. In this paper a method for determination of the Faraday rotation which can be used for studies on the gaseous medium and semiconductor materials is presented.

Experimental results.

We have realized a experimental setup to measure Faraday rotation angle of the polarization plane of the laser beam.

In Fig 1 is shown schematical diagram of the setup

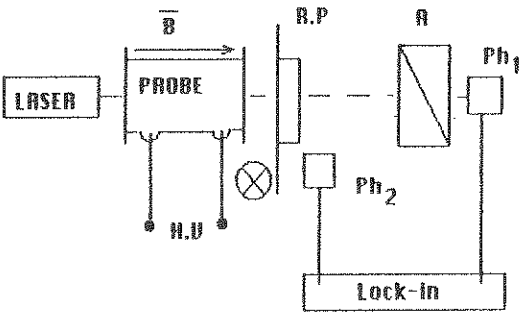

Fig. 1 Experimental setup

The optical active medium was an atomic gas (helium -neon mixture) . A linear polarized He- Ne laser beam (632,8 nm wavelength interact with optical active medium. A DC electric discharge realized a population inversion of a neon . The glass tube with mixture (probe) was introduced inside of the static magnetic field produced by a coil (this field is parallel to the propagation direction of a laser beam and to discharge electric field). After the interaction with Ne atoms , laser beam emerging the glass tube propagates through an rotating polarizer (R P) then laser beam propagates through an analyzer (A) and is received of an photocell (Ph_1 .). The photosignal from photocell synchronized with rotating polarizer is applied to a lock-in amplifier (Ithacomodel 353) . The rotating polarizer is of Leybold type and the analyzer is a Nicole prism mountated on a goniometer divided in hundredth of degree.

Using this apparatus we studied the dependence of rotation angle on the total pressure and on the discharged current . Also , we calculated population inversion existing between neon levels 3s and 2p .

This method can be used with successfully for the studies on semiconductors (the determination of the free carrier effective mass and the informations on the g- Lande's factor)

DOUBLE STIMULATED MANDELSHTAMM-BRILLUEN SCATTERING OF THE ELECTROMAGNETIC WAVES POLARIZED IN THE INCIDENCE PLANE.

V.G.Lapin
Radiophysical Reaserch Institute,
B.Pecherskaya str., 25, N.Novgorod, 603600 Russia
Fax: (8312) 369902; E-mail: lapin@nirfi.sandy.nnov.su

1.We shall discuss peculiarity of the nonlinear interaction of the system of waves, which appears during the process of the incident and reflected within plasma electromagnetic waves scattering on the same sound wave. Such a process is named Double Stimulated Mandelshtam-Brilluen Scattering (DSMBS) and has been intensively investigated recently because of it's low threshold in the laser-made plasma (A.A.Zozulya, V.P.Silin & V.T.Tikhonchuk Plasma Phys.Contr. Fusion, 1986,v.28,p.413; JETP,1984,v.86,p.1296; N.E.Andreev, V.P.Silin, V.T.Tikhonchuk Fizika plasmy,1988, v.14, p.851-858). In these articles full backside but not mirror reflection of the obliquely incident powerfull wave, has been demonstrated. Nevertheless, only the waves, polarized perpendiculary to the incidence plane were taken in to account. In the same time the existence of electric field component in the direction of plasma concentration gradient, caused by the sound wave, will produce additional plasma polarization. As a consequence the more complicated wave icidence angle dependence of the process will take place in this case.

2.Let the isotropic plasma uniform slab is located at $0 \leqslant Z \leqslant L$; and a powerfull electromagnetic wave, with wave"s vector $\vec{k}_1$, in the (X,Z) plane, incides to the $Z=0$ slab boudary. Suppose the incidence angle is equal to θ, and the wave magnetic field vector is collinear to OY-axes (TM-polarization). The $Z=L$ slab boundary reflects the wave and mirror reflected wave appears in the plasma. If a ion-sound wave propagates in the slab in OX direction, then the incident and reflected waves will produce two smaller frequencies scattered waves, which are directed backside with respect to the thirst two waves. Such a system of four electromagnetic and one ion sound waves is a closed one and has absolutely unstable character.

In the case of TM-polarization waves, it is covenient to deal with magnetic field complex amplitude $\vec{H}_y = H_y \equiv H$; $(H = 2Re[H_y \times \exp(-i\omega t)])$ or $\vec{A} = rot\, \vec{E}_y \simeq i\omega/c \times \vec{H}_y \simeq A_y \equiv A$. For the system of electromagnetic waves described above:

$$A = \sum_{j=1}^{4} A_j(\vec{r},t) \times \exp(i\vec{k}_j \times \vec{r}), \qquad (1)$$

where $k^2=\omega^2/c^2\times\varepsilon_0$, $\vec{k}_{1,2}=-(-k\times sin(\theta),0,\mp k\times cos(\theta))$, $\vec{k}_{3,4}=-(k\times sin(\theta),0,\ \mp k\times cos(\theta))$, we shall obtain in the stationary state:

$$\frac{\partial A_1}{\partial Z}=\alpha\times g\times A_3\ ;\ \frac{\partial A_2}{\partial Z}=\alpha\times g\times A_4$$

$$\frac{\partial A_3}{\partial Z}=\alpha\times g^*\times A_1\ ;\ \frac{\partial A_4}{\partial Z}=\alpha\times g^*\times A_2, \qquad (2)$$

where $\alpha\equiv\omega_0^2\times cos(2\theta)/(2kc^2\times cos(\theta))$ is a constant and g is proportional to ion-sound wave complex amplitude v: $\delta N/N_0=2\times Re(v\times exp(i\times\Omega\times(x/v_s-t)))$, N_0- electron concentration in the plasma, Ω and v_s-ion-sound frequency and velosity. The value of g is defined by the ion-sound wave equation, wich in the presence of energy dissipation γ may be writen in the form (stationary case):

$$(\gamma+i\times\Delta\omega)\times g=-\beta\times(A_1\times A_3^*+A_2\times A_4^*), \qquad (3)$$

where $\beta=e^2\Omega/(8\times m\times M\times v_s^2\times\omega^2)\times cos(2\times\theta)$.

The boundary conditions will be:

$$A_1(z=0)=A_{10}\ ;\ A_3(z=0)=0$$

$$A_2(z=L)=A_1(z=L)\times r\times exp(i\times\varphi);\ A_4(z=L)=A_3(z=L)\times r\times exp(i\times\varphi) \qquad (4)$$

where r and φ are the module and the phase of $z=L$ boundary reflection coefficient.

It is interesting that the equations (2)-(4) structure is analogous to that of in the case of TE-polarized waves. Nevertheless there are two differences between them. The thirst is that system (2) describes magnetic fields complex amplitude behaviour but not electric field as in the case of TE polarization waves. The second thing is that α and β coefficients has a factor $cos(2\times\theta)$. If $\theta=\pi/4$ then α and β is equal to zero. In this case the electromagnetic and sound waves does not affect each other, and DSMBS process is fully surpressed. This effect is absent in the case of TE polarized wave, because it is associated with the presence of electric fields components in the direction of plasma inhomogeneities gradient. The additional scattering takes place in this case and the full field can be substantionally diminished due to interference.

A NORMAL WAVES METHOD OF LF AND MF FIELDS CALCULATION IN THE EARTH-IONOSPHERE WAVEGUIDE

V.V. Kirillov, V.N. Kopeikin, Yu.V. Shtennikov
Physical Institute, St. Petersburg University,
198904,Stary Peterhoff,Russia

A normal wave series is being considered for an isotropic spherical stratified earth-ionosphere waveguide (EIW) on low and medium frequencies (LMF). The ray approximation is being applied for the field reflection from the ionosphere described by a smooth profile of electron density. In the medium under consideration, the ray pattern depends on height changeability of "spherical" permittivity

$$\varepsilon_s(r) = (r/a)^2\varepsilon(r)$$

where $\varepsilon(r)$ is the traditional permittivity of the ionosphere and a is the radius of the Earth. In the framework of the theory presented, sufficient attenuation in the ionosphere forces to give the ray turning points a complex character; for the same reason, the rays are complex, too. Is $\varepsilon(r)$ a monotonous function, the real part of spherical permittivity achieves its maximum at a complex height H_0 which has a physical meaning of the EIW axis height. $\mathrm{Re}H_0$ increases with a frequency by a near-logarithmic law: being equal to 50 km (day conditions) and 70 km (night conditions) on 30 kHz, on 3 MHz it increases up to 60 and 85 km, respectively.

The upper turning point H_u lies higher than the axis height ($\mathrm{Re}H_u>\mathrm{Re}H_0$); its value may be obtained from $1-\varepsilon(H_u)=C_2$, where C_2 is square of the incidence angle cosine determined for a corresponding normal wave at the H_u height level. The difference between $\mathrm{Re}H_u$ and $\mathrm{Re}H_0$ increases with a normal wave index. The most essential part of the ray beam includes modes with indices close to m_0, where m_0 is the index of the mode whose incidence is of a grazing character in reference to the earth's surface. For normal waves with indices $m<m_0$, the lower turning point lies at a height H_d between the earth's surface and the axis of the EIW (ionospheric waveguide), whereas for $m>m_0$ it comes to be under the surface, which has no direct physical sense and means the reflection of normal waves from the surface.

By any ray description of reflection from the ionosphere, the phase integral Φ is of particular significance. In this paper, an analytical model of Φ is being employed: as the first approximation, the integration is being made from H_d up to H_u with substitution of the real medium properties by these of free space (here $H_d=H_0$ $H_0>0$, otherwise $H_d=0$). Subsequent approximations are being computed with a quasiexponential form of $(1-\varepsilon)$ function calculated with parameters obtained from the real ionospheric profile at the upper turning point H_u. The phase height H_{ph} is defined as such a height that the "free space" phase integral from 0 up to H_{ph} is equal to the phase integral over the real medium for a given incident angle in reference to the earth's surface. Then the first approximation of the H_{ph} height is given by $H_{ph}\cong H_u-0.164/A_u$ (A_u being the derivative of $\ln(1-\varepsilon)$ with respect to r at the upper turning point), and the triangulation height H_{tr} (related with the derivative of Φ with respect to the spectral parameter) is given by $H_{tr}\cong H_u+1.386A_u$. As it was to be expected

in plasma, $ReH_{ph} < ReH_{\infty}$; on the contrary, $ReH_{gr} > ReH_{\infty}$: the difference makes some kilometers, and it is the larger the more diffuse are profiles of the ionosphere. The A_{∞} parameter has rather a small imaginary part on frequencies between MF and LF bands, which is the reason for imginary parts of all the characteristic heights to be approximately equal.

The key characteristic equation is being constructed on the strength of physical conditions which determine normal waves forming in the EIW. The sticking effect is essential for indices $m < m_{\infty}$, and corresponding eigenvalues may therefore be computed from $\Phi = (m+0.5)\pi$ and do not depend on conductivity of the earth's surface. Morover, this relation allows to estimate the value of m_{∞} as

$$m_{\infty} \cong (3\pi)^{-1} ka(2H_{ph}/a)^{3/2} - 0.5.$$

For example, on 300 kHz m_{∞} makes 17 by night conditions and 11 by day conditions. If the frequency dependence of H_{∞} may be neglected, m_{∞} changes with a frequency approximately linearly. The height distribution of electromagnetic field for $m \cong m_{\infty}$ is being described by the Airy functions which also figure in the description of reflection from the earth's surface.

For normal waves with indices $m > m_{\infty}$ (when the lower turning point comes to be under the earth's surface) the lower limit of the phase integral becomes equal to the Earth's radius, and the characteristic equation has to be transformed in a corresponding way. Further increase of the index makes it possible to make use of asymptotic formulae for the Airy functions, which leads to the description of reflection from the earth's surface by means of traditional Fresnel reflection coefficients. A starting approximation for each eigenvalue is being obtained consistently from a previous one. The logarithm branch fixation ensures a unique solution for each index m with the exception of night conditions on f>50 kHz over the earth's surface with sealand properties. In this exceptional case there is a wave falling out from the normal waves series; its eigenvalue weakly depends on properties of ionosphere and lies near the zero point of the earth's reflection coefficient. As to day conditions, there also are exceptions on f>300 kHz over marine or well conducting sealand regions. Corresponding isolate mode displays lower attenuation, and its eigenvalue is close to the first eigenvalue of a free sphere (no influence of the ionosphere).

ON THE EXPLOSIVE INSTABILITY STABILIZATION IN A MEDIA WITH RANDOM INHOMOGENEITIES.

V. V. Tamoikin*, S. M. Faishtein, A. G. Fakeev
Radiophysical Reaserch Institute, N. Novgorod
B. Pecherskaya st., 25, N. Novgorod, 603600 Russia
Fax: (8312) 369902, E-mail: toga@nirfi.sandy.nnov.su

It is well known (J. Weiland & H. Wilhelmsson, 1977, Pergamon Press), that in a nonequilibrium plasma such as a beam-plasma system, explosive instability is possible. The instability disscused takes place if the highest frequency mode has a negative energy while the other modes of the interacting mode triplet has a positive energies. Explosion will be stabilized in the presence of nonlinear frequency shift, or, in the other words if the cubic terms of weak nonlinearity are taken in to account.

In the present report the qualitative and quantitative characteristics are discussed of the system of three nonlinear equations for the slowly varrying complex wave amplitudes in the case of wave propagation in the media with large-scale refractive index random inhomogeneities. It is obtained that the presence of the random phase discrepancy leads to the unstable explosion with the power-dependence versus slab lehth of the mean waves intensities [in contrast to the situation described in (V. V. Tamoikin, S. M. Faishtein, A. G. Fakeev, JETP, 1990, v. 97, pp. 1159-11650) where is an exponential dependence].

The estimations obtained in the conditions of the cosmic plasma (the Earth and Solar atmospheres) are in qualitative accordance with the experimental Sollar flashes observations (R. Oran & Wite, 1977, Colorado Associated University Press, Boulder). These results are also userfull in constructing the powerfull noise generators in plasma electronics. Besides the results obtained has the theoretical meaning in the nonlinear waves propagation theory.

GENERATION OF POWER ALVEN RADIATION AS A RESULT OF DEVELOPMENT OF EXPLOSIVE INSTABILITY IN BEAM-PLASMA SYSTEM

Belyantsev A. E., Fainshtein* S. M. (Russia, Nizhny Novgorod 603600, ul. Minina, 24, Nizhny Novgorod State Technical University, chair of Applied Mathematics, E-MAIL: NSTU@nnpi, nnov. su. (RelCom), fax: (8312) 36-05-69).

Explosive instability in beam-plasma system was investigated in detail (J. Weiland, H. Wilhelmsson, Pergamon Press, 1977). However the analysis of that instability for alven modes is of interest for practical applications in thermo-nuclear fusion, astrophysics, etc. To present time only linear stage of development of beam instability with dense compensated stream of charge particles, permeating the plasma, has been studied (Dokuchaev V. P., JETPH, 1960, 39, p. 413-415).

In the present paper the dispersional equation for mono--velosity quasi-neutral particle stream, permeating "cold" plasma, is deduced and analysed on the basis of equations for ideal MHD. From the analysis of dispersional equation for normal modes of system the conditions of synchronism and energy of the triplet of waves, interacting owing to resonance, are found out. That is showed, that with weak concentration of particles linear stage of instability is absent and an explosive instability appears. That occurs since high frequency mode energy is negative and energy of other waves of the triplet is positive. With taking into account of cubic terms of expansion in approximation of weak nonlinearity the shorten equations for complex wave amplitudes are deduced and analysed. That is showed, that the "explosion" is stabilized owing to nonlinear breach of synchronism. In accordance of rough estimation received results are of interest for interpretation of flash phenomena in astrophysics, for creation of powerful generators (amplifiers) in solid (P. M. Platzman, P. A. Wolff, Academic Press, New York and London, 1973) and laboratory plasma, and for explanation of experiments in the problem of thermo-nuclear fusion.

AIR SURVEILLANCE RADAR AND REMOTE SENSING DIAGNOSTIC SYSTEMS USING ATMOSPHERIC BREAKDOWN

P. Kossey
USAF Phillips Lab/LID
Hanscom AFB, MA 01731-5000

G.M. Milikh, K. Papadopoulos*, R. Shanny, and R.D. Short
ARCO Power Technologies, Inc.
Suite 850
1250 Twenty-Fourth Street, N.W.
Washington, D.C. 20037

The development of new high power microwave sources in conjunction with advances in phased array technology make possible the creation, in a controlled manner, of artificially ionized regions in the stratosphere and lower ionosphere. The location, electron density, lateral extent and density gradient can be adjusted by controlling the characteristics of large, focused, ground based heater arrays. Such Artificial Ionospheric Mirrors (AIM) can be used as reflectors for VHF Over-The-Horizon (OTH) radar and communications systems [Short et al, GL-TR-90-0038, Geophysics Laboratory Air Force Systems Command, 1990], as well as for remote sensing of the stratosphere and lower ionosphere [Papadopoulos et al, J. Geophys. Res. (in press)]. A critical issue in the design of proof of principle as well as of operational systems that accomplish the detection, communication and remote sensing capabilities associated with AIM, concerns the design characteristics of the ground based focused heaters. The paper uses a combination of analytic theory, computer simulations and system analysis to design two strawman systems; one whose objective is to sense remotely the stratosphere at heights between 30-60 km, and the second to create a reflector at 70 km whose objective is to detect and track low flying aircraft and missiles.

The remote sensing is accomplished by observing from the ground or from space platforms the emission of minority atoms and molecules excited by the electrons produced during a pulsed breakdown [Figure 1]. The results indicate that a ground facility with 3-4 GW power and 100 nanosec pulse length at a frequency of 10 GHz, focused by a 34 m dish can detect minority species in the stratosphere with mixing ratios of one part per trillion. Furthermore, it can do so simultaneously for many species and altitude resolution better than 100 m. Alternatives utilizing more than one reflector and/or more frequencies will also be presented.

The surveillance system based on AIM [Figure 2] located at 70 km altitude requires a phased array with frequency in the UHF band, Effective Radiated Power (ERP) 156 dBW, duty cycle of .1-5%, frequency agility of about 10% and flexible and accurate control of the E field focus. An alternative approach based on an array of reflectors driven by high power L or S band klystrons will also be presented.

*Paper to be presented by K. Papadopoulos

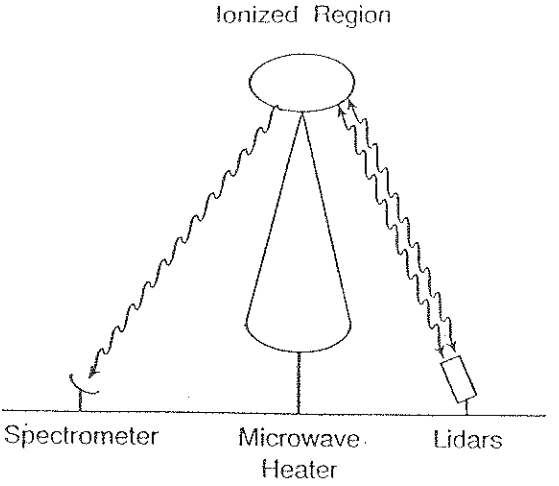

Figure 1

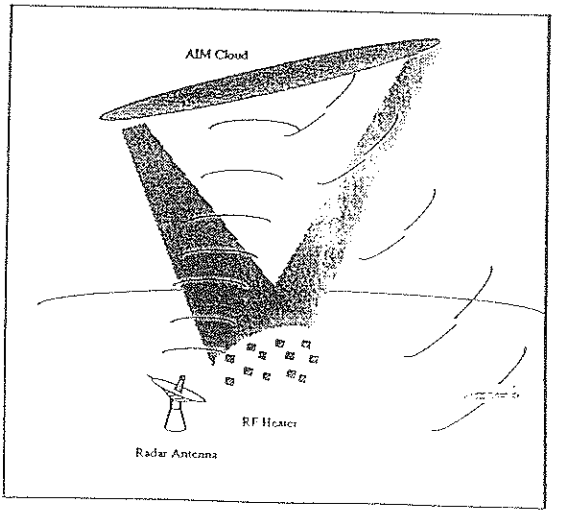

Figure 2

EMC in SMPS: a CAD tool

S. Piedra, E. Fernandez*, J. Basterrechea, M. F. Cátedra
Departamento de Electrónica. Universidad de Cantabria.
39005-Santander, Spain
Phone: +34 42 201493, Fax: +34 42 201402

A tool that forms part of a software package for the Computer Aided Design (CAD) of Switched Mode Power Supplies (SMPS) will be presented. The package is being developed under an ESPRIT project named POWERCAD. To have available efficient and reliable analysis tools of SMPS is being today and urgent necessity because most electronic and telecommunication systems are powered by more and more complex and integrated SMPS. The main objective of POWERCAD is to obtain computer tools that can provide a way to avoid the experimental try and error design cycles that are long and expensive. In order that POWERCAD tools be useful they must run with reasonable CPU times in affordable computers like workstations or top levels PC's.

To obtain this last feature the complete analysis of SMPS will be performed using an electrical simulator (ES) like ELDO, SPICE, etc. In order to obtain reliable results in the analysis (for instance accurate values for the current waves in the SMPS tracks), the input netlist for the electrical simulator is updated with the most significant parasitic phenomena, like layout parasitic capacitances, undesirable inductive coupling between tracks or between tracks and the magnetics (of transformers), parasitic resistance and capacitance in transformer windings, etc. These parasitics are obtained in POWERCAD by using rigorous methods like FE, MM, etc. In addition to these tools to obtain parasitic values, subroutines for the CAD of conducted and radiated noise will be incorporated in POWERCAD. These subroutines must provide predictions in such formats that can be directly comparable with the experimental data obtained from measurements performed following the European normative for EMC.

In particular in this communication the inductive parasitics between tracks and between tracks and magnetics and the models for radiated and conducted noise will be presented. These effects are quite important because SMPS support high levelled pulsating currents. Typically a frequency band between a few KHz and hundreds of MHz should be studied. A frequency domain analysis has been considered because in the HF band the magnetic materials of SMPS is very dispersive. In order to match to the input data format of the ES the circuit tracks are geometrically represented by long and narrow quadrilateral polygons. In nearly all the cases each one of these polygons are associated to each piece of tracks that joins the pads where are blended the terminals of the desired lumped elements. A pulse as basis current is associated to each one of these polygons. In this way an updated netlist

where each polygon is associated to a new branch is introduced to the ES. Also in this netlist-update the parasitic inductive coupling between the new branches is introduced by means of equivalent transformers. These equivalent elements are obtained from the part of the electric field that is due to the potential vector created by the current of the branches. Circuit tracks can be studied in free space or in multilayer environments. In the case of multilayer the potential vector is obtained from a Mixed Potential Integral Formulation that is easily formed in the Spectral domain. In all the cases and to increase the speed of computations, an expansion in terms of powers of the frequency is considered to compute the fields. This expansion allows to consider a quite broadband computing only a few integrals that only depend of the spatial coordinates. In practice our experience indicates that for the most part of the band under study the quasistatic approach is enough.

The computation efficiency is a priority as we are involved with pulsating currents that have a very large broadband. To accomplish with this priority a volumetric Conjugate Gradient Fast Fourier (CG-FFT) scheme has been considered for the analysis of the magnetic elements in transformers. The scheme is an adaptation of a previous formulation developed for scattering, (M.F. Cátedra et al., IEEE, AP-37, 528-537, 1989). This scheme is quite efficient in both CPU-time and computer memory requirements. In the adaptation the original integral equation has been substituted by a Magnetic Field Integral Equation (MFIE) where the unknown is an equivalent magnetic current that is proportional to the magnetic field and to the magnetic susceptibility. The impressed field in this MFIE is computed from the Fourier series expansion of the magnetic field created by the current waves in the transformers windings. Once the equivalent magnetic currents have been computed it is easy to compute the equivalent inductive parasitics between transformers and circuit tracks. Finally the radiated noise is calculated from a direct numerical evaluation of the near field or far field integral expressions considering all the currents (electrical currents in the tracks and equivalent magnetic currents in the transformers).

Now all these models are being validated by comparisons with measurements using a special SMPS designed specifically to test all the tools of the POWERCAD Project. First results of the validation indicate that the models considered provides reliable numerical predictions.

A RELIABLE METHOD TO STUDY CYLINDRICAL WAVEGUIDE TTC ANTENNAS WITH APERTURES

M. F. Cátedra+, J. Basterrechea+, J. de Frutos++, S. Piedra+*
+ Departamento de Electrónica. Universidad de Cantabria
Avda. Los Castros s/n. 39005 Santander. Cantabria. Spain
Phone: + 34 42 201493 Fax: + 34 42 201402
++ Instituto Nacional de Técnicas Aeroespaciales (INTA)

ABSTRACT

A scheme based upon a CG-FFT formulation is presented and applied to the analysis of TTC antennas with apertures. The revolution nature of the antenna and the presence of apertures in its surface make this tool very reliable compared with other techniques.

SUMMARY

Telemetry, Tracking and Control (TTC) antennas require omnidirectional radiation patterns except in the back region of the antenna where they are connected to the structure that uses them. Up to now they were designed using arrays of dipoles or with an obstacle in front of the antenna aperture. This work is concerned with the design of TTC antennas with symmetry of revolution fed by circularly polarized cylindrical waveguide with apertures in the side walls to increase radiation in the desired region and a skirt in the base to reduce radiation in the back region (see Figure 1).

The antenna geometry is defined by the turn of a generatrix around a symmetry axis. An arbitrary number of apertures can be placed at arbitrary positions in the walls.

The feeding system consist in the numerical model of two perpendicular dipoles placed in the symmetry axis and with a phase difference of 90° to obtain circular polarization.

The Conjugate Gradient in combination with Fast Fourier Transform (M.F.Cátedra et al., IEEE, AP-38, 286-289, 1990 and IEEE-AP-S, 790-793, 1991) is used to compute the induced currents in the antenna. This method has been chosen because its flexibility: it allows to consider discontinuities in the walls of the antenna (i.e., the apertures) on the contrary than other classical methods like the Body of Revolution formulation of Method of Moments in which the presence of apertures causes the coupling between the circular harmonics employed in the series expansion of the fields and destroys the method behaviour.

An important point in this type of structures is the antenna mismatching that can produce unacceptable losses. In order to improve the reflection coefficient, the code incorporates the possibility of including matching sections. A good estimate of the reflection coefficient can be obtained from the SWR of the currents in the antenna walls that provides the scheme presented here.

To validate the method, results have been successfully compared with the ones obtained using a BOR formulation of Method of Moments for circular horns.

RESULTS

To demonstrate the method capabilities, the structure shown in Figure 1 has been analyzed. It consists basically in a cylindrical waveguide of 22mm diameter with eight equidistant apertures 1.08mm wide by 5mm height and a section of waveguide that spreads out at an angle of approximately 85 degrees with eight apertures 18mm long shifted 22.5 degrees with respect to the first set. All dimensions including those of the skirt are shown in Figure 1.

The radiation patterns of this antenna are shown in Figure 2. Both copolar (dashed line), crosspolar (doted line) and total (continuous line) patterns are shown as a function of θ angle for the $\varphi=0$ cut.

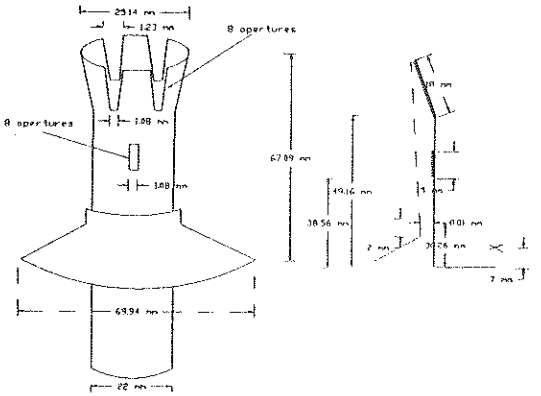

Figure 1. Geometrical dimensions of the TTC antenna analyzed.

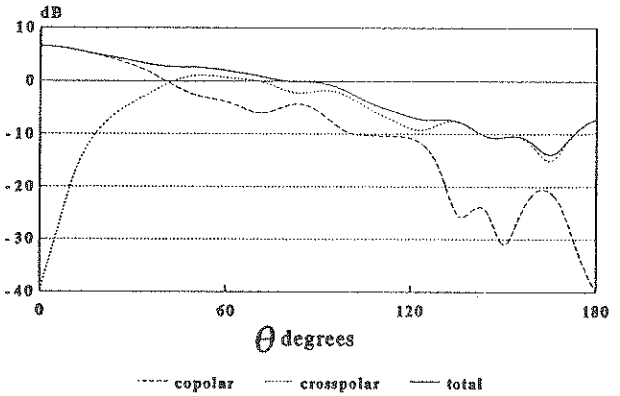

Figure 2. Radiation pattern for the $\varphi = 0$ cut.

Diffraction by a thin and thick slot in perfectly conducting body :

TATOUT F.

The physics of diffraction by a thin and thick slot of a given geometry for Maxwell equation is not easy to calculate. Of course, from a theoretical point of view, there's a long time since the fundamental ideas concerning small apertures and their coupling and scattering properties have been written. These ideas, in complete rupture with the old Kirchoff's approximation, lie in an article from Bethe [Bet] in 1944. Since then, everything has been calculated for some very special geometries : an exact formula for a semi-infinite guide in dimension 2 has been given, using Wiener Hopf or similar techniques, as extensively illustrated in [N] or [KH]. Then by this way, [W] has given an approximate formula for the diffraction through a thick plaque, by a perturbation technique. His formula is valid when the thickness L is much larger than the wavelength and the width d.
However literature doesn't talk much about the influence of geometrical characteristics such as curvature, edges or defaults or gratings in the slot for the diffraction or coupling-related phenomenons. Some other fields of problems appear if the slot is filled with a dielectric or an absorbing material.

In this speech we will concentrate on problems where

-L= 1to 10

-d << λ, typically 1/40 λ

-the hole space is divided in two domains, a perfect conductor and an homogeneous isotropic dielectric, or hollow.

Notice that the approximate formulae given by Weinstein are not valid here.
Few articles give good methods for computing the diffraction produced, and a poor taste of what can happen in such a configuration in general.

An interesting method used in [HA] permitted then to verify the following classical results for a thin slot in T.E illumination [1]:

-some resonances appear when L ~ n. /2.

-the effective width at resonance (i.e, the ratio (energy transmitted/energy density) for a plane incident wave) is about 1/ wavelength, regardless of the actual width, in the case of illumination by a normally incident plane wave .

Their calculation, presented from the point of view of electromagneticians, is based on the moment method together with a decomposition of the problem using some equivalence theorem, which is easily transposable in a mathematic formulation.
These remarks remind of a problem which has been widely (sometimes with some very unfortunate consequences) verified in experiments and in fact impedes the interest given to this type of study : near resonance frequency, or when the excitation is important, we can no longer assume that our material is perfectly conducting. There will appear, either deperdition by Joule effect, or the destruction of the dielectric material filling the slot. These phenomena are not easily computable, especially when the slot is coupled with a cavity, without the use of tremendous numerical calculations. To calculate inside the slot, we have indeed to refine in theory the spatial sampling at least to the scale of its width, assumed to be much smaller than in the remaining domain (which is already large enough for supercomputers!) where it is of 4 to 10 per wavelength, depending on the accuracy of the discretization . For an explicit time-volumic method s.a FDTD, time-sampling must be reduced by the same factor due to CFL

[1] For z-invariant problems, the incident electromagnetic field is said to be T.E (Transverse Electric) when B is z-directed. This corresponds to a 2-D scalar diffraction problem with Neumann bounary conditions. It is said to be T.M (Transverse Magnetic) when E is z-directed, whence corresponds to Dirichlet boundary conditions.

condition to be verified. In a 3D configuration it is conceivable that the processing of thin (planar in approximation) slots will slow down the general calculation to a non negligeable extent, because the density of samplings will be locally multiplied by a 100 to 1000 factor very easily.

This small presentation is as follows : as a motivation we describe the algorithm of Taflove and Umashankar. Then we first describe how we can reduce (time-)harmonic Maxwell equations to scalar wave equations, in a z-invariant problem of an infinite plaque with a slot . We then give some results of majoration of the solution of a 2D Helmholtz equation with Dirichlet, Neuman and impedance-type boundary condition. For Dirichlet there already exists a classical majoration saying that the solution is decaying far from the extrmities of the 2D slot. We adapt the demonstration to obtain a generalization for Neuman boundary condition : the solution approximately depends only on the distance from the extremities ; the error, oscillating in a cross-section, is also (exponentially) decaying. Moreover, the predominant term verifies a Helmholtz equation in the longitudunal coordinate, in a week form, up to a very small error. These two results,easy to generalize for a time-harmonic Maxwell equation, give a rigorous justification of the common approximation for electromagnetician engineers : "*nothing passes through in T.E mode, and the wave is constant in the cross-section for Neuman cindition*". Some numerical calculations using a FDTD method are in good concordance with this. F0or the complete calculus, we give the natural decomposition method, the theory of which is not formalised yet. But this would help us understand some phenomenons taking part in the propagation, and open the way for a fast and convenient method for calculationg the propagation for Helmholtz equation.

A few references:

[Bet] Bethe H.A Theory of diffraction by small homes, Physical Review, vol 66 n° 7&8, 1944, pp.163-182.

[HA] Harrington R.F, Auckland.D.T Electromagnetic transmission through narrow slots in thick conducting screens, IEEE Trans. Antenna Propagation, vol AP28, n°5, 1980, pp. 499-505.

[HM] Hislop P.D, Martinez.A Scattering resonances of a Helmholtz resonator, Indiana Univ. Math. journal, vol 40, n°2, 1991, pp.767-788.

[KH] Kashiap S.C, Hamid A.K Diffraction characteritics of a slit in a thick conducting screen, IEEE trans. Antenna Propagation, vol AP 19, n°4, 1971, pp. 499-507.

[N] Noble B Methods based on Wiener-Hopf technique, New York , Pergamon Press, 1958.

[TU] Taflove.A, Umashankar.K A hybrid moment method/finite-diffrence time-domain approach to electromagnetic coupling and aperture penetration into complex geometries, IEEE trans Antenna Propagation , AP 30, n°4, 1982, pp 617-627.

[VB] Van Bladel J Small hole couplig of resonant cavities and waveguides, Proc IEE, vol 117, n°6, 1970, pp. 1098-1104.

[W] Weinstein L.A The theory of diffraction and the factorization method, Boulder, the Golem Press, 1969.

NONLINEAR SCATTERING OF ELECTROMAGNETIC WAVES BY THIN NEAR-SURFACE FILMS

I.G. Kondrat'ev*, A.K. Kotov
Institute of Applied Physics Russian Academy of Sciences, 46 Ulyanov Str., 603600, N. Novgorod, GSP-120, Russia

A considerable amount of works have been devoted recently to a study of electromagnetic waves scattering on a variety of diffraction gratings (metal and dielectric) with a view to finding out the possibilities and concrete conditions for realizing specific nonmirror regime of scattering (autocollimation, equalpower distribution, etc.). This research is very timely not only for a broad range of general applied problems, but also in terms of solution of specific microwave and optical engineering problems, such as design of effective echelette resonators (applied, in particular, in powerful gyrotrons), power dividers and summators, etc. It is quite obvious that under nonlinear interaction of field and matter (at high power levels) periodic structures can form self-consistently. We find it interesting to evaluate the principle capabilities of nonlinear dynamic diffraction gratings in near-surface thin film coatings. Of course, these conditions limit the possibilities of structural realization (corrugation form), but on other hand, provide additional means of controlling the grating parameters (period, depth) at the expense of the field itself.

Here we illustrate nonstandard scattering capabilities of nonlinear diffraction gratings, using a rather simple model problem. Let two intensive monochromatic ($exp(i\omega t)$) plane waves of p-polarization incident at angles θ_1 and θ_2 to the normal from a vacuum onto a layer of plasma-like medium of thickness d, placed on an ideal metal substrate. Assume further, that the dependence of medium dielectric permittivity upon the amplitude of a high frequency electric field E is described by the expression $\varepsilon=\varepsilon_0+|E|^2/E_c^2$ which corresponds to the conditions of the local cubic nonlinearity. Note, that yexactly in the case of a p-polarized incident radiation when ε_0 is close to zero (plasma resonance) the regime of the most efficient resonance nonlinear field-medium interaction takes place.

Nonlinear interaction of the incident waves with the layer apparently gives rise to a periodic spatial modulation of permittivity along the layer, i.e. induces a self -consistent diffraction grating. In result, higher spatial harmonics with normalized propagation constants Γ_n ($exp(-i\Gamma_n k_0 x)$) equal to $\Gamma_n=sin\theta_1+n(sin\theta_2-sin\theta_1)$ appear in the scattered field. These harmonics can be both spatial (propagating from the layer), and localized (attached to the layer surface). Note, that the incident waves are involved in the general expression for Γ_n presented above and are described by the values of n equal to 0

and 1,respectively, i. e., in standard terms they correspond to the zero and first harmonics.

The problem of finding the stimulation coefficients of corresponding spatial harmonics has been solved in the approximation of a rather thin layer ($k_0 d \ll 1$), which permits the field presentation inside the layer in the form of series over the powers of $k_0 z$ (axis z is normal to the layer). In the result the system of coupled algebraic equations for determination of the indicated coefficients has been obtained, which permits one to realize both analytical consideration and numerical calculations.

Let us have a closer look at the simplest case when only one higher spatial harmonic with the number n=-1 is not localized and yields a plane wave propagating from the layer at an angle $\theta_{-1}=arcsin(2sin\theta_1-sin\theta_2)$; the rest of the higher harmonics (with numbers $|n|\geq 2$) are localized.

It was found out that in this case the energy of the wave incident at angle θ_1 (zero harmonic) is transferred by nonlinear interaction into waves reflected from the layer at angles θ_2 (first harmonic) and θ_{-1} (minus first harmonic). It is clear, that the amplitude of the wave reflected at angle θ_1 is decreasing, while for the wave incident at angle θ_2 the regime of the "superreflection" takes place. Moreover, it turns out that a wave mirror reflected at angle θ_1 can be completely suppressed. We have found the corresponding parameter values and shown that in this situation the energy flow of the wave incident at angle θ_1 is equally divided between two reflected waves (at angles θ_2 and θ_{-1}). Thus, even this simple case reveals original and rather interesting nonlinear regimes of nonmirror reflection. The presence of a large number of nonlocalized harmonics will, no doubt, open a variety of new possibilities.

NEMP HARDENING
THE HARDNESS VERIFICATION PROCEDURE

Jean-Claude BIOTTEAU
CENTRE D'ETUDES DE GRAMAT
46500 GRAMAT - FRANCE

Hervé GRAUBY*
GERAC - B.P. 505
31674 LABEGE CEDEX - FRANCE

1. INTRODUCTION

Whatever the electromagnetic threat considered, any hardening must be demonstrated. Concerning Nuclear ElectroMagnetic Pulse (NEMP), we must :

- show that the NEMP specification is reached,
- evaluate the margins really obtained.

The hardness verification is the procedure which tends to perform these two points. It might be considered for a period that a test performed at the end of the program on the hardened system was the solution. It is now, generally admitted that hardness verification is not only one step, but stretches out all along the hardening program.

This paper explains the methodology of hardness verification. It details the different stages, explains the documents which must be written. The tests are also taken up.

2. THE HARDNESS VERIFICATION PROCEDURE

The different stages are presented in figure 1.

We can see on the diagram some particulary important documents :

- the NEMP specification : it must define the threat, the survivability requirements ;
- the Hardening Definition File (HDF) : it must describe the hardening quite clearly, and how to achieve it ;
- the Hardness Verification Plan (HVP) : written in parallel with the HDF, this plan explains all the actions which must be done for hardness verification (studies, demonstrations, justifications, tests, ...). It also contains a schedule ;
- the Hardening Definition Justifying File (HDJF) : it collects all the justifications necessary for hardness verification, which is pronounced after examination of this file.

These three last documents are now described with more details.

3. HARDNESS DEFINITION FILE

The points to be justified are :

- margins which must be reached and threats considered,
- technical hardening specifications :
  - enclosure shielding effectiveness and equipements susceptibility to radiated transients,
  - cable shielding effectiveness and equipements susceptibility to conducted transients,
  - transient protection devices,
- tests procedures,
- tests results.

4. HARDNESS VERIFICATION PLAN

This document must contain the organization (responsibilities definition), the schedule, the points which will have to be justified and how they have to be (tests procedures, demonstrations, studies).

5. HARDENING DEFINITION JUSTIFYING FILE

It is constituted by the different justifications : theoritical studies, demonstrations, tests procedures, tests results.

6. TESTS

Concerning hardness verification, different kinds of tests can be distinguished, according to whether you want to check :

- compliance with specifications of each device,
- hypothesis considered at the conception of hardening (concerning the coupling or the attenuation of a structure for example),
- whole system performances.

The first ones are generally performed in a laboratory, on discrete devices (equipments, TPD, ...). The other ones are made on the global system. All of these tests allow to evaluate the real margin.

A GO-NOGO type test can be integrated in the hardness verification procedure, but cannot be considered self-sufficient.

7. CONCLUSION

The aims of the methodology presented here are :

- to homogenize the hardness verification procedure,
- to guide the hardness manufacturer in order to : - be more rigorous,
  - choose the most appropriated tests.

This methodology developped for NEMP hardening could also be used for other electromagnetic threats.

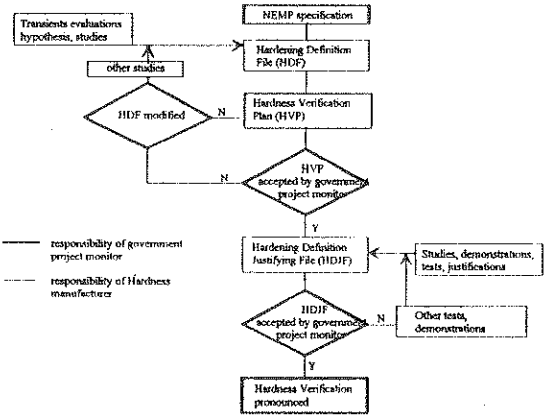

FIGURE 1 : The hardness verification procedure

EMP STANDARD: MIL-STD-188-125, VOL II (TRANSPORTABLE)

Youn M. Lee
U.S. Army Research Laboratory
2800 Powder Mill Road, Adelphi, MD 20783 U.S.A.

*Samuel A. Clark, Jr.
Sol Telecommunications Services, Inc.
4200 Daniels Avenue Suite 101, Annandale, VA 22003 U.S.A

Walter J. Scott
Defense Nuclear Agency
6801 Telegraph Road, Alexandria VA 23101-3398 U.S.A

Through the years, many techniques have been studied and developed to ensure that electronics survive when subjected to the potentially deleterious effects of various environments, including electromagnetic pulses resulting from high-altitude nuclear detonations. However, none of these mitigation techniques were universally standardized until the publication of volume I of MIL-STD-188-125, High-Altitude Electromagnetic Pulse (HEMP) Protection for Ground-Based C^{4}I Facilities (June 1990). This paper is a condensation of a new standard (volume II of MIL-STD-188-125) that covers HEMP hardening of transportable, ground-based C^{4}I (command, control, communications, computers, and intelligence) systems that require network interoperability during and after exposure to HEMP environments.

The standard is designed to integrate HEMP hardening measures with those of other electromagnetic disciplines (such as electromagnetic interference/electromagnetic compatibility, lightning protection, and TEMPEST) and with treatments for other hardening requirements.

The standard requires hardness program managers to develop design and engineering, fabrication, installation, and testing activities to accomplish the following objectives: (a) provide a low-risk HEMP-protected system design based upon verifiable performance specifications; (b) verify hardness levels through a cost-effective program of testing and analysis; and (c) during the acquisition process, develop a maintenance/surveillance program that supports the operational phase of life-cycle HEMP hardness.

System protection against the HEMP threat environment is achieved by the enclosure of all mission-critical systems (MCS) in electromagnetic barriers and also with special protective measures as required. If the transportable system is composed of separate transportable pieces (subsystems), each of the subsystems that is an MCS must be enclosed in an independent electromagnetic barrier. Special protective measures must be implemented when HEMP hardness cannot be achieved with an electromagnetic barrier alone and in other special cases.

The subsystem HEMP shields must be welded or brazed metallic enclosures that meet or exceed shielding effectiveness requirements and follow the construction requirements. The number of subsystem shield POEs is limited to the minimum required for operational life, safety, and habitability. Each POE is HEMP protected with POE protective devices that satisfy the performance requirements.

All intrasite cables are routed on the surface of the ground (or buried) when the system is deployed. Connections to long intersite lines are minimized. As a design objective, the system

design must enable the disconnection of long intersite metallic cables such as commercial power, telephone, and other signal lines from the system during operational deployment. A long line protection module can be used as a option for intersite line connections. The system is provided with HEMP-hardened electrical power generation and distribution capability sufficient to perform missions, without reliance upon commercial electrical power sources.

All MCS that will operate satisfactorily and compatibly within the subsystem shields are installed inside an electromagnetic barrier that meets the performance requirements of the standard. No HEMP-unique performance characteristics are required in the design/selection of MCS that will be housed within a barrier. MCS and rf (radio frequency) antenna subsystems that must be placed outside an electromagnetic barrier are provided with special protective measures as required to ensure HEMP hardness in the HEMP threat environment. RF communications equipment connected to an antenna whose signal line penetrates the electromagnetic barrier is housed in a separate subshield within the subsystem shield. Transient suppression/attenuation is provided to protect the rf communications equipment.

Special protective measures are implemented where HEMP hardness cannot be achieved with an electromagnetic barrier alone. Additional shielding, transient suppression or attenuation devices, and equipment-level protection are provided as required to achieve HEMP hardness.

The HEMP testing program demonstrates that hardness performance requirements have been satisfied and that the required HEMP hardness has been achieved. This program include quality assurance testing during system construction and equipment installation, acceptance testing for the electromagnetic barriers and special protective measures, and verification testing of the completed and operational system. Documentation requirements for test planning and test reporting are described in four appendices: A, B, C, and D. All data acquired during the HEMP testing program is stored on electronic media for ease of test reporting and subsequent use as a hardness maintenance/surveillance data base.

Quality program requirements are implemented during system construction and installation to demonstrate that the HEMP protection subsystem materials and components comply with the performance requirements. The quality assurance test procedures and results are documented for use as baseline configuration and performance data for the hardness maintenance/hardness surveillance program.

HEMP acceptance tests of the electromagnetic barriers and special protective measures are conducted after all related fabrication work has been completed. As a minimum, acceptance testing must consist of shielding effectiveness (SE) (appendix A) testing of all HEMP shields, and pulsed current injection (PCI) (appendix B) testing of all electrical penetrations. Acceptance test procedures and results are documented for use as baseline configuration and performance data.

After completion of the HEMP protection subsystems and installation/operational checks of the subsystem equipment, the HEMP hardness of the system is verified through a program of tests and supporting analysis. The verification program provides a definitive statement on the HEMP hardness of mission functions of the system under test. As a minimum, verification testing consists of SE or continuous wave illumination (CWI) (appendix C) for barrier shields, PCI and SE or CWI for electrical POEs and piping POEs, threat-level illumination (appendix D) and PCI for MCS outside the barrier, PCI for MCS within the barrier and MCS that failed during barrier PCI, and PCI plus SE for special protective barriers. In lieu of the minimum requirements, verification testing can consist of PCI for electrical POEs, piping POEs, and MCS outside the barrier, threat-level illumination for systems, and PCI for system elements too extensive for testing in existing threat-level illumination simulators.

DEDICATED MEASUREMENT SYSTEM FOR QUALIFICATION AND MAINTENANCE OF SHIELDING ENCLOSURES

J.Y. TOUCHAIS
ALCATEL CABLE, Département Electronique et Electromagnétisme,
35 rue Jean Jaurès, 95871 BEZONS Cédex

1. INTRODUCTION

This paper is an overview of the state of the art in shielding enclosures qualification and maintenance measurement systems.
The technology and performance of shielding enclosures are briefly reviewed before and then followed by an analysis of the main related standards. After describing the measurement systems usually used, we conclude with a description of the specific solutions we have designed and developed.

2. SHIELDING ENCLOSURES

Shielding enclosures are still widely used : they provide the best solution in terms of cost benefit ratio in protecting sensitive equipment from electromagnetic radiation (induced by lightning or NEMP) and in protecting access to classified information.

Today manufacturers build shielding enclosures that show a very high level of attenuation toward the electromagnetic fields, up to more than 130 dB in the 1 MHz to 1 GHz frequency range.

If the owner of a shielding enclosure is sure to find such a level of attenuation on the day of delivery, it is obvious that some time later the attenuation will begin to decrease. Therefore, shielding enclosures should be periodically inspected because their shielding effectiveness can deteriorate over a period of time and use.

3. TEST PROCEDURES

The test procedures used in shielding effectiveness measurements are well known and were established as early as 1956 in the American standard MIL STD 285.

All the usual standards have common points in their measurement methods :

- the measurement hardware is similar :
  - an emission system that creates the electromagnetic field by the means of a generator and an antenna,
  - a reception system that measures the level of the residual field with an antenna connected to a receiver.
- the procedure is identical :
  - during the first step (reference measurement) the level of the field created by the emission system is measured by the reception system in free space,
  - then a measurement of the residual field is made (attenuation measurement), with the two antennas (emission and reception) on each side of the wall to check.

The main differences observed among the several methods used by a large number of experts in this field lie in the hardware contents of the system.

4. SHIELDING EFFECTIVENESS MEASUREMENT SYSTEM

When the first standards were written, the recommended standard measurement equipment available was as follows:

- selective voltmeter, with poor frequency stability, and therefore poor selectivity and/or sensitivity - coupled to an external attenuator,
- signal generator with high energy consumption and large dimensions, providing relatively small power signals with poor frequency stability,
- passive antennas chosen among the basic following types : loop (magnetic dipole), rod (electric monopole), electric dipole.

Of course all the recommended equipment - except for the antennas - has long since become obsolete. Improvements come mainly from the use of synthesized oscillators in both emission and reception devices that provide a very good frequency stability and accuracy. More and more people today use a spectrum analyzer instead of a selective voltmeter for shielding measurement.

But this kind of shielding measurement system still presents three main drawbacks :

- heavy and bulky measurement system
- non battery operable system
- complex system

5. SPECIFIC MEASUREMENT SYSTEMS

The measurement systems developed by ALCATEL CABLE are dedicated systems which have been specifically designed for checking shielding effectiveness.

We have taken into account suggestions given to us by numerous laboratories which have many years of experience and possess significant knowledge in this domain, with specific mention to our own laboratory which has been of great help to us (20 years experience on many different sites and configurations).

As for measuring or monitoring shielding enclosures, we have designed a set of three systems that correspond to three different types of measurements :

- the shielding attenuation measurement system **MABE** is aimed at performing complete qualification and maintenance of shielding enclosures. The measurements are conducted in accordance with the procedures stated in the American standard MIL STD 285 and the French standard GAM T 20. This system can also be adapted to other specific standards.

- the device for Faraday's cage monitoring **DISCA** , designed with the technical support of the STEI, is based on a "go-no go" test for continuous surveillance and regular monitoring of Faraday cages.

- the feedthrough tester **SYVAR** enables the measurement of shielding enclosure leakages through all feedthroughs. This is done with a high voltage pulse generator and a specific set of probes and measurement equipment. Its principles have been established by the Centre d'Etudes de Gramat.

The major improvements provided by these systems are the following :

- lightweight and portable system
- battery operable system
- easy to use (not only reserved for highly trained specialists) due to a friendly interface user software.

THE UK'S REGULATIONS FOR COMPLIANCE WITH THE EC DIRECTIVE ON ELECTROMAGNETIC COMPATABILITY (89/336/EEC) AND EXPERIENCE TO DATE

A.E.J.Bond, Department of Trade and Industry (DTI)

1. INTRODUCTION

Given the completion of the legislative process, whereby on 28 October 1992 the EMC Directive 89/336/EEC was transposed into UK law, manufacturers of electrical and electronic products who elect to comply with the essential requirements of the Directive, during the transition period ending on 31 December 1995, are now in a position to do so.

The topics to be covered in this extended abstract which give support to the statement above are as follows:

- Outline of the United Kingdom's Regulations
- Appointment of Notified and Competent Bodies
- Guidance on the preparation of a Technical Construction File
- Continued dialogue with the EC Commission on clarification and implementation of the Directive
- DTI/Findlay Publications national EMC awareness campaign

2. UNITED KINGDOM'S EMC REGULATIONS

From its inception the basis of the EMC Regulations has been to give clear and unambiguous legal definition to the contents of the EC Directive and the means of complying with its essential requirements. This has necessitated going into detail on such matters as:

- Definition of terms and interpretations.
- Relevant apparatus, modified applications, transitional exclusions, general exclusions, specific exclusions, apparatus covered by other Directives - wholly or in part.
- Requirements for supply (placing on the market) or taking into Service.
- Conformity assessment requirements - the three routes to compliance.
- Presumption of conformity, the CE mark and EC declaration of conformity.

- The standards route to compliance.
- The Technical Construction File route to Compliance.
- The EC type-examination route to compliance.
- Enforcement authorities and powers, penalties and prohibition notices.

By virtue of the above descriptions, the Regulations are intended to give comprehensive guidance on the legal responsibilities which fall to a manufacturer, supplier, importer or user of electro-technical products under the terms of the EMC Directive and the penalties for violating national law. Equally, the Regulations stipulate the legal basis of enforcing the Directive and the limitations imposed upon the approved bodies, ie. Notified and Competent who are appointed by the Secretary of State for Trade and Industry, in exercising their responsibilities under the terms of the EMC Directive. (Copies of the Regulations can be obtained from HMSO and its outlets e.g. W H Smith. A booklet describing the main provisions of the Regulations and another giving guidance on their application are available from the Department of Trade & Industry).

3. APPOINTMENT OF NOTIFIED AND COMPETENT BODIES

For the purpose of issuing EC type-examination certificates under the terms of Article 10.5 of the Directive, and in respect of radio-transmitting equipment, the following bodies have been appointed and notified to the EC Commission:

- The Radio communications Agency of DTI.
- The Civil Aviation Authority.
- The Defence Research Agency (Maritime Division).
- The British Approvals Board for Telecommunications.

For the purposes of issuing reports or certificates under the terms of Article 10.2 of the Directive, and in respect of the Technical Construction File route to compliance, the bodies listed in Annex 1 to this extract have been appointed and also notified to the EC Commission for communication to the other EC Member States.

4. GUIDANCE ON THE PREPARATION OF A TECHNICAL CONSTRUCTION FILE (TCF)

In response to widespread demand for guidance to manufacturers, test laboratories and competent bodies on the preparation and content of a Technical Construction File, beyond the information given in Article 10.2 of the EMC Directive, the DTI has issued a document to be read in conjunction with its Regulations. It has no legal status and manufacturers are advised to consult with their chosen Competent Body on its contents and acceptability for use before embarking upon the preparation of their technical file. The document also points out in the foreword that changes to its content may be necessary in the event of the EC Commission issuing its own guidance.

5. EMC NATIONAL AWARENESS CAMPAIGN

Following invitations to tender the DTI has awarded a contract to Findlay Publications to run its national awareness campaign. The campaign will run from 1 January 1993 to 31 March 1995, and the launch was made at a special event hosted by Edward Leigh MP, Parliamentary under Secretary of State for Trade and Technology, at the Queen Elizabeth II Conference Centre on 12 January 1993.

The aim of the campaign is to draw to the attention of industry, business and commerce operating in the electro-technical field the details and legal implications of the EMC Directive and the mechanisms for achieving compliance. The campaign will include regional seminars, publications, magazine articles, text book and video material, local EMC clubs and a 'telephone hot line' for information on sources of practical help and guidance. It is intended that the campaign should build upon and interact with the many valuable initiatives which are taking place in the field of EMC awareness, and also to link with the various national and regional organisations offering technical advice and assistance at the levels of design and testing for EMC compliance.

A copy of Mr Leigh's speech together with details of the elements making up the awareness campaign are contained in a DTI booklet 'Eliminating Electromagnetic Interference - Background Notes - January 1993.

ELECTROMAGNETIC HARDENING SUSCEPTIBILITY and COUPLING : a PROBABILISTIC APPROACH

P. RIAUBLANC - G. BERREBI - J.C CURTINOT

THOMSON CSF / RGS DEN / DER
66 Rue du FOSSE BLANC 92231 GENNEVILLIERS FRANCE

This communication discusses how to tackle the electromagnetic hardening by using a probabilistic approach in the objective to optimize this hardening.

Components susceptibility as well as equipment susceptibility is characterized by a statistical distribution. It is the same for a conducted aggression (voltage , current) which comes from a conductor coupling (antenna, transmission line) with an electromagnetic pulse (EMP for example). These data knowledge allows to define a protection for a given survival equipment probability.

Before using this process it is necessary to have resources and methods. This communication proposes to describe THOMSON CSF / RGS used resources to reach this goal.

At first the equipment susceptibility determination (methodology aspect) is discussed . Calculated examples show this process. This methodology uses, at first, the susceptibility components knowledge by :

-- using previous works (by WUNSH , TASCA , PEDEN and component susceptibility THOMSON data base)

-- present works (experimental measurements results)

The second aspect deal with electromagnetic aggression determination in a probabilistic term. The aggression (current , voltage) may be characterized by standard deviation σ and a maximal value. EMP coupling with transmission lines is the example used in this article.

From a software using transmission line formalism and E.F VANCE model the probabilistic approach interest is showed with the help of numerical simulation results. Open circuit voltage and short circuit current induced by EMP are characterized by a distribution function with its standard deviation.

AEMC

COMPATIBILITE ELECTROMAGNETIQUE

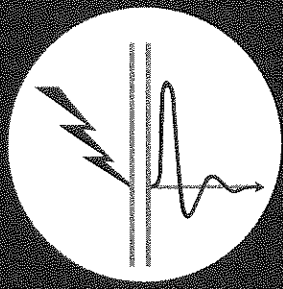

VOUS CONCEVEZ, INSTALLEZ :

Systèmes numériques	Automates
Cartes analogiques	Instrumentation
Electroniques de puissance	Automobiles

★ ★ ★

MAIS...

Des perturbations électromagnétiques et autres parasites s'insinuent au cœur des électroniques...

AEMC vous propose

- **DES COURS APPLIQUES : nombreux Travaux Pratiques.**
- **INGENIERIE : mise à disposition d'un ingénieur dans votre Société.**
- **DES CONSULTATIONS EFFICACES : AEMC MESURES (Paris et Lyon) est à votre disposition pour vous assister dans la mise en conformité de tous vos appareils électroniques aux normes CEM applicables en 1996.**

AEMC : 86, rue de la Liberté
38180 SEYSSINS
Tél. : **76 49 76 76**
Fax : **76 21 23 90**

NUMERICAL METHOD FOR EM SCATTERING ANALYSIS NONSPHERICAL ATMOSPHERIC PARTICLES

Yu.Eremin[1)]*, N.Orlov[1)], and V.Rozenberg[2)]

[1)]Faculty of Appl. Math.&Computer Sci. of Moscow St. Univ., Vorobjev's Hills, Moscow 119899, Russia
Fax: +7-095-939-2596; E-mail: eremin@cs.msu.su

[2)]Faculty of Appl. Math. of Russian St. Pedagogical Univ., Nab.reki Moiki, 48, S.-Petersburg 191186, Russia
Fax: +7-812-352-7531; E-mail: brondus@sovam.com

Problems of EM scattering by atmospheric particles are very important for researchers due to multiple practical applications. So, when investigate atmosphere by wheather radars the work wavelength happens to be very sensitive for presence of atmospheric particles. As result it arise such effects as attenuation of propagating field, scattering, depolarization, etc. At this report the method for simulation of multiple scattering by atmosphere hydrometeors is presented.

This method seems very efficient to calculate EM scattering by non-spherical atmospheric particles (Yu.EREMIN, N.ORLOV & V.ROZENBERG, Computer Physics Comm., accepted for publ.). The scattered field is represented as superposition of multipoles' fields. They satisfy analytically to the Maxwell' equations, radiation conditions and they are represented as a superposition of elementary functions. The efficiency of the method allows to employ personal computers only. We are able to investigate dielectrical particles having sizes up to 10 wavelengths and to control the accuracy of the calculated results.

This technique was applied to the scattering problem of TM/TE plane wave (wavelength is 3.2 cm) by atmospheric hydrometeors. The hydrometeor shape was chosen in accordance with (C.C. CHUANG

& K.V. BEARD, J. Atm. Sci., 47, No.11, 1990) and following to the real hydrometeor forms. The research of the scattering characteristics were performed for the different values of incline angle of the particles with respect to direction of plane wave propagation and also for the different particle shapes corresponding to the different values of external forces (electrostatic stress, surface tension, etc.). Comparison of scattering characteristics with results got from spherical approximation of the particle shape using was performed. We established there exists the diapason of the particle radiation angles for which the scattering characteristics strong differ from ones for the spherical particles. So, the limits of spherical particles' approximations for atmosphere hydrometeors were established.

The investigation of wave scattering using the dynamical model was performed. It allows to calculate the multiple scattering by the cluster of strong interacting particles. The particles differing one from others by shape and permittivity can be used as elements of the cluster. This model seems very useful when investigate the wave propagation through active atmosphere "melting layer" in that hydrometeors are in the state of fragmentation and coagulation. Results of complete EM analysis of such systems show the essentially different mechanism of scattering by cluster of strong interacting particles than by non-interacting ones. The class of scattering characteristics allowing for fixed radiation parameters and fixed sizes to determine the distance D over that cluster's particles become non-interacting was exposed. It was shown when distance between cluster's particles is less than D model of non-interacting particles is inapplicable.

So, the presented method was applied for numerical analysis of wave scattering by atmospheric hydrometeors and the limits of validity were established for: 1) spherical equivolume approximation for atmospheric particles' forms; 2) model of atmospheric particles' congestion as set of non-interacting particles.

THREE-DIMENSIONAL MODELLING OF LOWER IONOSPHERE PERTURBATIONS AND THEIR EFFECT ON SUBIONOSPHERIC VLF AND LF RADIO WAVE PROPAGATION

OLEG. V. SOLOVIEV
Radiophysics Department, St. Petersburg State University
198904, St. Petersburg, Russia.

The effect of large-scale 3D ionosphere inhomogeneities on VLF and LF radio wave propagation in the Earth-ionosphere waveguide proves to be rather complicated phenomenon. The impedance models of the Earth-ionosphere waveguide are investigated to evaluate this effect quantitatively. We assume our model guide to be of the height h and bounded by regular Earth surface S_0 with impedance δ_0 and by ionosphere wall Si. The last one is characterized by inhomogeneous surface impedance $\delta(R)=(\delta_0$ if $R \in S_p$ and δ_p if $R \in S_p)$, $S_p \in S_i$ and defines geometrical shape of perturbation. Thus two problems arise: the first is to determine the most valid parameters: h, δ_0, δ_p. The second problem is to obtain the field of a point source in the cavity with specified parameters.

From given electron density $N_e(z)$ and collision frequency $\gamma_e(z)$ height profiles of day-time unperturbed ionosphere we obtain h and δ_0. These values are found as solution of the following problem: we consider a plane wave obliquely incident (at an angle Φ) to inhomogeneous half space with plasma ($N_e(z)$, $\gamma_e(z)$). The nonlinear differential equation for $\delta(\Phi,z)$ is solved numerically in the height range 100-40 km which is of the most importance for VLF propagation. The impedance value $\delta^*(\Phi,z)$ corresponding to the limit of integration (40 km) is used to calculate the impedance on the height h. The effective height of a guide h is obtained as the minimum of derivative $\left| \partial\delta(\Phi,z) / \partial\sin(\Phi) \right|$. The eigenvalues of regular impedance waveguide ν_m, m=1,2,... are calculated using parameters h and δ_0. The above procedure is successively repeated until the following equality satisfies a given precision: $\sin(\Phi)=\nu_m$, m=1. These iterations lead to the value δ_0 that is very weakly depends on ν_m eigenvalue number. Hence, the obtained parameters of our model may be used to simulate multi-mode propagation.

In order to calculate δ_p we need $N_{ep}(z)$ and $\gamma_{ep}(z)$ profiles for perturbed ionosphere. Such data for the ionosphere illuminated by a powerful HF transmitter were published (M. A. ITKINA, D. S. KOTIK, Z. N. KROTOVA et al., Preprint NIRFI N162. Gorki, 1983). The same our procedure is employed to calculate the value δ_p. The impedance value $\delta_p^*(\nu_1,z)$ corresponding to the limit of integration is used to calculate the impidance δ_p on the height h. So the impedance model of irregular Earth-ionosphere waveguide is assumed to be completed. The location of irregular patch Sp on the surface Si may be arbitrary.

Let we proceed with the point source field in the considered model waveguide. In the scalar approximation we may relate unknown attenuation function V(R) and attenuation function for uniform waveguide $V_0(R)$ by the following integral equation:

$$V(R)=V_0(R)+(ikr/2\pi)\iint_{Sp}(\delta_p-\delta_0)V(R')V_0(R,R')\frac{e^{ikr(r'+r^*-r)}}{r'\,r^*}dS', \qquad [1]$$

where $R(r,\phi,z)$-observation point, $R'(r',\phi',z')$-integration point, k - free-space wavenumber, $r^*=\sqrt{r^2+r'^2-2rr'\cos(\phi'-\phi)}$.
The equation [1] admits various approaches for solution. In particular we have developed a asymptotic $(kr>>1)$ procedure allowing to study the case of large irregularity that was not treated with the aid of direct numerical approach (E.C.FIELD, Trans.IEEE.5,831-836,AP-30, 1982) and seems to be intractable by successive approximations technique. For the details and results of our method the interested readers are referred to our next paper presented herewith.

Here we continue to discuss the modelling of subionospheric propagation in irregular waveguide. The validity of our model was tested by considering the diffracting effect of a patch of ionosphere, illiminated by a powerful HF transmitter, on VLF radio wave propagation (O.V.SOLOVIEV, XX1Vth General Assembly URSI. Abstracts,639, 1993, Japan). Numerical simulation exhibited a good agreement with the measured field data.

To our knowledge the proposed scheme to compute perturbed impedance value δ_p corresponding to the same height h as that of regular guide becomes invalid when the perturbation is strong. The word "strong" means that the lower ionospheric layer in the perturbed area substantially descents (or ascents) thereby causing the effective height to change for more than 5-8 km. In such a case another model of localized ionosphere perturbation is proposed. We assume a truncated cylinder with a perfectly conducting lateral surface St standing on the surface Si. The base of cylinder Sp is characterized by two values: h_p - effective waveguide height, and δ_p - perturbed impedance value corresponding to h_p. These values are to be obtained from perturbed profiles $N_{ep}(z)$ and $\gamma_{ep}(z)$ exactly following the procedure which was used for calculating h and δ_0 from N_e and γ_e. The attenuation function in the waveguide with prominent cylinder is governed by the following equation:

$$V(R)=V_0(R)+(ikr/2\pi)\left(\iint_{Sp}V(R')\left[\delta_pV_0(R,R')-\frac{\partial V_0(R,R')}{ik\,\partial z'}\right]\frac{e^{ikr(r'+r^*-r)}}{r'\,r^*}dS'+\right. \qquad [2]$$

$$\left.+\iint_{St}V_0(R,R')\left[\frac{\partial V(R')}{ik\,\partial n'}+(1-1/ikr')\frac{\partial r'}{\partial n'}V(R')\right]\frac{e^{ikr(r'+r^*-r)}}{r'\,r^*}dS'\right)$$

where n' is the normal to St directed out of the cavity of waveguide. The lateral surface St contribution to diffracted field given by the second integral in [2] is shown to be not significant. This result of numerical experiment proves to be consistent with the physical theory: no one ray reflected from lateral surface of cylinder and received at any observation point located below the base of cylinder can be found. So we contemplate evaluating St contribution by using perturbation technique. As for integral equation on the surface Sp, here we are going to use our 3D asymptotic procedure mentioned above.

Broad-Band Detection of VLF-Atmospherics and Correlation with Meteorological Data

H. L. König*, R. Kulzer, A. Gerl
Technische Elektrophysik der TU München
Arcisstr. 21, 80290 München
and
H.-D. Betz
Sektion Physik der Universität München
Am Coulombwall 1, 85748 Garching

Similar to ELF-atmospherics, VLF-atmospherics (sferics) are caused by atmospherical electrical discharge processes which produce both pulse-shaped electric and magnetic alternating fields. The shape of the detected sferics-signal depends strongly on the kind of discharge and the conditions of transmission between the position of origin and detection. The frequency dependence of damping and dispersion along the transmission path becomes important because of the relatively extended band width (from below 1 to far above 100 kHz) of the original signals. In the past the basic properties of sferics have been mainly investigated with measuring techniques that sensed sferics-spectra in different frequency-ranges with a very small band-width. In contrast we developed an efficient computer-assisted broad-band measuring (low-cost) system which allows detection of the true shape of sferics-signals and immediate analysis.

The signals are characterized by low frequencies (and accordingly large wavelengths), so that the distant field conditions are not fulfilled for sferics which originate too close to an observation station. The newly developed wide-band antenna system, however, allows a completely separate registration of the electric and magnetic field components of the sferics-pulses.

In a first step, and by utilizing only a single receiver station, a computer code was developed to evaluate and display the angular distribution of sferics for chosen time intervals and, thus, to localize the direction of pronounced sferics-clusters with respect to the location of the station. In order to better assess the performance of the system and the significance of the recorded data, clusters of thunderstorms (lightning centers) were determined independently by purely meteorological techniques for the same observation time-intervals. The result was a very good correlation between the two types of data for the clusters.

In a second step, a total of three spatially separated, automatically operating receiver stations were set up. The data from the two additional stations is transmitted to the primary station, where the data processing takes place. While the data from a single station can only provide the direction towards the source of a sferic, application of triangulation techniques to the data from two or three stations allows to obtain the spatial coordinates of each sferic event and to map the source points on a continuous basis. Insofar, the resulting data is not expected to differ too much from the one obtainable by utilizing various other systems such as, for example, established lightning tracking systems.

Additional information, however, can be obtained from our system when each sferic pulse (i.e. the time-dependent signal) is fourier-analysed and when the resulting frequency-dependent spectra are compiled to groups representing the various spatially connected clusters of sferics activity. An analysis of these frequency distributions in the range between some 1 and 100 kHz has already revealed that different clusters may exhibit significant differences in the structure of the spectra. Beyond doubt, one of the reasons for this finding lies in the different transmission properties of the atmosphere between the cluster and the receiver stations. Further work is needed to disentangle this influence from characteristic emission properties of sferics clusters, and to possibly extract relevant meteorological information associated with these cluster areas.

AN ASYMPTOTIC 3D APPROACH TO THE PROBLEM OF ENVIRONMENTAL VLF AND LF RADIO WAVE PROPAGATION IN THE PRESENCE OF LOCALIZED IRREGULARITY

VYACHESLAV V. AGAPOV and OLEG V. SOLOVIEV
Radiophysics Department, St.Petersburg State University
198904, St.Petersburg, Russia

This paper is to present a three-dimensional approach to compute the point source field in irregular Earth-ionosphere waveguide. An irregularity is assumed to be of finite lateral extent. In this case the one-dimensional mixed-path approximation (E.L.FEINBERG, Radio Wave Propagation Along the Earth's Surface, 1961) proves to be inaccurate and the conventional two-dimensional integral equation turns to be too expensive for numerical implementation (E.C.FIELD, Trans IEEE. S,831-836,AP-30, 1982). We are aimed at employing asymptotic technique to simplify computational procedure and, nevertheless, to retain in solution all the features of field behavior that are intrinsic to three-dimensional diffraction problems.

We consider an impedance model of Earth-ionosphere waveguide consisting of two boundaries S_e and S_i characterized by surface impedances δ_e and δ_i. We suppose that one wall of our model waveguide contains an impedance discontinuity S_p of finite size (localized), so we may call it "patch" or "island". The irregularity S_p is characterized by inhomogeneous surface impedance $\delta_p(R)$.

In scalar approximation the unknown attenuation function $V(R)$ for vertical electric dipole in irregular impedance waveguide may be related to the attenuation function $V_0(R)$ for the same source in uniform waveguide by the following integral equation:

$$V(R)=V_0(R)+(ikr/2\pi)\iint_{S_p}(\delta_p-\delta_0)V(R')V_0(r^*,z',z)\frac{e^{ik(r'+r^*-r)}}{r'\,r^*}\,dS' \qquad [1]$$

where $R(r,\phi,z)$ - observation point, $R'(r',\phi',z')$ - integration point, k - free-space wavenumber, $r^*=\sqrt{r^2+r'^2-2rr'\cos(\phi-\phi')}$, $\delta_0=(\delta_i$ if $S_p\in S_i$ and δ_e if $S_p\in S_e)$. This equation [1] is rather versatile. If the suitable $V_0(R)$ is substituted it will govern the point source field above an inhomogeneous impedance plane or sphere, in a plane or spherical impedance model of irregular Earth-ionosphere waveguide.

First, we introduce elliptic coordinate system (u,v): $ch(u)=(r'+r^*)/r$, $\cos(v)=(r'-r^*)/r$ to perform the substitution of variables of integration. The asymptotic transverse integration with respect to u retains the terms up to the order of $O((kr)^{-1})$ (L.B.FELSEN & N.MARCUVITZ, Radiation and Scattering of Waves. 1975). The remained integral with respect to v may be represented as contour integral along the boundary of discontinuity ∂S_p:

$$V(R)=V_0(R)+\frac{\sqrt{kr/2}}{2\pi}(\delta_p-\delta_0)\oint_{\partial S_p} \exp(ikr(ch(u(v)-1))\, I(v)\, dv \qquad [2]$$

where $f(u(v),v)=V(R')V_0(R,R')$ if $R'\in \partial S_p$, $p=\sqrt{2kr}\ sh(u(v)/2)$,

$I(v)=e^{i\pi/4}\sqrt{\pi}\ f(0,v)\ W(e^{i\pi/4}p)+(f(0,v)-f(u(v),v)/ch(u(v)/2))/p$,

$W(x)=\exp(-x^2)[1+(2i/\sqrt{\pi})\int_0^x \exp(t^2)dt]$.

The integral operator in [2] may be splitted into two items: $V=V_0+AV+BV$, where A is the operator which acts on the function $f(0,v)$ performing the integration along the straight line from the source to the current observation point. The remained part is designated as B. We should stress that A is Volterra integral operator containing the main term of asymptotic expansion. A simple numerical procedure can be used to invert it (e.g. C. WAGNER, J. Math. Phys. 4,289-301, 1963). So, the following algorithm is proposed: $V^{(0)}=V_0$, $V^{(n)}=V_0+AV^{(n)}+BV^{(n-1)}$, $n=1,2,3,\ldots$ Unlike the Volterra operator from one-dimensional integral equation (E. L. FEINBERG) the operator A contains the $W(\exp(i\pi/4)p)$ function in the kernel. Thus, even in the first approximation we have noticeable three-dimensional effects such as backward reflection and oscillating transverse diffraction pattern. In addition, the convergence of our combined inversion-iteration procedure proves to be very rapid almost everywhere.

In order to employ the time-consuming advantage of our scheme we considered the groundwave propagation in the presence of comparatively large discontinuity. The following parameters were chosen: frequency 100kHz; impedance of the ground $\delta_0=(0.8334-0.83331)\cdot 10^{-9}$, impedance of the patch $\delta_p=(0.1871-0.08761)$; transmitter point $(x=0,y=0,z=0)$. The elliptic patch $((x-x_0)/a)^2+(y/b)^2=0$ was characterized by: $x_0=90$km, a=30km, b=9km and b=24km. The attenuation function values were calculated at the line x=180km, z=0km. The figures below illustrate these transverse diffraction patterns.

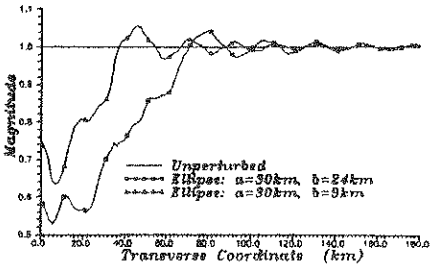

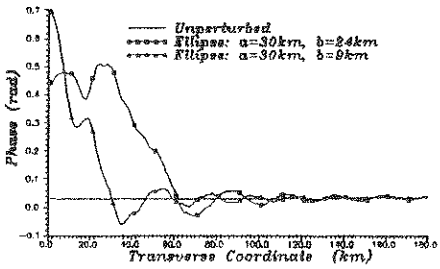

The developed asymptotic three-dimensional algorithm exhibits the very good agreement with earlier results obtained with the aid of the rigorous two-dimensional integral equation [1] (G. de JONG, Radio Sci. 11,925-933, 1976). Moreover, the drastic reduction of CPU time (varies as patch perimeter in square) in comparison with direct numerical procedure (varies as patch surface in square) is achieved.

THE RECEIVER ANTENNA PATTERN EFFECT IN MULTIPATH PROPAGATION ENVIRONMENT

Manuel García Sánchez(*)[1], Leandro de Haro Ariet[2], Antonio García Pino[1] and Miguel Calvo Ramón[2].
[1] Departamento de Tecnologías de las Comunicaciones. E.T.S.E. Telecomunicación. Universidad de Vigo. 36200, Vigo, Spain.
[2] Departamento de Señales Sistemas y Radiocomunicaciones. E.T.S.I. Telecomunicación. Universidad Politécnica de Madrid. Ciudad Universitaria. Madrid, Spain.

The characterization of the propagation mechanism is of great interest to compensate channel effects in radio digital communication systems. In many radio channels, propagation takes place by more than one path from transmitter to receiver, due to reflections and diffractions in the surrounding environment or refractions by the atmosphere.

Because of multipath propagation, the received signal is sum of attenuated and delayed versions of transmitted signal, so the existence of different paths causes diversity in time and the presence of frequency selective fading. Moreover, attenuation and time delay may be time variant by the medium changes or by the motion of the receiver, so a frequency diversity appears and the fading behavior also changes with time. Multipath channel is then characterized by the Power-Delay Profile and the Scattering functions defined by Bello (1: P. Bello, IEEE Trans. on Comm. Syst., Dec.1963) to study linear randomly-time-variant systems.

The receiving antenna effects should be added to the propagation channel mechanism to obtain a complete characterization of the radio channel. Signals propagated through different paths are received at different directions, so the radiation pattern of the directional receiving antenna adds an a different scaling factor. This scaling factor would depend on the angle at which each signal is received, so to account the effect of the antenna pattern in the received signal, the angles corresponding to each propagation path must be known.

To account for the receiving antenna effects sometimes very simple hypotheses about the distribution of these angles $p(\alpha,\tau)$, have been made (2: M.J. Gans, IEEE Trans. on VT, Feb. 1972), but these simple hypotheses may lead to errors in channel characterization if directional antennas are used (3: W.C.Y. Lee, IEEE Trans on AP, May, 1973). On the other hand measuring these angles may be difficult if not impossible (4: R. Steele, Pentech Press, 1992).

A novel method is proposed which avoids the referred problems and predicts the channel Power Delay Profile and Scattering Function corresponding to an arbitrary receiving antenna from those determined for another known antenna pattern.

First, the spatial distribution of the received signals is extracted from a measured Scattering Function, assuming that propagation takes place in a horizontal plane using the relation between Doppler shift and angle of signal arrival. If for a symmetric radiation pattern $G(\alpha)$ the Scattering Function $S(\nu,\tau)$ is (2:):

$$S(\nu,\tau)=\frac{2\cdot p(\alpha,\tau)\cdot G(\alpha)}{\nu_m\sqrt{1-\left(\frac{\nu}{\nu_m}\right)^2}} \tag{1}$$

$p(\alpha,\tau)$ can be solved from a measured Scattering Function:

$$p(\alpha,\tau)=\frac{1}{2\cdot G(\alpha)}S(\nu,\tau)\nu_m\sqrt{1-\left(\frac{\nu}{\nu_m}\right)^2} \tag{2}$$

Once the spatial distribution of the received signals is found, the Scattering Function corresponding to another receiving antenna pattern can be calculated using equation 1.

As an example of this method, figure 1 shows a Scattering function for hilly terrain. Figure 2 shows the corresponding spatial power distribution, and figure 3 the resulting Scattering function if a receiving antenna with the radiation pattern shown in figure 4 is used.

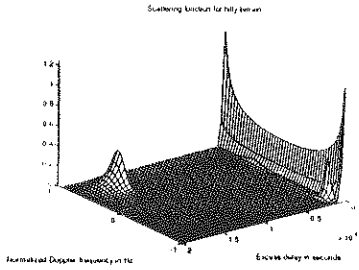

Figure 1

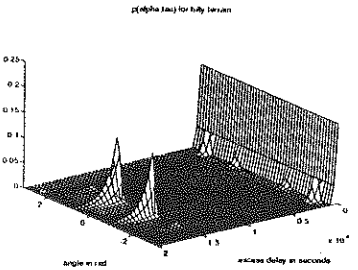

Figure 2

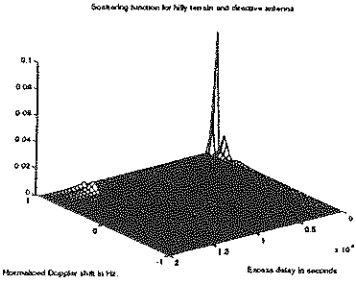

Figure 3

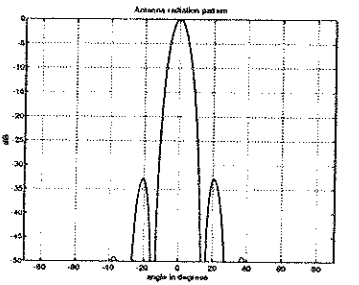

Figure 4

HEMP ENVIRONMENT POLARIZATION AND INCIDENCE ISSUES FOR COUPLING PROBLEMS

By

W. A. Radasky*
M.A. Messier
Metatech Corporation
Goleta, California

In recent years considerable progress has been made in standardizing the High-Altitude EMP (HEMP) environment, in particular by the International Electrotechnical Commission (IEC). Because this standard is defined for commercial purposes and because of the expectation that a future conflict may involve a small number of bursts, more interest has been shown in understanding the "statistical" behavior of the HEMP. This interest is especially aimed at the early-time ($t < 1$ microsecond) waveform and its use in performing coupling calculations.

For early-time HEMP coupling, there are two principal areas of interest. These include the polarization of the EM field and the angle of elevation of the line of sight above the Earth's horizon. The polarization is dependent on the HEMP generation mechanism which is due to the geometric field orientation in the high-altitude source region. Simple equations and graphs are provided that describe the polarization variations in different parts of the world.

The second issue involves the angle of elevation of the HEMP at an observer position of interest. For the assumption of a single high-altitude burst, we present a series of calculations that indicate the cumulative probabilities of particular elevation angles as a function of burst height. These calculations indicate that line of sight elevations of 10 degrees or less above the horizon are typical.

The paper concludes with a set of Earth reflection calculations performed using the IEC early-time HEMP environment for typical elevation angles and polarizations of interest. These results clearly demonstrate the range of environments that should be given priority in future analyses and testing.

CONSIDERATIONS CONCERNING EARLY-TIME HIGH-ALTITUDE EMP STANDARD WAVEFORMS

K.-D. Leuthäuser
Fraunhofer-Institut für Naturwissenschaftlich-Technische Trendanalysen (INT)
Appelsgarten 2
53881 Euskirchen, Germany

Calculations of the early-time HEMP show a considerable variability with yield and height of burst as well as with the observer location with respect to Ground Zero. In addition, the results are dependent on shape and energy spectrum of the gamma source. Further uncertainties arise from incomplete data on air chemistry, e.g. time lag in the formation of secondary ionization and electron avalanche coefficients.

The EXEMP code developed by the author (K.-D. LEUTHÄUSER, Theoretical Note 363, Oct 1992) was extensively employed to investigate the whole variety of HEMP waveforms. Absolute worst case results in terms of peak rate of rise and peak electric field magnitude are obtained for hypothetical delta function and decaying step function gamma sources. More realistic source functions may be described by a quotient of the sum of two exponentials (QEXP)

$$S(t) = S_0 / \left(\exp(-\alpha t) + \exp(\beta t)\right)$$

with rise-coefficients α assumed to be of the order of a few ns^{-1}, and decay coefficients $\beta \approx 0.1 ns^{-1}$.

For any height of burst and observer location, the EMP field can be characterized by the four quantities

(I) $\left(dE/dt\right)_{pk}$: peak rate of rise

(II) E_{pk} : peak electric field

(III) $\frac{1}{Z_0}\int_{-\infty}^{+\infty} E^2(t)dt$: energy fluence W_∞

(IV) $\int_{-\infty}^{-\infty} E(t)dt$: impulse I_∞

In order to derive a single worst case standard waveform covering the whole variety of conceivable individual waveforms, the heigths of burst and observer locations on ground are determined for which the quantities (I) to (IV) are maximized, keeping the gamma yield of the weapon (10 kt) and the average energy of gammas (2 MeV) constant. The results are summarized as follows together with the corresponding heights of burst and observer locations (LOC) with respect to Ground Zero in Cartesian coordinates:

	Gamma Source Function	Delta Function	QEXP $\alpha \to \infty$ [1]	QEXP $\alpha = 5\ ns^{-1}$	QEXP $\alpha = 1\ ns^{-1}$
(I)	$\left(\frac{dE}{dt}\right)_{pk}\left(\frac{kV}{m \cdot ns}\right)$	1.2×10^4	165	85	57
	T_r (ns)	.01	.31	.69	3.0
	HOB (km)	60	60	60	95
	LOC (km)	35 S [2]	43 S	63 S	153 S
(II)	E_{pk} (kV/m)	96	68	67	60
	HOB (km)	115	107	115	135
	LOC (km)	166 S	155 S	174 S	217 S
(III)	W_∞ (J/m^2)	.083	.093	.094	.094
	HOB (km)	200			
	LOC (km)	(650 E or W; 200 S)			
(IV)	I_∞ (Vs/m)	1.98×10^{-3}	2.0×10^{-3}	2.0×10^{-3}	2.0×10^{-3}
	HOB (km)	600			
	LOC (km)	2000 N			

1) corresponds to decaying step function

2) reads as : observer location 35 km southward of Ground Zero

Obviously, only one of the four quantities can be maximized for a single burst at a particular observer location. Each of these four electromagnetic pulses governs a particular frequency range in frequency domain: (I) maximizes the high-frequency part of the spectrum, (II) the high-intermediate, (III) the low-intermediate, and (IV) the low frequencies. The envelope of these curves in frequency domain can therefore be used to construct an analytic worst case waveform in time domain.

The data show that the maximum values (II) to (IV) are practically independent of the particular gamma pulse shape, except for the hypothetical delta function at lower HOBs. At the lowest altitudes considered, peak rate of rise and rise time T_r (10% to 90%), respectively, are essentially those of the gamma source function. Hence, some reasonable assumptions are required with respect to the source functions unless the lowest HOBs and observer positions near Ground Zero are excluded from consideration.

SOME CHARACTERISTICS OF THE ULF NOISE ELECTRIC ENVIRONMENT

S. V. Anisimov, S. S. Bakastov
Geophysical Observatory, Institute of Physics of the Earth
Russian Academy of Science, Borok, Yaroslavl, 152742 Russia
E. A. Mareev*
Institute of Applied Physics, Russian Academy of Science
46 Ulyanov st., Nizhny Novgorod, 603600 Russia

1.Short-period pulsations of electric field are an integral part of atmospheric electric noise environment. Their origins and spatio-temporal characteristics in the surface atmospheric layer remain an important and still unsolved problem, although it is studied for some recent decades.

For the investigation of short-period fluctuations in the frequency range $10^{-3} \div 1$ Hz, continuous measerements of electric field and vertical current density were performed at the Borok Geophysical Observatory ($58.03°N, 38.97°E$) since February, 1986. The observation conditions are characterized there by the absence industrial pollutions and low level of electromagnetic noise. An electric field is measured by an electrostatic fluxmeter of "Field Mill" type, specially constructed for these purposes. Its sensitivity is of order of 0.1 V/m.

Electric field in the the surface atmospheric layer can be considered as a locally homogeneous one with the smoothly changed average:

$$\mathbf{E}(\mathbf{r},t) = \mathbf{E}_0(z,t) + \Delta\mathbf{E}(\mathbf{r},t) \qquad (1)$$

where $\mathbf{E}_0$ is the averaged over the small scales electric field, which can change due to global generators and depends upon the vertical coordinate z owing to the electrode effect. $\Delta\mathbf{E}$ is the field of small scale pulsations, caused by local turbulent processes. We will refer below to the vertical component of electric field, which was measured in our experiments.

For the study of electric field pulsations in the surface atmospheric layer it is useful to find experimentally the structural function, being determined as a realization ensemble-averaged the squared modulus of a difference of electric field perturbations in remote points $\mathbf{r}_0 + \mathbf{r}$ and $\mathbf{r}_0$ at the moments $t + \tau$ and t respectively :

$$D_E(\mathbf{r},\tau) = \langle \mid \Delta E_z(\mathbf{r}_0 + \mathbf{r}, t + \tau) - \Delta E_z(\mathbf{r}_0, \tau) \mid^2 \rangle \qquad (2)$$

A system made to analyze spatio-temporal structures of the electric field of the near-Earth atmosphere, consists of five electrostatic fluxmeters of the "Field Mill" type placed in one line on the height $h \simeq 1.5$m at the distance r each from another; r was varied from 5 to 20 m in different experiments. The direction of the line was changed from the north to the south. The experimentally determined reduction coefficient was at this height $K_r \simeq 0.1$. The threshold sensitivity of the sensors was equal 0.1 V/m, the dynamic

range of measurements has been not less than 80 dB. The stripe filter unit separated out frequencies whithin the band $f = 10^{-3} \div 1$ Hz, and the differential amplifier has been used for obtaining corresponding differences of the analogue symbols. An IBM PC/AT with a program of digital representation permitted us to realize the algorithm for calculation of the structural function $D_E(r)$. The spectrum analyzer of the parallel type gave the possibility to find spectral characteristics in the real time-scale. The experiments on measuring structural functions and spectra were performed in the winter, spring and summer periods of 1990-1991. The basic meteorological parameters as humidity, temperature, direction and velocity of the wind, were recorded. The results, discussed in this paper, correspond to the fair weather conditions only. The total period of analysis has been more than 300 hours.

2.A typical structural function obtained by averaging over ensemble of differential signals from remote sensors (placed relative to the basic one at the distance no more than 20 m) , has the form of a smooth power function r^m with the index $m = 0.5 \div 1$ (under different experimental conditions), which rather differs from the common linear Kolmogorov's dependence of $[D_E(r)]^{1/2}$ on $r^{1/3}$ for scalar component.

For the distances $r = 20 \div 80$m two types of the structural functions have been obtained. The first of them is well approximated by the power function $r^{2/3}$ within all the range of r variations . However, the most probable case in the mentioned range of distances (in about 9 cases out of 10) is when the structural function becomes more flat at the scales of $r \simeq 20 \div 60$m and rises at scales longer than 60m. The relation between the scales L_0 and L_1 depends on the particular experimental conditions.

Analyzing empiric structural functions, one should conclude that the characteristic external scale L_0 of electric field pulsations in the surface layer lies within the limits $r \simeq 20 \div 60$m. Let us take into account that the the external scale of the turbulence L_0 is determined by the height of the Earth's surface layere h_*: $L_0 = \kappa h_*$, where $\kappa \simeq 0.4$ is the Karman's constant. So, one can state from the experimental results presented that the near-Earth layer were situated up to the heights $50 \div 150$m over the substrate surface, which is in accordance with early estimations. The rise of the structural function at the distances longer than 60 m emphasizes the existence of the corresponding scale of charge pulsations and is probably determined by the convection mechanism. Separation of large scales shows the possibility of volume charges generation in the Earth surface layer being carried up to the heights of the upper boundary of the atmospheric exchange layer.

3.We have presented here the results of investigation of atmospheric electric field pulsations in the frequency range from 10^{-3} to 1 Hz measured at a height 1.5 m above the ground under fair weather conditions. For the analysis of pulsation characteristics the concept of a structural function $D_E(r)$ is used. The found structural functions allow to single out an external turbulent scale $L_0 \simeq 20 \div 60$m, characterizing the height of the surface layer. On the other hand, our results testify to the existence of electric field perturbations with the scales $r \gtrsim L_1 = 60$ m, which are caused, probably, by convective cells. One can note that a volume charge, formed due to the electrode effect, could be transferred by these cells along the Earth's surface and carried off from it. It gives substantial contribution in the ULF electric noise environment.

ELECTROSTATIC DISCHARGE CALCULATIONS USING AIR CHEMISTRY MODELS DEVELOPED FOR NUCLEAR EMP

By

Michael A. Messier*
Metatech Corporation
Goleta, California

The calculation of the electromagnetic pulse (EMP) generated by a nuclear burst requires the use of air chemistry models which are accurate over the time frame of the pulse (sub-nanosecond to millisecond). These models have been developed over several decades of EMP research, but are not generally known outside the EMP community. This paper describes a prototype finite difference code (SPARK2D) which uses some of these air chemistry models in the calculation of an electrostatic discharge between two electrodes. The code assumes azimuthal symmetry, a bilateral symmetry plane between electrodes, and utilizes a simple outer boundary condition for the purpose of demonstration. The air chemistry models accept relative humidity and air density as parameters. A three-species calculation tracks electron and positive and negative ion densities. Processes considered are electron avalanching and attachment, electron-ion recombination, and ion-ion recombination. Avalanching and attachment are treated as functions of local electric field. For the purposes of these calculations, the recombination rates are considered independent of E-field.

The very act of attempting to set up a finite difference calculation of air breakdown is instructive and leads to several insights into the breakdown process. For example, it is well known that once a discharge commences, the risetime is very fast (sub-nanosecond). The discharge takes place on a time scale much shorter than the time over which converging electrodes can move any significant distance so that electrode distance can be considered constant over the time frame of the initial discharge. For a given initial charge (or potential difference, or electric field at the electrode tip), the discharge can occur over a relatively wide range of electrode separations; this distance can vary from one experiment to another as, for example, a charged electrode is brought closer to a metal plate. Therefore, one must ask the question: what is the mechanism that initially triggers the discharge? One possibility is background radiation. Random gamma rays and the high energy electrons generated by their collisions with air molecules can produce ionization trails along which a discharge develops.

SPARK2D allows the initial potential difference between electrodes to be specified. The electrode is a bump on a perfectly conducting plane; the plane forms the lower boundary condition (B.C.). The upper B.C. is also E-tangential = 0,

which can represent either a perfect conductor or a mirror image symmetry plane. In either case, there is an image electrode an equal distance on the opposite side of the plane. We choose to use this boundary condition as a symmetry plane. The difference is in how one defines the initial potential difference. In the case of SPARK2D, the potential difference is defined as that between the electrode and its image, rather than between the electrode and the plane. The electrode has the shape of a cylindrical pyramid. The user defines its radius and height above the conducting plane. The code approximates this shape using finite difference cells of the size defined by the user. The algorithm ensures that at least one cell will be used if the user defines a non-zero height. Of course, one always has the option of not using an electrode (zero height), in which case the calculation is equivalent to a 1-D geometry (no radial variation), as long as the initial conductivity is uniform over the grid and the outer radial B.C. is $H = 0$, where H is the magnetic field.

There is a choice of radial outer boundary conditions: $H = 0$ or one in which H decreases as $1/r$. The magnetic field is important in determining the time history of the discharge. This is an effect which is totally absent in 1-D calculations. The inductive E-field generated by the time derivative of H opposes the initial E-field between electrodes during the build-up of the discharge. However, energy stored in the H-field drives the discharge at later times as the H-field relaxes. This is responsible for the secondary current peak often seen in experiments, but absent from 1-D calculations.

One can optionally set up an initial global air conductivity and/or a column of conductivity (initial electron and ion densities) along the axis between electrodes (to simulate an ionized trail produced by a random gamma ray or charged particle). Representative calculations are presented for a specific electrode geometry which show the speed at which the discharge develops, the effect of several physical parameters, and the effect of the feedback of the large magnetic fields which are developed in a 2D geometry.

EVALUATION OF "FAST" GEOMAGNETIC STORM SIGNALS

By

W. A. Radasky*
M.A. Messier
Metatech Corporation
Goleta, California

J.G. Kappenman
Minnesota Power
Duluth, Minnesota

J.M. Pierre
Defense Nuclear Agency
Alexandria, Virginia

There has been significant interest over many years in the coupling of geomagnetic field fluctuations due to magnetic storms to the electric power system. The coupling process involves the creation of low frequency horizontal electric fields in the Earth which cause currents to flow through the neutral grounding of the power system. These currents in turn can produce transformer saturation leading to a power shutdown and under extreme situations damage to transformers themselves (both situations occurred during the Hydro-Quebec "event" on 13 March 1989).

Our interest in this problem results from the fact that complete analyses of past events have been incomplete because usually only low data rate magnetic field measurements ($\Delta t \sim 60$ seconds) have been available. We felt that higher data rates were needed as well as measurements related to the local induced electric fields. To that end we established a measurement system at a 500 kV substation in Northern Minnesota which provides:

(1) Fast ($\Delta t \sim 2$ seconds), 3-vector B-field measurements,

(2) Average E/W and N/S electric field measurements, and

(3) A neutral current measurement.

In addition, we have acquired data on the local ground conductivity to a depth of over 25 km.

Over the past two years, we have measured a substantial number of significant signals which indicate that data rates of at least 10 seconds are required for useful measurements. In addition, theoretical calculations indicate that the relationship between the B and E fields is well described by the measured Earth conductivity model for the region. Sample measured results and comparisons with analyses are shown in the paper. The paper concludes with a discussion of recent efforts with other researchers in examining measurements from the same storm at different Earth locations.

MAGNETOMETRIC DETECTION OF BURIED OBJECTS

Brian A. Baertlein and Kendall F. Casey*
Ballena Systems Corporation
5820 Stoneridge Mall Road, Pleasanton, CA 94588 USA

Magnetometry, the measurement of magnetic fields, is a standard tool for the detection and location of buried ferrous-metallic objects ranging from items of unexploded ordnance to submerged submarines and ore deposits. The local geomagnetic field is modified in the neighborhood of ferrous objects; these modifications are measured and used to infer the objects' sizes and locations. In applications related to environmental remediation, magnetometry is used to detect and locate buried unexploded ordnance, buried drums of hazardous and toxic materials, and like objects. In these applications, the detection problem is often confounded by the presence of clutter signals arising from such man-made sources as near-surface shrapnel and other ferrous debris, and natural sources such as rocks possessing intrinsic magnetization. These clutter signals tend to increase both missed detections and false alarms. In the remediation of ordnance contamination, missed detections increase the post-remediation risk and false alarms greatly increase the remediation cost. Improving the performance of magnetometric sensors operating in cluttered environments is therefore a worthwhile goal.

In this paper we first review the fundamental physics on which magnetometry and magnetic gradiometry are based. The quantity which is typically observed is the magnitude (or in gradiometry, one or more components of the gradient of the magnitude) of the total magnetic field which, in most situations of interest for environmental remediation applications, comprises the sum of the (essentially uniform) geomagnetic field and the field of the dipole moment induced in the object. The induced field is small in comparison to the geomagnetic field. Denoting the geomagnetic field by $B_0\vec{a}_0$, the dyadic magnetic polarizability of a given object by $\mathbf{M}$, and the position vector from object to observer by $r\vec{a}_r$, the total magnetic-field magnitude B_t is given approximately by

$$B_t \approx B_0 + \frac{B_0}{4\pi r^3}\vec{a}_0 \cdot (3\vec{a}_r\vec{a}_r - \mathbf{I}) \cdot \mathbf{M} \cdot \vec{a}_0 = B_0 + B_i$$

where $\mathbf{I}$ denotes the identity dyad. The induced component B_i can be shown to satisfy (1) Laplace's equation $\nabla^2 B_i = 0$ and (2) the Euler homogeneity condition $\vec{r} \cdot \nabla B_i + 3B_i = 0$. The latter property is the basis for the Euler deconvolution technique for processing magnetometric signature data. Matched-filter processing techniques are based on knowledge of the form of the expected signature.

The signatures of compact objects scale with the spatial coordinates in a

characteristic way. If $B_i(x, y; d)$ is the signature, as a function of x and y, of an object at depth d, we have

$$B_i(x, y; d) = \frac{1}{d^3} B_i(\frac{x}{d}, \frac{y}{d}; 1)$$

Thus an object's signature has a characteristic shape which is independent of its depth; the *amplitude* and the *spatial scale* of the signature change as the depth changes. This property can be used to estimate the depth of a detected object. It also forms the basis for the idea, which we explore extensively in this paper, that certain advanced signal-processing techniques may be particularly useful for the analysis of magnetometric signature data.

We will consider the composite signatures of objects in the presence of clutter and demonstrate that, under circumstances typically found in environmental remediation applications, the most significant differences between "target" and clutter signatures are not found in their magnitudes, but rather in their spatial scales. We will explore the use of two standard signal-processing techniques—matched filters and Euler deconvolution methods—for the extraction of desired signatures in these environments, and show that their performance is less satisfactory than one would desire.

Finally, we will present the results of an investigation of the use of advanced signal-processing techniques for signature extraction in clutter. These methods make use of spatial-scale resolution for signal decomposition and appear to be ideally suited for the analysis of magnetometric signature data. Our results indicate that the magnetometric detectability of ferrous objects in clutter can be greatly enhanced through the use of these techniques.

THE SEM REPRESENTATION OF SCATTERING FROM PERFECTLY CONDUCTING TARGETS IN SIMPLE LOSSY MEDIA

Carl E. Baum
Phillips Laboratory/WSR
3550 Aberdeen Ave SE
Kirtland AFB NM 87117-5776

This paper considers the general problem of the response of perfectly conducting targets in a lossy dielectric characterized by frequency-independent permittivity and conductivity, and free-space permeability. There are scaling relationships involving the propagation constant and wave impedance of the medium (as compared to free space) which can be used to relate the various parameters to the free-space case. Based on this one can use free-space parameters to find the singularity-expansion-method (SEM) representation of the target response in the lossy medium, including natural frequencies, natural modes, and coupling coefficients. There is also a branch-cut term introduced which is most significant for low frequencies (or late times).

There is also an entire-function contribution which relevant for early times. Such early times being related to the transit time across the scatterer, then in the high-frequency approximation this entire-function part can also be scaled. Basically the time for which this applies is scaled as c/v where v is the high-frequency propagation speed in the medium. A more general treatment would use the asymptotic treatment together with the general definition of the different SEM terms in terms of contour integrals. As in the free-space case, the currents on the perfectly conducting scatterer can be expressed without an entire-function contribution. However, the incident and scattered fields now include a branch-cut term which can considerably distort the propagated waveforms.

An important restriction concern the assumption of a perfectly conducting scatterer, so that the constitutive parameters of the target do not enter into consideration. More general targets (dielectric, lossy, magnetic) need a more general treatment allowing for the fields inside the target (as, for example, resonances inside a dielectric target).

Another restriction concerns the lossy medium which has been assumed uniform and isotropic. Real earth can have layers. If the medium in the immediate vicinity of the target is uniform and isotropic, then the scaling of the natural frequencies using the local parameters is an appropriate approximation. However, the propagation to and from the target (and hence the pole residues or coupling coefficients) can be significantly perturbed by the transmission of the incident and scattered waves through the various layers, including reflections at the interfaces.

While the present scaling results are quite general, the case

of low medium conductivity is particularly significant for detection, location, and identification of targets. Then the natural frequencies have $|s_a| >> \sigma/\epsilon$ and the scaling simplifies as a dilation and a shift in the complex frequency plane. Furthermore, the incident and scattered fields propagate at such frequencies in an approximately dispersionless manner with an attenuation given by $e^{-\frac{\sigma Z_m z}{2}}$ which can be tolerable for distances restricted such that $\frac{\sigma Z_m z}{2}$ is of order one or less. This also reduces the significance of the late-time distortion of the incident and scattered fields by the medium.

By suitable selection of the waveform launched by the transmitting antenna, the late-time distortion due to the medium can be compensated to some degree. This can also be allowed for in the processing of the scattered fields in the target-identification algorithms.

A MICROWAVE TOMOGRAPHIC EQUIPMENT FOR DETECTING BURIED OBJECTS

G.Cottard, Ph.Garreau, P. Berthaud
SATIMO, Le Pin, rue de la Terre de Feu, ZA Courtabœuf
91952 Les Ulis, France

J.Ch.Bolomey
SUPÉLEC, Electromagnetics Department, Plateau de Moulon
91192 Gif-sur-Yvette Cedex, France

ABSTRACT

This paper describes a new Microwave Tomographic Inspection Tool (MTIT) devoted to the detection of buried objects. An increasing number of applications requires remote detection, localization and identification of buried objects in ground, such as:

- mines, weapons or drug caches (police, military applications)
- pipes,cavities,voids,… (civil engineering and transportation)
- cables (telecommunications)
- etc…

For such applications, microwaves provide a very convenient investigation tool. The adequacy of microwaves mainly results from reasonnable penetration depth at acceptable dimensions, weights and costs of the equipments. Most of the existing equipments are directly derived from radar techniques and are based on monostatic or bistatic arrangements. The in-depth analysis results from the time separation of the echoes stemming from local discontinuities or inhomogeneities of the ground under investigation. This analysis can be performed, either directly in the time domain or in the frequency domain, via frequency sweeping and pulse synthesis. Such equipments are designated as Ground Penetrating Radar (GPR). Basically, GPR,s provide the reflected wave or, equivalently, the echoes integrated over the cross-section of the transmitted microwave beam. While in-depth spatial resolution is typically of the order of a few centimeters, according to the bandwidth of the transmitted wave, transverse resolutions are poor, due to the dimensions (a few ten centimeters) of the radar antennas. As well known, synthetic aperture processing of the reflected wavefronts can be used to improve spatial resolution. However, such a wavefront processing is usually performed after recording the echoes over a certain distance, excluding any real-time capability

The Microwave Tomographic Inspection Tool described in this paper is also based on the interrogation of a ground area with a

microwave beam. However, the reflected echoes are processed in view of obtaining a real-time tomographic display of the groung located under the equipment. Such a processing requires the spatial sampling of the reflected wavefront. The key element of MTIT is a 1 meter long linear array of 32 antennas which are used, successively, as transmitting and receiving antennas. During the transmitting mode, the antennas are fed by a frequency agile generator which delivers pulses at microwave frequencies extending between 400 MHz and 1.2 GHz. This frequency range has been selected to provide a maximum investigation depth of the order of 1 meter. The pulse duration is approximately 5 ns and the peak transmitted power is 100 mW. After an appropriate time delay for eliminating the ground echo, the antennas of the array are successively connected to a superheterodyne microwave receiver, via a microwave multiplexer. The 32 array elements are explored at 32 frequencies within 100 ms. Two observation modes are available. The "coarse" mode utilizes only 16 of the 32 antennas and provides 12 images per second time resolution. In the "fine" mode, the 32 antennas are effectively used, providing 2 images per second time resolution. The numerical processing involves appropriate space and time filtering and Fourier transforms. After preprocessing and autocalibration of the data, the tomographic view of the ground is obtained via so-called diffraction tomography reconstruction algorithms.

This equipment has been developped with the financial support of the French Police Nationale (Ministère de l'Intérieur). After in-laboratory adjustments, it has been engaged in an outdoor assessment procedure. The results obtained with metallic and dielectric burried objects illustrate the specific potentialities of the MTIT.

Oblique Scattering from Buried Homogeneous Cylinders Using the Multifilament Current and Discrete Complex Image Methods

K. A. Michalski* and J. Wu

Electromagnetics & Microwave Laboratory
Department of Electrical Engineering
Texas A&M University
College Station, Texas 77843-3128, USA

ABSTRACT

The problem of electromagnetic scattering from buried objects continues to be the subject of research because of its relevance to geophysical prospecting and remote sensing of underground tunnels, cables and pipes (J. S. IZADIAN et al., IEEE Trans. Geosci. Remote Sensing, GE-22, 52-61, 1984; L. CHOMMELEOUX et al., IEEE Trans. Microwave Theory Tech., MTT-34, 1064-1076, 1986). Recently, the multifilament current method (Y. LEVIATAN et al., Comp. Phys. Commun., 68, 331-345, 1991) was applied to efficiently analyze two-dimensional transverse magnetic (TM) and transverse electric (TE) scattering by homogeneous cylinders embedded partly or completely in a material half-space (Y. LEVIATAN & Y. MEYOUHAS, Radio Sci., 25, 1231-1244, 1990). In the present paper, this approach is extended to the case of cylinders in plane-stratified multilayer media and illuminated by obliquely incident plane waves, which is a vector problem involving a hybrid of the TM and TE partial fields Also, the multifilament model is combined with the discrete complex image method (D. G. FANG et al., IEE Proc., Pt. H, 135, 297-303, 1988), thus resulting in a more general and efficient approach.

In the multifilament current method (MFCM), as applied to a problem of time-harmonic electromagnetic scattering or guidance by two-dimensional homogeneous cylinders, the fields of suitably placed sets of fictitious electric and magnetic current filaments with adjustable complex amplitudes and a linearly progressive phase are used to represent the total field inside the cylinder and the scattered field outside. The source amplitudes are then found by point-matching the tangential field components across the cylinder surface. The advantage of the MFCM is its efficiency and ease of implementation, mainly because it obviates the need to numerically evaluate integrals with singular kernels, as is necessary, e.g., in the surface integral equation

approach. Its drawback is that the optimum location of the fictitious current filaments is not known a priori, and that a posteriori boundary conditions tests are necessary (more than in most other techniques) to discriminate spurious solutions, especially when the method is applied to a new structure. Also, the MFCM approach is best suited for smooth, convex objects, and may fail for bodies of complex shapes and with edges.

The discrete complex image method (DCIM) may well be the most efficient technique presently available for the evaluation of the spectral Sommerfeld-type integrals that appear in the Green functions for plane-stratified media. The basic idea of this approach (Y. L. CHOW et al., IEEE Trans. Microwave Theory Tech., 39, 588–592, 1991) is to extract from the spectral integrand its quasi-static form and any surface wave terms that may occur, and to approximate the remainder function in terms of a few complex exponentials. The last step, which is most easily accomplished by the Prony's method (S. L. MARPLE, Digital Spectral Analysis with Applications, Prentice-Hall, 1987), involves a deformation and truncation of the original integration path in the complex spectral wavenumber plane. All the so obtained integrals are then evaluated in closed form. The terms that arise from the complex exponential approximation may be interpreted as contributions from discrete image sources located in a complex space. If one discounts the small overhead cost of the surface wave and image extraction, which must be done once for each structure at each frequency, the resulting Green functions are essentially closed-form. The difficulty in applying the DCIM is that it is not known a priori where to truncate the integration path for the Prony's approximation. Also, in multilayer media, which at high frequencies support a large number of guided waves, it is difficult to automatically and reliably find the poles of the spectral integrands and the associated residues, as is necessary at the surface wave extraction stage of the DCIM.

The limitations of the two methods notwithstanding, the MFCM-DCIM combination is shown in this paper to be a very attractive solution technique for the class of problems considered here, because of its simplicity, ease of implementation, and computational efficiency. The formulation presented here consistently employs a transmission line analog of the layered medium, which has the advantage that the formulas are compact, yet valid for any number of layers. The numerical implementation, however, has only been carried out and results obtained for two- and three-layer media.

ELECTROMAGNETIC METHODS FOR IN-SITU SITE REMEDIATION

BY

RAYMOND S. KASEVICH
KAI TECHNOLOGIES, INC.
175 N NEW BOSTON STREET
P.O. BOX 3059
WOBURN, MA 01888-1859
617-932-3328
617-932-0927 FAX

AND

* PAUL F. CARPENTER
ARMSTRONG LABORATORY-OPERATING LOCATION
ENVIRONICS DIRECTORATE
SITE REMEDIATION DIVISION
(AL-OL/EQW)
139 BARNES DRIVE
TYNDALL AFB, FLORIDA 32403-5319

BACKGROUND

In the mid-1970's when the world was confronted with the rising prices of fuel oil, microwave and radio frequency systems were proposed and tested as a means for the in-situ retorting of oil shale, thereby eliminating the need for excavation and water resources. The rapid and efficient electromagnetic heating process could give a better oil product in large volumes as compared to the slower conventional heating of oil shale.

By the 1980's, more advanced hydrocarbon recovery efforts evolved from the work done to recover oil from shale and tar sands. Laboratory and full scale testing was accomplished under cooperative funding by the U.S. Air Force Civil Engineering and Services Center (AFESC), Tyndall AFB, Florida, U.S. Department of Energy and the U.S. Environmental Protection Agency. Pilot testing of in-situ soil remediation radio frequency systems by both IITRI (Illinois Institute of Technology Research Center) Chicago, and KAI Technologies, Inc., Woburn, Massachusetts conclusively demonstrated the ability of subsurface radio frequency systems to provide for the recovery of volatile and semi-volatile fuel and solvent hydrocarbon components as well as oil spills. The absorption of radio frequency energy by dielectric heating mechanisms create temperatures in the 125°C to 200°C range for in-situ volatilization of organic liquids. Transmitter power levels of 25 to 50 kilowatts in the frequency range of 6 to 13 MHz were employed for the pilot programs. Pilot scale test results at a site at the Volk Field Air National Guard Base in Wisconsin showed that the recovery of volatile and semi-volatile (aliphatic and aromatic compounds) ranged in the 85 to 99.9 percentile of chemicals removed from soil in a

13 day time frame. (L.Murdoch et. al., "Technologies of Delivery or Recovery for the Remediation of Hazardous Waste Sites", University of Cincinnati, Cincinnati, Ohio, EPA/600/2-89/066, January 1990.)

METHODS OF APPLICATIONS

Subsurface electromagnetic heating of soil for remediation involves a buried applicator geometry that efficiently couples the transmitter power to the soil matrix for the rapid and controlled release of liquid contaminants by volatilization. Temperatures in the range of 125°C to 300°C are required and are achievable through the appropriate choice of transmitter power, frequency and in-situ applicator design. The applicator design is the critical component in the overall design. KAI Technologies has developed a subsurface phased array antenna system that is applied through vertically or horizontally drilled boreholes. Widely spaced linear antenna elements in borehole become mutually coupled once the intrinsic soil moisture has been removed by antenna dielectric heating. For the temperature range of 100°C and above, current phasing of each antenna produces a steerable heating pattern for near uniform heating and process control. Each element is designed to efficiently couple energy into the earth "load" which depends on the complex dielectric constant of the soil as a function of temperature and frequency. Heating over a wide range of depths is achievable with this system as well as placement in difficult to access locations. Use in horizontally drilled wells under buildings and storage tanks are attractive in-situ soil treatment options to remove volatile organic compounds (VOC's).

IITRI has developed a tri-plate system that utilizes three rows of closely spaced electrodes to create a electric field between the center row and the two parallel outer rows. The systems act as a three-wire transmission line and is generally of low impedance. It requires careful tuning and electrode placement at the operating frequency to realize efficient power application to the soil matrix for remediation. The tri-plate system would normally be deployed at or near the earth surface because the feed point of the electrode array must be close to the matching transformer for purposes of efficiency. Excavation of soil would be necessary to position this system at significant depths.

Other electromagnetic methods for environmental remediation for ex-situ application involve microwave systems that heat and process a waste stream over a wide temperature range. A one megawatt microwave system for vitrification of waste is presently undergoing tests by DOE at the Rocky Flats Arsenal. Low frequency, 60 Hz systems are in development for site remediation. D.C. conductivity controls the heat absorbed in the soil matrix and dynamic impedance matching is necessary to maintain system efficiency.

KAI Technologies is developing an electromagnetic mixed waste system for the processing of radioactive mixed wastes in steel drums. It involves the combination of radio frequency heating for removing volatiles, electrokinetics (Westinghouse) for removing radionuclides and organic acids to reduce the volume of material (ABCOV method).

EXPERIMENTAL FIELD TESTING

Air Force Armstrong Laboratory test plans for two RF soil heating techniques, the IITRI Capacitor Technique and the KAI Antenna Technique, were drawn up in late 1992 and in cooperation with the DOD, DOE, EPA.

The antenna design approach was selected by the co-author for use in a follow-on field demonstration at Kelly Air Force Base under the guidance and assistance of the San Antonio Air Logistics Center Environmental Management Office (SA-ALC/EM), the DOE Office of Technology Development and their contract services of Westinghouse at the Savannah River Plant, and the AFCEE contract services of Halliburton NUS Corporation (now Brown & Root), of Oak Ridge, Tennessee. The IITRI electrode array design pilot test was completed at Kelly Air Force Base during the Spring of 1983. A Special field test and evaluation report comparing both the IITRI electrode array design and the KAI antenna system in two vertically drilled wells will be submitted for final publication in Fall 1994.

KAI Technologies, Inc. plans to use two antenna-like applicators in two vertically drilled well borings to achieve an elliptical-shaped electrical field capable of treating approximately 300 cubic feet of soil. In this manner, some comparisons can be made between the cubic-shaped IITRI results and the KAI elliptically shaped soil volume.

ELECTROMAGNETIC COUPLING TO CABLE BUNDLES

B. DEMOULIN, L. KONE and P. DEGAUQUE*
Université des Sciences et Technologies de LILLE
Laboratoire de Radiopropagation et Electronique
UA CNRS 837
Bâtiment P3
59655 VILLENEUVE D'ASCQ Cédex - FRANCE

The objective of this paper is to describe a theoretical and experimental approach of the coupling of disturbing electromagnetic waves to a cables bundle. The bundle is made of N_1 insulating wires and, more generally of N_2 multiwires shielded cables. Furthermore, it is assumed that this bundle is put parallel to a ground plane and that its height is much smaller than the wavelength so that the transmission line can be applied. Analytically, the problem can be solved from two approaches which seem very similar but, as we shall see later, can lead to quite different results. Indeed one of the main aspects is the choice of the voltage reference.

In the first model, which will be called in the following "multiple references" (M.R.), the induced voltages and currents on the cables are calculated in two steps. The reaction of the wires inside any shielded cables being neglected, the current distribution along the N_1 insulated wires and along the N_2 shields is expressed in terms of the incident electromagnetic field by applying the well-known transmission line theory. Then, from the knowledge of these currents, the voltages appearing at the ends of the inner wires of any shielded cables are determined by using the concept of transfer impedance.

In the second model, one can try to characterize all the voltages with a unique voltage reference (U.R.) which is the ground plane. It means that the system of coupled lines becomes a system of order $N = N_1 + N_2 + N_3$ where N_3 is the total number of wires inside the various shields. In this formulation, the shield is thus considered as any wire.

As an example, let us consider the simple case of a bundle reduced to only one coaxial cable. In Figure 1, the definition of the various voltages are indicated, case-a- corresponding to a multiple reference while in case-b- the voltage reference is the ground plane.

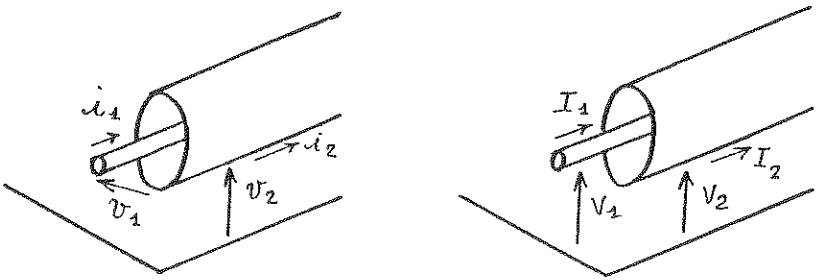

-a- M.R. model -b- U.R. model

Figure 1 : Definition of the various voltages.

Currents and voltages for the M.R and U.R cases are related by :

$$(v) = (T_v)(V)$$
$$(i) = (T_i)(I) \qquad (1)$$

where the T matrices are defined by :

$$(T_i) = \begin{pmatrix} 1 & 0 \\ 1 & 1 \end{pmatrix} \quad \text{and} \quad T_v = \begin{pmatrix} 1 & -1 \\ 0 & 1 \end{pmatrix} \qquad (2)$$

The main difficulty encountered in the U.R model is the determination of the (Z) impedance matrix since one cannot employ the usual coupling coefficients. The method consists in determining (Z) from the (z) matrix associated with the M.R model :

$$(z) = \begin{pmatrix} z_{11} & -Z_t \\ Z_t & z_{22} \end{pmatrix} \qquad (3)$$

z_{11} being the per-unit length impedance of the coaxial cable, z_{22} the one of the outer line made by the shield and the ground plane, Z_t the transfer impedance of the shield. This leads to :

$$(z) = (T_v)^{-1}(z)(T_i) \qquad (4)$$

However by replacing all the matrix elements by their analytical expressions and by carrying out all the calculation, it appears discrepancies between the two approaches.

In the more general case of multi-wire shielded cable, this paper will thus explain the reasons of these differences, their consequences and errors on the values of the induced voltages. Furthermore, we shall point out the advantage and drawbacks of a direct measurement at the (Z) coefficients.

ERROR ANALYSIS OF CROSSTALK AND ELECTROMAGNETIC INTERFERENCE BETWEEN BRAIDED CABLES.

S Sali*, University of Newcastle upon Tyne, UK.

The advent of microelectronics has enabled many complex electronic equipment to be used within a limited space. Braided coaxial cables are used as interconnects, in closely spaced bundles in such systems. The optimum operation of the equipments in such compact systems requires that close attention must be paid to the electromagnetic interference and coupling between the cables.

Braided coaxial cables have outer conductors made of criss-crossing belts of conductors to provide flexibility. Because of this the outer conductor contains a large number of diamond shaped holes and thus do not provide complete shielding against electromagnetic fields. A TEM wave generated inside the cable may couple to exterior and any external field may couple to the interior. At high frequencies magnetic field coupling is governed by transfer impedance per-unit-length (Z_T) and Electric field coupling by transfer admittance per-unit-length (Y_T).Transfer impedance at high frequencies is inductive and it is composed of braid and hole indiuctances. Hole inductance is caused by the direct leakage of magnetic field whereas the braid inductance is the result of magnetic flux linkage between the braid layers. Transfer admittance is purely capacitive. Recent theoretical models have already proven that the crosstalk between cables are quadratically related to these leakage parameters and hence any small errors in their experimental and theoretical determinations may cause large errors in the prediction of crostalk and interference effects between the cables.

The first objective of the paper is to investigate the sources and margins of different errors in the theoretical and experimental prediction of coupling parameters. Currently theoretical models used in calculating these parameters are not always successful. The two most widely recognised models used are those proposed by Tyni and Vance. Tyni's model covers both hole and braid inductances whereas in Vance's model the braid inductance is not accounted for. Because of this Vance's model yields poor agreements for all cable types. However we have combined the Vance's model for hole inductance with Tyni's model with braid inductance in our theoretical models. The results from these studies are shown for two cables: one over braided standard and the other optimised (where the braid is designed for lowest possible Z_T) in Figs 1 and 2.. It is seen that both models are successful for standard cable. For optimised cable Tyni's model is slightly better but still it does produce poor agreement against the measured values. It is clear that both approaches will produce large errors when used in crosstalk expressions for leakage parameters when leaky or optimised cables are used in the set up. This therefore leaves only other avenue which is to determine these parameters experimentally. The most commonly used device is the IEC's triaxial device which is shown in Fig.3. This device is not very accurate above 10MHz especially for cables with high Y_T content. This is typically illustrated in Figs.1 and 2 where it is seen that Z_T curve deviates. from linear line significantly at high frequencies for optimised cable because of its high Y_T content. There is a slight deviation in the curve for the standard cable although the error margin is much smaller. This error margin may be improved by using a more accurate high frequency matched triaxial device shown in Fig.4. The results from this device shown in Fig.5 for an optimised cable and projected to lower frequencies and compared against those obtained from the IEC device. The results show that there is an error margin of 20% between the two methods.

The axial and longitudinal torsions can also cause some significant errors in the experimental and theoretical predictions. This is illustrated in Fig.6 where Z_T values are plotted against frequency when torsion applied to the cable. These values are then used directly in the crosstalk expressions to study the effect of errors on the wave coupling and the results are shown in Fig.7, which clearly illustrates the scale of errors when the cable is subjected to torsion. It must be born in mind that the errors above can not be determined analytically and some kind of statistical approach must be used to predict their effect on interference and wave coupling. Thus the second objective of this paper is to develop statistical procedures where the effect of each error mechanisms on the wave coupling can be estimated.

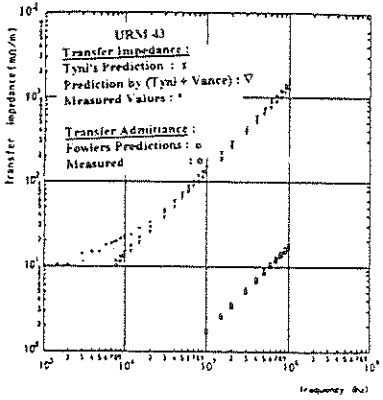

Fig.1 Measured and Predicted Z_T values

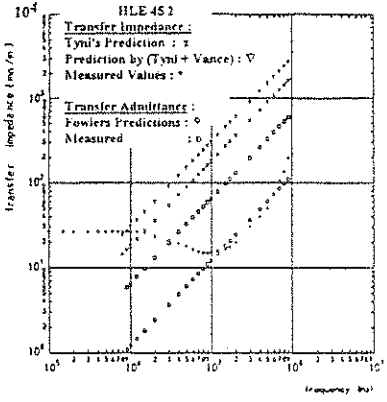

Fig.2 Measured and Predicted Z_T values

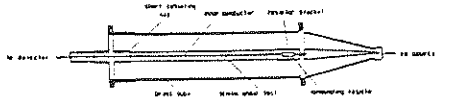

Fig.3 Low frequency triaxial apparatus.

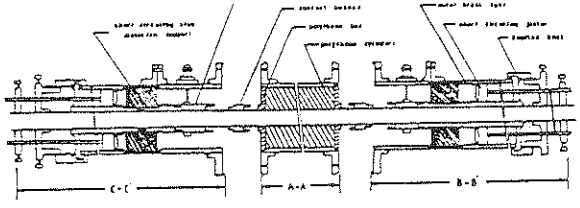

Fig. 4 High Frequency Matched Triaxial Device

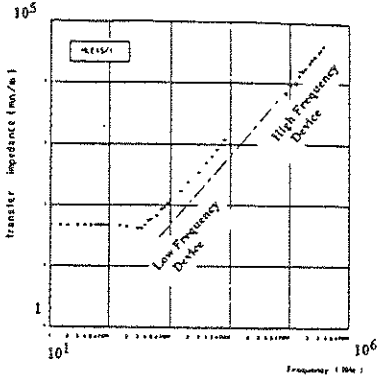

Fig.5 Measured Z_T values from Low and High Frequency Triaxial devices

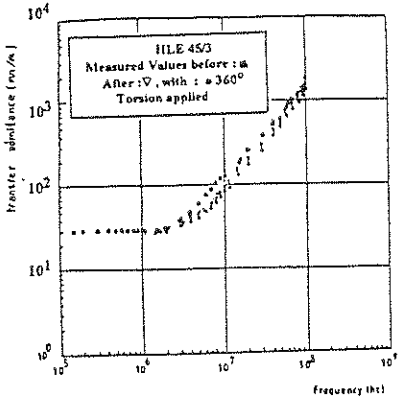

Fig.6 Measured Z_T / Frequency Curves

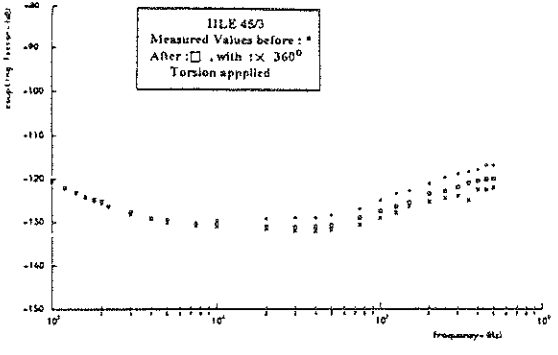

Fig.7 Coupling / Frequency Curves

EFFECTS OF TIME-DEPENDENT POLARIZED E-FIELD ON INDUCED CABLE RESPONSES

J.C. Chai
The Aerospace Corporation, P.O. Box 92957, Los Angeles, CA 90009, USA
Telephone (310) 336-8341; FAX (310) 336-5581

Summary

When a cable/wire is exposed to an incident electromagnetic field created by events such as lightning and nuclear explosionssome transient signal will be induced on the cable. This undesirable signal may be of sufficient amplitude and duration to upset or even permanently damage the delicate electronics connected to this cable. In order to understand this phenomenon, and thereby design the circuitry accordingly to protect the vulnerable parts, a great deal of efforthas been devoted to compute the transient signal using a linearly polarized incident E-field with a constant azimuthal polarization angle.

This paper generalizes the incident EM-field to be planarly polarized with the time-dependent azimuthal polarization angle, a more realistic case simulating the induced electromagnetic environment. Under this environment which varies with time-dependent polarization angles, the formal approach to calculate the cable response is to solve the second order differential equation for the induced current along the cable for a given frequency. The solution can usually be obtained only by numerical methods even for a simple incident E-field ($E^{inc}(t)$) and simple cable geometries. This paper also proposes to use an analytic (rather than a numerical) approach: calculating the induced open-circuit V_{oc} across cables of various geometries frequently encountered in practice. The quantity V_{oc} is calculated with both linearly and planarly polarized E-field for some common cable configurations (straight lines, circular arcs, helix cables and Archimedes spirals), and the ratios are taken to highlight the different temporal behaviors of the induced V_{oc} due to the time-dependence of the incident E-field polarization. Common factors in the ratios will cancel out, greatly simplifying the procedure. It was found that for most cases the effect of the time-dependent polarized E-field on cables is insignificant, but for some cases (e.g., long cables with large radius of curvatures in an oblique incident field) it can be much greater than that due to an incident E-field with a constant polarization angle. However, this approach is valid for cable lengths $L \ll vt$ where v is the propagation velocity in time t, for which the inductance of the cable and re-scattering of the waves are negligible. Under this new environment with time-dependent polarization angle, the induced voltage responses for some cable configurations as suggested above are calculated and

compared to those generated under the ideal (and less realistic) environment.

Some parametric studies were also performed for constants that were used in the calculation. Two values of α in $E^{inc}(t) = E_o e^{-\alpha t}$, $\alpha = 4\times10^6 \text{second}^{-1}$, and $\alpha = 100\text{second}^{-1}$, were considered and it was found that the results were fairly insensitive to the constant α. For straight cable with arbitrary orientation in space, it was found that the length of cable has only a minor influence on the ratio $R(t)$. However, for circular arc in the horizontal xy-plane with normal incidence, the effect of increasing arc length in the ratio $R(t)$ is very noticeable: as L increased from 6 meters to 20 meters, the ratio is above 2 at some time points, and as $L = 50$ meters the ratio becomes as large as 6.

The results obtained in this investigation can be summarized as follows:

1. For cables in a straight line configuration, regardless of angles of incidence, the ratio of V_{oc} produced by time-dependent polarized E-field to V_{oc} produced by a constant polarized E-field is almost always less than unity.

2. For cables in a slightly curved configuration with normal incident field, no significantly different effect due to time-dependent polarized E-field was noticeable.

3. For cables with large curvatures in an oblique incident field, the ratio $R(t)$ can be significantly greater than unity for some time points, suggesting that some more careful examination at the cable response of these configurations may be needed.

4. However, for all cases considered in this study with the exception of Archimedes spirals, even if the ratio $R(t)$ is greater than unity for some time points, the ratio of energy deposited in a load over the whole time range, will be more likely less than unity.

POWER LINE TRANSFER IMPEDANCE - A CASE STUDY

N. K. AGARWAL
VIKRAM SARABHAI SPACE CENTRE
TRIVANDRUM - 695022, INDIA

Very often interference signal from a culprit equipment is couple into a victim unit through a common power supply they share. Conducted emission from the culprit unit on its power supply lines is measured in terms of noise current (dBμA) using a current probe. On the other hand, susceptibility of the victim unit is measured in terms of voltage of the RF signal injected on its power supply lines. To corelate these measured data one should have knowledge of power line transfer impedance. The paper first defines power line transfer impedance and then describes a method of measuring it. This is followed by discussion of results and conclusion. Even though measurements are carried out by varying all the possible parameters and their effect on the impedance is studied, only a brief description of the method and a sample test result are given below.

A typical situation of interference signal being coupled from one unit to the other through a common power supply is shown in Fig.1. If I_n is the noise current generated by unit #1 (culprit) at its power input port and V_n is noise voltage developed at the power input port of unit #2 (victim) then power line transfer impedance Z_T is given $Z_T = V_n/I_n$. Z_T is a function of RF impedances of culprit and victim units at their power input ports, RF impedance of the common power supply, type and configuration of interconnecting cables, and frequency.

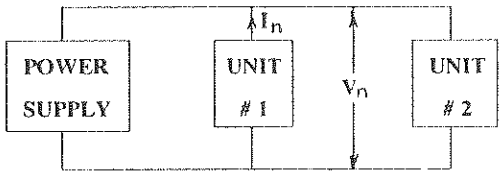

FIG. 1: CONDUCTED INTERFERENCE COUPLING THROUGH COMMON POWER SUPPLY

Schematic of measurement set-up is shown in Fig.2. Z_c (a resistor), coupling network (inductive for low frequencies and capacitive for high frequencies) and signal generator together simulate culprit unit. Z_v, a resistor, simulates victim unit. Noise current, I_n, at Z_c is measured using a current probe and EMI meter. Noise voltage V_n, is measured using an oscilloscope or selective microvoltmeter. Measurements are made for various values of Z_c and Z_v, different types of power supplies, all possible configuratiuons and types of inter connecting cables in 50 Hz to 400 MHz frequency range. One example of measured value of transfer impedance is shown in Fig.3.

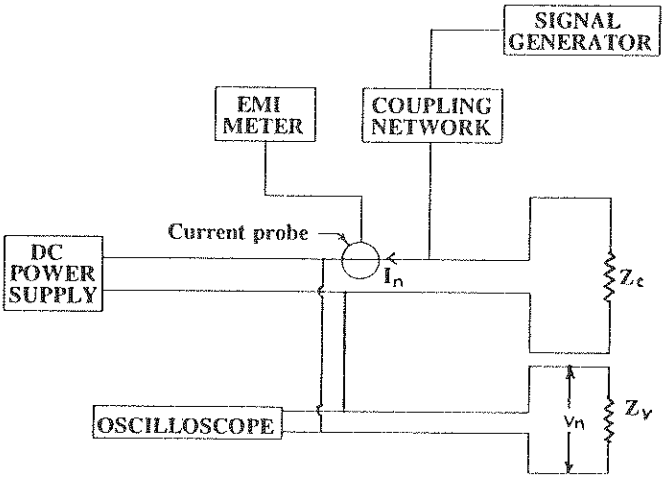

FIG.2: SCHEMATIC OF MEASUREMENT SETUP

At low frequencies (below 10KHz) value of transfer impedance is very low because in this freq. range effects of interconnecting cables can be neglected, impedances of culprit and victim units can be taken as equal to their dc resistances. Hence the effective transfer impedance is controlled by LF impedance (internal resistance) of the power supply which is low because of good regulation characteristics. As the frequency increases transfer impedance increases rapidly. This is true for all the parametersaffecting the impedance but rateof increase differ considerably.

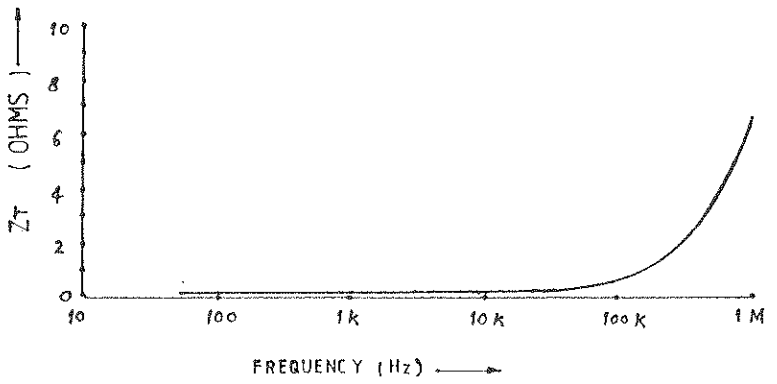

FIG:3 _ TRANS. IMP VS FREQUENCY

TIME-DOMAIN ANALYSIS OF FIELD-EXCITED CABLES WITH NONLINEAR PROTECTION DEVICES

S. Celozzi M. D'Amore M. S. Sarto
Department of Electrical Engineering
University of Rome "La Sapienza"
Via Eudossiana 18, 00184 Rome, Italy

I. Introduction

The analysis of the transient voltages induced by a pulse electromagnetic field in coaxial and multiconductor linear cables was performed in the past by means of Discrete Fourier Transforms. Recently, a hybrid frequency- and time-domain method has been proposed to analyse field -excited lossy networks with nonlinear loads (M. D'Amore, M. S. Sarto, *1993 IEEE EMC Int. Symposium*, Dallas). In this paper, the matrix procedure, based on the evaluation of Thevenin and Norton equivalent multiport circuits, is applied to predict the effects induced by an EMP plane wave in multiconductor cables with one- or two-stage nonlinear protective devices. The procedure has been tested by comparing the results for a coaxial cable with those obtained by means of a Finite Difference Time Domain approach. Cables constituted by two wires and a braided shield are considered. The influence of various grounding connections on the induced effects is investigated.

II. Modeling of Field-Excited Multiconductor Cables

A multiconductor dissipative cable illuminated by an EMP plane wave is simulated by taking into account the skin and proximity effects and considering a braided shield. A mesh representation is used to describe the following transfer equation between the input and output quantities:

$$\begin{bmatrix} \mathbf{V}_L(\omega) \\ -\mathbf{I}_L(\omega) \end{bmatrix} = \begin{bmatrix} \Phi_{11}(\omega, L)\ \Phi_{12}(\omega, L) \\ \Phi_{21}(\omega, L)\ \Phi_{22}(\omega, L) \end{bmatrix} \begin{bmatrix} \mathbf{V}_o(\omega) \\ \mathbf{I}_o(\omega) \end{bmatrix} + \begin{bmatrix} \mathbf{V}_s(\omega) \\ \mathbf{I}_s(\omega) \end{bmatrix} \tag{1}$$

in which Φ_{11}, Φ_{12}, Φ_{21} and Φ_{22} are the coefficients of the transition matrix. The voltage and current source vectors are given by:

$$\begin{bmatrix} \mathbf{V}_s(\omega) \\ \mathbf{I}_s(\omega) \end{bmatrix} = \int_0^L \begin{bmatrix} \Phi_{11}(\omega, L\text{-}x) & \Phi_{12}(\omega, L\text{-}x) \\ \Phi_{21}(\omega, L\text{-}x) & \Phi_{22}(\omega, L\text{-}x) \end{bmatrix} \begin{bmatrix} \mathbf{E}_s(\omega, x) \\ \mathbf{J}_s(\omega, x) \end{bmatrix} dx \tag{2}$$

where $[\mathbf{E}_s]$ and $[\mathbf{J}_s]$ are the series and shunt source terms distributed along axis x, in the mesh constituted by the external side of the shield and the ground return path.

The previous relations are used to determine the Thevenin equivalents of the field-excited multiconductor cable at both ends. The nodal approach is then applied considering the PI-type equivalent circuit of the cable. The following nonlinear integral matrix equation of Volterra-type is obtained in the time domain:

$$\mathbf{v}(t) = \hat{\mathbf{v}}(t) + \int_0^t \mathbf{z}(t-\tau)\, \mathbf{i}(\tau)\, d\tau \tag{3}$$

assuming that all the excitations begin after t=0 and v(t) and i(t) are the vectors including the input and output time domain quantities. The open-ended voltage vector $\hat{\mathbf{v}}(t)$ and the transient impedance matrix z(t) are computed by means of inverse DFTs:

$$\hat{\mathbf{v}}(t) = F^{-1}\{\mathbf{Z}(\omega)\, \mathbf{I}_{sc}(\omega)\} \tag{4}$$

$$\mathbf{z}(t) = F^{-1}\{\mathbf{Z}(\omega)\} \tag{5}$$

where $\mathbf{Z}(\omega)$ is the nodal impedance matrix of the cable and $\mathbf{I}_{sc}(\omega)$ the known short-circuit current vector in the frequency domain. Vector i(t) of the unknown currents in the nonlinear devices is related to the voltage vector by the following boundary condition:

$$i(t) = f_i(v(t)) \qquad (6)$$

in which f_i is supposed to be a nonlinear monotone function.

III. Applications

The numerical procedure is applied to predict the voltages induced in the cable by an EMP plane wave (E_o=50 kV/m, α=4 10^6 s^{-1}, β=5 10^8 s^{-1}, θ=30°) having a vertical polarization and a null azimuth angle (Fig. 1). The multiconductor braided shield cable, having a length of 5 m and a height of 1 m above an aluminium plane, is terminated at both ends on resistances of 100 Ω between the two wires, connected to protective devices. Fig. 2 shows the equivalent circuit of the cable terminations. The distributed source vectors are:

$$[E_s] = [\,0\;0\;E_s\,]_t \qquad (7a)$$

$$[J_s] = [\,0\;0\;J_s\,]_t \qquad (7b)$$

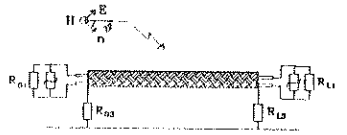

Fig.1 Cable configuration.

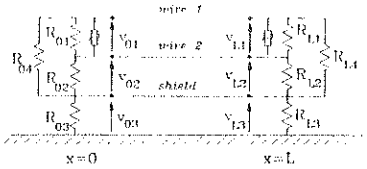

Fig.2 Equivalent circuit of the cable terminations.

In the first application the shield is grounded at both ends and wire 2 is connected to the shield at the left side of the cable only. In the second case wire 2 is connected to the shield at both ends and the shield is grounded at the right end only. The considered third configuration is obtained by grounding the shield and the wire 2 at right end only, being floating the opposite sides. Figs.3-5 show the induced voltages between wire 1 and 2 at right end in the described three configurations in case of 100 Ω unprotected loads (a); curves (b) are obtained by protecting the loads by a ZnO varistor having treshold voltage and current equal to 1 kV and 0.1 A, respectively. Finally, a two-stage protection device is cascade-connected to the loads at both ends of wire 1 and 2 in the second configuration. The coarse protection of the considered two-port nonlinear circuit is constituted by a ZnO varistor and the fine protection by two suppressor diodes connected in antiseries, having 20 V threshold voltage; the first and second stage are decoupled by means of a 20 Ω resistance series connected to a 10 μH inductance. Fig.6 shows the computed wire-to-wire voltages at left (a) and right (b) side.

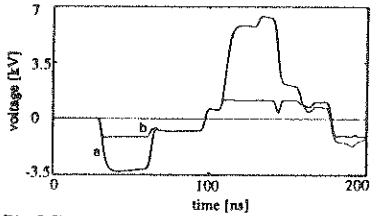

Fig.3 Terminal voltage without (a) and with (b) the protective device in the first configuration.

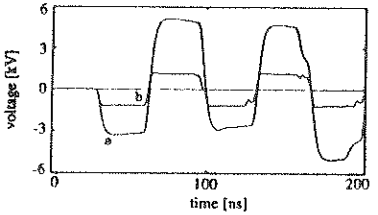

Fig.5 Terminal voltage without (a) and with (b) the protective device in the third configuration.

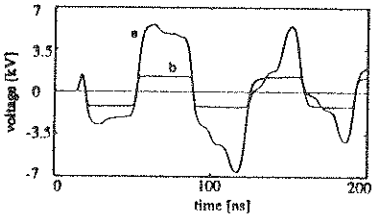

Fig.4 Terminal voltage without (a) and with (b) the protective device in the second configuration.

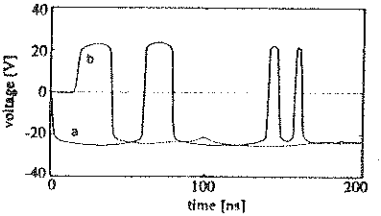

Fig.6 Terminal voltage at left (a) and right (b) side with the two-stage protective device.

ON THE USE OF MINIMUM PHASE ALGORITHM FOR DETERMINING RESPONSE TO UWB SOURCES

Captain Victor E. Martinez, Aircraft Research Group
WSM/Phillips Lab, Kirtland AFB, N.M., U.S.A. 87117

Dr. Chen-Shiang D. Lin, Lesli Research Facility
WSM/Phillips Lab Kirtland AFB, N.M., U.S.A. 87117

Dr. Tracey S. Bowen, Microwave Effects Group
WSM/Phillips Lab,Kirtland AFB, N.M., U.S.A. 87117
and
Dr. Shyam H. Gurbaxani*, Fiore Industries Inc.
Kirtland AFB, N.M., U.S.A. 87117

In the general procedure for experimentation with electromagnetic pulse illumination of large systems, convolution integral is utilized to obtain the response r(t) due to excitation e(x) using impulse response function h(t-x).

$$r(t) = \int_{-\infty}^{+\infty} e(x)h(t-x)dx = e(t) * h(t)$$

The magnitude as well as the phase information is necessary to compute the response in this classical formulation.

In this paper the response of some generic systems to a fast rise time (fraction of a nanosecond) short pulses (several nanoseconds) will be considered when only the magnitude data is available. Such situations, when the phase information is not known with sufficient accuracy, arise through either scalar data acquisition or non-linearity in wide frequency band components such as amplifiers. In order to minimize the experimental biases, the data presented will consist of two or three entirely different ultra wide band sources under two or three different configurations.

The Minimum Phase Algorithm as developed by E.G.G., T.R.W., B.D.M. and U.I.E. for the US Air Force under Micro-computer Signal Analysis program uses the property that of all the functions having the same Fourier transform, the minimum phase sequence has the least phase delay of the frequency components. The minimum phase can then be computed using the Hilbert transform property i.e. the logarithm of the magnitude of the Fourier transform and the phase form a Hilbert transform pair.

The algorithm used here to compute the minimum transform of the input sequence was developed by Quatieri and Tribolet as reported in "Programs for Digital Signal Processing", IEEE press (1979).

Computational approximation will be compared with the actual data and conclusions drawn as to the applicability of algorithm under various types of sources and/or systems under test.

ON A CERTAIN FILTERING APPROACH TO TARGET DISCRIMINATION

Sergey L. Primak* Serge Briskin
Department of Electrical and Computer Engineering
Ben Gurion University of the Negev, Beer-Sheva 84105, PO Box 653, Israel

Introduction. The increase in the use of experimental transient measurement facilities for target discrimination using the singularity expansion method (SEM) (C.E. BAUM, AFWL, IN-88, 1971) has generated considerable interest in the target discrimination methods based on the dominant complex natural resonances of radar targets (C.E. BAUM, et al., Proc. IEEE, 79, No 10, 1481-1491). Numerous efforts in this field were based upon Prony's method and its improvements (M.L. VANBLARICUM, R. MITTRA, IEEE AP-23, 777-781, 1975). Unfortunately these techniques can be significantly affected if the response is contaminated by noise, and the methods themselves become ill-conditioned.

In this paper we use a new filtering approach to the discrimination of radar targets by processing a mixture of the backscattered impulse response and white gaussian noise. The numerical simulations, which were carried out using models of F-104 and F-4 aircraft, verified the efficiency of this approach.

Method. The time-domain scattered field response of a conducting target has been observed to be composed of an early-time forced period, when the excitation field is interacting with the scatterer, followed immediately by a late-time period during which the target oscillates freely. The late-time period can be decomposed into a finite sum of damped sinusoids (excited by an incident field waveform), while their oscillating frequencies are determined purely by the target geometry.

We assume that the measured time-domain backscattered field is corrupted by white gaussian noise (WGN) $\xi(t)$ with zero mean and variance σ, so that

$$r(t) = \sum_{n=1}^{N} a_n e^{\sigma_n t} \cos(\omega_n t + \varphi_n) + \xi(t), \quad t < T_l \tag{1}$$

where a_n and φ_n are the aspect-dependent amplitude and phase of the n-th mode, T_l describes the beginning of the late-time period and N modes are taken into account. The natural frequencies $s_n = \sigma_n \pm j\omega_n$ can be found experimentally and are reported in (K.M. CHEN, et al., IEEE AP-40, 829-833, 1992).

Assume the case of two or more possible targets, characterized by sets of their natural frequencies $s_n^{(i)} = \sigma_n^{(i)} \pm j\omega_n^{(i)}$, where $1 \le i \le M$, and M is the number of the targets to be discriminated. We need to ascertain the number of the target having some measured backscattered response of the type (1). Let us confine ourselves to the case of $M = 2$ for the sake of simplicity. Since the mixture (1) must be composed mainly of the harmonics

of one of the given sets of natural frequencies, the discrimination of the two targets can be achieved by measuring amplitudes of the corresponding harmonics in the backscattered response.

To solve this task we propose using the filtering algorithm described in (V. LYANDRES, S. BRISKIN, Signal Processing, 34, No 2, 1994) in detail. We assume that the sets of the natural frequencies of any target are exactly known. Provided the incoming mixture is represented by a finite sum of sinusoidal segments, we can construct a filter invariant to amplitudes and initial phases of all sinusoidal components of the input, and this filter will let all given desired components of the input pass without distortion and will reject all interfering components. The advantage of the filter being invariant to amplitudes allows the successful application of this algorithm for processing segments of damped sinusoids of the form (1). So, if the case of identification of any target of the two possible is considered, the problem is to construct two filters, each of which is designed to identify (to pass without distortion) all the natural frequencies of one given target and to reject the frequency components of the other target. Then it is possible to decide which target is observed when comparing the responses of both the filters to the backscattered response coming from the target. As a simple means of comparing, and subsequently identifying the target, one can use for instance, the energetic characteristics of the processed response. In fact, let $a_i^{(1)}$ and $a_i^{(2)}$ be the measured amplitudes of the natural frequency components corresponding to the first and second target respectively. Then the decision is made depending on the value of

$$k = \sum_{i=1}^{M_1} \left(a_i^{(1)}\right)^2 / \sum_{i=1}^{M_2} \left(a_i^{(2)}\right)^2 \qquad (2)$$

where M_1 and M_2 are the number of the natural frequencies of the first and second sets respectively. If $k < 1$, the target 2 is identified; if $k > 1$, the target 1 is identified.

Now we would like to point out what, in our opinion, are the advantages of using this algorithm over the methods described in literature:

1) The filter's invariantness to amplitudes and initial phases of the mixture's frequency components, which principally allows the reconstruction of a useful signal with high accuracy, avoiding the necessity of taking these parameters into consideration.

2) The possibility of processing signal segments of a short duration.

3) The possibility of annihilation of a narrowband interference, removing it from the natural frequency components of the backscattered response.

4) The possibility of making a decision without using the whole set of the natural frequencies of a given target; the possibility of choosing the number of considered natural frequencies depending on circumstances.

5) The possibility of acquiring a well conditioned system of linear equations while processing a signal.

Numerical results. The numerical simulation was performed for two sets of natural frequencies corresponding to F-104 and F-4 aircraft. The WGN was approximated by 60 sinusoids, their frequencies ranging from 20 to 200 MHz with the step along the frequency axis equal to 3 MHz. The results of targets discrimination depending on the noise level σ in (1), as well as on a number of the natural frequencies considered, will be reported in the extended version of the paper.

INVESTIGATIONS ON THE EQUIVALENCE OF EMC EVALUATIONS IN TIME AND FREQUENCY DOMAIN USING RULE-BASED MODELLING

Lars Jendernalik*, Christian Pfeiler, Gregor Stricker, Universität Dortmund
Lehrstuhl für Hochspannungstechnik und elektrische Anlagen,
44221 Dortmund

An actual interference factor scenario includes in general both of continuous wave and of pulse signals. Due to economic considerations a limitation to one of the disturbance families is obvious for immunity test in laboratories. An analysis of the equipment used by industrial laboratories shows a nearly exclusive field exposure to the test object by means of continuous wave test quantities.

The immunity of an EUT hardened only in one way cannot be predicted concerning the other disturbance family. Furthermore EMC evaluation of a test object is mostly estimated due to the non-linear criterion of a malfunction. Consequently all efforts to build a relationship between time and frequency domain by superposing solutions of the Fourier transformation have to be considered critically in connection with EMC evaluation.

An approach to solve this problem is gained by applying the principle of rule-based modelling. This method is based on the analysis of input-output-behaviour. It can be described in the shape of rules appearing "IF situation at the input, THEN event at the output". Even complex systems can be characterized by a relatively simple set of rules. Typical system properties in frequency domain and characteristics of interference factors examined in time domain are selected as input. Output is the detected malfunction. The resulting set of rules yields the demanded relationship between time and frequency domain.

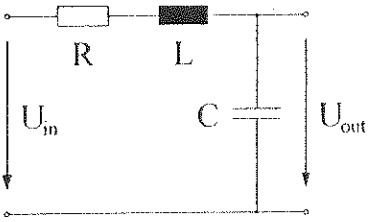

Fig. 1: Test circuit

A first application of rule-based modelling to the presented problem is deliberately realized with a simple object. A dampened series-resonant circuit (Fig. 1) represents the test system. The amplitude response maximum describing damping of the system is taken as an input variable. Front time T_1 and time to half-crest T_2 of the pulse being normalized to the resonant frequency of the circuit f_R serve as further input to the model. Overstepping a defined threshold of output voltage U_{out} represents the malfunction. Thus the rule-based model expresses what pulses excite a certain system. For a given RLC combination results of the rule-based modelling are shown in Fig. 2. Each single layer of the hatched columns represents a rule set of exceeding a certain output voltage U_{out}; hatching

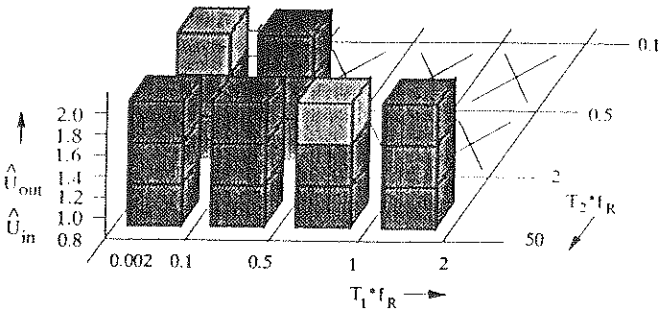

Fig. 2: Result of the rule-based model of the investigated test circuit in time domain

intensity corresponds with the statement certainty of rules in a particular range of time characteristics. To ensure reliability of the model, it is derived from 741 single time simulations. In comparison with measurements, rule-based modelling proves itself able as an appropriate evaluation method of the data amount required for a comprehensive time analysis. Due to this, knowledge of system characteristics in frequency domain allows statements about its behaviour in time domain, if linearity can be assumed before the malfunction occurs.

Experimental verification is done at the test object in connection with devices showing realistic failure events. As an example, the resonator circuit output is connected to the input of a flipflop. Its measured response can be interpreted as malfunction (Fig. 3). Neglecting the flipflop's own dynamic behaviour, Fig. 3 directly corresponds with Fig. 2. For a comparison, U_{out} is there to be replaced by the static switching voltage $U_{S,stat}$ of the flipflop and f_R must equal 300 kHz.

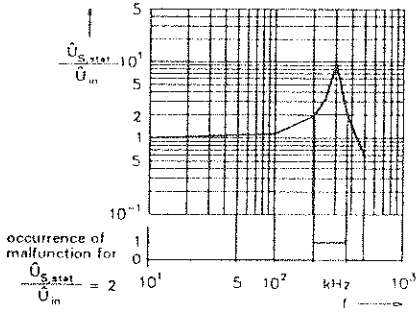

Fig. 3: Measured response sensitivity of the EUT over frequency

Special consideration is given to determining system characteristics in frequency domain to prepare and evaluate the time domain analysis. Presuming linear characteristics of an unknown system in frequency domain, this method appears to be transferable to more complex systems. In this sense rule-based modelling can be used as a general instrument to predict system behaviour in time domain by means of known frequency characteristics.

WAVEFORM BOUNDING AND COMBINATION TECHNIQUES FOR DIRECT DRIVE TESTING

Samuel Frazier
Edward Parimuha*
Naval Air Warfare Center Aircraft Division
Bldg 966, Code SY84
Patuxent River, MD 20670

Murali Tummala
Naval Postgraduate School
Code EC/TU
Monterey, CA 93943

Summary

The use of modern signal processing techniques and algorithms applied to the Electromagnetic Pulse (EMP) spectrum has created new opportunities to use all data gathered during aircraft system level EMP evaluations. Research into combining, compressing and storing transient waveforms is being conducted by the Naval Air Warfare Center Aircraft Division (NAVAIRWARCENACDIV) at Patuxent River, Maryland.

During current aircraft EMP evaluations, different simulator polarizations and aircraft configurations are tested to ultimately quantify system survivability. Measurements acquired at the Horizontally Polarized Dipole (HPD) and Vertically Polarized Dipole (VPD) simualtors during the system evaluation are stored in the Naval Air Electromagnetic Analysis System (NEMASYS). NEMASYS is a database, analysis tool and report generator used by the test engineers at NAVAIRWARCENACDIV.

Many individual waveforms are acquired during a system level evaluation, of which only 10 % are reused. These 10 % are selected to be inductively coupled onto system cabling during direct drive testing to evaluate system survivability margins. Initially, only the waveform with the highest peak amplitude per individual test point was selected for use during direct drive testing. The other waveforms, as many as five additional at each point, were not used although they contained important information. Through in-house signal processing and the help of the Naval Postgraduate School, transient waveform bounding techniques are being explored. The use of a waveform that contains all important test information from each of the waveforms collected in different polarizations and configurations for each test point, is referred to as a bounded waveform or stress envelope. The purpose using bounded waveforms (stress envelopes) is to: (1) Reduce uncertainty by bounding system/environment interaction; (2) Use all available system response data (polarizations, orientations); and (3 Improve on the aircraft survivability RDT&E

process. The bounded stress envelope must accurately reproduce the dominant time and frequency attributes of the original waveforms and must remain stable in the combination process. In the time domain, the bounded nature of the stress waveform is verified by performing a norm att ribute analysis. This analysis compares certain attributes of the stress waveform with those of the original waveforms for a close match. The actual bounding process is carried out in the frequency domain. The bounding of the stress waveform is accomplished by performing a wideband signal analysis approach that employs several spectral subband processing techniques. The spectral energy in each subband is selected to ensure that the in-band energy is representative of that of the original waveforms.

Research

Two stress envelope techniques have been used for combining and bounding test point responses: Pulse and Damped Sine Characterization and Autoregression. Details of these two techniques and a comparison of the norm attributes will be discussed.

Present research is focused on sinusoidal modeling, discrete wavelet transform, tree-structured quadrature mirror filter banks, composite sinusoidal modeling and wavelet transform, and combining low level continuous wave (LLCW) test measurements with HPD/VPD measurements to develop stress envelopes that encompass the frequency range from 100 kHz to 1 GHz. A brief discussion of each of these bounding techniques will follow.

Future research will extend the waveform envelope research from individual test points at the box level to system level modeling. The combination of additional transient and continuous wave threats will also be explored (Lightning, Electromagnetic Radiation, Power Switching Transients). A discussion of these topics will also follow.

Conclusions

The bounded electromagnetic stress envelope provides the maximum stress waveform regardless of the actual aircraft/threat scenario, allows waveform construction from multiple sources (high level pulse, LLCW and analysis) and creates a more complete characterization of the aircraft/threat interaction which increases test confidence. The benefits include use of all measured data to provide a better estimate of the maximum stress at a test point, optimization of survivability by incorporating "smart" margins, and design of custom envelopes that allows expanded use of present direct drive capabilities.

EMP SIGNAL MODAL ANALYSIS

S.YVETOT (*) - J.P. PERCAILLE
Centre d'études de Gramat
Dept ERI, Sce ES
46500 Gramat, France

C.MAILHES
GAPSE /ENSEEIHT
2, rue Camichel
31071 Toulouse cedex, France

Today, such a lot of EM perturbations exists like EMP or lightning, that we have to protect all sensitive electronic systems. In particular, the study of EMP effects on electronic systems is an important mission of the Centre d'études de Gramat, leading to validate the EMP hardening of systems.

For this case, the CEG is in possession of important simulators able to generate some electromagnetic states like EMP constraints with the plane-wave illumination. Then, measures and numerical processings of induced currents or voltages by coupling between EMP field and the system lead to characterize the electromagnetic behaviour of the object under test. This behaviour is defined through a modal decomposition (sum of damped sinusoids) of the induced currents (or voltages). Particularly, the peak magnitude, resonance frequency and quality factor are the main parameters which allow to consider some specifications both relating to protection methods and equipments use limitations.

With these parameters, we are able to generate the induced currents (or voltages) when injected on cables by special pulse generators ensuring the conformity of the materials to these specifications and the suitable hardening. Thus,as we can see, a good hardening is directly bound by the good estimation of the oscillant parameters.

The expansion of an EMP signal onto a linear set of damped and delayed sinusoids allows to identify the oscillant parameters by detecting the most energetic magnitude peaks of spectrum. Indeed, we can simply check that the spectral coordinates of these magnitude peaks (M_i, X_i) are dependant on magnitude and frequency parameters of sinusoids $\left(F_i = X_i \ , \ A_i \approx M_i . \frac{2\pi f_i}{Q_i}\right)$. Moreover, the inverse of the relative bandwith is an estimate of the quality factor.

Although the realization of this spectral method is easy , we have to consider some errors which involve a significant loss of accuracy on the measured parameters. Indeed, the above relations, are only valid for distant enough spectral components. Otherwise, the relative errors on the magnitude may reach 100 %, without forgetting the well-known limitations of the discrete Fourier transform when applied to truncated signals. Moreover,

this method cannot estimate the departure instants and thus any temporal computation is not available. So we present a new transient analysis method using up-to-date signal processing methods.

The required accuracy on the estimation of the oscillant parameters leads to a multi-model and multi-date approach, where the model is a Prony analysis (each Prony model having its own departure instants) like :

$$x(n) = \sum_{l=1}^{N_m} \sum_{m=1}^{P_l} B_{m,l} . Z_{m,l} . U(n - n_l)$$

The parameters $B_{m,l}$ et $Z_{m,l}$ are respectively the complex magnitude and pole of each oscillant mode. The Heaveside function $U(n)$ and the departure instant n_l allow to describe the reflexions of the incident wave. The total solution with respect to this formalism is difficult to obtain and leads to a non linear problem. Then, the global parameters computation is achieved in two steps:

1°) Detection of the departure instants

2°) Estimation of the components between each instant.

For the first step, we use the singularity detection properties of the wavelet transform realizing a signal segmentation. Then, in the second step, a deflation algorithm is used to fit the oscillant parameters (magnitude, phase, frequency and damped coefficient) of the successive Prony models. (S.Yvetot and al, 14th symposium of the gretsi, 14-16 Sept 1993, Juan les pins, France).

Results of this method are presented on figure 2, when applied to multi-date and multi-model Prony signals class like EMP signals illustrated on the figure 1. We have obtained a signal to modeling noise ratio about 10 dB.

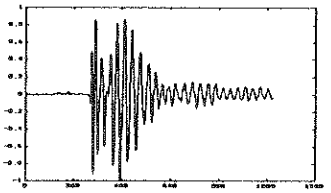

figure 1: EMP signal

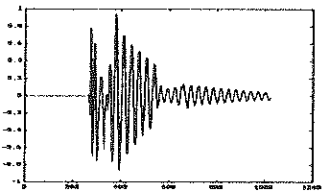

figure 2: result of analysis

The model presented here, is an adequat solution for analyzing the EMP signals and allows an approach of multi-transient signals with several unknown departure instants. The faster rise time of each transient is, the more efficient combined use of the wavelet transform and Prony modeling is.

GREEN'S DYADIC FORMULATION OF RADIATION IN THE PRESENCE OF GENERIC SCATTERERS

Captain Victor E. Martinez, Aircraft Research Group
WSM/Phillips Lab, Kirtland AFB, N.M., U.S.A. 87117

Dr. Shyam H. Gurbaxani*, Fiore Industries Inc.
Kirtland AFB, N.M., U.S.A. 87117

Theoretical and numerical considerations of the boundary value problems involving electromagnetic radiation from antennas in the presence of generic, finite and infinite, scatterers are investigated. The problem is handled in a completely generalized fashion using Green's dyadic $\underline{\underline{G}}(r_s, r_o)$ functions which are constructed to be appropriate to the geometry of the system. With conditions germane to the problem, the Green's dyadic can so simplify the problem as to limit the integration to antenna alone as given in the expression for the electric field intensity $E(r_o)$:

$$E(r_o) = jwu \int_{ant.surf.} K(r_s) \cdot \underline{\underline{G}}(r_s, r_o) dS$$

The surface currents induced on the scatterer are then obtained which satisfy the boundary conditions. The methodology of handling numerical sets of integer order, as well as real order, orthonormal eigenfunctions is developed with particular emphasis on the rapid convergence in order to be acceptable with reasonable computing power.

The truncation errors involved in such problems is checked by observing the continuity conditions at the boundary intersections. The symmetry of the problem is used in the particular case of a finite cone wherein the real and imaginary parts of the induced currents on the base converge to zero at the base center.

Numerical computation techniques used will be discussed. The accuracy of the algorithm is verified by the smooth continuity of the induced currents developed from entirely different eigenfuntions in the different regions of the system.

Finally the agreement of the theoretical/numerical results with the experimental and analytic work of Adachi, Kouyoumiam and Van Sickle at the University of Illinois will be presented.

Application of a Low Rank Approximations Based Iterative Method to the Electromagnetic Wave Scattering Problems.

Serge Kharchenko, Paul Kolesnikov,
Eugene Tyrtyshnikov, Alex Yeremin
Russian Academy of Sciences
Elegant Mathematics, Inc.
Michael A. Heroux, Qasim Sheikh*
Cray Research, Inc.

Abstract

It is well-known that the computational bottleneck in using boundary integral methods to solve the electromagnetic wave scattering problems is typically the solution, via LU decomposition, of dense linear systems $Ax = b$. This is especially true as the problem dimension grows large since the the arithmetic complexity of LU decomposition is $O(n^3)$, which is an order of magnitude greater than any other phase of the computation. In previous papers we have presented iterative methods with $O(n^2)$ computational complexity for solving linear systems of equations arising from application of boundary integral techniques to industrial class problems. These methods construct a block diagonally perturbed sparse preconditioner from the given matrix and use a stablized version of block GMRES method to solve the linear system. However, these methods still require $O(n^2)$ memory locations

*Corresponding Author: 655 Lone Oak Drive, Eagan, MN 55121 USA, email: qasim.sheikh@cray.com, Phone: (612) 683-3634, Fax: (612) 683-3699

to store the dense matrix. For dense linear systems of sizes close to 100k and more the disk space needed to store such matrices becomes unrealistic for todays storage technologies.

In this paper we present results from a class of iterative method for solving dense linear systems that have $O(n \log^2 n)$ computational and I/O complexity and need $O(n)$ memory locations. We briefly discuss the mathematical justification for the existence of such an iterative solver followed by the outline of the solution strategy. We use singular value decompositions of subblocks of A to create a block low rank approximation $\tilde{A}$. The memory requirements to store $\tilde{A}$ and the computational complexity of computing $\tilde{A}x$ are significantly less than the storage requirements for A and the computational complexity for computing Ax. These low rank approximations are computed after a certain gangster projector is applied to the matrix. This process ensures that the approximation is nonsingular whenever the original matrix is nonsingular. Our matrix compression and solution techniques are purely algebraic and no knowledge of the kernel of the integral formulation is needed. Also, the low rank approximation technique is embarrassingly parallel and lends itself well to a distributed memory implementation.

We show the efficiency of these methods by solving dense complex linear systems of sizes up to 100k with multiple right hand sides on CRAY C-90 vector/parallel computers. These linear systems are extracted from the simulation of electromagnetic wave scattering phenomenon in multi-layered dielectric medium using the boundary integral techniques for solving integral equation formulation of Maxwell Equations. Our experiments show an order of magnitude reduction in the memory requirement and an all most two orders of magnitude reduction in computation time taken by a fully optimized direct solver.

STUDY OF SCATTERING AND RADIATION BY ARBITRARY BODIES OF REVOLUTION WITH CG-FFT METHOD

S. Piedra*, M. F. Cátedra, J. Basterrechea
Departamento de Electrónica. Universidad de Cantabria
Avda. Los Castros s/n. 39005 Santander. Cantabria. Spain
Phone: + 34 42 201493 Fax: + 34 42 201402

ABSTRACT

In this work, the analysis of both scattering by conducting bodies of revolution (BOR's) and radiation patterns of dipoles in the presence of BOR's is tackled with the Conjugate Gradient Fast Fourier Transform Method (CG-FFT). The BOR can have arbitrary geometry (apertures, non contiguous metallizations, etc.).

SUMMARY

The first step to analyze the problem is to obtain the currents induced by the excitation (plane waves or dipoles) in the metallic surfaces of the BOR. From them the scattered fields can be computed by solving the electric field integral equation in its mixed potential integral form (MPIE):

$$n \times E^i = n \times \left[j\omega\mu \iint J(r')\, G(r,r')\, ds' - \frac{1}{j\omega\epsilon} \nabla \iint \nabla J(r')\, G(r,r')\, ds' \right]$$

To solve this MPIE a CG-FFT discretization scheme (M.F. Cátedra et al., IEEE-AP, 286-289, 1990 and J.C. Arredondo et al., IEEE-AP-S, 790-793, 1991) using modified rooftops as basis functions and modified razor-blades as testing functions has been developed. The following set of coordinates has been used to simplify computations: n: normal to the BOR surface at any point, ϕ: azhimutal coordinate and $t = n \times \phi$: normal to the previous ones at each point.

The periodic nature of the problem in the azhimutal direction leads directly to the use of the FFT to perform the cyclic convolution operations (that implies an uniform discretization step in this direction). In the other direction (t) convolutions must be computed numerically and hence nonuniform discretization steps can be used in it allowing a better geometrical model of the structure.

The resulting scheme is efficient compared with classical methods like the Body of Revolution formulation of Method of Moments concerning memory storage requirements and CPU times. This efficiency is increased when the problem under analysis is a metallic surface with arbitrary geometry conformed to a BOR like the shown in Figure 1 because apertures are directly included in the formulation.

The range of applicability of the resulting computational scheme is multiple. It can be used to solve typical scattering problems like Radar Cross Section (RCS) of BOR's by using plane wave excitation. It is also possible to use electric and magnetic dipoles with arbitrary polarizations placed anywhere in the space to simulate almost all practical situations. It can also be integrated as part of a more general tool in order to analyze particular fragments of a complex environment in an accurate way (ageneral surface can be locally modelled by a BOR surface). Finally, the results obtained with this rigorous method can be used to validate the results obtained with

other methods.

RESULTS

As an example, the results obtained with this method for the sphere section shown in Figure 2 with a $\lambda/10$ monopole excitation are presented in Figure 3. The sphere section has been obtained by cutting a 1m radius sphere with a cylinder of radius .5878m. The $\lambda/10$ monopole has been simulated with a $\lambda/20$ dipole. The radiation pattern obtained with this method (BOR) for the $\theta=90$ cut of this structure is compared in Figure 3 with the results obtained using a MM formulation (F. Rivas et al., URSI Symp., 154, 1993). In Figure 4, the results obtained with both methods for the $\phi=0$ radiation pattern cut are compared. In both cases the agreement is excellent.

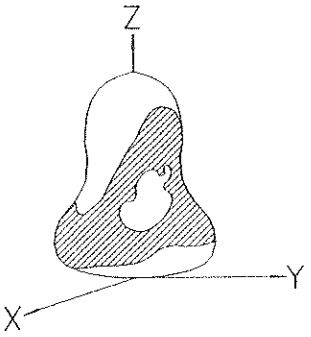

Figure 1: Arbitrary metallic surface conformed to a BOR.

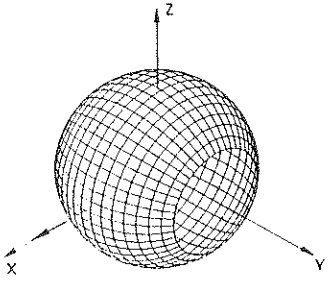

Figure 2: Sphere section analyzed in Figure 3 with the dipole placement shown.

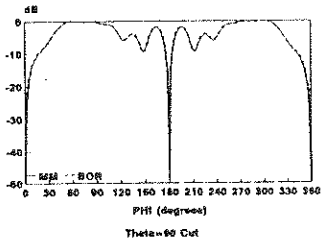

Figure 3: Radiation pattern of the sphere section shown in Figure 2 in presence of a $\lambda/10$ monopole: $\theta=90$ cut.

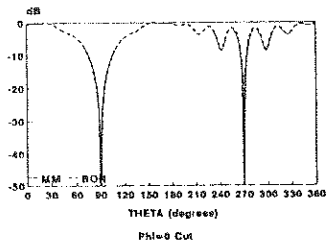

Figure 4: Radiation pattern of the sphere section shown in Figure 2 in presence of a $\lambda/10$ monopole: $\phi=0$ cut.

Polarizability matrix of layered chiral sphere

Murat E. Ermutlu, Ari H. Sihvola

Helsinki University of Technology
Faculty of Electrical Engineering
Electromagnetics Laboratory
Otakaari 5A, SF-02150 Espoo, Finland

Tel.: 358-0-451 2260
Fax: 358-0-451 2267
email: murat.ermutlu@hut.fi

Abstract

Using quasi-static analysis, this article solves the dipole moments that are induced by electromagnetic field in a layered chiral sphere, consisting of a spherical core and a spherical shell. The result is the low-frequency polarizability matrix of the sphere, and can be used to calculate the Rayleigh scattering of this object. Due to the chirality, the polarizability matrix has four components, electric and magnetic co- and cross-polarizabilities, that are functions of the permittivity, permeability, and chirality parameters of the core and shell materials and the ratio of their radii. The analysis is based on straightforward expansions of the field solutions in each region, and on making use of the boundary conditions, which leads to the inversion of a 8×8 matrix. The result can be shown to satisfy all the checks of previously known special cases of homogeneous chiral sphere and layered dielectric–magnetic sphere.

As a numerical example the effect of a dielectric layer on a chiral core is given. The polarizability matrix components are examined when the permittivity of the layer changes. The permeabilities of the both media are assumed to be those of free space and the chirality parameter of the core is taken as $\kappa = 0.1$. Fig. 1 shows the magnitude of the electric polarizability (α_{ee}) which is increasing when the permittivity increases. Fig. 2 shows an interesting effect of the chirality which is the appearance of magnetic polarizability in a chiral sphere without magnetic permeability. Finally, Fig. 3 shows the effect of permittivity on the crosspolarizability (α_{em}). The message is a rather strong shielding effect: α_{em} decreases strongly as layer permittivity inreases from the vacuum-permittivity value (no layer). On the other hand, α_{em} decreases with increasing core permittivity. The parameter δ is defined as $\delta = a_1^3 a_2^{-3}$ where a_1 is the radius of outer sphere and a_2 is the radius of the core.

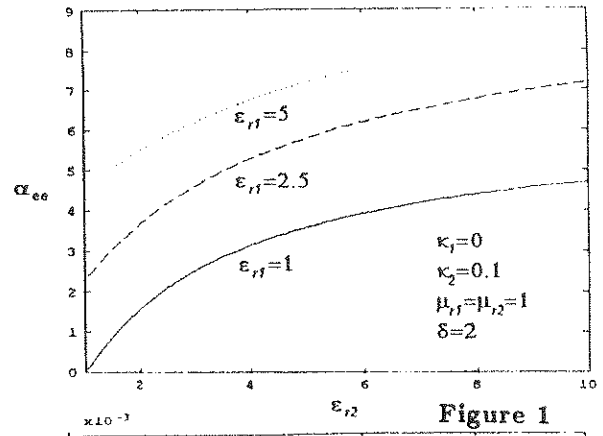

Figure 1

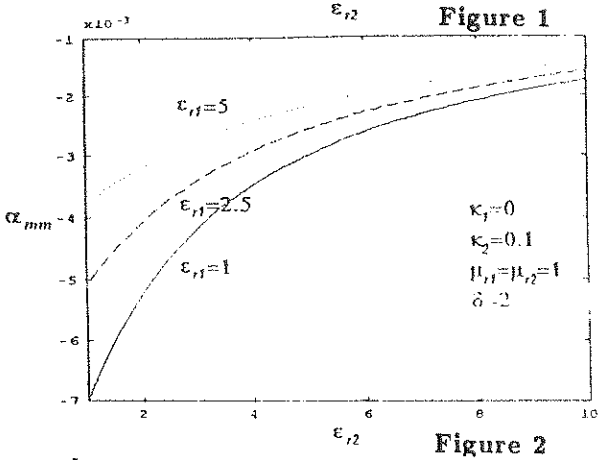

Figure 2

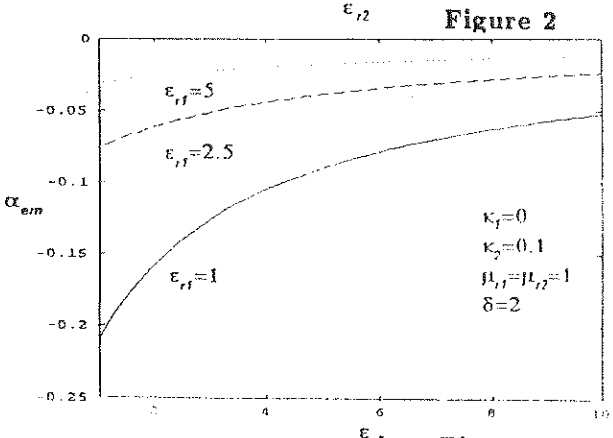

Figure 3

BOUNDARY-ELEMENT METHOD AS APPLIED TO DIELECTRIC OPEN-GEOMETRIES

S.M. Chehrehrazi* and A.R. Baghai-Wadji

Vienna University of Technology
Institute for Electrical and Electronic Engineering
Applied Electronics Department
Gusshausstrasse 27-29, A-1040, Vienna
AUSTRIA

Abstract: We consider N electrodes with arbitrary cross-section geometries, both in an isotropic and an anisotropic dielectric occupying the domain Ω with a boundary surface Γ. Γ is assumed to be the union of two subdomains Γ_m and Γ_f, which denote respectively the metalized and the non-metalized (i.e. free) boundary-areas. Some of the enclosed electrodes may float electrically. Our goal is the semi-numerical solution of the underlying boundary-value problem associated with open geometries, examples of which are given below.

The Laplace equation and the Poisson equation for the potential functions $\varphi^{ex}(\vec{r})$ and $\varphi^{in}(\vec{r})$ are respectively valid in the exterior and interior regions. Employing the infinite-domain Green's function related to the Laplace operator, and using Green's second integral theorem, it is possible to establish two singular surface-integrals: one for φ^{in}, its normal derivative $\partial\varphi^{in}/\partial n^{in}$ and the charge distribution ρ in Ω, and the other for φ^{ex} and its normal derivative $\partial\varphi^{ex}/\partial n^{ex}$. These integral equations have to be interpreted in Cauchy's sense and can be discretized by straightforward application of the method of moments. Incorporating the continuity conditions $\varphi^{in} = \varphi^{ex}|_{\Gamma_f}$ and $\partial\varphi^{ex}/\partial n^{ex} = \epsilon_r \partial\varphi^{in}/\partial n^{in}|_{\Gamma_f}$ in a discretized form and using the boundary conditions on the electrode surfaces in Ω, we obtain a matrix equation for the unknown potential-values on Γ_f and the charge distribution on electrodes.

Two characteristic examples are presented below. In each case the underlying geometry, the resulting equi-potential lines and the charge distributions on the selected electrodes are shown. In the paper we will show that the anisotropic properties and the 3D effects can be included in the analysis in a mathematically tractable way.

1.EXAMPLE:

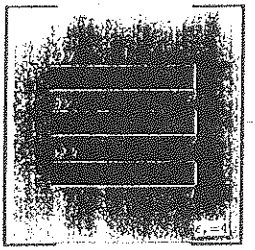

symmetric geometry of
an open structure

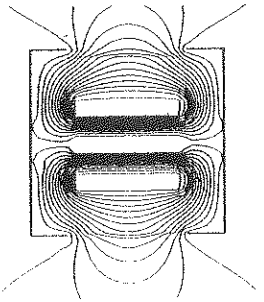

equi-potential lines

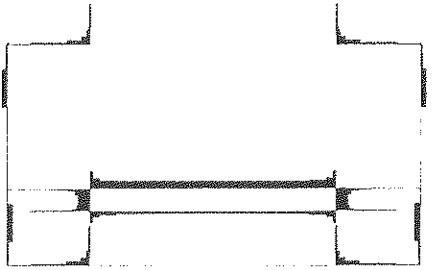

charge distribution on the grounded
electrodes and on the bounding
surface of the first electrode
in the interior region

2.EXAMPLE:

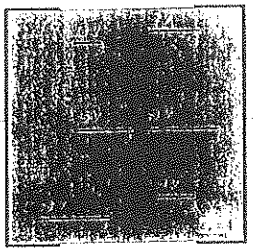

non-symmetric geometry of
an open structure

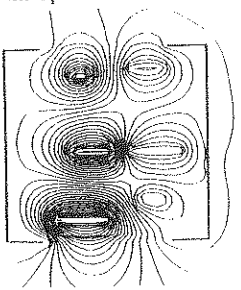

equi-potential lines

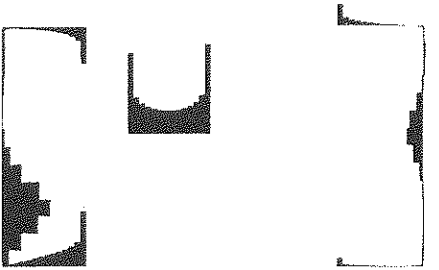

charge distribution on the grounded
electrodes and on the bounding
surface of the third electrode
in the interior region.

GERAC
ELECTROMAGNETISME

THE SENIOR PARTNER IN ELECTROMAGNETIC COMPATIBILITY

ENGINEERING : SOME OF OUR REFERENCES

- major participation in lightning and HIRF certification of AIRBUS planes,
- development of EMC specifications for Channel Tunnel electronic equipment,
- substantial engagement in preparing the HA-EMP Hardening Guide (French DOD).

DIGITAL SIMULATIONS : SOME OF OUR PRODUCTS

- **3D codes :**
  - structures in any material,
  - perfect or not perfectly-conducting floor,
  - non linear events,
  - ...
- **2D codes**
- **Cable coupling codes**
- **Modelling protection items**

TESTS : SOME OF OUR FACILITIES

- **Standard tests** : The whole equipment to run the major standard tests in lightning, EMC, HA and LA-EMP.

- **Non standard tests :**

  Double exponentials
  - shape (tm/td) : from 5 ns / 200 ns to 5 µs / 150 ms
  - amplitudes (Vco/Icc) : from 100 V / 20 A to 100 000 V / 10 A

  Damped sinusoids :
  - frequencies from 10 kHz to 100 MHz :
  - amplitudes up to 10 000 V / 100 A

GERAC - BP 19 - 46500 GRAMAT - Tél. 65 38 79 23 - PARIS : (1) 41 07 51 51 - TOULOUSE : 61 39 93 75

A Method of Moments Strategy for Calculating the Radiated Electromagnetic Field from Complex Multilayerboards

Stefan Öing *, Uwe Keller **, Mathias Künne **

* Siemens Nixdorf Informationssysteme AG · Cadlab – Analog System Engineering
** Universität GH Paderborn · Cadlab – Analog System Engineering
Bahnhofstrasse 32 · D-33094 Paderborn · Germany

Due to the increasing spectral content of digital and/or analog signals the problem of high frequency radiation is of serious concern to manufacturers and designers of electronic products. One of the most important aspects of 'electromagnetic compatibility' (EMC) is the compliance with radiation constraints (CISPR, FCC). In order to predict the radiation of Printed Circuit Boards (PCB), basically all effects related to scatterers on the board have to be considered.

In order to account for all relevant physical effects concerning radiation, the Maxwell equations are transformed into a suitable integral equation which can be solved numerically by the Method of Moments (MOM). Due to the tremendous number of variables obtained in that manner the problem renders a prohibitive demand of computer storage as well as long computation times. Therefore, to achieve a more tractable formulation enabling the evaluation of a practical multilayerboard, simplification schemes have been employed and embedded into the MOM-code of COMORAN (COMputation Of RAdiatioN).

One way to decrease the complexity of a given problem is the use of simple though appropriate geometrical models. The geometrical layout of such an adequate simple model might differ considerably from the original structure, where on the other hand care must be taken not to change the general orientation significantly with respect to the radiated fields. For example, a series of rectangular bends within an area can be replaced by one single bend, provided the area is small compared to the wavelength.

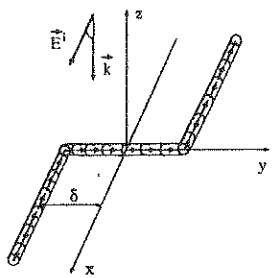

Figure 1: Wire ($\kappa \to \infty$) irradiated by a plane wave ($\varepsilon_r = 1$, $|E_x| = 1\,\mathrm{V/m}$, $\vec{k} = -\vec{e}_z$, $\vec{p} = \vec{e}_x$).

As a very elementary example the current distribution on a z-like structure was examined, figure 1. The excitation was assumed to be a plane electrical field wave of unit magnitude, x-polarization, and of perpendicular incidence. The total length of the structure was kept constant at $\lambda = 30cm$, the radius was chosen to be $1mm$.

The parameter δ, describing the extend in the y direction, was varied from 0 to $\lambda/4$. As can be easily seen from figure 2, where curves have been distinguished by that parameter, the current distribution begins to vary significantly if δ exceeds a certain length (for instance, the maximum deviation of the current at $\delta = \lambda/64$ from the current of a straight wire is less than 1.4%). The figures 3 displays the relevant components of the electric field intensity (x and y) within a plane $z = 0$ at a range of 3 meters. According to these observations, it is possible to specify a range of tolerance, which in turn for a given polarization could be directly transformed into a simplification scheme of the geometrical structure.

Since the MOM-techniques are verified by a great number of examples in various publications, adequate geometrical models for the evaluation of complex boards could be achieved by simply using a MOM code like COMORAN; in addition, the computations have been compared to measurements with satisfactory compliance.

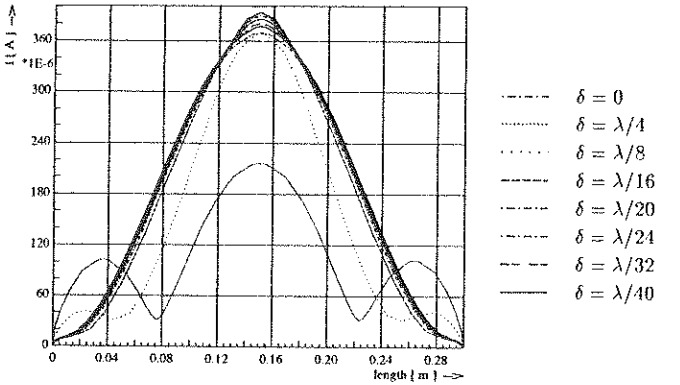

Figure 2: Current distribution on a z-like structure, variation of middle segment length 2δ.

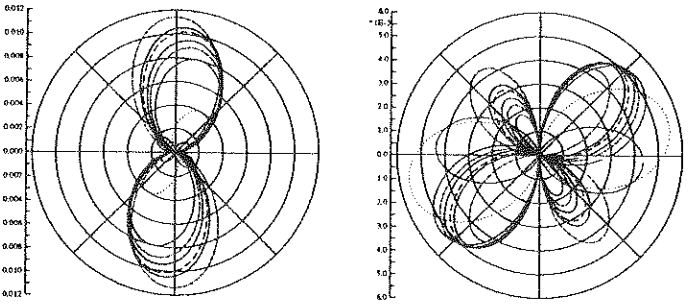

Figure 3: Characteristics of E_x and E_y within the plane $z = 0$ at 3 meters distance.

System-Theoretical Investigations on the Application of the Coupled-Wave Theory for the Diffraction Analysis of Dielectric Gratings

E. Griese

Siemens Nixdorf Informationssysteme AG · Cadlab – Analog System Engineering
Bahnhofstrasse 32 · D-33094 Paderborn · Germany

Introduction

The diffraction behaviour of optical gratings becomes more and more important in the area of modern communication systems. Examples of the field of application of optical gratings are optical multiplexers, demultiplexers, and of course grating couplers which can be used bidirectional. In the past many methods have been developed for analysing the diffraction behaviour of dielectric gratings. One of these methods is the Coupled-Wave Theory (M.G. MORARAM & T.K. GAYLORD, Rigorous Coupled-Wave Analysis of Planar-Grating Diffraction, Journal of Optical Society of America, 72(2):187-190, February 1982) which is a differential equation method.

1 The Coupled-Wave Theory

To solve diffraction problems in the frequency domain using the Coupled-Wave Theory the grating region is divided into a finite number of planar horizontal layers. Then, the permittivity within one layer depends solely on one coordinate which points into the direction of the grating periodicity. Introducing a coordinate system, this will be the x-direction, the unit vector in z-direction is the global grating perpendicular while the grating surface does not depend of the y-coordinate. Applying the Coupled-Wave Theory to the field strength within the nth layer, an ordinary system of coupled differential equations with an infinite dimension has to be solved. This system of differential equations can be derived directly from Maxwell's equations taking into account the pseudo-periodical behaviour of the field strengths.

$$\underbrace{\frac{d}{dz}\begin{pmatrix}\underline{\mathbf{s}}_E(z)\\ \underline{\mathbf{r}}_E(z)\\ \underline{\mathbf{r}}_H(z)\\ \underline{\mathbf{s}}_H(z)\end{pmatrix}}_{d\underline{\underline{\mathbf{u}}}(z)/dz} = \underbrace{\begin{pmatrix}\underline{\underline{\mathbf{0}}} & \underline{\underline{\mathbf{P}}}\\ \underline{\underline{\mathbf{Q}}} & \underline{\underline{\mathbf{0}}}\end{pmatrix}}_{\underline{\underline{\mathbf{A}}}} \cdot \underbrace{\begin{pmatrix}\underline{\mathbf{s}}_E(z)\\ \underline{\mathbf{r}}_E(z)\\ \underline{\mathbf{r}}_H(z)\\ \underline{\mathbf{s}}_H(z)\end{pmatrix}}_{\underline{\underline{\mathbf{u}}}(z)} \quad (1)$$

The $\underline{\mathbf{s}}_E(z)$, $\underline{\mathbf{r}}_E(z)$, $\underline{\mathbf{s}}_H(z)$, and $\underline{\mathbf{r}}_H(z)$ are vectors with infinite dimension which comprise the coefficient-functions of the field representation in the nth planar layer. The submatrices of $\underline{\underline{\mathbf{P}}}$ and $\underline{\underline{\mathbf{Q}}}$ again are built by submatrices with of course an infinite dimension.

The principal structure of the system matrix $\underline{\underline{\mathbf{A}}}$ is obtained because the arrangement of the coefficient vectors within the state vector $\underline{\underline{\mathbf{u}}}(z)$ has been choosen as given above. The numerical solution requires a reduction of this system to a finite dimension. This can be achieved by introducing a lower summing index $-M_l$ and an upper one $+M_u$ in the corresponding field approaches. Then, with increasing M_l and M_u the solution of the reduced system converges to the real solution.

2 Power Balance of the Reduced System

From the physical point of view it is obvious that in the case of lossless materials ($\kappa = 0$, $\varepsilon_r \in \mathbb{R}$) the original system of differential equations will describe a lossless system. But ist is not obvious, that the reduced system describes a lossless system as well.

Starting-point for the following investigations is Poyntings theorem. All materials are assumed to be lossless and without sources (charges, currents). Therefore, the integral of the time-averaged Poynting vector $\widehat{\mathcal{S}}(\boldsymbol{r})$ over an arbitrary closed surface has to vanish. As the geometrical arrangement does not depend on the y-direction, the complex Poynting vector $\mathbf{S}(\boldsymbol{r})$ depends solely on the x- and z-coordinate and it is periodical in x-direction with the grating period Λ. Considering this, a criterion for the lossless system characteristics is the integral of the z-component of the Poynting vector over the areas A_z^+ and A_z^-, which has to be zero:

$$\mathrm{Re}\left\{ l_y \cdot \int_{x_0}^{x_0+n\cdot\Lambda} \left[\mathrm{S}_z(x,z_2) - \mathrm{S}_z(x,z_1)\right] dx \right\} = 0 \,. \tag{2}$$

Here l_y, $l_z = z_2 - z_1$, and $n\,\Lambda$ are the dimensions of a rectangular cylinder, whose edges are parallel to the corresponding axis of the cartesian coordinate system introduced above (see also figure 1).

Applying the approaches for the field strengths to this criterion yields for arbitrary values of z_1 and z_2

$$\begin{aligned} &\mathrm{Im}\left\{\underline{\mathbf{r}}_H^*(z_1)\cdot\underline{\mathbf{s}}_E(z_1) + \underline{\mathbf{s}}_H^*(z_1)\cdot\underline{\mathbf{r}}_E(z_1)\right\} \\ &\quad = \mathrm{Im}\left\{\underline{\mathbf{r}}_H^*(z_2)\cdot\underline{\mathbf{s}}_E(z_2) + \underline{\mathbf{s}}_H^*(z_2)\cdot\underline{\mathbf{r}}_E(z_2)\right\} \,. \end{aligned} \tag{3}$$

This means that the imaginary part of the scalar product of two new introduced vectorial quantities $\underline{\mathbf{u}}_H = \left(\underline{\mathbf{r}}_H^T\ \underline{\mathbf{s}}_H^T\right)^T$ and $\underline{\mathbf{u}}_E \left(\underline{\mathbf{s}}_E^T\ \underline{\mathbf{r}}_E^T\right)^T$ has to be independent from the coordinate z.

$$\frac{d}{dz}\,\mathrm{Im}\left\{\underline{\mathbf{u}}_H^*(z)\cdot\underline{\mathbf{u}}_E(z)\right\} = 0 \tag{4}$$

The consideration of the field describing differential equation (1) yields

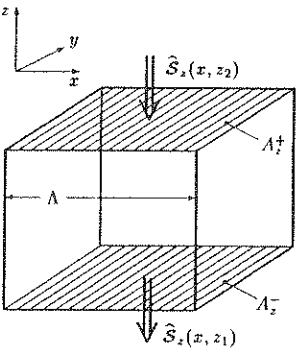

Figure 1: Rectangular Cylinder

$$\mathrm{Im}\left\{\underline{\mathbf{u}}_E^*(z)\cdot\underline{\underline{\mathbf{Q}}}^*\cdot\underline{\mathbf{u}}_E(z) + \underline{\mathbf{u}}_H^*(z)\cdot\underline{\underline{\mathbf{P}}}\cdot\underline{\mathbf{u}}_H(z)\right\} = 0 \,. \tag{5}$$

If the matrices $\underline{\underline{\mathbf{P}}}$ and $\underline{\underline{\mathbf{Q}}}$ are hermitian, this equation is satisfied because then both summands are real quantities. Therefore, the condition

$$\underline{\underline{\mathbf{P}}} = \underline{\underline{\mathbf{P}}}^* \qquad \text{and} \qquad \underline{\underline{\mathbf{Q}}} = \underline{\underline{\mathbf{Q}}}^* \tag{6}$$

is sufficient for the loss-free characteristics of the system. As equation (5) has to be valid for arbitrary and independent vectors $\underline{\mathbf{u}}_E(z)$ and $\underline{\mathbf{u}}_H(z)$ these characteristics of $\underline{\underline{\mathbf{P}}}$ and $\underline{\underline{\mathbf{Q}}}$ are necessary, too. It will be shown that for $M_l = M_u = M$ and for $\varepsilon_r \in \mathbb{R}$ the conditions given in (6) are satisfied for any M.

Conclusion

It can be pointed out, that the necessary reduction of the system to a finite dimension does not change the loss-free system characteristics if the infinite summing of the field approaches is reduced to a finite, but symmetric one. Furthermore, from eq. (2) a power criterion will be derived which allows the definition of a relative error for checking the accuracy of numerical results.

Method of Moments Analysis of Radar Scattering by Chiral Cylinders

Majeed Alkanhal* and Ercument Arvas
Department of Electrical and Computer Engineering
Syracuse University, Syracuse, New York 13244-1240

A numerical solution to obtain the radar cross section RCS of chiral cylinder of arbitrary cross section which is illuminated by TM and/or TE plane wave incidence is described in this paper. Chiral medium, defined by Jaggard et al., as consisting of macroscopic chiral objects randomly embedded in a dielectric is characterized by the constitutive relations of the form:

$$D = \varepsilon E - j\gamma B \quad \text{and} \quad H = (1/\mu) B - j\gamma E ,$$

where ε is the permittivity, μ is the permeability, and γ is the chirality admittance of the chiral medium. The chirality admittance γ is an indication of the degree of chirality of the medium. When we put $\gamma = 0$ in these equations they will reduce to the constitutive relations for simple (achiral) media, that is because the medium with ($\gamma = 0$) has no handedness. It is worth noting that according to the above equations the chiral media which is artificially made with chiral objects embedded in dielectric will exhibit optical activity. This property will cause a linearly or an elliptically polarized wave to rotate its axis of polarization as it propagates through the chiral medium.

The numerical solution presented in this paper is a method of moments solution to the surface E-field integral equations of the chiral cylinder. First, 2-D surface integral representation of the homogeneous chiral cylinder is developed. A more simplified form of surface integral equations for scattering by chiral cylinders which is feasible to numerical computations is, then, followed. The chiral surface equivalent principle is used to replace the surface of the chiral cylinder by equivalent electric and magnetic currents radiating in free space and in unbounded chiral medium. The use of the chiral surface equivalence principle results in a set of two coupled vector integral equations for the equivalent surface electric and magnetic currents. Due to the coupling between the longitudinal and the transverse components of the fields in chiral media, both longitudinal and transverse components of the surface currents are considered in the scalarization of the coupled vector equations. The resulting coupled scalar equations are, then, solved by a pulse basis and point matching method of moments solution. Once the equivalent surface currents are solved for, the RCS of the chiral cylinder can be obtained utilizing the surface currents in the field equation of the external equivalent problem.

Numerical results for circular chiral cylinders of different parameters show excellent agreement with the exact data found by eigne functions solution. Figure 1 compares the magnitudes of the computed and the exact bistatic echo width of a circular chiral cylinder of the shown parameters. The results of 44, 22 and 12 ($0.047\,\lambda_m$, $0.090\,\lambda_m$, $0.17\,\lambda_m$) segment approximations are in excellent agreement with the exact data. Also, this figure shows that as the number of segments increases, the MoM solution approaches the exact solution for both the co-polarized and the cross-polarized scattered fields. It is clearly noticeable that the cross-polarized scattering cross section of the chiral cylinder is of significant value which is a manifestation of the chirality of the cylinder even at small values of chirality admittance($\gamma = 0.0005$).

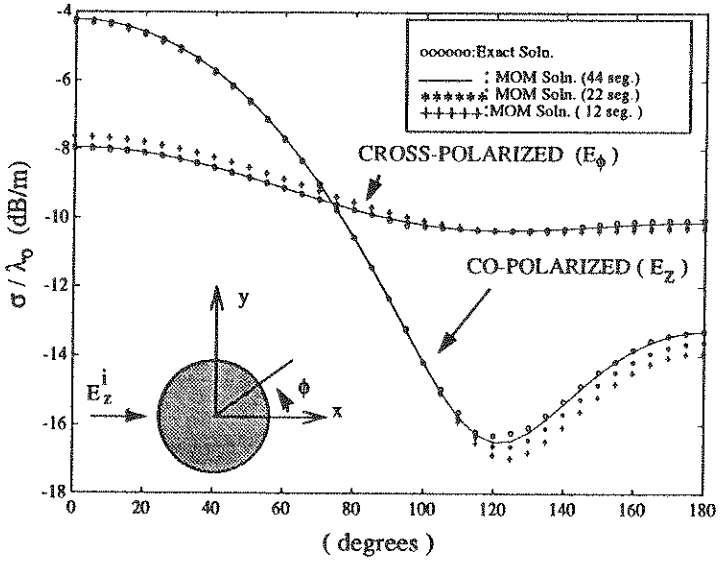

Figure 1: The co-polarized and cross-polarized bistatic echo width of a circular chiral cylinder for TM_z incident plane wave. (γ= *0.0005*, μ_r *= 4.0*, ε_r *=1.5*, δ_e *=0.0*, δ_m *=0.0*, *r=0.1* λ_o)

The effect of chirality in the scattered field for a square chiral cylinder is shown in figure 2. For chirality admittance varies from 0.0001 to 0.0005, the cross-polarized echo width has effected drastically by the increasing chirality added to the cylinder. Although the cross-polarized scattered field has almost the same pattern along the cylinder, it's magnitude evolves from zero-field at γ=0 and gradually, but significantly, increases with the increment of γ to reach a substantial magnitude even at, still small value of, γ=0.0005.

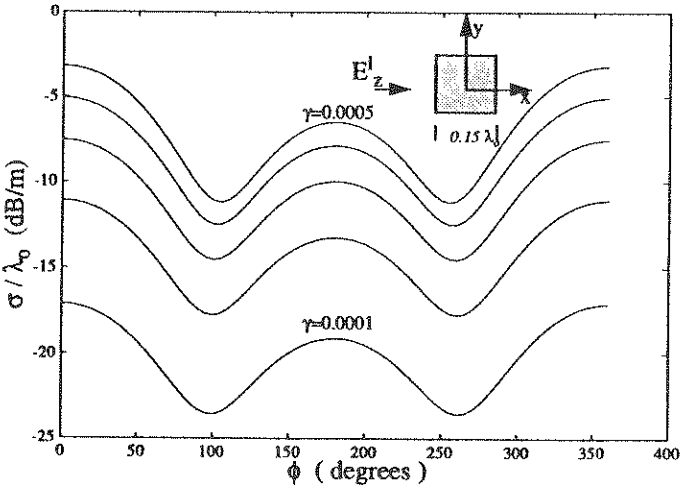

Figure 2 : The cross-polarized bistatic echo width of the square chiral cylinder illuminated by an incident TM_z plane wave (γ= *0.0001 to* γ= *0.0005*, μ_r *= 2.0*, ε_r *=3.0*, δ_e *=0.0*, δ_m *=0.0.)*

ELECTROMAGNETIC MODELING OF A POWER MODULE CASE.

E. CLAVEL, J.L. SCHANEN, J. ROUDET
ENSIEG-LEG CNRS-URA N°355
BP 46-38402 Saint Martin d'Heres cedex France

Introduction.

Nowadays the power levels required by a lot of industrial applications lead to the use of high power switches.
This function is achieved with the help of an hybrid architecture associating several elementary components in parallel.
This technology is more and more widespread and allows the integration of a whole inverter arm in a single module.
Due to the low switching times of the IGBT used and to the high power range, wiring and coupling inductances cannot be neglected anymore.
The aim of this paper is to present an hybrid module and its modeling using a simulation tool which is dedicated to inductance and resistance calculation: InCa. An equivalent electrical inductive circuit is obtained and the modeling is compared with impedance measurement.

I-The module.

The studied module is TOSHIBA MG300J2YS1. It is composed of four IGBT (two pairs of paralleled IGBT) and four free-wheeling diodes (two pairs of paralleled diodes) (Fig. 1.).

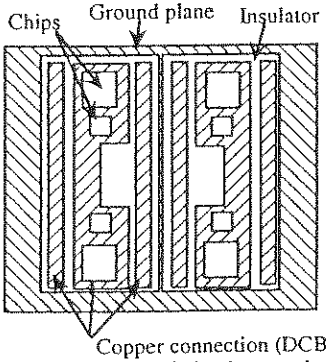

Fig. 1.The geometric implementation.

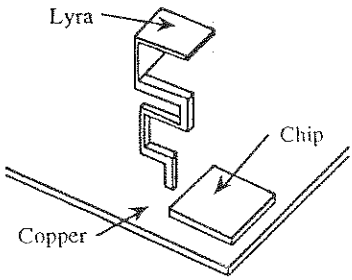

Fig. 2. A lyra.

The connections of the module in a converter structure are realised by three lyras C1, C2E1, E2. Fig. 2. gives an example of lyra.
The aim is to determine all wiring inductances, in order to obtain an equivalent circuit of the module case, which could be used in any power electronic simulator (PSPICE, PACTE) [B.ALLARD, H.MOREL, J.P.CHANTE "Power electronics circuit simulation using bondgraph and petri network techniques." IEEE PESC 1993].
The current waveforms will thus be available.

II-The electromagnetic model of the module case.

The three lyras and the copper connections between components have been modeled in order to find the values of the inductances and mutual inductances. The presence of the ground plane have been taken into account by using the magnetic image method.
We have used a simulation tool, developed in the laboratory InCa [J.L. SCHANEN "Intégration de la compatibilité électromagnétique dans la conception de convertisseurs en Electronique de Puissance." Thèse de doctorat INPG Janv.94]. It allows the determination of the different components of the electrical equivalent circuit (Fig. 3.).
Each straight part of circuit is modeled by a partial inductance coupled with the others [A.E. RUHELI. "Inductance Calculations in a Complex Integrated Circuit Environment." IBM Journal of Research and Development, Sept.72].

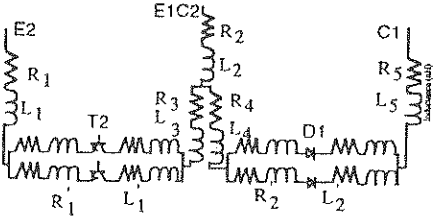

Fig. 3. The equivalent circuit (the mutual coefficients are not represented).

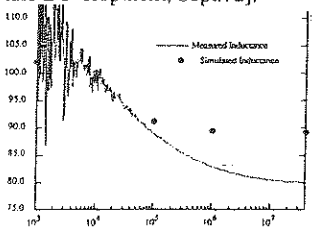

Fig. 4. Measured and simulated Inductance

III-The test structure.

In order to verify our modeling, we measured the total inductance of the module in a buck-converter configuration, replacing all semi-conductors devices by short circuits. In this structure only D1 and T2 functions are used.
Hence the mesh power inductance is :

$$Lm = L_1+L_3+L_4+L_5+2*(M_{13}+M_{14}+M_{15}+M_{34}+M_{35}+M_{45})+L'_1+L'_2+2*M'_{12}$$

The inductance values depend on frequency. As a result we simulated the module behavior for different frequencies (Fig. 4.).
For a large range of frequencies the results of simulations are closed to the measurements. For frequencies higher than 200 kHz, the number of subdivisions is insufficient. The simulation gives thus an overestimation of the value of the power mesh inductance. Nevertheless the difference between measurement and simulation is less than 10% for these frequencies.

Conclusion.

We have presented an electromagnetic modeling of a module case based on a simulated tool : InCa. The equivalent electrical circuit is obtained by replacing each straight segment of the structure by a R,L circuit and the results of simulations are in good agreement with measurements.
The code developed, InCa, is dedicated to inductance and resistance calculation. It is based on an analytical method and thus presents low computation time compared to the Finite Element Method.
All connection parasitic inductances and resistances may be evaluated with the help of this tool, which makes it very interesting for Computer Aided Design operations.

A GTD APPROACH TO OBTAIN RADIATION PATTERNS OF ANTENNAS ON BODIES MODELLED WITH NURBS SURFACES

J.Saiz, J.Pérez, M.T.López, O.Conde, R.Torres, M.F.Cátedra.
Grupo de Sistemas y Radio. Dpto. Electrónica. Universidad de Cantabria.
Avda. de los Castros s/n. 39005 Santander. Cantabria. SPAIN.

The knowledge and control of the effects of complex structures in the radiation patterns and coupling between on board antennas is a current requirement of the aerospace industries. The development of methods and compute codes is a sensible choice in contrast to the expensive measurements. In this communication a code called GONURBS, to analyze antennas on board of complex bodies is presented.

For the analysis of complex structures as satellites, ships, airplanes, cars, etc, one must have package consisting of a CAGD software, electromagnetic codes and post-processing programs. There is a strong dependency between the geometrical model of the bodies and the suitability of the electromagnetic approach used. In GONURBS the geometric description of the structures is given in terms of NURBS surfaces (W.Tiller, IEEE Computer Graphics Appl. 3, 61-69, 1983) which is a very optimized and powerful format for the complex bodies description available in most of the modern CAGD codes. In fact NURBS modelling is currently used in the aeronautic and automobile industries. NURBS are free-form parametric surfaces of arbitrary degree that provide a good accuracy with a low amount of information.

The Geometrical Optics (GO) and Geometrical Theory of Diffraction (GTD) have been used to analyze the effect of the structure in the radiation pattern of the antennas. GONURBS takes into account the following electromagnetic mechanism:

- Direct field
- Reflections
- Edge diffractions
- Double reflections
- Reflections-diffractions
- Diffractions-reflections
- Creeping waves.

The antennas are modelled using simple numerical models based on arrays of electric and magnetic infinitesimal dipoles. Therefore in the code the electromagnetic sources are dipoles.

The direct field is the field radiated by the dipoles in the direction where the rays do not find obstacles. In this case the obstacles are the NURBS surfaces of the body. For this analysis ray-tracing techniques as bounding-boxes for speed up the search are used (CHANG-GUY YANG, Computed-Aided Design, Vol.19, No.3, 1987). The reflected field is calculated by applying the GO method over the NURBS surfaces. In order to accelerate the calculations several algorithms are used previously for reject many of the surfaces which do not contain reflecting points in the search directions. The

Fermat principle in conjunction with the Conjugate Gradient Method (CGM) [6] is used for obtaining the reflection points. The diffracted fields from edges are considered by using the UTD method (R.G.KOUYOUMJIAN & P.H.PATHAK, Proc. IEEE, November 1974, pp.1448-1461). As in the reflected field computation, ray-tracing accelerating algorithms and the Fermat principle in conjunctions with the CGM are used for obtaining the diffraction points on the edges.

The major contribution to the total field is in general obtained from the above effects. However, for certain angles, frequency and polarization, mechanism of higher order, such double reflections and creeping waves are very important. Double interactions between surfaces and between edges and surfaces are treated using combinations of the single reflection and edge diffraction algorithms. UTD method (P.H.PATHAK, W.D.BURNSIDE, R.J.MARHEFKA, IEEE Trans. Ant. Prop. AP-28, No.5, pp.631-642, 1980) is used for calculate the creeping wave contribution. The geodesic curves are founded numerically, therefore the algorithm developed works efficiently for arbitrary geometries.

The individuals contributions are added for obtaining the radiation pattern of the antennas. The underlying contribution of this work in the application of the GO+GTD techniques on NURBS surfaces for the computation of the mechanism above. The developed method is quite efficient because it makes use of a small number of surfaces to model complex bodies, so it requires few memory and low computing time.

A NUMERICAL STUDY OF THE pxm RADIATOR

N.H. Younan*
B.L. Cox
C.D. Taylor

Department of Electrical and Computer Engineering
Mississippi State University
Mississippi State, MS 39762

W.D. Prather

Phillips Laboratory
Kirtland AFB, NM 87117

SUMMARY

For EMP applications, it is desired to design impulse-like transient radiating structures with cardioid patterns, where the structure is electrically small. One geometry that satisfies this requirement is a pxm structure. This antenna features an electric dipole moment, p, and a magnetic dipole, m, which are perpendicular and related in magnitude via $|\mathbf{m}| = c|\mathbf{p}|$, where c is the speed of light.

The performance of this structure is numerically analyzed to evaluate its suitability as a transmitting antenna, where an excitation source is applied to one end of the structure for various resistive loading. A similar type analysis is performed for the receiving case (N.H. Younan et al., IEEE International EMC Symposium, 420-424, 1993). Accordingly, a general method of moments code, developed by Sandia National Laboratory, called PATCH, has been used to numerically evaluate the performance of the pxm antenna over the frequency range of 10 KHz to 1 GHz. This code uses a configuration of triangular patches to represent complex shapes of conductor surfaces and determines the induced surface current density resulting from an incident field illumination.

Figure 1 illustrates the physical dimensions of the antenna structure. In order to guarantee the pxm conditions, $L \leq 0.1\lambda$ and $(h/L) < 0.2$ have to be satisfied. Analyzing this structure using the PATCH code requires that the size of the triangular patches are sufficiently small to model the geometry accurately. Also, the triangle edge lengths should be less than 0.1λ or even shorter. To ensure the convergence of the numerical solution, a "course" model with 53 edges in the top half of the structure with an average edge length of 6.23 cm is found to be suitable to use for this study.

In order to evaluate the suitability of the antenna structure as a transmitting antenna, the performance of the antenna is analyzed in terms of the front-to-back ratio and frequency response. The currents along the structure are also observed to

confirm that the numerical solution yields smooth current variations. Results for the front-to-back ratio, antenna patterns, and frequency response are examined for various loading terminations for frequencies up to 100 MHz. It is shown that the front-to-back ratios decrease from 27 dB for the matched case to 0 dB for the short-circuit case. Moreover, the current reveals a uniform behavior and increases in magnitude as the resistive loading decreases for a fixed applied voltage. For frequencies above 100 MHz, it is found that the pxm conditions are not satisfied.

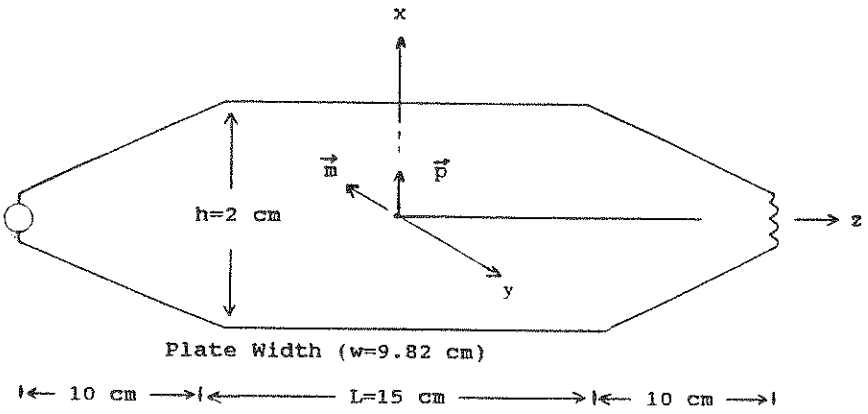

Figure 1. pxm Antenna Structure

"INDUCED CURRENTS ON LOADED AND SHIELDED ANTENNAS"

M. Courtot

CEA-Centre d'Etudes de Limeil-Valenton
94195 Villeneuve Saint-Georges, FRANCE

The finite difference time domain (FDTD)-method is applied to calculate the induced currents on loaded antennas which are located at different positions inside a cylindrical cavity lying above a mass plan. An electromagnetic pulse is propagated through an aperture of the cavity and coupled to straight thin wires inside.

The currents are calculated by solving the equations relating the electric field to the vector and scalar potentials. Let us connect the bottom end of the antenna to the mass plan through a resisitive, inductive and capacitive element. Then the current distribution can be calculated with Kirchoff's voltage law.

From a Fourier transform of the transient current evolution, we determine the spectral cross section.

This paper describes the methods and techniques implemented in a 3D-Code.

Numerical examples will be given as the transient currents on the load, the resonance frequencies, the cross-sections, etc..

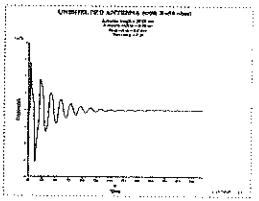

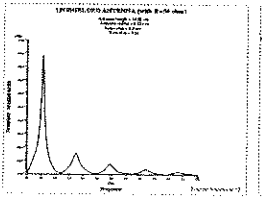

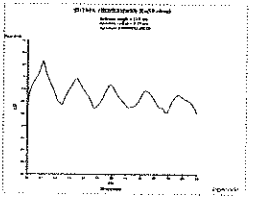

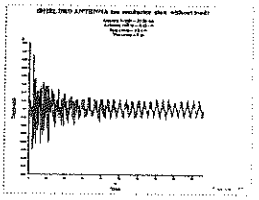

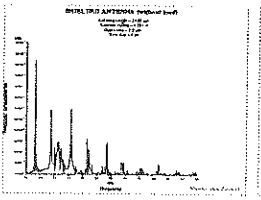

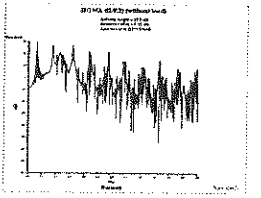

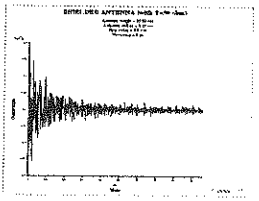

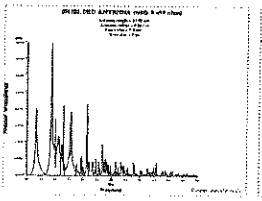

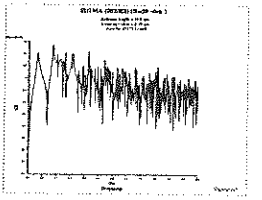

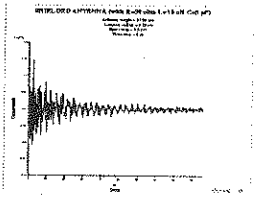

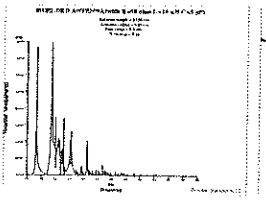

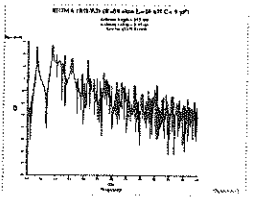

A LOW COST PARABOLIC REFLECTOR ANTENNA- AN UNDERGRADUATE PROJECT

* M. A.ABOUL-DAHAB AND N.M. ABD-EL-WAHAB
COLLEGE OF ENGINEERING STUDIES AND TECHNOLOGY,
ARAB MARITIME TRANSPORT ACADEMY,
P.O. Box 1029, ALEXANDRIA, EGYPT.

ABSTRACT

This paper describes a final year undergraduate project to set up a microwave antenna. It implies the design procedure as well as the implementation process of a low cost parabolic reflector antenna. The design procedure starts by knowing the required diameter of the reflector that fits a specific use, as well as the type of feeder at its focal point. Necessary surface geoemtry calculations are carried out and aperture efficiency is investigated for different f/d ratios. This is done via a computer software program that can display computational results in a variety of screen presentations.

After completing the design, a diagram of the reflector is drawn in full scale. A wooden pattern of the reflector is then made in the form of a number of segments. A metallic sheet of aluminum is made to take the shape of the wooden pattern by a hammering process. A polishing process is the followed to smooth the suface of the reflector. To simplify matters and to make it easy for feeding the reflector via a coaxial cable, a short dipole feeder is devised. The feeder being a wideband one, allows testing the reflector at the laboratory using the microwave (or antenna) bench available.

A parabolic reflector of 89cm diameter and a simple short dipole feeder has been designed and implemented by the undergraduate students at the College of Engineering Studies and Technology of the Arab Maritime Transport Academy. Experimental verification of the antenna has been carried out inside an anechoic chamber of the . A photo of the antenna is shown in the Fig.1 and its E-plane far field co-polar pattern at 3.8 GHz is shown in Fig.2. The feeder can further be modified to be a cross dipole one, a configuration that can be utilized in an IMARSAT standard-A land mobile terminal fitted on board ships (ship earth station).

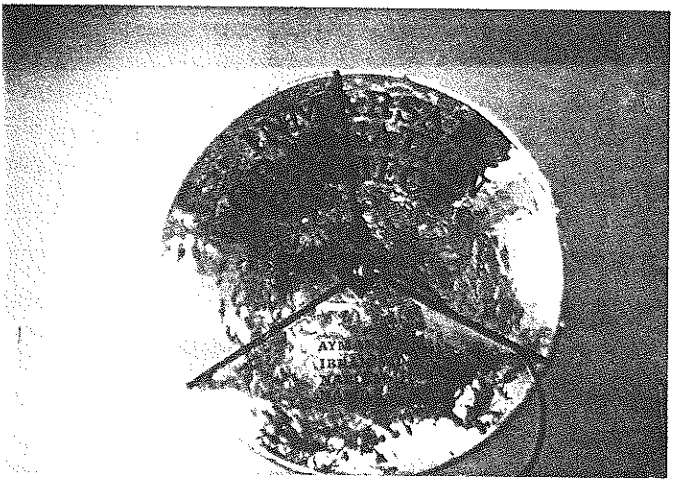

Fig.1. A photo of the parabolic reflector

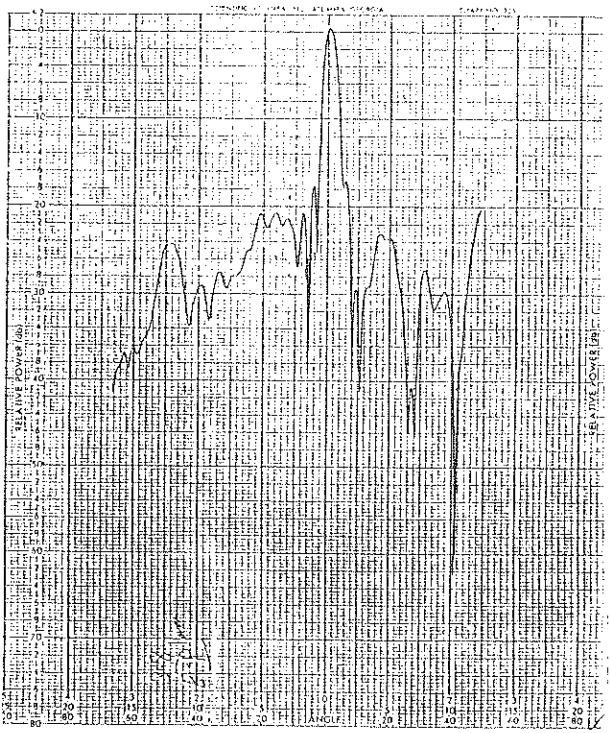

Fig.2. E-plane co-polar pattern at f= 3.8 GHz

SUSCEPTIBILITY OF LOGARITHMIC PERIODIC DIPOLE ARRAYS

R.Moini, R.Aghajafari and A.Tavakoli*
AmirKabir University of Technology
Electrical Engineering Department
No. 424, Hafez Ave., TEHRAN, IRAN
Phone:(+98) 216139480, FAX: (+98) 216406469

Introduction:

Since a few decads ago, broadband antennas such as logarithmic periodic dipole arrays (LPDA) have been investigated using frequency domain techniques in transmitting mode (D. E. ISBELL, IRE Tran. Ant. Prop., vol. 8, 260-267, 1961). However, behavior of these antennas in receiving mode specially due to transient electromagnetic waves such as NEMP (nuclear electromagnetic pulse) and LEMP (lightning electromagnetic pulse) has rarely been considered. In such few papers, the performance of LPDA due to an applied electromagnetic pulse has been studied in frequency domain and then the voltage-time and current-time charastristics of the antenna are obtained using Fourier transform (D. LECONTE, P. MOCCHI, & M. RENARD, 2e Colloque sur la C.E.M, D5-2, FRANCE, 1983).

Formulation of the problem:

Since narrow pulses in time domain have wide frequency spectrum, and noting that LPDA antennas have a wide frequency band, these antennas respond effectively to narrow pulses in receiving mode. Due to the widely use of these antennas in HF, VHF, and UHF frequency bands, the response of these antennas to such pulses and protection of electronic devices connected to the antennas are of great importance. Evidently, frequency domain techniques are not suitable for narrow pulses.

Figure 1 illustrates the antenna under consideration that is illuminated by an electromagnetic plane wave representing NEMP or LEMP pulses.

The electric feild amplitude of the wave is given by:

$$E(t)=E_0[\exp(-\alpha t)-\exp(-\beta t)]$$

Where t is the time and E_0 , α, and β are LEMP or NEMP parameters.

The direction of the incident wave is shown by three angles θ, ϕ, and η which are depicted in figure 2.

The antenna is modeled as wire conductors that are illuminated by the incident transient wave. The incident field induces a current on the wires that generates the scattered field.By the continuity of the electric field on the antenna, an integro-differantial equation for the induced current is derived. Then, the resultant integral equation is solved by the method of

moment in time domain. Consequently, the open circuit voltage Voc(t) and short circuit current Isc(t) at the feed can be evaluated. Using these two parameteres in the Thevenin model, the response of the antenna to NEMP or LEMP can be found (R. MOINI, B.KORDI, B. VAHIDI & M. ABEDI, A.C.E.S. 94 Monterey, CA,1994). Therefore, the appropriate protective devices against such pulses can be determined.

In this method, the effect of number,length, and the diameteres of the dipoles, and polarization and direction of the incident wave are investigated.

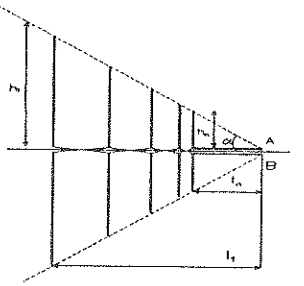

Fig. 1. The geometry of LPDA

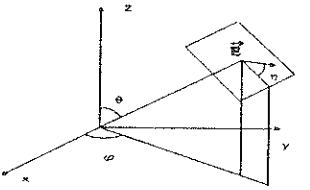

Fig. 2. Direction and polarization of incident wave

A NEW INTEGRAL EQUATION METHOD FOR THIN-WIRE CURVILINEAR ANTENNAS DESIGNING

Professor Dragutin M. Velickovic*, Member IEEE, D.Sc., Dejan M.Petkovic, D.Sc.
Department of Electromagnetics, Faculty of Electronic Engineering.
Beogradska 14, 18000 Nis, Serbia

The last decade is characterized by the intensive investigations on the geometry influence to the curvilinear wire-antennas performances, such as directivity and bandwidth. It has been pointed out by Landstorfer (John While & Sons Inc., Chicester, 1986.) hat properly shaped wire antennas of a length greater than a wavelength may yield a directivity considerably higher than that of straight dipoles. Optimization of the wire antennas is usually based on the corresponding integral equations solving, by example on the Mei's (IEEE Trans. Antennas Prop., Vol. AP-13, pp. 374-378, 1965.) or Pocklington's (E Camb. Phil. Soc. Proc., Vol. 9., pp. 324-332, 1897.) generalized equation. Unfortunately, a very complicated kernel of these equations contains quasi singularities of high order and practically restricts the use to limited number of antennas which have a simple geometry. The well known fact is that only three geometrical structures lead to the kernel of closed-cycle type (convolution kernel) which is necessary for replacement of derivatives between the current distribution function and the kernel, consequently for simplification of numerical treatment. The structures having this desirable property include straight wires, circular arcs, helical wires and no others. Apart from that, there is a sub-domain method in which the general shape of antenna is approximated by finite number of straight-line sections. The greater number of sections leads to better geometry approximation, but the nature of integral equation kernel then produce non-physical current oscillations near source region (invalid input admittance) which is numerically generated (Mittra,Springer-Verlag, New York, 1975.). Obviously, the curvilinear antennas should be treated as continual geometrical system and boundary value problem. This can be done only if an antenna problem is considered in conveniently chosen curvilinear coordinate system, which so enables entire-domain approximation for the current distribution . The purpose of this paper is to present a new integral equation, including numerical technique for its approximate solution.

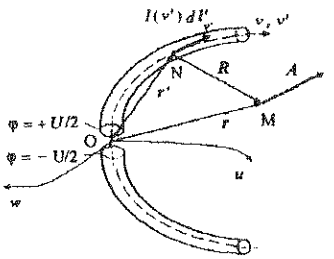

Figure–curvilinear antenna

Consider thin-wire curvilinear symmetrically driven antenna by δ-generator having voltage U and angular frequency ω. The antenna equivalent radius is a. The antenna axis coincide with v-axis $(u = u_0, v = v_0)$ of the curvilinear orthogonal coordinate system, u,v,w. Using boundary condition that the tangential component of the total electric field along the antenna surface vanish, the following differential equation can be established, $\frac{\partial}{\partial v}\operatorname{div} A + k^2 h_v A_v = 0$,where:

$A = A_u\hat{u} + A_v\hat{v} + A_w\hat{w} = \int_{-v_0}^{v_0} I(v')G(r,r')\frac{\partial r'}{\partial v'}\,dv'$ is the magnetic vector potential, $I(v')$ is the distribution of the current localized on the antenna axis and vanishes at the antenna ends, $I(v' = \pm v_0) = 0$. $G(r,r') = \frac{\mu_0}{4\pi}\frac{e^{-jkR}}{R}$ is free space Green's function; $R = |r - r'|$, r, r' are field and source point radius vector, respectively; $\hat{u}, \hat{v}, \hat{w}$ are unit vectors, h_v is Lame's coefficient and $k = 2\pi/\lambda = \omega\sqrt{\varepsilon_0\mu_0}$ is propagation constant and λ is the wavelength. Adding to both sides of dif-

ferential equation term $\frac{1}{h_s^2}\frac{\partial^2}{\partial v^2}(h_v A_v)$, where h_s is quite arbitrary constant, and applying the conventional method of constants variation, the following integral equation governing antenna current distribution on the upper arm $(0 \le v \le v_0)$ can be obtained:

$$kh_s \int_0^v (h_v A_v)\Big|_{v=s} \sin\left[kh_s(v-s)\right] \mathrm{d}s + h_s^2 \int_0^v \mathrm{div}\, A\Big|_{v=s} \cos\left[kh_s(v-s)\right] \mathrm{d}s = C\sin(kh_s v) \ .$$

The electric scalar potential is given as $\varphi = \frac{j}{\omega\varepsilon\mu}\mathrm{div}\, A = \frac{j}{\omega\varepsilon\mu}\int_{-v_0}^{v_0} \frac{\mathrm{d}I(v')}{\mathrm{d}v'} G(r,r')\mathrm{d}v'$ and the unknown constant $C = -jh_s \frac{U}{2}\sqrt{\varepsilon\mu}$ can be determined from the electric scalar potential condition in the upper arm driven point $\varphi(v \to 0) = U/2$.

An exact solution of the obtained integral equation does not exists. Because, the point matching method is used with polynomial current approximation.

The present integral equation technique is applied to several illustrative examples, the obtained numerical results are compared with the known values and the satisfactory agreement is found. Also, in the case when V-dipole degenerate in conventional straight dipole, integral equation reduces to the well known Hallen's integral equation if h_s=1. As the second example, the circular banded dipole having arm length h and diameter b and parabolic banded dipole is treated. The results for input admittance, $G + jB$, in $[\mathrm{mA/V}]$, are presented in the Table:

a) V-dipole antenna with h=0.25λ, Ω=10 and 2α=π/2, for h_s=1 and different order in current polynomial approximation, M.

b) circular dipole with Ω=10, h=0.5λ , for h_s=1, M=2 and different diameter, b.

c) circular dipole with Ω=10, b=0.2λ , for h_s=1, M=2 and different length of the dipole arm, h and

d) parabolic dipole with Ω=10 and h=0.5λ , for h_s=1, M=2 and different dipole shape, u_0. (The parabolic cylindrical coordinate system $x=uv$, $y=(u^2-v^2)/2$, $w=z$ is used.).

a			*b*			*c*			*d*		
$\frac{2h}{\lambda}$	G	B	$\frac{2h}{\lambda}$	G	B	$\frac{2b}{\lambda}$	G	B	u_0	G	B
0.1	0.001	0.826	∞	9.24	-4.26	0.1	0.001	0.826	0.1	0.094	0.922
0.2	0.023	1.867	5.0	9.24	-4.29	0.2	0.023	1.867	0.2	0.306	1.179
0.3	0.177	3.622	1.0	9.44	-4.55	0.3	0.177	3.622	0.3	0.556	1.390
0.4	0.645	8.630	0.8	9.56	-4.71	0.4	0.645	8.630	0.4	0.729	1.477
0.5	16.916	-17.510	0.6	9.83	-5.07	0.5	16.916	-17.51	0.5	0.823	1.508
0.6	0.770	-4.465	0.4	10.72	-6.22	0.6	0.770	-4.465	1	0.943	1.539
			0.2	16.82	-17.50						

Performance of the space factor by a secondary phased array

Rajhi Adnen
Depart. of Electric. Commun. Tohoku Univ. Japan

I- Introduction

Phased arrays are well spread in communication systems and in EM medical systems for therapeutic treatment and in order to improve their capabilities, a technique is proposed and demonstrated in this paper that the a secondary phased array can perform the role of side lobes , for that a process for calculating the weighting vector of the combined phased array has been established using an LMS algorithm.

II- Formulation of the problem

From the equivalence theorem, the EM sources can be replaced by their equivalent electric and magnetic surface currents expressed respectively by the vector J and M; a phased array of n discrete identic radiating elements separated by a distance (l) can be represented by the following sketch

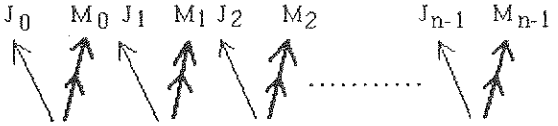

and the resulting space factor in an arbitrary point P can be given by

$|E| = |A_0 + A_1 z + A_2 z^2 + \ldots\ldots + A_{n-2} z^{n-2} + A_{n-1} z^{n-1}|$, with $A_m = a_m e^{j\alpha_m}$ (a_m is proportionnal to the current element and α_m is the phase of the discrete element) and $z = e^{j\psi}$, $\psi = \frac{2\pi}{\lambda} l \cos(\varphi) + \alpha$ (φ is the angle between the first discrete element and the point P).

But severe problems rise in this type of arrays such as the influence of the spacing in the active range, the location of the zeros of the associated polynomial within the active range, limitation on the space factor, the elements number effects on the side lobe levels. A solution for the mentioned problems require mainly the displacement of the active range to localize the zeros within the range. Since any linear array can be represented by a polynomial and each polynomial can be interpreted as a linear array, therefore some fundamental polynomial theorems can be applied:

Theo1. There exist a linear array with a space factor $S(\varphi)$ equal to the product of the space factor of two linear arrays if $f_1(z)$ and $f_2(z)$ are the associated polynomials then $S(\varphi) = S_1(\varphi)\, S_2(\varphi)$.

Theo2: The space factor of a linear array of n elements is the product of (n-1) virtual couplets with their null points at the zero of the space factor.

In order to solve the above mentionned problems of the phased array we find the necessity to design a double phased array constituted of a main and a secondary phased array; and by using theo1 and theo2, the two arrays can be treated as a conditioned phased array as will be explained in the following section.

III- Proposed technique and processing procedure

Any linear array designed for a desired space factor requires the solution of the weighting vector $[\omega_i]$ (ω_i is the weighting factor of the element i) which can be found by defining a cost function J as $J = D(f,T) - \sum_{i=1}^{n} \omega_i X_i(f,T)$ where $D(f,T)$, $X_i(f,T)$ are the finite fourier transform over a length T of the desired signal d(t) and the i^{th} radiating element $x_i(t)$ respectively, and the optimum choice of $\omega_i(t)$ will require to minimize the cost function, which is achieved by an LMS algorithm based on the steepest descent method and described by the following relation $\omega_i(j+1) = \omega_i(j) - 2kJ(j)\, X_i(j)$ as shown in Fig. 1. If we consider two phased array $[x_i(t)]$ and $[y_i(t)]$ which are not perfectly correlated, the weighting factor $\omega_i(f_1,f_2) = \omega_x^i(f_1) + \omega_y^i(f_2)\, \omega_{xy}^i(f_1,f_2)$ of the i^{th} element and the process can be divided into three major steps:

Step1: Optimize $[\omega_{xy}^i]$, by minimizing the finite fourier transform cost function of $[y_i(t)]$ under the condition that the linear effects of $[x_i(t)]$ are removed from $[y_i(t)]$ denoted by $Y_{/x}$.

Step2: Optimize $[\omega_x^i]$, by minimizing the cost function of the desired signal $[d(t)]$ under the condition that the linear effects of $[x_i(t)]$ are removed from $[d(t)]$, denoted by $D_{/x}$.

Step3: Then the two steps leads to a conditioned single phased array and the weighting process of $[\omega_y^i]$ is explained in Fig. 2.

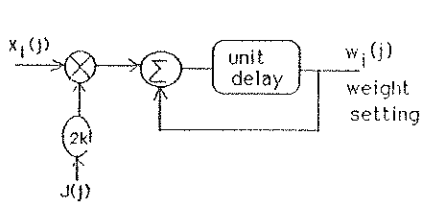

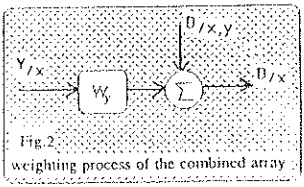

Fig.2 weighting process of the combined array

Fig 1 The steepest descent method

IV- Numerical results

First the LMS algorithm gives discrete fourier series of the amplitude and phase as defined sequences of the main phased array $\{a_d\}.\{p_d\}$; and for a desired space factor, the conditionned LMS gives the build sequences of the amplitude and phases for the secondary phased array $\{a_b\}.\{p_b\}$;

Fig.3 shows the space factor in an arbitrary point P for a single phased array (Fig. 3-a) and for the combined two phased array giving the possibility of suppressing the side lobe level if the arrays are operating at the same level (Fig. 3-b), or an improvement of the side lobe level (Fig.3-c) and possibility of beam steering (Fig. 3-d) if they are operating at different levels.

V-Conclusion

In order to preform the phased array capabilities, it has been shown that double phased array can overcome this difficulty; and this technique can widely be applied in communication systems in which the side lobe level is usually a problem or the necessity of beam steering, also it can be used in hyperthermia systems which requires an accuracy control of the beam involving focusing and uniformity of the space factor.

HIGH POWER MICROWAVE GENERATION FROM AN AXIALLY EXTRACTED VIRCATOR

J.M. ANGLES, M. ANGLES*, H. BOTTOLLIER-CURTET, G.GERMAIN

Commissariat à l'Energie Atomique (CEA) - Centre d'Etudes Scientifiques et Techniques (CESTA) - B.P. n°2 - 33114 LE BARP (FRANCE)

High power microwave radiations have been obtained with a virtual cathode oscillator, in the S band, in using the e-beam generator CESAR at CEA/CESTA. We performed experiments using 1200 kV, 100kA, 65 ns FWHM electron beam. The experimental set-up is shown in figure 1.

The configuration is axial symmetric. The microwave power is extracted in the same direction as the electron beam into a circular waveguide. The virtual cathode is formed when the beam current exceeds the space charge limited current. The sources of the microwave emission are both the reflexing electrons and the oscillating virtual cathode, which are conflicting. The virtual cathode operates as a free-running oscillator, and exibits frequency instability, and chirping.

Diagnostics have been developed for measuring the performance of this high power microwave source. The output power is diagnosed using receiving systems (horns). The operating frequency is measured using three methods: band pass filters, a heterodyne receiver and a frequency discriminator. An array of fluorescent tubes is used to verify the output mode. A first experiment,without frequency measurement, gives an estimation of a power of several hundred of MW in the TM01 mode around 3GHz.

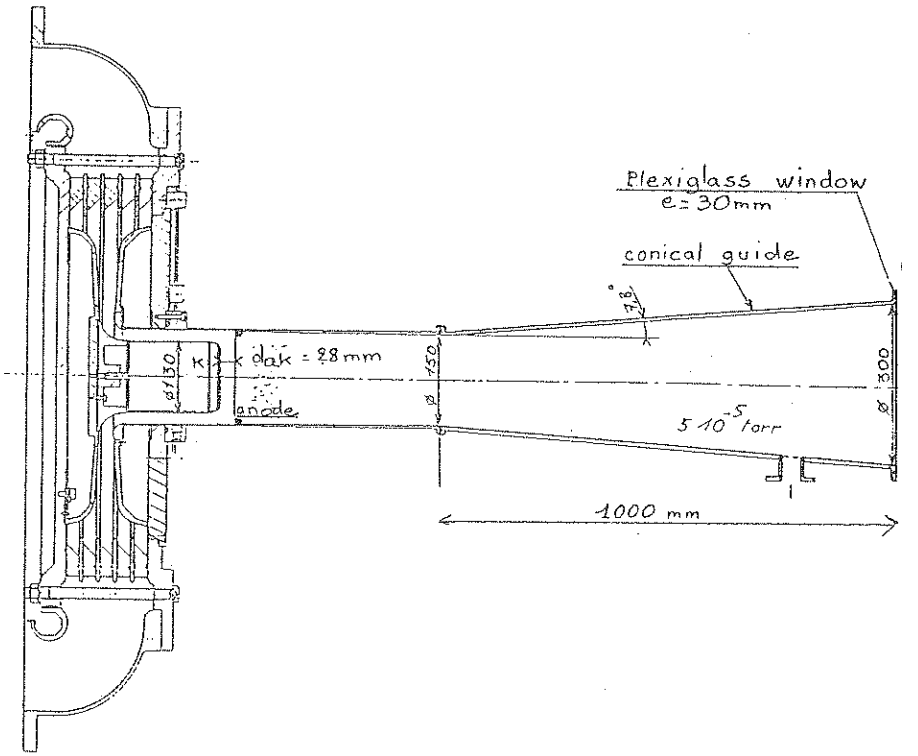

FIGURE 1 : THE VIRCATOR DIODE

RADIO FREQUENCY WEAPON AT THE FUTURE BATTLEFIELD

A.B.Prishchepenko
Central Scientific&Research Inst.for Chemistry&Mechanics
115487,Moscow,Nagatinskaja,16A,Russia,FAX(095)116-78-18
V.V.Kiseljov and I.S.Kudimov
Russian Defence Central Institute of Physics&Technology
141300,Moscow region.,Sergiev Posad-7,FAX(095)456-45-53

Incapaciing power of Radio Frequency Weapon(RFW)consists in inducing in target circuits of fatal for solid state elements(SSE)current and voltage.Though the energy required for such effects in SSE is small(microjoul's),there can't be any euphorie in the forecast of RFW's effectiveness.A specialist can easily estimate a SHF power required to burn out the radar at any distance,referring,from MIL,about minimal safe distance between the radars(with known radiating power)at the airfield.

An operational weapon must meet the requirement of high effectiveness in most wide range of battle situations.From this point of view,an application of a SHF radiation with substantial different from that of target wave length is expedient:orientation influence as well as protective properties of target's surge arresters are minimal.For microseconds range of pulse durations SHF power densities(PD)10-10 W/m are incapatiing most of targets,including infrared's and electrooptic's.At various PD many effects can be observed for same specimen (losing of target,complete malfunction etc.).This means a complicated character of damage and requires to protect many circuits(not only input).

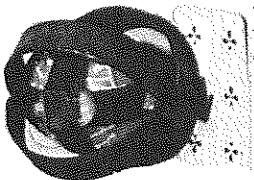

Fig.1.Outer view of SWSS

The PD can't be increased without limit.The discharge in surrounding air exhausts SHF power.If PD at the source surface is near to discharge treshold,the characteristic dimension(r) and strike range(R)of a source are bound(A.B.Prishchepenko.Morskoj Sbornik,1993,N7,p35):

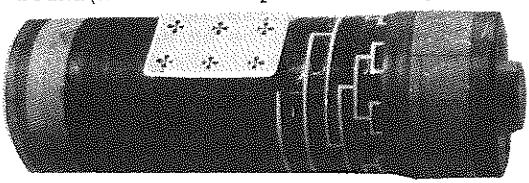

Fig.2.Outer view of IMGF.

$$R<r(PDD/PDI) \quad (1)$$

Here PDD-discharge treshold PD and PDI-minimal incapaciing PD. This bound doesn't depend from technical improvements.Dimensions of small,but too powerfull source are to be increased by layers of insulator to prevent discharge.For a direct beam r represents a length,and,if radiation space distribution is isotropic,r is source radius.

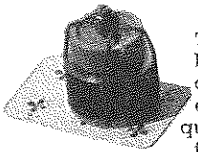

Fig.3.Outer view of FMGF.

The technical basic of RFW is represented by two classes of sources.A first one-traditional SHFgenerators(vircators,magnetrons etc.)with directed radiation and narrow frequency band.Realisation of an effective electron emission demands high(up to MV)voltage -that's why all dimensions are large and specific SHFenergy low(tens of mJ/l).The other class-devices of magnetic field's fast compression

1.Shock Wave Source(A.A.Barmin,A.B.Prishchepenko et.al Mechanika Zhidkosti i Gaza,1988,N6,p166)and,more effective,spherical modification,SWSS,(Fig.1).

2.Explosive Magnetic Generator of Frequency(A.B.Prishchepenko,M.V.Shchelkachev,Electrichestvo,1993,N8,p31) and more powerful implosive variant,IMGF,(Fig.2.).

3.Ferromagnetic Generator of Frequency,FMGF,(Fig.3.).

4.Superconductive Former of Magnetic Field Shock Wave (Fig.4.),which military application is doubtful.It needs cooling by liquid air,but is useful in the laboratory (doesn't contain explosives).

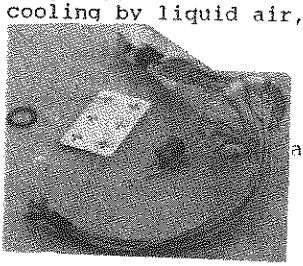

Fig.4.Main parts of SFMFSW:superconductive ring and feeder with Rogovsky loop

New generation principles allow to increase specific SHFenergy to 10 J/l ,to become isotropic radiation and enormous wave length band a some decades continuum(10 -100m).

Traditional source(with homing device)have to fulfil the mission similar to automatic gun.But it appears ,that source with length about 1m can knock out an average hardened target(sea-skimming missile)at a maximal distance about 1km (see 1),and even this wasn't demonstrated at yet.This distance is shorter than effective fire range of 30mm Gatling type gun with length of barrels about 1m as well.More favourable is a forecast of isotropic sources application as Electromagnetic Ammunition(EMA).An estimate(1)gives an incapacity radius of 130mm EMA about 60m-ten times larger than maximal distance of missile destruction by explosion of 130mm fragmentation shell.Similar result was sustained by experiment,but it will be an error to entrust to EMA too much.EMA can be effectively used against preciese weapon,which homing system is often enough to blind within a part of second.This requires far less energy,than complete malfunction.Similar effect produces a sequence of SHF-pulses,that's why a salvo firing of EMA is expedient.

RFW represents a logical answer to enormous role of electronics at the battle field.The appearance of RFW will upgrade the electronic warfare status from ensuring to the main one.

POWERFUL MICROWAVE OSCILLATOR OF MICROSECOND PULSE DURATION DRIVEN BY RELATIVISTIC ELECTRON BEAM

O.T.Loza*, P.S.Strelkov

General Physics Institute,
Vavilov Str., 38, Box 117942, Moscow, Russia

The present work continues experimental investigations of high-power microwave oscillator driven by relativistic electron beam (REB). We studied the possibility to prolong microwave pulse duration, usually restricted by plasma creation in a powerful vacuum device in different parts of it: cathode, diaphragm, slow-wave structure and collector. The increase of microwave pulse duration is possible only after complete elimination of plasma or, at least, its influence on the device operation.

To create REBs with high current (of a few kA) explosive cathodes are applied. We managed to generate a hollow circulant REB with invariant radius and thickness in a steady-state magnetic field. Having solved this problem, we got rid of plasma on the entrance diaphragm, and the collector plasma was merely removed with its originator far from the waveguide. The slow-wave structure remained the only area where plasma could appear.

It was shown earlier that plasma creation during the beam propagation by microwave discharge or collisions of relativistic electrons with the residual gas can be avoided by a proper choice of its pressure. Plasma can appear also by means of near-wall microwave secondary emission electron discharge. This effect may be obviated if REB space charge electric field on the wall is always more than electric component of microwaves. But if the surface was previously screened by sufficiently dense plasma layer, microwave discharge will develop.

Such an "ignition" plasma may appear after bombardment of the walls by a flux of relativistic electrons, that may appear either as the consequence of REB destruction in microwave field or after backscattering on the collector.

To eliminate the backscattered electrons completely, the method of spatial separation of the direct and the backstreaming electron fluxes was proposed. It uses the property of electrons to drift in an inhomogeneous (curved) magnetic field to the same side irrespectively to their longitudinal velocity. Backscattered electrons disappeared from the slow-wave structure, but nevertheless the radiation process terminated before the end of REB current.

A special experiment proved that in absence of all the deleted reasons for plasma appearance mentioned above, the two stage model of microwave breakdown does take place: first plasma "screen" is produced by wasted electrons of direct REB, and the following plasma accumulation is determined by microwaves with strong electric field on the wall. It would be hardly possible to prevent electron bombardment of the walls completely in a powerful device. Much more promising way to avoid fast breakdown it seems to be the next one. An axially-symmetrical TE-type mode of a circular waveguide has vanishing component of electric field on the wall. Hence, the initial plasma, created by relativistic electrons on the wall, will not have sufficient energy supply. Such type of electromagnetic wave can be generated in a gyrotron, for example.

The results of present investigation may be summed up as following. The breakdown of microwave radiation in a powerful oscillator driven by REB is determined by plasma creation inside the vacuum device. Numerous reasons for plasma appearance exist, overwhelming majority of them can be eliminated. On the base of experimental data, a mechanism of intensive plasma accumulation is proposed, comprising a few consequent processes.

First, strong microwave field causes destruction of REB, dispatching a part of electrons to the wall. The electron bombardment creates a layer of plasma on the surface. This plasma screens the electrostatic field of electron beam space charge, that initially had prevented secondary emission electron discharge in the microwave field. The discharge becoming possible, amount of plasma increases up to the moment of preliminary termination of microwave radiation, e.i. breakdown.

It is difficult (or maybe impossible) to avoid electron bombardment completely. To obviate the established mechanism of plasma accumulation it is proposed to use an axially-symmetrical TE-type mode of a gyrotron. Electron beams with invariant geometry are available.

Investigation of multicavity relativistic klystron with TW output section.

Aleksandr N.Sandalov, Victor M.Pikunov, Vladimir E.Rodyakin

Physics Department
Moscow State University
119899 Moscow, Russia

Multicavity relativistic klystrons with TW output cavity are cessary for the design of next generation of linear colliders. gorithms and numerical results of these devices are discussed.

The "large particle" electromagnetic models, based on "particle-in-cell" method, for simulation of intense relativistic electron beams dynamics are used. These models take into account the nonlinear processes in electron beam and wake fields of electron flow. Galerkin's method, orthogo- nalization method and integral equation method are used to simulate of electromagnetic fields in cavities and TW output structure.

The influence of intensity of electron flow on TW output structure dispersion characteristics was investigated. The researches of influence of relativistic electron beam on electromagnetic fields structure are presented. Phase volume transforming at interaction with electromagnetic fields in multicavity klystron was investigated .

THE COHERENT OPERATION OF TWO RELATIVISTIC MAGNETRONS IN THE NONSYMMETRICAL SYSTEM

A.S.Sulakshin, N.M.Filipenko, G.P.Pomenko, E.G.Furman, G.G.Kanaev, S.S.Novikov and V.V.Pozdeev

Microwave Centre
Institute of Nuclear Physics
Tomsk Polytechnical University
P.O.BOX 25, 634050, Tomsk, Russia

The present report envisages of theoretical and experimental investigations as well as a numerical simulation of the interaction processes for two high power relativistic magnetrons in nonsymmetrical system [1]. In particular, the system will be designed of two relativistic magnetrons system with power supply from two linear inductance accelerators.

The preliminary theoretical studies have shown that these systems due to the strong coupling have low phase locking time during some oscillation periods), significantly wider locking range and are not so critical to the parameters variations than symmetrical ones [2].

. The nonliniar osscillations of multifrequency autooscillated. Vladimirov S.V., Maidanovskii A.S., Novikov S.S. Tomsk University publishing: Tomsk, 1993.
. Alexandrovich D.V., Baranov S.V., Didenko A.N., Filipenko N.M., Fomenko G.P., Maidanovskii A.S., Novikov S.S., Pozdeev V.V., Sulakshin A.S., Relativistic magnetrons: optimization of parameters and modelling of phase locking process. Proc. of 9-th Int. Conf. on High Power Particle Beams, "BEAMS-92", Washington, DC, May 25-29, 1992, v.III, 1574-1579.

Spatial Mode Locking in a Corrugated Plasmaguide

A.M. Ignatov
General Physics Institute, 38, Vavilova st.
Moscow, Russia

Recently it has been shown that periodic corrugation of a cylindric waveguide filled with a magnetized plasma results in drastic modification of the Trivelpiece-Gould (TG) modes: the spectrum turned out to be an infinitesimally fine grid, called a dense spectrum, filling a band between zero and the plasma frequency ω_p (W.R. Low et al., Phys. Rev. Lett.,1991, 67, 2481). In the present report we implement the electrostatic approximation to study the wave propagation in a planar plasmaguide surrounded by perfectly conducting corrugated walls. At first sight, these simplifications can hardly change the argumentation resulting in the dense spectrum. However, here we solve the planar problem exactly for a plasmaguide of an arbitrary shape and observe numerous discrepancies with the results of numeric evaluation.

First of all, we note that the electric potential of any wave with the frequency ω in a magnetized plasma may be written as

$$\phi(x, z) = A(z + x/s) + B(z - x/s)$$

where A and B are arbitrary functions, $s = \omega (\omega_p^2 - \omega^2)^{-1/2}$ and the infinite external magnetic field is parallel to the z axis. Assuming that the plasmaguide is symmetric, i.e., its walls are at $x = \pm a(z)$, where $a(z+1) = a(z)$, and considering, for definiteness, the odd eigenfunctions ($B = -A$) we get

$$\varphi(z + a(z)/s) - \varphi(z - a(z)/s) = 1 \qquad (1)$$

where $A(z) = exp(2\pi i n \varphi(z))$. Here n is an arbitrary integer, therefore any solution of this equation results in an infinite number of eigenfunctions generalizing usual TG waves.

The wavenumber, k, is introduced by the periodicity boundary condition

$$\varphi(z + 1) = \varphi(z) + 2\pi k \qquad (2)$$

We show that due to Eqs.(1,2) the wavenumber is actually the inverse winding number of the circle map described by the function $f(z, s)$, such that $f(z, s) = z' + a(z')/s$, $z = z' - a(z')/s$. This map is continuous if $s > max|a'(z)|$; we restrict the discussion with this frequency range. The dependence of the winding number, i.e., k, on s is an example of the so-called devil's staircase: if k is some rational

number, $k = p/q$, then it is constant in a certain range of s ($\Delta_{p,q}$) . Thus, with an arbitrary periodic function $a(z)$, the entire frequency range is split into an infinite number of subbands, the wavenumber in each of them being a rational constant. Actually, this mode locking phenomenon is well-known in nonlinear physics but here we run it across in a linear problem.

The width of each step of the devil's staircase depends on the wall corrugation and q; generally, if $a(z) = a_0 + \varepsilon\ a\ (z)$ ($\varepsilon << 1$), then $\Delta_{p,q} \approx \varepsilon^q$. Therefore, with $\varepsilon \rightarrow 0$ the graph of the devil's staircase tends to the straight line , k(s) $\rightarrow$ s/ 2 , that obviously corresponds to the fundamental TG-mode of a smooth planar plasmaguide. The width of the sets of largest steps with $q = 1$ or 2 may be easily evaluated: $\Delta_{p,q} = (2 \min a(z)/ p\ ,\ 2 \max a(z)/ p)$. Figure 1 shows the steps of the devils staircase with q, p <100 evaluated numerically for $a(z) = 1/2 + \delta \cos (2 \pi z)$, $\delta = 0.05$. The corresponding spectral curve is shown in Figure 2.

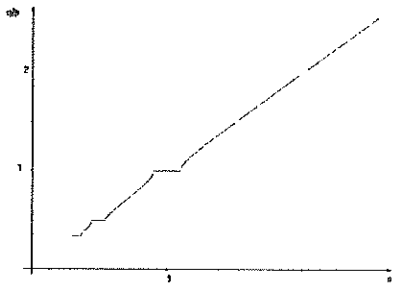

Figure 1

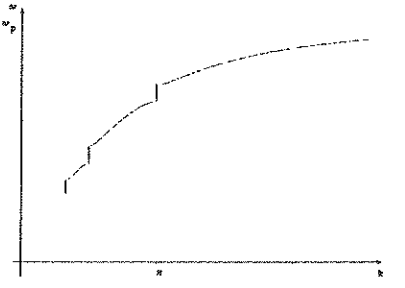

Figure 2

The general solution of Eqs.(1,2) is found in terms of the cycle elements of the circle map $f(z,s)$. Using this solution we consider the propagation of a wave packet of a finite spectral width . It is shown that generally the fractal character of the spectrum results in temporal damping caused by the phase mixing. The damping rate is determined by the width of the largest subband inside the wave packet. Moreover, if the packet contains the waves with $q = 1$ only, then the temporal evolution may be found explicitly for arbitrary initial conditions. We also consider the interaction of an electron beam with plasma waves. It is shown that the beam-plasma interaction is essentially modified by the spatial mode locking.

ASSESSING AIRCRAFT SURVIVABILITY TO HIGH FREQUENCY THREATS

SUMMARY

Mr. Samuel J. Frazier
Mr. Edward M. Parimuha*
Naval Air Warfare Center
Aircraft Division, Code SY84
Patuxent River, Maryland 20670-5304
Telephone (301) 826-3868

Mr. William Prather
Phillips Laboratory/WSR
Kirtland AFB, New Mexico
87117-5776

Mr. Michael Antley
United International Engineering, Inc.
2201 Buena Vista Drive SE, Suite 207
Albuquerque, New Mexico 87106

Mr. Donald McLemore
Kaman Sciences Group
6400 Uptown Blvd., Suite 300E
Albuquerque, New Mexico 87110

ABSTRACT

Throughout DoD, the need exists to assess and characterize aircraft system survivability to high frequency (HF) electromagnetic (EM) threats. These threats include the Electromagnetic Pulse (EMP) threat defined by DoD-STD-2169 and carrier shipboard environments. The Navy recognizes this need and is taking the initiative to investigate the feasibility of a realistic, low-cost test methodology to assess, characterize and validate aircraft survivability to threats that may range from a few hundred Kilohertz to the low Gigahertz region. The proposed Navy technical approach is based on established system-level RDT&E technology using existing high frequency test laboratories and equipment. The approach will be validated using a combination of High Level Pulse (HLP) testing at the Horizontally Polarized Dipole (HPD) and Vertically Polarized Dipole (VPD) free-field EMP simulators, electromagnetic effects generating equipment to simulate the carrier shipboard environment, low-level continuous wave (LLCW) testing to acquire the stress response data, and wideband direct-drive tests to characterize system strength. The Navy is developing a new wideband (up to 1 GHz) direct-drive technology and waveform combination techniques using stress response data to develop worst-case stress envelopes to be used during the direct-drive tests. Several technical issues must be addressed including recording test data at the high frequencies (> 1 GHz), quantification of the actual changes in coupling between previous EMP specifications and DoD-STD-2169, characterization of the effect that higher frequency EM fields have on weapon system survivability, and definition of the minimum required test capabilities to keep uncertainties within bounds.

INTRODUCTION

The Navy recognizes the need to address aircraft survivability to HF threats. Ideally, full-threat, free-field simulators, generators and emitters would be developed for system-level testing to DoD-STD-2169 and the multitiude of shipboard emitters. However, the costs associated with development and procurement of these facilities and types of equipment can be excessive with the ever-changing threat environments. Therefore, a low-cost alternative to assessment by simulated, full-threat illumination must be found and a realistic test capability for assessing aircraft and other weapons systems to HF threats developed. The technical approach described in this paper is based on using current HLP, EM generators and LLCW technology and resources, combined with significant improvements and enhancements to direct-drive current-injection test technology, to develop a low-cost test methodology to assess and validate aircraft EMP survivability to HF threats. The primary purpose of this effort is to develop an approach for validation of an abbreviated test methodology for assessing aircraft survivability to HF threat environments. The primary objectives of the assessment approach are to:

1. Assess the effect of the expanded EM threat defined by shipboard environments and EMP requirements on aircraft survivability;

2. Develop a realistic, low-cost test methodology needed to assess and validate aircraft survivability;

3. Develop an HF direct-drive current-injection capability (100 kHz-1 GHz);

4. Perform a system-level validation test (or multiple tests, as required) to evaluate LLCW test techniques to bound high frequency stress responses for aircraft,

5. Validate the feasibility of using waveform combination techniques to combine multiple high level pulse, shipboard environments, and LLCW measurements into composite waveforms (stress envelopes) to be used during direct-drive testing;

6. Define the minimum test capabilities needed to assess and validate aircraft survivability, including facilities, simulators, instrumentation, data processing and analysis techniques; and

7. Estimate tradeoffs between test fidelity and cost.

The paper and presentation will detail the technical approach and engineering views and judgements used for generating this test approach for assessing and validating aircraft survivability to HF threat environments.

HARDENING AS A FUNCTION OF FREQUENCY

W.D. Prather
Phillips Laboratory, WSR
Kirtland AFB, NM
G. Hoffer and D.P. McLemore*
Kaman Sciences Corporation, Dikewood Division
Albuquerque, NM and Alameda, CA

Concern about the effects of high power, broad band electromagnetic environments on the electronics equipment has, in the past, been limited primarily to frequencies below 100 MHz. Consequently, hardening techniques to protect systems against such environments have been designed to be efficacious at low frequencies. With the advent of potential threat environments with significant energy to 1 GHz and beyond, protection designs must begin to encompass a much wider frequency range of operation. Possible alternatives include the extension of existing low frequency techniques to higher frequencies or the development of novel approaches specifically aimed at high frequencies. Perhaps another element in this comprehensive hardening strategy is the determination of a maximum frequency above which no hardening is required.

An extensive set of CW coupling measurements were made on the Electromagnetic Effects Test Bed Aircraft in stepped frequencies from 100 MHz to 10 GHz at an outdoor range. Instrumentation for this test included B-dot probes to measure magnetic fields inside aircraft equipment bays and direct-contact voltage probes on circuit card inside electronics boxes.

Figure 1 shows data for several of the B dot probes inside the Test Bed equipment bays. The B-dot responses have normalized to the incident magnetic field to give the shielding effectiveness, displayed in the plot in dB. The fact the shielding efficiency of the cavity does not reach 0 dB indicates the presence of loss mechanisms for field energy in the cavity other than reradiation back through the POEs feeding into the cavity. At the highest frequencies the levels of the cavity fields converge to similar values. This probably represents a region beyond the fundamental resonance frequencies of the POEs into the cavities where the POE effective areas are similar for all cavities. The field levels also appear to be slowly declining at the highest frequencies. This may be due to a decrease in the POE effective area or an increase in the loss cross section.

The maximum, mean and minimum responses of several voltage probes measuring responses in electronic equipment within the aircraft are shown in Figure 2. The data have been normalized to the incident power density to give the effective area of the monitored circuit node in dB referenced to 1 cm^2. At low frequencies the effective areas display a wide range from one voltage probe to another: about 60 dB for the examples shown in the figure. There are several reasons for this wide spread. First, some points in the electronic circuits are connected directly to conductors that extend outside the metallic airframe. Next, the fields driving the "internal" cables wholly within the cavities inside the aircraft show variation with location as shown in Figure 1. Finally, some of the monitored circuit nodes are in interface circuits directly attached to a box connector while others are "buried" deep within the electronics circuits.

In order to get a more general picture of the coupling to the Test Bed than that provided by the curves for specific probes and incidence angles, the data for several probes and aircraft orientations were combined. The maximum, mean, and minimum values were obtained at each frequency, point by point, from a large number of coupling curves. The results for 54 (six probes times nine aircraft orientations) B-dot curves are shown in Figure 2. Below 0.5 GHz the mean and minimum curves are affected by the noise floor and are not shown in this range. The curves shown in the figure are relatively

constant with frequency. The straight lines shown a least-square fit to a constant value; numbers obtained for the shielding effectiveness are -8 dB, -26 dB, and -50 dB for the maximum, mean, and minimum, respectively.

Figure 3 shows a maximum, mean and minimum value of the effective area for 81 voltage probe data sets. As with the B-dot data, the mean and minimum for the voltage probe responses are affected by the noise floor, especially from 8 to 10 GHz and throughout the frequency range for the minimum. The general trend for the curves in the figure goes as f^{-2}; the straight lines show the least-square fits of f^{-2} curves to the data.

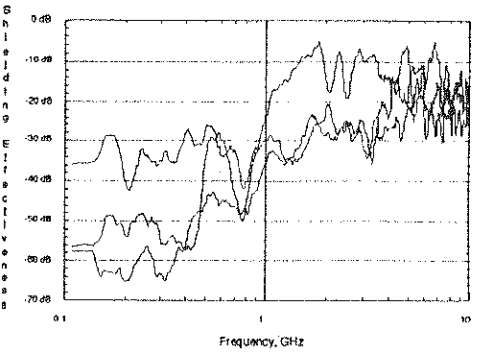

Figure 1. Examples of Test Bed internal B-dot probe data, normalized by incident magnetic field to give shielding effectiveness.

The coupling information described above allows us to make estimates of the power likely to be coupled to electronic components when a system is illuminated by a threat environment containing high frequency components. In order to obtain an upper-bound estimate on the high frequency coupled stresses in electronic circuits the following assumptions and parameters were used:

- The incident environment is monochromatic (this leads to an overestimate for a broadband environment) and has a power density of 1 kW/cm^2 (61 kV/m).
- The basis of the coupling to circuit nodes is the power received by interconnecting cables acting as long wire antennas with an effective area of $\lambda^2/8\pi$ (proportional to f^{-2}).
- The shielding effectiveness has a value of -10 dB and does not vary with frequency. (from the minimum shielding effectiveness data - see figure 2.)
- The reduction factor has a value of -30 dB and does not vary with frequency. (from the mean effective area data - see figure 3)

This leads to the coupled power curve shown in Figure 5.

In order to determine hardening requirements these coupled stresses must compared with the strength levels of electronic components, primarily semiconductor devices. A generic description of the strength levels of semiconductor parts is given in Figure 4 as a function of the frequency of the incident power. The strength is shown in terms of power absorbed in the part; the required incident power may be higher due to device reflectivity.

For the permanent damage more than 1 W of CW power is required, and thresholds for pulsed stresses are higher. The threshold level is essentially independent of frequency. The thresholds for upset are on the order of normal operating power levels, from

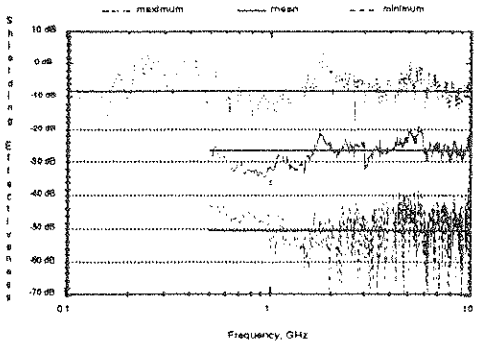

Figure 2. Maximum, mean and minimum values of shielding effectiveness from 54 test bed data sets (six probes times nine aircraft orientations).

microwatts to milliwatts. For frequencies within the operating bandwidth of the device the upset threshold is relatively frequency independent. Beyond the operating bandwidth, however, the rf signal must first be rectified by one of the semiconductor junctions within the component, and the remaining circuitry in the device responds to the rectified signal. Because the rectification efficiency decreases with frequency, the upset threshold increases.

Interference, upset and burnout data from semiconductor component testing were used to contruct the generic curves for failure, upset and interference thresholds for semiconductor devices shown in figure 5. The coupled power falls below the burnout threshold at about 600 MHz. This means that above that frequency *no circuit node will receive sufficient power to burn out a semiconductor component.* The leads to the

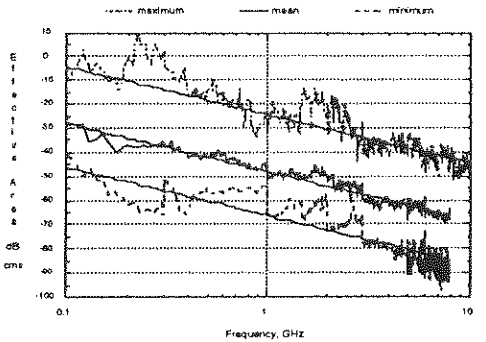

Figure 3. Maximum, mean and minimum values of effective area from 61 Test Bed data sets.

conclusion that no "high frequency" (e.g. above 600 MHz) hardening is required for protection against burnout.

The coupled power curve falls below the digital upset threshold at about 4 GHz. Above this frequency *no circuit node will receive sufficient power to switch the state of a digital device*. Some hardening may be required in the frequency range of a few gigahertz

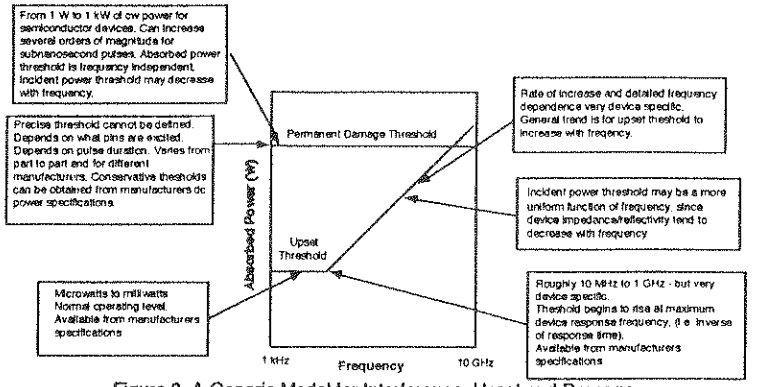

Figure 3. A Generic Model for Interference, Upset and Damage

to prevent digital upset of the system. Finally, the coupled power curve is above the analog interference threshold up to 10 GHz. As noted earlier, the significance of this threshold is more difficult to interpret than burnout or digital upset. The effect of the spurious offset voltages on system function depends on how they are processed. In addition, short pulse interference will have no effect on analog circuits with slow time constants. More detailed analysis with specific systems and environments is necessary to determine whether hardening to remove the possibility of these interference signals is required.

Thus, three frequency ranges emerge with differing degrees of hardening requirements. In the lowest range, up to close to 1 GHz, hardening should be done to remove the possibility of electronic burnout. In this range the necessary hardening techniques are relatively straightforward, and extension of existing low frequency hardening techniques will often suffice. The emphasis in this frequency range will be on the prevention of harmful signals generated on external (i.e., exposed to the incident environment) cables from reaching interface circuits in electronics boxes.

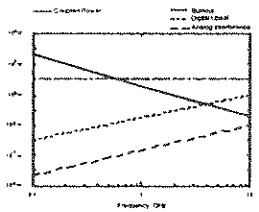
Figure 5. Comparison of maximum high frequency coupled stress with semiconductor device failure thresholds.

From about 1 GHz to a few gigahertz hardening may be needed to eliminate the possibility of spurious digital switching. Hardening in this frequency range will likely be more difficult than at lower frequencies but is probably feasible. Since electrical wavelengths in this range are comparable to aperture openings in systems, the notional idea of creating a closed shield may be impractical The hardening emphasis in this frequency range will likely be on the reduction of cavity field amplitudes and the suppression of harmful signals generated on any interconnecting cables.

Above a few gigahertz hardening may be desirable to avoid interference in analog circuits. Hardening may be difficult at these frequencies, especially in a retrofit situation, and further analysis with more specific details should be performed to determine whether hardening in this range is really appropriate.

A REVIEW OF THE HIRF PROBLEM FOR CIVIL AIRCRAFT

By

Rodney A. Perala

ELECTRO MAGNETIC APPLICATIONS, INC.
7655 West Mississippi Avenue, Suite 300
Lakewood, CO 80226
Phone: 303-980-0070
Fax: 303-980-0836

Modern commercial aircraft having critical and essential electronic systems are required to be certified against the effects of High Intensity Radiated Fields (HIRF). These fields are generally from non-hostile emitters, and include commercial and government radio transmitters and radars, and exist in the spectrum from 10 KHz to 40 GHz. Typical critical systems include full authority digital engine controller (FADEC), fly-by-wire control systems, and electronic flight instrumentation systems (EFIS). Because these systems depend upon low voltage semiconductor circuitry, it is necessary that systems of this type not be affected by HIRF environments.

The objective of this paper is to present an overview of the HIRF certification process and issues. The scope of the paper includes a review of:

- The HIRF environment
- HIRF coupling into aircraft
- The certification process and requirements
- Full vehicle test methods
- Bench test methods
- Analysis methods
- Outstanding technical issues

Ground test method for evaluating the internal electromagnetic environment of a large-size aircraft in the 10 kHz - 30 MHz range
Application to A340 and A330 aircraft

F. Flourens
GERAC

M. Crokaert
AEROSPATIALE AVIONS

E. Fanio*
AEROSPATIALE AVIONS

1. INTRODUCTION

The introduction on civil transport aircraft of electronic systems performing critical flight safety functions (fly-by-wire controls, engine control) is recent. These new technologies have led the aircraft manufacturers to ensure the immunity of the said systems to external electromagnetic aggressions which may be encountered by their aircraft in flight. These aggressions can be of a natural origin, such as lightning, or result from high-power sources of human origin (transmitters, radars, etc.). The latter aggression is identified by the generic name "HIRF" meaning High Intensity Radiated Fields.

The ad hoc working groups of organizations such as EUROCAE in Europe and SAE in the USA have established the spectrum (10 kHz - 18 GHz) and the HIRF threat level with regard to which the aircraft manufacturer must demonstrate the immunity of his aircraft during the certification process.

As the HIRF threat, brought to equipment and system level (ETDL: Equipment Transient Design Level), is specified before the aircraft is manufactured, it must be checked that a sufficient protective margin exists between the specified system test levels and the levels to which the systems will be subjected once installed on the aircraft. For this, the aircraft's electromagnetic transfer function is evaluated. This function characterizes the induced conductive constraints from 10 kHz to 100 MHz (ratio between currents induced on the internal cables/external field) and the induced radiated constraints from 30 MHz to 18 GHz (ratio between internal EM field/external EM field). Extrapolating the TF's to the spectrum of the HIRF external threat allows the effective threat levels to be determined (ATCL: Actual Transient Controlled Level) ; these are compared to the equipment test levels (ETDL) to evaluate the protective margin.

This paper concerns the HF frequency range (10 kHz - 30 MHz) in which the conducted coupling is predominant. For this low part of the HIRF spectrum, evaluating the transfer function by overall illumination of the aircraft is a difficult way because the homogeneity and the plane character of the incident wave are difficult to guarantee on account of the size of the aircraft, the presence of the ground and the absence of high-performance radiating facilities. In order to overcome this, Aerospatiale Avions has developed a current injection test method which reproduces on the structural elements on the ground the result of the incident EM wave/structure interaction in flight, that is, the surface current density distributions on the skin of the aircraft. This method is presented in the following paragraph and illustrated in the third paragraph by its application during the A340 certification.

2. METHOD FOR EVALUATION TRANSFER FUNCTIONS BY GROUND CURRENT INJECTION

In the method used for evaluating the transfer functions of an aircraft in flight in the low frequencies by means of current injection with the aircraft on the ground, we attempt to reproduce on the characteristic parts of the structure (fuselage, wing, engine), the result of the incident wave/structure interaction rather than the interaction itself. In the frequency range considered (10 kHz - 30 MHz) and provided that the apertures remain small when compared with the wavelengths, this interaction is mainly characterized by the current densities induced on the surface of the structure. The simulation therefore consists in reproducing as best as possible these densities or at least their topography in the considered frequency range. Five steps are required to evaluate the sought flight transfer function. These are:

1 • Characterize the electromagnetic response of the aircraft in flight subjected to plane wave illumination:
This step can only be performed using a theoretical tool allowing the surface current densities induced in flight to be determined by identifying the most penalizing angles of incidence and polarizations.

2 • Conceive ground simulation means:
This device must reproduce, on certain zones of the aircraft, the most stringent environment obtained from flight analysis. The zones considered must correspond to the parts of the structure where the greater part of the cable coupling occurs.

3 • Evaluate performance and optimize ground simulation means:
This step is performed using a theoretical tool. The resonance modes and the maps of the current densities induced by the simulation set up are compared to those identified in flight. The set up is modified to make the two results converge. The "good simulation" criterion is equality, at all points in the zone considered, in the ratio between the current densities induced by the simulator (J_{sim}) and the current densities calculated in flight (J_{flt}):

$$\frac{J_{sim}(\omega,P1)}{J_{flt}(\omega,P1)} \approx \frac{J_{sim}(\omega,P2)}{J_{flt}(\omega,P2)} \approx \ldots \approx \frac{J_{sim}(\omega,Pn)}{J_{flt}(\omega,Pn)}$$

4 • Manufacture the ground simulation device and make internal measurements:
The simulation device is manufactured and validated with regard to its definition by comparing several external measurement results to the theoretical predictions. The external domain/internal domain coupling is characterized by measuring the signals induced on the cables routed in the validity zone associated with the simulation set up and defined in 2 and 3.

5 - Extrapolate the internal measurements to obtain the flight transfer function:
An extrapolation function is obtained from the theoretical simulation results in flight and on the ground and allows the internal results in flight to be found from the internal measurements on the ground.

During the evaluation of the current injection simulation means, we found that a single injection on the aircraft with ground return was sufficient to reproduce the structure resonances with inhomogeneities with regard to free space not exceeding 6 dB. Identifying a reference signal allows the acquired measurements to be standardized, the best choice is current injected via aircraft structure $I_{inj}(\omega)$.

The measurements made in the experimental phase were of two sorts:

- External current density measurements;
  At least two current density measurements must be made in the complete frequency band and for each zone for comparison with the theoretical results. Correspondence between the two results guarantees that the simulation means and the hypotheses used in the theoretical modelling are correct. These measurements are referenced to the current measured at the injection point i.e. $\frac{I_{sim}(\omega,Bund_j)}{I_{inj}(\omega)}$.
- Internal measurements of the currents induced on the characteristic looms in terms of location, length, electrical loads: $\frac{I_{sim}(\omega, Bund_j)}{I_{inj}(\omega)}$

The transfer function is calculated by the definition of the correction functions. The internal measurements cannot be used directly and, even if the simulator was perfect, readjustment of the levels would be required. The readjustment depends on the frequency but is independent of the observation point. If, according to our initial hypothesis, the electromagnetic environment of the aircraft is entirely characterized by the external current densities, the readjustment coefficient will be the same for all the current densities of a simulation zone and, consequently, for the signals induced in the cables routed in this zone. Knowing the current densities in flight and those induced by the simulator, this coefficient will be equal to $\frac{J_{flt}(\omega,P_i)}{J_{sim}(\omega,P_i)}$. The internal currents induced in the bundles in flight can then be expressed as follows:

$$I_{flt}(\omega,Bund_j) = I_{sim}(\omega,Bund_j) \times \frac{J_{flt}(\omega,P_i)}{J_{sim}(\omega,P_i)}$$

We must now introduce the references of the various signals to build the extrapolation function applicable to the internal measurements, that is, the incident field module for the in-flight results and the current at the injection point for the results acquired with the simulation means. Thus, the flight transfer functions can be deduced from the ground measurements in the following way:

$$\frac{I_{flt}(\omega,Bund_j)}{\|E_{inc}(\omega)\|} = \underbrace{\frac{J_{flt}(\omega,P_i)}{\|E_{inc}(\omega)\|}\left(\frac{J_{sim}(\omega,P_i)}{I_{inj}(\omega)}\right)^{-1}}_{EXTR(\omega,P_i)} \frac{I_{sim}(\omega,Bund_j)}{I_{inj}(\omega)}$$

Ideally, the extrapolation functions EXTR (ω, P_i) are independent of the observation point P_i. In reality, certain defects subsist: the extrapolation function used is then the worst envelope of all the functions that can be defined in this zone:

$$CORR(\omega,Zone\ k) = MAX\ \{\ EXTR(\omega,P_i)\ \}\ \text{with}\ P_i \in (Zone\ k)$$

As the result of this operation is not really a measurable value but a worst envelope for this value, the CORR function is called the correction function. A correction function is built for each simulation zone and applied to the internal measurements made on the cables routed in the corresponding zone.

3. A340 PROGRAM

The results of the theoretical modelling of the coupling between an incident wave and the four-engine A340 underscore the following points:

- the normal and grazing incidences gave close results;
- the four main parts of the structure (right wing, left wing, front section of fuselage and rear section) resonate independently and at proper frequencies;
- a high resonance mode is related to the engines, interpreting this mode remains complex;
- the fuselage and engine resonances are maximized when field E is parallel to the fuselage, those related to the wings when field E is perpendicular to the fuselage;
- 5 main resonance modes were considered and concerned the rear section of the fuselage, the front section of the fuselage, each wing and the engine nacelle; the upper modes are complex to interpret as many parts of the structure are involved.

Two current injection configurations were defined: injection via wing tip and injection via the nose of the aircraft. In both cases, the center of the aircraft was connected to the ground plane to close the injection circuit. The injection cable supported a very high impedance load in order to simulate the conditions in free space (current node at resonance frequencies).

These two configurations were analyzed theoretically. After optimization of the test set-up, the efficiency of the simulation principle can be extended up to 18 MHz as shown on figure 1 where the extreme extrapolation functions calculated at two points in the wing zone are presented. These results confirm the good reproduction of the current density maps calculated in flight in this zone; the correction function will be the upward-adjustment envelope of these curves. It is thus demonstrated that injection via the nose is representative of illumination in flight with field E collinear to the fuselage. The cables routed in the fuselage will be considered in this test configuration. However, injection via the wing allows the cables routed in the wings and the engine nacelles to be dealt with.

The comparison between theory and experimentation can only be achieved for current injection. The correspondence between the two types of results for at least two points in each zone validates the realization of the test set-up and the electromagnetic model of the aircraft used for theoretical modelling.

A comparison example is given on figure 6. The slight differences which subsist between the two curves result from measurement inaccuracies and the fact that losses were not taken into account in the theoretical model.

Four correction functions were defined and applied to the internal measurements according to the test configuration and the cable routing zone. Remember here that the final results obtained are not exactly the signals that would have been measured during illumination in flight but an upward-adjustment envelope of these signals; this is because the maximizing parameters for flight illumination and the correction of the simulator defects by upward adjustment of the results.have been taken into account. An example of the final result is shown on figure 7.

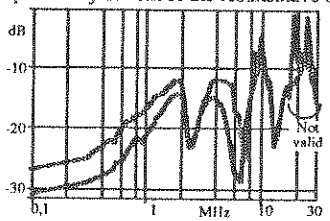

Fig. 5: Wing zone comparison

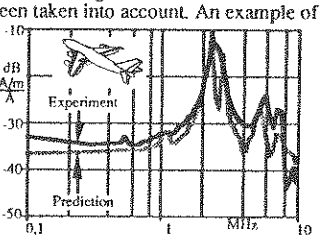

Fig. 2: Wing injection - Theory / Measure

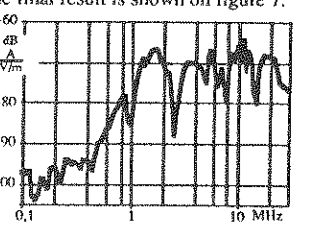

Fig. 3: Wing transfer function

4. A330 PROGRAM

The difference between the A330 and the A340 lies mainly in the fact that the two remaining A330 engines are different from those of the A340. The high similarity between the two aircraft deals us to use the A340 transfer functions for the A330 certification instead of performing a ground test. However, to obtain this goal, two conditions must be met and demonstrated: the coupling between the external domain and the cables must be very similar on the A330 and the A340 and the behavior of the A330 structure during illumination must be sufficiently close to that of the A340 in order not to call the result acquisition method into question.

Although the first point is acquired on account of the similarity between the two aircraft and the design rules used for the modified parts (engine pylons), the second point requires some theoretical modelling in order to conclude. The conclusions of this analysis are as follows:

- the current densities induced on the fuselage are identical for the two aircraft;
- for the wing zone, only the upper mode resonances are different, by 5 dB at the most; the densities induced on the A340 are higher than those induced on the A330 for this frequency range;
- the behavior of the A330 engine zone is similar to that of the A340 outboard engine zone (and not inboard) on account of the screen effect that the latter has.

Thus, it appears that the A340 transfer functions for the "fuselage" and "wing" cables can be applied to the A330 as they have an upward-adjustment effect and that, for the A330 engine cables, the transfer functions acquired on the A340 outboard engine cables can be considered as a worst case. The method used from the start again proves its efficiency: thanks to the understanding of the coupling phenomena that it requires, it allows us to go further in the analysis of the results and rigorously underpins a similarity analysis.

5. TOWARDS AN AIRCRAFT TEST SYNTHESIS

The HIRF transfer function characterization method in the low frequencies by a ground injection test requires knowledge at a given time in the process of the signals induced in the cables with regard to a current injected directly into the structure. These signals are to be compared to the values assessed for lightening. In effect, demonstrating the conformity of an aircraft with regard to lightening is supported by an evaluation of the internal constraints developed on the wiring and seen by the equipment. Primarily, the two types of measurements are identical except that one is made in the frequency domain and the other in the time domain.

Processing of the CW measurement results by Fourier analysis could allows the results acquired during lightning transfer function tests to be found under certain conditions.

The first results are encouraging and allow us to envisage the possibility of synthesizing the two aircraft tests into only one.

Lightning and EMP Protection for 2-Mbit/s Digital Networks

G. GIRARD *, Alcatel Cable / D.E.E.
B. AZUR, CNET LANNION

Telephone information transmission takes place very frequently on digital networks. The electronic circuits fitted at the ends of lines have become complex, sophisticated, and also more susceptible to electromagnetic disturbances. It is therefore necessary to have effective protection against overvoltage lightning and electromagnetic pulses (EMP) induced in cables.

The solution proposed here mainly concerns the protection of terminal transmission exchanges, where a large number of digital links are gathered.

Current Network Protection Technics

One of the protection methods would consist of distributing the information on fiberoptics links. This is the ideal solution, but is quite often it is difficult to implement, and much more costly than cable links.

Another solution would consist in using discrete protective components grouped in shielded boxes secured clamped directly to the wall of a Faraday cage with a clamp. The drawbacks of this solution are that it requires a large surface area on the Faraday cage wall. This can lead to many electromagnetic radiation leaks.

Proposed Solution

The product developed by Alcatel-Cable and CNET[1] can group 2048 protective devices in a remote hardened rack.

This rack (dimensions 2 m x 0.8 m x 0.7 m) is located inside the user's Faraday cage.

The cables carrying the overvoltages enter the cage through shielded flexible tubes that connect to the top of the rack. These cables enter through a plate as small as 0.3 x 0.2 m.

The rack contains 2048 plug-in type (for easier maintenance) protective modules. These miniaturized modules, whose compactness has been made possible by the technic of hybridization on substrate, contain two peak-clipping components (a spark arrestor and a low-capacitance diode) associated by a decoupling component. A low-pass LC filter is fitted at the output from the modules on the rack's sidewalls; this filter's capacitor is mounted acrosson the Faraday cage's wall to ensure electromagnetic leaktightness.

This feedthrough capacitor's output is equiped with a wire-wrap pin is to be used for direct connection of the protected cables outside the rack.

---

[1] Centre National d'Etudes des Télécommunications

The product's main features are the following:

- transmission of 2-Mbit/s digital signals, in compliance with the CCITT G.703 Recommendation;
- lightning wave handling capacity:
  8 x 20 µs; 5 kA; 10 times;
- lightning ripple voltage: < 25 V.

Shielding Effectiveness of Shielded Harnesses Terminated by Various Grounding Schemes

C. Goldstein, RAFAEL P.O.Box 2250 Haifa ISRAEL

A 1m long shielded harness was connected between 2 termination boxes. The harness contained different types of conductors such as shielded or unshielded cabels and shielded or unshielded twisted pairs. In one of the boxes the conductors were terminated by their characteristic impedance, in the other box the conductors were grounded. The stripline injection method (Goldstein & Mani IEEE EMC 34, 50-57, 1992) was used to inject on the harness shield a current pulse of double exponential shape and 100A amplitude. The injected current and the induced currents at the terminations were measured and recorded in a screened room. The experimental set up is shown in fig. 1.

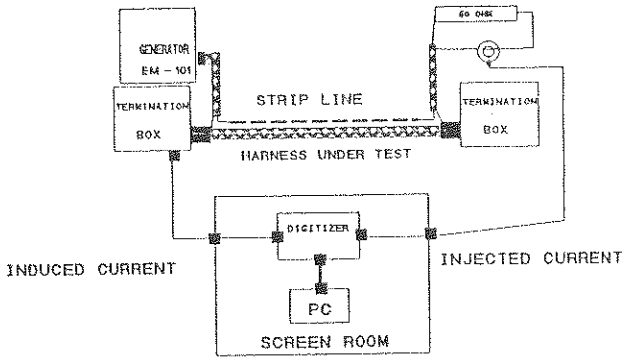

Fig. 1: The experimental set up

The harness shield was connected to the termination boxes by different schemes: a- circumferential connections to both boxes. b- pigtail connections to both boxes. c- pigtail connection to one box and open near the other box. Fig. 2 shows the injected current and the induced currents at the termination of an unshielded wire, for each of the above mentioned schemes. The amplitudes of the induced currents are: a- 80mA (ptp), b- 700mA (ptp) and c- 1.8A (ptp).

The corresponding energies at the terminations are: a- 4×10^{-9}J, b- 1.4×10^{-7}J and c- 8×10^{-6}J. the shielding effectiveness of the circumferential connections in scheme a shows an improvement of 33 dB over that of scheme c.

From the Fourier analysis of the injected and induced currents, the shielding effectiveness as a function of frequency was calculated for each of the above mentioned schemes.

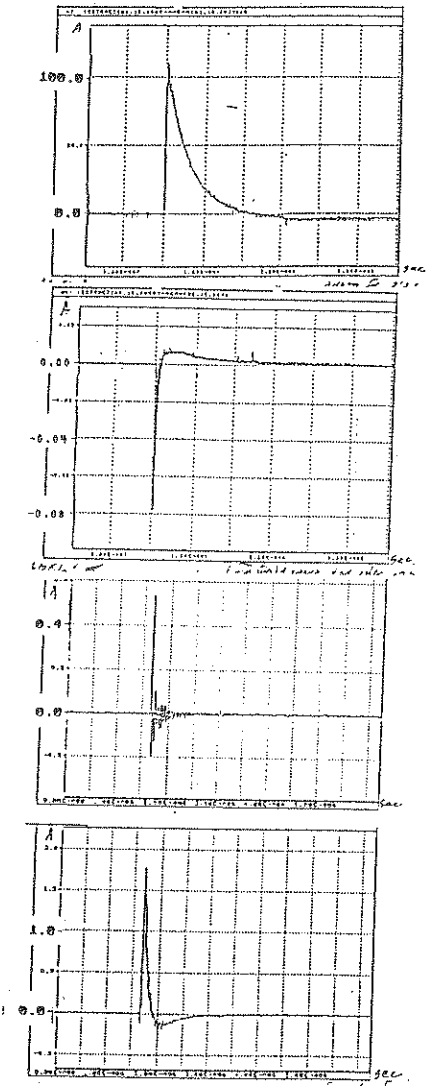

Injected shield current

Scheme a
Induced current

Scheme b
Induced current

Scheme c
Induced current

Fig. 2: Injected and induced currents

DECREASING THE IMPEDANCE OF RAISED-METAL-FLOOR TO UPGRADE SYSTEMS IMMUNITY

Michel Mardiguian *
EMC Consultant
78470 St Remy-les-Chevreuse
France

Alain Charoy
AEMC
38180 Seyssins
France

ABSTRACT

Creating a low impedance reference plane or grid reduces EMI effects onto an installed system. To attain this low impedance typically required the installation of a dedicated grid of wires, or straps, or a special type of raised metal floor (RMF). Often, the acceptance characteristics of the finished grids were ambiguous. This paper shows a practical way to use regular RMF as an excellent reference plane, provided the tiles /stringer /pedestal contact impedance is controlled. An easy way to reduce this impedance is described, which creates a grid impedance $< 10\Omega$ / sq. at 3 MHz. A criteria for the maximum allowable floor-grid impedance from DC to approximately 10 MHz is shown, along with a simple, practical, measurement set-up using only a Signal Generator and Oscilloscope.

SUMMARY

It is known for long that a room reference plane or grid is a sure way to reduce the effects of incoming conducted transients or ambient RF fields onto the installed electronic system (computer system, Telecom system or instrumentation). The "equipotential reference" between the various frames of a same system allows the circulation of :

- cable shields induced RF currents
- Power line spikes
- surge arrestors and filter currents

without objectionable Common Mode (CM) voltages between these frames.

A decent EDP equipment can generally withstand several tens of volt of transient CM ground shift between chassis, due a substantial CM rejection of its digital bus interfaces. Traditional ways of achieving this are the use of criss-crossing braids or straps, or raised metal floor (RMF) stringers with positive electrical bonding at intersections. This latter seems economical, but it is often expensive and time-consuming because regular RMF exhibit a rather poor tiles / stringers / pedestal contact. Pedestal heads are often equipped with plastic dampers which complicate the making of a good contact. Measured values of ordinary "computer-room grade" RMF show impedances in excess of $0,1\Omega$/ sq at few kHz, up to 20Ω or more at 3 MHz. By using finger-stock spring contacts to equip all pedestral heads, a better continuity is achieved :

- tile-to-tile
- tile-to-stringer
- grid-to-pedestal

After this simple treatment, the floor grid impedance between any nodes drops down to tens of milliohms (DC to kilohertz) raising to less than 10Ω at 3 MHz. The figure shows acceptable and unacceptable grid impedances for a 5m x 5m room with 0,60 x 0,60 m floor elements.

The zig-zagging braid (no gridding) is a 5 cm wide, daisy-chaining all pedestrals. Such earthing is mandatory for safety, in the absence of other positive earthing of tiles and pedestrals. But it totalizes a developed length of $\simeq$ 30 m, certainly unadequate for an RF ground. With such "ground", a single, rather common, transient of 10 A/ 1μs will cause a room ground shift of $\simeq$ 500v. Not often reported in literature is the fact that quasi-infinite grid whose each bar has an individual impedance Z_i; will show, between any two nodes, an impedance of $\simeq 0{,}5\ Z_i$; provided that the contacts at intersections are $< Z_i$.
To make practical RMF impedance measurement on-site, a simple test method has been devised. The method uses a signal generator a wide aluminium foil (5m x 0,5m) and an oscilloscope.

For a 5m, end-shorted line, the generator can be regarded as a constant current source up to approximately 6 MHz ($\lambda/10$) :

$$I_g = Vo/50\Omega$$

Z_1, the impedance of the wide 5m foil is measure first, once for all, from DC to 5 MHz, then, this foil is shorted to the unknown RMF, as shown on the figure. By measuring the terminals voltage V_2 at the signal Generator, the RMF impedance Z_2 can de derived by :

$$Z_2 = (V_2/I_g) - Z_1$$

The measurement results correlate extremely well with calculated results. This method and the RMF improvement hardware have been used successfully for all the technical rooms in the Trans Manche Link (TML), at UK side.

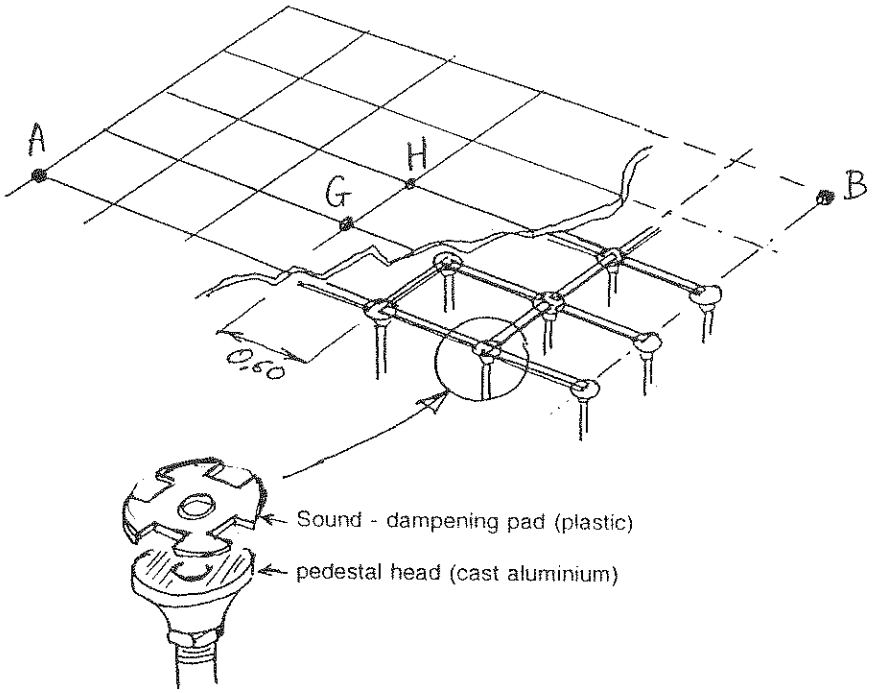

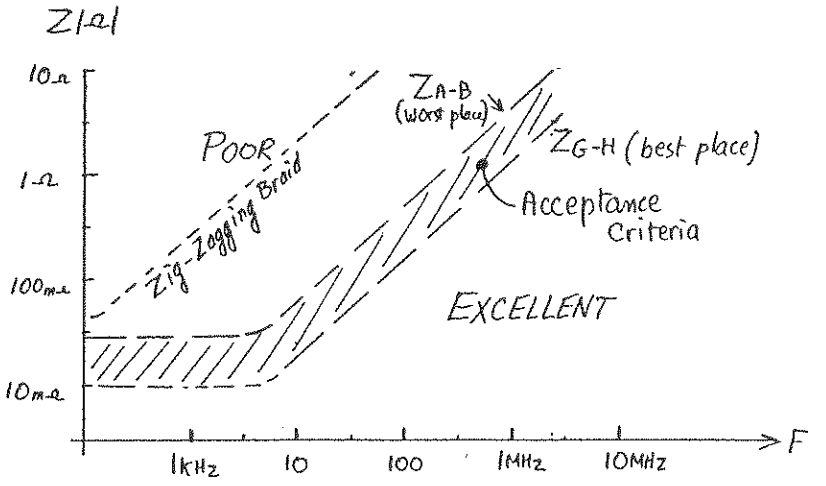

FIGURE: Raised Metal Floor Reference Grid, and Impedance criteria

MICROWAVE INTERFERENCE SUPPRESSION THROUGH ABSORPTION

Chaitanya Kumar M V, Nawal K Agrawal and Suresh C Gupta
Department of Electronics & Computer Engineering,
University of Roorkee, Roorkee - 247 667 India.

ABSTRACT : The lack of space available on modern weapon platforms, forces electronic systems to be placed in close proximity. Often a signal or harmonic from one system will interfere with an adjacent system leading to system degradation. This interference problem has become especially acute with the powerful broad band jammers currently being deployed. But this problem can be reduced significantly or eliminated by employing a coating of microwave absorbing layer. Depending on the systems requirements; single frequency, or a broad band microwave absorbing layer will have to be employed.

The coating of a planar surface with a thin absorber of thickness d, would constitute a three layered system.

Let a transverse electromagnetic wave propagating in the Z-direction be incident at an arbitrary angle θ, on the surface of the absorber. Part of this wave would be reflected back, giving rise to the primary reflected wave and part of it would be refracted into the absorber triggering a series of secondary reflected waves from the absorber surface as shown in the figure 1.

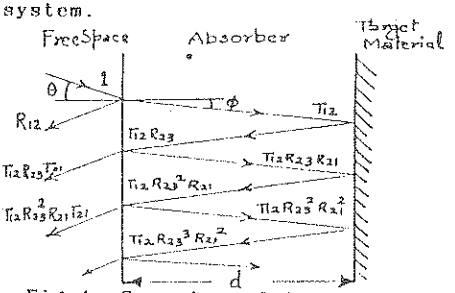

Fig 1. Geometry of the problem.

In order to remove the dependence on polarization within the absorbing media we impose the condition $n \gg 1$. Physically this assumption means that the wave inside the absorber is travelling in a direction, which is normal/near normal to the surface. With this restriction, $n^2 \gg \sin^2(\theta)$. Using this we define two variables α and β as

$$\alpha = 4\pi dp/\lambda \qquad .. (1)$$

and $$\beta = 4\pi dn/\lambda \qquad .. (2)$$

where n, p and λ are the refractive index and absorption index of the absorber and the free space wavelength.

Considering the medium 3 to be a good conductor, the overall reflection coefficient R, utilizing the binomial theorem and invoking the conservation of energy, can be written as

$$R = |R_{12} + e^{(-\alpha + j\beta)}|/|1 + R_{12}\, e^{(-\alpha + j\beta)}| \qquad .. (3)$$

then the reflection loss or absorption provided by the absorber is given by

$$A = -20\log_{10}|R| \qquad .. (4)$$

It can be observed from expression (3), that the major contribution to the overall reflection coefficient R, is the primary reflected wave. Hence (i) the overall reflection coefficient can be reduced by eliminating the primary reflected wave, leading to a matched absorber and (ii) the overall reflection itself can be reduced to zero leading to a resonant absorber.

Matched Absorber: It is desired that $R_{12} = 0$; and the conditions

to be satisfied are obtained as

$$n = \mu_r' \text{ and } p = \mu_r'' \quad \text{.. (5)}$$

$$\mu_r = \varepsilon_r \quad \text{.. (6)}$$

The thickness of the matched layer is given by $d = \lambda/(2\pi p)$ ..(7a)

Then the overall reflection coefficient for the matched layer is

$$R = e^{(-\alpha + j\beta)} \text{ and } |R| = e^{-\alpha} \quad \text{..(7b)}$$

Thus the overall reflection coefficient can be further reduced by making α larger or from (7a) increasing p, the absorption index. The absence of an explicit λ term in the conditions for the matched layer, makes these absorbers best suited for broad band operation.

Resonant Absorber: The resonant absorber is desired to provide zero reflected signal or R = Ø; the conditions to be satisfied are obtained as

$$d = (\lambda/8\pi p)\ \{\ln\ \{(\mu_r + n)^2 + p^2\}/\{(\mu_r - n)^2 + p^2\}\} \quad \text{..(8a)}$$

$$d = \lambda/4n \quad \text{..(8b)}$$

The thickness of the resonant absorber has to satisfy both the amplitude (8a) and phase conditions (8b) , which is seldom achieved in practice and only the phase condition is satisfied. Since the condition for the resonant absorber is λ dependent, this type can generally be employed for narrow band operation.

A design specification of minimum 10 dB absorption over Ku-band (12-18 GHz) was set for an absorber that can be employed for broadband operation, For an absorber that to could be employed as a single frequency interference suppressor, a design specification of ≥25 dB at 8.5 GHz. In both case a thickness constraint of 2 mm was also set.

The optimized values of 12.7 (8.5) GHz, 45%(52), Ø%(18%) and 1.78 (1.8) mm for the values of ferromagnetic resonance frequency of Cobalt substituted Barium Hexa Ferrite, concentration of the lossy material (Ferrite and Carbon)in the binder and thickness of the matched (resonant) absorber were obtained to meet the design specification.

The theoretically predicted and experimentally obtained absorption characteristics for the designed and fabricated matched and resonant absorbers are shown in the Fig 2 . The practical performance of the matched absorber over the entire Ku-Band follows very closely with the theoretically predicted values. Also, the experimentally determined resonant frequency and absorption for the resonant absorber behaves well with its theoretical counterpart.

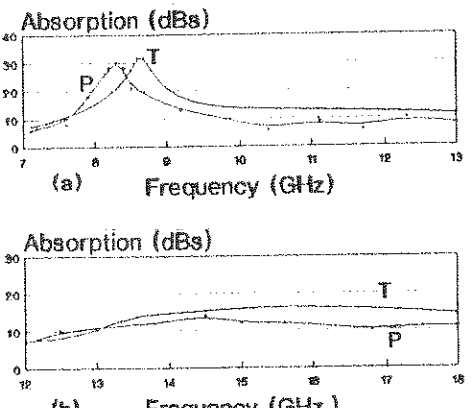

Fig 2. Absorption characteristics for (a) resonant and (b) matched absorbers. T: Theoretically simulated. P:Experimentally obtained

A mathematical model for the theoretical analysis and design of two types of interference suppressors has been considered. Their correctness has been validated by the design, fabrication, and experimental testing of an absorber for each type.

ACKNOWLEDGEMENT : The first author acknowledges the fellowship support from CSIR, Govt. of India.

ULTRAWIDEBAND RADAR: CURRENT AND FUTURE TECHNIQUES

P. R. Bellamy, Defence Research Agency, Malvern
UK

ABSTRACT

In recent years there has been a steadily increasing interest in Ultra Wideband (UWB) Radar with many research organisations attempting to exploit it for both civil and military applications. A fundamental property of radar systems is that the spatial resolution is dependent on the bandwidth of the transmitted signal (a true CW radar can only provide information about the velocity of a target).

Increasing the spatial resolution of conventional radars means modulating the carrier in some way in order to increase the transmitted bandwidth. In most types of UWB radar systems a special source is used to generate an impulsive signal which is inherently wideband. Typically, risetimes of 100ps can be achieved which allows range resolutions of the order of centimetres - sufficient to allow target detail to be resolved.

Analysis of returns from targets illuminated by UWB signals can also reveal natural resonances in a process similar to determining their impulse response. This combined with the high resolution spatial information offers the capability of accurate target discrimination. In order to extract this information in real time, new signal processing methods are being developed along with enhanced modelling techniques which allow a greater understanding of the processes involved.

The greatest technical challenges with most UWB radar systems are still associated with the source and antenna. Because the receiving system must be wideband in order to extract the most useful target information, achieving high sensitivity is difficult due to thermal noise limitations. One solution is to increase the source amplitude but this may mean peak powers in excess of 100MW for longer ranges. Increasing the antenna gain is another possibility, but the design of high gain wideband antennas for impulse applications is a difficult problem which has yet to be satisfactorily addressed.

This paper reviews the techniques used in current UWB radar systems, using results from the facility at DRA Pershore, and then examines the technological challenges still to be addressed.

Ultra-Wideband Noise Radar with Correlation and Double Spectral Processing of the Reflected Signals

K.A.Lukin

Institute of Radiophysics and Electronics,
Ukrainian Academy of Sciences,
12 Akad.Proskura St., 310085 Kharkov, UKRAINE
E-mail: ire%ire.kharkov.ua@relay.ussr.eu.net

Some characteristics of the Ultra-Wideband Radar using the regular video pulse series could be improved when correlation processing is made use. However, the uncertainty of the time delay value corresponding to the maximum correlation function and the false signals arising under the some conditions of the working of the correlator and regular pulses transmitter take place. Making use of noise signal with the same value of the frequency bandwidth one could avoid this difficulties.

In the paper the preliminary results of the possibility testing of the constructing Ultra-Wideband Noise Radar (UWBNR) with correlation and double spectral processing are presented. The laboratory model of the UWBNR constructed consists of the noise signals transmitter, generating the spread spectrum noise continuous signals, as well as transmitting and receiving antennas, connected to correlation receiver or in the case of double spectral processing - to the high frequency power spectrum analyzer and low frequency one in series. To provide the generation of the noise signals needed the special oscillator was designed and constructed on the base of the dynamical chaotisation of the oscillations in nonlinear circuits, using the modified Chua's diode (K.A. Lukin. Journal of Circuits, Systems, and Computers. Vol.3, Num.2, June 1993, pp.627-644). The oscillator was constructed on the base of operational amplifiers NE5539N, providing the negative resistance loaded by piece of delay line, which produce the noise signal oscillations with bandwidth about 100 MHz (from 10 KHz to 100 MHz) in continuous working regime. As a correlation receiver the Digital Analog Time-Integrating Correlator designed in was used. It provides the possibility of the correlation function measurement for the noise signals with frequency bandwidth from 10 MHz to 200MHz. The delay time step for measurements of the correlation function equals to 2.5 ns, the time of integrating could be varied from 10 mks to 1 ms. The double spectral processing was performed with help of series power spectrum analyzers. The main advantage of this method is in possibility of processing of the noise signals with very wide bandwidth up to 2 GHz, providing the distance measurements and additional information on the fine structure of the object .

The measurements conducted proved the possibility of the design and construction of the UWBNR, which will allow to solve the peculiar UWBR problems, possessing of the well known advantages of the noise radars.

OPTIMAL POLARIZATION STATES OF SIMPLE AND COMPOUND TARGETS

V. Sampath,* G.Y. Delisle, P. Luneau
INRS-Télécommunications
16, place du Commerce
Île-des-Soeurs, Québec
Canada H3E 1H6

The complex RCS-scattering matrix of a reciprocal target in the monostatic case is given by:

$$\begin{bmatrix} E_h^s \\ E_v^s \end{bmatrix} = \begin{bmatrix} RCS_{hh} & RCS_{hv} \\ RCS_{hv} & RCS_{vv} \end{bmatrix} \begin{bmatrix} E_h^i \\ E_v^i \end{bmatrix} \tag{1}$$

By simply knowing the RCS-parameters for a particular combination of receive-transmit polarization, one can foretell the same parameters for any arbitrary combination by using the following congruent transformation:

$$\underline{\underline{RCS}}^{\wedge} = \underline{\underline{Q}}(\psi_s, \tau_s)^{-1} \underline{\underline{RCS}}_{pq} \underline{\underline{Q}}(\psi_i, \tau_i) \tag{2}$$

The resulting polarization signature (or response) contains the power scattered back to the receiver for all linear, circular and elliptical polarizations, thereby condensing a considerable quantity of information into a compact, three-dimensional plot. It has been shown in the literature that, if the proper transforming factors are chosen, the matrix $\underline{\underline{RCS}}^{\wedge}$ will be in diagonal form in the new basis. Further, by considering the first derivatives of the power equations that issue from the elements of $\underline{\underline{RCS}}^{\wedge}$, the extrema of the polarization signatures can be found. It is these extrema (called the cross-pol maxima and cross-pol nulls, co-pol maxima and co-pol nulls and cross-pol saddle points) that constitute the optimal or characteristic states of the target and, on the Poincaré sphere, form the "polarization fork" or "Huynen fork." However, when the target cannot be described by a symmetrical RCS-matrix, i.e. the cross-diagonal elements are not equal:

$$\begin{bmatrix} E_h^s \\ E_v^s \end{bmatrix} = \begin{bmatrix} RCS_{hh} & RCS_{hv} \\ RCS_{vh} & RCS_{vv} \end{bmatrix} \begin{bmatrix} E_h^i \\ E_v^i \end{bmatrix} \tag{3}$$

employing eigenvalue techniques to diagonalise it will not be a straightforward task. In other words, a simple extension of the solution obtained in the symmetric case is not possible and the literature shows no evidence of such a transformation having been executed as yet. However, the practical significance would be enormous, since most targets, in practice, would possess distinct optimal states - a fact of considerable significance in target discrimination and recognition. Our intention, therefore, is to pursue the general case (equation 3) and present at the conference theoretical results for the optimal states of simple and complex targets, with the view of achieving some limited form of identification.

SIMPLE ANALYSIS OF ULTRASHORT PULSE INTERACTION WITH MATTER

H. WILHELMSSON**, J-H. TROMBERT*, J-F. ELOY*.

*CEA/CESTA , F-33114 Le Barp, France.

**CHALMERS UNIVERSITY OF TECHNOLOGY,IEFT, S-41296 Göteborg, Sweden.

An ultrashort electromagnetic pulse in general corresponds to a wide frequency spectrum covering low as well as high frequencies.

For describing the interaction of picosecond pulses with matter, we are here interested essentially in the behaviour of materials in the subpicosecond domain ($\Delta\tau < 10^{-12}$ s). In this case, the frequency band of interest $\Delta\nu$ extends over frequencies ranging from 10^{10} to 10^{13} Hz. For such a large band, the electromagnetic properties of matter depend on a number of resonances in dense media (metals, superconductors, dielectrics with 10^{26} m^{-3} < N < 10^{28} m^{-3}) or in less dense media (plasmas with 10^{18} m^{-3} < N < 10^{20} m^{-3}).

Even if a description of the propagation of ultrashort electromagnetic pulses does not encounter any difficulties in free space (index of refraction $n(\omega)$ constant), this is not the case for pulses penetrating media having high or low densities ($n(\omega)$ frequency dependent), since the spectra of the time profiles of the ultrashort pulses contain a broad range of frequencies (J.F. ELOY & F. MORIAMEZ, SPIE 1629, 298, 1992). Waves related to those frequencies propagate in the medium in such a way that for each frequency ν, the distance covered during a time t can be expressed by:

$$z(t, \nu) = ct / \mathrm{Re}[n(\nu)] \qquad (1)$$

Hence, it is necessary when analysing the interaction of ultrashort pulses with matter to take into account at the same time the space-time and the frequency dependence of the interaction of the waves with the medium characterized by an index of refraction $n(\nu)$.

A complete analysis of the problem of reflection for an ultrashort pulse by a metal, requires a consideration of these facts, which indeed involves considerable complications.

It should be emphasized, however, that the present work is not restricted to the calculation of the duration of the pulse interaction in the medium but to determine the relative shape of the reflected pulse as compared to that of the incident one. Such a change in shape may provide important information about the interaction and serve as a tool for diagnostic of the medium.

For the purpose, it is possible to introduce a simplified model which accounts for the essential features of the above mentioned processes.

The main steps of the model can be summarized as follows:

1) Assume that the time dependence of the incident ultrashort pulse in free space is described by A(t).

2) The spectral form of the incident pulse can be expressed, by the Fourier Transform, (A. SOMMERFELD, Partial Differential Equations in Physics, Acad. Press, N.Y. 1949):

$$A(\nu) = \int_{-\infty}^{+\infty} A(t)\exp(-i2\pi\nu t)dt \tag{2}$$

3) The spectral decomposition into a set of gaussian pulses, regarded as wave packets with central frequencies ν_m can be formulated as follows:

$$A(\nu) = \sum_{\nu_m=\nu_{min}}^{\nu_m=\nu_{max}} a_m g(\nu - \nu_m) \tag{3}$$

where a_m referes to the weight of each gaussian contribution $g(\nu - \nu_m)$.

4) The characteristic time of propagation of a wave packet associated with a certain frequency ν_m in the medium becomes:

$$t_m = 2\delta_s(\nu_m)n(\nu_m)/c \tag{4}$$

$n(\nu_m)$ being the index of refraction and $\delta_s(\nu_m)$ the skin-depth at frequency ν_m.

5) Reconstruction of the time dependence of the reflected pulse by associating a time delay with each gaussian component of the inverse Fourier transform. Each frequency ν_m determines the m^{th} time-shift t_m associated with the corresponding component of the reflected pulse:

$$A_{reflected}(t) = \sum_m \int_{-\infty}^{+\infty} \exp[2\pi i.\nu(t - t_m)].a_m.g(\nu - \nu_m).d\nu \tag{5}$$

Each part of the incident or reflected signal depends on all parts of the spectrum, and vice-versa. The structure in time of the reflected pulse also depends on each part in time of the incident pulse, as a result of the interaction with matter. It is thus not possible to define explicitly the duration of interaction of each time part of the pulse with the medium, even if the "average" time of interaction for the pulse may be estimated as $\langle t_m \rangle = \frac{1}{m}\sum t_m$.

The analysis by the Fourier transform technique accordingly seems indispensible for the understanding of these phenomena. The complexity of the general problem, however, suggests that for a more detailed description, it might be preferable to consider methods using variable time windows (Gabor transforms, wavelets, etc...) (H.N. KRITIKOS, PIERS Proc., JPL Publ, 93-17, 795, 1993),(Edt M. FARGE et al., Wavelets, Fractals and Fourier Transforms, Clarendon Press, Oxford, 1993),(C.K. CHUI, An Introduction to Wavelets, Vol 1, Acad. Press, 1992) which will be the aim of future investigations.

INVESTIGATION OF ULTRA-WIDEBAND ELECTROMAGNETIC PULSES IN DISPERSIVE MEDIA

Steven L. Dvorak and Donald G. Dudley*
Department of Electrical and Computer Engineering
University of Arizona
Tucson, AZ 85721

We have recently developed an efficient method for the analysis of ultra-wideband (UWB) electromagnetic pulses (e.g., double exponential pulse) propagating through dispersive media. Such a forward model is important in applications involving high-power, UWB radar systems. The initial results of this research were presented earlier (S.L. Dvorak & D.G. Dudley, Sec. Int. Conf. Ultra-Wideband Short-Pulse Electromag, Apr. 1994). In that paper, we demonstrated that the inverse Fourier transform representations for the electric and magnetic fields associated with an UWB double exponential pulse propagating through a waveguide or plasma (i.e., the ionosphere) satisfy second-order, non-homogeneous, ordinary differential equations. We have solved these differential equations, thereby obtaining analytical expressions involving incomplete Lipschitz-Hankel integrals (ILHIs). Since the ILHIs can be efficiently computed using known convergent and asymptotic series expansions, the expressions provide an efficient forward model for these complex dispersion problems. We demonstrated the usefulness of the ILHI expressions by comparing them with the fast Fourier transform technique (FFT). The comparisons were based on the numerical results obtained for an UWB double exponential pulse propagating in a plasma. Because of the long tails associated with these UWB pulses, a large number of points are required in the FFT to avoid aliasing errors. In contrast, the ILHI expressions provide accurate and efficient numerical results regardless of the number of points computed.

In the present paper, we use the ILHI expressions to derive relatively simple approximate expressions for the early and late-time responses. We utilize these results to critically examine the UWB pulse. In addition, short-time Fourier transforms and spectrograms are used to study multimoding effects in a waveguide where the pulse breaks down into packets traveling at different group velocities. Finally, we employ the ILHI expressions in an inverse problem where we estimate the shape of the pulse at the location of the source and the plasma cutoff frequency.

DETERMINATION OF THE ELECTROMAGNETIC FIELD GENERATED BY A MICROWAVE PROCESS. COMPUTATION OF THE TEMPERATURE FIELD BY CONDUCTION

D. CLEMENTZ *, IPEM company, Centre Condorcet,162 av. Dr Schweitzer,33600 PESSAC, France.
P. LEMASSON, Pr C. MARZAT,Master laboratory, University of Bordeaux I, 33405 Talence, France.

The increasing use of microwave requires a better knowledge of the electromagnetic field distribution in a cavity and its thermal consequences. The behaviour of the electric field **E** and magnetic field **H**, is given by the resolution of the **3D** Maxwell equations, and the temperature is estimated by the resolution of the conduction's equation. These resolutions are performed in **the time area**. The equations we solve, are the following ones:

$$(I) \qquad \begin{cases} \dfrac{\partial \mathbf{B}}{\partial t} = -\nabla \wedge \mathbf{E} \\ \dfrac{\partial \mathbf{D}}{\partial t} = \nabla \wedge \mathbf{H} - \mathbf{J} - \sigma \mathbf{E} \\ \dfrac{\partial T^{n+1}}{\partial t} + \operatorname{div} \lambda \nabla T^{n+1} = P \end{cases}$$

where $\mathbf{B} = \mu \mathbf{H}$ et $\mathbf{D} = \varepsilon \mathbf{E}$ and P = dissipated electric power

The above equations are discretized on unstructured and consistent meshes, by using a finite volume method. This principle enables us to consider in a natural way, different geometry curves and boundary conditions. This method allows to treat complex geometries, meaning that the space arround the product is meshed by unregular elementary volumes.
These vectorial equations (I) are available in a vacuum cavity as well as in one wich contains a sample. In each node, we set a particular value to each physical variable.

The principle of the coupling between electromagnetic and thermal equations allows to take into account the thermal variations of the physical parameters (ε', ε'', λ).

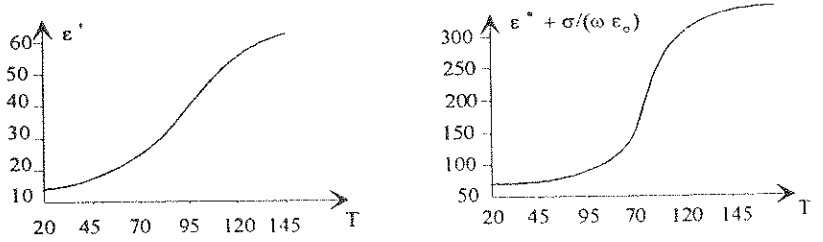

Variations of electrical parameters in function of the temperature

Moerover, we can follow the time evolution of the temperature during the heat of the sample.

With this software, we can determinate the electromagnetic and thermal fields in a closed cavity. It is also possible to treat open problems as antenna ones. We modelise the electric field generated by the magnetron in order to know the incident field settled into the cavity.

Now, we present an example concerning the heat of a matra inside a bounded cavity. The matra contains sulfuric acide and its characteristics depend on the temperature. On the two following graphics we can observe the electric and thermal fields. These pictures represent a cross-section of the fields, perpendicularly to the source of polarization.

Electric field (isovalues)

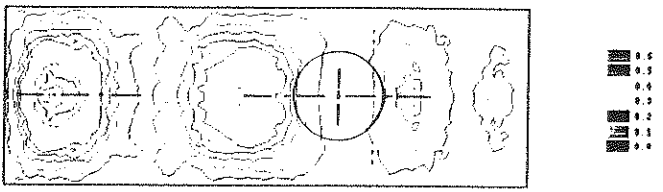

acid sample axis
(matra)

Temperature field (isovalues)

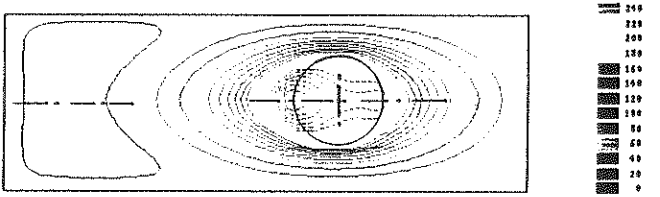

This article will present in the first part, the mathematical resolution method and in the second part, we explain through a few simulations the choice of the mesh, and we perform a few graphical visualizations of the electric and temperature fields.

EXTENSION OF TIME-DOMAIN SURFACE IMPEDANCE CONCEPT TO DISPERSIVE-MEDIA

S. KELLALI, Ph. LEVEQUE, A. REINEIX, B. JECKO
Equipe "Electromagnétisme" - Faculté des Sciences - URA CNRS n° 356
123, Avenue Albert-Thomas 87060 LIMOGES Cédex (FRANCE)

The use of surface impedance boundary conditions in the standard frequency independant finite-difference time-domain (FDTD), is very advantageous for studies of electromagnetic interactions with interfaces.

This method avoids the spatial quantization of the dielectric media (Figure 1) and thus provides a great computational savings, in addition with a lesser constraint on the space-time increments.

In this paper, this concept is extended to modelling of air-dispersive media interfaces.

These media are assumed to be frequency-dependent, with constitutive parameters : μ, σ and a complexe permittivity described by a Debye's model with a single relaxation :

$$\varepsilon(\omega) = \varepsilon_0 \left[\varepsilon_\infty + \frac{\varepsilon_s - \varepsilon_\infty}{1 + j\omega\,\tau_o} \right].$$

The complete time-domain expressions of the surface impedances for such media, are determined according to the formalism developed (KELLALI et al, IEEE Trans. on EMC, Vol. 35, n° 2, Aug. 1993).

Using these analytical expressions in a FDTD code, the results computed with this method agree very well with those given by the Fresnel or the frequency-dependent finite-difference time-domain (FD^2TD) methods.

When the media are assumed lossless ($\sigma = 0$), then those expressions are relatively simple, but for lossy media ($\sigma \neq 0$) they become more complex. Although these formulas take into account the incidence angle of T.E.M. plane waves, it is interesting to distinguish cases where the normal incidence expression of surface impedance may be used for both polarisations.

It emerges from this study that the cases where the surface impedance at normal incidence is available for both polarisations, are essentially fixed by the constitutive parameters of the media.

Then, for these cases of media, the surface impedance boundary conditions, may be used for studies of TEM plane waves illumination or current sources radiation over dispersive half spaces, since the incidence angle is not needed.

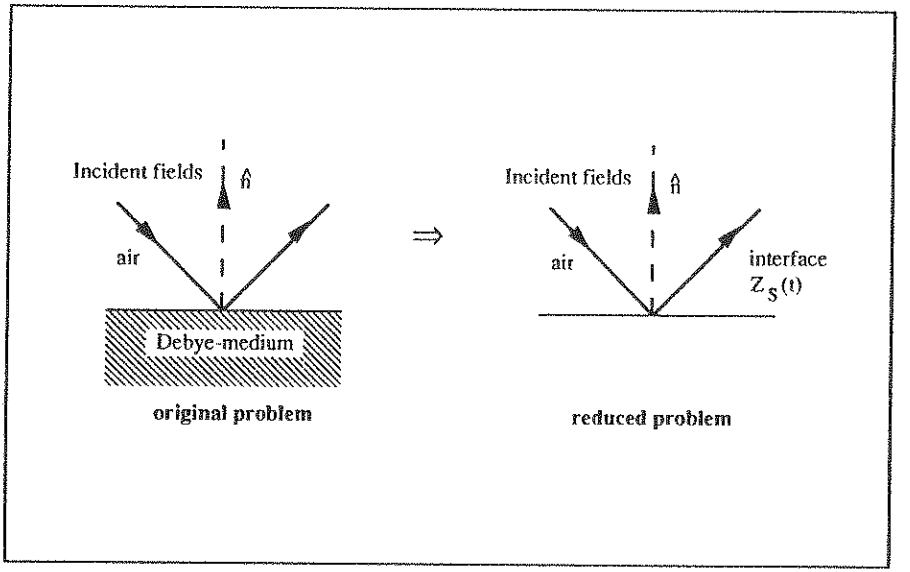

FIGURE 1

COUPLING BETWEEN NUMERICAL METHODS TO SOLVE BIG SIZE EMC PROBLEMS

Authors : B. JECKO - A. REINEIX
IRCOM - URA CNRS n° 356 - Faculté des Sciences
123, Avenue Albert-Thomas 87060 LIMOGES Cédex (France)

Most of electromagnetic problems can be formulated as the scattering problem of an incident wave by an obstacle. That is particularly the case in the EMC area where obstacles are often big size sturctures whose dimensions can be at the same time smaller, in the same order of length, and higher than the wavelengths appearing in the incident wave. Under these conditions, any approximative approach cannot be used to solve the EMC problem and consequently EM software are based on "full mode" methods. Moreover for big size problems, these rigorously formulated methods cannot be applied alone because they require usely prohibilitve computer time and memory place.

Then some authors [1, 2, 3] have developed hybrid technics which associate, in a complex formulation, two or more numerical technics. In this paper our approach is less complicate but also less rigorous. The space domain is devided into different regions as in a topologic approach. In each region, a suitable numerical software is applied and the equivalent principle is generally used to make the link between the different regions.

Some examples are presented which associate a "full mode" method (here the FDTD one) with other technics like assymptotic methods, thin wire integral equations, transmission line theory, and so on...

The first application deals with the radiation of antennas located on big size structures like cars, or missiles. In such problems, the FDTD algorithm permits to obtain the EM field in the vincinity of the antenna taking into account the car, and the assymptotic methods give, the radiation pattern. This technic is generalized to antenna for which the phase center is unknown.

The second application associates two full modes methods (the FDTD approach and a time domain integral equation technic) to solve EMC measurement modeling. For example, to evaluate EM susceptibility of mobiles illuminated by a large parasitic plane wave, measurements are usely performed in an anechoïc chambers using wire antennas (log periodic, Yagi, ...).It is very interesting to know how the experimental results are closed to these of the illumination by a plane wave. Then, a modelization of the experimentation must be done but it is obvious that the problem cannot be solved by introducing in the same computing volume both antenna and mobile.

Futhermore, the thin wire integral equation approach is more accurate than FDTD to model the antenna behaviour whereas the mobile scattering have to be treated with the FDTD algorithm. Then, these two methods are used together assuming that the mobile reaction does not modifie significantly the radiation of the antenna.

"Full mode" methods can also be associated with transmission line theory to simplify the analysis of wire structures located in a metallic box and illuminated via apertures by a parasitic incident wave. This problem is usely treated in aircrafts EMC problems.

All these associated technics involve numerical modifications of the softwares but permit to treat big size problems without introducing to much complexity.

COMPOSITE MATERIALS SHEET MODELING IN A F.D.T.D (3D) CODE

Asfaux D.* Negret D. Pecqueux B. Vézinet R.
Centre d' Etudes de Gramat
46500 GRAMAT (FRANCE)

Béniguel Y.
I.E.E.A.
13, promenade Paul Doumer
92400 COURBEVOIE (FRANCE)

ABSTRACT

In this paper, we will first describe two isotropic material sheet models usable in a finite difference time domain (F.D.T.D.) code, the material sheet being considered electrically thick or thin. Then, different applications using these models will be compared to an experimental approach and their validation discussed.

At last, a third sheet model for more complex materials implemented in a F.D.T.D. code will be presented as the expected improvements.

MATERIAL SHEET F.D.T.D. MODELS VALIDATION

In this part, the composite material must be considered as isotropic, homogeneous, linear and having constant (ε, μ, σ) electromagnetic characteristics values in the frequency bandwith of interest.

1st model - material equivalent electromagnetic characteristics model (ε_{eq}, σ_{eq})

Only the tangential electric field located on the sheet is computed /1/. According to the Yee 's F.D.T.D. formulation , the Ex (i,j,k) component is computed as follows (figure 1):

$$E_x^{n+1/2}(i,j,k) = AE_x^{n-1/2}(i,j,k) + B\left(\frac{H_z^n(i,j+1,k) - H_z^n(i,j,k)}{\Delta y} - \frac{H_y^n(i,j,k) - H_y^n(i,j,k-1)}{\Delta z}\right)$$

with : $A = \dfrac{\frac{\varepsilon_{eq}}{\Delta t} - \frac{\sigma_{eq}}{2}}{\frac{\varepsilon_{eq}}{\Delta t} + \frac{\sigma_{eq}}{2}}$ $\quad B = \dfrac{1}{\frac{\varepsilon_{eq}}{\Delta t} + \frac{\sigma_{eq}}{2}}$ $\quad \varepsilon_{eq} = \varepsilon_0\left(1 + (\varepsilon_r - 1)\right)\dfrac{d}{\Delta z}$ $\quad \sigma_{eq} = \sigma\dfrac{d}{\Delta z}$

d : material sheet thickness (m) , $\quad \sigma$: bulk conductivity (Siemens/m)
ε_r : relative dielectric permittivity , $\quad \Delta z$: F.D.T.D. spatial cell size (m).

2nd model - one way surface (Zs) and transfer (Zt) impedances model

Both external Es and internal Et electric field components are computed by means of the (Zs,Zt) impedances concept. The latter is defined in the frequency domain as below :

$$Es(f) = Zs(f)\ .\ Js(f) \quad \text{and} \quad Et(f) = Zt(f)\ .\ Js(f) \quad \text{where Js(f) is the current density (A/m) .}$$

In accordance with /2/, the impedances are expanded in the frequency domain by a series of exponential forms. Then, the (Es,Et) computations taking convolutions into account become in the time domain (figure 2):

$$E_s^n = \frac{1}{\sigma d}\left(J_s^n + 2\sum_{j=1}^{n} J_s^{j-1/2}\, S_s\,(n-j+1)\right) \qquad E_t^n = \frac{1}{\sigma d}\left(J_s^n + 2\sum_{j=1}^{n} J_s^{j-1/2}\, S_t\,(n-j+1)\right)$$

with : $S_s(m) = \sum_{k=1}^{k_{max}} \exp^{-\left(\frac{k\pi}{d}\right)^2\left(\frac{m-1/2}{\mu_0\sigma}\right)\Delta t}$ $\qquad S_t(m) = \sum_{k=1}^{k_{max}} (-1)^k \exp^{-\left(\frac{k\pi}{d}\right)^2\left(\frac{m-1/2}{\mu_0\sigma}\right)\Delta t}$

$$J_s^{j-1/2} = H_y^{j-1/2}(i,j,k) - H_y^{j-1/2}(i,j,k-1)$$

During the computations, only the E_s^n component is stored while E_t^n is an intermediate value used to calculate H_y^{n+1}. Besides, using the decreasing exponential forms aspect, computations are given in /3/ to avoid backstorage and minimize the CPU time .

Theory / experimentation confrontation

Numerical results obtained from the F.D.T.D. code GORF with 3D structures having composite material sheets are compared to measurements made on the same structures under E.M.P. simulators of C.E.G /3,4/. The figures (3,4) display a good agreement between the two approaches and consequently allow us to confirm the material sheet models validity.

The use domains of these two models versus material electromagnetic characteristics and frequency /3/ are finally given (figure 5).

TWO WAYS SURFACE AND TRANSFER IMPEDANCES CONCEPT GENERALIZATION IN THE CODE GORF /5/

According to the F.D.T.D. scheme, a material sheet behavior excited on both sides by electromagnetic fields can be rigorously modeled in the frequency domain by :

$$\begin{pmatrix} E_1 \\ E_2 \end{pmatrix} = \bar{Z}\begin{pmatrix} H_1 \\ H_2 \end{pmatrix} = \begin{pmatrix} Z_s & Z_t \\ Z_t & Z_s \end{pmatrix}\begin{pmatrix} H_1 \\ H_2 \end{pmatrix}$$

where (E_1, H_1) are the total electric and magnetic fields upon the sheet (respectively 2 above the sheet).

The (Zs, Zt) impedances are expanded into finite series of 3 different kinds of rational fractions in the frequency domain /6/ :

$$Z(\omega) = Z_0 + \sum_{i=1}^{N_1} Z_{i,1}(\omega) + \sum_{i=1}^{N_2} Z_{i,2}(\omega)$$

with : $Z_0 = \alpha_0 \qquad Z_{i,1}(\omega) = \dfrac{\alpha_{i,1}}{1 - \dfrac{j\omega}{\omega_{i,1}}} \qquad Z_{i,2}(\omega) = \dfrac{\alpha_{i,2}}{1 - \dfrac{j\omega\beta_{i,2}}{\omega_{i,2}^2} - \dfrac{\omega^2}{\omega_{i,2}^2}}$

Friendly dual time domain expressions for Zs(t) and Zt(t) make the convolution computation easier and avoid backstorage. The different constant coefficients $(\alpha_0,...,f_{2,i})$ are fitted by using a numerical optimization technique. Moreover, this transformation into canonical forms allows to take into account, in a F.D.T.D. code, a more complex composite sheet like multilayers or frequency dependent material .

REFERENCES

/1/ J. P. BERENGER " Thin sheet in a F.D.T.D. code " 6th International Symposium on EMC - Ecole Centrale de Lyon (FRANCE) 2-4 June 1992.

/2/ R. A. PERALA " A time domain representation of surface and transfer impedance useful for analysis of advanced composite aircraft " International Aerospace and Ground Conference- Orlando (Florida) June 1984 .

/3/ D. ASFAUX " Contribution to the study of composite structure modelisation " - Ph. D thesis from the University of LIMOGES (FRANCE) - January 28 , 1993 .

/4/ Y. BENIGUEL " Comparison between numerical and experimental results on a 3D CFC structure under EMP simulator " I.E.E.A. Report September 16, 1993 (under contract with C.E.G.).

/5/ N. ROUVRAIS " Rational fractions implementation for composite materials in the F.D.T.D. code GORF " GERAC Report December 23, 1993 (under contract with C.E.G.).

/6/ J. R. ELLIOTT " Time domain implementation of frequency dependent materials in finite difference calculations" EUROEM Symposium on EM Environments and Consequences Bordeaux (FRANCE) May 30, June 3, 1994.

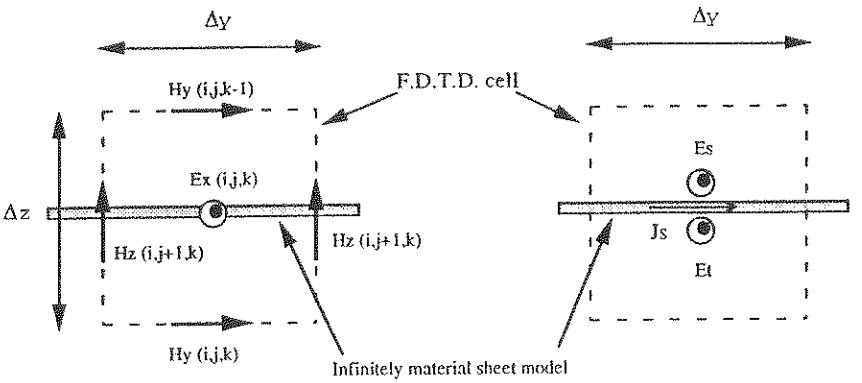

Figure 1 : (εeq, σeq) model

Figure 2 : (Zs, Zt) model

Fresnel transmission coefficient modulus

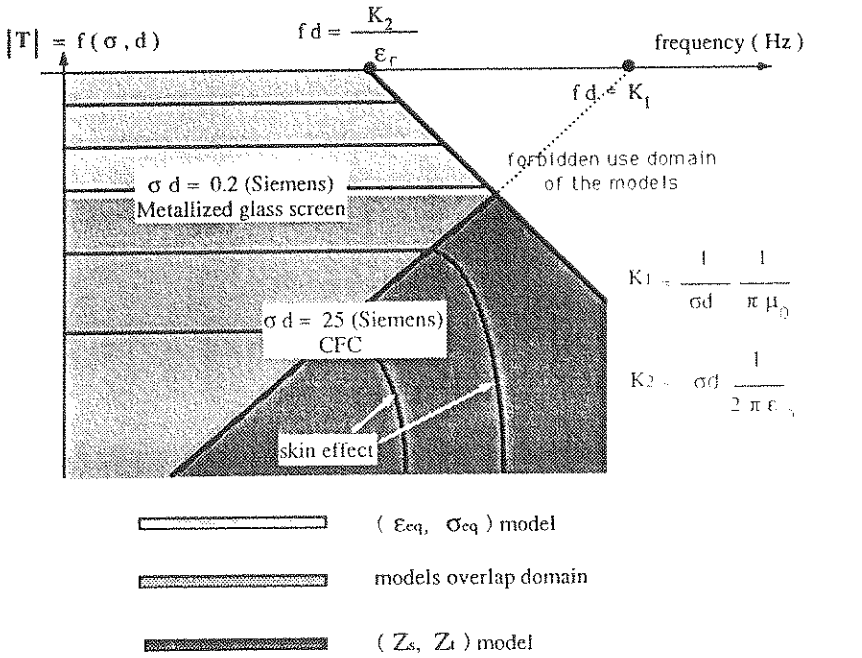

Figure 5: Material sheet models use domain

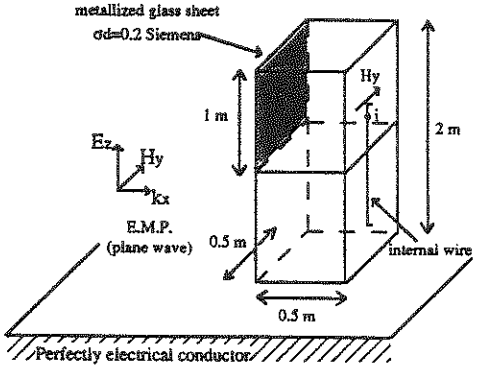

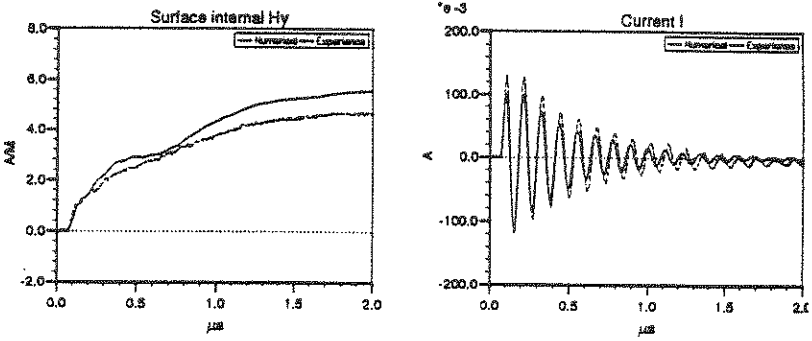

Figure 3 : 1st model / metallic structure with 1 sheet

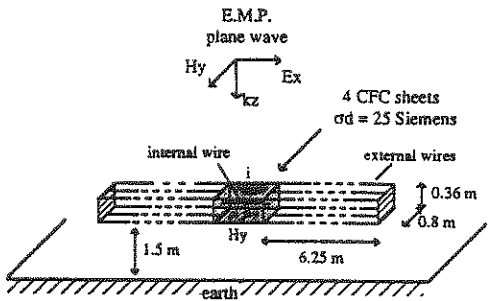

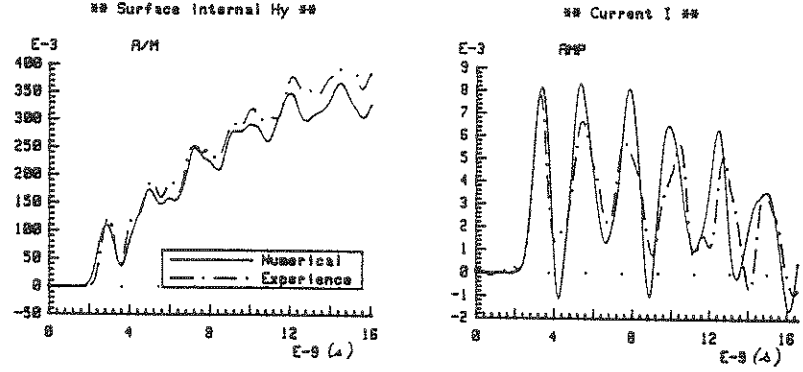

Figure 4: 2st model / composite structure with 4 CFC sheets

NUMERICAL SIMULATION OF ELECTOMAGNETIC WAVE PROPAGATION IN FERROMAGNETIC MATERIALS

Patrick JOLY Olivier VACUS*

INRIA Rocquencourt

In order to model ferromagnetic materials, we want to do both mathematical and numerical studies of Maxwell's equations coupled with the "Landau-Lifschitz-Gilbert" equation :

$$\begin{cases} \dfrac{\partial \mathbf{B}}{\partial t} = -\,rot(\mathbf{E}) \\ \dfrac{\partial \mathbf{E}}{\partial t} = rot(\mathbf{H}) \\ \dfrac{\partial \mathbf{M}}{\partial t} = \gamma \mathbf{H_T}(\mathbf{M}) \times \mathbf{M} + \dfrac{\alpha}{\|\mathbf{M}\|} \mathbf{M} \times \dfrac{\partial \mathbf{M}}{\partial t} \end{cases} \tag{1}$$

where we denote by $\mathbf{E}$ the electric field, $\mathbf{H}$ the magnetic field, $\mathbf{M}$ the magnetization.

In the third equation (LLG), $\mathbf{H_T}(\mathbf{M})$ is the total local magnetic field, that is to say the sum of $\mathbf{H}$, the solution of Maxwell's equation, and an effective field $\mathbf{H_{eff}}(\mathbf{M})$:

$$\mathbf{H_T}(\mathbf{M}) = \mathbf{H} + \mathbf{H_{eff}}(\mathbf{M}). \tag{2}$$

The effective field is a function of the magnetization $\mathbf{M}$, which increases the non-linearity of the problem. We decompose $\mathbf{H_{eff}}(\mathbf{M})$ into :

- $\mathbf{H_0}$, a static field,
- $\mathbf{H_{anis}}$, a field of anisotropy. ($\mathbf{H_{anis}} = -\dfrac{\partial F_a}{\partial \mathbf{M}}$)
- $\mathbf{H_{magn}}(\mathbf{M})$, a demagnetizing field.

This last one is a solution of a Laplace's problem :

$$\begin{cases} rot(\mathbf{H_{magn}}) = 0 \\ \mu_0\, div(\mathbf{H_{magn}}) = -\,div(\mathbf{M}) \end{cases} \Leftrightarrow \begin{cases} \mathbf{H_{magn}} = grad(\varphi) \\ \mu_0 \triangle \varphi = -\,div(\mathbf{M}) \end{cases} \tag{3}$$

A non-trivial difficulty is that the operator $(M \mapsto H_{magn}(M))$ is nonlocal in space.

The materials whose electromagnetic behaviour is described by the equation (LLG) are expected to be "absorbing materials". After giving a new formulation of (LLG), we show it corresponds to the decay of an electromagnetic energy. This decay is due to the second term in (LLG) and is of course linked to the sign of α. Another important result is that the norm of the magnetization $\|M\|$ is constant at each point in the ferromagnetic domain.

Concerning numerical aspects of our problem, we have constructed a numerical scheme for which we have proved the explicit nature and a stability result, provided that some CFL condition is satisfied.

This scheme is shown to preserve the decay of a discrete energy and the fact that the norm of the magnetization is constant.

We will present results of a one-dimensional computation, which illustrate the following physical phenomena : the Larmor precession, influence of the different parameters, existence of a resonnant frequency, ... We also compare these results to those obtained after linearization.

ANALYSIS OF RADIATION EMISSIONS FROM PRINTED CIRCUIT BOARDS

M. DRISSI*, J. CITERNE*, P. HERVE*, and M. ROCHDI**
* URA CNRS 834, INSA , 35043 RENNES CEDEX, FRANCE
** CNET/PAB/SHM, 92131 ISSY-LES-MOULINEAUX, FRANCE

The considerable increase of electronic equipments multiplies the electromagnetic interference caused by the radiation from cables and/or printed circuit boards (PCB). Furthermore, the use of fast digital circuit families makes the radiated emissions, according to CISPR regulation, a very difficult task for digital circuit designers. So, the present paper gives a rigorous analysis to evaluate the radiation emission from the PCB due to common mode and differential mode currents.

The approach is based on the use of integral equations technique solved by the method of moments. From the obtained differential-mode or common-mode currents, the components of the radiated field are calculated by modelling the current distributions as an array of elementary dipoles. The feeding generator is considered as a trapezoidal wave form with a 50% duty cycle and a rise time *ton*. Using the Fourier transform, each spectral pulse component is used as a feeding field in the integral equations. In order to compute the load impedances corresponding to the component inserted at the end of the conductor strip, some extra boundary conditions are used on the currents computation .

The mentioned technique is applied on two strip lines of the configuration given in figure 1. The microstrip line of length 150 mm is excited from one end by trapezoidal wave form generator and is loaded by an open circuit at the other end. Figure 2 shows the variation of the radiated field calculated at 1m from the PCB circuit. Our calculated results are compared to the measured ones performed in the anechoic chamber. The comparison shows a very good agreement.

The present analysis has the advantage of being capable to determine also the radiated field created by common-mode currents when the ground plane of the previous structure is removed (fig.1 a). Fig. 3 gives an example of such a results. Again, one can see the good agreement between the theory and the measurement except around 300 MHz. This is due to the contribution of the radiation of the power supply which has a half wave length at this frequency. This problem was avoided in the microstrip structure by putting the power supply behind the ground plane. It can be noticed that the radiated field due to common-mode currents is 20 dB higher than the one due to differential-mode currents.

Fig. 4 presents the magnitude of the radiated field calculated for two different rise time values. The obtained results show that the radiation emission increases when the ton decreases either for differential-mode and common-mode. The effect of varying the load conditions of the interconnection line on the radiated field is also investigated and will be presented.

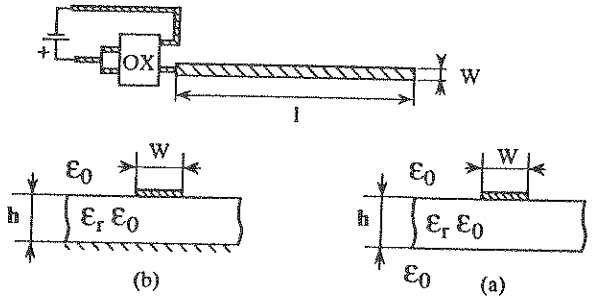

Fig. 1 Strips conductor feeded by an oscillator
(h = 0.635 mm, εr = 4.5 , W = 1 mm)

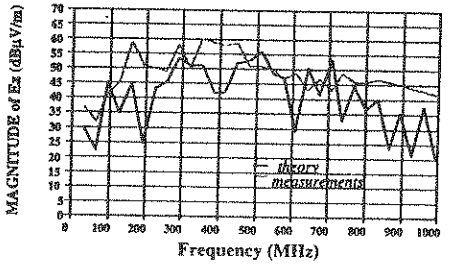

Fig. 2 Radiated field due to differential - mode currents
(clock signal 32 MHz, t_{on} = 2ns, duty cycle = 50%)

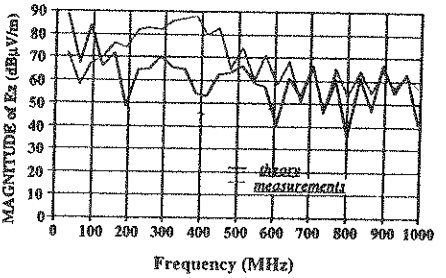

Fig. 3 Radiated field due to common - mode currents
(clock signal 32 MHz, t_{on} = 2ns, duty cycle = 50%)

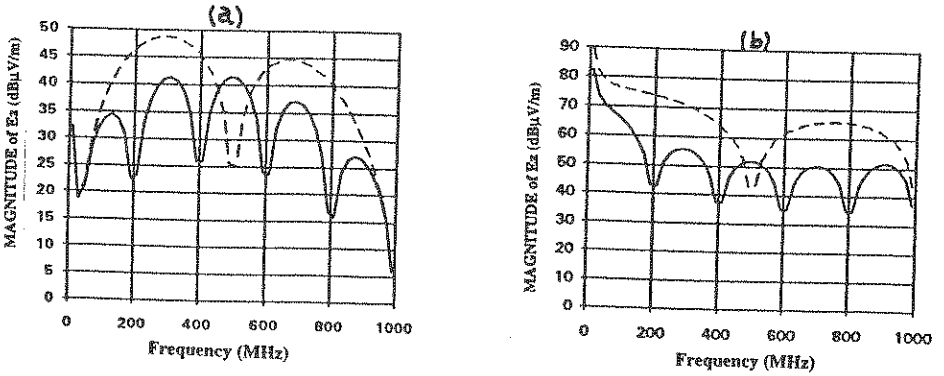

Fig. 4 : Radiat ed field (clock signal 32 MHz, duty cycle = 50%)
(a) differential-mode , (b) common-mode

———— ton = 5 ns
— — - ton = 2 ns

Computation And Reduction Of The Magnetic Field Outside Electromagnetic Devices

B. Belhoucine*,**, M. Besseau**, H. Kermorgant** and A. Foggia*

* Laboratoire d'Electrotechnique de Grenoble (U.R.A 355-C.N.R.S) ENSIEG, BP 46, 38406 Saint Martin d'Hères, France
** Société E.C.A, rue des Frères Lumière Z.I Toulon-Est, BP 242, 83078 TOULON Cédex, France

Abstract **- This paper is devoted to the computation and reduction of the magnetic field radiated by a rotating axial airgap variable reluctance machine. The authors used a 3D finite element program in which the open boundary space was represented either by a geometrical transformation or by the coupling of finite element and boundary integral methods.**

INTRODUCTION

The electromagnetic field produced by electromagnetic devices with finite dimensions, cancels at infinity. However in the given applications, this field may be disturbing source; indeed beyond certain limits, it can perturb its environment. So it is necessary to know the radiated field produced by the electromagnetic systems.

However, to calculate the electromagnetic field it is not an easy task because of the open boundary problem and the needs of Maxwell's equations to be solved. So evercome this difficulty and to take into account infinity, we used two techniques of resolution. The techniques which gave satisfactory results, based on modelling of the electromagnetic structures by the finite elements method, and take account infinity by two methods:

- bijective transformation method;
- boundary integral equations method.

METHODOLOGY USED

These two methods are implemented in our FLUX3D program. The problem that has been solved in this paper has consisted in computing the 3 components of the flux density outside the bounded domain of resolution. This is a new aspect of magnetic device modelling, where the knowledge of the flux density distribution outside the device is required.

THE SYSTEM UNDER INVESTIGATION

The system under investigation concerns a rotating axial airgap variable reluctance machine. It consists of two non-magnetic material discs with nine ferromagnetic studs per disc. Each stator has eight U shaped magnetic circuits equipped with coils representing four phases of the stator.

RESULTS

Figure 2 shows the electromagnetic field outside the motor by bijective transformation method. And figure 3 shows the reduction of the electromagnetic field by the compensation loops.

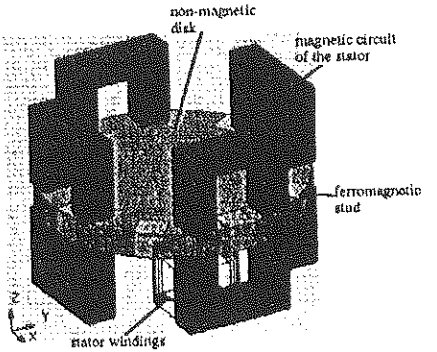

Fig. 1. Geometry of the half motor

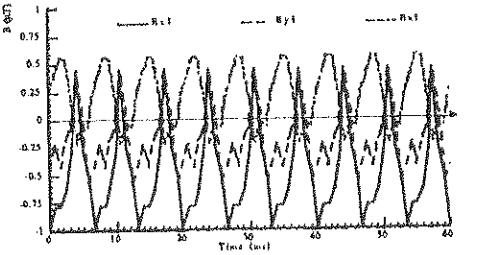

Fig. 2.

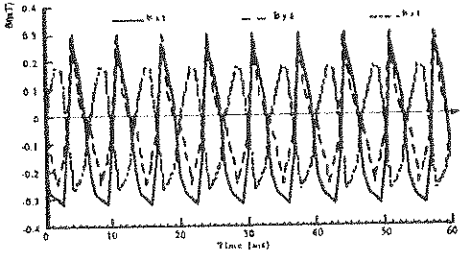

Fig. 3.

CONCLUSION

In conclusion, this paper presents comparisons between values of far away magnetic fields computed using two different methods of solving Maxwell's equations in 3D open boundary space. Its presents also the reduction methodology of the magnetic field radiated by electromagnetic devices.

RADIATED EMISSION FROM TRANSMISSION LINE IN PCBs*

Fang Han [1] and S. Sali [2]
Dept. of Telecom. and Control Eng., Northern Jiaotong Univ., Beijing, 100044, CHINA
Dept. of Electrical and Electronic Eng., Univ. of Newcastle upon Tyne, NE1 7RU, UK

Radiated emission from digital printed circuit boards (PCBs) may cause narrowband and broadband interference with surrounding electronic equipment, as well as leakage of data information. In general, the emission effect may vary with structure or layout in a PCB. Exciting source is also a significant factor affecting the emission feature. In recent years, the emission from PCBs have been studied by some publications, in which, several methods were discussed for simplified analysis (*C. R. Paul, IEEE Trans. on EMC, 2, 189–93, 1989, R. Raul, et al., IEEE Trans. on EMC, 1, 88–9, 1988*). However, because of difference in layout and exciting parameters, it is difficult to find a universal model for analysing radiated emission from PCBs. For example, the electric diode and magnetic diode model are valid only for the case, in which, the length of circuit is much shorter than both the wavelength of interest and the distance between source and field point.

In many cases, the track in PCBs or the line connecting a PCB and other devices may be treated as an equivalent transmission line. As such, emission from a PCB can be discussed on the basis of emission from a transmission line. This paper is to discuss far zone field radiation from a PCB circuit which can be equivalent to a transmission line.

Fig.1 shows a pair of transmission line circuit of differential mode current and common mode current. Suppose $d \ll r$, $l \ll r$, $\lambda \ll r$, for far zone field, $r > 2l^2/\lambda$. Thus, the vector potential at point P, produced by entire differential mode current, can be given by

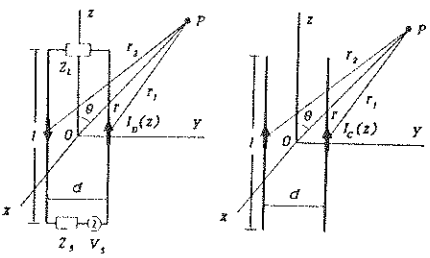

Fig.1 (a) differential and (b) common, mode circuit

$$A_z = \frac{\mu_0}{4\pi}\int_{-\frac{l}{2}}^{\frac{l}{2}} I_D(z')\left[\frac{e^{-j\beta(r_1 - z'\cos\theta_1)}}{r_1} - \frac{e^{-j\beta(r_2 - z'\cos\theta_2)}}{r_2}\right]dz' \qquad (1)$$

in which, $r_1 \approx r - \frac{d}{2}\sin\theta$, $r_2 \approx r + \frac{d}{2}\sin\theta$, $\cos\theta_1 = z/r_1$, $\cos\theta_2 = z/r_2$, $\cos\theta = z/r$. Noticing that $d \ll r$, it could be assumed that $\theta_1 = \theta_2 = \theta$, then, (1) can be approximated as

$$A_z = \frac{j\mu_0 e^{-j\beta r}}{2\pi r}\sin\left(\frac{\beta d}{2}\sin\theta\right)\int_{-\frac{l}{2}}^{\frac{l}{2}} I_D(z')e^{j\beta z'\cos\theta}dz' \qquad (2)$$

The electric field at far zone can be thus obtained as

$$E_D = -\frac{\mu_0 \omega \sin\theta e^{-j\beta r}}{2\pi r}\sin\left(\frac{\beta d}{2}\sin\theta\right)\int_{-\frac{l}{2}}^{\frac{l}{2}} I_D(z')e^{j\beta z'\cos\theta}dz'\ \theta \qquad (3)$$

* This project is supported in part by The Royal Society of UK and The National Natural Science Foundation of China

If field point $P(x,y,z)$ is not in the circuit plane, the following relations hold as shown in Fig.1 (a)

$$r_1 \approx r - \frac{d}{2}\sin\theta\sin\varphi, \quad r_2 \approx r + \frac{d}{2}\sin\theta\sin\varphi$$

Thus, the electric field at far zone produced by differential mode current can be calculated by

$$\mathbf{E}_D = -\frac{\mu_0 \omega}{2\pi r \sin\theta e^{-\beta r}} \sin\left(\frac{\beta d}{2}\sin\theta\sin\varphi\right)\int_{-\frac{l}{2}}^{\frac{l}{2}} I_D(z')e^{\beta z'\cos\theta}dz'\ \vec{\theta} \tag{4}$$

where, φ is the angle between normal direction of the circuit plane (x) and direction in projection of r on xoy plane, and $I_D(z')$ is distribution of the differential mode current, which can be calculated by transmission line theory as follows.

$$I_D(z) = V_S \frac{Z_C \mathrm{ch}\gamma\left(\frac{l}{2} - z\right) + Z_L \mathrm{sh}\gamma\left(\frac{l}{2} - z\right)}{Z_C(Z_S + Z_L)\mathrm{ch}\gamma l + \left(Z_S Z_L + Z_C^2\right)\mathrm{sh}\gamma l} \tag{5}$$

where, γ, representing complex propagation constant, is not the same with β. Inserting (5) into (4), the general solution of the radiated field at far zone produced by differential mode current becomes

$$\mathbf{E}_D = -\vec{\theta}\frac{\mu_0 \omega \sin\theta e^{-\beta r}}{2\pi r}\sin\left(\frac{\beta d}{2}\sin\theta\sin\varphi\right)F \tag{6}$$

where

$$F = \frac{(A+B)e^{\frac{\gamma l}{2}}}{\gamma - j\beta\cos\theta}\mathrm{sh}\left[(\gamma - j\beta\cos\theta)\frac{l}{2}\right] + \frac{(A-B)e^{-\gamma l/2}}{\gamma + j\beta\cos\theta}\mathrm{sh}\left[(\gamma + j\beta\cos\theta)\frac{l}{2}\right] \tag{7}$$

$$A = \frac{V_S Z_C}{Z_C(Z_S + Z_L)\mathrm{ch}\gamma l + (Z_S Z_L + Z_C^2)\mathrm{sh}\gamma l}$$

$$B = \frac{V_S Z_L}{Z_C(Z_S + Z_L)\mathrm{ch}\gamma l + (Z_S Z_L + Z_C^2)\mathrm{sh}\gamma l}$$

V_S represents source voltage, and Z_C, Z_S, Z_L represents characteristic impedance, input impedance and output impedance, respectively.

For common mode current $I_C(z)$, the radiated field at for zone can be obtained in similar way, i.e.

$$\mathbf{E}_C = \frac{j\mu_0 \omega}{2\pi r}\sin\theta e^{-\beta r}\cos\left(\frac{\beta d}{2}\sin\theta\sin\varphi\right)\int_{-\frac{l}{2}}^{\frac{l}{2}} I_C(z')e^{\beta z'\cos\theta}dz'\ \vec{\theta} \tag{8}$$

where, the expressive form in $I_C(z)$ will be depend on distributed parameter of the transmission line (*F. Han, IEEE Trans. on EMC, 3, 345-8, 1992*).

If condition $l \ll r$, $d \ll r$, $\lambda \ll r$ are satisfied, (4) and (8) can be also applied to calculate electric field at far zone produced by common mode and differential mode current of other kinds of transmission line.

An Approach for a Fast Preanalysis of Reflection Effects on Printed Circuit Boards

J. Müller*, E. Griese**

* University of Paderborn · Cadlab · Analog System Engineering
** Siemens Nixdorf Informationssysteme AG · Cadlab · Analog System Engineering

Bahnhofstrasse 32 · D-33094 Paderborn Germany

Introduction

Increasing demands on circuits and PCBs results in faster component technologies, increasing clock rates, and PCBs with a higher complexity. Therefore, the design of PCBs has to be supported by fast analysis methods, otherwise EMC effects like reflection and crosstalk will occur. Aim of the presented preanalysis is an approximative determination of the maximal voltage overshoot for a two-point-net without a time extensive simulation. Two-point-net means a layout constellation being a direct connection between two active components. It may contain passive components and the connection may consist of sections with different characteristic impedances. The reflection behaviour of digital circuits depends on the matching of the transmitter and receiver to the characteristic impedance of the transmission line, the reflection coefficents effected by discontinuities of the characteristic impedance, and the propagation time of the transmission line. First principle of the introduced method is, that the result shall represent a worst case investigation.

Maximum Overshoot at the Receiver

Figure 1 presents the used model for the determination of the amplitudes of the first propagating voltage wave V_1. It results from the voltage divider of the characteristic impedance Z_L and the resistance R_{out} of the ideal voltage source. When a series resistance R_s is used for matching the output to the characteristic impedance Z_L of the transmission line, it has to be added to the resistance R_{out}. At the receiver the termination is given by the input resistance of the receiver and if necessary by a matching measures. Figure 1 shows the equivalent circuits.

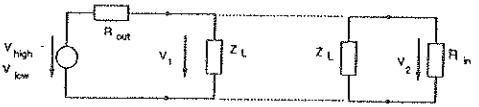

Figure 1: Equivalent circuits for transmitters and receivers

$$V_2 = \rho(r) \cdot V_{1,high} \qquad (1)$$

$$V_1 = (V_{high} - V_{low}) \frac{Z_L}{R_{out,low/high} + Z_L} \qquad (2)$$

As at the most IC-technologies the output resistance of the high/low transition differs from the low/high transition, both cases have to be investigated seperately. The associations will be given as example for the low/high transition. The function $\rho(r)$ is a characteristic equation describing the reflection behaviour on transmission lines.

Determination of the Characteristic Equation for Piecewise Homogeneous Transmission Lines

As the most PCBs have more than one signal layer, many transmission lines will extend over more than one layer. A jump of the characteristic impedance has to be expected at the via. Compared to the maximum overshoot of a homogeneous transmission line this case yields to a larger overshoot. Figure 2 shows the ringing at the termination of a long transmission line for three different arrangements. The lengths of the line sections were choosen unrealistically long, which means that the amplitude is independent from the rise-time and the transmission line length.

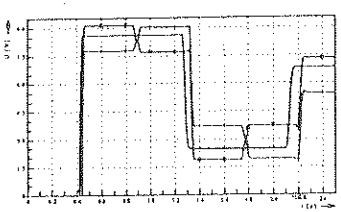

Figure 2: Voltage ringing of a long line without (net1:-) and with a layer change (net2:*), (net3:+)

Hereby, the following data were taken for the simulation at all three circuits:

$$V_{low} = 0\ V\ , \quad R_{out,low/high} = 10\ \Omega$$
$$V_{high} = 5\ V\ , \quad R_{in} = 100\ k\Omega$$

The characteristic impedances were choosen as:

net1: $Z_{L1} = 60\ \Omega\ , \quad Z_{L2} = 60\ \Omega$
net2: $Z_{L1} = 50\ \Omega\ , \quad Z_{L2} = 60\ \Omega$
net3: $Z_{L1} = 60\ \Omega\ , \quad Z_{L2} = 50\ \Omega$

Now it can be shown that for a 'worst case' approximation the function $\rho(r)$ can be determined for n arbitrarily arranged characteristic impedance changes as follows:

$$\rho = (1 + r_{in}) \prod_{i=1}^{n} (1 + r_i), \qquad r_i = \left| \frac{Z_{L(i+1)} - Z_{Li}}{Z_{L(i+1)} + Z_{Li}} \right|, \quad r_{in} = \left| \frac{R_{in} - Z_L}{Z_L + R_{in}} \right| \qquad (3)$$

The voltage, determined in equation (1), does not consider the influence of the line length (figure 3).

The calculated maximum voltage amplitude is only achieved in the two-point-net if $2t_d \geq t_r$ (t_d: propagation delay of the transmission line, t_r: rise time of the digital signal). The approximated voltage has to be multiplied with the term $\frac{2t_d}{t_r}$ for shorter transmission lines. Considering the practically important mixed resistive/capacitive terminations one gets an exponential rise that differs from that in figure 3 presented curve depending on the capacitive load. Comparing the resulting voltage amplitude with the given boundary value (static noise margin), it can be decided whether measures to avoide reflections are necessary for the examined net.

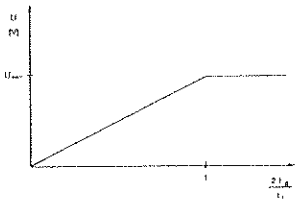

Figure 3: Voltage amplitude of the overshoot versus $2t_d/t_r$

This research is part of the JESSI project AC-5 *Development of an EMC-Workbench for Microelectronic Application*. The project is supported by the BMFT (Bundesministerium für Forschung und Technologie) under grant 01 M 2886 D8 and 01 M 2886 D0. The responsibility for this publication is held by the authors only.

PROXIMITY EFFECTS IN CYLINDRICAL CONDUCTORS FOR APPLICATIONS IN A WIDE RANGE OF FREQUENCIES

M. Kane, A. Ahmad* and Ph. Auriol
Centre de Génie Electrique de Lyon, URA CNRS 829, E.C.L.
BP 163, 69131 Ecully cedex, FRANCE

In many applications of circular conductors, high accuracy is required for the computation of flux densities and cable parameters. Various approaches to the problem of determining skin and proximity effects have been described in the literature (E.S.M. MOK & G.I. COSTACHE, IEEE Elect. Compat., 34,1992), (M. KANE & PH. AURIOL, IEE CEM,1994), (A. KONRAD & M.V.K. CHARI & Z. CSENDES, IEEE MAG, 18, 1982). Analytical methods provide good results in a short time of computation. This paper deals the analytical modelling of cylindrical conductors. The skin and proximity effects are taken into account for frequencies from 0 Hz to 100 MHz. Fig. 1 shows the general configuration of the investigated problem. A local cylindrical coordinate system (r,θ,z) is defined for parallel current carrying conductors. The total current I flows in the k-th conductor in the z direction. The permeability μ and conductivity σ are assumed to be linear in this paper. The electric (magnetic) field intensity inside and outside the conductor are obtained from Maxwell's equations assuming there are no displacement currents inside the conductors :

$$\frac{\partial^2 E_{zk}}{\partial r_k^2}+\frac{\partial E_{zk}}{r_k\,\partial r_k}+\frac{\partial^2 E_{zk}}{r_k^2\,\partial\theta_k^2}-j\,\mu\sigma\omega E_{zk}=0;\ r_k\le r \qquad ; \qquad \frac{\partial^2 E_{zk}}{\partial r_k^2}+\frac{\partial E_{zk}}{r_k\,\partial r_k}+\frac{\partial^2 E_{zk}}{r_k^2\,\partial\theta_k^2}=0;\ r_k>r_a$$

where ω, (ω=2πf), is the angular frequency and j is the complex operator. The solution of the wave equation is expressed in the following form by separation of variables :

$$H_{\theta k1}(r_k,\theta_k)=\frac{\partial E_{zk1}}{j\,\omega\mu\partial r_k} \quad ; \quad E_{zk1}(r_k,\theta_k)=\sum_{n=0}^{\infty}C_n J_n(j\,r_k\sqrt{j\,\omega\mu\sigma})\,\mathrm{Cos}\,(n\theta_k+a_{nk})$$

$$H_{\theta k2}(r_k,\theta_k)=\frac{\partial E_{zk2}}{j\,\omega\mu_0\partial r_k} \quad ; \quad E_{zk2}(r_k,\theta_k)=U\ln(r_k)+G+\sum_{n=1}^{\infty}((S_n r_k^n+O_n r_k^{-n})(\mathrm{Cos}\,(n\theta_k+a_{nk}))$$

The numbers 1 and 2 denote the inside and outside of the k-th conductor. J_n is the Bessel function of the first kind of order n. Also,U, G, S_n, O_n, C_n and a_{nk} are the parameters to calculated by the boundary surface conditions. A special technique is used to calculate the unknown parameters in the above equations. In order to evaluate G and O_n as functions of U and S_n, the following conditions are considered : the continuity of E_z and the tangential component of the H at the k-th conductor boundary. Next, the U and S_n are evaluated by using a decomposition of the external total field magnetic H, for each configuration considered. a_{nk} is evaluated according to system geometry. Due to the space limitation, we describe briefly the procedure to calculate U and S_n without the equations. At the point c, outside the conducting domain, the total field $H_{t,k}$ with regard to coordinate system k can be decomposed into M parts (M is the number of conductor) : $H_{t,k}=H_k+H_{k+1}+H_{k+2}+.....+H_M$
where H_k, H_{k+1},... and the H_M are the field contribution of the k-th, k+1-th, ... and the M-th conductors respectively. We continue this process for all conductors. Then,

$H_{t,k+1}=H'_k+H'_{k+1}+H'_{k+2}+.....+H'_M$; $H_{t,k+2}=H''_k+H''_{k+1}+H''_{k+2}+.....+H''_M$; .....

Therefore, U and S_n can be computed by considering :

$H_k=H'_k=H''_k=H'''_k=....$; $H_{k+1}=H'_{k+1}=H''_{k+1}=...$; .....

To confirm the validity of the proposed method, we have analyzed some applications. We show here some of them. First, two identical conductors A and B, are considered to be

separated by an axial distance D. Each conductor has a radius a and carries a total current I that flows in the z direction.The current direction in conductor A is opposite that of conductor B. The internal impedance of each conductor is computed via complex power per unit length.

A) Fig.2 shows the resistance and internal inductance of the conductor by two methods. One is the present method and other is the Finite Element Method (FEM). The results are good agreement. In this case, a=1 mm., D=4 mm, and the conductivity of the conductor is considered to be $\sigma = 5.8\ 10^7$ S/m.

B) Another comparison between FEM and the present method is given for a frequency range from 1 kHz to 1 MHz. Table I confirms the accuracy of the results calculated for high frequencies by comparison with those obtained by empirical formulae. The system geometry is the same as for previous example.

Secondly, a three identical conductors are considered (Fig.3). Table II shows a comparison between results obtained by the present method and those obtained by FEM. All results are also in good agreement. Other comparisons for different configurations will be presented in the final paper.

The results presented here indicate the validity of the method. One important application of the method is to compute the conductor system parameters over a large range of frequencies.

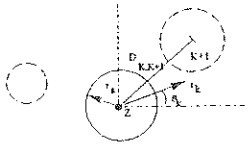

Fig.1. Investigated problem.

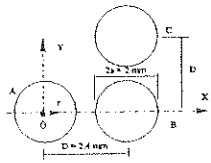

Fig.3. Configuration used of three identical conductors.

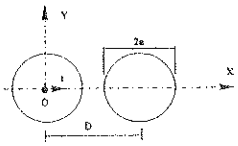

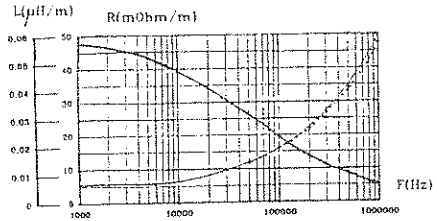

Fig.2. Comparisons of two methods for high frequencies, R and L_i are the resistance and internal inductance of the conductor. _____Present method, **** FEM

TABLE I, Comparison between empirical formulae and the present method, $X=2\pi f L_i$. R and L_i are the resistance and internal inductance of the conductor.

Frequency	F (MHz)	1	10	20	50	100
Empirical formula	R (Ω/m) 10^{-2}	5.25	16.6	23.5	37.1	52.5
Present method	R (Ω/m) 10^{-2}	5.41	16.8	23.8	37.5	53.0
Empirical formula	X (Ω/m) 10^{-2}	5.25	16.6	23.5	37.1	52.5
Present method	X (Ω/m) 10^{-2}	5.23	16.7	23.6	37.3	52.8

TABLE II, Internal impedance of conductor A near two conductors B and C.

Frequency	F (kHz)	1 10^{-3}	1	10	100	1000	5000	10000
Present method	R (Ω/m) 10^{-3}	5.49	5.53	7.9	23.2	71.3	158	223
FEM method	R (Ω/m) 10^{-3}	5.68	5.71	7.84	22.2	68.4	158	235
Present method	L (H/m) 10^{-8}	9.53	9.52	8.12	3.32	1.1	0.496	0.352
FEM method	L (H/m) 10^{-8}	9.2	9.16	7.76	3.16	1.04	0.472	0.323

Long Conduction Time Plasma Opening Switch for a New High Power Generator

A. Chuvatin, B. Etlicher, F. Douieb, V. Frolov, Ya.E. Krasik†, C. Rouillé, H. Lamain, and P. Auvray.

Laboratoire de Physique des Milieux Ionisés, Laboratoire du C.N.R.S.,
Ecole Polytechnique, 91128 Palaiseau, France
† Weizmann Institute of Science, 76100, Rehovot, Israel

A long-conduction-time Plasma Opening Switch is studied on MAG-1 and MAG-1P generators, using coaxial and strip-line geometry, (400 kA, 100 ns rise-time in the inductive load after a one-stage 0.7 μs-conduction-time POS). In this paper, we will emphasize the coupling between the two modules of MAG-1P which improve the synchronization of the load current. This concept can be used for a multi-megajoule multi-module new high power generator.
Comparison of the conduction and opening phases in the two geometry will be given. The experimental 2-D shock-like process occuring during those phases will be shown and compare with existing theories.

The authors wish to thank Dr. L. Zakatov and Dr. G. Dolgachev from RRC Kurchatov Research Center for their suggestions about the synchronization of POS and very fruitful discussions.

Work partially supported by DRET under contract #92.134 and ETCA/CEG under contract #420/115/01.

PROJECT OF A MICROWAVE AMPLIFIER BASED ON A COMPACT HIGH VOLTAGE MODULATOR

E.B. Abubakirov, M.I. Fuchs, N.F. Kovalev, N.I. Zaytsev
Institute of Applied Physics,
46, Ulyanov str., Nizhny Novgorod, RUSSIA
J-P. Brasile, G. Jean-François, M. Simon
Thomson Shorts Systèmes
9, rue des Mathurins - BP 150 - 92223 Bagneux cedex (FRANCE)

1 - ABSTRACT

This report presents a project version of microwave amplifier adapted to a high voltage compact modulator with output voltage 1 MV, current 20 kA and energy 3 kJ at pulse duration about 150 ns. Supposed outputs of the X-band amplifier are microwave power about 1 GW, gain about 40 dB, wave pattern being Gaussian beam.

2 - AMPLIFIER CONCEPT

The choice of the scheme of X-band amplifier is based on the following considerations :

a) To provide a sufficiently low energy spread in high-current electron beam, the most simple method is to use a coaxial diode with cold (field emission) cathode immersed in strong magnetic field.

b) The rectilinear electron beam determines Cherenkov type of the device, where electrons interfact with slow electromagnetic waves (or their slow harmonics)

c) To avoid the RF breakdown at high output power it is necessary to use oversized electrodynamic systems.

d) The use of oversized systems increases a risk of parasitic excitation of the amplifier. Effective way to suppress the parasitic excitation is divide the interaction space into a set of sections coupled by the common electron beam.

An effective scheme of sectioned Cherenkov amplifier is a cascade joint of a modulating backward wave and an amplifying following wave sections. Such a relativistic amplifier with output power up to 100 MW at the X-band was developped and tested experimentally at the IAP, RAS (N.I. Zaitsev et al, 4-th Symp. High-Current electronics, Tomsk, abstr., part 3, pp.26-28, 1986. A.B. Volkov et al., Pis'ma v ZhTF, vol.18 no.12, pp.6-10, 1992). The same scheme is proposed for the design under consideration.

3 - AMPLIFIER DESIGN

A power supply for the device will be the high-current modulator with output voltage up to 1.2 MV and pulse duration about 150 ns (O. Becie et al., 8th IEEE Int. Pulse Power Conf. pp. 998-100. San-Diego. 1991). Low inductance (less then 1μH) of the compact modulator provides a possibility to feed the electron injector without additional pulse formation. The amplifier is planned to be driven by hollow electron beam with particle energy 0,8 MeV and current 7 kA.

The proposed scheme of the amplifier is shown in Fig. 1.

Input microwave signal for the amplifier will be delivered by standard magnetron oscillator with central frequency 9,2 GHz and output power up to 200 kW. The quasi-optical mode converter transforms the input signal from the magnetron to the rotating mode TE_{41} of a cylindrical waveguide which is the operating mode of the backward wave amplifier (BWA).

The BWA represents backward wave oscillator operating below the self-excitation threshold. Thus the BWA will work in the regime of regenerative amplification (amplification with positive feedback) near the start regime of the operating mode.

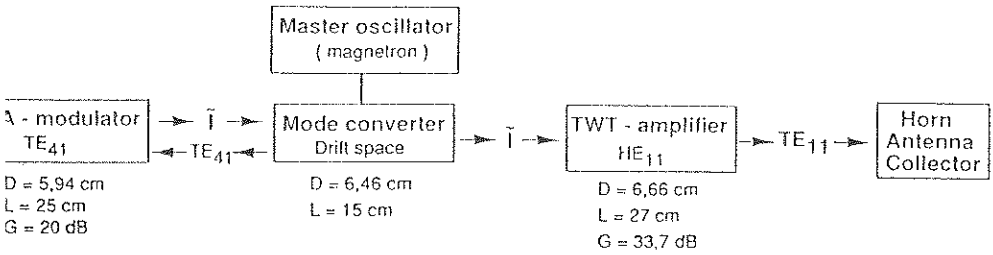

Fig. 1 - Block diagram of the amplifier project design.
D is waveguide diameter, L is effective section length, G is "linear" amplification

The regenerative regime provides efficient narrow-band modulation, which minimizes the influence of inherent noise of the electron beam. We suppose that in the working regime the stability of the high-voltage modulator will allow us to control parameters of the electron beam with accuracy sufficient to provide the amplification of the order of 20 dB in the BWA-section. The electrodynamic system of BWA based on corrugated cylindrical waveguide is chosen so that in this section modulation of the electron beam is produced as the result of synchronous interaction with a dipole space harmonic of the whispering gallery mode TE_{41}.

The electron beam modulated in the BWA undergoes additional free bunching in the drift space which length ($\sim$ 5 l) is chosen to provide effective excitation of the TWT section. TWT section operates at the slow hybrid wave HE_{11} of the cylindrical waveguide with axis-symmetrical corrugation of the sinusoidal profile. This electrodynamic system makes it possible to have amplification rate about 1 dB/cm. The output wave HE_{11} of the TWT section is transformed to the Gaussian beam in the output conic waveguide which simultaneously serves as a collector for electrons.

4 - ANALYSIS OF AMPLIFIER OPERATION

Amplifier operation was analyzed on base of solving of the equations of relativistic Cherenkov devices (NF Kovalev et al., in : Microwave relativistic electronics, issue 1, pp.76-113 ; IAP RAS, 1979). Nonlinear analysis of the described version of the amplifier shows the possibility to provide total amplification up to 45 dB with efficiency over 30 % and output power over 1 GW (Fig. 2).

This work is performed with support of "Direction des Recherches, Etudes et Techniques" (DRET, France).

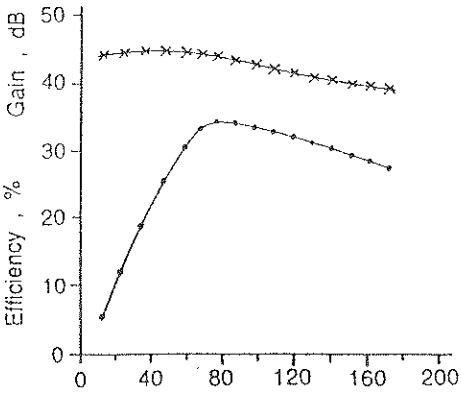

Fig. 2. - Gain ( ) and efficiency (•) of the amplifier vs input power (kW)

METHOD OF THE STRAIGHT CHANNEL ELECTRON MULTIPLIER GAIN EVALUATION

Yu.M.Saveljev*, A.Maitland

University of St Andrews, Department of Physics and Astronomy
North Haugh, St.Andrews, Fife, KY16 9SS, Scotland, UK

The continuous channel electron multiplier (CEM) is a well known device that may be used in many applications such as radiation, particle detection and image intensification. A straight CEM consists of a dielectric or semiconductive tube with a length much greater than its diameter. A voltage of a few kV is applied between the ends of the tube and may be distributed along the channel by means of a semiconducting layer on the inner surface. This layer serves also as a secondary emissive material. Primary radiation enters the negative end of the channel and produces some secondary electrons with a transverse velocity which are accelerated in the longitudinal electric field and strike the tube wall with sufficient energy to produce futher secondaries. If the secondary emission coefficient is greater than unity then electron multiplication occurs.

One of the most important questions concerning the CEM behaviour is the total channel gain G. So far there have been three main strategies to calculate G: these are numerical simulation of the multiplication process, numerical solution of the integral equations which take account of the electron energy distributions, and analytical models based on simplistic assumptions. Unfortunately, these methods tend to be very complicated and time-consuming or not reliable enough. In the present work we combine a semiempirical approach with elements from the methods involving integral equations and analytical models to produce equations which agree well with published experimental results.

In the strategy we introduce we proceed as follows. First, the gain is expressed in a monochromatic approximation. Then we use the semiempirical analytical model introduced by Manley et al (Adv.EEP, 28A, p.471, 1969) to calculate the secondary emission coefficient δ. Thirdly, we give semiempirical expressions for the exponent β that controls the shape of δ dependences. Fourthly, electron emission energies are described in terms of non-Maxwellian distributions. Finally, by introducing the notion of effective initial electron energy together with the above steps, we avoid the need to solve integral equations to obtain the CEM gain.

Simple formulae for CEM gain may be deduced by using a monochromatic approximation in a method similar to that described by Oba and Maeda (Adv.EEP, 33A, p.183, 1972). We obtain

$$G = \exp(g_0 \gamma) \tag{1}$$

where the gain parameter g_0 is

$$g_0 = \frac{4V_0}{V_d} \ln \delta \tag{2}$$

and $V_d = U / \gamma$ is a normalized voltage applied to the channel. The parameter γ is the channel length-to-diameter ratio, $\gamma = L / d$, and δ is a secondary emission coefficient.

For present purposes we use δ in a form given by Manley et al (ibid) that is convenient for fitting to experimental data. The equation we use is

$$\delta = \delta_m \left(\frac{V}{V_m} \sqrt{\cos\theta} \right)^{\beta} \exp\left\{ \alpha(1-\cos\theta) + \beta\left(1 - \frac{V}{V_m}\sqrt{\cos\theta}\right) \right\} \qquad (3)$$

where $V = V_0(1 + V_d^2 / 4V_0^2)$ is an electron collision energy, θ is the angle of incidence according to $\cos\theta = \sqrt{V_0 / V}$, δ_m is the maximum value of the secondary emission coefficient achieved at $V=V_m$, and α is a constant of the material. Parameter β in (3) controls the shape of the curve δ(V). Unlike Manley et al who used descrete values for β, we suppose β to be a smooth function on V and determine the following three approximations that allow us to match experimental data with high accuracy:

$$\begin{aligned} &\beta(V) = 0.25 + 0.35/(V/V_m + 1)^3, \\ &\beta(V) = 0.3 + 0.7/(V/V_m + 1)^3 \\ &\beta(V) = 1 - 0.65(V/V_m)^5 / [(V/V_m)^5 + 1]. \end{aligned} \qquad (4)$$

In accordance with the shapes of the δ(V) curves obtained, the β-functions may be named as "broad", "narrow" and "intermediate".

Models for secondary electron distributions of initial energy which fit experimental data are of the form

$$N(V_i) = \frac{k_0}{V_s}\left(\frac{V_i}{V_s}\right)^{n_1} \exp\left\{ -k\left(\frac{V_i}{V_s}\right)^{n_2} \right\} \qquad (5)$$

where $n_1 \approx 1.4\text{-}1.8$, $n_2 \approx 0.35$ and $V_s \approx 0.05V$. Since the distributions $N(V_i)$ are important for accurate evaluation of the gain parameter, conventionally, we must solve the integral equation

$$\int_0^{\infty} \exp\left\{ -g_r \frac{V_d}{4V_i} \right\} N(V_i)\,\delta(V_i)\,dV_i = 1 \qquad (6)$$

However, we can avoid solving (6) if we introduce the notion of effective initial energy of secondary electrons defined by $V_0(V_d) = V_a f(V_d/V_{d0})$ where V_a is an average value of $N(V_i)$ and V_{d0} is the normalized voltage at which the gain parameter is equal to zero. The function f is deduced from equation $g_r(V_d) = g_0(V_d)$ and may be approximated to any desired accuracy by polynomial functions. We note that the normalized effective initial energy V_0/V_a depends but weakly on the main secondary emissive material properties.

The effect of the secondary electron angular distribution has little effect on the channel gain and so it may be neglected in view of the uncertainties in the experimental data of the initial energy distribution. In Figure 1, experimental gain dependence (curve 4) and theoretical models at $V_m=350V$, $\delta_m=2.6$, $\alpha=0.6$ and "broad" β-function are represented. Curve 1 is calculated in the monochromatic approximation at $V_0=2.8V$. Curve 2 takes into account effective initial energy $V_0(V_d)$ and curves 3 and 5 are obtained from integral equation (6). The last curve is calculated at $\beta=1$ and is shown to

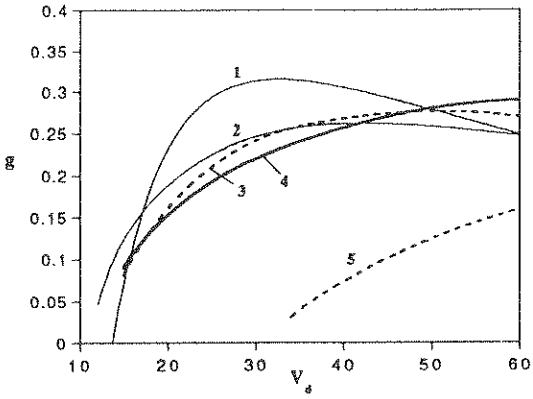

Fig.1

emphasize the importance of making a correct choice of β-function. We conclude that the monochromatic approximation with effective initial energy allows the channel gain to be determined with high accuracy (slight differences between curves 2 and 3 are due to the very simple $V_0(V_d)$ approximation used).

The suggested method may be recommended as a quite reliable and simple tool to determine the CEM gain. It may be used not only for straight channels but for curved ones too if the radius of curvature is large enough to allow electron trajectories to be similar to those in the straight channel.

THE DEVELOPEMENT OF HIGH PEAK POWER SOLID STATE PULSE GENERATORS

A.K.L. Dymoke-Bradshaw*, J.D. Hares, P.A. Kellett
Kentech Instruments Ltd. U.K.

Kentech Instruments Ltd. has been building and developing high power solid state based pulse generators for ten years. The applications were originally in high speed photography and the driving of pockels cells. Recent developements in rise time, peak power, repetition rate and channel synchronisation have lead to the developement of systems useful for Ultra Wideband and Impluse Radar applications. The modular structure and low trigger jitter of the pulse generators makes them particularly suitable for driving arrays of loads. Modules of a few tens of megawatts peak power and repetition rates to several kHz, have been constructed. Mass parallelism should be able to achieve high far-field electric fields. Such a system also lends itself well, to the possibility of adjusting the focus and of steering the radiated energy.

MECHANICAL PROPULSION FROM UNSYMMETRICAL MAGNETIC INDUCTION FIELDS

Rex L. Schlicher *
Defense Nuclear Agency
Test Directorate/RSET
1680 Texas Street SE
Kirtland AFB, NM 87117-5669

Albert W. Biggs
Electrical and Computer Engineering Dept.
The University of Alabama at Huntsville
Huntsville, AL 35899, USA
(Phone: 1-205-895-6459, Fax: 1-205-895-6803)

A means of generating mechanical propulsion from unsymmetrical magnetic induction fields is described in detail. It is an extremely low frequency (ELF) antenna excited by a pulsed high current source. The ELF antenna is a modified three dimensional multiple loop antenna designed for optimal reaction thrust instead of electromagnetic radiation.

Rigid three dimensional geometrical asymmetry is achieved with strip electrical conductors to create a partially closed space in the antenna around a central coaxial conductor. This space enclosed magnetic flux to create a flux density gradient along an axis collinear with the central conductor.

This magnetic flux density gradient creates forces from interactions from the antenna internal magnetic induction field with currents in the antenna conductors. Other forces result from pressures on electrically isolated prismatic conductor surfaces projecting into the internal magnetic field.

The latter forces contribute to pressure thrust in a partial differential equation equivalent to the Newtonian rocket thrust equation. For this propulsion, these forces are significantly greater than the radiated electromagnetic thrust forces in the first part of the

preceding paragraph. The rise time and shape of the inner current wave is critical in maximizing conversion of the internal magnetic field momentum and energy density to mechanical propulsion.

The Nonlinear Electromagnetic Propulsion System, or NEMPS, is designed with physical boundary conditions which generate an unsymmetrical magnetic flux density B when excited with source currents I. Lorentz forces F,

$$\oint F = I \times B \, dl \, ,$$

between the magnetic flux density B and the currents I in the flat strip conductors with lengths dl results in a net mechanical force on the conductors for acceleration of NEMPS.

After describing electromagnetic interactions, models of the ELF antenna array are presented. Calculations are derived for Lorentz forces on the flat conductors, with discussions and estimations of canceling forces. The net force is then found by adding individual forces.

CONCEPTION AND MODELLING OF AIRCRAFT ELECTROMAGNETIC SIMULATORS

Yves RAINGEAUD*, Jean PAILLOL, Joël ANDRIEU, Alain REINEIX, Bernard JECKO
IRCOM - URA CNRS n° 356
123, Avenue Albert Thomas
87060 LIMOGES CEDEX (France)

The increase of ground transmitters such as RADARS and other electromagnetic disturbances imposes that safety of aircrafts flying in a High Intensity Radiated Fiels should be demonstrated. The purpose of this paper is to define experiments on the ground allowing to reproduce the coupling phenomena of an electromagnetic wave form with an aircraft in flight. No direct measurement can be performed on the cables connected to sensitive systems of a flying airliner. Therefore simulators are proposed to reproduce on the ground the behaviour of the flying plane in order to recreate goods currents on the cables.

So, the analysis of the aircraft electromagnetic behaviour is achieved in three steps:

- the theoretical modelling of the coupling between an electromagnetic plane wave and a plane in flight. The current densities representative of the coupling are computed on the external surface of the plane,

- illuminated flying plane behaviour understood, three simulators able to reproduce these current densities are proposed. A theoretical simulation of the simulator with the plane on the ground is carried out and the current densities are compared with those computed in the previous step,

- as proposed means are capable to correctly reproduce the flying aircraft behaviour, they are built and experimental measurements are made.

Therefore the response of an airliner is reproduced from 10 KHz to 100 MHz with three simulators:

The injection simulator ($f \leq 10$ MHz)

A plane is placed on a metallic grid that simulates the perfectly conducting ground. In order to reproduce the coupling between an E.M. wave and the plane, an injection current device is designed. Two injection points are needed to reproduce all families of resonance observed when the plane is illuminated : one at the end of the wing and the other at the end of the fuselage. (A coaxial cable joints the grid and the connection region between the fuselage and wings). Note a very good agreement between theoretical an experimental results.

Two illumination simulators (10 MHz $\leq f \leq 100$ MHz)

- a resonant antenna in the bandwidth [20 MHz - 100 MHz] which is a log periodic antenna. The position of this simulator can easily be changed in order to illuminate wings or body of the plane.

- a progressive wave aerial, with novel design suitable for the bandwidth [1 MHz - 30 MHz]. The frequency bandwidth is chosen in order to compare results with other simulators in the lower and the upper part of the spectrum.

Theoretical simulation and a comparison with experimental results has shown a good agreement (figure 1).

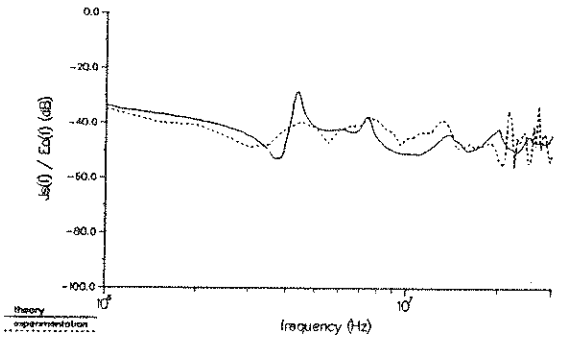

Results on a wing point

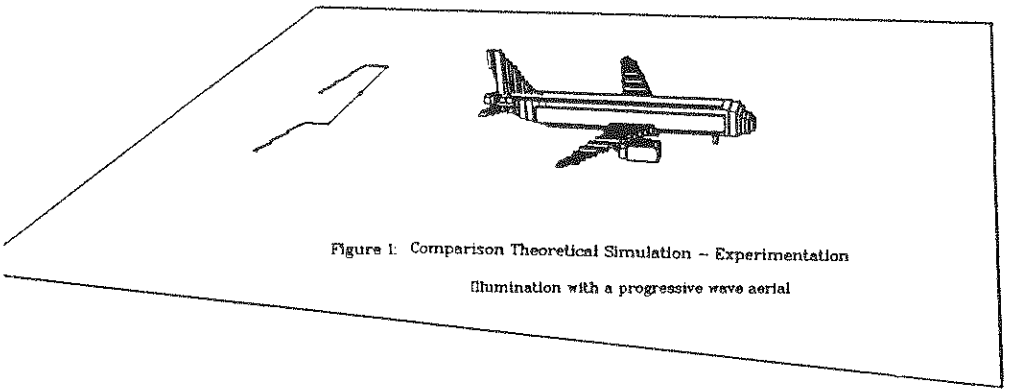

Figure 1: Comparison Theoretical Simulation – Experimentation

Illumination with a progressive wave aerial

The experiment has been made in Toulouse (France) by "Aerospatiale" and this work has been supported by "Aerospatiale", the "Direction Générale - Aviation Civile" (D.G.A.C.) and the Service Technique des Télécommunications et des Equipements Aéronautiques" (S.T.T.E.). The theoretical analysis has been carried out at the "Institut de Recherche en Communications Optiques et Microondes" (Limoges - France).

COMPARISONS OF THE LOW LEVEL CW ELLIPTICUS AND HIGH LEVEL PULSE HPD CURRENTS ON THE EMPTAC AIRCRAFT

D. Lawry, W.D. Prather, R. Torres and T. Tran
Phillips Laboratory, WSR
S. Langdon, S. Gutierrez and W. Walton
Phillips Laboratory, WSM
Kirtland AFB, NM
S. Kokorowski, J. Martinez and D.P. McLemore*
Kaman Sciences Corporation, Dikewood Division
Albuquerque, NM and Santa Monica, CA

The Phillips laboratory has recently designed and constructed a CW, low-level simulator (ELLIPTICUS) for use in determining coupling of electromagnetic energy to aerospace systems.(D. McLemore, J. Martinez, G. Sower, C. Baum, T. Tran, and W. Prather, "The Phillips Laboratory Broadband, High Frequency CW Simulator," National Radio Science Meeting, Boulder, CO, 1993). This antenna is designed to make the field patterns similar to those produced at the high level pulse simulator, HPD.

A diagram of the ELLIPTICUS antenna is shown in Figure 1. The simulator is constructed of two solid jacketed coaxial cables which are joined at the top of the antenna with a balun. The inside conducting surfaces of one of the coaxial cables acts as a feed to the balun, and currents from the output of the balun are delivered to the outside of the outer conductors of the coaxial cables. These currents are responsible for the fields created by the simulator.

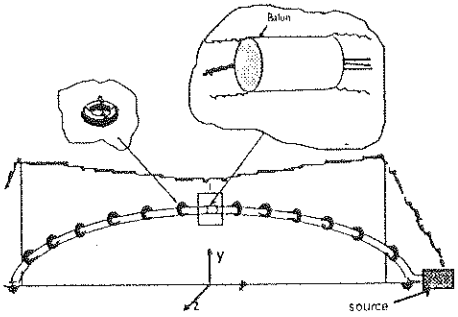

Figure 1. The ELLIPTICUS Simulator

This simulator was intentionally crafted to make the field patterns for this antenna much like those of the HPD simulator. Because the high level pulse simulator, HPD, has a resistive loading to control the low frequency ratio of the Electric-to-Magnetic field amplitudes, a method to achieve this criteria for the ELLIPTICUS antenna was also needed. In order to accomplish this, ferrite beads made of material number 77 were used. Figure 2 shows the real and imaginary loading presented by one of these beads to a current passing through it.. As can be seen in the figure, the impedance of a single bead is both resistive and reactive.

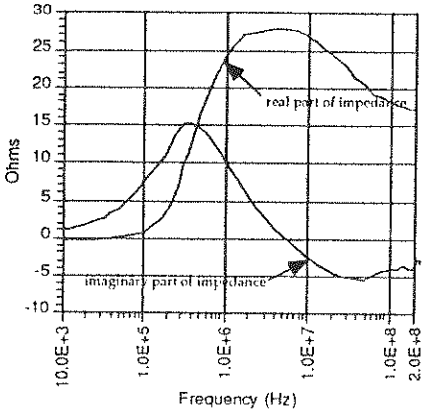

Figure 2. The Loading Characteristics of a Ferrite Bead with no Resistors

In order to achieve a resistive loading over the frequency range in which radiation resistance does not dominate losses in the antenna, resistors were used with the ferrite beads. By combining in parallel to the bead impedance a resistor whose resistance is far less than the impedance of the ferrite, the dominant impedance of the combination will be that of the resistor. Extending this notion to many resistors in parallel to the ferrite impedance (reducing the inductance of the resistor wires), four, forty ohm resistors wrapped symmetrically around each bead offered a predominantly resistive load (6-7 ohms) to the antenna over the frequency range of interest (100 kHz to approximately 200 MHz). This is illustrated in figures 3 and 4. The Ellipticus antenna was outfitted with these beads-plus-resistors with a density per unit length to match the HPD resistive loading.

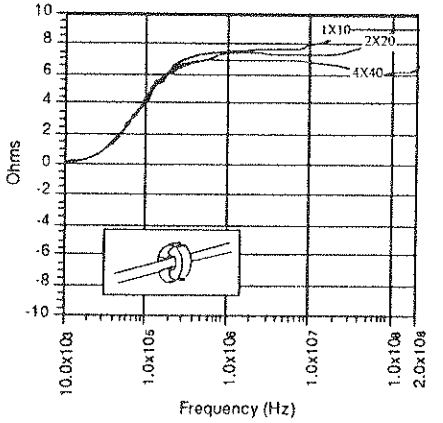

Figure 3. The Real Part of the Loading of a Ferrite Bead with Resistors Symmetrically Wrapped on the Bead

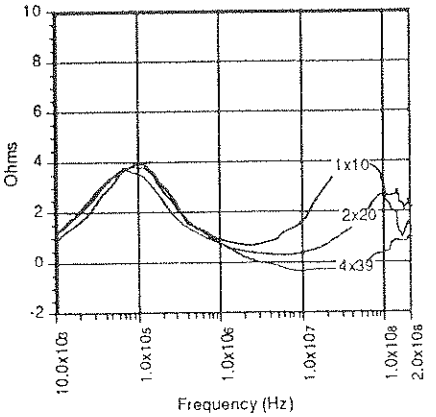

Figure 4. The Imaginary Part of the Loading of a Ferrite Bead with Resistors Symmetrically Wrapped on the Bead

The HPD antenna with the HAG I pulser, at Kirtland AFB, was used to obtain the high level pulse responses on the EMPTAC aircraft. Although this simulator was capable of producing energy above the noise level up to well above 100 MHz; however, the high frequency fiber optic system dynamic range effectively limited the measurement bandwidth to 100 MHz.

Figure 5 shows the excellent frequency domain comparisons of the measured and CW predicted responses of test point 2142, a relatively well shielded bulk current measurement in the midsection of the aircraft.

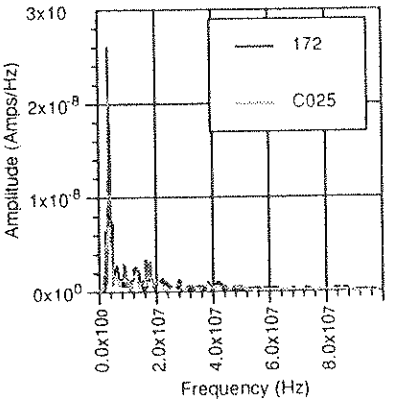

Figure 5. A Frequency Comparison of the Ellipticus Prediction (C025) and HPD (172) Responses for EMPTAC

Frequency conversion microwave / VHF associated to the formation of a plasma

*JL. VAGNEUR * / M. SIMON ** / G. LABAUNE **

Coupling phenomena between electromagnetic waves and aircraft harness are well understood when the signals are in the VHF-UHF range (cases of NEMP - lightning ...).

In the range of microwaves, these coupling phenomena are poorly described in the open literature.

It is well known that, in some cases, damages can occur in equipments implemented in structures when these structures are illuminated by high power microwaves. We can assume two ways for the energy penetration in the equipments. The first one is a direct penetration in this case, only the radiated modes have to be taken into account because the conducted ones can't propagate on the harness.

The second one uses a frequency conversion of the energy linked with the plasma formation in holes or slots in which the electric field becomes higher than the breakdown threshold. In this case the spectral content of the energy is typically bounded within one gigahertz.

In this paper, we shall estimate the characteristic values associated to the second mechanism :

- electromagnetic fields radiated by the plasma formation,
- currents and voltages induced in the equipments by the previous electromagnetic field.

Experimental and calculated results will be presented as well as derived characteristic values.

* Thomson-CSF/RCM
** Thomson-CSF/DSE

DEVELOPMENT OF AN EMBEDDED TERMINAL PROTECTION DEVICE (TPD) TESTER

Lothar O. Hoeft* and Thomas M. Salas
BDM Federal, Inc.
1801 Randolph Rd., S. E.
Albuquerque, NM 87106
Voice: (505) 848-5399 Fax: (505) 8484029

William D. Prather
Phillips Laboratory (WSR)
3550 Aberdeen Ave., S. E.
Kirtland AFB, NM 87117
Voice: (505) 846-0416 Fax: (505) 846-0417

Many modern aircraft use Terminal Protection Devices (TPDs) installed or embedded in the Line Replaceable Units (LRUs) that they are meant to protect. The electrical characteristics of these devices must be periodically measured to ensure that the system's electromagnetic hardness is being maintained. Embedded TPDs are more difficult to characterize than external TPDs since input/output or transfer function measurements are not possible. Furthermore, circuits that are supposed to be protected by the TPD could be damaged if the TPD is no longer functional and some of the usual test methods, such as measuring clamp voltages with constant current sources or high level pulses, are used.

A technique for characterizing embedded TPDs in-situ has been developed that is quick, effective and safe. This technique injects a fast (few tens of nanoseconds) rise time trapezoidal pulse of moderate duration (a few hundred nanoseconds for most interface circuits) into the LRU at the connector. The voltage is measured as close to the connector as possible so that the measured voltage is the algebraic sum of the injected, or incident, and reflected pulses. For non-linear voltage clamp TPDs, the voltage near the end of the measured pulse is the clamp voltage. The measured voltage is related to the reflection coefficient and the amplitude of the injected pulse. Therefore, the input capacitance and/or inductance of linear TPDs can also be measured.

Measurements on a wide range of TPDs installed in a simulated LRU showed that the technique was capable of characterizing both embedded voltage clamp and linear filter TPDs. These measurements showed that the clamp voltage could be measured if appropriate pulse characteristics were used. In particular, the pulse duration must extend beyond the response time of the reactance of the TPD, wiring, and associated circuitry in order for their effects to be disregarded. The initial effort was extended and refined by using a test set-up that was representative of that which could be used in an automated tester and demonstrated the technique on a real LRU.

Embedded terminal protection devices in an Alarm Control LRU were measured using the high voltage pulse test technique or TPD Tester. A preliminary circuit analysis of the protected circuits determines the test parameters that are best suited for measuring the TPDs. The pulse duration, amplitude, and rise time need to be specified before the test can be safely performed by an automated or semi-automated system.

The importance of choosing the appropriate parameters was demonstrated by the analyses and measurements performed on the two different types of circuits in the same LRU; a signal interface circuit and a power supply circuit All circuits have effective shunt capacitance to ground and require a finite time interval to charge before the Zener voltage is reached. This implies that the pulse must be longer than a few RC time constants or cable transit times and that the voltage be measured during the later part of the pulse. The calculated RC time constant for the signal interface circuit was on the order of 50 ns; therefore, a pulse width between 100 ns and 250 ns was used. In contrast, the power supply circuit had a large capacitor to ground in series with a large inductor. For times less than the L/R (inductor/source impedance) time constant, the inductor isolates the Zener diode from the large capacitor. Therefore, the pulse must be less than the L/R time constant, or 200 ns. This was confirmed by the laboratory measurements. Even though a pulse width of 450 ns was used, only the first 200 ns were meaningful for a test pulse whose open circuit voltage was about twice the clamping voltage of the protection device.

Using an open circuit voltage level that is about twice the Zener voltage, only one pulse is necessary to test the functionality of the diode and measure its clamping voltage. If the measured voltage far exceeds the expected clamp voltage, then it may be an indication of a failed protection device and the LRU should be tagged for a complete and thorough examination. The use of a single short pulse minimizes the possibility of damage to the circuit. By understanding the circuit behavior before the TPD Tester is applied, the test parameters can be determined that will ensure credible measurements. The parameters should be verified through laboratory experiments before they are put into practice, but once they have been established, there should be no need to repeat this step again.

The laboratory demonstration used the same basic hardware elements as the proposed TPD Tester. That is to say, the equipment used in the laboratory has features that are essential for an automated or semi-automated TPD Tester. A square pulse generator was used which has an adjustable output voltage and pulse width. It was seen that a pulse generator with a 50 ohm output impedance reduces unwanted reflections, thereby simplifying the measurement task. The pulse generator fed into an interface box which contained a circuit switch to apply and measure the test pulse to various pins on the LRU. The inductance of the switch and the short lead lengths are negligible when the appropriate rise times and pulse widths are chosen. An oscilloscope and a digitizing camera system were used for the voltage measurement system in the demonstration. A test port was provided by the interface box to keep the measurement close to the circuit pin on the LRU. An automated system would have a triggered sample and hold circuit built-in with data transfer capabilities or a display to inform the operator of the results. The only element that was missing in the laboratory demonstration was the logic performing hardware and software to provide a pass or fail indication of the test results. By integrating these elements into one unit, it is possible to devise a TPD Tester small enough to be used in flight-line maintenance activities.

SUBJECT CATEGORY : AUTOMATIC TEST BENCH FOR HARDENED AIRCRAFT TERMINAL PROTECTION DEVICES

**Y. Gallety - J.L. Lair - J.C. Remaud*
ROCKWELL INTERNATIONAL
ROCKWELL-COLLINS FRANCE
6, Avenue Didier Daurat
Parc Industriel Aéroportuaire - B.P. 8
31701 Blagnac Cedex, FRANCE
Téléphone (33) 61-71-77-00 Fax (33) 61-71-51-69

The surveillance and checking of the aircraft hardness need several test equipment. A product line of such testers has been developed to measure periodically the parameters of the Terminal Protection Devices (TPDs) installed in Terminal Protection Module (TPMs). These test benches are used to measure the following parameters for each TPM :

Transfer curve
Serial resistance
Leakage current
Capacity
Inductance
Firing voltage for the non linear devices

This paper describes two applications :

- The TBNH-160F (Test Bench for Nuclear Hardening) which is in operation in the Astarte Program for the french Air Force to test the TPDs of the C-160 aircraft.

- The TBNH-6F which is in operation in the TACAMO Program for the US Navy to test the TPDs of the E-6A aircraft.

The measurements performed with these test benches are used to check the performances of the TPDs but also to analyse the trend of the TPDs quality over time. This analysis is used to improve the periodicity of the preventive maintenance of the aircraft.

ELECTROMAGNETIC SCATTERING FROM CONTINUOUS AND INHOMOGENEOUS CYLINDERS AT OBLIQUE INCIDENCE (Application to Wake Echo Radar Cross Section)

* Magali. JEAN
Société MOTHESIM

Christian TESSIERAS
C.E.A.-C.E.S.T.A

The turbulent part of reentry vehicule wake can be approximated by an infinite cylinder with radially variable permittivity. Further more this caracteristic is a random variable in space. We split it in the mean value and the fluctuating part :

$$\varepsilon(\rho) = \langle \varepsilon(\rho) \rangle + \varepsilon_f(\rho).$$

The incident wave is assumed to be a plane wave with oblique incidence in relation to the cylinder axis.

The topic of the presentation is the field diffracted by the mean medium. Its permittivity is less than the permittivity of the vacuum.The permittivity profiles have the following form :

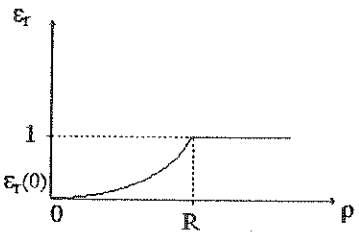

where $\varepsilon_r(0) = \left(1 - \frac{\omega_p^2}{\omega^2 + \nu_c^2}\right) - j * \left(\frac{\omega_p^2 \, \nu_c}{\omega^2 + \nu_c^2}\right)$

$\omega_p = 3.18 \ 10^9$ Ne : plasma frequency,

$N_e = 10^9$ cm^{-3} : electron density,

$\nu_c = 10^8$Hz : collision frequency,

$\omega = 2\pi f$ with f : frequency.

R : cylinder radius.

We consider the mean medium as a multilayer cylinder. We are thus able to use the potential theory. This approch leads for each layer to a Helmholtz equation in terms of electrical (G), and magnetical (F) axial vector potentials. (R.F HARRINGTON Time-Harmonic Electromagnetic Fields, Mac Graw-Hill).

Using the method of separation of variables, the potentials and in consequence the fields can be written in the following form :

$$U(\rho,\varphi,z) = \int_{-\infty}^{+\infty} \sum_{m=-\infty}^{+\infty} U^m(k_z,\rho)\ e^{jm\varphi} e^{jk_z z}\, dk_z$$

The modal coefficients E^m and H^m are easily obtained in solving an ordinary differential equation in ρ by a method of Finite Difference. It's better to solve in terms of fields. It avoids us indeed to impose at each interface the continuity of field tangential components. Moreover we have thus to solve only a 4x4 linear system instead of a (2KC+2)x(2KC+2) system with KC the number of layers. So it remains to take into account the boundary conditions. Those conditions are imposed on the potential coefficients which are constant in an homogeneous area. At infinity, the steady-state component of the total wave is equal to the incident wave, and on the cylinder axis, the fields are finite.

The diffracted field is derived from the asymptotic form of the potentials. We deduce then the mean scattering width.

$$\sigma = 2\pi \lim_{r\to+\infty} r \frac{\left|\mathbf{E}^d.\,\mathbf{E}^i\right|^2}{\left|\mathbf{E}^i\right|^2}$$

Some validations have been established through comparisons with the code SHFC2D of the CEA-CELV (R. LEMARTRET, B. STUPFEL). This code is based on a coupled formulation : Finite Elements and Integral Equation.
A typical result for the case of an homogene cylinder is :

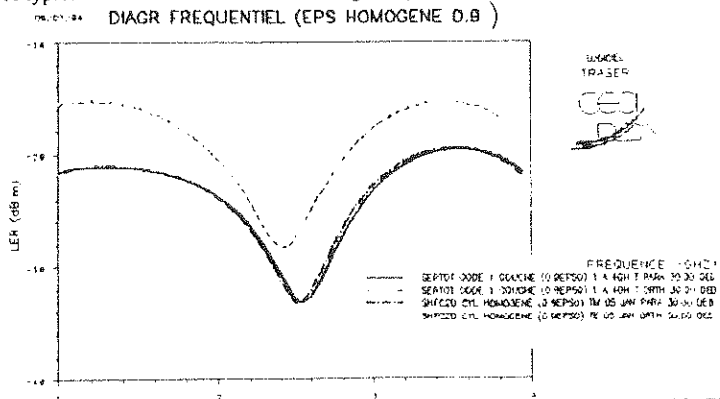

Our main goal is to determine the mean value of the wake echo RCS. The method utilised is the Born approximation. The source equivalent to wake fluctuations will be expressed in terms of the near field, we obtained above.

SCATTERING BY AN INFINITE WEDGE

* CANTON Aymeric
CEA-CESTA
PUJOLS Agnès
MOTHESIM
VERMERSCH Sébastien
CEA-CESTA

As yet, no exact solution has been found for diffraction by an arbitrary wedge. In fact, only some particular wedges had been already treated:

- wedges with a circular rounded edge,
- wedges with a sharp edge.

That's why we develop an hybrid method to compute the diffraction by wedges with arbitrary edges, whatever the frequency and the incidence are.

The chosen method is a combination of integral equations and Physical Optics: the integral equations calculate the currents created by the incident wave at the top of the wedge Γ_0 while we impose the current given by the Physical Optics on the semi-infinite planes Γ_∞.

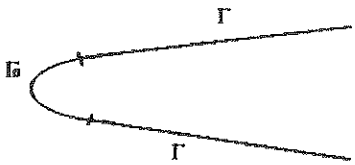

The beginning point is the Stratton-Chu integral representation of the scattered field in terms of $\vec{j}$ the electric current and $\vec{m}$ the magnetic current defined on the boundary $\Gamma = \Gamma_0 \cup \Gamma_\infty$ by the relations:

$\vec{j} = \vec{n} \wedge \eta_0 \vec{h}$, $\vec{m} = -\vec{n} \wedge \vec{e}$

with $\vec{n}$ the outward normal of the wedge and η_0 the free-space impedance.
Then we write the boundary conditions on the Stratton-Chu integrals :

$$\vec{m} = -Z\vec{n} \wedge \vec{j}$$

where Z is the surface impedance; we recognize the perfectly conducting condition for Z=0.
The current of the Physical Optics is imposed on Γ_∞:

$$\vec{j} = \begin{cases} \vec{j}(x,y) \text{ si } (x,y) \in \Gamma_0 \\ \vec{j}^{op}(x,y) \text{ si } (x,y) \in \Gamma_\infty \end{cases}$$

We construct a variational formulation by taking the inner product of the obtained integral equation with a testing current defined on Γ_0 and by enforcing the conditions of continuity:

$$\vec{j}.\vec{t} = \vec{j}^{op}.\vec{t} \text{ sur } \partial\Gamma_0$$
$$Z\vec{n} \wedge \vec{j}.\vec{t} = Z\vec{n} \wedge \vec{j}^{op}.\vec{t} \text{ sur } \partial\Gamma_0$$

The variational problem is solved by a finite element method. We lay on the code of integral method SHF2D developped by P. Bonnemason and B. Stupfel in the research center of Limeil-Valenton. We add to their formulation the integral terms containing the Physical Optics.
The implementation of this hybrid method consists on putting these additional terms which are integrals of the form:

$$\int_{\Gamma_\infty} \vec{j}^{op}.\text{grad}\Phi \, dl \quad \text{et} \quad \int_{\Gamma_\infty} \vec{j}^{op}.\Phi \, dl$$

with the Green function in the two dimension :

$$\Phi(\vec{\rho}-\vec{\rho}') = -\frac{1}{4i} H_0^2\left(k(\vec{\rho}-\vec{\rho}')\right)$$

To calculate these integrals,we distinguish two areas of Γ_∞:

- an area Γ_∞ on which the product k*p is enough large such that we can take the asymptotic approximation of the Hankel functions and evaluate these integrals by the method of the stationnary phase.
- a intermediate area Γ_1 beetween Γ_∞ and Γ_0 on which the integrals are numerically computed by the Gauss technical.

The results of the hybrid method are compared to the results avalaible in the literature.

CHANGING OF PROPERTIES OF MATERIALS AFTER HIGH POWER MICROWAVE IRRADIATION.

A.N.Didenko.
Russian Academy of Science, 117334,
Moscow, Russia

The exploration of new and unique concepts for high-power icrowave generation (HPM) with the pulse power about several igawatts has progressed rapidly in recent years.

Electromagnetic waves of high strength may produse various hermal and deformation processes. It was shown that properties f materials can change during irradiation by HPM. For exemple ıe conductivity of materials during HPM-interaction differes from that before and after irradiation. It is pessible that unter ıfluense of HPM metal acquires the properties of dielectric. It ıkes place when magnetic component of HPM is so high that Larmor ıdius is less not only than depth of skin-layer, but also less ıan electron free path. In that case reflection of HPM from ·tal becomes sufficiently less and major part of HPM is absorbed · metal.

There is good agreement between theoretical and experimental sults.

High-power microwaves may be of sufficient interest for rious technological purposes. Pulse character of interaction fluences processes in materials. This espesially takes place en HPM interacts with the system of two or more layers terials with different physics-chemical properties. The culiarities of HPM interaction with materials was investigated r dielectric or low- conducting layers (e.g. rust) on surface such metals as Cu, Al and Fe. It was shown that optimum ration of pulse varies from one to a few tens nanoseconds. mination of dielectric layers from metals, surface cleaning-off ı change of metals mechanical properties occur when density of microwave energy is equal to 0,15-0,4 J/cm2.

EMP Response of Conductor Structures in Ionospheric Plasma

Jean-Jacques Laurin* and Dominique Dubouil
Department of Electrical and Computer Engineering
École Polytechnique de Montréal, P.O. Box 6079, Station Centre-Ville
Montreal, Quebec, Canada, H3C 3A7

I. Introduction

For conductor structures mounted on spacecrafts in low-earth orbit, the transient response to EMP waves can be significantly different than in free space due to the finite free-electron density present in the ionosphere. Cylinders immersed in a magnetized plasma support a surface wave mode (Y. MUSHIAKE, Radio Science, 69D(4), 503-510, 1964) having an upper cutoff frequency equal to the electron cyclotron frequency (f_c). If there is an ion sheath covering the cylinder, the surface waves, so-called sheath waves, can propagate up to $f_{uh}/\sqrt{2}$, or to $f_p/\sqrt{2}$ when there is no magnetic field ($f_{uh} = \sqrt{f_p^2 + f_c^2}$, f_p = plasma frequency) (J.-J. LAURIN et al. Radio Science, 24(3), 289-300, 1989). Well below the cutoff frequency, the sheath waves can be weakly attenuated. Therefore, a transient disturbance could possibly excite long-duration sheath-wave travelling pulses on cylinders. In this paper, we will examine this conjecture by simulating the effect of an EMP event incident on a sheathed cylinder in ionospheric plasma.

II. Model and Simulation

The antenna model is a symmetric linear dipole with passive load (linear or nonlinear) at its terminals. The incident EMP wave's electric field is parallel to the dipole. In order to simplify the analysis, and to focus as much as possible on the EMP-sheath-wave interaction, we have considered a zero-temperature isotropic plasma and a vacuum sheath. The waveform of the applied transient is the same as a typical EMP waveform measured on the ground but with a peak amplitude of 1 V/m. Finally, a linear behavior is assumed for the sheath-plasma system.

Following the time-stepping procedure of Liu and Tesche (IEEE Trans.

AP-24(2), 131-139, 1976), the current i_L in the load at time $t = n\Delta t$ is given by:

$$i_L(t) = i_{sc}^{EMP}(t) + \sum_{i=0}^{n-1} y_{in}(t - i\Delta t)\, v_L(i\Delta t)\, \Delta t + y_{in}(0)\, v_L(t)\, \Delta t$$

where $i_{sc}^{EMP}(t)$ is the current at the short-circuited antenna terminals exposed to the EMP wave and $y_{in}(t)$ is the current response to an impulse voltage generator feeding the unloaded antenna. The load voltage v_L is related to i_L through the load characteristic. Impulse responses $y_{in}(t)$ and $i_{sc}(t)$ are the inverse Fourier transforms of $Y_{in}(f)$ and $I_{sc}(f)$ calculated in the frequency domain with the Richmond-Tilston moment method program (M.A. TILSTON & K.G. BALMAIN, IEEE Trans. AP-38(10), 1636-44, 1990). Convolution of $i_{sc}(t)$ with the EMP waveform is the necessary to obtain $i_{sc}^{EMP}(t)$. In the moment-method calculation, we used a cylinder radius of 5.5 cm, a sheath thickness of 1.8 cm (5 Debye lengths), and a length of 16 m broken into 64 segments for the dipole.

III. Results

The center-current response to the EMP under various load conditions with and without the plasma were simulated. Results for the zero-impedance load are shown in Figure 1. Without plasma, rapid oscillations decay within 1 μs due to radiation losses. For the cylinder in plasma, these rapid oscillations decay at about the same rate but slower oscillations continue for a much longer time (up to 200 μs according to other results). These slow oscillations contain a superposition of the frequencies corresponding to the sheath-wave resonances of the dipole. Since sheath wave oscillations have a very slow decay, they could be more susceptible to affect the EMI immunity of spacecrafts in the ionosphere.

FIGURE 1: Z(load)= 0

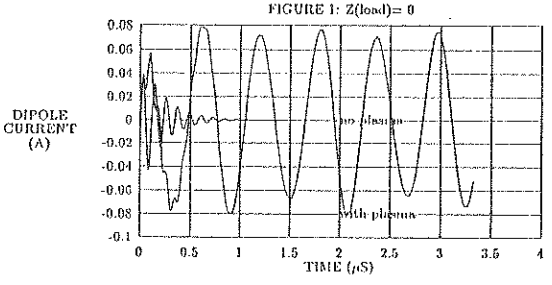

THE EFFECTIVE METHOD USED FOR THE ANALYSIS OF THE FAST TRANSITION EMP COUPLING TO THE CONDUCTING SCREENING ENVELOPES

Loudmila V.Vavriv*, Andrey E.Serebryannikov
Molniya Research and Engineering Institute ,Kharkov, Ukraine
Nicolai P. Zhuk
Kharkov State University, Kharkov, Ukraine

The subject of investigation was the mechanism of electromagnetic noises' penetration through the apertures, cable inputs, technological irregularities of screening envelopes of aerospace engineering. Along with the diffusion through the walls this mechanism is considered to be the main one in the case of such noises as fast transition LEMP and NEMP (IEEE Trans.Vol.EMC-30,1,1989,p.46-52). It was assumed that the dimensions of the irregularities were small in comparison with the effective wavelength of the noise. Then the envelope is considered to be a regular one at the first stage of calculations. For the estimation of the internal elec tromagnetic situation (EMS) we shall use the method of small perturbations. Thus the problem is reduced to simpler where the EMP scattering on the 3D envelope can be estimated. Since the most rigid requirements are referred to the "start conditions" we shall consider that the object is located near the Earth surface. The case has been considered in detail, when the object is approximated by the model of thin perfectly conducting cylinder. The problem was solved taking into consideration the influence of the Earth ionosphere. Both the ionosphere and Earth surface are simulated by the perfectly reflecting surface parallel to the Earth.

In the thin-wire approximation the problem is reduced to the solution of integral equation relative to the spectral components of the induced current. The analytic solution of the equation is obtained by the method of sequential approximations. The compact formulae for the natural waves' amplitudes have been suggested. In application to the symmetric and antisymmetric current components the direct formulae for the resonant frequencies and for the object lengths embracing the resonances both of the lower and of the higher types have been determined. The calculations' results of the currents induced on the objects were compared with the results for the case of pulses scattering on the object located in the free space when ionosphere was taken into account. As a result, the dimensions of the object and the lightning pulse parameters under which the influence of the ionosphere can be significant have been determined. The influence of ionosphere leads not only to the noticeable change of maximum value of currents induced on the object but also to the noticeable change of the shape of induced current in space and time as well as to the redistribution of electromagnetic field. If the distribution of currents on the regular envelope is known it is very easy to determine EMS inside the envelope through the solution of an excitation problem (G.T.Markov, A.F.Chaplin Electromagnetic waves' excitation, Moscow,1967). Let us note that resonance character of amplitude-frequency response of induced currents makes the use of FFT for the transform to the time domain very effective.

KMP ELECTRONICS

SPÉCIALISTE DES ÉQUIPEMENTS D'ÉMISSION DE PUISSANCE ET RÉCEPTION POUR LA COMPATIBILITÉ ÉLECTROMAGNÉTIQUE ET LES TESTS DE SUSCEPTIBILITÉ

Amplificateurs de puissance MOS-FET

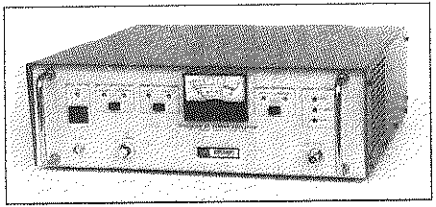

Large bande :
10 KHz à 1 GHz
Forte puissance :
1 Kwatt et plus
selon la bande - Interface IEEE, contrôle à distance
Selon norme IEC Pub 801-3 et 6.

Antennes d'émission/ réception

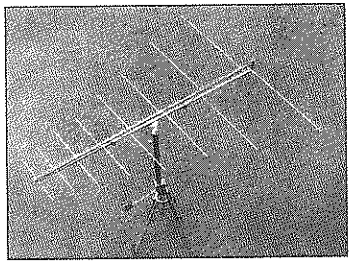

Log-périodiques,
log-spirales, biconiques,
dipoles, boucles, cornets.

Instrumentations IEM/IRF/TEMPEST

Récepteurs de détection
Tempest - Applications
toutes normes.

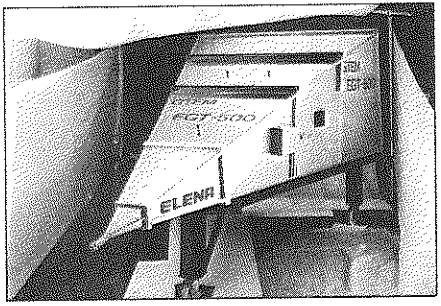

Cellules TEM et GTEM

8 modèles TEM,
DC à 1 GHz
300 watts
de puissance
admissible,
3 modèles GTEM,
DC à 2 GHz
100 à 1000 watts
de puissance admissible - 16 Kvolts pulse.

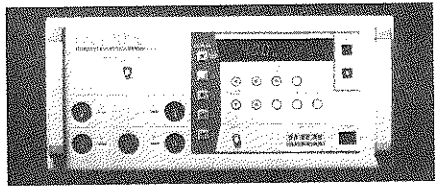

Générateurs de décharges électrostatiques

0,2 à 30 Kvolts,
temps de montée
0,7 à 1 nsec.

Générateurs de bursts rapides

250 à 4500 volts, cycle 2,5 - 5 et 10 KHz.

Simulateurs de perturbations IEM

Selon norme IEC Pub 801-5.

BP 64 - 9, allée Beausoleil - 92145 Clamart Cedex - Tél. : (1) 46 45 09 45 - Fax : (1) 46 45 24 03

ANALYSIS OF ELECTROMAGNETIC SCATTERING FROM FINITE COMPOSITE STRUCTURES

Tapan K. Sarkar*
Department of Electrical and Computer Engineering
Syracuse University
Syracuse, New York 13244-1240, USA
e-mail: TKSARKAR @ RODAN.SYR.EDU

Sadasiva M. Rao
Department of Electrical Engineering
Auburn University, Auburn, Alabama 36849, USA

ABSTRACT

An integral equation technique is presented for the analysis of arbitrary shaped composite conducting and dielectric structures in the frequency domain. In this paper the surface/surface formulation is presented for the analysis of printed circuit antennas and radiation from linear taper slot antennas on finite substrates. Scattering from finite composite structure is also presented.

In the surface/surface formulation, all the finite conducting structures are replaced by surface equivalent electric currents $\mathbf{J}_c$ located and radiating in free space as required by the equivalence principle. All dielectric structures are replaced by equivalent surface electric and magnetic currents. However, the equivalence principle needs to be enforced both for the external region to the dielectric and in the internal region. By the application of the equivalence principle, the material body is encapsulated by two surface electric and magnetic currents of equal magnitude and opposite in direction. So that the original problem is not changed. One of the current sources is located on S_d^+ and the other on S_d^-, where S_d is the dielectric surface. The magnitude of the unknown currents are related to the

$$\mathbf{J}_d = \hat{n} \times \mathbf{H}_{tan} \tag{1}$$

$$\mathbf{M}_d = \mathbf{E}_{tan} \times \hat{n} \tag{2}$$

The magnitude of the unknown currents are related to the total tangential components of the electric and magnetic fields at the material interface and $\hat{n}$ is the direction of the outward normal. The original

problem is now split into two parts, the external equivalence and the internal equivalence. For the external equivalence due to (2.1) & (2.2), the fields internal to S_d^+ should be zero as the surface currents $\mathbf{J}_d$ and $\mathbf{M}_d$ take care of the discontinuities in the tangential components of the fields. Since the fields internal to S_d^+ is zero, the dielectric material can be removed and is replaced by free space without changing the external field equivalence. $\mathbf{J}_d$ and $\mathbf{M}_d$ are now located in free space and the fields radiated by them can easily be calculated by the free space Green's functions. For the internal equivalence, since, fields external to S_d^- is zero due to the presence of the surface currents - $\mathbf{J}_d$ and - $\mathbf{M}_d$, the exterior region can be replaced by the same materials of the interior region and therefore - $\mathbf{J}_d$ and - $\mathbf{M}_d$ radiate in a homogeneous region and produce the proper internal fields. The completeness of this representation is guaranteed by the uniqueness theorem.

If instead of the dielectric region, we have a conductor, then we apply the same principle as before, and in addition, recognize the facts that the fields interior to a conducting region is zero and the total tangential component of the electric field on a conductor surface is zero. Hence for conductors only the external equivalence exist. Moreover since $\mathbf{E}_{tan}$ is zero on S_c^+, there is no need to put a magnetic current as the electric current is sufficient to represent the external fields. Therefore, by the terms of the external equivalence,

$$\mathbf{E}^{inc} + E^{sc}_{ext}(J_c, J_d, M_d) = E^{sc}_{int}(-J_d, -M_d) \quad on \quad S_d \tag{3}$$

$$\mathbf{H}^{inc} + H^{sc}_{ext}(J_c, J_d, M_d) = H^{sc}_{int}(-J_d, -M_d) \quad on \quad S_d \tag{4}$$

$$\mathbf{E}^{inc} + E^{sc}(J_c, J_d, M_d) = 0 \quad on \quad S_c \tag{5}$$

Next the method of moments is applied to discretize the unknowns $\mathbf{J}_c$, $\mathbf{J}_d$ and $\mathbf{M}_d$. The triangular basis functions are chosen as they can represent any arbitrary surface. The details are available in (T. K. SARKAR, S. M. RAO & A. R. DJORDJEVIC, IEEE Trans. on MTT, Nov. 1990, Vol. 38, pp. 1568-1575) and application to radiation/scattering from a bent-dipole on a finite slab is compared with experimental data in (S. M. RAO, T. K. SARKAR, P. MIDYA & A. R. DJORDJEVIC, IEEE Trans. AP, pp. 1034-1038, July 1991).

NL-FDTD MODELING OF LINEAR AND NONLINEAR GRATING-ASSISTED COUPLERS

Richard W. Ziolkowski † *and Justin B. Judkins*

Electromagnetics Laboratory
Department of Electrical and Computer Engineering
The University of Arizona
Tucson, AZ 85721 USA
(602) 621-6173 (office) (602) 621-8076 (fax)
ziolkowski@ece.arizona.edu

Finite-length corrugated waveguide output couplers constructed from a dispersive (Lorentz), nonlinear (Raman and instantaneous) material are characterized for multiple-cycle and single-cycle, ultra-short optical pulses using a multi-dimensional, nonlinear finite difference time domain simulator.

With the continuing and heightened interest in linear and nonlinear semiconductor and optically integrated devices, more accurate and realistic numerical simulations of these devices and systems are in demand. Such calculations provide a testbed in which one can investigate new basic and engineering concepts, materials, and device configurations before they are fabricated. The time from device conceptualization to fabrication and testing should therefore be enormously improved with numerical simulations that incorporate more realistic models of the linear and nonlinear material responses and the actual device geometries. It is felt that vector and higher dimensional properties of Maxwell's equations that are not currently included in existing scalar models, in addition to more detailed materials models, may significantly impact the scientific and engineering results.

In this paper we describe numerically obtained, multi-dimensional, full-wave, vector Maxwell's equations solutions to problems describing the interaction of ultra-short, pulsed beams with a dispersive, nonlinear material having a finite response time. These numerical solutions have been obtained in two space dimensions and time with a nonlinear finite difference time domain (NL-FDTD) method which combines a generalization of a standard, FDTD, full-wave, vector, linear Maxwell's equations solver with a Lorentz linear dispersion model and two nonlinear (Raman and instantaneous) material models. In particular, we are solving in a self-consistent manner the system of equations:

$$\frac{\partial}{\partial t}\left[\mu_0 \vec{H}\right] = -\nabla \times \vec{E} \tag{1}$$

$$\frac{\partial}{\partial t}\left[\epsilon_L \vec{E}\right] = \nabla \times \vec{H} - \frac{\partial}{\partial t}\vec{P} \tag{2}$$

$$\frac{\partial^2}{\partial t^2}\vec{P}^L + \Gamma_L \frac{\partial}{\partial t}\vec{P}^L + \omega_L^2 \vec{P}^L = \epsilon_0 \chi_0 \omega_L^2 \vec{E} \qquad \text{Lorentz Model} \tag{3}$$

$$\frac{\partial^2}{\partial t^2}\chi^{NL} + \Gamma_R \frac{\partial}{\partial t}\chi^{NL} + \omega_R^2 \chi^{NL} = \epsilon_R \omega_R^2 |\vec{E}|^2 \qquad \text{Raman Model}, \tag{4}$$

where $\vec{P} = \vec{P}^L + \vec{P}^{NL}$ and $\vec{P}^{NL} = \epsilon_0 \chi^{NL} \vec{E} + \epsilon_0 \chi^{Kerr} |\vec{E}|^2 \vec{E}$, χ^{Kerr} being the instantaneous Kerr susceptibility. Thus, the NL-FDTD simulator models pulse propagation under the influence of linear and nonlinear dispersive, linear and nonlinear diffractive, and time retardation effects in the medium.

By coupling the linear and nonlinear dispersion models together simultaneously, as well as using the natural boundary conditions arising from dielectric discontinuities, for example, at gratings and corrugated interfaces, we are trying to design ultrashort pulsed beam steerers and all-optical switching devices for ultrashort pulses. The NL-FDTD approach can readily handle complex, realistic structures. This allows a thorough investigation of the wave propagation in the presence of complicated scatterers built into a nonlinear waveguiding structure.

Ultra-short pulses are single-cycle or multiple-cycle envelopes containing fewer than 15 cycles. Sources in the laboratory have produced pulses compressed to as short as three optical cycles. By using these sources we illustrate two advantages of the time domain approach: (1) the ability to carry phase information over a wide spectrum, and (2) the ability to model transient effects which occur either quickly or slowly relative to the time scale of the pulse. Steering and output coupling of these types of pulsed beams with finite corrugation sections of the waveguide requires one to take advantage of interference effects and the material's linear and nonlinear transient responses. The corrugation structures also allow for more complex interplay amoungst the fields, the materials, and the geometries. Polarization and intensity dependent beam steering and output coupling result.

We will specifically present NL-FDTD results obtained for the interaction of multi-cycle and single-cycle pulses with grating assisted couplers in linear and nonlinear waveguides. Interest in these waveguide corrugation problems follows from our desire to design nonlinear guided wave couplers and beam steerers. The basic corrugated waveguide geometries we will show results for are shown in Figures 1 and 2. The corrugations have been both dielectric (an extension of the dielectric waveguide) and metallic (deposited into or on top of the dielectric waveguide) teeth. A variety of TE and TM field structures will be presented; effects depending on the medium response time, the polarization, and the material parameters, will be discussed. The multi-cycle results represent behaviors that could be observed with optical systems currently under investigation; the single-cycle results represent those being developed for future studies by the international optics community. However, in either case, the full pulse is modeled with the NL-FDTD approach rather than only the envelope of the carrier wave, as it is with the nonlinear Schrödinger equation models. This enhanced modeling capability of the NL-FDTD approach allows one to model and distinguish the effects that arise in both the single- and multiple-cycle TE and TM polarization cases.

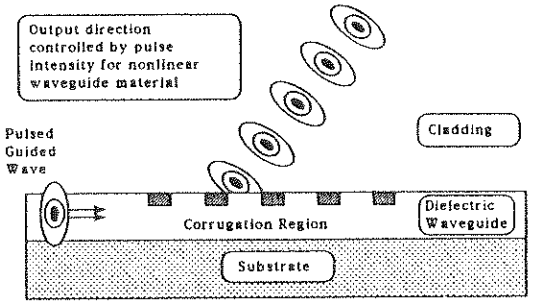

Figure 1. Grating-assisted beam steering output-coupler configuration.

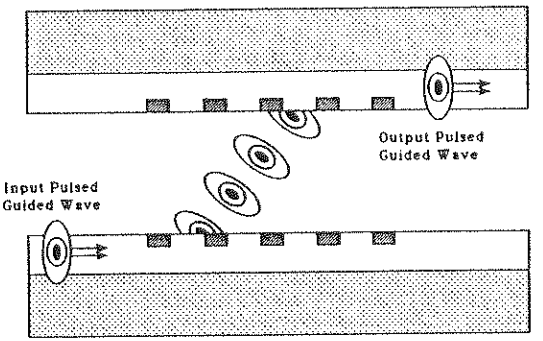

Figure 2. Grating-assisted waveguide coupler configuration

INCREMENTAL DIFFRACTION COEFFICIENTS FOR THE EXTENDED PHYSICAL THEORY OF DIFFRACTION

A. Michaeli, Research Consultant
Tchernihovsky St. 61, Haifa 35704, Israel

The essence of the Physical Theory of Diffraction (PTD) as formulated by P.Ya. Ufimtsev (*Method of Edge Waves in the Physical Theory of Diffraction*, Air Force Systems Command, Foreign Tech. Div. Doc. ID No. FTD-HC-23-259-71, 1971) was to augment the radiation integral for the physical optics (PO) current on the surface of an edged body by the radiation integral for the fringe current excited by the edge diffraction. The latter integral, in Ufimtsev's formulation, reduced asymptotically to contributions from isolated stationary phase points on the edge, making this formulation invalid at and near the caustics of the diffracted field. This shortcoming was removed in a later development (K.M. MITZNER, Aircraft Div. Northrop Corp., Tech. Rep. AFAL-TR-73-296, 1974) wherein the PTD field was represented by a line integral along the edge with an integrand expressed in closed form in terms of incremental diffraction coefficients (IDC). An elaborated version of this formulation, eliminating singularities from the integrand, was developed by A. Michaeli (*IEEE Trans. Antennas Propagat.*, **AP-34**, 912-918, 1986) in the form of equivalent edge currents.

The mentioned formulations pertain to integration over a *body's* surface. However, according to the equivalence theorem, the radiated or scattered field by a body can be represented by an integral over an *arbitrary* surface encompassing the body (but not the observation point). This theorem is employed in practical calculations for bodies with concavities or apertures (reflectors, open waveguides, horns), where the surface of integration is usually stretched over the edges of the body, traversing, at least in part, free space. Instead of the true surface current, one deals in this case with equivalent electric and magnetic currents related, respectively, to the magnetic and electric fields on the surface of integration as $\mathbf{J}=\mathbf{n}\times\mathbf{H}$, $\mathbf{M}=\mathbf{E}\times\mathbf{n}$, where $\mathbf{n}$ is the exterior normal to the surface. Just as the Kirchhoff integral is an extension of the PO integral to an aperture surface, one can conceive a similar extension of the PTD integral; the latter would involve the fringe equivalent currents $\mathbf{J}^f=\mathbf{n}\times\mathbf{H}^d$, $\mathbf{M}^f=\mathbf{E}^d\times\mathbf{n}$ on this surface, where $\mathbf{E}^d$, $\mathbf{H}^d$ are the edge-diffracted fields. Indeed, such an extended PTD (EPTD) solution was recently constructed (A. MICHAELI, *Radio Sci.*, 20, 1537-1548, 1985) for a 2-D canonical problem of a half-plane aperture terminating at the edge of a perfectly conducting wedge. In the context of a 3-D aperture with isolated stationary-phase diffraction points, that solution provides the necessary PTD diffraction coefficients. A formulation of EPTD in terms of IDC, which would help overcome the caustic problems, is, however, still lacking, and the present paper comes to fill up this gap.

The derivation of IDC for the problem in question is similar to that employed in the previous paper by Michaeli (*IEEE Trans. Antennas Propagat.*, **AP-34**, 912-918, 1986) and can be understood with the aid of the figure below. The aperture terminating at the edge of a wedge occupies the half-plane $z=0$, $x>0$. For a given edge point, chosen as origin, we consider the skewed co-ordinate σ measured along the diffracted ray traversing the aperture, which makes the same angle β with the edge as the incident ray. The integration of $\mathbf{J}^f$, $\mathbf{M}^f$ with respect to σ from 0 to ∞, which is performed by interchanging the order of integration with the Sommerfeld integrals involved in $\mathbf{J}^f$, $\mathbf{M}^f$, yields closed-form expressions which constitute a part of IDC for the edge. These expressions vary with the angle Φ between the aperture plane and the wedge face. To complete the expressions for IDC, one has to add the contribution from the second aperture extending from the edge "to the left". In particular, that aperture may coincide with the second face of the wedge.

A typical problem where the new IDC can be employed is the radiation from an open-ended waveguide. The enveloping surface for the calculation of the radiation integral can be composed of the aperture and the exterior surface of the waveguide. Alternatively, it can be chosen to be the infinite plane containing the waveguide's aperture. In the latter case, one may use the versions of the radiation integral appropriate to a half-space with an electrically or magnetically perfectly conducting wall, which eliminate, respectively, the magnetic or electric equivalent currents and thus simplify the calculation.

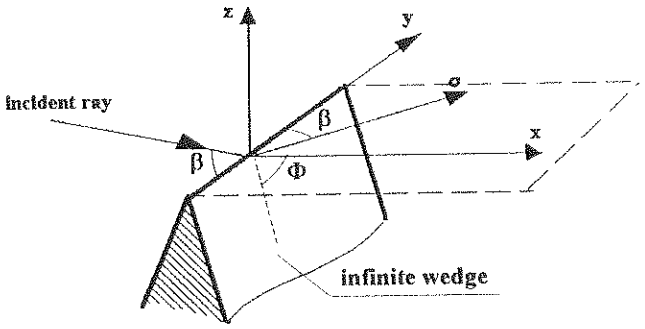

INTEGRAL EQUATIONS TECHNIQUE IN THE TIME DOMAIN

Y. BENIGUEL

IEEA, 13 promenade Paul Doumer, 92400 COURBEVOIE, FRANCE

INTRODUCTION

The integral equation technique to solve scattering problems is presented in the time domain. This technique is particularly useful to calculate the response of a structure to an electromagnetic pulse. The structure may be of an arbitrary complexity, including antennas and dielectric parts.

For a perfectly conducting surface, we may use either the magnetic field integral equation for a closed surface or the electric field integral equation for antennas and opened or closed surfaces. For a non perfectly conducting structure, both equations must be solved simultaneously.

The method of solution is the method of moments. The antennas are approximated by dipoles. The structure is approximated by triangles. Two families of expansion functions are used with respect to time and space. The space functions are linear and similar to those defined by Rao, Wilton and Glisson (IEEE Transactions on antennas and propagation, may 1982) in the frequency domain. Time functions are second order. Both explicit an implicit algorithms may be developed.

METHOD OF SOLUTION

The derivation is briefly presented hereafter for the electric field integral equation. To avoid calculating the charge density, we use the derivative of this equation:

$$\frac{\partial E^{i}}{\partial t} = \frac{\partial}{\partial t} \Phi + \frac{\partial^{2} A}{\partial t^{2}}$$

With linear space expansion functions, we obtain as an intermediate result:

$$\rho^{c+} \cdot \frac{\partial E^{ic+}}{\partial t} + \rho^{c-} \cdot \frac{\partial E^{ic-}}{\partial t} = \left[\rho^{c+} \cdot \frac{\partial^{2} A^{ic+}}{\partial t^{2}} + \rho^{c-} \cdot \frac{\partial^{2} A^{ic-}}{\partial t^{2}} \right] - \frac{\partial \Phi^{c+}}{\partial t} + \frac{\partial \Phi^{c-}}{\partial t}$$

where $A^{ic+(-)}$, $\Phi^{ic+(-)}$ are the potentials at the centers of the + (-) dipole/triangle corresponding to point i.

Derivatives are centered for the time derivatives. This provides an $A_i(t+1)$ value and consequently allows to compute the current density $J_i(t+1)$ on the structure. A second order time basis function is chosen to calculate the potentials with respect to the current on the structure.

Increasing the time step increase the number of patches interacting each others at the same time step and consequently fill the "influence matrix". For a time step such that

$$\Delta t \quad < \quad \text{Min} \frac{R_{ij}}{c}$$

the algorithm is explicit. It becomes implicit on the contrary. A similar development may be achieved for the magnetic field integral equation. For a simultaneous resolution in the case of a non perfectly conducting material, a magnetic current density has to be taken into account. The number of unknowns is doubled in that case.

The results presented below apply to a reception problem. A square plate is illuminated by a gaussian plane wave. The curves shown are those of the current densities at three points on the plate due to the incident pulse. Both the time domain result and the inverse Fourier transform of the frequency result at the same points have been plotted.

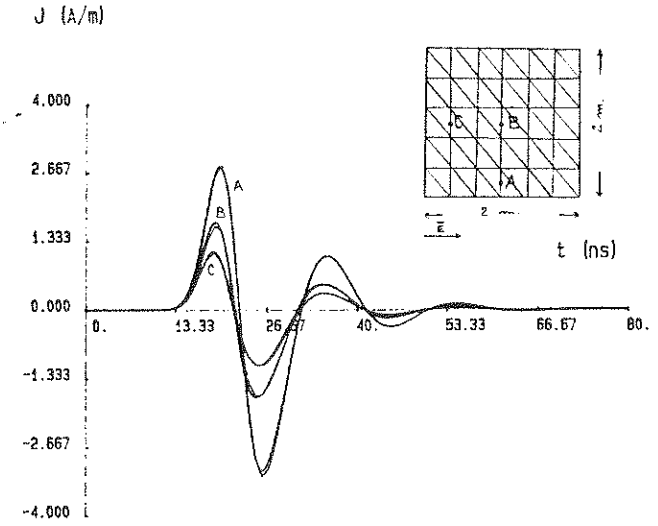

More complicated structures are presently under test and the results will be presented.

MMP-3D: A Survey on Recent Improvments

Stéphane Kiener
Mothesim, La Boursidière
Plessis Robinson, France

Abstract:
If the GMT (General Multipole Technique) principles and the code MMP-3D (Multiple Multipoles Program) are already well known, there has been recently new developments which allows the code to compute new geometries and materials in an even more efficient way.
These improvments, different choices of basis functions, new boundary conditions or an improved solving method for the matrix equation have been implemented in the MMP-3D code.
The subject of this presentation is to show these developments pointing out which features are standard and which have been developed whith little effort from the basis code.

1. Introduction:

The MMP-3D code has been first been written by Klaus [1] on the ideas of Hafner for the 2D code [2]. Now a 3D code exists on a commercial basis [3].
This code has been widely used by researchers from the Swiss Federal Institute of Technology in Zurich. It has been very successful for smooth geometries made of dielectrics or perfect conductors in the resonant region (dimension of the bodies from 0.1 to 10 wavelengths).
However, the progress in computer's performances and the need for more general shapes and materials which are usual in the technical field made a generalization necessary.
This has lead to the recent improvments which will be described in the following.

2. Basic principles of the MMP-3D:

It is well known that a program, especially when it is for general usage, is composed of multiple features. Still, using a block structure, it is possible to separate the "intrinsic essence" of the code.
The following three principles are the basis of the code and build a common platform for neighbor codes, like SPEX of Ludwig, the Yasuura method (Okuno in Japan) or the equivalent sources (Leviatan in Israel).

1) The basis functions used are analytical solutions of the field equations. In the 3D dynamical case, Helmholtz equations are to be solved.
2) The boundary conditions are written on discrete points (Matching Points or MP) and solved numerically. For perfect conductors, the electric tangential field and/or the magnetic normal field are zero and in the case of dielectric materials the tangential components must be continuous and/or the normal components jump.
3) The matrix equation is overdetermined (more equations than unknowns) and solved in the least square sense.

For the reader who is not familiar with the MMP-3D code, this is still not enough to be able to write his own program, as nothing is said about the location of the multipoles or the MP, but the space of this communication does not allow to go in details and the interested reader will have to read the more detailled references. Still, these three principles build the basis of the codes.

In the original MMP-3D code, the basis functions where essentially of three kinds:
- Multipoles, which gave the name to the code, in the sense of Jackson, are a combination of Hankel functions (of non integer order), Legendre polynomials and harmonic functions. Therefore, anlytical solutions of the Helmholtz equation in spherical coodinates, i.e. well adapted to smooth structures.
- "Normal expansions" which differs from the multipoles only by the replacement of Hankel functions by Bessel functions. This is especially useful for dielectric bodies with, again, the restriction of smooth bodies.
- Plane-waves which are mostly used to describe the source of the field and eventually the reflection on flat structures.

For the boundary conditions, there is not much to say, except that the impedance condition of Shelkunof for the outside problem of non-perfect conductors was also implemented and that all boundary conditions were carefully weighted.

The overdetermined system of equations is solved, in MMP-3D, with an improved Linpack subroutine using the Givens plane of rotation.

3. Improvments:

As it has already been mentioned this method works fine for smooth geometries and for a large class of materials but problems appeared when large flat plates (even if possible as shown in [4]) or very thin, wire similar, structures were computed. Also, the problem of shielding by "good" conductors was not solved and finally the behavior of the matrix solver for large problems (bigger than ten wavelengths) was not excellent.

For thin or large flat structures, the solution was to implement new basis functions:

- Thin wire expansion were only the longitudinal component of the current on a wire is considered. This has been done in [5]. Following, boundary conditions were applied as for perfect conductors with "special" locations for the MP. This is now a standard feature of the code.

- For large flat plates, roof top functions for the current were implemented. One should notice that these basis functions were not placed on the surface of the conductor but inside the geometry to avoid any singularity .

For the "inside" problem of closed cavities made of good conductors (or even superconductors), new boundary conditions were implemented [6]. This allowed the computation of shieldings for "SQUIDS" but also for classical and multi-layers materials.

And finally, for big and complicated geometries, an interactive process, called "connections" is used to improve the convergence of large matrices. This is also a standard feature of the code, even if it requires a certain know-how to use it properly. Also, the "a priory" knowledge of certain parts of the result is easy to implement to improve the convergence of the solution.

4. Conclusion:

The promoters of MMP-3D were always very careful to keep the code open to useful ideas coming from other well known codes as NEC (in the case of thin wires) and in a near future with GTD. This allowed to implement new sub-routines for more general geometries and materials to improve even more the power of the code.

References

[1] G. Klaus, *3D Streufeldberechnungen mit Hilfe der MMP Methode*, Thesis ETH, Zurich, 1985.

[2] Ch. Hafner, *Beiträge zur Berechnung der Ausbreitung Elektromagnetischer Wellen in Zylindrischen Strukturen mit Hilfe des "Point Matching" Verfahren*, Thesis ETH, Zurich, 1980

[3] Ch. Hafner & L. Bomholt, *MMP-3D: A Scattering Program for Computational Electromagnetics*, John Wyley, 1993

[4] St. Kiener, *Les limites du modèle de Maxwell: Applications aux discontinuités géométriques résolues par les codes MMP*, Thesis ETH, Zurich, 1990

[5] P. Leuchtmann, "The Thin Wire Expansion in the MMP code", *Aces Proc.*, 1992

[6] A. Nishikata & St. Kiener, "Modeling and Analysis of the Electromagnetic Shielding Behavior of Superconductors, Conductors and Magnetic Materials", *To be published in IEEE Trans. on Magnetics*, 1994

THE TWO-DIMENSIONAL FINITE INTEGRAL TECHNIQUE COMBINED WITH THE MEASURED EQUATION OF INVARIANCE APPLIED TO OPEN REGION PROBLEMS

Griffin K. Gothard and Sadasiva M. Rao*
Department of Electrical Engineering
Auburn University, Auburn, Alabama 36849

Tapan K. Sarkar
Department of Electrical and Computer Engineering
Syracuse University, Syracuse, New York 13244

In this work, we present a new numerical technique capable of calculating the electromagnetic scattering/radiation from electrically very large arbitrarily shaped inhomogeneous structures. The technique combines all the advantages of the existing methods which are primarily based either on the integral equation solution method or the differential equation solution method. In this procedure, the first step is to approximate the object and the surrounding space by a regularly shaped finite element mesh. Since we are dealing with two-dimensional structures in the present work, triangular shaped finite elements are utilized for modeling. The triangular elements have the ability to conform to any plane boundary and hence provide accurate approximation of the actual geometry.

However, in the present scheme, the mesh is extended only two layers away from the object boundary and at this outer boundary, the so-called measured equation of invariance (MEI) termination condition is utilized. The MEI condition is derived from the integral equation solutions utilizing Green's functions which enforce the radiation condition automatically. The most important advantage of the MEI termination condition is the generation of a sparse matrix which can be efficiently solved using iterative techniques such as the conjugate gradient method. This is in contrast to conventional finite difference/finite element methods applied to open region problems. In the conventional scheme, in order to obtain accurate results, the mesh needs to be extended to a much larger number of layers. Thus, the present scheme results in a highly reduced size for the generating matrix which implies that electrically very large problems can be handled rather easily.

The next step in the solution procedure is to apply the finite integral technique (FIT) to the triangular grid in order to solve

the scattering problem. The FIT technique involves solving the Maxwell's equations in the integral form. This scheme again differs from the conventional finite difference/finite element techniques where the differential form of Maxwell's equations are routinely solved. The solution of Maxwell's equations in integral form is more suited for numerical manipulation particularly when dealing with conformal grids. In addition, the unknown electric and magnetic fields are explicitly expressed in terms of well defined basis functions with unknown coefficients. This explicit definition enables us to determine accurately the required field quantities anywhere in the solution space without using interpolation techniques.

The advantages of the present solution scheme may be listed as follows:

1. The method requires much less computer storage than the conventional methods to solve a similar size problem.

2. Each unknown cell in the numerical model is related to only the immediate neighbors as in all differential equation solution schemes.

3. The radiation condition is automatically enforced because the grid termination condition is derived from integral equations and Green's functions.

Typical numerical results are presented for the solution of the two-dimensional Helmholtz's equation to illustrate the accuracy of the technique.

TEMPOREL GEOMETRICAL THEORY OF DIFFRACTION : SIGNIFICATION AND NUMERICAL ASPECTS

Thierry GEORGE

Frédéric MOLINET

MOTHESIM

La Boursidière, Rn 186

92 357 Le Plessis Robinson Cedex

This work was supported by the CEG under contract CEG/93 40 008 00 402 94 51.

In harmonic domain, the Geometrical Theory of Diffraction (GTD) is an hight-frequency asymptotic approximation, used when characteristic dimensions of objects are large in respect with the wavelength. This method is employed when the numerical method implementation no longer is possible. This theory proposes approximations for each elementary problem (reflection, diffraction...). Solutions are established from the study of canonical cases. They are well studied in Fourier domain. The first asymptotic solutions (J. B. Keller, J. Opt.SC. Am., Vol. 52, 1962) following two types of singularities: transition zones and vicinities of caustic of rays. Transition zones are defined when one of components of the asymptotic field disappears. In the case of a diffraction by a wedge, transition zones correspond to the shadow and reflection boundaries. Uniform solutions have been introduced (R. G. Kouyoumjian & P. H. Pathak, Proc. IEEE, Vol 62, 1974) to avoid disadvantages linked to transition zones. They are known under the term of Uniform Theory of Diffraction (UTD). Uniform solutions exist also to calculate the Airy caustic (P. H. Pathak & M. C. Liang, IEEE Ant. Prop., 1990). Spectral methods or equivalent current methods (PTD) allow to deal with the most general caustic case. The numerical implementation of asymptotic solutions need a research of rays. The electromagnetic contribution of a ray is obtained by the dyadic product of elementary solutions along the ray.

In time domain, explicit solutions have been obtained from harmonic solutions by inverse transform (in the case of the wedge diffraction: T. N. Veruttipong, IEEE Trans. Ant. Prop., Vol. 38, n°11, 1990). The unilateral Laplace transform and the principle of causality are necessary tools for these developments. The influence of a caustic can be expressed far of the caustic (T. George & F. Molinet, CEM 1993, Toulouse). In time domain, high-frequency approximation transforms by an approximation to the vicinity of the time of arrival of the wave. The spectral range of the incident signal has to be to high frequency: the signal has to be sufficiently impulsive and its duration has to be sufficiently small. This approach in the time domain allows a direct physical meaning of the phenomena. Indeed, the signal is decomposed in elementary contributions that correspond to rays (figure 1). This example will be developed in the presentation.

The far field of the caustic will be examined in the speech. This situation is interesting because the approximation is non causal. The form of the signal is however well represented in the vicinity of the ray time.

From the plane wave diffraction by a perfectly-conducting wedge, we compare the time expressions obtained with the classic asymptotic method (GTD), the uniform theory (UTD) and an exact solution that is valid if the incident field is normal to the wedge (L. E. Felsen & N. Marcuvitz, Prenctice-Hall, 1973.). The numerical solution behavior is illustrated in figures 2 and 3. In this case, the wedge angle is 270 degree. Points of observation are situated on one of the faces, to two meters of the edge (figure 2) and to 20 meters (figure 3). The incident signal has an approximate duration of 30 nanoseconds. The first calculation corresponds to a very small travel time (7 nanoseconds) what explains the bad result of the GTD. The results of GTD are best in the second calculation (travel time of 66 nanosecondes). We notice the

agreement of the uniform solution results with the exact solution for any observation position. On the other hand, the solution predicted by the GTD is singular on the shadow or reflection boundary. The interest of the uniform theory appears clearly.

The numerical implementation consists in a series of convolutions that correspond to interactions along the ray. In the case of a reflection, the convolution is analytic : this operation is reduced to a delay of the signal and to an algebraic multiplication. Each other canonical solution is a singular Green function and a particular attention must focus on the choice of the time sampling. It is necessary to avoid the correspondence between a signal time sample and the travel time of a ray where applies the singularity. The convolution has been envisaged with a numerical integration and with a Fast Fourier Transform. Precisions of the two approaches are equivalent but the speed plays in favor of the Fast Fourier Transform.

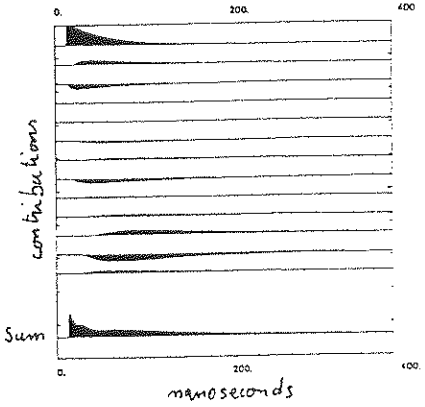

Figure 1

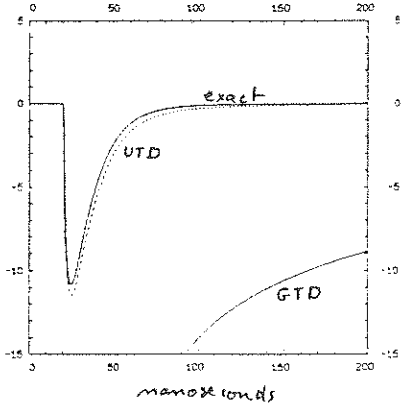

Figure 2

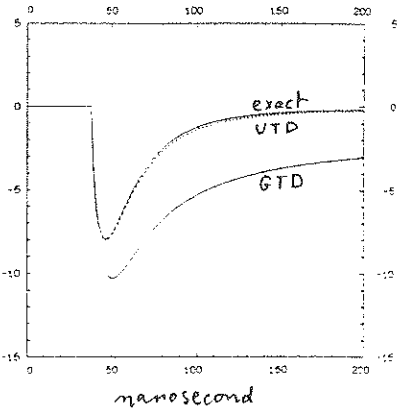

Figure 3

ON REGION OF VALIDITY OF SHORTWAVE APPROACH TO A PLANE WAVE DIFFRACTION BY A SINUSOIDAL GRAITING.

D.Maystre, Laboratoire d'Optique Electromagnetique, Faculte des Sciences et Techniques, Centre de Saint-Jerome, Marseille.
M.Popov, Departement de Geophysique Appliquee, Universite Pierre et Marie Curie, Paris.
V.Zalipaev. V.A.Steklov Mathematical Institute. St.-Petersburg.

Consider the following problem of diffraction of a plane wave by a smooth periodic boundary. Suppose the plane wave $U_{in}=\exp\{ik(x\cos\chi - y\sin\chi)\}$ illuminates sinusoidal grating S having period L.We assume the total wave field U satisfies the reduced wave equation above S, Dirichlet's boundary condition on S and corresponding radiation conditions.Then the diffracted field U_d above S can be presented as a series of diffracted plane waves outgoing from the graiting.

$$U_d = \sum_{n=-\infty}^{n=\infty} R_n \exp\{ik(x\cos\varphi_n + y\sin\varphi_n)\} \qquad (1)$$

where φ_n is the diffraction angle of corresponding plane wave and R_n is its amplitude. This problem has been envestigated by V.Zalipaev & M.Popov (J.Sov.Math. 50,N6, 1990, and 55,N3, 1991) under the following assumptions: i) the wave length $\lambda = 2\pi / k$ is small in compare with the period L, height of the humps and radius of curvature of the boundary, so that we are in the frame of shortwave approximation, ii) the grazing angle χ is small, so that only tops of humps are illuminated while all other part of the boundary remains to be in deep shadow. Both these assumptions were caused by an application of the problem to the problem of radiolocation near ocean surface.

Using both the ideas and mathematical technique developed in shortwave approach to diffraction problems asymptotic formulae for the diffracted field and amplitudes R_n of the outgoing plane waves have been obtained. For example, formulae for Rn can be presented in the form :

$$R_n = R_n^{(0)} + R_n^{(1)}\, 1/p + O(p^{-2}) \qquad (2)$$

where $p = (k\rho/2)^{1/6}$ should be considered as a large parameter (ρ is the radius of curvature of S at the top of hump of the boundary) and n remains to be in a vicinity of mirror reflection ($n = 0, \pm1, \pm2, \ldots$). Note that $R_n^{(0)}$corresponds to Fresnel's diffraction while $R_n^{(1)}$ involves background (formulae for them are cumbersome to be presented here).To apply the asymptotic formulae we have to know what means that p is large, or in other words, for what value of the large parameter asymptotic formulae will provide sufficient accuracy.To this end we compare results of caculation on the base of asymptotic formulae for sinusoidal grating with exact numerical approach developed by D.Maystre (Topics in current physics. Electromag.Theory of Graitings, ed. R.Petit,Springer, Berlin,1980.).

The results obtained for different relations between the period L and wave length λ are presented in Table, where n is the number of diffracted plane wave, by E_n and $\widetilde{E}_n$ we denote reflected efficiencies computed with the help of exact numerical approach and asymptotic formulae respectively To estimate coincidence between both these methods parameter :

$$\sigma = \frac{\sqrt{\sum_{n=0}^{13}\left(E_n - \tilde{E}_n\right)^2}}{\sum_{n=0}^{13} E_n}$$

has been computed in each case, see the last line in the Table. It follows from the results that coincidence between the methods increases with increasing of the ratio L / λ. We can expect the shortwave asymptotic formulae to be reliable for studing of radiolocation problems near ocean surface, because L/λ is rather large in the case.

TABLE

L / λ	50		100		150	
n	E_n	$\tilde{E}_n$	E_n	$\tilde{E}_n$	E_n	$\tilde{E}_n$
0	0.522	0.658	0.432	0.453	0.239	0.227
-1	0.076	0.095	0.095	0.110	0.062	0.062
-2	0.054	0.059	0.075	0.074	0.043	0.042
-3	0.043	0.045	0.083	0.058	0.035	0.034
-4	0.034	0.038	0.091	0.049	0.031	0.029
-5	0.026	0.033	0.084	0.043	0.029	0.026
-6	0.024	0.029	0.063	0.038	0.028	0.024
-7	0.029	0.026	0.040	0.035	0.027	0.023
-8	0.037	0.024	0.021	0.032	0.026	0.021
-9	0.041	0.023	0.010	0.031	0.025	0.020
-10	0.038	0.021	0.004	0.030	0.023	0.019
-11	0.030	0.020	0.001	0.030	0.020	0.018
-12	0.021	0.020	0.000	0.030	0.019	0.017
-13	0.012	0.020	0.000	0.030	0.019	0.017
σ	0.143		0.096		0.026	

ON THE USE OF WAVELET LIKE BASIS FUNCTIONS FOR EFFICIENT SOLUTION OF ELECTROMAGNETIC PROBLEMS

Luis Emilio García Castillo[1], Tapan K. Sarkar[2], Magdalena Salazar Palma[1]
[1]Grupo Microondas y Radar. Dpto. Señales, Sistemas y Radiocomunicaciones.
E.T.S.I. Telecomunicación. Universidad Politécnica de Madrid
Ciudad Universitaria s/n. Madrid 28040. SPAIN.
[2]Dept. Electrical and Computer Engineering, Syracuse University.
121 Link Hall, Syracuse, New York 13244-1240, USA.

ABSTRACT: The introduction of "wavelet" concepts for solving differential form of Maxwell's equations allows to reduce the computational effort. This technique is applied to one dimension (1D) and two dimensions (2D) differential equations. Numerical examples are presented showing the features of the method.

INTRODUCTION: Present microwave technology requires an accurate electromagnetic simulation in order to take care of coupling between lines, packaging and other effects. On the other hand, a wide and complex variety of geometries, material and configurations are used nowadays in the designs. This complexity means a considerable computational effort when numerical approaches are employed.

The finite difference and the finite element method have been developed over the last few years in the microwave area to solve practical engineering problems. However, one of the problems of the Finite Difference and the Finite Element Method lies in the solution of a large matrix equation (either a deterministic or an eigenvalue problem). The problem here is that as the number of unknowns increase (and hence the dimension and size of the matrix) the condition number of the matrix also increases, affecting directly the solution procedure as, for example, a highly ill conditioned matrix prohibits application of a direct solver like Gaussian Elimination [G. Golub, C.F. Van Loan, "Matrix Computations"] and more sophisticated techniques like Singular Value Decomposition may have to be introduced. Several methods have been presented; for example, in [M.A. Krasnoseliskii et.al, "Approximative Solution of Operator Equations", S.G. Milkhlin, "The Numerical Performance of Variational Methods", Wolters-Noordhoff Publishing] where the choice of basis functions can control the growth of the condition number. In this paper, that principle has been used together with new wavelet concepts [B.K. Alpert, in Wavelets - A Tutorial in Theory and Applications, in C.K. Chui (ed), pp. 181-216, Academic Press, 1992], [S.Jaffard, in Probabilistic and Stochastic Methods in Analysis with applications, by J.S.Byrnes et.al (eds.), pp.3-13, Kluwer Publishers, 1992], [R.A.H. Lorenz, W.R. Madych, in Applicable Analysis (to appear)] to solve differential form of Maxwell´s equations.

The basic philosophy of this paper lies in the choice of a particular set of basis functions, "wavelet basis", which attempts to diagonalize the system matrix that arises when a discretization is applied to the differential form of Maxwell´s equations. The ideal situation will be to make the sparse matrix diagonal. Then the solution of such a matrix problem becomes trivial. However, because of various boundary conditions this goal can not be achieved. Therefore the next best procedure is an attempt to make the major part of the system matrix diagonal.

WAVELET BASIS AND NUMERICAL RESULTS: Different wavelet basis functions have been employed to illustrate the features of the present approach. In order to easily explain the basic philosophy, the 1D case is first considered.

Figure 3 shows the basis functions employed in 1D to solve the Poisson equation. Basically, functions ϕ_i (i=1..n) satisfy the Dirichlet homogeneous boundary conditions and ϕ_{e1}, ϕ_{e2} take care of any other boundary conditions. Note that these basis functions are not the classical subdomain ones, corresponding to ϕ_2, ϕ_3, ϕ_4, ϕ_5 and the three dotted line triangular functions shown in the same figure.The basis functions of Fig. 3 are termed "wavelet basis" as they are the dilation and the shifted version of the same function. The main reason for the choice of the "wavelet basis" functions is that as the dimension of the problem increase, the condition number of the solution matrix does not go up as fast as when employing the classical ones. Effectively, it is easy to find that the introduction of basis functions shown in Fig. 3 in the Poisson equation, via Galerkin method, provide a system matrix of the following form:

$$[S]=\begin{bmatrix}[D]_{n\times n} & [G]^{*}_{n\times 2}\\ [G]_{2\times n} & [B]_{2\times 2}\end{bmatrix} \qquad (1)$$

where [D] is a diagonal matrix. The reason of the use of "wavelet" functions is now clear: since a major part of the system matrix is diagonal computational effort can be strongly reduced. In addition, in this particular case $[G]=[G]^{*}=[0]$ and the solution is

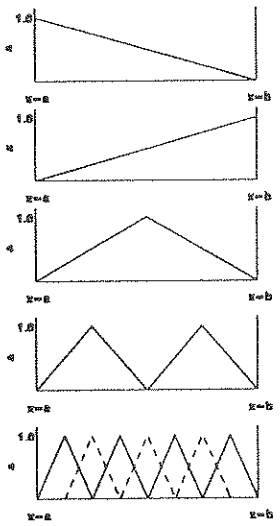

Fig. 3 Third Order Wavelet Basis in 1D
a)(b): Matching Functions
c)1st d)2nd e)3rd Order Functions

	TE_{10}	$TE_{20}=TE_{01}$	TE_{11}	TE_{21}
N=2	1,57	3,16	3,53	4,46
N=4	1,57	3,14	3,52	4,45
N=6	1,57	3,14	3,51	4,44
N=8	1,57	3,14	3,51	4,44
N=10	1,57	3,14	3,51	4,44
Exact	1,57	3,14	3,51	4,44

Table 3.Cut-off Wavenumbers of the TE modes of the Rectangular Waveguide

	Row Size of Matrix	Row Size of Diagonal Block	% Diagonal
N=2	28	8	28,57
N=4	66	32	48,48
N=6	120	72	60,00
N=8	190	128	67,37
N=10	276	200	72,46

Table 4. Percentage of Diagonality for TE case of Rectangular Waveguide

	Mode 1	Mode 2	Mode 3	Mode 4
N=2	6.95	6.96	8.68	8.72
N=4	6.94	6.95	8.66	8.70
N=6	6.94	6.95	8.66	8.70
N=8	6.94	6.95	8.66	8.70
Sarkar et. al.	6.91	6.96	8.50	8.51

Table 5.Cut-off Wavenumbers of the TM modes of the Coaxial Rectangular Waveguide

	Row Size of Matrix	Row Size of Diagonal Block	% Diagonal
N=2	48	32	66.67
N=4	160	128	80.00
N=6	336	288	85.71
N=8	576	512	88.89

Table 6. Percentage of Diagonality for TM case of Coaxial Rectangular Waveguide

	Mode 1	Mode 2	Mode 3	Mode 4
N=2	1.90	2.84	3.91	5.18
N=4	1.89	2.84	3.91	5.16
N=6	1.89	2.84	3.91	5.16
N=8	1.89	2.84	3.91	5.16
Sarkar et. al.	1.85	2.81	3.89	5.05

Table 7.Cut-off Wavenumbers of the TE modes of the Coaxial Rectangular Waveguide

	Row Size of Matrix	Row Size of Diagonal Block	% Diagonal
N=2	96	32	33.33
N=4	240	128	53.33
N=6	448	288	64.29
N=8	720	512	71.11

Table 8. Percentage of Diagonality for TE case of the Coaxial Rectangular Waveguide

trivial. This is not true in the general case.

The extension of this concept to 2D problems has been done using rectangular regions (Ω:0≤x≤a 0≤y≤b). Any arbitrary region is discretized into rectangular ones. "Wavelets" concepts have been also applied to the choice of the basis functions ψ_{ij}. As in 1D case it is necessary to add new functions to take care of boundary conditions (either external or interface between regions). The unknown is approximated as given in (2) where N_{ij}, N_{ij}, N_{ij} and N_{ij} are edge matching functions and T_1, T_2, T_3 and T_4 are vertices matching functions. These matching functions will generate the non diagonal part of the system matrix.

$$u(x,y) \approx \hat{u} = \sum_{i=1}^{M}\sum_{j=1}^{N} A_{ij}\psi_{ij}^{(x,y)} + \sum_{i=1}^{4}\sum_{j=1}^{P} B_{ij}N_{ij}^{(x,y)} + \sum_{i=1}^{4} C_i T_i^{(x,y)} \qquad (2)$$

This last approach has been applied to obtain the cut-off wavenumbers of several waveguides with excellent accuracy. For the TM modes (homogeneous Dirichlet boundary condition) the row size of the matrix becomes $LxN^2 + NxN_{ie} + N_{iv}$ where a LN^2 x LN^2 submatrix is diagonal. Then the matrix is mostly diagonal and the computation is greatly reduced. N_{ie} is the number of internal edges and N_{iv} of the internal vertices. L is the number of rectangular regions and N is a parameter related to the degree of approximation in each region (M=N=P for comparison purposes). For the TE case (homogeneous Neumann boundary condition), the row size of the matrix becomes $LxN^2 + NxN_E + N_v$ where N_E is the total number of edges and N_v of the vertices. Again, a mayor portion LN^2 x LN^2 of the system matrix has been made diagonal by a suitable choice of the basis functions. Note that the diagonality is higher in the TM case for the same value of N due to the lower number of matching functions (those corresponding to the internal boundaries). Results for several cut-off wavenumbers of the TE and TM modes of rectangular (Tables 1 and 3) and Coaxial Rectangular (Tables 5 and 7) waveguides are presented. Percentage of diagonality achieved in each case is shown in Tables 2, 4, 6 and 8. To illustrate the flexibility and accuracy of the procedure the rectangular waveguide has been divided into two regions (Fig. 1; A1=1.33, A2=0.66). Coaxial Rectangular waveguide has been divided into three regions (Fig. 2; a=1.25, b=1, d=0.25, s=0.25). In both cases results show excellent accuracy and convergence. The obtained results have been compared with the analytical solution for the rectangular waveguide and with those from [T.K. Sarkar et. al, Journal of Electromagnetic Waves and Applications", Vol. 3, No. 2, pp. 143-165, 1989] in the case of the coaxial estructure. The computation efficiency of the wavelet basis now becomes clear. High percentage of diagonalilty can be achieved and this percentage goes up with the number of unknowns. Other structures have been analyzed showing also excellent results. The accuracy and efficiency of this preliminary results are promising. In future work this technique will be applied to more complicated structures.

CONCLUSIONS:The application of "wavelet" concepts for solving 1D and 2D problems has been presented. Its main advantage is the generation of almost diagonal system matrices reducing the computational effort. This concept has been applied to find the cut-off wavenumbers of certain waveguides showing the features of the method.

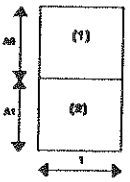

Fig. 2 Rectangular Waveguide

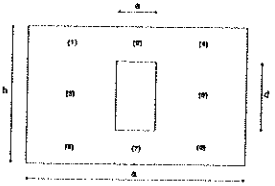

Fig. 2 Coaxial Rectangular Waveguide

	TM_{11}	TM_{21}	TM_{01}	TM_{31}
N=2	3,51	4,45	5,66	6,48
N=4	3,51	4,44	5,66	6,48
N=6	3,51	4,44	5,66	6,48
N=8	3,51	4,44	5,66	6,48
N=10	3,51	4,44	5,66	6,48
Exact	3,51	4,44	5,66	6,48

Table 1. Cutoff Wavenumbers of the TM modes of the Rectangular Waveguide

	Row Size of Matrix	Row Size of Diagonal Block	% Diagonal
N=2	10	8	80,00
N=4	36	32	88,89
N=6	78	72	92,31
N=8	136	128	94,12
N=10	210	200	95,24

Table 2. Percentage of Diagonality for TM case of Rectangular Waveguide

Reflection and Transmission of Well-Focussed General Astigmatic EM Gaussian Beams

H.T. Chou, G. Zogbi and P.H. Pathak*
The Ohio State University ElectroScience Laboratory
1320 Kinnear Road, Columbus, Ohio

The transformation of a well-focussed, general astigmatic EM Gaussian beam (GB), which is incident obliquely on an arbitrary curved interface, into corresponding general astigmatic GB's that are reflected and transmitted at the interface is obtained. The resulting closed form expressions for the reflected and transmitted fields in terms of general astigmatic GB's are obtained using two different approaches. One of these approaches involves the use of proper matching conditions for these GB's and the other is based on the use of radiation integrals together with paraxial approximations. Thus, a beam optics solution is developed which in some sense may be viewed as a geometrical optics type theory for the reflection and transmission of well-focussed GB's.

The results obtained here may be useful in the analysis/design of large reflector antennas with an array feed, or phased arrays, especially in focal regions, and in the analysis of the radiation and propagation of millimeter (mm) waves including interactions with mm wave components, etc. The diffraction of such general astigmatic GB's is currently in progress and will be reported separately in the future.

It is noted that an astigmatic GB and a rotationally symmetric GB are special cases of the general astigmatic GB. In the general astigmatic GB case, the curves of constant amplitude and phase terms in the exponent are ellipses which are rotated with respect to each other. Such a general astigmatic GB can be produced, for example, by reflecting a rotationally symmetric GB, or a conventional astigmatic GB, which is incident obliquely on a general curved reflector. It is further noted that conventional complex source point (CSP) techniques, which are sometimes used for mathematically generating a 2-D GB, and also a rotationally symmetric 3-D GB, cannot be directly applied to represent a general 3-D astigmatic GB. Hence, it becomes necessary to develop useful techniques different from the CSP-based methods to deal with the reflection (and diffraction) of general astigmatic GB's as is being developed here.

Some numerical results illustrating the accuracy of the expressions developed for reflected /transmitted general astigmatic GB's will be presented.

RANGE & RADIATION HAZARD ZONES ESTIMATION OF HIGH POWER LF WARSAW BROADCASTING STATION

Daniel J. Bem, Wojciech J. Krzysztofik

Technical University of Wroclaw, Institute of Telecommunication & Acoustics
Wybrzeze Wyspianskiego 27, 50-370 Wroclaw, *POLAND*

In recent years, there has been a tendency to increase the range of LF broadcasting stations by means of extremely high power transmitters. In view of need to ensure perfect receiving conditions throughout the country, it has been decided to erect a very high power LF broadcasting station in Poland. The projected, broadcasting station is to be rebuild up after disaster and damaging of the antenna tower on August 1991. The operating frequency of 225 kHz remains unchanged and total output power was 2 MW is planed to be decreased to satisfy actual radiation hazard regulations.

The correct use of the transmitter output power means selecting appropriate transmitting antenna. The increase in radiated power, and hence the greater ground-wave range (dominant mode of transmission at LF) , calls for antenna with narrowed vertical radiation patterns for reduced sky-wave. The antifading pattern can be obtained by an array (e.g. ring-type) or by increasing the antenna high up to approximately half wavelength. On 1970th it was decided to select the half-wave vertical mast (about 645 m high), the first half-wave antenna in the LF range in the world (Fig. 1).

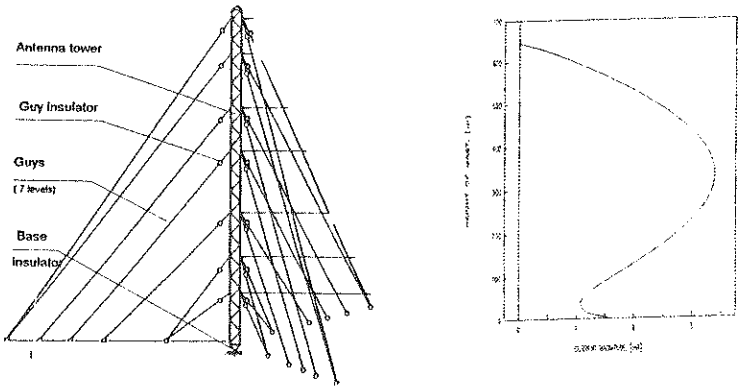

Fig. 1. Antenna mast (about 645 m high) of LF Warsaw broadcasting station (a) and the current distribution along the mast (b)

To prepare the background for re-building of the mast it was vital to carry out a thorough theoretical analysis concerning the antenna high optimisation (with respect to assumed vertical pattern), variety methods of feeding (base, shunt, folded dipole, etc.), new ideas for mast insulation (minimisation the number of guy insulators), ground-wave range, radiation hazard zones, etc.
The present paper discuss the results of these studies. The initial design calculations were based on the current antenna model solved by the methods of moments.
The current distribution along the antenna mast is presented in Fig. 1b, and calculated vertical radiation pattern of the antenna is shown in Fig. 2a.

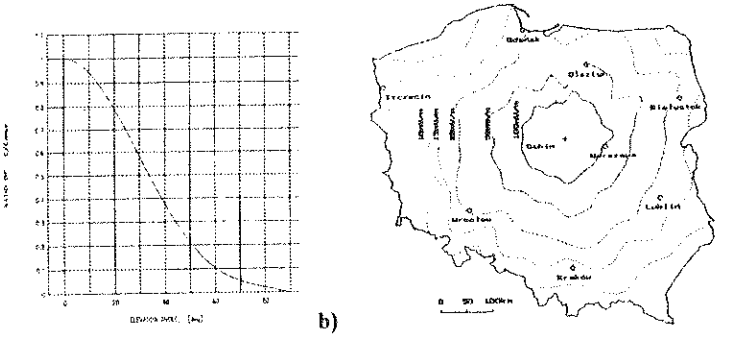

a) b)

Fig. 2. Vertical radiation pattern of the antenna (a) and the ground-wave distribution on the territory of Poland

The antenna mast, triangular in shape, was replaced in theoretical calculations by an equivalent cylinder. The current amplitude at the antenna input is 92.7 A (for 2 MW carrier wave). Most time of calculations was spend on the analysis of new solutions of the antenna insulation. The main idea concerns to the minimisation of the guy insulators number. It is important from at least two points of view: first one is the cost of the antenna construction and second - the static discharge problem on the insulators during the exploitation time (especially due to atmospheric lightening). It is decided to eliminate most of insulators along the guys and leaving only two of them on each guy (one on the mast-end and the second on the ground-end).
Separate consideration were done on evaluation of the ground-wave range of the station. It is done by the use of the Millngton procedure and applying the numerical map of the Poland territory ground conductivity. An example of the ground-wave distribution on the Poland territory, determined for 747 kW transmitter power AM-modulated with DCC (Dynamic Carrier Control) is shown on Fig. 2b. Radiation hazard zones were determined using the antenna current model. It was concluded that the first zone (E=5 V/m) is placed around the broadcasting station bounded by circle of 1.5 km for P= 747 kW (AM-DCC).

RF EXPOSURE IN A SHORTWAVE TRANSMITTER ENVIRONMENT INCLUDING THE INFLUENCE OF BUILDING STRUCTURE AND HUMAN BODY

R. Coray*, Swiss Telecom PTT, Directorate Radiocom, 3030 Bern, Switzerland
F. Gassmann, EMC BADEN Ltd., 5405 Baden-Daettwil, Switzerland

According to a Swiss government survey (1993) the RF exposure in a shortwave environment might be a source of insomnia, reduced concentration, high blood pressure and a general anxiety. A detailed interdisciplinary follow-up study (1993/94) performed specialised measurements and numerical predictions of the electromagnetic environment near the shortwave transmitter 'Schwarzenburg' including an investigation of the RF exposure inside buildings and bedrooms, which have been correlated with objective medical data. In a further step the influence of the human body on field perturbation and attenuation was calculated. This allowed certain measurement guidelines and precautions to be deduced. This paper gives an overview of the significant results.

SUMMARY

A maximum of three shortwave transmitters in the frequency range 6.1 - 21.8 MHz with an output power of 150 kW operate simultaneously at the 'Schwarzenburg' station which is located 20 km south of Bern. The facility is owned by the Swiss Telecom PTT and is programmed by Swiss Radio International. The village 'Schwarzenburg' and its surrounding farm houses lie within a short distance from the transmitter antennas. Some buildings are located very close to the outer bounds of the transmitter antennas. The population in the neighbourhood felt continuously annoyed and submitted a petition to the Swiss Government that measures be taken. The institutes for Social and Preventive Medicine at the University of Bern, which carried out the health study, asked 215 people, divided approximately equally among three zones A, B and C around the Schwarzenburg station, to keep a diary of how they felt for an average of 25 days. The RF radiation levels were measured by the Swiss Telecom PTT and the population's weighted 24-hour average exposures were estimated. The very complex near field situation around a shortwave transmitter antenna necessitates specialised measurement equipment and numerical calculation. Figure 1 shows a calculated electric field pattern around a typical HF curtain array at 12 MHz in V/m. The study showed that subjective complaints about psycho vegetative disturbances are significantly higher in the proximity of the transmitter antennas than in the control group C (unaffected by transmitter radiation).

In a follow up study, with the goal to acquire objective medical data (blood pressure and melatonine levels), measurements were performed at night inside numerous (60) bedrooms within zones A, B and C. Consequently a highly sophisticated measuring system (method) as well as corresponding prediction tools (numerical calculation of field variation inside bedrooms including persons) had to be developed.

The international standards on personnel safety limits recommend the measurement of the magnetic and the electric fields in the shortwave frequency range. The electromagnetic field measurement equipment used for

the follow up study was a fully isotropic, optically isolated probe for simultaneous electric and magnetic field measurements. The probe, originally developed by EMC BADEN in co-operation with the Swiss PTT, has been modified for higher sensitivity. Thus an electric field range from 0.1 V/m up to 60 V/m and a magnetic field range from 0.5 mA to 0.15 A/m could be accurately measured. For psychological reasons the probe has been mounted inside a plexi glass enclosure. The measurement was fully automated by computer control.

Within a building, metallic objects including the human body can significantly perturb the electromagnetic fields; thus some bedrooms were numerically modelled and the expected field variations were calculated. Figure 2 shows a model of a typical bedroom with two sleeping people. Figure 3 shows one example of the relative electric field variation caused by the metallic objects and the human bodies. The combination of measurement data, exact location of scatterers, probe position and the numerical prediction of the field variation provides a good idea of the expected measurement uncertainties. The calculation showed that in typical bedroom a 20 dB field strength variation can occur. Depending on electric field polarisation the human body itself can act like a dipole with a typical increase of electric field strength of more than 12 dB on its ends (head and foot). The bodies and objects may also couple with each other which is another source of perturbation.

Since not only a whole body average RF exposure might be the cause of change in melatonine production, the local field strength on the body surface and the attenuation of human tissue at shortwave frequencies may be of importance. Because there are very few epidemiological studies on the chronic effects of exposure to low-level (non thermal) RF radiation, the confirmation of the observed biological effects could force a major reevaluation of health standards.

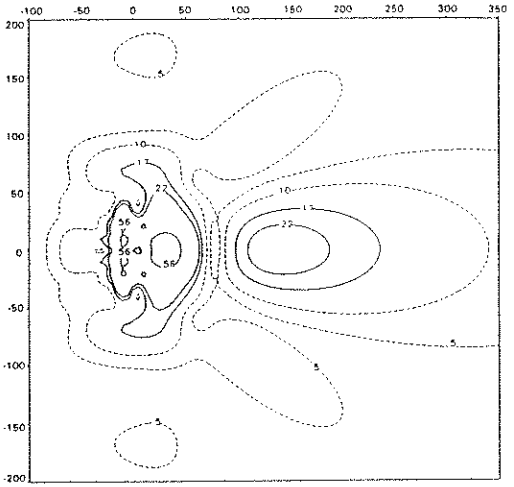

Figure 1: Near field electric field pattern of a HF curtain array antenna at 12 MHz and 500 kW input power at 1.5 m above ground. Scale: meters, E-field: V/m rms.

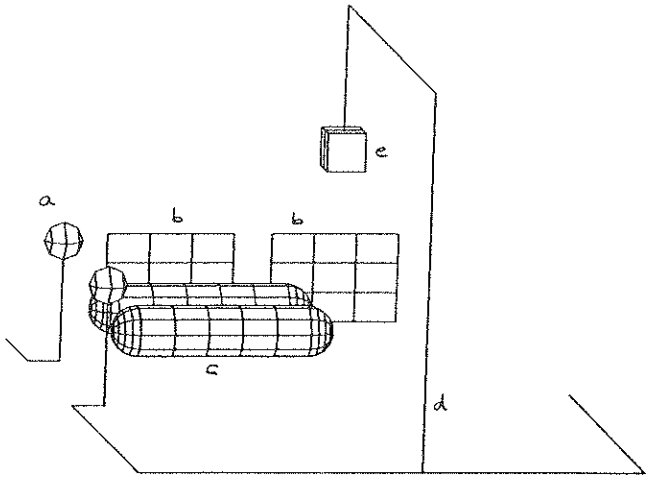

Figure 2: Model of a typical bedroom including (a) bedside table light , (b) radiators, (c) two lying people , (d) electrical power lines and (e) main light

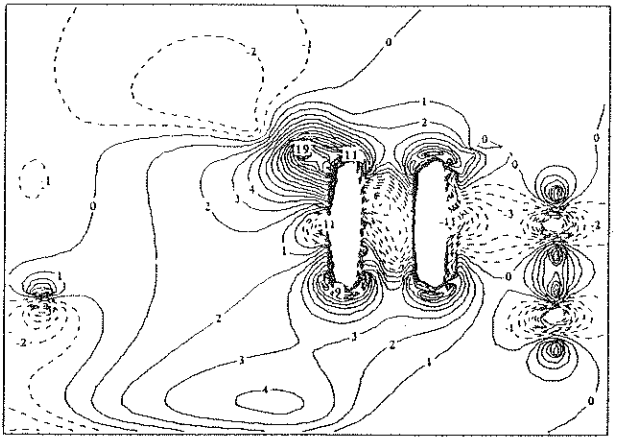

Figure 3: Contour plot of relative electric field variation (in dB) at 15 MHz in a typical bedroom (horizontal plane, 1 m above ground). Through lines: field increase (1 dB steps), dashed lines: field reduction (1 dB steps).

A Case Study of Compatibility Between Radioastronomy and Mobsat

F. Broydé *, E. Clavelier
EXCEM
12, Chemin des Hauts de Clairefontaine
78580 MAULE - FRANCE

E. Gérard, J. Pezzani, B. Clavelier
OBSERVATOIRE DE MEUDON
5, place Jules Janssen
92190 MEUDON - FRANCE

The present abstract describes some preliminary computational results obtained in the prediction of interferences between two ITU authorized services with primary status (following decisions at the WARC-92) in the 1610,6 MHz to 1613,8 MHz frequency band. In this band, a mobile of the Mobsat service acts as a transmitter, and may disturb radiotelescopes. Radiotelescopes are large antenna connected to a sensitive receiver, able to measure input signals weaker than the noise in their bandwidth. Our paper is limited to the case of the Nançay radiotelescope. Three coupling paths will be investigated : ground wave coupling, atmospheric scatter coupling, and diffraction by airplanes.

Ground wave coupling was investigated experimentally, and was found to compare well with path loss predicted by the EPM73 model, provided a correction factor was included to take into account an additional propagation loss attributed to the forest surrounding the Nançay radiotelescope. For distances exceeding 3 km, this correction factor approximately takes on the value of 30dB. Such an additional factor can be explained by the larged attenuation for any propagation path inside the forest and the (qualitative) results given by a propagation model describing successive diffraction by the top of the trees. Our quantitative empirical data were used to design a Great Electromagnetic Screen (GES) to be built around the radiotelescope.

Atmospheric scatter coupling was only consider in two particular cases (assumed to be extreme cases) of tropospheric scatter : rain scatter and cloud scatter. Establishing the coupling value is not a common bistatic scattering problem because the very high gain of the radiotelescope (about 63 dB) brings the rain or the clouds in the near field of the radiotelescope antenna. We have therefore introduced a near-field aperture efficiency η_{pr} that includes the loss due to imperfect focussing of the spherical wave scattered by a water droplet. The power P_{rec} received by the radiotelescope receiver from a Mobsat mobile radiating the power P_{ant} with an antenna gain G_2 takes on the form :

$$P_{rec}(\theta_1,\varphi_1)=k^2 V_0 P_{ant} \int_{r_{1min}}^{r_{1max}} \frac{G_2(\theta_2,\varphi_2) f(\theta_1,\varphi_1,\theta_2,\varphi_2,\xi,\zeta)}{r_2^2} \left(\frac{r_1}{r_1+D}\right)^2 \eta_{pr}(r_1,\theta_1)\, dr_1 \qquad (1)$$

where k is the wave number, V_0 a volume characteristic of the cloud or rain, f an angular function describing polarization mismatch, r_1 the distance from the radiotelescope to the integration point, r_2 the distance from the Mobsat source to the integration point, and D an offset distance of the radiotelescope. The integration is carried out on the part of the radiotelescope antenna beam that falls into the rain or cloud. For a heavy rain, and a single 40 W Mobsat source connected to a low gain antenna (4 dB maximum gain) with circular polarization, we obtained for instance the computational result of figure 1, where the X-axis and Y-axis are the position in km of the source, with the radiotelescope at the origin, observing a source low on the horizon, to the south.

If one takes into account the assumed emission bandwidth of a Mobsat source (16,5 MHz) and the assumption of perfectly uniform power density in this bandwidth, the resulting typical noise of -123 dBm is equivalent to a noise temperature contribution of about 2 K, which adds to the radiotelescope system noise of 45 K. One may consider that

a radiotelescope is affected by interference when the received noise exceeds 10 % of its system noise fluctuations (CCIR 2/199-F report). This shows that there might be an interference if many sources are active during an observation.

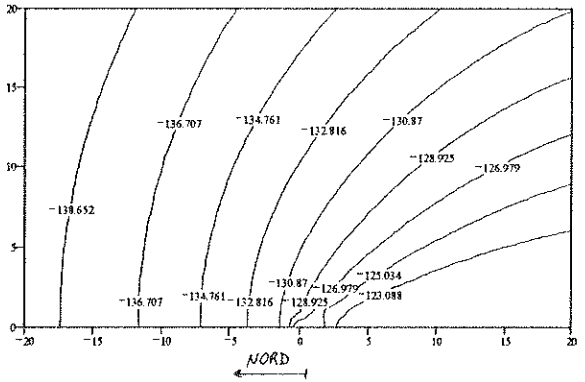

Fig. 1 Contour plot, showing the level in dBm delivered by the radiotelescope antenna, as a function of the Mobsat antenna position (in kilometer).

The problem of the scattering of the Mobsat emission by airplanes was more difficult to assess because we lacked data on the bistatic radar cross-section of the commercial airplanes found (quite high) in the sky of Nançay. We did two calculations with very simple assumption. The first was to use the bistatic radar cross-section formula :

$$P_{rec} \approx \sigma P_{ant} \frac{\lambda^2 G_1 G_2}{(4\pi)^3 r_1^2 r_2^2} \eta_{pr} \qquad (2)$$

with an arbitrary 100 m^2, typical of monostatic RCS data of such airplanes at those frequencies. An other was to assume a perfect specular reflexion which led us to :

$$P_{rec} = P_{ant} \frac{\lambda^2 G_1 G_2}{(4\pi)^2 (r_1 + r_2)^2} \eta_{pr} \eta_{refl} \qquad (3)$$

where η_{refl} is a reflexion efficiency. We then considered that the occurrence of an airplane inside the radiotelescope beam was too unlikely to be considered, and mostly focussed our interest on the occurence of an airplane on a sidelobe of the radiotelescope, with an assumed gain of 0 dBi. In this case, assuming $r_1 = r_2 = 20$ km, (2) gives a (negligible) noise temperature contribution of 3,8 mK at the radiotelescope antenna output, and (3) a noise temperature contribution of 48000 K in the case of $\eta_{refl} = 1$, a realistic hypothesis in most cases. Though (3) gives an enormous noise contribution, specular or near specular incidence might be an exceptional phenomenon. This, however is not *a priori* garantied, if one considers a reasonable source density of 0,1 km^{-2} and the length of standard radioastronomical measurements (defined as 2000 s in CCIR 2/199-F report).

Our conclusion is that more work is required, that should include the statistical distribution of sources and their activity, in order to establish the probability of interference between Mobsat and radioastronomy. Our preliminary study shows at least that there are many questions worth asking.

CONCEPTION OF CREATING A RADIOMONITORING SYSTEM

I.P. Kharchenko*,V.A. Solonnikov,E.M. Vinogradov
EEU, Popova 5, 197376, St. Petersburg, Russia.
Fax + 7 (812) 311-95-66

One of the most important problems in the EMC field is the problem of efficient spectrum utilization. The radio-monitoring service in National Communications coordinates frequency assignment and takes inspection of parameters for authorized stations. The main aim of those procedures is to keep satisfactory performance of communication links and prevent them from arising unintentional disturbances.

Based on analytic survey of papers and documents regarding radiomonitoring and modern point of view on this problem, a list of conceptual problems arising before the monitoring service and principles which may be used to complete measurement posts at monitoring stations are substantiated in the article.

Criteria chosen as conceptual ones are:

- economic self- repayment,
- step-by-step realization,
- orientation to national technologies and know-how.

Critical analysis of papers concerning the radiomonitoring problem indicates that they don't contain only partial information about such problems as

- the problem of emitting source identification through a signal spectrum portrait;
- the problem of finding the frequency of an interference source affected the receiver performance through spurious receiver channels;
- a set of measurements which is necessary and enough to reach radiomonitoring goals;
- the problem of creating radiomonitoring expert systems;
- correlation between volumes of problems being solved and material expenditure to realize them;
- self - repayment of investments for realization of radiomonitoring programmes.

In natural way formulated criteria determine five conceptual problems for monitoring stations. These problems are given in Fig. 1 in the order of their priority and with some steps of their solutions.

It is proposed a structure of measurement post that should be utilized to solve the problems mentioned. The post possesses some redundancy to keep its reliability.

The post has two test receivers of the same type tunable by frequency code and a personal computer, systems for matching, commutation and control of antennas and measuring devices, digital device to register interference sources, a FFT device and a series of common measurement devices.

Control, collection of information and information processing are made by terminals of the personal computer that, in many cases, may eliminate the spectrum analyzer and plotter.

Use of standard devices permits step -by - step realization of the post that does not demand extraordinary large financial investments.

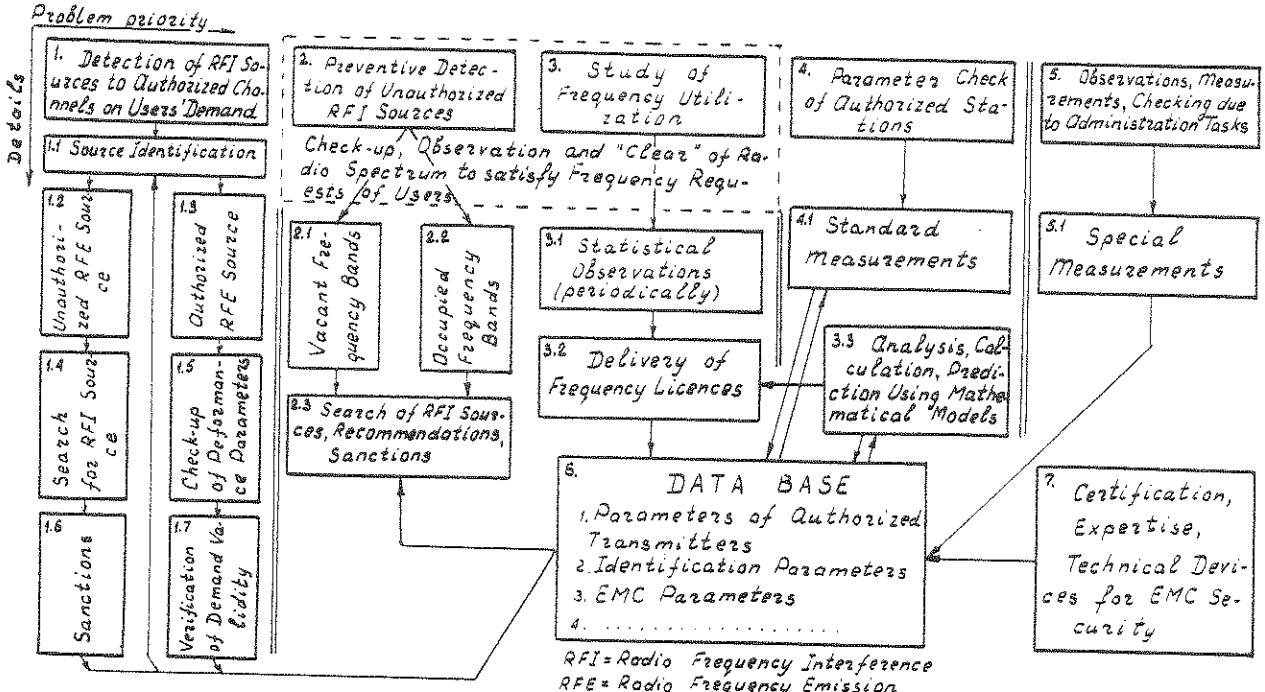

Fig. 1 Conceptual problems of radiomonitoring.

IMMUNITY OF CARDIAC PACEMAKERS AND RISK POTENTIAL OF PACEMAKER PATIENTS, WITH SPECIAL REGARD TO HIGH-POWER MEDIUM- AND SHORT-WAVE TRANSMITTERS

R. Coray *, Swiss Telecom PTT, Directorate Radiocom, CH 3030 Bern, Switzerland
H. Schaer, EMC Baden Ltd, CH 5405 Baden-Daettwil, Switzerland

A cardiac pacemaker's response to electromagnetic interference (EMI) is highly dependent on the pacemaker's mode and sensing polarity, as well as the characteristics of the EMI source. The latter can be classified as conducted currents or voltages and electric, magnetic or electromagnetic fields. Modern pacemakers may be assumed to be sufficiently immune in typical electromagnetic environments such as in households, within urban areas or at working places. In special industrial environments, however, pacemakers may be temporarily upset or even damaged under severe conditions.

Various complaints from the population located near to the Swiss PTT transmitters have exerted heavy pressure on the Swiss authorities to examine possible adverse health effects. These epidemiological studies, however, do not include aspects related to cardiac pacemakers. The Swiss Telecom PTT therefore decided to also investigate the pacemakers more closely.

The aim of this paper is to examine the susceptibility of pacemakers in a very broad frequency range (dc up to Gigahertz) and also to analyze the restrictions (limit values) given by the European standards. In particular the situation for Swiss medium and short-wave transmitters is evaluated, including a mapping of the near-fields around the antennas and an estimate of the possible risks for persons with a pacemaker (fig. 1).

Although obligatory European standards do not yet exist for the institutions operating such transmitters, the Swiss Telecom PTT has attempted to inform the population and has marked the high field areas around their medium and short-wave transmitters by using a caution sign according to DIN 40023 part 1, June 1987.
The conclusions of this paper are the following.

National standards or draft standards at present only cover the frequency range from 50 kHz to 50 MHz. Obligatory European standards do not yet exist.

Pacemaker manufacturers' data suggest susceptibility values in the range 50 ... 200 V/m for the medium- and short-wave region, whereas the limit values given by National standards may be as low as 3 ... 10 V/m.

The limit value used by the Swiss Telecom PTT for the caution sign took into account technical criteria (such as actual electromagnetic field values and manufacturers' pacemaker data), standards limit values (e.g. EN 50061) and also pragmatic considerations.

Low-frequency magnetic fields or voltages and currents must not be neglected as potential risk sources for persons with a pacemaker.

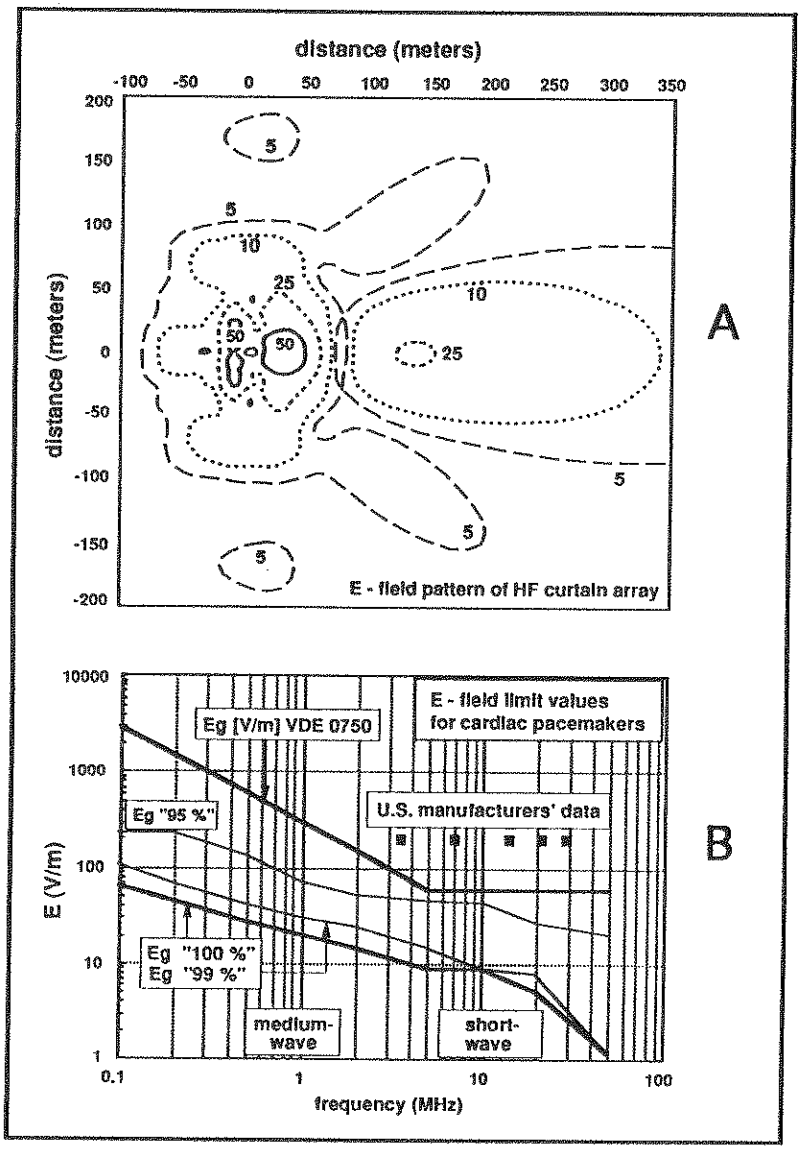

Figure 1. A: Electric field pattern 1.5 m above ground near to a HF curtain array operating at 12 MHz with 500 kW.

B: Electric field susceptibility values for cardiac pacemakers. Various values of European (national) standards and new U.S. manufacturers' data.

COMPARISON OF NEMP AND LIGHTNING VULNERABILITY TESTS ON AIRCRAFT

Maurice CANTALOUBE *Jean-Pierre CLERC

DGA / CEAT

23, Avenue Henri Guillaumet

31056 TOULOUSE - FRANCE

This paper analyses the main characteristics of the lightning impulse and the NEMP threating an aircraft; taking into account that the lightning characteristics are not yet completely determined. Although the coupling mechanism between NEMP or lightning and the aircraft is completely different (radiated electromagnetic wave vs injected current), the skin parameters (E_N and H_T) or even the short-circuit currents or open-circuit voltages on bundles inside the aircraft, can be compared.

	Lightning		NEMP/HA
	Waveform A	Waveform H	
Peak value	200 kA	10 kA	50 kV/m
Rate of rise	140 kA/µs	200 kA/µs	
Rise time	6.4 µs	100 ns	<10 ns
T 50%	70 µs	4 µs	<200 ns
Current	Constant for each section of the aircraft		Zero at the extremities
Resonances	Dependent on the arc impedence at the extremities		Close to 2L and 2L/3
Test generator	Connected to the aircraft- (injected current)		radiated or guided EM wave
Test set-up			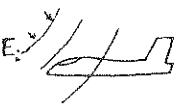
	Aircraft = central conductor of the coaxial return		Aircraft floating in the simulator

The NEMP test simulators are now able to duplicate rather well the electromagnetic aggression on the aircraft. The main resonances of the aircraft structure are obvious on the skin parameters and on the currents or voltages on bundles. The main wavelengths of the resonances are then closed to 2L and 2L/3, L being the length of the aircraft. [1]

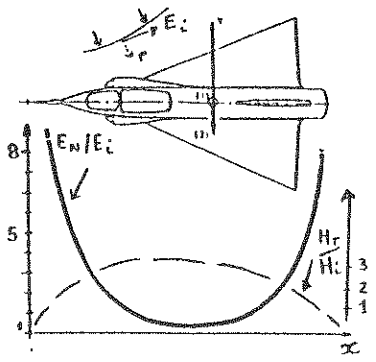

E and H fields along the fuselage (NEMP aggression)

Lightning impulse test generators need a return path. The usual way to make it, is to build a coaxial return path around the aircraft structure which becomes the central conductor. The coaxial return may be short-circuited or matched. In both cases, the set-up response is highly dependent on the generator characteristics, but short-circuited returns seem to create some resonances of the skin parameters or voltages on bundles. Unfortunately the wavelength of the resonance is closed to 4L and 4L/3.

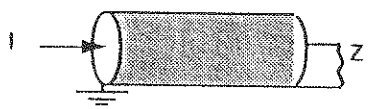

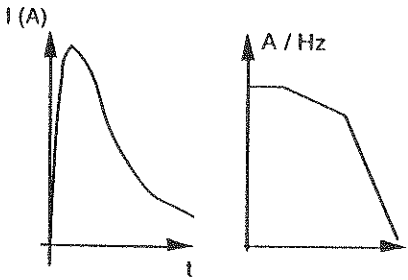

Short circuited coaxial return

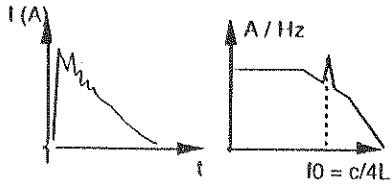

Matched coaxial return

The level of the short-circuit current on bundles is higher by a 6 dB factor in the short-circuit set-up than in the matched set-up for a metallic structure. In carbon structure, both set-up give almost the same peak levels but higher and non-oscillatory waveforms than in the metallic case.

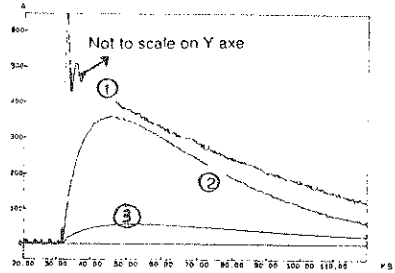

Induced currents on the same wire inside a metallic box (3), a carbon box (2), under an injected(1) current of 40 kA (D wave).

A better understanding of the internal coupling mechanism between the aircraft and the lightning arc could reduce the safety margins which are applied to the design of airborne equipements.

References

1 Principe de simulation des environnements E.M. : dominance E ou H résultant de l'interaction d'une IEMN avec une structure : C EG publication at ASTE LAB 90 by D NEGRET and PECQUEUX.

2 Influence on configuration effects on "multiple burst" simulation Testing. J.L. EMANUELLY, M CANTALOUBE - CEAT Report : ICOLSE 91 - USA -

THE EFFECTS OF LARGE STATIC MAGNETIC FIELDS UPON AIRCRAFT

By

Rodney A. Perala
ELECTRO MAGNETIC APPLICATIONS, INC.
7655 West Mississippi Avenue, Suite 300
Lakewood, CO 80226
Phone: 303-980-0070
Fax: 303-980-0836

Large low frequency or static magnetic fields may be created by pulse power circuits, electromagnetic guns, magnetic resonance imaging systems and electrical energy storage devices. The magnetic fields from energy storage devices, in particular, are of special significance because of their large spatial extent and long time duration. It is of interest to know what effects these fields have on nearby electronic systems.

The objective of this paper is to report the results of a preliminary study of the effects of large static magnetic fields produced by the Superconducting Magnetic Energy Storage -- Engineering Test Model (SMES-ETM) upon civil aircraft. The static fields from the SMES-ETM are quite large and extend great distances from the site; e.g., its magnetic field is the same size as the earth's background field (~.5 Gauss) at an altitude of 3300 feet, and is 160 Gauss at 500 feet, the legal flight altitude for fixed wing aircraft. An important fact is that there presently exists no standards, test methods, or qualification requirements regarding the certification of either civil or military aircraft to static magnetic fields. Therefore, the effects of these fields on aircraft must be fundamentally treated as unknown.

As part of an Environmental Impact Statement, however, the author performed an analysis of the expected magnetic field levels which may possibly cause problems for civil aircraft. The study was generic, in that potentially sensitive devices and components were identified, and a threshold magnetic field which may affect these devices and components was identified. The results are summarized in Table 1. The left column lists the items of concern which were studied. The rest of the table identifies the threshold magnetic field and the threshold spatial boundary. It is clear that expected effects could occur well above minimum legal flight altitudes for fixed wing aircraft (500 feet, VFR), and the situation is even worse for rotorcraft, which theoretically could legally fly more closely to the site.

It should be noted that even though Table 1 indicates possible effects, there is no experimental data indicating that the effects really will happen. In addition, even if these devices and components are affected, one cannot presently say that these effects actually adversely affect aircraft flight safety.

In this paper, the methods of aircraft certification to electromagnetic effects are described, and applied to the static magnetic field environment. The approach to evaluating the effects upon possibly vulnerable critical systems as given in the table are summarized. Recommendations for future technical investigations are given.

Table 1

Summary of Possible Effects with Corresponding Aircraft Component Effects Threshold Boundaries

Item of Concern	Aircraft Component Effects Threshold Boundary		
	Magnetic Field Level, Gauss	Altitude ft	Radius Statute Miles
1. Motion Induced Voltages		No Concern	
2. Energy Dump Voltages		No Concern	
3. CRT for 1 cm Deflection	5 Assumes 20 dB magnetic field shielding	1550	0.25
4. Hall Effect Switches	100	530	0.08
5. Magnetization of Steel	50	690	0.12
6. Relays	8	1324	0.20
7. Bubble Memory	20	980	0.17
8. Magnetic Media	75 (for 10% signal loss)	600	0.10
9. Compass Errors Inflight, 2° Worst Case Location	0.020	11,000	2.10
10. Compass Errors Approach, .5°	0.005	17,500	3.33
11. Compass Errors Calibration	0.0006	N/A	5.0

LIGHTNING INDUCED CURRENT EVALUATION APPLICATION TO A FIGHTER AIRCRAFT

I. JUNQUA* – R. POUZALGUES
D. SERAFIN
Centre d'Etudes de Gramat
46500 GRAMAT

Because of the extensive use of composite materials and digital electronic, current aircrafts are more and more sensitive to high frequency lightning electromagnetic threat. In-flight campaign measurements revealed lightning currents whose frequency spectrum content, significant up to a few tens of MegaHertz, could be damageable for the equipments inside an aircraft.

In order to evaluate high-frequency lightning induced currents on the inner cable network, the "Centre d'Etudes de Gramat" (C.E.G) develops a study program on a fighter aircraft real scale model, fitted out with its real harness running inside the aircraft and connected to "false" equipment, constituted of 2 outputs (hot point and cold point).

In this context, a simulator (PARSIFAL), based upon a coaxial return path technique, has been designed. This simulator is driven by a generator, delivering a current whose frequency spectrum content is similar to the one observed during in-flight experimental campaign. The comparison of electromagnetic fields mappings on the aircraft skin, obtained , first, experimentally under the simulator, and, secondly, numerically by means of a 3D code (GORF) in-flight lightning simulation and a transfer function concept, proves the potentiality of this real scale simulator.

This simulator reproducing correctly the electromagnetic environment on the aircraft skin, the coupling of the electromagnetic perturbation on the inner "false" equipment is analysed. During normalized qualification process, induced perturbations on the equipment are expressed in terms of open-circuit voltages and short-circuit currents in common and in differential modes. Nevertheless, direct measurements of differential voltages and of currents are uneasy in high frequency, since the metrology commonly used is not fitted to this kind of application.

To overcome this experimental limitation, a method, based upon a generalized Thevenin model, is developed. The system, seen from any equipment, is considered as a "black box" which is completely characterized by its repartition [S] parameters. The Thevenin impedance [Zth] can be, then, derived from the expression of these [S] parameters, easily measured by means of a network analyser, as follows:

$$[\,Zth\,(f)\,] = 50\,.\,[\,1 - S\,(f)\,]^{-1}.\,[\,1 + S\,(f)\,]$$

When the aircraft is submitted to an electromagnetic perturbation, induced open-circuit voltages on any equipment represent the equivalent Thevenin generator and can be directly related to voltages measured in time domain on the equipment loaded with 50 Ohm by the following expression:

$$[\,Eth\,(f)\,] = [\,1 - Zth\,(f)\,/\,50\,]\,.\,[\,V_{50}\,(f)\,]$$

From the definition of Thevenin model, voltages and currents at both output of any equipment are defined as:

$$[\,V\,(f)\,] = [\,Zth\,(f)\,]\,.\,[\,I\,(f)\,] + [\,Eth\,(f)\,]$$

Open-circuit voltages and short-circuit currents in common and differential mode are, then, derived from the previous equation.

The normalized high frequency lightning current, elementary pulse of a multi-burst, is defined as an ideal current generator having the following characteristics:

– Magnitude = 10.572 kA
– Rise time (10% to 90%) = 100ns
– Pulse width = 4 µs

In the coaxial return path simulator, the current existing at the nose of the aircraft can not be likened to the normalised high frequency lightning current, since the generator is not ideal. This measured current depends on the total impedance of the aircraft and on the internal impedance of the generator. The significant parameters (open–circuit voltages and short–circuit currents), deduced from measurements, responses to the current at the aircraft nose under the simulator, are normalised to the elementary pulse of a multi–burst:

$$[\, V_{Norm}(f) \,] = [\, V_{simulator}(f) \,] \,.\, [\, I_{multi\text{-}burst}(f) \,] \,/\, [\, I_{simulator}(f) \,]$$

The previous procedure enables the determination of induced signals, during an in–flight lightning and is applied to numerous equipment for a statistical approach. Indeed, any signal in time domain can be expressed as a infinite sum of damped sines. In order to analyse the whole set of datas, the characteristics (frequency, joined magnitude and quality factor) of the 5 most significant terms of the infinite sum and the magnitude in time domain are extracted from each signal. The process of the data base, constituted of these characteristics, underscores 2 main areas on the aircraft and a dominant frequency relative to the aircraft resonance ($\lambda / 2$).

Various examples will illustrate the different steps of this procedure while the communication. This program enables the validation of a whole optimized procedure applied to the evaluation of induced signals during an in–flight lightning and can be generalised to any kind of system, submitted to an electromagnetic perturbation.

This work is supported by the "Direction des Recherches, Etudes et Techniques" (D.R.E.T).

HIRF-TESTING OF THE SAAB 2000 AND THE JAS39 GRIPEN AIRCRAFT

H. Frennberg*, T. Martin, M. Eriksson, M. Bäckström, B. Wahlgren*
Environmental Engineering, Saab Military Aircraft,
Linköping, Sweden

In the certification process of a modern aircraft, civil or military, more emphasis has been put on the immunity to High Intensity Radiated Fields (HIRF). The route to compliance includes numerical analyses, equipment/system testing, testing of whole aircraft at full threat levels and coupling measurements at low levels. This paper summarizes the whole aircraft testing performed in order to show compliance with the HIRF requirements for the Saab 2000 commuter aircraft and JAS39 Gripen military fighter aircraft.

Since the HIRF requirements cover the frequency spectrum from a few kHz to tens of GHz, it was judged necessary to use different test and verification methods in different parts of the frequency range. Both coupling measurements and high level testing have been used. The aim of the coupling measurements was to show that the external fields do not induce cable bundle currents that are higher than the current levels achived at the equipment/system tests. At higher frequencies fields in equipment bays were measured instead of currents. High level testing was performed on a fully operational aircraft with the relevant functions continuously monitored.

Numerical analyses have been performed to verify requirements regarding equipment test levels and also for development and support of whole aircraft test methods. A three dimensional Finite Difference Time Domain code (FDTD) was used for the main part of this work.

For frequencies below 400 MHz a method called Low Level Swept Coupling (LLSC) was used to determine the coupling between external fields and cable bundle currents. Where necessary, break-out boxes were used when measuring the currents. At lower frequencies, typically below a few MHz, the generation of high quality excitation fields becomes difficult. This can be solved either by specially designed antennas or by using a different test procedure, Low Level Direct Drive (LLDD). Presuming that magnetic coupling is dominant in this frequency region, it is sufficient to produce relevant surface currents at important points of entry. This can be accomplished by direct injection of current into the airframe.

On the Saab 2000 aircraft LLDD was performed using two different test setups in order to expose cable bundles and equipment boxes belonging to critical systems such as the elecrical flight control system and the Full Authority Digital Engine Control system (FADEC). The test configurations consisted of ten return conductors positioned around the aircraft connecting the signal generator to the exit point (tail or propeller spinner).

LLSC measurements were performed illuminating the aircraft from all four sides with a uniform swept RF field. Prior to the measurements the field at the aircraft location was measured for normalization purpose. Both horizontal and vertical polarization was used.

Both the LLSC and the LLDD measurements were supported by extensive numerical analyses of the test setups and their ability to reproduce in-flight conditions. The modelling was done using an FDTD code where in-flight illumination from above, from below and from all four sides were simulated. Two different polarizations were used in all directions. The two LLDD test set-ups were also modelled. Surface currents from the analyses were then used to form a generic injection current corresponding to the worst case of free flight illumination at a specified fieldstrength.

During LLSC, surface currents were measured at several locations on the aircraft. The corresponding information was also extracted from the modelling. The ratio beween the surface currents measured on the ground and those calculated in free flight was used to create a compensation factor. This compensates for effects such as ground reflections, near field effects and the fact that the aircraft were only illuminated from four directions during the LLSC measurements.

An example of the consistency of the LLDD and LLSC methods is shown in figure 1 where measured current on a cable bundle, normalized to 1 V/m external electric fieldstrength, is presented. The solid line shows results obtained by the LLSC method and the dashed line results from LLDD measurements.

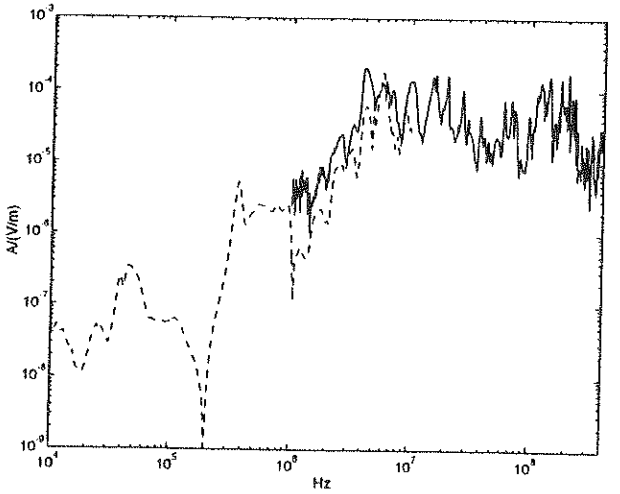

Figure 1. Current on a typical cable bundle. LLSC solid. LLDD dashed.

Above 400 MHz both Low Level Swept Field (LLSF) measurements and high level testing were performed. During the LLSF measurements the relation between the external electric field and the electric field inside avionic bays were determined. High level testing was done at five discrete frequencies in the L, S, C, X and Ku band respectively, using the Microwave Test Facility (MTF) at Saab. Peak field strengths reaching tens of kV/m can be achieved at a distance of 15 m. The aircraft were illuminated from several different angles of incidence and with both horizontal and vertical polarization. During exposure the direction of the antennas was varied slightly to avoid the influence of local minima in the coupling between external field and equipment.

E-6A HARDNESS ASSURANCE, MAINTENANCE AND SURVEILLANCE PROGRAM

William DePasquale and Bernd Lubosch
DUAL Incorporated
745C Great Mills Road
Lexington Park, Maryland USA 20653
Telephone (301) 737-2784 Fax (301) 862-5043

Joel Haines and Mark Mallory
Naval Air Warfare Center Aircraft Division
Code: SY84
Patuxent River, Maryland, USA 20670-5304
Telephone (301) 826-3872 Fax (301) 862-3786

The challenge facing aircraft program managers and the Fleet is to ensure that the electromagnetic hardness of design is maintained throughout the aircraft life cycle. The electromagnetic pulse community must work closely with aircraft program managers and aircraft design contractors to properly integrate the logistics elements necessary to accomplish this effort. This process must begin early in the acquisition phase and be dynamic enough to evolve as changes in life cycle mission requirements occur.

This paper identifies the Hardness Assurance, Maintenance and Surveillance Program for the U. S. Navy's E-6A aircraft. The program includes various test techniques that are used to monitor aircraft hardness integrity and maintenance procedures to direct the hardness critical process. A database was also developed which integrates all test and maintenance data to aid aircraft hardness surveillance.

The E-6A Hardness Assurance, Maintenance and Surveillance Program was developed to meet the needs of the TACAMO Fleet and serves as a model for the U.S. Department of Defense.

FIELD CONFIGURATION OF BEAM EXCITED MODES IN THE ADVANCED PHOTON SOURCE (APS) STORAGE RING WAVEGUIDES*

S.O. Brauer[†], R.L. Kustom, P.L.E. Uslenghi
Advanced Photon Source
Argonne National Laboratory
9700 S. Cass Ave, Argonne, IL 60439, USA

The RF system for the Advanced Photon Source (APS) storage ring uses 16 cylindrical Tm010-like, reentrant cavities operating at 351.93 MHz to resupply energy lost by the beam due to synchrotron radiation. The stored beam will have approximately 60 bunches, 5 mA per bunch, for a total beam current of 300 mA. Calculations of the threshold current for coupled-bunch instabilities in the storage ring have indicated that several beam-induced higher-order modes (HOM) will reduce the threshold for beam stability and therefore should be damped. The twelve HOMs of concern are listed in Table 1. Some of these modes couple, through the coupling loop, from the storage ring cavity into the waveguide. This study investigates the electric and magnetic field configuration of each HOM present in the waveguide. A pillbox cavity and a prototype storage ring cavity, together with various WR2300 waveguide components, are used to obtain the measurements needed for the determination of the mode configuration of the HOMs at the frequencies of interest. To avoid the development of beam instabilities due to the existence of these HOMs in the rf cavity, damping of the modes will be required. The possibility of the HOMs present in the rf cavity coupling into the loop coupler and traveling through the coupler into the waveguide, may allow damping of some of the HOMs by the insertion of dampers into the waveguide adjacent to each cavity.

Using a prototype single-cell rf cavity, verification of the HOMs' field configuration in the cavity was done by performing a bead-pull measurement which is based on perturbation theory. Measurements were performed at the frequencies of interest in the experimental setup shown in Figure 1.

Out of the twelve HOMs, two frequencies (585.763 and 1144.108 MHz) were not found in the waveguide. Three additional frequencies (538.548, 1021.275, and 1232.375 MHz) were found but the strength of the measured E-field was lower than expected. These results may be due to the construction of the prototype cavity, which was copper-plated stainless steel. Additional measurements are being taken with an all-copper prototype single-cell cavity to further verify the data. Previous measurements taken using an aluminum pillbox cavity did show that four out of five of these frequencies were found in the waveguide.

The seven remaining frequencies were found in the waveguide. E-field was measured on both the broad-wall and side-wall of the waveguide as shown in Figures 2 through 5. These data indicate that these modes may be damped by using a simple antenna placed inside the waveguide through the side-wall of the guide. The measurements also show that an H-loop damper positioned on the broad-wall may also damp five of the seven modes. Both dampers, the side-wall antenna, and a prototype H-loop damper for the broad-wall are being tested.

*Work supported by U.S. Department of Energy, Office of Basic Energy Sciences under Contract NO. W-31-109-ENG-38.

Table 1

Longitudinal Modes (Monopoles)		Transverse Modes (Dipoles)	
freq HOM (MHz)	Ithresh (mA)	freq HOM (MHz)	Ithresh (mA)
336.7	80	588.7	80
922.5	130	761.1	43
939.0	340	962.0	190
1173.2	340	1017.4	435
1210.8	130	1145.1	410
1509.1	130	1219.2	315

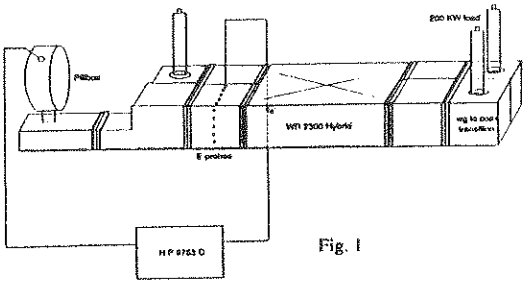

Fig. 1

Fig. 2

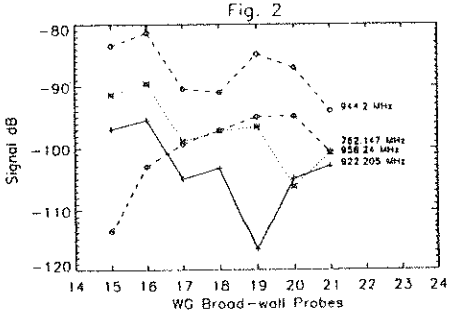

Fig. 3

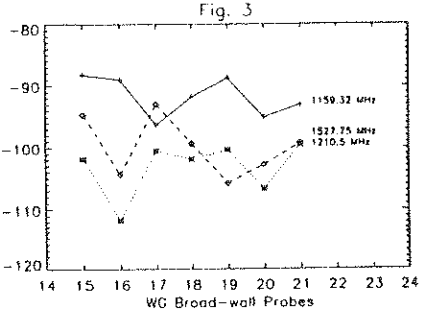

Fig. 4

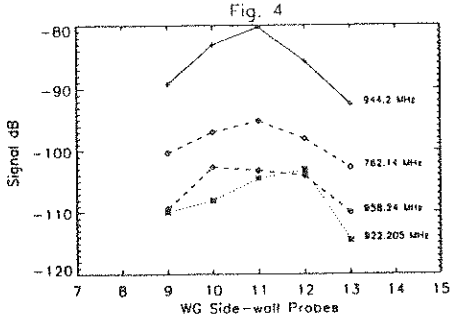

Fig. 5

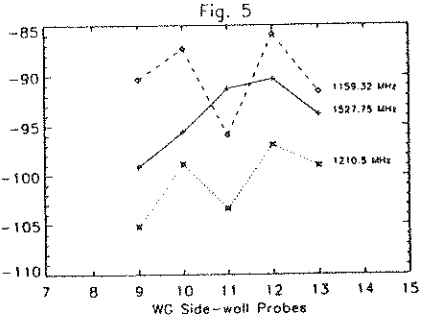

TR CELL CHARACTERISTICS AT HIGH RATE OF RISE OF INCIDENT POWER

Dr David Mellor
Mr P Hackney*

EEV
Carholme Road
Lincoln
LN1 1SF

In conventional gas filled TR cells, a knowledge of the spike leakage from the device and its effect on radar system front end components is essential to allow the design of reliable systems. Many studies of this have been undertaken, however, little attention has been given to the effect of varying the rate of rise of the incident power pulse. In this work the effect of short bursts of pulses having enhanced rise time on the protection capability of gas filled TR cells is reported.

Initially the paper describes techniques used to generate 50KWp X band pulses having a risetime of the order of 1us.

Two types of gas filled X band TR cells have been studied, one containing a conventional DC primer and the other a primerless TR limiter. A qualitative understanding for the results obtained is also included.

Other results are presented for the change of characteristics of both balanced mixers and low noise amplifiers when subject to spike leakage pulses resulting from high rate of rise inputs.

HIGH POWER MICROWAVE EFFECTS ON LOW NOISE HEMTS & MESFETS

D. Lazaro* [1,2], J.C. Mollier[1,2], A. Roizes[1]

[1]: ONERA CERT/DERMO
2, Avenue E. Belin 31055 TOULOUSE CEDEX
[2]: ENSAE
10, Avenue E. Belin 31055 TOULOUSE CEDEX

1. INTRODUCTION

Among the different technologies of low noise Field Effect Transistors, performances of HEMT devices make them attractive for use in radar front end low noise amplifiers. However data from some manufacturers could suggest that HEMTs may be more sensitive than conventional GaAs FETs. This paper describes experimental test of failure from H.P.M. on commercially available HEMTs and MESFETs operating in common source configuration and low-noise biasing conditions. Three steps of failure depending on microwave power and energy level have been observed and found quite different for the various transistors technologies investigated : low level effect, gradual and catastrophic failures.

2. EXPERIMENTAL SETUP AND PROCEDURE

The experimental setup shown in figure 1 allows to overstress and to characterize the device under test. The S-band magnetron is capable of generating up to 200 W of pulsed RF power. Repetition rate of the pulses can be ajusted as well as their time width (over 10 ns). During the pulse, incident, reflected and transmitted powers as well as drain and gate currents shifts are stored. Before or following the pulse, either DC-characteristics or scattering parameters [S_{ij}] of the FET can be measured. A first step gives an order of magnitude of the failure peak power (Table I) by increasing the incident power level of a 100ns pulse until the device fails. Then an other device from the same lot is submitted to a 100 ns single pulse which peak power level is lower than the failure peak power. This test procedure is repeated keeping the incident power level constant until the FET is degraded.

3. FAILURE ANALYSIS

3.1. Low level effects

The non-linear behaviour of the Schottky diode during the RF pulse induces a high DC forward current in the gate. Deep levels in depletion region can capture electrons and lead to a decrease ΔIds of the drain current just after the end of the RF pulse. Then the total charge is recovered with a time constant τ (V.V. Antipin, V.A. Godovitsyn, etc., Scripta Technica, 66-68, 1992). The drain current shifts and recovery time constants are listed in table I for all the tested samples.

3.2. Gradual failure

Gradual failure has only been observed with HEMTS (H1 & H2) . After a longer delay than the low level recovery time, the drain current is not completely restored. The output DC-characteristics Ids(Vds,Vgs) are slightly shifted down (Fig. 2) and the intrinsinc gain S_{21} decreases while the cumulated energy increases (Fig. 3 - Gradual Failure).

3.3. Catastrophic failure

Catastrophic failure always occurs suddenly without any forewarnings for all tested samples. The intrinsic gain S_{21} falls down to 0 dB and the gate current increases to a few milliamps at the bias point. The channel cannot be pinched after the stress because the voltage breakdown is shifted near the pinch-off voltage.

3.4. Annealing effects

After catastrophic failure, two kinds of recovery effects are observed for all sets of components except for M1 transistors :

3.4.1 Spontaneous recovery (right part in Fig.3)

The still biased component recovers naturally a fraction of the lost gain S_{21} and at the same time the gate current falls to a few microamps. It can be noticed that the time constant is of the same order of magnitude as the one observed at low level.

3.4.2 Electronic stimulation

According to the components, a forward or reverse continuous polarisation allows to recover a part of the missing gain S_{21} (H1 & H2) and the microamps gate current (H3). Similar effects can be observed on the M2 sample, after a reverse diode Schottky characterisation by impulsions.

4. CONCLUSION

Table I shows the difference of behaviour between HEMTs and MESFETs, especially regarding the high time constants associated with gradual degradation of H1 and H2 samples. Although annealing effects exist, the FET's structure seems to be deeply alterated by HPM effects. Effectively, the new failure peak power has decreased by 20 or 30 dB.

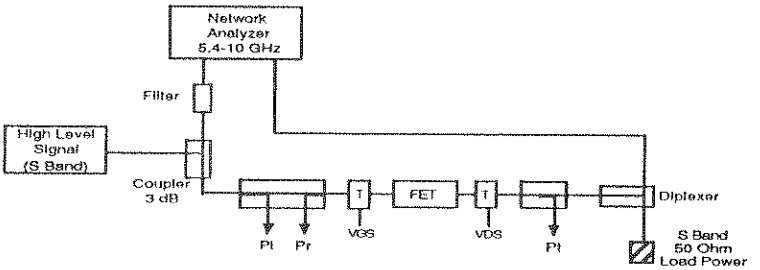

Figure 1: Experimental Setup

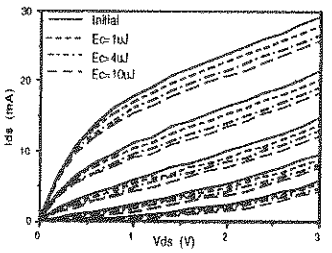

Figure 2: Gradual Degradation of Ids(Vds)

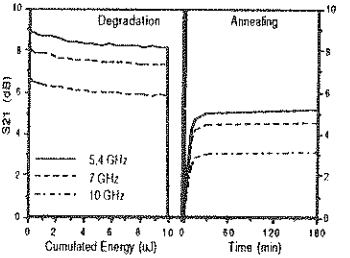

Figure 3: Degradation & Annealing of S_{21}

Table I: Tested Transistors Synthesis

Samples	Gate Structure	Low-Level Effects (τ/ΔIds)	Gradual Degradation	Peak Power Degradation	Annealing Effects
M1 MBE	Π	0.5s/0.9mA	no	3 to 10 W	/
M2 MBE	T	40s/0.08mA	no	30 W	Electronic Stimulation
H1 MBE	Π	80min/0.8mA	yes	2.5 W	Spontaneous+ Stimulation
H2 MBE	Π	90min/0.3mA	yes	8 W	Spontaneous+ Stimulation
H3 MOCVD	Π	2s/0.4mA	no	4 to 5 W	Continuous Polarisation

We would like to thank the Centre d'Etudes de Gramat for helping and supporting during this study.

PERSPECTIVES OF APPLICATION OF HIGH POWER MICROWAVE IN AIRCRAFT MATERIAL RESEARCH.

A.N.Didenko*, V.A.Shulov, A.S.Sulakshin, A,S.Nochovnaya.

Russian Academy of Science, 117334, Moscow, Russia

It was shown that not only electron and ion beams but also high power microwave (HPM) can change mechanical propertits of materials.

HPM have many advantages in comparison with influence particle beams on materials. The purpose of report is to investigate influence of HPM on heat strength titanium alloys VT18 and VT8M waidely spread in aircraft generator bilding.

Microhardness, roughness, fatigue strength, thermal resistrance of salt corrosion was stadied with using of the various physical methods (Auger-spectroscopy, X-ray diffraction, electron microscopy, optical metallografy and other) before and after influence of HPM. It was shown that above characteristics sufficiently improved after HPM influence that means that HPM can have great interest for various technological applications.

HIGH POWER MICROWAVE PULSES GENERATION FROM VIRCATOR WITH INDUCTIVE STORAGE

K.V.Gorbachev, A.N.Didenko, A.B.Ivanov, E.V.Nesterov, V.A.Stroganov, V.P.Tarakanov, V.E.Fortov, E.V.Chernykh, V.P.Shumilin
Russian Academy of Science, High Energy Density Research Center, Moscow, Russia, e-mail:frt@hedrc.msk.su

The high power microwave generation is strongly connected with problems of the high current relativistic electron beams accelerators. The main physical volume of such accelerators are: energy storages and electrical pulse formation systems. Quasistationary electromagnetic energy accumulation is possible by using either electric or magnetic fields. The utmost energy density storaged in the magnetic field can be substantially(by 3 or 4 orders) higher than that in the electric field. In the modern capacitors this utmost magnitudes can be up 10^6 V/cm; i.e.energy densities about 0.1 J/ccm. The utmost magnetic fields can be up to 5*10^5 Oe, i.e. energy density about 1000 J/ccm.

Most microwave generation carried out the capasitors bank and forming lines are used. But the inductive storage using makes possible to simplify substantially scheme and decrease bulk of accelerator. However, to realise these advantages one needs using of the some current opening swithes. When working with the inductive storage it is enough in the quasistationary regime to provide the neccesery current in the inductace and then to disrupt it sharply. When using exploding wires opening swiches as disrupter, for example, it can provide load voltage increasing with regard to initial one up to ten times. To realize these advanges one needes using of primary energy source with adequate densities characteristics. Magnetic flux compressor may be used as that source(Brodkij A.Ya., Vdovin V.A.,et.al.,Dokl.Acad.Nauk USSR, v.314,No.4,846-849,1990, Azarkevich E.I., Didenko A.N.,et.al.-Microwave pulses >from chemical energy of high explosive. Preprint, Chernogolovka,1992). However , it is one short device. For this reason the investigation of the problem of coordination between the inductive storage and the microwave generator must be produced by imitator of magnetic flux compressor - pulse current generator.

The succesful decision of the problem of the coordination between inductive storage and the microwave generator should bring to the creation of the compact powerful systems with record parameters produced under the laboratory conditions.

USING LOW LEVEL CW ILLUMINATION TO PREDICT HIGH POWER MICROWAVE EFFECTS

Clayborne D. Taylor, Stephen L. Langdon, and Samuel J. Gutierrez
Phillips Laboratory (AFMC), PL/WSME
Kirtland AFB, NM 87117-6008

ABSTRACT

Determining the effects on systems from high power microwave (HPM) illumination is not a simple procedure. Nonlinear and irreversible processes may occur that depend upon the peak field strength, the incident fluence, the incident power density, or perhaps a combination of factors. Reproducing these effects and identifying the coupling mechanisms may be very difficult and prohibitive in terms of the cost and the time required. It has been shown that these problems can be overcome through low-level continuous wave (CW) illumination and high-level direct drive application. Data are provided for a generic test-bed aircraft to illustrate the application of the presented techniques.

By exposing a system to low-level CW illumination, it is possible to identify electromagnetic coupling paths and to establish the relative importance of the various coupling mechanisms for large systems. Supplementing these results with high-level direct drive applications will allow the exercise and study of nonlinear effects. Low-level CW studies can be performed with relatively few personnel, with relative little danger to personnel, and with a relatively small investment in equipment and facilities when compared to full scale studies using high-level or threat exposures.

The expected effects resulting from illumination with a narrow band HPM source can be obtained by the appropriate scaling of the low-level responses. For completeness in some cases it may be necessary to implement direct drive excitations at levels determined by the scaled low-level responses. When the illumination is from a wideband or ultra wideband source, the response of the system can be determined via Fourier frequency superposition utilizing Fourier transform applications. These computed responses can be used to establish the appropriate pulse excitation to be emulated in the direct-drive applications.

Generally the HPM illumination may come from a variety of sources, deliberate and inadvertent. Consequently the low-level CW illuminator may have a variety of polarization and incident angle requirements. Often these may be satisfied by using one of two illuminator configurations - the rhombic nonuniform transmission line illuminator and the impedance loaded elliptical loop illuminator. The rhombic transmission line configuration can provide horizontal propagation with a vertical electric field and a horizontal magnetic field or horizontal propagation with a vertical magnetic field and a horizontal electric field. The impedance loaded loop illuminator can provide vertical propagation with horizontal electric and magnetic fields. By using the freedom of orientation of the system under illumination a veritable infinity of illumination scenarios are available where the illumination field is nearly uniform over the target. Moreover the frequency range of the illumination can be varied

from dc to a few GHz.

A typical measurement performed in the Rhombic illuminator uses an automatic network analyzer to drive the antenna as shown in Figure 1.

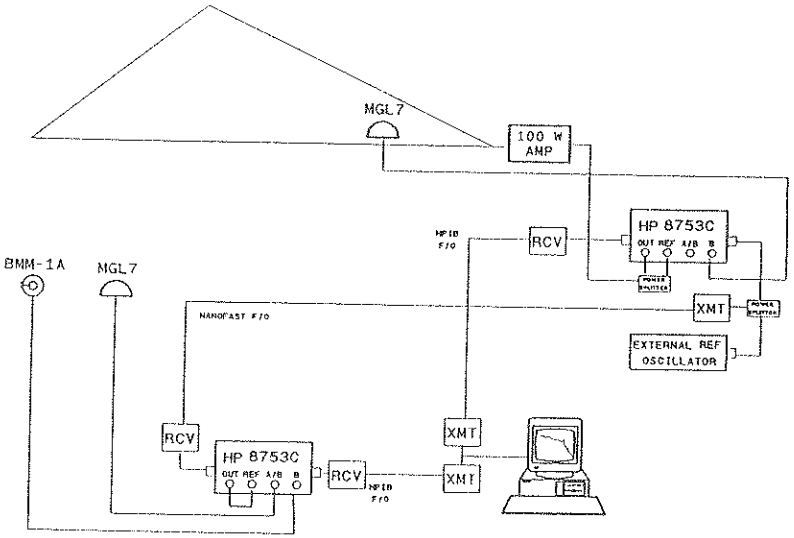

Figure 1. A Schematic of the Instrumentation for Measurements in the Rhombic Illuminator.

Here an HP 8753C is used to drive the rhombic array through a 100W wideband amplifier. A second analyzer may be located in a screen box inside the system under illumination or a safe distance away. Fiber optic data links are used to connect and synchronize the network analyzers as well as to provide the connection to the computer controlling the instrumentation. Included in Figure 1 are three sensors, a high frequency current probe and two magnetic field sensors. One magnetic field sensor is located in the launch section of the rhombic transmission line illuminator. Its response is directly proportional to the time derivative to the magnetic field incident on the system under study. A simple field mapping exercise can quantitate that relationship as well as determine the variation of the incident field over the system under illumination. Consequently the internal measurements recorded by the other two sensors can be used to obtain the transfer functions relating internal responses to the illumination field.

Measurements are performed with the elliptical loop illuminator using basically the same instrumentation setup as shown in Figure 1. The reference sensor located in the launch region of the rhombic is replaced by a sensor installed on the ground plane at a convenient location when the elliptical loop illuminator is used.

Using Low Level CW Testing in the Development of An Integrated Approach to Aircraft testing

CARTER N.J.

DEFENCE RESEARCH AGENCY

UNITED KINGDOM

With the rapidly increasing costs in applying an Electromagnetic Hazard Protection requirement to aircraft, there is considerable effort to Integrate all aspects of the requirement to reduce costs both in design and test. This paper gives an overview of the UK work in this area with special reference made to the application of low level frequency domain coupling measurements in generating an integrated threat response of a vehicle.

ANALYSIS OF SITE ATTENUATION
-In case of Vertical Polarization-

Haruo KAWAKAMI* and Gentei SATO
(Laboratory, Antenna Giken Co.,LTD.)

1. Introduction

In our previous paper ([1]), we discussed the characteristics of site attenuation on an infinitely large reflector and also on finite reflectors. By using the Sommerfeld formula for vertical polarization ([2]). We calculated theoretical site attenuation levels on dry soil with the application of the moment method compared the result with the data calculated for an infinitely reflector and for free space, and made a comparative examination between the theoretical levels and experiment data.

2. In the case of an antenna on dry ground earth

We analyzed the effect of reflected waves for a linear antenna existing on dry ground earth (Figure 1) by using the Sommerfeld formula. When the flat ground is assumed to be the X-Y plane and a linear antenna is placed at (x', y', z'), the vertical Hertz vectors Π_z are expressed as follows:

$$\Pi_z = \Pi_z^{direct} + \Pi_z^{reff}$$

where:

$$\Pi_z^{direct} = P\frac{e^{-jk_1R_1}}{R_1}$$

$$\Pi_z^{reff} = P\left[\frac{e^{-jk_1R_2}}{R_2} + 2\varepsilon\int_0^\infty \varepsilon \frac{J_0(\lambda\rho)e^{-\sqrt{\lambda^2-k_1^2}(z+z')}}{\sqrt{\lambda^2-k_1^2}+\sqrt{\lambda^2-k_2^2}}\lambda d\lambda\right]$$

3. Results of computation

We calculated the theoretical site attenuation level of vertical polarization for an assumed site where the transmitting and receiving antennas are on an infinitely large reflector and also on dry ground earth. Figure 2 (a) to (d) show the height patterns of site attenuation with respect to changes in the receiving antenna height h2 and Figure 3 gives the frequency characteristics. For comparison purposes, we also included the values calculated by assuming that the transmitting and receiving antennas exist in free space.

4. Conclusion

Our data showed that in the case of vertical polarization, the amount of site attenuation was close to the level calculated by assuming that the transmitting and receiving antennas exist in free space, proving that the influence of reflected waves is small in a wide range of frequencies.

We plan to examine cases of horizontal polarization with finite reflectors placed on the ground .

Reference:
(1)Gyoda,K., Kawakami,H. & Sato,G.:IEICE,J74-B-II,11,616-623,1991 (in Japanese).
(2)Sommerfeld,A.:"PARTIAL DIFFERENTIAL EQUATIONS IN PHYSICS", Academic Press,N.Y.1964.

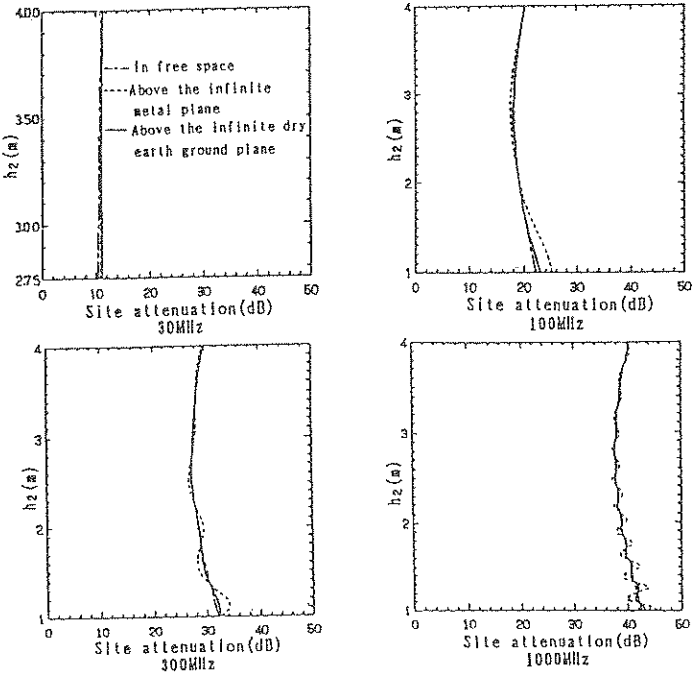

Fig. 2 Height pattern of site attenuation. (in case of vertical polarization)

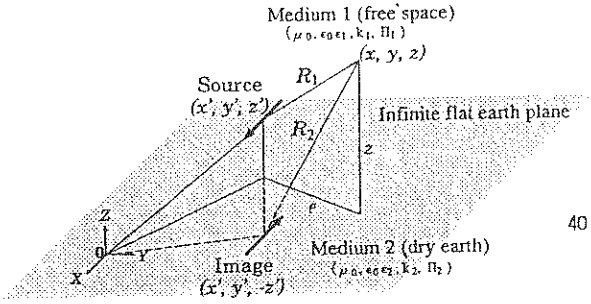

Fig.1 Hertz vector and its coordinate system

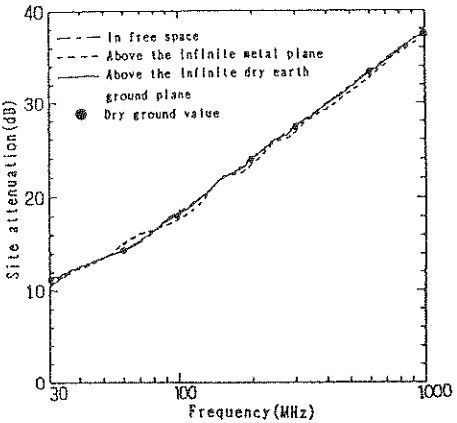

Fig. 3 Frequency characteristics of site attenuation. (in case of vertical polarization)

CORRELATION BETWEEN SPECTRAL ATTENUATION DATA OF SHELTERS OBTAINED WITH A NEW FAST EMP-SIMULATOR AND FROM CONTINUOUS WAVE EXPERIMENTS (MIL-STD 285)

* G.J.J. Remkes, A. Kranghand
Fokker Special Products b.v.
Edisonstraat 1, 7903 AN Hoogeveen,
the Netherlands

1. Introduction

EMP-simulators add information to CW-experiments in that the combined effect of cable coupling and EM-field exposure can be tested experimentally. Current CW-attenuation values guarantee that the maximum field inside the shelter does not exceed a critical value when exposed to a simulated EMP. However, in a few aspects simulator testing is quite different from CW-experiments. For example Mil-Std-285 measurements yield considerable more local information about the shielding performance of enclosures than simulator experiments do. Furthermore, the source field is 'plane wave like' in a simulator whereas it is of the near field type, E- or H- field in the continuous wave experiments (below 100 MHz). Thus an answer is wanted to the question: "In which respects is the spectral transmission function of shelters as observed with simulator experiments different from what can be deduced from CW-experiments". A first step to answer this question are the comparative observations on a empty shelter as we performed them.

Our observations add important new information because the simulator tests were performed with the upgraded EMP-simulator EMIS 3. This simulator has especially been designed to meet the new NATO requirements. The test object is a new type Fokker N-EMP shelter. However, the presented correlation is probably correct for all balanced constructed screened enclosures.

2. Results

The simulator, EMIS 3 of FEL-TNO, (Physics and Electronics Laboratory of the TNO-institute in the Netherlands) is a transmission line device which has a rise time just below 1 ns and a maximum field amplitude of several 10 kV/m. The transmitted field in the shelter is observed with H-field and E-field antennas in the frequency ranges of 10 kHz to 20 MHz and 10 MHz to 1 GHz, respectively. Transmission measurements were performed for all four orientations of the shelter and on all important locations such as close to the door, the entry panel, the honeycomb filter, the trimangles and of course a blind wall. It was found that the observational results do not vary strongly with shelter orientation or with location of measurements. Such a result is the best guarantee of the craftmanship by which the shelter has been manufactured because it implies that walls, joints and openings form one entity, one closed Faraday cage. In our vision the electromagnetic field sticks to the shelter walls and penetrates through all joints and openings, irrespective of shelter orientation. An averaged electromagnetic field is reconstructed from the individual transmitted waves inside the shelter. Therefore, the observed data are always the result of an averaging effect over the entire shelter. Consequently, the data do not vary much from location to location.

Mil-Std 285 attenuation measurements were carried out on all important locations of the N-EMP test shelter, similar to the simulator experiments. H-field, E-field and plane wave measurements were performed in the frequency ranges from 10 kHz up to 320 MHz, from 25 MHz to 100 MHz and from 0.4 GHz to 10 GHz, respectively. As usual a considerable spread is found in the measuring data. This confirms that Mil-Std 285 measurements are rather local.

To compare the results of H-field Mil-Std 285 measurements with those of simulator experiments they are subjected to an averaging procedure. The result is given in Fig. 1 by the fat dots. To demonstrate that the chosen averaging procedure yields a reasonable result, the lower and upper boundaries of the observed values are indicated in the same figure by the two straight lines (a dotted line means above the observational limit). A typical result of simulator H-

field observation is given by the curve in Fig. 1. Above 20 MHz noise is observed only. Comparing H-field attenuation data obtained with Mil-Std 285 and with simulator experiments it can be concluded that the results of both methods are rather the same, in spite of their fundamental differences. The simulator results lie within the range of Mil-Std 285 observed values, close to the averaged values.

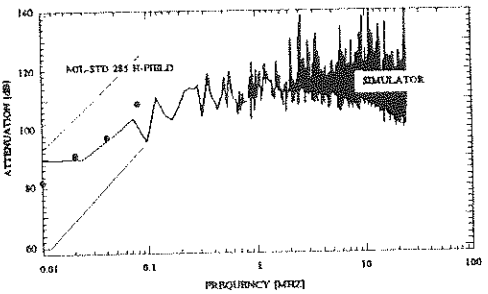

Fig. 1: Results of H-field measurements obtained with Mil-Std 285 and with a new fast simulator.

A typical result of E-field measurement obtained with the EMP simulator is given in Fig. 2. E-field data obtained with Mil-Std 285 all lie on the observational limit of 110 dB. Therefore, a comparison between both methods is not possible (the data are not contradictory). Mil-Std 285 obtained plane wave attenuation data have been added in Fig. 2 (the dots). Near 1 GHz, and probably for higher frequencies as well, the plane wave measurements yield a similar result as the E-field simulator measurements. This tends us to the conclusion that within the shelter a far field situation is present for these frequencies. Thus, plane wave like attenuation values are ob-tained with the simulator in the GHz region. The discrepancy between the decay of the simulator obtained attenuation data and the Mil-Std 285 data below 700 MHz can be explained by the fundamental differences in both methods: one method measures E-field attenuation and the other method plane wave attenuation.

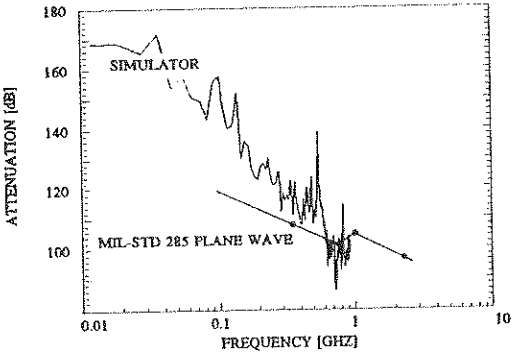

Fig. 2: Results of plane wave measurements according to Mil-Std 285 and of E-field measurements with a new fast EMP-simulator.

The attenuation values as they are shown in figures 1 and 2 are sufficient to meet new requirements for shelters.

3. Conclusions

Shielding attenuation data have been presented for the new Fokker shelter which is certified under the new requirements. Data were obtained with a new fast simulator and with Mil-Std 285 measurements to determine possible differences in the spectral attenuation functions. Concerning H-field measurements with both methods, the results are correlated. The plane wave measurements yield a similar result as the E-field simulator observations from a few 100 MHz. Probably, a plane wave like result is obtained with the simulator in the formerly mentioned frequency region. The discrepancy between the decay of the simulator obtained attenuation data and the Mil-Std 285 data can be explained by the fundamental differences in both methods: one measures E-field attenuation and the other plane wave attenuation.

ELECTROMAGNETIC EFFECTS OF THE FOUR-TOWER SUPPORTED CATENARY WIRE ARRAY LIGHTNING PROTECTION SYSTEM

J.C. Chai*, H.A. Heritage, and R. Briët
The Aerospace Corporation, P.O. Box 92957, Los Angeles, CA 90009, USA
Telephone (310) 336-8341; FAX (310) 336-5581

Summary

Four-Tower supported Catenary Wire Array Lightning Protection Systems (FTCWALPS) have been built for Launch Complexes 40 and 41 at Cape Canaveral Air Force Station (CCAFS) in Florida, USA. The main purpose of the overhead lightning protection system is to provide direct lightning strike protection to the launch vehicle and payload, and protection for personnel remaining in the vicinity of the Mobile Service Tower (MST) during lightning storms. Because of the height of the catenary wire array elevated by the towers, it is expected that direct lightning strikes to the proximity will be attracted to the protection system and be dispersed through diverging array down conductors in a controlled manner to remote areas.

However, due to the radiation generated by the return stroke along the catenary wires, it is highly desirable to know the indirect effect, e.g., the amplitude and duration of the induced electromagnetic field under the newly erected FTCWALPS. Furthermore, due to the sensitive electronics on board the launch vehicle and satellite vehicle (LV/SV) system, and recent evidence about the existence of the VHF and UHF components in the lightning spectrum, an analysis of the lightning coupling to the LV/SV system over a broader frequency spectrum is needed and US Air Force/Space and Missile Systems Center is seeking this information.

This paper discusses the results obtained by using the Numerical Electromagnetic Code (NEC), a method of moments code in the frequency domain, for the scattering/coupling analysis. The LV/SV system, the umbilical cable from the Umbilical Mast Tower to the LV/SV, the FTCWALPS, and the finite-conducting ground are modelled in the framework of NEC. The impedance of the FTCWALPS system is found, and unit voltage sources at various locations of the structure, each representing a different lightning scenario, is used to drive the entire system. The impulse response functions, in terms of both induced charge densities (E-fields) and currents (H-fields) on the surface of the LV/SV system, are obtained for any desired segment of the model. The impulse response function is then convoluted with the current attributable to the return

stroke waveform of Component A in the US military standard 1795A. The responses of the system in the frequency domain are inverse-fourier-transformed to the time domain, using an inverse integral Fourier transform algorithm. Typical results are presented in Figures 1 and 2 which show the induced H-field and E-field on the surface of the top region of the LV/SV system. These results can be used in the effort to mitigate indirect effects induced by lightning on the LV/SV system within the FTCWALPS.

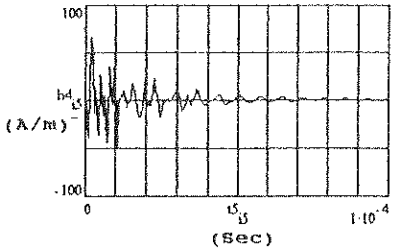

Figure 1. Induced H-field (h4) on the surface of LV/SV in the time domain.

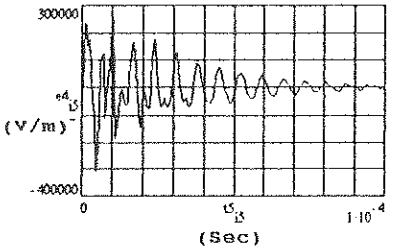

Figure 2. Induced E-field (e4) on the surface of LV/SV in the time domain.

AN EFFICIENT TECHNIQUE FOR THE MEASUREMENT OF SHIELDING EFFECTIVENESS USING NARROW BAND WHITE GAUSSIAN NOISE

Captain Thomas A. Loughry, Electromagnetic Research Lab WSM/Phillips Lab, Kirtland AFB, N.M., U.S.A. 87117

Mr. Hector Del Aguila, Electromagnetic Research Lab WSM/Phillips Lab, Kirtland AFB, N.M., U.S.A. 87117
and
Dr. Shyam H. Gurbaxani*, Fiore Industries, Inc. Kirtland AFB. N.M., U.S.A. 87117

In this paper we wish to present a new technique for rapidly acquiring shielding effectiveness data using the method of nested chambers. This technique has the same advantages of reverberation chamber of obtaining the data with a relatively low power (compared to anechoic chamber), uncostrained by the angle of incidence, etc.. Further more introduction of the narrow band white Gaussian noise eliminates the mechanical paddle wheel required for altering the boundary conditions in the case of a reverberation chamber.

The procedure consists of introducing a smaller chamber with a window inside the outer chamber. Each chamber has an antenna. The antenna of the outer chamber serves to introduce the electromagnetic fields while the inner chamber antenna senses the signal for the calculation of the shielding effectiveness of the window material. If the window aperture is large compared to the wavelength at which the test is conducted, the measurement approximates the field in the outer chamber. The window is then covered with the material of interest and the received power measured again.

Using first principles, it will be shown that the sheilding effectiveness (SE) is given by:

$$SE = 10 \log(\frac{S_1}{S_2}) - 10 \log(\frac{4}{A_w}) \ (2A_g\delta_g\frac{\omega}{3c} + \pi\frac{c^2}{2\omega^2})$$

where S_1 and S_2 are the power densities in the outer and inner chamber respectively, A_w and A_g are the areas of the window and the inside surface of the inside chamber respectively, δ_g is the skin depth of the inside surface of the inside chamber and c and ω are the velocity and test angular frequency. Recent measurements underway at the National Institute of Standards and Technology will be reported.

In-situ Measurement Techniques of Circuit Impedance: S_{11} vs. Shunt Resistor

Kenneth R. Calahan
Los Alamos National Laboratory

Dr. Walter L. Atchison
Field Command, Defense Nuclear Agency

Dr. Roger Colvin
Field Command, Defense Nuclear Agency

Mr. Micheal D. Rogers
BDM Federal, Inc.

Abstract

An assessment of a new technique to measure the approximate impedance of an in-situ test point is presented.

Contemporary EMP and HPM testing has incorporated low level, frequency-domain measurements of a test object to predict the response of a test object to various incident waveforms. Typically, the low level measurements are in the form of a frequency domain transfer function which represents the coupling efficiency of the radio frequency (RF) energy from the exterior of the test object to the interior test point at which the measurement was made. This transfer function (T.F.(f)) is then convolved with the frequency domain Fourier transform of the incident waveform of interest (E(f)) to create a test point response. The numerical process is then taken one step further by performing an integral across the frequency domain to estimate how much energy would be delivered to the test point as shown in Equation 1. In the equation, one typically uses 50 ohms as the circuit impedance (R), independent of frequency. Because circuit impedances

$$W(\text{joules}) = \frac{2}{R}\int_{f_{low}}^{f_{high}} [E(f) * T.F.(f)]^2 \, df \qquad (1)$$

are rarely 50 ohms across four decades of frequency, the LANL test team

searched for a measurement technique which would provide test point impedance as a function of frequency (R(f)).

Initially, the LANL test team used an S_{11} impedance measurement technique to provide a frequency-dependent value required for the integral. While the S_{11} measurement technique worked moderately well, this method is very intrusive and requires significant changes in the test configuration. This introduces additional assumptions concerning the applicability of the S_{11} results to the problem at hand. Additionally, S_{11} measurements require the injection of a signal at the test point from a source which characteristically has a source impedance of 50 ohms. This is to be compared with the test configuration which has the source external with a 1000 ohm voltage probe at the internal test point measuring what energy diffuses down to the test point. Figure 1 illustrates the two measurement schemes.

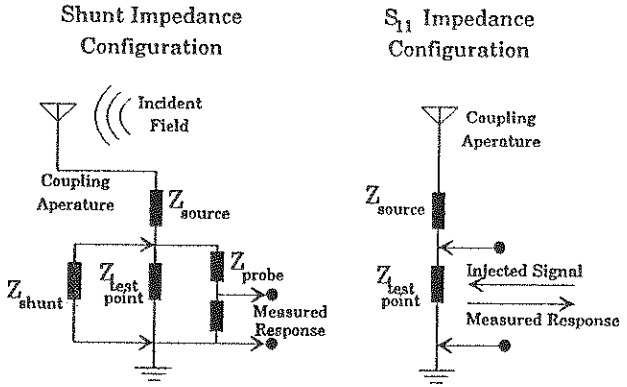

Figure 1. Schematic Representation of the S11 and Shunt Resistor Measurements.

This paper reports on the application of a different technique wherein a shunt resistance is connected in parallel to the test point and a 1000 ohm voltage probe. Three unique shunt resistances are used. The resulting three transfer functions are then ratioed to reveal the test point impedance. The results of the shunt resistor impedance technique are discussed and compared to S_{11} measurements taken at the same test point.

EFFICIENT METHOD FOR MEASURING PARTIAL DISCHARGE USING ROGOWSKI COIL

ROBERTO LINARES Y MIRANDA
Department of Electrical Engineering, Communication Section
CINVESTAV, Mexico

The partial discharge measured under in-situ condition are superposed by various interfering signals, which are coupling via conduced, induced and radiated into the experimental set-up. The use Rogowski coil is a very efficient measuring method of partial discharge in high voltage equipments and can overcome some EMI problems.

The continuous supply of electric energy is world wide of great important. The high voltage components (e.g., generators, transformers and cables) installed in the energy supply network have to work reliably in any situation. In order to get this objective, it is necessary to assure the test are carried out by the manufactures. Additionally several important components are periodically or permanently monitored to avoid an unpredictable or interruption of the power supply in most case. In order to recognize insulation faults in high voltage equipment a monitoring of the partial discharge is needed. At present is used standard method /1/(e.g., TETTEX) whose sensitivity is too low and the

measurements are disturbed by interferences. The main problems during discharge measurements occur due: measuring signals of low level, large width band and high level of interferences are presented /2/. In addition, measuring signals are contaminated with a variety of noise signal from the test voltage source, the measuring circuit itself and the surrounding area. The partial discharge measuring is the most power full method to detect even small insulation faults in the electrical power components. It has been used since various decade for quality control at manufacture's plant. The high voltage test laboratory for partial discharge measurement is well filtered. Therefore, disturbances are reduced.

This paper will describe an efficient measuring method of partial discharge using the Rogowski coil. In comparison with using standard equipment /1/ are obtained:

	Standard Equipment	Rogowski Coil
sensibility	≈ 1.5 nV/pC	≈ 1.5 μV/pC
wide band	≈ 500 KHz	≈ 70 MHz
high immunity to interference	Low	High
compatibility measurement in-situ	No	Yes
opening the high voltage circuits	Yes	not necessary

These characteristics are gotten because the Rogowski coil can see as: transmission line, an antenna with shielding and can be built of open form.

The measuring system is shown in the figure 1.

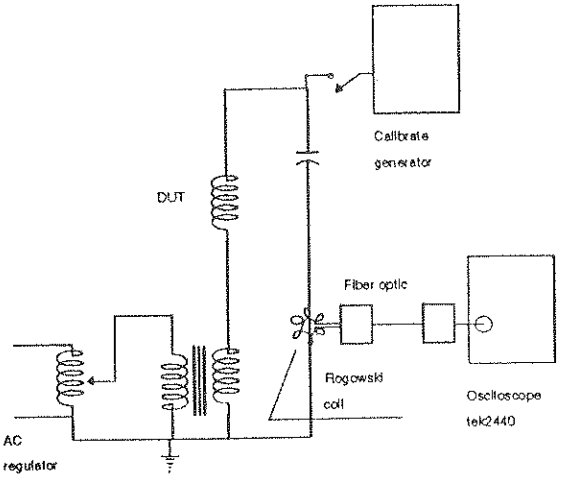

Figure 1. Measuring System.

One result of partial discharges measurements on a power transformer with 6.9 KV, is shown in figure 1. The channel 1 shows the result obtained using the Rogowski coil. The channel 2 shows the results obtained using the TETTEX equipment. Both systems were calibrated with a charge generator. The measured charge was 2800 pC.

From figure 2 and other results can do the following observations: The Rogowski coil has more sensitivity and it is faster than TETTEX equipment. Also it has higher immunity to interference, can be used in-situ and there is not necessary to open the high voltage circuit.

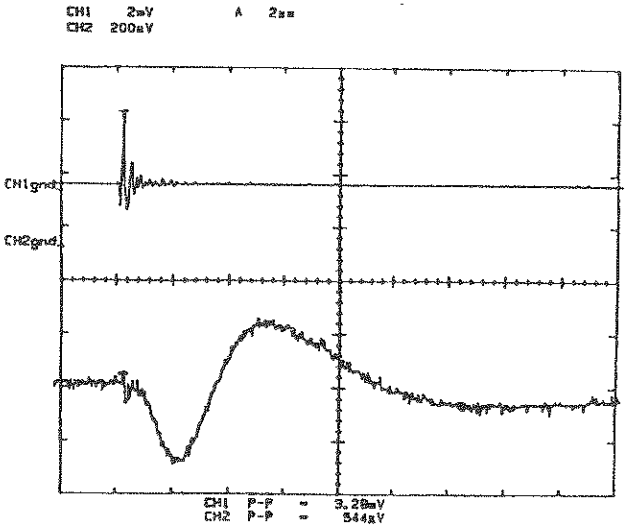

FIG. 2. The values Peak from a partial discharge of a transformer with 6.9 KV. Channel 1 Rogowski coil, Channel 2 TETTEX equipment.

Bibliography

1. W. Rogowski and W. Steinhaus. Arch Electrotech, 1 141 (1912).

2. F. H. Kreuger "Partial Discharge Detection in High-Voltage Equipment" Chapter 6. 73-76, Butterwoeths and Co., 1989.

MEASUREMENT OF THE PARALLEL AND AXIAL TRANSFER IMPEDANCES : THEORY, PRACTICAL METHODS, AND RESULTS

F. Broydé *, E. Clavelier
EXCEM
12, Chemin des Hauts de Clairefontaine
78580 MAULE - FRANCE

Throughout the present abstract, we will only study shielded multiconductor cables having any number n of internal wires and one overall shield. Several authors have already developped concepts and measurement techniques for shielded multiconductor cables, including (lineic) transfer impedance and (lineic) transfer admittance for each indidual wire. In some cases the concepts of common-mode and differential-mode transfer impedance have been introduced and those quantities directly measured. However those quantities could theoretically be deduced from the knowledge of the complex transfer impedance for each wire contained in the shield.

A recent paper (Broydé & Clavelier, IEEE Trans. on EMC, Nov. 1993) outlined that other coupling mechanisms indeed exist in multiconductor shielded cables, and gave a mostly theoretical introduction to three new types of coupling, called type 3, type 4 and type 5. According to this nomenclature, type 1 and type 2 coupling are the usual mechanisms respectively characterized by the lineic transfer impedance (in Ω/m) of the cable, and the electric coupling coefficient (the latter being related to lineic transfer admittance). The present paper will be focussed on type 3 coupling (or axial transfer impedance coupling) and type 5 coupling (or parallel transfer impedance coupling) only.

Fig. 1 illustrates type 3 coupling. Here the current is orthoradial (i.e. around the cable), and is caused by an axial magnetic field on the cable. This is typically what would be observed if the cable is placed on the axis of a coil. Coupling with the internal wires will not occur if those conductors are straight. However, a voltage will clearly be induced on skewed wires, an example of which is the twisted pair. It does not seem natural to relate the induced voltage to the current. We use instead a quantity that relates the voltage per unit length on a given wire to the axial magnetic field H (in A/m). This quantity is called the axial transfer impedance Z_{AT} (in Ω), and one need n axial transfer impedances to characterize the cable with respect to type 3 coupling. Fig. 2 illustrates type 5 coupling. A magnetic field passes through the cable, penetrates the shield and directly induces voltages between the cable's conductors. Unlike the four other types of coupling, this coupling places the magnetic field in a « forbidden » orientation : the laws of electromagnetics say that magnetic fields must run parallel to good conductors. In fact this should not disturb us too much because we are obviously dealing with imperfect shields, made of imperfect conductors. This type of coupling could be produced if we install the cable inside an Helmholtz coil, orthogonal to its axis. We describe this phenomenon with a quantity defined for each inner wire as the ratio between the per-unit-length voltage induced with respect to the cable shield, to the amplitude of the impinging magnetic field (in A/m). This quantity is called the parallel transfer impedance Z_{PT} of the cable (in Ω). As previously, we need n complex parallel transfer impedances, which are *a priori* dependant on the orientation of the magnetic field.

For cables with an homogeneous shield, axial transfer impedance and parallel transfer impedance can easily be computed theoretically, as shown by Broydé and Clavelier (1993) with the help of results obtained by H. Kaden. Also, these quantities must be introduced in the formulas for field to wire coupling, and this can be done easily. The relevance of these parameters can be proved by an experiment where a cable is installed on the floor of a Crawford Cell, orthogonal to the cell axis. Considering the geometry of the cable and the measurement set-up, calculation with transfer impedance only predicts that the cable

response should be negligible. We in fact obtained a very significant response only below 15 dB of the transfer impedance response obtained with the cable parallel to the cell axis. Because we checked that the response could not be caused by transfer admittance coupling, such an experiment demonstrate the necessity of including Z_{AT} in most calculations. For a single-braid multiconductor cable with 19 internal wires, this experiment allowed the assessment of Z_{AT}. At 1 MHz, we measured -89 dB(Ω) and at 10 MHz our result is -73 dB(Ω) for the axial transfer impedance.

We have developped a new kind of clamp that is especially designed to produce on a cable the field configuration shown on fig. 2. This so-called « parallel H-field probe », is appropriate for Z_{PT} measurements on a multiconductor cable. For instance, on a single braid cable with 14 internal wires, we measured -63 dB(Ω) at 1 MHz and -51 dB(Ω) at 10 MHz for the parallel transfer impedance. A similar device was also designed for the measurement of Z_{AT}, and is called the « axial H-field probe ». One of the most interesting characteristic of these measurements is that they are perfectly local, i.e. there is no necessity to terminate the outer circuit. Figure 3 shows measurement results for Z_{PT} obtained with a passive parallel H-field probe. This curve is reliable in the 200 kHz to 10 MHz frequency range. A single measurement with an active parallel or axial H-field probe may cover the entire 10 kHz to 200 MHz range. This is for instance appropriate for HEMP hardening control.

The work presented here has two main consequences :

— many previous calculations for field-to-cable coupling on critical systems will have to be revisited ;

— high immunity cables will have to be characterized for axial and parallel transfer impedance.

The good news is that axial and parallel transfer impedances are easy to measure, and can provide useful local measurements on cable, applicable to shield-fault location.

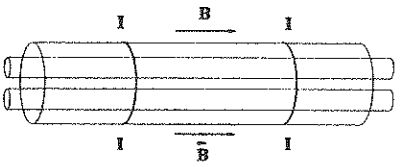

Fig. 1. Type 3 coupling on a shielded multiconductor cable.

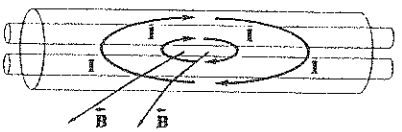

Fig. 2. Type 5 coupling on a shielded multiconductor cable.

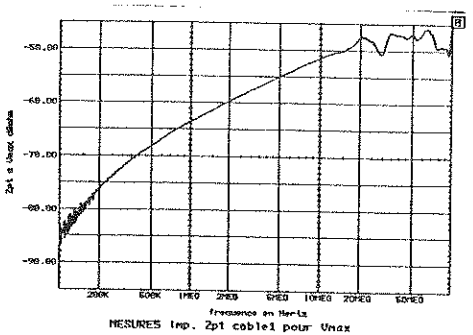

Figure 3 : measurement results for ZPT on a 14 conductors single-shield cable

FIBER-OPTIC DATA LINKS FOR ELECTROMAGNETIC PULSE AND HIGH POWER MICROWAVE TESTING

Bruce T. Benwell
US Army Research Laboratory
2800 Powder Mill Road
Adelphi, MD 20783

ABSTRACT:

When RF vulnerability assessments are performed on electrical devices (whether it be HEMP or HPM), it is often necessary to optically transmit measured currents and voltages from the device under test, to remotely located instrumentation. Optical transmission of measured signals is required to prevent contamination of the measured signal from the intense ambient electromagnetic (EM) environment.

The US Army Research Laboratory (ARL), has developed prototype analog fiber-optic links based on two optical technologies, miniature InGaAsP diode lasers as well as state-of-the-art integrated-optical modulators (IOM).

The first optical link design, is based on the direct modulation of an ultrahigh-speed miniature diode with the signal to be measured. Specifications for the link include an analog bandwidth from 10 kHz to 2 GHz, dynamic range of 40 dB (tangential noise over full bandwidth to 1-dB compression), minimum detectable signal of 20 uV (tangential noise floor over full bandwidth), input/output impedance of 50 ohms, fiber lengths >200 m, and an operating time of three hours with rechargeable battery packs. The transmitter also includes a remotely controlled 30 dB front-end attenuator, end-to-end calibrator, and on/off control. The entire transmitter is contained within a metallic cylindrical case measuring 3.5 cm in length with a diameter of 3.2 cm. The optical link consists of an InGaAsP miniature diode laser as a source, a single mode optical fiber, and an InGaAs PIN photodiode. Important features of the laser transmitter include dc-bias and network matching of the rf input, automatic control of the dc laser bias, and remotely controlled calibration and rf attenuation using a digital demultiplexing technique.

The second optical link design is based upon an integrated-optical modulator(IOM). The main advantage to externally modulating a continuous wave laser is that modulating frequencies as high as 15 GHz can be achieved with present electro-optic integrated modulators. The size of these devices (typically 20x20x40mm) and their electrical performance make these modulators an ideal choice for the basis around which a wideband fiber-optic link is developed. Recent advances in the fabrication of these modulators, based on an annealed proton exchange process, have produced IOMs that are extremely stable for high optical power levels of a few hundred milliwatts. The specifications for the link being developed include an operational bandwidth from 10 kHz to 5 GHz, a sensitivity of 100 μV, an input/output impedance of 50 ohms, and a dynamic range of 40 dB. A small transmitter size of 40x40x40 mm is necessary to minimize perturbation of the EM fields as well as allow the placement of this transmitter within a device under test.

A fully operational 2GHz fiber-optic link based on diode lasers as well as a 5 GHz breadboard prototype system (constructed of discrete components) using integrated optical modulators have been assembled and extensively tested. The results of these tests will be presented.

A SIMPLE TECHNIQUE FOR DETERMINING TRANSMISSION LOSSES IN SAW DELAY LINES

T. E. TAHA
Fculty of Electronic Engineering
32952, Menouf, Egypt

Abstract:

Experimental data are analysed in order to determine the synchronous frequency at which the minimum insertion loss occurs in a Surface Acoustic Wave (SAW) delay line. The insertion loss of a locally fabricated delay line is measured to be 29.23 dB at a synchronous frequency in the order of 6 MHz. The transmission losses are deduced as a result of the comparison between the experimental data of the total insertion loss of the delay line and the theoretical results of the transducer losses.

Summary:

SAW devices are now used in considerable range of applications in modern electronics, and they play a key rol in consumer communication applications. (C. K. CAMPBELL, Proc. IEEE, 77, 1453-1484, 1989),(C. W. RUPPEL et al.,IEEE Trans. Ultrason. Ferroelec. Freq. Cont.,40 ,438-452, 1993). One of the most important factors that infulance the characteristics of these devices is the transmission loss. It is therefore, necessary to understand all the mechanisms contributing to the total insertion loss to accomplish the optimum design of such devices. Fig.1 shows diagramatically various contributions that make up the total inseration loss. This loss is devided into two parts: trancducer losses (L_T) and the transmission losses (L_P). L_T are losses due to the conduction loss, the electrical mismatch loss and the bidirectional loss.

According to the circuit model of the uniform geometry transducers (W. R. SMITH et al., IEEE Trans., Microwave Theory Tech., 17, 856-864,1969) the loss L_T is given by:

$$L_T = 10 \log\left[4 \left[1 + \frac{R_c}{R_a(\omega)} + \frac{1}{2 R_a(\omega)} \left| (\omega L - \frac{1}{\omega C_T}) + X_a(\omega) \right|^2 \right]\right] \qquad (1)$$

where $R_a(\omega)=(4K^2N/\pi\omega_0C_T)(\sin x/x)^2$, $X(\omega)=(4K^2N/\pi\omega_0C_T)[(\sin 2x-2x)/2x^2]$, and $x=N\pi(\omega-\omega_0)/\omega_0$. K^2 is the electromechanical coupling consant, N is the number of the interdigital periods, R_c is the conduction loss, L is the tuning inductance, and C_T is the trancducer capacitance. On the other hand, L_P is the loss due to the interaction between the surface waves and thermal lattic wave, the effect of air loading , the presence of surface imperfections, radiation of bulk waves, beam steering and diffraction (D. P. MORGAN, Surface-Wave Devices for Signal Processing, New York, Elesevier, 1985). It is difficult to derive a theoretical loss L_P because it depends on the fabrication conditions of the device.

In this paper, we estimate the value of L_P experimentally. The experimental data of the total inseration loss (IL) against the frequency for a locally fabricated delay line are given in Fig. 2. The following cubic polynomial form is found to fit the experimental points by the least-squares approximation:

$$IL = 61.936 - 9.919\ F + 0.557\ F^2 + 0.031\ F^3 \qquad (2)$$

Putting the first derivative of eqn. 2 equal to zero gives the synchronous frequency F_o= 5.93 MHz. and the minimum inseration loss IL_{min} = 29.23 dB. At this frequency the transducer losses L_T is determined to be 24.5 dB as shown in Fig. 2. In order to obtain the experimental value of L_p at the synchronous frequency of the device, we should substract L_T from the

minimum insertion loss IL_{min}. The transmission losses L_P of our specimen are found to be 4.73 dB (see Fig.2).

The technique presented here can be regarded from a double point of view: On the one hand, we propose a simple method for determining the transmission losses, and used also to demonstrate the fundamental behavior of SAW devices using the delay line structure; On the other hand , this technique can be considered as a base to the development of laboratory experiments to acquaint the undergraduate communication engineering major with SAW techonolgy. It is the first appraoch indicated which has guided our work.

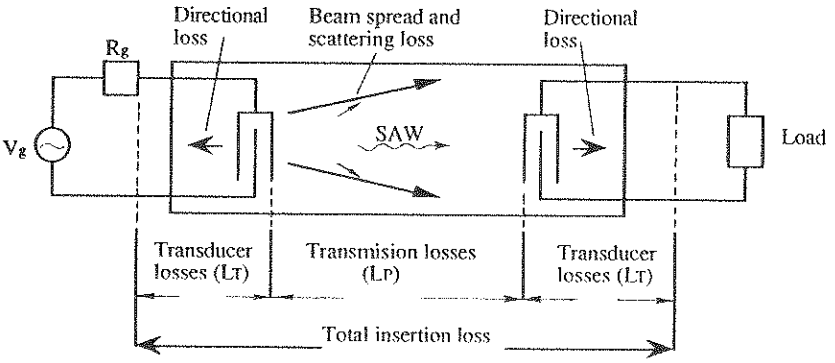

Fig.1 Losses in a SAW delay line

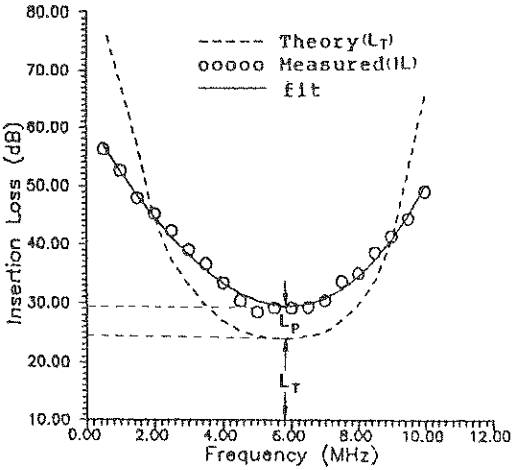

Fig.2 Theoretical and measured insertion loss versus frequency for a 6MHz $LiNbO_3$ SAW delay line.

TDAS CONDUCTED COMPATIBILITY ANALYSIS

V. Basile*(1), G. Gervasio *(1), L. Inzoli* (2)

1 - ALENIA Spazio TORINO, Corso Marche 41, 10146 TORINO, Tel. 011 7180 ext. 263/256, FAX # 011 73307/011 724807
2 - ESA-ESTEC XEE, P.O. BOX 299, 2200 AG NOORDWIJK NL, Tel. 31-17198 ext. 3660/3932, FAX # 31-171983660

"The increasing complexity of electromagnetic models and the power of new computational tools invite an ambitious effort towards a new generation of electromagnetic tools targeted at a wider range of application and aimed to substitute or substantially reduce experimental activity [1st announcement and Call for Paper III ESA European Workshop on EMC and Computational Electromagnetics]"

As a function of the increasing complexity, on the one hand, while time and money available for projects tend to decrease, on the other, the availability of powerful S/W tools may become of fundamental importance in the engineering development of the product.

Analysis, as well as test, must provide reliable results, that essentially means the results must be repetitive, within a known interval of confidence. Provided that the available interval of confidence is commensurate with the purpose, an activity of analysis must be associated to a "cost function"; thus its effectiveness is a function of accuracy, time, "installation" and cost.

Very often , "very simple" questions like "what I'm doing" , "when I'm doing it" and "where I'm doing it" have to be considered. I may find convenient one method, instead of another, and vice versa, depending on I'm in the bread boarding or in qualification phase, whether I' m "more close" to a test facility or to a S/W house.

In some cases, there are no chances, analysis, or test, is the only possibility and the probability of success might be, a priori, completely unknown.

There are absolute "values " which make an analysis tool attractive, as follows:

- Capability of taking advantage of other experiences (which may be very old, e.g. measurement and data acquired up to yesterday, and/or not belonging to your organisation) and to leave something that can be further reused by that analysis or by others.
- Possibility to improve continuously the early model, which has been based on specification figures and assumptions, until the condition in which the early input data have been completely replaced with the measured EMI data and circuit characteristics.
- Usage of models which have been validated, without changing the framework (i.e. the modifications are transparent).
- Standardisation of the data.

This last aspect has a significant and self-standing role.
It may be that now the time is right to proceed with the process of standardisation of the measurement methodology.
Everybody should agree that the normal problems of comparing the data from different laboratories directly, (because different people made different choices in representation), would be no longer tolerated.

ALENIA Spazio Torino, as Prime Contractor of many Space projects of different contents, need to be sensitive to new issues, even if continuing to operate in reliable scenarios.

In this frame new (and old) S/W tools are being used and evaluated; the "mixture" with respect to other methodologies is a function of the state-of-the art.

The TDAS concept, represented in figure 1, is considered herein. This paper provides our original contribution in the understanding of the boundary conditions of applicability of this methodology, inside an industrial environment.

The TDAS performance have been evaluated in a "scaled down", real, application; in particular the electromagnetic conducted noise, steady state, frequency domain, of one (of the three) SAX AOCS power buses has been investigated.

The main steps of the activity are the following:

I. As usual, the Equipment are being qualified by the relevant Suppliers. In particular the AOCS equipment investigated in this activity are PDU, ACC and MRU (SAS and Watchdog). Figure 3a is a typical plot of conducted emission.

II. This "scaled down" System, sketched in Figure 2, has been modelled with TDAS.
   - The input circuitry has been derived from the Supplier data .
   - The specified conducted emission have been included in the model.
   - A first prediction have been performed.

III. The selected Equipment have been tested again, one by one, in house via an internal developed process , able to provide data in a format suitable for processing by TDAS. Figure 3b shows the noise measured in ALENIA; a comparison has been made with the previous measurements. Filtering of data has been performed (as a DEMO), in order to show how the data can be manipulated to subtract undesired "filtering" which was present during the measurement.

IV. The above data have been loaded in TDAS and the prediction updated.

V. The "scaled down" System has then been integrated and the measurement of the conducted noise at PDU input has been performed (see figure 4). For the sake of clarity, this measurement has been performed two times; first it has been performed following the same method of point III, then the measurement has been performed using standard probes PCL11 and PCL30. The two measurements have been compared.

VI. Predicted noise (IV) has been finally compared with the measured one (V). For the sake of completeness, a comparison has been performed also between prediction in point II (based on Equipment specification) and VI (based on measured Equipment data) in order to evaluate the under or overdesign.

The paper will be completed with a general view about TDAS, in particular with regards to those aspects related to our findings.
Future activities, including discussion about possible further improvements in the methodology are briefly discussed also, for example the open issues regarding, parasitic entities and phase measurement.

In conclusion, ALENIA judge that a considerable effort has still to be spent in this area; this would be "paid" only by reaching the target of standardisation of data acquisition (which would allow implementation of a reliable ESA data base of conducted emissions).

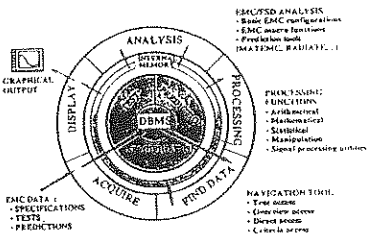

Fig. 1. TDAS FUNCTIONAL OVERVIEW

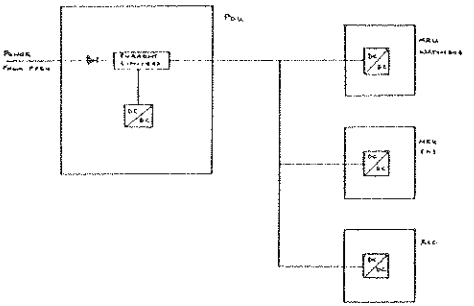

Fig. 2. "SCALED-DOWN" SYSTEM ARCHITECTURE

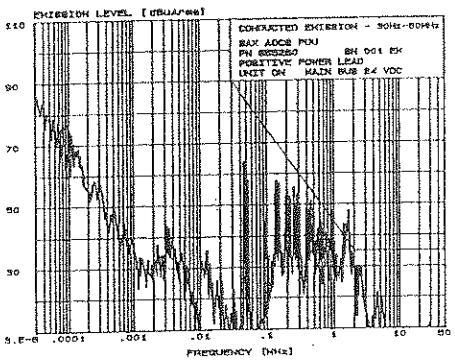

Fig. 3a. UNIT LEVEL MEASURED BY SUPPLIER

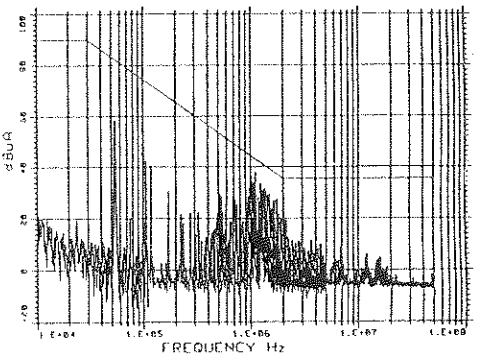

Fig. 3b. UNIT LEVEL MEASURED BY ALENIA

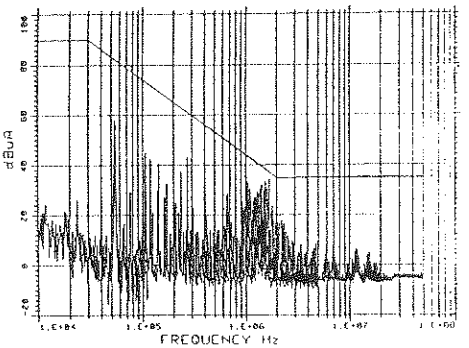

Fig. 4. "SCALED-DOWN" SYSTEM MEASUREMENT

An Approach Considering EMC-Aspects During System Planning

D. Frei *, W. John **, J. Schrage *, M. Gutzmann *

* University of Paderborn · Cadlab – Analog System Engineering
** Siemens Nixdorf Informationssysteme AG · Cadlab – Analog System Engineering
Bahnhofstrasse 32 · D-33094 Paderborn · Germany

Overview

System planning considering EMC-effects means designing a system according to economical as well as environmental consideration. Within this article a system is defined as an abstract term for electronic equipment. It may be divided into different subsystems (e.g. mother board, I/O card) which are interconnected by transmission systems. In the following the discussion will concentrate on EMC-problems of conducted interference at system level. The work is focused on the relation between the model of an EMC-optimization-process and a generalized design process. The target is to illustrate the iterative design process with necessary support- and analysis tools, which will be introduced. The first step of this discussion will be a global description of the general design process. In a second step the coupling of the EMC-optimization-process to the generalized design process will be described.

Generalized Design Process

The design of systems can be mapped onto a generalized design process. In vertical direction figure 1 shows the design process which is divided into eight different design stages.

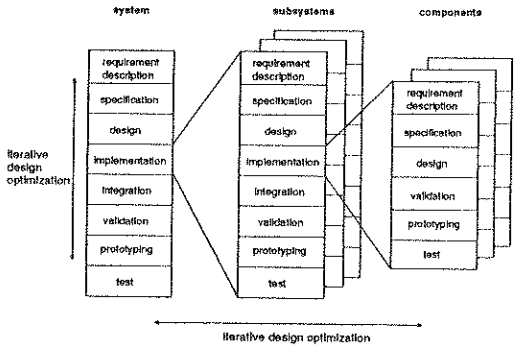

Figure 1: Generalized Design Process

In addition the division of a system into subsytems and components is illustrated in horizontal direction. The characteristics of this view of a design process are:

- characteristical design stages,
- recursive structures,
- arbitrary number of partitioning levels.

A detailed description of the design process is given in: cadlab report # 04/94.

EMC-System-planning

The model of an EMC-optimization-process which will be introduced in the following, is split into two steps: EMC-system-planning and EMC-validation (see figure 2). It seems practical to divide the EMC-system further into the areas *results/targets* and *activities*. Within the scope of *results/targets* EMC-boundary-conditions and characteristics of the system are determined. The EMC-concept describes the relevant EMC-parameters of the system. The *activities* of the EMC-system-planning area contains the procedure to achieve the *results/targets*. Furthermore, the required tools for the single design stages are introduced and described.

Requirement Description: Within the stage of the EMC-requirement-description technical, legal, and economical contexts of the complete system are discussed. Therefore, a concept of a support-tool, which reduces the data to a relevant part, has been developed.
Specification: The target of the EMC-sytem-planning in the specification phase is the EMC-prediction.

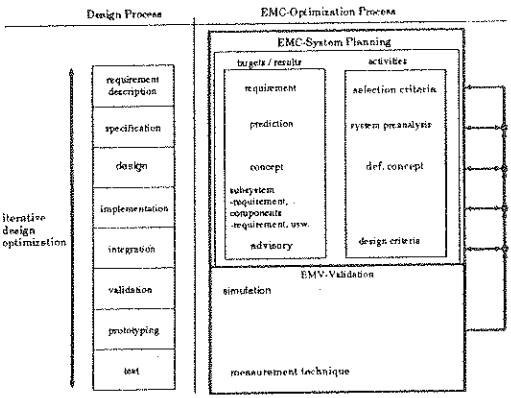

Figure 2: Model of EMC-Optimization Process

It contains a qualitative statement on the EMC-situation and an EMC-risk-problem-presentation. Moreover, it is the basis for the solution of EMC-problems. Tools for the system preanalysis can only be applied effectively, if they are used iteratively and first data from the implementation stage are already available. Such a preanalysis tool will set up influence-matrices, frequency- and level schemes as well as coupling matrices, and therefore will give an overview on the EMC-situation of the system.

Design: The EMC-concept is set up at the design level. Within this concept the EMC-subsystem-groups and intra-system-measure are determined.
Implementation: The task in the implementation stage is the partitioning of the system into subsystems and components. The subsystems and components within equivalent EMC-system-planning steps are performed, based on subsystem- and component conditions.
Integration: Within this stage layout plans are established and single transmission lines are placed. Therefore, EMC-rules are necessary for the design criteria of routing.
EMC-Validation: The results of the integration stage are the layout data which allow the simulation of signal propagation as well as radiation and irradiation analysis. This tool is one of the most important elements of the optimization process.
Iterative Process: In an iterative process an effective EMC-system-planning can be achieved. Preconditions are feedbacks and corresponding information flow between the single stages. The efficiency depends on the analysis tools, especially the simulation in the validation phase. With the aid of this tool a possibility is achieved to generate data for the concretisation of EMC-sytem-planning before prototyping. The data flow with the EMC-system-planning area *activities* puts the *results* and *targets* into concrete terms.

Summary

This article showed how the model of an EMC-optimization-process supports the generalized design process (see figure 2). This EMC-optimization-process provides an effective and efficient contribution for the system planning under EMC-contraints based on the application of the introduced help- and analysis-tools.

This research is part of the JESSI project AC-5. The project is supported by the BMFT (Bundesministerium für Forschung und Technologie) under grant 01 M2886D8, 01M2886D0 and 01M2886H9. The responsibility for this publication is held by authors only.

EMI X EMC IN THE INSTALLATION OF ELECTRONIC SYSTEMS

Roberto Menna Barreto
MARCONI - Companhia Portuguesa Rádio Marconi, SA
Av. Columbano Bordalo Pinheiro, 70 D
1000 Lisboa
Portugal
Fax: (351-1) 726.5700
Phone: (351-1) 7269163

In the first part of this paper it is introduced a kind of **DILEMMA** that exists between Manufacturers (Supplyers) and Users when EMC is considered for a particular installation. The point is that although the pieces of equipment are developed under a large support regarding EMC (literature, products, standards, tests, etc.) it should be expected that this same sofistication would be reflected in their installation, even if the EMC capabilities of the equipment are there to allow a more free installation. However, the EMC technology regarding system installation is not as well developed as in what concerns equipment development and the dilemma comes up when the installation of an electronic system is considered: should the Manufacturer be responsable for the user's installation (power system, lightning protection, cable runs, etc.) in order to provide the adequate configuration for the electronic system or should the user be the one who will have to overcome all the EMI problems through a consistent study of the EMC characteristics of the Manufacturer system?

Assuming the user as the one who used to take care of this sort of problems, it is analysed in the second part of this paper some draw-backs that normally exist inside any organization when EMC is considered. The set of those factors which tends to postpone EMC analysis for system installation was called ' **EMC INERTIA**' and includes: **The Ideal System Syndromme**, that is that kind of thoughts in which we are used to consider the electronic system as an ideal system, fed by a clean power system, operating in a quiet neighbourhood, etc.; **The EMC Complexity**, which is the complexity inherent to the EMC area that makes it difficult to be included in current plannings or easilly talked about; **The EMC Uncertainity**, which means that we may know exactely how much it will cost the implementation of a specific EMC protective measure in many cases but we cannot be sure on how much it will save in the future; **The Electronic X Logic** engineering divergence meaning that nowadays electronics is more related to logic than phisics itself; and finally the '**Descartes' Thinking**' where it is often difficult to integrate the various parts considered for a system installation.

In the third part it is introduced the concept of an **Interference Control Plan** for system installation as a quite usefull tool to overcome the EMI scenery considered so far. It is done through an example of such a Plan which is composed of four main chapters: INTRODUCTION (System Description, Parts which are Envolved and Training), ANALYSIS (Electromagnetic Environment and Potential Situations of Interference), INTERFERENCE CONTROL (Connections to Earth/Grounding, Electrostatic Discharge, Cabling, etc.) and TESTS.

In the fourth part it is presented some **Practical EMI Situations** concerning electronic systems installation where the importance of an Interference Control Plan is enphasized in order to guarantee a proper EMC configuration for the electronic system to be installed. Those examples are referred to the design of the earth electrodes subsystem, power system connections and lightning protection subsystem.

Finally, in the fifth and last part of this paper some **Conclusions** are considered: EMI is a reality; there should exist more standards / recommendations concerning EMC system installation; Manufacturers are invited to go more inside the houses of their clients to solve/analyse EMI possibilities; and the development of an Interference Control Plan is a must for a proper electronic system installation.

A LEAST ABSOLUTE VALUES METHOD FOR ADAPTIVE SPATIAL SUPPRESSION OF INTERFERENCE IN A LOW FREQUENCY RECEIVER

P. V. Gorev, "Poljot" Scientific - Production Association,
Nyzhny Novgorod, Russia 603000

The paper presents a least absolute values (LAV) approach for enhancing the performance of low frequency communication receiver through the suppression of interference. The typical antenna system for this application consists of H-field crossed loops and an E-field monopole. RF amplification of the narrow-band antenna outputs and conversion into complex digital form is performed. Each complex number is represented by a 2x2 matrix which is incorporated into a real MxN data matrix $\mathbf{A}$, $M \geq N$, where N is doubled number of antenna elements.

By weighting and summing of the matrix $\mathbf{A}$ columns with an N-size vector $\mathbf{w}$ it is possible to create a new output $\mathbf{Aw}$ which provides the minimum norm for the residuals vector $\mathbf{r}=\mathbf{d}-\mathbf{Aw}$, where $\mathbf{d}$ is a reference signal vector. Using the Euclidean norm leads to the least squares (LS) problem $\mathbf{Aw} \cong \mathbf{d}$, which solution may be found from the normal equations $(\mathbf{A}^T\mathbf{A})\mathbf{w}=(\mathbf{A}^T\mathbf{d})$. Calculation of $\mathbf{A}^T\mathbf{A}$ includes a lot of multiplications, besides, the condition number of $\mathbf{A}^T\mathbf{A}$ is the square of the condition number of $\mathbf{A}$, hence numerical solutions of the normal equations will be less accurate than algorithms which use orthogonal representations of $\mathbf{A}$.

An alternative to the orthogonal representation approach to overcome such difficulties is to use the 1-norm of the vector $\mathbf{r}=(r_1,\ldots,r_M)^T$: $\|\mathbf{r}\|_1=\sum_{m=1}^{M}|r_m|$. Let us define a function $n1(\mathbf{d},\mathbf{a},c) = \|\mathbf{d}-c\mathbf{a}\|_1 \;/\; \|\mathbf{a}\|_1$ and its derivative with respect to c: $p1(\mathbf{d},\mathbf{a},c)$. We will say, that $\mathbf{r}$ is 1-orthogonal to $\mathbf{a}$ if $c=0$ is the point, where $p1(\mathbf{d},\mathbf{a},c)$ changes its sign. Minimization of $\|\mathbf{d}-\mathbf{Aw}\|_1$ is equivalent to finding such $\mathbf{w}$ that $\mathbf{d}-\mathbf{Aw}$ is 1-orthogonal with every column of $\mathbf{A}$. This condition yields a system of equations

$$p1(\mathbf{d}-\mathbf{Aw},\mathbf{a}^n,0) \cong 0,\ n=\overline{1,N} \qquad (1)$$

which are nonlinear with respect to $\mathbf{w}$. This system is replaced by another one which includes $\mathbf{w}$ linearly:

$$p1(\mathbf{a}^n,\mathbf{d}-\mathbf{Aw},0) \cong 0,\ n=\overline{1,N} \qquad (2)$$

Some simplifications lead to the equations, which may be called as 1-norm normal equations:

$$(\mathbf{J}\mathbf{A}^T\mathbf{A})\mathbf{w} = (\mathbf{J}\mathbf{A}^T\mathbf{d}) \qquad (3)$$

where $\mathbf{J}\mathbf{A}$ is a sign matrix with columns of kind of $\mathbf{J}\mathbf{a} = (sgn(a_1), sgn(a_2), \ldots, sgn(a_M))^T$. Because of replacing (1) by (2) the solution of (3) provides only some approximation to the exact 1-norm solution. Nevertheless we have a sufficient reason to hope that this approximation is satisfactory for zero mean processes at least. This assumption has been corroborated by the numerical simulation for the frequency manipulated (f_0 and f_1) desired signal with the signal-to- (thermal noise) ratio $S=20$ dB and the direction of arrival azimuth (DOAA) φ_S, which is received with two H-field crossed loops. The narrow-band noisy interference was generated by the point source with the interference-to-(thermal noise) ratio $I=60$ dB and the DOAA φ_I. The reference vector $\mathbf{d}$ contained the real and imaginary parts of the complex sinusoid with the f_0 frequency.

Figure 1 shows the output signal-to-(interference + thermal noise) ratio (dB) in dependence from $\varphi_S - \varphi_I$ (deg.) for the conventional LS method (solid line) and for the LAV approach, i.e. for the solution of (3) (dashed). The maximum value of the degradation of the LAV from the LS is about 0.7 dB.

Thus the paper has presented an adaptive method that is based upon the 1-norm minimization. Special normal equations have been derived, yielding an approximate solution to the problem. The preference of the method proposed is the absence of multiplications in $\mathbf{J}\mathbf{A}^T\mathbf{A}$. Besides, this matrix has the condition number which is comparable with that of $\mathbf{A}$.

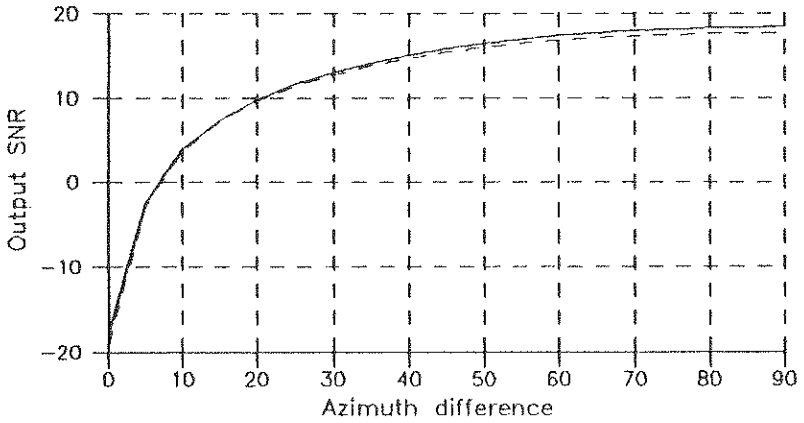

Fig.1. Output SNR with respect to azimuth difference

SOFTWARE AS A TOOL TO CONTROL EMI/EMC IN DESIGNING COMPUTER SYSTEMS

G.K. SAHA
Electronics Research & Development Centre,(ER & DC),
Calcutta, INDIA.

ABSTRACT

E ³ Design Engineers building today's speed hungry electronic equipment must have electromagnetic compatibility [EMC] uppermost in their minds. The high - frequency clock that runs applications at lightning speeds is responsible for unwelcome electromagnetic radiation. As a result, random errors may occur within computer systems. Computer systems may experience annoying interference. To combat existing and potential problems stemming from electromagnetic emissions, most nations have set guidelines for allowable disturbance generated by electronic equipment. These guidelines are commonly known as electromagnetic compatibility [EMC]. There are two aspects to EMC. First, the equipment must be able to withstand certain levels of electromagnetic interference [EMI] without degrading performance. Second, equipment must not emit excessive amounts of electromagnetic energy. Creating software that guides and helps in controlling EMI is a complex challenge. This software which is properly designed and developed has some advantages like the EMC- rule checks are easier to understand and they can be performed on a partial or unrouted design. When problems are found , users are guided on their demand, to a solution. Design practices suggested by this software system will be useful even to more knowledgeable users. This Software Tool functionally behaves as an EMC Guide in designing Computer Systems. This EMC Guide's main function is to provide a measure of compliance a selected set of differential and common - mode rules along with various guidelines to the E ³ designers . This software is a fully - integrated , and menu driven on - line system. Computer Systems Designers can " tune " a design with continuous measure of EMI control. With this EMC Guide software E ³ engineers can review their EMC design at any point in the design process even it can be used much earlier in the design process. After analysis, designers may alter the

layout to improve performance and re-analyze the design in one or more categories and thus the designers can establish maximum EMI immunity to computer systems. Thus this software, being used as a tool, can guide a design engineer to establish maximum EMI immunity at every stage of design cycle of computer systems against noises like crosstalk, ESD, EFT, RFI etc. The following steps show how this EMC Guide software helps in reducing EMI in the design-cycle of computer systems.

Algorithm. This algorithm shows the logic how this EMC Guide Software can be a very useful tool to a computer systems design engineer to control EMI in the different places of the design cycle.

Step 1. Complete Design Specification.
Step 2. Design.
Step 3. Schematic Capture.
Step 4. Review EMC Design. [Using EMC Guide S/W]
Step 5. If Review Result .NOT. Satisfactory, then:
Go to Step 2.
[End of if structure]
Step 6. Layout (placement).
Step 7. Review EMC Design. [Using EMC Guide S/W]
Step 8. If Review Result .NOT. Satisfactory, then:
Go to Step 2.
[End of if structure]
Step 9. Layout (routing).
Step 10. Review EMC Design. [Using EMC Guide S/W]
Step 11. If Review Result .NOT. Satisfactory, then:
Go to Step 2.
[End of if structure]
Step 12. Simulation of EMC.
Step 13. Review EMC Design. [Using EMC Guide S/W]
Step 14. If Review Result .NOT. Satisfactory, then:
Go to Step 2.
[End of if structure]
Step 15. Test EMC.
Step 16. Review EMC Design. [Using EMC Guide S/W]
Step 17. If Review Result .NOT. Satisfactory, then:
Go to Step 2.
[End of if structure]
Step 18. Prepare Technical Documentation.
Step 19. EMC Guide S/W automatically expands the knowledge table.

EUROEM 94, Bordeaux, May 1994

MILO EXPERIMENTS AND COMPUTER SIMULATIONS

by

D E T F Ashby*, J Allen, J W Eastwood, K C Hawkins and L M Lea

AEA Technology, Culham Laboratory, Abingdon, Oxfordshire
OX14 3DB, England

A variety of MILO configurations have been investigated using a combination of experiment and computer simulation. The MILOs used were made from a set of standard parts which enabled the configurations to be changed rapidly. The MILOs all operated at around 1 GHz and were powered by a 20 ohm, 600 kV, 200 ns pulser. In one set of experiments the MILO consisted of two sections with different dispersion properties separated by a attenuator; the first second acted as a driver for the second section. See Fig 1. Computer simulations showed good agreement with experiment.

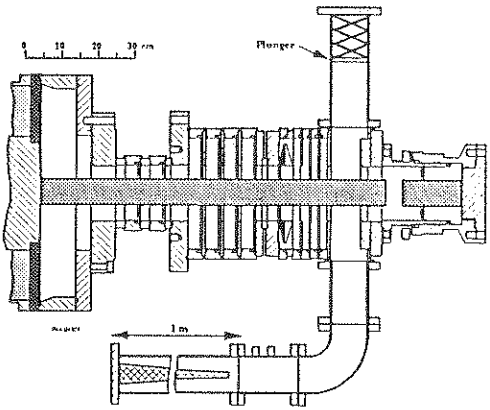

Figure 1: *Diagram showing a MILO consisting of two sections separated by an attenuator.*

In a second set of experiments the behaviour of a series of simple axisymmetric MILO structures was compared with computer simulations. In these experiments the behaviour varied considerably as the geometry and number of cavities were changed. Good agreement between experiment and the modelling was obtained except near the end of the pulse when the microwave signal from the cavities tended to decay; this decay increased with applied voltage. The effect was attributed to plasma formation and subsequent electron emission from the resonator structure; it was drastically reduced when the aluminium resonator vanes were replaced by polished stainless steel vanes. The electron emission hypothesis was consistent with computer modelling.

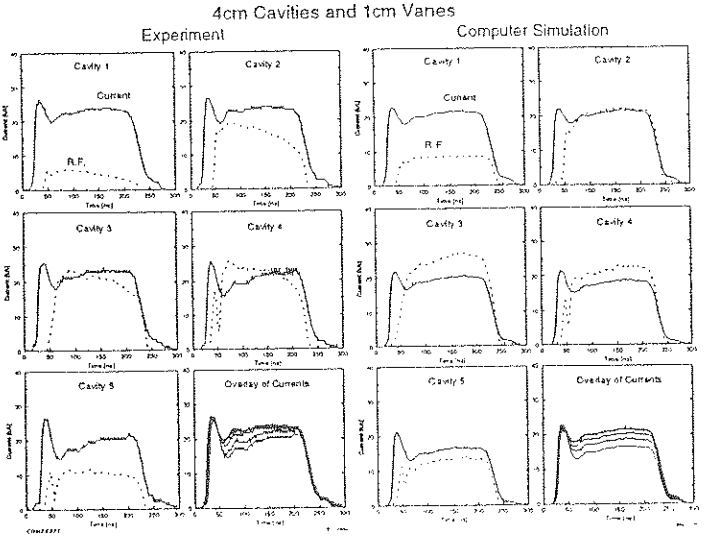

Figure 2: *Comparison between experiment and simulation for a simple 5-cavity MILO. The oscillograms are based on the output from magnetic loops in each cavity.*

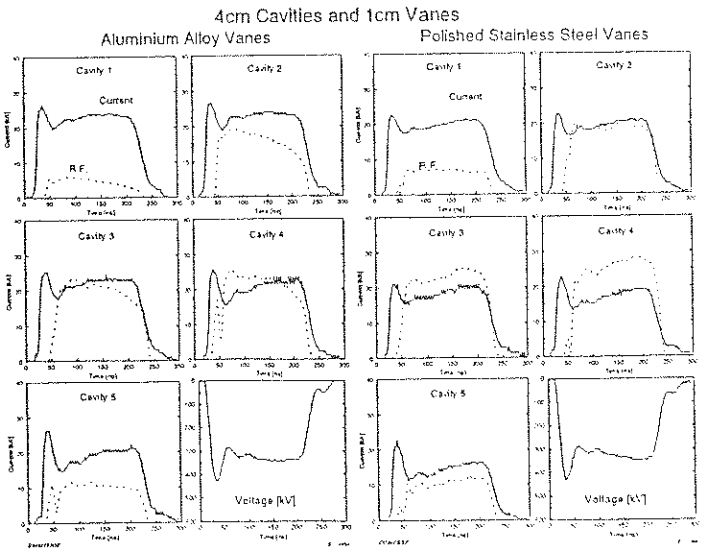

Figure 3: *Experimental oscillograms showing the effect of vane material on MILO behaviour.*

Design and Operation of a Novel Field Emission Array (FEA) Gyrotron Cathode

M Garven, SN Spark and ADR Phelps

Department of Physics and Applied Physics
University of Strathclyde, Glasgow, G4 0NG, U.K.

This paper presents the design and operation of a novel field emission array (FEA) gyrotron cathode utilising GEC-Marconi Ltd silicon FEAs. Gyrotrons operate with electron accelerating potentials of typically ~50kV. The design of an FEA gyrotron cathode will be described, which has thus far been tested up to a potential of 50kV. This design allows the FEAs to be individually addressed while protecting the chip mount and bond wires from high voltage breakdown. Results will be presented which will demonstrate electron beam formation at accelerating potentials of up to 25kV. It has also been experimentally determined that field penetration into the corona shield beam holes is sufficient that 100% of the FEA current appears in the high energy electron beam. As the gyrotron is a crossed field device, FEA damage from back ion bombardment is expected to be considerably less than in linear tube designs using FEAs.

Design Considerations

Several gyrotrons have been developed at Strathclyde with more recent work involved in the development of a gyrotron based on a thermionic magnetron injection gun (MIG). To allow a direct comparison with the operation of the thermionic MIG, the FEA gun design was developed such that it would fit directly into the existing experimental framework. Design parameters of the FEA gun were kept at approximately the same values as in the successful thermionic device. Typically with average cathode radius 13.0mm, slope angle 4° and the spacing factor between the cathode and intermediate anode of the MIG 5.0mm, Figure 1.

Silicon wafer fabrication of FEAs implies that the final emitters are produced on flat semiconductor chips which are mounted in an annular arrangement as shown in Figure 1. Previous experiments[1,2] investigated various chip designs and the most suitable chip for a gyrotron application was determined in terms of maximum emission current with each chip achieving a reproducible emission current of 10mA. The final design used was a 2.25x2.25mm chip containing 5x6000 Si tip arrays. Design considerations dictated that an optimum of 10 chips would fit into the gun geometry, implying that a beam current of up to 100mA is feasible from the FEA gyrotron cathode.

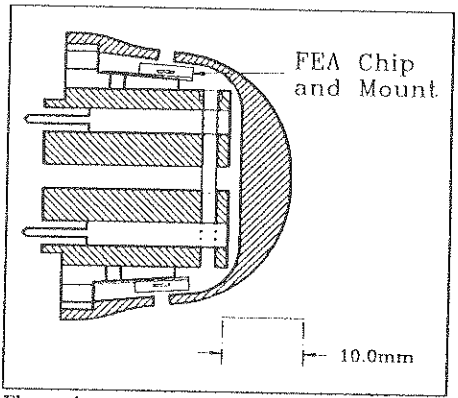

Figure 1. Cathode section of FEA gun showing emitter chip and support structure.

One of the main advantages of this new type of FEA gun, over its traditional counterparts, is in the ability to control the electron beam and more significantly the individual components of the beam. This was achieved by individually addressing each of the 10 chips via the Nb metal grid potential. A PTFE spacer and 10 wires isolated each chip whilst applying the grid voltage. The multiple cathodes of the device, the Si tips of the 10 chips, were held at the same potential. The chips were activated by applying the Nb metal grid voltage, typically ~ +80V. A smooth corona shield with 10 holes was accurately aligned with the 10 emission sites. This shielding contoured the high electric field and eliminated any high voltage breakdown of the fine 25μm

bond wires.

Gyrotron Development

In the gyrotron electron gun (Figure 2), the FEA cathode structure was held at potentials of up to -50kV hence the 10 channel grid voltage supply floated and was addressed via fibre optic control. The intermediate anode of the device was held at up to -25kV and was similar in design to that used in the thermionic MIG. The cavity walls, interaction region and millimetre wave output taper were all at ground potential. Electron beam current from the cathode to the intermediate anode was measured with a cathode-intermediate anode accelerating potential, V_{cin}, of up to -25kV. The cathode tuning coil was a conventional, water-cooled 0 to 0.3T magnet and a superconducting magnet capable of producing 0 to 11T was used to generate the cavity B-field.

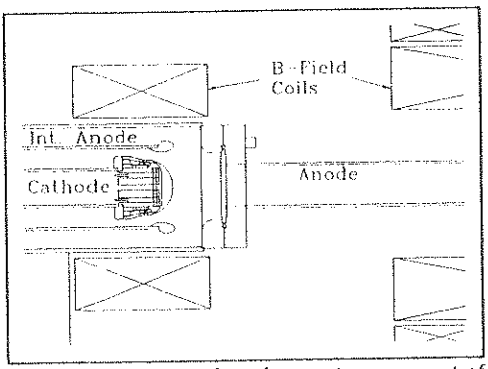

Figure 2. Electrode and magnet arrangement of the FEA based electron gun

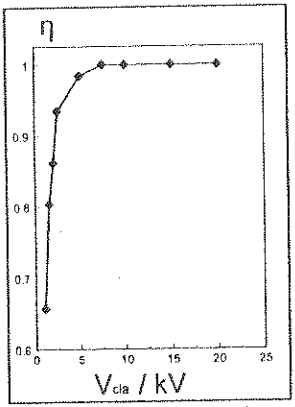

Figure 3. FEA electron beam parameter η as a function of cathode-intermediate anode gap potential V_{cin}.

As the cathode corona shield is at the same potential as the FEA emitting points, electric field penetration into the shield holes will determine the fraction of FEA current, I_{FEA}, extracted into the cathode/intermediate anode gap, I_{GAP}. Figure 3 shows that at low accelerating gap potentials of <7.5kV field penetration initially limits the ratio of I_{GAP}/I_{FEA} ,defined as η, to <1.0. However, as the gap potential is increased to >7.5kV and field penetration into the holes increases, the ratio of I_{GAP}/I_{FEA} increases to a measured maximum of 1.0. Experiments on differing hole sizes are planned. Methods of individually addressing the FEAs by fibre optic control, novel experimental techniques and recent results will be presented at this meeting.

Acknowledgements

Support for this research was provided by the DRA and an SERC/CASE award with GEC-Marconi Ltd. Helpful discussions with N Cade, DM Parkes, K Trafford, B Kerr, J Lyons and DF Howell are gratefully acknowledged.

References

1 M Garven, ADR Phelps, SN Spark and N Cade, *Vacuum*, **45** (1994)
2 M Garven, SN Spark, ADR Phelps and N Cade, *Proc. 18th Int.Conf.Infrared and Millimeter Waves*, SPIE **2104**, 452-453 (1993).
3 SN Spark, ADR Phelps and PR Winning, *Int.J.Infrared and Millimeter Waves*, **12**, 885-894 (1991).
4 SN Spark, AW Cross and ADR Phelps, *Proc. 17th Int.Conf.Infrared and Millimeter Waves*, SPIE **1929**, 466-467 (1992).

A Novel Scaling of the Gyrotron/CARM Equations of Evolution

B W J McNeil, G R M Robb and A D R Phelps,
Department of Physics and Applied Physics,
University of Strathclyde, Glasgow G4 0NG.

We show that a set of five coupled equations describing steady state single TE_{mn} mode gyrotron/CARM evolution reduce to a universally scaled set of three equations identical in form to those of the steady state high gain Compton regime free electron laser (FEL). We do this using the approximation of slowly varying amplitude and phase over a cyclotron period and neglect space-charge effects. We also assume a thin annular beam concentric with a circular waveguide in the limit $k_\perp r_L \ll 1$, where $k_\perp$ is the perpendicular wavenumber and r_L is the Larmor radius.

Starting from the coupled Lorentz-Maxwell equations, the following equations can be derived using the above approximations :

$$\frac{d\phi_j}{d\bar{z}} = p_j - i\frac{\mu}{\bar{u}_\perp \bar{u}_\parallel}(Ae^{i\phi_j} - c.c.) \quad (1)$$

$$\frac{dp_j}{d\bar{z}} = (\rho p_j - 1)\frac{\bar{u}_{\perp j}}{\bar{u}_{\parallel j}^2}(Ae^{i\phi_j} + c.c.) \quad (2)$$

$$\frac{d\bar{u}_{\perp j}}{d\bar{z}} = -\frac{\mu}{\bar{u}_{\parallel j}}(Ae^{i\phi_j} + c.c.) \quad (3)$$

$$\frac{d\bar{u}_{\parallel j}}{d\bar{z}} = -\rho\frac{\bar{u}_{\perp j}}{\bar{u}_{\parallel j}}(Ae^{i\phi_j} + c.c.) \quad (4)$$

$$\frac{dA}{d\bar{z}} = \left\langle \frac{\bar{u}_\perp}{\bar{u}_\parallel} e^{-i\phi} \right\rangle \quad (5)$$

where:

$$j = 1..N_e,\ \bar{z} = \frac{k_\perp^2}{k_\parallel}\rho z,\ \phi = \omega t - k_\parallel z + tan^{-1}(\frac{u_y}{u_x}) - (m-1)\theta_0 - \frac{\pi}{2},\ u_\perp = \gamma v_\perp,\ u_\parallel = \gamma v_\parallel,\ \bar{u}_\perp = \frac{u_\perp}{\langle u_{\perp 0}\rangle}$$

$$\bar{u}_\parallel = \frac{u_\parallel}{\langle u_{\parallel 0}\rangle},\ |A|^2 = \frac{1}{\rho}\frac{U_w}{U_{b0}}\frac{v_g^2\langle\gamma_0\rangle}{\langle u_{\perp 0}\rangle\langle v_{\parallel 0}\rangle},\ \alpha = \frac{\langle u_\perp\rangle}{\langle u_\parallel\rangle},\ \omega_c = \frac{eB_0}{m_e},\ k_{c0} = \frac{\omega_c}{\langle u_{\parallel 0}\rangle},\ \nu = \frac{k_\parallel}{k_{c0}}\alpha_0^2,\ \mu = \frac{\rho}{\nu}$$

$$\rho = \left(\frac{e\mu_0}{8m_e}\frac{k_\parallel^2\langle u_{\perp 0}\rangle^2}{k_\perp^2\langle u_{\parallel 0}\rangle^3} I D_{mn}^2 J_{m-1}^2(k_\perp R_0)\right)^{\frac{1}{3}},\ D_{mn} = \left(J_m(\chi'_{mn})\sqrt{\pi(\chi'^2_{mn} - m^2)}\right)^{-1},\ \langle ... \rangle = \frac{1}{N_e}\sum_{j=1}^{N_e} ...$$

and : j is the electron index number, N_e is the total number of (macro) electrons, subscripts $\perp$ and $\parallel$ represent vector components perpendicular and parallel to the waveguide axis, ω is the radiation frequency, $(k_\perp, k_\parallel)$ are the wavevector components of the TE_{mn} mode, γ is the electron relativistic factor, (R_0, θ_0) are the polar coordinates with respect to the waveguide axis of the electron guiding centres, $(v_\perp, v_\parallel)$ are the electron velocity components, v_g is the radiation group velocity, B_0 is the axial magnetic guiding field, A is a scaled complex radiation field strength, U_w is the energy per unit waveguide length of the radiation, U_b is the energy (including rest mass) per unit waveguide length of the electron beam, I is the electron beam current, χ'_{mn} is the nth root of $J'_m(k_\perp R_w) = 0$, R_w is the waveguide radius, and subscripts 0 indicate initial values at $\bar{z} = 0$. Other symbols have their usual meaning. An identical set of equations results for TM mode evolution but with different scaling [1]. Note that

$$\rho|A|^2 = \eta\frac{v_g}{\langle u_{\parallel 0}\rangle}(\langle\gamma_0\rangle - 1) \quad (6)$$

where η is the efficiency. It can be seen from equations (2..4) that there is a functional relationship between p, $\bar{u}_\perp$ and $\bar{u}_\parallel$, so the number of equations can be reduced from five to just three. In the low efficiency limit $\rho \ll 1$ these equations become:

$$\frac{d\phi_j}{d\bar{z}} = p_j - i\frac{\mu}{\sqrt{1+2\mu(p_j-\delta_j)}}(Ae^{i\phi_j} - c.c.) \quad (7)$$

$$\frac{dp_j}{d\bar{z}} = -\sqrt{1+2\mu(p_j-\delta_j)}(Ae^{i\phi_j} + c.c.) \quad (8)$$

$$\frac{dA}{d\bar{z}} = \left\langle \sqrt{1+2\mu(p-\delta)}e^{-i\phi} \right\rangle \quad (9)$$

where: $\delta = p(\bar{z}=0)$ and for clarity we assume a cold electron beam (ie. $\bar{u}_{\parallel 0_j} = \bar{u}_{\perp 0_j} = 1 \; \forall \; j$).

Using equations (3..5), a constant of the motion can be derived and rearranged to give :

$$\rho(|A|^2 - |A_0|^2) = \frac{\nu}{2}\left(1 + \frac{\sigma_{\perp 0}^2 - \langle u_\perp^2 \rangle}{\langle u_{\perp 0} \rangle^2}\right) \quad (10)$$

where $\sigma_{\perp 0}$ is the standard deviation of the spread in $u_{\perp 0}$. A physical interpretation of the parameter ν can be obtained using this equation. Maximum energy would be transferred from the electron beam to the radiation if all transverse electron motion were exhausted, that is $\langle u_\perp^2 \rangle = 0$. Assuming this electron beam state and that $|A_0|^2 \approx 0$, then

$$\rho|A|^2_{max} = \frac{\nu}{2}(1 + \frac{\sigma_{\perp 0}^2}{\langle u_{\perp 0} \rangle^2}) \quad (11)$$

Hence, using equation (6), we have an upper efficiency limit for the system of

$$\eta_{max} = \frac{\nu}{2}\left(1 + \frac{\sigma_{\perp 0}^2}{\langle u_{\perp 0} \rangle^2}\right)\frac{\langle u_{\parallel 0} \rangle}{v_g}\frac{1}{\langle \gamma_0 \rangle - 1} \quad (12)$$

Sufficiently small values of the parameter ν will then limit the energy of the electron beam available for transfer to the radiation. As such, we call ν the '*free energy parameter*'.

Neglecting free energy depletion by taking the limit $\mu \ll 1$, the set of equations (7..9) reduce to:

$$\frac{d\phi_j}{d\bar{z}} = p_j \quad (13)$$

$$\frac{dp_j}{d\bar{z}} = -(Ae^{i\phi_j} + c.c.) \quad (14)$$

$$\frac{dA}{d\bar{z}} = \left\langle e^{-i\phi} \right\rangle \quad (15)$$

These universally scaled equations are identical in form to those describing the high gain Compton FEL([2] and references therein). By universal scaling we mean that the solution depends only upon the initial conditions δ and A_0.

Linear stability analysis of the above equations for an initially unbunched, monoenergetic resonant ($\delta = 0$) electron beam gives an intensity growth of $|A(\bar{z})|^2 \approx |A_0|^2 exp(\sqrt{3}\bar{z})$ for $\bar{z} > 1$. The parameter ρ then determins the growth rate. Also, as $|A|^2 \approx 1$ at saturation, this implies the saturation intensity scales as $I^{4/3}$. Using the analogy with FEL theory we call ρ the '*Fundamental Gyrotron/CARM Parameter*'.

Clearly, many of the results of Compton FEL theory now become applicable to gyrotrons and CARMs within the above assumptions and limits. We believe this to be a powerful statement, particularly with regard to effects not yet fully considered in the gyrotron/CARM literature e.g. superradiant effects and development of coherence. Work is currently underway to relax, or remove, the assumptions outlined above.

References

[1] G. R. M. Robb, in preparation.

[2] R. Bonifacio, N. Piovella and B.W.J. McNeil, Phys. Rev. A, 44, 3441-3444 (1991)

COMPUTER AIDED ANALYSIS OF INFINITE WAVEGUIDES

D. Muller*, L. Nicolas, A. Nicolas

Centre de Génie Electrique de Lyon - URA CNRS 829
Ecole Centrale de Lyon
BP 163 - 69131 ECULLY - Cedex
phone: +33 - 72.18.60.89
e-mail: muller,laurent,nicolas@trotek.ec-lyon.fr

Introduction

mWave is a software package solving in real time the analytical field equations to show the electric or the magnetic field - for either TE or TM modes - inside an infinitely long wave-guide of circular or rectangular cross-section. *mWave* is particularly usefull for the analysis of complex field topologies like those appearing inside of overmoded waveguides. (D. MULLER et al., Records of Compumag Conf. pp. 360-361, Miami, Florida Oct.31-Nov.4, 1993).

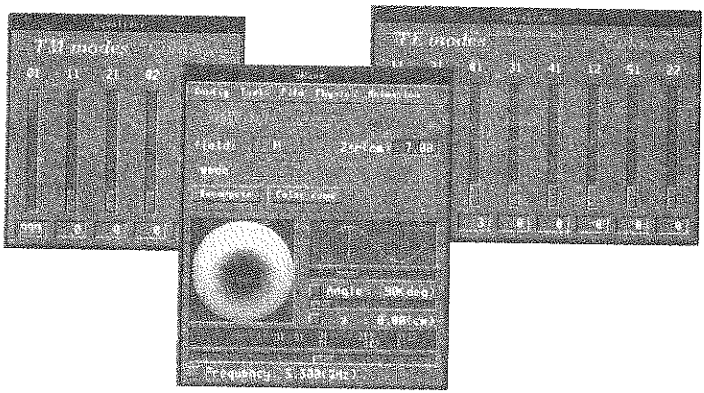

Figure 1: A typical screen layout of the *mWave* environment

The high order modes may be due for example to the geometric singularities of the guide and the field topologies of the overmoded waveguide may be computed by simulation programs taking into account its real geometry. Analyzing the results of such programs, attempts are made to determine which are the evanescing or propagating modes and which are their respective amplitudes - but until now, no tool existed allowing to examine the resulting field topology.

The user interface of *mWave* – conforming to the industrial standards X-windows and Motif – allows the end user to interactively specify the modes he wants to propagate and their relative amplitudes, and the solver is fast enough to provide instant feedback to these interactions.

Background

The COLOS project – where COLOS stands for "COnceptional Learning Of Science" – consists of ten groups from universities of seven European countries, whose goal is to use the potential of modern computer technology for a better and more direct approach towards presentation and understanding of basic concepts in science and technology.
This paper will present a contribution to that project. *mWave* is an environment for a better understanding of waveguides, intensively using the power of fast modern RISC-workstations to offer the students and the research staff a highly interactive environment allowing them to examine any desired configuration of the studied system with instant feedback.

Results

In this section we show an example of how we used *mWave* to identify the magnetic field modes appearing inside a Vlasov-type antenna.

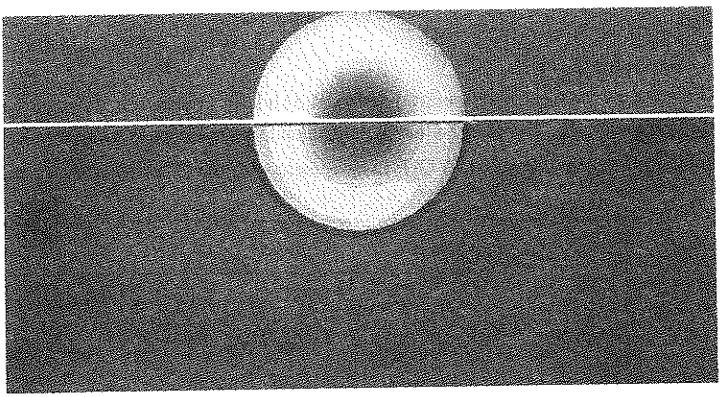

Figure 2: Comparison of *wave3d* (finite element software) and *mWave* results

The lower part of Figure 2 shows the instantaneous magnitude of the magnetic field inside a circular waveguide (Vlassov-type antenna) with a sixty degrees slant-cut angle, at the aperture of the guide and at time $t = 0$, as computed by the finite element *wave3d* package (L. NICOLAS et al., IEEE Trans. on Mag., MAG29 n°2, 1642-1645).

The upper part shows how we could obtain the same field topology by identifying the propagating modes using the *mWave* package. The mode with highest amplitude is TM_{01} which is the mode the antenna is developed to propagate, but we identified also additional modes TE_{01} and TE_{11}.

NUMERICAL SIMULATIONS OF THE VIRCATOR

Ph. Gouard*, O. Henry and F. Sellem
C.E.A./C. E. L.-V. 94195 Villeneuve-Saint-Georges Cedex, France

ABSTRACT

The VIRCATOR (virtual cathode oscillator) has been studied by the simulation code M2V. This two-dimensional particle-in-cell code resolves the Maxwell-Vlasov equations. Actually, it calculates only the emitted microwave frequencies. The microwave power from Poynting vector is in progress.

The code M2V has permitted to simulate the experiments following:

- Physics International experiments.
- CESTA experiments.

The simulation, described below, corresponds to the P. I. experience.

Fig. 1 and 2 display respectively the particle plots in both real (r versus z) and momentum space (P_z versus z). The momentum plot shows the formation of a strong virtual cathode situed at a distance of the anode equal to the anode-cathode gap. This virtual cathode has a strange form as a "shell-hole". The electrons, about this cathode, can only flow to:

- the real cathode.
- the waveguide internal wall.
- the symmetry axis.

Fig. 3 represents the frequency spectrum obtained by taking Fourier transform of the time history of the component E_r. The point, where is calculated this spectrum, is located to waveguide end. The dominant frequency is about 10 GHz in agreement with the experimental measures.

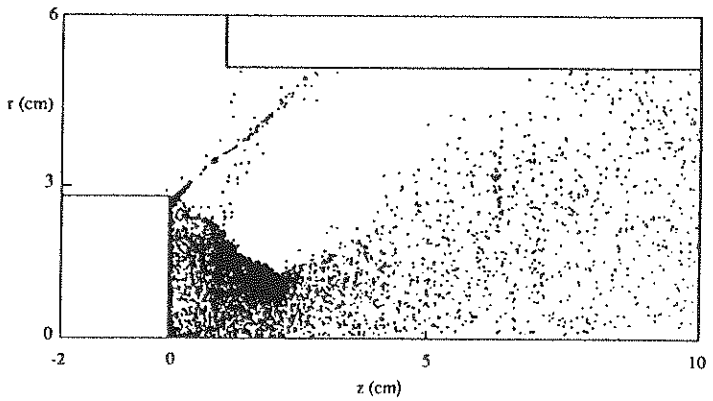

FIG. 1. Real-space (r-z) diagram of the electron beam.

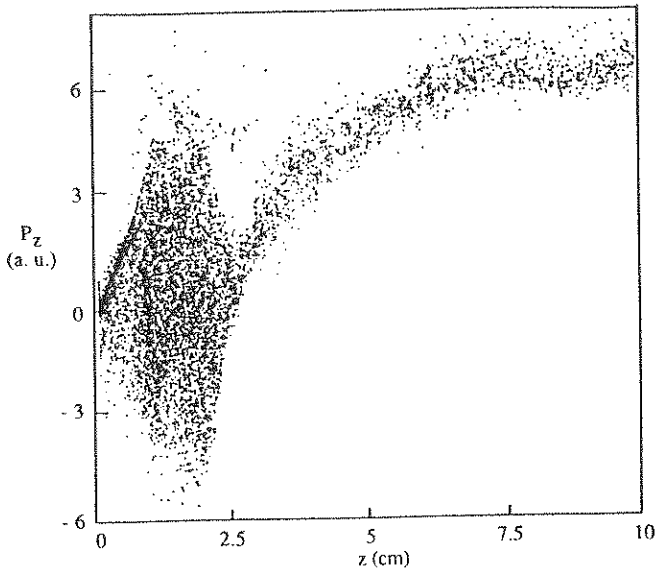

FIG. 2. Phase-space (P_z-z) diagram of the electron beam.

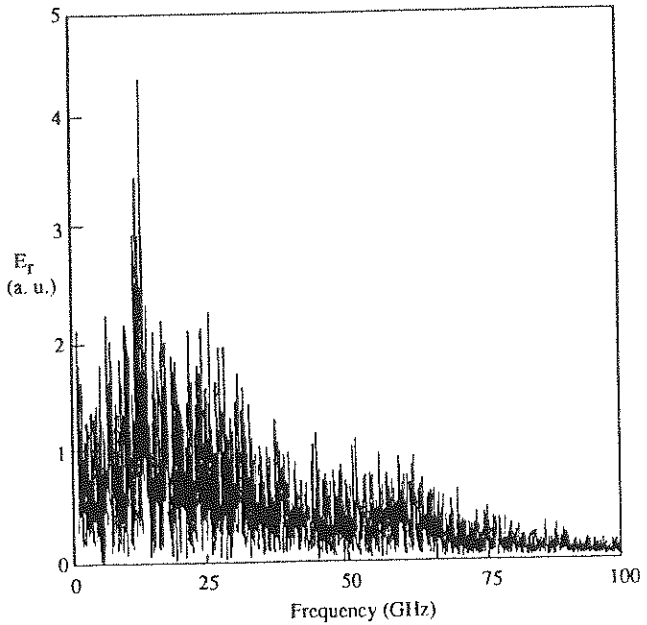

FIG. 3. Frequency spectrum obtained by taking Fourier transform of the time history of the radial electric field.

OPTIMIZING THE RADIATED PULSE OF TRANSIENT ANTENNAS

S.M. Booker*, A.P. Lambert, P.D. Smith

**Department of Mathematics and Computer Science,
University of Dundee,
Dundee, DD1 4HN, Scotland, UK.**

Antenna structures capable of supporting, essentially, transverse electromagnetic (TEM) spherical waves are characterized by their frequency independence over a wide bandwidth. This makes them ideal candidates for ultrawideband applications, such as transient field generation and reception.

The triangular plate configuration of the TEM horn (together with structures which may be derived from this) is of particular interest for a variety of *directive* wideband applications. These include: nuclear EMP simulation (J.J.A. KLAASEN, Proceedings of 10th International Zurich Symposium on Electromagnetic Compatibility, 317-322, 1993); impulsive field detection (M. KANDA, IEEE Trans. Antennas and Propagat., AP-31, 438-444, 1983); ultrawideband radar pulse transmission (D.M. PARKES, M.F. LEWIS, R.L.S. DEVINE, K. TRAFFORD & D. RICHARDSON, SPIE Vol 1631, 232-242, 1992); and feeds for paraboloidal reflector antenna systems (E.G FARR & C.E. BAUM, Sensor and Simulation Notes, Note 337, 1992). The basic design for such structures is based upon that of idealized, infinitely long, conical antennas. However, in producing practical antennas, which optimize the required characteristics of the radiated pulse train, several modifications to the initial design are possible. This paper will discuss two particular features of the TEM horn design: the prediction of the characteristic impedance for a given structure; and the effect of the horn profile on the output pulse.

Accurate estimation of the characteristic impedance of a given transient antenna is desirable for two main reasons. Firstly, by ensuring that the structure is correctly matched to the rest of the system, maximum power transfer to the active radiating elements is guaranteed. Secondly, the (possibly corruptive) effects of late-time reflections, due to mismatch at the antenna - free space interface, can be reduced by suitably tailoring the characteristic impedance towards the radiating aperture of the antenna. The original theoretical work on this topic, using conformal mapping techniques, was by Carrel, (R.L. CARREL, IRE Trans. Antennas and Propagat., AP-6,

197-201, 1958). However, experiment and subsequent re-examination of the analysis has shown his results for the TEM horn to be in error. Consequently, two alternative methods for estimating the characteristic impedance have been developed. The first is a new conformal mapping technique (A.P. LAMBERT, S.M. BOOKER & P.D. SMITH, submitted to IEEE Trans. Antennas and Propagat.) which is entirely self-consistent. The second is a numerical treatment, based upon a consideration of the feed region characteristics of the antenna (S.M. BOOKER, A.P. LAMBERT & P.D. SMITH, submitted to Journal of Electromagnetic Waves and Applications); this approach, which involves a time-marching solution of the Electric Field Integral Equation (EFIE), is suitable for a variety of TEM structures. An alternative numerical approach to the problem of transient antenna impedance, based upon an integration of the radiated electric near-field, may also be adopted in order to verify this technique. It will be shown that the results of both methods, theoretical and numerical, are in excellent agreement with those obtained experimentally, using time domain reflectometry (TDR).

A second parameter of considerable importance to the design of efficient, transient pulse radiators is the specific profile of the antenna. Given that the radiated power is related to the effective aperture of the antenna, flaring of a TEM horn can result in an increase in peak radiated power. However, modifications of this type also affect the shape of the resultant wavefront and the radiation pattern of the antenna and so a balance must be struck in order to obtain the maximum power increase, while still conforming to the required directivity and radiated waveform specifications. Numerical calculations of the electric far-field produced by a variety of horn profiles have been carried out, using a time-marching approach to the solution of the EFIE. It will be shown that, by a suitable selection of the horn profile, significant increases in the peak power can be obtained without significantly degrading the radiated waveform.

TIME DOMAIN ANTENNA MEASUREMENT TECHNIQUE

S. Skulkin

Radiophysical Research Institute, B. Pecherskaya 25/14, Nizhny Novgorod 603600, Russia
tel.: (8312) 360.129, fax: (8312) 369.902, e-mail: skulkin@nirfi.sandy.nnov.su

One of the most promising trend in the development of antenna technique is the measurement of antenna parameters using wideband sounding signals. Apart from determination of antenna characteristics at different frequencies the application of wideband signals can improve the measurement accuracy due to suppression of spurious signals scattered by surrounding objects (for instance, by elements of auxiliary equipment) and in some cases promote getting an additional information on the antenna tested. An effective way of wideband signal formation is generation of ultrashort (20-70ps) video pulses. The high accuracy of time domain (TD) signal measurements is provided by specially designed stroboscopic transformers. Such signals and transformers are used in the method of far field TD signal restoration by the measurements of near field TD antenna response (so called time-pulse method (TPM) of antenna pattern (AP) measurements). The set of AP in frequency domain is obtained by Fourier transformation of far field TD distribution.

This method is differed from known ones by some peculiar features. The use of "time window" in TD measurements make it possible not only to estimate the contribution of each element to the AP, but also to avoid errors due to elements of construction and surrounding objects. So, if one takes a time dependence of the field amplitude distribution and knows distances to the sources of spurious signals, then using "time window" it can be obtained more clear response of the antenna tested. The advantages of the "time window" (in connection with release of reflection) are usually regarded to have no sense for narrowband antennas since the time duration of the antenna transient process is sufficiently large as compared with the time duration of wave propagation up to surrounding objects. In fact, even in the room with a distance of about 2-3m to the surrounding objects the parameters of narrow band antennas can be measured at frequencies up from 2GHz. The same is true for narrow-beamed antennas with $D/\lambda \geq 10 \div 50$ (where D -the size of the antenna, λ-wave length). Actually the size of the measurement unit are usually comparable with the antenna size D. So the difference between time delays of sounding and scattered signals is $\sim D/c$ (by the order of magnitude). To separate these signals it is sufficient to have a passband of antenna-feeder system of about $\Delta\nu/\nu \sim c/D\nu = \lambda/D$. Besides, the time window duration can be reduced for some antennas. A complete release of reflection makes it possible to restore AP in full solid angle by near field measurements.

TPM can simplify a physical realisation of antenna parameter measurements at an arbitrary scanning surface. The transformation of near field measurement data is usually difficult for an arbitrary scanning surface. This problem is essentially simplified

in the case of sounding video pulses. The processing algorithm given in the report makes it possible to reduce the measurement data processing to vector adding of delayed bulks that saves a lot of computer time because it does not require calculating of special functions for each angle on the scanning surface and in the far field. The source of pulse signal must be matched only with a sounding antenna that helps greatly in solving problems of the measuring set and widens the types of antennas, studied without additional matching with a source of the pulsed signal. Therefore, the measurement set becomes versatile for a large class of antennas. When it is not desirable to disclose the operating frequency of the antenna, the TPM may also simplify measurements. This is because the information on the antenna operating frequencies is in pulse signals propagated in closed transmission channel connecting the antenna and the stroboscopic transformer and is inaccessible for a side observer at any power levels of sounding signals transmitted.

One of the interesting points in the development of the TPM is the design of a "flexible scanner" which is a measuring set consisting of 4 pulse antennas; one sounding and 3 reference ones. Since the pulse is always localized in time and, therefore, in space, then knowing cable lengths and coordinates of fixed antennas one can determine the location of the sounding antenna in space by the triangulation method. Such opportunity reduces greatly the requirements to the scanner accuracy and might be very promising in the cases impeding a precise scanner due to antenna size or other reasons. It should be also noted an appearance of an additional time coordinate in TPM measurements. Data redundancy appeared for some antennas give a possibility under definite conditions to get rid of one coordinate in the scanner, i.e. to carry out measurements along a line instead of a surface.

One more principal advantage of proper measurements in TD is a possibility to avoid an error of near field measurements usually encountered so far. It is connected with the fact that in real measurements the distance between a scanning surface and an aperture is not zero ($z > 0$). But for plane surface measurements the Fourier transformation procedure used for AP calculation it is supposed $z = 0$. An optimum distance between the aperture and the sounder is about 10λ. In fact, to hold this optimum distance is possible only at the measurements on a plane of plane antenna arrays. For mirror antennas this distance is limited by a mirror focal length. There are the similar errors at the measurements on a sphere or cylinder. Some results of estimation of this error by an example of circular plane aperture are given in this report.

There are some difficulties to be encountered in TPM practice. As a rule, a complicated design of ultrawideband sounding antennas with a ratio of frequencies $f_{max}/f_{min} > 100$ and generators. The problem of electromagnetic compatibility should be mentioned here, i.e. impossibility to carry out simultaneously precise radio measurements next to each other.

EVALUATION OF VANE STRUCTURES FOR APPLICATION IN MINIATURE TRAVELING WAVE TUBES

Thomas M. Wallett, NASA Lewis Research Center, Cleveland, OH 44135
A. Haq Qureshi*, Cleveland State University, Cleveland, OH 44140

NASA Lewis Research Center is interested in the development of a 30 GHz traveling wave tube (TWT) of reduced size and weight for a phased array antenna. Several potentially viable slow-wave structures, such as, vane type, disk-loaded, and tunnel ladder structures are being investigated. Results of our findings on the disk-loaded structures have been recently reported (T. M. Wallett and A. H. Qureshi, "Characteristics of a Cylindrical Disk-Loaded Slow-Wave Structure Found by Theoretical, Experimental, and Computational Techniques," *Int. Journal of Microwave and Millimeter-Wave Computer-Aided Engineering*, vol. 4, 1994, to be published). The vane type structures are frequently used as slow wave structures for linear magnetron tube devices but there is no evidence in the literature of their use in traveling wave tubes. This report presents results of ours investigations aimed at assessing the suitability of periodic vanes as the slow wave structure in traveling wave tubes in terms of their interaction impedances and losses. The ease with which these structures can be fabricated allows us to experimentally determine the characteristics of their scaled models and compare them to those obtained by general theoretical analysis and computer generated results.

A simplified TM mode analysis of a general vane structure with a roof has been carried out by Collin (R. E. Collin, "Foundation for Microwave Engineering", pp. 383-390, McGraw-Hill Book Company, New York, New York, 1966) and Watkins (D. A. Watkins, "Topics in Electromagnetic Theory", pp. 16-19, John Wiley & Sons, New York, New York, 1958). Assuming that the vane width is much larger than the roof height, the dispersion relation can be written as

$$\frac{1}{k_0 d \tan(k_0 c)} = \frac{s}{d} \sum_{n=-\infty}^{\infty} \left[\frac{\sin(\beta_n s/2)}{\beta_n s/2} \right]^2 \cdot \frac{1}{h_n d \tanh(h_n (b-c))}$$

where, b and c are, respectively, the roof and vane heights, d is the period, s is the slot spacing, k_0 is the free space wave frequency, $\beta_n = \beta_0 + 2n\pi/d$ is the n-th axial wavenumber, and $h_n = \sqrt{\beta_n^2 - k_0^2}$.

For slow waves, $\beta_n > k_0$ and $h_n \approx \beta_n$. The theoretical dispersion characteristics for a general vane structure without a roof ($b \to \infty$) can then be found from the relation

$$\frac{1}{k_0 d \tan(k_0 c)} = \frac{s}{d} \sum_{n=-\infty}^{\infty} \left[\frac{\sin(\beta_n s/2)}{\beta_n s/2} \right]^2 \cdot \frac{1}{\beta_n d}$$

Figure 1 shows a frontal view of all the tested circuits.

	A	B	C	D
Height/Width	*2.5"/2.5"*	*2.5"/2.5"*	*1.645"/1.11"*	*2.2"/1.11"*

Figure 1 - Profiles of four vane structures investigated

All vanes were 0.075" thick with 0.15" gap spaces between vanes. The holes for structures B,C, and D are centered 1.645" above the base with a diameter of 0.59". Resonance frequency measurements were taken for all structures with and without a 0.25" radius alumina dielectric rod using a Hewlett-Packard 8510C network analyzer. The alumina rod was placed at the top center of structure A and at the center of the holes for the other structures.

The four vane structures were also modeled and analyzed using numerical techniques. The resonance frequencies of the simulated structures were found with and without a simulated perturbing dielectric rod having a cross section equal to that of the actual alumina rod. Interaction impedances were then calculated for all four structures.

The dispersion characteristics of all the four circuits exhibit the familiar pattern of gradual increase with frequency. The dispersion characteristics of circuits A and B are found to be almost identical as expected. The theoretical, experimental, and computational results for each of the four structures are in favorable agreement with each other.

The interaction impedance of all the structures calculated from the cold test results show, in general, a decreasing trend with frequency. Structure A exhibits the highest impedances both experimentally and computationally. However, the agreement between the experimental and computed results for this structure is not as close as in the other three structures.

An important parameter is the circuit loss per wavelength. It is inversely proportional to the quality factor Q of the structure and directly proportional to the ratio between the phase and group velocities (v_p/v_g) of the signal. Its value is experimentally measured using two circuits of different lengths to negate the effect of coupling losses. The parameter Q was obtained analytically and v_p and v_g were determined from the dispersion characteristics. Losses for the four structures were measured as well calculated. These results enable us to assess the suitability of these structures for use in miniature microwave devices.

RADIATION OF NONSINUSOIDAL WAVES BY APERTURE ANTENNAS

S.P.Skulkin*, V.I.Turchin

Radiophysical Research Institute, Nizhny Novgorod, Russia
Institute of Applied Physics AS, Nizhny Novgorod, Russia.

Introduction of wideband radars radiating complex time signals as well as the development of ultrawideband radars (UWBR) with large aperture antennas require a new approach to the analysis of antenna systems used. The presence of such a main parameter as an antenna pattern (AP) may be insufficient for the analysis of a field produced by such systems even if the set of AP are measured at many frequencies. UWBR designers become interested in time relations (TR) of radiated signals and it being not only in the far field zone. If radars are placed at complex objects, then for their optimum arrangement one needs to know field TR in the near-field zone. A practical need in the analysis of field TR arises also in measurements of antenna parameters by time domain near field zone method. As it will be shown in the report, the calculation of the aperture antenna field TR is more simple than that of the antenna field at a fixed frequency and the form of pulse radiated characteristic (PRC) is easy to interpret. A calculation method is proposed for PRC of plane apertures. Strict formulas are given for PRC of circular and rectangular plane apertures for any point of half-space before the aperture under the condition that every aperture point radiates a δ-pulse. The real PRC of the signal is obtained as a result of convolution of the radiated signal, PRC of radiating elements (or PRC of a feed in the case of mirror antenna) and PRC of an aperture. According to the reciprocity principle the same time dependence will be observed at the output of the antenna receiving a signal of point pulse source having the same coordinates as the observation point in the case of the radiating aperture. When deriving the resulting time domain PRC $E_s(t, \vec{r})$ (here $\vec{r}$ is radius-vector of the observation point) we neglect the vector character of the field, use the Kirchhoff integral up to terms decreasing as $(1/r)$ and take into account that the radiating surface is inphase, the aperture size is much more than the wavelength ($D >> \lambda$) as well as the directivity factor of the Huygens element. The use of δ-function in the subintegral expression makes it possible to come from a two dimensional integral to one-dimensional one over a line of cross-section of the radiating surface and a sphere with a center at the observation point and radius $c * t$ (c-light velocity, t-time). The result is presented in a form of elementary functions. A detailed analysis is given for PRC of circular and rectangular plane apertures for near and for far field zones. Here the near-field zone is understood as an area from the aperture up to a distance a bit larger than the aperture size, i.e. a region between the aperture and the Fresnel zone. PRC is shown to have different form in a zone of projector area (a geometrical extension of the aperture) and in the region outside the limits of the projector area.

The qualitative space-frequency characteristics of the inphase antennas at fixed frequency in the near field is studied in detail. The corresponding formulas are rather cumbersome. Even for apertures of the simplest form (circular, rectangular) at distances permitting expansion of $|\vec{r}-\vec{r}_a|$ in a series with only quadratic terms (Fresnel approximation) the field is represented in a form of either special function expansion for the circular plane aperture or combination of Fresnel integrals for the rectangular aperture. An expression obtained in time domain are turned out to be simpler than well known ones of aperture antenna fields for a monochromatic signal and can be used for calculation of the space-frequency field characteristic of the aperture antenna.

STUDY OF SCHOTTKY- CONTACT COUPLED MICROSTRIP DIRECTIONAL COUPLER

M. El-Kordy and A. A. Abou El-Fadl
Electrical Commu. Dept., Fac. of Electronic Eng.Menouf, EGYPT

Summary:

An accurate study of Schottky- contact coupled microstrip lines is presented. Green's function has been used to determine the depletion layer capacitance of the even and odd modes. This technique has been applied to calculate the propagation chracteristics and the coupling coefficient of the coupled lines . The dependence of the slow wave factor and the attenuation on the resistivity of the semiconductor substrate has been studied. It is found that the resistivity 1Ohm.cm is convinient with minimum attenuation. It is also noticed that, in the even mode more field lines passed through the conductive layer than those in the odd mode. With this technique, the calculated predictions of the coupled microstrip lines are in good agreement with the published data.

The spectral domain method SDM (T.C.MU et al., Electron. Lett., 21, 946-947, 1985) was used to determine the propagaton characteristics of the coupled lines printed on semiconductor medium. In the SDM the doped region of the semiconductor substrate is treated as a dielectric layer with constant resistivity. The field which was far from the conductor is also assumed to have little effect on the propagation characteristics.

In this paper, the fringing field capacitance is involved in our calculation. Green's function (M. El-Kordy, Ph.D. Thesis, Menuofia University, EGYPT) has been used to transfer the two-dimensional Possion's equation into the following integral equation.

$$V(x,y) = \frac{1}{\epsilon} \int_{x_o} \int_{y_o} G(x/x_o, y/y_o)\ \rho(x_o, y_o)\, dx_o\, dy_o \qquad (1)$$

Eq.1 could be solved for the coupled lines of Fig.1, at y >0.0 and y <0.0, ρ_{ij} can be calculated at the respective applied biased potential and consequentially the following capacitances are calculated:

$C_{11} = \delta Q_{11}/\delta V_{11}$, $C_{12} = \delta Q_{12}/\delta V_{12}$,....., $C_{21} = \delta Q_{21}/\delta V_{21}$ and $C_{22} = \delta Q_{22}/\delta V_{22}$

The even mode capacitance is given by $C_e = C_{11} + C_{12}$

The odd mode capacitance is given by $C_o = C_{11} - C_{12}$

The elements values of the equivalent circuit (M.El-Kordy et al., Proc. URSI, B6,(1-10), 1993, Cairo, EGYPT) can be calculated using the previous depletion layer capacitances at the even and odd modes, then the propagation characteristics has been determined.

Fig.2 shows the frequency behavior of the slow wave factor for the even and odd modes. The figure includes also the results obtained using SDM (T.C. MU et al., Electron. Lett., 21, 946-947, 1985). The curves are plotted for the semiconductor resistivity of 1 Ohm.cm (doping concentration 5.1E+15 /cm.

The attenuation constant of the even and odd modes as a function of resistivity of the substrate is displayed in Fig.3 to compare it with the data obtained by SDM. The attenuation obtained by both techniques exhibit some discripancies for the determination of the optimal resistivity value. The difference between the resistivity calculated by the two techniques at the minimum attenuation not exceed 0.2 Ohm.cm.

The variation of the real and imaginary parts of the characteristic impedance with the frequency are illustrated in Fig.4 , while Fig.5 indicats the frequency dependence on the coupling coefficient. It is noticed that the coupling is reduced by increasing the frequency because the difference between the resistivity in the even and odd modes is reduced.

Conclusion:

Schottky contact coupled microstrip lines have been analized using Green's function technique. The propagation characteristics of both even and odd modes are obtained with good accuracy over a wide range of frequencies and resistivities of the semiconductor. With this technique the best value of the substrste resistivity has been determined. The validity of our technique has been proved by the comparison with SDM. The discrepancy between our findings and SDM is due to the effect of the fringing field.

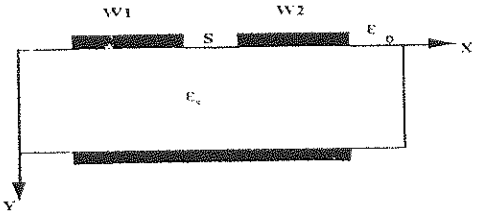

Fig.1 Coupled microstrip directional coupler

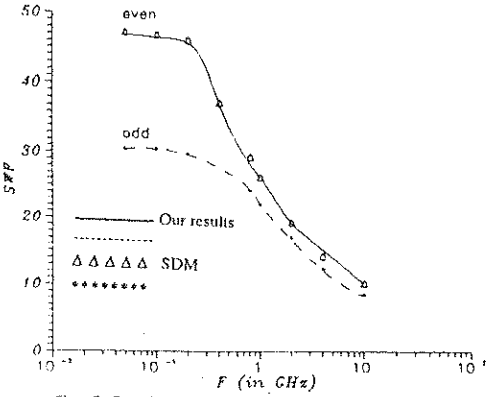

Fig. 2 Relation between SWF and frequency of Schottky contact coupled microstrip lines
W=0.1mm S=0.5mm ρ=1 Ohm.cm εs=12

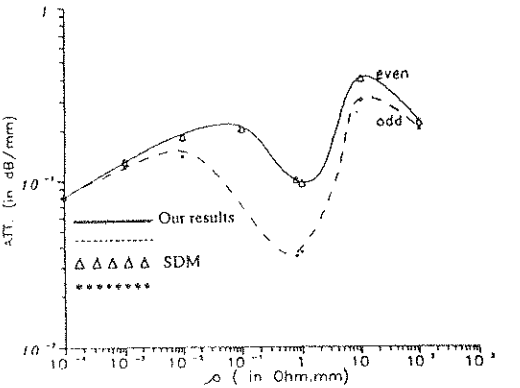

Fig. 3 Relation between attenuation and resistivity of Schottky contact coupled microstrip lines
W=0.1mm S=0.1mm F=1GHz

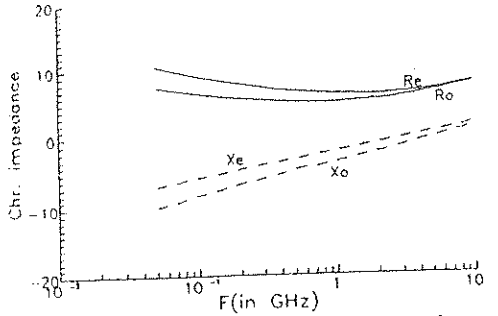

Fig. 4 Relation between char. impedance and frequency of Schottky-contact coupled microstrip lines
W=.1mm S=.5mm ρ=1 Ohm.cm , εs=12

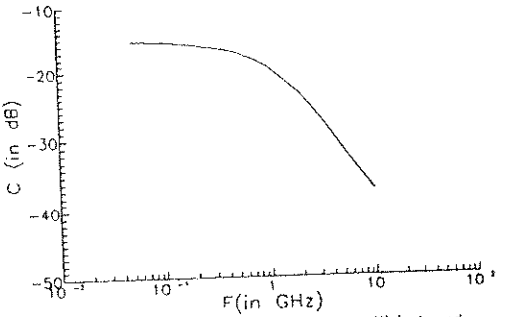

Fig. 5 Relation between coupling coefficient and frequency of Schottky-contact directional coupler
W=.1mm S=.5mm ρ=1 Ohm.cm εs=12

MUTUAL COUPLING IN A FINITE PLANAR ARRAY OF CIRCULAR MICROSTRIP ANTENNAS

P.S.Bhattacharjee (India)

This communication describes a solution to the problem of computing mutual coupling of a finite planar array of circular microstrip antennas fed by coaxial probes. Equations have been presented for the calculation of inter-element mutual coupling in a finite size planar array of circular patches. The general expression for mutual impedance (1.Mutual Impedance Between Circular Microstrip Antenna-P.S.Bhattacharjee ;MOT Letters,vol.6,April'93) is used for calculating coupling between different elements of the two dimensional array excited in TM_{11} mode. An agreement between the calculation for 10X10 array and experimental results establishes the validity of the theoretical model.

The use of microstrip antennas in arrays is becoming increasingly popular owing to its low profile,light weight and low cost. But the inter-element coupling is of paramount importance and it is required while designing an array. An appreciable level of coupling can result in mismatch of individual element with the feed and distortion of the radiation pattern.

Mutual coupling effects are caused by radiation through free space and space waves launched through the dielectric material. Mutual coupling arising out of the first way gas been talen into account here. The assumption that surface wave is not so predominant compared to the radiation is valid so long the substrate used is of low dielectric constant and the patch antenna is electrically thin. Moreover it is tacitly assumed here that the field configuration remains unperturbed owing to anther resonator in vicinity. The inter-element spacings, d_x and d_y respectively along X and Y axes, albeit different are uniform along a particular direction (Fig. 1).

Here,each circular patch is replaced by an equivalent magnetic current source distribution placed along the circumference of each patch over a grounded dielectric slab derived from the electric field on the wall of the element, predicted by cavity model. Based on the reaction theorem, mutual impedance (1) is calculated. from the knowledge of the port impedance matrix the scattering matrix is formulated for elements at different positions i.e. along the X axis, the Y axis and diagonally also. The coupling coefficient defined as, $C_p = 20 \log_{10} |S_{12}|$ has been computed for different elements of the planar array. Scattering parameters are measured using HP-8410B network analyzer. Calculated and measured E-plane coupling coefficients typically agreed to within 1.4dB for frequency upto 2.0GHz (Fig. 2(a) & 2(b)).

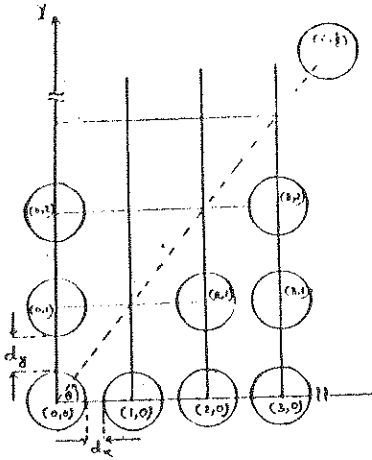

$$\theta_{ij} = \tan^{-1}\left(\frac{j \cdot 2a + j \cdot d_y}{i \cdot 2a + i \cdot d_x}\right)$$

d_{ij} = distance between circumferences of the elements at (0,0) and (i,j)

$$= \left[\{i(2a + d_x) - 2a\cos\theta\}^2 + \{j(2a + d_y) - 2a\sin\theta\}^2\right]^{1/2}$$

$1 \le i \le n$

$1 \le j \le m$

Fig 1 Position of elements in an n×m array

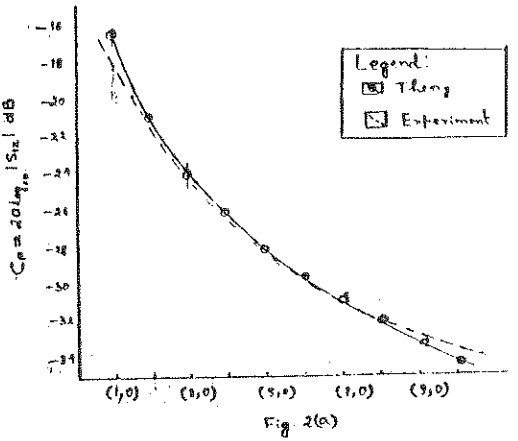

Fig 2(a)

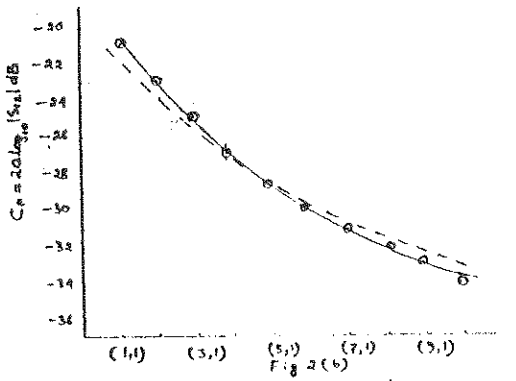

Fig 2(b)

$\epsilon_r = 2.55$; $a = 0.01831$ m ; $t = 3.0480 \times 10^{-3}$ m.

Fig 2(a), 2(b) Variation of coupling with position of elements

3D VHF MAPPING OF LIGHTNING DISCHARGE

P. Laroche*, A. Bondiou, P. Blanchet, B. Deltour and J.Pigère

Office National d'Etudes et de Recherches Aérospatiales
B.P. 72, 92322 Chatillon Cedex, France

Electromagnetic measurements in HF and VHF range are the more efficient way to obtained complete and detailed information on intra cloud and cloud to ground lightning processes. To interpret observations of VHF signals related to lightning activity, ones needs to consider how each single component of a flash radiates in a selected frequency range. Above few tens of MHz, it appears that only negative leaders and recoil streamers radiates a power which magnitude provides a good detectability over large spatial area. The positive leaders which exhibit lower current and higher rise time do not radiate significantly in VHF. ONERA had set up a 3D VHF high resolution interferometer designed to provide a continuous monitoring and location of lightning activity during a storm life cycle. Large amount of data had been obtained during experiment conducted with MIT (Massachusetts Institute of Technology) near the International Airport of Orlando (Central Florida) during the summer 1992 and 1993.

First, we give in this paper a description of the natural lightning phenomenology within cloud. Observations are used to describe the organisation of the lightning activity within a storm. They confirm that the lightning channels have an important horizontal extension. Three altitude ranges of lightning activity appear:

- the negative stepped leader between ground level and the lower part of the cloud,
- the horizontal recoil streamer in the negatively charged part of the cloud,
- the horizontal recoil streamer in the upper positively charged part of the cloud.

We then present and discuss a comparison between 3D VHF location and the low frequency wide band field variations measured simultaneously with capacitive antenna.

LIGHTNING STRIKE EFFECTS ON COMPOSITE-HYBRID CONNECTORS AND CABLE WIRING SYSTEMS

Clarence D. Bond*
U.S. Naval Research Laboratory
Washington, DC 20375

and

David P. Smith
SFA, Inc., Landover, MD 20785

and

Matthew R. Maier and Mike Whitaker
U.S. Naval Air Warfare Center, Aircraft Division,
Patuxent River, MD 20670

The development of composite airframes that employ nonconductive or partially conductive materials has greatly reduced the conventional protection of the all-metal airframe against the high current surges of lightning strikes. This problem has become particularly critical with the simultaneous use of the more vulnerable fly-by-wire control systems and the introduction of new composite-hybrid connectors and cable wiring systems.

The composite-hybrid connector systems were developed to reduce weight and improve corrosion resistance, while the development of ROI (Ribbonized-Organized-Integrated) type wiring harness systems was introduced to provide a lighter-weight non-random wire spacing with improved control of EMC and EMI. The introduction of these new cable-connector technologies has necessitated an independent evaluation of the vulnerability of these new systems under the lightning strike environment encountered in the operation of naval aircraft.

This paper specifically addresses the electrical effects of the indirect high-current transient surges that pass through the low impedance conduction paths of cable harness shields, connector shells and chassis enclosures, as might be found in composite airframes or in composite-metal airframes. The indirect pulse current is simulated by the pulse waveform 5B as recommended by the SAE-AE4L Committee and is a

unipolar double exponential pulse having a rise-to-peak time of 50 μs ± 20% and a 50% decay time of 500 μs ± 20%.

Six different cable-connector systems have been subjected successively to ground injection currents of 0.5, 1.0, 3.0, 10.0, 15.0, and 20.0 kA. The resulting electrical effects of thermal/mechanical damage, degradation of electrical parameters and induced waveforms on the internal wiring are presented for the six systems.

FRICTIONAL ELECTRIFICATION ON ICE

HISASHI SHIO
Department of Physics, Faculty of Education, Hokkaido University of Education

Abstract

Since it is considered that the mechanism of the main charge generation in thunderclouds is related with the electrical property of ice (snow crystals, graupel, and hail stones), the property has been studied bymany meteorologists. Latham (1963) reported that when two pieces of ice of different temperature were slided together, the ice block with lower temperature was electrfified positively against the other with higher temperature. The same result was found independendently by Reynolds, and Gourley (1967) Moreover, Latham and Mason (1961) attempteo to explain these results theoretically based on different mobility between HO_3^+ and OH^- in steady temperature gradient in ice. Recently, however, it was noted that the charge separation in ice could not alway be expained by this theory, but was influenced by other factors, even if the ice was produced from pure water; for example Shio and Magono (1971) indicated that the sign of frictional electrification was mainly determined by change in contact spot from a uniform surface to a surface of irregular cell boundaries (poly crystal), namely, there is past history on frictional electrification. In this paper we made the trial to investigated the effects of the crystallographic characteristics of the surface of specimen on frictional charging phenomenon. As a result, the following new facts were revealed; 1. In the case of an asymmetric rubbing between a pair of face differently orientated with respect to crystal axes, the rubbed face with prism plane was invariably positively electrified against that of the basal plane, regardless of the temperature difference between pairs of the rubbed faces. 2. However, at about -6°C the electric potential of the prism plane against the basal plane was greatly reduced and became so little as to be neglected. 3. As regards pairs of faces identically orientated with respect to crystal axes, the electric potential of the rubbed face with a cold spot against that of a hot spot was reversed from positive to negative at -6°C or thereabouts as the ambient temperature rose. Since the magnitude of the scratch hardness of ice were dependent on the difference of crystallographic orientation of the rubbed surface, in order to check whether the sign of charging was dependent on the anisotropy of the scratch hardness or not, the author investigated the frictional electrification on ice specimens hardened by a thermal shock. At sliding speeds of as 3.4 cm/s the sign of charge of the hardened surfaces was always positive regardless of the temperature difference and the anisotropy of crystal faces. The mechanism for this behaviour is considered to be as follows: The usual surface

is deformed plastically by rubbing to a higher degree than the hardened surface; excessive dislocation then occurs in the deformed surface layer, and a part of this dislocation may be separated into a dislocation-jog sharged negatively and H_3O^+; the deformed surface with the remains of the dislocation-jog may be negatively electrified as against the hardened surface with increasing of H_3O^+, according to the differece of mobilities.

COUPLING OF ELECTROMAGNETIC PULSES LIKE LIGHTNING ON LARGE GROUND NETWORKS OF BUILDINGS

Jean-Luc BABIGEON - société CHELTON FRANCE - 12 Rue Charles de Gaulle - 78350 JOUY EN JOSAS - tel/fax : 16 1 46 30 91 74

INTRODUCTION

Until now, the theoretical study and calculation of electromagnetic coupling were limited by the complexity of structures and networks. A lot of work has been done on well defined objects, like towers, antennas, unique cable, etc... EMP, LEMP and ESD are considered as the most dangerous sources of perturbations on electronic equipments inside buildings. Our approach is confined to LEMP, but could be generalized to NEMP, with some precautions. We have based our analysis on the following ideas :

- the EM coupling of LEMP in a ground network can be reduced to a conduction problem,
- the new generation of grounding networks can be represented by 2D networks made of RLC components.

DESCRIPTION OF LEMP PROPAGATION INSIDE A BUILDING

The typical grounding of a building is shown by the following figure :

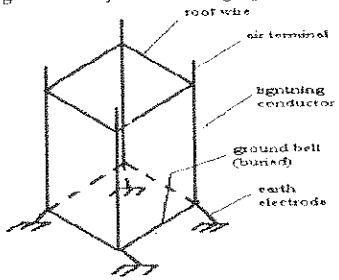

We have considered the simplest type of building, constituded of a unique floor, but our method can be repeated for a complex building. LEMP can couple by two ways :

- direct struk on a wire of the network, basically air terminal or roof wire if the protection is well concepted,
- indirect effects by induction on down conductors.

The primary pulse is then distributed partly in the meshes of the grounding network, partly in earth electrodes. If the voltages or currents appearing in the meshes are important, all references of electronic equipments and alimentations will be suddenly raised. The picture sometime presented, is these one of all the grounding network floating upon its earth electrodes, but there are at least two reasons for thinking that it is probably wrong. The goal is then to calculate the electric stresses applied at the nodes of the grounding network, previously defined.

APPROXIMATIONS

We have used the following approximations :

- the treatment of the problem can be restricted to conduction aspects only, with the Kirchhoff tool

- capacitive part of soil and transmission lines responses are neglected

We avoid the prior time effects of LEMP, say HF radiations on unintentional antennas. The result is to assimilate the return strike like a current or voltage source, which is connected to a node, or accros a mesh of the network. Recent experiments have been realised with current source which waveform was $1/40\mu s$, where we mean here the rise time and width. We have computed the spectra of that waveform, and we see easily that the maximum frequency generated is 50 kHz (10 % of the voltage remaining). Other experiments may be driven with shorter waveforms, but we emphasize the limit of generaly used spectra : 1 MHz max. It's well known that below 1 MHz, capacitive effects of soil are neglected.

REPRESENTATION OF THE NETWORK

We have also determined a set of electrical properties for the wires of the network : resistance, inductance of meshes, resistance and inductance of earth electrode, with the hypothesis of mean soil of 10000 Ohm/cm.

The precedent schematic of network is drawn in 3D dimensions. We have imagined to "unfold" it in a 2D sheet, and the result is represented by the following figure :

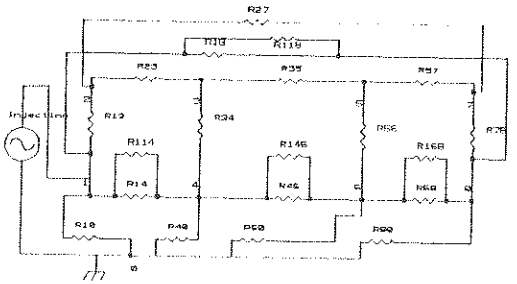

R27 and R18 are then relative to the fourth side of the building. We have only represented the (DC) resistances of the wires, but it is easy to complete it with the inductances, inserting them serially with the resistances. The four earth electrodes are R10, R40, R60, R80. The grounding interconnecting belt is represented by R114, R146, and R168. The source is connected either to node 1 (base of mesh 12 and start of earth electrode R10), or to node 2 (top of the roof and one of the air terminal). All earth electrodes are strongly coupled. Calculations have been made in time and in frequency.

RESULTS

We have obtained amplitudes of the currents at all the nodes, especially at earth electrodes. The data seem consistent with experiments and the previous literature. For instance, the injected waveform being a current pulse, with a peak current really injected of 1,7 kA, the peak current at first earth electrode is 400 A, and the peak current at a mesh "far from injection", is 70 A. CHELTON FRANCE has gained the experience permitting the prediction of LEMP response of real grounding networks, knowing the electrical drawings. We have also tried to acquire a more comprehensive description of these data. That supplemental work could be exposed in a more detailed paper.

EQUIVALENT SCHEME (WITH LUMPED PARAMETERS)FOR A NODE WITH N LINES AND IMPEDANCE TO GROUND,STRUCK BY LIGHTNING.

M.W.KOSTENKO

ST.PETERSBURG,RUSSIA

ABSTRACT

Quasi-linear partial differential equations for return-stroke lightning during initial stages of transformation from last streamer-leader step to return stroke were obtained in the form:

$$-\frac{\partial i}{\partial x}=\frac{\partial q}{\partial t}+G*u=C_d*\frac{\partial u}{\partial t}+T_d*\frac{\partial i}{\partial t};\ C_d=\frac{\partial q}{\partial u}\ ;\ T_d=\frac{\partial q}{\partial i};$$

$$-\frac{\partial u}{\partial x}=\frac{\partial \Phi}{\partial t}+E=L_d*\frac{\partial i}{\partial t}+Z_a*\frac{\partial i}{\partial x};\ L_d=\frac{d\Phi}{di}=\frac{\partial \Phi}{\partial i}+\frac{\partial \Phi}{\partial r_L}*\frac{dr_L}{di}, \qquad (1)$$

where i and u are the current in lightning channel and voltage with respect to the earth,q is the total line charge density(also taking into account the surrounding volume charges),Φ is the magnetic flux,$E_a=du_a/dx$ is the longitudial component of the electric field on the lightning channel surface, $G\geq 0$ is the conductivity to the earth, $u_a=A*i^{\alpha}$ is the active voltage drop($A=Const$, $\alpha=Const<1$) at the last streamer - leader step, $Z_a=du_a/di=f_a(i)$ is dynamical impedance, $r_L=B*\sqrt{i}$ is the radius of lightning channel; $C_d=f_C(i,u)$, $T_d=f_T(i,u)$, $L_d=f_L(i)$ are dynamical capacitance, delay and inductance. These parametrs have to take into account heating, expansion and negative arc impedance of return stroke channel and neutralization of space charges surrounding leader channel.

One solves equations (1) by the method of characteristics and obtains:

$i(t,x) = i(\xi)$; $u(t,x) = u(\xi)$; $\xi = t - x/v$; $v = f_v(i,u)$, (2)

where v is return stroke phase velocity. It is equal to:

$$v = \left\{ Z_a - T_d/C_d - \left[\left(Z_a - T_d/C_d \right)^2 + 4 * L_d/C_d \right]^{1/2} \right\} / (2 * L_d). \quad (3)$$

Respective dynamical du/di and equivalent Z_{eq} impedances of the returne stroke channel are:

$$du/di = F(i) = v * L_d - Z_a \; ; \; Z_{eq} = u/i = \left[\int_0^i F(i)\,di \right] / i. \quad (4)$$

Numerical integration of equations (4) are performed for Z_a, T_d, C_d and L_d dependances of i and u according to laboratory results with variations over wide ranges.

One gets the following empirical approximate formula:

$$Z_{eq} = 140 * (i + 240/i_\lambda) \quad \text{if } i_\lambda < I_\lambda(\max) \text{ and } t < t_f, \quad (5)$$

where Z_{eq} and i_λ are expressed in ohms and kiloamperes.

One determines u_x voltage in X-node with respect to ground according to equivalent scheme in fig.1, with current sources i_λ, i_n and lumped impedanses Z_x, Z_Σ, Z_{eq}:

$$u_x = (i_\lambda + i_n) * \left[Z_x^{-1} + Z_\Sigma^{-1} + Z_{eq}^{-1} \right]^{-1}; \quad (6)$$

$Z_\Sigma = \left(\sum_{j=1}^{n} Z_j^{-1} \right)^{-1}$ is the equivalent impedance of n lines,

Z_j is impedance of line j=1,2...n,

Z_x is the impedance in X - node to ground,

i_λ is calculated lightning current for $Z_x \to 0$,

$$i = \begin{cases} 0 & \text{before waves reflected from neighbouring} \\ \sum_{j=1}^{n} 2 * u_{jx}/Z_j & \text{nodes enter in X-node,} \\ & \text{after this moment.} \end{cases}$$

Voltages u_{xj} of waves, leaving X-node along j= = 1,2...n lines are equal to:

$$u_{xj} = u_x - u_{jx}. \quad (7)$$

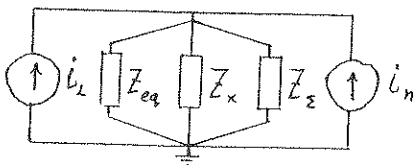

fig. 1

USE OF THE TIME DOMAIN ANALYSIS FOR THE MICROWAVE CHARACTERIZATION OF MATERIAL WITH RELEVANT PERMITTIVITY AND PERMEABILITY IN A TRANSMISSION LINE

Thanh-Tuyen NGUYEN*, Geneviève MAZE-MERCEUR, Jeanne GARAT
CEA-CESTA, BP n°2, 33114 Le Barp - FRANCE

Microwave characterization is of great interest in a number of microwave and millimeter-wave applications. This is carried out either in free space, in cavities, or in a transmission line and waveguide, depending upon whether the material is thick or thin, homogeneous or heterogeneous, isotropic or anisotropic. The Transmission/Reflection method in a circular coaxial line is well adapted to the broad-band characterization of isotropic, homogeneous material of dimensions of several square centimeters. However, it does not work well for materials having relevant value of index $((\varepsilon_r.\mu_r)^{1/2}$ because at frequencies where the sample length is a multiple of one-half wavelength in the sample, the equations for ε_r and μ_r are algrebraically unstable. To bypass this problem, a time domain analysis is performed.

The reflection coefficient (S_{11}) of a sample inserted in a transmission line can be interpreted as the infinite summation of optical rays: the first one is reflected on the first interface air/sample, and all the others are transmitted, arising from multiple reflections inside the sample. The transmission coefficient (S_{21}) can be interpreted as the infinite summation of the rays transmitted on the second interface sample/air. Consequently, the reflection and transmission coefficients are computed using the Inverse Fourier Transform (IFT) as a means to exhibit the mismatching at the interfaces in the time or space domain.

According to the nature of the material (lossless or low-lossy, and frequency dependent or independent), the IFT of S_{11} or S_{21} can be expressed analytically. In certain cases, ε_r et μ_r can be derived from it.

As an example, the IFT of the scattering parameters of an amagnetic sample (sample ①: $\varepsilon_r \cong 100$ -j0, thickness = 2.0 mm) is processed and shown in figure 1. The constant distance between the Dirac peaks as well as the constant slope confirm that the real part of the dielectric constant is equal to 105 (±5%) and the imaginary part is less than 10^{-3}.

Generally speaking, this time domain analysis treatment leads to the following conclusion:

- The IFT enables us to determine ε_r and μ_r corresponding to lossless or low-lossy, and frequency independent materials.

- The Sliding Short Fourier Transform (SSFT) leads to the permittivity determination corresponding to low-lossy and frequency weakly dependent materials.

Application to another material (sample ②) having a dielectric constant equal to about 3200 is carried out: its characteristics have to be determined on a required wide frequency band (0.5 to 18 GHz). However, measurement results realized on this same sample at discrete frequencies up to 5 GHz in a resonant cavity are known and mentioned in table 1. The problem is that the dielectric constant determination at high frequencies turns out to be impossible by the perturbation method in a resonant cavity. The knowledge of these results shows that the Transmission/Reflection method cannot be applied because of the sample length limitation as explained above, which shows the interest of this time domain technique.

Consequently, a 2mm sample ② has been characterized using the time domain analysis. The transmission coefficient SSFT has been performed and result corresponding to the real part of the dielectric constant is given in figure 2. A good agreement is obtained with discrete values measured in a resonant cavity at frequencies up to 5 GHz. This time domain analysis using the IFT or SSFT processing can obviously compete with the perturbation method in a resonant cavity thanks to use of the broad-band characterization.

In the final paper, the mathematical derivation will be addressed. It will be shown that owing to this method, it is possible to give a priori information on unknown samples.

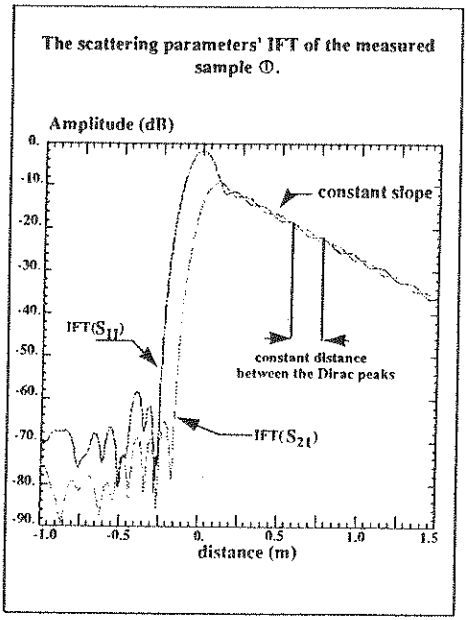

- figure 1 -

f(GHz)	1.4	2.5	3.4	4.6
epsilon	3203	3015	3450	2942

- table 1-

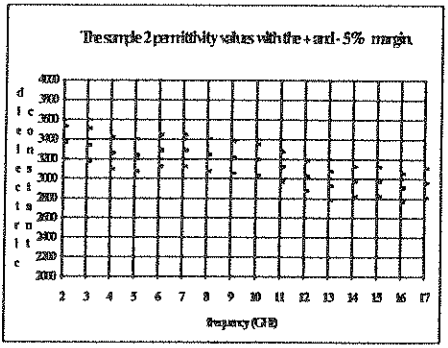

- figure 2 -

FREE-SPACE MEASUREMENT OF COMPLEX PERMITTIVITY OF LOSSY MATERIALS AT MICROWAVE FREQUENCIES

M. Van Craenendonck *, J. Dauwen and H. Pues
Grace N.V., Nijverheidsstraat 7, 2260 Westerlo, Belgium

This paper describes a free-space technique to measure the complex permittivity of planar lossy materials between 2 and 18 GHz. The technique is based on a simple transmission measurement between two broadband horn antennas using a vector network analyser. The complex permittivity is calculated starting from the measured complex transmission coefficient (S21). This free-space measurement method has several advantages in comparison with standard transmission line techniques : it is fast, broadband and non-destructive as the samples do not need to be machined.

A common technique for measuring permittivity and/or permeability of solid materials is the so-called transmission line technique. It implies the use of a coaxial line or waveguide and the samples need to be machined very accurately in order to completely fill the cross section of the transmission line. The accuracy of the measured material parameters is very high. Although this technique has proven its usefulness, for quick and routine testing a non-destructive method would be more suitable. Several non-destructive measurement methods have been described in the literature : the open-ended coaxial probe technique (J.P. Grant et al.,J. Phys. E:Sci. Instrum. 22, 757-770, 1989), a free-space technique using two spot-focusing horn lens antennas (D.K. Ghodgaonkar et al.,IEEE Trans. Instrum. and Meas. 37(3), 789-793, 1989) and a free-space technique using two spot-focusing reflector antennas (M. Maurens et al.,Progress in Electromagnetics Research 6, Chapter 11, 345-385, 1992). With all these methods as well as with the standard transmission-line method only small test samples can be investigated. This implies that the obtained information is only valid for that particular part of the material where the sample has been taken. In order to develop a technique which allows measurements over a larger sample, to obtain an average value of the permittivity, a new measurement set-up has been designed.

A schematic view of the measurement set-up is given in Figure 1. It consists of two broadband antennas (2-18 GHz dual-polarised quadruple-ridged circular horn antennas), a vector network analyser (HP8510B), microwave switches and a computer. The material under test, which has to be flat having a uniform thickness, is laid on a styrofoam table which is transparent to microwaves in the 2-18 GHz frequency range. The upper side of the table is located in the middle between transmit and receive antenna. The table, having dimensions 200cm x 80cm (length x width), can rotate to change the angle of incidence. Measurements can be done in either perpendicular or parallel polarisation.

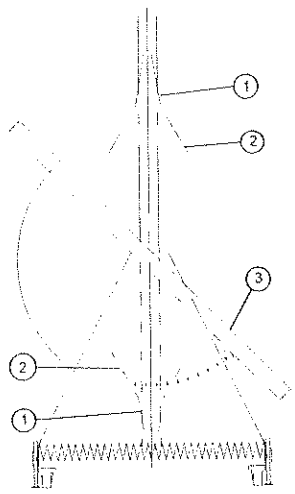

Fig 1. Free-space Measurement Setup Consisting of Antennas (1), Absorbing Shrouds (2) and Styrofoam Table (3).

Diffraction effects at the edges of the sample are minimized by using special designed absorbing shrouds on both transmit and receive antenna. The measurement set-up has been designed in such a way that a circular area with a diameter of about 50 cm of the material under test is illuminated.

In order to reduce multiple reflections between the antennas and the test sample, measurements are done at off-normal angle of incidence (45°). Time domain gating is applied to remove the remaining multiple reflections and other errors.

A simple response (THRU) calibration is done to set the reference level. Conversion from the measured transmission coefficient S21 to the complex permittivity is accomplished by reading the trace data into the computer, performing the required conversions and then plotting the measurement results. The software algorithm is based on a plane wave assumption.

In order to validate the measurement set-up, comparative measurements between this free-space and the conventional transmission line technique have been done on a large number of lossy sheets. These sheets, consisting of a polyurethane foam impregnated in a carbon dispersion, differ from each other by the carbon loading. The layer dimensions are 180cm x 60cm x 0.33cm (length x width x height).

Free-space measurements on these sheets have been done at parallel polarisation and an angle of incidence of 45 degrees. Measurements have been done at three different locations of the layer and the mean value of these measurements has been calculated.

These results have been compared to measurements using the transmission line technique. For each sheet, three samples have been measured in S-band en X-band waveguide. The software algorithm to convert the measured S-parameters (S11 and S21) is described in the literature (Hewlett-Packard, Product note 8510-3, Measuring the Dielectric Constant of Solids with the HP8510 Network Analyzer). Afterwards, an average result of these measurements has been calculated for each layer.

Figure 2. shows measurements on a lossy sheet for both the free-space and waveguide setup. A good correlation between free-space and waveguide measurements is obtained.

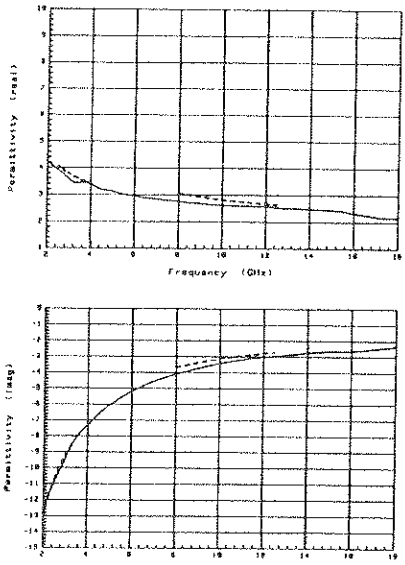

Fig 2. Measured Complex Permittivity using Free-space (——) and Transmission line (· · · ·) Technique.

A new free-space technique to perform permittivity measurements on lossy materials has been developed and an experimental set-up has been built. The validity of this technique has been proven by comparing the measurement results with standard transmission line techniques.

MICROWAVE CHARACTERIZATION OF HOMOGENIZABLE MATERIALS IN A TRANSMISSION LINE : A MODEL WITH RESONATORS

S. LEFRANCOIS*(1), D. PASQUET(2) AND G. MAZE-MERCEUR(1)
(1) C.E.A. / C.E.S.T.A., 33114 Le Barp, FRANCE
(2) E.N.S.E.A., Laboratoire Microondes, 95014 Cergy, FRANCE

New materials are used for specific studies (stealthness, ...), such as composite materials. So their microwave characterization has to be carried out. Classical methods, such as the reflection/ transmission method, provide accurate results only for homogeneous materials (J. BAKER-JARVIS / E. J. VANZURA / W. A. KISSICK - IEEE MTT, 1990, pp 1096-1103). These methods have to be extended to the measurement of heterogeneous materials.

In most general case, these materials are constituted with a host material containing inclusions. To consider this mixing as homogenizable, the dimensions of the inclusions must be small enough compared to the wavelength and the dimensions of the sample, and the concentration of these inclusions must be low enough to prevent the development of aggregates. In that case, an effective permittivity ε_{eff} and an effective permeability μ_{eff} can be defined as functions of permittivities and permeabilities of the different components as well as their geometrical parameters. So the classical measurement method should be adapted to the determination of complex ε_{eff} and μ_{eff} in the microwave frequencies. But, although the material is homogenizable, measurements of the scattering parameters (reflection and transmission coefficients : S_{11} and S_{21}) versus frequency in a waveguide or a circular coaxial line exhibit perturbations. They can be linked to the excitation of higher order modes in the sample by diffraction on the heterogenities. So, the parameters ε_{eff} and μ_{eff} cannot be deduced in the classical way.

To bypass this problem, two approaches are introduced: a circuit approach and a propagation approach.

On the one hand, a model for the perturbed line is introduced. The measurement cell containing the sample is represented by an unperturbed cell containing an equivalent homogeneous sample in series with symmetrically diffracting parallel resonators. So, the obtained model is shown in figure 1 :

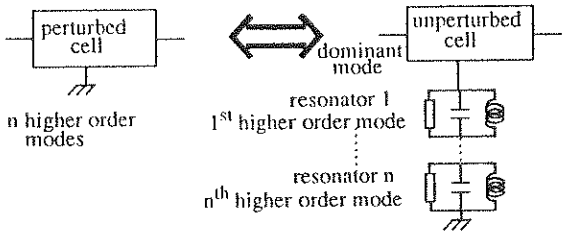

- figure 1 -

In this model, each higher order mode in the perturbed cell is associated with a resonator. The unknowns are the equivalent resistance R, inductance L, capacitance C. They are computed from the amplitude, width and frequency of the observed perturbation on measured curves (D. KAJFEZ / P. GUILLON - «Dielectric Resonators» - Norwood, MA : Artech House, 1986).

The equivalence between both formulations, measured quadripole and equivalent model, leads to the computation of the S-matrix of the unperturbed cell (S_c). The S-matrix of the perturbed cell is expressed from the measured data and the S-matrices of the resonators are deduced from R, L, C. So, S_c is the only unknown matrix. Finally, the classical calculation provides ε_{eff} and μ_{eff} from S_c.

On the other hand, by considering the sample as a dielectric resonator in a measurement cell (waveguide or transmission line), the modes allowable to resonate in the sample can be computed (H. Y. YEE - IEEE MTT, vol. 13, 1965, p 256).

When expressing the modes inside and outside the sample and the continuity relations of the fields, a system of three complex equations is found. The unknowns are the attenuation outside the sample (α_0), the resonance pulsation (ω_0) and the propagation constant in the sample ($\gamma=\alpha+j\beta$). They are obtained by a numerical solving. Consequently, the modes able to propagate in the sample can be determined in this way. But the coupling coefficient stays inaccessible because it depends on the microscopic structure of the material and our point of view on the sample is only macroscopic.

According to the first approach, results for ε_{eff} versus the frequency are shown in figures 2 and 3. A case with one resonance and a case with two resonances are studied. The first material (fig. 2) is a mixture of dielectric inclusions (with $\varepsilon\#\varepsilon_0(5000\text{-}j30)$) in a dielectric resin (with $\varepsilon\#\varepsilon_0(3\text{-}j0)$). The second material (fig. 3) is a mixture of carbon fibers in a dielectric resin. The above mentionned conditions for a homogenizable sample are verified.

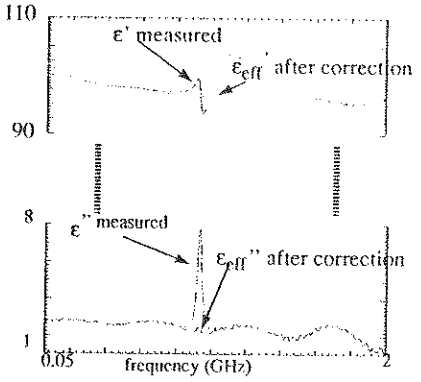

- figure 1 -

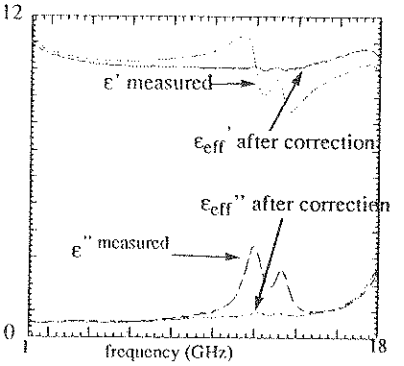

- figure 2 -

This new model takes into account the higher order modes. So, measurements of homogenizable composite materials can be processed correctly. The advantage of this model is to be directly built on the physical phenomenon appearing in the cell during measurements. For instance, the metallic losses are accounted for in the quality factor. Our method works for any kind of waveguide structure, in particular for coaxial and rectangular waveguides.

FERROELECTRIC THIN FILMS MICROWAVE INVESTIGATION AND ANNEALING

Yu.M.Poplavko, Yu.V.Prokopenko and V.A.Rakityansky
Kiev Polytechnic Institute, 252056 Kiev, Ukraine

It is well known that ferroelectric devices for computer use will have to be integrated with semiconductors. For various techniques of ferroelectric film preparation, the sol-gel processing is one of the most promising.This method includes the stage of precursor coating heating up to the temperature of 400 - 700°C in order to obtain good crystalline-structured ferroelectric film on semiconductor Si or GaAs wafer. As this takes place, the less heating of wafer the better, to keep complicated semiconductor structures from becoming blured. It is a powerful infrared radiation that is usually used for synthesis of ferroelectric film which is no more than a superficial mixed oxide layer on the wafer. It is significant that infrared-absorbing properties of mixed oxides and semiconductors are close. The principle idea of proposed new method is to use the significant distinction between microwave absopsion of ferroelectrics and semiconductors in order to apply microwave radiation for integrated ferroelectric film synthesis simultaneously with their investigations.

Only by the microwave methods the films electrical parameters could be obtained from distance and even during the technological process. In a sol-gel method the last is especially informative due to the microwave absorpsion of water,alcohol and other components of various precursor mixes: all of them have the superhigh-frequency dielectric dispersion parameters of which are extremely sensitive to the temperature, viscosity, chemical composition etc. Proposed in this report microwave method of measurements and anneaing is compatible with another chemical thin films techniques (CVD, MOCVD, MOD).

Specific feature of any structural disordered, polycrystalline or polydomain ferroelectric is a strong dielectric dispersion at microwaves. Whereas in a bulk ferroelectric the center of this wide range dispersion is usually observed at 1-10 GHz, thin ferroelectric films on various substrates show a blurred dielectric absorption maximum in the range of 10-100 GHz (I.S.REZ and Y.M.POPLAVKO. Dielectrics: Main Properties and Electronics Applications. Moscow, 1989, p.400, Russian). Microwave absorpsion is very sensitive to domain walls mobility, degree of structural disordering and to a peculiarities of interface between film and wafer. High-resistance silicon or semi-insulated gallium arsenide adds a little to microwave absorbsion or reflection at 300 K: in both crystals dielectric permittivity are practically independent on frequency up to 300 GHz. The microwave conductivity of Si varies slightly and should be considered as a constant at the given temperature. But GaAs microwave conductivity increases at high frequencies especially above 500 K. Microwave temperature dependencies show that the properties of ferroelectric films deposited on silicon could be controlled up to 700 K while for semi-insulating GaAs this limit is about 1000 K.

Consequently,microwave measurements is of profound importance for integrated ferroelectric films examination. Being non-contact and non-electrode, microwave study of thin films electric parameters could be used during the various steps of their fabrication.

At the latest stage of film's technology millimeter wave power could be used for the most high-temperature burning and annealing process. It seems that this method could provide the highest temperature difference between semiconductor wafer and ferro- or paraelectric film heated inside due to its microwave absorption. Ferroelectric film parameters could be investigated simultaneously with its annealing. Consequently, microwave pulse parameters could be adapted to the electric and thermal properties of film and would be controlled by processor. The advantages of this method is the possibility of microwave heating pulses precision control: their rise and fall times, duration, periodic duty and power. Microwave radiation is operate with a complex sandwich consist of para- or ferroelectric thin film, conductive coating of In_2O_3 or Pt which is semitransparent for millimeter waves and thick semiconductor Si or GaAS wafer with a good metallized back served as a reflector for microwave. As in ferro- so in paraelectric phases the film is the main absorber of millimeter wave energy from this complex sandwich. In ferroelectric phase microwave absorption is produced by domain walls vibration and in a paraelectric phase this absorption is caused by the overdamped soft lattice mode. In the temperature interval usually used for sol-gel process fabricated film microwave dielectric loss factor far exceeds the microwave losses of Si or GaAs semiconductor wafer. The absorption and transparency of interface coating depends on many factors.

A device under development allows for pulse microwave heating of ferroelectric film and its microwave reflection measurement during the interval between powerful heating pulses that makes possible to modify pulses' parameters as may be required. Special-purpose antenna provides a homogeneous power distribution on 6 inches diameter circular section. Various electrodynamic methods including microwave source frequency change could be used in order to obtain the minimum microwave reflection from ferroelectric film. The device could be used also for examination and annealing of Pt-coating.

Authors are indebted to Prof. A.Sigov for integrated on Si ferroelectric films PZT and $(Ba,Sr)TiO_3$.

A NEW KIND OF LIGHT BULK STORAGE IN MATERIALS

Saparin G.V.(*),Obyden S.K., Perlovski G.A.
Department of Physics, Moscow State University.
119899, Moscow, RUSSIA

In some materials such as GaN Zn (epitaxial layers), LiF (single crystal), polyethylenetherephthalate (PETF) films, etc the activation effect of local cathodoluminescent (CL) emission was discovered after preliminary action on these materials by the electron flow with high energy. The CL intensity from areas exposed by the electron flow with energy over 5-10 keV increases for some samples by 100 times over in comparison with CL-intensity in initial time of radiation. A new state of materials with induced high quantum yield has been retained several years under the room temperature. The induced state can be canceled by annealing and the new cycle of activation is available.

As the GaN Zn-epitaxial layers are more studied the main details can be described. We have been exposed such heterojunctions by the immobile 20 keV electron beam with a current 10 nA during 5 sec in the scanning electron microscope (SEM). Experiments show that the activation effect is realized in the deep trace of electron beam propagation. The time dependence of CL intensity increasing has a saturation and a rate of the CL-intensity variation depends on the electron beam current density significantly. The local CL-spectra of activated samples show that the emissive line peaked at 2,85 eV at the same position as for nonactivated areas. So this factor allows to suppose that the light radiative centers into activated and nonactivated areas are identical and attributed at the Zn acceptor level in the forbidden zone.These Zn- atoms are located in the

sublattice of Ga. It is possible to represent some mechanism explained the activation effect of GaN Zn under bombardment by the electrons. This effect is observed on the doped layers deposited in the hydrogen atmosphere and therefore it is available to suppose that it is related by existance Zn and H-atoms in GaN. The probability of H-atoms location into the same lattice cell where Zn atom is placed is very high as the hydrodgen concentration in the layer is high too. Such aggregation is profitable energetically as it is availaible the bonding between the hydrogen and nonpaired electron of N. In this case all bonds are saturated and a level of bonded hydrogen in the forbidden zone is formed. The electron flow destroys the N-H bonds and a new effective radiative recombination H-Zn center is created. This transformations increase the quantum yield. Thermal annealing stimulates the H-atoms diffusion and regeneration of destroyed bonds.

Above effect can be used for creation of a new kind of bulk storage (probably archival storage) and a detector of charge particles with topographycal memory. The last detects a space distribution of flow density. The direct writing and reading of information by electron beam are availaible with digital and analogue modes with density over 10^8 bit/cm^2 in binary code. The use other known materials leds to widening of bit space as the action of electron beam varys the CL spectra in visual wavelength interval. The CL-spectra position and colors of SEM-images depend on the charge value induced by writing electron beam.

AEMC

COMPATIBILITE ELECTROMAGNETIQUE

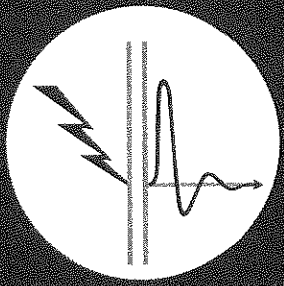

VOUS CONCEVEZ, INSTALLEZ :

Systèmes numériques	Automates
Cartes analogiques	Instrumentation
Electroniques de puissance	Automobiles

★ ★ ★

MAIS...

Des perturbations électromagnétiques et autres parasites s'insinuent au cœur des électroniques...

AEMC vous propose

- **DES COURS APPLIQUES : nombreux Travaux Pratiques.**
- **INGENIERIE : mise à disposition d'un ingénieur dans votre Société.**
- **DES CONSULTATIONS EFFICACES : AEMC MESURES (Paris et Lyon) est à votre disposition pour vous assister dans la mise en conformité de tous vos appareils électroniques aux normes CEM applicables en 1996.**

AEMC : 86, rue de la Liberté
38180 SEYSSINS
Tél. : **76 49 76 76**
Fax : **76 21 23 90**

COMPARISON OF NUCLEAR HEMP STRESSES WITH SELECTED STANDARD TEST PULSES

By

William A. Radasky*
Michael A. Messier
Metatech Corporation
Goleta, California

New work is underway in the IEC to provide guidance to builders and operators of civilian systems with regard to the protection from High Altitude EMP (HEMP). There are substantial differences in the approaches used to protect civilian systems as compared to military systems. In particular, civil systems are not necessarily required to operate through a nuclear attack and may be able to be reset manually if upset. In addition, it is not possible from a cost point of view to build in a large amount of EM shielding and/or surge protection to handle the worst case HEMP fields that may be present. Given these differences, the IEC is approaching the problem in terms of providing protection guidance that is incremental in terms of the usual hardening and testing approaches for EMC/ESD/Lightning.

One point that should be noted at the beginning is the fact that the EMC specifications are usually defined at the "box" level, not at the system level as usually preferred by the HEMP community. This is of course due to the fact that other subsystems can be emitters of noise which will interfere with other boxes. Interestingly, because other emitters may be close by, some of the compatibility levels for boxes in "noisy" environments can be quite high.

It appears from the preliminary work accomplished thus far in the IEC, that it will be possible to take advantage of many of the new test requirements that have been defined for EMC immunity testing. We plan to present several simple calculations in this paper which will compare the expected HEMP transients at the subsystem level with existing tests methods and levels defined for EMC.

The first set of calculations and comparisons involves the conducted stresses that could reach a box interface due to HEMP. The external HEMP contribution to this internal stress is assumed to be from two sources. The first is due to the long line coupling to power lines which pass through a local transformer into a home or factory. We assume that a standard lightning protector is present on the transformer. The input to this problem comes from the IEC common mode conducted currents provided as a function of probability (assuming a single burst and a random, early-time HEMP coupling). Using a simple model for an arrestor-protected transformer, the current waveform inside the building is calculated. A second stress source is also considered -- that due to the field coupling through the walls of a concrete building. Using approximations found for different construction techniques and the IEC description of the external

HEMP environment, it is possible to estimate the internal HEMP fields within a facility. These internal fields are used along with some typical geometries to calculate bulk cable currents leading to electronic boxes.

Given the results provided above, the paper continues with a comparison of these calculated HEMP stresses with several well-established standard EMC tests waveforms. In particular, we have examined the IEC 801-4 fast transient (noise) and the 801-5 surge tests. In addition, we have considered the new MIL-STD-461/462 tests. It is clear that the new EMC immunity tests are considerably faster than similar tests specified in the past. This leads to the conclusion that with modest adjustments, it should be possible to provide reasonable HEMP protection for many subsystems which are well protected from higher levels of EMC/ESD/lightning transients.

Future C4I Electromagnetic Protection Standards and Requirements for Global Operations Developed in Canada

Dr. Andrew S. Podgorski
ASR Technologies
332 Crestview Rd.
Ottawa, Ontario, K1H 5G6
Tel: (613) 737-2026, FAX: (613) 737-3098

Abstract

The rapidly increasing reliance on electronic and electrical equipment has led to dramatic increases of interfering electromagnetic field levels which in turn has resulted in widely spread electromagnetic interference problems. In the past, the designers of electronic and electrical equipment had to deal with naturally generated threats such as inter- and intra-system interference, lightning (LEMP), and electrostatic discharges (ESD). Later on, man made threats such as jamming and nuclear electromagnetic pulse (NEMP) had to be considered. During the last few years discussions regarding addition of another electromagnetic threat - the high power microwave (HPM) threat - are taking place.

In the past, realizing the cost associated with the development of new man made electromagnetic threats, Canada had to rely on the information released by other countries regarding the newly developed threats. Such dependance made Canada vulnerable to total reliance on standards, testing methods and testing equipment from other countries and not being able to improve the value added content to the equipment produced or maintained in Canada. The reliance on threat knowledge from other countries would also made Canada unprepared for possible world wide electromagnetic threats.

Since 1981, the author has been conducting a scientific program supported by the Canadian Department of National Defence that was to permit an independent electromagnetic threat assessment and development of new testing facilities and methods in order to allow

Canada to tailor its standards and specifications. The newly developed Canadian based testing technology, resulted in order of magnitude cost savings for system testing, versus similar tests conducted by other countries. Also, the knowledge gained during the scientific studies will in the future allow Canada to play a major and an independent role in the prediction of possible future electromagnetic engagements.

Short Biography

Dr. Podgorski is a leading edge thinker and a recognized authority in the area of Electromagnetic Compatibility and Electromagnetic Protection. Over the years he conducted interdisciplinary theoretical (numerical modelling) and experimental technology related research in diverse areas including Electromagnetics, High Power Microwaves, Lightning, High Voltage Engineering, Satellite Communication, Semiconductor Technology, Fibre and Integrated Optics, Measurements and Standards.

Dr. Podgorski has published over sixty scientific papers and over twenty classified and unclassified reports. He has served on many international inter-governmental military and civilian panels of experts representing Canada in USA, Europe and Australia and was a consultant for the new EH-101 helicopter project. Last year he was elected, as a first Canadian ever, to the Board of Directors of the Electromagnetic Compatibility Society of IEEE. His name is listed in the Canadian "Who's Who".

STANDARDS FOR COMPONENT EMC REQUIREMENTS

Ms S Nensi, Assessment Services Ltd, Titchfield, Hampshire UK PO15 5RH

This paper presents the results of a study commissioned by the Ministry of Defence Directorate of Standardization and Safety Policy on the standardization requirements of EMC performance of components used to:

a) control electromagnetic emissions and
b) to protect equipment from the effects of extraneous electromagnetic interference (EMI).

The study was regarded as a prelude to the preparation of a family of standards for components used to achieve electromagnetic compatibility (EMC). The task was to identify the extent of existing standardization for electrical and electronic components used primarily for EMC purposes. These components would have many applications (equipments, sub-systems, etc.) and be required to operate in varied environments (EMI, EMP, TEMPEST, Lightning, ESD). To this end, the Study was divided into three parts. The first part was to identify the components, their application and probable environment. The second part was to identify the extent and suitability of current standardization for the identified components. The third part was to identify further work in those areas where standardization is not adequate, and to recommend the content of new standards to overcome present inadequacy with respect to 'EMC components'.

A number of EMC component manufacturers, suppliers and users of EMC components were invited to present their views on, and support for, the standardization of EMC performance, and their response documented.

For EMC components the main conclusion was that the majority of EMC components require further specification in terms of EMC performance. The order of priority for further action is as follows:

1. Screening materials and enclosures.
2. Connectors and cable fitting accessories.
3. Cables, particularly looms and harnesses.
4. Suppression components.
5. Bonding devices.

This paper reports the progress to date of the work carried out in meeting the objective of the MoD's requirements with respect to standardization of these devices.

Screening/shielding materials: There is a need to define the EMC performance of planar materials and conductive coatings, loaded plastics, mesh screens, honeycomb panels, wire mesh air filters and perforated metals. Conduits, trunking and sheaths require suitable EMC test methods. Gaskets are the subject of an Interim Defence Standard, but caulking compounds and adhesives require standardization for EMC purposes. Shielded enclosures, cabinets, cases and laminates require suitable standards.

Connectors and cable fitting accessories: Connectors have been divided into three categories - RF coaxial, circular multi-way and non-circular multi-way. RF coaxial connectors are already suitably covered by British Standards. Circular multi-way are covered in general by MIL-C-38999, and a draft British Standard BS9520G. However, non-circular connectors are not addressed, for which there is an urgent requirement.

Backshells, glands and adaptors are often manufactured independently from the connector producer and it may therefore be prudent to take this into consideration when preparing standards for connectors.

Cables: The EMC performance of cables is divided into two areas, firstly cable and secondly connectorised cable assemblies.

Connectorised cables are being addressed in existing standards, however, cables are not. It is felt that this requires urgent attention to provide a standard which includes a common acceptable measurement method.

Suppression components: Capacitors, inductors and filters already have standards applied to them which relate to their EMC performance. However considering the vast array of component types, configuration and application, it may be appropriate to examine the standards for completeness. It is felt that this activity is less urgent than some of the other areas.

Spark/Transient suppressors and isolation transformers together with ferrites and lossy lines are a group of components where the need for standards has been established. Of these, ferrites and lossy lines are the least specified, particularly for transient performance.

Bonding devices: These include ground rods, bonding straps and shield ground adaptors. It is not felt that Defence Standards for the procurement of ground rods and bond straps are appropriate, but rather codes of practice defining their installation. Within the codes of practice standard performance test methods could be extremely useful.

Acknowledgements: The Study was supported by the DELSC L8 Sub-committee. The author wishes to thank the Chairman, Mr D G Wilkinson for his cooperation.

PRACTICAL ASPECTS OF RS TESTING OF AUTOMOTIVE ELECTRONICS

Wolfgang Bittinger
Robert Bosch AG, Diesel Injection Development
Geiereckstraße 7, A-1110 Vienna, Austria
Phone: 0043-1-79722-9201, Fax: 0043-1-79722-9299

ABSTRACT

1. INTRODUCTION

Some radiated susceptibility (RS) test methods are not sufficiently well defined, so that there exists the danger that an engineer not so expert in the field of high frequency technology might jump to wrong conclusions by administering tests physically improperly. In some cases, also the physics of test methods for automotive electronics are not well understood. This paper presents some critical comments for the better understanding of subsequently described measurement methods.

2. STRIP LINE TEST METHODS

The operation of strip lines for susceptibility testing inside a shielded enclosure can cause large errors because of room resonances. The repercussions of these resonances upon the field inside the strip line are investigated. A desired field strength level versus frequency can be obtained only when no high Q room resonances impede the proper operation of a closed control loop. For an experimentally optimized arrangement of strip line and small pyramid absorbers, significant improvement of the control quality is achieved. As a conclusion, a strip line not only has to be operated in a shielded room in order to avoid radiation of high frequency energy, but also has to be operated in an anechoic room.

When using a parallel plate transmission line system as a field generating device for vehicle RS tests, its properties have to be considered: First, an anechoic room is required in order to avoid measurement errors caused by room resonances (see previous paragraph). Second, line resonances may occur as soon as the wavelength of the interfering RF signal approaches the dimensions of the line structure. Typical field inhomogeneities between plates as a result of such line resonances can be observed. Third, horizontal E-field polarization is not possible since the vehicle cannot be rotated 90^{o} around its length axis while in operation.

3. BULK CURRENT INJECTION

Theory and special aspects of bulk current injection (BCI) in combination with the EMC of automotive electronics are treated. The influence of geometrical and electrical parameters in a typical test arrangement is investigated. The only parameter subjected to variation in practical equipment handling when applying this test method, i.e. the distance between injection and measuring probes, has negligible influence on the transfer function. The transfer function accounts for the impedance mismatch between generator and injection probe and for the coupling between injection and measuring probes.

BCI tests must be performed inside an absorber-lined shielded room in order to avoid repercussions of room resonances. Their negative effect can be demonstrated by measuring $|S_{11}|$ of the injection probe loaded by a transmission line: Strong variations of the input reflection coefficient are observed due to room resonances. Calibration of the current injection probe in a special jig is based on a nearly constant wave impedance of this system. To ensure this, an electrical connection is absolutely necessary between both parts of the calibration jig, i.e. ground plate and cover plate have to be made of conductive material.

4. TEM CELL TEST METHODS

TEM cells feature properties which limit their application: Among them, cell resonances produce strong field inhomogeneities. Placed inside the TEM cell, the typical automotive equipment under test (EUT) forms a capacitor, and the harness forms an inductor, which both together act as a series resonant circuit with a resonant frequency well below the cutoff frequency of the cell. The series resonance frequency can be computed by proper modelling. Good agreement between theory and measurements is observed. In conclusion, TEM cells are not proper test tools for susceptibility measurements unless certain precautions are taken.

5. GENERAL CONSIDERATIONS

The maximum frequency step size Df for the frequency sweep usually is chosen too high in order to uncover resonance effects of the EUT and its periphery, of the harness and the car body. Therefore, Df has to be equal or smaller than Df_R associated to the 3 dB bandwidth of a resonance f_R. Defining a representative environment for an individual vehicle requires the determination of an amplitude probability distribution of field stength values for all natural and man-made radiation sources. A properly selected probability of abscissa exceedence, combined with an estimate of confidence level of RS tests in anechoic chambers yields the order of magnitude for RS test limits of vehicle electronis.

6. CONCLUSIONS

Finally, typical RS test standards for automotive electronics are checked for the topics treated above. In all cases, measures have to be taken in order to avoid unwanted resonance effects for repeateable results. Mandatory use of absorber-lined shielded rooms will improve RS test results considerably.

EMC/EMP ACTIVITY IN RUSSIA

Dr. Alexander A. Worshevsky
ELEMCOM LTD, Lotsmanskaya, 3
St. Petersburg 190008 RUSSIA

Standardization

Russian EMC standards are based upon the work of the CISPR, IEC and national EMC Technical Committee. State Center for standardization, certification and metrology on EMC coordinates the work in this area. Specialists from different institutes and organization prepare national EMC standards. New EMC Norms will be harmonized with European Norms. In 1991-1993 immunity standards IEC 801-1 - IEC 801-5 and some product EMC standards have become mandatory throughout Russia. Many immunity and emission Norms are planed for enactment in the future. Russian Register of Shipping set requirments for shipboard automatic equipment immunity to harmonics, ESD, bursts, surges, radiofrequency voltages, magnetic and electromagnetic field. There will be requirments for immunity of any electronic equipment. Technical Committee prepares EMC standard for nuclear power plant systems. Lightning and EMP are important testing.

Laboratory facilities

EMC testing is carried out in accredited laboratories. Good equiped laboratories are situated near Moscow and St. Petersburg. Russian test centers can test equipment in accordance with national and international EMC/EMP standards.

Powerful electrical generator with frequency converter in rotor circuit give possibility to test equipment with power up to 400 kW, voltage 0 - 8 kV, frequency 40 - 60 Hz. It can simulate voltage modulation, voltage drop with any duration and harmonics up to 10%.

There were made portable ESD, bursts and surge simulators for testing of electronic equipment in accordance with IEC 801-2, 801-4, 801-5.

Different coils and current generators are used for magnetic field immunity testing. The maximum magnetic field is 1000 A/m.

Test radiofrequency electromagnetic field is generated by different antennas, lines, EM cells up to 10 V/m.

EMP are generated by transmission lines and cells. Pulsers give voltages up to 5 MV. The largest working volume is 50 x 20 x 15 m.

Transmission line with height changing (2.5 - 10.5 m) can generate wave up to 200 kV/m, 450 A/m with rise time 0.25 - 0.6 μs and duration up to 6 ms. In underground part of line EMP can be up to 16 kV/m, 400 A/m. Line is drived by 3 synchronized pulsers.

Transmission line with specialized back wires simulates (15-30)/(80-450) ns EMP up to 80 kV/m, 200 A/m in air and to 20 kV/m, 150 A/m in ground with vertical or horizontal polarization.

Cylinder EM chamber has 250 m^3 working volume. It is possible to fill it with water or ground. Coils generate pulse magnetic field up to 2700 A/m with duration up to 5 ms. System of electrodes can simulate horizontal electrical field.

Different installation can be used for testing of large or small equipment under EMP up to 200 kV/m, 400 A/m with duration up to 10 ms. The minimum rise time is 9 ns.

One kilometer power transmission line can be used for investigation of its influence on cables or equipment.

Pulsers can simulate lightning up to 5 MV with the following forms: 1.2/50 μs, 1.2/(1.4-6) μs, 250/2500 μs and pulse current up to 100 kA.

Specialized small lines are made for metrology testing of measuring probes. The minimum rise time is 3 ns. Amplitude can be reproduced up to 400 kV/m, 1000 A/m with 3-5% accuracy.

Measuring systems include probes, fiber optics and digital recording equipment. Transient time is 3 ns.

Mathematical models

Software give possibility to simulate the following processes:

- voltages and currents induced by EMP in metal constructions, cables and circuits of equipment,
- crosstalk of power transmission line and undeground cables. Induced voltages in cables caused by transients and lightning process,
- pulse voltages in shipboard electrical systems. Generation and propagation of pulses in cables and through filters, transformers,
- design of EMP simulators, calculation of EM field.

ELECTROMAGNETIC DIAGNOSIS TECHNIQUE USING SPHERICAL NEAR-FIELD PROBING

F.Thérond*
Centre d'Etudes de Gramat, 46500 Gramat, France

J.Ch.Bolomey / N.Joachimowicz
Supelec, plateau du moulon, 91190 Gif-sur-Yvette, France

F.Lucas
Satimo, Z.A de Courtaboeuf, 91952 Les Ulis Cedex, France

In the context of electromagnetic compatibility (EMC), a knowledge of potential leakage points on structures is of great interest; we present here a method aiming at identifying, locating and characterizing such points on metallic objects.We search for the point(s) through which a given object is the most sensitive to a micro-wave attack in the frequency range 100MHz - 4 GHz.This study is closely related to the spherical near-field facility SOCRATE (Centre d'Etudes de Gramat) working in the same frequency range and primarily devoted to coupling analysis by means of cross-sections measurements.

Our approach consists in a near-field (NF) to very-near-field (VNF) transformation using the induced current as an intermediate step.The radiated near-field of the object, considered as a transmitting antenna, is either measured or simulated in spherical coordinates; these near-field data are then inverted to yield the induced current at the object surface. This inverse linear scattering diagnosis problem is solved by a full 3D vectorial "pseudo-inverse" approach.

Having the induced current we can compute the field at any point in space and in particular in a very close range, a typical calculation distance being a tenth of a wavelength.The very-near-field so computed allows for determining the most important areas of radiation of the object. Indeed, the very-near-field is expected to be almost zero except in front of the radiating apertures. In return, the choice of such a method compells to deal with ill-conditioned systems and great numerical heaviness.

The various steps involved in the diagnosis procedure, using both experimental data and numerical modeling, are described on figure 1.

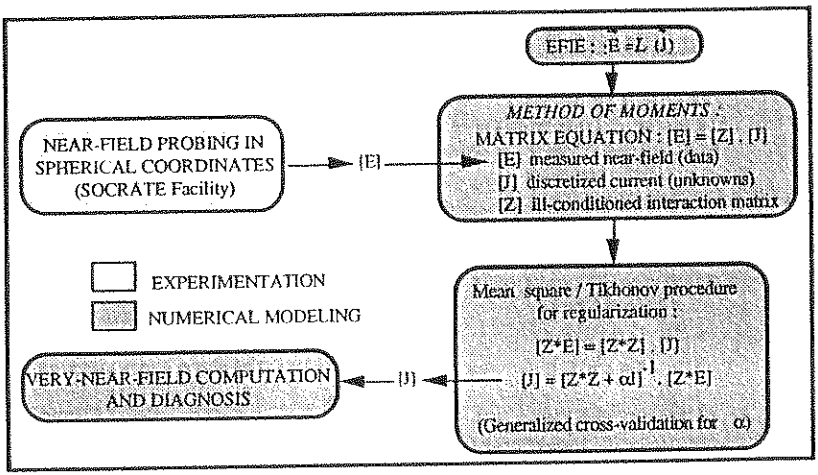

Figure 1 : the diagnosis process and its different steps

The feasibility of such a diagnosis technique has been assessed at first on simple wire structures numerically easy to handle. During this first phase the Numerical Electromagnetics Code (NEC) was used as a reference providing both the near-field data and the ideal current on the wires.This phase was successfull in demonstrating the diagnosis algorithm capabilities and in evaluating its performances with respect to random and systematic errors. Besides, it helped to establish a regularization strategy to apply to more complex objects.

The implementation of our approach using real measurements from the SOCRATE facility has been performed on a generic cylindrical structure exhibiting one circular aperture.The height and diameter of the cylinder are respectively 50 and 30 cm as illustrated on figure 2.

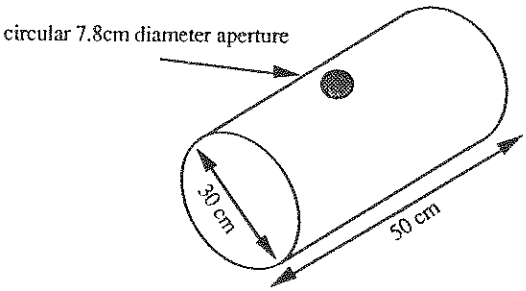

Figure 2 : object under test geometry

Tests on the previous structure have been conducted from 600 megahertz up to a few gigahertz, frequencies for which the wavelengths and the object dimensions are of the same order of magnitude.We show on figure 3 a typical meshing and the associated very-near-field result at 1 GHz. At that frequency and for such an object, the matrixes sizes are typically (1000*1000), the computations lasting about 8 hours on a Sun work station Sparc 10.

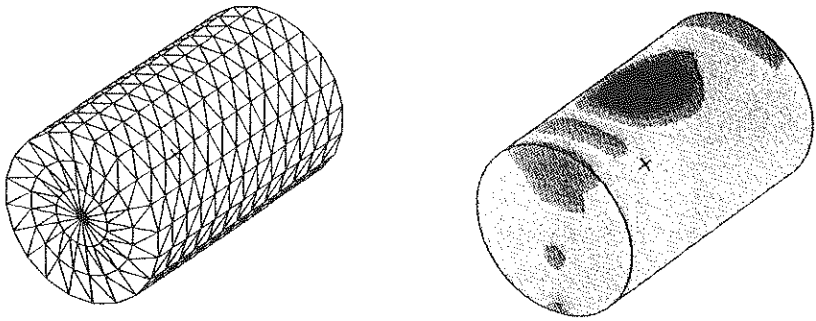

Figure 3 : meshing and very-near-field (1cm) of the object at 1GHz

Results on other generic cylindrical structures exhibiting few apertures of different sizes, shapes and locations will be presented.They testify of the diagnosis procedure capabilities to locate and characterize, in terms of polarizations, the main radiating areas on the objects surfaces.

HORIZONTALLY POLARIZED DIPOLE II ELECTROMAGNETIC PULSE SIMULATOR

Russell Blundell, U.S. Army White Sands Missile Range, Nuclear Effect Directorate, Nuclear Operations & Support Division

The change in Department of Defense requirements governing the testing of military systems has dictated the necessity for the Test & Evaluation Commands to provide EMP simulators with faster rise times and narrower pulses. U.S. Army White Sands Missile Range, Nuclear Effects Directorate accepted the challenge and with the assistance of the U.S. Air Force Phillips Laboratory, Advanced Weapons and Survivability Directorate (WSR) have constructed a simulator to meet the requirement. The Horizontally Polarized Dipole II (HPDII) is actually a high level pulse, high frequency simulator based on the same design as the Horizontally Polarized Dipole (HPD) Simulator, a semi-elliptical antenna with the end terminated at ground and a high-voltage pulser.

The HPDII is a hybrid EMP simulator which combines some of the features and qualities of the radiating simulators with those of transmission line/bounded wave simulators. The HPDII simulates the EMP environment that exists outside the high-altitude nuclear source region, specifically for weapons systems or test objects located on the earth surface.

The HPDII consists of a half toroidal antenna with a major radius of six meters and a minor radius of .77 meters, with the antenna cage formed of six resistively loaded one-eighth inch diameter aircraft cables supported by circular hoop rings. The resistive load on the aircraft cables achieves a low-frequency ratio of electric to magnetic fields at the center of the half-torus that approximates the free space plane wave impedance of 377 ohms. The High Altitude Generator-1 (HAG1) is a 16 stage Marx generator with an erected Marx capacitance of 3.1 nano-farads and a charging resistance of 480 kilo-ohms with a maximum voltage of 1.6 mega-volts. When the Marx is discharged it drives a 150 micro-henry inductor and a 750 pico-farad peaking capacitor that serves as an intermediate storage area for the energy. The energy is then switched onto the antenna by means of a self-breaking gas-filled main output switch.

The field mapping of the HPDII simulator was done in September 1993 to determine the average rise time and peak amplitude performance. The field map data was acquired with a MGL-6 free field sensor and a DMB-4 balun. A 1 giga-hertz fiber optic link was used to transfer the data to a SCD-1000 digitizer to record the data. A computer controlled data acquisition system was used to store and analyze the data. Results show a consistent sub-nanosecond rise time with a 70 kilo-volt per meter pulse, 2 meters off the ground directly underneath the pulser.

Input impedance of grounding systems with arbitrary shape

Y.Bourdet *-S.Lamesch
Alcatel cable
35, rue Jean Jaurès
95870 BEZONS

Y.Beniguel
I.E.E.A
13, promenade Paul Doumer
92400 COURBEVOIE

1. INTRODUCTION

Ground systems (G.S) are of primary interest for many electric systems. The problem is to design such a system with a low input impedance both at low and high frequencies (up to 30 MHz), as a function of ground characteristics, conductivity and dielectric constant. To achieve this, we may use a set of ground rods electrically connected in a parallel network ; or a more complicated structure composed of a ground rod connected to a structure of arbitrary shape such as a plate, a disc, or a sphere .

The objective of this paper is to present state of the art measurement methods and theory .Computations are made solving for the electrical field integral equation with the method of moments. The electric field is developed as a function of Hertz vectors. At low frequencies, the problem is the same as when calculating the input impedance of an antenna located inside a conducting medium. At high frequencies, Sommerfeld integrals have to be added to the equations. Conversely, measurement technics have been developed both at low and high frequencies. Fundamentals of the theoretical method, measurement technics, and results obtained are presented hereafter.

2. THEORETICAL APPROACH

2.1. Solution methods

The electric field is calculated as a function of the Hertz vectors

$$\vec{E} = k_1^2 \vec{\Pi} + \nabla\nabla.\vec{\Pi}$$

where k_1 represents the wave number in the ground.

Usually, the ground system is composed of a ground rod electrically connected to a structure. To solve the electromagnetic problem, the ground rod is divided into dipoles and the structure is approximated with triangles. Test functions used in the moment method are linear both for the ground rod and the structure in order to implement junctions between current elements. The latter may be one of two different types: linear elements (goose foot arrangement fig.1a) or a linear element and structure (fig.1b). An overlapping technic is used in a similar way in both cases.

wire to wire junction

fig.1a

wire to surface junction

fig.1b

The Z_{mn} term of the impedance matrix is equal to:

$$Z_{mn} = I_m\left[k_1^2\left(\frac{\bar{\rho}_m^{c+}}{2}\cdot\bar{\Pi}_m^{c+} + \frac{\bar{\rho}_m^{c-}}{2}\cdot\bar{\Pi}_m^{c-}\right) - B_m^{c+} + B_m^{c-}\right]$$

$$\text{with } \bar{\Pi}_m^c = \int f_n(r')\cdot\bar{\Pi}ds \text{ and } B_m^c = \int f_n(r')\nabla\cdot\bar{\Pi}ds$$

To calculate the two integrals above, we use the following procedure. Each current element (dipole or triangle) is divided into a horizontal and a vertical element. A vertical electric dipole (VED) creates a vertically oriented Hertz vector :

$$\Pi_{1z} = \frac{j\omega\mu_1 p}{4\pi k_1^2}\left(G_{11} - G_{12} + k_2^2 V_{11}\right)$$

A horizontal electric dipole (HED) gives rise to both a horizontal and a vertical Hertz vector:

$$\Pi_{1h} = \frac{j\omega\mu_1 p}{4\pi k_1^2}\left(G_{11} - G_{12} + U_{11}\right) \text{ and } \Pi_{1z} = \frac{j\omega\mu_1 p}{4\pi k_1^2}\cdot\nabla_h W_{11}$$

where G_{11} and G_{12} are the Green's functions associated with the source and image points, with respect to the interface. U_{11}, V_{11} and W_{11} are Sommerfeld integrals. We finally obtain:

$$\bar{\Pi}_m^c = \frac{j\omega\mu_1 p}{4\pi k_1^2}\int \bar{f}_n(r')\left(G_{11} - G_{12}\right)ds + f_n(r')\left[\left[\cos\theta k_2^2 V_{11} + \sin\theta\nabla_h W_{11}\right]\hat{z} + \sin\theta U_{11}\hat{h}\right]ds$$

A similar equation may be obtained for B_m^c

2.2. Numerical technics

The most convenient way to handle the G_{12} term consists of doubling the structure with respect to the interface. The problem is then one of a classical antenna problem. The index of the medium is the ground index. Proceeding this way gives excellent results as compared to measurements for frequencies up to approximately 1 MHz. Beyond this value, the Sommerfeld integrals render a significant contribution. They are calculated by using different approximations depending on the value of the horizontal distance as compared to characteristic values, function of the frequency and ground resistivity :

-the quasi-static approximation
-the intermediate range approximation
-the asymptotic approximation

3. MEASUREMENT TECHNICS

Today, you can find four different methods for measuring input impedance of ground systems. They are different in principle and in their frequency ranges. Two types of methods can be identified: the range of low frequencies up to approximately 1 MHz, and the range of high frequencies up to 40 MHz or 100 MHz.

3.1. Voltage method at low frequency

The principle is based on the measure of the rising voltage of the ground system when we connect a generator between the ground system and an auxiliary ground rod. The reason why we can limit the frequency up to 500 kHz is due to the difficulty in measuring the voltage drop between two distant points, and to the value of the high input impedance of auxiliary ground rods compared to the value of the ground system.

3.2. three point method at low frequency

The principle is based on three measures of impedance with two auxiliary ground rods. This can be accomplished by only measuring the current at each point of frequency for the

three impedance only if we know beforehand the value of the equivalent supply voltage in open circuit and the supply output impedance. Consequently, we can obtain three equations :

$$\begin{cases} \overline{Z}_{XA} = \dfrac{\overline{E}_{th}}{I_{XA}} - \overline{Z}_{th} = \overline{Z}_X + \overline{Z}_A \\ \overline{Z}_{AB} = \dfrac{\overline{E}_{th}}{I_{AB}} - \overline{Z}_{th} = \overline{Z}_A + \overline{Z}_B \\ \overline{Z}_{XB} = \dfrac{\overline{E}_{th}}{I_{XB}} - \overline{Z}_{th} = \overline{Z}_X + \overline{Z}_B \end{cases}$$

The impedance is deduced from measures by relation :

$$\overline{Z}_X = \frac{\overline{Z}_{XB} + \overline{Z}_{XA} - \overline{Z}_{AB}}{2}$$

This method has the advantage of taking into consideration the length of the measure cable. However, we cannot measure with good precision beyond 1 MHz, because the impedance of the cable is too significant with regards to the impedance of the ground system.

3.3. Loss lines method at high frequency

This method has been developed by the "Centre d'Etudes de Gramat" and is protected by a patent. The principle is the same as for the three points method but the cables and auxiliary ground rods are replaced by loss lines. The loss coefficient of the lines allow to remove the standing wave state and if the input impedance of the lines is low or about equal to that of the ground system impedance, the precision is accurate within 500 kHz to 40 MHz.

3.4. Reflectometry method at high frequency

This method which has been developed by "Alcatel Cable" explores the possibility of the ground system as an antenna in a lossy medium. At a given frequency, it is therefore characterized by the standing wave ratio. From this measure, the impedance can be determined if we know the characteristic impedance of the cable. This method has a frequency range starting at a few MHz up to 100 MHz. Before using the network analyzer, one must first conduct the calibration process (open circuit, short circuit, 50 Ohms load).

4. RESULTS OBTAINED

The following diagram shows the results for a spherical ground system obtained by calculation and measurement (3 points method and reflectometry) The dimensions of the sphere are 0.5 m radius and it is connected to the interface with a 0.85 m length and 10 mm diameter conductor.

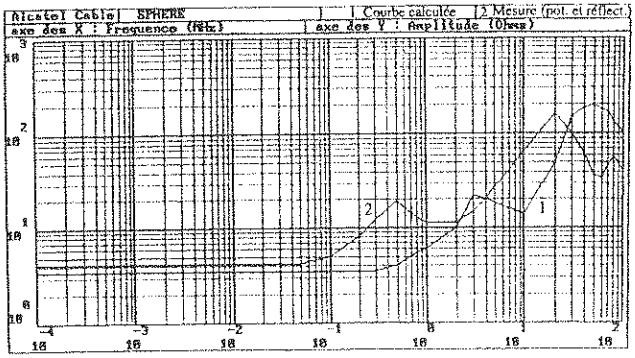

To compare the different methods, we have measured different ground systems. Measured values of the input impedance of a disc ground system (1m radius at 1m depth connected by its center to the interface with a 30*2mm section conductor) versus frequency are plotted below. These results have been obtained by using the reflectometry method (curve 1) and the loss lines method (curve 2).

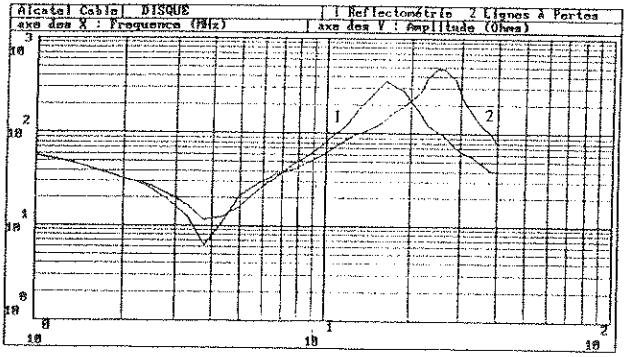

5. CONCLUSION

Comparisons between calculated results and measurements are similar up to 1 MHz. Beyond this value, slight differences occur especially at resonant frequencies. Further developments are in progress for the theoretical methods with regards to choice and method of calculation of the Sommerfeld integrals.

BEHAVIOUR AND OPTIMIZATION OF TRANSMISSION LINE NEMP SIMULATORS

O. DAFIF - Ch. BARDET - B. JECKO
IRCOM "Electromagnétisme" - Faculté des Sciences
URA CNRS n° 356 - 123, Avenue Albert-Thomas
87060 LIMOGES Cédex (FRANCE)

J.J. RODARO
CEG - 46500 GRAMAT
(FRANCE)

I - INTRODUCTION

The experimental simulation is introduced in the construction and demonstration of the EMC, during the creation of a system. This consists of realizing experimentally through the means of guided or radiated wave simulators, a parasitic coupling case (NEMP, etc) with a "to be tested" structure (aircraft, shelter, missile, transmission center, line, antenna, ...), so it would achieve the most realistic perturbation effect in the most penalizing configuration.

This approach implies the most reliable representation of the perturbing E.M. wave in its form (generally a plane wave), and its evolution in function of the time and therefore its spectral content.

However, the difficulties encountered with the structures of the transmission lines result essentially from radiation generated by two phenomenous (figure 1) :

- Diffraction by the angular points (discontinuity radial lines-flat line)
- Reflection by the horizontal layer.

This parasitic radiation (apparition of non TEM modes related to the discontinuities) reduces the test zone and decreases the high frequency content of parasitic resonances following the observation points.

II - STUDY AND THEORITICAL OPTIMIZATION OF THE EM CARACTERISTICS OF A TRANSMISSION LINE SIMULATOR

A theoretical optimization of a strip line antenna (SSR : Half-Rhombic simulator) (figure 1) that has been the subject of a convention with the CEG, this lead to discover new ways and original solutions [Patent IRCOM (DAFIF - JECKO) DRET - CEG (RODARO) n° 93044 27 of 15 / 04 /1993] which able to avoid these drawbacks (deterioration of the rise-time due to the parasitic radiation generated by the discontinuities and the flat lines, especially at high frequencies of the NEMP considered) without changing the horizontal inclination part (the reflecting can be avoided by limiting the aerial with a structure cornet type).

This optimization is based on the principal component of this parasitic radiation by artificial radiations produced by addition of distributed or localized load situated on the level or on both sides of discontinuity (figure 2b).

The study of the simulator theoretical is solved using a space-time "integral equation" [Dafif : Doctorat - University of Limoges, February 1983]. This rigorous method allows to analyse:

- This current induced by the generator (NEMP) on the wire simulator;
- the electric and magnetic fields (maximum, vector, rise-time, etc, ...).

This study allows to analyse E.M. simulator behaviour and to evaluate the perturbation generated by the transition of the radial line and the flat line on the current induced along the wire, and on the electric and magnetic fields $\left(\vec{E}, \vec{H}\right)$ in the test zone, with and without optimization device (figures 2 and 3) patented before.

A comparison between experiment and theory on a simulator (small-scale) will be considered.

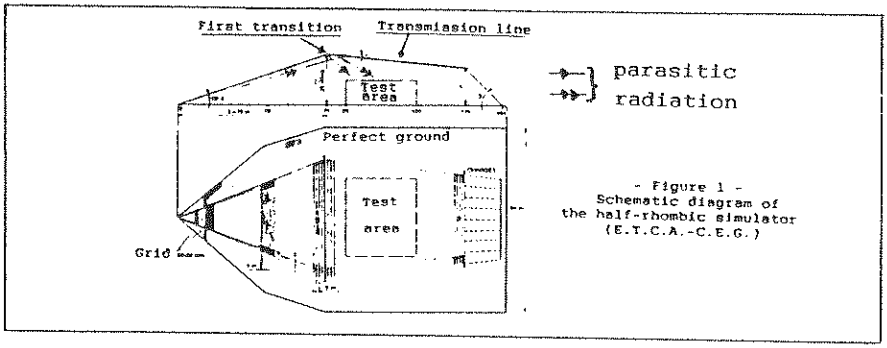

- Figure 1 -
Schematic diagram of the half-rhombic simulator (E.T.C.A.-C.E.G.)

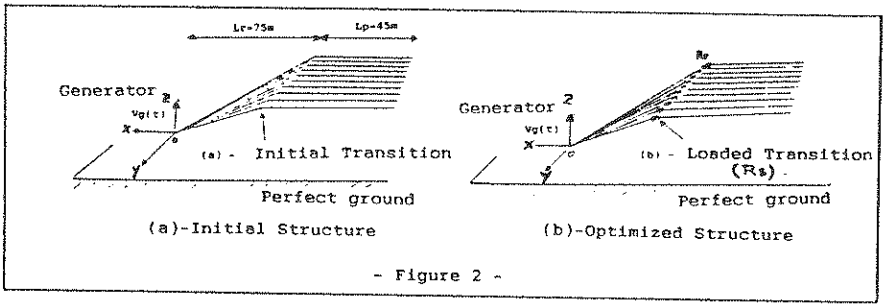

(a)-Initial Structure (b)-Optimized Structure

- Figure 2 -

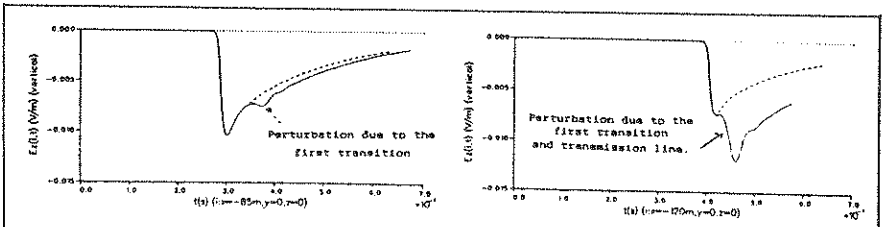

——— (a)-Initial Structure

------ (b)-Optimized Structure

- Figure 3 - Ez component of the electric field at two points of the test area.

FLAT BROADBAND ABSORBERS : "REFLECTIVITY vs. SITE ATTENUATION"

Dr Ferdy MAYER.-

Mr Jean-Pierre CHAUMAT.-

Mr Manfred KIRSCHVINK.-

LEAD

"Quarter-wave broadband flat absorbers" have become practically available, for the implementation of 30-1000 MHz Absorptive Open Air Test Sites (AOATS) and Absorber Lined Chambers (ALC's).

For the basic absorber/material, vertical incidence reflectivities of 20 dB and better, over this frequency range, can be achieved. Off-perpendical wave reflectivities are clearly worse and sensitive to the em wave polarisation. In addition both are sensitive to the practical implementation of the absorptive material, as all air-gaps (between tiles, due to uneven tile surface, etc) have a strong influence on the realworld reflectivity performance.

It has been shown (IEEE-EMC Cherry Hill 1991), that for such non ideal absorbers, the site attenuation deviation (S.A.D.) achieved, in an absorptive ground plane Open Air Test Site (OATS) and an Absorber Lined Chamber (ALC), are not related to the scalar value only of the reflectivity, but to the reflexion phase angle as well. As a consequence site attenuation is sensitive to the geometrical implementation of the site.

More recently, (IEEE-EMC Anaheim 1992), a "generic" SAD behaviour has been shown, existing in a similar way, with all imperfect absorber : Related insights on the physics involved on wave compositions between direct and absorber reflected waves, have been described, as related to site attenuation.

With such knowledge and the use of an overall modelization and optimization of SAD (given a certain max. SAD, determine the number of layers and their composition and geometry), a new flat multilayer absorber "CUNICO" has been developed, covering the 30 MHz-5 GHz range, with an SAD of about ± 1 dB and allowing emission testing with a fixed receiving antenna.

PRACTICAL APPLICATIONS OF EMC SIMULATIONS IN PRODUCT DESIGN

Andrew Sleeper, PE, Member, IEEE
Woodward Governor Company, Loveland, Colorado, USA

Simulation models for EMC events are typically complex; even so, achieving agreement between simulation results and real-life results is difficult. This paper proposes using simple simulation models which are not absolutely accurate, so one simulation run may not be very useful. Instead, making changes in the model and comparing results from different simulation runs can give useful information about the relative performance of different circuits. Using only the relative results from sets of simulation runs, the following issues can be evaluated early in the design cycle, entirely in the realm of simulation:

1. Design guidelines can be established by investigating various configurations of shielding, grounding and filtering, to determine which measures are most cost-effective.
2. Once a problem has been identified in testing, the relative merits of different fixes can be evaluated in a simulation before implementing them in hardware.
3. The impact of production and usage variability, including tolerances and temperature, can be evaluated in a simulation.

Besides the obvious cost and schedule advantages of using simulation, measurements of circuit parameters are easy in a simulation, while they may be impractical in real life. Of course, simulation has potential numerical problems which could yield unreasonable results. Caution and verification is advisable whenever simulation is used.

To demonstrate the first of above applications, the author created a simple model of a shielded twisted pair cable carrying an unbalanced signal from one piece of equipment to another. Forty combinations of filtering and grounding configurations were tested, to include all combinations of the following levels of three factors:

> Wire Termination: No filter, Cap to chassis, Bead, Bead + Cap, and Cap + Bead
> Shield termination (EUT): Open, Gnd to chassis, Cap to chassis, Bead to chassis
> Shield termination (field end): Open, Grounded to chassis

The capacitor is 1000 pf in all cases; the ferrite bead model represents a commonly used surface mounted bead. Not all combinations of these factor levels are sensible; however, to estimate the impact of each factor independent from the others, a full factorial experimental design involving all forty combinations is useful.

These forty circuit models were each subject to three simulated EMC tests, as follows:

1. IEC 801-4: The prescribed fast transient pulse is applied to the cable shield through a 171 pf capacitor, which simulates the capacitive clamp. The simulator produces transient analysis plots of voltages in the EUT vs. time.

2. IEC 801-6: To simulate this test, an AC source with 150 Ω resistance is tied directly to the cable shield, with both the eut and field device connected to earth through 150 Ω resistors. The simulation produces plots of the AC voltages at points inside the EUT as the AC source sweeps from 150 kHz to 1 GHz.

3. CISPR 11: Instead of attempting to simulate radiated emissions, the author makes an assumption that the received signal will be roughly proportional to the AC voltages seen on the shield of the cable. With a noise source (simulating a CPU clock) inside the EUT, the simulation gives plots of the shield voltages vs. frequency.

To show that simple simulation models are sufficient, all these simulations have been done using the evaluation version of PSpice, which has a circuit size limitation of 64 nodes. This is sufficient to create reasonable models of the eut, field device, and a lossy transmission line for the cable. The evaluation version of PSpice is freely distributed, or it can be purchased for a nominal fee from MicroSim Corporation in Irvine, CA.

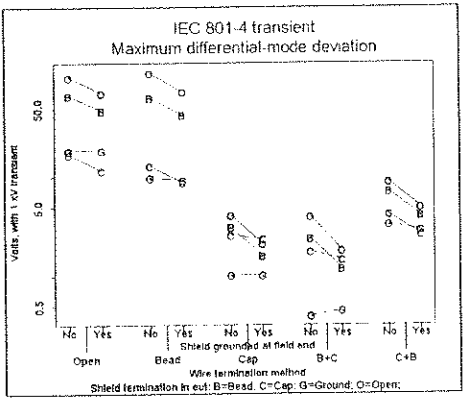

The results of each group of simulations show clear differences between the various options of cable termination and grounding. As an example, the figure shows the maximum differential-mode voltage seen in the EUT during the IEC 801-4 transient, for all forty simulations.

The five clusters of points represent each of the five methods of wire termination; the plotting characters O, G, B, and C represent the four shield terminations at the eut end; the short lines show the effect of grounding the shield at the field end.

The complete paper and presentation will include the following information:

- Full description of the models used for the cable, ferrite bead, and the overall circuit configuration.
- Plots and tables showing summarized results from the 120 simulation runs.
- Design-oriented conclusions drawn from the simulation results
- Discussion of statistical tools used to set up and analyze the results.
- Cautions and advice for the effective use of circuit simulators
- Further applications.

Determination of Minimum-Phase Conditions and Justification of the use of the Bayard-Bode's Relationships in the Construction of a Test Device Operating on Continuous Waves

Marcel BLANCHET, Consulting Engineer, MB et Associés
Jean-Louis BRAUT *, Engineer, Alcatel Cable/D.E.E.
Alain PARISELLI, Engineer, Alcatel Cable/D.E.E.

Abstract

In this paper, the authors intend to explain some paradoxical concepts whereby certain transfer functions that are theoretically stable non-minimum phase functions, may turn out to be minimum-phased during actual use. This justifies that the Bayard-Bode's relationships be applied to such functions whenever required.

The authors will deal with transmission lines, with regards to their transition from a lumped-constant structure (i.e. a minimum-phase structure) to a distributed-constant structure. They will also explain how the boundary transition results in the disappearance of the minimum-phase properties.

Conversely (and of greater interest, from an experimental point of view) they will show that no such thing as an "ideal line" cannot exist. This implies that those lines are always minimum-phased.

They will also examine how this astounding conclusion can be applied to propagation in linear media, as to the type of propagation (in free space, close to the ground), the nature of obstacles, the kind of reflections (dielectric or metallic) and dispersion in dielectric media.

They will briefly describe a design for a test device that operates on pure or encoded continuous waves.

DOUBLE BULK CURRENT INJECTION : A POSSIBLE SUBSTITUTE TO FIELD-TO-WIRE COUPLING

Marco KLINGLER*, Marielle SZELAG & Marc HEDDEBAUT

INRETS - CRESTA
20, rue Élisée Reclus
59650 VILLENEUVE D'ASCQ
- FRANCE -

- Abstract -

Bulk Current Injection (BCI) is a convenient qualification method since it is easy to use and of relatively low cost. Unfortunately, the current distribution on the cables and through the termination loads does not respect the current levels that can be encountered when the same equipment is placed in an electromagnetic field such as in a TEM cell.

This paper proposes a new qualification method based on a Double Bulk Current Injection (DBCI) which reproduces the same current distribution as in the case of a field-to-wire coupling by an incident plane wave. Qualifications using a TEM cell or this new DBCI method become therefore comparable.

The theoretical approach considers a lossless conductor placed over a perfect conducting ground plane. This conductor is connected to ground at its ends by two loads. If the wavelength of the incident field is much greater than the height of the conductor and if we neglect the coupling on the vertical conductors at each end, the transmission line model (TLM) can be applied. The propagation equations expressing the coupling of an incident plane wave can be therefore expressed by :

$$\begin{cases} \dfrac{\partial V(z,t)}{\partial z} + L\dfrac{\partial I(z,t)}{\partial t} = \displaystyle\int_0^h \frac{\partial B_y^i(x,z,t)}{\partial t}\,dx \\ \dfrac{\partial I(z,t)}{\partial z} + C\dfrac{\partial V(z,t)}{\partial t} = -C\displaystyle\int_0^h \frac{\partial E_x^i(x,z,t)}{\partial t}\,dx \end{cases} \qquad (1)$$

where $V(z,t)$ and $I(z,t)$ are respectively the total voltage and the total current at a position z of the transmission line at an instant t, $B_y^i(z,t)$ the y component of the incident magnetic field and $E_x^i(z,t)$ the vertical component of the incident electric field. In the case of $Ez = 0$ (figure 1), it is shown that equations (1) can be written as a function of the total current $I(z,t)$ and the scattered voltage $V^s(z,t)$ as follows :

$$\begin{cases} \dfrac{\partial^2 V^s(z,t)}{\partial z^2} - L\,C\dfrac{\partial^2 V^s(z,t)}{\partial t^2} = 0 \\ \dfrac{\partial^2 I(z,t)}{\partial z^2} - L\,C\dfrac{\partial^2 I(z,t)}{\partial t^2} = 0 \end{cases}$$

where

$$V^s(z,t) = V(z,t) + \int_0^h E_x^i(x,z,t)\,dx$$

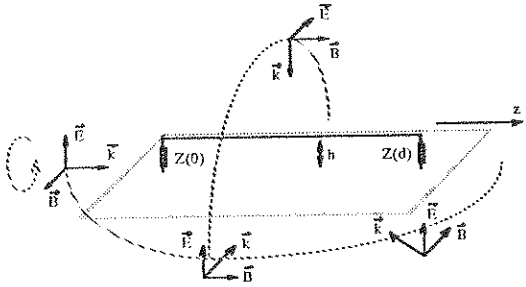

Figure 1 : Case of Ez = 0.

When Ez = 0, the electromagnetic coupling on a transmission line can be then summarised by the following equivalent electric model :

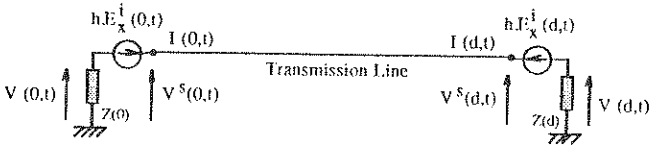

Figure 2 : Equivalent electric model in the case of Ez = 0.

The basic idea of the DBCI method is to reproduce artificially the voltage sources inserted at each end of the transmission line by using two injection probes fed by a single RF generator (figure 3). To reproduce a field-to-wire coupling on the cable, the difference of length of the two coaxial cables $\Delta\ell = L2 - L1$ must compensate the propagation delay between one end of the transmission line and the other. In the case of an unique electric coupling the length of the two coaxial cables L1 and L2 are equal.

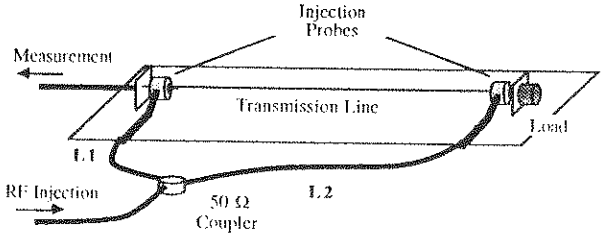

Figure 3 : The DBCI test method.

Comparative measurements and numerical simulations have also been carried out in a TEM cell and using the DBCI method on a single conductor and a twisted 3-conductor cable including right angle bends. As shown in graphs 4, very good agreement has been obtained between theoretical results, measurements using the DBCI approach and results using the conventional TEM cell method.

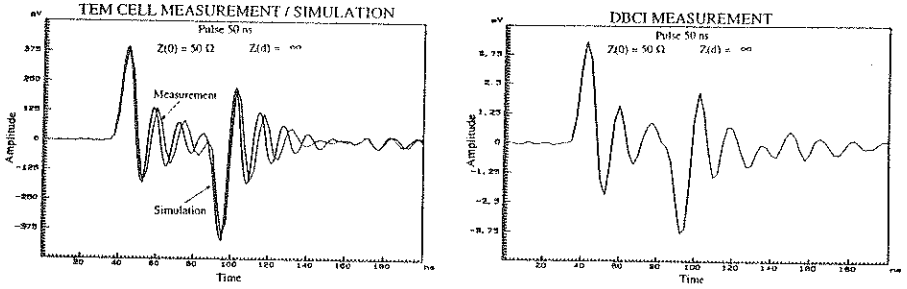

(a) TEM cell and simulation results.

(b) DBCI results.

Graphs 4 : Comparison between the different approaches.

This paper will detail the theoretical and experimental points of this method. The results obtained by the different approaches will also be compared to conventional BCI results. The advantages of this new qualification method compared to the TEM cell qualifications will then be discussed.

CONDITIONS OF FQUIVALENCE OF VARIOUSLY SHAPED NOISE PULSES

K.A.ROCHKOV

The Belorussian State University of Transport
The Department of Electrical Engineering

Expensive modelling apparatuses are needed to test the effects of nuclear electromagnetic pulses. Commonly these tests are performed using variously shaped pulses.

In order to save significant costs of such tests it is a very pressing task to deduce the conditions of equivalence of variously shaped pulses. In the case when it is nesessary to perform tests using variously shaped pulses the shape of apulse is selected such which can be easier implemented in the modelling apparatus. Then the conditions of equivalence are used to verify the behavior of other pulses by recalculation.

To solve the problem it is necessary to determine which pulses can be assumed equivalent and thento obtain specific conditions of equivalence of variously shaped pulses expressed through relationships between their parameters.

Such variously shaped equivalent pulses are assumed to have such relationships of the parameters of their amplitude and duration that the linear circuit output would respond identically to these equivalent pulses.

The author has demonstrated(K.A.Rochkov. The theory and techniques of monitoring electromagnetic compatibility of microelectronic circuits controlling safe railway traffic. Doctor's Dissertation,Moscow,1993,47 pp.) that the requisite and sufficient conditions to produce the equivalent effects of pulses are the equality of their active spectral bands f and their full energies W.

The active spectral band is assumed as the frequency band width covering 95% of the pulse energy.

The appended Table lists the conditions of equivalence of nine differently shaped pulses in relation to the rectangular pulse, as the author has deduced them.

The presentation discloses the theorem of equivalence of variously shaped noise pulses formulated and validated by the author and gives an example how the conditions of equivalence are deduced.

The results of the theoretical investigation performed by the author allow to reduce significantly the cost of testing the effects of nuclear electromagnetic pulse.

For more information you are welcome to address:

246653,the Republic of Belarus, Gomel, Kirov St.,bld.34.

Table

Pulse shA	Time function	Pulse W	$\Delta f_{0.05}$	Conditions of
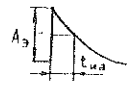	$A_э e^{-\beta t}$	$\frac{A_э^2 t_{иа}}{1,4}$	$\frac{1,41}{t_{иа}}$	$\begin{cases} 1,41 A_п = A_э \\ 0,7 t_п = t_{иа} \end{cases}$
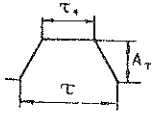	$2A_т \frac{\tau/2 + t}{\tau - \tau_1}$, $-\frac{\tau}{2} < t < \frac{\tau_1}{2}$ $A_т$, $-\frac{\tau_1}{2} < t < \frac{\tau_1}{2}$ $2A_т \frac{\tau/2 - t}{\tau - \tau_1}$, $\frac{\tau_1}{2} < t < \frac{\tau}{2}$	$\frac{A_т^2}{3}\tau(1+2\xi)$	$\frac{0,9}{\tau}$	$\begin{cases} 1,83 A_п = A_т \\ 0,45 t_п = \tau \end{cases}$ для $\xi = 0.5$
			$\frac{1,59}{\tau}$	$\begin{cases} 1,2 A_п = A_т \\ 0,795 t_п = \tau \end{cases}$ для $\xi = 0.8$
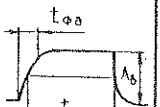	$A_б (1 - e^{-\beta t})$	$0,8636 A_б^2 t_{иа}$	$\frac{0,9}{t_{иа}}$	$\begin{cases} 1,6 A_п = A_б \\ 0,45 t_п = t_{иа} \end{cases}$ для $t_{фа} = 0,2\, t_{иа}$
			$\frac{1,37}{t_{иа}}$	$\begin{cases} 1,25 A_п = A_б \\ 0,685 t_п = t_{иа} \end{cases}$ для $t_{фа} = 0,1\, t_{иа}$
	$A \cos \pi \frac{t}{t_и}$	$\frac{A^2 t_и}{2}$	$\frac{0,94}{t_и}$	$\begin{cases} 2,063 A_п = A \\ 0,47 t_п = t_и \end{cases}$
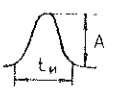	$\frac{A}{2}\left(1 - \cos \frac{2\pi}{t_и} t\right)$	$\frac{3}{8} A^2 t_и$	$\frac{1,14}{t_и}$	$\begin{cases} 2,163 A_п = A \\ 0,57 t_п = t_и \end{cases}$
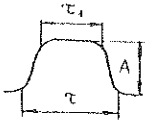	$A \cos^2 \frac{\pi}{\tau - \tau_1}\left(t + \frac{\tau_1}{2}\right)$, $-\frac{\tau}{2} < t < \frac{\tau_1}{2}$ A, $-\frac{\tau_1}{2} < t < \frac{\tau_1}{2}$ $A \cos^2 \frac{\pi}{\tau - \tau_1}\left(t - \frac{\tau_1}{2}\right)$, $\frac{\tau_1}{2} < t < \frac{\tau}{2}$	$0,6875 A^2 \tau$	$\frac{1,07}{\tau}$	$\begin{cases} 1,7 A_п = A \\ 0,505 t_п = \tau \end{cases}$ для $\xi = 0.5$
		$0,875 A^2 \tau$	$\frac{1,59}{\tau}$	$\begin{cases} 1,2 A_п = A \\ 0,795 t_п = \tau \end{cases}$ для $\xi = 0.8$
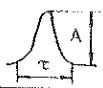	$A \cos^3 \frac{\pi}{\tau} t$, $-\frac{\tau}{2} \le t \le \frac{\tau}{2}$ 0, $\lvert t \rvert > \frac{\tau}{2}$	$\frac{5}{16} A^2 \tau$	$\frac{1,33}{\tau}$	$\begin{cases} 2,19 A_п = A \\ 0,665 t_п = \tau \end{cases}$
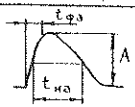	$kA\left(e^{-\beta_1 t} - e^{-\beta_2 t}\right)$	$0,752 A^2 t_{иа}$	$\frac{1,28}{t_{иа}}$	$\begin{cases} 1,44 A_п = A \\ 0,64 t_п = t_{иа} \end{cases}$ для $t_{фа} = 0,1\, t_{иа}$
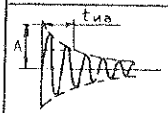	$A e^{-\alpha t} \sin \omega_0 t$	$\frac{A^2 \omega_0^2}{4\alpha(\alpha^2 - \omega_0^2)}$	$\frac{1,41}{t_{иа}} + f_0$	$\begin{cases} A_п^2 t_п = \frac{A^2 \omega_0^2}{4\alpha(\alpha^2 - \omega_0^2)} \\ \frac{2}{t_п} = \frac{1,41}{t_{иа}} + f_0 \end{cases}$

ON THE CONDITIONS OF EVALUATING THE SHIELDING EFFECTIVENESS IN THE PLANE WAVES REGION BY MEANS OF COAXIAL MEASURING CELLS WITH TEM MODE

Mihai Th. Bădic[t], MEMBER, IEEE, Research Institute for Electrical Engineering, Bucharest, Romania
Mihai-Jo I. Marinescu, Research Institute for Electrical Engineering, Bucharest, Romania
Cristin Păun, Polytechnic University Bucharest, Romania

The determination of shielding effectiveness or insertion loss for any materials is of great importance in the EMC field. Excepting the well-defined materials from the point of view of macroscopic parameters ϵ, μ, σ, the materials shielding capability is difficult to be calculated. Because the shielding effectiveness of a complex material is difficult to predict, it often must be measured. On the other hand, experimental reproduction of the theoretic calculus conditions (infinite plane shield placed in the Fraunhoffer region for a wide band of frequency) is hard, and for this reason, equivalent methods are used to obtain the similarity conditions and the identical results with the initial case. The full paper deals with the foundations of the modelling method by means of coaxial cells with TEM propagation mode, which have been already applied in the last decades, at first being used even usual coaxial lines (R.A.WECK, Proc. of the IEEE, Feb.1966). The publications of the American standardisation institutions, ASTM and NBS, have contributed to the generalisation of the method based on the expanded coaxial cells with TEM mode (P.F.WILSON & M.T.MA, NBS Tchnical note 1095-1986).

The full paper includes a complete demonstration of the modelling possibilities of the ideal state including thin ($|\gamma d|<<1$) and thick shields, conductive and dielectric, depending on incident radiation frequency; it is emphasized the fact that the correct simulation and the results identity given the modelled case do not mean phenomenological identity.

In some cases differences may appear between the phenomena that take place in the infinite plane shield and the material test from the coaxial cell. General demonstration starts, obviously, from the similarity of the transmission lines propagation equations with the plane waves equations, of the reflexion and transmission factors expressions and from the equivalence established between the secondary constants Z and γ of the material of a plane shield and those which characterize a coaxial line with the same material between the inner and the outer conductor (Fig.1). It is observed that in chosen example (for a conductive material, $\sigma >> \epsilon\omega$), there is an identity of the propagation constant expressions and a non-identity of the wave impedances expressions. Since the propagation constant describes the phenomenology inside of the material and the wave impedance the one on the separation surfaces, it seems that the reflection properties of the plane shield do not coincide with those of the coaxial cells. Startig from the general expression of the transmission factor for a configuration with two regions and two separation surfaces :

$$T_{E,U}=\frac{4Z_1Z_2}{(Z_1+Z_2)^2} \qquad (1)$$

it is seen that an identity of this factor is obtained, for the two

situations, because of the reduction of the "(1/2π)·ln(a/b)" factor, which appears both in Z_{0c} and that of Z_{Lc} :

$$T_E = T_D = 4\sqrt{\frac{\mu_0}{\varepsilon_0}}\sqrt{\frac{j\omega\mu}{\sigma}} \Big/ \left(\sqrt{\frac{\mu_0}{\varepsilon_0}} + \sqrt{\frac{j\omega\mu}{\sigma}}\right)^2 \qquad (2)$$

The demonstration agrees to the principle according to what the formal equivalence must be verified for all the cases that may occur starting from the general relation :

$$SE_{dB} = R_{dB} + A_{dB} + B_{dB} = 20\log e^{\alpha d}\left|\frac{(Z_0+Z_m)^2}{4Z_0Z_m}\right|\left|1-\frac{(Z_m-Z_0)^2}{(Z_m+Z_0)^2}e^{-2\gamma d}\right| \qquad (3)$$

Relation (3) describes the losses by reflexion, absorbtion and re-reflection respectively, for the most general case of the normal incidence of the plane waves with an infinite plane shield (D.R.J.WHITE, Electromagnetic Shielding, Don White Consultants, 1980).

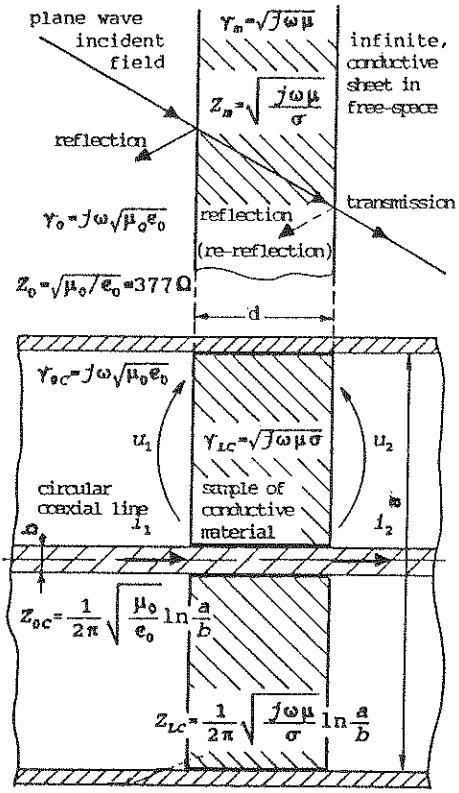

Fig.1. Similarity between the infinite plane shield behaviour and the conductive material sample from the coaxial measuring cell ($d \cong \delta$).

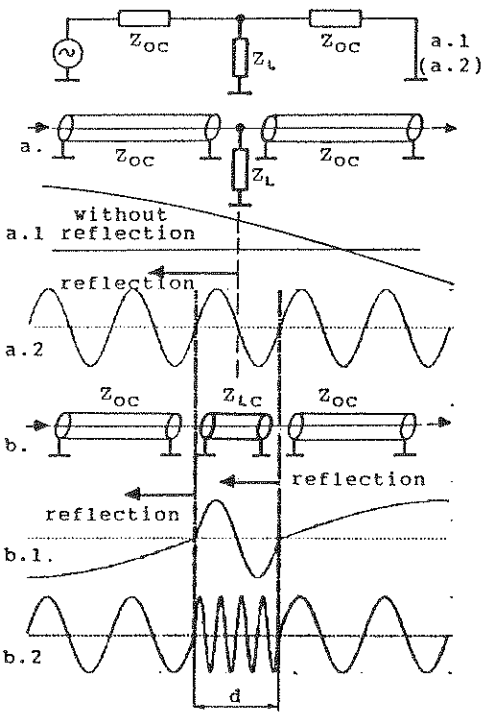

Fig.2. Shielding effectiveness modelling phenomenology with coaxial lines, related to the work signal frequency.
(a) Thin samples. (b) Thick samples.

Because, at present, expanded coaxial cells with TEM mode are used for a wide frequency band (0.01÷1000 MHz) the demonstration is presented, as it is shown in Fig.2, for separate frequency ranges. Besides the classification in thin and thick samples, from electric point of view it must be accepted the separation into frequency ranges for which the measureing cell appears as a lumped constant circuit or a circuit with distributed parameters. The thin sample and low frequency case (a.1) accepts a modelling with lumped constant circuit, which, formal, is demonstrated to be valid for the case a.2 (thin samples and high frequency) too. Moreover the complete demonstration for the specified cases and the emphasis of the connection with the transfer impedance of materials (J.A.BIRKEN, IEEE Int.Symp. on EMC, Colorado 1981), the paper contains the similarity limitations as, for example, those involved by the incidence angle of the radiation at the separation surfaces between media. Also are given experimental results obtained by using the expanded coaxial cell (Fig.3), in comparison with the theoretic ones (relation (3)) for thin and thick samples.

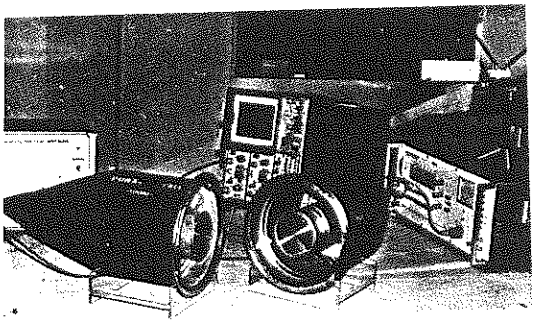

Fig.3. Expanded coaxial measuring cell with TEM mode used at the measurements.

HIGH-POWER MICROWAVE PRODUCTION USING A REDITRON

M. Angles[1],J.M. Angles[1], G. Germain[1],F. Piro[2] *
1 C.E.A./CESTA, 33114 Le Barp
2 Alcatel Cable/D.E.E., 35 rue Jean Jaurès 95871 BEZONS Cedex

1. Introduction

The VIRCATOR has many advantages (easy frequency adjustment within a broad band, simple mechanical construction, high output power). This has led laboratories working in the field of high-power microwaves to develop this type of source, while researching to minimize its drawbacks, (low yield, broad bandwidth and frequency shift in time).

In the framework of this research effort, several laboratories, including the C.E.A./CESTA in cooperation with ALCATEL CABLE/D.E.E., have tested a new type of diode named REDITRON (REflected elecTRON DIscrimination).

2 REDITRON Features

The REDITRON is a microwave source consisting of a diode placed in an axial magnetic field. This diode has a fairly thick (approx. 1 cm) anode which prevents the electrons located in the virtual cathode space from coming back to the space between the anode and the cathode.

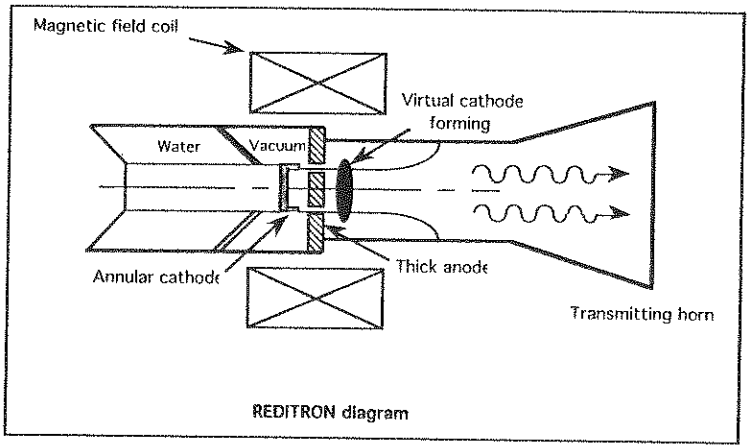

REDITRON diagram

As shown on the diagram, the magnetic field guides the annular electron flow through the circular slit in the anode towards the space where the virtual cathode is created. The Larmor radius of that part of the beam which is reflected off the virtual cathode increases. The affected electrons can no longer travel through the circular slit in the anode and they are absorbed by it. Thus, a part of the reflected electrons is eliminated, and the virtual cathode oscillations only produce microwave radiation.

The tested REDITRON has the following features:

- anode-to-cathode distance variable in the range of $10 < d_{AK} < 32$ mm
- cathode diameter, approx. 100 mm,
- graphite anode, thickness approx. 10 mm.

A clever system is used to accurately locate the circular slit in the anode in relation to the cathode (which is annular in shape). This is a stringent requirement, as incorrect centering of the anode relative to the cathode would result in a drastic drop in transmission power.

3. Experimenting with the REDITRON

The REDITRON has been tested at the C.E.A./CESTA in Bordeaux,on the electrons generator named CESAR which adjustments have been made for the use of a REDITRON. We have observed the following features:

- Output power, between 1 and 1.2 MV;
- Diode current, between 80 and 150 kA.

The coaxial line connected to the Marx output device enables 100-ns wide pulse approximatively at half size to be generated at the diode.

Contrary to the conventional Vircator, the REDITRON's thick anode can withstand a large number of firings before needing to be replace (which would imply "breaking" the vacuum). Therefore, a higher firing rate can be achieved.

Instruments were located approximately 3 m in front of the transmitting horn. They were used to measure the power and frequency of the diode microwave radiation.

4. Results

The frequency is equal or proportional to the plasma frequency depending on the applied magnetic field:

$$fp = \sqrt{\frac{n.e^2}{\pi.m.\gamma}} \qquad \text{GHz}$$

Furthermore, these tests have highlighted the following advantages:

- higher yield,
- reduced chirping,
- higher firing rate.

REP-RATE, EXPLOSIVE WHISKER EMISSION CATHODE STUDIES*

Marc S. Litz
Army Research Laboratories

Jeffry Golden
Berkeley Research Associates

An experiment is underway to study the usefulness of several cathode materials as field-emission cathodes for low voltage (≤ 100 kV), rep-rate (< 1 kHz) electron accelerators. A thyratron-switched Blumlein line modulator with a 70Ω characteristic impedance, and 1 us pulse width, is operated between 20 and 100 kV, from single-shot to 300 Hz rep-rate. This provides a high average power (50 kW) test bed for the study. A comparison is made of cathodes fabricated from velvet, carbon, diamond coatings, niobium wire nanocomposite, and poly-crystalline tungsten. Surface emission is monitored by an array of Faraday Cups. The 'turn-on' time, the uniformity of the emission, and closure time are measured as a function of the spatially-averaged, macroscopic electric field at the cathode.

A cold cathode capable of > 100 A/cm^2, fabricated from a robust material for long lifetime, and reproducible from shot-to shot would be useful in the new generation of repetitively pulsed sources useful in both industrial and military applications.

The goal of this effort is to find high-current-density cathodes that have reproducible and uniform emission, under low voltage (< 100kV) electron beam accelerator operation. In addition, this cathode should provide high durability in repetitive (≈ 1kHz) operation. Applications for such cathodes range from industrial processing of materials, robust x-ray lithography sources, to high average power RF sources. The lithography application is difficult because diode operation at low-voltage ($\approx$ 10 kV) is typically below threashold for cathode emission, and high current density (≈ 1kA/cm^2) also necessary. The RF sources present issues in durable, robust cathodes that can operate at high average power scenarios (≈ 100kW).

Thermionic cathodes do not generate more than 60 A/cm^2 with long lifetime, and require clean, high vacuum conditions to operate at that level. A common cold cathode in use for low-voltage operation is velvet. The liftime of velvet cathodes is

*Work supported by the Army Research Laboratory HPM Technology Management Office

rarely more than several hundred shots. Use of these cathodes in repetitive sources would be impracticle since they would last only several seconds before failure.

Experimental Setup

A resonantly charged, 5-stage, 70 ohm, Blumlein line is triggered by a thyratron. The E-type Guilleman network configuration of the PFN was chosen because the capacitors in each stage are identicle, while pulse shape variations are achieved through adjustment of the inductors of each stage. This is easily accomplish when the inductors in series are tapped off of one large inductor. The modulator configuration is shown in figure 1.

The 25 cm diameter coaxial vacuum vessel is 75 cm long. The negative 100 kV pulse is applied to the cathode stalk, while the outer conductor and titanium-wire anode screen are at ground potential. Local measurements of electron flux are made across the cathode surface with an array of Faraday Cups that are fabricated inside of female SMA connectors. These small Faraday Cups enable quantitative measurements of fast current-density variation throughout the electron beam cross-section.

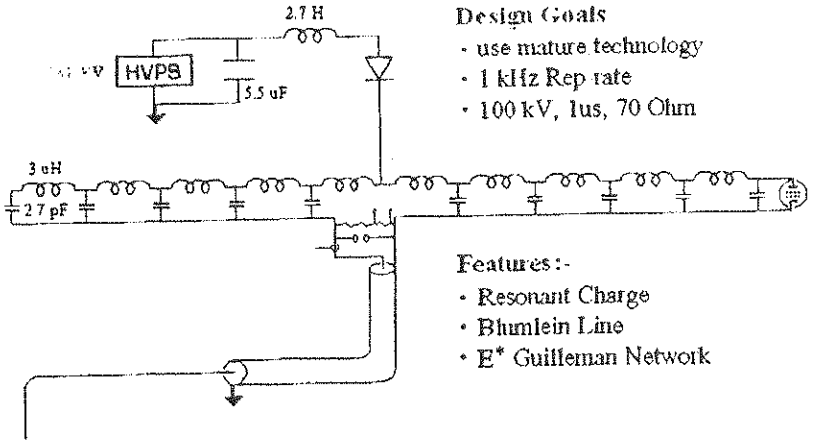

Figure 2. The circuit model for the pulsed modulator used in the cathode studies is shown above.

EFFICIENCY ENHANCEMENT OF HIGH POWER VACUUM BACKWARD-WAVE OSCILLATORS DRIVEN BY SHORT PULSE AND LONG PULSE ELECTRON BEAMS

E. Schamiloglu,* L. Moreland, R. Lemke, J. Gahl, and C. Grabowski

University of New Mexico
Department of Electrical and Computer Engineering
Albuquerque, NM 87131, USA

The efficiency of high peak power microwave generation in X-band backward-wave oscillators (BWOs) is being studied. In the short pulse regime, nonuniform slow wave structures are driven by a Sinus-6 repetitively-pulsed, relativistic electron beam accelerator. Peak microwave power exceeding 500 MW at 9.6 GHz has been measured in a 10 ns pulse with corresponding beam-to-microwave conversion efficiency exceeding 25%. A high power serpentine mode convertor is used to transform the TM_{01} mode of the BWO to a Gaussian-like TE_{11} pattern, resulting in power densities as large as 450 kW/cm^2 being measured 1.7 m from the radiating conical horn antenna, as indicated in Fig. 1. The experimental results are compared with 2.5 D particle-in-cell computer simulations and analytic models. There is good agreement between experimental measurements and computer simulations for certain configurations, whereas there are significant differences for others. These results are explained in terms of the cavity Q's in the computer simulations. Furthermore, simulations reveal that, in addition to the backward propagating transverse magnetic surface mode, backward and forward propagating volume modes with wavelengths twice that of the surface mode play a critical role in high power microwave generation and radiation.

In a companion set of experiments, nonuniform slow wave structures developed using the Sinus-6 are driven by a modified PI-110A long pulse, single shot electron beam accelerator. The voltage and current parameters of this accelerator are comparable to the Sinus-6, although the pulse duration is much longer, about 450 ns FWHM. The goal of these studies is to investigate whether the large peak powers radiated in 10 ns bursts can be extended to longer pulses to achieve greater radiated energies. Preliminary results from the long pulse BWO experiments indicate that microwave radiation terminates after 100 ns using the nonuniform slow wave structure developed using the short pulse accelerator.

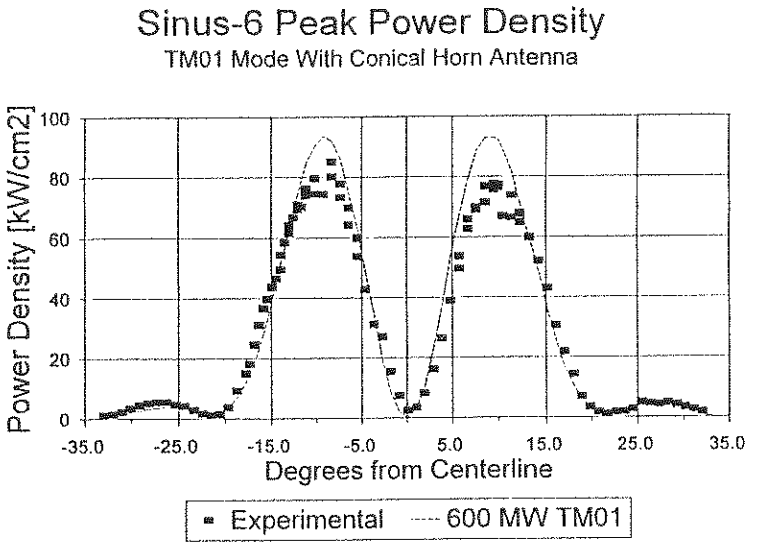

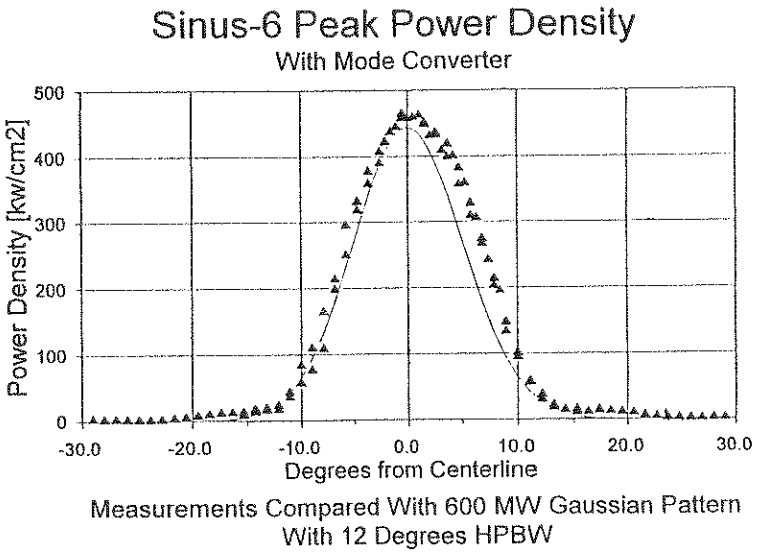

FIGURE 1. Radiation pattern from short pulse high power BWO without (top) and with (bottom) a serpentine mode convertor.

OPERATION OF A RELATIVISTIC MAGNETRON IN MARX RUN DOWN

`JP.BRASILE, G. JEAN-FRANCOIS, M. SIMON '
THOMSON SHORTS SYTEMES
9, Rue des Mathurins - BP 150 - 92223 BAGNEUX CEDEX (FRANCE)

1 - Introduction

In the objective to produce High Power Microwaves with a compacness assembly using a relativistic magnetron, we have designed , built and tested a fast compact high voltage modulator (marx generator 1.2 MV /3 kJ ,low inductance - O Bècle et al ,8th IEEE International Pulse Power Conf. pp998-1000 San Diego 1991) that allowed the magnetron to operate in "Marx Run Down" mode .

The HPM source is an S band Magnetron directly connected to the Marx

To have a good operation of the magnetron it is necessary to feed it with the shortest rise time pulse voltage .The marx satisfied this condition and we have experimented a good efficiency in marx run down mode.The apparatus has shorts dimensions that are.: diameter 0.78 m ; length : 3 m ; weight 200 Kg .

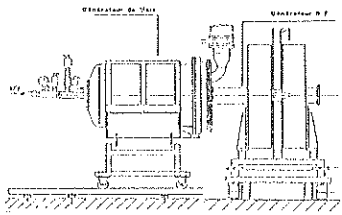

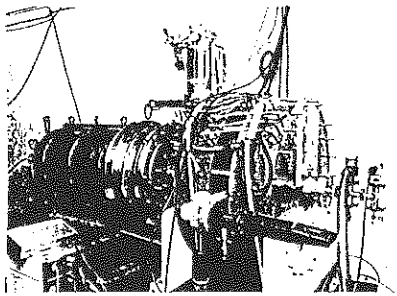

2 - Description

MARX GENERATOR : The main characteristics of the marx are :

-large operating voltage range of :300 kV to 1.2 MV

-rise time less than 50 ns on 50 Ω resistive load for 900 kV

-SF6 gas insulation

-total energy 3 kJ ; equivalent capacitance 4.17 nF(twelve stages specially designed by THOMSON - CSF / LCC for 100 kV input voltage)

-dimensions : diameter 0.78 m ; length 1.12m

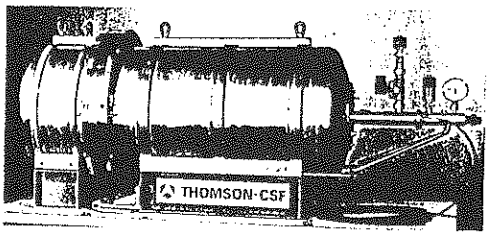

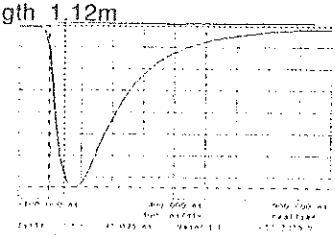

V_{charge} = 95 kV (P = 2,8 bars)

V_{out} = 900 kV

Rise time < 50 ns

MAGNETRON : The RF generator is a standard six vanes magnetron purchased at Physics International with a washer or modified cathode.The axial B field is provided by two coils .The shematic apparatus is the following :

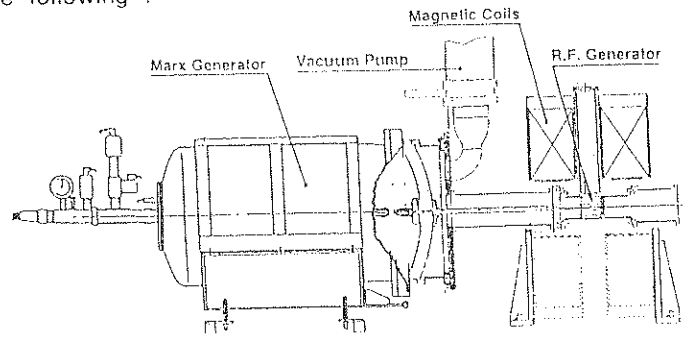

3 - Results

The magnetron can be fed by 300 kV to 800 kV pulse voltage .The magnetic field range is 0.4 T to 1T .The results show a power range from 60 MW to 600 MW ; a pulse length range from 20 ns to 100 ns and a rise time range from 3 ns to 15 ns.
For illustration of the results,typical traces are as follows :

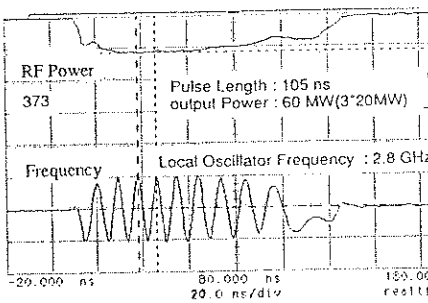

Crystal detector pulse shape and frequency spectrum

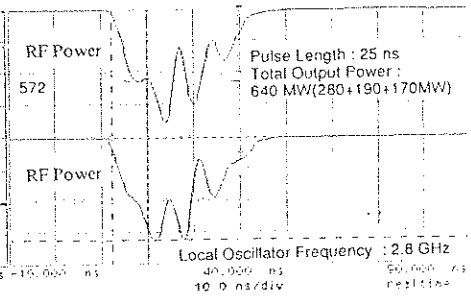

Pulse shape with 2 outputs for the same shot

4 - Conclusion :

Intense relativistic beam generator such as magnetron doesn't require pulse forming line to have good operation when directly connected to a high performance marx generator.

A STUDY OF VIRTUAL CATHODE INDUCED ELECTRON BUNCHING[b]

Marc S. Litz*
Army Research Laboratories

Jeffry Golden
Berkeley Research Associates

A variety of methods have been employed to modulate electron beams in RF power applications. This paper discusses the use of a non-reflexing electron, virtual cathode system to generate a chopped beam. This technique requires no external magnetic fields, and is experimentally uncomplicated. A 100 kV, 1.5 kA beam experiment is compared to PIC calculations. Capacitive electric field monitors measure RF power in radial waveguide arms, while fast Faraday cups measure beam flux modulation. This modulated beam technique results in 0.9 to 3 GHz microwaves.

Reflexing vs Bunched Electrons

A virtual cathode generated from a space-charge limited beam can be used to generate an electron barrier such that most of the electrons are scattered to the side walls of the cell (in the absence of magnetic fields) or reflected backwards towards the cathode by the virtual cathode. In this device (reflex diode), the energy stored in the potential barrier generated by the space-charge electric field at the position of the virtual cathode is periodically larger than the kinetic energy of the electrons accelerated by the anode. The potential barrier height and postition fluctuates with time throughout the pulse. The amplitude of fluctuations vary with andode-cathode (AK) gap. This effect is seen in figure 1. There are 3 regions of operation observed. The first region (8 to 12 mm AK) is characterized by a wildly varying amplitude and position of the virtual cathode, where the maximum of the potential barrier height is 30% of the initial accelerating potential. In the second region (12 to 16 mm) the fluctuations are reduced to 10% of the accelerating voltage, and vary about the zero. Beyond 18 mm, the potential barrier of the virtual cathode is reduced by as much as half of the accelerating potential. In general, an increase in AK gap decreases the fluctuation in the amplitude of the virtual cathode, and approaches its long-term stability. Judicious choice of the AK gap and cathode size determines the mode of operation of the virtual cathode oscillator (ie. beam buncher, reflex diode, or vircator).

Maximum beam bunching is observed when the product of velocity and transit time is matched to one-half wavelength, a distance corresponding to the anode/potential barrier-peak distance.

Experimental Setup

A resonantly charged, 5-stage, 70 ohm, Blumlein line is triggered by a thyratron. The E-type Guilleman network configuration of the PFN was chosen because the capacitors in each stage are identicle, while pulse shape variations are achieved through adjustment of the inductors of each stage. This is easily accomplish when the inductors in series are tapped off of one large inductor.

---

[b]This work is supported by the Army Research Laboratory - High Power Microwave Technology Office.

The 25 cm diameter coaxial vacuum vessel is 75 cm long. The cathode stalk is pulsed with a negative 100 kV, 1 μs duration applied potential, while the outer conductor and titanium-wire anode screen are at ground potential. Locations of voltage and current diagnostics are shown in figure 2. Local measurements of electron flux are made with Faraday Cups that are fabricated inside of female SMA connectors. These small Faraday Cups enable fast (> 2.5 GHz bandwidth) quantitative measurements of current-density variations throughout the electron pulse.

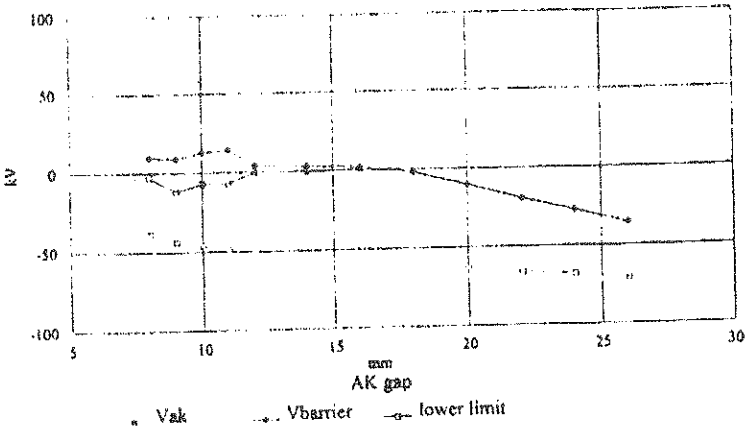

Figure 1. The accelerating potential (Vak) and the barrier potential (potential of the virtual cathode) are plotted as a function of anode-cathode (AK) gap. The operating region beyond 16 mm AK produces stable bunches with the deepest modulation at 24 mm AK.

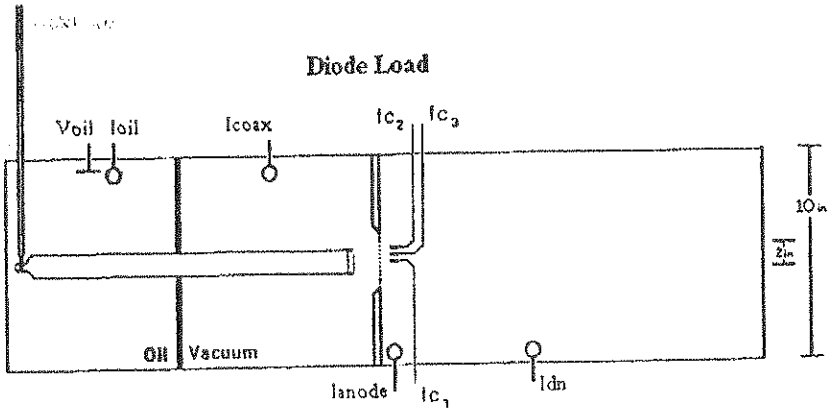

Figure 2. The vacuum diode load of the 100 kV. pulser is shown with the voltage, current, and current-density diagnostics in place. These positions are monitored in PIC simulations as well as the experiment.

NUMERICAL MODELING OF LIGHTNING PROTECTION SYSTEMS

*O. Daguillon,
Laboratoire d'Electronique
URA CNRS n°830
Complexe Scientifique des Céseaux
63170 AUBIERE Cedex

A. Karwowski
Silesian Technical University
44-100 GLIWICE
POLAND

A. Zeddam
France Telecom, CNET
2, route de Trégastel
BP 40
22301 LANNION Cedex

Typical lightning protection system (LPS) consists of air terminations, down conductors and earth terminations. Down conductors usually form a three-dimensional cage of wires connected at crossing points. The LPS is installed adjacent to the structure to be protected or incorporated within. To protect the equipment inside this mesh from an excessive electromagnetic stress, the control and reduction of coupling effects to acceptable level is required.

The provisions for lightning electromagnetic pulse (LEMP) should be included in the integral system concept, and should be a part of the initial design of the system. Therefore, availability of efficient technique is highly desirable for the purpose of predicting LEMP effects and thus optimising the LPS topology.

A general efficient method for analysing transient currents on LPS is based upon the frequency-domain electric field integral equation (EFIE) formulation combined whit the method of moments. The frequency-domain response of the structure can be then Fourier transformed to obtain the time-domain response. The main goal of this study is to determine the distribution of the current induced on the LPS conductors; the current distribution is a parameter of primary importance, since all other parameters of interest can be derived from this current in a conventional way.

In order to establish an efficient, reliable tool for modeling the LPS installations, the validation of the theoretical results is of primary importance. Thus, we have made an extensive comparison of theoretical and experimental results derived from a laboratory model measurements to demonstrate the accuracy and versatility of the method. Some results of the analysis of direct and indirect effects on a complex structure (Fig. 1) are given for 2 conductors.

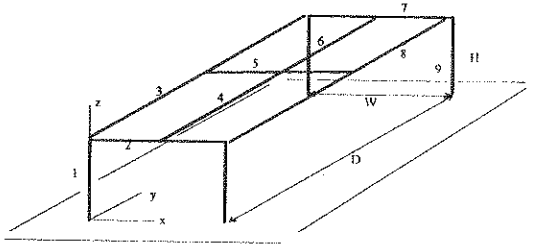

Fig. 1 : Geometry of the LPS
(H * W *D = 1 * 1 *2 m)

In the first case (Fig.2), a current was injected directly on the structure and then, we observe experimental and theoretical currents at the centre of the conductor 5.

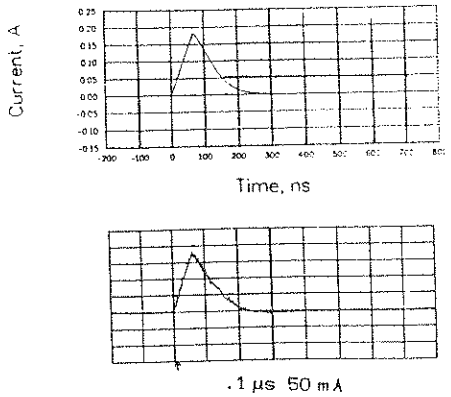

Fig. 2 : Current induced on the conductor 5

In this case (Fig.3), the structure was illuminated by the double exponential pulse plane wave. In the experiment, the parameters of the pulse were as follows :

$E_0 = 75$ kV/m, $\alpha = 4\ 10^6\ s^{-1}$, $\beta = 4.76\ 10^8\ s^{-1}$

Now, we compare theoretical and experimental currents on the conductor 9.

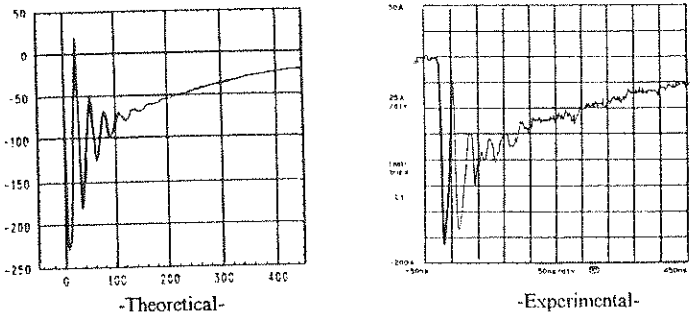

Fig. 3 : Current induced on the conductor 9

To study the potentiality and reliability of the approach, numerical results are compared with the experimental data derived from a laboratory model measurements. The comparison shows that the theory gives fair results and, therefore, the proposed approach can serve as a useful tool for predicting the lightning electromagnetic pulse effects and thus optimising the lightning protection system.

ON THE PROCESSING OF MEASURED SYSTEM-LEVEL CW TEST DATA

F. M. Tesche*
Electromagnetics Consultant
6714 Norway Road, Dallas, TX, 75248, USA

A. W. Kälin, B. R. Brändli,
Defence Technology and Procurement Agency
NEMP Laboratory, CH 3700 Spiez , Switzerland

As a relatively inexpensive alternative to pulse testing for determining a system-level response to a high altitude nuclear electromagnetic pulse (HEMP), the concept of a swept continuous wave (CW) test has seen increased popularity (T. Karlsson and L-I. Sundberg, *CW Test Technique - A Preferable Method for Assessing the Electromagnetic Vulnerability in Large Telecommunication Facilities*, NEM 1990 Record). This test method has been applied to both ground-based facilities and aircraft in the past several years.

The basic concept behind this test method is to measure a CW transfer function T(ω) of a specified electromagnetic (EM) field quantity outside the test object to a similar quantity inside the object. For example, if the magnetic field is selected as the observable quantity, a transfer function between the j^{th} and k^{th} vector components of the internal and external H-fields can be defined as $T(\omega) = H_j^{in}(\omega) / H_k^{out}(\omega)$. Generally, this is a complex-valued function of frequency (having both a magnitude and phase), and it is measured by a network analyzer over a specified range of frequencies. For HEMP testing purposes, the frequency range is usually between 10 kHz to 200 MHz, although recent improvements in measurement technology has increased the upper frequency to 1 GHz in some cases.

With a suitably measured transfer function, the HEMP response inside the system can be inferred by calculation. This requires a knowledge of the HEMP-produced H-field spectrum outside the facility, which is denoted by $H_k^{EMP}(\omega)$. The internal system response spectrum to HEMP $H_j^R(\omega)$ is computed by $H_j^R(\omega) = T(\omega) H_k^{EMP}(\omega)$. Once this spectrum is determined, the corresponding transient response is computed by either a fast Fourier transform (FFT) or by a Fourier integral transform (FIT).

Often, problems arise in this process at high frequencies in the numerical evaluation of the Fourier transform. If the FFT is used, the measured data must be interpolated into uniformly spaced samples in the frequency domain. Because the phase can be varying rapidly at high frequencies, this extrapolation process can be the cause of serious error in the computed response. One way to minimize this extrapolation error is to try to reduce the rapid variation of the phase shift in the measured spectrum by multiplying the spectrum by the complex function $e^{-j\omega\tau}$. This amounts to a simple shift of the time domain response by the time τ. In this manner, the resulting frequency domain spectrum can be interpolated more

accurately. Figure 1 illustrates the phase of a measured transfer function and the same phase after multiplying the transfer function by the time-shift exponential factor for $\tau = 0.85$ μs. Clearly the rapid variations of the phase have been reduced, and the resulting smooth phase may be interpolated more accurately.

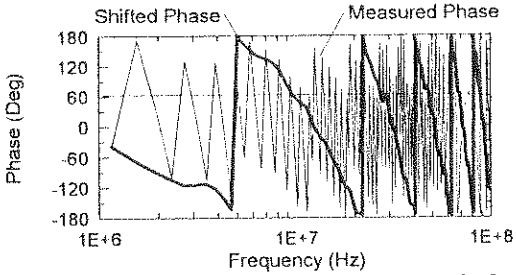

Figure 1. Measured and shifted phases of a system transfer function.

As an example of the time-domain error introduced by an improper phase sampling and interpolation, Figure 2 illustrates the inverse Fourier transform of a measured system-level CW transfer function (i.e., the δ-function response) for the cases of no phase shifting (part a) and for the phase shift (part b). The effect of improper phase interpolation appears as a "phantom" response occurring later in the time record.

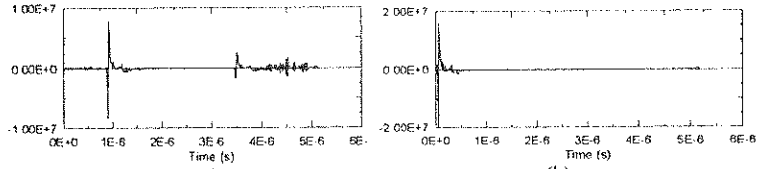

Figure 2. Delta-function transfer function responses without phase shifting (a) and with phase shifting (b).

Figure 3 illustrates the error in the final extrapolated CW test result, after the δ-function responses above have been convolved with a typical HEMP waveform. The errors in the interpolation process are evident. In this paper, additional details of this phase interpolation process will be provided.

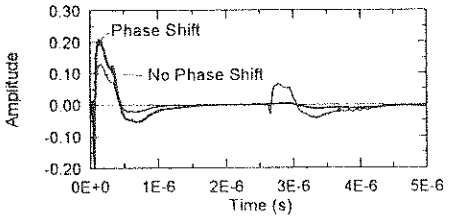

Figure 3. Extrapolated HEMP responses showing the false, late-time pulse response arising from phase extrapolation errors.

CALCULATION OF QUASI-STATIC PARAMETERS OF ARBITRARILY-SHAPED MULTI-CONDUCTORS IN $\mu\varepsilon$-ANISOTROPIC MEDIA

M.T. Manzuri-Shalmani* and A.R. Baghai-Wadji

Vienna University of Technology
Institute for Electrical and Electronic Engineering
Applied Electronics Department
Gusshausstrasse 27-29, A-1040, Vienna
AUSTRIA

Abstract: The quasi-static inductance and capacitance matrices of a system of ideal-conductive electrodes with arbitrary cross-sections are computed using the boundary-element method. The electrodes are embedded in an air-surrounded anisotropic medium which is specified by general $\underline{\underline{\mu}}$ and $\underline{\underline{\varepsilon}}$ tensors, and the system is assumed to be uniform in z-direction (Fig. 1a). The formulation has been derived from our *recently developed infinite-domain anisotropic Green's function* in conjuction with the condition of total-current (or charge) neutrality. As the reader will see the proposed method can be easily extended to cover *multi-layered* anisotropic problems.

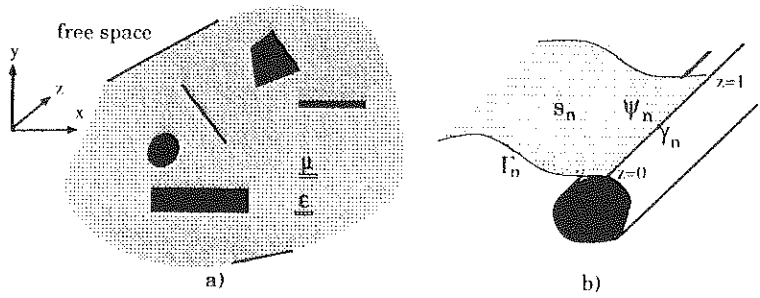

Figure 1: a) Geometry of interest b) n^{th} electrode in detail

The inductance matrix $\underline{L}$ can be introduced by $\underline{\psi} = \underline{L}\,\underline{I}$ where the n^{th} component of the $\underline{\psi}$ (i.e. ψ_n) can be expressed in the following way: based on the well-knowen equations $\vec{B} = \nabla \times \vec{A}$ and $\psi = \int\int_s \vec{B} \cdot \vec{ds}$ we obtain $\psi = \oint_\Gamma \vec{A} \cdot \vec{d\Gamma}$. Let s_n be a semi-plane intersecting n^{th} electrode along a z-directed line γ_n ranging from $z = 0$ to $z = 1$ (Fig. 1b). Futhermore, let γ_n denotes the contour of s_n. The total magnetic flux surrounding n^{th} conductor is then given by:

$$\psi_n = \oint_{\Gamma_n} \vec{A} \cdot \vec{d\Gamma} = A_{zn} - A_\infty. \qquad (1)$$

A_{zn} and A_∞ are values of A_z on γ_n, and in the far-zone, respectively. As the

current-density vector is assumed to have a z-component only, H_z vanishes and consequently, the value of A_{zn} (and thus ψ_n) does not depend on a particular position of the intersection line γ_n. It is instructive to introduce the following vectors:

$\underline{A}_z = (A_{z1}, ..., A_{zN})$, $\underline{I} = (I_1, ..., I_N)$ and $\underline{U} = (1, ..., 1)$, where N is the number of electrodes. Using these vectors and substituting Eq.(1) and the current neutrality condition in $\underline{\psi} = \underline{\underline{L}}\,\underline{I}$ we obtain:

$$\begin{bmatrix} \underline{A}_z \\ 0 \end{bmatrix} = \begin{pmatrix} \underline{\underline{L}} & \underline{U} \\ \underline{U}^T & 0 \end{pmatrix} \begin{bmatrix} \underline{I} \\ A_\infty \end{bmatrix}. \tag{2}$$

Assuming the following form for $\underline{\underline{\mu}}$

$$\underline{\underline{\mu}} = \begin{pmatrix} \mu_{11} & \mu_{12} & 0 \\ \mu_{21} & \mu_{22} & 0 \\ 0 & 0 & \mu_{22} \end{pmatrix} \tag{3}$$

$\nabla \cdot \underline{\underline{\eta}} \nabla A_z = -j_z$ can be derived from the Maxwell equations, with

$$\underline{\underline{\eta}} = \frac{1}{\sqrt{\mu_{11}\mu_{22} - \mu_{12}\mu_{21}}} \begin{pmatrix} \mu_{22} & \mu_{21} \\ \mu_{12} & \mu_{11} \end{pmatrix}. \tag{4}$$

Using the aforementioned infinte-domain anisotropic Green's function, and applying the method of moments to $\nabla \cdot \underline{\underline{\eta}} \nabla A_z = -j_z$ we obtain a system of equations, which after a few algebraic manipulations, gives

$$\begin{bmatrix} \underline{I} \\ A_\infty \end{bmatrix} = \underline{\underline{M}} \begin{bmatrix} \underline{A}_z \\ 0 \end{bmatrix}. \tag{5}$$

Comparison of $\underline{\underline{M}}^{-1}$ with the matrix involved in Eq.(2), leads *directly* to the values of the elements of $\underline{\underline{L}}$. The capacitance matrix can be computed by an analogous approach. Below a glimpse at our numerical results are presented. The first example has been chosen to compare our results with available data. The second one serves to illustrate the generality of our method.

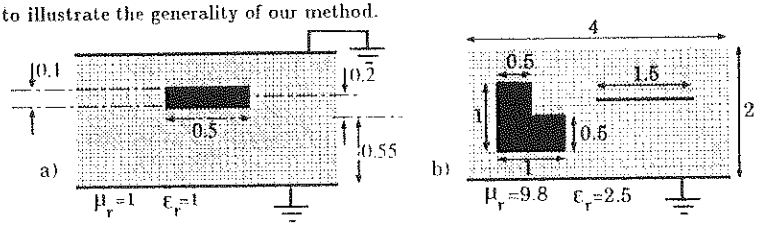

Figure 2: Geometry and data for the examples considered. Both of above structures are open and air-surrounded.

First example: $\frac{C}{\varepsilon_0} = 4.764$ (conformal-mapping method)

$\frac{C}{\varepsilon_0} = 4.770$ and $\frac{L}{\mu_0} = 0.209$ (present method).

Second exmple: $\frac{C}{\varepsilon_0} = \begin{pmatrix} 48.50 & -16.80 \\ -16.80 & 23.18 \end{pmatrix}$ and $\frac{L}{\mu_0} = \begin{pmatrix} 0.25 & 0.15 \\ 0.15 & 0.49 \end{pmatrix}$

(present method).

Field Penetration In Complex Objects By An Hybrid Finite Element / Geometrical Theory of Diffraction Method

Benoit Roturier[1]*, Bernard Souny[1], Henri Baudrand[1]

[1]E.N.A.C Dept. Electronique
7, av E. Belin 31055 TOULOUSE CEDEX

[1]E.N.S.H.E.E.I.T
2 rue Camichel 31071 TOULOUSE

INTRODUCTION

In this paper a method is outlined to compute electromagnetics fields inside complex objects of resonant size when large external scatterers are present. The first step is to divide the problem in an internal and an external part using the theorem of equivalence (R.F.Harrigton "Time Harmonic Electromagnetic Fields"). The internal part associated to the inside of the complex object is described and computed by a Finite Element (FE) method and may be of complex shape and constitution, while the external part must be large in term of wavelength so that its interaction with fields might be computed by Geometrical Theory of Diffraction (GTD). In a second step, the radiation of the equivalent sources introduced during the first step allows computation of the fields inside the complex object with the Finite Element method. In this communication we use a time harmonic dependance of fields.

FORMULATION

The equivalence theorem allows us to divide the original problem into two independant problems by the introduction of equivalent electric and magnetic sources on a separation surface S which separate the problem in a zone of FE analysis and a zone of GTD analysis. These sources must radiate the same field as the original field in one half of the problem and radiate zero field in the other half. With this condition, it is possible to close each one of the half problems by any condition of convenience: metallic or magnetic wall for finite element analysis, free space for the external problem for example.

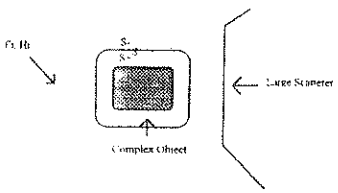

1) FE analysis of internal problem

The FE analysis is performed using a commercial software (J.R.Brauer, B.E.MacNeal "MSC/EMAS User's Manual"), whose functionnal has been modified to adress properly the problem of spurious solutions (L.Bardi, O.Biro "An efficient finite element formulation without spurious modes for anisotropic wave guides" IEEE Trans on MTT vol 39 n°7 July 1991). The internal problem is enclosed by a magnetic wall and the FE software is used to compute the Green function of the internal problem, that is the relationship between a unit source of electric current on each element on S- and the electric field everywhere on S. Since we postulate a null electric field in the external part of the problem, we introduce a source of magnetic current on the magnetic wall which allows the step discontinuity between the internal tangential electric field and the external null field.

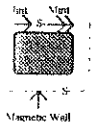

If we have N elements on the boundary, we are able to compute an N×N matrix Z_{int}, and we then have a weak formulation of the relationship between the unknown electric (J_{int}) and magnetic (M_{int}) sources so that the external fields be zero:

$$\langle M_{int}|\varphi\rangle = \langle J_{int}|Z_{int}|\varphi\rangle + \langle E^i_{int}|\varphi\rangle, \quad \forall|\varphi\rangle \quad \text{weighting function} \quad (1)$$

2) GTD analysis of external problem

A similar approach is used for the external problem, however to allow a practical calculation, the electric (J_{ext}) and magnetic (M_{ext}) sources must be chosen so that they

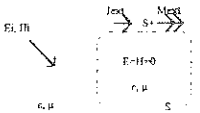

radiate a GTD field, and also the internal body will be changed either for free space or perfect metallic or magnetic body depending on problem geometry. This is possible because we impose to J_{ext} and M_{ext} a relation to nullify the field in the internal problem.

Then one is able to compute with GTD the electric and magnetic fields on S due to these sources. Hence we also have a weak formulation of the relationship between the unknown electric (J_{ext}) and magnetic (M_{ext}) sources which nullify the internal fields:

$$\left.\begin{aligned}\langle M_{ext}|Y_{ext}|\varphi\rangle+\langle J_{ext}|L_{ext}|\varphi\rangle+\langle H^{i}_{ext}|\varphi\rangle=0 \quad (2)\\ \langle M_{ext}|K_{ext}|\varphi\rangle+\langle J_{ext}|Z_{ext}|\varphi\rangle+\langle E^{i}_{ext}|\varphi\rangle=0 \quad (3)\end{aligned}\right\} \quad \forall\varphi$$

Yext and Lext are the operators which relate the magnetic and electric sources on S+ to the magnetic field on S and Kext and Zext are the operators which relate the magnetic and electric sources on S+ to the electric field on S.

3) Problem Solution

The solution of the problem is obtained by cancelling in a weak sense the equivalent sources:

$$\left.\begin{aligned}\langle J_{int}|\varphi\rangle+\langle J_{ext}|\varphi\rangle=0 \quad (4)\\ \langle M_{int}|\varphi\rangle+\langle M_{ext}|\varphi\rangle=0 \quad (5)\end{aligned}\right\} \quad \forall\varphi$$

The set of equations (1) to (5) is an overdetermined matricial system which allows us to solve for the 4 unknown sources. We need more equations than unknown to adress the problem of internal resonnances. One should also note that the representation of internal and external sources are different since different methods are utilised for the internal and external problem. For the geometry shown in Result part for example, the internal sources are represented by pulses function which are the natural sources for the finite element software while the corresponding external ones are represented by dirac delta distributions whose radiation is easily computed by GTD.

RESULTS

The method has been validated by computing in the external domain the Radar Cross Section of simple shapes in free space and comparing with analytical results. We show below an application for the internal domain: the magnetic field calculated around a perfect metallic cylinder with a TM incident plane wave at .47 Ghz coming from the left and a vertical perfect metallic infinite plane located at 1 m of the cylinder center on the right. The radius of the cylinder is 5 cm and the separation surface S between GTD and FE is here a circle arbitrarily situated at 10 cm of the center of the cylinder. This field is by radiated by the calculated J_{int} on a magnetic wall boundary condition within the FE software.

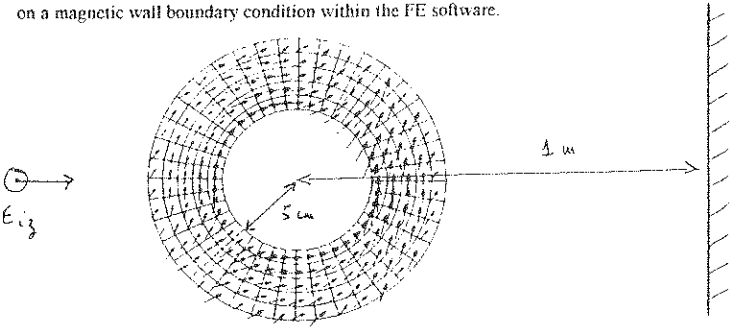

INDOOR ELECTROMAGNETIC WAVE PROPAGATION MEASUREMENTS AND MODELLING

Wiart joe
France Telecom CNET PAB/SHM
38 40 rue du général leclerc F 92131 Issy les moulineaux cedex
tel 33 1 45 29 58 44 fax 33 1 45 29 63 07

Indoor radio propagation has been an active area of research in recent years. The attenuation of radio waves propagating into building is a crucial factor in the design of portable radio telephone systems and in the electromagnetic compatibility studies. A large range of wall and floor loss has been reported. Much work has been done to characterise statistically propagation inside buildings . In some cases discrepancies are observed with measurements. Because of the potential implementation of wireless lan and personal communication network it is important to understand indoor propagation.

Building represents a complex environment of very large dimensions compared to the wavelength. Radio waves are propagating by reflections, transmissions and diffractions. The resulting multipath causes the received signal to exhibit strong variations. Environment is times varying: people move and furnishing change so prediction accuracy is limited and systems have to consider these characteristics. Waves propagation mechanisms are studied and modelled in that conditions. To get the mean field traditional practice has been to average the signal by moving the receiver over a spatial area having linear dimensions of 10 to 20 wavelength (often in circular path). The fast fading distribution is often described by Rice-Nakagami distribution for one strong dominant path and the Rayleigh law when all the paths have same strength. In case of indoor propagation estimation of fast fading distribution functions show that fast fading are often governing by Rice law. A strong dominant path exists and so determinist approach is needful. In this paper the propagation mechanisms in indoor environment are analysed.

The contribution of the reflected, transmitted and diffracted waves in the received field are studied using high frequency methods and in particular ray theory and geometrical theory of diffraction.The finite conductivity has been studied by Maliuzhinets, approximated form has also been studied by Luebbers through heuristic coefficients. Diffraction is often forgotten in indoor propagation studies. For some receiver location the geometric optic rays must pass through many walls or floors, whereas paths exist whereby the waves reach the receiver with less loss after diffraction. To get accurate model this phenomenon have to be taken into account. The received field is a mixture of reflection transmission and diffraction.

Measurements had been done to show that if transmission model (loss of straight ray) gives accurate results in specifics cases, in most cases diffraction must be take into consideration. Measurements were done in a building of "Club Méditéranée" in Avoriaz.

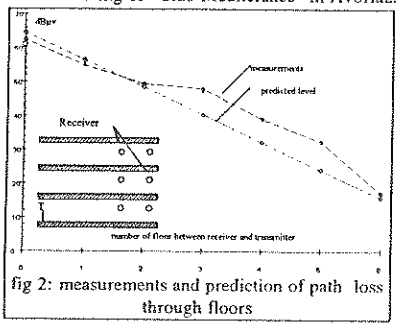

fig 2: measurements and prediction of path loss through floors

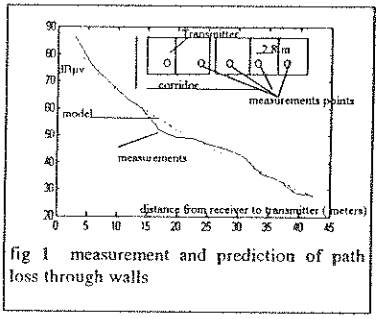

fig 1 measurement and prediction of path loss through walls

Bedrooms are line up, partitions walls are made of concrete (thickness 17 cm). There is no piece of furniture in the rooms. Figure 1 and 2 show that in some case power carried by diffracted ray is less than that carried by the straight ray.

In some case (fig 3) diffraction must be taken into account because the power carried by diffracted rays is the major contributor to the total received power. Attenuation does not linearly increase with the number of floor. Using Felsen approach diffraction path loss was calculated.

The transmission model is close to the measurements at the beginning. When the number of floor increases the received level does not more and more decrease. The received level has an asymptotic behaviour. The diffracted field become to be the major contributor.

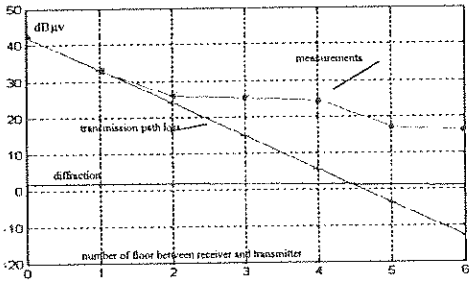

fig 3 received power versus number of floor between receiver and transmitter

Propagation in corridor also shows that diffraction is often the major phenomenon, especially in bend corridor. We have done simulations to studied propagation in dielectric canyons, they showed that if we consider the finite width of the walls the field is very close to those yields by infinite width. In corridors measurements , in good agreement with simulations, showed that when the receiver is in line of sight of the transmitter an accurate approximation of the path loss is given by the free space loss When the receiver turn around a corner the received field is a sum of reflected and diffracted waves.. A program based on a typical corridor was developed when the receiver is in line of sight 8 reflections are permitted, when the receiver is not in line of sight 8 reflections without diffraction and two reflections with one diffraction on the corner are permitted. We study the contribution of the reflected and diffracted wave at the corner. The model gives an understanding of the basic phenomena. Received power when the receiver is no line of sight (after the corner) is a sum of reflected and diffracted rays. The reflected power decreases rapidly with a quasi-linear slope. The diffracted power yields by reflections and Maliuzhinets approach is close to the field given by the Felsen absorbing wedge

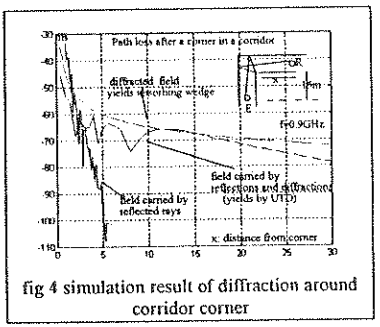

fig 4 simulation result of diffraction around corridor corner

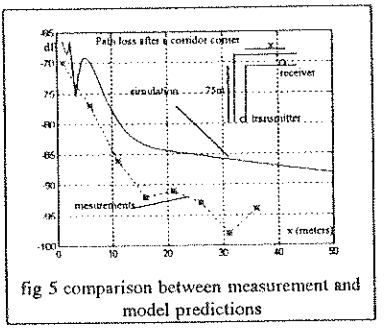

fig 5 comparison between measurement and model predictions

This study shows that indoor propagation model must take into account diffraction. When the receiver is not near the transmitter in spite of high diffraction path loss the diffracted rays could carry most important field. Measurement confirm this approach

SLIT CABLE CALCULATION

Professor Dragutin M. Velickovic*, D.Sc., Member IEEE, Alenka M. Dekic
Department of Electromagnetics, Faculty of Electronic Engineering.
Beogradska 14, 18000 Nis, Serbia

The radio link space-time continuum is necessary in the contemporary railway transport. The practical solutions use the SW transmitters placed along the railway-track on the distances less then 100 [km] and corresponding receiver on the locomotive. In regard to the used frequency band in mobile telecommunications between a locomotive and a dispatcher center, the tunnels and the bridges cause serious difficulties, because they act as waveguides whose cut-off frequency, in the train presence, is greater then the operating frequency. Two following practical solutions have been used to solve these problems: a) setting directional antennas at the ends of the tunnels, and b) setting the slit cable along the whole route of the tunnel, as close as possible to the locomotive receiving antenna on the train roof (D.M.VELICKOVIC, A.Z. DORDEVIC, A.M.DEKIC, VI International Scientific Conference: Problems of Integrating of the Eastern-European Railways into the European Transport System, November 10-12, 1993, Sofia, Bulgaria).

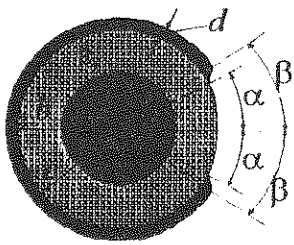

Fig.1–Slit cable cross-section

The slite cable cross-section is presented in Fig.1. a is radius of internal conductor. b and c, $c = b + d$ are radii of the shield. d denotes shield thickness. α and β are angular openings of the internal and external shield side.

The analysis of slit cable with zero shield thickness can be founded on the following point matching procedure in numerical solving of Laplace's equation:

The electric scalar potential, φ, inside and outside slit cable, satisfies well known Laplace's equation, $\Delta\varphi = 0$, and boundary conditions:

$$\varphi = U,\ r = a,\ 0 \le |\theta| \le \pi,\ \varphi = V,\ r = b,\ \alpha \le |\theta| \le \pi \text{ and } \varepsilon_r \left.\frac{\partial\varphi}{\partial r}\right|_{r=b-0} = \left.\frac{\partial\varphi}{\partial r}\right|_{r=b+0},\ 0 \le |\theta| \le \alpha,$$

where r, θ, z are cylindrical coordinates and $r = 0$ coincides with cable axis. U and V are potential, with respect to the infinite referent point, of internal and external electrode. The approximate potential solution, witch automatically satisfies Laplace's equations and first boundary condition, can be put in the following form:

$$\varphi = \begin{cases} U\dfrac{\ln(b/r)}{\ln(b/a)} + \sum_{n=1}^{N} A_n \dfrac{\mathrm{ch}(nk\theta)}{\mathrm{ch}(nk\pi)} \sin\left(nk\ln\dfrac{r}{a}\right) + \sum_{n=1}^{M} B_n \dfrac{\left(\dfrac{r}{a}\right)^n - \left(\dfrac{a}{r}\right)^n}{\left(\dfrac{b}{a}\right)^n - \left(\dfrac{a}{b}\right)^n} \cos(n\theta), a \le r \le b \\ \sum_{n=1}^{M} B_n \left(\dfrac{b}{r}\right)^n \cos(n\theta), b \le r < \infty \end{cases}$$

where $k = \pi/\ln(b/a)$ and A_n and B_n are unknown constants. The total number of unknowns is $K = N + M + 2$ $(A_n, n = 1, 2, \ldots, N, B_n,\ n = 1, 2, \ldots, M, U$ and $V)$.

By using known cable tension, $U_0 = U - V$ and cable charge condition, $q_1' + q_2' = 0$ (where q_1', and q_2' are charges per unit electrodes length.), the remained $N + M$ necessary equations can be obtained by matching second and third boundary condition in N and M points. So the system of linear equations can be put. After solving this system, capacitance per unit length can be calculated as $C' = q_1'/U_0$ and characteristic impedance is $Z_c = \sqrt{\varepsilon_r \varepsilon_0 \mu_0}/C'$. The convergence is very good and satisfying accuracy can be achieved when $N, M \le 4$.

The dependence of the characteristic impedance to the relative permitivity, ε_r, for $b/a = 3$ and $d = 0$ is presented in the Fig.2.

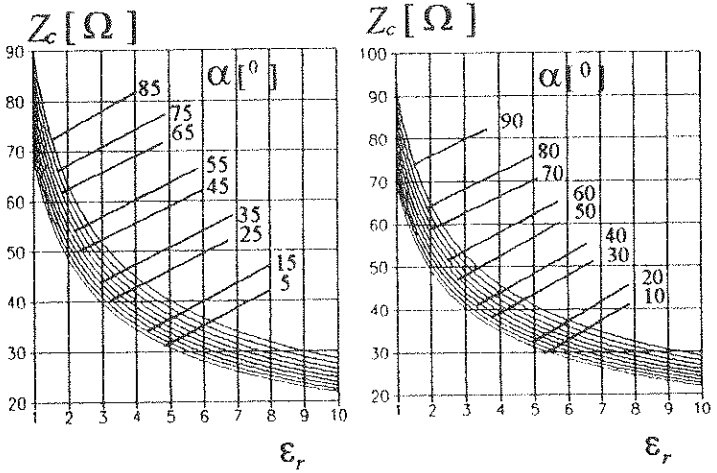

Fig.2– Characteristic impedance, $Z_c[\Omega]$, for $d = 0$, $b/a = 3$, and different values of angle α, as function of the relative permitivity, ε_r

Protecting Building Power & Communication Lines Against Lightning Currents

Michael F. Stringfellow
EFI Electronics Corporation
Salt Lake City, Utah, U.S.A.

Abstract

Introduction

This paper considers the mechanisms that couple lightning currents into building power, communication and data lines and the effects of the resulting transient voltages.

Techniques for protecting against these lightning currents and mitigating their effects on electrical and electronic equipment are discussed. In particular, the benefits of cascaded non-linear and hybrid surge protective devices and shielding of communication lines are discussed in detail.

Lightning Current Coupling

Lightning currents enter power and communication lines in buildings in three main ways:

1. Directly into overhead or underground lines entering the building

2. Indirectly through the structure, particularly structural steel

3. Indirectly by electromagnetic induction

Effective protection against lightning currents must take into account all three modes of coupling.

The most severe lightning currents involve direct lightning striking overhead or underground lines entering the building. These include ac power, telephone, cable tv and similar communication lines. Lightning strikes to roof-mounted equipment should also be included in this category. The latter commonly include air-conditioning equipment, lights, security cameras and radio antennas.

In the worst cases, surge currents exceed 10 kA, voltages exceed wiring flashover levels, and severe damage to electrical and electronic equipment may result.

Lightning currents which enter the building structure frequently couple into internal wiring indirectly, either through induction or through "ground skew". Ground skew, or differential ground voltages, occur when lightning currents pass through the building steel or its grounding system. Momentary voltages exceeding several kilovolts may result. Although surge currents are much lower than those encountered in direct strike events, damage frequently occurs to data and communication systems and sometimes to electrical equipment.

Direct induction from the lightning channel results in the lowest energy surges in building wiring, and rarely results in damage to electrical installations. Nevertheless, damage is often reported from this cause to the more sensitive data communications systems.

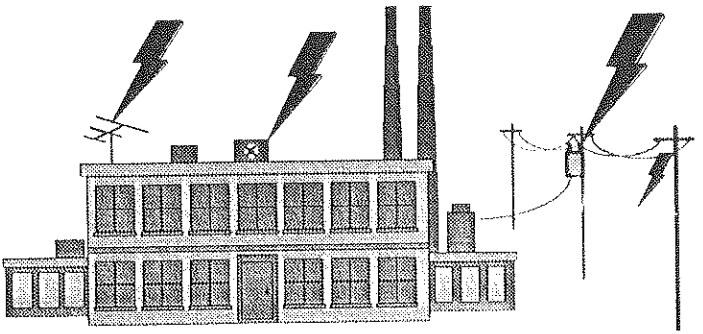

Protection techniques

Effective protection requires a three-step procedure:

1. Install lightning protection systems which divert direct lightning strikes away from the power and communication lines. In sensitive structures, this may include protecting the building itself.

2. Install cascaded surge protective devices on all vulnerable power, data and communication lines. Cascaded protection requires primary protection at the point the service enters the building, secondary protection at a distribution or intermediate point, and final protection at any sensitive electronic equipment. Communication lines may require special hybrid protectors or may be isolated through transformers or fiber-optic cable.

3. Shield sensitive data lines to minimize the effects of electromagnetic induction and properly ground the shields.

LIGHTNING WARNING STATION
Active lightning protection methodology

P. RICHARD* and F. BROUTET,
DIMENSIONS, 13790 Rousset, FRANCE

The active lightning protection of sensitive sites proves to be an efficient, reliable and cost effective solution.

The principle is to isolate, during lightning risk periods, the sensitive equipments from the main sources of overvoltages and perturbations. The isolation can be either performed manually or triggered automatically by a lightning warning device.

The efficiency of the active protection relies on the quality and early warning capability of the lightning warning equipment and on the proper implementation of active protection equipments.

For application on local sites a well adapted technique is based on the early detection and identification of thunderstorm through the measurement and analysis of its electrostatic field. The strong convective activity which occurs within the thundercloud is at the origin of the electrification mechanisms and consequently of the lightning discharges. These lightning discharges first occur within the thundercloud during the growing phase and then between the cloud and the ground during mature and decay phases. Electrification mechanisms and lightning discharges modify the atmospheric electrostatic field in the vicinity of the thundercloud. Electric field modifications can be detected and analysed in real-time as soon as the thundercloud builds up and a warning issued before the first lightning strikes to the ground.

Evolution of thunderstorm electrical activity:

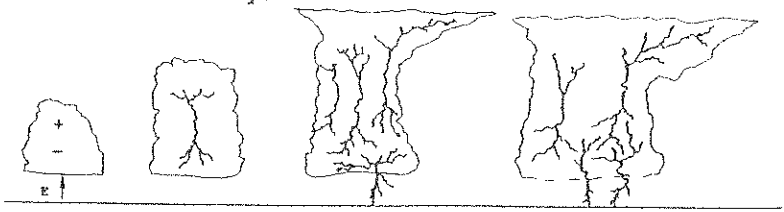

Evolution of electrical field on the ground:

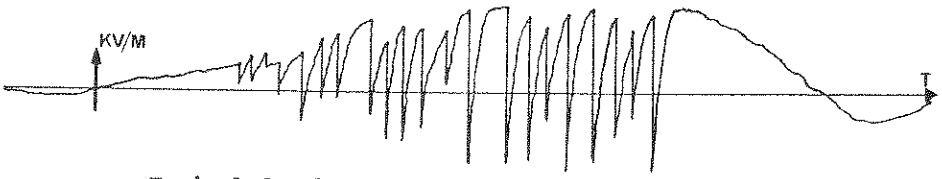

Typical development of a thunderstorm cell

The lightning warning algorithms used by the "Lightning Warning Station" is a result of ONERA research program in the field of thunderstorm electrical phenomenology. It integrates a real-time dynamic analysis of electric field evolutions in order to give improved performances compared to standard criteria based only on electric field threshold. It results in a real "intelligent warning" giving better operational results in terms of early warning leading time, detection efficiency and false alarm rate.

A gradual warning depending on the hazard level is provided according to 3 lightning warning levels:

Warning 1: **Early warning;**
tendency towards thunderstorm activity.

Warning 2: **Distant active thunderstorm;**
possible disturbances on electric lines and data transmission.

Warning 3: **Local thunderstorm;**
lightning strike hazard on the site.

The advantages of this gradual warning is to enable the progressive protection of sites and equipments, and to adapt the protective measures to the real situation in order to maintain operational activities.

This type of warning protection methodology is in operation on sites where the continuation of activities is of prime importance such as telecommunication centers (France Telecom), military sites, radar and detection systems (French Civil Aviation) as illustrated in the figure below.

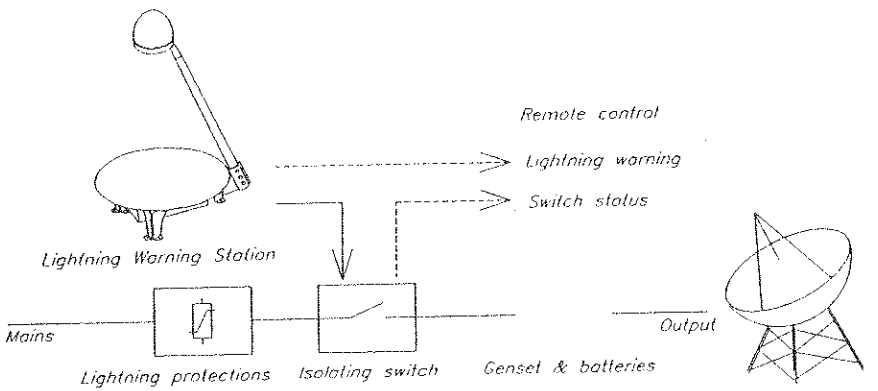

Active lightning protection

RESPONSE OF GAS DISCHARGE TUBES TO THE FOLLOW ON CURRENTS OF SIMULATED LIGHTNING STROKES

Charles S. Field, III*
Lawrence R. Shapnek
Sandia National Laboratories
Arming and Firing Department 9332
Albuquerque, New Mexico 87185-1157

Gas discharge tubes (known as over-voltage gaps, gap tubes and gas-filled spark gaps) are high-energy, voltage-controlled switching devices capable of repeatably switching currents of thousands of amperes. These operating capabilities make the gas discharge tube useful in mitigating the effects of lightning and large electrical transients on components and systems. The gas discharge tube typically consists of two metal electrodes separated by a specific distance and placed within a gas-filled chamber. With the application of sufficient voltage across the electrodes, an electrical arc breakdown occurs between the electrodes. When formed, this electrical arc is capable of carrying currents of thousands of amperes while the voltage developed between the electrodes during the arcing process remains relatively independent of the arc current. A voltage considerably higher than the gap tube arcing voltage must be applied to initiate breakdown. The gas discharge tube is a bipolar device, conducting current of either polarity.

While artificially triggered lightning tests of gap tubes and associated circuitry have been performed by Lawrence Livermore National Laboratory and Sandia National Laboratories, limited follow-on current amplitudes and pulse widths were obtained. Controlled and repeatable testings of gas discharge tubes in the high-energy region of the lightning follow-on environment were needed. This report describes the electrical testing of various gas discharge tubes (produced by Reynolds Industries, Incorporated, Los Angeles, California), with high-energy current pulses up to a maximum of 1.5KA for durations up to 1.0 second. These current pulses represent the 99 percentile level of electrical charge and energy as found in the follow-on portion of natural lightning.

The test objective was to establish performance thresholds for these specific gas discharge tubes, i.e., the points at which their characteristics permanently change and no longer exhibit the functional characteristics of gas-filled gap devices. Our goal was to identify failure modes of the gap tubes and to characterize, in the follow-on lightning environment, the performance of the different types of Reynolds gap tubes, and to determine how differing breakdown voltages, amperage ratings and electrode materials affect gas discharge tube performance.

A 48-volt current source, composed of four deep-cycle marine lead/acid batteries connected in series, was applied to the gas discharge tube under test by an automotive starter relay. The amplitude of the current pulse was controlled by a selectable series resistance. The time duration of the current pulse was determined by an adjustable electronic timer that controlled the operation time of the relay. A high-voltage, capacitive-discharge unit was used to initiate breakdown of the gap tube. A LeCroy Model

7200 Oscilloscope with internal computational capabilities was used to record gap voltage and current as function of time. From these inputs, the LeCroy 7200 generated additional computational outputs of electrical charge and energy deposited in the gap tube as a function of time. Data was entered into a database for reduction and processing. Performance equations were derived for the gap tubes using least squares analysis methods. The various analyses of voltage, current, charge and energy waveforms enabled the attainment of the stated goals and provided insights for enhancement of the energy-absorbing capabilities of gas discharge tubes.

INJURIES FROM LIGHTNING - A REVIEW

by

Dr Chris. ANDREWS
BE MBBS MEngSc PhD GradDipCompSc EDICM

University of Queensland, Australia
and
Royal Brisbane Hospital

Lightning injuries are a fascinating example of multisystem trauma and are unlike other electrical injuries. This paper reviews the spectrum of injury and briefly examines treatment modalities in the light of new knowledge of the injury.

Four mechanisms of injury are pertinent - the direct strike, side flash and contact potential, and earth potential rise. Models are presented estimating the current flowing through a person under these circumstances, and also estimating its time course. The models are supported with early experimental results.

The major consequences of the injury from the point of view of life threat are those in the cardiorespiratory systems. The progress of cardiorespiratory arrest is traced giving recent experimental findings. The importance of the cranial special sense orifices as portals of entry to the body is stressed, and thereby mechanisms of special sense damage are given. Pathways of current passage involving the cardiorespiratory system are given, and histological examination of damaged tissue is also offered.

In injury to other systems, burns are presented, as is peripheral neurological damage and the phenomenon of keraunoparalysis. A short speculative resume of psychiatric consequences is given.

Finally indications of treatment of the injury are given.

LIGHTNING PROTECTION CERTIFICATION OF EFIS NBELL 412 ROTORCRAFT

Sigit Hardjanto - Harlina

Lightning Protection Group
Flight Test Center - IPTN
Jl. Pajajaran No. 154, Bandung - 40174, Indonesia
Telp. 62 - 22 - 633900 ext. 2433
Fax. 62 - 22 - 632132 & 62 - 22 - 631873

Abstract.

The paper describes the lightning protection certification process of Electronic Flight Instrument System (EFIS) installed in IPTN - BELL 412 (NBELL 412) rotorcraft.

The tests have been performed to demonstrate compliance with DGAC and FAA regulations.

The rotorcraft was injected by the lightning simulation currents (reduced level) to determine the levels of voltages and currents expected to be induced in interconnecting wiring which were extrapolated to find the Actual Transient Levels (ATL's). Laboratory testing was performed on the EFIS equipments to verify the Equipment Transient Design Levels (ETDL's).

Comparisons between the Transient Control Levels (TCL's) to the ETDL's were made to verify adequacy of protection against damage or upset due to lightning induced transients.

The proposed paper shows protection from indirect lightning - effects for certification purposes.

MONOCHROMATIC AND TRANSIENT SCATTERING OF CHAFF

Yanping Guo[1] and Herbert Überall*
Dept. of Physics, The Catholic University of America, Washington, DC 20064

The electromagnetic scattering of a chaff cloud has been investigated both in the case of monochromatic waves and in the case of transient waves. Chaff usually consists of a large amount of thin conducting wires dispersed in the atmosphere, and these wires form a cloud of scatterers to protect a target from being detected by radar.

In the case of monochromatic scattering, the bistatic radar cross section of the chaff cloud is evaluated. From a practical point of view, instead of using the traditional scattering-plane-based system, we consider the problem here in the ground-based system and relate the scattered field to the incident field through the Stokes parameters. In the evaluation Einarsson's second order formula has been used to calculate the scattering of a single wire. The statistical characteristics of the wires in the cloud are realized and described in their distribution functions. It is assumed that the wires are uniformly randomly distributed in the atmosphere in this case of monochromatic scattering, and the orientation of each wire is considered in two patterns, one with the spherically random orientation and one with Gaussian in elevation and uniform in azimuth. The bistatic radar cross section is obtained for arbitrary polarizations of the transmitter and the receiver in the ground based system.

The numerical results show that different orientation pattern that the wires are in have different effect on the radar cross section in certain polarizations of the transmitter and the receiver. Figure 1 is one of the examples showing the average bistatic radar cross section for vertically to vertically polarized transmitter and receiver with the spherically random orientation (a) and with the Gaussian orientation (b). In this example the radar cross section in the latter case is generally about two orders smaller than the one in the former case.

In the investigation of the transient scattering of the chaff cloud, its response to incident pulses is evaluated in the time domain. The responses are obtained by means of the Fourier transform method. In this case of transient scattering, the relative phase difference among the wires caused by their locations has been taken into account. It is assumed that the wires are located according to a Gaussian radial distribution with the densest part in the center of the cloud. The wires orientation may be either one of the patterns described in the monochromatic case. The bistatic response is obtained for various polarizations of

---

[1] Present address: Johns Hopkins University Applied Physics Laboratory, Laurel, MD 20723.

the transmitter and the receiver in the ground-based system.

Figure 2 is a calculated backscattered response of the chaff cloud to a 40-cycle sine waveform.The chaff cloud consists of one thousand wires which are located according to the Gaussian distribution and oriented spherically randomly. In the calculation each of the wires' location and orientation parameters are generated and assigned by the computer according to the assumed distribution functions. The result shown in Fig. 2 is from one of the random parameter data sets.

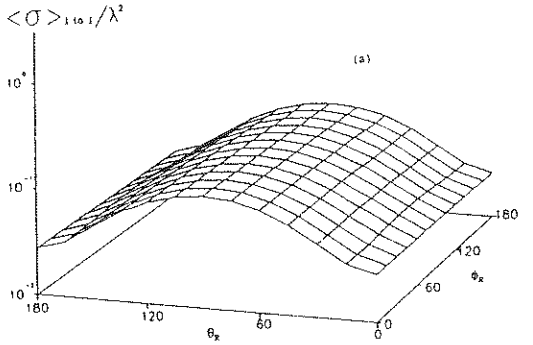

Fig. 1

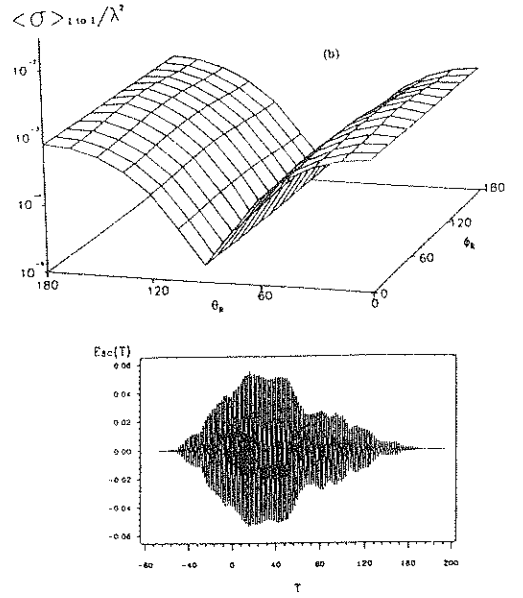

Fig. 2

STATISTICAL ELECTROMAGNETIC FIELD IN REVERBERATING CHAMBERS

P. CORONA
Istituto Universitario Navale (Naval University)
via Acton, 38 -80133 Naples- ITALY

The reverberating chamber. In a metallic (with low loss walls) cavity the electromagnetic field fed by a source is by far larger than the corresponding free space field, due to the high quality factor, Q, of the chamber; such a situation has been considered with interest for EMC applications, where high intensity fields are necessary for susceptibility measurements (on the other hand, high sensitivity is also required for emission tests). For large cavities (referred to the wavelength) a multimode field is assessed, but this field is very sensitive to the smallest change of position of the items under test, and sometimes also to the vibrations of the structure. Such a field cannot be used for measurements. Looking toward the possibility of taking advantage of this instability, the idea is of enhancing it, by introducing movable mode stirrers in the cavity; such provision allows to obtain a mode mixing which results in an "average" uniform field. The more recent evolution of reverberating chamber can be referred to seventies, in two different approaches independently followed by an US group (Navy, McDonnel Douglas, NBS and Colorado University) and by an Italian group (Naval University of Naples). The purpose of the first of them was basically to improve shielding effectiveness test procedure for MIL/STD, and "stepped mode" stirrers operation, in the purpose of obtaining some tuning (leading to a "worst case" evaluation) was presented, while the purpose of the second group was to propose a reliable method for testing leakage by microwave power equipment (f.i. microwave ovens), and, since its starting, was based on "continuos mode" stirrers operation. The two approaches showed to be each other consistent and some cooperation was established.

Isotropy versus Uniformity. The electromagnetic field inside a reverberating chamber can be seen in two different manners: as plane waves (rays) incoming isotropically (in the statistical, time average sense) toward the interior of the chamber, or as modal fields summing up in the chamber to generate (again in the statistical, time average sense) an uniform field across the chamber. As a consequence of the first viewpoint, the directivity of a matched sensor (i.e. an antenna), either receiving or radiating, is lost, and the received power is related only to the insertion loss of the chamber (and to the mismatch, or to the shielding, of the sensor). Some simple mathematics can relate the energy level in the chamber, the flowing power density, and the chamber losses, all parameters whose meaning is based on the "energy and power" concepts, but some difficulty can arise in the attempt to relate such a concepts, with the customary, steady state concepts, such as quality factor and number of modes. Furthermore, latter parameters are uneasy to be computed, considered the structure of the chamber itself. A fully statistical approach has to be considered, if appropriate, as a better procedure to evaluate the reverberating chambers performance.

Measurement set-up. A network analyser has been put in operation as a fixed frequency, time domain sampler, fig. 1, in order to sample the insertion loss as coupling of the receiving and transmitting antennas in the chamber. Typical statistical probability density pattern are in fig.2 and 3. They well fit the predicted statistical behaviour and can be considered as the basic reference for the statistics in the reverberating chamber. Many tests have been performed, in a research activity supported by the European Space Agency, using the receiving sensor

enclosed in a cabinet with a wall open and suitable to be covered (fig. 4 and 5) with nets simulating various coupling degrees. Some conclusions can be drawn. Loosely coupled equipments give smooth, regular statistics, better approaching the predicted ones. Less regular statistics are given by equipments exhibiting too tight coupling with the field (unlikely to occur in EMC evaluations), or in conditions of poorly operated (f.i. frequency too low to ensure an adequate modal coverage) chamber.

Conclusions. The statistical field in a reverberating chamber can be considered a reliable reference condition suitable for many EMC evaluation. Many tests, as well as theory, showed the possibility to correlate the reverberating chamber results to other reference conditions, such as a plane wave. But the stability of the statistical representation, referred to many operating conditions, suggests to look at this representation as suitable to typify also the natural behaviour of electromagnetic fields in an enclosed, partially reactive, non free space condition.

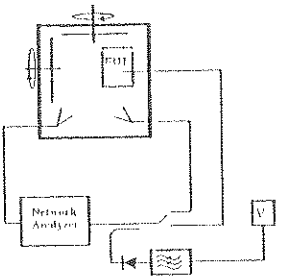

fig. 1

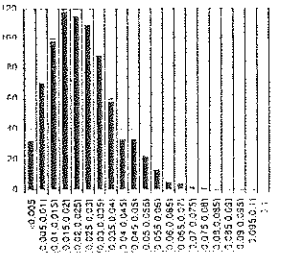

fig. 2

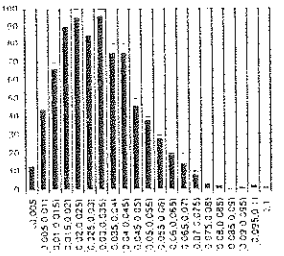

fig. 3

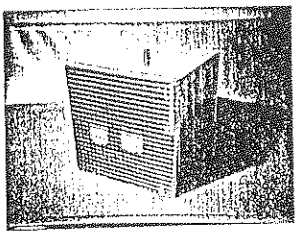

fig. 4

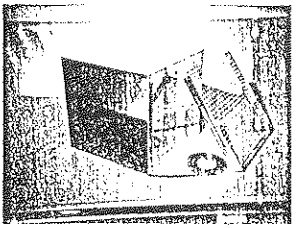

fig. 5

A RATIONALE FOR DEVELOPING AND USING STEM (STATISTICAL ELECTROMAGNETICS)

E. K. Miller*, 3225 Calle Celestial, Santa Fe, NM 87505, 505-820-7371
T. H. Lehman, 221 S. Main, Suite 205, Belin, NM 87002, 505-861-0280

Classical electromagnetics has been pursued as an almost wholly deterministic discipline. Although contrary examples can be found, for example, rough-surface scattering and random-medium propagation, where problem conditions are truly statistical, the vast majority of analysis and computation has followed deterministic lines. That is, problems are approached as though all necessary details concerning object and boundary geometries, media electrical parameters, excitation, etc. are specified or known as accurately as desired.

This approach seems reasonable when problems are small enough in electrical size and simple enough in geometrical complexity to permit definition with arbitrary accuracy and resolution. However, when a problem's size and/or complexity increase beyond some threshold, our ability to describe it completely and accurately enough for a deterministic solution to be practically achievable or meaningful is proportionately diminished. Furthermore, when a problem's rank, or number of degrees of freedom, exceeds some corresponding threshold, our ability to describe and interpret its associated observables is similarly reduced. Thus, even when problems are deterministic in principal, their descriptions and solutions in practice can be so numerically demanding that a statistical framework becomes mandatory.

The purpose of this discussion is to present a rationale for STEM as a logical parallel in electromagnetics to that of statistical mechanics in physics. Both areas, by definition, deal with problems whose ranks are so large that the law of large numbers can be invoked (i.e., for sufficiently large values of n, the relative frequency of occurrence of the event E in n observations differs from the probability p for the occurrence of the event by less than e, with a probability that is arbitrarily close to 1, from Bernoulli). When the number of possible outcomes exceeds some lower limit, it becomes simpler and more useful to describe problems in statistical terms, such as expected values, variances, etc. as derived from the moments of probability density functions (PDFs). In particular, we argue that when the PDFs can be determined from first-principles physics, as opposed to estimating candidate PDFs from fitting them to data, the use of statistics in electromagnetics for many applications is substantially more productive than are deterministic predictions.

INDOOR PROPAGATION: A STATISTICAL APPROACH

M. Tobin, and J. Richie*

Department of Electrical and Computer Engineering
Marquette University
Milwaukee, WI

Abstract

The study of propagation of microwave signals within rooms and buildings has become an important part of microwave engineering due to the proliferation of wireless systems such as wireless networks, other wireless communication systems, and security systems. A number of path loss models have been developed and investigated to predict the propogation characteristics for indoor systems and mobile systems (outdoors). In addition, recent interest in STatistical ElectroMagnetics (STEM) has arisen in the solution to highly overmoded cavities of complex shape.

The path loss models can be broadly seen as utilizing the following procedure. A suitable model of the problem is formulated, possibly with parameters to be determined through experimental measurement. The model is then used to compute the field strength at particular locations. We shall denote this approach as modeling the problem. Another possibility is to disregard location completely and obtain only statistical information regarding the problem. The statistical information may begin by predicting only the average value of the field strength in the selected environment. However, accurate knowledge of the probability density function (pdf) of the electric field strength also provides a relatively equal amount of information when compared to the path loss prediction models.

In addition, it will be argued that the number of degrees of freedom is the only important quantity necessary to characterize the pdf, i. e., once the number of degrees of freedom is large enough, one can usually disregard the details of the geometry when describing the pdf.

The presentation will describe experimental evidence obtained from a mockup of the Space Station Freedom and a simulation of the two-dimensional Green's function for a rectangular room. It will be seen that once the density of the modes is sufficiently high, both an empty mockup of SSF and a full mockup of SSF admit a Rayleigh pdf, and the 2-D Green's function also exhibits field strength statistics that follow a Rayleigh pdf until the walls of the room are nearly transparent.

MEASURED STATISTICAL CHARACTERISTICS OF THE ELECTROMAGNETIC ENVIRONMENT IN REVERBERATION CHAMBERS

Gustav J. Freyer
Universal Systems Inc
Monument, CO USA

There has been an increasing interest in the use of reverberation chambers for system radiated emission and radiated immunity testing. Reverberation chambers provide an all aspect angle and polarization test without the requirement to rotate the system-under-test (SUT). The high quality factor, Q, values of most reverberation chamber test facilities yield high test power density to input power ratios. This enables testing at the higher power densities required for certification of some systems without requiring kilowatt (or higher) amplifiers. Reverberation chamber tests also provide working volumes which are a significant fraction of the total enclosure volume.

The basic concept of a reverberation chamber requires that the cavity be highly moded and that a mechanism be available to sufficiently perturb the modal structure to provide isotropic and randomly polarized fields throughout the working volume. Thus unlike most other test techniques, reverberation chamber testing is intrinsically a statistical process.

The requirement for sufficient mode density determines the lowest useable frequency for reverberation chamber operation in a specific enclosure.

There are at least two methods for perturbing the modal structure which have been sufficiently investigated to warrant acceptance. The first is mechanical mode mixing which uses a rotatable metal tuner to change the cavity boundary conditions. The second is band limited, white gaussian noise which randomly excites the intrinsic cavity mode structure within the noise bandwidth. This paper will use data obtained with mechanical mixing to investigate the statistical characteristics of a reverberation chamber immunity test.

The tuner should be asymmetric and have a minimum dimension of one wavelength at the lowest usable frequency. The common test for proper operation is the empirically derived guideline of a stirring ratio of 20 dB. Figure 1 shows a typical data trace for a discrete frequency measurement with a continuously rotating tuner. The data was taken at 500 MHz, well above the lowest useable frequency for the chamber. The input power was constant and inserted into the chamber using an in-band log spiral antenna. The chamber power density was measured using an in-band, log periodic receive antenna. The power received is plotted against the rotation time of the tuner. The average received power, - 8.1 dB is a function of the input power and the cavity Q. The time for one complete tuner rotation

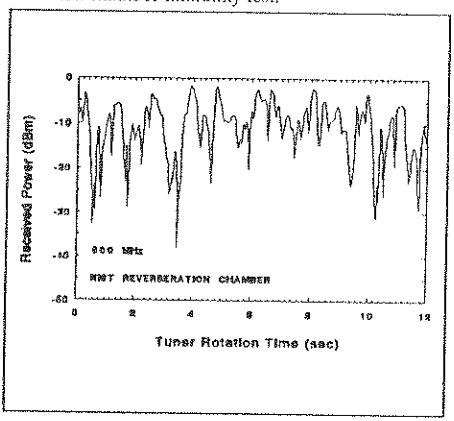

FIGURE 1 Discrete Frequency Received Power With Mode-Stirring

is 9.7 sec after which the pattern in the received power repeats. The stirring ratio is defined as the ratio of the maximum received power to the minimum received power over one complete tuner rotation and is 36 dB for these data. An adequate test requires that the SUT be exposed to a sufficiently large number of discrete field variations. An empirically derived guideline of 200 discrete data points per tuner rotation is commonly used. The data in Figure 1 represent more than 400 data points.

The data in Figure 1 can be compared to the predicted distribution for randomized fields in a highly moded, complex cavity. The probability density function has been shown to be (Lehman, TL, Note 494, Interaction Notes, USAF Phillips Lab)

$$F(x) = C\,EXP\{C(x-\mu)\}\,[EXP\{-EXP\{C(x-\mu)\}\}] \qquad (1)$$

where x is the received power in dB, C is a constant, $(10\ Log\ e)^{-1}$, and μ is the arithmetic mean expressed in db. This one parameter distribution function depends only on the mean of the experimental data. Figure 2 plots the cumulative theoretical distribution as the solid line. The abscissa is the received power referenced to the mean. The dotted line shows the cumulative distribution of the data from Figure 1. Several statistical tests indicate that the two distributions can be considered the same. For reference, the paper compares the measured distribution to several other common distribution functions. Statistical goodness-of-fit tests reject the applicability of these other distributions. These results imply that a reverberation chamber electromagnetic environment (EME) can be considered to be isotropic and randomly polarized which corroborates the results of direct electric field measurements by multiple, three axis probes. Data from other reverberation chambers and complex cavities are compared to each other and to the theoretical distribution.

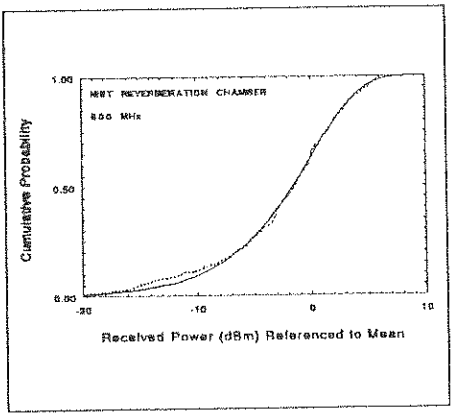

FIGURE 2 Cumulative Received Power Distribution.

The average power density characterizes the EME in a reverberation chamber. However many systems will respond to the peak value of the power density rather than the average value. In a reverberation chamber the peak to average ratio is a random variable. Statistical variations in the peak to average ratio as a function of the specific cavity, the number of discrete data points, the stirring ratio and the cavity quality factor are presented. Statistical parameters obtained for internal excitation of several mode stirred aircraft cavities are compared to those of reverberation chambers.

In summary, this paper investigates the statistical nature of the EME of a reverberation chamber and other complex cavities.

A PROBABILISTIC METHOD FOR THE MODELING OF AN EMP CONDUCTED ENVIRONMENT

M. IANOZ*
Ecole Polytechnique
Fédérale de Lausanne
CH-1015 Lausanne
Suisse

B. NICOARA
Facultatea de Energetica
Universitatea "Politehnica"
Bucuresti
Roumanie

W. RADASKY
Metatech
Goleta Ca 93117
USA

The International Electrotechnical Commission (IEC) decided in 1988 to produce a civil standard on the electromagnetic effects of a High Altitude EMP (HEMP). Two environments, a radiated and a conducted must be defined. For this civil standard a curve fit by Radasky (C.E. Baum, "From The Electromagnetic Pulse to High-Power Electromagnetics", Proc. IEEE, vol.80, No. 6, June 1992, p. 789-817) based on calculations performed by Longmire has been chosen as radiated environment. A conducted environment dependent on many parameters is more difficult to define. However this environment is of major importance for defining tests and protection concepts. The aim of this work is to present a probabilistic approach which has been adopted to define a typical current shape for the conducted environment.

This environment, represented by currents or voltages induced in conductors by the electromagnetic field due to the burst and propagating to loads representing sensitive components or installations, is a consequence of the radiated environment and cannot exist without it.

Depending on the position of the victim (line, installation, system) on the ground, the electromagnetic wave can have different polarizations. Depending on the direction of the earth magnetic lines of force, the electromagnetic field due to a high altitude nuclear burst can be completely horizontally polarized (near the magnetic north or south pole).In the other parts of the world, the wave is partially horizontal and partially vertical polarized. The polarization angle γ is defined as the angle between the plane containing the electric field component and the plane formed by the the normal to the earth surface at the observation point and the direction of propagation (Poynting vector) of the wave.

This angle depends on the angle of the line of sight from the burst and the dip angle of the earth's magnetic field which is measured from the local horizontal plane in the downward direction.

In addition to the dip angle, two more parameters depend on the relative position of the burst and of the victim. They are the elevation and the azimuthal angles

One possible approach for defining a protection concept against transient phenomena is to calculate the open circuit voltage which permits one to determine the breakdown level of the protection element and the short-circuit current which permits to determine the capability of the protection element to conduct to the ground the current after breakdown has occured.

These two values have been calculated for a typical aerial line of 1 km length, illuminated by the above defined radiated field, using a probabilistic method which includes the possibility of occurence of the Ψ and ϕ values.

A number of 1'710 cases resulting from 90 values of the elevation angle (from 1^0 to 90^0 with a step of 1^0) and 19 values of the azimuthal angle (from 0 to 90^0 with a step of 5^0) have been calculated for both the horizontal ($\gamma = 90^0$) and vertical ($\gamma = 0^0$) polarizations.

The distribution functions of the peak current value, rise time and time to half amplitude are presented and discussed. By combining the calculation results for both polarizations, probabilities for these parameters at different geomagnetic dip angles have been obtained.

As an example, the result of this process applied to the current peak values is plotted in fig. 1. The dip angles corresponding to the most populated parts of the world are larger than 50^0. In the figure it can beseen that curves corresponding to dip angles greater than 45^0 are well grouped.

From fig.1 it can be seen that there are no large differences in the peak current values for dip angles larger than 45^0 and that it is relatively easy to chose an average curve corresponding for instance to a dip angle of 67^0 in order to define a normalized conducted environment.

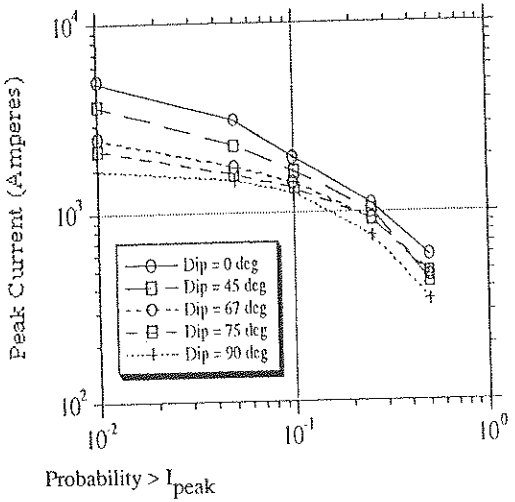

Fig. 1 - Probability to exceed different values of the peak current for a number of dip angles

DETECTION OF RANDOM PULSED PROCESSES IN LOCALLY STATIONARY NOISE UNDER A PARAMETRIC *A PRIORY* UNCERTAINTY

O.M.Isaeva
Radiophysical Reasorch Institute,
8.Pecherskaya st., 25, N.Novgorod, 603600 Russia
Fax: (8312) 369902

The detection problem of random pulsed processes in additive random noise is discussed, when intensities of noise and pulsed processes and a constant probability of pulse action in each moment of observation time are unknown. Noise process intensity changing during the time is assumed to be relatively slow and described by a function, which can be step-like approximated, such that envelope of the received process within the observation time T can be divided into M parts, each of which has the constant background intensity σ_{0i}^2, $i = \overline{1,M}$. Each such part of the noise process envelope is described by a Rayleigh distribution. The pulsed process is meant to be a process with random moments of noncovering pulses arising and a Rayleigh pulse amplitude probability density function. Both atmospheric and some artificial pulsed clutters are described by such processes. With these assumptions, the detection problem can be formulate in terms of binary hypotheses testing procedures as the following.

Let $x_{11},\dots,x_{1n_1},\dots,x_{M1},\dots,x_{Mn_M}$ be M independent samples from the envelope of the received process within the time T, where $x_{i1},\dots,x_{in_i}$ is an independent sample from the i th part of the envelope $x(t)$ with the constant background intensity σ_i^2. Then, two hypotheses to be tested are

$$H_0:\ f_0(\bar{x};\ \sigma_{01},\dots,\sigma_{0M}) = \prod_{i=1}^{M} \frac{x_i}{\sigma_{0i}^2} \exp\left\{-\frac{x_i^2}{2\sigma_{0i}^2}\right\},$$

$$x_i > 0,\ \sigma_{0i} > 0,\ i=\overline{1,M}\ .$$

$$H_1:\ f_1(\bar{x};\ \sigma_{01},\dots,\sigma_{0M},\sigma_{11},\dots,\sigma_{1M},\gamma) =$$

$$= \prod_{i=1}^{M}\left[(1-\gamma)\frac{x_i}{\sigma_{0i}^2}\exp\left\{-\frac{x_i^2}{2\sigma_{0i}^2}\right\} + \gamma\frac{x_i}{\sigma_{1i}^2}\exp\left\{-\frac{x_i^2}{2\sigma_{1i}^2}\right\}\right],$$

$$x_i > 0,\ \sigma_{0i} > 0,\ \sigma_{1i} > 0,\ 0<\gamma<1,\quad i=\overline{1,M}\ ,$$

where $\bar{x} = (x_1,\dots,x_M)$, σ_{0i}^2 is a noise intensity on the i th part of the envelope, $\sigma_{1i}^2 = \sigma_{0i}^2 + \sigma_{pi}^2$, σ_{pi}^2 is a pulse in-

tensity on the i th part of the envelope. γ is a probability of pulse action in the moment t_{ij}, $x_{ij} = x(t_{ij})$, $i=\overline{1,M}$, $j=\overline{1,n_i}$. Parameters σ_{0i}^2, σ_{1i}^2, $i=\overline{1,M}$ and γ are unknown.

Similar problem has been considered in (A.A.Gorbachev & O.M.Isaeva & A.P.Koldanov. Radiotehnika, 7, 21-25, 1983) in assumptions of a stationary background and a constant intensity of pulses, where relatively simple for technical realization detection algorithms have been proposed. These algorithms have consistency in tests and similar critical regions. The test statistics are functions of received process envelope extremes. The paper provides generalization of this results for the locally stationary background and different pulse intensities on the different stationary regions of the background.

The test of the hypotheses H_0 and H_1 is formulated as

$$\delta = \begin{cases} d_0, & \text{if } \max\limits_{i=\overline{1,M}} T_i \le C, \\ d_1, & \text{if } \max\limits_{i=\overline{1,M}} T_i > C, \end{cases}$$

where d_0 and d_1 are decisions to accept H_0 and H_1 respectively, threshold C is determined from the condition $Pf\ d_1|H_0) = \alpha$, according to the acceptable false alarm probability α, T_i is the test statistics of the hypotheses

$$H_{0i}: f_{0i}(x_i, \sigma_{0i}) = \frac{x_i}{\sigma_{0i}^2} \exp\left\{-\frac{x_i^2}{2\sigma_{0i}^2}\right\},$$

$$H_{1i}: f_{1i}(x_i; \sigma_{0i}, \sigma_{1i}, \gamma) =$$

$$(1-\gamma)\frac{x_i}{\sigma_{0i}^2}\exp\left\{-\frac{x_i^2}{2\sigma_{0i}^2}\right\} + \gamma\frac{x_i}{\sigma_{1i}^2}\exp\left\{-\frac{x_i^2}{2\sigma_{1i}^2}\right\}\Bigg].$$

STATISTICAL ANALYSIS OF CODED SIGNALS

Dr. ATEF ABOU EL-AZM

Faculty of Electronic Engineering
Menouf,32952 Egypt

ABSTRACT

One of the problems encountered in designing digital transmission systems is the choice of line code. There are many key factors that influence the choice of these codes. The main factors discussed in this paper are the spectral analysis and error detection in the coded signals. A universal and simple method of finding the spectral density for a large number of commonly encountered will present. Simplified mathematical models and statistical analysis of various methods of error detection are also introduced. These methods can be utilized for error detection at dependent repeaters and at receive terminals of digital transmission systems. General formulae of a parameter called effectiveness (η) of error detection (as a function of statistics of transmitting data (q) and error rate (e)) have been derived to each code in each method of detection. General algorithms of computations are described which have general validity and can be used for any coding scheme provided that the block codes are have bounded running disparity.

The paper , is organized as follows: First, a general algorithm of spectral analysis which provides a detailed characterization of the spectral properties of large number of commonly encountered codes. Next, is concerning with two classes of error detection called: symbol-by-symbol detection ,and word-by-word detection. In the first class we present the analysis of two methods of error detection called Running Digital Sum method (RDS-method) and Forbidden sequences method (FSM-method). Since the codes have a bounded running disparity they allow the error detection at dependent repeaters during normal operation by checking the bounds of the running disparity itself without decoding the line signal. This can be achieved by an up-down counter that follows the running disparity and detects violation whenever the bounds allowed are exceeded. By this method it is possible to perform a sufficiently precise measure of error rate: the second method (FSM-method) is basically depends on that each code has forbidden sequences which are not belonging to its encoding rule in case of lack of transmission error. Thus detection of such forbidden sequences during the transmission means detection of error. In the second class we present the analysis of a three methods of error detection. These methods are based on the detection of the unexpected transition for the encoder states . This class is used only in the presence of word synchronizing at the receive terminal, while the first class does not need this synchronization.

Generally, in this paper properties of a substantial number (nineteen) of commonly encountered digital block codes have been examined. An extensive set of results and supportive data of the effectiveness of error detection (η) as function of the statistic q , the probability of symbol zero in the transmitting data, and as function of transmission error rate (e) are presented. While no such collection can hope to be complete, that presented here is considerably more comprehensive than any known to be available elsewhere in the literature. The presented results are useful in providing data for the designer for calculations the performance of the digital transmission systems. Thus this paper is considered as a useful reference for digital transmission system studies. It is concluded that no one monitor is signaled out as the best since the final choice depends largely on the specific requirements of a given application. This work is based on the reference (A.A.El-Azm, Ph.D. thesis, W.T.U, 1990, Poland).

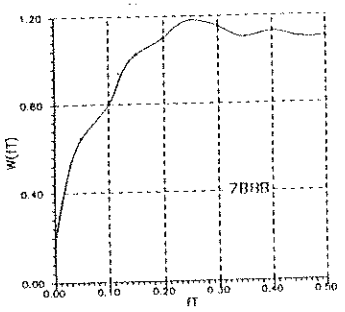

Fig.1 Power spectra of the code 7B8B (q=0.5)

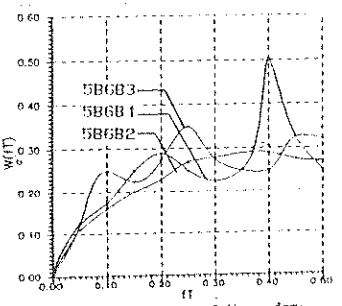

Fig.2 Power spectra of the codes: 5B6B(1),5B6B(2),5B6B(3)-(q=0.3)

Results of (η) using the (FIRST) class of error detection
e = 0.001

code\q	0.05	0.20	0.35	0.50	0.65	0.80	0.95
AMI1	0.997	0.997	0.997	0.997	0.996	0.994	0.979
3B4B(1)	0.977	0.991	0.993	0.993	0.993	0.991	0.977
3B4B(2)	0.995	0.995	0.994	0.993	0.994	0.995	0.995
3B4B(3)	0.907	0.969	0.975	0.976	0.975	0.969	0.907
3B4B(4)	0.907	0.970	0.978	0.981	0.986	0.989	0.992
5B6B(1)	0.942	0.977	0.981	0.982	0.981	0.976	0.942
7B8B	0.328	0.504	0.642	0.708	0.721	0.647	0.387
AMI	0.998	0.998	0.998	0.997	0.997	0.994	0.980

Results of (η) using the (SECOND) class of error detection
e = 0.001

code\q	0.05	0.20	0.35	0.50	0.65	0.80	0.95
AMI1	0.46	0.40	0.32	0.25	0.15	0.10	0.05
3B4B(1)	0.04	0.16	0.22	0.25	0.22	0.16	0.04
3B4B(2)	0.46	0.34	0.28	0.25	0.28	0.34	0.46
3B4B(3)	0.28	0.38	0.42	0.44	0.44	0.38	0.28
3B4B(4)	0.28	0.38	0.42	0.44	0.44	0.38	0.28
3B4B(5)	0.29	0.37	0.42	0.44	0.42	0.37	0.28
5B6B(1)	0.30	0.22	0.21	0.21	0.22	0.22	0.31
5B6B(2)	0.19	0.22	0.23	0.21	0.21	0.22	0.19
AMI	0.05	0.20	0.35	0.50	0.65	0.80	0.95

AN OVERVIEW AND CRITIQUE OF THE NEW MIL-STD 461/462 REV"D"

Michel Mardiguian *
EMC Consultant
78470 St Rémy-les-Chevreuse
(France)

J.Marie Hutin
EMC Manager
AEROSPATIALE Missiles
92322 Chatillon (France)

1.Introduction

More than an evolution,the revision "D" of Mil-Std 461(test requirements) and 462(test methods) released in 1993 brings a small revolution. They contain drastic modifications from the former 461 "B" or "C" versions. The "one-limit-one-bandwidth" concept,the use of a 50 ohm/50µH LISN instead of the traditional 10µF capacitors,the measurement of Conducted Emissions up to 10MHz only,instead of 50MHz, all are fundamental changes in the philosophy of the Spec. All these aspects are more or less justified by an ad-hoc Appendix in each Standard document. However,some of the rationale are not obvious and need clarification or critique.

2.The essential new CE limits

The following list shows the principal features of old vs. new limits for CE testing :

Mil Std461C		Mil Std 461D	
CE01	15kHz dBuA , NB & BB	CE101	10kHz dBuA, fixed BW
CE03	50MHz dBuA, NB & BB	CE102	10MHz dBuV,fixed BW
CE07	Spikes,time domain		Deleted

The new CE101 limit remains in dBµA. The reason invoked is that actual power sources impedances in test facilities are uncontrolled,so a measurement in current will be somewhat independent of actual mains impedances variations. This is only true as long as emissions source impedance itself is much larger than power source impedance. This is the case for Comm.Mode (CM) emissions driven through the EUT parasitic capacitance to ground, but certainly not for Diff.Mode (DM) emissions ,like those due to poor ESR of front-end capacitors in Switch Mode Power Supplies. In fact,the rationale for the 10µF capacitors (old CE01) was to force the maximum possible emission current into an RF short. The new LISN impedance is certainly not a short below 15kHz and may cause an under-estimate of the DM emissions.

The CE102 limit is now in dBuV,measured at LISN port.There are no longer dual NB/BB limits.The reason invoked is a simplification of the test interpretation. However,it is well known (Ref CISPR works ,and later, the CBEMA ESC-5 study which the FCC-15j and EN55022 are based upon) that a single limit with only one type of detector (here the peak detector) will pose the following dilemna:

- a single limit based on a NB interference scenario will overprotect the radio reception in BB cases.

-a single limit based on a BB interference scenario will underprotect radio-reception in NB cases.

Comparing old and new limits require a double conversion :

a) One to translate dBuV into equivalent dBuA,using the LISN impedance:
I(dBuA) = V(dBuV) - Z(dBohm)

b) One to translate the dBuA into dBuA/MHz using the BW correction:
IdBuA/MHZ=IdBuA + 20Log(1MHz/ CE102 Bw)

When performing these adjustments and comparisons,the following results :

	Old CE03 (Part 2,Aircrafts) (NB)	New CE102 (for 28v supply *) (NB)	New/Old
15kHZ	86 dBuA	74 dBuA	-12
500kHz	38dBuA	26 dBuA	-12
2MHz	20dBuA	26 dBuA	+6
10MHz	20dBuA	26 dBuA	+6
	(BB) dBuA/MHz	(BB equivalent) dBuA/MHz	
15kHz	130	134	+4
500kHz	72	66	-6
2MHz	50	66	+16
10MHz	50	66	+16

An other significant change is that the CE102 stops at 10MHz. The reason given is that, for a cable length of 2,5m, conducted measurements become questionable above 10MHz. This is a rather arguable statement since CISPR,VDE,FCC etc measurements,all in accordance with IEEE or ANSI are carried up to 30MHz without unsurmountable problems.

3.The new Conducted Susceptibility Limits

The following list shows the essential features of old vs.new limits for CS testing.

Mil 461C	Mil461D
CS01 CW ----50kHz	CS101 CW----50kHz
CS02 CW------400MHz (Voltage injection)	CS114 CW ---400MHz(Curr Inject)
CS06 Spikes (Voltage)	CS 115 Spikes (current)
CS09 Structure current	CS109 idem
CS10/CS11 Damped oscillat.,10kHz-100MHz	CS116 idem.Cable injection only
(or CS12/13) Pin & cable injection	

The new set of limits seems approximately equivalent and somewhat simpler,more logical than the old one.From the experience gained in civilian testing with Electrical Fast Transients like IEC801-4,the CS115 test,an offspring of the chattering relay test,seems ridiculously low since it injects the equivalent of 250v CM voltage (500v open ckt) spikes into the cable bundle.The deletion of the pin injection oscillatory test (old CS10 & 12) will be certainly welcome since it simplify the test work.An option is left to test individual wires or pairs if needed.

4. The new Radiated Emissions limits.

The following list shows the essentials of old vs. new limits for RE testing:

Mil 461C	Mil 461D
RE01 H field --- 50kHz	RE101 Hfield --- 100kHz
RE02 E field --- 10GHz	RE102 E field --- 18GHz

A same correlation has been attempted as for CE102/CE03 to compare new vs old limits.The result is a much tighter match,with generally less than +/- 6dB difference.

5. The new Radiated Susceptibility Limits

The following list shows the essentials of old vs new limits for RS testing.

Mil 461C	Mil 461D
RS01 H field --- 50kHz	RS101 --- 100kHz
RS03 E field --- 40GHz	RS103 --- 40GHz
RS05 /RS06 EMP	RS105 EMP

Radiated Susceptibility seems the area where Rev.D shows the lesser changes,with basically similar limits and methods. A significant novelty is the requirement for absorbing materials on chamber walls,with a prescribed minimum attenuation.Also, frequency scanning steps and time intervals are precisely defined, resulting in a more thorough exploration, but also a longer test duration.

6. Discussion and conclusion

With its test limits and methods evolving in a same,coordinated update, the Rev.D brings significant clarity and simplification compared to the former thick and somewhat scattered set of specifications.All limits are called-out in a single requirement set,with adjustment notes for Army,Navy etc.. specifics,instead of repeating the same text in Part 2,3.... up to #10 as in 461B or C.

On the other hand,the rationales exposed in the Appendices to justify the simplifications are sometimes questionable and need to be reviewed/revisited for anyone willing to tailor a test requirement for specific applications. For instance the suppression of the NB/BB dichotomy makes the new limits more liberal at certain frequencies.This leaves the radio reception less protected in certain bands.Also the use of the 50 ohm/50uH LISN,perfectly appropriate for commercial testing where typical mains lines are long and inductive seems unjustified for military platforms such as tanks,aircrafts,ships etc... where power cable lengths and characteristic impedances are typically lower.

DEVELOPMENT OF E^3 INTEGRATED BOX LEVEL TEST ENVIRONMENTS FOR ARMY HELICOPTER AVIONICS

By

Rodney A. Perala* and Gregory J. Rigden
Electro Magnetic Applications, Inc.
7655 W. Mississippi Avenue, Suite 300, Lakewood, Colorado 80226 USA
303-980-0070

In the next decade military equipment will be required to operate in severe electromagnetic environments. These environments are expected to contain most non-ionizing frequencies (D.C. to GHz), from hostile and/or non-hostile sources, and be severe enough to cause temporary upset or even catastrophic failure of electronic equipment.

Over the past thirty years considerable emphasis has been placed on hardening critical systems to one or more of these non-ionizing radiation environments, the most prevalent being the nuclear-induced electromagnetic pulse (EMP). From this technology development there has evolved a hardening philosophy that applies to most of these non-ionizing radiation environments. The philosophy, which stresses the application of zonal shields plus penetration protection, can provide low-cost hardening against such diverse non-ionizing radiation as p-static, lightning, electromagnetic interference (EMI), EMP, high intensity radiated fields (HIRF), electromagnetic radiation (EMR), and high power microwaves (HPM).

A unified E^3 standard provides numerous advantages. Beneficial aspects are realized with considerable reductions in costs, time, and complexities associated with testing and implementing the required hardening techniques. Presently, there exists numerous tests for each individual E^3 threat. Integration will greatly reduce this quantity due to the removal of test redundancies or test elimination due to other procedures that require a more severe environment. In addition, the box test methods are developed explicitly for helicopters which permit bench tests during development and prior to installation which is extremely cost-effective when compared to full-vehicle tests and retrofit procedures.

The objective of the effort documented here is to develop an example unified E^3 standard for Army helicopter avionics. The standard integrates the effects of HIRF, high altitude nuclear electromagnetic pulse (HEMP), and lightning to an upper frequency limit of 200 MHz. The standard contains test waveforms of varying severities and avionics box bench test methods. The test waveforms address the avionics radiated and conducted environments. The test methods were devised to utilize existing equipment, test setup configurations, and known procedures, when possible, to reduce the expenditures of test modifications.

The approach to determine the test waveforms is based upon numerical analysis techniques applied to three representative Army helicopters. The helicopters are the AHIP (OH-58D), the Blackhawk (UH-60A), and the Apache (AH-64A). Numerical analysis provides a cost-effective means of accomplishing the objective when compared with experiments and tests. Other advantages realized by numerical analysis is the capability of providing a complete description of helicopter response behavior. All locations are easily monitored simultaneously with no distortions caused by measuring procedures or devices. All geometrical configurations and relationships of the EM source and the helicopter are easily provided. This is especially advantageous for plane wave illumination where the presence of a ground plane causes response distortions and renders certain incident angles and electric field polarizations virtually impossible to obtain experimentally. In addition, numerical procedures afford an exact plane wave source (for HIRF and HEMP) thereby providing uniform illumination across the frequency band. The results obtained

from numerical analysis were compared to experimental results when available to provide reality checks.

Figure 1 illustrates one of the results. It shows a set of box current injection test waveforms which integrates both NEMP and lightning environments. It is shown in the paper that these waveforms can be thought of as existing lightning test waveforms, modified only slightly to accommodate the NEMP environment.

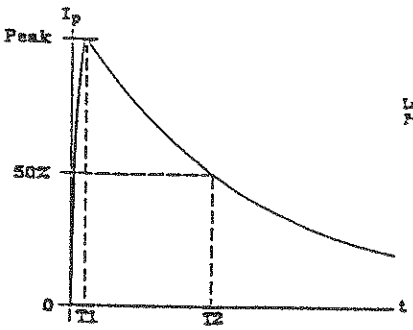

Amplitude decreases 37% of peak amplitude in N cycles. The peak amplitudes and N are provided in the tables below.

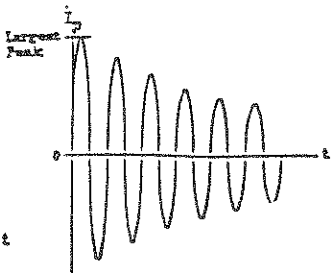

Waveform Sets 1 through 5

Current Waveform Set	Current Test Waveform	Severity Level	Ip(A)	T_1 (Nanoseconds)	T_2 (Microseconds)
1	1-1	1	47	220	69
	1-2	2	2500	1800	69
	1-3	3	25000	4700	69
2	2-1	1	12	110	35
	2-2	2	620	1200	35
	2-3	3	6200	2300	35
3	3-1	1	3.3	9	4.0
	3-2	2	130	100	4.0
	3-3	3	1200	200	4.0
4	4-1	1	16	3.0	4.4
	4-2	2	70	6.0	4.4
	4-3	3	250	13	.340
5	5-1	1	47	33	69
	5-2	2	2500	520	69
	5-3	3	25000	2100	69

Waveform Set 6

Current Waveform Set	Current Test Waveform	Severity Level	Ip (Amperes)	N	Frequency (MHz)
6	6-1	1	2	5000	10-200
	6-2	2	20	3000	10-200
	6-3	3	20	3000	10-200

Figure 1 **An Example of Transient Box Current Injection Test Waveforms which Integrate NEMP and Lightning Environments**

THE THEORY OF WAVEFORM NORMS AND THEIR APPLICATION IN MILITARY STANDARDS

Jerry I. Lubell
Mission Research Corporation

Introduction. The purpose of this paper is to provide an overview of the theory of waveform norms and how they are used in U. S. military standards and specifications for electromagnetic pulse (EMP) hardening and testing. First an initial set of waveform norms is suggested and a theory is presented showing the importance of the suggested attributes in causing transient upset and permanent damage in electronic circuits. Next, the ability of the set of norms to cover the important characteristics of EMP induced transient waveforms is discussed. The issue of coverage is addressed by comparing the coverage provided by the norms to characteristics of a data base of measured waveforms. The paper is concluded by showing how the waveform norms concept is actually used in U. S. standards and specifications for EMP hardening and testing of fixed and transportable command, control, communications, computer, and intelligence systems.

Initial Set of Norms. The initial suggested norms are divided into three categories, amplitude, variation, and content as shown in Table 1. The norms can be calculated

Table 1. Initial Set of Norms

DEFINITIONS	NAME	TYPE
$N_1 = \lvert f(t) \rvert_{max}$	Peak Value	AMPLITUDE
$N_2 = \lvert df / dt \rvert_{max}$	Peak Derivative	VARIATION
$N_3 = \left\lvert \int_0^t f(x)dx \right\rvert_{max}$	Peak Impulse	CONTENT
$N_4 = \int_0^\infty \lvert f(x) \rvert dx$	Rectified Impulse	CONTENT
$N_5 = \left\{ \int_0^\infty [f(x)]^2 dx \right\}^{1/2}$	Root Action Integral	CONTENT

from time domain data. Moreover, corresponding frequency domain formulas provide the capability for using frequency domain data and are particularly useful for hardness maintenance/surveillance applications.

The plausibility of the initial set of norms can be established using the simple two port model shown in Figure 1 and limiting cases. In this model, f(t) is the stress waveform at an external interface, g(t) is the resulting response at a vulnerable port inside the

equipment, and T( ) is the frequency domain transfer function relating these two signals. Malfunction is assumed to occur if the norms at the vulnerable port exceed either peak or energy bounds on g(t).

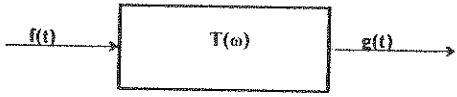

Figure 1. Two Port Model to Establish Norm Plausibility

Based on this failure model, and assuming different limiting case pass band characteristics for the transfer function, it can be shown that the stress norms that control malfunction includes the set of initial norms in Table 1, thereby establishing the plausibility, but not sufficiency, of the set.

Norm Coverage and Sufficiency. Coverage and sufficiency address the minimum number of norms needed to characterize EMP-induced waveforms. Once the minimum number is established, the minimum set can be used to develop EMP specifications and standards. There is no formal way to establish this minimum number mathematically. It is possible, however, to show that specifying bounds on a few descriptors implicitly places bounds on the unspecified descriptors. In other words, directly controlling a few norms adequately constrains other norms of EMP responses as well.

Norm coverage and sufficiency was established by directly comparing 10 norms to a measured EMP stress data base. The 10 norms were selected to include 2 in the amplitude category, 3 in the variation category, and 5 in the content category. The stress data base was comprised of about 900 data records of responses measured inside communications facilities. This direct comparison approach showed that 90 percent coverage of all 10 norms is obtained if only 3 norms are controlled, as long as at least one norm from each of the amplitude, variation, and content categories is used.

Use of Norms in U. S. Military Standards

The norms concept is used in MIL-STD-188-125 for fixed C^4I systems and in the draft MIL-STD-188-125 for transportable C^4I systems. The hardening and testing approach in these standards is based on an electromagnetic barrier concept. As shown in Figure 2. The

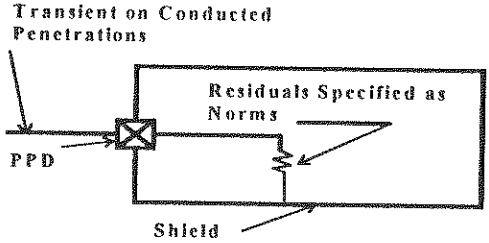

Figure 2. Norms in MIL-STD-188-125

electromagnetic barrier consists of a shield and penetration protective devices for all penetrations. Norms are used to control the residual stresses on conducted penetrations inside the barrier. External transients are specified outside the penetration protective devices. The allowed residuals on the clean side of the protective devices are specified in terms of norms. The values of the norms were chosen to balance the attenuation achievable by the protection devices and the upset/burnout susceptibilities of the interior circuits.

SPECIFICATION AND MEASUREMENT OF THE PERFORMANCE OF A SHIELD BOND.

Laurent PECQUEUR,
Direction des Constructions Aéronautiques, STPA,
26 boulevard Victor, 00460 ARMEES.

Michel RENARD *,
Direction des Constructions Aéronautiques, STTE,
129 rue de la Convention 75731 PARIS CEDEX 15.

1 - OBJECTIVE.

Within this paper, a "shielded bond" involves both the shielded cable and the attached extremity connectors. Both "simple" shielded bonds (two extremities) and "complex" shielded bonds (more than two extremities) are dealt with.

The very purpose of the paper is to provide a consistent answer to the two-sided question : how to manage in order to
1) fully and consistently specify the required performance of a shielded bond,
2) and then make sure that the provided shielded bond does actually meet the required performance ?

2 - PARAMETERS GOVERNING THE PERFORMANCE OF A SHIELDED BOND.

When specifying the required performance of a shielded bond, none among the following parameters may be overlooked:

Transfer impedance $Z_T(\omega) \leq R_0 + j\omega M_{12}$
R_0 (ohm per meter) and M_{12} (henry per meter) are characteristics of the cable shield.

Transfer admittance $Y_T(\omega) = j\omega C_{12}$
C_{12} (farad per meter) is not a characteristic of the sole cable but the combination $(Z_0)_{EXT}(Z_0)_{INT}C_{12}$ (henry per meter) does.
$(Z_0)_{EXT}$ (ohm) is the characteristic impedance of the external transmission line (outer shield against ground return) the propagation celerity of which is V_{EXT} (meter per second).
$(Z_0)_{INT}$ (ohm) is the characteristic impedance of the internal transmission line (inner conductors taken as a whole against inner shield) the propagation celerity of which is V_{INT} (meter per second).

Transfer impedance of connections $Z = R + j\omega L$
At every extremity of the shielded bond, R (ohm) and L (henry) are characteristics of both the connector itself and its attachment on the cable.

Transfer impedance of would-be local defects $Z_d = R_d + j\omega L_d$
R_d (ohm) and L_d (henry) are characteristics of a defect which may occur at any location z_d along the shielded bond.

Note. The case of a simple shielded bond the two connections of which ($\neq 1$ at $z = 0$ and $\neq 2$ at $z = l$) exhibit different transfer impedances Z_1 and Z_2 is treated (assuming for example $Z_2 > Z_1$)
as the case of two identical connections with $Z = Z_1$ plus a local defect at $z_d = l$, with $Z_d = Z_2 - Z_1$.

3 – SPECIFICATION OF THE REQUIRED PERFORMANCE.

In order to fully and consistently specify the required performance of a shielded bond, it is recommended to proceed in sequence:

1) Specification of R_0 (ohm per meter).
No default value can be accepted.

2) Specification of M_{12} (henry per meter), with reference to R_0 and frequency.
A default value is acceptable.
The recommended default value is such that $2\pi 30\,10^6\, M_{12} = 10 R_0$.

3) Specification of the maximum value (ohm) that can be tolerated for 2R, with reference to both R_0 and l.
A default value is acceptable.
The recommended default value is $(2R)_{MAX} = MIN\left[\frac{R_0 l}{5}, R_0 l_{CRITICAL}\right]$
with $l_{CRITICAL} = 1{,}0$ m.

4) Specification of the maximum value (ohm) that can be tolerated for ΣR_d, with reference to $(2R)_{MAX}$.
A default value is acceptable.
The recommended default value is $(\Sigma R_d)_{MAX} = (2R)_{MAX}$.

5) Specification of the maximum value (henry) that can be tolerated for 2L, with reference to both M_{12} and largest frequency $(f_0)_{MAX}$ which is involved in the considered application.
A default value is acceptable.
The recommended default value is $(2L)_{MAX} = \frac{M_{12}}{10} \frac{V_{INT}}{2\pi (f_0)_{MAX}}$
Typical values for $(f_0)_{MAX}$ and V_{INT} are respectively
$100\,10^6$ Hz and $0{,}75c$, with $c = 3\,10^8$ m/s.

6) Specification of the maximum value (henry) that can be tolerated for ΣL_d, with reference to $(2L)_{MAX}$.
A default value is acceptable.
The recommended default value is $(\Sigma L_d)_{MAX} = (2L)_{MAX}$.

7) Specification of the maximum value (henry per meter) that can be tolerated for $(Z_0)_{EXT}(Z_0)_{INT}C_{12}$, with reference to M_{12}.
A default value is acceptable.

The recommended default value is $\left[(Z_0)_{EXT}(Z_0)_{INT}C_{12}\right]_{MAX} = \frac{M_{12}}{2}$.

4 – EXPERIMENTAL TESTS.

The principle of tests is:
– driving extremity $\neq 1$ ($z = 0$) of the external transmission line with CW generator the open circuit voltage of which is $V_{OC}(t) = (V_{OC})_{MAX}\sin 2\pi f_0 t$,
– and measuring currents $i_{INT}(0,t)$ and $i_{INT}(l,t)$ respectively induced at both extremities of the internal transmission line.

Both external and internal transmission lines need to be matched at both extremities. V_{EXT} needs to be chosen very close to V_{INT}.

Experimental procedure involves two steps.

1) Using first a low frequency f_0 ($f_0 = 100$ kHz), measurements allow direct access to:

$$\begin{cases} R_{BOND} = (R_0 l) + (2R) + \Sigma R_d, \text{as} \\ R_{BOND} = \dfrac{1}{S_{MAX}}\left[i_{INT}(0,t)\right]_{MAX} = \dfrac{1}{S_{MAX}}\left[i_{INT}(l,t)\right]_{MAX} \end{cases}$$

with $S_{MAX} = \dfrac{(V_{OC})_{MAX}}{2(Z_0)_{EXT}\,2(Z_0)_{INT}}$.

Relative uncertainty $\Delta R_{BOND}/R_{BOND}$ has to be estimated.

2) Choosing then f_{OC} high enough ($f_{OC} \geq 30$ MHz) and such that
$X_{OC} = \text{tg}X_{OC}$, with $X_{OC} = \pi f_{OC} l\left(\dfrac{1}{V_{INT}} + \dfrac{1}{V_{EXT}}\right)$, measurements allow direct access to both L_{BOND} and k_{BOND}.

$$\begin{cases} L_{BOND} = (M_{12} l) + (2L) + \dfrac{kX_{OC} + 1}{2}\Sigma L_d \\ L_{BOND} = \dfrac{1}{S_{MAX}}\dfrac{1}{2\pi f_{OC}}\dfrac{1}{2}\left\{\dfrac{X_{OC}}{\sin X_{OC}}\left[i_{INT}(0,t)\right]_{MAX}, \left[i_{INT}(l,t)\right]_{MAX}\right\} \end{cases}$$

$$\begin{cases} k_{BOND} = 1 + \dfrac{2(Z_0)_{EXT}(Z_0)_{INT}C_{12} l + (kX_{OC} - 1)\Sigma L_d}{\left[M_{12} - (Z_0)_{EXT}(Z_0)_{INT}C_{12}\right] l + (2L) + \Sigma L_d} \\ k_{BOND} = \dfrac{X_{OC}}{\sin X_{OC}}\dfrac{\left[i_{INT}(0,t)\right]_{MAX}}{\left[i_{INT}(l,t)\right]_{MAX}} \end{cases}$$

Relative uncertainties $\Delta L_{BOND}/L_{BOND}$ and $\Delta k_{BOND}/k_{BOND}$ have to be estimated.

In the above relations k is a coefficient which is not exactly known. Depending on the would-be defects locations and on the test frequency, k may be either positive or negative. What is sure is that $|k| \leq 1$.

5-CRITERION FOR ACCEPTANCE.

Considered as a whole, the set of combinations R_{BOND}, L_{BOND}, k_{BOND} takes into account every parameter which is involved in the performance of the shielded bond.

To make sure that the provided shielded bond does actually meet the required performance, four conditions need to be simultaneously fulfilled:

$$\begin{cases} R_{BOND} + \Delta R_{BOND} \leq (R_0 L) + (2R)_{MAX} + (\Sigma R_d)_{MAX} \\ L_{BOND} + \Delta L_{BOND} \leq (M_{12} l) + (2L)_{MAX} + \dfrac{X_{OC}+1}{2}\left(\Sigma L_d\right)_{MAX} \\ k_{BOND} - \Delta k_{BOND} \geq 1 - \dfrac{(X_{OC}+1)(\Sigma L_d)_{MAX}}{(M_{12} l) + (\Sigma L_d)_{MAX}} \\ k_{BOND} + \Delta k_{BOND} \leq 1 + \dfrac{2\left[(Z_0)_{EXT}(Z_0)_{INT}C_{12}\right]_{MAX} l + (X_{OC}-1)(\Sigma L_d)_{MAX}}{\left\{M_{12} - \left[(Z_0)_{EXT}(Z_0)_{INT}C_{12}\right]_{MAX}\right\} l + (\Sigma L_d)_{MAX}} \end{cases}$$

6-EXAMPLES.

As a first example, let us consider $l = 2{,}53$ m and $V_{INT} = 0{,}75c$ and let us specify $R_0 = 10^{-3}\ \Omega/m$ plus the recommended default values.

Hence,

$M_{12} = 5{,}30\,10^{-11}$ H/m, $(2R)_{MAX} = 5\,10^{-4}\ \Omega$, $(\Sigma R_d)_{MAX} = 5\,10^{-4}\ \Omega$, $(2L)_{MAX} = 1{,}90\,10^{-12}$ H,

$(\Sigma L_d)_{MAX} = 1{,}90\,10^{-12}$ H, $\left[(Z_0)_{EXT}(Z_0)_{INT}C_{12}\right]_{MAX} = 2{,}65\,10^{-11}$ H/m,

$X_{OC} = 4{,}4935$ and $f_{OC} = 63{,}601$ MHz.

The criterion is:
$$\begin{cases} R_{BOND} + \Delta R_{BOND} \leq 3{,}5\,10^{-3}\ \Omega \\ L_{BOND} + \Delta L_{BOND} \leq 1{,}4\,10^{-10}\ \text{H} \\ k_{BOND} - \Delta k_{BOND} \geq 0{,}92 \\ k_{BOND} + \Delta k_{BOND} \leq 3{,}04 \end{cases}$$

As a second example, let us consider $l = 9{,}72$ m and $V_{INT} = 0{,}75c$ and let us specify $R_0 = 10^{-3}\ \Omega/m$ plus the recommanded default values.

Hence,

$M_{12} = 5,30\,10^{-11}$ H/m, $(2R)_{MAX} = 10^{-3}\Omega$, $(\Sigma R_d)_{MAX} = 10^{-3}\Omega$, $(2L)_{MAX} = 1,90\,10^{-12}$ H, $(\Sigma L_d)_{MAX} = 1,90\,10^{-12}$ H, $[(Z_0)_{EXT}(Z_0)_{INT}C_{12}]_{MAX} = 2,65\,10^{-11}$ H/m, $X_{OC} = 10,9041$ and $f_{OC} = 40,172$ MHz.

The criterion is:

$$\begin{cases} R_{BOND} + \Delta R_{BOND} \le 11,7\,10^{-3}\Omega \\ L_{BOND} + \Delta L_{BOND} \le 5,3\,10^{-10}\,H \\ k_{BOND} - \Delta k_{BOND} \ge 0,95 \\ k_{BOND} + \Delta k_{BOND} \le 3,06 \end{cases}$$

EME INTEGRATION: SPECULATION ON A PROPER NORM FOR LIGHTNING

Richard W. Sutton
Science Applications International Corporation
McLean, Virginia, USA

Examination of lightning waveforms given or referenced by governmental military and commercial standards shows that each reference is unique and specific. The specificity is good to the extent that one must design equipment to only one requirement; satisfaction to the one appropriate waveform has essentially given waiver for all possible natural variations of lightning waveforms. Note of the growing need to design for dual use equipment, increased utilization of commercial products in military environments and reminders that lightning waveforms are far more complex than those given in specifications leads to a desire for a more sound set of design and test criteria.

The mathematical notion of the Norm, $\|f(x)\|$, has previously been expanded for use in characterizing strength-stress margins (DAVIS, 1989). The attractiveness of the Norm lies in its simple scalar representation of rather complex waveform vectors. Other properties guarantee conservative addition and linear scaling of the waveform which allows a Norm algebra. However, another underlying assumption is that a particular form of the Norm is a good estimator of the likely or observed failure mechanism threshold.

One would like to associate the onset of failure with the magnitude of the scalar, then safety margins can be assigned on the basis of the corresponding Norm of the stress waveform. Each of several failure mechanisms would be assessed with different Norms and margins expressed for each. Design and acceptance testing could proceed based on the appropriate Norms without need to reference a standard waveform, but with assurance that any particular test waveform would maintain the safety margin.

Failure mechanisms found for lightning have been direct mechanical damage such as puncture holes, fusing of wiring or burning of insulation. For this class of damage the root action integral seems appropriate; its square describes energy delivered in extended time frames. Some damage is in the form of non-equilibrium processes such as fuse link blowing or IC thermal failures. Here the energy required for damage may be a function of the time in which it is delivered. The Norm might reflect the natural energy dissipation rate of the class of test objects. The small time scale end point is the adiabatic case where only energy delivered within the time scale is effective. Finally, there is the voltage dependant breakdown which destroys insulating properties or allows follow-on current to flow and accomplish damage.

A class of functional failure modes could be considered where transitions of digital signals are induced. The appropriate Norm might be charge transferred within the clock or data cycle. In highly oscillatory situations, the rectified impulse must have

an important role to play, especially in high gain analogue circuits.

An epoch is needed to define many of these Norms. The epoch is moderately dependant on the nature of the object to be certified and heavily dependant on the mechanisms for failure. It may also be an epoch which allows us to incorporate the other EMEs within the Norm format. Candidate epochs for lightning are the "stroke" times, the "flash" time and a "follow-on current" time previously described by Uman, 1968.

Several of the Norms of several published specified waveforms are shown in the table.

Lightning Specification	Root Action Integral $A^{1/2}s$ ($x10^{-3}$)	Maximum Rate of Rise A/s, ($x10^{-12}$)	Peak Current kA	Rectified Impulse A-s
Mil B 5087 (ASD)	.8	.1	200	3.6
Mil Std 1542A				
Mil-Std-1757A	1.4	.025	200	1.3
RTCA/DO-160 C	1.4	.004	200	1.3

Although there are significant differences in dwell and magnitudes, there is relatively small difference in the value of the associated Norms.

In consideration of the above, the standards community and the test and evaluation community should be encouraged to evaluate this admittedly more complex means of setting requirements. The benefits would be in having uniform requirements which could be enforced without, however, dictating test setups. The form of specification would be simplified thus reducing the amount of confusion over implementation. These benefits would accrue while maintaining a strong grounding of the specification in the underlying phenomenology which allows setting of economical safety margins.

Ultimately, consideration of the these Norms must be based on a robust set of data. Modern instrumentation should be used to recapture the lightning statistics base. A second need will be extensive verification of the relation between each failure mechanism and its corresponding Norm. This is quite necessary to build confidence that the right orm has been chosen. The final basis necessary is evaluation of cross terms between failure Norms to find any confounding features of multiple failure mechanisms.

If these steps are completed, a more useful paradigm for safety and protection will be constructed leading to easier enforcement and more economical implementation.

SUB-PROTONOSPHERIC ELF WAVEFIELDS FROM NUCLEAR EXPLOSIONS AND LIGHTNING

Dr Hal J. Strangeways, Department of Electronic and Electrical Engineering, University of Leeds, Leeds LS2 9JT, U.K.

Introduction. It is well known that whistlers are excited by nuclear explosions. It has also been found that explosion-excited whistlers generally have similar properties to natural whistlers, limiting their use as a means of detection of nuclear explosions. Further, the propagation mechanism of whistlers is such that they would only be observed in very restricted regions such as the geomagnetically conjugate point to the latitude of entry into a duct. However, one unusual feature which has been seen for a high altitude explosion-excited whistler is an additional delayed trace at very low frequencies (400Hz - 1kHz), (Helliwell and Carpenter,J.geophys.Res,68,4105,1963). Delayed traces below 1kHz have also been seen for natural whistlers and so do not necessarily constitute a unique feature. These have been explained by wave-energy in this lower frequency range following a different ducted path at a little higher invariant latitude than the rest of the whistler trace. This can explain the increased dispersion which results in a discontinuity or low upper cut-off in the whistler trace.

There are, however, significant problems with this explanation. Frequencies of about 1kHz are below the cut-off of the earth-ionosphere waveguide (typically about 1.8kHz) and so are attenuated greatly for propagation below the ionosphere. Thus it seems very surprising that if these frequencies propagate in a separate higher L-value duct, the frequencies above 1 kHz should have been much more attenuated so that they are not seen at all for this duct. Further, for the case of the whistler received from the starfish prime explosion in Wellington, the distance from source to duct entry point at the geomagnetic conjugate to Wellington is about 3000km for which very considerable attenuation would occur for the frequency range 400 Hz to 1kHz and yet the whistler trace shows no wave energy and thus much greater attenuation for the higher frequencies above 1kHz. Thus what is really required is an explanation of how wave-energy at these frequencies could follow a lower attenuation path from the explosion site or lightning flash to the duct entry point and how this could result in a greater dispersion than occurs for higher frequencies. Strangeways et al. (J.atmos. terr. Phys,45,387,1983) have shown how some whistlers received at about 66° latitude resulted from a normal whistler path followed by a sub-protonospheric path, explaining why their exit point (determined by triangulation is significantly higher (by about $\Delta L=2.9$) than their ducted propagation (determined by their nose frequency). At these latitudes, the sub-protonospheric path is aided by the electron gradient associated with the equatorward side of the high latitude trough. Thus, it is not clear that such paths can exist at lower latitudes. At least for the starfish prime whistler, it is also necessary for the sub-protonospheric path to come before the ducted path as this whistler was received close to the duct exit point. Thus the possibility of such sub-protonospheric paths and their coupling to ducted paths to explain delayed whistler traces below 1kHz is investigated by ray-tracing.

Ray-tracing calculations. These were performed in a realistic model of the magnetospheric plasma incorporating hydrogen, helium and oxygen ions in diffusive equilibrium and latitudinal gradients of electron density and temperature corresponding to winter night (WN) conditions. Although the anisotropy of the magneto-ionic medium introduced by the geomagnetic field generally limits upgoing VLF paths to an angle of about 20° to the geomagnetic field, at frequencies below

the LHR (lower hybrid resonance frequency), the refractive index surface becomes closed, enabling propagation at right angles to the geomagnetic field. Thus an upgoing ray can be reflected below the protonosphere and return to the earth at a few degrees higher or lower latitude rather than arriving in the conjugate hemisphere after propagation through the plasmasphere as for whistlers. Rays were started upgoing at 300 km altitude over a range of initial latitudes with frequencies in the range 400 Hz to 2kHz and with wave-normal angles to the vertical up to 30°. It was found that the larger the initial wave-normal angle to the vertical ϕ (pointing to higher latitude) the higher the upper frequency limit for the sub-protonospheric path. For, example for rays from 30° latitude, the highest frequency reflected back was 800Hz for $\phi = 18°$, 1 kHz for $\phi = 20°$ and 1.4kHz for $\phi = 22°$. Initial wave-normal angles of 15° or less did not result in sub-protonospheric reflection. Although wave-normal angels of about 20° to the vertical at 300 km altitude are greater than can be explained by Snell's law for a uniform horizontally stratified medium, experimental observations such as those of the VLF transmitter FUB aboard the FR-1 satellite show that wave-normal in this range exist in the upper ionosphere arising from either horizontal gradients or scattering. The latter mechanism would seem quite likely following a nuclear explosion since this will also perturb ionisation levels in the D region and above.

The height of reflection increased with frequency and varied from 550 to 800km. If the wave-normal angle to the field had not increased to 90° by 800 km altitude, then the ray-path continued on into the conjugate hemisphere as the wave-normal angle was found to decrease above this altitude. The typical frequency range reflected is comparable with the range of frequency of the delayed low frequency traces (below 1kHz) such as that seen for the whistler following the starfish prime explosion and natural whistlers recorded at Eights and Byrd stations, Antarctica (Helliwell and Carpenter,*op.cit.*). The final latitude of the sub-protonospheric paths at 300 km altitude were generally about 4-6° higher than the initial latitude and the time delay associated with the path varied in the range 150 to 300ms. The final wave-normal angle was typically close the direction of the geomagnetic field and would thus be reflected back upwards in the ionosphere rather than penetrating to the ground. It could then undergo another sub-protonospheric reflection or become trapped in a duct. For the delayed whistler component resulting from the starfish prime test, it would need to make 3 or 4 sub-protonospheric hops from the site of the explosion to the conjugate point to Wellington where the starfish prime whistler was received. The total time for these would be about 850 ms at 1kHz which is in good agreement with the extra delay of the low frequency portion of the trace observed.Thus it can then be assumed that this low frequency delayed trace propagated in the same duct as the higher frequency part and that the extra delay is due to the extra time taken for propagation from the explosion site to the duct below the protonosphere. Theoretical whistler have been constructed by adding together time delays for ducted propagation in the WN model with additional delays for the lower frequencies due to sub-protonospheric propagation. These are then compared with observed traces of starfish prime and natural whistlers.

Conclusions. A new mechanism has been suggested to explain the extra delayed very low frequency traces that can follow explosion excited and natural whistlers. It has been shown that the extra delay results from a sub-protonospheric propagation mode. This is therefore a new mechanism for coupling of ELF energy in the frequency range up to about 1kHz from lightning or nuclear explosions into the region above the ionosphere and below the protonosphere, up to about 800 km altitude. Propagation in this region may occur for a few thousand km due to multiple reflections and thus may have EMC consequences for low altitude satellites.

DIPOLE DEPTH VARIATION OF LOW-FREQUENCY ELECTROMAGNETIC FIELDS PRODUCED AT THE EARTH'S SURFACE BY SUBMERGED DIPOLES

Aziz S. Inan
University of Portland
Portland, Oregon

The quasi-static electromagnetic fields generated along the Earth's surface by a vertical dipole are evaluated numerically and the results are plotted as a function of dipole depths ranging from 0 to 30 kilometers for various observer locations. The curves indicate the existence of interference minimums between the direct and lateral wave components for some of the field components. For example, the following curves are showing the variation of the magnitude of the vertical component of the magnetic field, B_z, (in picotesla) as a function of the depth of a vertical magnetic dipole at various observer locations. The observer locations are ranging from 0. to 80 kilometers, as indicated. There is a sharp minimum around 6-7 kilometers of dipole depth as seen in the curve corresponding to an observer location $\rho = 17.5$ kilometers. Similar interference minimums exist in some of the other components.

The last part of this presentation is to further investigate this interference between direct and lateral waves by looking at the terms in the mathematical expressions and identifying the direct and the lateral terms from one another. The results of this work could be used for various applications such as communication through the Earth, geophysical prospecting, and undersea communication.

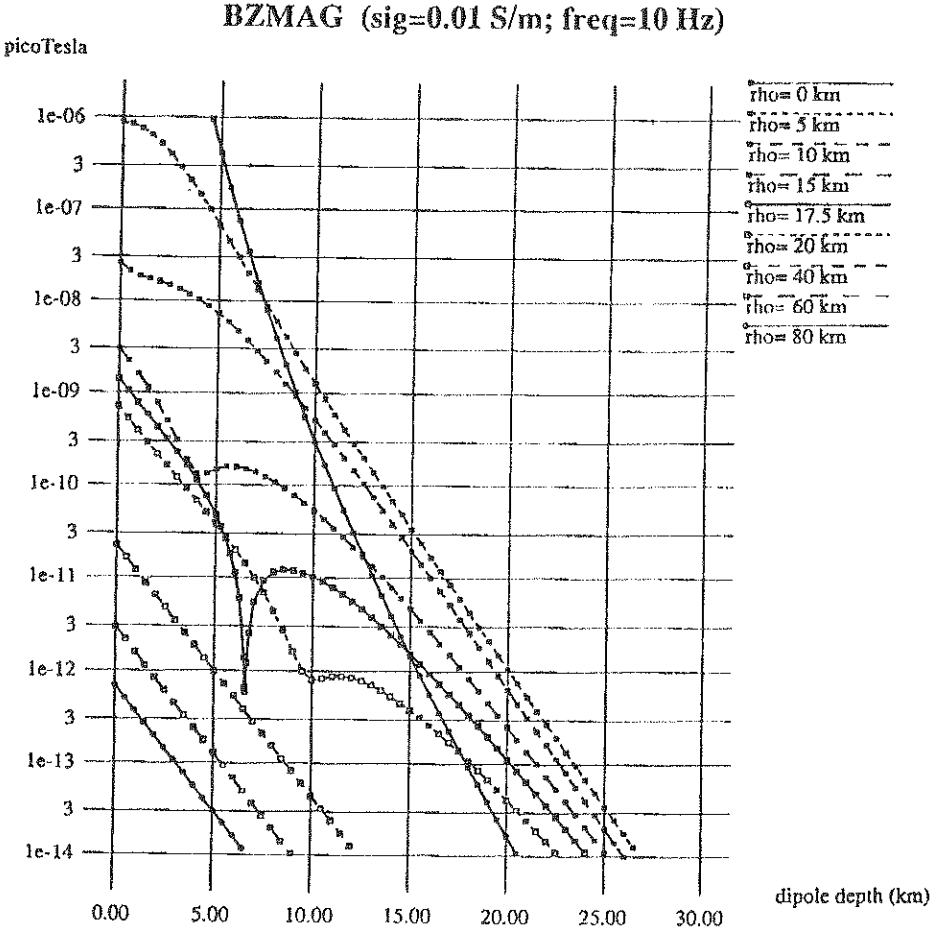
BZMAG (sig=0.01 S/m; freq=10 Hz)
picoTesla
1e-06
3
1e-07
3
1e-08
3
1e-09
3
1e-10
3
1e-11
3
1e-12
3
1e-13
3
1e-14
0.00
5.00
10.00
15.00
20.00
25.00
30.00
dipole depth (km)
rho= 0 km
rho= 5 km
rho= 10 km
rho= 15 km
rho= 17.5 km
rho= 20 km
rho= 40 km
rho= 60 km
rho= 80 km

EXTENSIVE EXTREMELY LOW-THRESHOLD OPTICAL DISCHARGE

M.Yu. Klimov and Yu.M. Sorokin*
University of Nizhni Novgorod, Russia

The propagation of high-intensity laser radiation in gas-dispersive media (such as atmosphere) gives rise to a wide class of nonlinear phenomena affecting as energy, duration, focusing and wavelength of the beam so the type and characteristics of aerosol component. Whereas for water aerosols (fogs, clouds) the main nonlinear processes connected with evaporation and fragmentation, in the case of solid chemically inertive aerosols (natural or man-made ones) optical plasma formation processes are usually initiated which limit both the peak intensities and pulses energies of powerful beams. The last processes of various types are generally known as the optical breakdown phenomena which result in optical discharge formation, i.e. the appearance of isolated plasma speckle, ensemble (train) of speckles or extensive plasma channel (Yu.D. Kopytin, Yu.M. Sorokin, A.M. Skripkin, N.N. Belov and V.I. Bukatyi. Optical discharge in aerosols. Nauka. Novosibirsk, 1990). We have realized the last object in laboratory under the extremely low intensities (10^6W/cm^2 in near infrared band) in relatively long ($\sim$ 1 ms) pulse due to the collective processes in a high density aerosol ensemble.

The threshold quasilocal (TQL) model of such extensive collective optical discharge (ECOD) is analogous to the known compact one (COD) model (Yu.M. Sorokin, Atmospheric Optics (USSR), 1, 1, 73-80, 1988). The main physical differences between COD and ECOD connected with the ECOD propagation mechanisms and beam-plasma interaction effects. The main difference in experimental setup is in the fact that the focal region length L_F and the homogeneous dense aerosol cloud depth L_a are now of the same order ($L_a \geq L_F$) contrary to the case of compact COD where $L_a \ll L_F$. The TQL model energy condition of nonoptimized COD (Yu.M. Sorokin et al., Quant. Electron. (USSR), 13, 2464-2473, 1986) connects the power density of energy input into a strongly absorbing aerosol $P_a = \pi I a^2 n_a$, defined by intensity I of the beam, the radius a and concentration n_a of aerosol particles, with the characteristic time τ of beam-particle interaction and the pressure p of buffer gas (air for example):

$$P_a \cdot \tau \geq 2p\left[1 + \sum_i \gamma_i\right] = Q_a^* ; \quad \tau = \min\,(2R_F/v_a\,,\ \tau_p), \qquad (1)$$

where γ_i are parameters depending on the physical properties of the buffer gas and aerosol matter, R_F is the radius of the focal spot, v_a is the light reactive ejection velocity, τ_p is the pulse duration.

As for the corundum-like materials in air at the pressure of order of atmospheric one $Q_a^* \cong 14$ J/cm ^{3} and the typical value of $v_a \sim 30$ m/s, the estimation of τ for moderately focusing optical or near infrared beams ($R_F \sim 0.3$ cm) is $\tau \simeq 2\ 10^{-4}$ s $< \tau_p$. So for intensity I ~ 1 MW/cm^2 we have $n_a \cdot a^2 \sim 2\ 10^{-2}$ cm^{-1}. The technical problem of laboratory ECOD is to create such homogeneous quasistationary ($t \gg \tau_p$) aerosol ensemble along the sufficiently extensive line. We achieve this aim with the bunker-type aerosol generator for the SiC aerosol with a~ 70 μ so that $n_a \sim 10^3$ cm^{-3} and $L_a \cong 30$ cm.

The location of ECOD was determined according to the objective spectroscopic criterion (CaII lines 393,37 nm, 386,85 nm) with the use of the fiber plait. For the focal length F=1 m under the intensity I $\cong$ 0.7 MW/cm^2 (pulse energy W $\cong$ 130 J) of Nd-laser the ECOD length was about 25 cm, which is the same order with the continuous extensive laser spark (CELS) initiated earlier in high-intensity (I > 10^4 MW/cm^2) axicon formed caustic (L. Polonski et al., Sov. Phys. JETP, 73,969-975,1991). The plasma channel of ECOD is sufficiently cold ($T_e \sim 1$ eV), moderately ionized ($N_e \sim 10^{17}$ cm^{-3}) and long lived ($\tau_e \sim 2$ ms) with respect of CELS one (T_e~10 eV, $N_e \sim 10^{18}$cm^{-3}, $\tau_e \sim 0.1$ μs).

The absorption of powerful beam in ECOD channel was about 50% and strongly depends on W. The preliminary investigations disclose the new mechanisms of optical discharge propagation in ECOD: the gas dynamic ejection mechanism (forward) and the light reactive ejection mechanism (backward).

SPREADING OF CHAOS IN MAGNETOSPHERIC PLASMA

V.I.Larkina, Ja.I.Likhter
Institute of Terrestrial Magnetism, Ionosphere and Radio Wave Propagation of Russian Academy of Sciences
Troitsk town, Moscow Region, 142092 Russia
Phone (095) 334 09 13. Fax (095) 334 01 24.
Telex 412623 SCSTP SU

Data of different plasma parameters (concentration N_α (α different kind of particles), fluxes of electrons (U) having different energies from lukewarm to MeV energies, plasma temperature T, quasiconstant magnetic B_o and electric E_o fields, b and e components of ELF/VLF wave fields in broad frequency band and some others) measured at certain "Intercosmos" satellites in different geophysical conditions were utilized for calculating the auto and cross probability characteristics. Analysis of correlation effects give the possibility to find cause and effects properties of the interaction.

Between the experimental results obtained we would like to mention:

a). The modulation of b and e amplitudes of ELF/VLF wave fields, the U electron fluxes and the B_o of quasiconstant geomagnetic field with the ULF frequencies. Such effect is seen at satellites and on the Earth observatories.

b). Simultaneous and quasisynchronous chaotic fluctuations of e,b and B_o in the high lalitudes where the longitudinal currents are seen usually.

c).Quasiperiodic and chaotic variation of e and b amplitudes of waves and N_α and T of plasma.

d). The cross corelation coefficients of the e_i and b_j mutual perpendicular wave components undergo spatial variations not only because of changing the amplitude but also because of the spatial changing of probability density.

For the interaction of the mentioned experimental facts one have to use the kinetic Vlasov equation. The dispersion equation is a consequence of kinetic equation and established a connection between the e and b amplitude components of the wave which propagate through the plasma and the plasma parameters N_α, T, U, E_o and B_o fields. So we have the functions $e(N_\alpha, T, U, E_o, B_o, f)$ and $b(N_\alpha, T, U, E_o, B_o, f)$. If for example, one find experimentaly or theoreticaly the probability density for, say N_α and T, so it is possible to find the probability density and the moments of the casual variables e and b. That is a more simple way to solve the problem of transport of the stochastic fluctuations of say N_α to the e and b amplitudes.

For example, from wave dispersion relation we get $e(f,N_e)=\gamma_e N_e^2$ and $b(f,N_e)=\gamma_b N_e^{5/2}$ and supposing that probability density (prodens) of N_e is a Maxwell one

$$p_N(N_e)dN_e=\sqrt{2/\pi}\,\frac{N_e^2}{\eta_N^3}\exp\left\{-N_e^2/2\eta_N^2\right\}dN_e,$$

we can find the prodens of the e and b and the first and second moments for these stochastic quantities. So the e-prodens is

$$p_e(e)de = \sqrt{2/\pi}\ \frac{\gamma_e}{2\,\gamma_e^{3/2}\,\eta_N^3}\ \exp\left\{\frac{-e}{2\gamma_e\eta_N^2}\right\}de$$

and the b-prodens is

$$p_b(b)db = \frac{2}{5}\cdot\sqrt{2/\pi}\ \frac{b^{1/5}}{\gamma_b^{6/5}\,\eta_N^3}\ \exp\left\{\frac{b^{4/5}}{2\gamma_b^{4/5}\,\eta_N^2}\right\}db.$$

In the Table we have placed the characteristic values for fluctuation of N_e, amplitude e and b of the VLF field.

Table

	Fluctuating quantity N_e	e	b
Mathematical expectation $(ME)_i$	$1,59\eta_N$	$3\gamma_e\eta_N^2$	$2,048\ \gamma_b\eta_N^{5/2}$
Dispersion $(D)_i$	$0,453\eta_N^2$	$15\gamma_e^2\eta_N^4$	$14,956\ \gamma_b^2\eta_N^5$
σ_i	$0,673\eta_N$	$3,873\gamma_e\eta_N^2$	$3,867\ \gamma_b\eta_N^{5/2}$
Range of fluctuations $\alpha_i = \sigma_i/(ME)_i$	0,423	1,291	1,888
Relative range α_i/α_N	1	3,052	4,475
α_b/α_e	-	-	1,463

From the Table one may see that:
1). the first and the second moments of e and b quantities are proportional to the characteristics value (η_N) of N_e prodens in the same way as it follows from the dispersion relation for the harmonic wave amplitudes;
2). The fluctuations of the b-amplitude is more sensitive to the fluctuation in N_e then the e-amplitude.

In the same way it is possible to get the notion about the spreading of chaotic fluctuations, say of the energetic particles and of the plasma temperature. Of course the results mentioned are the stationary one. To find the nonstationary development of the spreading of chaos in the magnetospheric plasma it is necessary to solve the kinetic differentional equation.

Solving the kinetic differential equation one may find how the stochastic fluctuations of, say e, b, E_o and B_o and other foreign phenomena, pass on the N_α and T. Such problem is usually known as a heating of plasma by the waves.

GEOELECTRIC SECTIONS MAP OF EUROASIA

Yu.B. Bashkuev*, V.S. Dorzhiev, L.H. Angarkhaeva
Buryat Institute of Natural Sciences Siberian Division of Russian Academy of Sciences, 6 Sakhyanova str., Ulan-Ude, 670042, Russia

The problem of investigating electric properties of earth and earth covering (i.e. forest, rivers, lakes, glaciers) is of great importance for the EMC practice since many electromagnetic systems (communication, electrical engineering, control) are located on earth and are electrically connected with it. Operational effectiveness of different telecommunication systems depends considerably on good knowledge of electrical characteristics of underlying medium and it's time and space variations.

Electrical properties of rock depend on many factors such as material and mechanical structure, humidity, temperature, ground water mineralization so it is impossible to obtain these values only theoretical calculations. They can be determined more accurately by special measurements taken under conditions of rock natural bedding. A convenient model of underlying medium in the local point is a geoelectric section (GES) differentiated with respect to electrical resistance ρ_i ($\rho_i = 1 / \sigma_i$), dielectric constant ε_i and thickness h_i of each layer. Underlying medium with depth up to 50-100 metres usually consists from 2-4 layers with different ρ_i and ε_i . The Earth crust with the depth up to 30-40 km can have 10-15 layered geoelectric section.

The influence of the underlying medium on the electromagnetic field is often taken into consideration by value of surface impedance Z_s , definited by the electric parameters and structure of the medium. Prediction maps and area propagation diagrams of different GES types are basis for making of frequency dependent surface impedance maps, which allow to calculate electromagnetic fields in wide frequency range (ELF-VLF-LF-MF). Forest vegetation, ice-cover and seasonal layer of freezing and thawing are taken into consideration on the GES maps by the introduction of the additional semiconducting layer. The connection between the electric properties of the mountain rocks and there lithological structure and geocryological conditions forms the basis of the GES maps composing method. In spite of this are widely used different geological maps and data about many executed vertical electric soundings (VES).

The conductivity map of the globe composed by R. Morgan and E. Maxwell doesn't often satisfy the needs of EMC practice, because in some regions there are considerable differences with measuring results. In the report there is given an experimental estimation of Morgan-Maxwell's map for the Siberia region. It has been shown that ρ values on this map are, as a rule, overestimated in 2-3 and more times and geoelectric boundaries don't coincide with real electric boundaries. In the report a new prediction geoelectric sections map of Euroasia at the scale of 1:15000000 included 95 different types of geoelectric sections has been considered and founded.

Recently radioimpedance methods of investigating the Earth crust and cryolitic zones have been developed. Their advantage is due to the lack of contacts and the possibility to get information about the borders and the thickness of the frozen condition of the ground. In the studies of cryolitic zone remote radioimpedance methods with the use of aircraft allowing to investigate areas diffi-

cult of access are of special importance. Elaboration and wide use of underlying medium's local electrical characteristics measuring methods with the help of apparatus being installed on an aircraft or a car (Yu.B. Bashkuev at al., VIII Int. Wroclaw Symp. on EMC, part 1, 281-290, 1986) presents an urgent scientific and technical problem for geoelectric mapping.

In 1980-1987 large-scale experimental work on determining underlying medium's effective resistivity with the use of airvariant of REMP in VLF band was carried out. It's aim was geoelectric mapping of areas with complex geological structure and estimating REMP airvariant validity in mountainous regions. The area of more than 120000 sq. km was mapped from AN-2 airplane. On the whole electrical boundaries of various rock complexes (Archaean, Cambrian, Jurassic and others) coincide rather well with geological ones. Classification of the major geoelectric structures of the area under investigation has made possible to establish regularities of underlying medium's electrical properties space change and make geoelectric prediction of the areas that have not been studied. The fragment of geoelectric sections map of Euroasia is presented in Fig. It has been mapped by the results of the remote sounding and ground measurements data.

Creation of data banks of electromagnetic medium characteristics (electric properties of the earth and atmosphere, electromagnetic noise, etc.) and hard-software means for modelling electromagnetic characteristics of concrete communication systems demand elaboration of automatic numerical methods of solution direct and inverse geoelectromagnetic problems for heterogeneous semiconducting media. On the basis of regularization A.N. Tikhonov's method has been grounded a method of definition parameters (ρ_i, ε_i, h_i) of stratified semiconducting medium on surface impedance frequency dependence, measured by REMS method.

The portable apparatus for surface impedance frequency dependence measurement with the use of electromagnetic fields of VLF-LF-MF radiostations and the worked-out procedure of solving the inverse problem for stratified impedance medium could take the place of the low productivity method of VES while solving many practical problems of EMC in communication system, power engineering and radioengineering (e.g. calculations of grounding, a choice of cable line paths, radiostation location).

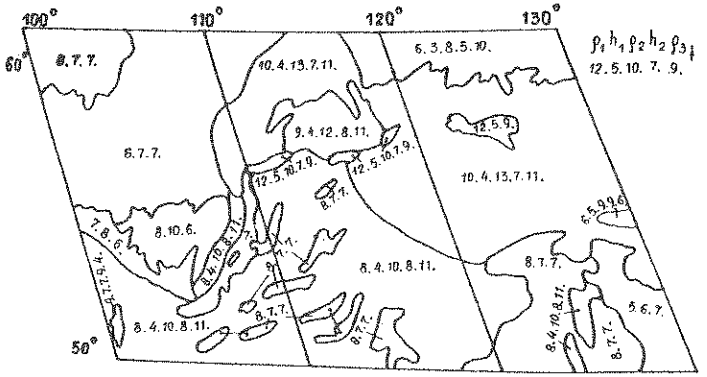

code	average value	
	ρ_i, Ohm·m	h_i, m
0	0.68	—
1	1.47	0.147
2	3.16	0.316
3	6.8	0.68
4	14.7	1.47
5	31.6	3.16
6	68	6.8
7	147	14.7
8	316	31.6
9	680	68
10	1470	147
11	3160	316
12	6800	680
13	14700	1470

Fig. The fragment of geoelectric sections map of Euroasia.

A NUMERICAL CODE TO ANALYZE WIRE ANTENNAS ON COMPLEX STRUCTURES MODELLED WITH NURBS SURFACES USING THE METHOD OF MOMENTS

F. Rivas, L. Valle, M.F. Cátedra
Grupo de Sistemas y Radio
Departamento de Electrónica. Universidad de Cantabria
Avda. Los Castros s/n. 39005 Santander. Cantabria. SPAIN
Phone: +34 42 201493, Fax: +34 42 201402

ABSTRACT

Recently a paper presents a Moment Method technique using NURBS surfaces and Bézier patches to represent the geometry of arbitrarily shaped scatterers. Modelling that way implies that fewer basis functions are needed to obtain a precise representation of complex bodies. In this approach, a basis function is associated with each one of the boundary lines between pairs of Bézier patches. These new basis functions can be considered as a generalization of the planar rooftop functions introduced by Glisson (A.W. Glisson, D.R. Wilton. IEEE-AP, 593-603, 1980). The well-known blade-razor functions were considered as testing functions. This method was successfully validated when the obtained RCS values of several objects were compared to other methods, (L. Valle, F. Rivas, M.F. Cátedra. To appear in IEEE Transactions on Antennas and Propagation).

SUMMARY

The purpose of the present communication is to present a technique for analyzing radiation and coupling between wire antennas mounted over conducting surfaces starting from the method mentioned above. With the aim of establishing continuity of current at the wire-surface junction, an special kind of subdomain (junction subdomain) has been introduced. The radius of the antennas analyzed in this work is assumed to be much smaller than the length. A piecewise-linear approximation can be made to model an arbitrary curved antenna. With this thin-wire approximation, a linear rooftop basis function is associated with each one of the subdomains on the wire. As in the case of the boundary lines between Bézier patches, blade-razor functions are used as testing functions.

The junction subdomain shares the characteristics of both kinds of subdomains defined above: subdomains over a Bézier patch and on electrically small wire. For this reason, the basis function associated with the junction subdomain is a linear rooftop on the wire and a generalized curved rooftop on the Bézier patch. The idea is to impose a total charge of $-1/jw$ on the wire and a charge of $1/jw$ on the patch (a pulse-doublet of charge is associated to the

junction subdomain). Because one part of the junction subdomain is a Bézier patch of the whole geometry, is not necessary a testing function on the patch. Only on the wire a blade-razor function is defined as a testing function.

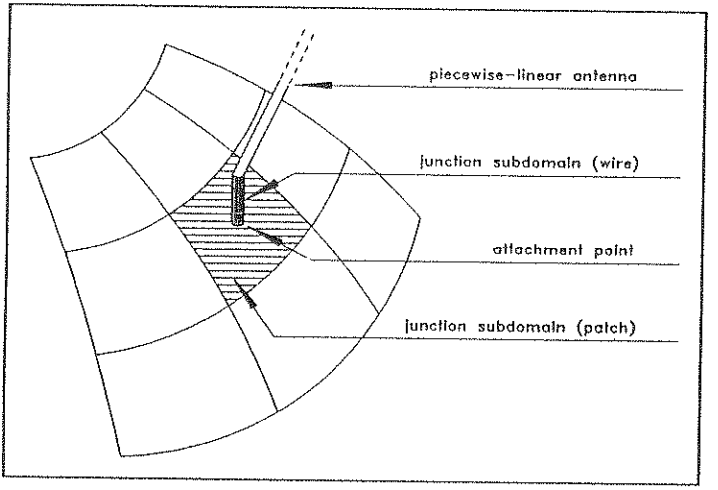

Definition of the junction subdomain.

Once the expansion and testing functions are defined for all the three kinds of subdomains in the geometry, the computation of the impedance matrix of the MM is carried out.

To compute the coupling between antennas the reaction theorem is considered. The approach here presented has been validated considering radiation and coupling values of wire antennas on board of canonical shapes like plates, boxes, spheres, etc. Now is being applied in the analysis of antennas on an aircraft. The method appears to be quite accurate and efficient.

RECENT DEVELOPMENTS IN HIGH FREQUENCY METHODS

Roberto Tiberio[1]*, Stefano Maci[2], Alberto Toccafondi[1], Filippo Capolino[1]

1 College of Engineering
University of Siena, via Roma 77, 53100, Siena, Italy.

2 Department of Electronic Engineering
University of Florence, via S. Marta 3, 50139, Florence, Italy.

High-frequency techniques which describe dominant electromagnetic scattering phenomena, are found to be highly efficient and accurate for treating a variety of antenna and RCS problems, and provide insight into the physical mechanisms. In these paper a brief overview on these techniques is presented, and some recent developments are high lighted.

First, the background of both the Geometrical Theory of Diffraction (GTD) (J. B. Keller, *J. Opt. Soc. Am.* , 52, 116-130, 1962), (R. G. Kouyoumjian, P. H. Pathak, *Proc. IEEE*, 62, 1448-1461, 1974) and the Physical Theory of Diffraction (PTD) (P. Ya. Ufimtsev, *Electromagnetics*, 11, 125-159, 1991) are illustrated in order to give evidence to the similarities and the differences between these two theories, expecially in the use of the solutions of local canonical problems.

Next, the Incremental Theory of Diffraction (ITD) (R. Tiberio, S. Maci, to be published on *IEEE Trans. Antennas Propagat.*) is discussed, which provides a unified framework for describing high-frequency phenomena. This method essentially consists of a localization process, based on a rigorous Fourier transform analysis of canonical problems. To this end, the solution of a cylindrical canonical configuration is thought of as a superposition of an infinite uniform distribution of incremental field contributions, that are localized along a directrix of the cylinder. The pertinent element factor is extracted by establishing a Fourier transform pair relationship between the incremental contribution and the solution of

the cylindrical canonical problem. Next, these incremental field contributions are adiabatically distributed and integrated along the actual shadow boundary line (SBL). The total scattered field is represented as the sum of a generalized Geometrical Optics (GGO) field plus incremental diffracted fields.

This method is applicable to any local shape, where a uniform, cylindrical, local canonical configuration with arbitrary cross-section is appropriate. Also, its formulation is uniformly valid at any incidence and observation aspects, including caustic of the corresponding ray-field representation.

This method naturally includes the uniform GTD ray field representation of the scattering phenomenon, when it is applicable. It is suggested that this method may provide a self-consistent, high-frequency description of a wide class of scattering phenomena within a unified framework.

Several numerical examples are presented and discussed to demonstrate the validity of the ITD. These example include radar cross section of polygonal plates, pattern of dipoles on finite ground planes and the corresponding near field distributions.

Beltrami-Moses Fields in Electromagnetism

Pierre Hillion

Institut Henri Poincaré.Paris.

The Beltrami-Moses vectors used in many parts of physics for many years are eigenfunction of the curl operator and they were introduced in electromagnetism in a particular way by Moses (SIAM J.Appl.Math.21,114,1971).

The Beltrami-Moses fields are complex vectors $u(\underset{\sim}{x},\underset{\sim}{p};\lambda)$ depending on $\underset{\sim}{x}\in R^3$ and on a vector $\underset{\sim}{p}$ in the momentum space such as

$$curl.\ u(\underset{\sim}{x},\underset{\sim}{p};\lambda)=\lambda|\underset{\sim}{p}|\,u(\underset{\sim}{x},\underset{\sim}{p};\lambda)\quad,\quad \lambda=0,\pm 1\ , \tag{1}$$

and any well behaved vector $V(\underset{\sim}{x})$ has the representation

$$V(\underset{\sim}{x})=\sum_{\lambda}\int u(\underset{\sim}{x},\underset{\sim}{p};\lambda)\,f(\underset{\sim}{p},\lambda)\,d\underset{\sim}{p}\ , \tag{2}$$

where $f(\underset{\sim}{p};\lambda)$ is a scalar function.
Then the complex electromagnetic vector ($i=\sqrt{-1}$, $x_0=ct$)

$$\Lambda(\underset{\sim}{x},x_0)=\sqrt{\varepsilon}\,E(\underset{\sim}{x},x_0)+i\sqrt{\mu}\,H(\underset{\sim}{x},x_0)\ , \tag{3}$$

has according to (2) the representation

$$\Lambda(\underset{\sim}{x},x_0)=\sum_{\lambda}\int u(\underset{\sim}{x},\underset{\sim}{p};\lambda)\,f(\underset{\sim}{p},x_0;\lambda)\,d\underset{\sim}{p}\ , \tag{4}$$

where of course f depends now on x_0 and satisfies a partial differential equation obtained by substituting (4) in Maxwell's equations.We discuss the solutions f in a homogeneous isotropic medium.Then,it is shown that the Beltrami-Moses transform (4) competes successfully with the covariant Fourier transform of

the electromagnetic field.

We give an application to time harmonic fields for which

$$f(\underline{p}, x_0; \lambda) = e^{i\lambda|\underline{p}|x_0}\, g(\underline{p}; \lambda) \tag{5}$$

when the spectral function $g(\underline{p}; \lambda)$ is a surface harmonic. This supplies the electromagnetic field in terms of a series of spherical Bessel functions generalizing the well known multipole expansion of plane waves (J.D.Jackson Classical Electrodynamics Wiley 1975). The Beltrami-Moses fields are also a powerfull tool to discuss the Cauchy problems as well as the initial-boundary value problems for Maxwell's equations.

GREEN'S FUNCTION OF SPHERICAL BODY

Professor Dragutin M. Velickovic, D.Sc, Member IEEE
Department of Electromagnetics, Faculty of Electronic Engineering.
Beogradska 14, 18000 Nis, Serbia

The conventional image theorem application gives one solution in closed form in low frequency electromagnetic field theory, when point sources are in surroundings of dielectric plane, cylinder and perfectly conducting sphere. In the case of dielectric sphere having permitivitty ε and conductivity σ, the Green's function in closed form is unknown. The present paper proposes one new solution of Green's function for dielectric sphere. The expressions for electric field density and for electric current density are in closed form.

Spherical body $(\varepsilon_2, \sigma_2)$ with radius a and current point source I at a distance d of the body center, in the exterior region $(\varepsilon_1, \sigma_1)$, is presented in the Figure.

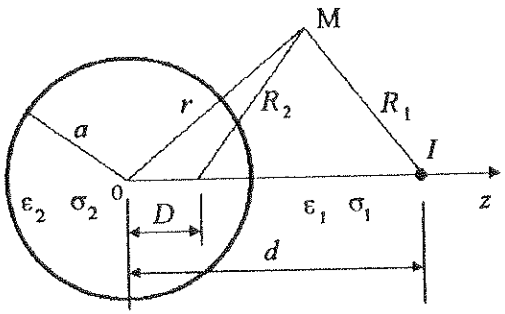

Figure – Point current source and dielectric body

In order to determine electric scalar potential distribution, φ, the following Poisson's equation and boundary conditions can be used:

$$\Delta\varphi = \frac{1}{r^2}\frac{\partial}{\partial r}\left(r^2\frac{\partial\varphi}{\partial r}\right) + \frac{1}{\sin\theta}\frac{\partial}{\partial\theta}\left(\sin\theta\frac{\partial\varphi}{\partial\theta}\right) = \begin{cases} -\dfrac{I}{2\pi\underline{\sigma}_1}\dfrac{\delta(r-d)\delta(\theta)}{r^2\sin\theta}, & a < r \\ 0, & r < a \end{cases},$$

$$\varphi(r=a-0) = \varphi(r=a+0) \text{ and } \underline{\sigma}_2\left.\frac{\partial\varphi}{\partial r}\right|_{r=a-0} = \underline{\sigma}_1\left.\frac{\partial\varphi}{\partial r}\right|_{r=a+0},$$

where:

r,θ are spherical coordinates,

$\delta(r-d)$ and $\delta(r-d)$ are Dirac's δ – functions and

$\underline{\sigma}_1 = \sigma_1 + j\omega\varepsilon_1$ and $\underline{\sigma}_2 = \sigma_2 + j\omega\varepsilon_2$ are complex conductivities.

ω is angular frequency.

By combining standard image theorems, the potential can be expressed as:

$$\varphi=\begin{cases}\dfrac{I}{4\pi\underline{\sigma}_1 R_1}+\dfrac{I}{4\pi\underline{\sigma}_1}\dfrac{a}{d}\dfrac{\underline{\sigma}_1-\underline{\sigma}_2}{\underline{\sigma}_1+\underline{\sigma}_2}\left(\dfrac{1}{R_2}-\dfrac{1}{r}\right)+\dfrac{I}{4\pi d}\dfrac{\underline{\sigma}_2-\underline{\sigma}_1}{(\underline{\sigma}_1+\underline{\sigma}_2)^2}\sum\limits_{n=1}^{\infty}\dfrac{1}{n}\left(\dfrac{D}{r}\right)^n P_n(\cos\theta)\ , & a\le r\\ \dfrac{I}{2\pi(\underline{\sigma}_1+\underline{\sigma})R_1}-\dfrac{I}{4\pi\underline{\sigma}_1 d}\dfrac{\underline{\sigma}_1-\underline{\sigma}_2}{\underline{\sigma}_1+\underline{\sigma}_2}+\dfrac{I}{4\pi d}\dfrac{\underline{\sigma}_2-\underline{\sigma}_1}{(\underline{\sigma}_1+\underline{\sigma}_2)^2}\sum\limits_{m=1}^{\infty}\dfrac{1}{n}\left(\dfrac{r}{d}\right)^n P_n(\cos\theta)\ , & r\le a\end{cases}$$

where:

$R_1=\sqrt{r^2+d^2-2rd\cos\theta}$, $R_1=\sqrt{r^2+D^2-2rD\cos\theta}$, $D=\dfrac{a^2}{d}$ and $P_n(\cos\theta)$ are Legendre's polynomials of the first kind.

The electric field components can be put in the closed form:

$$E_r=-\frac{\partial\varphi}{\partial r}=\begin{cases}\dfrac{I}{4\pi\underline{\sigma}_1}\dfrac{a-d\cos\theta}{R_1^3}+\dfrac{I}{4\pi\underline{\sigma}_1}\dfrac{a}{d}\dfrac{\underline{\sigma}_1-\underline{\sigma}_2}{\underline{\sigma}_1+\underline{\sigma}_2}\left(\dfrac{a-d\cos\theta}{R_2^3}-\dfrac{1}{r^2}\right)+\dfrac{I}{4\pi d}\dfrac{\underline{\sigma}_2-\underline{\sigma}_1}{(\underline{\sigma}_1+\underline{\sigma}_2)^2}\left(\dfrac{1}{R_2}-\dfrac{1}{r}\right), & a<r\\ \dfrac{I}{2\pi(\underline{\sigma}_1+\underline{\sigma}_2)}\dfrac{a-d\cos\theta}{R_1^3}-\dfrac{I}{4\pi r}\dfrac{\underline{\sigma}_2-\underline{\sigma}_1}{(\underline{\sigma}_1+\underline{\sigma}_2)^2}\left(\dfrac{1}{R_1}-\dfrac{1}{r}\right), & r<a\end{cases}$$

$$E_\theta=-\frac{\partial\varphi}{r\partial\theta}=\begin{cases}\dfrac{I}{4\pi\underline{\sigma}_1}\dfrac{d\sin\theta}{R_1^3}+\dfrac{I}{4\pi\underline{\sigma}_1}\dfrac{\underline{\sigma}_1-\underline{\sigma}_2}{\underline{\sigma}_1+\underline{\sigma}_2}\dfrac{aD}{d}\dfrac{\sin\theta}{R_1^3}+\dfrac{I}{4\pi dr\sin\theta}\dfrac{\underline{\sigma}_2-\underline{\sigma}_1}{(\underline{\sigma}_1+\underline{\sigma}_2)^2}\left(\dfrac{D-r\cos\theta}{R_1}+\cos\theta\right), & a\le r\\ \dfrac{I}{2\pi(\underline{\sigma}_1+\underline{\sigma}_2)}\dfrac{d\sin\theta}{R_1^3}+\dfrac{I}{4\pi dr\sin\theta}\dfrac{\underline{\sigma}_2-\underline{\sigma}_1}{(\underline{\sigma}_1+\underline{\sigma}_2)^2}\left(\dfrac{r-d\cos\theta}{R_1}+\cos\theta\right), & r\le a\end{cases}$$

In the practice, the series in potential formulas can be transformed as:

$$S=\sum_{n=1}^{\infty}\frac{p^n}{n}P_n(\cos\theta)=\sum_{m=1}^{M}\frac{S_m(m-1)!}{p^m}-\sum_{m=1}^{M}\frac{1}{m}+M!\sum_{n=1}^{\infty}\frac{p^n P_n(\cos\theta)(n-1)!}{(n+M)!}\ ,\ 0<p<1\ ,$$

where:

$$S_m=\sum_{n=1}^{\infty}\frac{p^{n+m}n!}{(n+m)!}P_n(\cos\theta)=\begin{cases}\displaystyle\sum_{k=1}^{m-1}(-1)^{k+1}\frac{p^k S_{m-k}}{k!}-\frac{(-1)^m}{(m-1)!}J_{m-1}\ , & m\ge 2\\ J_0\ , & m=1\end{cases}$$

and

$$J_m=\begin{cases}\ln\dfrac{\sqrt{1+p^2-2p\cos\theta}+p-\cos\theta}{1-\cos\theta}\ , & m=0\\ \sqrt{1+p^2-2p\cos\theta}-1+\cos\theta J_0\ , & m=1\\ \dfrac{p^{m-1}\sqrt{1+p^2-2p\cos\theta}+(2m-1)\cos\theta J_{m-1}-(m-1)J_{m-2}}{m}\ , & m\ge 2\end{cases}$$

By example, it is:

$$S=\frac{1}{p}\ln\frac{\sqrt{1+p^2-2p\cos\theta}+p-\cos\theta}{1-\cos\theta}-1+\sum_{n=1}^{\infty}\frac{p^n}{n(n+1)}P_n(\cos\theta)\ .$$

EM COUPLING TO TRANSMISSION LINES COMPUTED BY DIFFERENT METHODS AND COMPARED WITH EXPERIMENTAL RESULTS

A. W. Kälin, B. R. Brändli*
Defence Technology and Procurement Agency
NEMP Laboratory, CH-3700 Spiez , Switzerland

F. M. Tesche
Electromagnetics Consultant
6714 Norway Road, Dallas, TX, 75248, USA

P. Wilson
EMC Baden, LTD.
CH-5405 Baden, Switzerland

When examining the excitation of a transmission line by an incident electromagnetic (EM) field for nuclear electromagnetic pulse (EMP) or electromagnetic compatibility (EMC) studies, one is generally interested in getting a rapid overview of the influence of numerous parameters, such as the electrical conductivity of the soil, the transmission line geometry, the incident EM field parameters, and the terminating impedances of the line.

For this purpose, a computer code that executes rapidly is important, especially if extensive parametric studies are to be undertaken. For line calculations, an approximate quasi-transverse electromagnetic (quasi-TEM) transmission line model can often be used. An alternative is to use a more rigorous, integral equation solution for the induced line currents, although this option requires significantly longer computation times.

For the approximate quasi-TEM theory, the code NULINE is available, and is very efficient in computation time. This program models a single, straight conductor over a lossy earth, with excitation in the form of either an incident EM field or by lumped voltage or current sources along the line. Although the calculations are performed in the frequency domain, transient results are available through the fast Fourier transform (FFT). As long as the basic requirements for such quasi-TEM modelling are met (i.e., $h << \lambda$ and $L >> h$), this code provides reasonably accurate results.

In order to ascertain the usable range of parameters of the NULINE transmission line code, several different line geometries and excitations have been calculated with this code and compared with results of two other integral equation codes, the Numerical Electromagnetics Code (NEC2) and the CONCEPT code. Figure 1 illustrates the line geometry used for this comparison.

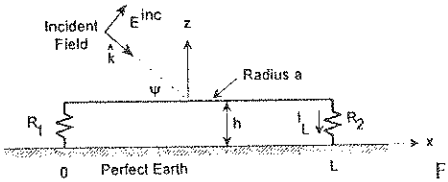

Figure 1. Line geometry.

Figure 2 compares the results of the excitation of a line with L = 30 m, h = 0.1 m, and a = 0.15 cm by a standard HEMP incident field - the Bell Laboratory double exponential. In this case, the results of the calculations are practically identical. Figure 3 illustrates the corresponding results for a line with h = 5 m and the same excitation.

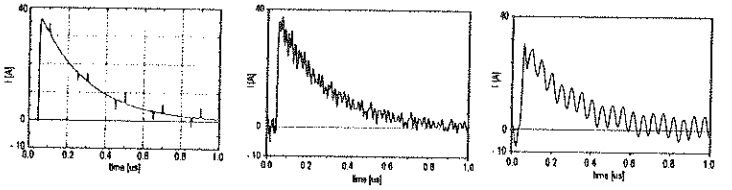

(a) NULINE (b) NEC c) CONCEPT

Figure 2. Comparison of the transient load #2 currents for L = 30 m, h = 0.1 m, a = 0.15 cm, $\psi = 45^{o}$, and $R_1 = R_2 = 20\ \Omega$

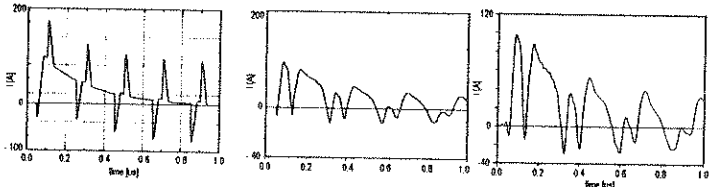

(a) NULINE (b) NEC c) CONCEPT

Figure 3. Comparison of the transient load #2 currents for L = 30 m, h =5 m, a = 0.15 cm, $\psi = 45^{o}$, and $R_1 = R_2 = 20\ \Omega$

In this paper, the deviations between the accurate calculations and the transmission line model which appear in Figure 3 are discussed and demonstrated with calculations for other geometries and excitations. One major reason for the inaccuracy of NULINE at increasing line heights is that the vertical line segments (i.e., the risers) are not treated as transmission lines. This deficiency can be eliminated by adding small transmission line sections at the end of the horizontal line, as suggested by De Gauque. Results for such a modified model will be presented.

Finally in this paper, results from all analysis methods will be compared with experimental data obtained in an EMP simulator. The details of the results will be discussed, and the influence of various parameters will be demonstrated.

DETERMINATION OF CURRENTS IN WIRES FROM THEIR SCATTERED FIELD.

by A. Bacha, P. Saguet*, F. Ndagijimana
LEMO - CNRS URA 833 - ENSERG BP 257 38016 GRENOBLE CEDEX - FRANCE

Introduction

In many electromagnetic compatibility problems, electromagnetic impulses induce currents in wires or in conductor strips. These currents may lead to an improper working or even to a destruction of the devices. Often, we can't perform a direct measurement of currents. On the other hand, sensors can give the value of the electric (or magnetic) field close to the wires.
We propose a theoretical method to evaluate currents in a number of coupled wires from their diffracted field. Indeed, in the vicinity of the conductors, the total field which can be measured by sensors can be assimilated to the diffracted field.
Here, the structure is simulated with the TLM method which has been extensively validated in the past. The simulation gives all the components of the electromagnetic field throughout the structure (and acts as a sensor) and in particular, the tangential component of the magnetic field on the surface of conductors from where we can easily deduce the current density. So, we can compare the current obtained with the proposed theoretical method and those obtained with the TLM method.

Theory

In a very classical way, we discretize a thin wire or antenna in N elementary parts which are small enough so that the current can be considered as constant for each element. Each element Z_j radiates a magnetic field toward a point P_i at a distance R_{ij}. If the magnetic field is measured at N points P_i, we get the matrix equation:

$$[K][I] = [\mathcal{H}_d]$$

where [K] is a matrix which describes the relation between current and scattered field. It is representative of the antenna kernel. This kernel can be calculated in a close form or in an approximated form for fast calculations on a computer.
In the case of two antennas, two "series" of measured fields are required (Fig. 1).
Then, the following system can be built

$$\left[\mathcal{H}_1^d\right] = \left[K_{11}\right]\left[I_1\right] + \left[K_{12}\right]\left[I_2\right]$$

$$\left[\mathcal{H}_2^d\right] = \left[K_{21}\right]\left[I_1\right] + \left[K_{22}\right]\left[I_2\right]$$

and currents in both antennas can be derived from :

$$\left[I_1\right] = \left[\left[K_{12}\right]^{-1}\left[K_{11}\right] - \left[K_{22}\right]^{-1}\left[K_{21}\right]\right]^{-1}\left[\left[K_{12}\right]^{-1}\left[\mathcal{H}_1^d\right] - \left[K_{22}\right]^{-1}\left[\mathcal{H}_2^d\right]\right]$$

$$\left[I_2\right] = \left[\left[K_{11}\right]^{-1}\left[K_{12}\right] - \left[K_{21}\right]^{-1}\left[K_{22}\right]\right]^{-1}\left[\left[K_{11}\right]^{-1}\left[\mathcal{H}_1^d\right] - \left[K_{21}\right]^{-1}\left[\mathcal{H}_2^d\right]\right]$$

This procedure can easily be generalized to N wires. Then, N series of measured fields are required.

Results

We give in this summary the results obtained with the proposed method, for two antennas opened at each end and immersed in a dielectric box (Fig. 2), when a plane wave illuminates the box.
Fig. 3 shows a good agreement between results. Other results obtained for three or more antennas are also in good agreement with TLM results. In the final paper, more

theoretical details will be given and also CPU time and memory-size required on a Personnal Computer.

Conclusion

The proposed method could be an efficient tool to determine when an electromagnetic impulse is dangerous for a device, even though this device is not directly accessible to measurement. Of course, the device must be entirely defined but this is often the case.

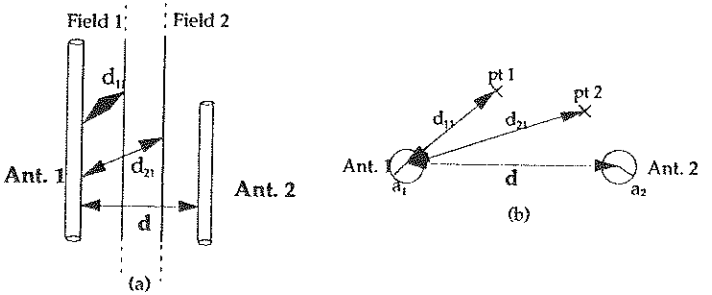

Fig. 1 Case of two antennas.

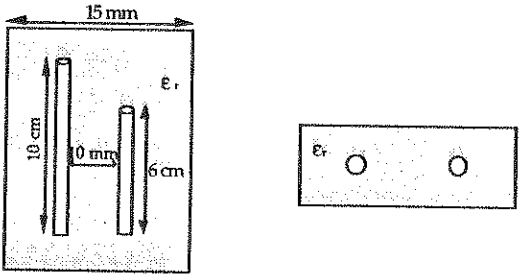

Fig. 2 : Two open antennas in a dielectric box.

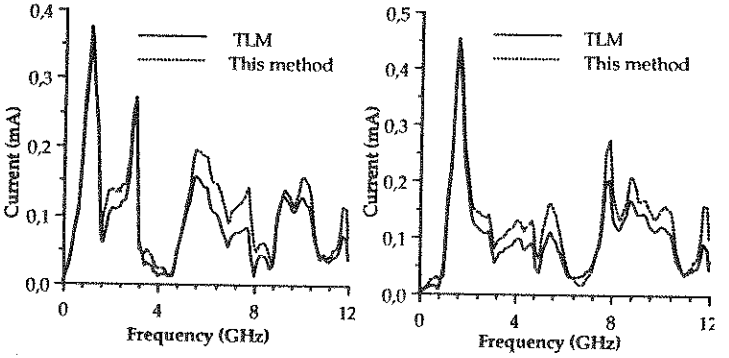

Fig. 3 : Current in antennas as a function of frequency.
(a) : Antenna 1, (b) : Antenna 2

RESPONSE OF CABLES TO DIRECT INTERACTIONS WITH PHOTONS

Dr. James R. Elliott* , Dr. T. Rudolph, P.M. McKenna, Dr. R.A. Perala
Electro Magnetic Applications, Inc.
P.O. Box 260263
Denver, CO 80226
USA
(303) 980-0070

and

Dr. Walter Kornahl
Wehrwissenschaftliche Dienstelle der Bundeswehr für ABC-Schutz
Postfach 11 42
3042 Munster
Deutchland

The response of cables to the direct photon environment associated with the tactical nuclear source region was investigated using both modeling and testing at a flash X-ray machine. A variety of cables were examined, including coaxial and twisted pair configurations, both with and without application of a biasing voltage.

Radiation transport modeling used the Integrated Tiger Series Monte Carlo codes to determine charge displacement and energy deposition within a cable sample. Geometry and material properties appropriate to each cable type was used. Both the simulator spectrum and alternative source region spectra were used. In addition, monochromatic sources were used to study the energy dependence of the cable response. The location of the displaced charge was input to an electrostatic problem solver to determine the size and sign of the replacement charge needed to reestablish equilibrium.

Simulator testing consisted of a series of shots on three samples of each cable type. The three specimens of a given cable type had -50 V, 0 V or + 50 V initially. Strong stored charge effects were observed for some but not all cables; this was usually exhausted after a few shots. The applied bias voltage significantly modified the response for some cables, especially if it was changed after a number of shots.

An heuristically derived circuit model was constructed in order to extract such parameters as source strength, initial stored charge, air gap and enhanced charge/conductivity region geometry. This model could then reproduce a sequence of as many as 11 consecutive shots on a cable sample. This included 100% changes in bias voltage. Figures 1-4 show the response of a 50 Ohm coaxial for its first four shots.

The parameters derived from the short simulator test cables were then used in a transmission line model to examine the response of cables up to 1000 m in length.

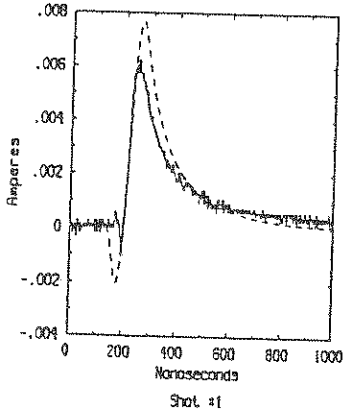

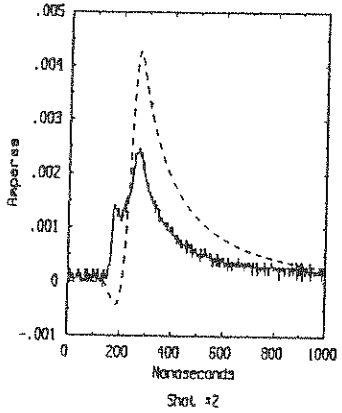

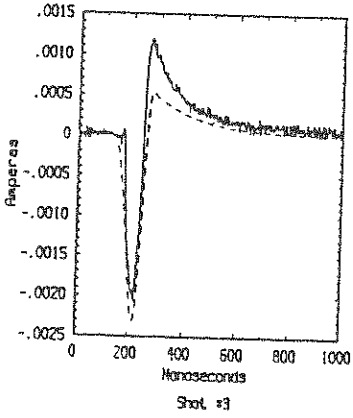

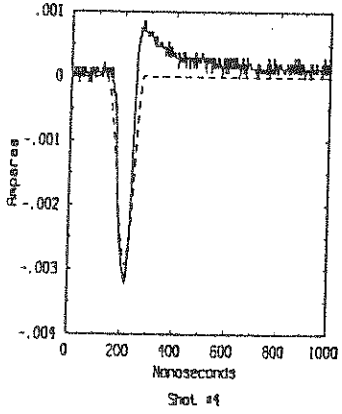

Figures 1-4 RG58C/U-1 Responses for 11 Consecutive Shots with Positive
_____ Measured Response
- - - - - - Modeled Response

THIN WIRES IN 3D SREMP COUPLING CODES

Y. LE GUILLOU*, P. BREUILH
NUCLETUDES -BP 117, 91944 LES ULIS , FRANCE

There is a need to predict the response of thin conductors like wires, cables, antennas, on or within large systems. To be realistic, models used to compute the effects of SREMP environments must be 3D. Concequently, the number of cells describing a system in FDTD 3D SREMP coupling codes is very large, and the limit in computer resources forces the cell size not to be too small. As the cell sizes are larger than the thin conducteur radius, they cannot accomodate them. Then there is a need for a special treatment of thin-struts in 3D FDTD EM codes.

We consider first a thin wire formalism using an "in-cell inductance" model of the wire (R.HOLLAND, L.SIMPSON, IEEE T. EMC , may 1981), with the modifications adequate in conducting SREMP medium (J.P.BERENGER, 3ème colloque sur la Compatibilité Electromagnétique, 1985). In this model, it is assumed that the wire radius is much smaller than the cell size, and that the stability of the time stepping algorithm is the same as without the presence of the wire .

However, in some practical cases, the wire radius is not much smaller than the cell size, and the time step must be decreased to insure stability (J.GRANDO et al, APS meeting ,1993). Moreover, the results are sensitive to the position of the wire inside the cell.The figure 1 shows the EM response for a single isolated "fat" dipole in free space, placed in the midle of a cell, and figure 2 shows that when it is placed along edges, there is a 30% decrease for the maximum.

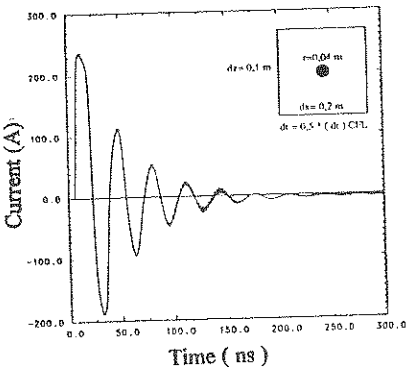

FIGURE 1: wire in the middle of the cell
Midpoint dipole current. (Holland formalism)

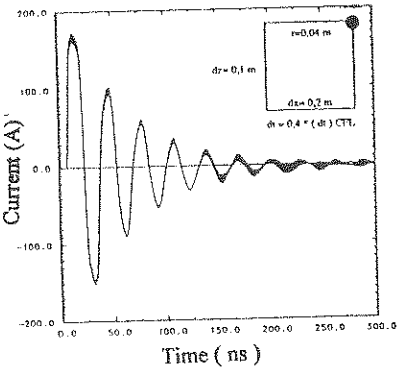

FIGURE 2: wire along edges
Midpoint dipole current. (Holland formalism)

In order to prevent divergences, the time step is about the half of the free space CFL (COURANT-FRIEDRICH-LEVY) time step limit, and there are still some numerical noise .

By changing the thin-strut model, the sensitivity to the wire position in the cell can be alleviated, and the free-space CFL limit can be used, wihout any reduction. Moreover, as appears on figure 3, the results are less noisy than on figures 1 or 2 .

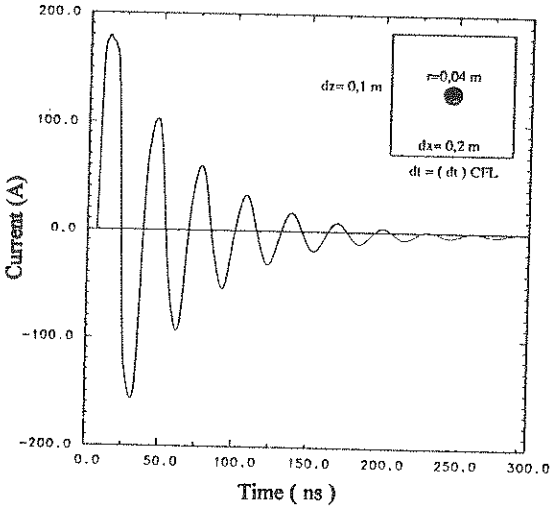

FIGURE 3: Midpoint dipole current. (Model based on the new formalism)

A stability analysis shows the conservation of the free space CFL limit for that thin strut model .The corresponding algorithm can be used for parametric studies on the responses of elongated structures , like in-flight missiles , or poles on the ground , in SREMP environments , with a substantial saving in computing time .

DEVELOPMENT OF CABLES MODELS FOR SYSTEM ANALYSES APPLICATION TO SPACE AND DEFENCE POWER BUS SIMULATIONS

C. LEONARD, G. CHAMBERT
AEROSPATIALE Espace et Défense
66, route de Verneuil, 78130 LES MUREAUX
Tél : (1) 34.92.10.08 , Fax : (1) 34.92.17.34

J. SEILLE, J.P. GRANGER
MATRA MARCONI SPACE FRANCE
31 rue des Cosmonautes, 31077 TOULOUSE
Tél : 62.24.74.99 , Fax : 62.24.77.90

ABSTRACT

This paper deals with the methodology used to perform multi-cable systems simulations within an EMC simulation framework.

First, the theoretical background associated to the cable modelling is briefly reviewed together with the method of integration of the model in a network analyzer based on the nodal admittance matrix method.

Then, an example of validation of the model is presented just before the application to a typical system power bus. Typical results are given for elementary cable level simulations and for system level simulations.

1- INTRODUCTION

The increasing complexity of spacecrafts, and the non availability of measurements at system level for some of them, impose to develop new EMC engineering tools. These tools are designed for centralizing a large variety of functionalities in order to help engineers to handle complex EMC configurations and to ensure the electromagnetic compatibility of an electrical system at any stage of its development.

Developed in the frame of an European Space Agency (ESA) project, TDAS-EMC constitutes one of these new types of engineering tools. The purpose of this framework is also to organise the EMC data, thanks to a standardisation of data formats and to offer EMC prediction capabilities.

In this paper, one mainly focus on the use of this EMC workbench for multi-cable systems simulations. In particular, the software was experimented to simulate a typical power bus. The backbone of such a simulation was the accurate modelling of the harness which was constituted of overshielded twisted shielded pairs.

Therefore, a special effort was made on the validation and on the improvements of the corresponding models in the simulation framework.

Also, in the first part of the paper, the general principles of the cables modelling are reminded.

Then, typical simulation results are given and some of the foreseen improvements are presented, just before the conclusion.

2- THEORETICAL BACKGROUND

The numerical evaluation of the response of any cable can be split into the following elementary steps :

- Evaluation of the electrical parameters of the line starting from the geometrical parameters and from the materials characteristics (metal resistivity, electrical permittivity of dielectric, ...)
- Solving of the transmission lines equations via an electrical network analyzer based on the admittance matrix method.
- If necessary, computation of the equivalent conducted sources for external electromagnetic coupling simulation.

The main features of these elementary steps are now briefly presented.

2.1- Generalized transmission line equations

In the case of a multi-conductor line, the transmission lines equations can be written by means of matrices :

$$\begin{cases} \dfrac{\partial [V]}{\partial x} = [Z]\,[I(x)] + [V_S(x)] \\ \dfrac{\partial [I]}{\partial x} = [Y]\,[V(x)] + [I_S(x)] \end{cases} \quad (1)$$

where :

- $[V]$ is the vector of the voltages of the conductors w.r.t. reference
- $[I]$ is the vector of the currents in the conductors
- $[Z]$ is the impedance matrix of the cable
- $[Y]$ is the admittance matrix of the cable
- $[I_S]$ and $[V_S]$ are the equivalent voltage and current source terms representing external electromagnetic coupling.

In the following explanations, we only focus on conducted mode effects and source terms are neglected.

2.2- Calculation of the electrical parameters of the line

When the electrical parameters of the line are not known, the impedance and admittance matrices of the cable must be evaluated starting from its geometrical parameters and from the electrical characteristics of the materials (electrical permittivities, resistivities, ...).

Two main types of methods can be used for this evaluation :

- use of analytical formulae,
- numerical solving of the Laplace's equation.

Use of analytical formulae

Analytical formulae can be used to evaluate the electrical parameters of simple cables geometries such as single cables, flat/ twisted pairs and coaxial cables.

The interest of such formulae is obviously that the electrical parameters are very easily deduced from the geometrical parameters. Such formulae are also easy to integrate in a simulation framework such as TDAS-EMC.

The main drawback of the method is that the formulae become difficult to establish when the number of conductors increases and for complex geometries.

Therefore, when the number of conductors increases (twisted pair shielded, multi-conductor lines, ...), an intermediate solution consists of computing approximate analytical formulae.

In this case, one must verify that the approximate formulae are compliant with the quasi-TEM approximation (2) otherwise substantial errors can be made on the resonance frequency values when using the model.

$$[L].[C]_{\varepsilon_R=1} = \frac{1}{c^2}[Id] \quad (2)$$

where

$[L]$ is the inductance matrix of the cable

$[C]_{\varepsilon_R=1}$ is the generalized capacitance matrix of the cable computed with the dielectric material removed ($\varepsilon_R=1$).

c is the light velocity (m/s)

$[Id]$ is the identity matrix

In the special case of the twisted shielded pair modelling, the mutual capacitances values evaluated via the approximate formulae were not accurate enough to reproduce the cable behaviour. Thus, theoretical developments were needed to establish very accurate formulae. These formulae are still valid when the two conductors are close to each other and close to the shield. These formulae were integrated in the simulation framework and, as it will be shown in the last part of this paper (§3 and §4), they allowed to get quite accurate predictions at system level.

Numerical solving of the Laplace's equation

Complex configurations can be analyzed via a numerical solving of the Laplace's equation based either on finite differences or finite element algorithms.

The principle of the analysis consists first of a 2D meshing of the cross section of the cable.

The potential values in each mesh are then computed by solving the Laplace's equation for a given set of potentials on the conductors. The total charge on each conductor is deduced from the potential by applying the Gauss' law [2] :

$$\oint_S -\overrightarrow{\text{grad}}(V).d\vec{S} = \frac{Q}{\varepsilon} \quad (3)$$

S is a close surface surrounding the conductor

V is the potential

Q is the total charge on the conductor

ε is the electrical permittivity of the dielectric material

The capacitance matrix of the cable is then deduced from the computed charge using the following formula:

$$\begin{bmatrix} Q_1 \\ Q_2 \\ \vdots \\ Q_n \end{bmatrix} = \begin{bmatrix} C_{11} & C_{12} & \cdots & C_{1n} \\ C_{21} & C_{22} & \cdots & C_{2n} \\ \vdots & \vdots & \ddots & \vdots \\ C_{n1} & C_{n2} & \cdots & C_{nn} \end{bmatrix} \cdot \begin{bmatrix} V_1 \\ V_2 \\ \vdots \\ V_n \end{bmatrix} \quad (4)$$

where

Q_i is the per unit length charge on the ith conductor (C/m)

V_i is the potential on the ith conductor (V)

The capacitance matrix terms can thus be calculated by the following relation:

$$C_{ij} = \frac{Q_i}{V_j}\Big|_{(V_1, \ldots, V_{j-1}, V_{j+1}, \ldots, V_n)=0} \quad (5)$$

Therefore, the determination of all the capacitance matrix parameters for a n conductors line requires the solution of the potential distribution n-1 times for n-1 sets of potential boundary conditions on the conductors.

The inductance matrix $[L]$ of the cable can also be evaluated using this method by computing the capacitance matrix with all the dielectric materials removed and by applying the formula (2).

The advantage of this method is that the geometrical configuration of the cable cross-section can be complex and that non homogeneous dielectric materials can be taken into account.

In a practical point of view, the computation of the cable parameters requires the use of a solid modeller and of a mesher to prepare the analysis.

2.3- Principle of the numerical solving of the transmission lines equations

A rather analytical solution of the transmission lines equations can be computed for the system (1) using well-known mathematical methods of eigenvectors computation. On the contrary of the lumped models (meshing of the cable in several RLC cells), the accuracy of the computation is independent from the length of the cable. In addition, it allows to save memory blocks and CPU time.

Moreover, starting from this modal analysis, the nodal admittance matrix of any cable can be computed.

In a theoretical point of view, the three following elementary steps [1] allow to establish the nodal admittance matrix of any cable :

- Computation by modal analysis of the general solution of the propagation equation on [V] derived from (1).
- Application of the boundary conditions on [V] on line terminations.
- Computation of the general solution on [I] using the first equation of the system (1) and the expression of [V].
- Application of the boundary conditions on [I] to derive the admittance matrix of the cable.

2.4- Dielectric losses modelling

In the particular case of the simulation of the multi-cable system composed of overshielded twisted shielded pairs, the model lead to over-estimated responses at high frequencies, due to unexpected dielectric losses in the bundle.

Also, a model of distributed dielectric losses was developed.

In a theoretical point of view, the losses of an homogeneous dielectric are characterized by the tg(δ) factor which can be calculated at frequency F using the following formula :

$$tg(\delta) = \frac{\sigma}{\omega . \varepsilon} \quad (4)$$

where

σ is the conductivity of dielectric $(\Omega^{-1}.m^{-1})$

ε is the electric permittivity of dielectric (F/m)

$\omega = 2\pi F$ is the pulsation (rad/s)

Due to these losses, the conductance matrix [G] of a cable, which is the real part of the cable admittance, can no more be neglected. The conductance matrix is also deduced from the capacitance matrix [C] of the cable using the formula (7).

$$[G] = [tg(\delta)] . [C] . \omega \quad (7)$$

where

$[tg(\delta)]$ is a matrix which characterizes the losses of the different domains of cable (dielectrics, vacuum, ...).

3-VALIDATION ASPECTS

The verification phase of the twisted shielded pair model has consisted first in the simulation of canonical EMC situations (impedance matching, resonance frequencies, ...): Model predictions have been compared with literature and with other models predictions (lumped models, ...).

Then the model has been validated by comparison with test measurements performed at elementary cable level for various loads values and for several shield grounding configurations.

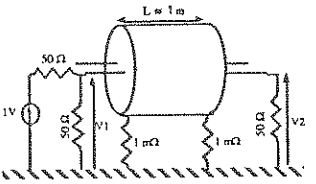

Figure 3.1 : Typical configuration used to validate the twisted shielded pair model

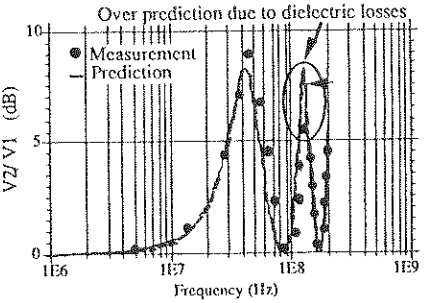

Figure 3.2 : Cable transfer function - Comparison between prediction and test results

Figure 3.1 represents a typical test configuration which has been simulated using the EMC workbench. The computed transfer function of the cable (ratio V2/V1) is represented on Fig. 3.2 together with the corresponding measurement results. A fairly good correlation is obtained.- although the calculated response appears to be over-estimated at high frequencies, due to unexpected dielectric losses. A model of distributed dielectric losses (§2.4) was developed since then.

4- APPLICATION TO POWER BUS SIMULATION

The TDAS-EMC tool was applied to the modelization of a complex power bus. This power bus is constituted of twisted shielded pairs, routing in complex multiconductor overshielded bundles. The system of interest features five interconnected bundles and an umbilical connector. The whole system runs over approximatively 8,50 metres.

As stated above, a model of twisted shielded pair was first developed and tested, giving a very good agreement between prediction and measurements up to 200 MHz (i.e. in the frequency range of most conducted EMI specifications).

This elementary cable model was then integrated in a more complex one, including connectors, which was assumed to be representative of the system bundles (i.e. roughly a twisted shielded pair inside a cylindrical shield). The calculated transfer functions (see schematic on fig. 4.1) have shown a fairly good correlation between theory and measurement.

An elementary model of the umbilical device was also assumed, and gave a fairly good agreement between computation and measurement - although a lot of parameters were ignored and taken *a priori*. Fig. 4.2 shows a comparison between theory and experimental data (the umbilical connector being connected to a one-metre long bundle).

As the dielectric losses appeared to be rather important at high frequencies, crosstalk inside the bundles was assumed to be a second-order phenomenon and thus was neglected in this first approach.

Fig. 4.3 shows the comparison of the calculated transfer function for the whole power bus and the experimental data. The agreement between the predicted response and the measurement is rather good (one should keep in mind that dielectric losses could not be modelized, leading to an over-estimated calculation). Drastic resonances that appear on both calculated and measured responses are due to redundant cables kept open-circuited during the measurement - and taken into aount for the prediction.

The whole system has finally been simulated by connecting the models of the equipments on the power bus. Also, the noise levels at the input of each equipment has been evaluated and compared to the corresponding specifications.

5- CONCLUSION

This study has demonstrated that the methodology used was able to accurately predict the behaviour of complex multi-cable systems in the conducted mode, even in the very early stages of development, when few information is available on the system.

As usual when the behaviour of specific cables must be simulated, a validation campaign has been set-up to assess the validity of the mathematical models used and to evaluate their applicability domain. During this campaign, measurements have been made at both elementary cable level and subsystem level.

Moreover, specific theoretical developments were carried out to improve the model of the twisted shielded pair.

6- FUTURE TRENDS

New developments are foreseen in order to extend the applicability domain of the cables models and of the cable to cable coupling models.

In particular, the effects of the cable conductance variations at high frequencies (>100 MHz) will be simulated.

Moreover, a 2D Laplace's equation solver is under development in order to compute the electrical parameters of complex lines configurations (multi-conductor lines, cable/ cable coupling configurations, non homogeneous dielectric materials, ...).

As far as radiated mode analysis is concerned, several models of cables (single, coaxial, triaxial, ...) have already been developed for simulating the coupling of external electromagnetic fields on multi-cables systems. Additional models such as the twisted shielded pair are still under validation.

More complex EMC situations, such as the coupling between cables and structure elements will be handled using advanced numerical techniques based on a direct solving of Maxwell's equations via Method of Moments algorithms.

REFERENCES

[1] Development of radiation susceptibility models for systems.
J. SEILLE, R. LACRESSE, J.P. GRANGER, J.P. ESTIENNE - 3rd ESA European workshop on EMC and computational electromagnetics. Pisa 26-28 October 1993.

[2] Finite Element Method Applied to Modeling Crosstalk Problems on Printed Circuit Boards.
R. L.Khan and G. I. COSTACHE- IEEE Trans. on EMC,Vol. 31, No 1 Feb. 1989

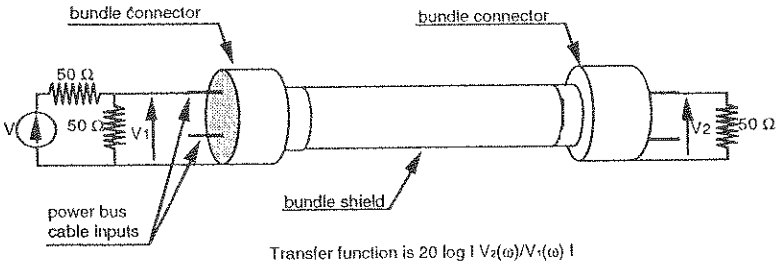

Fig 4.1 - Measurement schematic (one bundle case)

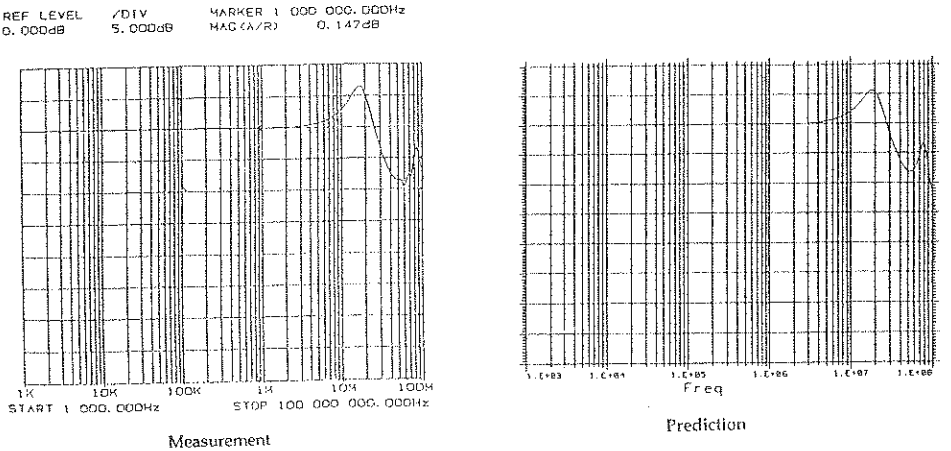

Fig 4.2 - Comparison of predicted and measured transfer functions
(umbilical connector + 1 metre-long bundle)

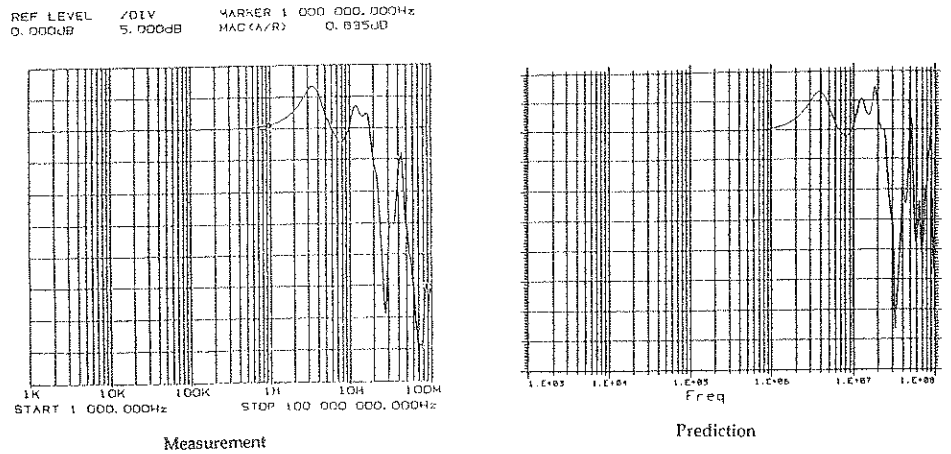

Fig 4.3 - Comparison between prediction and experimental data
for the whole power bus

GERAC
ELECTROMAGNETISME

THE SENIOR PARTNER IN ELECTROMAGNETIC COMPATIBILITY

ENGINEERING : SOME OF OUR REFERENCES

- major participation in lightning and HIRF certification of AIRBUS planes,
- development of EMC specifications for Channel Tunnel electronic equipment,
- substantial engagement in preparing the HA-EMP Hardening Guide (French DOD).

DIGITAL SIMULATIONS : SOME OF OUR PRODUCTS

➢ **3D codes :**
- structures in any material,
- perfect or not perfectly-conducting floor,
- non linear events,
- ...

➢ **2D codes**

➢ **Cable coupling codes**

➢ **Modelling protection items**

TESTS : SOME OF OUR FACILITIES

➢ **Standard tests** : The whole equipment to run the major standard tests in lightning, EMC, HA and LA-EMP.

➢ **Non standard tests :**

Double exponentials
- shape (tm/td) : from 5 ns / 200 ns to 5 µs / 150 ms
- amplitudes (Vco/Icc) : from 100 V / 20 A to 100 000 V / 10 A

Damped sinusoids :
- frequencies from 10 kHz to 100 MHz :
- amplitudes up to 10 000 V / 100 A

GERAC - BP 19 - 46500 GRAMAT - Tél. 65 38 79 23 - PARIS : (1) 41 07 51 51 - TOULOUSE : 61 39 93 75

TRANSIENT RESPONSE ANALYSIS OF GAS ARRESTERS

M. S. Sarto *
Department of Electrical Engineering
University of Rome "La Sapienza"
via Eudossiana 18 - 00184 Roma - Italy

J. L. ter Haseborg
Department of Measuring Engineering/EMC
Technical University Hamburg-Harburg
Schloßstr. 20 - 21071 Hamburg - Germany

1. Introduction

The suppression of transient overvoltages and electromagnetic overstresses in electrical and electronic equipment is an issue which arouses great interest in the Electromagnetic Compatibility field. In particular, the analysis of the transient response of nonlinear protective elements is a fundamental step in the design, optimization and coordination of protection apparatus. In this context, gas arresters are commonly used to prevent failures, permanent degradation and temporary malfunction of sensitive systems stressed by high energy surges such as lightning or electromagnetic pulses. Moreover, in low voltage signal transmission networks (M. D'AMORE, M. S. SARTO, Proc. ICEAA, pp. 85-88, Turin, Sept. 14-17, 1993), gas arresters generally realize the first stage or coarse protection of multi-stage nonlinear circuits because of their high energy capability.

In this paper, the transient response of gas arresters will be investigated with reference to the steepness and energy rate characterizing the transient overvoltage. The analysis will be carried out by defining an equivalent simulation model of the protection element and by using measured data to characterize its high-frequency behaviour.

2. Simulation Model and Application

The dynamic response of a gas arrester is described by defining the impulse spark-over voltage (V_{si}) which is the threshold voltage when the excitation is a voltage pulse with stepness greater than 100 V/s (H. SINGER, J. L. TER HASEBORG, F. WEITZE, H. GARBE, "Response of arresters and spark gaps at different impulse steepness", Proc. 5th Int. Symp. on High Voltage Engineering, Braunschweig, Aug. 24-28, 1987) and developing a suitable simulation model which takes into account the nonlinear time-varying behaviour (R. B. STANDLER, Protection of Electronic Circuits from Overvoltages, John Wiley & Sons, 1989, pp. 117-132).

Let consider the configuration shown in Fig.1 in which a gas arrester protects the sensitive load represented by R_{ou}. The surge is simulated by the pulse source $v_s(t)$ which supplies the device through the linear resistance R_s. The analysis of the transient response of the system, the energy transferred to the protection device and to the linear load can be obtained by solving the following nonlinear equation system:

$$v(t) = v_s(t) - R_s\, i_{in}(t) \quad , \quad v(t) = R_{ou}\, i_{ou}(t) \quad , \quad v(t) = f\{\, i(t)\,\} \quad , \quad i(t) = i_{in}(t) - i_{ou}(t) \qquad (1)$$

in which $i_{in}(t)$ and $i_{ou}(t)$ are the unknown currents flowing through R_s and R_{ou} respectively, $v(t)$ and $i(t)$ are the unknown voltage and current involving the gas arrester.

The dynamic characteristic of the protection device is described by the nonlinear monotonic function f in eq.(1) which represents the Toepler's law during the ignition of the gap

$$v(t) = \frac{k_T\, V_b\, i(t)}{E_b \int_{t_b}^{t} i(\tau)\, d\tau} \qquad (2)$$

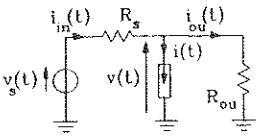

Fig.1

and the arc resistance when the gap is firing (H. GARBE, H. SINGER, Proc. 7th Int. Zurich Symp. on EMC, Zurich, March 9-11, 1987). In eq.(2) K_T is the Toepler's constant, E_b the critical electric field of the dielectric between the electrodes, V_b the actual breakdown voltage of the gas arrester corresponding to V_{si}, t_b the breakdown time.

The described simulation model is solved numerically by using the trapezoidal rule to integrate eq.(2) and by developing an iterative procedure which allows to compute the transient voltages and currents with good

accuracy. The computation algorithm is based on the following expressions:

$$v^k(t) = \frac{R_{ou}}{R_{ou} + R_s} \left[v_s(t) - R_s\, i^k(t) \right] \qquad v^k(t) = \frac{k_T\, V_b\, i^k(t)}{E_b \left[0.5\, \Delta t \left[i(t-\Delta t) + i^{k-1}(t) \right] + I(t-\Delta t) \right]} \tag{3}$$

where k is referred to the kth iteration, Δt is the time step and $I(t-\Delta t)$ is given by:

$$I(t-\Delta t) = \int_{t_b}^{t-\Delta t} i(\tau)\, d\tau \tag{4}$$

The proposed model is applied to the analysis of the transient response of the 230 V gas arrester in Fig.1 stressed by the voltage pulse $v_s(t)$ having maximum amplitude V_0 and time-constants τ_1, τ_2. The impulse spark-over voltage of the protection device depends on the steepness of the transient surge and can be deduced from the measured breakdown voltage - breakdown time curve represented in Fig.2. Fig.3 shows the transient currents flowing through R_s, R_{ou} in case of $R_s = R_{ou} = 50\ \Omega$, $V_0 = 8$ kV and $\tau_1 = 2$ ns, $\tau_2 = 250$ ns or $\tau_1 = 1.67$ ns, $\tau_2 = 25$ ns; the breakdown voltage of the protection element is assumed to be $V_b = 2.5$ kV or $V_b = 2$ kV, respectively. The energy transferred to the gas arrester and to the linear load is represented in Fig.4 for a 2 / 250 ns voltage pulse.

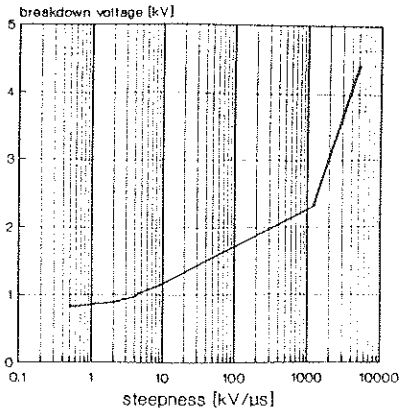

Fig.2

Figs.5a and 5b show the experimental set-up and the measured currents $i_{in}(t)$, $i_{ou}(t)$ respectively. Let notice that there is a good agreement between computed and experimental results. For instance, both Figs.3 and 5b show a peak of the current $i_{in}(t)$ when the gas arrester discharges; the following oscillations of $i_{in}(t)$ in Fig.5b cannot be observed in Fig.3 because they are due to the parasite inductances and capacitances of the real configuration which have not been taken into account in the modelling.

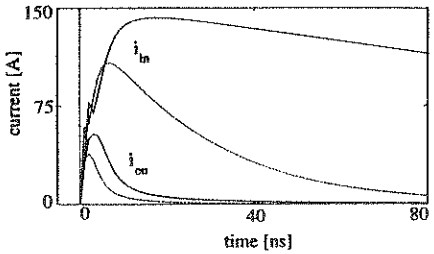

Fig.3 - Currents $i_{in}(t)$ and $i_{ou}(t)$ in case of a 2 / 250 ns (—) and 1.67 / 25 ns (---) pulse.

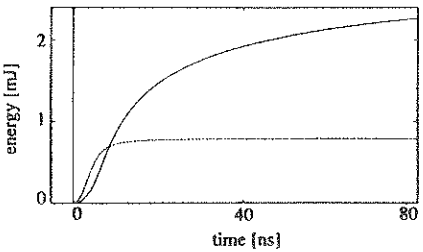

Fig.4 - Energy transferred to the gas arrester (—) and to R_{ou} (---) in case of a 2 / 250 ns pulse.

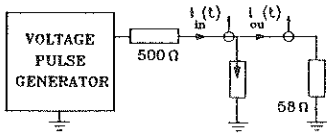

(a)

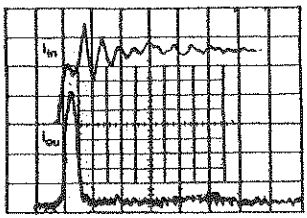

(b)

Fig.5 - Experimental set-up (a) and measured currents $i_{in}(t)$ (20 A/div - 10 ns/div), $i_{ou}(t)$ (10 A/div - 10 ns/div) (b).

SPICE Model of Excited Transmission Lines with Nonlinear Loads

S. Celozzi* M. Feliziani* K. Borgeest**

* Dept. of Electrical Eng., Univ. of Rome "La Sapienza", Via Eudossiana 18, 00184 Rome, Italy
** Dept. of Measurement Eng., Tech. Univ. of Hamburg-Harburg, Harbirger Schloss-strasse 20, 2100 Hamburg 90, Germany

1. Introduction

The use of SPICE code is illustrated to analyze EMC problems of field-to-wire coupling in presence of nonlinear loads. The transmission line equations with distributed voltage sources are analytically solved in the time domain for exponential waveforms of the incident electric field, so that the interaction with EMP, LEMP and ESD can be easily modeled. Overvoltage nonlinear protection devices, as sparkgaps and varistors, are also considered by means of specifically-designed equivalent circuits. SPICE implementation is illustrated in the solution of the coupling between an EMP plane wave field and a lossless wire terminated on nonlinear protection devices above a ground plane.

2. Lossless Transmission Line with Distributed Sources

Considering the configuration shown in Fig.1, wave propagation in terms of the scattered voltage $v^s(z,t)$ and the total current $i(z,t)$ is given by [1-2]:

$$\frac{\partial v^s(z,t)}{\partial z} = - L \frac{\partial i(z,t)}{\partial t} + E_z^i(z,t) \tag{1a}$$

$$\frac{\partial i(z,t)}{\partial z} = - C \frac{\partial v^s(z,t)}{\partial t} \tag{1b}$$

where L and C are the p.u.l. line parameters, $E_z^i(z,t)$ is the distributed voltage source due to the coupling with the incident field. After some mathematical manipulations of (1), the scattered voltages at the terminal ends of the transmission line are given by:

$$v^s(0,t) = Z_c\, i(0,t) + v^s(l,t-T) - Z_c\, i(l,t-T) + 2\, E^{s-}(0,t) \tag{2a}$$

$$v^s(l,t) = - Z_c\, i(l,t) + v^s(0,t-T) + Z_c\, i(0,t-T) + 2\, E^{s+}(l,t) \tag{2b}$$

where $T=l/c$ is the line transit time, l the length of the line and c the free space velocity. $E^{s+}(l,t)$ and $E^{s-}(0,t)$ are obtained by integrating the distributed voltage sources along the line. For double exponential waveforms of the incident electric field, such as those occurring in EMP and ESD studies, closed-form expressions can be obtained [1].

The total voltages $v(0,t)$ and $v(l,t)$ at both the ends of the transmission line are given by:

$$v(0,t) = v^s(0,t) + v^i(0,t) \tag{3a}$$

$$v(l,t) = v^s(l,t) + v^i(l,t) \tag{3b}$$

being $v^i(0,t)$ and $v^i(l,t)$ the incident voltages.

Equations (2) and (3) allow to model the coupling between the conductor and the external field by means of the equivalent lumped circuit shown in Fig.2.

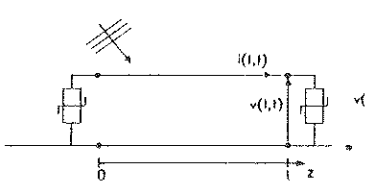

Fig.1 - Examined configuration

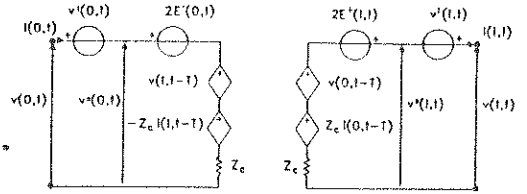

Fig.2 - SPICE equivalent circuit

2. Nonlinear Loads

a) Sparkgaps

If the transient behavior needs to be accurately described, the arc resistance R(t) can be modeled by Toepler's equation [3]:

$$R(t) = k / \int_0^t i_a(t)\, dt \qquad (4)$$

being k the Toepler constant and $i_a(t)$ the arc current. An integrator can be realized by a controlled current source loading a capacitance. The voltage on the capacitance controls the time-dependent resistance. There are several ways to realize time-dependent resistances, i.e. a controlled switch, a MOSFET and a controlled current source, but some of them cause great numerical problems. The use of a controlled current source is the most suitable method.

b) Varistors

The behavior of a varistor can be described by

$$i_V(t) = \alpha\, v_V(t)^{\beta} \qquad (5)$$

where $v_V(t)$ and $i_V(t)$ are the varistor voltage and current, α and β known coefficients. This formula can be implemented in a SPICE code by means of a controlled current source.

References

[1] S. Celozzi, M. Feliziani, *"On the exact time-domain solution of lossless field-excited transmission lines equations"*, submitted for publication.

[2] S. Celozzi, M. Feliziani, "FDTD analysis of the interaction between an EM field and a lossy shielded cable", Proc. of 10th EMC Zurich Symposium, March 9-11, 1993, Zurich, Switzerland.

[3] S.A. Boggs, F.Y. Chu, N. Fujimoto, A. Krenicky, A. Plessl, D. Schlicht, "Disconnect switch induced transients and trapped charge in gas-insulated substations", *IEEE Trans. on PAS*, Vol. Pas-101, No. 10, Oct. 1982.

SIMULATING THE FREQUENCY RESPONSE OF NON-LINEAR PROTECTION CIRCUITS WITH SPICE

K. Borgeest*, J.L. ter Haseborg
Technical University Hamburg-Harburg
Department of measurement engineering/EMC
Harburger Schlosstrasse 20
21071 Hamburg

F. Wolf
C. Plath GmbH
Company for Nautical Electronics
Gotenstrasse 18
20097 Hamburg

Nonlinear protection circuits with one or more stages are necessary in order to suppress steep interfering transients. These circuits are expected on the one hand to protect the following circuitry from failure or damage, on the other hand it should ideally be transparent for the passing signals, particularly in the RF-range. The development of such circuits requires expensive tests of both aspects. One can cut down development costs and time by computer simulation of these circuits, which of course can't substitute tests totally. The easiness with which modifications can be tried on a computer makes a more sophisticated design possible. For these simulations the widely used circuit analysis software SPICE has proven its suitability.

Here simulation results with a dual-stage protection circuit are presented and discussed. The method described here can also be applied to circuits with more stages. The circuit is shown in fig 1. Only the frequency domain and small signals are considered. Under these conditions the spark gap can be represented by its capacitance. The diodes are represented by a self designed model which realizes the voltage dependent junction capacitance characteristics by interpolation of measured values. The parallel nonlinear ohmic resistance can be neglected, because with signal amplitudes of a few millivolt the real component of current through an avalanche diode is in the range of some pico-ampere. The serial resistance caused by the leads and the semiconductor material has to be considered, because it amounts up to 10 Ω. Hence the circuit is regarded linear here, the diode model can be simplified drastically as a series circuit of the resistance R_d and a constant capacitance C_d. Fig. 2 shows the RF equivalent circuit.

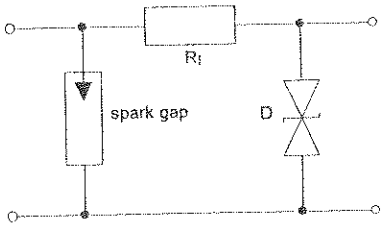

Figure 1: The examined nonlinear protection circuit

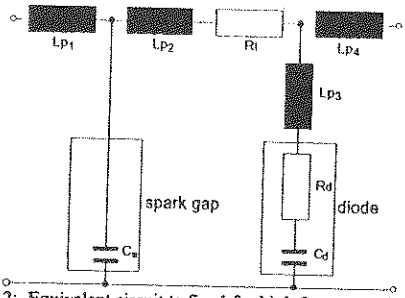

Fig. 2: Equivalent circuit to fig. 1 for high frequency signals

Investigated circuit parameters were the scattering parameters S_{11} (input reflection factor) and S_{21} (ratio of output power and available input power). Whereas the first one has to be close to 0, the second one has to be close to 1. Theoretically both should be constant, which in reality is impossible. Following techniques are compared:

1. Measurement with a network analyzer using an S-parameter set,
2. Coarse SPICE simulation considering concentrated elements only as in fig. 1,
3. Precise SPICE simulation considering additionally parasitic effects due to wiring inside the circuit (especially inductance as in fig. 2).

A good conformity between measurement and the precise simulation can be shown. The simulation results without parasitic effects are quite different from the measurements. Therefore parasitic effects must not be neglected in any case. The inductances proved to be most important. There is only a small influence of resistance, capacitance and conductance.

A practical problem is the correct estimation of the equivalent parameters. A too large effort to get them would counteract the simulation aim to save time. So an efficient method combining quickness with a sufficient precision is necessary.

Determining the diode parameters is quite simple. In linear circuits the bias-free C_d can be considered voltage independent. It is usually specified by the producer and can be found in data sheets. Otherwise it can be obtained together with R_d by a measurement of the complex impedance, e.g. with a vector impedance-meter. Neglecting the skin effect, R_d can also be assumed constant. The internal inductance should be handled like a part of the wiring inductance L_{p3}.

The spark gap capacitance is another parameter which can be taken from a data sheet or measured easily.

The most difficult problem is the estimation of the parasitic wire inductances $L_{p1}...L_{p4}$. This is a central problem which has to be considered furthermore, so some approaches and the obtained results will be presented.

DETERMINATION OF THE SHIELDING EFFICIENCY OF CABLE ASSEMBLIES FROM A COMBINED APPROACH THEORY-EXPERIMENT

H. RANAIVOARISON, L. KONE, B. DEMOULIN, and P. DEGAUQUE*
Université des Sciences et Technologies de LILLE
Laboratoire de Radiopropagation et Electronique
UA CNRS 837
Bâtiment P3
59655 VILLENEUVE D'ASCQ Cédex - FRANCE

H. TATER, D. HANIA
LABINAL-DSA
17 rue de Clichy
93400 SAINT OUEN - FRANCE

In many problems dealing with the characterization of the efficiency of shielded lines between electronic systems, usually called "harness", preliminary measurements are usually made by putting the harness at a given height above a ground plane and by injecting a disturbing current at a given point of the structure. However it appears in many cases that the experimental results cannot be easily extrapolate from one case to another one and thus the global interpretation is difficult. Some examples will illustrate this fact. In this paper, we successively consider the coupling in the various zones of the cable assembly in order to define intrinsic transfer impedances which can then be included in a global numerical model to predict the voltages when such a cable assembly is illuminated by a disturbing wave. Usually most of the measurements are carried out in the frequency domain, up to 100 MHz or few hundred MHz but the results can be extropolated up to 1 or 2 GHz, i.e. up to the limit of validity of the quasi T.E.M. approximation. In the numerical model, the current flowing on the shield can be either uniformly distributed or propagation effects with various boundary conditions at the ends of the cable under test can be taken into account. A typical cable assembly can be represented, as described in Figure 1, by various lumped or distributed elements contributing to the penetration of the energy inside the structure. The region 1 corresponds to the cable shield, 2 to the connectors and 3 to the connection between the cable shield and the connectors. To simplify the presentation, let us consider in this summary the simple case of a short cable having a length much smaller than the wavelength. The voltage V_c appearing at the end of the cable assembly can be easily related to the current I_p flowing along the shield and on the outer part of the connectors :

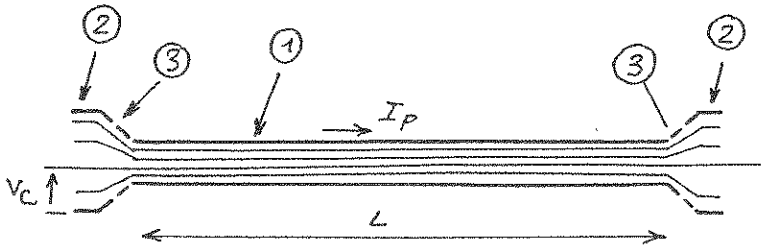

Figure 1 : Typical cable assembly.

$$V_c = \frac{1}{2} Z_{t1} L I_p + Z_{t2} I_p + Z_{t3} I_p \qquad (1)$$

This expression is valid only if the inner conductor is connected at both ends on identical loads. Furthermore Z_{t1}, Z_{t2} and Z_{t3} characterize the transfert impedance of the shield (Ω/m), of the connectors (Ω) and of the link between the cable shield and the connectors (Ω) respectively. From experimental data, it appears that these terms can be put in the following form :

$$Z_{t3} = R_3 + j L_{t3} \omega \qquad (2)$$

where R_3 is an equivalent resistance,

$$Z_{t2} = Z_{td2} + j L_{t2} \omega \qquad (3)$$

L_{t2} is a transfer inductance corresponding to the increase of Z_{t2} linearly with frequency while Z_{td2} is a transfer impedance associated with the penetration through homogeneous cylindrical shields. The model used to describe the behavior of the cable shield is more complicated and the following formula is proposed as a starting point :

$$Z_{t1} = Z_{td1} \pm k_1 \sqrt{\omega} \exp(-3j\pi/4) \pm j L_{t1} \omega \qquad (4)$$

The various coefficients allow to take the coverage ratio and the weave angle into account. The signs + or - are determined from a preliminary experiment in time domain, the cable under test being excited by a short pulse of current. Then, the precise values of k_1 and L_{t1} are deduced from measurements in frequency domain and in a wide frequency band. This paper will present the experimental results showing the relative influence of the connectors and of the cable shield on the inner voltages. Furthermore both in the low frequency range and at high frequency, when propagation effects are important, we will point out the influence of the cable length since all these effects do not add in phase.

TRANSPARENT CONDUCTING THIN FILMS FOR RF HARDENING

Glenn L. Brown
Resource Engineering And Planning
El Paso, Texas 79912

*Felicia Hereford-Kaigler
U. S. Army Missile Command
Redstone Arsenal, Alabama 35898

Benjamin L. Lowe and Bryan L. Woodham
Engineering Systems and Planning
Huntsville, Alabama 35816

Investigations of the effects of electromagnetic fields on guided missiles and smart munitions have demonstrated that modulated RF fields can disrupt or degrade the performance of ultraviolet (UV), visible, infrared (IR), and millimeter wave (mmW) sensor systems. The major port of entry by which an external electromagnetic field penetrates into the interior of a tactical guided missile to disrupt missile functions is the missile dome. The MICOM CM/CCM Center has therefor developed techniques for producing missile domes, and aperture windows, which shield against RF fields but are transparent in the frequency band or bands over which the seeker is designed to operate. The hardening techniques are applicable to all types of windows which act as ports of entry for RF fields.

The hardening approach taken by the MICOM CM/CCM Center is to install thin film electromagnetic filters on the aperture window of the sensor to be protected. The filters are deposited directly on the window. Filters have been fabricated and tested for use with both single mode and dual mode (two band) sensor systems. Filters can now be deposited with selective transmittance over one or two frequency bands selectable from ultraviolet to millimeter wavelengths. Coating materials range from single layer semiconductor materials to dielectric stacks. The coatings can be applied to plastic, glass, ceramics and crystals with flat or curved surfaces. Typical window transmittance losses in the filter pass bands are 5% to 20%.

The technique for creating a dual bandpass filter is to coat the window with a conducting tri-layer film which is transparent over the shorter wavelength band and then photo-etch or ion-etch holes in the film to create a frequency selective surface (FSS) which is transparent over the longer wavelength band. The center of the FSS band is adjusted by varying the distance between the holes and the width of the

bandpass is determined by the hole size. Hardened domes and windows have been produced for UV/IR, NIR/IR, and IR/mmW sensor systems. Transmittance curves are presented for dual bandpass filters.

An extensive test program has been conducted at the MICOM CM/CCM Center to measure the shielding effectiveness of conducting thin films over the frequency range from .1 to 10 GHz. Measurements are made using a generic missile which has the external dimensions of the Copperhead missile. An electric field probe is mounted inside the nose cone. The signal from the probe is rectified, amplified, and input to a fiber optics transmitter located inside the missile. An air driven generator supplies the internal missile power. A fiber optics link transmits the probe signal to an external receiver. The missile is positioned on a rotatable non-reflecting pedestal in an anechoic chamber. The missile is illuminated with a modulated RF field and the probe signal recorded as a function of the incidence angle of the field. The probe signal is recorded first with a standard transparent dome on the missile and then with a hardened dome installed.

Shielding effectiveness data have been acquired for a large number of tranparent conducting films with various sheet resistances. The data shows that shielding effectiveness varies with sheet resistance exactly as predicted by plane wave theory. Photo-etching holes in the film to create a frequency selective surface has no measurable effect on shielding effectiveness. Films with sheet resistances of 10 ohms per square provide of the order of 30 dB RF hardening. Measurements made on an outside RF range at power densities as high as 140 W/cm^2 show no change in filter performance. Thin film electromagnetic filters provide protection from RF, HPM, and Ultra Wide Band environments.

DISPERSION AND ACCURACY IN FINITE DIFFERENCE CALCULATIONS

Jim Gilbert
Metatech Corporation
Goleta, California

Many calculations are best performed using time domain finite difference techniques instead of frequency domain techniques. These include situations where the conductivity of materials are time dependent, such as calculations of radiation coupling to systems, or when the properties of materials are nonlinear, such as the calculation of coupling to long lines where breakdown is important. The principal difficulties that the use of time domain finite difference introduce are the need for absorptive outer boundary conditions and dispersion due to the use of the finite difference approximation to Maxwell's equations. This paper discusses both of these effects in one and three dimensional finite difference techniques. The one dimensional methods are important in that they are commonly used for the calculation of EMP coupling to long lines.

The analysis of dispersive effects on an evenly spaced finite difference mesh is performed by considering an initial value problem where introduce the basis functions

$$e^{ik_x x + ik_y y + ik_z z - i\omega t}$$

We then use the finite difference equations to determine ω as a function of k and then determine the group velocity $d\omega / dk$. The actual group velocity depends on the specific finite difference method employed - for the explicit Yee method in one dimension, where the electric and magnetic fields are interleaved, the group velocity is

$$\frac{d\omega}{dk} = c\frac{\cos(k\Delta x/2)}{\cos(\omega\Delta t/2)}; \qquad \sin(\frac{\omega\Delta t}{2}) = \frac{c\,\Delta t}{\Delta x}\sin(\frac{k\Delta x}{2})$$

It should be noted that the frequency ω becomes complex when $c\Delta t > \Delta x$, and the Yee method becomes unstable. A useful representation of dispersion characteristics is to show the group velocity in a three dimensional surface plot for a specific time step and frequency. An example for the explicit Yee method for three dimensions is shown in figure 1.

Implicit techniques involve the inversion of matrices, but have the advantage that the time step can be taken to be arbitrarily large. For an alternating direction implicit technique, for example, the dispersion relation becomes

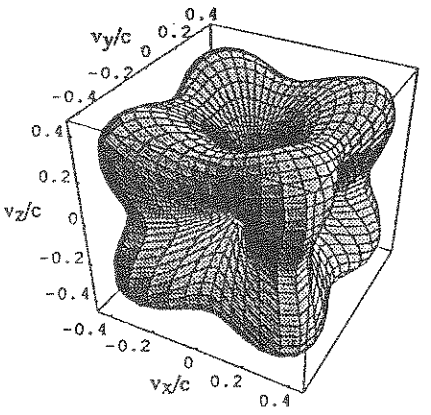

Figure 1. Group velocity of high frequency waves.

$$W^2 = \frac{X^2 + Y^2 + Z^2 + X^2Y^2 + Y^2Z^2 + Z^2X^2}{(1+X^2)(1+Y^2)(1+Z^2)}$$

$$X = \sin(\frac{k_x \Delta x}{2}); \qquad W = \frac{\Delta x}{c\Delta t}\sin(\frac{\omega \Delta t}{2})$$

which is seen to produce real values of ω for all values of k and is therefore unconditionally stable. The accuracy of the technique, however, falls for time steps much greater than $c\Delta t > \Delta x$. This paper will present the dispersion analysis for the following techniques in both vacuum and in a finitely conducting medium.

1. Explicit Yee method in one dimension.
2. Explicit Yee method in three dimensions.
3. Fully implicit technique in one dimension.
4. Fully implicit technique in three dimensions.
5. Alternating direction technique in three dimensions.

The presence of dispersion also affects the performance of outer boundary conditions - this occurs because many outer boundary conditions use the electric or magnetic fields one cell inside the mesh to determine the fields on the surface of the mesh by extrapolation. If the extrapolation process assumes that the fields propagate at the velocity of light, significant errors are made, and the outer boundary conditions is ineffective at high frequencies. An example of this is an outer boundary condition where the tangential electric field is assumed to fall as $1/r$ in retarded time from the center of the mesh. (This outer boundary has been

used in aircraft EMP simulations.) The reflection coefficient which is produced by dispersion is shown in figure 2.

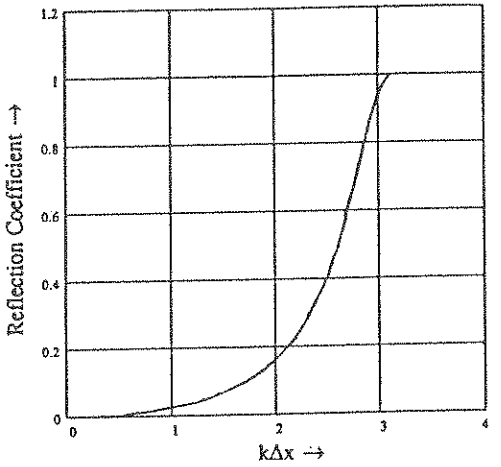

Figure 2. Reflection coefficient from extrapolation outer boundary.

This reflection depends on the spatial centering of the finite difference equations and on the type of extrapolation (electric field extrapolation, or impedance condition where the outer tangential electric field is obtained from the magnetic field 1/2 cell inside the mesh). Numerical examples of the effect of outer boundary conditions will be shown.

TIME DOMAIN IMPLEMENTATION OF FREQUENCY DEPENDENT MATERIALS IN FINITE DIFFERENCE CALCULATIONS

Dr. James R. Elliott
Electro Magnetic Applications, Inc.
P.O. Box 260263
Denver, CO 80226 USA
(303) 980-0070

Time domain finite difference modeling is a versatile and computationally efficient technique useful for many problems involving time varying electromagnetic fields and arbitrarily shaped objects. Historically, the technique has had limited ability to incorporate the frequency dependence of materials. If an analytic form is known for the frequency dependence of a material, it is possible to obtain a time domain representation by means of standard Fourier or LaPlace transform techniques. However, the implementation of the frequency dependence in the time domain gives rise to a convolution term which, in general, is very expensive to evaluate on a computer. Only a few particularly convenient frequency dependences have been usefully implemented in time domain finite difference codes.

Frequency dependence in electromagnetic problems can arise from several different mechanism and on different scales. In some objects, the frequency dependence of a material can be considered to be a bulk property due to local microscopic characteristics but insensitive to macroscopic dimensions. A simple example is the index of refraction of light traveling in a mono-atomic gas. The classical formulation of this results in the second order equation for as damped harmonic oscillator. Similar second order behavior is observed in dielectrics and lossy magnetic materials in addition to first order relaxation phenomena.

In other objects, there is no frequency dependence of any microscopic characteristic, but a frequency variation due to the over all dimensions of the object is observed. Simple examples of this type of behavior are the reflection and transmission coefficients for a thin dielectric layer. Conducting layers also exhibit a sharply decreasing transfer impedance at frequencies for which the layer thickness is greater than the skin depth in the material. This will be the primary example used in this paper. A transfer impedance, Z, can be defined by

$$\vec{E} = Z\,\vec{H} \qquad \text{Eq. 1}$$

where the frequency dependence is embedded in the quantity Z. It is possible to associate the frequency dependence with a hypothetical set of physical processes, similar to those discussed above. If we further restrict ourselves to a canonical form, say a first order relaxation, for the frequency dependence, E may be written as

$$\vec{E} = \vec{H} \sum_{i=1}^{N} Z_i \qquad \text{Eq. 2}$$

where

$$Z_i = \frac{\alpha_i}{1 - i\omega/(2\pi f_i)} \qquad \text{Eq. 3}$$

This canonical form chosen is causal, has an easy interpretation in terms of physical processes and has a convenient form for transformation to the time domain. If Eq. 1 is transformed to the time domain using Eq. 3, a finite difference representation is easily obtained.

To obtain the α_i and f_i parameters in Eq. 2, a fit to the known dependence of Z is performed. The results are then incorporated in the finite difference code. Figure 1 shows a transfer impedance with a strong frequency dependence. In Figure 2 the transmitted pulse resulting from the implementation of the transfer impedance algorithm just described is compared to the results from a fully gridded model. The agreement is quite good, corresponding to the accuracy of the fit for the frequency dependence of Z.

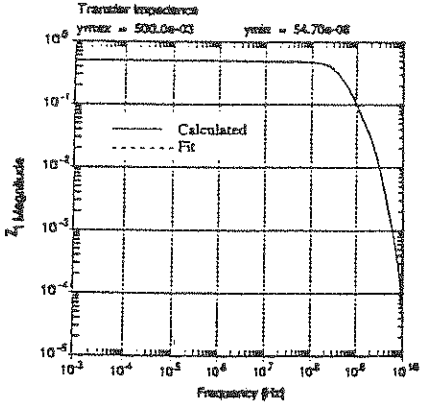

Figure 1 Comparison of the Calculated Fitted Frequency Dependence of the Magnitude of the Transfer Impedance

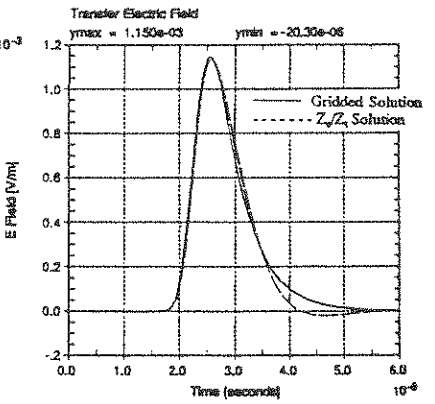

Figure 2 Time Domain Comparison of Second (Transfer) Surface Electric Fields as Computed by a Fully Gridded Finite Difference Code and by a Frequency Dependent Surface/Transfer Impedance Formalism in a Finite Difference Code

Study of TE_0 to Z Modes in Rectangular Dielectric Resonators by the Method of Finite Difference in Time-Domain

Terry K. C. Lo*, Albert K. Y. Lai
Dept. of Electronic Engineering, The Chinese University of Hong Kong

The numerical method of finite difference in time-domain (FDTD) (K. Umashankar & A. Taflove, IEEE Trans. on EMC-24, 397-405, 1982) has been applied, coupled with the fast Fourier Transform (FFT), to determine the resonant frequencies of the TE_0 to z modes of free rectangular dielectric resonators with different dielectric constant ε_r. Good agreement with Okaya's first order approximation is obtained. This method can be used to compute the field quantities in different modes or a range of frequencies in a single computation process and thus allows faster computation of the field distribution on the frequency spectrum. Assume at t = 0, a Gaussian pulse source is started at the center of the rectangular dielectric resonator as shown in Fig. 1.

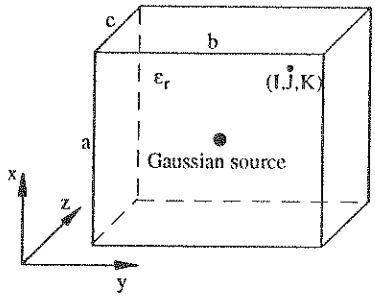

Fig 1 Rectangular dielectric resonator

The width of the Gaussian pulse source must be set carefully so as to include a wide range of frequencies. The whole geometry can be covered by the usual rectangular finite difference grid. The ratio of the spatial and temporal increment should be chosen to satisfy the stability criterion. In accordance with the discretized Maxwell's curl equations, the field components can be computed through the Yee's time-stepping algorithm. Mur's second order absorbing boundary condition (G. Mur, IEEE Trans. on EMC-23, 377-382, 1981) has been employed to truncate the computational domain. A spatial point (I, J, K) is chosen inside the region of rectangular dielectric resonator on the finite difference grid and the field variation $\{\phi^n (I, J, K)\}$ at successive time step, n = 0, ... , N-1, is obtained. The field distribution on the frequency spectrum can be found by applying the FFT to the time series $\{\phi^n (I, J, K)\}$. Since the magnitude of the field quantities will be maximum when resonance occurs, the frequency values at which the magnitude of $\Phi^u = \mathcal{F}\{\phi^n (I, J, K)\}$, where u = 0, 1, ... , N/2, acquires a local absolute maximum correspond to the resonant frequencies at different modes and the corresponding harmonics.

One of the frequency spectra obtained after the FFT is shown in Fig 2. The maxima of these spectra corresponding to different dielectric resonators with ε_r ranging from 5.0 to 20.0 have been identified and compared with the first order approximation in (A. Okaya & L. F. Barash Proc. of IRE, 2081-2092, 1962). In Fig 3, the relation between the resonant frequencies and ε_r for 3 modes have been shown. The resonant frequencies decreases as ε_r increases in these modes. The value of Δf used is 84.514 MHz and Δt is 2.889 ps. The size of the resonator is 3.0 cm times 3.0 cm times 1.5 cm.

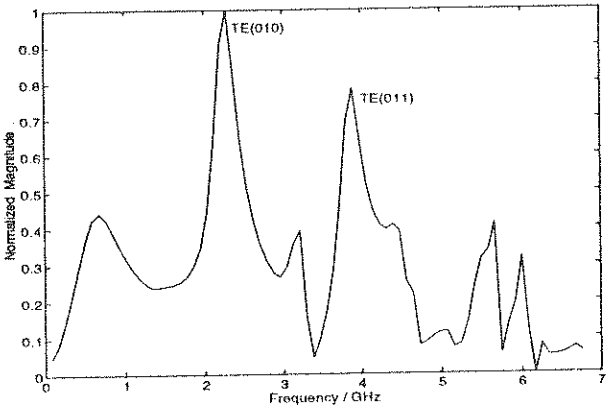

Fig 2 Frequency spectrum of E_y with $\varepsilon_r = 8.0$

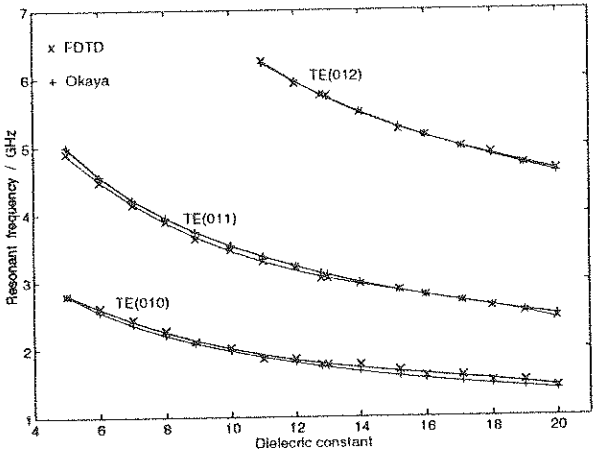

Fig 3 Comparison between data from FDTD and Okaya's 1st order approximation

High order absorbing boundary condition for Maxwell equations in free space and lossy media.

R VEZINET *
Délégation Générale pour l'Armement
Dir. des Recherches, Etudes et Techniques
Centre d'Etudes de Gramat
46500 GRAMAT

F. COLLINO - P. JOLY
Institut National de Recherches en
Informatique et en Automatique
Domaine de Voluceau - Rocquencourt
BP 105 78153 LE CHESNAY CEDEX

ABSTRACT

A new Absorbing Boundary Condition (ABC) for Maxwell equations in free space and lossy media has been developed; it makes use of a double space and time high order approximation of the dissipative one way wave equation. A new condition for the corner is given. Comparative results with classical second order ABC demonstrates the efficiency of the new ABC for 2D and 3D FDTD problems.

INTRODUCTION

Time domain finite difference method has become a classical tool to investigate electromagnetic coupling in EMC, EMP and lightning areas. Simulation of "open problems" requires the use of Absorbing Boundary Conditions (ABC). The most popular, for cartesian problems, involves the approximation of the "one way" wave equation. The accuracy of the numerical solution and, on the other hand, the complexity of the formalism are strongly dependent of the order of the approximation witch is usually limited to two for most of the 3D available codes. The FDTD code GORF at CEG uses the two order Joly and Mercier ABC for free space. The treatment of devices located near or into a lossy soil and the needing of higher accuracy with the aim to reduce computational volumes have justified the development of a new high order ABC and his generalization to lossy media (F. COLLINO INRIA Research Report # 1790 November 1992),(R. VEZINET Centre d'Etudes de Gramat Technical Note # T 93-33/CEG/AE June 1993).

APPROXIMATION OF THE GENERALISED ONE WAY WAVE EQUATION

The one way wave equation for lossy media ($\sigma>0$) which absorbs perfectively the outgoing waves traveling to the y^+ direction in the 2D space $\{(x,y)\in\Re^2\}$ takes the familiar form:

$$\frac{\partial U}{\partial y}=\frac{i\omega}{c}GU \quad \text{with} \quad G=\sqrt{1-\eta} \quad \text{and} \quad \eta=\left(\frac{kx\,c}{\omega}\right)^2-\frac{i\sigma}{\omega\varepsilon} \qquad (1)$$

The wavenumber in the x direction, kx, satisfies the relation $kx=\omega/c \sin\theta$ with θ angle of propagation respect to the y direction.

Time and space localization of the pseudo differential operator G is provided by a rational fractions expansion in the form:

$$G \simeq 1-\sum_{k=1}^{nk}\frac{\beta_k\eta}{1-\alpha_k\eta} \qquad (2)$$

which was initially introduced by Lindman for the approximation of 1/G for $\sigma=0$ (free space).

Literal expression for α_k and β_k can be derived to obtain an equivalent Pade expansion of (2) but it's more efficient to use optimum coefficients which minimize the 2D reflection coefficient modulus versus frequency and angle of incidence:

$$(\alpha_k,\beta_k) \quad \text{minimising} \quad \sum_{l=1}^{l_{max}}\sum_{j=1}^{j_{max}}|R_{2D}(f_l,\theta_j)|^2 \qquad (3)$$

$$\text{with:} \quad R_{2D}=\frac{\cos\theta\sqrt{1+s}-A}{\cos\theta\sqrt{1+s}+A}, \quad A=1-\sum_{k=1}^{nk}\frac{\beta_k(1-\cos^2\theta(1+s))}{1-\alpha_k(1-\cos^2\theta(1+s))} \quad \text{and} \quad s=\frac{j\sigma}{\omega\epsilon} \qquad (4)$$

ABC FOR THE 2D PROBLEM (Side Y+)

A friendly form of the ABC allowing discretization is obtained by using auxiliary functions defined on the boundary:

$$\varphi_{ky}=\frac{\eta}{1-\alpha_k\eta}U \qquad (5)$$

where U represent the E or H boundary tangential field component under investigation. The ABC takes the form of a set of nk+1 equations :

$$\frac{1}{c}\frac{\partial^2\varphi_{ky}}{\partial t^2}+c\sigma\mu\frac{\partial}{\partial t}(\alpha_k\varphi_{ky}+U)-c\frac{\partial^2}{\partial x^2}(\alpha_k\varphi_{ky}+U)=0 \qquad (6)$$

$$\frac{\partial U}{\partial y}=-\frac{1}{c}\frac{\partial U}{\partial t}+\sum_{k=1}^{nk}\frac{\beta_k}{c}\frac{\partial\varphi_{ky}}{\partial t} \qquad (7)$$

CORNER CONDITION

A new corner condition has been developed by considering a family of particular solutions satisfying the wave equation, the ABC of the two sides and some regularity criterium. Using 2 nk auxiliary functions:

$$\Psi_{kx}=\alpha_k\varphi_{kx}+U \quad \text{and} \quad \Psi_{ky}=\alpha_k\varphi_{ky}+U \qquad (8)$$

and 2 nk² double indexed auxiliary functions (for $\sigma>0$):

$$\Psi^x_{ml} \quad \text{and} \quad \Psi^y_{ml}$$

the corner condition takes the form

$$\frac{\partial\Psi_{1y}}{\partial x}+\left[1+\sum_{m=1}^{nk}\frac{\beta_m}{\alpha_m}\right]\frac{\partial\Psi_{1y}}{\partial t}-\sum_{m=1}^{nk}\frac{\partial\Psi_{1y}}{\partial t}-\sum_{m=1}^{nk}\frac{\beta_m\alpha_l}{\alpha_m}\frac{\partial\Psi^y_{ml}}{\partial t}-\sum_{m=1}^{nk}\beta_m\frac{\partial\Psi^x_{lm}}{\partial t}=0 \qquad (9)$$

$$\frac{\partial\Psi_{1y}}{\partial x}=(\alpha_l+\alpha_m-\alpha_l\alpha_m)\frac{\partial\Psi^y_{ml}}{\partial t}+\alpha_l\alpha_m\sigma\Psi^y_{ml} \qquad (10)$$

NUMERICAL RESULTS

Numerical 2D FDTD tests have been done with a five terms expansion (nk=5) making use of optimum coefficients ; they reveal a perfect absorption until 70 degrees in free space and 60 degrees for a typical lossy soil.

As examples we give free space results compared to exact and second order ABC results. First we simulate a punctual source (Bell NEMP standard double exponential) located at the center of a square computational domain (18x18 cells) (Fig.1) and we observe the field at the center of one of the absorbing sides (Fig. 2).

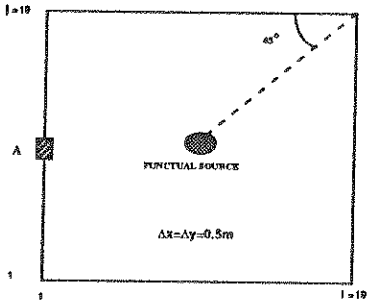

Fig. 1 - 2D Punctual source test geometry

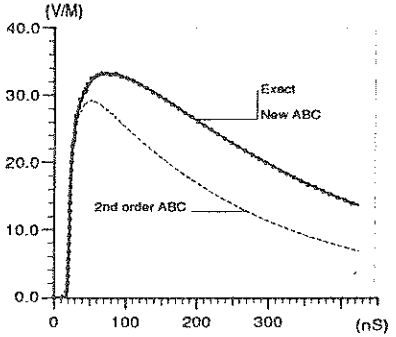

Fig. 2 - Ez field at test point A

The second test concerns the simulation of the coupling between a plane wave (Bell NEMP) and a rectangular metallic object (8x1 meter) for two different computational domain sizes corresponding to 65 and 70 degrees maximum incidence angles (Fig. 3). Results for H field component at the extremity of the object confirm the very good efficiency of the new ABC.

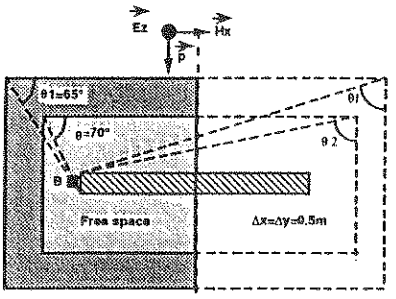

Fig. 3 - 2D Plane wave coupling test geometry

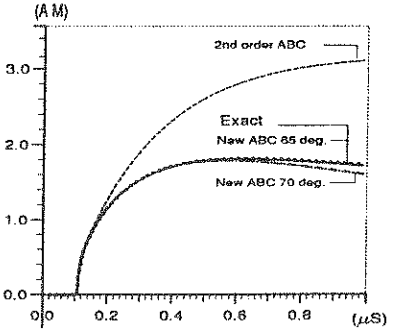

Fig. 4 - Hy field at test point B

The generalization to 3D has been done (F. COLLINO INRIA Research Report # 1991 July 1993) and the the implementation in GORF is in progress ; comparative results will be shown during the presentation.

EXTENSION OF THIN SLOT FORMALISM FOR SLOTS OF COMPLICATED SHAPE

*I.B.Baholdin, N.I.Kozlov, A.I.Kondrat'eva
Keldysh Institute of Applied Mathematics
Russian Federation Acad. of Sciences

We use three-dimensional finite difference time domain method of solution of Maxwell equations. Our program complex permits to do calculations with one or several perfectly conductive solids of complicated shape placed in calculation volume. It contains main program and programs for data files preparation which describe these solids as constructions made of rectangles and struts. This program complex has showed its effectiveness in many practical calculations of electromagnetic pulse interaction with aircraft, sphere, cylinder, box, system of boxes.

In some cases it is necessary to calculate penetration of electromagnetic waves through narrow slots. Basic algorithm permits to solve this problem only if the width of the slot α is one or several spatial steps $\alpha \approx n\Delta$. Increasing time and memory needed for calculations we can solve this problem for a slot of arbitrary width. But it is more effective to use thin slot formalism (J.GILBERT & R.HOLLAND IEEE Trans. on Nucl. Sci. 28,6,4269-4274,1981). If $\alpha << \Delta$ we can introduce artificial electrophisical constants ε_r and μ_r for internal points of the slot. All other calculations must be fulfilled as if $\alpha = \Delta$.

Let us assume the slot to lie in YZ plane and continue in Z direction

$$\varepsilon_r = \Delta y / \Delta x \cdot Q / V \quad , \quad \mu_r = 1/\varepsilon_r$$

where Q is charge per unit of length of the strip between the edge of the slot and boundary of the cell, V is potential through the slot. Quantity Q/V was called capacitance in cell. It can be calculated as capacitance per unit of length between two strips on the plane (C.D.TURNER & L.D.BACON IEEE Trans. on Electromagnetic Comp. 30,4,523-528,1988)

$$C_{in-c} = K\left(\left(1 - \alpha^2/\Delta y^2\right)^{1/2}\right)/K(\alpha/\Delta y) = F(\alpha/\Delta y)$$

where K is full elliptic integral.

Earlier explorers used this method only for isolated slots on plane surfaces. In basic program complex we have introduced subroutines that permit us to use thin slot formalism for system of arbitrary intersecting slots. Slots on curved surfaces which are simulated by a system of rectangles were described as systems of intersecting strait line slots. We used this method for practical

calculations for circular slot between two cylindrical surfaces.

We also extended thin slot formalism for the case of two surfaces which are perpendicular to each other. Locally one of these surfaces can be treated as infinite plane (surface 1) the other as half of a plane (surface 2). Let us assume 1 to be XY plane, 2 half of YZ plane. Let us continue all fields from $y>0$ to $y<0$ region so that $\bar{E}(-y)=-\bar{E}(y)$, $\bar{H}(-y)=\bar{H}(y)$. Half of the plane YZ, $y<0$ is surface 3. There are narrow slots between surfaces 1,2 and 2,3. We have derived two modifications of thin slot formalism.

1. We can treat the system of surfaces 1,2,3 as a system of two equal capacitances

$$C_{1-3} = 1/2\, C_{1-2} = 1/2\, C_{2-3} = F(2a/2\Delta y) = F(a/\Delta y)$$

We must increase ε_r two times and fulfill all calculations as usual. Calculation of electromagnetic pulse interaction with the cylinder without bottom surface lifted at low altitude over the plane has shown a good agreement with results obtained by increasing number of cells.

2. In this modification the centers of cells lie on plane 1. Modification 1 was derived assuming that nodes of cells lie on plane 1. We have used "cross" numerical method in which $\bar{H}$ components are corresponding to centers of sides of the cell, $\bar{E}$ components are corresponding to centers of edges of the cell. Boundary condition

$$\bar{E}_{tan}(0) = 0$$

on plane 1 was replaced by condition

$$\bar{E}^{-}_{tan}(-\Delta y/2) = -\bar{E}_{tan}(\Delta y/2)$$

where index - denotes imaginary boundary quantity. The width of the slot must be increased two times. All other calculations must be fulfilled as usual. This modification is more proofed mathematically but it needs some changes in basic program complex.

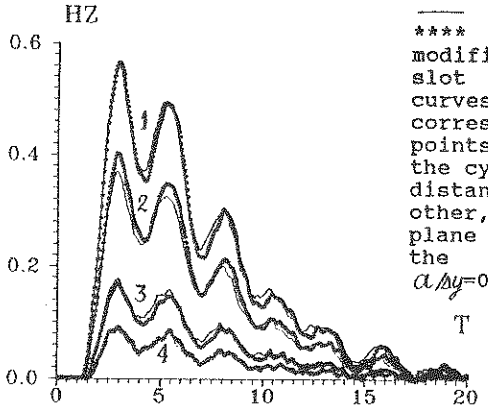

—— basic method, **** first modification of thin slot formalism, curves 1,2,3,4 are corresponding to four points on the axis of the cylinder at equal distances from each other, 1 is near the plane 1, 4 is near the top surface, $a/\Delta y=0.5$, $a=0.04$

ENVIRONMENT AND CIRCUIT MODEL FOR CAPACITOR-BASED RAIL GUN

I. Kohlberg*
Kohlberg Associates, Inc.
5375 Duke Street, Unit 1603
Alexandria, VA 22304

W.O. Coburn
US ARL (AMSRL-WT-ND)
2800 Powder Mill Road
Adelphi, MD 20783

Electromagnetic launchers such as rail guns (see Fig. 1) are relatively new devices for generating hypervelocity projectiles. As indicated in this figure, the projectile is accelerated between the rails by a "$\vec{I}x\vec{B}$" force until it exits at the muzzle. The magnetic field, $\vec{B}$, is created by the current in the rails, and the $\vec{I}$ is the loop current flowing through the rails and armature. Although the acceleration issues concerning these devices have been studied for some time, the electromagnetic compatability (EMC) issues related to their integration into a system remain to be examined. This paper addresses the salient features of the electromagnetic enivronment under live-fire conditions, including muzzle arcing and switching transients. It includes a discussion of the instrumentation techniques used to measure the electric and magnetic fields, the representation and modeling of this inherently nonlinear device as a circuit element, and a comparison of theoretical predictions of the fields with selected experimental results.

In the absence of friction the equation of motion of the armature is

$$m\frac{d^2x}{dt^2} = \frac{l}{2}L_e'I^2 \quad , \tag{1}$$

where m is the combined armature-plus-projectile mass, x is the position of the armature, and L_e' is a theoretically derived "effective" inductance per unit length which takes into account the transmission line inductance per unit length of the rails and the efficiency of magnetic field force coupling to the armature. When Eq. (1) is combined with the rail gun driving circuit model (see Fig. 2) and a transmission line model for the rails, a system of nonlinear time-dependent equations is developed whose solution provides the time-dependent current and associated electromagnetic fields. The equations are solved and the resulting electromagnetic fields are determined in the region around the rails. Figure 3 shows a sample comparison between a measurement of the magnetic field and a theoretical prediction. We have also obtained agreement between calculated and measured muzzle velocities approaching 5%.

In addition to the deterministic fields generated by the rails and moving armature, whose frequencies range from DC to tens of kHz, we have also estimated the electric fields due to arcing at the muzzle and compared it to the field of a dipole radiator under transient arcing conditions. Comments regarding shielding are also rendered.

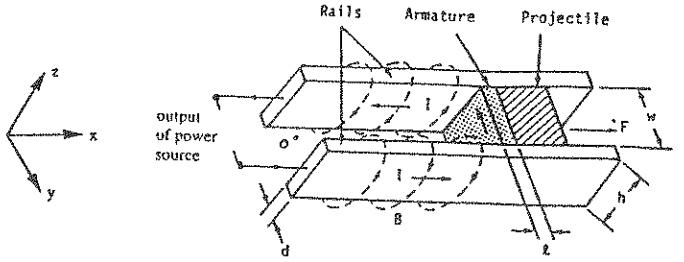

Figure 1. Rail gun geometry and coordinate system

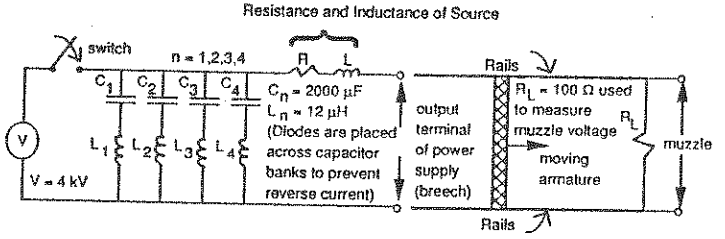

Figure 2. Rail gun driving circuit

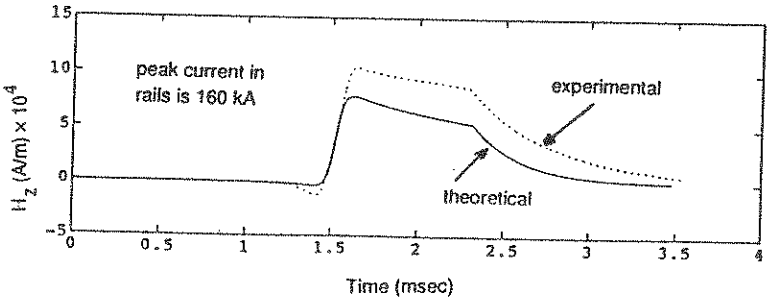

Figure 3. Comparison between experimental and theoretical behavior of vertical component of magnetic field in plane of symmetry at 2-inches above the rails and 28-inches from the breech.

Plasma Diagnostic Observations in Pulsed, Cold Cathode, Gyrotrons

K Ronald, SN Spark, ADR Phelps, W He and H Yin

Department of Physics and Applied Physics
University of Strathclyde
Glasgow, G4 0NG, U.K.

Results are reported of plasma formation in the diode of a pulsed cold-cathode gyrotron. High speed photography has been used to provide direct evidence of certain aspects of the plasma behaviour. Streak photography coupled to measurements of the simultaneous millimetre wave output of the gyrotron and the collapsing electrical impedance of the diode gap, these experiments demonstrate the rôle of the plasma in terminating the millimetre wave output pulse. Framing photographic observations of the spatial distribution of the cathode 'hot spots' as a function of insulating magnetic field strength, during the low voltage arc discharge, subsequent to the termination of the gyrotron output. Measurements of the dynamic impedance of the gyrotron diode fitted with cathodes of different materials reveals that the electron emission is in general from a cathode plasma, but at lower levels of applied electrical power the diode impedance is initially a strong function of cathode material.

The cold-cathode gyrotron using a two-electrode field immersed diode has been regarded as a 'single shot' microwave source in contrast to the MIG configured devices using thermionic cathodes capable of very long pulse or D.C. operation. Interest in cold cathode gyrotrons has been spurred by recent experiments demonstrating the possibilities of operating these devices at high pulse repetition frequencies[1] ($\sim$300Hz) whilst maintaining high power outputs $\sim$6MW, and the inherent simplicity and robust nature of the plasma flare cathode, with beam currents $>$100A.

In the plasma flare gyrotron the maximum duration of the millimetre wave output pulse is limited by plasma disruption of the diode geometry. As the plasma expands outwards from the cathode so the required compression of the electron beam increases. The distortion of the beam results in inferior spatial coupling between the waveguide mode and electron beam. Ultimately the oscillations will terminate when the relativistic electron beam (which is essential to the gain mechanism) is grossly distorted.

It was the aim of these experiments to obtain a better understanding of the fundamental processes occurring at the cathode. Specific objectives were to establish if use of different cathode materials could significantly enhance either (a) the PRF performance of the gyrotron (where load matching of the diode, $\sim$200Ω with a stainless steel cathode, and the power supply are of great importance), (b) the reproducibility and stability of the millimetre wave output pulse, and (c) the maximum duration of the millimetre wave pulse.

The photographic observations of the cathode were made by placing a high speed camera at the output window of the gyrotron and focusing along inside the waveguide, thereby forgoing the necessity of potentially detrimental modifications to the gyrotron[2]. Streak photography of the cathode was achieved using a Hadland IMACON 500 camera operating typically at 50ns/mm giving a 2μs observation time. Using a series of calibrated optical time reference signals, the millimetre wave output of the gyrotron could be compared synchronously on the same timescale as the photographic observations. Such a result is shown in Figure 1. Framing photographic observation of the cathode was obtained using a Hadland IMACON 790 operating at 2×10^6 frames per second during the later low voltage arc discharge phase of each pulse. Results obtained from these experiments are phenomenologically consistent with the process which Mesyats has described as the screening effect[3].

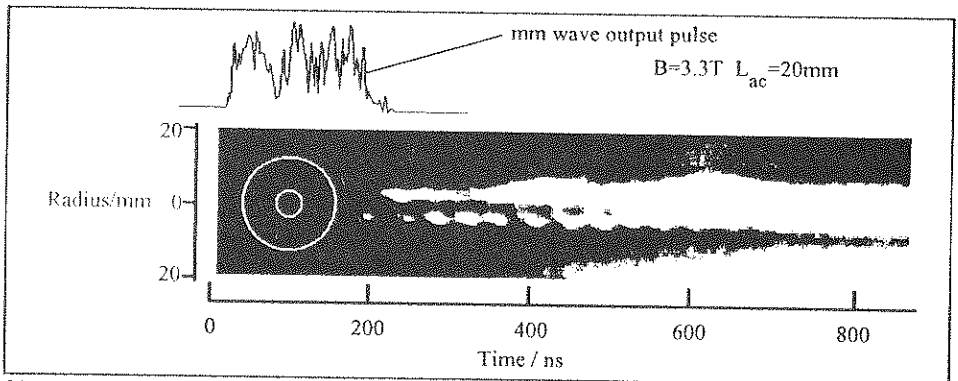

Figure 1. Streak photograph of plasma formation with simultaneous millimetre wave output pulse, plotted on the same horizontal time axis. Circles show spatial location of cathode (inner) and anode.

Electrical measurements of the diode impedance were obtained using a self-balancing copper sulphate voltage divider and a current shunt connected between the diode and ground. Figure 2 shows the peak electrical impedance of the diode for each of three cathode materials as a function of the applied electrical power. The convergence of the impedance lines as the power increases is consistent with a transition from field enhanced emission to plasma flare space charge limited emission. At lower levels of power it is clear that the plasma formation is preceded by a period of field emission dominated by material characteristics

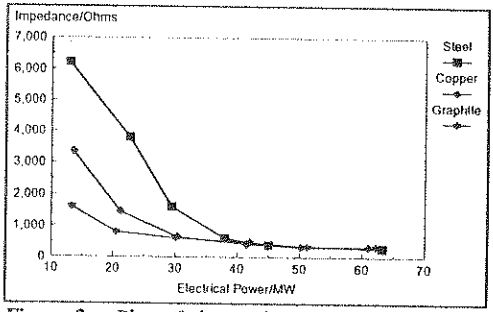

Figure 2. Plot of the peak of the dynamic diode impedance for each of three cathode materials at increasing electrical power levels.

Acknowledgements

The SERC and the MoD supported this research. DM Parkes, K Trafford and SJ MacGregor provided encouragement and stimulating discussions.

References

1. Spark SN, Cross AW and Phelps ADR, 1992, Proc. 17th Int. Conference on Infrared and Millimeter Waves, SPIE **1929**, 466-467.
2. Spark SN, Ronald K, Cross AW, He W and Phelps ADR, 1992, Proc. 17th Int. Conf. on Infrared and Millimeter Waves, SPIE **1929**, 322-323.
3. Mesyats GA, 1991, IEEE Trans. on Plasma Science, **19**, 683-689.

HIGH MICROWAVE PULSED POWER MEASUREMENT USING HOT ELECTRON PHENOMENON IN SEMICONDUCTORS

M.Dagys, Ž.Kancleris, V.Orševski and R.Simniškis
Semiconductor Physics Institute, Goštauto 11, Vilnius 2600, Lithuania

Nowadays various physical and technical investigations are carried out making use of high power short microwave (mw) pulses. To measure them direct couplers or attenuators with high attenuation (60-90 dB) are usually used since the standard power heads are mainly designed for a low power mw pulse measurement. On the one hand, big attenuation results in the decrease of the measurement accuracy. On the other hand, a small signal is detected by the head, and some difficulties could arise to measure such a signal in the presence of the hard stray pick up and the electromagnetic field interference which are usual at a high power mw.

Therefore the problem of great importance is to develop the power heads which can detect high power short mw pulses without using high additional attenuation and produce high output signal. To solve this problem new types of sensors manufactured from semiconductors, ferrites and other materials are designed.

In this report the resistive sensor being one of the most perspective sensor for high power mw detection is presented. The resistive sensor is made from n-type Si, and the performance of it is based on the semiconductor bulk resistance change in the strong electric field (E.M. Conwell, "High field transport in semiconductors", New York and London: Academic Press, 1967).

We had investigated transfer function, temperature dependence of the output signal, frequency response and reliability of the resistive sensors, and on the basis of these investigations resistive power heads have been designed.

The diaphragm type resistive sensor has been developed for high mw pulsed power measurement in the waveguide. The sensor is a rectangular parallelepiped shape piece of n-Si with Ohmic contacts on the ends which is placed between the wide wall of the waveguide and the special diaphragm. Dimensions of the sensor and the diaphragm as well as the specific resistance of n-Si are chosen making an optimization of the frequency response of the sensor, decreasing electric field perturbation in the transmission line and improving sensor's thermal characteristics. The sensor is also connected into DC circuit together with current generator. When mw pulse reaches the sensor electrons are heated by mw electric field, the resistance of the sensor increases, and DC pulse appears. The resistance change is proportional to the mw electric field strength in the sensor's volume. The latter, in turn, is proportional to the mw power. Thus, by measuring the amplitude of the DC pulse mw pulse power in the transmission

line can be determined.

Two modification of the diaphragm type power heads were designed. SF series is devoted to detect short mw pulses, the duration of which lies in the interval from 5 to 100 ns. The response time of that heads is of the order of 1 ns. Low specific resistance of Si is used for the resistive sensor's manufacturing, so the resistance of it is of the order of 20 Ω. To avoid lattice heating pulse DC supply is used, therefore the output signal of a few tens of volts on 50 Ω matched load is obtained. The power heads of SF series for various waveguide's dimensions in the frequency range 0.8-37.5 GHz were designed. They were used to detect short mw pulses generated by relativistic microwave devices in the former Soviet Union's microwave centers.

The resistive sensor made from higher specific resistance of Si is used in the heads of IA series, so they are employed to detect high power mw pulses the duration of which lies in the range of 0.5-300 μs. Lower perturbation of electric field in the transmission line and lower value of VSWR is achieved, therefore pulse power measurement accuracy is increased. It is ±10% in the waveguide's frequency band and in the temperature range -20 +50 C. It can be done even lower for a fixed frequency (usually high level mw sources generates at a fixed frequency or in a narrow frequency band). Power heads of IA series for various waveguide's dimensions in the frequency range 0.8-37.5 GHz were designed. Making use of the power head connected to the matched load and the horn antenna high level pulse power density in a free space of the order of 1 MW/m^2 has been measured in S, X and Q frequency bands. Parasitic signal induced in the measurement circuit by the external electromagnetic field ranges less than 1% of the useful one. Contrary to usual measurement systems, which measure electric field strength, such device measures mw power density, can observe single or low repetition rate mw pulses and detects power density more that three orders higher than can be measured using standard electric field probes.

Preliminary investigation have been performed to use the resistive sensor as a sensitive element in a dipole antenna to measure very high pulsed electric field strength in a free space. Using such probe electric field strength up to 2 kV/cm was measured in S frequency band.

Concluding the following advantages of the resistive sensor in comparison with Shotkey or point contact diode, which is also used for mw pulse power measurement, has to be mentioned: (i) possibility to measure high mw pulse power directly in the transmission line without using direct couplers or attenuators, (ii) high value of output signal from the sensor is available (up to a few tens of volts), (iii) high reliability and overload resistance is characteristic to the resistive sensor, (iv) switching off DC supply of the resistive sensor the parasitic signal induced in the measurement circuit by the external electromagnetic field can be determined. These features made resistive sensor irreplaceable for high level mw pulse measurement at a hard external conditions.

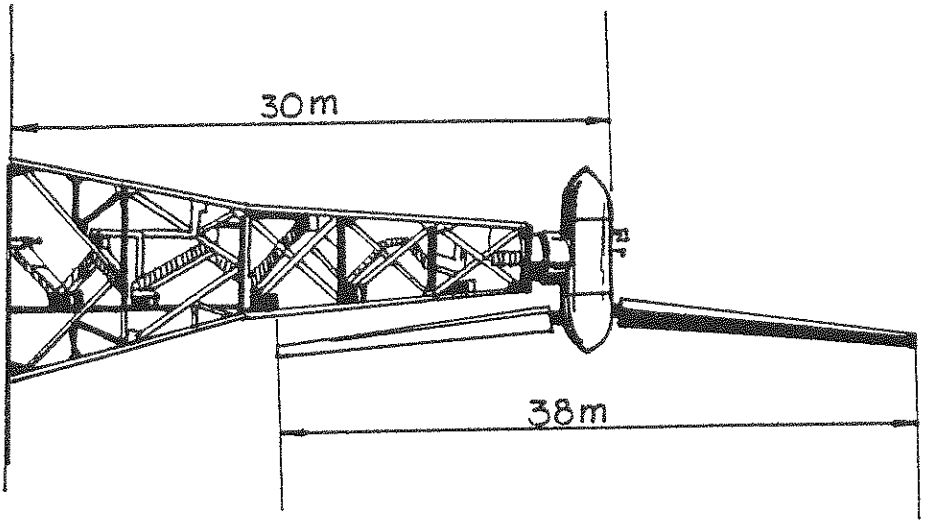

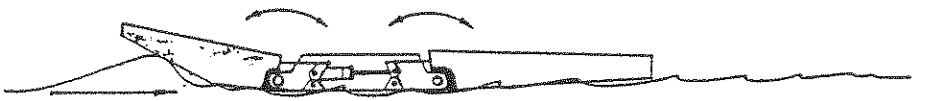

bangos judėjimo kryptis

Academy of Sciences of the Russia
GENERAL PHYSICS INSTITUTE
Vavilov str. 38, Box 117333, Moscow, Russia

Pulse of High Power EMI by Scanning REB.

Kazanskii L.N., Rukhadze A.A., Rybak P.V.
Theoretical Department, General Physics Institute,
Vavilova str., 38, Moscow, 117942, Russia

A possibility of excitation a short pulse of high power ($\leq 10^{-12}s$, $\geq 10^{10}Watt$) EMI by scanning REB is presented which is interest for many scientific applications. Traditional pulse technology can provide for such short pulse EMI the power only less then $10^7 Watt$. For excitation of such EMI the high voltage relativistic electron beams (REB) is proposed. If a REB with voltage $\approx 10^6 - 10^7 V$ and current $\approx 10^3 A$ ($a \simeq 0,1sm$, $b = 1sm$) is scanning on the conductive surface of coaxial chamber sinchronic with velocity equal to the light speed then the very effective EMI pumping takes place. After the time interval τ the pumping processes stopped when

$$2\pi j a^2 \frac{\tau}{2} = \varepsilon$$

Here $j = 10^4 A/sm^2$ is the current density of REB and $\varepsilon = 10^6 - 10^7 eV$ is the energy of beam electrons. From this relation follows the estimate of EMI power $P \simeq (0,4 - 4)10^{12} Watt$ and $\tau \simeq 3ns$. Then $\tau_u \simeq a/c \simeq 3 * 10^{-12}s$ and total energy $\approx (1 - 10) Joul s$. This estimate is very optimistic and therefore for proving it the numerical modeling of the processes is performed.

NEW SEMICONDUCTOR DEVICES FOR HIGH POWER PULSERS OF MICRO, NANO AND PICOSECOND RANGES

I.V.Grekhov, Ioffe Institute, St.Petersburg, Russia

Limited switching capability of usual power switches leads to the restrictions in application a number of novel electromagnetic technologies. For instance, gas discharge devices can switch very high electric power but have usually too short lifetime to fit well for industrial applications; from the other side usual power semiconductor devices have practically unlimited lifetime but rather low switching capability.

Topic of this presentation is to report some new ideas in power semiconductor device physics and new results of investigations which completed by working out several types of new power semiconductor switches for micro, nano and picosecond ranges. Switching capability of this devices surpass the gas discharge devices capability in many aspects.

- The new devices RSD(reversely switch-on dinistor) are switched uniformly over he whole device area and RSD with 80 mm silicon wafer diameter can switch ~ $7.5 \cdot 10^8$W (3 kV, 250 kA, 20 μs pulse width). A number of RSD connected in a stack can be switched simultaneously without RC voltage dividers. High switching capability of RSD and simplicity of series connection give an opportunity to design of megampeers current, tens kV, repetitive mode pulsers.

The small switching losses permit to use RSD for designing of the high frequency (up to 100 kHz) generators in the range of several megawatts mean power, where MOSFET and bipolar transistors cannot be used.

High voltage, high power submicrosecond pulsers are the other very promising area of RSD aplication. Circuit of this pulsers consist of low voltage RSD pulse generator (1-5 kV, several kA, several μs pulse width), high voltage pulse transformer and one or two magnetic compressing cells. Such approach give us an opportunity to fabricate rather cheap and

compact pulsers with pulse voltage 30-100 kV, 100-200 ns pulse duration and repetition rate 10^1-10^4Hz (pulse power up to 10 MW) for replacing the hydrogen thyratrons.

- Nanosecond range devices (drift step recovery diodes, DSRD) are based on the recently discovered effect of superfast recovery of a high voltage silicon diode when it is switched from the forward to reverse bias. These devices are the opening switches with a switching power of $\sim 2 \cdot 10^6$ W (2 kV, 1 kA) or more, off-time 2-3 ns, repetition rate up to several kHz and jitter less than 50 ps. DRSD may be connected in a stack without any voltage dividers, so high voltage (up to 100 kV) DRSD nanosecond generators are available. Because small jitter a number of DSRD-generators can be synchronized very precisely and very high power (several MW average) installations may be designed.

- Subnano and picosecond ranges devices are based on the new phenomenon of reversible wave breakdown in semiconductor diodes. These diodes (silicon avalanche shapers, SAS) with switch-on time less than 0,1 ns (0,05 ns min) and jitter less than 30 ps, can switch the power $\sim 10^5$ W (2,5 kW, 50 A) and more at reprate up to several kHz. SAS can be connected in series without any voltage dividers when specially selected. The most powerful SAS-generator designed up to now has the following characteristics: 20 kV, 400 A ($8 \cdot 10^6$ W), 200 Hz, 0,1 ns pulse front.

KMP ELECTRONICS

SPÉCIALISTE DES ÉQUIPEMENTS D'ÉMISSION DE PUISSANCE ET RÉCEPTION POUR LA COMPATIBILITÉ ÉLECTROMAGNÉTIQUE ET LES TESTS DE SUSCEPTIBILITÉ

Amplificateurs de puissance MOS-FET

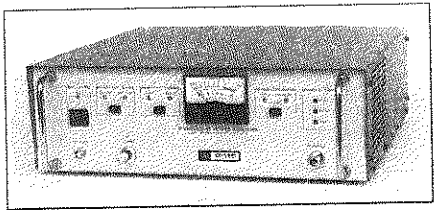

Large bande :
10 KHz à 1 GHz
Forte puissance :
1 Kwatt et plus
selon la bande - Interface IEEE, contrôle à distance
Selon norme IEC Pub 801-3 et 6.

Antennes d'émission/ réception

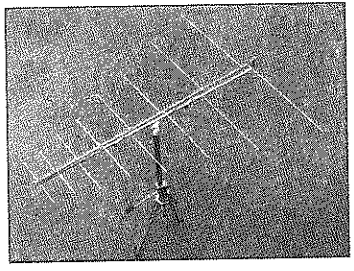

Log-périodiques,
log-spirales, biconiques,
dipoles, boucles, cornets.

Instrumentations IEM/IRF/TEMPEST

Récepteurs de détection
Tempest - Applications
toutes normes.

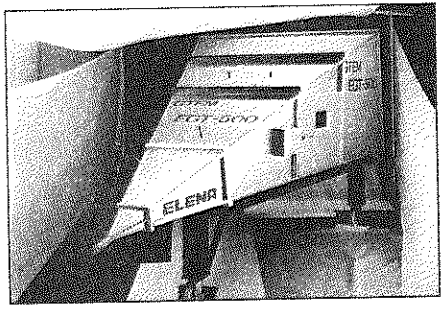

Cellules TEM et GTEM

8 modèles TEM,
DC à 1 GHz
300 watts
de puissance
admissible,
3 modèles GTEM,
DC à 2 GHz
100 à 1000 watts
de puissance admissible - 16 Kvolts pulse.

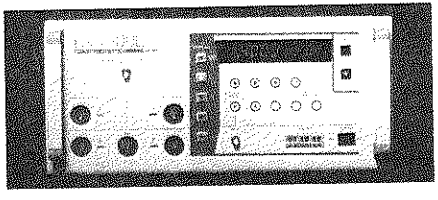

Générateurs de décharges électrostatiques

0,2 à 30 Kvolts,
temps de montée
0,7 à 1 nsec.

Générateurs de bursts rapides

250 à 4500 volts, cycle 2,5 - 5 et 10 KHz.

Simulateurs de perturbations IEM

Selon norme IEC Pub 801-5.

BP 64 - 9, allée Beausoleil - 92145 Clamart Cedex - Tél. : (1) 46 45 09 45 - Fax : (1) 46 45 24 03

FINITE-DIFFERENCE COMPUTATION OF VLF-LF PROPAGATION IN THE EARTH-IONOSPHERE WAVEGUIDE

JEAN-PIERRE BERENGER

Centre d'Analyse de Défense 16 bis, Avenue Prieur de la Côte d'Or 94114 Arcueil, France

In past years, two methods have been used for computing propagation of VLF-LF radiowaves on the earth surface, respectively the waveguide and wavehop methods. These techniques are very efficient in term of computational time, but they cannot take into account continuous variations of radiopath parameters such as ground conductivity or electronic profile. So, in order to remove that inconvenience we have developped a new computer code based on the finite-difference method.

In a first step the finite-difference time-domain technique FDTD, widely used in EMC and RCS computations for many years, will be briefly described. The special implementation needed to solve the propagation problem will be provided.

A second step will be devoted to validation of the method and to evaluation of its possibilities. It will be shown the FDTD results are in sharp agreement with those computed using the waveguide and wavehop codes. A discussion of the computational time will be presented for frequencies in the range 10-100 kHz.

In the last step, some results of FDTD computations will be presented for problems which could not be solved by the previously used two methods. Such problems show that the FDTD method allows to compute VLF-LF propagation through graduated terminators, over ground conductivity varying continuously, or over realistic ground taking into account mountains.

The conclusion will be that the FDTD method is a reliable one for solving propagation problems, it allows possibilities not available by the previously used methods, at a computational cost not prohibitive at frequencies up to 100 kHz.

CIVIL AIRPORT'S PROTECTION AGAINST A HIGH FIELD

Gilles BERREBI - Louis TAILLER - Jean-Claude CURTINOT
THOMSON-CSF/RGS Département DEN

The aim of this paper is to consider, with an example, the use of a numerical method, as one of industrials means, to assess the electromagnetic protection feasibility of a system.

This paper discusses a civil airport exposed in a near field of H.F antennas. The electronic equipment of the communication system is vulnerable to this hostile electromagnetic environment. The susceptibility of component, equipment package, which is defined as the level of electrical/electromagnetic excitation causing a temporary or permanent disruption in its operation, is known.

Accordingly, it's asked to propose electromagnetic protection design.
The simple way to protect vulnerable equipment to high level electromagnetic disturbance is to enclose them in a shielded building.
This protection design is highly efficient to solve the above problem but many others constraints must be taken into account :

- future system modifications
- users (claustrophobia, functionality...)
- shielding building maintenance
- the public architectural design.

A better way to tackle these constraints is the sensible use of a protection zone method which utilizes the natural shielding effectiveness of the building and the system.

To guarantee an efficient protection design, it's necessary to base it on performant numerical simulation which is able to give an accurate solution to problems.
The used code solves MAXWELL's equations in time-domain by the finite difference method. This code determines the diffracted field of a pulse or continuous plane wave by a conducting structure (wires or metallic plates). These impose to mesh the structure (here the building) and the space around with the help of elementary parallepipedical meshes.

So this numerical code determines the shielding effectiveness of :

- wire-netted concrete walls;
- metallic nets in front of windows;
- wave guide (simulating the building's front door, ducts).

The novelty of this feasibility study is :

- in regard with customer's requirements, to propose efficient and optimized (quality/cost) electromagnetic protection design;
- in an approache with a numerical code as a compulsory step, to allow realistic solutions proposals.

QUADRAXIAL SYSTEM FOR MEASURING CIRCUIT PARAMETERS

by
Joseph Capobianco & Robert L. Atkinson
Army Research Laboratory

ABSTRACT
(Poster Paper)

An understanding of electromagnetic (EM) coupling through shield penetrations and mutual coupling to adjacent conductors is necessary for determining the survivability and vulnerability of a system to a nuclear electromagnetic pulse (EMP), a high-energy radiation field (HERF), a lightning strike, high-power microwave (HPM) weapons, and electromagnetic interference (EMI).

A research investigation was conducted into the shielding effectiveness (SE) of various materials and the coupling associated with conductors within the shield. Efforts focused on understanding the resistive, inductive, and capacitive (RLC) parameters associated with the division of shield current and coupling on multiple inner conductors. This work culminated in a measurement system that can reduce the complexity of such measurements and the time necessary to perform them.

The system, made up of a radio-frequency (rf) driver, a quadraxial test fixture and software-controlled data acquisition equipment, can measure distributed, circuit-element cable parameters, including surface transfer impedance and surface transfer admittance, from 1 khz to 1 GHz. Conductor-conductor coupling parameters can be measured under variable loading (terminating) conditions.

Research efforts are on going to measure the electric properties of advanced composite materials with this system. Modifications to the test fixture allow the shielding effectiveness of various composite materials to be measured via a slotted aperture approach. These measuring techniques, along with analytical modeling, are necessary to assess Army system design and for evaluating new technology used to protect Army systems from electromagnetic threats or interferences.

This poster illustrates the quadraxial measuring system, system features and measuring parameters.

Quadraxial System for Measuring Lumped Circuit Parameters
Army Research Laboratory
SLAD/WTD Directorates

Joseph Capobianco
and
Robert L. Atkinson

ABSTRACT

[illegible]

SYSTEM FEATURES

- Measures RLCM Coupling Parameters
- Measures Shield Effectiveness
- Useful to 1 GHz
- Flexible input/output peripherals & cable harness
- Adaptable to connectors
- Can be extended for longer cables
- Compares EMI composite material to a slotted aperture

SYSTEM UNIQUENESS

- Computerized EM Hardness Test Tool
- PC-Based Software/Hardware
- IEEE-488 GPIB control & data acquisition

APPLICATIONS/USES

- Apply to HEMP, HERF, HPM type Environments
- Hardness Maintenance/Spec compliance tool
- Standards tool
- Design Practices for composite structures

SYSTEM MENUS

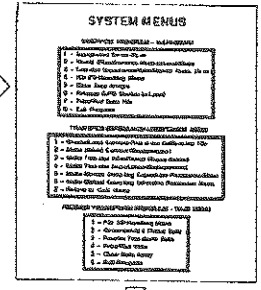

SHIELDING EFFECTIVENESS: The ratio of electric or magnetic field strength at a point before and after the placement of the shield in question. Equation is defined as: SE = 20log(E1/E2)

SURFACE TRANSFER IMPEDANCE: The voltage drop across the inside of the shield per unit length, divided by the current flowing on the outside of the shield surface. Eq. : Zt = [dV/dx] /dI/dz) for kr > 0

SURFACE TRANSFER ADMITTANCE: The short circuit current induced on the cable conductor for an electric field per unit length on the external surface of the cable shield.
Equation: Yt = -(1/W) (dI/dx)] for W > 0

TYPICAL DATA PLOTS

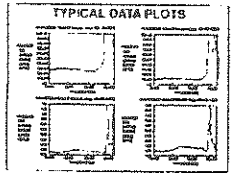

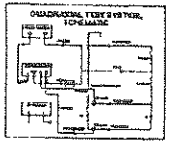

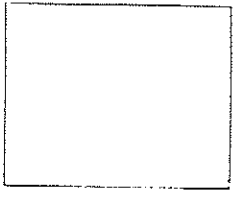

QUADRAXIAL TEST FIXTURE

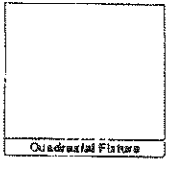
Quadraxial Fixture


Side View

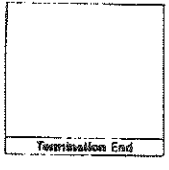
Termination End


Drive & Measurement End

EMC study of transmission network integrated in a mobile shelter

François CHASSAGNE / Jean-Michel CORTES
THOMSON-CSF/RGS
66, rue du Fossé Blanc
92231 GENNEVILLIERS - Cédex (FRANCE)

This paper presents an electromagnetic compatibility (EMC) study of a transmission network node. The basic item composing this transmission network node is a mobile shelter in which more than twenty different equipment, including receivers/transceivers are integrated. Radiocommunication system is completed by several analog and numerical lines.

The electromagnetic compatibility of such complicated system cannot be let to chance, it must be treated as earlier as design.

There are many probable self-interference coupling paths available in transmission network node, including antenna/antenna, antenna/equipment, cable/antenna, cable/equipment and apparatus in the shelter between themselves.

To get optimum electromagnetic compatibility in the design and shelter integration of transmission network node, we manage EMC study with three principal tools :

- EMC methodology,
- Numerical simulations,
- EMC engineering - installation guidelines.

EMC methodology is divided into six stages :

1. Definition of EMC performance objectives.
2. Functional analysis.
3. Electromagnetic and topological analysis.
4. EMC general design (pre-design phase).
5. Identification and study of potential performance deficiences.
6. EMC design.

Then, EMC study is treated with top to down analysis.

Numerical simulations (FDTD code, NEC) are acheived to obtain first orders of magnitude and afterwards, improved to obtain an optimisation of :

- Shelter's architecture,
- Antennas arrangement,
- Electromagnetic protection,
- Equipment EMC design.

The fundamental "How-to's" of EMC engineering and installation completes the numerical simulations to define industrial EMC design.

Some results obtained during the study of the transmission network node will be presented in the article.

Design Of Digital and Analog Error Detector Systems

By
Dr. ATEF ABOU EL-AZM
Faculty of Electronic Eng.
32952-Menouf, Egypt

ABSTRACT

In this paper, measurement of bit error rate in systems with binary block codes of bounded digital sum is described. Any crossing to such bounds due to an error leads to violations after a certain time. Moments of detecting these violations as well as the time spacing between them are computed. Design of an error detector system is also presented. The detector system is designed in both analog and digital circuits with acceptable circuit complexity and low power consumption.

The paper interested in detecting overflow of bounds of running digital sum (RDS violations) of a code combination, i.e. a combination of a codes elementary symbols. Fig.1 shows four block sections of a line signal and accompanying RDS-curve in a time representation. Curve a shows the RDS-change in case of an error-free line signal and curve b in case that the first symbol of the second block in the line signal has a positive error (F). This error leads after a certain time to the first crossing (violation) F1 of the upper bound, which also represents the upper limit of the signal during the crossing time curve c. The same thing happens in case of the second crossing F2. Moments of detecting the violations F1 and F2 after the faulty symbol are determined for the code ,e.g.3B4B and shown in Figs.(2.3). The RDS violation detector system can be realized in either a digital or an analog system.

a-The digital detector system-(Fig.4)

The two registers have the following functional possibilities: "parallel registration" and "shifting information". The system runs as follows: an appearance of a symbol "1" within a code combination causes a registration of 1 into the stages A_2 and B_2 of the register R_2. and at the same time a shift of previous register contents by one position toward C_1 of R_1; an appearance of symbol "0" in a code combination causes the registration of a 0 into C_1 and D_1 of the register R_1 and a simultaneous shifting the contents of the register by one position toward A_2 of the register R_2. Table 1 shows relations of values assignments a running digital sum of the register contents taking zeros as a starting state contents of the registers. Such initial state corresponds to a value of RDS=-3 (error signaling). After crossing the lower or the upper bound of RDS the system will remain in a state corresponding to a value of RDS=+3 or -3. till a moment of appearing an opposite symbol to the symbol causing that crossing in code combination. Appearance of such opposite symbol causes the system to return to a state corresponding to RDS value equal +1 or -1. Appearance of a state "1" in C_1 of a register R_1 is a proof of crossing the RDS value to the upper bound. on the other hand appearance of "0" state in A_2 of R_2 means crossing the lower

bound. Both crossings are summed up in a gate G, and manifested themselves by a change of its output from lower to upper level. To calculate the bit error rate , it is necessary to define the number of appearing RDS-violations in time intervals of fixed lengths. It is assumed that such an interval is 1 second, which corresponds with the number of transmitted symbols and equal about X Mbits where X depends on the design of transmission system. In a digital circuit, RDS violation counter should be applied which is cleared every 1 second. For the signaling of error rate 10^{-3} (i.e. error intensity equal about X 10^{-3} errors), the capacity of such counter should be very great and should be cleared in a definite time which in turns requires the use of a frequency divider to determine these time intervals which based on the code clock.

b-The Analog Detector System-(Fig.5)

Figure 5 shows the basic schematic diagram of the analog detector system. The input signal is isochronous rectangular pulse train with time period T and with the amplitude A. This input signal generates a voltage corresponding to the RDS violation which will charge the capacitor C. The capacitor discharge through the resistor R in the period equal to the gap between two pulses. It is assumed that $T \ll rC \ll RC$, and the voltage across the capacitor is always less than the amplitude A. Greater in capacitor voltage means greater in the frequency of RDS violation which in turn means greater in bit error rate. A finite excess in the capacitor voltage causes an excess in the error rate. Thus comparing that voltage with an original voltage, it is possible to detect the excess in the error rate.

Table I : Contents of the registers R1 & R2

signal	Q_{C1}	Q_{D1}	Q_{D2}	Q_{C2}	Q_{B2}	Y_2	Y	RDS
initial	1	0	0	0	0	0	1	-3(viol.)
0	1	0	0	0	0	0	1	-4(viol.)
1	1	0	0	0	1	1	0	-1
1	1	0	0	1	1	1	0	0
1	1	0	1	1	1	1	0	+1
1	1	1	1	1	1	1	0	+2
1	0	1	1	1	1	1	0	+3(viol.)
1	0	1	1	1	1	1	0	+4(viol.)
0	1	0	1	1	1	1	0	+1

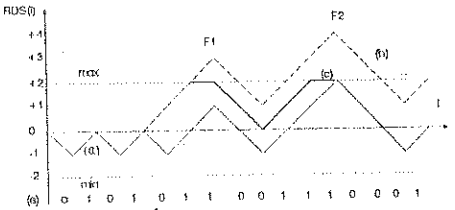

Fig.4 Error detection for a 3B4B coded signal

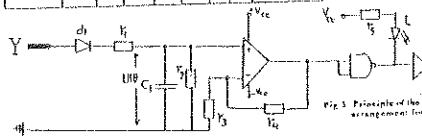

Fig.5 Principle of the analog circuit arrangement for error detection

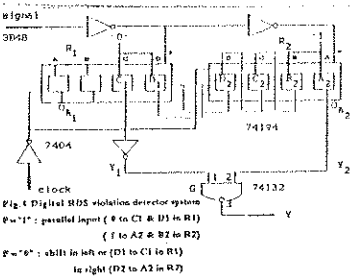

Fig.6 Digital RDS violation detector system
"1" : parallel input (0 to C1 & D1 to R1)
(1 to A2 & B2 to R2)
"0" : shift in left or (D1 to C1 to R1)
in right (D2 to A2 to R2)

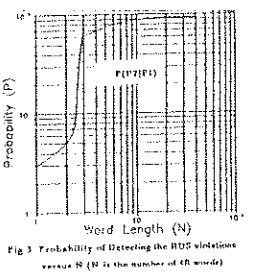

Fig.7 Probability of Detecting the RDS violations versus N (N is the number of 4b words)

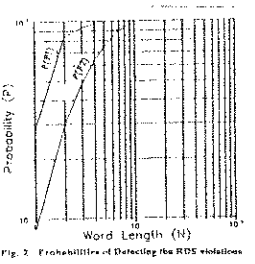

Fig. 8 Probabilities of Detecting the RDS violations versus N (N is the number of 4b words)

STUDY OF ACOUSTOELECTRIC MEMORY FOR SPREAD-SPECTRUM COMMUNICATION USING GREEN'S FUNCTION

A.A. ELFADL , M.EL-KORDY* and T.E.TAHA
Electrical communications Engineering,
Faculty of Electronic Eng., Menouf, EGYPT

Summary:

A study of the acoustoelectric strip-coupled real-time convolver and memory correlator using Schottky diode as storage element is presented. This study involves utilization of Schottky diode charges which are estimated by using Green's function in the calculation of the device efficiency and output power. The theoretical predictions of this calculation are compared with the published experimental results, in which the experimental point of the efficiency is verified at different values of the input power. The dependence of the output power on the depletion depth gives good results in comparison with the published data.

In this paper, we present an accurate method in which the depletion layer boundary under Schottky diode as well as static and dynamic charges are calculated by using Green's function. Green's function is used to invert Laplacian's operator of Poisson's equation (H.Baudrand et al.,Electronic Lett., 22, pp.(1263-1265), 1986) into integral equations whose solution are done by using the moment method. To determine the diode dynamic charge, a formula of Green's function is developed (M.El-Kordy, Ph.D. Disseration, Menoufia Uni. 1991) at the boundary condition of the electric field which accompanies the acoustic signal. The efficiency of the real-time convolver has been calculated by using the output equivalent circuit which is proposed by (Becker et al., IEEE vol. Su-29, no.6, p.289).

The open circuit voltage (at 2ω) is given by:

$$V_{o.c.}=\frac{Q_r Q_s}{2\varepsilon_1 q\, ND\, (p\, L_d)^2}$$

where Q_S is the charge due to signal (reading wave) and Q_r is the charge due to refrence (writing wave). In our calculation Q_r and Q_S are calculated at the given diode potential by using Green's function (see fig.(1)) rather than the approximate expression of Becker. The conversion efficiency of the convolver is defined as:

$$F=10\log\frac{P_o}{P_s P_r} \qquad \text{dBm}$$

where P_O is the output power in mw, P_r is the reference input power in mw and P_S is the signal input power in mw.

The experimental point of efficiency (0.95 as given by Becker) is calculated at different values of the input power Table 1.

The efficiency is greatly affected by the depletion depth which varies from its minimum value (built-in depth) to the deeper value as a result of the storage impulse. In the case of real- time convolver, there is no storage of SAW and therefore the increased depletion depth that would occur as a result of storage interaction can be ignored. But in the case of memory correlator the device is impulsed for storage of the reference chrage. By varying the impulse amplitude the depletion depth is determined as well as the charge, the efficiency as a function of the depletion depth is calculated and plotted in Fig.(2) in comparison with Becker's experimental results.

The theoretical prediction of Becker give F=-74.8dBm at built-in depth while our method gives -71.4dBm which agrees well with the experimental value of Becker (-71.3dBm).

Conclusion:

The study of strip-coupled real-time convolver and memory correlator are carried out by using Green's function which is used to calculate Schottky diode charges and the depletion layer boundary. The experimental point efficiency of the convolver has been verified at different values of the input power. The effect of the depletion depth on the efficiency of the convolver and memory correlator gives good results in comparison with the published experimental data.

L_d in cm	P_i in mw	V_a / UT	Q in C/cm^2	EFF. %
.01	.1	2.41	.133 E-8	95.10
.01	1.	7.63	.559 E-8	95.42
.01	2.	10.79	.845 E-8	95.16
.01	10.	24.0	2.31 E-8	95.20

Table (1) Experimental point of efficiency at different values of the input power

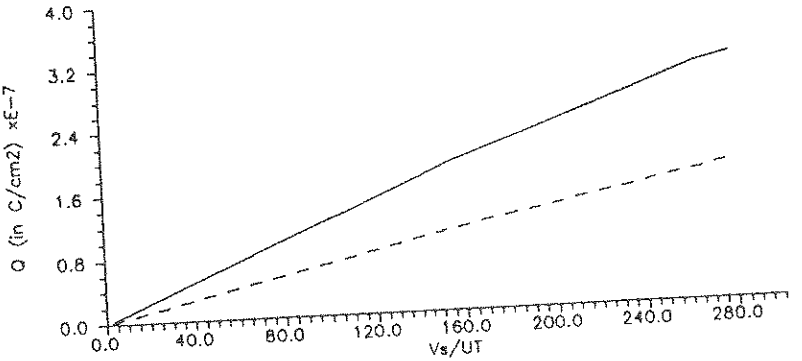

Fig. 1 Amplitude of the dynamic charge as a function of piezoelectric potential at:
——— ND=1.e15 cm-3
– – – ND=5.5e14 cm-3

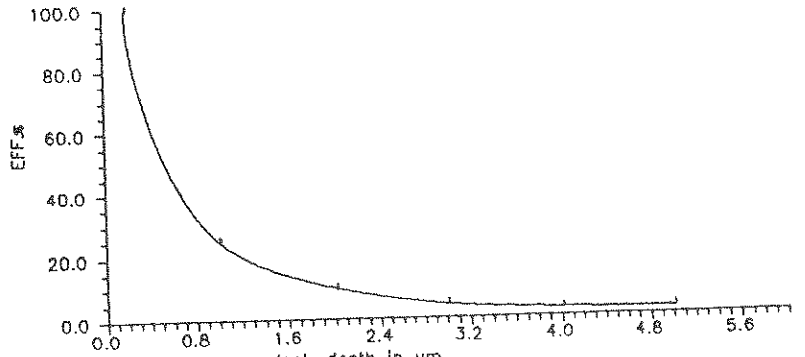

Fig. 2 Efficiency as a function of the depletion depth of strip-coupled convolver
F=416MHz
ND=5.5 E14 cm-3
——— Green's function
ɔ ɔ ɔ published results

THE EXCITATION OF SURFACE PLASMA OSCILLATIONS IN LIMITED SEMICONDUCTOR STRUCTURES BY THE CHARGES MOVING ALONG THE BOUNDARY

T.Yu. Fedchenko*, I.V. Yakovenko
Kharkov Technical University
Ukraine

At present time the study of electromagnetic radiation influence on the capability for work of semiconductor devices presents certain interest. This is connected with the necessity of solution of practical problems, that deal with the creation of electroradio equipment (ERE) stable to the electromagnetic radiation.

This paper studies the influence of currents induces by the external electromagnetic pulses inside of ERE on the wave processes in the limited solid structures. The obtained results can be used in the creation of semiconductor devices stable to EMP action and designated for the generation and conversion of SHF electromagnetic oscillations.

The coordinate system is chosen in such a way that the plane Y=0 is a semiconductor (Y<0) - dielectric (Y>0) media boundary.

The current

$$\vec{J}(x,y,t) = J_0(t)\delta(y-a)\delta(x-v_0 t)\vec{e}_z \qquad (1)$$

is excited in the dielectric at a distance a from the boundary along the conductive line (OX axis).

In OZ direction the structure is supposed to be homogeneous. Let us consider the case when the current as a function of time has biexponential shape with the arbitrary chosen parameters

$$J_0(t) = J_0(e^{-\alpha t}-e^{-\beta t}) \qquad (2)$$

The generality of the problem being solved is not lost. This is true for the cases of EMP influence on the communication lines.

This formulation of problem gives an opporunity to estimate the external EMP influence on the functioning of the solid-state structures of ERE in whose elements flow the currents induced by EMP. The paper consideres the MDS (metal-dielectric-semiconductor) structure as an object of investigation.

To describe the electromagnetic properties of structures we use for each media the Maxwell equations.

Let us consider the surface polaritones of TM-type.

This choice was made because of the localization of surface oscillations near the dielectric-semiconductor media boundary. The availability of the

moving electromagnetic radiation source (current induced by EMP on the surface of solid-state structure) can cause the excitation of these oscillations. The energy losses of charged particles are described in this case by the following expression

$$\frac{dW}{dt} = -\frac{J_0^2 (\beta^2-\alpha^2)(\varepsilon_0+\varepsilon_{02})^2}{V_0^2(\omega_0^2+\alpha^2(\varepsilon_{01}+\varepsilon_{02}))(\omega_0^2+\beta^2(\varepsilon_{01}+\varepsilon_{02}))} \qquad (3)$$

where ε_0 is medium permittivity, indexes 1,2 is a dielectric or semiconductor, accordinly, ω_0 is a ion plasma frequency.

The possibility of plasma oscillations excitation in solid bodies by the flows of charged particles has been investigated by now widely enough both theoretically and experimentally. In most papers the transformation machanism of beam energy into medium oscillation energy is explained as a cosequence of relationship between electromagnetic oscillation in a beam and in a solid body; similar interaction of the "wave-wave" type is described within the frame of hydrodynamic instabilities theory.

There is another excitation mechanism of electromagnetic oscillations: when charged particles of a beam do not possess collective plasma properties. In this case each perticle is an independent source of electromagnetic radiation. Such interaction is described within the frame of Vavilov-Cherenkov effect and occurs in case of coincidence of particle velocity and phase velocity of wave not much attention was paid to this possibility of excitation in solid bodies due to the low drift velocity of particles in such medium in comparison with the phase velocities of oscillations being excited. This paper compensates this blank to a certain degree. It consideres the possibility of a similar resonance interaction which is realized for higher particles velocities of a beam during its motion above the surface of solid body and the ecxitation object, i.e. the surface waves are localized in the same space domain.

The dependence of the power losses quantity (10) on the process parameters (frequency, carrier velocity and so on) is qualitatively analogous to the results obtained in paper (Pafomov V.E., DG.E.T.F.,t. 33, № 7, 1074-1078, 1960) for Vavilov-Cherenkov effect in unlimited geseous medium under excitation of volumetric oscillations.

The obtained solution allows for the estimation of energy amount carried by the external current and dissipated in a semiconducting element destabilizing its operation.

PATTERN TRACKING OF EXTERNAL MAGNETIC NEAR-FIELD FOR SURFACE-SAR IN REALISTIC HEAD MODEL FOR MICROWAVE EXPOSURE

* Osamu FUJIWARA and Michihiko NOMURA
Faculty of Engineering, Nagoya Institute of Technology, Nagoya 466, Japan

At the present time it is difficult to compute or to measure the specific absorption rate (SAR) at microwave frequency for a realistic human body model. On the other hand, a simple formula for approximating the localized SAR by an incident magnetic far-field was proposed, which was also validated experimentally on a flat phantom (N.Kuster and Q.Balzano, IEEE Trans.VT-41, 1, 17-23, 1992). From this result, we infer that the localized SAR pattern on a living body could be predicted if the external magnetic fields close to the body surface would be measured. In this sense, for a realistic head model, this paper shows the pattern tracking of the external magnetic near-field for the surface-SAR due to microwave exposure.

The finite-difference time-domain (FD-TD) method was used to compute the external magnetic near-field and surface-SAR in a realistic human head model for 750 MHz and 1.5 GHz plane waves of the 1990 ANSI specified safety levels (power densities: 2.5 mW/cm^2 for 750 MHz and 5.0 mW/cm^2 for 1.5 GHz). Figure 1 shows the head model and the computation region. This model was constructed by our group on the basis of the anatomical chart of the Japanese adult head. The abscissa and ordinate of the figure show the number of the cubic cell with the side of 2.5 mm. The computation region is comprised of 6,766,000 (=199x200x170) cubic cells, while the actual cell-number for the computation is 3,400,000 (=100x200x170) for symmetry. Figure 1 also shows on the right-hand side the examples of the horizontal cross section. Table 1 summarizes the electric parameters of the head model.

Figure 2 shows the spatial patterns of the squared external magnetic field H^2 and the one-gram averaged SAR <SAR> on the cross sectional perimeter shown in Figure 1(a). The solid and broken curves in the figure show the H^2 and <SAR> on the perimeter, respectively. Here, the H^2 and the <SAR> on the cross sectional perimeter are normalized to their peak values. Figure 2 shows that the magnetic field patterns roughly track the surface SAR, which means that there exists the strong correlation between them. We therefore computed the H^2 and <SAR> values on the fifty-five cross sectional perimeters from the forehead to the chin, and obtained the following regression relationships between them: $<SAR>[W/kg]=C\times H^2[A^2/m^2]$ where C is the correlation coefficient (C=1.59 for 750 MHz and C=2.27 for 1.5 GHz). We also confirmed that these C-values are similar to the theoretical correlation coefficient for the slab model having the same electrical properties as the skin.

We have examined numerically the pattern tracking of the external magnetic near-field for the one-gram averaged surface-SAR in the realistic head model for 750 MHz and 1.5 GHz microwave far-field exposures, and have found that the strong correlations between them are observed.

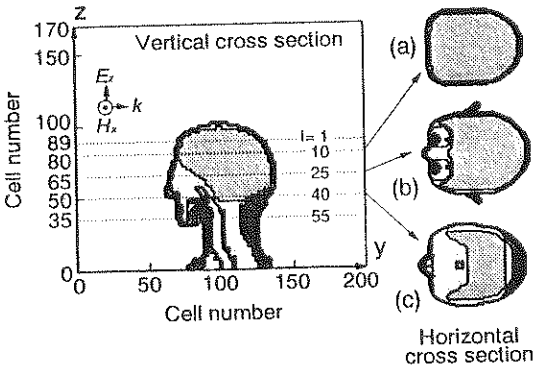

Figure 1 Realistic head model and computation region.

Table 1 Electric parameter of head model.

	750 MHz		1.5 GHz	
	Relative permittivity ε_r	Conductivity σ [S/m]	Relative permittivity ε_r	Conductivity σ [S/m]
Skin, Muscle	52.0	1.54	49.0	1.77
Fat, Bone	5.60	0.09	5.60	0.12
Brain	49.0	1.20	46.0	1.40
Eyeball	80.0	1.90	80.0	1.90

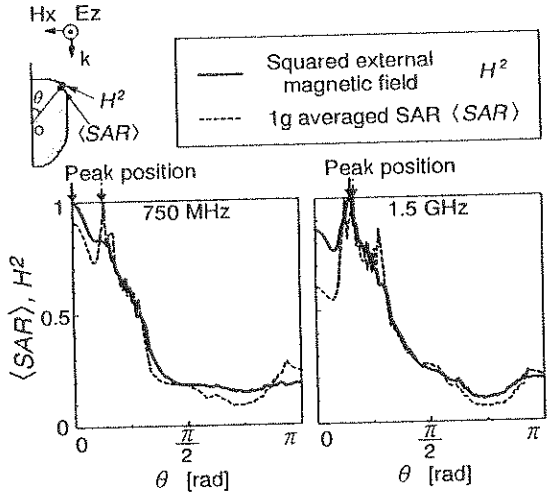

Figure 2 Comparison between the spatial patterns of the squared external magnetic field and the surface SAR.

On the Electromagnetic Measurement (ε^*, μ^*) of Solids and Liquids using Waveguides at Large Scale of Frequencies (0.5 to 100 GHz).

S.GUIROUS JUNIOR MEMBER, IEEE , MEMBER CNISF

Abstract-With the general use of the computer and automatic test equipment, the techniques for measuring complex dielectric constant (ε^*) and permittivity (μ^*) become more accurate. In this paper, a method is presented for determining simultaneously the both intrinsic properties of linear or composit materials using a waveguide with high level of accuracy.

Introduction

Actually the measurements of complex permittivity (ε^*) and permeability (μ^*), both vector quantities of dielectric or absortive materials, has gained increasing importance with expanding use of RF and microwave spectrum, particularly in communications and electromagnetic countermeasure applications. The industrial requirements on this topic are:

- -The permittivity and the permeability must be measured simultaneously on the same sample.
- -The measurements must be made at large scale of frequencies from 40 MHz to 40 GHz and up to 100 GHz.
- -The technique must be efficient for linear materials as for composit materials.

In order to reach those requirements, several solutions have been proposed in the literature which use TEM transmission line, microstrip line, coplanar line, waveguides or time-domain techniques but they suffer from lack of accuracy and speed processing. An automatic method using vectorial network analyzer is developped in this paper showing ways to reach these requirements.

Automatic Measurement System

A computer-controlled network analyzer is used to measure the parameters of a network consisting of a section of waveguide containing the sample of material. Under computer control, network analyzer system calibration and measurements are obtained at the reference planes indicated in Fig 1a, 1b. On the Fig.1.a the calibration reference planes and the measurement planes are the same: avoiding phase corrections Fig.1.b on the S_{11} and S_{12} parameters and then insuring more accuracy. This is obtained by the Thru-Reflect-Line (T.R.L) calibration <3> which consist of measuring the correction factors (12 parameters) with a delay, a short-circuit, and matching the ports of the analyzer. The four S-parameter are corrected with the correction factors over a number of predetermined frequencies at which the complex values of ε^* and μ^* are to be determined.

Fig.1.a.

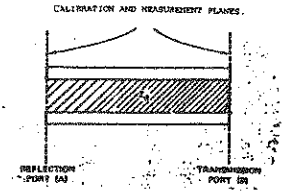

Fig.1.b.

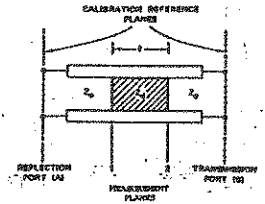

Fig.1. Transmission line section containing material sample with (a) and without (b) T.R.L calibration.

Data Processing Techniques

The equations used to compute complex ε^* and μ^* from the measured S_{11} and S_{12} parameters are known <1,2,6> and are not developped in this article.
For waveguides and TE_{01} mode with fictitous material parametres:

$$\varepsilon^*_f = \varepsilon'_f - j.\varepsilon''_f = -j.(\lambda/2.\pi.d).((1-\Gamma)/(1+\Gamma)).\mathrm{Ln}(T)$$

$$\mu^*_f = \mu^* = \mu'_f - j.\mu''_f = -j.(\lambda/2.\pi.d).((1+\Gamma)/(1-\Gamma)).\mathrm{Ln}(T)$$

Where: $T = (S_{11} + S_{12} - \Gamma)/(1-(S_{11} + S_{12})).\Gamma$

Γ is the first reflexion on the material sample.
d: length of the sample.

The results obtained for the Teflon are shown on the Fig. 2

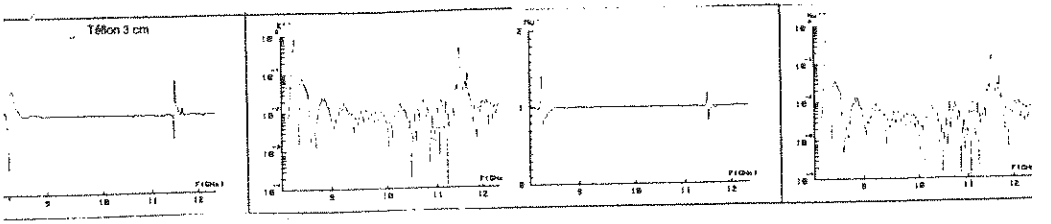

Fig.2. Teflon parameters (ε', ε'', μ', μ'').

SYSTEMATIC ERROR PARAMETERS

After having calibrating the network analyzer, we can obtain the 12 systamatic error parameters <5> and computing the error on the S_{11} and the S_{12} parameters by usin B.DONECKER's model <4>:

$$\Delta|S_{11}| = |D + Tr.S_{11} + MsS_{11} + Ml.S_{12}.S_{21}|.$$

$$\Delta\phi_{11} = \text{Arcsin}(\Delta|S_{11}| \;/\; |S_{11}|).$$

$$\Delta|S_{21}| = |C + Tt.S_{21} + MsS_{11}.S_{21} + Ml.S_{11}.S_{21}|.$$

$$\Delta\phi_{21} = \text{Arcsin}(\Delta|S_{21}| \;/\; |S_{21}|).$$

Where: D = Directivity; Ms = Source Match; Tr = Reflection Tracking; C = Crosstalk;
Tt = Transmission Tracking.

Then we compute the worst case error on the couple (ε^*, μ^*) as follow:

$$S_{ij} \pm \Delta S_{ij} \Rightarrow \begin{matrix} \varepsilon^* \pm \Delta\varepsilon^* \\ \mu^* \pm \Delta\mu^* \end{matrix}$$

The worst case error on the couples (ε^*, μ^*) is obtained by calculating the 16 couples and then taking the maximal and minimal value of both parameters Fig.3.

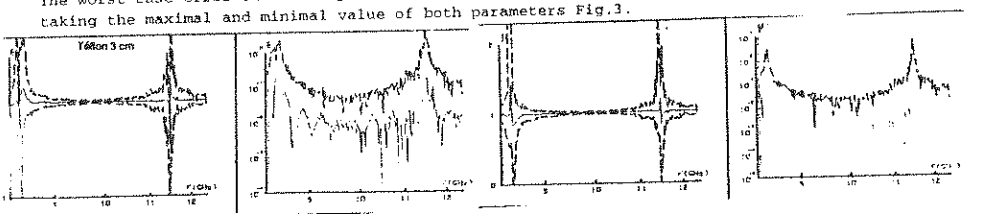

ACCURACY IMPROVEMENT

In the case of dielectric and magnetic material with low loss factor (μ^*), it is possible to improve the accuracy in the measurement of the parameter ε^*. This improvement is obtained by doing the cross between ε^* and μ^*.

$$\mu^* = \mu' = -j.(\lambda o g / 2.\pi.d).((1 + \Gamma)/(1 - \Gamma)).LnT$$

Then:

$$\varepsilon^*_f = \varepsilon^*_\varepsilon.\mu'/\mu' = (-j.(\lambda o g / 2.\pi.d).LnT)^2$$

ε^* is more accurate as shown on Fig.4.

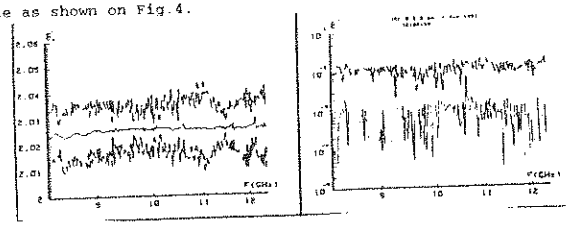

CONCLUSIONS

A method has been demonstrated to measure simultaneously ε^* and μ^* by using analyzer network.
A new calibration technic has been used avoiding the use of correction factors in the measurements of S-parameters.
Error parameters have been discussed and a worst case error calculation on ε^* and μ^* have been implemented.
A technic has been shown to improve the accuracy in the measurements of the parameter ε^*

REFERENCES

<1> A.M.NICOLSON, G.F.ROSS "Measurement of intrinsic properties of materials by time-domain techniques". IEEE TRANSACTIONS ON INSTRUMENTATION AND MEASUREMENT, NOVEMBER 1970.

<2> William B.WEIR "Automatic measurement of complex dielectric constant and permeability at microwave frequencies." PROCEEDINGS OF THE IEEE, VOL. 62, NO. 1, JANUARY 1974.

<3> G.F ENGEN and C.A.HOER "Thru-Reflect-Line: An improved technique for calibrating the dual Six-Port automatic Network Analyzer." IEEE TRANSACTIONS MICROWAVE THEORY AND TECHNIQUES, Vol. MTT-27, N.12, DECEMBER 1979.

<4> Bruce DONECKER "Accuracy predictions for a new generation Network Analyzer." MICROWAVE JOURNAL, JUNE 1984.

<5> G.DAMBRINE "Caractérisation des transistors à effet de champ: mesure précise de la matrice de répartition et détermination directe du schéma équivalent." Thèse de Docteur, Lille, MARCH 1989.

<6> S.GUIROUS "Sur la caractérisation électromagnétique (ε^*,μ^*) de matériaux solides et liquides en structure guide d'ondes rectangulaire à large bande de fréquences (0.5 à 100GHz)." Mémoire de D.E.A, Lille C.H.S, JULLY 1991.

On the Use of GTEM Cell in EMP-Threat Testing

Jarosław M. Janiszewski, Tadeusz W. Więckowski

Technical University of Wrocław, Institute of Telecommunication and Acoustics,
Wybrzeże Wyspiańskiego 27, 50-370 Wrocław, POLAND
phone: +4871 214998, fax: +4871 223473

The application of LSI and VLSI systems to a variety of electronic devices (including those installed in aircrafts) has become increasingly frequent in the past few years. But this has led to a noticeable decrease in the threshold of electromagnetic (and particularly EMP) vulnerability, thus creating an urgent need of investigating not only interferences produced by different sources, but also the sensitivity of electronic devices to such interferences. As far as the aircraft is concerned, the main source of EMP-threat is lightning (both cloud-to earth and cloud-to-cloud). And this implies joint investigations of aircraft vulnerability to EMP exposure and extensive testing of the electronic devices installed on the board of the aircraft.

EMP vulnerability tests should be conducted under conditions simulating real phenomena. For this purpose, it is necessary to construct a generator for simulating the shape and amplitude of the EMP and to design a measuring set-up for the needs of the simulation test. The available standards (both national and international) define the shape and the amplitude of the electromagnetic fields that are to be generated.

Simulation tests often raise serious problems, particularly when EMP fields are involved. They require simulators of special design, as well as suitable location of the testing set-up in order to provide safe operating conditions.

The Institute of Telecommunication and Acoustics (ITA), Technical University of Wrocław has designed and constructed an EMC Laboratory which has been equipped with measuring set-ups according to national and international standards. The EMC Laboratory provides conditions for continuous threat tests and EMP threat tests. There are also set-ups for the testing of radiating and conducting interferences. The description of the EMC Laboratory can be found in: Bem D.J., Janiszewski J.M., Więckowski T.W., Zieliński R.J., Int. Wrocław Symp. on EMC, 1990, pp. 313-318 and pp. 627-633. Investigations on the improvement of relevant methods and on the extension of the scope of the tests are underway.

One of the various measuring techniques made use of in the EMC Laboratory is the TEM cell method which has been applied to EMC tests. At the first stage of the study we designed a Crawford-type cell which is used for continuous threat tests. The objective of this study was to design and implement a GTEM cell.

The TEM cell is a transmission line with a fundamental mode of the TEM field. The electromagnetic field in the working space of the cell is similar to that in the free space (the characteristic impedance 120π i.e. 377Ω). The electric field vector is perpendicular, and the magnetic field vector is parallel to the conductors. GTEM cells (Gigahertz TEM) do not radiate electromagnetic fields to the environment.

The GTEM cell operated by the EMC Laboratory provides cooperation with both continuous-signals and pulse generators. To control the electromagnetic field in the measuring space and to investigate electromagnetic field distribution variations due to the presence of the device under test, probes involving linear antennas or loops have been designed. There have also been developed numerical procedures which enable not only calculation of the transfer functions for the measuring probes of the cell, but also reconstruction of the real shapes and real electromagnetic field values in the vicinity of the antenna. A major advantage of introducing such probes into the cell is that they enable measurement of the electromagnetic field parameters in the time domain and in the frequency domain. This is of paramount importance, since the GTEM cell acts as a set-up for testing the vulnerability of electronic devices to continuous and pulse-type threats.

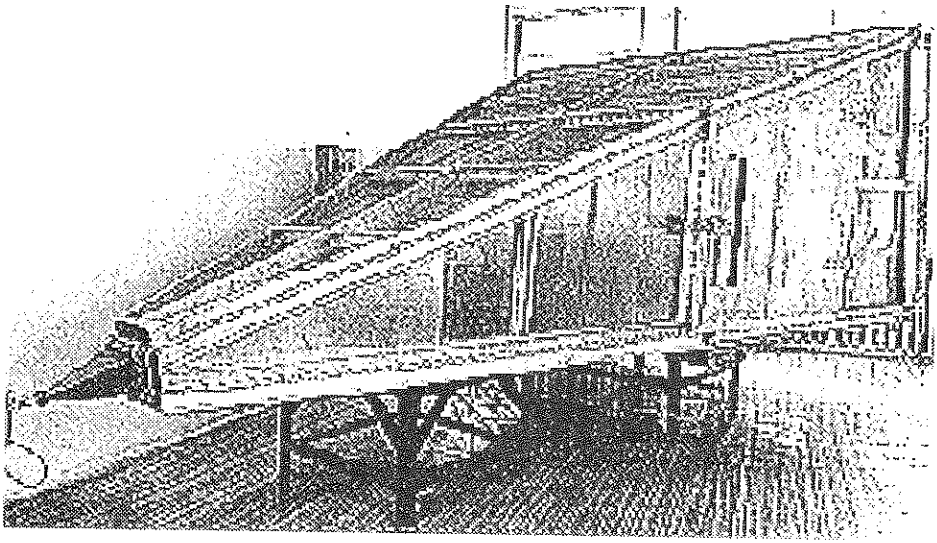

Fig. 1. GTEM cell designed in EMC Laboratory in Wrocław

The GTEM cell presented in this paper was designed and constructed by the research and engineering staff of the ITA, and was part of the set-up for electromagnetic vulnerability tests.

The paper will include the measured values of the electric properties of the GTEM cell (impedance, SWR), as well as the measured values of the EMP parameters in the cell.

Summing up, the GTEM cell of the design described in this paper makes it possible to investigate the vulnerability of electronic devices to pulse-type electromagnetic fields which are particularly difficult to simulate. The design proposed in this study enables generation of EMPs with rise times varying from several picoseconds to several milliseconds.

HOW TO IMPROVE SPECTRUM EFFICIENCY BY ADVANCED METHODS OF DETERMINING COUPLING BETWEEN TRANSMITTERS

A.Knälmann*, A.Quellmalz, Südwestfunk Baden-Baden

1. Current problems in transmitter network modelling

Spectrum management is one of the most important tasks in communication engineering today, because frequencies for wireless transmission of information must be considered as rare, exhaustible resources. The basic task for the frequency planner is to evaluate carefully the coupling between the transmitters to be planned, because these relations serve as the basis for the following frequency assignment. The coupling relations have to be determined so that with a minimum amount of spectrum the wanted coverage area of each transmitter can be protected against interference. Modern planning methods often use a special graph structure, the coupling graph, to describe the coupling relations between transmitters in the network. But the planning methods currently in use suffer from the fact, that the underlying model of the transmitter network is often to simple to describe reality. This results in wrong evaluation of the coupling between the tranmitters. Coupling is either under- or overestimated. Of course this has an effect on the use of spectrum. If the coupling between the transmitters is overestimated the frequency planner will waste more spectrum than he really needs to achieve the wanted coverage in the planning area. On the other hand if the coupling is underestimated the planner will think that with a smaller amount of spectrum he can achieve the wanted coverage, but after the network will be put into operation he will see that the planned coverage areas are destroyed by interference.
In this contribution we present new, sophisticated methods to evaluate coupling between transmitters. We will show, that by the use of these method the problems described before can be resolved. Hidden reserves in spectrum space can be found with the help of the new, more realistic coupling method.

2. Advanced coupling methods

Current coupling methods use only the interfering fieldstrength at transmitter sites for the determination of the coupling relations. In our new method coupling between transmitters is considered not only at transmitter sites, but in the whole wanted coverage areas of each transmitter. In the first approach the wanted coverage areas

are modelled by an area around each transmitter, which is formed by a contour, on which the desired fieldstrength of the transmitter is constant. Between each pair of transmitters a critical point on this contour is determined, where the difference between the desired and the interfering fieldstrength takes a minimum. This signal-to-interference ratio is taken as the coupling value between the transmitters. By this method coupling relations can be determined much more realistic than before, but one disadvantage of the method is that modern wave propagation models, which take into account topography and morphography of the planning area can not be used. For that reason in our second approach we model the wanted coverage area of the transmitters by testpoints. At these testpoints the fieldstrengths of the transmitters can be calculated with every available wave propagation model. The coupling relations are again taken from the difference between desired and interfering fieldstrengths at critical testpoints in the wanted coverage areas. One problem we had to solve was, that because of the statistical nature of the fieldstrength calculated with a topographical wave propagation model we often found extreme values of the fieldstrength at the critical testpoints. The coupling between two transmitters was overestimated very often, which as described before results in a waste of spectrum. For that reason we considered not only one critical testpoint but made a statistical analysis of the whole testpoint area in our final coupling model. From this analysis we derived the coupling relations between transmitters. It could be found that this last approach is an optimal compromise between realising the wanted coverage and efficient use of spectrum.

3. Results

Several different coupling models have been developed and tested. For a practical example of a transmitter network in the Black Forest in the South Western part of Germany we will show the characteristics of the different coupling models and their often great difference to the model where coupling is only considered at the transmitter sites. Also we will demonstrate the possibility of finding hidden topographical spectrum reserves by use of the new coupling method in combination with a topographical wave propagation model.

REPRESENTATION OF THE ELECTROMAGNETIC COMPATIBILITY OF STATIC CONVERTERS BY MEANS OF INTERFERENCES ENERGY AND JOULE LOSSES

*M. Lardellier°, G. Rojat°, E. Labouré°°, F. Costa°°

° CEGELY - Ecole Centrale de Lyon
CNRS - URA 829
36, Av Guy de Collongue
BP 163, 69131 ECULLY Cedex

°° LESIR - ENS CACHAN
CNRS - URA 1375
61, Av du Pdt WILSON
94235 CACHAN

1. INTRODUCTION

Earlier works on generated high frequency electromagnetic disturbances, in static converters have addressed the influence of commutation mode, cabling parasitic effects, and the parasitic behaviour of active components according to their technology. (F. COSTA and A. PUZO Doctoral thesis 1992)

In order to characterise cells according to these parameters, and in addition to temporal and frequential studies of interferences, we suggest a two dimensional method of representing the operating point from the electromagnetic compatibility point of view : we define a reference whose co-ordinates are representative of energies :

- in abscissa : $\frac{W_{int}}{W_{load}}$: energy due to conducted interferences dissipated in 50 Ω resistors of Line Impedance Stabilisation Networks (LISN), as per load energy.

- in ordinate : $\frac{W_{elec}}{W_{load}}$: electrical energy of joule losses in active components as per load energy (W_{load}).

This study is made with per unit values of load energy, and allows us to choose the parameters of the cell : voltage supply, load current, control speed, type of switches, technology ... A good compromise between component heating and interferences levels is thus achieved.

2. ENERGY MEASUREMENT

The test bench is shown figure 1. This is a commutation cell in forced commutation working at 100 kHz, without snubbers.

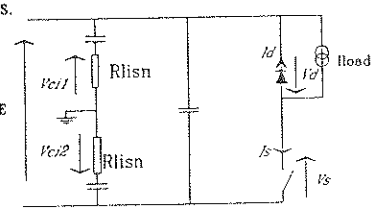

Fig 1. test bench.

We use a digital signal analyser to calculate :

- The electrical losses in the diode and in the switch : $W_{elec} = \int_0^T v_d i_d dt + \int_0^T v_s i_s dt$

v_d and v_s are measured with a voltage probe and i_d and i_s are measured with a high performance current probe (current probe : I_n = 40 A , high frequency cut-off : 250 MHz). Oscillations occur around 30 - 50 MHz.

- The interference energy is calculated using V_{ci1} and V_{ci2} voltages by the formula :

$$W_{int} = \frac{1}{R_{rsil}} \left(\int_0^T V_{ci1}^2 dt + \int_0^T V_{ci2}^2 dt \right).$$

3. ANALYSIS OF RESULTS

The test bench works under the following conditions (figure 2.):

- switch : IGBT (IPGPC 50U) and diode (BYW 30PI400) :
* voltage supply 100 V , load current from 3 A to 10 A curve n° 1.
* voltage supply 50 V , load current from 3 A to 10 A curve n° 2.
* load current 10 A, supply voltage from 30 V to 130 V, curve n° 3.

- switch MOSFET (IRFP 250) and diode (BYW 30PI400) :
* voltage supply 100 V , load current from 3 A to 10 A curve n° 4.
* voltage supply 50 V , load current from 3 A to 10 A curve n° 5.

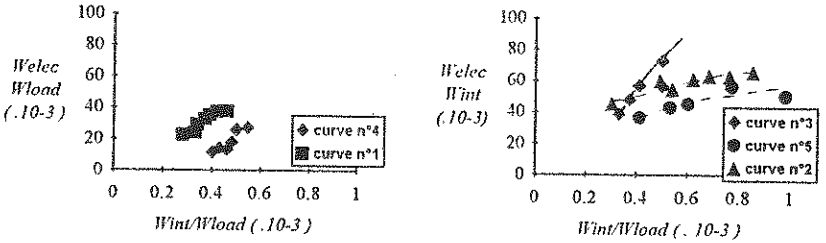

Fig 2. Electromagnetic behaviour of the cell.

Supplied by 100 V, the interferences and losses of an IGBT cell vary in the same proportions : for a 3.3 ratio of W_{load}, the relative values of W_{int} and W_{elec} vary in a ratio equals to 2. however, under a 50 V supply voltage, interferences vary much more rapidly than Joule losses ($\Delta \frac{W_{int}}{W_{load}} = 3$ and $\Delta \frac{W_{elec}}{W_{load}} = 1.5$). The behaviour of MOSFET is different : the curves show cell sensitivities to load current for different supply voltage levels.

We notice that cells using MOSFET generate less Joule losses, this component being able to work at high frequency control. On the other hand, IGBT cells are less polluting in conducted interferences.

The curves show that MOSFET and IGBT cells losses as per load energy vary in the same porportions but interferences energy as per load energy vary much more in IGBT cells than in MOSFET ones (1.5 times more).

4. CONCLUSION

The study of commutation cell sensitivities as regards to parameters which are called into play in the generation of electromagnetic interferences is facilitated by the representation of the operating point in the suggested plane.

We have shown in this paper that cell sensitivity as per load current is increased when supply voltage decreases. In the same way, we can vary each parameter one at a time in order to determine which ones are preponderant.

Example : curve n° 3 : variations of supply voltage with constant load current I = 10 A.

The curves have shown that the ratio of losses and interferences are lower when components are used under high voltage and high current, and that the variations of the operating point depend on the parameters changed in the cell : variations of electrical losses as per load energy are higher in the case of current variations as compared to voltage variations, variations of conducted interference energy as per load energy are higher in the case of voltage varations as compared to current variations.

The use of a LISN has permitted a global approach for conducted interferences. For radiated interferences, we are limited to a local approach of radiated fields in a fixed point of space and we calculate the energy density of radiated field by the formula :

$$w_H = \frac{\mu_0}{2}\int_0^T H^2 dt \text{ and } w_E = \frac{\varepsilon_0}{2}\int_0^T E^2 dt \ .$$

It will be interesting to develop a global method in order to quantify the total energy radiated by the cells.

TWO-DIMENSIONAL METHODS FOR CALCULATION OF MAGNETIC FIELD TRANSMISSION LINE AND COMPARISON WITH MEASUREMENT VALUES

Luis Ortiz N. and Roberto Figueroa B
Department of Electrical Engineering
Santiago of Chile University
Santiago of Chile, Chile

Abstract - This paper present two-dimensional methods for calculation of magnetic field transmission lines more used. These methods are comparison between theirs and with measurement values. The methods: complex distance image, corrected complex distance image, real distance image and the method that not considers soil resistivity are presented. These methods are applied to specific 220 kV power line and their soil resistivity effect and precision are evaluated.

I. INTRODUCTION

The magnetic field produced by transmission, distribution and utilization systems of electrical energy have been a considerable interest during the last years. The interest has been originated by possible biological effects suggests for some researches (I. E. Bridges and M. Preasche, Proc. IEE, 1092-1119, Sep. 1981).

Magnetic fields are originated for natural sources and man-made electrical systems. Some principal artificial sources are the electric power lines (IEEE Trans. on Power Delivery, Vol. 3, N° 4, October 1988).

There are several two-dimensional deterministic methods for calculating of magnetic field produced by electric power lines. The more used method is based to image representation of quasi-static fields of a current line source above the resistive ground (J. R. Wait and K. P. Spies, Canadian Journal Physic, Vol. 47, 2731-2733, 1969). These methods are: complex image distance, corrected complex image distance (EPRI Transmission Line Reference Book, 2th Edition, 1982), real image distance (D. W. Deno, EPRI EL-802, Project 556, 2-12, June 1978) and not considered soil resistivity effect method (IEEE Trans. on Power Delivery, Vol. 3, N° 4, Oct. 1988).

These methods are presented, soil resistivity effect and their precision are evaluated. Theoric and measured values are comparison.

2. CALCULATION METHODS

The well-known complex image distance method, replace the soil with resistivity ρ for the current image with inverse direction at complex distance of surface soil (EPRI Transmission Line Reference Book, 2th Edition, 1982). A method more precise designed corrected complex image distance is obtained added a term obtained for adequate truncation of Carson series (IEEE Trans. on Power Delivery, Vol. 3, N° 4, October 1988). A hardy simplification, sometimes used, located image at real distance of the surface soil (D. W. Deno, EPRI EL-802, Project 556, 2-12, June 1978). The more simple method, but available on the right-of-way not considers resistivity soil effect (IEEE Trans. on Power Delivery, Vol. 3, N° 4, October 1988). The general mathematical expresion are:

$$B_x = -\sum_{i=1}^{n} \frac{\mu_o I_i}{2\pi}\left\{\frac{y-h_i}{R_i^2} - \frac{y+h_i+\alpha}{R_i^{*2}}\cdot\beta\right\} \qquad (1)$$

$$B_y = \sum_{i=1}^{n} \frac{\mu_o I_i}{2\pi}\left\{\frac{x-d_i}{R_i^2} - \frac{x-d_i}{R_i^{*2}}\cdot\beta\right\} \qquad (2)$$

donde:

$$R_i = \left[(x_i-d_i)^2 + (y_i-h_i)^2\right]^{1/2}$$

$$R_i^* = \left[(x_i-d_i)^2 + (y_i-h_i+\alpha)^2\right]^{1/2}$$

$$\alpha = \delta(1-j), \quad \delta = 2/\sqrt{\mu_o\sigma\omega} \approx 503\sqrt{\rho/f}$$

The conditions for diferent methods are:

Complex image distance method: $\beta=1$

Corrected complex image distance: $\beta = 1+(1/3)(\alpha/R_i^*)^4$

Real image distance method: $\beta=1$ and $h+\alpha = D_e = 660\sqrt{\rho/f}$

Not considered soil resistivity effect method: $\beta=0$.

3. APPLICATION METHODS

These methods presented on section 2, are applied to 220 kV line Alto Jahuel-Los Almendros of the company Chilectra Metropolitana of Chile. This line has two circuits in vertical configuration with two shield conductors. The current is 336 Ampere for each phase with 5 % unbalanced.

The soil resistivity effect on the magnetic field calculated for corrected complex image distance method. This effect for several values of soil resistivity is shown in Fig. 1. Typical values for soil resistivity range from 1 to 10000 ohm-meters

The errors of each method in function of lateral distance from axe line are shown in Fig. 2 The reference is corrected complex image method.

The theoric and measured values of the magnetic field at 1 m over soil surface are shown in Fig. 3. The EFM Model Magnetic Field Meter of the Electric Field Measurements were used.

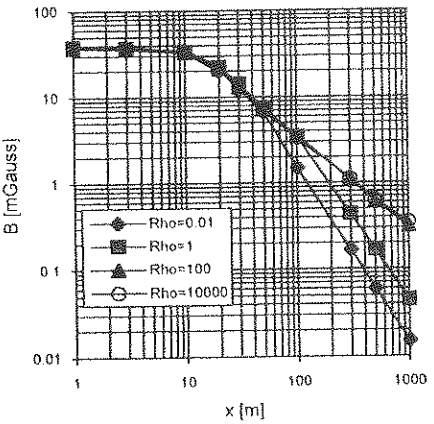

Fig. 1. Effect of resistivity on the magnetic field of the 220 kV electric power two circuit line.

4. COMPUTER PROGRAM

An interactive program with four magnetic field calculation methods was developed. This program calculated the components of magnetic field, maximum value, angle and error relative to corrected complex image method. The program can be applied for any geometry lines.

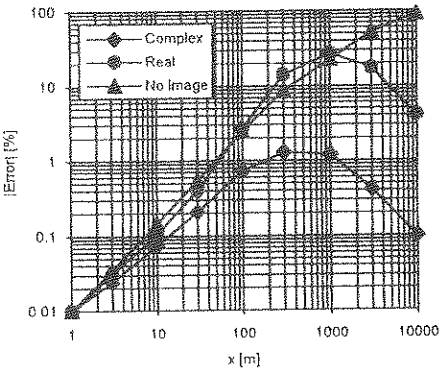

Fig. 2. Magnetic field error of 220 kV electric power two circuits line for 100 ohm-m soil resistivity.

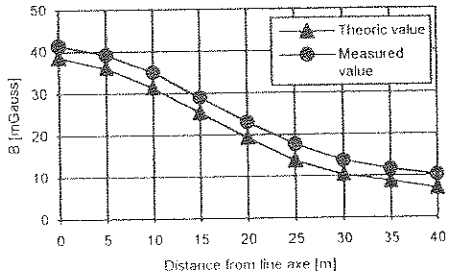

Fig. 3. Comparison of calculated and measured values of magnetic field lateral profile on 220 kV lines.

5. CONCLUSIONS

On the right-of-way for soil resistivity much larger than 1 ohm-m, or for radial distance from conductor to the calculated point much less than the skin depth of the earth, the soil resistivity effect can be neglected.

The difference between corrected complex image distance method to complex distance method is not significative (minor than 1.5 %). The complex distance image is recommended for general proposes. The other methods real image and not consider soil effect are valid only the right-of-way

ACKNOWLEDGMENT

The autos wish to express their indebtedness to the FONDECYT of Chile in the project numbers 500-92.

ANALYSIS OF LIGHTINING PROTECTION DEVICES

Emilio Mino & José Emilio Vila*

TELEFONICA INVESTIGACION Y DESARROLLO

Tel. 34 1 3374428 - Fax. 34 1 3374212

28043 MADRID (SPAIN)

1 INTRODUCTION

This paper shows the results of the strenght to surge voltage tests carried out on different discharge protection devices, with application in telecom equipment.

The objetives of this study were to determine the discharge resistance of these components against a standard surge voltage, to compare the results with the manufacturer specification (usually for a different waveform) and to perform measurements of the transients voltages transmited, that can affect the circuit to protect, and the leakage current.

2 TEST DESCRIPTION

Series of 10 positive and negative voltage pulses were applied with a 1/1000μs waveform, from 500 V to 6000 V, in steps of 500 V, until the failure of the component. The time between pulses was 1 min. The discharge generator was a Haefely P6T with an output resistance of 25Ω.

The voltage pulse 1/1000 μs is the standard requirement for surge protection in telecommunication equipment in Spain (the raise time of this pulse is 1 μs and the fall time to half peak voltage is 1000μs). In shortcircuit the discharge generator gives an approximate current waveform of 2/500μs.

The leakage current was a measured with a Semiconductor Parameter Analizer HP 4145B.

3 TEST SAMPLES

Tests were carried out on crowbar devices (trisils and gas arresters) and clamping devices (transils and varistors) with a breakdown voltage about 200 V for all devices. All of them have similar size.

4 TEST RESULTS

Table 1) resumes the strength discharge test showing the maximum peak voltage and current before the component failure, and the data sheet specification.

Tabla 1

STRENGTH DISCHARGE TEST

	VARISTOR	GAS ARRESTER	TRISIL	TRANSIL
DATA TEST	4500V/86A	>6000V/>140A	>6000V/>140A	<500V/<6A
DATA SHEET	15A (1)	10 000 (2)	90A (3)	2.2A (3)

1 . Rectangular current waveform of 2 ms.

2 . Exponential current waveform of 8/20 μs.

3 . Exponential current waveform of 10/1000 μs.

The obtained results were the following:

- The trisil and the varistor show more strenght than the specified, although the vendor specified tests define waveforms with higger energy.
- The transil failed at the first discharge at 500 V. It's a device with application in low voltage protection. The reason is that the peak power dissipation is constant for the same serie of devices, then for high voltage components the current available is very small.
- The trisil and specially the gas arrester show the higgest resistance to discharges and they didn't fail during the test.

Figure 1, Figure 2 and Figure 3 show the current (I) and the voltage (V) waveforms obtained when a discharge 1/1000 μs and 1500 V was applied to different devices.

The varistor peak voltage raised to 320 V, a 56% more than the data sheet breakdown voltage at 1 mA (205 V).

The voltage duration is 3.7 ms, and the current duration is 1.8 ms that correspond with the time when the voltage is higger than 200 V. The ohmic value at maximun peak voltage varied from 50Ω to 4Ω, depending on the transient amplitude (500 V to 4500 V).

The gas arrester peak voltage raised to 650 V, a 317% more than th data sheet dc spark-over voltage (230 V). The pulse voltage duration is 400 ns.

The ohmic value presented by the gas arrester, when fired, varied between 1568 mΩ at 500 V and 102 mΩ at 6000 V.

The trisil peak voltage raise to 160 V, that is smaller than the data sheet breakdown voltage (200 V), because the intrinsic trisil capacity help to fire it, for this reason the circuit to protect will not suffer pertutbation. The pulse voltage duration is 2 μs.

The ohmic value presented by the varistor, when fired, varied between 342 mΩ at 500 V and 74 mΩ at 6000 V.

Table 2 shows the leakage currents measured for the test samples at 200 V, and the maximun specified by the manufacturer data sheet.

Tabla 2

Leakage current at 200 V

	VARISTOR	GAS ARRESTER	TRISIL
TEST	25 μA	2.5 pA	100 nA
DATA SHEET	1mA	no spec.	1 mA

The results evidence the low leakage current for the gas arrested and the trisil, the high varistor leakage current can limit its aplication in circuit with low leakage requirements.

5 CONCLUSIONS

As a result of the test we can come to the following conclusions:

1. The more resistant devices are, in this order: gas arrester, trisil, varistor and transil. The high voltage transils show very low resistance to surge voltage, they are not suitable to be used in telecom applications.

2. The gas arrester and the varistor transmit voltage peaks dangerous to the circuit to protect. The gas arrester peak has a short duration (~0.4 μs) and very high voltage (~650 V), the varistor peak has a large duration (~1.8 ms) and high voltage (~320 V). The trisil doesn't transmit perturbations.

3. The leakage current must be taken into account in the designs using varistor (25μA at 200 V), the trisil has a lower value (100 nA) and the gas arrester has a neglectible value (2.5 pA).

Figura 1

Varistor voltage and current

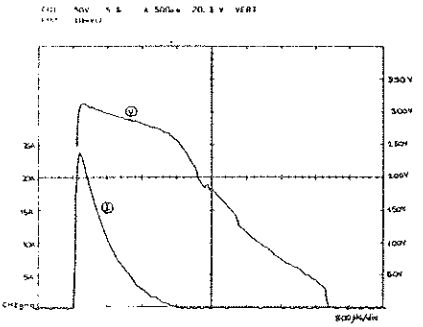

Figura 2

Gas arreter voltage and current

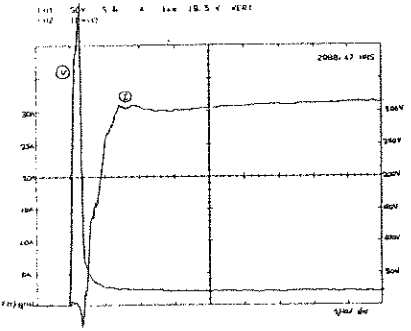

Figura 3

Trisil voltage and current

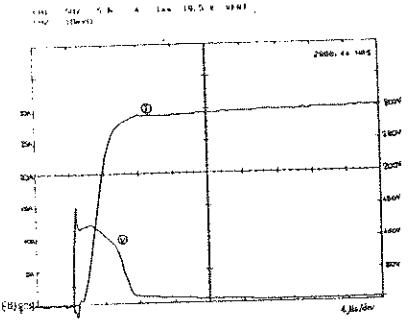

CAPACITY ESTIMATION OF METROPOLITAN AREA MOBILE RADIO NETWORKS

Mostafa Nofal
Dept. of Electrical Communications
Faculty of Electronic Engineering: Menouf, EGYPT.

Metropolitan areas present the greatest challenge to mobile radio network planners due to the ever-growing user demand and the shortage in frequency spectrum. Microcellular technology was evolved to overcome this problem. The microcells are tailored to cover streets where teletraffic sources (vehicles) are localized. The estimation of capacity and congestion parameters of mobile radio networks implemented in metropolitan areas is highly complex as a result of the increased handover rate and the fact that the behavior of telephone traffic is strongly correlated to vehicular traffic flow which is basically dependent on the traffic lights controlling techniques.

The movement behavior of vehicles within the service area is governed by the road topology, the vehicular traffic flow and the controlling traffic lights. A one-way system of straight cross roads that is controlled by two sets of traffic lights is considered. When a channel is assigned to a call, the system holds the call on that channel until completion within the microcell or the MS leaves the service area of the microcell. By positioning the BS antenna at the lamp post levels, the propagation characteristics are largely determined by the shape of the street.

Let n represents the number of lanes in the street and L defines the microcell length. With each idle user independently generates call attempts with exponentially distributed inter-arrival time of mean $1/\lambda_u$ sec, the new call rate attempted per microcell is given by

$$\lambda_n = [Mu - j\ ]\ \lambda_u$$

where Mu=(n.L.q / V) is the number of users in a microcell, q is the traffic volume, V is the mean speed of vehicles and j represents the number of active calls in a microcell. Consider $P_{nb}=(1-P_{ns})$ represents the blocking probability of new calls and the probability that a new call will cross the microcell boundary and need handover is P_1. If P_h denote the probability that a handover call needs more handover and the probability of handover failure is $P_{hb}=(1-P_{hs})$, the handover rate per microcell is

$$\lambda_h = (\lambda_n\ P_{ns}\ P_1)\ /\ (1 - P_h\ P_{ns})$$

Due to handover process, the occupation time of a channel by a call is equal to the least of either the time a MS spends in a microcell or the call duration. The time spent in a microcell is mainly dependent on the type of the traffic lights controlling technique. In green wave progression the approaches to intersections are provided with advisory speed indication signs which, if obeyed, ensure that the vehicle arrives at the traffic lights on green indication and is not delayed there. With $\bar{T}_c=1/\mu_c$ represents the average call duration, v represents the vehicular speed and h expresses the fraction of handover requests to the total requests, the average channel holding time is

$$\bar{T}_H = (1/\mu_c) - (h/\mu_c)\exp(-\mu_c L/v) - [(1-h)v/\mu_c^2\ L][1-\exp(-\mu_c L/v)]$$

When vehicles move randomly, they may suffer delay at intersections. The average occupation time of a voice radio channel under this vehicular traffic condition can be obtained as

$$\overline{T}_H = (1-h)\left[\frac{1+b1}{\mu_i+\mu_c} - \frac{b1}{\mu_d+\mu_c}\right] + h\left[\frac{1+b1}{\mu_o+\mu_c} - \frac{b2}{\mu_d+\mu_c}\right]$$

where $b1 = \mu_i P_d/(\mu_d-\mu_i)$ & $b2 = \mu_o P_d/(\mu_d-\mu_o)$ and $\overline{T}_i = 1/\mu_i$ is the mean travelling time from the onset of a call till the microcell boundary while $\overline{T}_o = 1/\mu_o$ is the mean travelling time from one microcell boundary till the next. The mean delay time and the probability of delay are respectively $\overline{T}_d = 1/\mu_d$ and P_d.

The time congestion, i.e., the probability that the N channels of the microcell are found busy is given by

$$P_N = \binom{M_u}{N} \left(\frac{(\lambda_n+\lambda_h)\times\overline{T}_H}{M_u - A_c}\right)^N P_o$$

where P_o is the probability that all channels are free and A_c is the carried traffic. The period and frequency of congestion during a busy hour are given respectively by

$$T_{cong} = P_N \times 3600 \quad \text{seconds}$$

$$F_{cong} = P_{N-1} \times (\lambda_n+\lambda_h) \times 3600.$$

The new or handover call congestion is given by

$$P_B = P_{nb} = P_{hb} = \binom{M_u-1}{N} \left(\frac{(\lambda_n+\lambda_h)\times\overline{T}_H}{M_u - A_c}\right)^N P_o$$

As the traffic carried by a microcell $A_c = [\lambda_n+\lambda_h)\times\overline{T}_H](1-P_B)$, the capacity of the system in terms of the average number of users served by a channel during a busy hour is

$$M_h = (A_c \times 3600) / (N \times \overline{T}_H) \quad \text{users/BH/ch.}$$

Numerical results for the two vehicular traffic progressions can be obtained based on the established analytical model. Some of these results are displayed in Figures (1-3) for nominal system parameters.

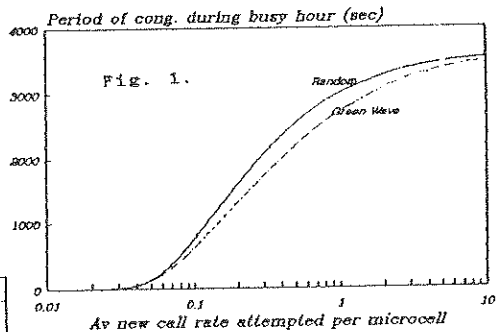

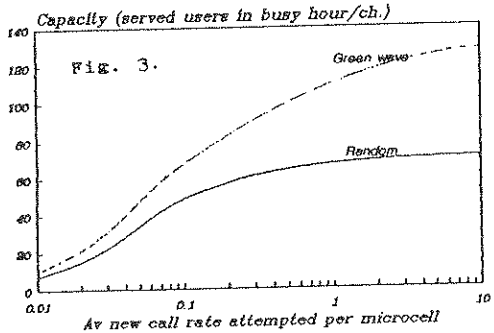

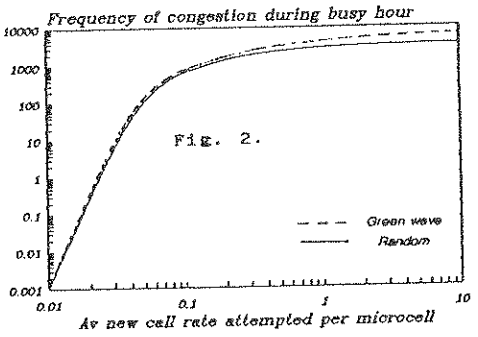

A NEW FACILITY FOR PIECE PART DOSE RATE TESTING **

D. PENE-BAVEREZ*, M. VIE - DGA/CEG 46500 GRAMAT, Tél. 65.10.54.32
Y.M. COIC, J.L. LERAY - CEA/BIII F-91680 BRUYERE-LE-CHATEL
J.C. BRION - EUROPULSE 46400 CRESSENSAC

Performance and concept improvements for a new 1.5 MeV pulsed electron beam facility are assessed in order to help contractors for piece part dose rate testing with a fair simulation fidelity to gamma energy deposition.

Evaluation of electronic behaviour under high dose rates is supported both by testing and calculations. Most of the work for testing is done with high energy X ray facilities. Use of small pulsed electron sources would give to contractors a smart tool in order to evaluate by their own with a cheaper method in the cursory of hardening development phase their electronic. Before taking this step it is necessary to solve the question of simulation fidelity starting from electrons instead of photons. It is also necessary to take into account the specific electronic irradiation restraints : because of the short electron ranges, discret devices under test must be bare to reach the active ship, and the test bed has to be shielded to avoid charge collection and noise.

We did calculations with a model of semiconductor structure including metallizations in order to evaluate the kind of energetic electron spectrum necessary to give a deposition depth profile representative of the dose rate profile corresponding to the gamma ray threat (Fig. 1).

Experimental data from the GENETRON source have shown that :

- The energy spectrum is too much soft,
- The current density is too low for good simulation.

In fact this facility seems to give an electron beam with less than 200 keV maximum energy and a total current in the range of 150 A for the experimental setup used.

Figure 1

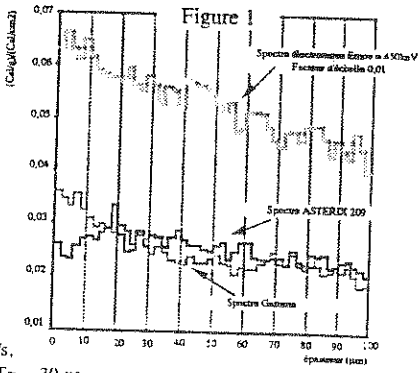

We have enhanced an effort to improve the concept of the source with the following performance objectives :

- Maximum electron energy 1.5 MeV, Dose rate range 10^8 to 10^{13} cCy(Si)/s,
- Electron mean energy > 500 KeV, Total current 2500 A, FWHM ~ 45 ns, T_R ~ 30 ns.

The improvements deal with dielectric interface design and diode geometry to allow and maximise axial electron production and avoid electric breakdown due to radial field distribution. The dielectric interface is made of polyvinyl chloride, cathod can be removed and has a truncated cone shape

The test chamber has been designed to allow irradiation testing through a large area titanium window closest to the source preserving the ability to vary the pressure in the transport chamber and the diode gap space and shape (Fig. 2).

We can record shot to shot reproducibility for :

- Current and voltage on the facility, Electron energy spectrum at the diode, Dose rate,
- Current density in the test chamber with a 1 cm^2 spatial resolution on the axis using a Faraday cup,

---

** This work has been supported by the french Delegation Generale pour l'Armement.

FIG. 2 : Encombrement du générateur d'électrons

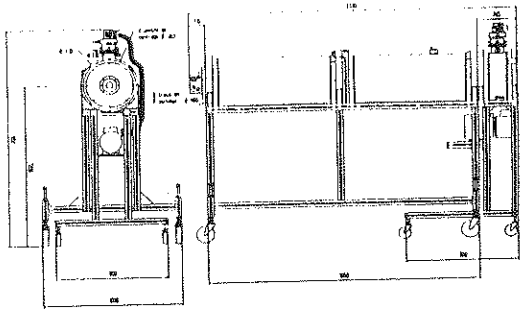

This paper showes the experimental set up and its performances.

We first recorded the facility working parameters : MARX voltage, diode voltage, diode current and electron current at the test chamber entrance.

This data were taken with sensors manufactured and calibrated by the vendor :

- A capacitive divider gives the MARX voltage pulse shape and magnitude (V_M),
- A coaxial capacitive divider gives the diode voltage pulse shape and magnitude (V_D),
- A Rogowski coil measures the cathode total current - I (D),
- The coaxial divider and current monitors are located in between the diode gap,
- Finally another Rogowski coil at the top of the source monitors the transmitted electron current through the titanium window (I_F).

The delivered pulse has a rise time of about 7 ns and a total duration of about 100 ns. Its shape is illustrated (Fig. 3).

The following results were collected for nominal working conditions with 30 kV charge for each of the 50 solid MARX stages with 250 Joule stored total energy.

	V_M (MV)	V_D (MV)	I_D (kA)	I_F (kA)
Peak	- 1,3	- 1,86	8,8	6,4
% Discreapancy (±) over 17 shots	4	3,5	5,8	10,4

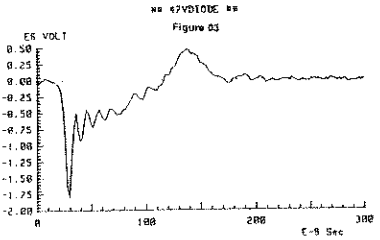

Roughly 2/3 of the total amount of electrons get more than 500 keV energy over these 17 shots at diode level. Mean electron energy is about 630 keV.

We will present the Faraday cup and dose rate data and analyse these results in terms of overall performance and simulation fidelity regarding the gamma ray threat.

Transient Over-voltage Test Wave forms: state space representation, p-norms and fuzzy logic attributes.

Valerii Ya. Kontorovich,
Centro de Investigacion y de Estudios Avanzados del I.P.N., Apartado Posaal 14-740, Mexico 07000. D.F.

Sergey L. Primak,
Electrical and Computer Dep., Ben Gurion University of the Negev, PO Box 653, Beer-Sheva, 84105, Israel

Transient overvoltages, which, for example may be produced by lightning or switching reactive loads, are a common reason of damage or upset of electrical circuits and systems. It is important to assess the vulnerability of electronic systems to damage and upset by transient overvoltage as well as calculate the bounds of the system's reaction on these distributions. To this end, standard publications describe several test wave forms that are representative of transient overvoltages (E. BENNISON E, A.J. GHAZI, and P.FERLAND, IEEE COM-21, 1136-1143, 1973.). In the paper (R.B. STANDLER, IEEE EMC-30, 1, 69-71, 1988) the simple analytical expression were presented to describe these forms. According to "combined approach" which was presented in (V. KONTOROVICH *et.al*, Zirich-93, 307-310) one needs the system of differential equations to model input signals - transient overvoltages as well as their p-norms (C.E. BAUM MN-63, 1979) to estimate the bounds of complex system reaction on these distributions.

We use the following set of p-norms to present all aspects of penetration transient overvoltages inside the complex systems, firstly proposed by C. Baum:

Peak Absolute Amplitude $$\left|f(t)\right|_{max} \quad (1)$$

Peak Absolute Derivative $$\left|\frac{df(t)}{dt}\right|_{max} \quad (2)$$

Peak Absolute Impulse $$\left|\int_0^t f(x)dx\right|_{max} \quad (3)$$

Rectified Impulse $$\int_0^\infty \left|f(x)\right|dx \quad (4)$$

Root Action Integral $$\sqrt{\int_0^\infty [f(x)]^2 dx} \quad (5)$$

In addition to the norm concept the fuzzy logic advisor to estimation of the electromagnetic environment was suggested in (J. LOVETRY & G. COSTASCHE, IEEE EMC-33, 3, 241-251, 1991). Their HardSys/HardTop software requires the database of the fuzzy logic attributes for different type of the excitation.

The state space representation, p-norms and fuzzy logic attributes are developed for the $0.5\mu s-100-kHz$ ring, $8/20-\mu s$, $1.2/50-\mu s$, and $10/1000\mu s$ test wave forms. Here we give only one example for $0.5\mu s-100-kHz$ ring wave form.

Example. 100-kHz Ring Wave form. The simple numerical expression for the $0.5\,\mu s-100-kHz$ kHz ring wave is specified by (6):

$$V(t)=AV_p(1-exp(-t/\tau_1))exp(-t/\tau_2)cos(\omega t) \qquad (6)$$

where $\tau_1=0.5334\,\mu s$, $\tau_2=9.788\,\mu s$, $\omega=2\pi\cdot10^5 s^{-1}$, $A=1.590$, t is the time, and V_p is the maximum or peak value of $V(t)$. Let us rewrite the (6) in the following form

$$V(t)=AV_p\{exp(-t/\tau_1)\cdot cos(\omega t)-exp(-t\cdot(1/\tau_1-1/\tau_2))\cdot cos(\omega t)\}$$

It is easy to show that the state equations for dumped sine $exp(-t/\tau)cos(\omega t)$ has the form

$$\frac{dx}{dt}=\begin{pmatrix}-1/\tau_1 & -\omega\\ \omega & -1/\tau_1\end{pmatrix}x,\quad x_1(0)=1,\ x_2(0)=0; \qquad (7)$$
$$V(t)=(AV_p\ 0)x$$

where $x=(x_1,x_2)$ - is the state vector. Using the block (7) one can easily construct the full equation for the wave form (6) in the following form:

$$\frac{dx}{dt}=\begin{pmatrix}-1/\tau_1 & -\omega & 0 & 0\\ \omega & -1/\tau_1 & 0 & 0\\ 0 & 0 & -1/\tau_1-1/\tau_2 & 0\\ 0 & 0 & 0 & -1/\tau_1-1/\tau_2\end{pmatrix}x,$$
$$x(0)=(1,0,1,0)^T;\ y=(AV_p,0,AV_p,0)x;$$

where x is the state vector, $V(t)=y$ is the output vector. The plot of (7) is shown on the fig.1. Using the following definition of constants $\alpha_1=1/\tau_2=1.4658\cdot10^5$ and $\alpha_2=1/\tau_1+1/\tau_2=2.6012\cdot10^6$ one can find all of the norms (1)-(5)

$$\|V(t)\|_{1)}=V_p(V);\ \|V(t)\|_{2)}=2.3141\cdot10^6V_p(V/s)$$
$$\|V(t)\|_{3)}=1.5765\cdot10^{-6}V_p(V\cdot s);\ \|V(t)\|_{4)}=9.2091\cdot10^{-6}V_p(V\cdot s) \qquad (8)$$
$$\|V(t)\|_{5)}=4.8491\cdot10^{-6}V_p(V\cdot s)$$

According to fuzzy logic levels introduced in (J. LOVETRY & G. COSTASCHE) this wave form can represented as set of fuzzy logic levels:
$f<100\,Hz-medium$; $100\,Hz<f<1\,kHz-high$; $1\,kHz<f<10\,MHz-extreme$; $10\,MHz<f<100\,MHz-high$; $100\,MHz<f<1GHz-medium$; $1GHz<$ $<f<10GHz-low$; $10GHz<f$ $-very\ low$.

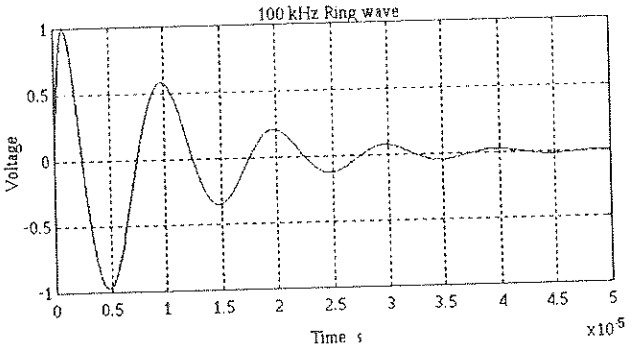

APPLICATION OF SIMULATED ANNEALING ON THE FREQUENCY ASSIGNMENT PROBLEM

A. Quellmalz*, A. Knälmann, Südwestfunk Baden-Baden

1. Current problems in spectrum managment

Spectrum management is one of the most difficult tasks in communication engineering today, because frequencies for wireless transmission of information must be considered as rare, exhaustible resources. The most important tasks for todays frequency planners are to complete, to expand or to reorganize existing transmitter networks. For each of these planning tasks it is necessary to take into account the influence of the electromagnetic environment. The goal is to decouple the transmitters by assigning appropriate operating channels under consideration of all extern constraints. The frequency planner has to protect the coverage area of each transmitter in the network against interference with a minimum amount of spectrum available. In this contribution we will demonstrate the application of a new stochastic approach to solve the frequency assignment problem. Also we will compare the new algorithm to several heuristic optimization algorithms at a realistic planning problem.

2. Channel assignment as a combinatorial optimization problem

The problem to assign each transmitter in a network an appropriate operating channel out of a limited amount of channels available, can be considered as combinatorial optimization problem. Solving a combinatorial optimization problem amounts to finding the "best" or "optimal" solution among a finite or countably infinite number of alternative solutions. Unfortunately the channel assignment problem belongs to the complex class of NP-complete problems. A direct consequence of this property is, that optimal solutions cannot be obtained in reasonable amounts of computation time. For that reason several aproximation algorithms have been developed to find at least a nearly optimal solution of the problem.

3. Stochastic approaches to solve channel assignment problems

One strategy which has been applied to the solution of NP-hard combinatorial optimiziation problems is the gradual "Simulated Annealing" of less than optimal combinations. The concept of "Annealing" is derived from solid state physics, where it is used to describe the process of eliminating lattice defects in crystals, i.e.

minimizing the free energy of the crystal, by a procedure of heating followed by slow cooling to room temperature. In present context every possible assignment of channels to the transmitters in the network corresponds to one configuration of the system. Each configuration is assigned a special value indicating the resulting interference in the network. This value is interpreted as the energy of the system which has to be minimized. During the optimization we search the configuration space for the optimal solution by randomly generating new configurations. A new configuration is only accepted if a special acceptance criterion, which is known as Metropolis Algorithm, is fulfilled. By this acceptance criterion the optimization process should not be trapped in a local minimal solution but should find the optimal solution or at least a near optimal solution for the problem. Hard constraints and the electromagnetic environment can be taken into account by adding special penalties. The channel assignment results in a transmitter network in which occuring interference is minimial.

4. Results

The new optimization algorithm will be demonstrated for the FM-Broadcasting system which is due to high transmitter density and low quality of the receivers very susceptible to interference problems. We will show that the new algorithm reacts flexible to fulfil hard constraints and to consider the electromagnetic environment. A comparison to several heuristic optimization algorithms will show the superiority of the Simulated Annealing Algorithm.

OPTIMISATION of SHELTER ARCHITECTURE "THIN PLATES MODEL" LIMITATIONS for GASKET MODELISATION

P. RIAUBLANC - L. TAILLER - G. BERREBI

THOMSON CSF / RGS DEN / DER
66 Rue du FOSSE BLANC 92231 GENNEVILLIERS FRANCE

This communication takes place within general works with the goal of hardening cost reduction. The example showed in this article deals with shielding aspect over :

-- Optimisation of shielding needs
-- Gasket modelisation (knowledge of internal electromagnetic environment and damaged gasket modelisation the aim of which is optimizing maintenance).

The studied system is composed of integrated equipment in a mobile shelter . The study is realized with the help of numerical simulation. The calculation tool is a three dimensional software using finite-difference in time domain (FDTD code).

At first, the interest to take into account electromagnetic zones into the shelter is showed. Numerical simulations results display natural electromagnetic attenuations given by :
-- coffer laying-out
-- doors laying-out
-- internal partition laying-out

The radiated impulses taken into account are :
-- 10 ns rise time
-- 1µs rise time

In a second time gasket modelisation (good quality gasket and damaged gasket) is discussed. We deal briefly with gasket modelisation using " thin plates model " in a FDTD code.

Numerical results show :

-- gasket modelisation possibilities to take into account good quality and uniform gasket
-- model limitations for the modelisation of medium quality and damaged gaskets.

The calculations realized with a FDTD code will be compared with other numerical simulation results (integral equation formalism) and experimental results.

MODIFICATIONS TO THE 1 MV EMP SIMULATOR AT WWD Bw

H. Schilling* and J. Schlüter
Wehrwissenschaftliche Dienststelle der Bw
für ABC-Schutz (WWD Bw)
and
K. Nielsen, T. Naff and J. Hammon
Physics International Company

The EMP simulator at WWD Bw, Munster, Germany, was developed during the late 1970s. The pulsed power system, supplied by Physics International Company (PI) of San Leandro, CA, includes a Marx generator and a peaking circuit/transmission line pulse launch system contained within a plastic housing (gas box) filled with the insulating gas R-12 (freon). Two major concerns have developed over the years since the WWD Bw simulator was first dedicated: (1) The venting of freon-12 into the atmosphere is considered harmful to the natural environment. (2) The most recent EMP studies show that simulated field risetimes might need to be considerably faster than the 10 ns requirements of ten years ago.

WWD Bw has contracted with PI to provide modifications as necessary to eliminate R-12 from the gas house and to design and develop a pulser providing faster risetimes.

The EMP simulator can be operated over a range of output voltages from 125 kV up to 1 MV and in either polarity. The Marx generator operates in a tank filled with transformer oil. A urethane diaphragm provides the oil/gas interface between the Marx and the gas box housing the peaking section. The peaking circuit (peaking capacitors, an output switch and water capacitors across the output switch) is necessary to produce the early-time, fast-rising load current that the Marx cannot supply because of its series inductance. To prevent flashover on the diaphragm and capacitor surfaces, the gas box is filled with about 26 cubic meters of R-12 freon at atmospheric pressure. This freon gas must be vented to the atmosphere during periodic maintenance procedures. Present environmental regulations prohibit the use of R-12 for this facility and after 1995 the manufacture of freon gases is prohibited. Consequently, the EMP simulator in its original configuration can only be operated at about half the maximum output voltage.

In principle, there are several methods by which the simulator can be reconfigured to operate at the full 1 MV output voltage without use of R-12. For example, the gas could be replaced by SF_6 or transformer oil or the pulser replaced by a complete modification. These solutions, however, were rejected as too complicated and costly.

PI has undertaken an approach by which it is possible to operate the pulser at near 1 MV using air only in the gas enclosure. The chosen method is to reduce time of voltage stress by reducing Marx and peaking capacitances. The pulser circuit is given in the figure with the revised component values shown in parentheses. The erected Marx capacitance of 20.2 nF results from the series-parallel combination of 30-nF, 50-kV tubular capacitors. Each of the Marx stages consists of two groupings of 16 parallel tubular capacitors.

For operation in air, the time of voltage stress is reduced by using only two capacitors in each grouping of parallel capacitors, yielding a Marx capacitance of 2.52 nF. The peaking capacitors were also changed, from 0.69 nF to 0.41 nF. The output pulse, which in the original configuration decayed with a 1.8 μs e-fold, now decays in near one-eighth that time.

An estimate of the breakdown voltage may be obtained from the empirical relationship developed by J. C. Martin and colleagues at the Atomic Weapon Research Establishment (AWRE) for impulse waveforms applied to gaps with a single highly field-enhanced electrode. The PSpice™ simulation, using the 2.52 nF Marx and 0.41 nF peaker, suggests an effective time of 32 ns at the oil/gas diaphragm and 6.5 ns across the output switch. Using the spacings of 50 cm at the diaphragm and 38 cm at the switch, one obtains V = 1017 kV and V = 1050 kV for the predicted breakdown voltage at these two locations, respectively.

Reliable, reproducible operation at 970 kV in an air environment has been achieved. Attempts to achieve 10% higher voltages, by using higher pressures or larger gaps in the output switch, have not been successful. Apparently an inductive closure occurs, most likely on the outside surface of either the output switch or on the parallel water capacitors. Energy dissipated in the breakdown is limited by the 90 Ω series transmission line and termination. As a result, when breakdown does occur, it leaves no visible track, and subsequent pulsing is successful.

In additional to the above work, PI has recently begun the task of designing a pulser for risetimes of 1 ns, 300 to 500 kV output voltage, and 30 to 100 ns pulsewidth. The pulser will be compatible with the I MV pulser interface so that either pulser can be used to drive the 90 Ω waveguide.

The fast risetime pulser will use the existing Marx to charge a transfer capacitor similar to the existing peaking capacitors. Upon closure of the transfer switch, a very low inductance peaking capacitor will be charged. Subsequent closure of a low inductance output switch will launch the fast risetime wave. Hardware will be fabricated later this year with installation and checkout scheduled for late 1994.

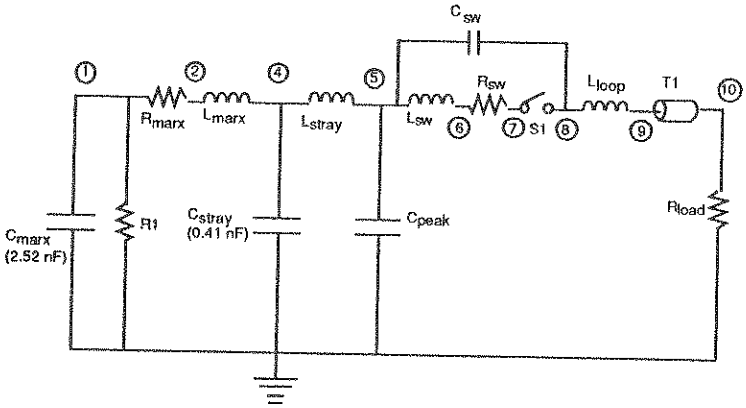

IMPROVED MATCHING OF ANTENNA SYSTEM FOR RECEIVING MANY CHANNEL TV WAVES

TOSHIHARU FUJIWARA HIROSHI UJIIE

TOHOKU INSTITUTE OF TECHNOLOGY

ABSTRACT

For TV broadcasting in Japan, two frequency bands of waves are in use presently: VHF(CH1-CH12) from 90 MHz to 220 MHz and UHF(CH13-CH62) from 470 MHz to 770 MHz. In each band, to receive with one antenna this many channels of waves in high quality is diffcult. Both bands cover a wide range of frequency and this makes it hard to satisfy the following conditions which are essential for reception of TV waves in high quality: the sharp directivity of the antenna and matching between the antenna and the feeder line. lack in directivity permits reception of unnecesary waves and poor matching creates an unbalanced suface currents on the feeder line which transmits undesired waves. Popular YAGI antenna aim at reception of a wideband waves which can be done only at the expense of the directivity and/or the antenna-feeder matching. In this paper, we propose a technique to satisfy both of these conditions. Our technique takes advantage of the fact that different channels are used in different service area and is to find the minimum number of antennas required for reception of high quality of TV waves in each area. This technique does not sacrifice the ability of the YAGI antenna but makes the best use its features, high gain and narrow bandwith. Our technique is described in detail, as follows. Let us consider two channels of area CH. A and CH. B at frequency Fa and Fb. Suppose we design a high gain antenna tuned at a frequency F_0 which is at the center of the two frequencies,

$$F_0(\mathrm{MHz}) = \frac{Fa + Fb}{2}.$$

Now, we found that the antenna/feeder matching can be attained satisfactory degree if the difference between the two frequenies falls within about 10% of F_0. The following is a more concreate description of our technique. In the city of Sendai, six channels of TV broadcasting waves are used(Table 1). The difference between CH. 1 and CH. 12 is 126 MHz which is 82% of the centre frequency of these two channels. Reception of all these twelve channels with one YAGI antenna forces degradation of some channels in picture quality or a considerable degree of loss in gain of every channel. However, reception of CH. 1

and CH. 3 with one antenna can be done without sacrifice in picture quality nor in gain. The frequency difference between these two channels is 12 MHz which is 11.8% of the centre frequency, 101.7 MHz. A YAGI antenna is designed at this centre frequency and the antenna-feeder matching is done only at the frequencies CH. 1 and CH. 3 . Thus, we can anticipate to have a high gain and low VSWR receiving antenna for these two channels. likewise, we can design high gain/high matching antennas for the pair of CH.5 and CH.12 and also of CH.32 and CH.34, respectivily.

Table 2 presents evaluation of the improved YAGI antenna in terms of picture quality. Fig. 1 shows an example of performance of an antenna by our design. In this case, the design was aimed at reception of pictures of Rank A quality. As we expected, the impedance as close to 75 ohm and VSWR was low (not more than 1.5). For any of the channels in the area of Sendai, quality of pictures by our improved antenna was evaluated A or A′ , higher than the evaluation of the general popular antennas which is B.

Table 1 Channels of TV waves in Sendai

Channel	Frequency(MHz)
1CH.	I.F. 91.24
	S.F. 95.74
3CH.	I.F. 103.25
	S.F. 107.75
5CH.	I.F. 177.25
	S.F. 181.75
12CH.	I.F. 217.25
	S.F. 221.75
32CH.	I.F. 585.25
	S.F. 589.75
34CH.	I.F. 597.25
	S.F. 601.75

I.F.: Image Frequency

S.F.: Sound Frequency

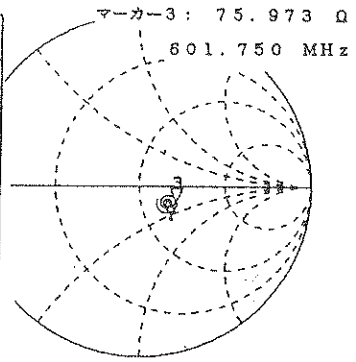

Fig. 1 Smith chart of improved antenna

Table 2 Rank of picture quality

Rank	A	A′	B	C
Evaluation	Excellent	very good	good	poor

METHODOLOGY OF EMC CONTROL FOR PAYLOAD ELECTRONIC EQUIPMENTS

Patrick ZEMLIANOY
Jean-Claude POURTAU

ALCATEL ESPACE, Industrial Development Department
26, Avenue J.F. Champollion - 31037 TOULOUSE CEDEX - FRANCE
Tél.: (33) 61.19.50.50
Fax: (33) 61.19.59.20

ABSTRACT

The electromagnetic compatibility of space programs must be practically insured at payload level with adequate protections against conducted and radiated interferences (shielding, filtering, ...) which are implemented inside the electronic equipments.

This paper takes aim to describe the EMC control methodology, applied at ALCATEL ESPACE, which combines:

- Software tools for EMI prediction.
- EMC design rules.
- EMC tests.

This methodology are illustrated by relevant applications in the frame of the poster - sessions.

KEYBOARDS

Electromagnetic Compatibility, Methodology, Simulation, Test, Payload, Equipment.

1 - EMC CONTROL METHODOLOGY DEFINITION

Due to specific of space activities (High reliability, lot of technical documentation, few models for each system, no maintainability, ...) a strong EMC control methodology (see figure 1.1) from preliminary study design and development, manufacturing and test is applied at equipment level.

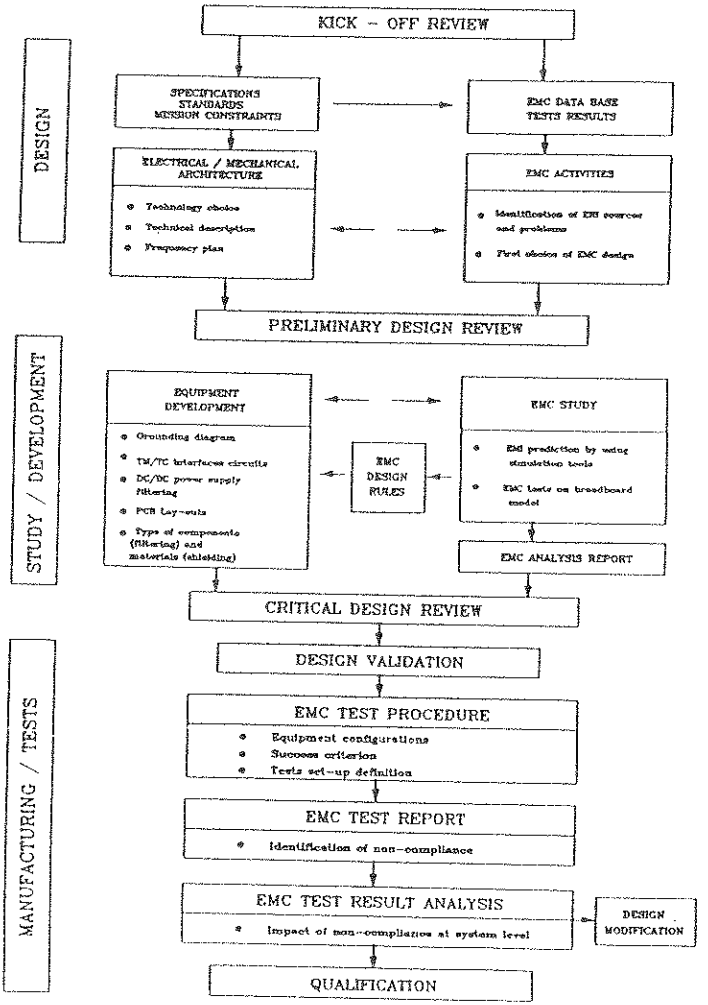

FIGURE 1.1: DEVELOPMENT PLAN / EQUIPMENT QUALIFICATION

2 - SOFTWARE TOOLS FOR EMI PREDICTION

A more systematic approach to EMC design is necessary, using simulation tools, starting at system or subsystem level and going down to the most basic level (i.e. equipment / component level).

The global objective is the reduction of the development time of products by introduction of modelling tools in the early design stage before building prototypes.

Alcatel Espace analyse of EMC point of view the subsystem and equipment hardware drawings, using the following software tools:

2.1 - EMC / CNES software

Analysis of conducted electromagnetic coupling in electrical circuit of equipment or system (common mode impedance coupling, cross-talk between wires, ...)

2.2 - MSC / EMAS software

Electro-Magnetic Analysis System, for electrical engineers who require comprehensive analysis capabilities. MSC / EMAS is a general purpose two and three dimensional finite element program for solving electric and magnetic field problems for linear, non-linear and anisotropic materials. The program includes DC, AC and transient solution capabilities and encompasses eddy current and resonant mode analysis.

MSC / EMAS includes a state of the art interactive graphics interface available for electrical engineers. The interface is based on MSC / XL, a program which makes the interface to finite element analysis as efficient and effective as possible. This closely integrated pre and post processor combines a modern menu structure, powerful command language, advanced graphics and integration with MSC's family of finite element analysis tools.

MCS / EMAS has replicated the data processing efficiencies of MSC / NASTRAN while incorporating MSC's a new unified formulation of Maxwell's equations. The program offers comprehensive capability to mix three and two dimensional elements. In addition, circuit analysis can be included in the model by using scalar elements such as resistors, capacitors and inductors.

Using MSC / EMAS, we can solve a wide variety of practical problems in analysis applications involving EMI and cross-talk, antennas, RF and microwave components, cavities and electrical apparatus.

Some applications, presented in the frame of the poster - sessions shows the capability of these software tools to analyse EMI problems.

3 - HARDWARE ASPECTS

EMC design rules are developed to allow designers to incorporate into the equipment design the necessary EMC measures from the beginning.

In addition EMC training is organized inside Alcatel Espace for study engineers; electrical and mechanical designers and manufacturing technician.

A example of "EMC design rules" at equipment level is shown in figure 3.1

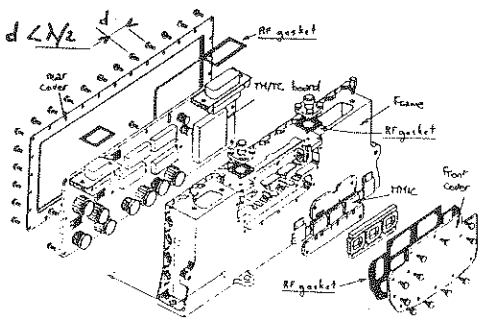

FIGURE 3.1: KU-BAND CHANNEL AMPLIFIER MMIC TECHNOLOGY

The shielding effectiveness is better 100 dB at ku-band frequencies.

4 - EMC TESTS

During subsystem or equipment development, testing for EMC design checking and demonstrating compliance with appropriate standards and specifications is necessary.

In the frame of the poster - sessions EMC tests are illustrated both a payload level and at equipment level.

A example of electrostatic discharge test set up at equipment level is shown in figure 4.1.

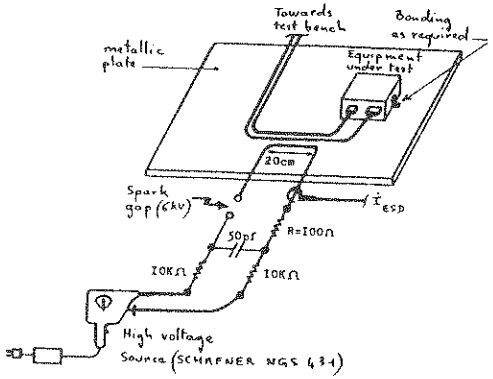

FIGURE 4.1: ELECTROSTATIC DISCHARGE TEST SET-UP FROM AN EQUIPMENT

5 - CONCLUSION

EMC control will take a growing importance in future satellite according to:

- A larger number of payloads integrated to the same satellite.
- Pulsed radar instruments.
- Demand for ON board Processing.

These trends will require from EMC domain huge efforts in term of:

- Capability to predict EMI for complete system.
- Electronic components modelling.
- Data base of EMC tests results needed for experience capitalisation.

EMC ANALYSIS OF SATELLITE EARTH STATIONS WITH SMALL ANTENNA (VSAT)

Ryszard J. Zieliński
Technical University of Wroclaw, Institute of Telecommunication and Acoustics
Wybrzeze Wyspianskiego 27
50-370 Wroclaw, Poland
phone: (+48) 71 214 998, fax: (+48) 71 223 473

ABSTRACT

In the past few years the use of telecommunication systems in the frequency range above 1 GHz has increased considerably. A mass production of the equipment used in those systems has already been started or will be started in the near future. The stations work in frequency ranges which are granted to special services exclusively or are shared by other services. To coordinate the operation of those services in the given frequency ranges, CCIR has developed special coordinating procedures. The method worked well only when majority of the communication systems were controlled by the Administration which solved the interfering problems according to relevant CCIR recommendations. But with the appearance and ever increasing number of small terminal systems (which may be used by anybody at any place), the method failed to bé effective.

The objective of this paper was to present method and result of analysis interference to satellite earth stations. Interference is generated by the set of VSAT terminals. The basic parameter for such analysis is the interfering signal level at the input of the interfered receiver. The determination of this level requires a mathematical model.

MODEL OF INTERFERENCE

It is assumed that interfering signals are caused by spurious radiation of VSAT terminals. The bandwidth of interfering signals is limited by receiver bandwidth. The duty factor for TDMA operation of VSAT terminals is not taken into account. The worst case situation is analysed i.e. when VSAT terminals operate continuously (duty factor =1). It is also assumed that there is no obstacles along the propagation path (free space propagation) and that interfering signals are not correlated. Last assumption enables to calculate total interfering power level as a sum of power levels of the interfering signals generated by each VSAT terminal.

It was assumed that all interfering stations operates with the same satellite. This assumption allows to determine azimuth as well as elevation angle γ for all considered antennas. These data with information about location of the interfered station in relation to interfering station allows to calculate all necessary angles. The detailed analysis is presented in the full paper.

The interfering VSAT terminals are distributed uniformly in the nodes of rectangular net. Distance between interfering and interfered stations is determined on the basis of density of VSATs / km^2. Two variants A and B of distribution are considered. They are presented in Fig. 1.

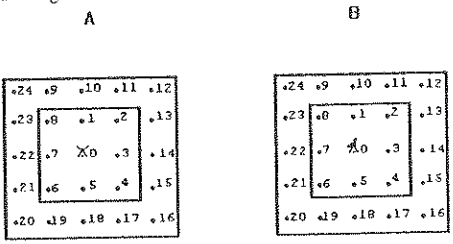

Fig. 1. Two variants of distribution interfering VSAT stations in relation to interfered VSAT station

The interfering stations were grouped in the zones. There are only two zones shown in Fig.1.

INTERFERED STATION CHARACTERISTICS

It is assumed that interfered station is typical VSAT receive station with receiver bandwidth normalized to B_r=64 kHz. The antenna gain is rigorously defined by the ETSI recommendation for VSAT terminals (Satellite system operators, e.g. those of EUTELSAT, have their own requirements.). For the purpose of analysis, the characteristics proposed by the ETSI standard ETS 300 159 was taken.

RESULTS OF ANALYSIS

The model was used for determining the total interference level at the input of the receiver for various density of interfering VSAT terminals. The free space propagation model was adopted. Typical parameters of all the stations considered were selected for the model. The analysis were performed for each interfering terminal. Results were processed to obtain results for each zone. In the table 1 the interference levels at the input of the receiver produced by interfering terminals located in the first zone are presented.

Table 1 Interference level [dBpW] from terminals located in the first zone,
variant A, $\gamma = 20°$, fr = 12.5 GHz, b = 64 kHz (N - density of terminals per km^2)

N station number	1	10	100
1	-53.91	-43.91	-33.91
2	-66.39	-56.39	-46.39
3	-63.38	-53.38	-43.38
4	-66.39	-56.39	-46.39
5	-63.38	-53.38	-43.38
6	-66.39	-56.39	-46.39
7	-63.38	-53.38	-43.38
8	-66.39	-56.39	-46.39
Σ	**-51.96**	**-41.96**	**-31.96**

Table 2 presents interference levels produced by terminals located in each zone (Σ). The value named max corresponds to the level of interference generated by dominant terminal in each zone.

Table 2 Interference level [dBpW] from particular zones.
variant A, $\gamma = 20°$, fr = 12.5 GHz, b = 64 kHz

N zone number		1	10	100	%
1	Σ max	-51.96 -53.91	-43.91 -43.91	-31.96 -33.91	49.1
2	Σ max	-55.83 -59.93	-45.83 -49.93	-35.83 -39.93	20.1
3	Σ max	-57.69 -63.45	-47.69 -53.45	-37.69 -43.45	13.1
4	Σ max	-58.95 -65.95	-48.95 -55.95	-38.95 -45.95	9.8
5	Σ max	-59.91 -67.89	-49.91 -57.89	-39.91 -47.89	7.9
1..5	Σ	**-48.87**	**-38.87**	**-28.87**	**100.0**

CONCLUSIONS

The analysis shows that the total interference level at the receiver input depends mainly on the interfering signals radiated from VSAT terminals located inside the first zone. Additionally there is one station dominating in this zone. It is possible to asses the level of total interference taking into account the level of interference radiated from dominant terminal and adding factor which depends on the geometry of the terminals (density of terminals) and elevation angle. The full set of results, formulas and detailed discussion can be found in the full text of the paper.

ANNEX

HIGH PRECISION FACILITIES AND MEASUREMENT MEANS FOR DETERMINATION OF METROLOGICAL CHARACTERISTICS OF EMP-SENSORS

A.V.Chikurov, L.N.Ivanov*, D.N.Ushanov, D.A.Yerokhin
Russian Federation Defence Ministry

For the metrological measurements ensuring during the tests of the equipment on EMP-simulators, complex of sample measurement means and check-up settings was made on the experimental base of the Russian Federation Defence Ministry.

As is known, two basic methods for the determination of metrological characteristics of sensors are in practical use: the method of direct easurements of the responces of investigated sensors on sample pulses generated by check-up settings (CS), and the method of immediate comparison of the responses of investigated and sample measurement means on the same testing signal. The first method is employed in the complex of "Delta-1" and "Delta-4" check-up settings to form pulsed electromagnetic fields; "Delta-2" and "Delta-3" settings to form pulsed magnetic fields; "Progress-1" setting to determine the parameters of the sensors transient performance. For the realization of the second method, IPPL-19M, IPPL-5L and INMP-BFK, DMP-1H sample measurement means (SMM) for pulsed electric and magnetic fields are used respectively. Metrological characteristics of the check-up settings and SMM are listed in Tables 1, 2.

The "Delta-1" check-up setting is made in the form of TEM-cell with splitted lateral conductors. CS may function in two operational modes: the mode of reproduction of the EMF single pulses with exponential form ("A"), and the mode of reproduction of the EMF single pulses with the stepped form ("B") for etermination of the decay of transient performance of electric field sensors.

For determination of the decay time constant of magnetic field ensors, the "Delta-2" check-up setting with field-forming system in the form of Maxwell's ings is used, which reproduces magnetic field intensity pulses with the stepped form. Amplitude-time characteristics of pulsed magnetic field of this setting allow to carry out metrological certification of MM with the decay from 5-7 microseconds to several tens seconds.

Investigation and certification of the sensors with transient performance rise time less than 5 ns may be carryed out in the "Delta-3" setting (Helmholz's rings) and the "Delta-4" setting (GHz-TEM-cell with splitted conductors and high-voltage generator with the frequency of signals repetition of 20-100 Hz).

The measurement means high-performance may be determined in the "Progress-1" setting (GHz-TEM-cell), which reproduces electromagnetic pulses with rectangular form with the front duration of 0.1-0.5 ns and total pulse duration of 200 ns.

Table 1

Metrological characteristics of the check-up settings

Name of the setting	Range of the reproducted field intensiti		Pulse rise time, ns	Decay time constant, mks	Error of amplitude reproduction, %
	kV/m	A/m			
"Delta-1"					
mode A	2-400	6-1000	5	145	1-2
mode B	2-400	---	10		1
"Delta-2"	----	14-140	10		2
"Delta-3"	----	1-250	1	total duration 0.04	5
"Delta-4"	1-42	2-110	1	total duration 0.11	5-7
"Progress-1"	10^{-4}- 1.2	$3*10^{-4}$-3	0.1-0.5	total duration 0.2	----

Table 2

Metrological characteristics of the sample measurement means

Name of SMM	Range of measured field	Rise time of the transient performance	Decay time constant of the trasient performance	Error of transform coefficient
INMP-FK	1-2500 A/m	3.7 ns	1.44 mks	4.5%
DMP-1H	7-1500 A/m	1.1 ns	11.6 mks	4%
IPPL-19M	0.1-500 kV/m	0.14 ns	total duration 0.02 mks	3.5%
IPPL-5L	0.1-500 kV/m	0.18 ns	total duration 0.005 mks	4%

Metrological characteristics of the sample measurement means (see Table 2) allow to carry out certification of MM for pulsed electromagnetic field measurements with the transient performance rise time of 0.2-1.5 ns and the decay time constant of 5-400 ns. Connection lines of the sensors allow to carry out measurements not only near grounded surfaces, but also in thevolume of the field-forming systems of the EMP-simulators. The length of connection lines (up to 50 m) allows to carry out metrological certification of large-size EMP-simulators as well.

Thus, the complex of the sample MM and check-up settings allows to carry out, on the experimental base, metrological certification of the pulsed electromagnetic field sensors with the transient performance rise time of 0.2 ns, unlimited decay time constant of transient performance in amplitude range of 10-500 kV/m and 3*10-2500 A/m.

METHOD OF THE MEASURING DATA TREATMENT TO BROADEN THE CAPABILITIES OF THE EXPERIMENTAL FACILITIES AND MEASURING EQUIPMENT USED IN THE ELECTROMAGNETIC COMPATIBILITY STUDIES

A.V.Vasenin*, V.A.Plygach, Y.F.Chibisov

Russian Federation Defence Ministry

There exists the problem of electromagnetic field, current or voltage parameters measurement at any point of the tested unit, subjected to the pulsed electromagnetic interference of various configuration during the electromagnetic compatibility studies. A deficiency of the experimental method is the necessity to produce the pulsed electromagnetic interference of the set form during the experiments.

The suggested method of the measuring data treatment is intended to eliminate the indicated shortcomings. The method works only when there are no non-linear effects; it allows to determine the induced currents, voltages and electromagnetic fields parameters at any other pulsed electromagnetic interference form using the recordings of the pulsed electromagnetic interference, induced currents, voltages or electromagnetic fields parameters inside the tested unit.

Let's consider the method algorithm to determine the current pulse $i(t)$, which would have been induced by the pulsed electromagnetic interference with the amplitude-temporary dependence $f(t)$ in some electrical curcuit of the tested unit. It is known, that the current pulse $I(t)$ is induced in the circuit unit under the influence of the pulse electromagnetic interference with the amplitude-temporary dependence $F(t)$.

The following statements are true, if there are no non-linear effects and the system characteristics do not depend on the reference time momentum setting:

- the current pulse $A*i(t)$ will be induced under the influence of the pulsed electromagnetic interference, expressed by the relation $A*F(t)$, where A is constant;

-the current pulse $i(t+T)$ will be induced in the circuit under the influence of the pulsed electromagnetic interference, expressed by the relation $F(t+T)$, where T is constant.

It follows from the statements, that $i(t)$ is expressed by presentation $f(t)$ as a sum of n functions $F(t)$, each of them is multiplied by the corresponding coefficient and is displaced for the corresponding time. Then the sum of n functions $I(t)$ is determined, each function is multiplied by the same coefficient and displaced for the same time, as the fuction $F(T)$, corresponding to it. The final sum will determine the real current pulse $i(t)$.

Such a solution of the problem is possible only if there are no errors in the initial data. When there are errors in the initial data, the problem in indelicately set from the very beginning. Besides, the error of the result becomes indeterminate. In this case the set of the problem is advisable to be altered: to seek for not a function $i(t)$, but the functions, determining with the set probability the confidence interval upper and lower boundaries, in which the function $i(t)$ values lie. The problem is solved by the direct statistical modelling method: the unknown pulse is repeatedly determined, and it is supposed, that there are no initial data errors, and initial data values change randomly every moment according to the given distribution in the range, determined by the appropriate parameter measurement errors. The definite portion of the results is excluded according to the given criteria. The remained maximum and minimum values of the results for every moment will determine with the set probability the upper and the lower boundaries of the confidence interval, where the function $i(t)$ values lie.

LIGHTNING INDUCED BY SURFACE TERMONUCLEAR BURST

A.A. Shvedov

Russian Federation Defence Ministry

Sometimes lightning may be induced by surface termonuclear burst. Photographs show that lightning flashes occur at ranges typically from 900 m to 1380 m and at the interval of time 1..75 ms [Uman M. et al. " Journal of Geophysical Research " V.77, N9, N9, March 20, 1972].

Estimates of electromagnetic pulse environment, given in all papers, indicate that static theta directed electrical field E_θ is not more than 30 kV/m. This magnitude is essentially lower than the uniform field breakdown of air. That's why authors have to make many additional assumptions to explain lightning occurance.

Calculations of quasistationary electromagnetic fields with the help of DIF two-dimensional program, using the approximate source of γ-radiation, show that theta directed electrical field considerably exceeds radial electrical field at 1 ms after a 10 Mt burst. It may achieve 60 kV/m at the standard air moisture of $\varkappa \approx 70\%$ (Fig. 1). Fig. 1b shows that maximum of $E_\theta(r)$ is namely in the range of 900...1400 m and we can observe it at $t \sim 1$ ms. Electrical field strength of about 60 kV/m is also considerably lower than breakdown. The most distinctive feature of " MIKE " burst is that it was carried out at the place which is characterized by increased air moisture (Eniwetok Atolls).

Investigations show that variation of air moisture from 0 to 96 % increases theta directed electrical field strengh in 4 times. Calculations, done for air mousture of 96 %, indicate that E_θ strengh achieves 100 kV/m. Taking into account that lightning discharges namely occured in the places where the apparatus with high ahtennas were, electrical field strengh is sufficient for breakdown (according to an emperical rule $E_\theta \cdot h \geq 1$ MB, $h \approx 10$ m).

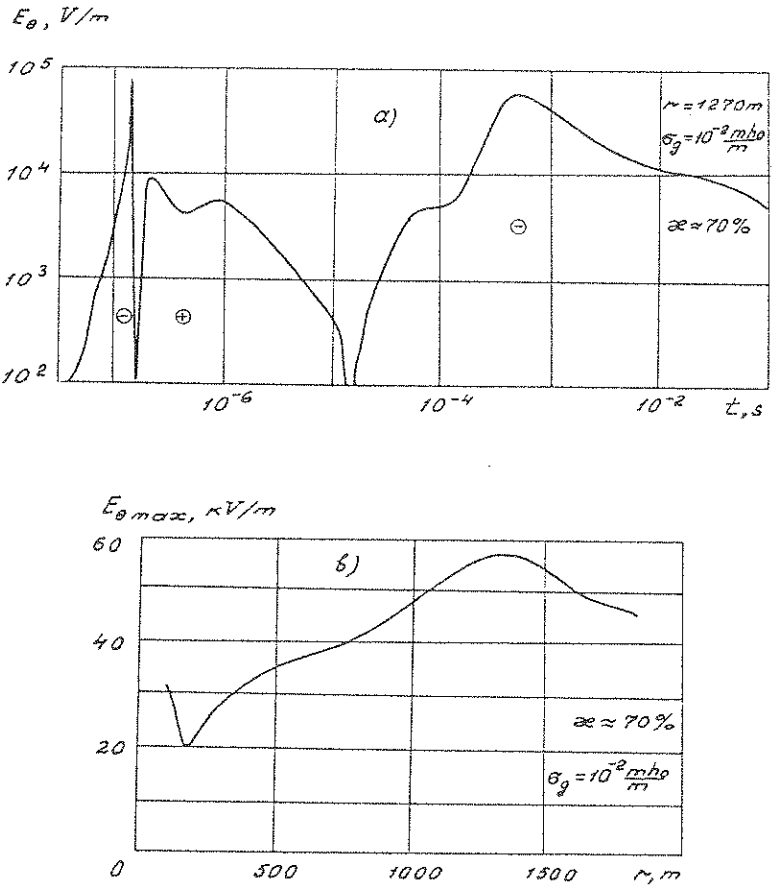

Fig.1 Theta directed electrical field as a function of time (a) and amplitude distribution (b)

THE SET OF CALCULATION METHODS FOR OBTAINING THE SURFACE BURST ELECTROMAGNETIC PULSE PARAMETERS

I.G. Chernishov, V.M. Kuvshinnikov., V.I. Pankov, A.A. Shvedov*

Russian Federation Defence Ministry

For obtaining electromagnetic pulse parameters in surface burst case the set computer codes is used. Each code based on a spesific method taking into account the main features of the field generation and evolution processes. Due to this approach the calculation method based on finit differencies may be efficiently used. The ranges of code application are show in fig. 1, 2.

Code FAG , worked out for solution Maxwell's equation, uses only one simplification- the axial simmetry. Discritization along characteristics in r-direction and conservative discritization in θ,z-direction are used. Iterativ procedure using two-dimentional discrete conservation law is applied to control accuracy.

The initial phase of EMP generation near the ground-air interface may be considered with help of TBA code. The retarded time and conservative discritization in θ,z-direction are used; $\partial / \partial r$ is omitted.

The equations to be solved by DIF and DIFER codes are similar to those of the two-dimentional diffusion problem. Nevertheless the retarded time is used to calculate the Compton current and the ionization rate. Code DIFER also takes into account the main features of the initial phase of EMP generation due to additional members in equations.

Sperical garmonics instead of the mesh in θ, z-direction are used in the POL and FORD codes. The POL code takes into account the real air conductuvity by finite difference approximation in r-direction. The FORD code is based on analitical expressions for a case of the non-conducting air and a real ground conductivity.

Self-consistent effect and ground stratification may be regarded by the code consideration.

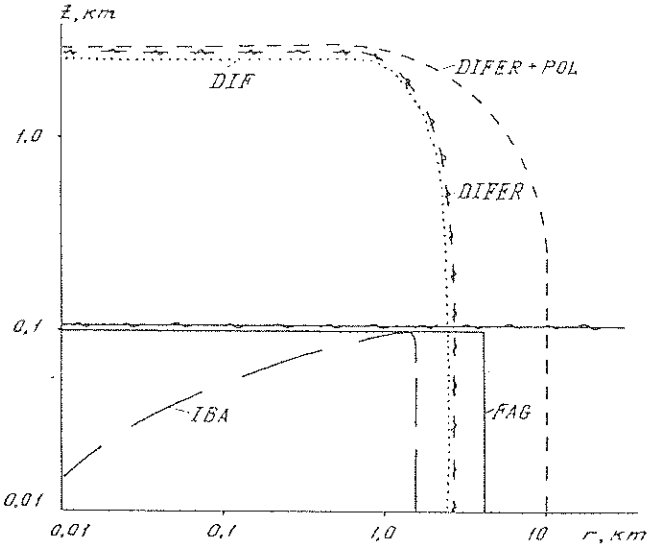

Fig. 1 Code ranges of effective calculations of EMP-parameters in ground:(z-depth,r-distance from burst)

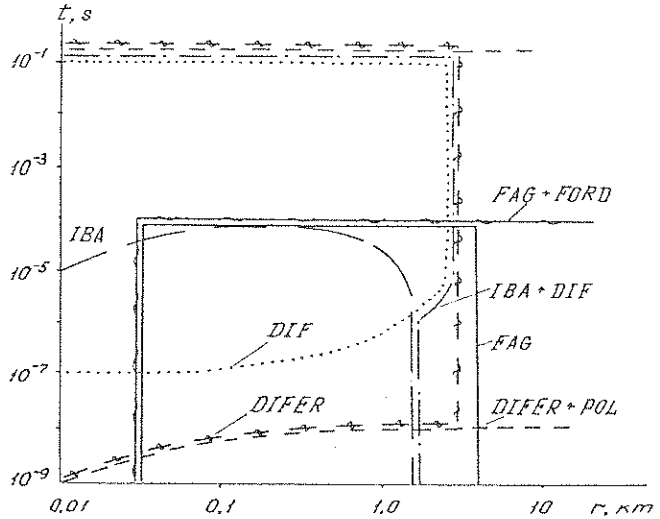

Fig.2 Code ranges of effective calculations of EMP-parameters in air:(t-retarded time,r-distance from burst)

ELECTROMAGNETIC FIELD EFFECT ON THE UNIT, PLACED IN THE SIMULATION FACILITY WORKING CAMERA

I.B.Baholdin, A.V.Vasenin, N.I.Kozlov, A.I.Kondrat'eva, D.D.Matveev, A.V.Miheev, V.A.Plygach*, V.I.Solovarov, Chikurov A.V.

Russian Federation Defence Ministry

To study the electromagnetic field effects on the units, equipped by electronic and electrical devices a problem of EMP field effects reproduction with the help of the simulation facilities arises. The simulation facility usually consists of high-voltage pulse generator and the field-generating system. Usually the field-generating system consists of two horizontal plates - the upper and the lower one. The tested unit is placed in the volume between these plates.

The electromagnetic fields, produced by the simulation facility, induce currents in the tested unit which, in its turn, cause the occurence of the so called "dispersed" field. The "dispersed" field is reflected by the plates and once again induces currents. These multiple repeating reflections may considerably alter the EMP effects on the unit, especially when the distance between the unit and the plates is too small.

The working volume of the simulator may be incresed to lower multiple repeating reflection effects. But this causes the complication of the field-generating system and the generator construction, wich brings about the simulating facility cost increase. It is impossible to place a large-scale facility indoors, and this fact considerably complicates the tests.

The important problem therefore is to set optimal requirements to the simulation facility working camera dimensions.

To solve this problem the computation method was created being the modernized version of the existing one (Baholdin I.B., Kozlov N.I., Kondratjeva A.I. "The 3-D computation of surface currents and charges, induced by electromagnetic fields in arbitrary configuration bodies", Preprint No 131, 1991, The Applied Mathematics Institute, Russian Academy of Sciences). The modern computation method differs from the previous one by the fact, that the calculation is performed in the calculation volume and its height corresponds to the field-generating system height. The electric field tangent constituent is set to be equal to zero to forse the upper and the lower plates influence on the measuring volume upper and lower borders. The new calculation method was approved by comparison with the experimental results of electromagnetic field distribution near the metal cylinder surface measurements. The results of the calculations and the experiments differ no more than 30% and are in the range of experiment error.

The research shows that the simulation facility working volume height decrease causes the EMP effect increase . The upper plate most of all effects the electric field parameters in the upper part of the unit, if it is placed on the lower plate surface. The greater the unit dimensions are the stronger is the effect. For example, electric field amplitude in the upper part of the unit increases by approximately 2,5 times, if the upper plate is fixed at the height of 1,5 times more than the cylinder with the height of 0,8 meters and the diameter of 2 meters. The electric field amplitude increases only by 20% if the cylinder of the same diameter and the height of 10 meters is tested, and if the upper plate and the tested unit hights ratio are similar.

Thus, the upper plate influence is neglegible, if the units with small transverse dimensions are tested. When the units with relatively large transverse dimensions are tested, the upper plate influence is to be taken into account even if it is placed at the height of 2 times more than the unit maximum height.

COMPUTER PROGRAM FOR NUMERICAL ANALYSIS OF THE EMP SIMULATOR.

M.G. Vakhnin, V.D. Gubarev*, O.V. Izotov
Russian Federation Defence Ministry

The computer program for numerical analysis of a Transmission Line EMP Simulator will be described in this paper briefly. The Simulator is composed of three transmission line sections consisting of wires. The fist and third sections are tapered to accomodate, respectively, a generator and a terminating resistor. The program is based on the numerical solution by moment methods (Galerkin) of an Electric Field Integral Equation (EFIE) for currents induced on the structer by local source of voltage. The output may include: current density, input impedance, near or far electric or magnetic fields. Using the well-known approximation for the thin wire,i.e.,

a. Transverse currents can be neglected relative to axial currents on the wire;
b. The circumferential variation on the axial current can be neglected;
c. The current can be represented by a filament on the wire axis;
d. The boundary condition on the electric field need to be enforced in the axial direction only,

EFIE for thin wires may be changed EFIE for the infinitesimally thin conducting plate (conditions a,b,c), but unknown current density vector is assumed to be one-dimensional vector (condition d).

Then, the EFIE used in the programm is given by

$$-\mu p \iint_s J(\overline{R'})G(\overline{R},\overline{R'})dS' + \frac{1}{\varepsilon p}\nabla_t \iint_s \nabla_t J(\overline{R'})G(\overline{R},\overline{R'})dS' = -\overline{E}^i_{tan} + Z_t J(\overline{R'}),$$

where

p=a+j*ω, ω- radian frequency, a- real part of Laplas tranformation process;

μ,ε- the permeability andpermetivity of the free space, respectively;

$G(\overline{R},\overline{R'})$ – Green's function of free space;

$\overline{R}$ - vector at the observation point;

$\overline{R'}$ - vector at the source point;

∇_t - the gradient operator in the direction tangent to S;

$\overline{E}^i_{tan}$ - the tangential component of the excitation electric field, which is zero everywhere on S except across the source gap, where it is assumed known.

In the numerical solution of the EFIE, the surface is devided into N strips less than about λ/8 in length to obtain an adequate representation of current distribution. The current density is next expanded in a set of triangular basis functions Jn as follows:

$$\bar{J} = \sum_{n=0}^{N} I_n \bar{J}_n$$

where N represents the number of subintervals.
If the inner product is taken with Jm, EFIE may be transformed into a set of algebraic equations given by

$$[\ Zmn + Zlmn\ ] \times [\ In\ ] = [\ Um\ ],$$

where [Zmn],[In] and [Um] are the generalized impedance,current, and voltage matricies, respectivly, and [Zlmn] is matrix determined by the terminal load.

This equation is solved using LU-transformation method, which involves a decomposition of Z in lower and upper triangular matricies.The integrations over S and S' are reduced to one integration after change of variables in the integrals.

Pulses of currents and fields in time domain can be obtained using inverse Laplas transformation procedure after solving EFIE for all frequencies interested.The program is written in FORTRAN-77 and realized on VAX3550. The obtained results lead to errors of less than 15% for experimental dates.The CPU run time for the transmission line with the size (width x perimeter) $5\lambda \times 65\lambda$ was about 15 hours.

OPTOELECTRONIC EMP-SENSORS

V.I.Bzyta, L.N.Ivanov*, A.N.Kornev, D.A.Yerokhin
Russian Federation Defence Ministry

For the measurement of amplitude-time parameters and structure of the field in EMP-simulators, optoelectronic measuring channels (MC) have found wide application on the Experimental Base of RFDM. The advantages of such channels are high disturbance protectivity, possibility to transmit measuring information at long ranges, and also galvanic outcome of recording equipment and sensor. Optoelectronic MC usually consists of sensor, amplifier, voltage-to-light-converter (VLC), optical fiber, photodevice and recorder.

The problem of measurement of the parameters of EMP with subnanosecond front duration arised lately. To ensure the possibility of EMP parameters measurement in subnanosecond range by the optoelectronic MC the necessity has arised to ensure required rapidity of measuring channel components.

The use of extensively applied capacitive and induction initial sensors for measuring EMP parameters in subnanosecond range was difficult due to resonance oscillations generated in the elements of sensors when geometrical sizes of sensor and corresponding upper critical frequency in the spectrum of EMP being measured are comparable. Strip sensors are without faults inherent in capacitive and induction sensors. The rise time of transient performance of strip sensors is 0.1 ns, which allowed to use them in the measurements of EMP in subnanosecond range.

Semiconductor lasers and optical diodes are usually applied as electricity-to-light converters. However, optical diodes have unsufficient rapidity. In this connection, low-mode semiconductor laser ILPN-216 with upper critical frequency of 2 GHz was used. Input electric resistance of ILPN-216 is 50 Ohm, which facilitates its co-ordination with an amplifier or sensors. The main disadvantages of these semiconductor lasers making difficult their use in VLC, were great noise intensity and low dynamic range (20-25 dB). Noise power of the VLC having semiconductor laser as a component is defined by the expression:

$$P_n = J_n \times I_{og}^2 \times R_g \times G \times \Delta f \qquad (1)$$

where J_n - respective noise intensity of semiconductor laser; I_{og}- constant component of the current from laser; R_g - input resistance of the amplifier; Δf - frequency band of VLC; G - gain of the amplifier.

From this expression it is seen that engaging the amplifier before VLG decreases noise power and increases dynamic range of the optoelectronic MC transmission part. Due to outer optical closed-loop

control and "jumping" of laser radiation modes the noise makes principal contribution to the relative noise intensity of low-mode semiconductor laser. The introducing of low-power high-frequency harmonic signal with the frequency exceeding upper critical frequency of the useful signal in 1,5-2 times into measuring signal given to the laser became the most acceptable way to reduce these noise components. High-frequency "sub-feeding" of the laser allowed to stabilize noise level of laser diode and to reduce signal distortion arising due to the alternations in the mode composition of the laser radiation.

The designing of the photodevices with rise time of transient performance of 0,3-0,5 ns was performed applying avalanche germanium photosensitive diode LFD-119 as photodetector. Full shot noise of LFD-119 was not make principal contribution to the noise performance of optoelectronic MC under recorded levels of the power of 200-600 μW. For further amplification of the signal, super-wide-band amplifiers with the gain of 20-40 dB were used.

Proposed principles of the designing of rapid optoelectronic measuring channel, and also optimization of the performances of MC carried out on the base of experimental investigation of the elements MC allowed to develop optoelectronic measuring channel for pulsed electric field of subnanosecond range.

MC consists of:

- strip sensors;
- voltage-to-light converter on the base of the low-mode ILPN-216 semiconductor laser with automatic adjustment of power and high-frequency sub-feeding;
- optical one-mode gradient fiber;
- photodevice with avalanche photosensitive LFD-119 diode and super-wide-band amplifier on the base of two M42177-1 microassemblies.

The tests of optoelectronic MC were carried out on the TEM-cell. Voltage pulse with the front of 200 ps was applied to the input of the cell from high-voltage cable of the hercon generator. The signal at the output of the measuring channel was recorded by stroboscopic oscilloscope C1-70.

Following performances of MC were obtained by the tests:

- rise time of transient performance - 0.85 ns;
- duration of measured pulse - 20 ns;
- amplitude range - 0.2 - 80 kV/m;
- coefficient of transform - 0.235 mV/V/m.

Thus, the developed optoelectronic measuring channel allows to determine time performances and amplitude of the pulsed electric fields with the front of 1 ns.

MULTICHANNEL AUTOMATIZED MEASURING COMPLEX FOR THE TESTS OF THE EQUIPMENT IN THE SIMULATORS OF HIGH POWER ELECTROMAGNETIC PULSES

V.I.Bzyta, L.N.Ivanov*, D.A.Yerokhin, V.M.Zhikharev
Russian Federation Defence Ministry

During the testing of great-size objects in the simulators of high power electromagnetic pulses (EMP) it is necessary to determine parameters of the electromagnetic fields in many points of simulator volume. Besides, the measurements of the electromagnetic fields, currents and voltages in the screens and electric circuits of equipment of tested objects are required. It is possible to enhance the effectiveness and to reduce the execution time using a multichannel automatized measuring complex (AMC).

The "Pamir-M" AMC located in RFDM Experimental Base is intended for the measurement of single pulses of the electromagnetic field, current and voltage in a wide range of amplitude-time parameters by way of the equipment testing in EMP-simulators. The AMC consists of 50 measuring channels for the detection of electromagnetic field, current and voltage, digital recorders for single pulses, two IBM PC AT computers, the devices for feeding and for synchronization. The number of channels may be increased up to 100 depending on the problem formulation. The devices with a resolution time down to 60 ps and effective discretization frequency up to 250 GHz such as SUPI24, S9-6, S9-27, SRG7 are used as digital recorders in AMC. The structure of the complex is modifiable depending on the problem under consideration and measuring conditions, which allows to use any number of measuring channels in variors combinations.

The technical characteristics of the measuring channels contained in AMC are listed in Table I. The values of parameters of transient performance are determined by level 0.1-0.9 (for a rise time) and by level 0.368 (for a decay time constant).

The devices and equipment of the complex are placed in the shielded room with attenuation coefficient for pulsed disturbances of 80 dB in frequency range of 0.01-1500 MHz. The communication lines of the measuring channels and feeder of the complex pass through special ports which prevent the penetration of the disturbances from inducted on lines signals in the shielded room. The AMC feeders filters reduce the pulsed disturbances by 60 dB in frequency range of 0.001-1500 MHz. It allows to carry out the measurements in a complicated electromagnetic environment at tests of the objects in great-size EMP-simulators.

The basic operations carried out by automatized measuring complex are follows: the tracollection, nsmission, storage, reflection and output of the registrated measuring information in the required form; the program-

registrated measuring information in the required form; the program-algorithm data processing; the checking of the complex operating capability; the self-calibration and self-checking of the measurement channels; the control of the measuring process, configuration changing, system composition and its self-checking control.

Table I

Characteristics of the Measurement Channels of Complex "Pamir"

Type of the measuring channel	Ampltitude range	Rise time, ns	Decay time, μs	Number of channels	Communication line and its length, m
IPPL	0.1 - 500 kV/m	0.14	0.02	2	Cable, 20
KIKEP	1 - 1000 kV/m	0.8 - 1.5	0.1	8	Cable, 150
KIKMP	3 - 2000 A/m	1.0 - 1.9	0.1	6	Cable, 150
IKMP SUPI21	1 - 1000 A/m	8 - 20	10	8	Fiber cable, 200
IKEP SUPI21	0.1 - 250 kV/m	7 - 17	15	8	Fiber cable, 200
IKEP SUPI27	0.1 - 250 kV/m	8 - 30	150	4	Fiber cable, 200
IKMP SUPI27	1 - 2500 A/m	13 - 22	150	4	Fiber cable, 200
DN-1	0.1 - 2 V	7	100000	2	Fiber cable, 200
ODN-1	0.01 - 50 kV	7	10000	2	Fiber cable, 200
IPT7	100 - 2500 A	7.6	1000	1	Fiber cable, 200
RPR-1	0.07 - 3 A	6	2.7	2	Fiber cable, 200
KSH-1	1 - 5000 A	7	1000	3	Fiber cable, 200

The program-mathematical and device ensuring of the complex allows to operate the registrating and measurement devices, inclusion, readiness establishing, calibration etc., to process the registrated signals (reconstruction of the given metrological characteristics of the measuring channels, Fourier-analysis, integration, differentiation); to carry out the measurements of the pulse parameters; to document the measuring information on the magnetic or paper carriers. The program creates a structured data base and the report of the experiment carrying out. The time of the processing of information from fifty measurement channels is not more than three minutes.

The software is made using module principle which allows to use the individual program modules and to supplement the software by new modules according to experiment conditions.

INVESTIGATION OF POSSIBILITY OF DEVELOPING HIGH-RAPIDITY ELECTROOPTICAL MEASUREMENT MEANS ON THE BASE OF FRANZ-KELDYSH EFFECT

L.N.Ivanov
Russian Federation Defence Ministry

The problem of metrological ensuring of measuring the EMP-parameters of nanoseconds and subnanoseconds ranges calls forth the necessity of measurement means (MM) development on the base of new physical effects, which allows to achieve greater rapidity, precision and reliability of measurements. In this plane the electrooptical Franz-Keldysh effect (FKE) in the semiconductor crystals is of interest. The essence of the effect is the appearance of the absorption of light, which has passed through the crystal, with photon energy hν, less than the width E_g of semiconductor forbidden zone, if the electric field E is applied to the semiconductor. In this case electrons of valent zone can get over to the conductivity zone, having absorbed the photon with energy $h\nu < E_g$ and then tunneling through triangular potential barrier with the width $d=E_g/eE$, where e - the electron charge. With the decreasing of the field, the barrier width is increased, the part of tunelling electrons is decreased and, accordingly, the number of absorbed photons is decreased too. So, intensity of ligth, that passed through the crystal, depends on the electric field intensity. This dependence can be almost linear when high Ohm (~ 10^8 Ohm×m) compensated semiconductors are used. The inertness of FKE is defined by tunneling time τ:

$$\tau = \frac{\sqrt{m_n\left(E_g - h\nu\right)}}{eE}, \qquad (1)$$

where m_n - reduced effective mass. Value of τ in the fields of 10^5 - 10^6 V/m comes to 10^{-12} - 10^{-13} s. Experimentaly linearity of FKE frequency chracteristic exists up to frequences 20 GHz.

Block-diagram of MM on the base of FKE is shown in Fig.1. The base elements of it is the sourse of light 1; transmitted and received optical tracts (optical fibers) 2, 3; sensor 4; photodetector 5. The functioning of MM is based on modulation of optic radiation intensity, which passed through it, when the measured electric field or voltage influence it. High Ohm semiconductor crystal is sensor.

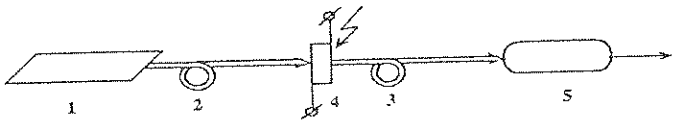

Fig.1. Diagram of measuring channel on FKE.

Since electric field makes amplitude modulation of light directly, but not phase modulation as in Kerr and Pockels effects, there is no need to use in sensor polarizators and focus facilities. This simplifies the design and allows to easily make sensor in integral-optic implementation. In addition, the crystal size in the direction of light penetration can be smaller by order than sensor based on Pockels effect with the same intensity and the same input signals.

Experimental study of possibility of application of FKE for measurement of nanosecond range pulses, was carried out using high Ohm compensated crystals of GaAs with the sizes of 0,1×3×4 mm. An electric field with the amplitude up to 2,5 MV/m was created in the crystal by generator of powerful nanosecond pulses (G5-33 type). The light came to the crystal from monochromator by quartz optical fiber with the diameter 200 mkm.

The amplitude modulated radiation, which passed through the crystal, was applied to the input of 14ELU-FK photoreceiver by optical fiber too. To increase sensor electric strength, stability of characteristics and optimum operating mode, the crystal was placed to the vacuumized volume and was cooled to 120 K.

The results of facility investigation have shown that it has linear amplitude characteristic in the range of intensity E = 0,4 - 2,5 MV/m and allows to measure the form of field pulses with the front duration of 5 ns. The forms of field pulses in semiconductor crystal and output signal of MM on the base of Franz-Keldysh effect are shown in Fig. 2. The limitation of time resolution was the result of imperfection of line structure, which brings the voltage to crystal. It can be removed in future.

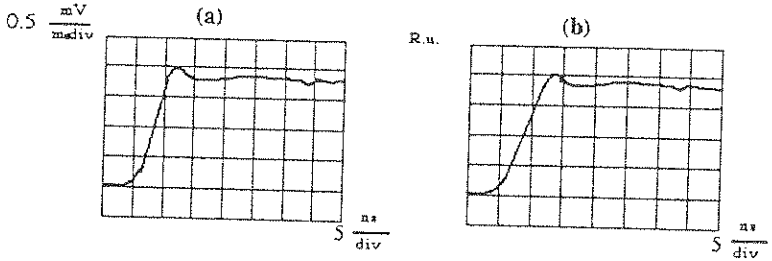

Fig. 2. (a) Form of pulse of measured field, and, (b) form of output signal of MM based on FKE.

Application of capacitive sensor, with the semiconductor crystal as load, allows to increase the MM sensitivity on the base of FKE.

Thus, MM on the base of Franz-Keldysh effect can be used to measure pulsed electric fields and voltages in nanosecond range. There is a perspective to increase MM rapidity on the base of FKE up to tens picoseconds.

ELECTROOPTICAL SENSOR BASED ON THE KERR EFFECT FOR PRECISE MEASUREMENT OF THE PULSED ELECTRIC FIELD AMPLITUDE UNDER NON-LINEAR CONDITIONS

V.I.Bzyta, L.N.Ivanov*
Russian Federation Defence Ministry

One of the ways to increase the pulsed electric field's amplitude measurement accuracy is application of the sensors using quadratic electrooptical Kerr effect. Important advantage of such measuring means (MM) is their high obstacle immunity and low-inertness.

Block diagram of the device for the measurement of electric field's amplitude is given in Fig. 1. Continuous radiation of the laser 1 is supplied to the polarizator 3 through optical-fiber transmission line 2. The main axes of the polarizator 3 and analyzer 6 are orthogonal and form the angle of 45 degrees with the direction of the electric field in the Kerr cell (4). During the supply of the pulsed voltage from primary sensors (PS) 5 to the electrodes of the Kerr cell, optical anisotropy arises in the cell. Linear-polarized radiation entered into the cell undergoes double ray-refraction: phase shift gathers between the extraordinary and ordinary rays during the passing through the cell. The analyzer 6 placed behind the cell transforms this phase modulation into amplitude one in accordance with an expression:

$$I = I_{max}\sin^2[(\pi/2)\times(U/U_0)^2] \qquad (1)$$

Here I and I_{max}- radiation intensity on the output of the analyzer at the given time moment and its maximum value; U- the voltage at the input time moment; U_0 - half-wave voltage defined by the cell structure and the Kerr constant. For the Kerr cell made in the form of flat capacitor

$$U_0 = \frac{d}{\sqrt{2lB}}, \qquad (2)$$

where d - distance between the electrodes; l - electrodes length in the direction of the radiation propagation; B - the Kerr constant.

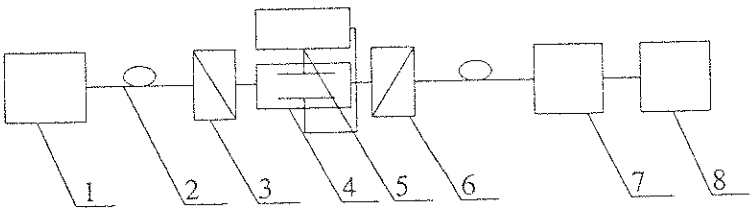

Fig. 1. Block diagram of electrooptical sensor.

At the moment of the voltage U supply on the cell, transmission of modulator is maximal, and, under further increase of the voltage, radiation intension on the analyzer output varies in accordance with (1). Thus, under the voltage supply of exceeding U_0, during τ time, radiation intensity at the analyzer output will be represented in the form of the section of guasisine function with constant amplitude, but with changing frequency. This function will fill the time interval of τ. The modulation frequency is defined by the expression

$$f(t)=\frac{U(t)}{U_0^2}\times\frac{dU(t)}{dt}. \qquad (3)$$

It is seen from this that modulation frequency is proportional to the voltage value at the PS output and the rate of its variation at a given time moment t. Formula (3) defines the frequency range, where the photoreceiver 7 and detector 8 must work when measuring pulsed fields.

The measurements of the pulsed electric field are carried out as follows. First, transform coefficient k_n of primary measuring converter and half-wave voltage U of the Kerr cell are defined. In this case, the Kerr cell must be selected in such a way that its half-wave voltage was less than or equal to minimum output PS voltage. Then, PS with Kerr cell is placed into measured pulsed electric field, and the signal at the photoreceiver output is recorded. When the signal is registrated, number of extremums n of the guasisine function is determined, and then the value of pulsed electric field intensity E is defined by the formula

$$E = k_n\times U_0\sqrt{n\pm\frac{2}{\pi}\arcsin\sqrt{\frac{I}{I_{max}}}}, \qquad (4)$$

where $\frac{I}{I_{max}}$ -relative intensity of the light beam registrated by photoreceiver; $n = 0,1,2,3,...$, n - number of the extremums of the guasisine function; k_n - PS transmission coefficient. Calculation of the amplitude and the reproduction of the pulse form are made by a computer.

Important advantage of the measurement method is that the measurement accuracy of the electric field amplitude does not depend on the transmission line coefficient of the light signal and parameters of the Kerr cell active media.

THE EFFECT OF THE SYSTEM GENERATED ELECTROMAGNETIC PULSE ON THE WIRE ANTENNAS

Y. V. Parfenov, O. A. Tarasov *

Russian Federation Defence Ministry.

As is generally known at interaction between X-rays and an object the so-called system generated electromagnetic pulse (SGEMP) is forming about it. If the object has an antenna-feeder arrangement then the SGEMP induces currents and voltages in antenna circuits.

This paper is concerned with the effect of the system generated electromagnetic pulse on a helical antenna, one of the most complex wire antennas. Two mechanisms of impact are considered: electromagnetic and radiative ones (Fig.1). First (electromagnetic) consists in that X-rays influence on antenna surrounding structures, in particular on its reflector initiating emission of photoelectrons from it which form radiation-extraneous current (REC). REC forms impulsed electromagnetic field affecting antenna. Second mechanism (radiative) is governed by the emission of electrons from antenna itself. In that case the antenna receives some potential with respect to the frame and the current flows through antenna load. Since the antenna is in the REC formation zone the nonlinear effects related to antenna impact on photoelectron current were been taken into account. Calculation of interference parameters in complex wire antennas was accomplished through solution of Fredholm's integral equation of the first kind by a self-regularization method.

The results of our investigation demonstrated that energy release at 50-ohm load of the helical antenna (the radius of the helix is 0.03 m, the pitch of a turn is a 0.05 m, the number of turns is 5, the radius of the conductor is 0.001 m) increases with increasing X-rays density at 20-ns length and quantum energy of 10 keV but it should be noted that at low levels ($\leq$0.01 cal/sq.cm) predominant contribution to energy release is introduced by the electromagnetic mechanism (Fig.2).

The obtained results demonstrate that the level of interference in the wire-type antennas is very high and for support of load conservation the use of shielding is necessary.

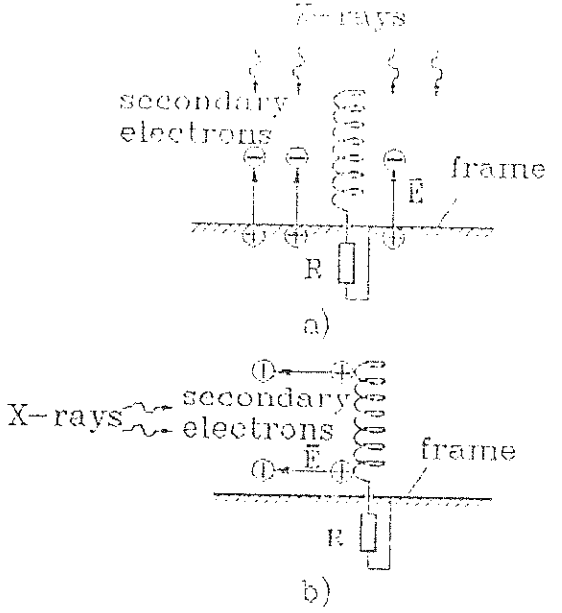

Fig.1 The effects of X-rays on an antenna:
a) electromagnetic
b) radiative

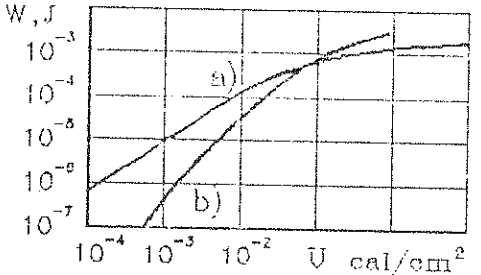

Fig.2 Energy release in antenna lood us function of X-ray energy density:
a) electromagnetic mechanism
b) radiative mechanism

THE MOBILE " ZENIT " COMPLEX SIMULATORS OF CURRENTS AND VOLTAGES

U.F.Chibisov *, Y.V.Parfenov, V.A.Plygach, L.N.Zdouhov
Russian Federation Defense Ministry

To realise the tests of radio-electronic and electrotechnical equipment, signal and electropower lines, antenna-feeder devices and tracts, facilities to depend from the effects of pulse currents and voltages, which are conditioned by outside electromagnetic field influence, the mobile complex of ZENIT simulators has been developed.

There are three plants which form the ZENIT complex , the output parameters of which have the wide amplitude-temporal ranges, which make it possible to realise the tests of various kinds objects of pulsed currents and voltages impact, generated by electromagnatic fields, i.e EMP, lightning, industrial disturbances and so on.

The tests are realised by way of supply of currents (voltages) pulses with parameters defined in advance on inputs of equipment or into cable lines. The plants output pulses are formed at the pulsed voltage generator launch. The generator is their integral part.

The required amplitude-temporal parameters are provided by the schemes switchings and the use of special forming appliances.

Said plants consist constructively of the pulsed voltages (currents) generators, the forming and management systems which are placed on automobile platforms.

The complex plants outward appearance and their basic characteristics are shown in Table 1.

The advantage of the described complex is his mobility and the wide amplitude-temporal range of the reproduced currents and voltages, which make it possible to realized the tests of objects, including stationary ones on the impacts of electromagnetic fields of different nature.

TABLE 1

ZENIT Complex Plants Outward Appearance and Their Basic Characteristics

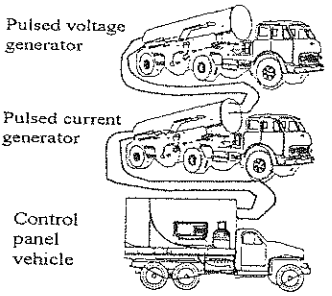

" Zenit-K " Simulator

" Zenit-K " Simulator critical parameters
Um =100...1200 kV
$t_{R}^{0.5}$ =3...10 ns
t_P =10...100 ns
Imax =20...80 kA

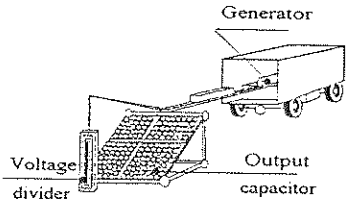

" Zenit-A " Simulator

" Zenit-A " Simulator critical parameters
Um =100...800 kV
t_R =10...80 ns
t_P =2 μs
Imax =10 kA

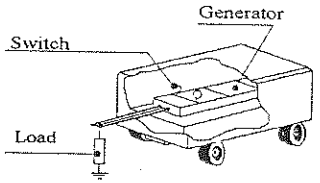

" Zenit-R " Simulator

" Zenit-R " Simulator critical parameters
Um =50...200 kV
t_R =15; 500 ns
t_P =1 μs; 20...100 μs
Imax =3...20 kA

Legend :

t_R - impulse rise time in the range of 0.1-0.9 from maximum

$t_P^{0.5}$ - impulse duration at the level of 0.5Um

t_P - impulse duration at the level of 0.1Um

ELECTROMAGNETIC PULSE EXPERIMENTAL AND TEST FACILITIES

V.M.KONDRAT'EV, V.M.LOBOREV*, V.V.PARFENOV, L.N.ZDOUHOV

Russian Federation Defence Ministry

EMP simulators modelling, with one or another degree of approximation, the nuclear explosion real electromagnetic fields (EMF) or currents and voltages induced by them in various systems are used at present to test the nuclear explosion EMP impact on military and civil materiel and equipment.

EMP simulators are available in a number of research and testing centers of Russian Federation, including the Defence Ministry Institutes. A complex of research and test facilities for various purposes is available at the Defence Ministry . Here large stationary and mobile simulators are included and also laboratory facilities generating pulsed EMFs, currents and voltages. Using these a wide variety of problems can be resolved, for instance:

- investigation of impact mechanisms of EMFs of diverse nature (nuclear explosion EMP, lighting discharges, commutation and emergency voltages in energy systems, static electricity) on diverse objects and systems;
- effectiveness investigation on EMF impact shielding techniques and means;
- testing of military and civil materiel, equipment, devices, separate apparatus elements and assemblies.

For these purposes stationary EMP simulators are used (SEMP-6, EDF-2M, EDF-0.4M) which reproduce EMP direct impact on large-size objects and systems. These simulators generate electric fields with the tension of $E_m \leq 200$ kV/m, magnetic fields with $Hm \leq 400$ A/m in operating volume of field-forming system V=600...15,000 m^3 or on the line L=1000 m long. Time characteristics of EMF reproduced pulses change in the following ranges: impulse front duration on a level of 0.1...0.9 of the amplitude τ_r=2...500 ns , and total pulse duration on a level of 0.5 of the amplitude τ_w=0.4...$3 \cdot 10^4$ μs. The simulators of this class are used to investigate and test objects and materiel that can be delivered to the test site.

There is a complex of mobile simulators to test equipment and diverse systems that cannot be delivered to the test site. Among these mobile simulators of currents and voltages induced in antenna-feeder devices (Zenith-A), currents and voltages in extensive communication lines (Zenith-K), in objects cases (Zenit-R) and also mobile simulating facility for EMF generation (SF-M) can be mentioned. The SF-M facility operating volume is $V=16\,m^3$, $E_m \leqslant 100\,kV/m$. The "Zenith-A-K-R" simulators output voltages are $U_m \leqslant 1\,MV$, peak currents - $I_m=80\,kA$, time characteristics of the pulses - $\tau_r=15...800\,ns$, $\tau_w=2...100\,\mu s$.

The available laboratory facilites (SEMP-1...5, SFIEP-1,2, SFIEC-1,2,3) and other ones can be used to study and test small-size radioelectronic apparatus, its elements and assemblies, radioelectric articles. The laboratory facilities major specifications are as follow: $V=0.1-2.4\,m^3$, $E_m \leqslant 750\,kV/m$, $U_m \leqslant 150\,kV$, $I_m \leqslant 30\,kA$, $\tau_r=0.5-15\,ns$, $\tau_w=10...10^7\,ns$.

As has been noted above simultaneously with the tests on nuclear explosion EMP impacts the experimental and test facilities of the Defence Ministry can be used to test the impacts of electromagnetic effects of natural and technogenic origin. These include testing on a direct lightning stroke on the object, lightning discharge field effects, short-circuit currents, commutation disturbances, fields and currents of electric transmission lines, harmonic fields effects, static electricity fields effects.

Measurements of loading parameters on objects being tested and their response to electromagnetic impact is carried out using automated measuring and processing complexes.

The Defence Ministry experimental and test facilities base is of a complicated infrastructure (spur-tracks, water-supply, power-supply, transportation, test objects depots). The test objects can be delivered by automobile, railway and air transport. Tests on the equipment of ships and other sea or river objects can also be carried out using experimental and test facilities of the Institute, for which purposes a special test proving ground is available.

ELECTROMAGNETIC FIELDS GENERATED BY GAMMA- AND X-RADIATION OF HIGH-ALTITUDE NUCLEAR EXPLOSION

V.M. KONDRAT'EV*, A.G. KOZLOVSKY, V.M. LOBOREV
Russian Federation Defence Ministry

An effective technique has been developed to calculate the parameters of electromagnetic pulse (EMP) generated as a result of simultaneous impact of a high-altitude nuclear burst gamma- and X-radiation on the atmosphere. The basis of the physical model is a current systems formation mechanism suggested by O.I. Leipunsky and A.S. Kompaneets; the mathematical model is based on the HF approximation of W.J. Karzas and R. Letter. The technique takes into consideration major physical factors having influence on the EMP formation and propagation, i.e. the fast Compton and photoelectrons twirl in the Earth's magnetic field, heterogeneous density of the atmosphere by altitude, primary distribution, ionization brake and fast electrons multiple dispersion, their delay in relation to photon flux as well as self-consistence effects and secondary electrons energetic spectre disbalance.

The Compton electrons current density is determined from the kinetic equation solution for the compton electrons distribution function whilst photoelectron current is basing on quasihydrodynamic approach, assuming electron flux medium characteristics definition from the equation for distribution function moments. Here, a part of physical factors is being taken into exact account, the other - approximately. The secondary electrons flux is calculated in the Lorentz model limits.

The EMP parameters determination is based on the numerical integration by the finite difference system technique of integral-differential equations including the equations for electromagnetic field and those of Compton, photo- and secondary electrons. The calculation time for one of the variants does not exeed 10 processor time minutes for a computer having internal performance in the order of 10^6 operations per second.

The report show that X-rays combined with gamma-radiation lead to transverse electrical field amplitude ($E_{\perp M}$) decrease at a ground surfase (Fig.1), and especially in the EMP source region (Fig.2). The fact is stipulated by a relatively great contribution of X-rays in the air conductivity as

compared with the flux density because of small velocity and weak anisotropy of the photoelectrons output diagram.

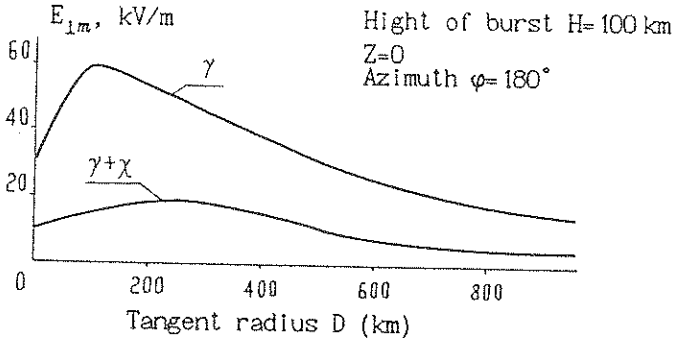

Fig. 1.

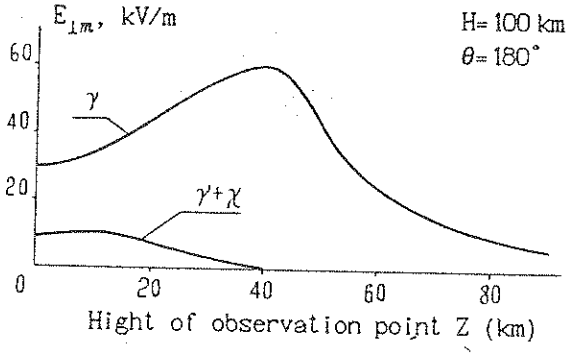

Fig. 2.

Dr. Ferdy MAYER - IEEE (PAR 1128)

IEEE RECOMMENDED PRACTICES FOR RF ABSORBER EVALUATION IN THE RANGE 30 MHz TO 5 GHz

1. Introduction

1.1 Scope

The purpose of this Practice is to recommend realistic and repeatable criteria, as well as recommend test methods to characterize the absorption properties of typical anechoic chamber lining applied to a metallic surface. The Practice covers the parameters and test procedures for evaluation of RF absorbers to be used for radiated emissions and radiated susceptibility testing of electronic products in the absorber manufacturer and/or absorber user environment over the frequency range of 30 MHz to 5 GHz.

The recommended methods approach the RF absorber evaluation at three levels:
(1) RF absorber materials bulk parameters
(2) Arrays of commercially available RF absorbers
(3) RF absorbers in actual applications as in anechoic or semi-anechoic chambers, and lined open test sites.

The evaluation measurements can be performed in frequency and/or time domain. However, the present Practice does not cover the correlation of absorber evaluation results obtained using different test methods. Such correlation, as well as new absorber evaluation methods to be developed in the course of new R&D programs, will be addressed in future revisions of this Practice.

1.2 Applications

With the proliferation of RF absorber lined shielded rooms, and their wide utilization for testing equipment for radiated emissions, and radiated susceptibility, there is a need to provide repeatable, and realistic performance figures of such RF absorbers in the frequency range of 30 MHz to 5 GHz.

The data provided by many manufactures is usually only for normal incidence. This immediately eliminates the effect of polarization on the RF absorber performance. For RF absorbers using a pyramidal structure, the reflection coefficient is also a function of the alignment of the incident wave with the pyramidal structure, specially for high frequencies, and large angles of incidence. The lack of these kinds of data precludes the accurate calculation of the performance of RF absorber materials in the great majority of applications.

This Practice is intended as an aid to RF absorber users and manufacturers. It will indicate what kind of data is required by the design engineer and various methods of how to obtain such data. Hopefully, in the future, both manufacturers and users, will utilize the same or accepted equivalent methods to estimate the performance of RF absorbers.

Where the word "shall" is used in this practice, it is considered to be mandatory. The words "should and may" are advisory only.

STUDY OF HIRF EFFECTS ON A LARGE CIVIL AIRCRAFT IN THE BAND 500 MHz - 40 GHz

CUILLER Claude *
GERAC
BP 505
31674 Labège Cedex

CROKAERT Michel
Aerospatiale Division Avion
316 Route de Bayonne
31060 Toulouse Cedex 03

ROUQUETTE Jean Alain
Aerospatiale Division Avion
316 Route de Bayonne
31060 Toulouse Cedex 03

1- INTRODUCTION.

High Intensity Radiated Fields are included in the environmental conditions to which a civil aircraft can be subjected. The sources which produce these fields are generally high power radio transmitters and radars. The threat is defined in the 10 KHz to 40 GHz frequency range in terms of "average" and "peak" values, and the higher field levels can reach several kilovolts by meter. The coupling phenomenon between the external threat and the aircraft is responsible for induced current on bundles or for the internal electromagnetic field. On the other hand, in last generation aircraft, the majority of the critical functions are vested in electronics equipment which potentially could be disturbed by electromagnetic threat. A demonstration of the good behaviour of the aircraft when it is subjected to HIRF threat is done on both the equipments and the aircraft.

A study has been launched in order to improve the method for demonstrating compliance in the 500 MHz - 40 GHz frequency range for a large civil aircraft. This requires a review of the present method on the basis of a better understanding of the coupling phenomenon and electronic disturbances. This abstract expounds the study philosophy and gives a summary of the initial results and the associated conclusions. On the basis of these conclusions the outline of further work will be presented in the last chapter. The study is carried out by Aerospatiale Aircraft Division, and it is sponsored by the Direction Générale de l'Aviation Civile (DGAC).

The 10 KHz - 500 MHz frequency range has already been discussed in a previous study (F. Flourens, JC. Albouy, M. Crokaert "Definition of a method for demonstrating conformity with HIRF threat in 10 KHz - 400 MHz range" Aerospatiale Aircraft Division, document CEDOCAR).

2- STUDY PHILOSOPHY.

The study is divided into three steps corresponding to the different levels of threat progression, towards the electronics components, and to the effects on these components.

- The first step concerns the coupling phenomenon between the HIRF external threat and the aircraft structure. The objective is to analyse the electric field penetration process inside the fuselage and to define the internal threat.
- After the definition of the internal threat, the following step concerns the coupling between this threat and the electronics equipment. This part defines the electric field seen by the electronic components or the power induced on the cables connected to the equipment and the worst illumination conditions for the equipment.
- The two first steps allow the threat inside an equipment box to be assessed, this third deals with electronics component behaviour, under radiation. Considering the complexity of the task, with respect to the number and type of components and the upset analysis, the objectives are to give an order of magnitude of the susceptibility levels and to define the severest threat characteristics.

To conclude a synthesis will be made between the threat seen by the electronics components and their susceptibility levels. It will highlight the threat characteristics and the illumination conditions which are the severest and which will have to be reproduced during equipment or system qualification tests. Test methods for aircraft transfer function measurement and equipment or system tests will be proposed.

3- PRESENTATION OF THE INITIAL RESULTS.

3.1- COUPLING BETWEEN THE EXTERNAL THREAT AND THE AIRCRAFT.

The aircraft structure electromagnetic behaviour analysis is based on theoretical results coming from coupling phenomenon simulation, and on A300, A320 and A340 experimental results. In the first step the simulation highlights the parameters related to the threat (frequency, polarisation) or to the aircraft structure (apertures), which control the electric field penetration inside the fuselage. In the second step the aircraft measurements are analysed with the help of simulations with an objective of generalization to define an internal environment applicable to a large aircraft. The internal environment is defined through transfer function between the external electric field (in free space) and the electric field inside the aircraft. These transfer functions are related to aircraft zones in which the electronic equipment are located, the cabin , the cargo zone and the cockpit.

The transfer functions related to the cabin and cargo zones have been simulated with models integrating the main apertures, windows and slots between the doors and the fuselage. The following figures present the simulation results and a comparison with the measured transfer functions.

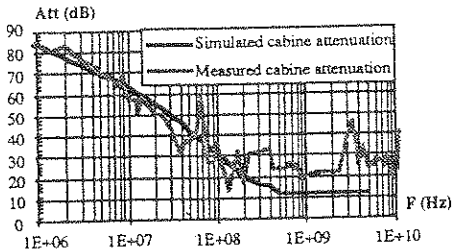

Figure 1
Cabin transfer function

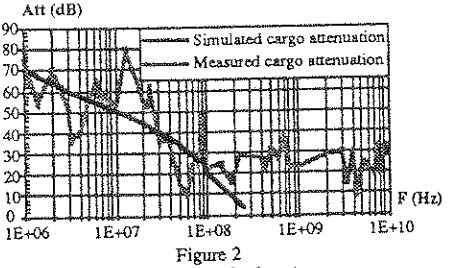

Figure 2
Cargo zone transfer function

The conclusions which have been drawn from the theoretical and experimental results are the following :
The windows and slots around the doors are the main apertures which control the electric field penetration.
The transfer function behaviour is equivalent to that of an isolated aperture and can be broken down into two steps according to the frequency range. A decreasing stage up to a limit around 200 MHz with a slope between 20 and 40 dB/decade and, beyond that, a stabilization stage. The frontier between these two stages corresponds to the aperture resonance frequency.
The minima in the experimental transfer function below 100 MHz are due to the field radiated by the cables at the current resonance frequency.
Above the aperture resonance frequency the differences between the measured transfer function minimum and maximum have the same amplitude as the simulated fuselage resonance phenomenon (not taken into account in figures 1 and 2).

3.2- COUPLING BETWEEN THE INTERNAL THREAT AND AN EQUIPMENT BOX.
The objective of this part of the study is to define the threat seen by the electronics inside an equipment box. This threat can be broken down into a radiated part, which penetrates into the equipment through the box apertures, and a conducted part induced on the cables connected to the equipment.
The study of the electric field penetration through the box apertures is based on simulation and measurement carried out on an A340 flight warning computer (FWC). The box transfer function has been established through electric field measurement in free space and inside the box in the 400 MHz - 18 GHz frequency range. The following figures present the first theoretical and experimental electric field transfer functions, for an equipment box without electronic inside.

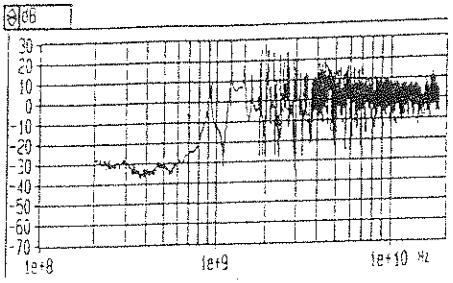

Figure 3
Simulated equipment box transfer function

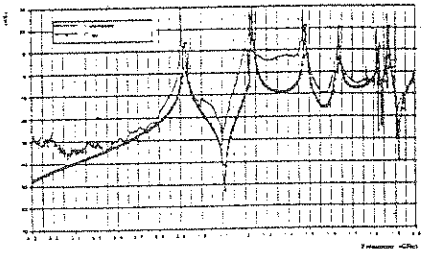

Figure 4
Measured equipment box transfer function

The initial results show that the simulation make it possible to find the resonance related to the box and the general behaviour of the transfer function. The stabilisation stage in the low frequency range presented by the measured transfer function can be explained by a sensitivity limitation of the measurement apparatus. As regards the high frequency range, as for the aircraft transfer function, the stabilisation appears beyond aperture resonance frequency.

The theoretical and experimental results will make it possible to characterize the coupling phenomenon and the influence of each kind of aperture, ventilation hole, slot between the different box parts, specific hole to receive memory module, and to assess the transfer function applicable to another equipment box different from the FWC. The severest illumination conditions for the equipment test will also be defined.
The conducted threat coupled on the cables will be assessed during the FWC tests.

3.3- ELECTRONIC COMPONENT SUSCEPTIBILITY.

The susceptibility levels of the electronics and the identification of threat parameters (level, pulse duration and repetition rate) will be defined through radiated tests. These tests will be carried out on a flight warning and system data acquisition computers. This computer will be modified in order to illuminate its printed circuit boards one by one. A monitoring bay connected to the computer under test will allow a failure analysis and an identification of the functions responsible for the upset to be made.
Preliminary radiated tests were carried out on isolated components, transistors and AND gates to assess the susceptibility levels of different technologies (High speed CMOS, Advanced complementary MOS, Fast bipolar, Advanced complementary MOS TTL levels, Advanced low power shottky). The threats used during these tests were CW and pulsed emissions.
The main conclusions drawn from these tests are the following :
- Most of the susceptibility occurred around 1 GHz.
- Above 1 GHz there is less susceptibility at higher field levels.
- The Advanced low power shottky is the most susceptible technology and the High speed CMOS the least susceptible.
- The lowest susceptibility level has been recorded at 600 V/m for a pulsed emission.

4- FURTHER WORK.

The initial results on the transfer functions show that if we take worst attenuation, the external electric field could be reinforced to reach values higher than the susceptibility levels of the electronics. The experience gained by Aerospatiale shows that this is not true. These discrepancies are due to elements not taken into account in the simple models used during the initial work such as :
- the bad Q factor inside the boxes which attenuates the resonance phenomenon,
- the characteristics of the threat inside the aircraft or the boxes which is not a plane electromagnetic wave,
- the equipment location and environment inside the aircraft. The metallic parts such as electronics bay and racks provide protection for the equipment.

The on going work will assess the influence of these factors on the coupling phenomenon. The definition of the internal threat will also be given in terms of power density.
As regards the sensitivity of the electronics, the initial work tends to correlate results obtained during aircraft and equipment radiated tests. Further work will give confidence on these results.

5- CONCLUSION.

The initial results on the coupling make it possible to identify, with simple models, the parameters related to the aircraft or to the boxes, which control the electric field penetration. Nevertheless, complementary work is necessary to evaluate the influence of parameters such as the Q factor, the equipment location and environment, not taken into account in the initial models. The tests carried out on the components make it possible to assess the sensitivity of different technologies. The influence of the threat parameters on the sensitivity of the electronics will be assessed through further aircraft computer susceptibility tests.
The better understanding on one hand of the coupling between the HIRF threat and the aircraft / equipment boxes and, on the other, of the threat parameters which are responsible for the electronics upset, will enable us to define more representative equipment tests as regards the bench test configuration, the frequency sweeping, pulse width, repetition rate and time exposure. If it is shown that these tests are representative of the HIRF effects on the aircraft and on the electronic equipments, the radiated test on the whole aircraft with the full threat could be eliminated.

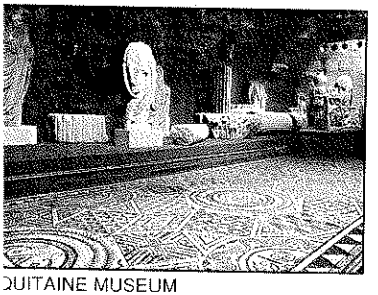

DUITAINE MUSEUM

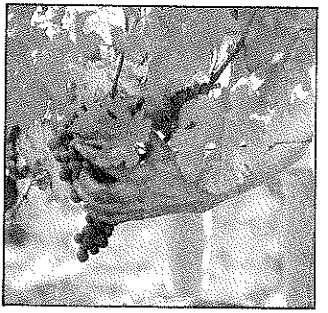

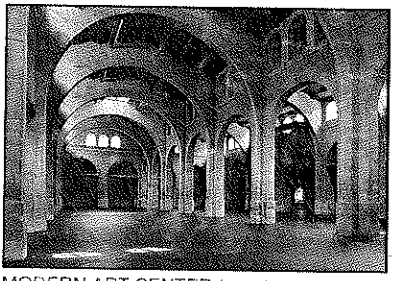

MODERN ART CENTER (capc)

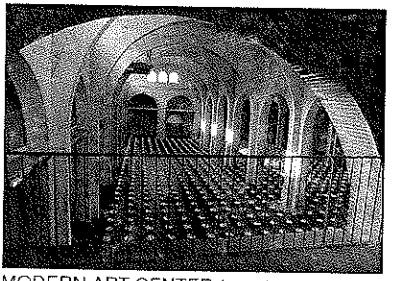

MODERN ART CENTER (capc)

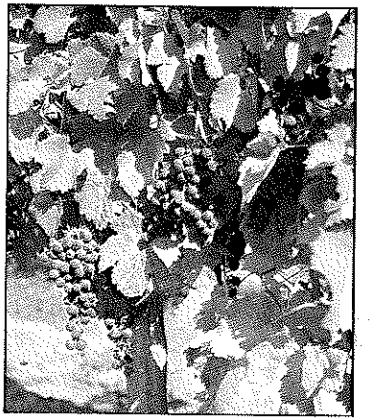

GA

AIR FRANCE

EDF
Electricité de France

CNRS
CENTRE NATIONAL
DE LA RECHERCHE
SCIENTIFIQUE

France Telecom

Imprimerie
BOOSENAAR